ORIGIN PHYSICAL AND CHEMICAL PROPERTIES, OF THE BENTONITE DEPOSITS FROM THE AEGEAN ISLANDS OF MILOS, KIMOLOS, AND CHIOS, GREECE

Thesis submitted for the degree of
Doctor of Philosophy
at the University of Leicester

by

George Christidis B.Sc (Athens) M.Sc (Hull)
Department of Geology
University of Leicester

June 1992

Στους γονεις μου
και στο Μαράκι που περίμενε

αἱ δ᾽αὐτοφυεῖς καί ἅμα τῷ περιττῷ τό᾽
χρήσιμον ἔχουσαι σχεδόν τρεῖς εἰσίν ἤ τέτταρες
ἥ τε Μηλιάς καί ἡ Κιμωλία καί ἡ Σαμία καί
ἡ Τυμφαική τετάρτη παρά ταύτας ἤ γύψος

Θεόφραστος "Περί Λίθων "

ORIGIN PHYSICAL AND CHEMICAL PROPERTIES, OF THE BENTONITE DEPOSITS FROM THE AEGEAN ISLANDS OF MILOS, KIMOLOS, AND CHIOS, GREECE.

George Christidis B.Sc (Athens), M.Sc (Hull).

ABSTRACT

More than 20 bentonite deposits crop out on the islands of Milos, Kimolos and Chios, Aegean Sea, Greece many of which are currently under exploitation. The bentonite deposits have been formed at the expense of volcaniclastic rocks, probably pyroclastic flows in the majority of the deposits, under subaqueous conditions. The presence of abundant authigenic K-feldspar in most deposits suggests that alteration was diagenetic and took place at very low temperatures.

Alteration of the glass involves mobilization of alkalis, and uptake of Mg and S. Al and Ti are essentially immobile while the behaviour of Si and Ca is controlled by both the nature of the parent rock and the composition of smectite. Fe displays small scale migration controlled by the prevailing redox conditions. Zr, Nb, Cr, Ni, V and the LREE are essentially immobile, while Ba, Sr, Rb, Zn, Y and the HREE are mobile. The behaviour of Th is controlled by the phase which hosts the LREE. The mobility of chemical elements has caused variation in the chemistry of the microenvironment in which smectites formed, resulting in large variations in the chemistry of smectites. Smectites might have been formed through an Ostwald Ripening-like process affecting the pore fluid chemistry and thus the chemistry of other phases like zeolites. Beidellites coexist with Cheto- but not with Wyoming-type montmorillonites. The crystal chemistry of smectites is affected by the nature of the parent rock, but the conditions prevailing during alteration might modify this "inherited" factor, as indicated by 1000 EPMA microanalyses which complement XRF, XRD, IR, DTA/TG, SEM, TEM and HRTEM data.

Almost all deposits have been affected by a later hydrothermal alteration which has effectively "diluted" the original smectite content either by conversion of smectite to illite/smectite, kaolinite/halloysite and/or alunite or by precipitation of new phases (carbonates, phosphates, sulphides). Illitization of smectite probably proceeds by an Ostwald ripening-like mechanism characterized by low supersaturation conditions.

The Greek bentonites have good swelling properties after Na-activation, and cation exchange capacity which ranges from 40 to 105meq/100gr. These properties are closely related in bentonites containing smectites with similar crystal chemistry. The bentonites with low CEC contain abundant opal-CT. The rheological properties vary and are probably related with the degree of disaggregation of the smectite tactoids. Low grade bentonites might be suitable for the drilling industry.

Acid activation increased the surface area of the bentonites up to 5 times and rendered them suitable for decolourization of crude edible oils. However, the maximum bleaching efficiency is not associated with maximum surface area. Mg-smectites are activated easier, but their decolourization properties deteriorate faster than Al-smectites. High grade Greek bentonites have foundry properties comparable to those of commercial products after Na-activation. This treatment increases the wet tensile strength but its effect on the other foundry properties is unpredictable.

The properties of the bentonites have been degraded by the superimposed hydrothermal alteration, in general, although in some cases limited kaolinization of smectite seems to have a positive effect on the rheological properties.

ACKNOWLEDGEMENTS

This project wouldn't have been carried out without the continuous help of a lagre number of people from the University of Leicester and elsewhere whom I would like to thank.

First I would like to to thank my supervisors Profs. A.C. Dunham and P.W. Scott for their patience, help and understanding. Their door was always open and we spent many hours discussing the interesting topics of my work.

Dr. Mike Norry had time for some long, fruitful discussions about the... behaviour of trace elements (what else?!!!) and Dr Kevin Pickering gave important clues about some sedimentary structures present in the bentonite deposits.

Nick Marsh with his vast knowledge on XRF analytical techniques helped to overcome the peculiar character of the bentonites and to obtain reliable results. His contribution also in the form of scientific talks was very important. I would like also to thank Brian Dickie and Addy Holmes who helped with the ICP analyses and "beared" me for a further month while I was doing CEC measurements. I would like to inform them that I have not dissolved yet!

Rob Wilson was always there when the microprobe had any problem. I really do not believe that I would have ever done so good microanalyses on smectites without his help. Colin Cunningham suffered until my polished blocks were ready. I would like to thank him for his patience. Rod Branson was always willing to allow me work on the SEM.

I would like to thank Mrs E. Roberts from the department of Biology, University of Leicester for her patience and help on matters concerning TEM and HRTEM. Dr. A. Low allowed me to use his computer program for particle size measurement. It helped very much. Also Drs J. Haynes and G. Adams from the department of Chemistry helped to carry out Infra Red Analysis. Mrs Sutherland from the same department allowed me to carry out my absorption measurements for ß-carotene.

It is certain that this project wouldn't have been completed without the help and understanding of my colleages. To Amit, Soma, Andy and Jullian who shared the same room with me and probably suffered, many thanks. Jez almost managed to make me a "Mack-Man", but my IBM instinct prevailed in the end!. I do not know how I would have presented my data without his help and patience. Migrac, Arif, Changlin and Salim had always their door open.

A part of this work was carried out outside the University. I would like to thank Dr. D.J. Morgan for the permission to work, and Simon Inglethorpe and Clive Mitchell for their help in the laboratories of the BGS. I would also like to thank BCIRA for their permission to perform foundry tests in their laboratories. Grand Holt and Joss James shared much of their experience.

Prof. Marcopoulos from the Technical University of Crete allowed me to use the XRD facilities of the University during the time I could not go for field work in the Aegean Islands.

This saved time which was valuable. I would also like to thank him, together with his wife Sylvia, for the wonderful hospitality they offered me the time I was in Chania.The Silver and Barytes Ore Mining Company allowed me to work in their quarries and kindly provided accomodation and transportation during the period I was in Milos. Roussos Brothers allowed me to work in the bentonite deposit at Prassa. I am grateful to all of them.

However, it is certain that I would not be able to submit this Thesis, if my beloved Eleni, Yiannis and Maria did not support me morally the difficult night of the 14th January, 1992. and thereafter. I thank them with all my heart.

And last but not least I would like to thank the State Scholarships Foundation for the economic support, without which this project would not have been carried out.

TABLE OF CONTENTS

LIST OF FIGURES

LIST OF TABLES

LIST OF PLATES

The plates are located in the end of the relevant chapters.

Chapter 3

Plate 1	1. Southern face of the Tsantili deposit, Area 1, Milos.
	2. Aspro Horio deposit, Area 1, MIlos.
Plate 2	1. Zoulias deposit, Area 1, Milos.
	2. Lower bentonite horizon of the Ano Komia deposit, Area 3, Milos.
Plate 3	1. Ankeria deposit, Area 2, Milos.
	2. Koufi deposit, Area 2, Milos.
Plate 4	1.Higher horizon of the Ano Komia deposit, Area 3, Milos (white bentonite)
	2. Garyfalakena deposit, Area 3, Milos
	3. Kato Komia deposit, Area 3, Milos.
Plate 5	1. Mavrogiannis deposit, Area 3, Milos
	2. Rema deposit, Area 3, Milos.
Plate 6	1. Kastriani deposit (kaolin), Milos
	2. Agrilies deposit, Milos.
Plate 7	1. Prassa deposit, Kimolos
	2. Loutra deposit, Kimolos
Plate 8	1. Fanara deposit, Kimolos
	2. Bonatsa deposit, Kimolos
	3. Agios Tryfon deposit, Kimolos.
	4. Bentonite outcrop in Chios Island.
Plate 9	1. Stockwork textures in Zoulias deposit, caused by hydrothermal alteration
	2. Syn-sedimentary fault in Zoulias deposit.
	3. Opal-CT-bearing bed in the Ankeria deposit, Milos.
	4. Pillow-lava-like texture in the Koufi deposit.
Plate 10	1. Concentric alteration to bentonite. Koufi deposit, Milos.
	2. Sedimentary structures (dewatering structures) in the bentonite of Ano Komia deposit.
	3. Contact between the Rema bentonite and the "Green lahar".
	4. Herring-bone structures in the Prassa deposit, Kimolos.
	1. Bivalve fossil in the bentonite of Loutra deposit, Kimolos.
	2. Typical "pop-corn" texture characteristic of bentonite outcrops, Bonatsa deposit, Kimolos.

CHAPTER ONE

INTRODUCTION

The Greek bentonites have been utilized since ancient times. However systematic extraction did not take place before the mid-fifties when the first bentonite quarries began their operations. Since then, the quality of these materials has become famous worldwide and Greece became the second producer in world scale with a total production of 1.3 million tonnes in 1988 (O'Driscoll 1988). Several companies, many being multinational, are currently operating on the two major extractive centres, the islands of Milos and Kimolos.

Despite the huge economic and scientific interest of the deposits the first and also the most recent investigation took place in the end of sixties with the Ph.D thesis of Wetzenstein (1969) on the bentonites of Milos. Since then, many of the conclusions of this work have been reviewed critically by several workers (see section 1.5). The bentonites of Kimolos and Chios islands have never been studied systematically and only sporadic references have been reported.

1.1. Objectives of the project.

The lack of knowledge about one of the most important industrial minerals of Greece gave the motive for this project, the objectives of which can be summarized as follows:

-Establishment of the environment in which the parent materials were deposited and understanding of the processes which caused their alteration.

-Complete mineralogical and geochemical investigation of the Greek bentonites in order to establish the principal parageneses in the different deposits.

-Attempt to correlate the different deposits so that the exploration cost for new ones might be reduced.

-Determination of the useful physical and chemical properties of the bentonites, especially those for which no previous data have been presented (for example the deposits of Chios island).

-Attempt to activate the Greek bentonites with acids in order to evaluate their potential in decolourizing oils. Greece does not currently produce any acid activated clays but imports them.

1.2. Structure of the Thesis.

The thesis has been divided into eleven chapters. It can be separated into two equal parts. The first part consists of the first six chapters and deals with the geology, mineralogy

and chemistry of the deposits. The second part which consists of five chapters deals with the industrial evaluation of the Greek bentonites.

The first chapter is the introduction of the thesis. It includes sections about the terminology used in both the theoretical and industrial applications, the crystal structure of smectites, the useful properties of the smectite minerals which are valued by industry, and the main applications of bentonites in the various sectors of industry. It includes also, the previous scientific contributions on the geology, mineralogy, chemistry and physical properties of the Greek bentonites.

The second chapter deals with the regional geotectonic environment where the islands of Milos, Kimolos and Chios occur. Also an account of the evolution of the Aegean region and the subduction of the African Plate under it and its connection with the volcanism in the South Aegean area is discussed.

The third chapter is involved with the geological features of the three islands, their structural features and the geological characteristics of the individual bentonite deposits, including stratigraphic columns of the deposits wherever necessary.

The fourth chapter examines the mineralogical characteristics of the deposits including bulk mineralogy, clay mineralogy, as well as the mineral-chemical characteristics of the smectites and other authigenic minerals.

The fifth chapter deals with the geochemical characteristics of the deposits, from both the major and trace element point of view. Special attention is given to cases where profiles from the fresh glass to the altered bentonite are observed in order to establish the relative mobility of the various chemical elements. Also a correlation between the deposits of Milos island is attempted using simple geochemical plots and discriminant function multivariate statistics.

In the sixth chapter a synthesis of the geological, mineralogical and geochemical data is attempted. This is done in order to establish the mode of origin of the bentonites and the formation of smectites, the nature of alteration, and the use of the information obtained in the exploration of new deposits in the area.

The seventh chapter deals with the evaluation of quality and grade of the bentonite deposits. The properties which are used are the swelling index and the cation exchange capacity respectively.

The eighth chapter examines the rheological properties of the Greek bentonites, including viscosity and thixotropy. The variables measured are apparent viscosity, plastic viscosity, and yield. Also thixotropic loops of some selected bentonites are presented.

The ninth chapter involves the acid activation of representative samples under conditions of different time and acid strength. The acid activated clays are examined for their suitability in the clarification of rape seed oil, in comparison with commercial products already used in industry for that purpose. They are also examined by various analytical

techniques for the crystal-chemical changes caused on smectite by the acid treatment.

The tenth chapter deals with the applications of Greek bentonites in foundries. The raw materials are examined in both their natural state as well as in alkali-activated state for properties like green and dry compression strength, wet tensile strength, shatter index, compactability and permeability.

Finally the eleventh chapter includes the conclusions obtained from the thorough examination of the Greek bentonites.

1.3. What is bentonite? -Terminology.

Accorrding to Grim & Güven (1978) and Patterson & Murrey (1983), the term bentonite was used for the first time by W.C.Knight in the end of 19th century, to describe a clay-rich rock found in the Fort Benton Cretaceous formations in Wyoming, USA. In the subsequent years, bentonites have been valued for their unique physicochemical properties; they are used in many sectors of industry including drilling industry, foundries, mineral and vegetable oil industry, ceramics, and pharmaceutical industry. Notwithstanding their intensive utilization there is confusion about the terms used to describe bentonites in various places of the world.

To begin with, the necessary feature a rock must have in order to be characterized as bentonite is the predominance of a clay mineral belonging to the **smectite group**; montmorillonite in the majority of cases. Although the term is usually used for clays derived from the alteration of a volcanic glassy rock (volcanic ash or tuff in most cases), there are deposits where the parent material is not known with certainty. This led Grim (1972 as quoted by Patterson and Murrey, 1983) to define bentonite as a clay consisting essentially of smectite minerals regardless the way of origin. Previously, Wright (1968, as quoted by Grim and Güven 1978) had defined bentonite as "a clay composed dominately of a smectite clay mineral, whose physical properties are dictated by this mineral". This definition was adopted by Roen & Hosterman (1982). Also it covers the process proposed by Bates (1969) about redeposition of material transported from the site of its original deposition. A different definition has been given by Fisher & Schmincke (1984) which was adopted by Chamley (1989). According to this definition which does not include the necessity for existence of a particular clay mineral, bentonites are laterally widespread clay rich, thin beds of altered volcanic ash. This definition is favoured by several clay mineralogists (Dr. W. Huff oral communication, Manchester, July 1990). According to the clay mineral present they are named *smectite bentonites*, *kaolinite bentonites* or *tonsteins* and *illite bentonites*. However, according to Roen & Hosterman (1982) the term bentonite should include the characteristics described by Knight in the type-locality. Since these characteristics are associated with the presence of smectites, the term bentonite should be

Table 1.1

Nomenclature used to describe smectite-rich materials

(modified after Anonymous, 1978).

Principle Mineral	Synonymous terms	Regional terms
Sodium montmorillonite	Synthetic bentonite	Wyoming bentonite (USA)
	Sodium bentonite	Western bentonite (USA)
	Swelling bentonite	Bentonite (UK)
	Sodium-activated bentonite	
	Sodium-exchanged bentonite	
Calcium montmorillonite	Calcium bentonite	Southern bentonite (USA)
	Sub-bentonite	Texas bentonite (USA)
	Non-swelling bentonite	Fuller's earth (UK)
Magnesium smectite	Saponite	
	Armagosite	
Potassium smectite	Metabentonite	
	K-bentonite	
Lithium-magnesium smectite	Hectorite	

restricted only to smectite-bearing clays.

Except for the aforementioned definitions a large number of other terms, mainly empirical, are currenly used in the various countries. Thus, in the U.K bentonites are clays rich in Na-smectites; the Ca-rich ones are called *fuller's earths*. This is a historical empirical name for clays suitable to adsorb grease used for cleansing ('fulling') wool (Highley 1972, Robertson 1986, Harben & Bates 1984, 1990). However in the USA the term fuller's earth is used for sepiolite-attapulgite-rich clays (Highley, 1972, Harben & Bates, 1984, 1990). Furthermore, in the U.K the term fuller's earths also has stratigraphic meaning, which describes a particular Middle Jurassic horizon containing montmorillonite. In the USA the Ca-rich smectitic clays are called *non-swelling bentonites*, while the Na-rich ones *swelling bentonites* (Highley 1972, Patterson & Murrey 1983). Since the Ca-varieties occur arround the Gulf of Mexico and the Na-varieties in Wyoming and adjacent States the former are also called *Southern bentonites*, while the latter *Western bentonites* (Patterson & Murrey 1983). The term *sub-bentonite* is used to describe the low to moderate swelling bentonites, while *metabentonites* or *potassium bentonites* are clays composed mainly of mixed layered illite-smectite (Patterson and Murrey 1983). The term *naturally active clay* is used as a synonym to fuller's earth, when the latter is used in oil processing.

Other terms used for smectitic clays which have been treated with acids or alkalis in order to improve their properties in certain applications are *activated clays*, *bleaching clays* (synonym to *absorbent clays*) or *bleaching earths* (Patterson & Murrey 1983). The latter two are used for both the naturally active and the activated clays but they also include activated bauxite. *White bentonites* are Ca-bentonites with high brightness, while *organophilic bentonites* or *organoclays*, or *bentones* (Grimshaw, 1971, Patterson & Murrey, 1983) are Na-bentonites treated with organic compounds which have special properties (O'Driscoll, 1988). Finally, a number of terms have entirely empirical origin; these terms are used directly in the market and include drilling mud bentonite, foundry bond bentonite, taconite bond bentonite, high and low-yield bentonite, high and low-strength bentonite, and high and low-gel bentonite (Patterson & Murrey 1983). In Table 1.1 the terminology used for the different varieties of bentonites in the various regions is presented.

In this project the terminology which will be used follows the definition given by Grim (1972), because it is not restricted only to altered volcanic ash beds but also includes smectite-bearing rocks derived from other precursors. As it will be shown in the following chapters, in most cases Greek bentonites have considerable thickness and have been derived from rocks other than volcanic ash beds. In order to describe differences in the characteristics of the materials imparted by the different exchangeable cations the prefixes Na- (for the sodium smectite-rich variety) and Ca- (for the calcium variety) will be added. The term K-bentonite will be used in the cases where mixed layered illite-smectite instead for smectite is present.

1.4. Crystal structural characteristics of smectites.

The smectites are clay minerals (the "princess" of the clay minerals according to Moore and Reynolds, 1989) with unique physical and chemical properties, which are evaluated by the industry. The reason for this behaviour is closely related to the structural features of these minerals. Smectites are phyllosilicates with a 2:1 layer structure, *i.e* two **tetrahedral** sheets linked with an **octahedral** sheet in between (Fig.1.1). The structure is based on pyrophyllite or talc (Deer *et al.* 1962), with the tetrahedra pointing towards the centre of the structure sharing one oxygen with the octahedral units. The model proposed by Edelman & Favejee (1940), about inversion of some tetrahedra and replacement of the apical oxygens by hydroxyls has been rejected by Schultz (1969). As well as the common oxygens, the plane of junction between the tetrahedral and the octahedral sheet also contains two unshared hydroxyl groups which belong to the octahedral sheet. The octahedral cations are usually Al, Mg, Fe^{3+} and Fe^{2+}, but other medium sized cations like, Li, Ti, Mn, Cr, Zn, V, Co, Ni may also occur (Bailey 1984). The main tetrahedral cation is Si which might be replaced by Al or Fe^{3+}.

The smallest structural unit contains three octahedra, sharing edges. If two out of three are filled with octahedral cations then the structure is called dioctahedral (gibbsite-type sheet); if all three positions are occupied then it is trioctahedral (brucite-type sheet). The octahedral sheet strongly affects the other structural elements and is very important for the formation of the mineral, since it is believed that it is the metal-hydroxyl which precipitates first acting as a template for the silica monomers (Güven 1988). There are two types of octahedral sites, namely M1 and M2; the former being on the miror planes of the mineral and the latter on both sides of the miror (Fig. 1.2). The M1 sites have <u>trans</u> configuration (<u>trans</u> octahedra) because they have hydroxyls in both sides, while the M2 sites have <u>cis</u> configuration (<u>cis</u> octahedra) having hydroxyls in one side of the coordination polyhedron (Güven 1988). The occupancy of the trans sites is different in the various types of smectites. Obviously, in the case of trioctahedral smectites all the available octahedral sites are occupied. Consequently this is only relevant in the dioctahedral smectites. Trans-site occupancy varies between 0 and 100% in montmorillonite (Tsipursky & Drits 1984, Güven 1988). In this mineral octahedral Fe^{3+} occupies trans-sites. In beidellite it is generally minimal (Güven 1988, Tsipursky & Drits 1984) although exceptions might occur (*e.g* Unterrupsroth beidellite) (Güven 1988). Finally, in nontronite trans-sites are vacant (Besson *et al.* 1983). Generally speaking, in well-formed smectites the trans sites tend to be vacant (Güven 1988).

The tetrahedral sheets consist of pseudo-hexagonal rings composed of Si-tetrahedra linked with the neighbouring tetrahedra by sharing apical basal corners (Bailey 1984). Three of the apical oxygens occur in the same plane and one points towards the

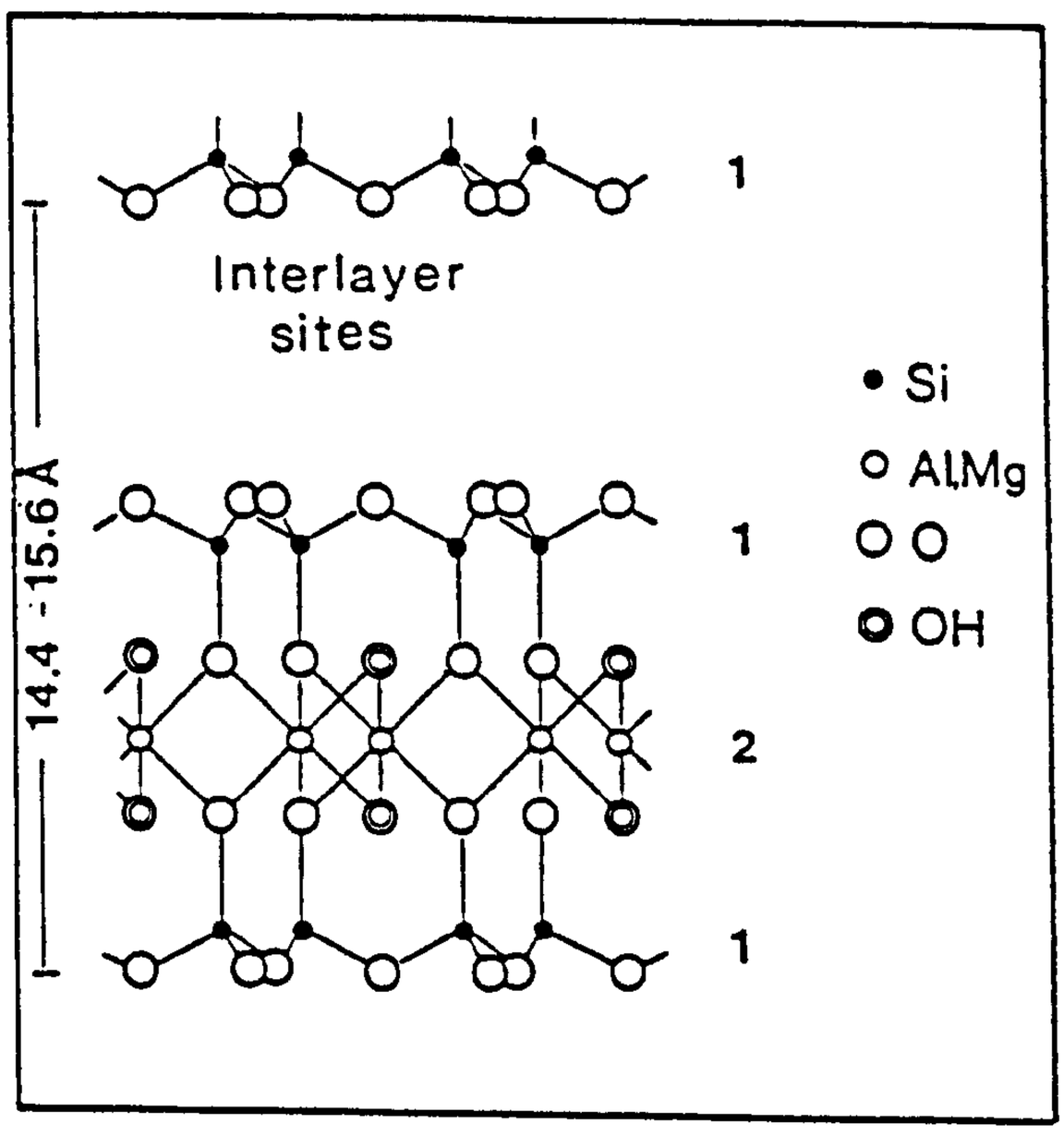

FIGURE 1.1. Schematic structure of the smectites adopted from Hoffman *et al.*, (1933) and Bailey (1984). The structure presented belongs to montmorillonite. Key to the numbers: 1= tetrahedral sheet 2= octahedral sheet.

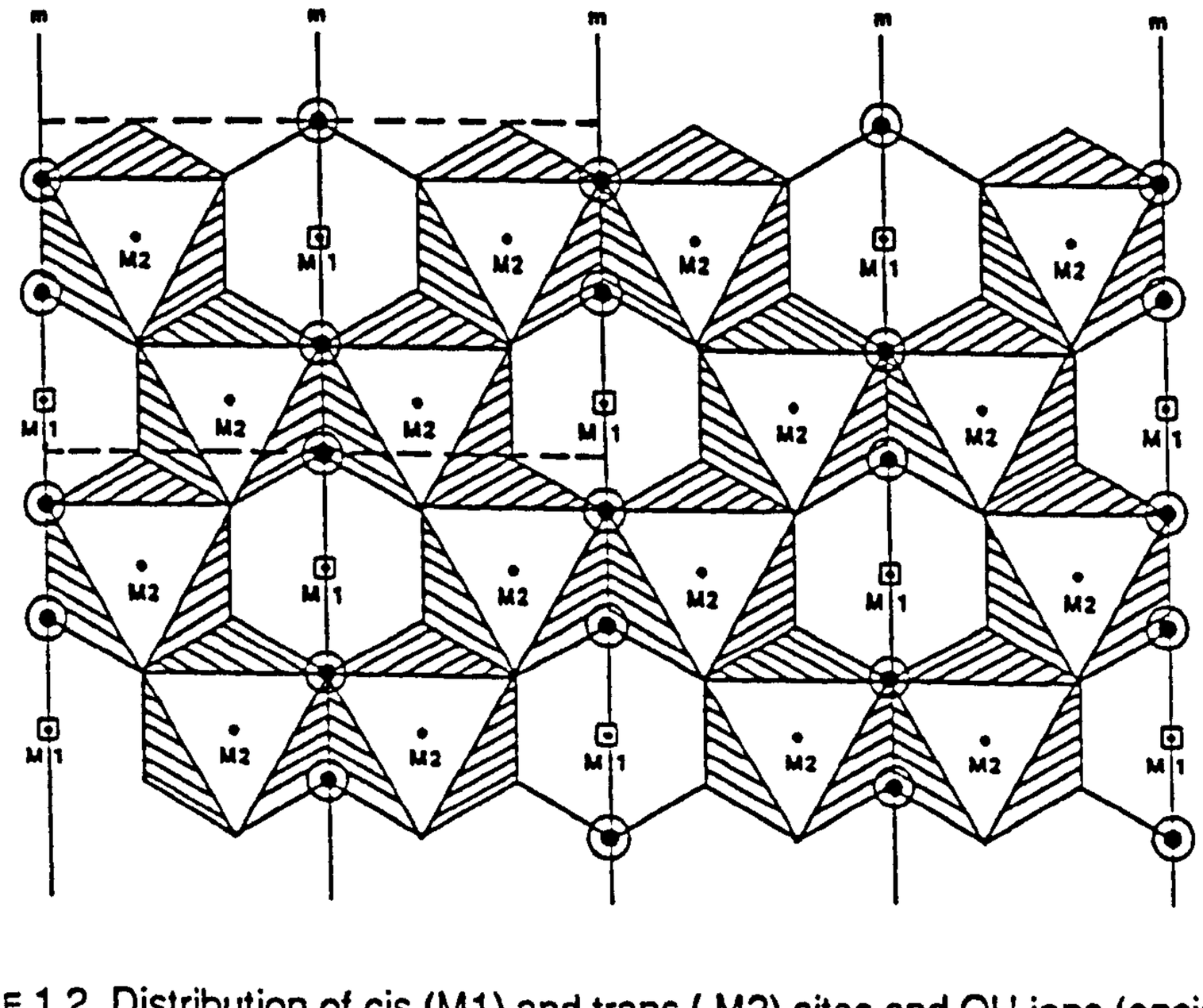

FIGURE 1.2. Distribution of cis (M1) and trans (M2) sites and OH ions (encircled dots) in an ideal octahedral sheet. m = mirror planes. The dashed lines indicate a unit cell.

octahedral sheet (Fig. 1.1). The main geometrical features of the tetrahedral sheet are the angle of the tetrahedral sheet are the angle of rotation α of the sheet (measure of the deviation from the ideal hexagonal ring), the tetrahedral tilt and the tetrahedral sheet thickness (Bailey 1984, Güven 1988).

The dimensions of the octahedral and the tetrahedral sheet are different. The dimensional descrepancy between the octahedral and the tetrahedral sheets is represented by the ratio $d_{M\text{-}O}/d_{T\text{-}O}$, where $d_{T\text{-}O}$ is the length of the Si- (and/or Al^{IV}-)* O bond and $d_{M\text{-}O}$ the length of the metal-oxygen bond in the octahedral sheet (Güven 1988). The ideal ratio where no discrepancy takes place is 1.33. In the case of trioctahedral smectites it ranges between 1.25 and 1.29 while in dioctahedral smectites between 1.16 and 1.25 (Güven 1988). In other words the discrepancy is greater in dioctahedral smectites.

In order to fit one on the top of the other structural rearrangements must take place among the various units (Bailey 1984, Güven 1988). These rearrangements involve mainly the tetrahedral sheet; the only distortions that may occur in the octahedral sheet are not associated with the fit over the tetrahedra but with the ionic repulsions between the octahedral cations. These distortions include shortening of the shared edges and lengthening of the unshared ones (Güven 1988). The modifications in the tetrahedral sheet involve either rotation of the tetrahedra in opposite directions if the tetrahedral sheet is larger than the octahedral one (Bailey 1984, Güven 1988), or tilting of the sheet if it is smaller. The latter case is not common in smectites. The angle of rotation varies between 1 and 10^{o} in the dioctahedral smectites and between 1 and 8^{o} in the trioctahedral ones.

As noted above, the structure of smectites is based on that of pyrophyllite for the dioctahedral and talc for the trioctahedral ones. The major difference between the two mineral species is the ionic substitutions in the former. Substitutions may occur in both the tetrahedral and the octahedral sheets. In the former the major type of substitution is that of Al^{3+} for Si^{4+}. In the octahedral sheet substitutions involve both replacements of divalent for trivalent cations (the most common case), for example Mg and/or Fe^{2+} and/or Fe^{3+} for Al^{3+} in the dioctahedral and univalent and/or divalent or trivalent for divalent cations (Li and/or Fe^{3+} and/or Fe^{2+} for Mg) in the trioctahedral ones (Grim, 1962, Deer *et al.*, 1962, Grim, 1968, Grimshaw 1972, Weaver & Pollard, 1973, Grim & Güven, 1978, Bailey, 1984, Brindley, 1984, Odom 1984, Newman & Brown 1987, Güven 1988). The above substitutions result in a charge deficiency, which varies between 0.2 and 0.6 charge units per half structural formula, and which is balanced by the introduction of cations in the **interlayer** sites. These cations are hydrated and can be replaced by others providing thus the **cation exchange capacity** which is one of the more characteristic properties of smectites used in their industrial applications (Deer *et al.*, 1962, Grim, 1962, Grim 1968, Highley, 1972, Odom, 1984, Hall, 1987, Newman & Brown, 1987, Güven 1988, Moore &

---

* Al^{IV} stands for tetrahedral Al.

Reynolds, 1989). The location of the exchangeable cations in the interlayer space is dictated by the location of the charge deficiency (Odom, 1984, Güven, 1988). In the case of cation substitutions in the octahedral sheet the charge deficiency is localized to distances 7Å apart in the 110 direction and 9Å apart in the Y direction. In the case of tetrahedral substitutions the charge deficiency is again localized to distances equal to the b distance in the Y direction and 2a in the X direction (Güven 1988). The charge deficiency in the tetrahedral charge is expected to have more profound effects on the distibution of the interlayer cations since the tetrahedral sheet is close to the interlayer space. The interlayer cations might be located in the hexagonal cavities created by the tetrahedra rings, or might be linked with two oxygens from the adjacent layer above the cavities (Farmer & Russell, 1971, Suquet *et al.*, 1975, Brindley 1984, Güven, 1988). In this way they act as bridges between the different layers. The hydration and the swelling of smectites will be examined in Chapter 7.

The stacking of the different smectite layers can generate three different types of crystal order (Güven, 1988):

-"Regular stacking" with zero degree of rotation and a perfect 3-dimensional periodicity. This structure is very rare in dioctahedral smectites (Black Jack mine beidellite is an exception) and occurs in some saponites (Suquet *et al.* 1975).

-"Semi-random stacking" with random n x 60^{o} rotations while the pseudohexagonal holes remain intact between the layers. In this type of stacking, only the hkl reflections with k=3n are observed; those with k=3n are diffuse.

-"Turbostatic stacking" with completely random translations and rotations between adjacent layers. The pseudohexagonal holes are not preserved. This type of stacking destroys the 3-dimensional periodicity; only the basal reflections and some hk diffraction bands are observed in X-Ray Diffraction diagrams. Turbostatic stacking is very common in smectites, especially in montmorillonites

1.4.1. Classification of smectites

Several workers have attempted to classify smectites according to chemical and structural criteria, including Grim, 1962, Grimshaw 1972, Weaver & Pollard, 1973, Brindley 1984, Güven, 1988, and Moore & Reynolds, 1989. From these classification schemes the most complete is considered to be the one proposed by Güven (1988). According to this scheme the criteria to differentiate smectites can be summarized as follows:

-The di-and trioctahedral nature of the octahedral sheets (di- and trioctahedral subgroups)
-The sources and sites of the layer charge of the mineral (tetrahedral (x_t or octahedral x_o)
-The predominant octahedral cation and
-The proxy ions in octahedra like Mg in montmorillonite.

Table 1.2.

Classification of natural and synthetic smectites (modified after Güven, 1988).

Ratio between tetrahedral (x_t) and octahedral (x_o) charges	DIOCTAHEDRAL SMECTITES Predominant octahedral cation(s)	Smectite species	TRIOCTAHEDRAL SMECTITES Predominant octahedral cation(s)	Smectite species
$x_o/x_t > 1.0$ (octahedral charges dominate)	$Al(R^{+2})$	montmorillonite	Mg	stevensite
			Mg(Li)	hectorite
			AlMg(Li)	swinefordite
			single or mixed transition metals	transition metal "defect" trioctahedral smectites
$x_t/x_o > 1.0$ (tetrahedral charges predominate)	Al	beidellite	Mg	saponite
	Fe^{3+}	nontronite	Fe^{2+}	Fe-saponite
	Cr^{3+}	volkonskoite	Co	Co-smectite
	V^{3+}	V-smectite	Zn	sauconite
			Mn	Mn-smectite

The classification scheme with the different types of smectites is presented in the Table 1.2. The more common of the smectites shown in Table 1.2 are montmorillonite and beidellite.

1.5. Properties and uses of smectites.

Smectites are known to have been in use since the ancient times. Robertson (1986) in an extensive review mentioned the use of bentonites (fuller's earths) from the times of the ancient Egyptians and Greeks since today. It is well known that the unique diversity of applications of smectites is closely associated with their structural characteristics, which in turn determine their physicochemical properties (Highley, 1972, Grim, 1968, Grim & Güven, 1978, Patterson & Murrey, 1983, Odom, 1984). In this chapter only a brief outline of the characteristic properties of smectites, is presented. A thorough discussion will take place in the following chapters.

1.5.1. Properties of smectites.

-a) Crystal size and shape. According to Grim & Güven (1978) the size of the smectite flakes varies from 0.1 to 2μm with an average size of 0.5μm. The small crystal size imparts large specific surface area to the smectites which can increase even more with suitable treatments (acid activation, formation of pillared smectites), imparting thus high adsorptive capacity. Smectites tend to form aggregates in suspensions. This event affects the colloidal properties of bentonites because decreases the free or effective surface area and increases the effective particle size. According to Odom (1984) the smectite particles are inheritedly interlocked and it is difficult to be separated except by a strong shear force. Generally, the natural Na-smectites have the smallest effective crystal size and the larger effective surface area because of the high swelling pressures developed when they are dispersed in water (Odom, 1984).

-b) Cation exchange capacity. The most important part of the smectite structure which determines the suitability for the various applications is the interlayer region. This is because the interlayer cations can be exchanged providing the required properties. An example of this is the so-called alkali-activation of smectites, which involves replacement of the original interlayer cations (usually Ca) with other cations, mainly Na (Patterson & Murrey ,1983, Odom, 1984). For the pure smectites the cation exchange capacity (CEC) varies from 70 (mainly soil smectites) to 130 meq/100gr. According to Grim, (1962, 1968) and Weaver & Pollard (1973), 80% of the total CEC results from charges due to substitutions in the structure of smectites with the remaining 20% from charges due to broken bonds.

-c) Hydration and swelling. One of the most characteristic properties of smectites is the uptake of water in the interlayer space (hydration) and the resulting swelling of the mineral, *i.e* smectites have high absorptive capacity. Swelling is a measure of the quality of bentonites (Highley, 1990, Morgan, 1990a). There are two stages of swelling; the so-called innercrystalline swelling (Norrish, 1954, Madsen & Muller-Vonmoos, 1989) in which smectites can take gradually from one to four water layers, and the osmotic swelling (van Olphen 1963, 1977, McEwan & Wilson, 1984, Madsen & Muller-Vonmoos 1989) which causes the complete dissociation of the smectite layers. Swelling strongly depends on the type of the exchangeable cations, the magnitude of the layer charge and the interaction between water, interlayer cations and the clay mineral interlamelar surface (McEwan & Wilson 1984). Usually Na-smectites develop higher swelling than Ca and Ca-Mg ones; thus alkali activation is applied to improve the properties of those poor bentonites (Odom 1984).

-d) Rheological properties. Smectites have the ability to impart high viscosity and develop thixotropy when added in amounts 5-6% in water. This is because they tend to form an homogeneous rigid gel structure. Several workers believe that this structure result from flakes linked together due to attractions between their positive charged edges and negative charged faces it is called card-house structure. However, the card-house model has been disputed (see Chapter 8).The development of viscosity is used in the drilling industry. Natural Na-smectites usually develop higher viscosity and thixotropic properties than Na-activated Ca-smectites or Ca-smectites.

-e) Dehydration and hydration. There are two types of water bound in smectites; that adsorbed on the surface and in the interlayer space, and the crystalline water located in the octahedra within the structure. The adsorbed water is lost at temperatures between 100 and 200^{o}C in one or two (usually) stages. The crystalline water is lost at higher temperatures ranging between 550 and 750^{o}C depending on factors like chemical composition, crystal structure and structural defects (Green-Kelly, 1957, Schultz, 1969, Odom, 1984). The way that the structural water is lost affects the performance of smectites in industrial applications like foundries and iron ore pelletization. Smectites tend to absorb water and rehydrate even when they have been subjected to high temperatures close to the dehydroxylation range, affecting the re-using process in foundries. Also, some dehydrated smectites are used as dessicants (Odom, 1984).

-f) Plasticity. It is the property of a material which permits deformation under stress without rapture and ability to retain the shape obtained after the stress has been removed (Grim, 1962, Grim and Guven, 1978). Bentonites develop higher plasticity than all other clay materials. On this ground, Bain (1971) proposed a chart using plasticity as a means of identification of the different clay materials. Plasticity is evaluated in applications like mortar and putty formulation, and in ceramics (Highley, 1972, Grim, 1962, Grim & Guven, 1978).

-g) Bonding properties. Na-smectites have very good bonding properties which are used in

industrial applications like taconitic iron ore and animal feedstuff pelletization, and foundries.

-h) Organic reactions. Smectites react with organic compounds which are either adsorbed on their surface and/or replace the interlayer cations. This type of reaction has increased the potential of smectites for use as toxic pollutant adsorbent. They are also important for the production of organoclays (Clarke, 1985) or bentones (Grimshaw, 1971, Patterson & Murrey, 1983).

1.5.2. Uses of bentonites.

The versatile character of bentonites have been described by many authors in the past, including Grim (1962), Hartwell (1965), Grimshaw (1971), Highley (1972), Hofstadt & Fahn (1976), Grim & Güven (1978), Patterson & Murrey (1983) Odom (1984), Clarke (1985), Robertson (1986) and O'Driscoll (1988). They all presented the fields where the bentonites find applications. Generally speaking, the applications can be divided into those which use large tonnages of bentonites and those where bentonites are used in small quantities (Odom, 1984, O'Driscoll, 1988). The most important uses of bentonites are presented in the following paragraphs.

-Oil drilling industry. The rheological properties (viscosity and thixotropy) displayed by natural Na-rich, or Na-exchanged smectites are used in the drilling industry. During the rotary drilling bentonite-bearing drilling fluids lubricate the bit and rods, bring the drill cuttings to the surface when the drilling is in progress and prevent them from settling in the bottom of the hole when the operation has ceased, due to development of yield stress. (Grim, 1962, Highley, 1972, van Olphen, 1977). The suspension also helps to make impermeable barriers when drilling cuts permeable strata, keeps the formation fluids from entering the pit (Grim, 1962) and supports both the sides of the drill hole and the weight of the drilling equipment (Highley, 1972). There are many types of inorganic and organic additives used to improve the properties of drilling muds (Odom, 1984). In the high temperature environment encountered in geothermal fields of high enthalpy, the viscosity may increase drastically. To cope with these difficulties specially formulated Na-smectites have been introduced (Odom, 1984).

Bentonites face competition from sepiolite and attapulgite in drilling applications. Attapulgite has inferior thixotropic properties but shows small variations in viscosity and gel strength with large variations in salt content. However it has high water losses in cases were fresh water formations are drilled (Grim, 1962, Patterson and Murrey, 1983). However, these difficulties are overcome with the addition of organic substances.

-Foundry applications. Due to their good bonding properties bentonites are used as binding agents in silica sand ("greensand") moulds for molten metal casting. The smectite

crystals due to their large surface area cover the quartz grains acting as a cementing agent (Grim, 1962, Highley, 1972). The greensand becomes plastic and cohesive and thus can be moulded around a pattern. The mould must have sufficient strength to withstand filling with molten metal and to retain its shape after the metal has solidified. The required properties for smectites are green compression strength, dry compression strength, wet tensile strength, hot compression strength, flowability and durability (Odom, 1984). The greensand must also have good permeability to allow gases to escape when the hot metal is poured. Natural Na-bentonites or Na-activated bentonites are preferred from Ca-bentonites. Na-bentonites have slightly lower green strength but have higher dry strenth (Patterson and Murrey, 1983, Odom, 1984) and much higher wet tensile strength and hot compressive strength than their Ca-rich counterparts (Odom, 1984). The strength of the mould depends on the milling time, on the amount of clay added as well as on the amount of tempering water.

The major competitor for greensand is the so called synthetic-sand which uses synthetic binders, mainly organic resins. The advantages of the synthetic sands include among others high production rates, improved dimensional accuracy, reduced handling and fast turn-round of pattern and moulding boxes (BCIRA report, 1985). However, greensands are preferred in medium and large foundries.

-Iron ore and animal and poultry feed pelletization. Taconitic iron ores (B.I.F. ores) are the main sources of raw Fe-rich material used in the production of metal iron. Bentonite is used in small amounts (0.5-1% or even smaller according to Hartwell, 1965) to bind the the fine grained ore. According to Jones (1979), the materials are then introduced into a rotary (balling) drum to aquire the desired spherical shape. Water is added in small amounts so that the resulting pellets contain 85-90% iron ore, 0.7-1% bentonite and 8-10% moisture. The small spheres are then dried and subsequently fired at 1200-1300^{o}C. During firing the iron ore crystals (hematite and/or magnetite) undergo sintering while the bentonite melts providing a good binding agent for the pellet. These events impart the physical strength nesecary before entering the blast furnace. The pellets must be strong enough to withstand handling and the desired properties required are fairly uniform size range, high green and dry compression strength, abrasion resistance, high reducibility and low swelling and uniform chemical composition for satisfactory hot metal analysis and blast furnace control (Patterson and Murrey, 1983, Jones, 1979). Natural Wyoming bentonites and/or Na-activated Ca-bentonites are used for iron ore pelletization. (Grim, 1962, Jones, 1979, Odom, 1984).

Bentonite is used in small amounts (1-2% according to Hartwell, 1965 and Odom, 1984) in the pelletization of animal and poultry feed mixtures, in order to increase the nutritional benefits to the animals and to assist with the handling of the feeds (Hartwell, 1965, Watson, 1982, Odom, 1984, O'Driscoll, 1988). However, bentonites face competition from

lignosulphonates which are wood derived products (Watson, 1982). Both Na and Ca-bentonites are used for animal feed pelletization.

-Civil engineering applications. Na-bentonites (natural and alkali-activated) find ample use in civil engineering applications because of their lubricity, sealing ability (impermeability according to Highley, 1972), thickening and gelling properties (O'Driscoll, 1988). They are used in the construction of diaphragm walls, in soil sealing and lining especially in environmental applications like waste disposal, in grouting applications, in lubrication of caissons and piles etc. For use in civil engineering applications bentonites need to be tested for their flow properties and gel strength, their water or filter loss, density, solids and sand content and hydrogen ion concenrtation.

The above uses consume the main part of the bentonites produced. There are however some growing markets with liquid absorbents (especially pet litters) being a very promising one especially in Europe (O'Driscoll, 1988). According to Robertson (1986) the desirable properties required are easy recognition of the saturated granules by the animal (fauld granules), high absorptive capacity and rate of absorption, odour prevention, resistance to "tracking" and lack of "dusting" (O'Driscoll, 1988). The bentonites are used either untreated (Highley, 1972, O'Driscoll, 1988), or heated (Grim, 1962, Grim and Güven, 1978). Other uses of bentonite as absorbent include removal of grease and oil from floors (Odom, 1984, Harben & Bates, 1984,1990).

Bentonites which have been previously undergone treatment with acids (acid activation) to increase their decolourizing properties are used for the decolourizing of edible and industrial oils and fats, and waxes (Grim, 1962, Hartwell, 1965, Highley, 1972, Grim & Güven, 1978, Clarke, 1985). According to Clarke (1985) the total production in the "western" world was about 550.000 tonnes. Ca-bentonites are usually activated in order to increase their surface area, and to develop microporosity which enchance the decolourizing ("bleaching") capacity of the raw material.

Na-bentonites treated with organic compounds (mainly amines) are rendered hydrophobic. In this condition they are used for their special rheological characteristics (effective gellants in organic fluids) in applications where rheology is important, like the grease paint and ink industries. Finally, another type of special treatment includes the formation of pillared smectites which can be used as catalysts. Pillaring agents reported are alkylammonium and bicyclic amine cations, and hydroxy-Al and Zr cations (Rupert *et al.* 1987).

In addition to those already mentioned, bentonites are used in a large number of applications including among others medicines pharmaceuticals and cosmetics, anti-stick and drying agent applications, soil conditioning, water clarification, ceramics (especially white bentonites), soaps, mortar mixes and nuclear waste disposal both as absorbers and sealants.

Table 1.3
Uses of bentonite (modified from O'Driscoll, 1988).

Crude bentonite			
	Naturally active (Na/Ca bentonite)	**Alkaline activated (Na-exchanged bentonite)**	**Organically activated bentonites (organophillic bentonites)**
Foodstuffs industry	Refining, decolourising, purifying and stabilizing of vegetable oils and fats		
Sulphur production	Refining, decolourizing, bitumen extraction		
Forest and water conservation	Powder fire-extinguising agents/binding agents for oil in water		
Mineral-oil industry	Refining, decolourizing anf purifying of mineral oils, fats, waxes, parraffin/catalysts for oil cracking.		
Beverages and sugar industry		Fining of wine, must and juices/beer stabilization/purifying of saccharine juice and syrup.	
Chemical industry		Catalysts/catalyst carriers, incecticides and fungicides/fillers, dehydrating agents/water and waste water purification/absorbents for radioactive materials	Grease thickening
Paper industry		Pigment and colour developer for carbonless copying paper/adsorption of impurities in white water systems.	
Cleaning and detergents		Polishes and dressings/additives for washing and cleaning agents and for soap production	
Pharmaceutical industry		Medicaments/bases for creams and cosmetics	
Ore production		Binding agents for ore pelletizing	
Building industry		Construction of diaphragm walls and shield tunneling/subsoil sealing (dumps)/anti-friction agents for pipejacking and shaft sinking/additive in soil concrete, mortar	
Ceramics industry		Plasticizing of ceramic compounds/strength improvement/fluxing agents	
Agriculture, animal husbandry		Soil improvent/cat litter/composting/animal-feed pelletizing/liquid manure treatment	
Drilling industry		Borehole scavenging for salt water	Thixotropic suspensions for borehole scavenging
Tar exploitation			Emulsification and thixotroping of tar-water emulsions, tar and asphalt coatings
Paint and varnish industry			Thickening, thixotroping, stabilizing and anti-setting agents for paints, varnishes, coating materials, sealing cements, waxes, adhesives.
Foundries		Binding agents for special moulding sands	Binding agents for synthetic moulding sands, core sands/binding agents for anhydrous casting sands/for thickening blackwashes.

In Table 1.3 the major areas of application for bentonites is presented (O'Driscoll, 1988). The uses of acid activated bentonites are examined separately in Chapter 9.

1.6. Previous work.

1.6.1. Milos-Kimolos.

The geological, mineralogical and geochemical investigations of the rocks exposed on the both islands started in the previous century. Sauvage (1846) and Ehrenburg (1889) gave the first geographic and geological informations about the islands including some references for earthquakes (Ehrenburg, 1889).

The first complete investigation of the geological features of the islands was provided by Sonder (1924-25). He first distinguished the four major geological units, namely in geochronological order, the metamorphic basement, the sedimentary sequence, the volcanic sequence and the alluvial deposits. He also stressed the significance of the hydrothermal alteration for the silicification of the original tuffs ("Bimsteintuffs") and lavas and the formation of sulphur, alunite, baryte and manganese outcrops observed on the islands for the first time.

Voreadis & Mourambas (1935) examined the Ag-bearing barytes (with or without galena) deposits of Milos; their work was based on the geological background established by Sonder.

Liatsikas (1949) dealt with the geological features and the economic deposits of the island of Milos. He accepted the structure proposed by Sonder, with changes of minor significance. His contribution is important because he was the first to describe the existence of a type of "clays" different from kaoline in several places of Milos. This "clay" was probably bentonite.

Porphyris (1955) gave the first unpublished report about the physical properties of the Greek bentonites and compared them with commercial products used in the industry.

Marinos (1958) and Voreadis (1956) studied the hydrothermal kaoline deposits occuring in the NW part of Milos island.

The most important contribution on the study of the bentonites of Milos was provided by Wetzenstein (1969, 1972). Based on geological observations he concluded that the parent volcanic rocks were deposited under marine conditions and were transformed into bentonites via the action of the sea water and the supply of Mg cations by submarine hot springs. He also postulated that the kaolinitization, alunitization and silicification phenomena observed in several bentonites are products of hydrothermal alteration events posterior to the formation of bentonites. Finally, he assumed that the bentonite deposits of Milos are members of a single horizon. Patterson & Murrey (1983) used this model of bentonite formation for the deposits of Milos. In a later contribution (1975) Wetzenstein

studied the effects of the hydrothermal alteration on the baryte and manganese deposits observed on Milos.

Stul & Mortier (1974) and Lagaly & Weiss (1975) in their experiments on inhomogeneous charge distribution in smectites, examined some montmorillonites from Milos and found that their layer charge varies between 0.24 and 0.38 charge units per $O_{10}(OH)_2$.

Angelier *et al.* (1977) studied the neotectonic regime and related the different tectonic episodes with the different geochemical characteristics of the volcanics croping out on the island.

Fyticas (1977) carried out the first comprehensive geological, structural, and volcanological synthesis of Milos and produced the geological map of the island. He divided the geological formations of Milos into four groups like Sonder, but he found that the sedimentary sequence is of Neogene age (U.Miocene-L.Pliocene) and not Cretaceous-Eocene as Sonder had assumed. He also distinguished the volcanic episodes which occured on the island and described the pyroclastic formations. He contradicted Wetzenstein about the existence of a single bentonite horizon because he did not observed a constant marine horizon anywhere in Milos. According to Fyticas, bentonites and kaolins are products of the same hydrothermal system and were formed in different geochemical environments controlled by pH; bentonites at greater and kaolines at shallower depths. The same origin is invoked by Harben & Bates (1984, 1990).

Kanaris & Minopoulos (1979) in a preliminary report presented a comprehenive list of the kaoline and bentonite deposits of Milos which are not owned by the the Silver and Barytes Ore Mining Company, without further geological, mineralogical, or geochemical investigation.

Kornprobst *et al.* (1979) and Hoffmann & Keller (1979) investigated the mineralogical and petrological features of the metamorphic rocks of the basement.

Minopoulos (1980, 1981) examined some useful raw materials of Kimolos including some bentonites. He reported for the first time the existence of clinoptilolite in a bentonite deposit of eastern Kimolos.

Marcopoulos & Kraniotis (1982) reported the formation of analcime, mordenite and clinoptilolite in bentonites at the Phyropotamos area in northern Milos.

Alberti & Brigatti (1982) studied the mineral chemistry of 14 montmorillonites from Kimolos and using statistical methods found that most of them can be classified as Otay-type montmorillonites.

Kalogeropoulos & Mitropoulos (1983) studied the sulphur and oxygen isotopic composition as well as fluid inclusions of some baryte deposits from Milos. They concluded that they have been formed in an environment similar to that of the Kuroko-type barytes.

Zagalis (1983) examined the mineralogical and crystal-chemical characteristics of some bentonites and kaolines from Milos without further information about the location where the

samples were collected from.

Andseta (1983) described the geomorphological characteristics of Milos, Kimolos and Polyegos islands and provided informations about the hydrographic network of the islands.

Thanasoulas (1983) applying geoelectrical methods in the SW part of Milos island reported the existence of three main geological formations: the metamorphic basement, a pyroclastic horizon which in places contains clayey material (possibly smectites) and surficial lavas.

Thanasoulas & Tsocas (1985) applying geoelectrical methods in Kimolos found three main geological formations below the alluvial cover. The deeper corresponds to the crystalline basement of the island, the intermediate probably corresponds to pyroclastic sediments while the stratigraphically higher one possibly to the lavas observed on the island.

Simeakis (1985) studied the neotectonic evolution of the islands of Milos Kimolos and Polyegos and proposed a model describing the rotations of the various neotectonic blocks he assigned on the island of Milos.

Robertson (1986) in his monograph about the fuller's earths gives an extended account on the history of extraction of bentonites in Milos and Kimolos in both the ancient and the modern times.

Fyticas *et al.* (1986) a revised the original model about the volcanological evolution of Milos and Kimolos proposed by Fyticas (1977). The major improvements are the establishment of the chronological order of the several volcanic episodes on the island and the redefinition of the term "green lahar" as a phreatic horizon rather than a mud-flow.

Marcopoulos & Katerinopoulos (1986) studied the formation and the paragenesis of the alunites of Milos and attributed their genesis on the oxidation of ascending S-bearing hydrothermal solutions at very low pH.

Briqueu *et al.* (1986) studied the Sr, Nd and O isotopic ratios of some volcanic rocks of Milos and Kimolos and gave informations about the possible petrogenetic processes which prevailed during the magma genesis.

Liacopoulos (1987) studied the alterations of the wall rocks in the basement of Milos island caused by hydrothermal alteration. Based among the isotopic composition of siderites he attributed the formation of clay deposits (kaolins, bentonites) to the circulation of hydrothermal fluids, in agreement with the model of Fyticas (1977).

Mitropoulos *et al.* (1987) used rocks from Milos among other Aegean islands to establish their petrogenetic model of the volcanic rocks of the South Aegean Sea.

Marcopoulos & Christidis (1988) in a preliminary study of the bentonites of Kimolos reported the existence of mordenite in Prassa Qyarry and clinoptilolite in the Loutra area. They attributed the formation of the bentonite-bearing deposits on diagenetic processes, and the formation of kaolinite and alunite to posterior hydrothermal activity.

Papanicolaou (1988) studied the neotectonic characteristics of Milos and described the kinematic charactereristics of the faults observed on the island.

Tsoli-Kataga & Mavronichi (1989) studied the kaoline occurences of south Kimolos and proposed a hydrothermal model for their origin. Although they did not observe any spatial association between kaolines bentonites and zeolite-bearing bentonites they assumed that bentonites with or without zeolites are products of this hydrothermal process.

Lüttig & Wiedenbein (1990) in their account about the bentonite market worldwide, stressed the role of the bentonite deposits of Milos and described their origin as hydrothermal being affected by a later halmyrolysis process.

1.6.2. Chios island.

Chios island has received great geological interest because it is one of the few Greek areas with lower Palaeozoic outcrops. The geology of the island was investigated in depth by a recearch team from the University of Marburg/Lahn (Germany) who produced six Ph.D theses, a number of scientific contributions in the form of research papers and the geological map of the island. Besenecker *et al.* (1968) and Kauffman (1969) distinguished two geological units, the autochthonous and the allochthonous one. Herget & Roth (1968), Besenecker *et al.* (1968), Roth (1968) and Herget (1969) studied the Palaeozoic rocks of the NW part of the island and proposed a stratigraphic column for these rocks. Besenecker *et al.* (1968) Kauffman (1969), Tietze (1969) and Lüdke (1969) provided data about the mesozoic rocks of the two geological units of the island.

Kreatsas (1964), Besenecker *et al.* (1968) and Besenecker (1973) studied the Neogene rocks which crop out in the SW sector of the island. Besenecker (1973) gave the detailed stratigraphy of these Neogene rocks and divided them into four stratigraphic formations, namly the Thymiana layers, the Zyfia layers, the Keramaria layers and the Nenita limestones. The age of these Neogene rocks was determined by palaeontological means as Upper Miocene-Lower Pliocene.

Besenecker & Pichler (1974) studied the Neogene volcanic rocks of the island. They distinguished two volcanic cycles the age of which was determined as Upper Miocene-Pliocene.

Bellon *et al.* (1977) provided geochronological data for the volcanic rocks of the island which proved that the age of these rocks is Lower-Upper Miocene and not younger as Besenecker *et al.* (1968), Besenecker (1973) and Besenecker & Pichler (1974) assumed.

Papanicolaou & Sideris (1983) and Sideris (1986) studied the Palaeozoic rocks of the island provided an alternative model for their occurence. They proposed that they represent a wild flysch probably of Permian age.

The bentonite deposits of Chios island which have been described by Kreatsas (1964)

were studied by Andronopoulos (1961). The latter determined that the smectite present is Ca-montmorillonite, described the existence of dolomite in them, but failed to determine the existence of opal-CT which was present in these materials. He also gave some incomplete data about the major element geochemistry. Finally, Kanaris (1978) in a more detailed work determined the presence of quartz, chlorite, and illite and carried out a semi-quantitative analysis of the bentonite. He proposed that the bentonite extends over a considerable area.

1.7. Location of the field areas.

The islands of Milos, Kimolos and Chios are situated in the Aegean Sea, Greece. Milos and Kimolos are situated in the SW part of the Cyclades group of islands (Fig. 1.3). They are about 90 sea miles south of the port of Piraeus. The area of Milos is 150.9 km^2 while that of Kimolos 36.4 km^2. Both islands are part of a greater island group, called "the island group of Milos", which includes also the islets of Polyegos (or Polivos) and Antimilos.

Chios island is situated in the eastern Aegean Sea close to the Turkish borders (Fig 1.3). Its area is about 900km^2 and it is about 150 sea miles away from the port of Piraeus.

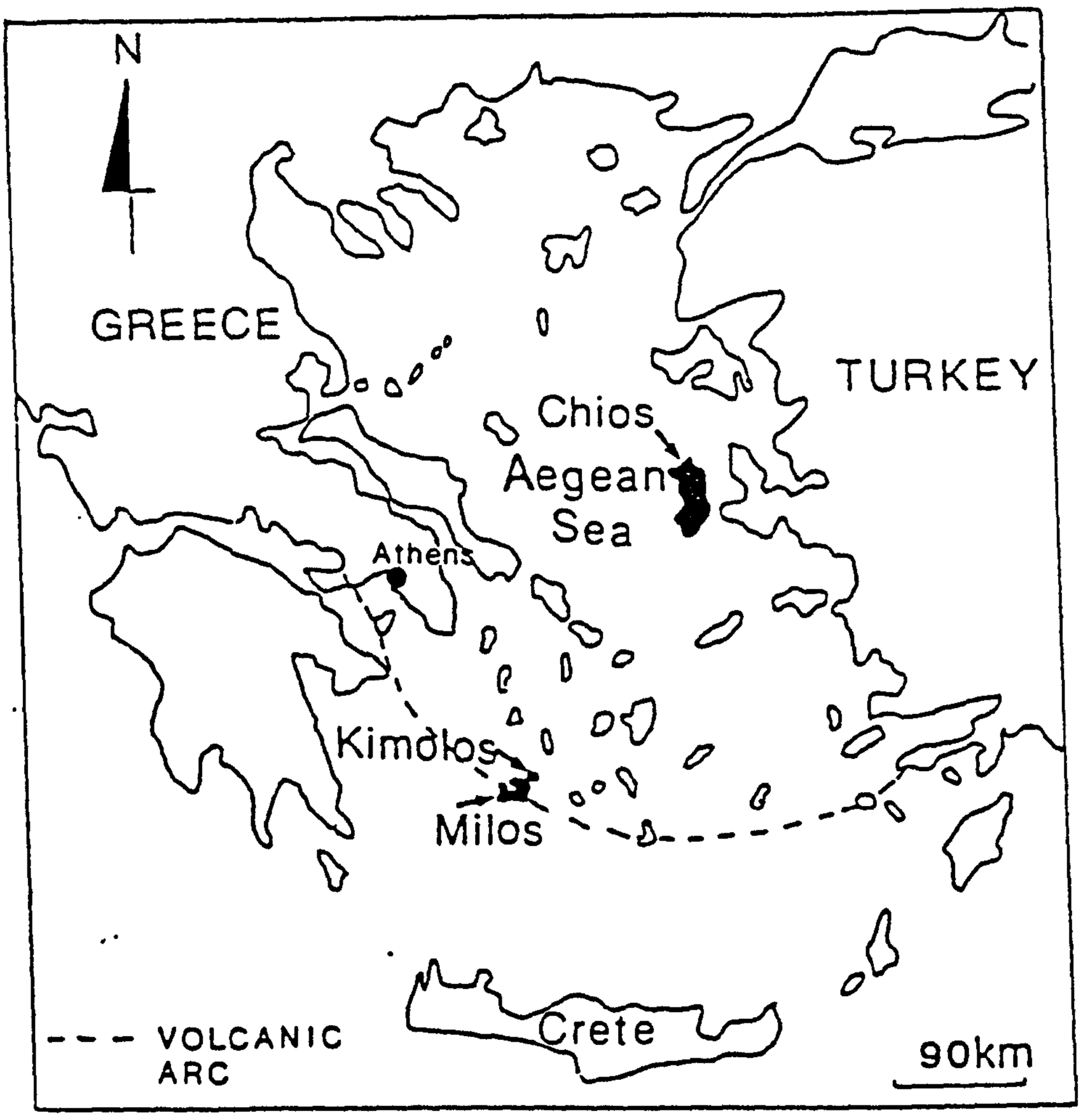

FIGURE 1.3. Location of the study areas in Greece.

CHAPTER TWO

REGIONAL GEOTECTONICS: EVOLUTION OF THE AEGEAN. VOLCANISM AND GEOTECTONICS

2.1. Geotectonic setting and evolution of the Aegean Sea.

The islands of Milos, Kimolos and Chios belong to the Aegean area, the greatest part of which is submerged under the Aegean Sea. (Fig. 2.1). The Aegean Sea has several characteristics of a typical marginal sea (Berckhemer, 1978, 1980) is seen from a physiographical point of view. These are (Berckhenmer, 1978, 1980):

-A deep sea trench with a pronounced free-air gravity anomaly -130 to -250mgal.

-An inner island volcanic arc above hypocentres in 100-150km depth, at a distance of about 200km from the trench.

-Tensional tectonics in the back-arc region.

-High heat flow, up to 2.7 H.F.U, in the central Aegean and low in front of the arc.

-High absorption of seismic waves in the upper mantle behind the island arc.

However there are differences from typical marginal seas. These include:

-Small size of the sea.

-Lack of typical oceanic crust in the Eastern Mediterranean (the thickness of the crust is roughly 20km including some 10km of Neogene sediments), and existence of a huge sedimentary chain in front of the Hellenic Trench. There is evidence for the existence of oceanic crust burried under 8-15km sedimentary strata (Makris & Stobbe, 1984).

-A thick continental crust below Crete and the Cyclades which becomes thinner under the Cretan Sea (about 20km).

-Low sub-Moho Vp (7.7-7.9 $km.s^{-1}$).

-Lack of true sea-floor spreading.

-Existence of scattered deep-intermediate shocks in the North Aegean region.

-The frontal non-volcanic sedimentary arc dominates, while the volcanic arc is poorly developed.

According to Karig's classification (as quoted by Berckhemer, 1978, 1980), it is a small, young, inactive (with respect to sea-floor spreading) marginal sea, with high heat flow and a hampered state of development .

The whole area is characterized by the active subduction of the African lithospheric plate, and more specifically of the Eastern Mediterranean crust which is considered to be one of the last sections of the Tethyan Ocean (Papanicolaou, 1986), in front of the Hellenic Trench (Fig 2.2) (Papazachos 1973, 1976, Richter & Strobach, 1978). The subducted slab is about 280km long and is dipping with an angle between 30 and 40^{o} (Papazachos, 1973,

FIGURE 2.1. Map showing the essential geographic and bathymetric features of the Aegean area (after Mercier, 1981).

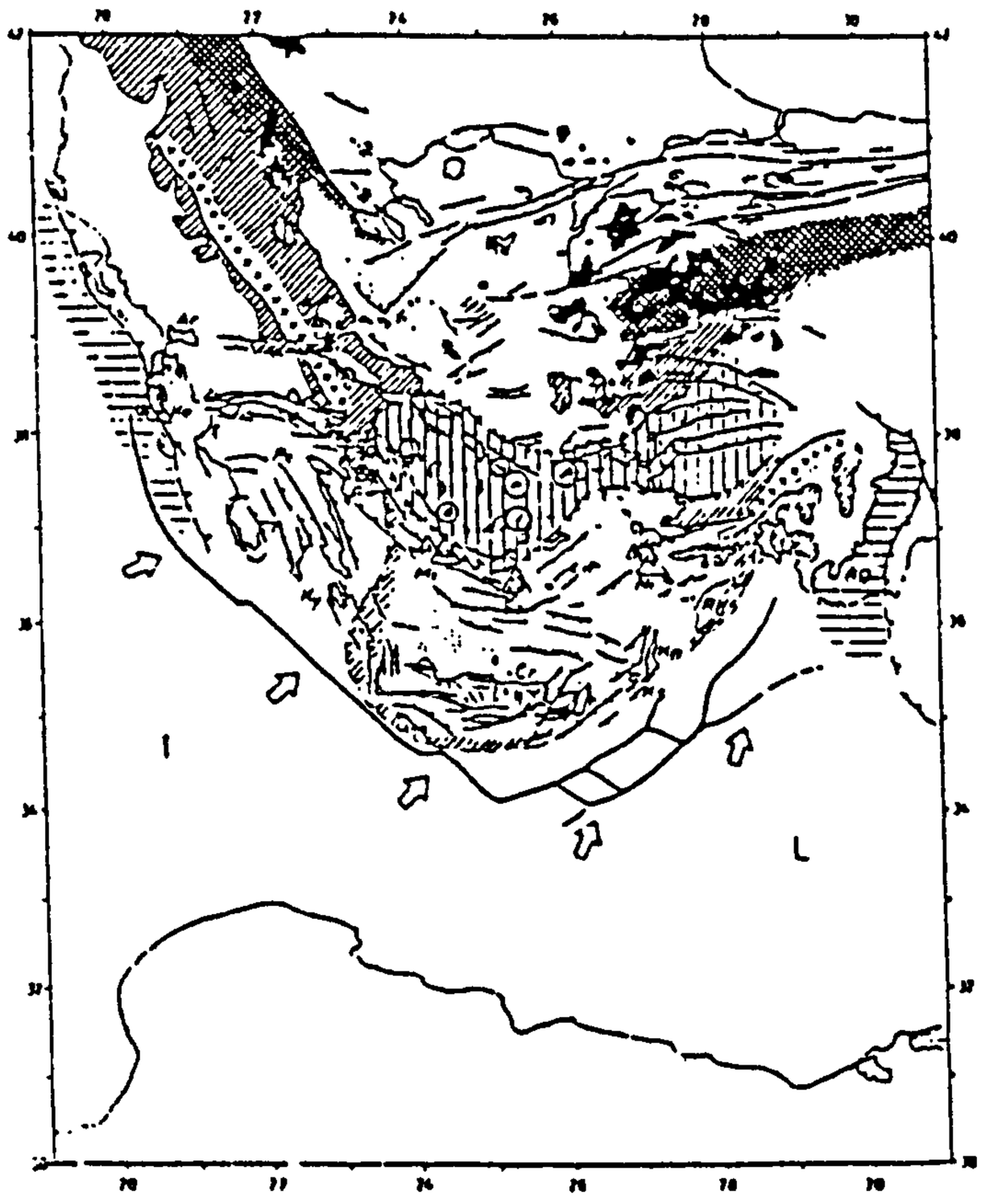

FIGURE 2.2. General framework of the Aegean region. The arrows indicate the direction of subduction of the African plate in front of the Hellenic Trench (after Mercier, 1981)

LePichon & Angelier, 1979), reaching a maximum depth of 180km (Richter & Strobach, 1978). The speed of the subducted slab is 3.5cm/year (McKenzie, 1978) although it has been considerably lower during the last 3 my (1.8cm/year according to Fyticas *et al.*, 1976).

The direction of the subduction is not the same throughout the whole extent of the Hellenic Arc (Fig. 2.2). It is perpendicular in the westem and SW part of the Arc, becoming subparallel in the SE section (LePichon & Angelier, 1979, 1981, Huchon *et al.*, 1982). Consequently, the relative motion of the the two plates changes from convergence with slip-vector perpenticular to the arc, when projected horizontally, in the western and SW sector of the Arc, to a motion having component subparallel to the direction of the Arc (LePichon & Angelier, 1979, Huchon *et al.*, 1982).

The orientation of the Hellenic Trench follows that of the Hellenic Arc. It is striking in a NW-SE direction in the western sector changing to a ENE-WSW direction south of Gavdos Island (Huchon *et al.*, (1982). It has a rather complex structure and in the SE sector it breaks up to several subparallel en-echelon trenches (South Cretan, Pliny and Strabo Trenches) (Fig.2.3).

The Aegean is dominated by extensional tectonics throughout the entire area, except in the NW and westem parts of the Hellenic Arc where compression dominates (Fig. 2.4) (Mercier, 1981, LePichon & Angelier, 1979, McKenzie, 1972, 1978, Jackson & McKenzie, 1988). Compression events have also been reported in the northernmost part of thew Aegean Sea (Papazachos, 1976) and in the NW Greece, (McKenzie, 1978). This regime dominates at least since the Uppermost Miocene (Mercier, 1981, Jackson & McKenzie, 1988), while LePichon & Angelier (1979, 1981) consider Upper Serravallian (12-13 Ma) as the time for the beginning of the extension, and Sengör *et al.* (1985) postulate Middle Miocene. This type of tectonism has been interrupted twice since the Uppermost Miocene (Mercier, 1981). The first time was in the boundary between the Uppermost Miocene and Lower Pliocene and coincides with the " jump" of the convergence zone west of the Ionian Islands. The second time was during the Lower Quaternary. LePichon & Angelier (1979) mention one additional phase of compression which occured before the uppermost Miocene before the deposition of the Pikermi-type layers (*i.e* between 12 and 9 Ma) and affected the central Aegean. Crete was dominated by extension throughout the time between Lower Miocene-Early Pliocene.

However, more recent research and detailed field work have questioned the existence of compression events between extension tectonism. The tectonic discontinuities described by LePichon & Angelier (1979) and Mercier (1981) as reverse faults and thrusts are in fact listric normal faults, which have undergone rotation about an horizontal axis (Jackson *et al.* 1982). Similar observations were made by Price (1989) in western Anatolia which has

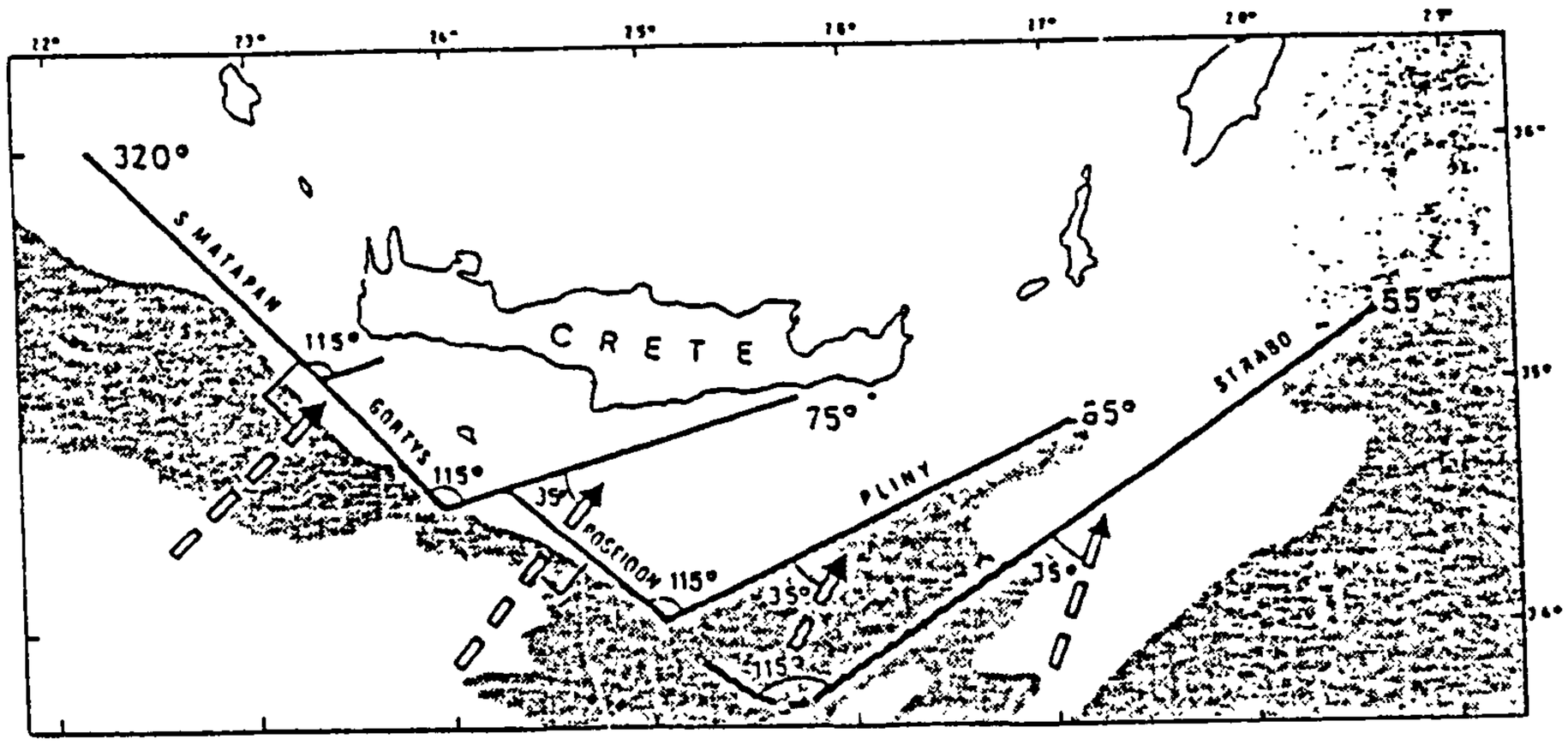

FIGURE 2.3. Schematic gross-structural and kinematic map of the Hellenic Trench system showing the angular relationships between tslip vectors (thin dashed arrows) and trenches. (after Huchon et al., 1982)

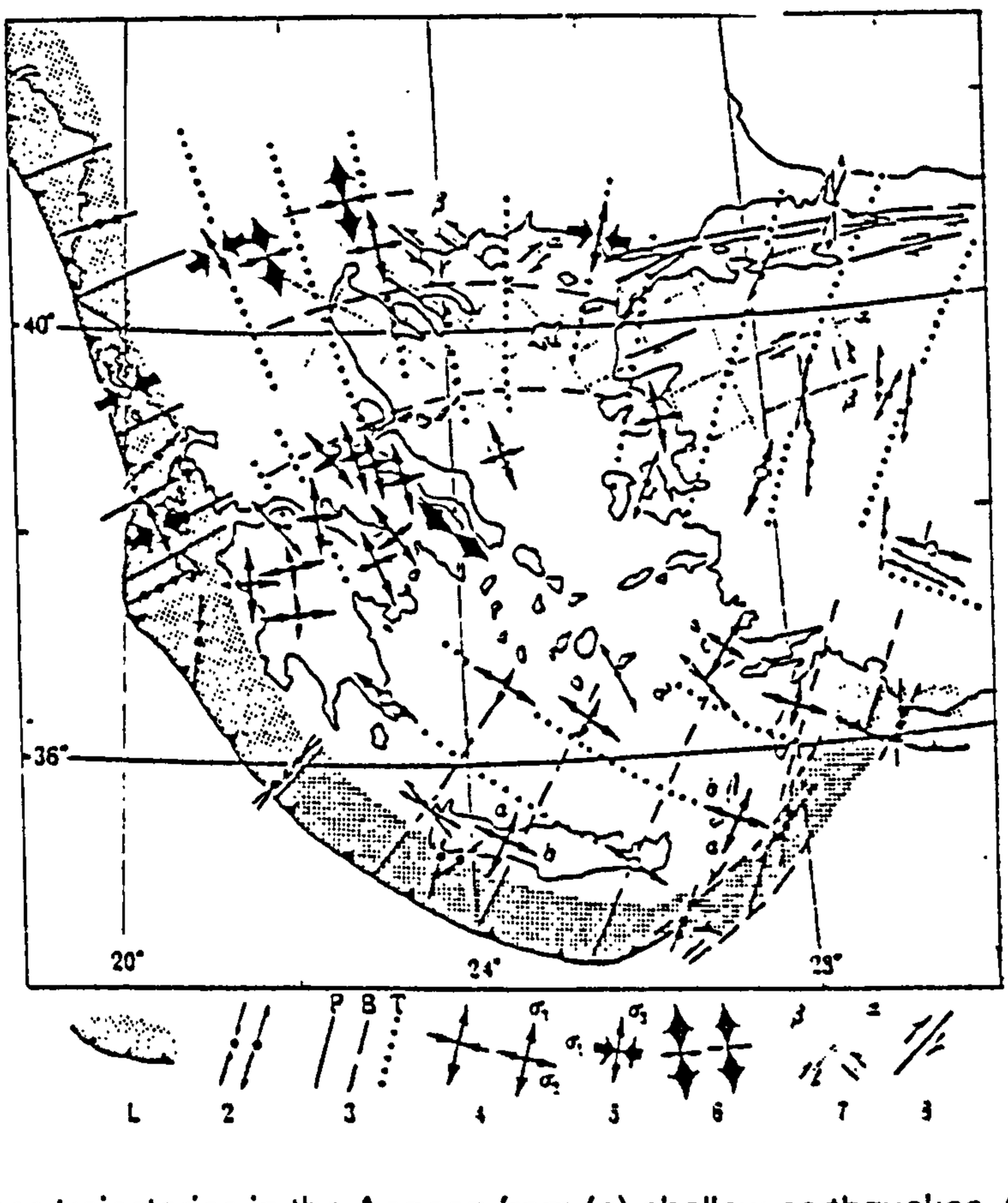

FIGURE 2.4. Stress trajectories in the Aegean from (a) shallow earthquakes, (b) neotectonic and active faults, and (c) *in situ* measurements. 1= Aegean subduction. 2= Horizontal projections of the slip vectors determined from compressional (convergent arrows) and extensional (divergent arrows) shallow earthquakes. 3= (P, B, T) Regional principal directions of compressional, intermediate and tensional stresses. 4,5= Deviatoric compressional σ_1, intermediate σ_2 and extensional σ_3 principal directions determined from structural analysis of neotectonic and active faults. 6= Principal extensional stress directions from *in situ* measurements. 7= Slip lines drawn bisecting at a 45^{o} angle the P and T trajectories. 8= Strike slip faults (after Mercier, 1981)

undergone a similar tectonic evolution to that of the Aegean, at least since the Lower Miocene (Seyitoglu & Scott, 1991).

Before the initiation of the extension mentioned above, the Aegean was land levelled by erosion. An epicontinental sea transgressed periodically from the NE while the Mediterranean invaded in some areas during Tortonian and Messinian from the south (Mercier, 1981). In the area where the Cretan Sea is developed today, the initial altitude was about 300m o.d decreasing towards the east to the sea level (Angelier *et al.*, 1982). Today the sea depth is greater than 2.5km in some places.

The aforementioned extension regime is responsible for the considerable thinning of the Aegean crust, the thickness of which is reduced from 40-45km in the continental Greece and Western Turkey, to 23-26km in the central Aegean (Makris, 1978a,b, Makris & Vees, 1977). Furthermore, the crust between Santorini and Crete has undergone maximum extension having a thickness as low as 20km (Makris, 1978). Geophysical prospecting revealed traces of Quaternary intrusions of possibly volcanic origin in the Cretan Sea, which however are not considered as evidence for active sea-floor spreading (Jongsma *et al.*, 1978).

The extension observed in the Aegean has been quantified (LePichon & Angelier, 1979, 1981, Angelier *et al.*, 1982, McKenzie & Jackson, 1986). It was found that the crust below the Cretan Sea has undergone as much as 80% extension while the average extension of the whole area must be between 30 and 50%. Furthermore, the streching factor and the coefficient of expansion is maximum in the area of the Cretan Sea. Extension rates have been estimated to be in the range 30-110 $mm.y^{-1}$, with a probable value of 62.5 $mm.y^{-1}$ (McKenzie & Jackson, 1986; 70 $mm.y^{-1}$ according to McKenzie, 1978). Extension has a N-S direction with very little E-W motion (McKenzie & Jackson, 1986). The factors which caused this regime are points of controversy between different researchers. LePichon & Angelier (1979), Berckhemer (1978, 1980) and Segitoglu & Scott (1991) consider gravitational forces to be the most plausible explanation, while Mercier (1981), although he believes that such forces may be responsible to a minor degree. proposes crustal deformation described by means of the slip-line theory as the most important reason for the extension tectonics. McKenzie (1978) suggests motions in the boundary between the asthenosphere and the lithoshere, while Makris (1976) believes that tectonism can be explained by means of the uprise of a mantle plume in the central Aegean.

In addition to extension, the crust of the Aegean area has undergone significant uplift and subsidence in different sectors during the last 12-1Ma (LePichon & Angelier, 1979, Angelier *et al.*, 1982). The area in the central Aegean has subsided while areas which belong to the Hellenic Arc have been uplifted. Crete has been uplifted as much as 4 km. The vertical motion was calculated to be about 1-3cm/century (Angelier et al., 1982). It has been suggested (LePichon & Angelier, 1981, Angelier *et al.*, 1982), that this uplift has been

caused by the accumulation of the lower sedimentary strata which is scraped off the subducted African plate. The upper sedimentary strata is not being subducted but is accumulated in the form of an accretionary ridge (Mediterranean ridge) 100-200km south of the trench (Huchon et al., 1982). Similarly, the Messinian evaporites have not been subducted but have been trapped in front of the trenches (LePichon & Angelier, 1981, Angelier *et al.*, 1982, Huchon *et al.*, 1982).

Several models have been proposed to describe the tectonic motions of the broader area in terms of regional geotectonics. McKenzie (1970, 1972) introduced the term **microplates** to describe the observed regime. More specifically, he considered that the **Aegean microplate** is forced to move southeastwards, because of the westward movement of the **Turkish microplate** along the North Anatolian Fault, as a result of the collision between the Arabian and the Eurasian plates in the area of Caucasus (Fig. 2.5), which occurred in the Middle-Upper Miocene. Simultaneously, there is active subduction of the African plate beneath the Aegean microplate. He also considered Aegean and Turkey to behave as rigid blocks. Dewey & Sengör (1979) used the term **Peloponnesian microplate** for the Aegean microplate of McKenzie and also introduced the **Cretan microplate**, a term which has not been used since then. they also considered that the North Anatolian Fault has moved westwards 80-90km since the Upper Miocene (110-120km according to LePichon & Angelier, 1979) and that this motion is taken up by a system of grabens in the north Aegean and the continental Greece. The latter hypothesis has been accepted by McKenzie & Jackson 1983, 1986).

However, McKenzie (1978) considered that plate tectonics cannot explain several features observed in the area. Furthermore, the transform fault, which had been assumed by McKenzie (1970, 1972) as the boundary between the Aegean and the Eurasian plates was never found in the continental Greece (Mercier, 1981). Consequently, Lepichon & Angelier (1979) and Mercier (1981) consider the Aegean to be the deformed margin of the Eurasian plate (Fig. 2.6). It has also been considered that the Aegean has been rotated in a clockwise direction relatively to Europe (Fig. 2.7) about a pole located close to Arta town in the NW Greece (LePichon & Angelier, 1979, 1981, Angelier *et al.*, 1982). This rotation, which was initiated in the Middle-Upper Miocene has been modified by further extension (LePichon & Angelier, 1979, 1981, Angelier *et al.* 1982).

In all the aforementioned models, the initiation of the present plate-tectonic regime is put in the Middle-Upper Miocene. However, Mercier (1981) questioned this dating and suggested the Uppermost Miocene or even the Miocene-Pliocene boundary i.e during the "jump" of the convergence zone west of the Ionian islands. McKenzie & Jackson (1988) suggest a similar age for the beginning of subduction with the form that is observed today, based on calculations about the streching rates in the Aegean area.

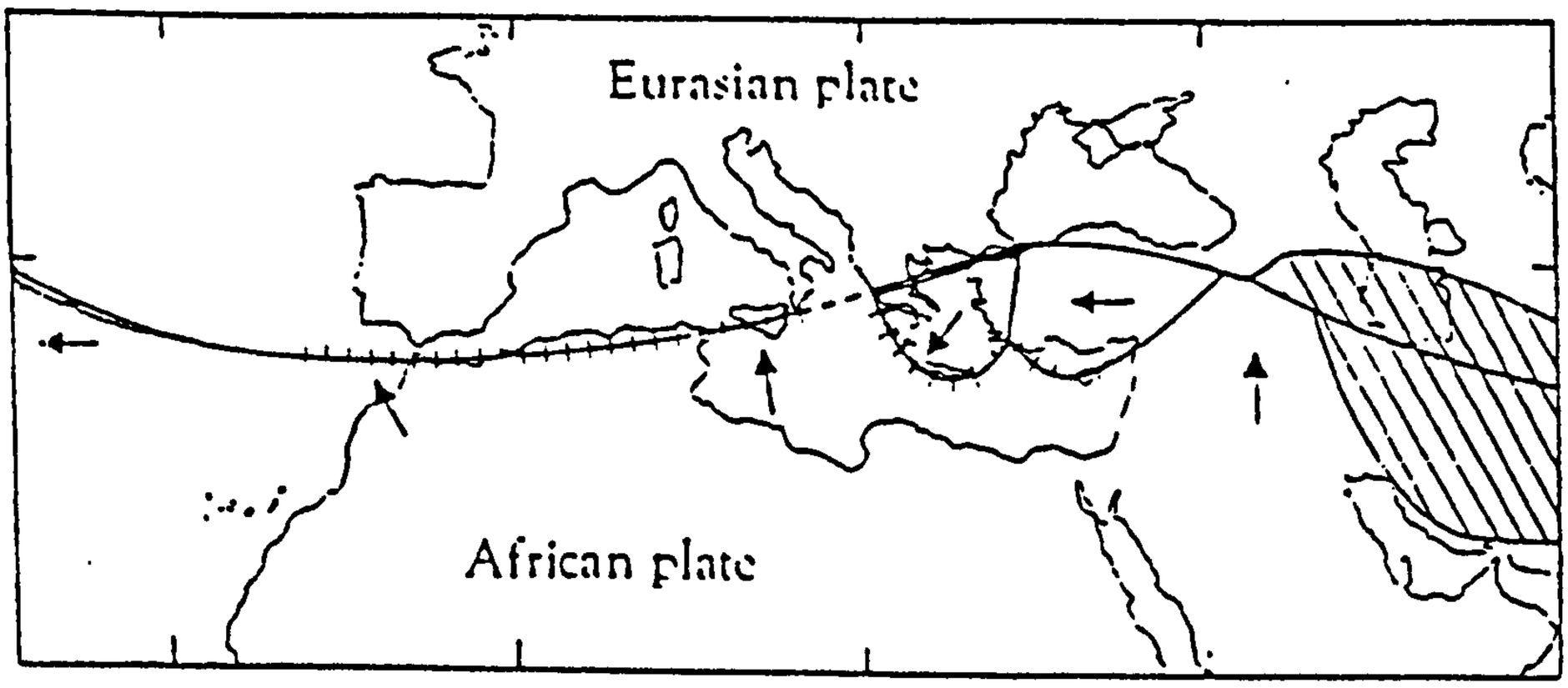

FIGURE 2.5. Approximate positions of the plate boundaries and relative plate movements in the "microplate model" of MacKenzie (1970).

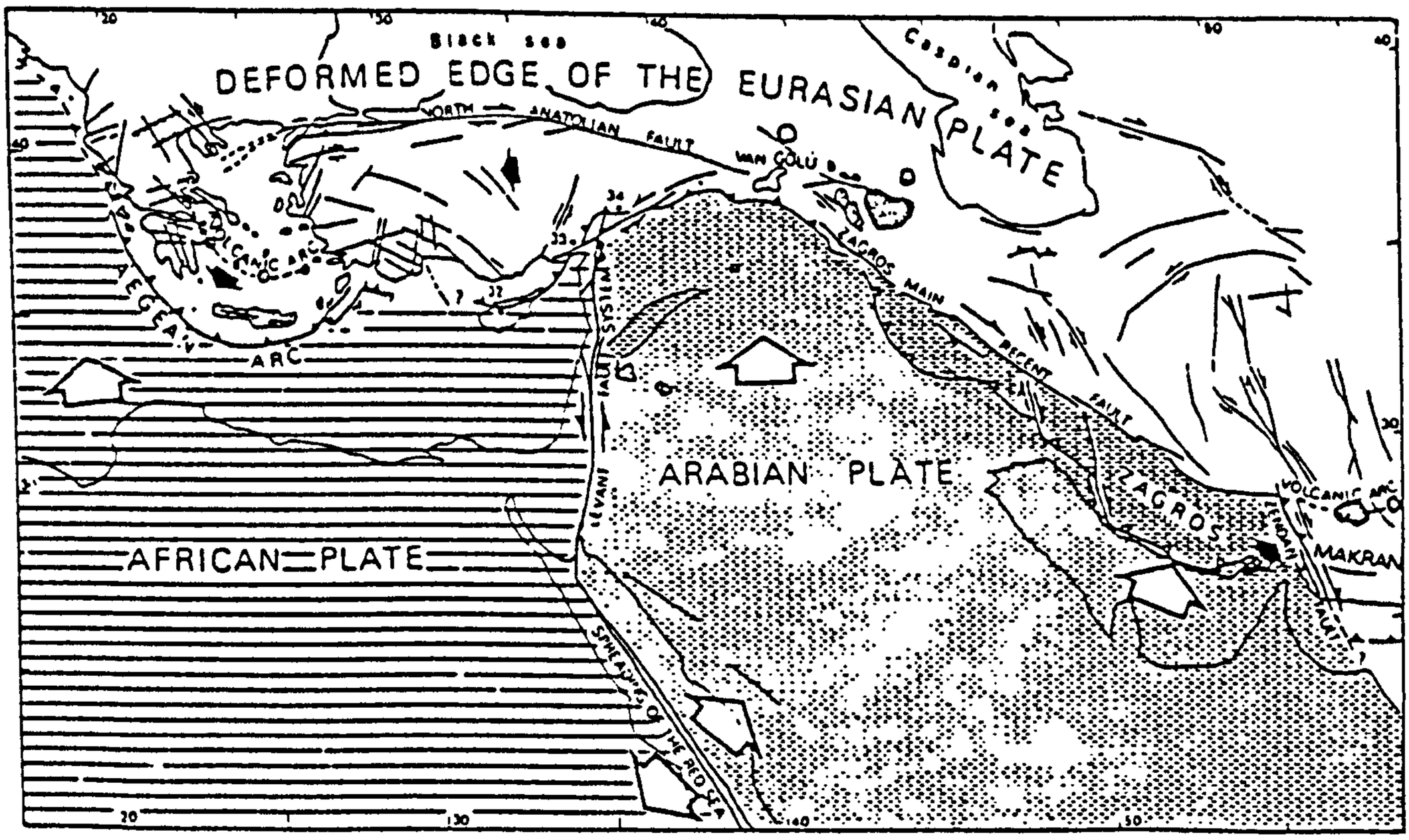

FIGURE 2.6. Location of the Aegean Arc with respect to the major deformational units of the Middle East and the Eastern Mediterranean (after Mercier, 1981).

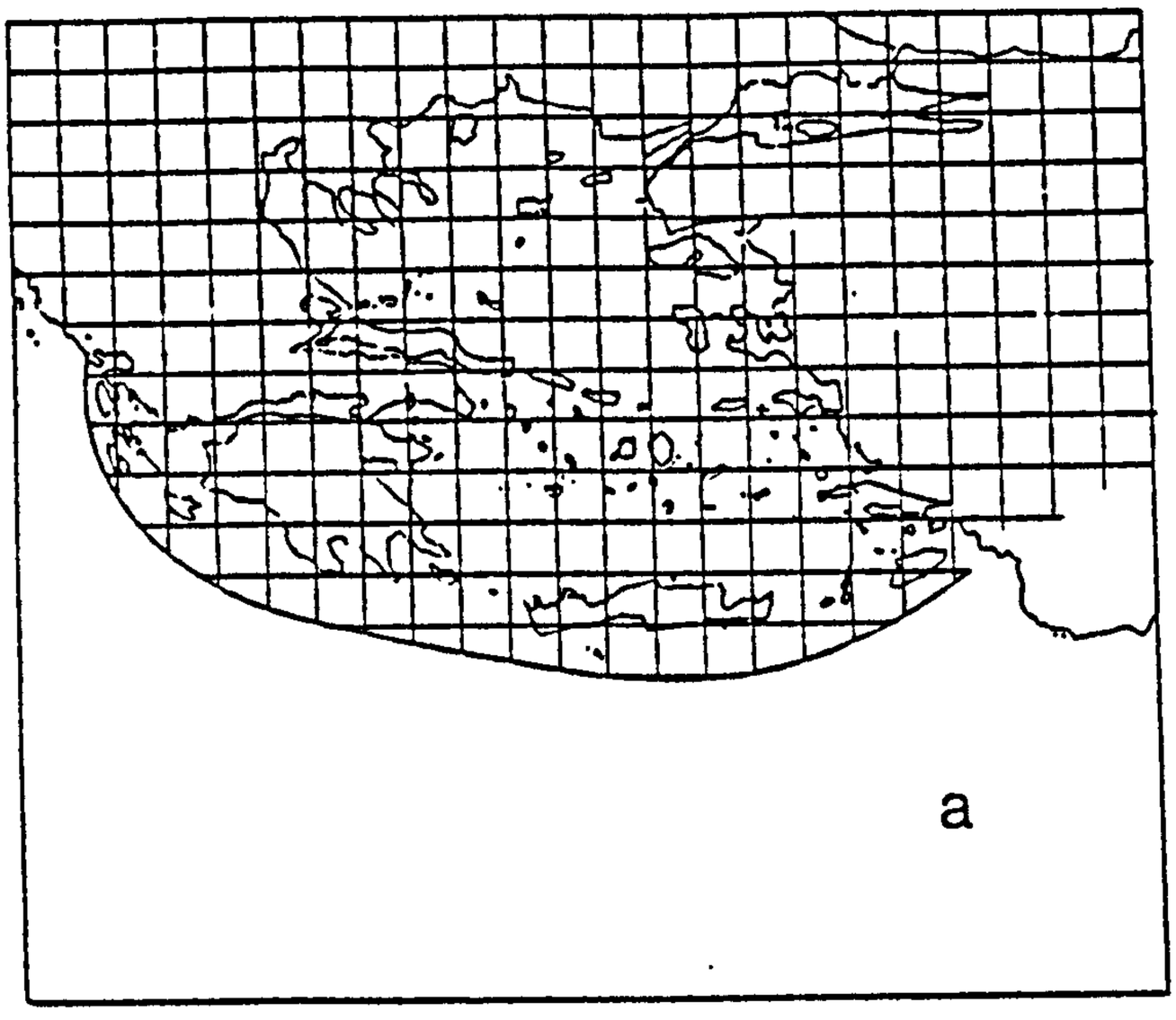

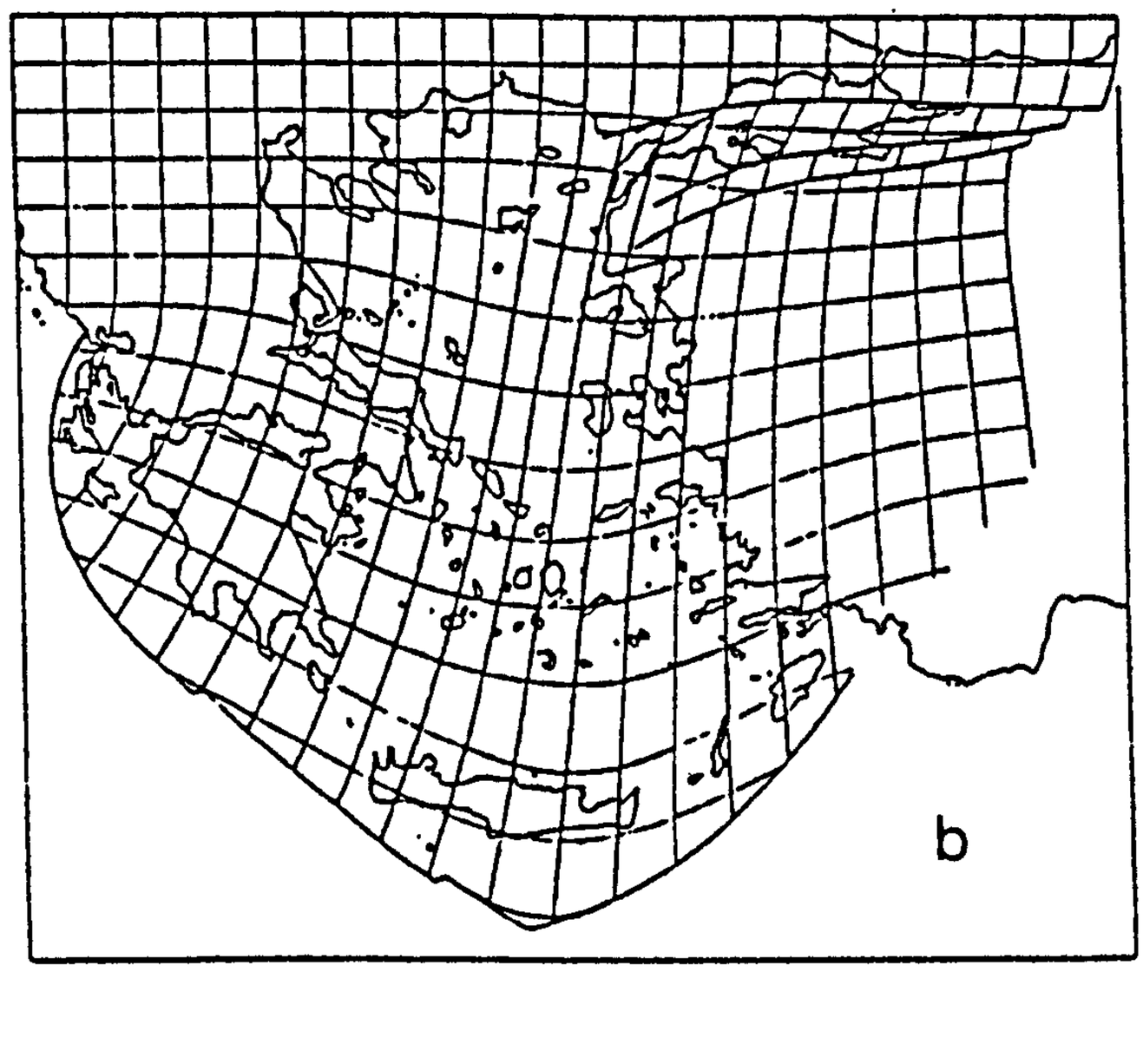

FIGURE 2.7. (a) Reconstruction of the Aegean region before Hellenic subduction and associated Aegean expansion Configuration 13Ma ago. (b) Present configuration of the Aegean region (after LePichon & Angelier 1981).

Paleomagnetic data have demonstrated that rotation indeed occurred, but it was not constantly clockwise throughout the Aegean and Western Anatolia (Laj *et al.*, 1982, Kissel *et al.*, 1985, 1986a,b, Kissel & Laj, 1988). More specifically, it was found that Western Greece has been rotated clockwise as much as 45^{o} since Burgigalian, and that this rotation took place in two equal steps; the first between Burdigalian and Middle Miocene, and the second between Upper Miocene and Recent. Between these two stages there is a time gap of about 7 Ma, during which no rotation occurred. The second stage of rotation is related to the "jump" of the convergence limit between the Aegean and the African plate west of the Ionian Islands (Mercier, 1981). Crete has not undergone any significant rotation since Tortonian (Laj *et al.*, 1982, Angelier *et al.*, 1982), while Rhodes at least since the Lower Pliocene (Laj *et al.*, 1982).

The clockwise rotation decreases from west to the east and becomes anticlockwise in Western Anatolia (Kissel *et al.*, 1985, 1986a,b, Kissel & Laj, 1988). The high rotation angles recorded in Euboea Island, central Aegean, were explained with the model of McKenzie & Jackson (1983, 1986), for deformed zones confined by rigid blocks (Kissel *et al.*, 1986b, Kissel & Laj, 1988). However, Price (1989) in a similar situation in Western Anatolia, which has undergone similar tectonic evolution as the Aegean at least since the Upper Miocene, found that this model cannot be applied satisfactorily. Instead he concluded that the Aegean should be considered as a region subdivided into many smaller areas deforming independently from one another.

Kissel & Laj (1988) presented a model for the configuration of the Hellenic Arc in the Lower Miocene, i.e when rotation according to their data began. It was assumed that the Arc was rectilinear having an E-W orientation (Fig. 2.8), while today it is subangular. LePichon & Angelier (1979, 1981) considered a similar situation (Fig. 2.7) but with three differences:

a) The E-W orientated arc is considered to be in the Lower Miocene in the model of Kissel and Laj. On the contrary, LePichon & Angelier consider it in the Middle Miocene in their model.

b) The arc has migrated southwards since the Middle Miocene. Kissel & Laj consider a northward migration.

c) The area north from the pole of rotation in the model of LePichon and Angelier have not undergone any significant rotation, whereas according to the model of Kissel & Laj those areas have undergone maximum rotation.

It is obvious that more work needs to be done before a broadly accepted model about the evolution of the Aegean area can be proposed. However, it seems possible that the Aegean does not behave like a rigid block, as was assumed in several of the models quoted, but it should be treated in terms of separate tectonic blocks moving independently from one another (Dr. B.Scott pers. communication, 1990).

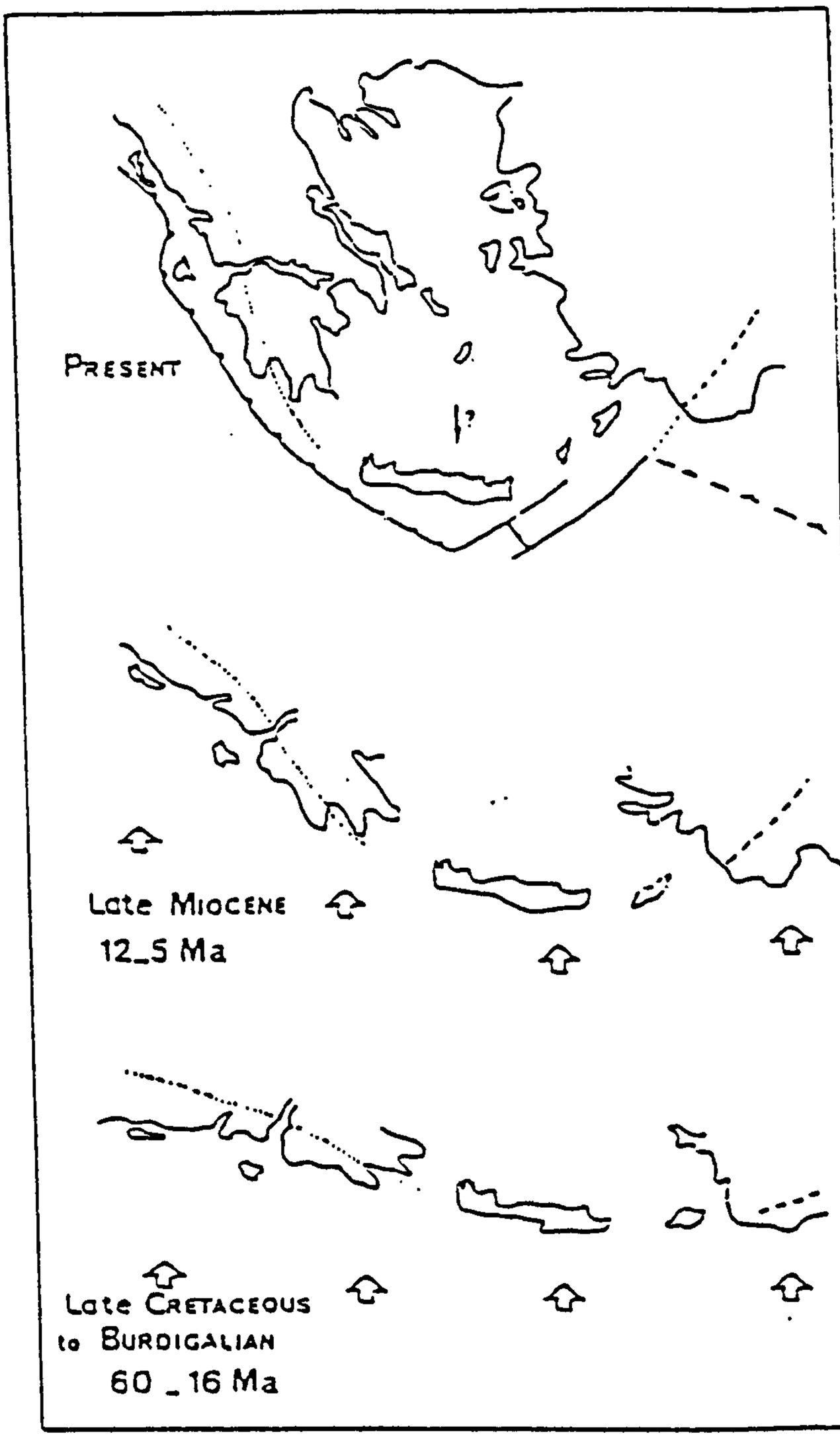

FIGURE 2.8. Evolution of the curvature of the Aegean Arc during the Cenozoic. The large arrows illustrate the northward drift of Aegea since at least Early Palecene to Middle Miocene times. The dotted line represents the Pindus overthrust and the dashed line, the front of the Lysian nappes. The original arc was almost rectilinear and trending E-W. (after Kissel et al., 1988).

2.2. Evolution of the volcanic activity in Aegean and its relationship to the geotectonic regime.

Milos, Kimolos and Chios are volcanic centres with complex volcanological characteristics. Kimolos, especially, is an almost entirely volcanic island, while in Milos more than 70% of the exposed outcrops are volcanic. Volcanic centres are widespread throughout the Aegean (Fig 2.9), and volcanic activity still takes place in the form of fumaroles. Gaseous activity occurs in almost every volcanic centre of the so-called Volcanic Arc of the Southern Aegean Sea and more specifically, in Krommyonia, Milos, Kimolos, Santorini and Nisyros. Two main stages of volcanic activity distinct from one another have been described (Fyticas *et al.*, 1976, 1984):

-The Oligocene-Miocene volcanic phase which took place in the north and central Aegean, known as **North Aegean Tertiary Activity.**

-The Pliocene-Quaternary volcanic phase, known as the **South Aegean Active Arc.**

Between these two main stages there are a number of volcanoes which erupted from the Upper Miocene to Quaternary and which, because of their individual petrological and geochemical characteristics, cannot be included in any of the aforementioned categories. The volcanic rocks of Chios island were erupted during the first phase, while these of Milos and Kimolos during the second.

The first stage (Fig. 2.9) includes volcanic rocks occuring in Thrace, NNW Anatolia and in several islands in the north and central Aegean, including Samothraki, Lesvos, Limnos, Agios Eustratios, Skyros, Chios, Psara and Euboea (Fyticas *et al.*, 1976, 1984). There is evidence that this type of activity was initiated in the Late Eocene, although its culmination took place during Oligocene and Miocene (Fyticas *et al.*, 1984). The volcanism has orogenic characteristics, but the pure calk-alkaline products are restricted in Thrace and the central Aegean islands Skyros and Euboea. The other areas in which rocks of this volcanic phase occur, include high-K calk-alkaline volcanites and shoshonites (Fyticas *et al.*, 1979, 1979). Rocks with the highest K_2O content are rare in the northern part of the area, but are relatively abundant in the central and southern sectors. This event implies an increase of K_2O towards the south (Fyticas *et al.*, 1984). The oldest rocks are exposed in Thrace (Oligocene age). Radiochronological data gave the following ages for the different volcanic centres (Fyticas *et al.*, 1984):

Thrace	33.1-23.6 Ma	Chios	17.0-14.3 Ma
Limnos	22.7-17.8 Ma	Psara-Antipsara	17.7-15.0 Ma
Ag. Eustratios	22.7-18.0 Ma	Skyros	15.0 Ma
Lesvos	18.0-15.5 Ma	Euboea	14.8-13.2 Ma

It seems that the volcanic activity migrated towards the south with time (Fyticas *et al.*, 1984), but it is difficult to estimate the absolute migration, because of the intense extension

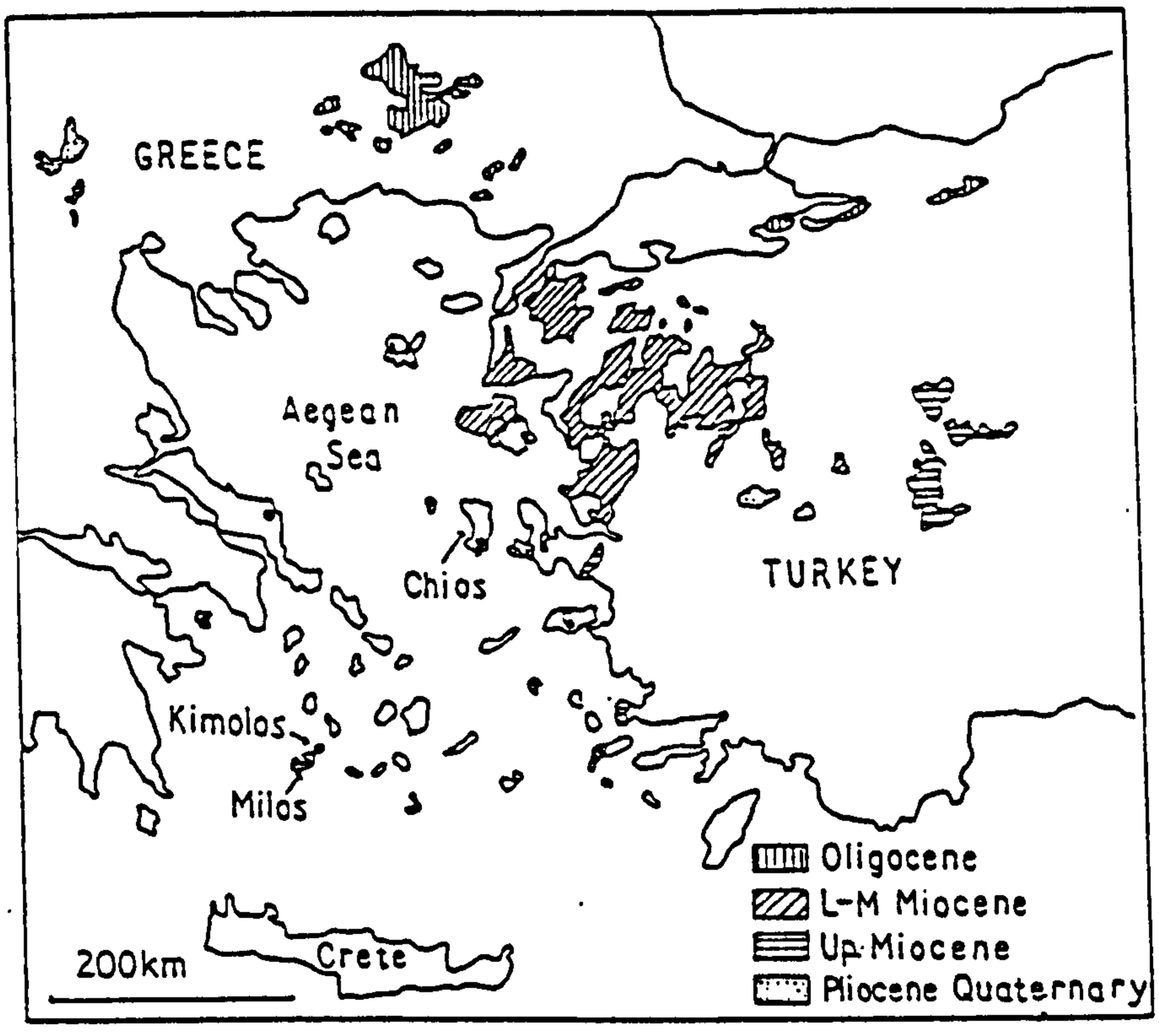

FIGURE 2.9. Distibution of the volcanic products from the Oligiocene to present time in the Aegean area including Westem Anatolia (after Fyticas *et al.*,1984)

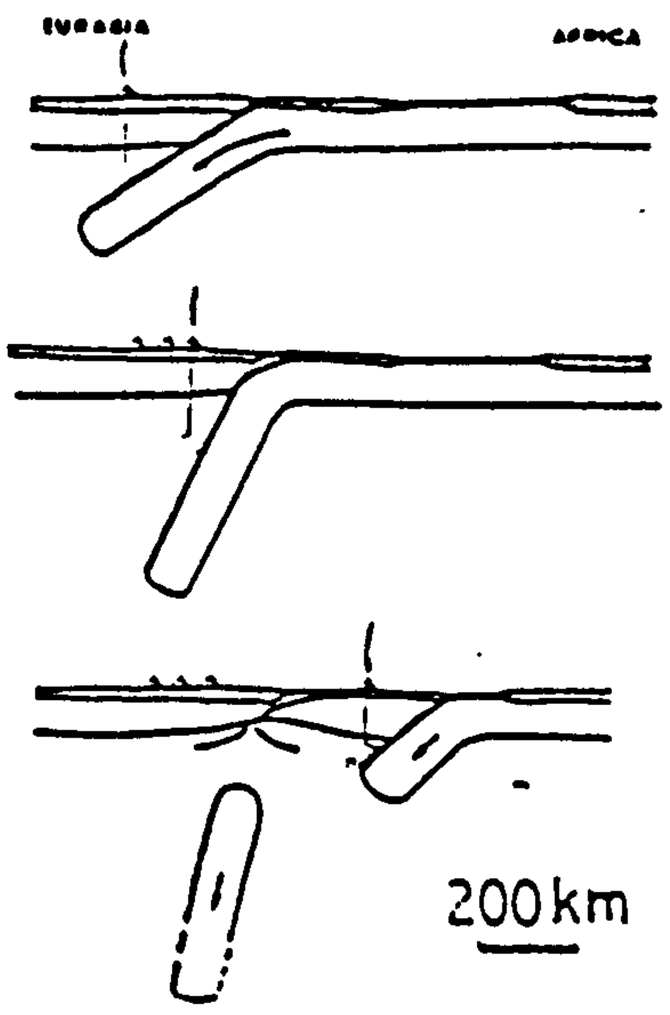

FIGURE 2.10. Schematic cross section depicting inferred geodynamic evolution and southward migration of orogenic volcanism in the Aegean. During the Eocene to Oligocene the southern margin of Eurasia (Rhodope Massif) collides with the Appulian microplate located between Africa and Eurasia (after Fyticas *et al.*, 1984).

of the whole area. al least since the Uppermost Miocene (Mercier, 1981) or even earlier (LePichon & Angelier, 1979, 1981).

The second stage (Fig. 2.9) includes the volcanic products erupted in the fairly narrow zone of the South Aegean Volcanic Arc which includes the volcanoes of Krommyonia, Aegina, Methana, Poros, Milos, Antimilos, Polyegos, Kmolos, Santorini, Christiana Islands, Nisyros, Gyali, Tilos and Kos. The arc is considered to be the surface expression of the still active subduction of the African plate beneath the Aegean. According to Fyticas *et al.* (1976), the arc is composed of two smaller ones; the main outer arc and the inner arc which is not well developed. However, more recent data (Innocenti *et al.*, 1979, 1982b) have demonstrated that the volcanoes of Antiparos and Kalogeri, as well as those of the Volos-Atalanti group are connected with processes which are not related to subduction.

This volcanic activity was initiated in the Upper Pliocene, about 3my ago (Fyticas *et al.*, 1976, Angelier *et al.*, 1977, Innocenti *et al.*, 1979, Ferrara *et al.*, 1980). The older products occur in Krommyonia in the NW part of the arc. The calk-alkaline activity (Fyticas *et al.*, 1976, Innocenti *et al.*, 1981, Fyticas *et al.*, 1984) has K_20/Na_2O ratios closer to the values of the island-arc type than to Andean-type calk-alkaline rocks (Innocenti *et al.*, 1981).

The structures of the volcanoes which erupted in the Southern Aegean Volcanic Arc are not the same throughout the entire area of the arc (Innocenti *et al.*, 1981). In the WNW sectors small lava domes predominate (Krommyonia, Aegina, Methana, Poros), while in the central and eastern sectors large composite volcanoes generally associated with caldera structures occur (Milos, Santorini, Nisyros). These characteristics have been attributed to differences in time and space, of the tectonic regime prevailing during the evolution of the arc (Innocenti *et al.*, 1981, Fyticas *et al.*, 1984), and more specifically to the intensity of the extensional tectonism in the various parts of the arc.

Between the two main volcanic phases, local volcanic events have occurred all over the Aegean area except in the northern sector (Fyticas *et al.*, 1979, 1984). This eruptive activity took place between the Upper Miocene and the Quaternary, and the eruptive products are limited in volume. Firthermore, their characteristics are distinctively different from those of both the previous categories and have been classified in four groups (Fyticas *et al.*, 1984):

a) Sodic-alkaline products localized mainly in the Eastern Aegean area and the Western Anatolia. They crop out in the island of Samos (8.3-7.8 Ma), Patmos (3.5-4.1 Ma), Kalogeri (6.0 Ma), Psathoura (0.5 Ma) and tne Western Anatolia (Innocenti *et al.*, 1982a).

b) Highly potassic alkaline lavas with shoshonitic affinity never continous in space or time with the volcanics of the two previous phases. They crop out in Kos, Patmos, and Bodrum (10.6-7.0 Ma), as well as in the NW Greece (Voras mountain; age ranging from 5.0 to 1.8 Ma).

c) Rhyolites formed from crustal anatexis outcropping on the island of Antiparos with age ranging from 5.4 to 4.0 Ma (Innocenti *et al.*, 1982b), connected with the Upper Miocene intrusives present everywhere along the southern margin of the Attic-Cycladic Massif.

d) Volcanics of the Volos-Atalanti group (3.4-4.0 Ma; Innocenti *et al.*, 1979).

To explain the distribution of volcanic activity in both time and space, Fyticas *et al.* (1984) and Papanicolaou (1986) considered that a migration of the subduction zone towards the south has taken place in time. According to Fyticas *et al.* (1984), increase of the angle of subduction is responsible for the enrichment of the volcanic products of the first stage in K_2O during the evolution of volcanism (Upper Eocene to Middle Miocene). Orogenic activity was interrupted in the Middle Miocene, because the subducted plate was cut off. Consequently, the volcanic arc migrated to the South Aegean Sea, since subduction started again and the South Aegean Volcanic Arc which is still active today was formed (Fig. 2.10).

However, Robertson & Dixon (1984) based on data of Altherr *et al.* (1982) questioned the aspect of the southward migration of the volcanic arc from the area of Thrace and North Aegean to its present position. Altherr *et al.* (1982) considered the Oligocene-Miocene High Pressure/Low Temperature metamorphic rocks of the Phyllite-Quartzite series in the external tectonometamorphic zone of the Hellenides, cropping out in South Peloponnese and Crete, known also as Arna Geotectonic Unit (Skarpelis, 1982, Papanicolaou, 1986), and the Plattenkalk series as a result of the subduction of a southern strand of the Neotethys under Eurasia. Thus considering the space distribution of volcanism at that time, it is difficult to assume that this subduction process accounts also for the volcanic activity in Thrace (Robertson & Dixon, 1984). Instead, they accepted the assumption of Papavasilliou & Sideris (1982) who proposed subduction of the Axios zone (Vardar zone) under the Rhodope Massif to be the most plausible explanation for the Thracean volcanism of Oligocene-Miocene.

The existence of a second subduction zone in the area of the North Aegean, either within the area of the Rhodope Massif or north of it, has also been assumed by Kissel & Laj (1988) in an attempt to explain their paleomagnetic data. This subduction zone was active at least between the Early Paleocene and the Middle Miocene. Finally, Papazachos (1976) suggested the existence of a Benioff zone under Rhodope dipping northwards with an angle of about 30^{o}, based on scarce seismic data. However, recent geochemical data (Jones *et al.*, 1992) suggest that the Cenozoic magmatic activity in the area of Northern Greece is not associated with an active subduction zone, but is related to the extensive regime prevailing in the area. Also, the Upper-Middle Miocene volcanism in the central and Eastern Aegean is probably associated with the crustal extension-related volcanism in Western Anatolia. The north-south directed extension was triggered by the collapse of the

Alpine orogen which probably began as early as the Lower Miocene or even the Upper Oligocene (Seyitoglu & Scott, 1991).

The scattered volcanic activity which took place between the Upper Miocene and Quaternary in central and eastern Aegean is also associated with the same intra-plate extensional regime (more recent products), which created a series of E-W orientated lineaments (Fyticas *et al.*, 1984). The more pronounced features of this tectonic regime are the roughly E-W orientated grabens which have formed since the Upper Miocene in the Western Anatolia (Sengör *et al.*, 1985). Similarly, the volcanoes of the Volos-Atalanti group and those of Voras mountain are related to intense extensional tectonics in continental Greece (Fyticas *et al.*, 1984)

2.3. Summary

The islands of Milos, Kimolos and Chios are situated in the Aegean in the deformed Eurasian margin. Milos and Kimolos are members of the Volcanic Arc of the Southern Aegean Sea characterized by calk-alkaline activity, which is probably related with the subduction of the African plate under the deformed Eurasian margin. This activity began in the Upper Pliocene and continues to the present in the form of fumarolic activity in most of the volcanic centres. The volcanic activity in the island of Chios is older (Lower to Middle Miocene) and is probably connected with the intraplate extensional regime due to the collapse of the Alpine orogen.

CHAPTER THREE

GEOLOGICAL FEATURES

3.1. Regional geology of the study areas.

3.1.1. Milos island

Milos is a volcanic island which, in terms of the geology of its basement, belongs to the Northern Cyclades geotectonic unit (Papanicolaou 1986). This unit belongs to the Intermediate-Tectonic-Metamorphic Zone of the Hellenides; its main characteristic is the existence of crystalline rocks metamorphosed under conditions of High Pressure/Low Temperature (glaucophane schists, eclogites), which underwent a retrograde metamorphic event under conditions of greenschist facies.

The stratigraphic sequence of the island is composed of four distinct geological formations (Sonder 1924, Fyticas 1977):

-The alpine metamorphic basement.

-The Neogene sedimentary sequence.

-The volcanic sequence of Upper Pliocene-Quaternary age.

-The alluvial cover.

The most important of these formations in terms both of volume and economic significance is the volcanic sequence. It occupies more than 70% of the total area of the island (Fig. 3.1) and is associated with a number of mineral deposits including bentonite, kaolin and barytes.

3.1.1.1. The alpine metamorphic basement

The metamorphic rocks of the basement are known only from small outcrops in the southern and SE part of the island (Fig. 3.1). Their limited volume and number of outcrops do not allow the description of the total stratigraphic column of the unit. Generally it is difficult to give a definite stratigraphic sequence representative of the whole Northern Cyclades geotectonic unit because it changes from place to place (Papanicolaou 1986). However, in the island of Andros, where more stratigrphic horizons of this unit are exposed Papanicolaou (1978) described the existence of a carbonate sequence, the depositional characteristics of which change from those of shallow marine water in the base to a pelagic environment in higher horizons. In the intermediate horizons the presence of clastic metasediments and metavolcanics associated in places with Mn-deposits and hematite-rich schists is very common. In the upper horizons of the stratigraphic column the pelagic carbonate sequence evolves into

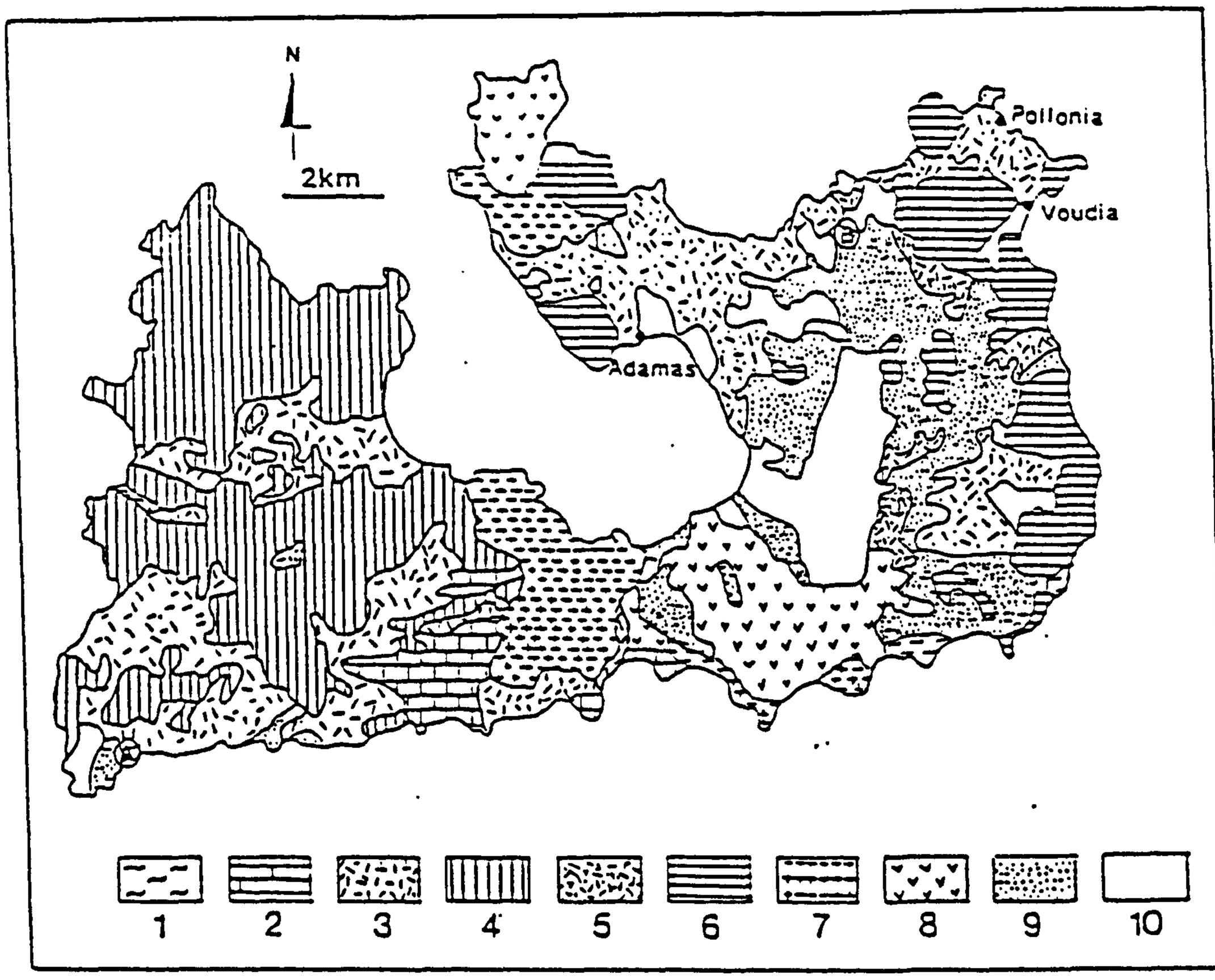

FIGURE 3.1. Geological map of Milos Island (modified after Fyticas *et al.*, 1986). Key to the numbers: 1 = metamorphic basement, 2 = Neogene sedimentary sequence, 3 = basal pyroclastic series, 4 = complex of lava domes and lave flows (Upper Pliocene), 5 = Lower Pleistocene pyroclastics, 6 = Lower Pleistocene lava domes, 7 = Halepa and Plaka domes, 8 = Rhyolitic complexes of Trachilas and Phyriplaka, 9 = products of phreatic activity, 10 = Quaternary sediments, A= Kleftico area, B=Agia Irini area.

a wild metaflysch. According to Papanicolaou (1986) the metamorphic grade increases in a north-south direction (8Kb/320^{o}C in the Southern Euboea, 10Kb/480^{o}C in Andros island and 14Kb/500^{o}C in Syros island. Since the whole sequence has been metamorphosed under conditions of high pressures and moderately high temperatures there are not sufficient paleontological data preserved (Papanicolaou 1986). The age of the marbles in the base of the sequence is Upper Triassic (Melidonis 1980), while the wild-flysch is probably Upper Cretaceous-Eocene (Papanicolaou 1986). The above limited data indicate that the Geotectonic Unit of Northern Cyclades is of Alpine Age and might belong to the so called External Hellenides.

In Milos island, the metamorphic basement has been studied in detail by Hoffmann & Keller (1979) and Kornprobst *et al.* (1979). Kornprobst *et al.* (1979) distinguished three stages of recrystallization of the metamorphic rocks:

-The first is characterized by lawsonite-free jadeite eclogites metamorphosed under High-Temperature/High Pressure conditions (15Kb/500-600^{o}C).

-The second is represented by lawsonite-eclogites and glaucophane schists corresponding to metamorphic conditions of high pressure/low temperature (6-11Kb/300-350^{o}C). Hoffmann & Keller (1979) suggested temperatures around 350^{o}C and depth of burial at least 15km.

-The third stage is dominated by low-pressure/high temperature assembages (greenschist facies mineralogy).

The second and third stages are considered to be the beginning and end of the same event (Kornprobst *et al.* 1979). Thus, the rocks which were crystallised within the jadeite-eclogites field, due to rapid subduction, were recrystallized in the lawsonite stability field (lawsonite-eclogites and glaucophanites) under lower temperatures. Finally, recrystallization within the greenschists metamorphic conditions was characterised by low pressures and increasing temperatures. According to Fyticas (1977) the metamorhic rocks of the basement cropping out in the SE Milos compose a type of wild metaflysch. If this is the case, then they might belong to the Upper horizons of the Northern Cyclades Unit.

Geochronological data for the first metamorphic event suggest a Middle Eocene age (45±5my in Naxos, 42my in Siphnos according to Altherr *et al.* 1979). Similar data for the culmination of the second event which is represented by the greenschiet facies assemblages indicate an Upper Oligocene-Low Miocene age (Altherr *et al.* 1979, Andriessen *et al.* 1979). The later metamorphic event might be related to the high pressure/low temperature event recorded on rocks in the Southern Peloponnese and Crete, which according to Seidel *et al.* (1982) also took place in the boundary between Oligocene and Miocene.

3.1.1.2. The neogene sedimentary sequence

The Neogene sedimentary sequence has been described in detail by Fyticas (1977). The members of this series crop out in the southern part of the island (Fig. 3.1) in the so called isthmus of Provatas. It is believed that it continues in the north and east under the rocks of the volcanic sequence and the alluvial cover (Fyticas 1977), because rock fragments belonging to this series have been found in pyroclastic horizons in several occasions.

The series begins with a **basal conglomerate** up to 30m thick, which is composed mainly of pebbles belonging to the metamorphic basement. This indicates a marine transgression over a land consisting of metamorphic rocks. Often, thin beds of cemented sand-size crystalline material are interbedded with the conglomerates, while sporadically thin yellow or red intercalations of clayey material are present. The source of the cementing agent is terrestrial; generally calcitic cement is absent.

The basal conglomerate is followed by a **shallow marine carbonate sequence**, the thickness of which varies up to a maximum of 150m. The limestones are relatively pure without significant marly and/or sandy impurities. They are well bedded and have undergone a mild diagenesis. Sporadically they are interbedded with thin beds of conglomerates, while in places coral reefs are present. Characteristic microfossils (Fyticas 1977) are *Elphidium crispum* (CINNE), *Globorotalia puncticulata* (DESHAYES) and *Sphaeroidinellopsis Seminulina* (SCWAGER). These microfossils indicate that the age of the carbonate series is Miocene-Low Pliocene. This means that the carbonate sequence is post-Alpine and that the Alpine (Cretaceous-Eocene) age determination of Sonder (1924) is false.

3.1.1.3. The Volcanic Sequence

The volcanic sequence of the island was first studied by Sonder 1924, but the it was the work of Fyticas (1977) and Fyticas *et al.* (1986) which provided detailed information about the evolution of the volcanic activity on the island.

The volcanic rocks occupy more than 70% of the outcrops observed on the island (Fig. 3.1). The volcanic activity was initiated in the Upper Pliocene (Fyticas *et al.* 1976, 1986, Ferrara *et al.* 1980) and is considered to be triggered by the subduction of the African Plate under the deformed margin of the Eurasian Plate (Ninkovich & Hays 1972, Boccaletti *et al.*, 1974, Fyticas *et al.*, 1976, Fyticas 1977, Ferrara *et al.*, 1980, Fyticas *et al.*, 1986). Volcanism was first manifested in the western sector of the island; it was then transferred to the eastern part before its last migration in the central areas of the island (Fyticas *et al.*, 1986).

The oldest volcanic products deposited on the island are pyroclastic rocks mainly of submarine origin, and belong to the **basal pyroclastic series** (Fyticas *et al.*, 1986). The age of this series varies between 3.5 and 3.0 my i.e Middle-Upper Pliocene. It is exposed mainly in the SW part of the island and consists of pyroclastic flows, submarine tuffs, pumice flows and occasionally, pillow lavas and pillow breccias (Fyticas *et al.*, 1986). A typical stratigraphic column of the unit from the area of Kleftico (Fyticas *et al.* 1986) is shown in Figure 3.2. The sequence begins with well stratified tuffite layers forming thin beds and evolves to strata composed of pyroclastic flows. Within these horizons thin diatomite-rich beds are often intercalated. Locally the series is terminated with basic volcanic rocks (basaltic andesites) products of submarine volcanic activity, with characteristic structures (pillow lavas, pillow breccias, hyaloclastites). The tuffaceous horizons of the series do not extend to the eastern part of the island as Fyticas (1977) had initially assumed.

The rocks of this sequence have been substantially altered by secondary hydrothermal alteration associated principally with the lava domes which were emplaced later (see below) (Fyticas 1977). This resulted in the formation of small kaolin deposits and a Mn-deposit in the NW part of the island at the area of Cape Vani. The hydrothermal activity has often obliterated the initial structural characteristics of the original tuffs.

The basal pyroclastic series is followed by a **complex of lava flows and domes** (Fyticas *et al.*, 1986) of intermediate composition (andesitic-dacitic) which covered the rocks of the previous series. This complex is also restricted in the western part of the island. The major feature of this volcanic episode is the change of its character from submarine to subaerial. The age of this complex varies between 2.4 and 2.0 my i.e Upper Pliocene. The lavas are associated with small volumes of pyroclastic rocks which are the products of small volcanic centres. According to Fyticas *et al.* (1986) the largest domes are associated with NNE or NE structural faults confirming the relation between extension tectonism and volcanism observed by Angelier *et al.* (1977). These volcanic centres are also associated with hydrothermal activity which altered the pyroclastic rocks belonging to the basal pyroclastic series. This hydrothermal activity has caused extensive silicification of some of the lava domes; for example the volcanic complex of Profitis Elias (Fyticas 1977).

Petrologically, the andesitic rocks are characterized by porphyritic and/or (less often) microlitic texture, with basic plagioclase phenocrysts associated with augite and hypersthene, and occasionally common and/or basaltic hornblende phenocrysts. Biotite and olivine are very scarce. Accesory minerals are magnetite, apatite and zircon. The groundmass is principally glassy and occasionally microlitic with crystals similar to the phenocrysts.

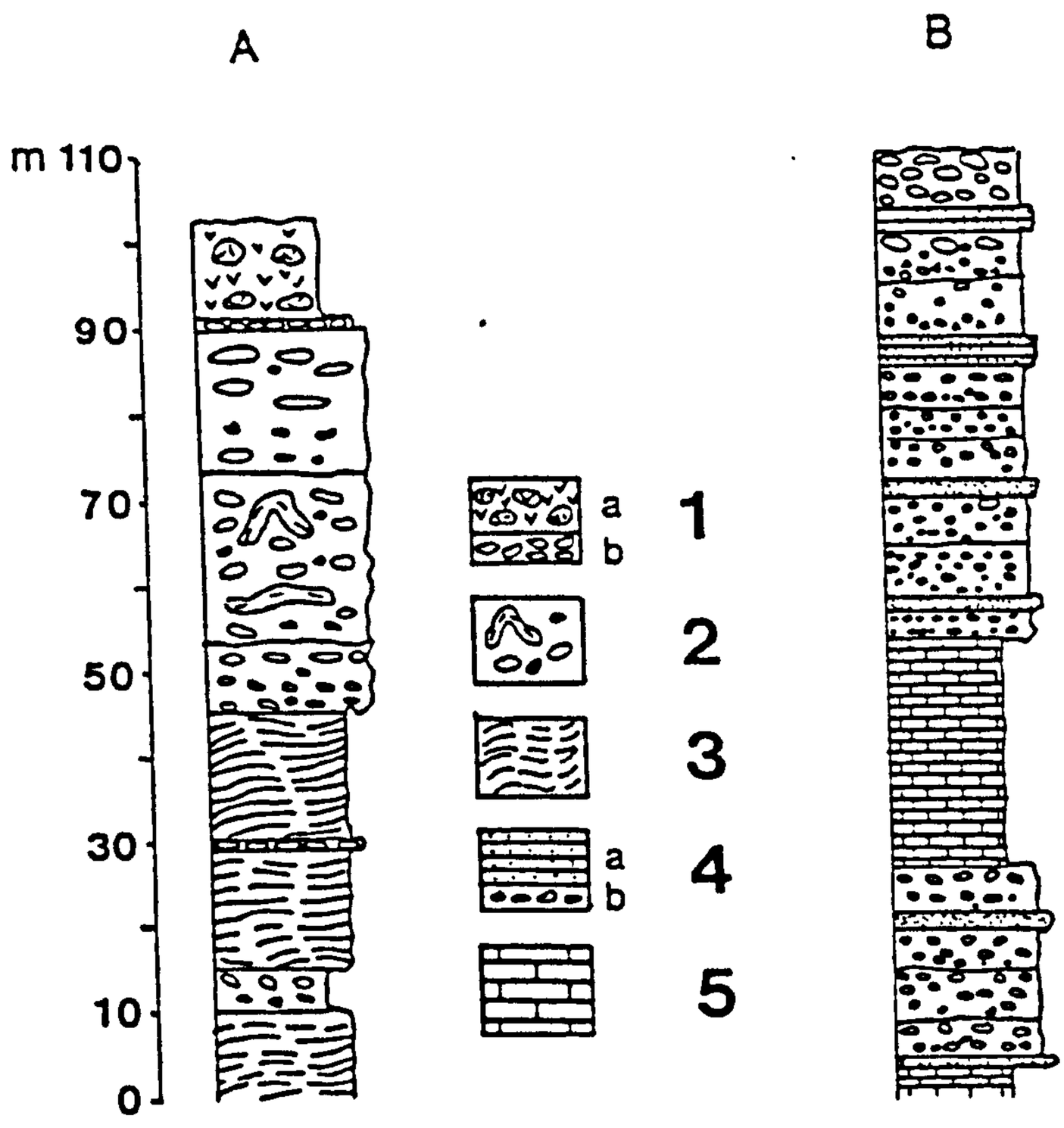

FIGURE 3.2. Stratigraphic sections in the areas a) Kleftico and b) Agia Irini (after Fyticas *et al.*,1986).. Key to the numbers: 1= pillow lavas (a) and pillow breccias (b), 2 = pyroclastic flows including tuffite layers, 3 = thinly stratified and ondulated tuffite layers, 4 = ash flow deposits (a) and with fossils (b), 5 = diatomite-rich ash deposits.

The dacitic rocks are dominated by porphyritic texture (less often microlitic), with phenocrysts predominately of acidic plagioclase and subordinate quartz, common hornblende, biotite, and sometimes pyroxenes. Magnetite is present as an accessory mineral. The groundmass is either glassy characterised by perlitic texture, or microlitic, with microlites of plagioclase, quartz hornblende and biotite.

After the emplacement of the complex of lava flows and domes, the volcanic activity migrated to the eastern and northen sector of the island. **A series of lava domes,** mainly acidic were emplaced, **and submarine pyroclastic rocks** were deposited in those areas. The oldest rocks of these series compose the rhyolitic dome of Demenegaki in the eastern part of the island (1.84±0.08 my). The pyroclastic rocks are exposed mainly in the northern part of the island. Typical stratigraphic columns of the pyroclastic rocks are shown in Figure 3.2. The stratigraphic sequence of these rocks changes from place to place. It is mainly composed of different horizons of pyroclastic flow deposits which locally include tuffite layers. They are interbedded with ash flow deposits and diatomite-rich ash deposits. Locally, the pyroclastic rocks of the sequence are covered by hyaloclastites of andesitic composition.

The composition of the lava domes varies between broad limits (from rhyolites to andesites), although the acid materials predominate. The rhyolitic rocks are characterized by vitrophyric texture with phenocrysts of acidic plagioclases, quartz and occasionally sanidine embedded in glass. Hornblende phenocrystals are always present while biotite and pyroxenes are scarce. Magnetite is present as an accessory mineral. The glass commonly has perlitic textures. The andesitic and dacitic rocks of the series have mineralogical composition similar to that of the intermediate rocks in the western part of the island described above.

By the end of Pleistocene the volcanic activity migrated to the central part of the island and formed the **acid centres of Trachilas** in the northern and **Fyriplaka** in the southern part of central Milos (Fyticas, 1977, Fyticas *et al.*, 1986). Both complexes are very recent (0.38 my and 0.14-0.09 my respectively). In the acid complex of Trachilas pyroclastic surge deposits products of interaction between magma and water, formed the wide basal ring of the volcano. The volcanic activity gradually changed character and converted to effusive; eventually lavas of rhyolitic composition closed the volcanic cycle.

The volcanic complex of Fyriplaka was formed by two separate events which are dominated by explosive activity (Fyticas *et al.*, 1986). The first one started with the formation of a wide basal ring-tuff followed by a pyroclastic cone made of blocks and lapilli. This phase was terminated with the effusion of acidic lavas. This cycle was followed by a series of intensive phreatic explosions which brought on the surface material from the metamorphic basement.

The second cycle started with the formation of a wide ring-tuff which is a surge deposit, indicating the presence of phreatomagmatic activity. The lower parts of this horizon include blocks of the metamorphic basement. This activity was continued by the formation of an inner ring-tuff evolving to a cone of blocks and lapilli similar to the first cycle. In the depression which resulted from the coalescence of these cones, a series of small cones associated with lava flows were formed. These lava flows are mainly perlitic and flowed towards the gulf of Milos in a NW direction.

The initial stage of the different cycles is often phreatic evolving into a phreatomagmatic one. The later phases are usually dominated by the effusion of lavas. According to Fyticas *et al.* (1986) the initial phreatic phase causes fracturing of the country rocks, allowing circulation of water and interaction with the magma; consequently the hydromagmatic stage takes place. In the later stages, the water-magma interaction decreases significantly, and effusive products (lavas) dominate. In other words, in both the two acid volcanic centres, the water/magma interaction decreases towards the later stages of their development.

Petrologically, the rocks in both the volcanic centres are rhyolites. In the Trachilas complex rhyolites have vitrophyric texture with phenocrysts of quartz, sanidine, acidic plagioclase, biotite and Fe-hydroxides and glassy groundmass. In Fyriplaka, the rhyolites of the main crater have perlitic texture and are characterised by phenocrysts of acidic plagioclase, quartz sanidine and occasionaly pyroxenes.

In the eastern sector of the island there is a widespread formation dominated by a "chaotic" structure i.e it lacks any internal structural organization. It includes blocks and agglomerates belonging to various volcanic rocks as well as to the metamorphic basement. The main part of this formation corresponds to the characteristic horizon of **green lahar** proposed by Fyticas (1977). However, this term has been reappraised by Fyticas *et al.* (1986) and this chaotic formation is considered to be the product of several phreatic explosions. The thickness of this formation varies from place to place and becomes maximum close to volcanic centres and its age is certainly Quaternary; probably younger than 0.2 my (Fyticas *et al.*, 1986).

3.1.2. Kimolos island

Kimolos is an almost entirely volcanic island (Fig. 3.3). with geological evolution similar to that of Milos island. The volcanic products are predominately pyroclastic rocks which were erupted between the Upper Pliocene (3.5 my) and the Middle Pleistocene (0.9 my) (Fytikas & Vougioukalakis, 1992). Two cycles of volcanic activity have been recognized (Fytikas & Vougioukalakis, 1992): The first between 3.5 and 2.0 my which produced the ignimbrite of Kastro which occupies more than half of the entire

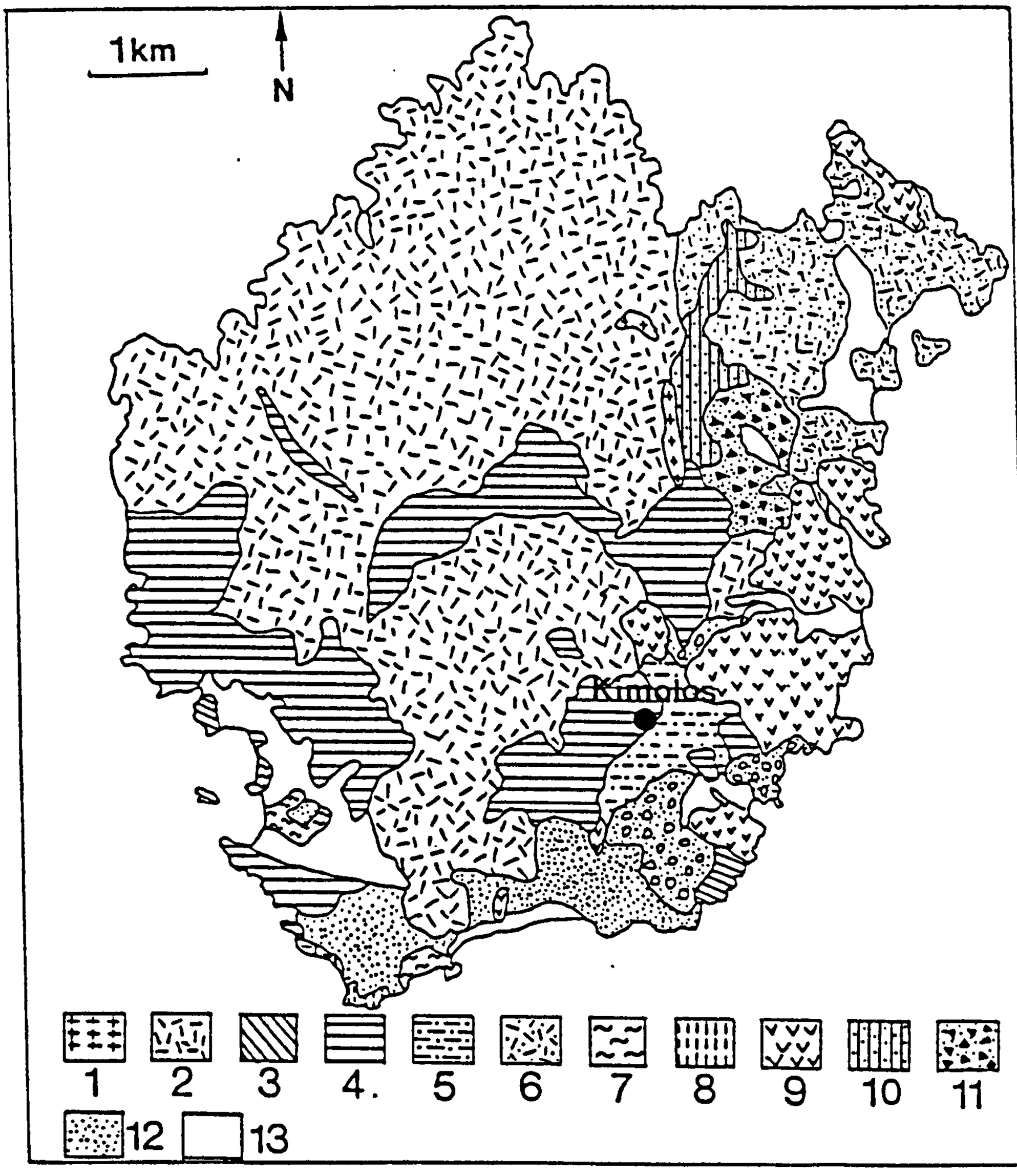

FIGURE 3.3a Schematic Geological map of Kimolos Island (modified after Fyticas & Vougioukalakis, 1992). Key to the numbers: 1 = granitic body, 2 = Kastro ignimbrite, 3 = hydrothermally altered volkanic rocks, 4 = andesitic and dacitic dykes and lava flows and domes, 5 = Kimolos village breccia, 6 = ignimbrite of Prassa area (NE Kimolos), 7 = pumice flows, 8 = hydrovolcanic pyroclastics of Maar type, 9 = lava flows of the Geronikola area and domes and lava flows of the Psathi area, 10 = nuee' ardente pyroclastic breccia of the Korakies area, 11 = reworked pyroclastic breccia of the Korakies area, 12 = alluvial deposits, 13 = scree, elluvial and beach deposits.

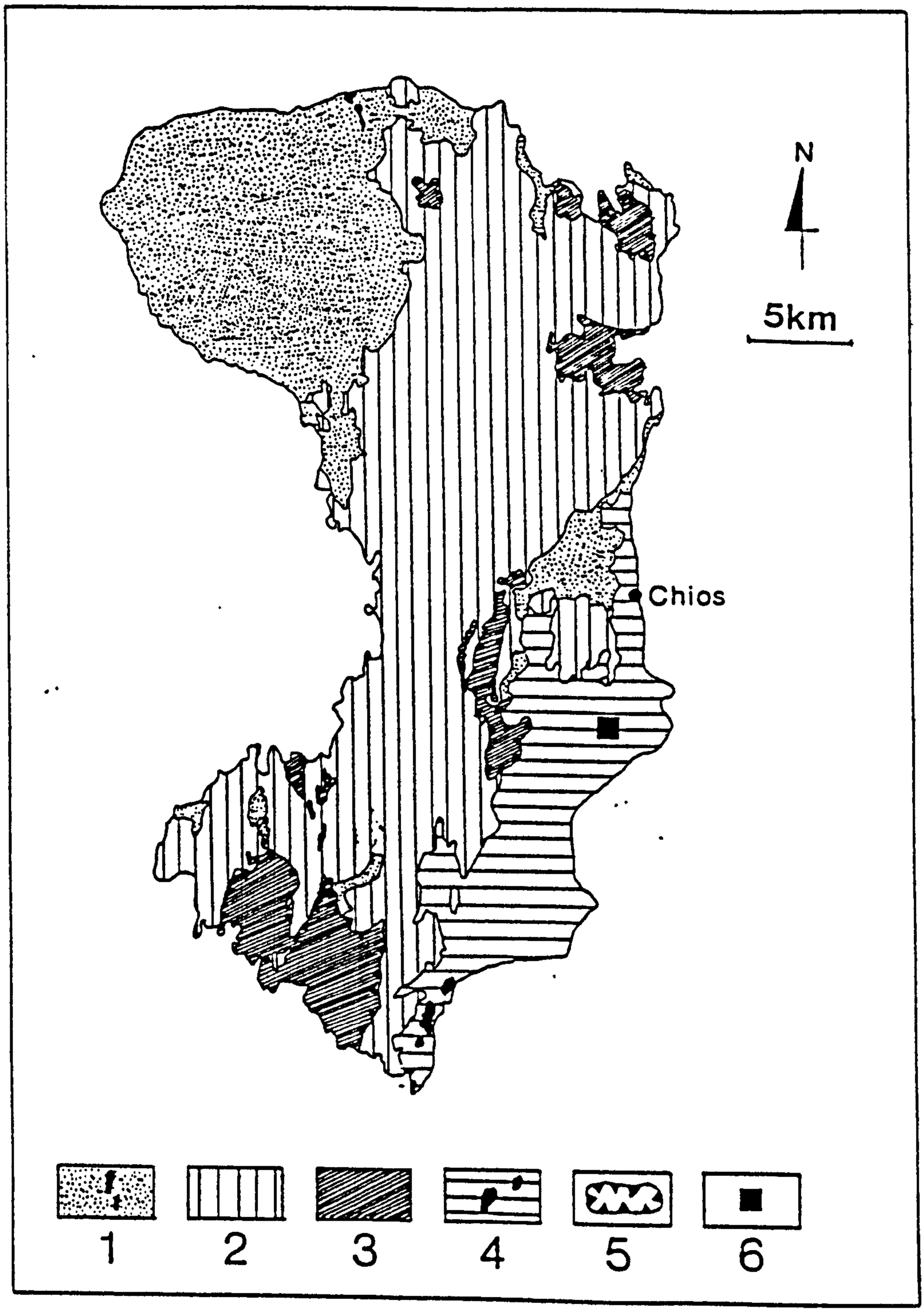

FIGURE 3.3b. Schematic geological map of Chios Island (modified after Besenecker *et al.*, 1968). Key to the numbers 1= paleozoic rocks and associated volcanics (autochthonous unit), 2 = paleozoic rocks (autochthonous unit), 3 = allochthonous unit, 4 = Neogene rocks and associated volcanism, 5 = thurst, 6 = study area.

area of the island (Fig. 3.3) and the andesitic and dacitic lavas cropping out in the central and eastern part of the island.

The second cycle was active between the Lower and the Middle Pleistocene (2.0-0.9my) and produced the ignimbrite at Prassa, the andesitic pyroclastics and lavas of Geronikola, the rhyolitic pyroclastics of Psathi and Myrsini in the southern part of the island and finally the rhyolitic domes of Psathi, Xaplovouni and Mersini. After the extrusion of these domes the volcanic activity ceased.

The source of the magmas which gave rise to the volcanic rocks in both islands is a matter of controversy among different workers. Nicholls (1978) proposed a complex model for the volcanic rocks of Santorini, according to which partial melting of the underlying oceanic slab produced magmatic fluids enriched in Large Ion Lithophile (LIL) elements. Those fluids reacted with the upper mantle wedge causing its subsequent melting and generating basic magmas with calc alkaline characteristics. The latter magmas underwent fractionation during their ascend to higher levels, giving rise to more acid products. Innocenti *et al.* (1981), based on trace elements relationships, rejected the idea of a magmatic contribution from the subducted oceanic slab. Instead they proposed a model which attributes the variability in LIL elements among the various volcanic islands of the South Aegean Volcanic Arc (SAVA), including Milos and Kimolos, to the inhomogeneity in the composition of the upper mantle, probably caused by hydrous fluids.

Fyticas *et al.*, (1986) and Briqueu *et al.*, (1986) agreed that the less evolved rocks of Milos have been derived from mantle derived magmas which underwent contamination with crustal material, while the more evolved ones are products of simple fractionation processes of intermediate magmas. However, Mitropoulos *et al.*, (1987) rejected the possibility of crustal contamination, or any contamination from subducted pelagic or terriginous sediments. They attributed the trace element patterns observed throughout the SAVA to inherited LILE enrichment which took place during the long period of subduction processes in the area.

3.1.3. Chios Island

The geological formations which crop out on Chios island can be divided into two distinct groups: the pre-Neogene rocks and the rocks of the Neogene sequence. The pre-Neogene rocks have been further subdivided into two tectonic units (Besenecker *et al.*, 1968, Kauffmann, 1969): **an autochthonous** one characterized by a discontinuous sedimentary succession from Silurian to Jurassic, and **an allochthonous** unit comprising a discontinuous sedimentary succession from the Carboniferous to the Jurassic (Fig. 3.3b).

3.1.3.1. The autochtonous unit

It covers the larger part of the island. It begins with a clastic sequence dominated by grey or occasionally reddish sandstones, the age of which is not known with certainty due to the lack of fossils (Besenecker *et al.*, 1968, Herget & Roth, 1968, Roth 1968, Herget 1969 Papanicolaou & Sideris 1983, Sideris 1986). It includes blocks of various lithologies (limestones, flints, slates, volcanic rocks), sizes and ages. The origin of this sequence has been a point of controversy between different geologists. Two possible modes of origin have been postulated. The old one suggests a normal stratigraphic sequence with some stratigraphic hiatus mainly in Lower and Middle Devonian, beginning in Silurian (Llandovery) and terminating in the Upper Carboniferous (Besenecker *et al.*, 1968, Herget & Roth, 1968, Roth, 1968, Herget 1969). The second hypothesis supports the idea of a wild flysch with a possible Permian age, which includes olistoliths of various ages and sizes (Papanicolaou & Sideris 1983, Papanicolaou 1986, Sideris 1986). The latter hypothesis seems more plausible as it was proven from observations of the contacts and the different type of deformation between the various olisthostromes and the sandstone matrix (Papanicolaou & Sideris, 1983, Sideris 1986), the lack of systematic time and phase-sequence between the various blocks (shown by the admixture of blocks of different ages and depositional environments, Papanicolaou & Sideris 1983, Sideris 1986), and the nature of the mineralization connected with the volcanic blocks (Lambropoulos & Kaminari 1989).

According to this model, the olistoliths are distributed in four distinct formations dipping towards the east and appearing again in the eastern part of the island, i.e they form a synclinal structure with the older olistoliths in the centre of the structure (Sideris 1986). The four formations from east to the west are the following (Sideris 1986):

-Melanios formation (mainly limestone and volcanic blocks of the Lower Carboniferous)

-Nenitouria formation (volcanic, schists, and limestone blocks of the Lower Carboniferous)

-Drymonas formation (volcanic, and shallow water limestone blocks of Lower Carboniferous, pelagic limestone blocks of Devonian age)

-Agrelopos formation (mainly large limestone blocks of Silurian age)

The transition to Trias is again another point of controversy among the various workers. Besenecker *et al.* (1968) consider a discontinuous succession, associated with a hiatus, characterized by a basal transition series composed of three different horizons:

-A basal conglomerate having a thickness varying from 0 to 40m followed by

-a sandstone horizon having a thickness up to 20m and a

-basal limestone which in its lower levels alternates with sandy-marls, having a thickness varying from a few tens of metres up to 100m.

The total transition series is preserved only in the northern part of the island. The conglomerates first and then the sandstones disappear towards the south; consequently, in the central areas of the island the basal limestones are in direct contact with the Paleozoic rocks.

However, Sideris (1986) considers a gradual transition from the Upper Permian to Scythian without any discontinuities and consequently without any hiatus. This assumption is based on the fact of the existence of conglomerates in the uppermost sectors of the Permian wild-flysch like horizon which have similar characteristics to those of the transition series.

The age of this transition series is Scythian.

Above the basal limestones of the transition series a thick sequence of massive limestones and dolomites follows, having an Upper Scythian-Low Anisian age. Its thickness varies between broad limits reaching 500m in places and it is closely associated with the underlying basal limestones. In the higher sectors of this carbonate sequence the limestones are converted to red limestones with characteristics of **the Hallstatt facies** (i.e rich in cephalopod fossils especially ammonites). Towards the end of the carbonate sequence, the limestones appear to be brecciated.

In the Upper Anisian the character of sedimentation changed due to tectonic instability (Besenecker *et al.* 1968). This situation lead to the deposition of a variety of rock types including limestones, marls, sandstones and conglomerates. Also, volcanic activity produced a number of tuffaceous horizons. Stratigraphic hiatus of very small scale are present, but generally the series can be considered as being continuous. In the upper horizons of this series the sedimentary conditions changed again, leading to the deposition of marly limestones.

From the beginning of the Ladinian up to the Lias the stratigraphic column of the autochthonous unit is composed of a thick carbonaceous sequence consisting of massive and locally thick-bedded limestones and dolomites characteristic of a shallow depositional environment. The sequence has a maximum thickness of 1000m. In several stratigraphic levels during the Upper Ladinian-Karnian local emergence caused the formation of small bauxitic horizons without any economic importance. Also, during the Lias another emergence caused the change of the character of sedimentation to a clastic one. This led to the deposition of conglomerates and sandstones which later evolved to limestones as the sedimentary conditions changed again (Besenecker *et al.*, 1968).

The abrupt changes of the depositional environments during the Trias and the Lias, most probably due to tectonic events (Besenecker *et al.*, 1968, Sideris 1986) as well as

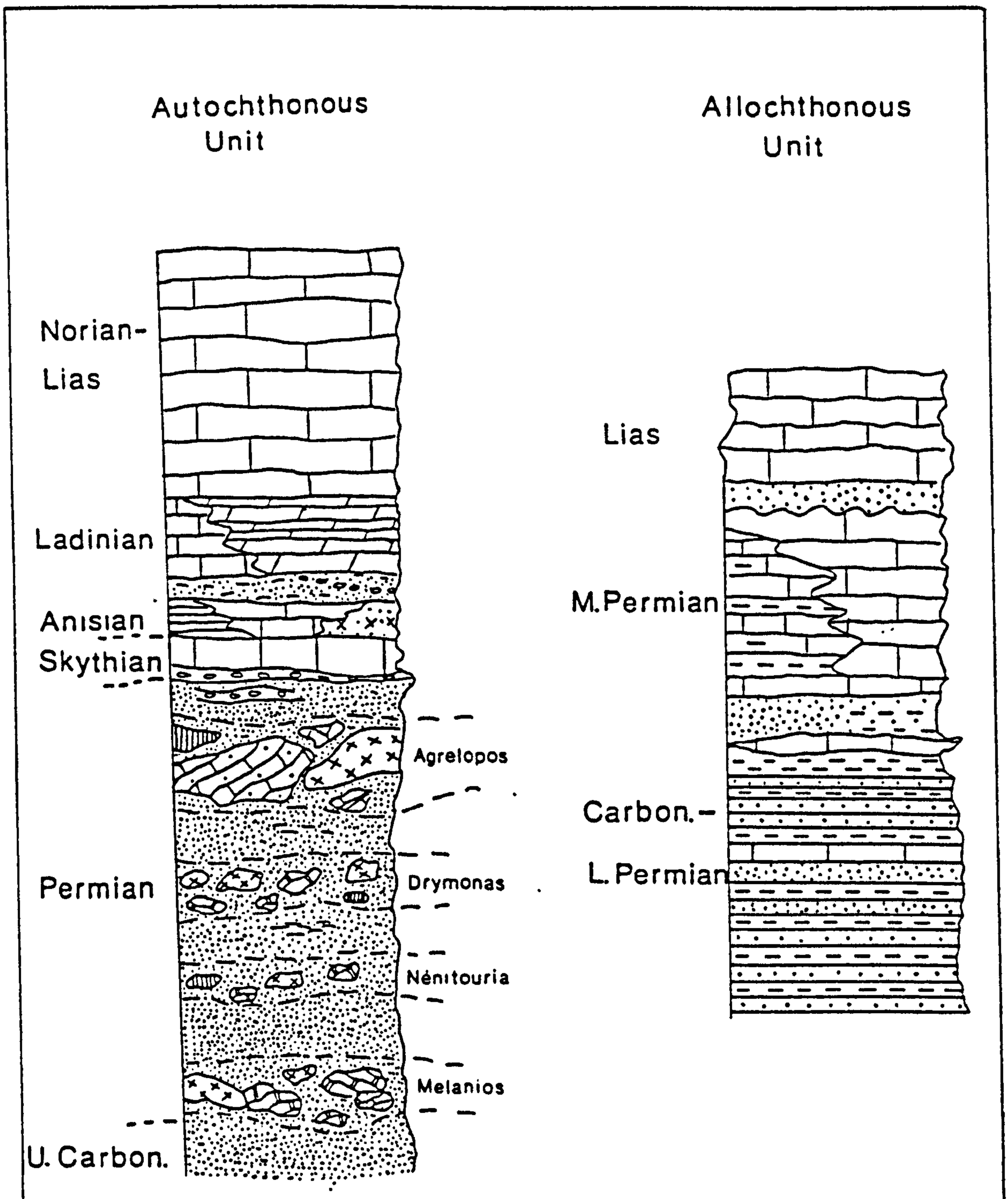

FIGURE 3.4. Stratigraphic columns of the geotectonic units of Chios (after Sideris, 1986).

the manifestations of volcanism in several areas of the island during that period, have been attributed to regional tectonic events associated with the relative movements of the Cimmerian continent with respect to the Eurasian margin, as the Neotethys ocean was opening (Monod & Akay 1984, Sideris 1986).

Finally, at the southern end of the island a clastic horizon consisting of conglomerates, associated with marly sandstones is developed, forming an unconformity with the underlying horizons of Lower Mesozoic. The age of this horizon is not known with certainty but it is believed to be Paleogene, since some of the pebbles of the conglomerate include Maastrichtian fossils (Upper Cretaceous), belonging to the allochthonous series (Besenecker *et al.*, 1968, Ludke 1969). A schematic stratigraphic column of the autochthonous unit is depicted in Figure 3.4 (Sideris, 1986).

3.1.3.2. The allochthonous Unit.

It constitutes a discontinuous succession from the Lower Carboniferous to the Upper Cretaceous, with large hiatus in the Lower and Upper Mesozoic (Besenecker *et al.*, 1968, Kauffmann 1969, Sideris 1986).

The Lower Carboniferous is represented by dark bedded bituminous limestones with conodonts, the thickness of which is not known with detail. These limestones are isolated from the higher placed stratigraphic members of the succession.

The Upper Carboniferous is represented by a sequence of clastic sediments alternating with massive marine limestones. The sequence begins with products of clastic sedimentation, greywackes and shales, evolving into a carbonate succession consisting of massive and in places bedded limestones in which thin sandstone and quartz-conglomerate beds locally occur. The thickness of these limestones reaches up to 70m.

Above the Upper Carboniferous, a predominately clastic sequence of Lower Permian age follows. It consists mainly of greywackes and shales with intercalations of reef-limestones containing corals, foraminifera, and algae fossils, as well as limestone-rich conglomerates and breccias without fossils. These rock-types imply a complex depositional environment consisting of small reefs amidst a basin where clastic sedimentation was taking place (Besenecker *et al.*, 1968).

In the Middle and the Upper Permian the sedimentary environment changed again and limestones become again the main lithofacies (Besenecker *et al.*, 1968). They are thin- bedded, dark brown bituminous limestones which occasionaly include thin beds of marls. The thickness of the sequence reaches up to 60m in the Northern part of the island, but it decreases dramatically towards the south and is completely absent south

of the area of Langada in the NE part of the island.

The Upper Permian is followed directly by Lias due to the existence of a large hiatus which includes the whole Triassic. An exception to that is a small outcrop of Karnian rocks (Upper Triassic) which are exposed in the NE part of the island (Marmaro area). Consequently, the Lias transgression caused the deposition of a thin basal formation a few metres thick, composed of red shales, sandstones and conglomerates. This basal series is followed by a carbonate sequence a few hundered metres thick consisting of thick-bedded limestones and dolomites. The age of this sequence is Lower Lias.

Finally, in southern Chios a thin (20m) sequence of marly-limestones and marls with a thin conglomerate deposited with a small unconformity over the Lias carbonates has been reported by Besenecker *et al.* (1968) and Ludke (1969). The age of this horizon has been determined by rudist fossils as Santonian-Maastrichtian (Upper Cretaceous).

The stratigraphic sequence of the allochthonous unit of Chios island, does not occur in any other area of Greece. Sideris (1986) considers that it might be a part of the Cimmeririan continent. A schematic stratigraphic column of the allochthonous unit is depicted in Figure 3.4 (Sideris, 1986).

3.1.3.3. The Neogene Sequence

The Neogene sedimentary succession crops out in the SW part of the island. Lithologically it is divided in three horizons from bottom to the top (Besenecker *et al.*, 1968, Besenecker, 1973):

-A sandstone sequence up to 150m thick.

-A sequence composed of alternations between clays and sands 100-250m thick.

-A lacustrine marly-limestone sequence more than 250m thick in places.

The sandstone sequence has been deposited with an angular unconformity over the Mesozoic-Palaeozoic rocks of the basement. It consists of brown-red medium to fine grained poorly sorted fluviatile and/or lacustrine sandstones, with calcareous or argillaceous cement. Amidst the mass of the sandstone a thin, yellow-red marly horizon is present. This sequence corresponds to the **Thymiana-layers** described by Besenecker (1973).

The aforementioned sequence evolves to fine-grained sand beds alternating with red and green clay horizons of Upper Miocene age dipping with 10^{o}-15^{o} in a south eastern direction. These beds include a very characteristic tuffaceous-horizon which Besenecker *et al.* (1968) describe as "Bimstuff" i.e light tuff, while Kreatsas (1964) characterizes it as bentonite. The sequence has been divided by Besenecker (1973) into two units, the lower **Zyfia layers**, up to 150m thick, which are richer in sand relative to clay, and the upper **Keramaria layers** 60-130m thick, where the clay

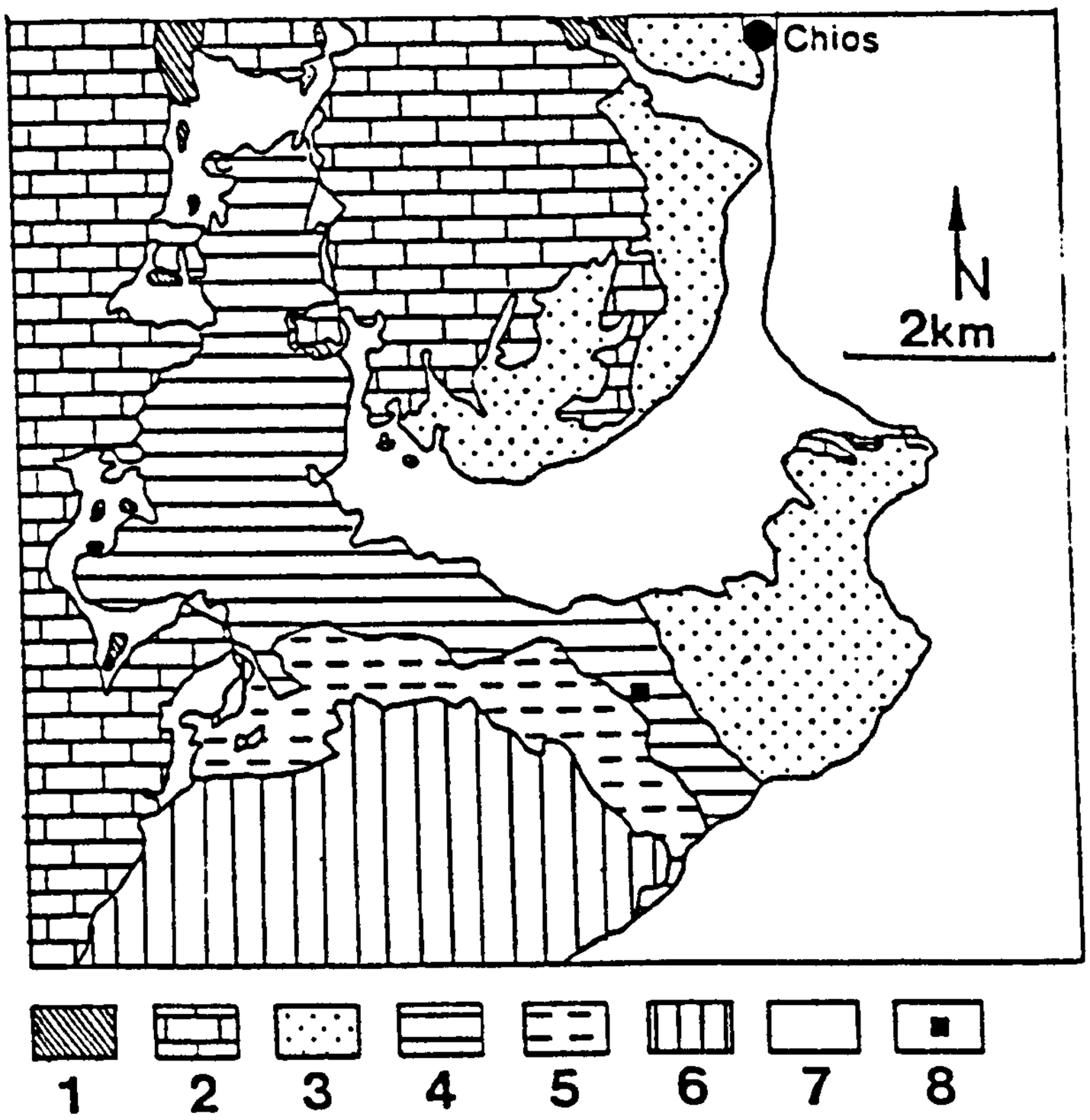

FIGURE 3.5a. Geological map of the Neogene rocks of Chios in the field area (modified after Besenecker, 1973). Key to the numbers: 1 = Paleozoic rocks (greywackes) 2 = Mesozoic limestones and dolomites 3 = Thymiana layers, 4 = Zyfia layers, 5 = Keramaria layers, 6 = Nenita layers, 7 = alluvial deposits, 8 = main bentonite occurrence (field area).

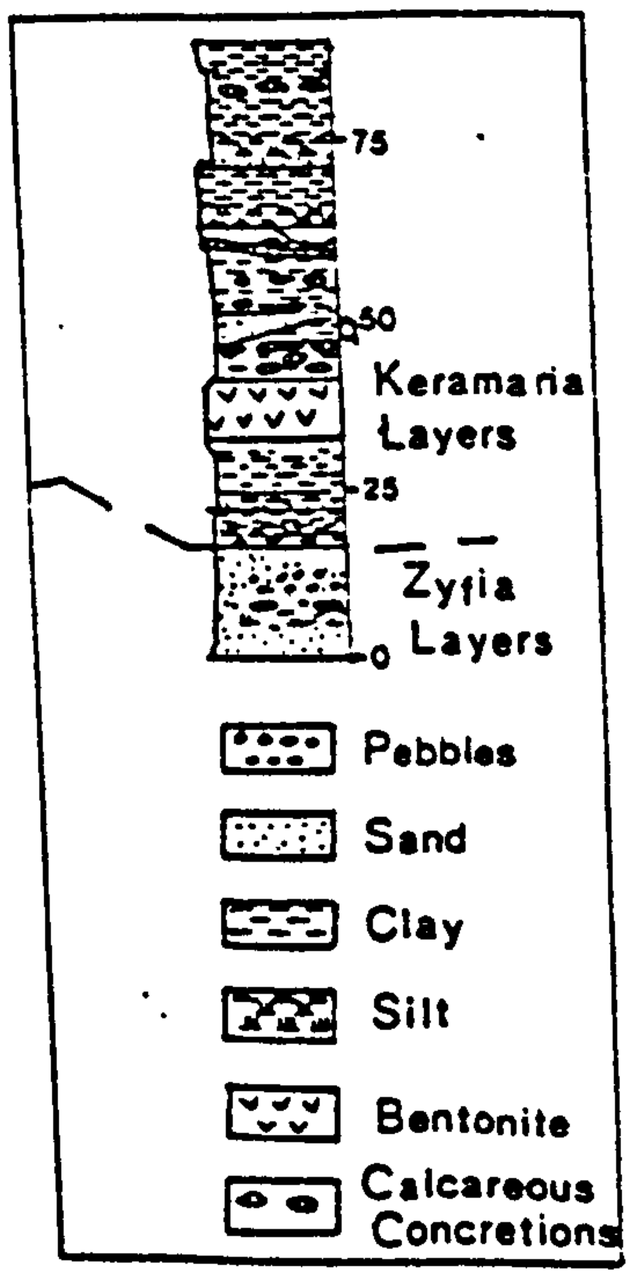

FIGURE 3.5b. Location of the bentonite bed in the transition between the Zyfia and Keramaria layers (after Besenecker, 1973).

horizons predominate. The bentonite horizon is situated a few metres above the boundary between these two sub-units (Fig. 3.5), and in some cases determines their contact (Fig. 3.11b).

The Neogene succession terminates with a lacustrine, marly-limestone formation, which Besenecker (1973) named **Nenita layers**. It is a white to silver-white thin bedded formation which includes intercalations of clay or sand bands and thin coal beds.

The age of the Neogene succession has been determined as Upper Miocene-Early Pliocene mainly from paleontological evidence (Besenecker *et al.*, 1968, Besenecker, 1973). However, radiometric data from the volcanic rocks cropping out on the island, including data from the tuffaceous horizons associated with the Neogene sediments, determined a Lower to Upper Miocene age (Burdigalian-Tortonian), *i.e* 17-11 my (Belon *et al.*, 1979). Very similar ages have been determined in volcanic rocks associated with Neogene basins in Western Anatolia (Seyitoglu & Scott, 1991).

The volcanic activity produced a number of small-volume outcrops the geochemical characteristics of which are calc-alkaline (Besenecker & Pichler, 1974). An exception to this trend is exhibited by a lati-basalt (basalt according to Ludke, 1969) cropping out in the southern part of the island (Pirgi area) which exhibits alkaline characteristics containing normative nepheline (Besenecker & Pichler, 1974). The age of this alkaline episode was estimated as Upper Miocene. Acording to Besenecker (1973) and Besenecker & Pichler (1974), the calc-alkaline volcanism postdated the alkaline episode and has been divided into an rhyolitic one (Upper Miocene-Lower Pliocene), followed by an andesitic episode (Upper Pliocene-Pleistocene). However, more recent geochronological data (Belon *et al.*, 1979, also see Fyticas *et al.*, 1984) showed that the volcanism is older (17-11 my i.e Lower-Upper Miocene) and that the different volcanic outcrops belong to a single volcanic cycle, being closely associated with the volcanic rocks of the Western Anatolia.

Detailed petrological investigation of the volcanic rocks has been carried out by Besenecker & Pichler (1974). The rhyolitic rocks have porphyritic texture, with phenocrysts of plagioclase having an oligoclase to acidic andesine composition (An_{20-35}), sanidine and quartz, with subordinate biotite. In the glassy (cryptocrystalline in places) groundmass microliths of the same mineralogical composition as the phenocrysts, with the addition of hornblende and possibly some pyroxene, are present.

The andesitic rocks are characterized by a porphyritic texture with phenocrysts of plagioclase of labradorite composition (An_{60-70}), augitic pyroxene, and occasionaly olivine and hypersthene. The groundmass has hyalopilitic texture consisting of microlites of plagioclase, clinopyroxene and opaque minerals.

Finally, the lati-basalt exhibits porphyritic texture with phenocrysts of Ti-augite with

characteristic hour-glass texture (Besenecker & Pichler, 1974), olivine (mainly replaced by serpentine and iddingsite) and occasionally plagiclase of bytownite composition (An_{70-75}), embedded in a hyalopilitic groundmass. The latter consists of microlites of plagioclase and clinopyroxenes with opaque minerals.

3.2. Structure

3.2.1. Milos-Kimolos

The tectonic features of Milos and Kimolos Island have been studied with detail by Fyticas (1977), Angelier *et al.* (1977), Simeakis (1985) and Papanicolaou (1988). Both islands have been affected by the same tectonic events since they are situated closely in space (Fig 3.6a).

Since the Alpine metamorphic rocks outcrop only in a small number of places occupying minimal areas, the alpine tectonic events have not played an important role on the tectonic characteristics observed on the island. On the contrary, the neotectonic events, especially those after the Upper Miocene, are very important since they are responsible for the configuration of the structure of the total Aegean area. Consequently the major structural characteristics of both islands are governed by fault tectonics.

The most detailed description of the tectonic features of Milos island has been given in the recent report of Papanicolaou (1988). After a measurement of 452 fault orientations he proposed four major fault sets in accordance with Fyticas (1977):

-A fault set having NW-SE direction (130-310^{o}) accounting for 29% of the total fault population. This system is responsible for the formation of the gulf of Milos and the Straits of Pollonia which separate Milos from Kimolos. It was observed also in Kimolos during the field work.

-A second set with E-W direction (90-270^{o}) including 19% of the fault directions measured.

-The third set has a N-S direction (0-180^{o}) accounting for about 18% of the faults.

-The fourth fault set has a ENE-WSW direction (60-240^{o}) and includes 16% of the faults measured. This set continues also in Kimolos island being observed in bentonites at the NW and SW parts of the island.

In several sites structural features caused by other than neotectonic events can be observed; for example syn-sedimentary faults formed during the deposition of volcanic material of different strength one on the top of the other, and/or from volcanic explosions (Papanicolaou 1988), or textures formed from slumping of hard volcanic blocks within soft tuffaceous material.

Each one of the four sets described includes faults characterized by different

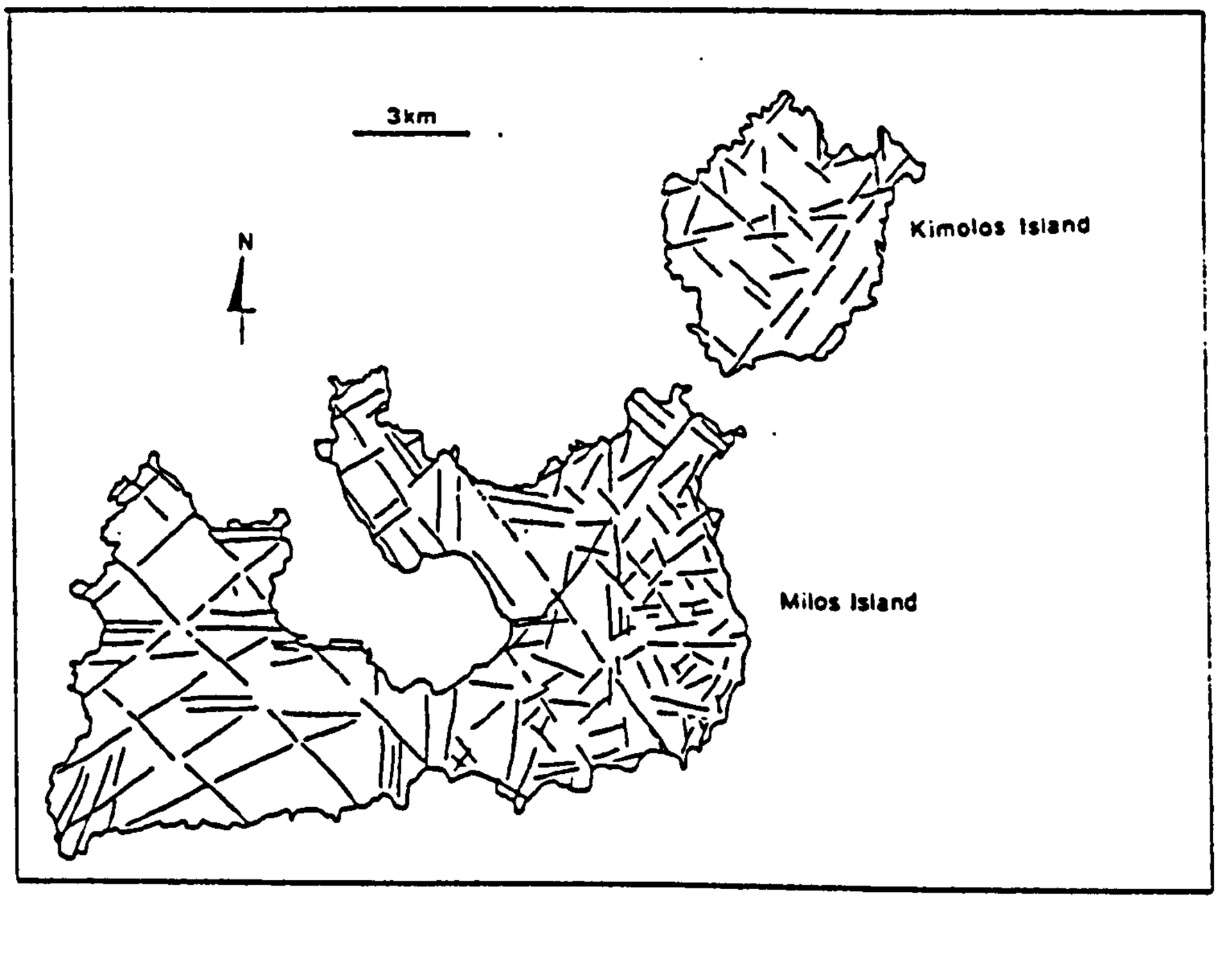

FIGURE 3.6a. Structural map of Milos and Kimolos Islands (after Simeakis, 1985)

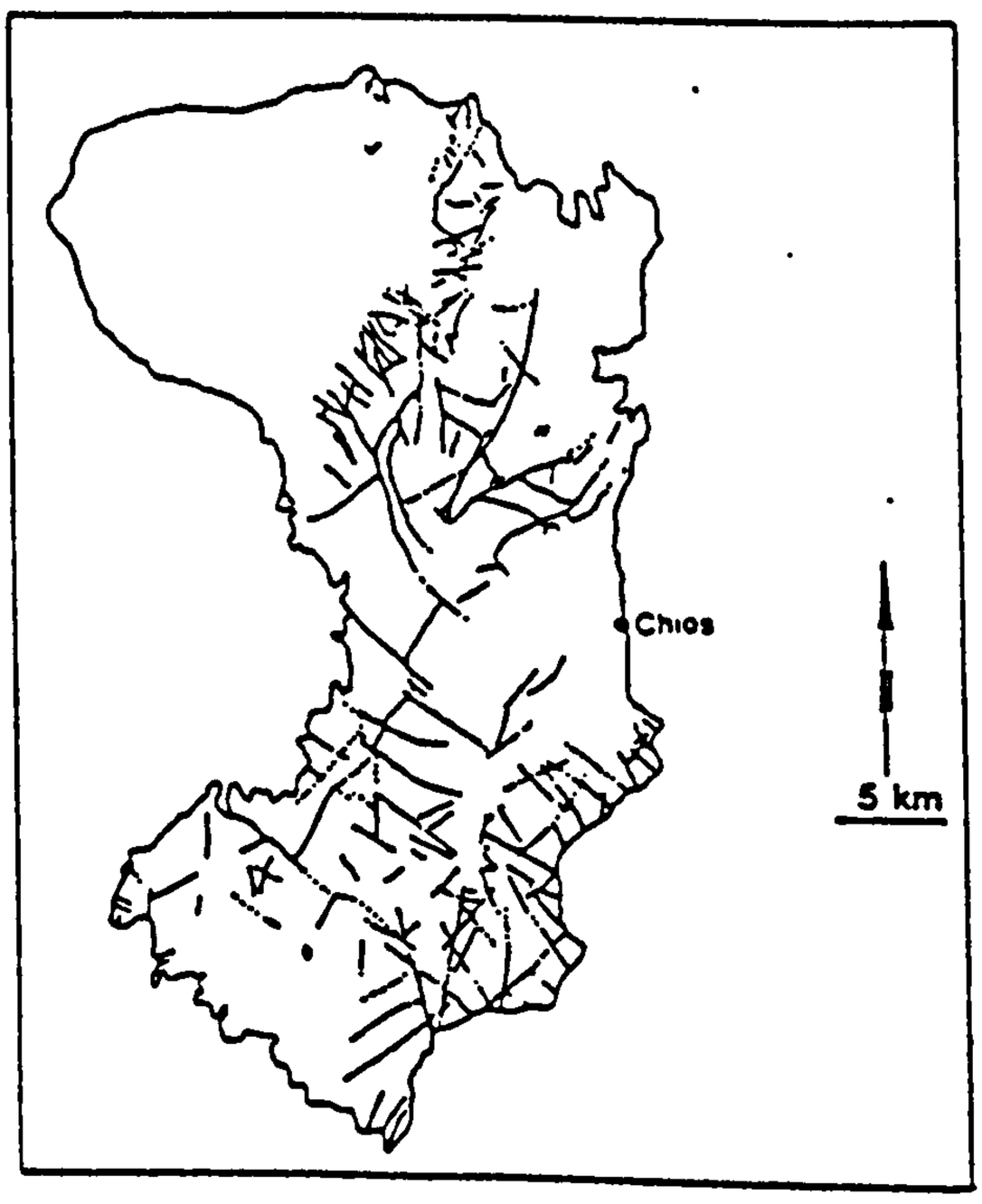

Figure 3.6b. Structural map of Chios Island (after Besenecker *et al.*, 1968).

kinematics, throw, length and age (Papanicolaou 1988). The faults can be classified into normal and strike slip ones with respect to their kinematic and dynamic features (Papanicolaou 1988). This means that no reverse faults have been identified in Milos (Angelier *et al.*, 1977[1], Papanicolaou 1988), indicating lack of any compression events on the island, al least from the Miocene-Pliocene boundary onwards (see also Chapter 2). According to Papanicolaou (1988) the E-W fault system was the most active one during the Pliocene but it has gradually been rendered inactive. Thus, during the Quaternary, the N-S and the NW-SE fault systems dominated, with the latter being active during the whole neotectonic evolution of the island, although its activity was restricted during Pliocene.

3.2.2. Chios Island

Both geotectonic units observed on the island have been affected by Alpine compressional orogenic events. Besenecker *et al.*, (1968), Kauffman (1969), Tietze (1969), and Ludke (1969) distinguished three main compressive events associated with the formation of three fold systems:

-The older one which has an age older than the Upper Cretaceous is characterized by fold axes striking NNE to NE. This system is associated with overthrusts exhibiting small scale movements.

-The second compression event is associated with the superposition of the allochthonous unit as a tectonic nappe over the autochthonous unit. The allochthonous unit "travelled" in a N-S direction for at least 50km; its original position should be located somewhere between the islands of Chios and Lesvos (Besenecker *et al.*, (1968). The allochthonous unit is characterized by a fold-system with axes striking in an E-W direction, probably associated with the N-S movement of the nappe. The age of this compressive event might be the boundary between Cretaceous-Eocene, or the Lower Tertiary.

-The third compressive event is observed mainly in the allochthonous unit and is associated with folds having axes srtiking in a NNE direction. The age of this event is considered to be the Late Paleogene or the boundary between Paleogene and Neogene (i.e Lower Miocene).

The Neogene beds have not been affected by any compressive cycles because they are post-Alpine formations. However, they have been intensively fractured by fault tectonics. Besenecker (1973) dlstinguished three fault systems which affected the

---

[1]Although they did not observe reverse faults in Milos they assumed the existence of a compressional event in the Lower Pleistocene based on observations in other Aegean islands.

Neogene rocks (Fig 3.6b):

-A NNE and NNW (less often) system which controls the development of the Neogene basin and is probably associated with the extrusion of volcanic rocks in the SE parts of the island. It was probably initiated during the Neogene and has certainly been active in the post-Neogene period. Faults of this direction occur in the Alpine rocks also.

-A second NE and NW system probably of Plio-Pleistocene age which is also observed on the Alpine rocks. It is responsible for the formation of the coast lines and the Pleistocene valleys of the island.

-The third system has an E-W direction and its age is not known with certainty. This direction is very important for the tectonic development of the whole area, since it is the predominant one found in the Western Anatolian grabens.

However the above dating of the fault systems needs revision since the age of the Neogene beds is older than was assumed by Besenecker *et al.* (1968) and Besenecker (1973) as shown by the geochronological data of Belon *et al.* (1979). It seems more probable that they became active within Miocene (probably since the Lower Miocene) similar to the Western Anatolian fault systems.

Most faults examined by Besenecker *et al.*, (1968), and Besenecker (1973) are normal as regards their kinematic characteristics, although some reverse ones have been reported. However, these could be lystric faults similar to those described by Jackson *et al.*, (1982) in the central Aegean and Price (1989) in W. Anatolia (see Chapter 2). Since the geotectonic regime which has prevailed since the Lower Miocene in the area is characterised by extension, this type of fault-kinematics is expected.

3.3. Geology of the bentonite deposits.

This section describes the geological features of the bentonite deposits. The full mineralogical and geochemical characteristics are presented in the following chapters.

3.3.1. Milos Island

The bentonite deposits of Milos island can be separated into three groups according to their geographical distribution (Fig. 3.7a). The first group includes the Aspro Horio, Tsantili, and Zoulias deposits (designated as Area 1 in this work), the second the deposits of Ankeria and Koufi (Area 2), while the third the Ano Komia, Garyfalakaina, Mavrogiannis and Rema deposits known as the deposits of the area of Komia (Area 3). The general geological characteristics of the bentonite deposits can be summarized as follows:

-Stratiform development which is best shown in the deposits of the Areas 1 and 2.

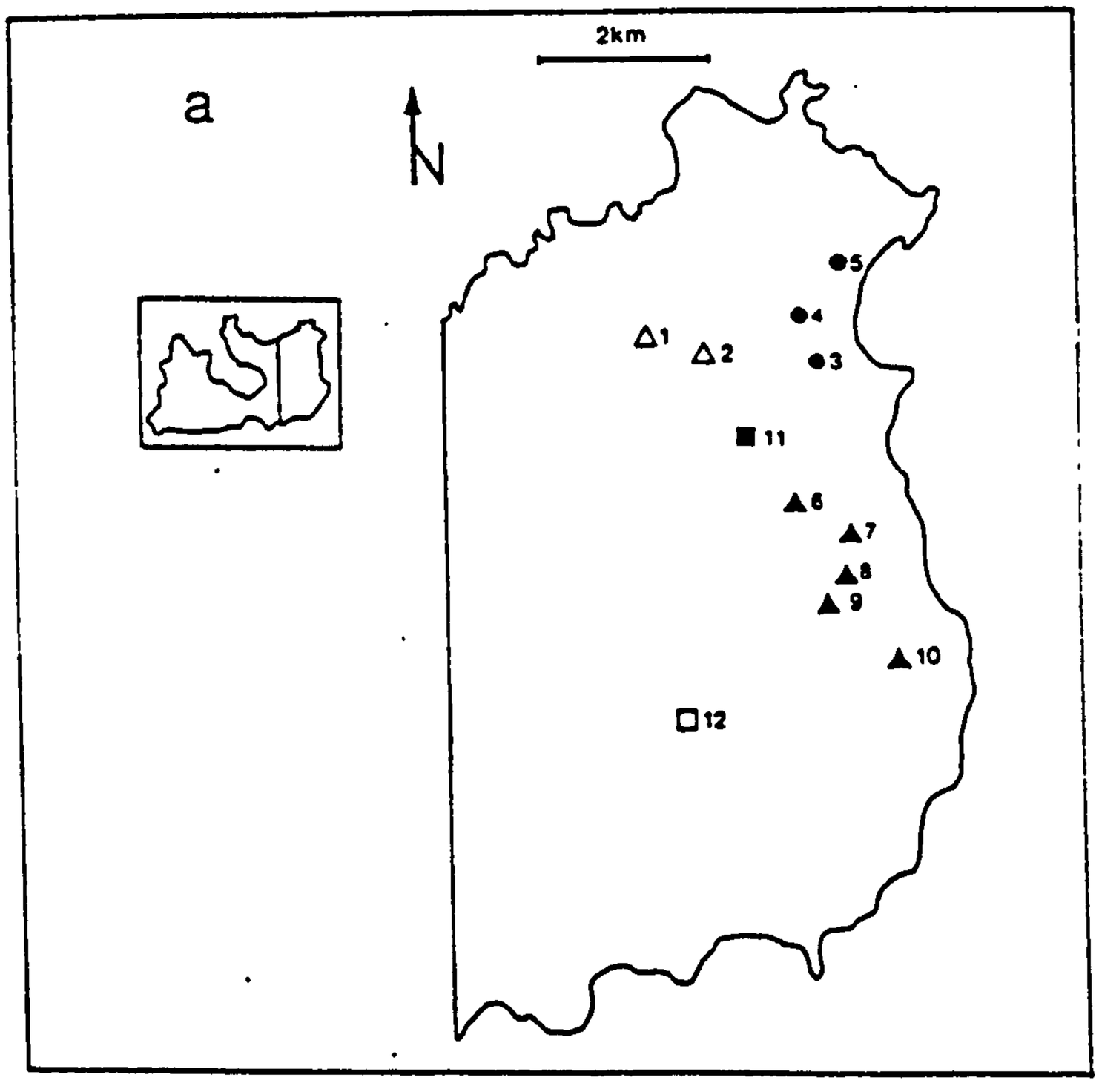

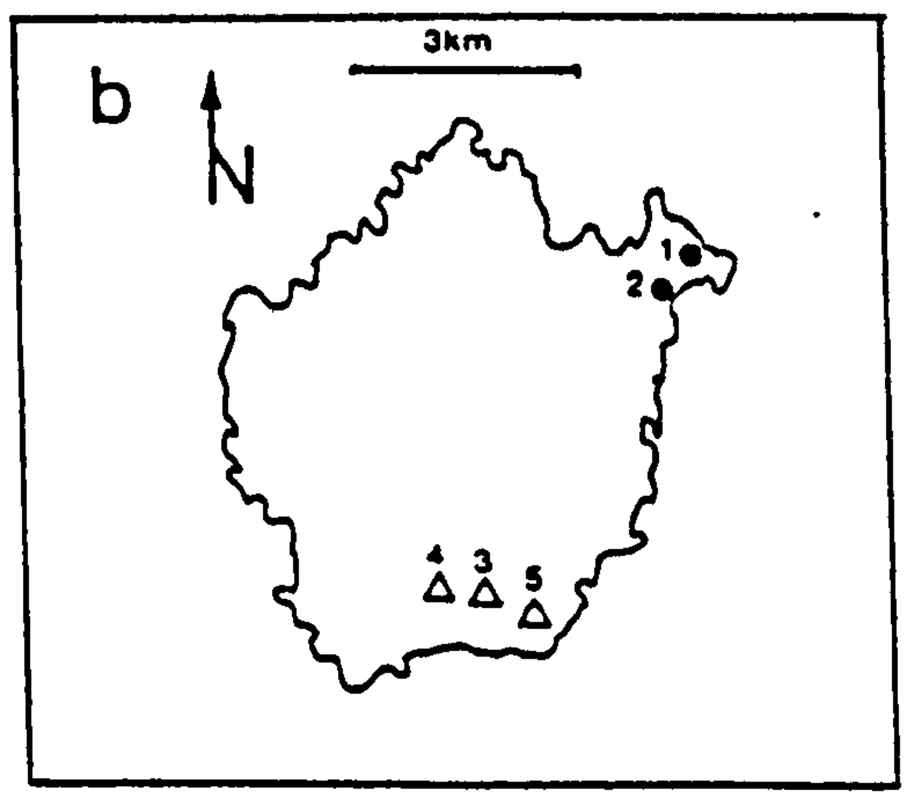

FIGURE 3.7. Location of the bentonite deposits of Milos (a) and Kimolos (b). Key to the symbols: solid circles: area 1 in both islands, open triangles: area 2 in both islands, solid triangles: area 3 , Milos, solid square: Agrilies deposit, Milos, open triangle Kastriani deposit (kaolin), Milos. Key to the numbers. Milos: 1 = Ankeria deposit, 2 = Koufi deposit, 3 = Tsantili deposit, 4 = Aspro Horio deposit, 5 = Zoulias deposit, 6 = A no Komia deposit, 7 = Kato Komia deposit, 8 = Garyfalakena deposit, 9 = Mavrogiannis deposit, 10 = Rema deposit, 11 = Agrilies deposit, 12 = Kastriani deposit. Kimolos: 1 = Prassa deposit, 2 = Loutra deposit, 3 = Fanara deposit, 4 = Bonatsa deposit, 5 = Agios Tryfon deposit.

-Well defined upper boundaries of the deposits.

-Lack of evidence about the nature of the underlying rocks in the active quarries.

-Existence of partly devitrified glass amidst the totally altered materials.

-Development of separate opal-rich stratiform horizons in several levels.

-Predominance of one bentonite horizon with similar macroscopic characteristics in most deposits. This does not mean that a single horizon extends throughout the area where the bentonites occur.

-Evidence of intense hydrothermal activity which has significantly affected the deposits and which still is active with the form of fumaroles (Ankeria).

-Intense fracturing of the bentonite horizons by fault systems having N-S and NE-SW direction. Veins of gypsum and/or Fe-oxides are common along such discontinuities.

3.3.1.1.Deposits of Area 1.

3.3.1.1.1. Aspro Horio deposit.

The deposit is characterised by the predominance of a basal green-blue volcaniclastic lapilli-tuff with texture similar to a volcanic breccia. Wetzenstein (1969, 1972) described this rock as "brocken tuff". This term will be used to describe similar textures in this thesis. The exact thickness of this horizon is not known, but it is exposed for at least 15m (horizon 1 in Fig. 3.8a). It is composed of light-coloured subangular-angular fragments, embedded in a green groundmass, showing normal grading. The upper sectors are well bedded (see Plate 1). The entire rock has been converted to bentonite. Pyrite crystals are present throughout the entire horizon. The green bentonite is followed by a well defined pink-reddish bed (horizon 2 in Fig. 3.8a), 1m thick, with similar texture, above which a grey bed having maximum thickness 1.2m occurs (horizon 3 in Fig. 3.8a). This grey bentonite is the base of a 15m thick yellow bentonite which follows (horizon 4 in Fig. 3.8a). The latter is a moderately sorted lapilli tuff having a texture which resembles a pyroclastic flow. However, since the rock has been completely altered, this texture might be the result of the bentonitization process, which might have overprinted the original one. In the higher stratigraphic levels of this horizon, two thin, discontinuous lensoid opal beds, having 0.25 and 0.15m maximum thickness, occur. No pyrogenetic minerals are visible throughout the bentonite succession. In the southern sector of the deposit a small glassy rhyolitic lava dome occurs within the bentonite bed. The lava is fresh and is only altered along fault fractures.

Two main fault systems are observed in the quarry: a dominant one having a N-S direction and a second, minor one, having a NE-SW direction, both belonging to the main fault systems observed in the island. The stratigraphic column of the deposit is

depicted in Figure 3.8.

3.3.1.1.2. Tsantili deposit.

The deposit is composed of a single bentonite horizon, the visible part of which is more than 30m thick (Plate 1). The bentonite is a massive lapilli tuff lacking any type of bedding, with "brocken tuff" texture *i.e* resembling that of a volcanic breccia. There are two main geological characteristics observed in this deposit: a) the very intensive hydrothermal alteration associated with sulphur-rich solutions, which is ubiquitous throughout the entire bentonite mass and b) the existence of a thick silicified horizon in the upper parts of the deposit (Plate 1). The colour of the bentonite varies substantially due to the influence of hydrothermal alteration. It is grey in the lowermost parts, becoming red, green, brown or yellow (depending on the alteration mineral phases present and possibly on the oxidation state of iron) in the higher levels. The deposit is cut by numerous veins of gypsum and sulfur-rich minerals dipping with an 70-80^{o} angle and striking in an ENE-WSW direction, obviously filling fault fractures.

3.3.1.1.3. Zoulias deposit.

It is the most complex deposit as far as geological evolution is concerned, since it is composed of a large number of volcanic and volcaniclastic horizons (Fig 3.8b), most of which have been converted into bentonites.

The succession begins with a lava dome (horizon 1 in Figure 3.8b) the total volume of which is not exposed. It is an andesitic-basic dacitic porphyritic lava with pseudomorphosed phenocrysts of feldspars and amphiboles, embedded in a blue-green groundmass, the initial nature of which (i.e glassy or micro/cryptocrystalline) is not known due to intense alteration. In places, there are "pockets" of relatively fresh lava, and a transition from the fresh to the completely altered material is often present. The rock has undergone additional hydrothermal alteration as it can be seen from the ubiquitous "stockwork" structures (Plate 8); they consist of veins rich in sulphurous compounds crossing the bentonitized lava. Locally, horizontal, opal-rich horizons are observed. This lava dome has provided the topographic relief upon which all the following horizons have been deposited. In the following descriptions the terms upslope and downslope refer to the slopes of the lava dome-basement (Plate 2).

The lava dome is followed by a well bedded, dark-green lapilli-tuff with a maximum thickness of 1.5m, which wedges off on the underlying formation (horizon 2 in Figure 3.8b). The rock has been completely converted into bentonite. It is characterized by the alternation between fine grained and coarse grained material, which might correspond

to graded bedding. However, the extensive bentonitization does not allow a positive characterization of the bedding, although in places there are traces of gradual transition from the coarse grained to the fine grained material.

This bentonite horizon passes to a 7.25m thick, well bedded, yellowish-white lapilli-tuff, which resembles the coarser parts of the previous horizon. Locally, there are stainings of Fe-oxides. In the upper 0.5m it evolves to a coarser lapilli-tuff (horizon 3 in Figure 3.8b).

Above the previous bentonite, a fine grained, thin and well bedded, off-white bentonite, probably derived from a fine grained lapilli-tuff or volcanic ash, occurs (horizon 4 in Figure 3.8b). The maximum thickness of this horizon is 5.75m decreasing upslope. The off-white, thin layers of this bentonite alternate in places with thin dark green to black, very hard layers. This bentonite has been affected by syn-sedimentary fault tectonism (Plate 9).

The previous bentonite is followed by a thick (8.6m) bentonite layer (horizon 5 in Figure 3.8b). It consists of thin, hard, green layers, encompassing white elliptical boulders, the size of which increases in higher stratigraphic levels and upslope on the flanks of the lava dome. More specifically, the large diameter of the boulders increases from a minimum value of 0.3-0.4m in the lower stratigraphic levels of the horizon, to greater than 1.5m in the higher ones. Their texture consists of elongated, almost filamentous units completely converted into clay, which might have been derived from welded pumiceous material. In that sense, this bentonite horizon has probably been formed at the expense of an ignimbritic rock. The thin, green layered units resemble similar ones found in the previous bentonite horizon.

The succession continues with a relatively poor bentonite which contains relatively large amounts of grit content (horizon 6 in Fig. 3.8b). It is a yellow, 3.10m thick lapilli-tuff including small white boulders having a pumice-like texture, which resemble those observed in the previous horizon. Thin, hard, greenish lenses of clay material are present throughout the entire mass of this bed.

Above the previous layer, a yellowish, 2.30m thick lapilli-tuff, with large grit content develops (horizon 7 in Fig. 3.8b). This bed has been affected by syn-sedimentary-fault-tectonism during the deposition of the volcanic material.

The previous tuff is followed by an unwelded, lapilli-tuff which has not been altered to bentonite (horizon 8 in Fig. 3.8b). It has a maximum thickness of 2.55m. It is followed by a 0.45m thick volcanic sandstone, which is fresh and well bedded, showing graded bedding in places. Above this sandstone is found, a glassy, fresh, welded, light-grey pumice flow (ignimbrite), the thickness of which increases downslope reaching 9m (horizon 9 in Figure 3.8b). The texture of the welded pumiceous material is similar to the structure of the boulders occuring in the previous bentonite horizons.

The volcanic sequence of the Zoulias quarry has been disrupted by a kind of land-slide which occured after the deposition of the pumice flow described before (horizon 10 in Fig 3.8b). The rock which resulted from this land-slide or possibly avalanche has a chaotic structure composed of large blocks of volcanic rocks, cemented by pumiceous material. This glassy material is fresh in the higher levels of this chaotic horizon, but it is altered to bentonite in the lower levels. On the other hand, the volcanic fragments and the blocks are fresh throughout the entire volume of this horizon. This formation cuts all the previous horizons (Plate 2) and its boundaries are well marked by the presence of Fe-oxides.

Finally, the latter chaotic horizon has been covered by a lapilli tuff with structure very similar to the "brocken tuff"-type observed in the deposits of Aspro Horio and Tsantili (horizon 11 in Fig. 3.8b). The parent glassy material has not been altered thoughout the entire mass of the rock, but there are cores where the original glass is preserved.

3.3.1.2. Deposits of Area 2.

3.3.1.2.1. Ankeria deposit.

It consists of 4 distinct stratiform horizons (Fig. 3.8c, Plate 3) striking in an E-W direction and dipping towards the north with a 10^{o}-12^{o} angle in the western and a 20^{o} angle in the eastern face of the quarry.

The sequence begins with a high quality plastic, green-blue bentonite with minimal amount of grit content, the total thickness of which is not known (horizon 1 in Fig. 3.8c). The texture of the parent rock has not been preserved but it is very possible that it was a volcaniclastic rock since there is no indication for a lava precursor. The rock is friable in the lower stratigraphic levels of the horizon, becoming compact in the higher ones. The contact with the overlying bentonite is sharp.

The previous bentonite is followed by a 4m thick bright-yellow bentonite of the same quality. In places it is stained with red Fe-oxide colorations (horizon 2 in Fig 3.8c). It has probably been derived from devitrification of a volcaniclastic precursor. The material has a texture similar to that occurring at the the lower levels of the previous horizon.

The succession continues with a faded-yellow bentonite which has characteristics similar to those of the higher levels of the basal green bentonite (horizon 3 in Fig. 3.8c). The rock wedges out towards the east. Its maximum thickness in the western face of the quarry is about 10m. Again, striations of Fe-oxide stainings are present in several sites. In places it contains considerable amounts of opaline silica. The opaline material itself has formed a lensoid siliceous layer at the higher stratigraphic levels of the horizon.

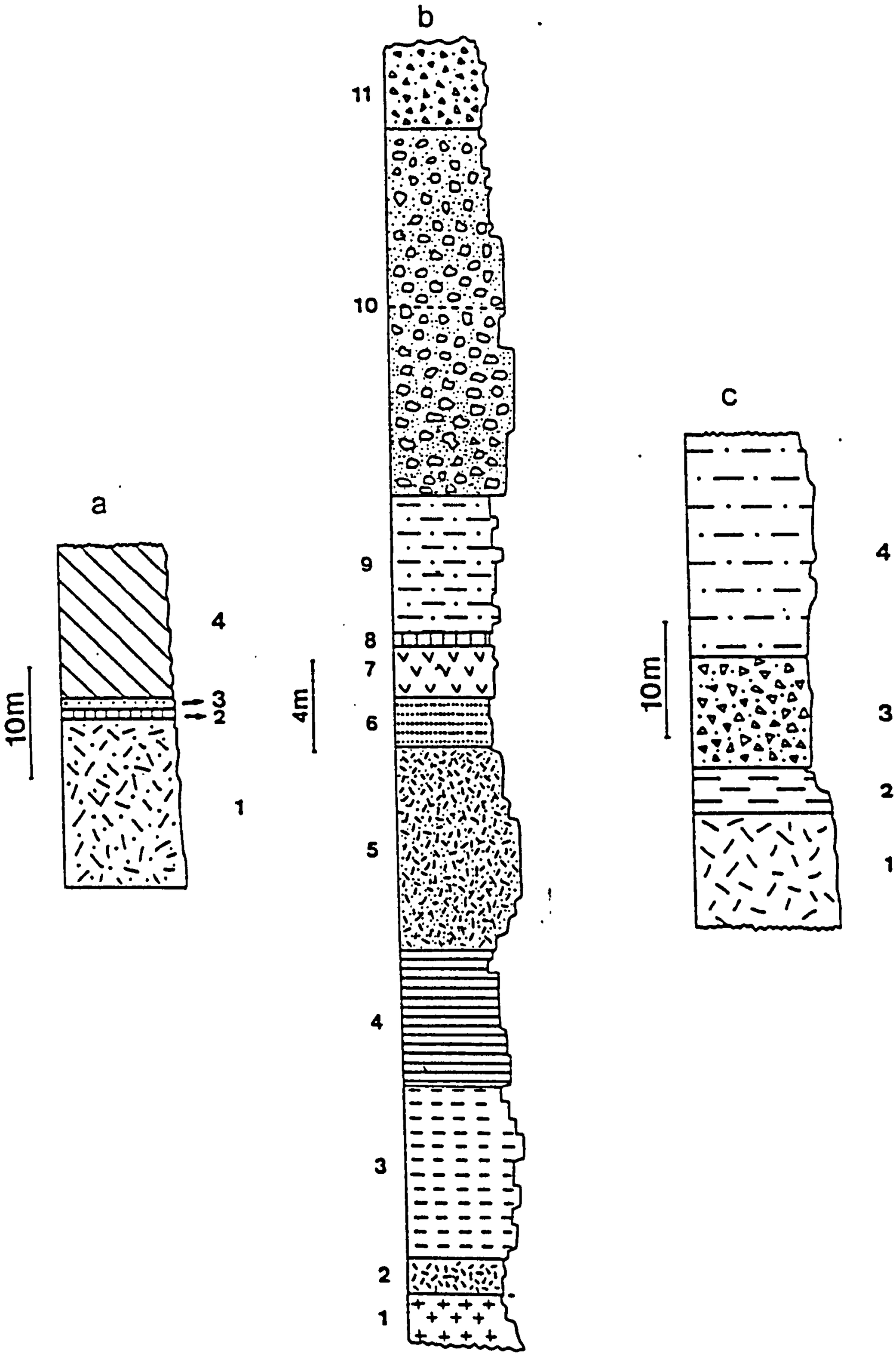

FIGURE 3.8. Stratigraphic columns of the Aspro Horio (a) , Zoulias (b), and Ankeria (c) deposits. Description of the individual bentonite horizons is given in the text.

The three previous bentonite horizons have been affected by hydrothermal alteration which is still active today in the form of a hot solfatara spring (Plate 3). The circulation of sulphur-rich hydrothermal solutions through fault fractures has affected both the texture and the mineralogical characteristics of the bentonites; it has converted them into sand-like friable materials and has deposited native sulphur and sulphate minerals. The temperature of the hot springs was estimated to be 50-60^{o}C on the surface.

The faded-yellow horizon is followed by a grey bentonite with yellow striations, the thickness of which increases eastwards (horizon 4 in Fig. 3.8c). In its higher stratigraphic levels the devitrification is not complete and transitions from the relatively fresh rock to completely altered bentonite are frequent. The parent rock might be a lapilli-tuff, which in places includes larger blocks having various colours. In the western face of the quarry, the texture resembles that of a volcanic breccia, thus being similar to the bentonites of the group i. In the same quarry face, thin opal lenses the maximum thickness of which reaches 0.4m are common (Plate 9).

The bentonite horizons are covered by a red lapilli tuff which contains fossils belonging to the *Cardium sp.* Thus, at least in the case of the Ankeria deposit, since the transition from the bentonite beds to the overlying red-tuff is continuous (i.e without unconformity), it is certain that the deposition of the parent material took place under subaqueous conditions.

The stratigraphic column of the deposit is presented in Figure 3.8.

3.3.1.2.2. Koufi Quarry.

It is a large deposit consisting of 3 bentonite horizons (Plate 3). The sequence begins with a green basal horizon derived from a lapilli-tuff (horizon 1 in Fig 3.9a). Since only the upper sectors are exposed its entire shape thickness and size is not known. It is followed by a stratiform, 30m thick green high-grade bentonite with only small amount of grit content owed to the present of pyrite crystals disseminated throughout the entire mass of the rock (horizon 2 in Fig. 3.9a). It is characterized by a "porphyritic" texture, with white fragments embedded in a green groundmass. The spacial distribution of this horizon and its texture implies that its precursor might be either a completely devitrified glassy lava or an ash flow (ignimbrite). In places the material presents textural features resembling pillow lavas (Plate 9). However, it is not certain whether these textures are remnants of the original lavas or have resulted from the intense bentonitization. There is evidence that hydrothermal solutions which circulated through fractures might have played some role to the alteration of the parent rock (Plate 9).

The higher horizon of the bentonite sequence is a yellow, partially bentonitized acidic lava, showing transitions from relatively fresh rock to bentonite (Plate 10). It is a

porphyritic rock with feldspar phenocrysts embedded in a yellow groundmass (horizon 3 in Fig. 3.9a). The material has been affected by hydrothermal alteration caused by the circulation of hydrothermal solutions along N-S striking vertical faults, which deposited Fe-oxides and sulphates.

The stratigraphic column of the deposit is depicted in Figure 3.9.

3.3.1.3. Deposits of Area 3.

3.3.1.3.1. Ano Komia deposit.

It consists of two bentonite horizons separated by a well bedded fresh lapilli-tuff showing low angle cross-bedding (Fig. 3.9b). The latter is the parent material from which the lower horizon was derived.

The lower bentonite bed is a grey friable rock with high grit content. Its visible thickness is 7.2m but the total thickness is greater (horizon 1 in Fig 3.9b). The dewatering deformation structures shown in Plate 10 imply that the original tuffaceous material was deposited under subaqueous conditions. The main characteristic of this horizon is the superimposed sulphur-dominated hydrothermal alteration, which has created "stockwork" structures crossing the bentonite (Plate 10). These structures caused changes to the coloration of the originally grey bentonite.

The higher bentonite horizon is a white bentonite with high silica content (Plate 4). It is characterized by the presence of off-white/white fragments of lapilli size embedded in a white groundmass, i.e it is possible that the parent material was a lapilli tuff. In places it has been stained reddish/pink due to the presence of Fe-oxides. The exact thickness of this bentonite is not known (horizon 2 in Fig. 3.9b).

3.3.1.3.2. Kato Komia deposit.

It is a small deposit consisting of a single grey bentonite horizon. The exact thickness of the deposit is not known. It has been formed at the expense of a lapilli-tuff with the same "broken-tuff" texture described before, which had been deposited in a depression of the overlying relief dominated by the lave dome of Demenegaki. The deposit has been affected by hydrothermal alteration (Plate 4), and veins filled with sulphur-rich compounds are ubiquitous throughout the deposit. This alteration is superimposed on the bentonite.

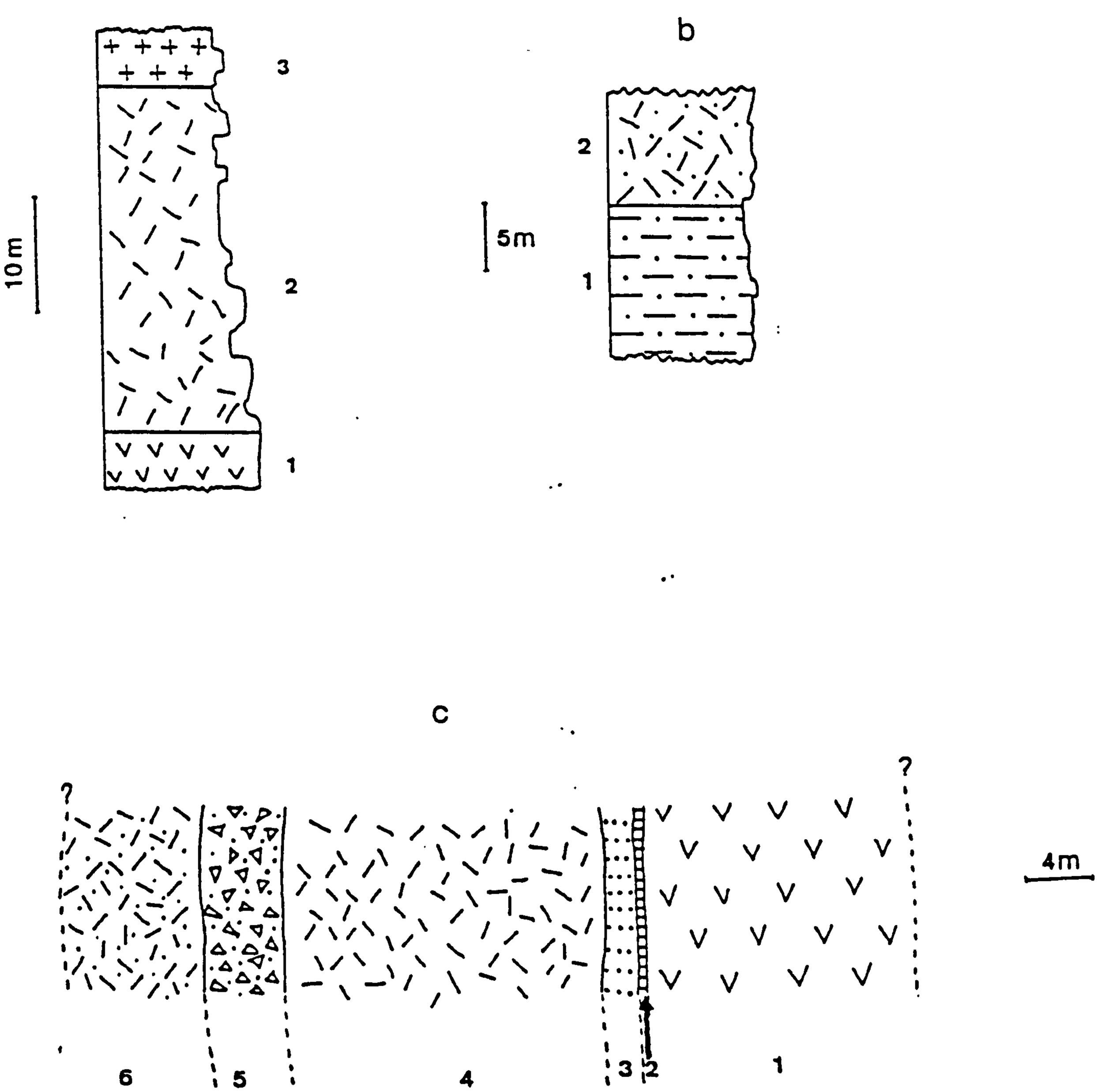

FIGURE 3.9. Stratigraphic columns of the Koufi (a), Ano Komia (Milos) (b), and Prassa (Kimolos) (c) bentonite deposits. Description of the individual horizons is given in the text.

3.3.1.3.3. Garyfalakaina deposit.

It has very similar characteristics compared with the Kato Komia deposit. It consists of a single grey bentonite horizon (light grey at the stratigraphically higher weathered levels) having a "brocken-tuff" texture. It occurs in a depression at the lower slopes of the Demenegaki dome. Therefore it is very probable that it has been derived from the similar parent material as the Kato Komia deposit. The exact thickness of the deposit is not known. In the higher stratigraphic levels there is evidence of intense silicification, i.e existence of essentially opaline material. The deposit has been affected by hydrothermal alteration involving deposition of sulphur-rich compounds (Plate 4).

3.3.1.3.4. Mavrogiannis deposit.

It has characteristics very similar to those of the Garyfalakaina and Kato Komia deposit. Again the deposit consists of a single grey bentonite horizon (Plate 5), having a "brocken-tuff" texture. The thickness of the deposit is not known. It has undergone intense hydrothermal alteration which is superimposed on the original bentonite. The alteration has involved deposition of sulphur-rich compounds.

3.3.1.3.5. Rema deposit.

It occurs at the southern lower slopes of the Demenegaki rhyolitic dome. It has very similar characteristics to the previous deposits occurring at the lower slopes of the same dome. Thus it is a single horizon bentonite deposit, consisting of a grey bentonite, having a "broken-tuff" texture. It is possible that it has been formed at the expense of the same parent material as the previous deposits occurring in the northern lower slopes of the Demenegaki rhyolitic dome. The exact thickness and the extent of the bentonite are not known because the extraction operations are superficial (Plate 5). At the eastern side of the deposit silicification phenomena caused by high opal-concentrations are very obvious. In the same area the "brocken tuff" is clearly overlain by the so-called green lahar mentioned by Fyticas (1977), and Fyticas *et al.* (1986) (Plate 10).

3.3.1.4. Agrilies deposit

This deposit is isolated and does not belong to any of the three groups described before. It consists of a single grey stratiform bentonite horizon having a "brocken tuff" texture. It was derived by a lapilli tuff, the exact thickness of which is not known. The

deposit exhibits clear indications of hydrothermal alteration with deposition of native sulphur and sulphate minerals. This alteration is probably associated with the formation of a silver-bearing barytes deposit which is exploited in the vicinity of the Agrilies deposit. The bentonite horizon is followed by the **green lahar** (defined after Fyticas, 1977). The contact between the two horizons is sharp and well defined, similar to the bentonite-green lahar contact in the Rema deposit (Plate 6).

3.3.1.5. Kastriani deposit (kaolin).

It is a small lens-shaped deposit which has been formed by hydrothermal alteration of lapilli-tuffs and possibly the "green lahar" (Plate 6), although this is not very clear because kaolinitization has obliterated the original texture competely, and has formed dissolution cavities on the rock. However alteration of the "green lahar", with very similar characteristics has been observed in the Agia Kyriaki site, close to this deposit. In its higher stratigraphic levels it contains red stainings caused by Fe-oxides. The fact that the "green lahar" is a very young formation (Fyticas *et al.*, 1986) and also that it overlies the bentonites of the Rema and Agrilies deposits suggests that there is not any obvious connection between the formation of the two types of clay deposits.

3.3.1.6. Indications concerning the depositional environment of the bentonites.

The environment under which the deposition of the parent material of bentonites took place has been a point of controversy between the different workers as has already been stated in Chapter 1. The geological data collected after detailed field work which included extensive sampling and observation of the relationships among the different bentonite deposits as well as between bentonites and the surrounding rocks give the following information:

1) The parent materials were deposited under subaqueous conditions. There is paleontological as well as textural evidence supporting this idea. This is certainly the case for the deposits of Area 2 (Ankeria and Koufi), where fossils were found. The parent material of the lower horizon of the Ano Komia deposit was certainly deposited under water conditions (presence of dewatering deformation structures). There is no reason to assume that the other deposits of Area 3 were not deposited under similar conditions, since they occur very close to the previous deposit, and there is no indication implying that any change in the depositional environment has taken place. The subaqueous environment for the deposits of Area 2 is supported from the work of Fyticas *et al.* (1986) in Agia Irini area close to the deposits, where submarine tuffaceous sequences have been described.

However, there is not unambiguous evidence about the depositional environment for the deposits of Area 1. The existence of thin bedding in several of the bentonite horizons of the Zoulias and Aspro horio deposits does not necessarily imply a subaqueous environment (see Fisher & Schmincke, 1984, and Cas & Wright, 1988). Also the indications for graded bedding do not automatically exclude the possibility of subaerial deposition. Wetzenstein (1969, 1972) reported the existence of a thin limestone horizon in Zoulias quarry. This was not confirmed during the field work because it was dangerous to visit the site quoted. However, there is not any reason to reject the possibility for the occurrence of the limestone horizon. Therefore, it is accepted that the bentonites of Area 1 were deposited in a subaqueous environment.

2) The subaqueous deposition of the parent material does not necessarily mean that the **eruptions** which produced the rocks took place under water. The alternative possibility is to have a subaerial eruption leading to a subaqueous deposition. In the case of the deposits of Area 3 (the lower horizon of the Ano Komia deposit is excluded) which have very similar characteristics it is possible that the parent materials might have been the products of a pyroclastic flow formed by subaerial erruptions, which moved downslope along both flanks of the Demenegaki rhyolitic dome and deposited into the sea. This idea is favoured by the model of Papanicolaou (1988) for the neotectonic evolution of Milos island, who proposed that the Demenegaki dome was subaerial while the area in the north (*i.e* where the deposits of Area 3 occur) was submerged under seawater during the Lower Pleistocene. The assumption that the parent material might be a pyroclastic flow is supported from the fact that the bentonite deposits of group iii occur in depressions along the lower slopes of the dome. The subaqueous deposition has been proved already by the dewatering deformation structures found in Ano Komia deposit. The proposed model for the deposition of the parent material in Area 3 is presented in Figure 3.10a. Nevertheless, the possibility of a subaqueous eruption cannot be rejected. Also the possibility that the parent materials were not erupted from the Demenegaki rhyolitic dome should not be ignored, especially if their emplacement was prior to the extrusion of the dome (see Fig. 3.10b). In this case the vent where they were errupted from might not necessarily be in the vicinity of the area in which they occur today.

The passage of a pyroclastic flow into subaqueous environments has not been studied so far *in situ* and the interaction between water and pyroclastic material is a matter for speculation among different workers. Cas & Wright (1988) addressed the problem and assumed that in the case of a large, single pyroclastic flow, the material reaching the sea level will still have sufficient momentum and density to continue to deeper levels but rapidly and perhaps explosively, it quenches. Eventually the chilled debris will form an ash turbidite. In this model welding might occur aided by the gasses

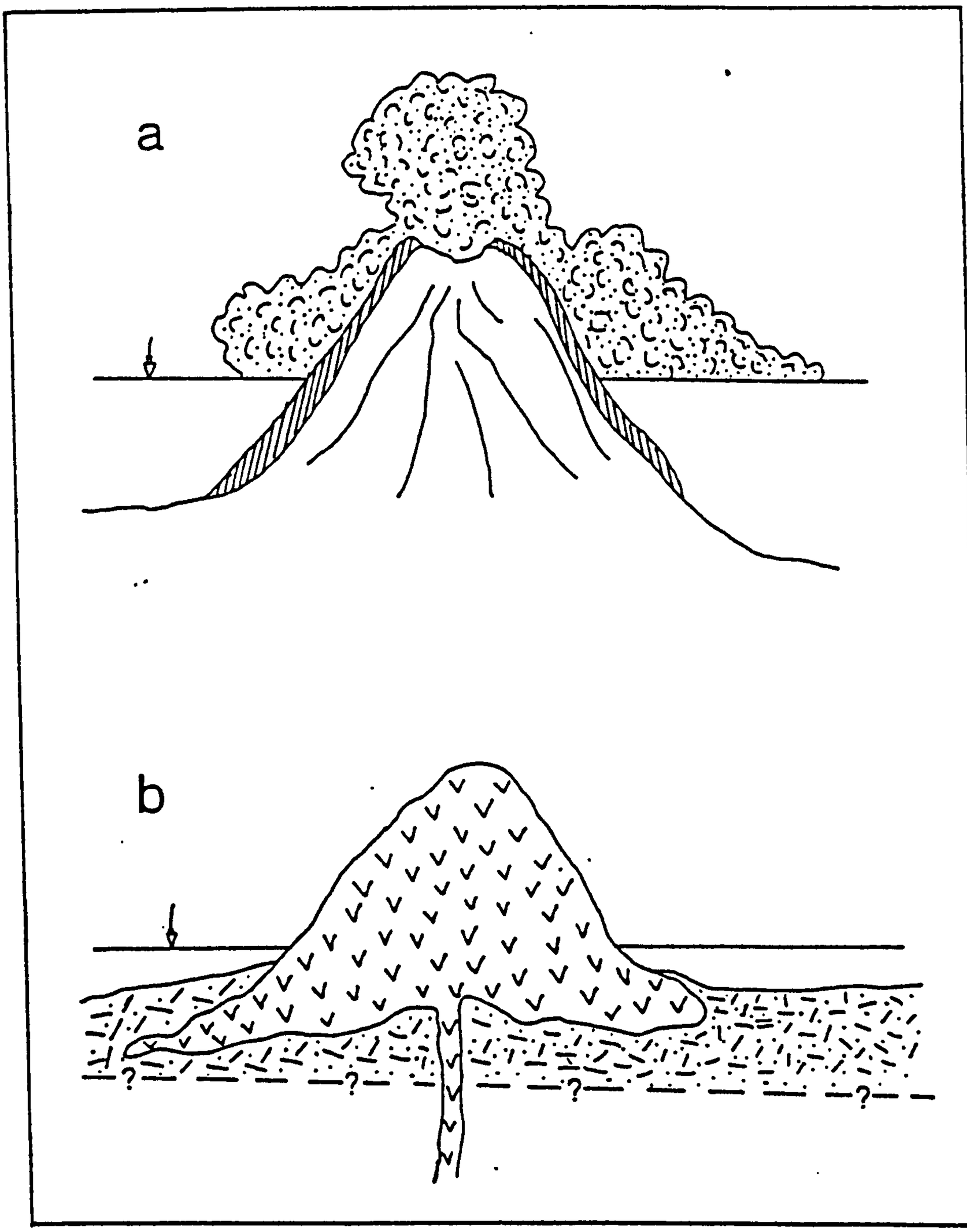

FIGURE 3.10. Alternative models proposed for the deposition of the parent materials of the bentonite in the area 3 of Milos a) Eruption from the Demenegaki rhyolitic dome, b) eruption before the xtrusion of the Demenegaki dome.

trapped within the mass of the flow. Smaller pyroclastic flows will eventually form ash turbidites. Fisher & Schmincke (1984) discussing the possibility of submarine welding accepted the theoretical model of Sparks *et al.* (1980) about this type of welding. According to Cas & Wright (1988), the most probable case for passage to a subaqueous environment is that provided by epiclastic processes and slumping (volcaniclastic rocks). In the case of the bentonite deposits of Milos, because of the intense alteration it is not possible to say whether the parent material was **pyroclastic** or **volcaniclastic** (i.e whether it contained juvenile volcanic material or was simply the result of the collapse of a lava dome, or even a large scale slumping).

Similar assumptions can be made for the deposits of Area 1. In this case the localization of the deposits is different. Some of them like the highest horizon of Zoulias might have been formed from the alteration of a pyroclastic flow which originated from the volcanic centre of Korakia. The same might be true for the lower horizon of Aspro Horio deposit and the breccia-type material of Tsantili deposit. This "brocken-tuff" type horizon occurs in many sites arround the Korakia dome implying that it might extend over a wide area. This fact can be used as a criterion for further exploration. Again the possibility that the eruption of the parent materials took place from another vent cannot be excluded. Also, it is not certain whether the eruption was submarine or subaerial. Certainly, the advanced degree of alteration does not allow an unambiguous assumption for the mode of origin and deposition of the parent material.

Knowing the paleogeographic evolution of the Aegean area, it is certain that the subaqueous environment where the original materials were deposited was marine. This is supported also from the paleontological data presented by Fyticas (1977) and Fyticas *et al.* (1986).

3) All deposits examined have been affected by hydrothermal alteration, which in some areas has altered completely the original characteristics of the rock. It is certain from the geological observations that this alteration has been superimposed on bentonites. The case of the Kastriani kaolin deposit and (especially) the Agia Kyriaki site close to this deposit provide some evidence for the time relationship between the kaolinitization and bentonitization processes. The "green lahar" is probably one of the precursors of the kaolin deposit. According to Fyticas *et al.* (1986) this formation is very young; probably younger than 0.2my. Consequently, kaolinitization might be a recent alteration process. On the other hand it has already been shown (see Plates 5, 6, 10) that the "green lahar" clearly overlies the bentonite deposits of Rema and Agrilies. The same is valid for the deposit of Ankeria also. This suggests that kaolinitization is a later process than the formation of bentonites.

4) The shape (stratiform), morphological characteristics of the parent rocks, (predominance of the "broken-tuff" rock-type regardless of the area of occurrence) and

spacial distribution of the bentonite deposits (horizontal or inclined following bedding planes), suggest that hydrothermal alteration might not be the process through which they were derived. It is known that the hydrothermal alteration patterns associated with argillitization might include either concentrations of the clay around structural features (faults, joints, thrust surfaces) or massive changes of the parent rock like those in Kuroko type deposits (Chamley 1989). The first possibility is immediately rejected if one takes into account the distribution patterns of the Miloan bentonites which are controlled by stratigraphic rather than structural criteria. In Kuroko type deposits the alteration pattern is concentric around the ore body, with the smectite zone following the mica/montmorillonite zone and followed by the zeolite zone. In the case of the Milos bentonite deposits there is not any evidence for concentric alteration patterns. The smectite-type alteration is isolated with respect to time since kaolinitization is posterior to it. Kalogeropoulos & Mitropoulos (1983) found that the baryte hydrothermal deposits of eastern Milos which are situated close to some of the bentonite deposits studied, belong to the Kuroko type and were probably formed when the hot hyrdothermal fluid came in contact with the cold sea water close to the sea floor. However, their occurrence is controlled by structural criteria. Moreover, in most cases bentonites are not associated with baryte deposits.

In conclusion, the geological characteristics of the bentonite deposits of Milos, their relationship with the surrounding rocks and the hydrothermal activity patterns observed, suggest that hydrothermal alteration might not be the mechanism which led to their formation, although it has certainly affected them. Deposits other than bentonites which have certainly been formed through hydrothermal processes, like kaolin, baryte and native sulphur deposits, are hardly associated genetically with bentonites. This suggestion is examined further in the following chapters using other criteria.

3.3.2. Kimolos Island.

The bentonite deposits investigated in Kimolos island can be separated into two groups according to their geographic distribution. The first group includes the Prassa and Loutra deposits situated in the NE area of the island, while the second the deposits in Agios Tryfon, Fanara and Bonatsa areas situated in the southern part of the island (Fig 3.7).

3.3.2.1. Deposits of Group I.

3.3.2.1.2. Prassa deposit.

It is the most important deposit occuring on the island and includes the famous white bentonite of Kimolos. The deposit has been formed at the expense of an unwelded ignimbrite (Plate 7). The parent material had been deposited under submarine conditions (Plate 10), but it is not known, whether the eruption was submarine or subaerial. The deposit is controlled by structural criteria and consists of relatively small "pockets" of high quality bentonite restricted around faults. The larger outcrop is a 30mx35mx10m body which continues in depth which can be divided into six distinct zones including the fresh glass zone (Fig. 3.9c):

-The fresh glass zone. It surrounds the deposit and its thickness is greater than 20m. It is used as raw material in the cement industry (horizon 1 in Fig. 3.9c).

-A thin, 30-40cm, transition zone where the glass begins to alter to bentonite (horizon 2 in Fig. 3.9c).

-A 1.5-1.8m thick yellowish, hard when dry, very plastic when wet, bentonite. The original macroscopic characteristics of the glass have been completely obliterated due to the alteration. The same is true for the other zones also (horizon 3 in Fig. 3.9.c).

-The grey bentonite zone. This is the main bentonite horizon, consisting of a 20m thick, very plastic, without noticeable grit content, material (horizon 4 in Fig. 3.9c).

-The white bentonite horizon. It is a high-quality 5m thick white bentonite, very plastic without noticeable grit content. This is the main horizon which is extracted (horizon 5 in Fig. 3.9c).

-The opal-rich white bentonite which is not extracted. Its thickness is not known (horizon 6 in Fig 3.9.c).

In other sites of the quarry there are more occurrences of white bentonite, without the zonation observed in the main horizon. In every case the smectite-rich material is restricted around faults. This individual characteristic of this deposit can be used in the future for the exploration of new deposits in the same area.

The fault systems observed in the deposit can be classified into two groups; one having a N-S direction and one having a NE-SW direction.

3.3.2.1.2. Loutra deposit.

It is a small stratiform well bedded deposit consisting of a light-grey bentonite (Plate 7) derived from fine grained volcanic material (probably volcanic ash). It can be subdivided into two horizons which differ in the degree of devitrification, the lower being richer in smectite content. The deposit has been affected by fault tectonism. Along the

faulted zones the bentonite has been altered further to a red hard fine-grained material possibly due to the influence of Fe-bearing solutions. The material is hard and rich in grit content. The parent rock had been deposited under submarine conditions, as proved by the presence of bivalve fossils (Plate 11)

3.3.2.2. Deposits of the second group.

3.3.2.2.1. Fanara deposit.

It is a small deposit which has been destroyed by a land-slide. Therefore its faces are only partially exposed and its thickness is not known (Plate 8). It was formed at the expense of a lapilli tuff with conglomerate texture indicating deposition of the parent material in very shallow seawater depths and epiclastic reworking. The pebble size becomes smaller in the lower topographic levels of the quarry and eventually the material becomes a volcanic sand. This indicates an increase of the depth of deposition. At the higher topographic levels of the deposit the pebbles have been partially converted to bentonite. The higher stratigraphic horizons of this rock have been silicified (Plate 8). At the lower topographic levels of the quarry, a small outcrop of a high quality white bentonite derived from an unwelded ignimbrite is noticeable. The parent material of this horizon might have been erupted under submarine conditions.

3.3.2.2.2. Bonatsa deposit.

It has been derived at the expense of a submarine acid lava. It is a yellow bentonite which has not been devitrified completely. The material is cut by numerous faults, along which the devitrification is more intense (Plate 8), with frequent transitions from the fresh rock to bentonite. The extent of this deposit is not known. Next to this deposit, a partly devitrified pumiceous material yielding white bentonite which shows typical "pop corn" texture, occurs (Plate 11).

3.3.2.2.3. Agios Tryfon deposit.

It is a small kaolin deposit formed next to extended bentonite beds similar to those found in Fanara deposit. It has undergone small scale underground extraction in the past (Plate 8), but the activities have now ceased. Due to the intense alteration it is not possible to establish the nature of the parent material, but the preservation of bedding indicates a volcaniclastic precursor. The smectite-rich rock has a texture identical to that of the lower levels of the Fanara deposit, being a volcanic sand. The deposit is characterized by a transition from the greenish-grey bentonite to the white-yellowish

kaolin. Fe-oxides have imparted red colorations on the rock (Plate 8). Gypsum crystals several cm long as well as alunite (alum-taste of the altered rock) are common throughout the transition zone.

3.3.2.3. Indications about the depositional environment of the bentonites of Kimolos.

Geological observations on Kimolos Island have provided secure indications about the depositional environment of the bentonite deposits on the island. These indications are derived from geological as well as paleontological evidence. The conclusions can be summarized in the following points:

1) The parent materials from which bentonites came from were deposited under submarine conditions. This is valid for the deposits of both groups. The evidence is provided from fossils (Loutra deposit) and sedimentary structures for the other deposits (Plates 7, 11). In the case of the Prassa deposit where the alteration is controlled by structural criteria (*i.e* faults), there is not any indication about the influence of hydrothermal alteration. It is believed that if hydrothermal alteration was the reason for the formation of this deposit, then characteristic minerals (kaolinite, gypsum, baryte and other sulphates, sulphides) should be abundant. This view is supported from the fact that in areas where hydrothermal alteration is obvious, Mn-rich mineralization is observed. It is also interesting that although the parent rock is very susceptible to alteration (unstable glass) the alteration does not extend far from the faulted zones. This topic will be discussed extensively in Chapter 6.

The deposit of Fanara presents a good example of preservation of the paleogeographic conditions where the original material had been deposited. The altered volcanic conglomerate contains pebbles the size of which decreases downslope. Eventually the rock becomes volcanic sand in size and extends to the coast in the area of Agios Tryfon. This might indicate a progressively increasing depth of the depositional environment, along the continental shelf (Fig. 3.11a). It is believed that the matrix of the conglomerate which has now been altered to bentonite was derived from a volcanic ash which was deposited into sea water. Due to the action of sea waves and currents this ash was intimately mixed with the rounded pebbles which occurred in the sea-shore yielding the conglomerate. However, as on Milos island it is not certain whether the eruptions which produced the parent materials of bentonites were subaerial or subaqueous.

2) Hydrothermal activity, like the case of Milos island, has been superimposed on bentonites. However its influence is less obvious than in Milos. It is strictly associated with structural criteria and is characterized by the deposition of mineral phases like baryte,

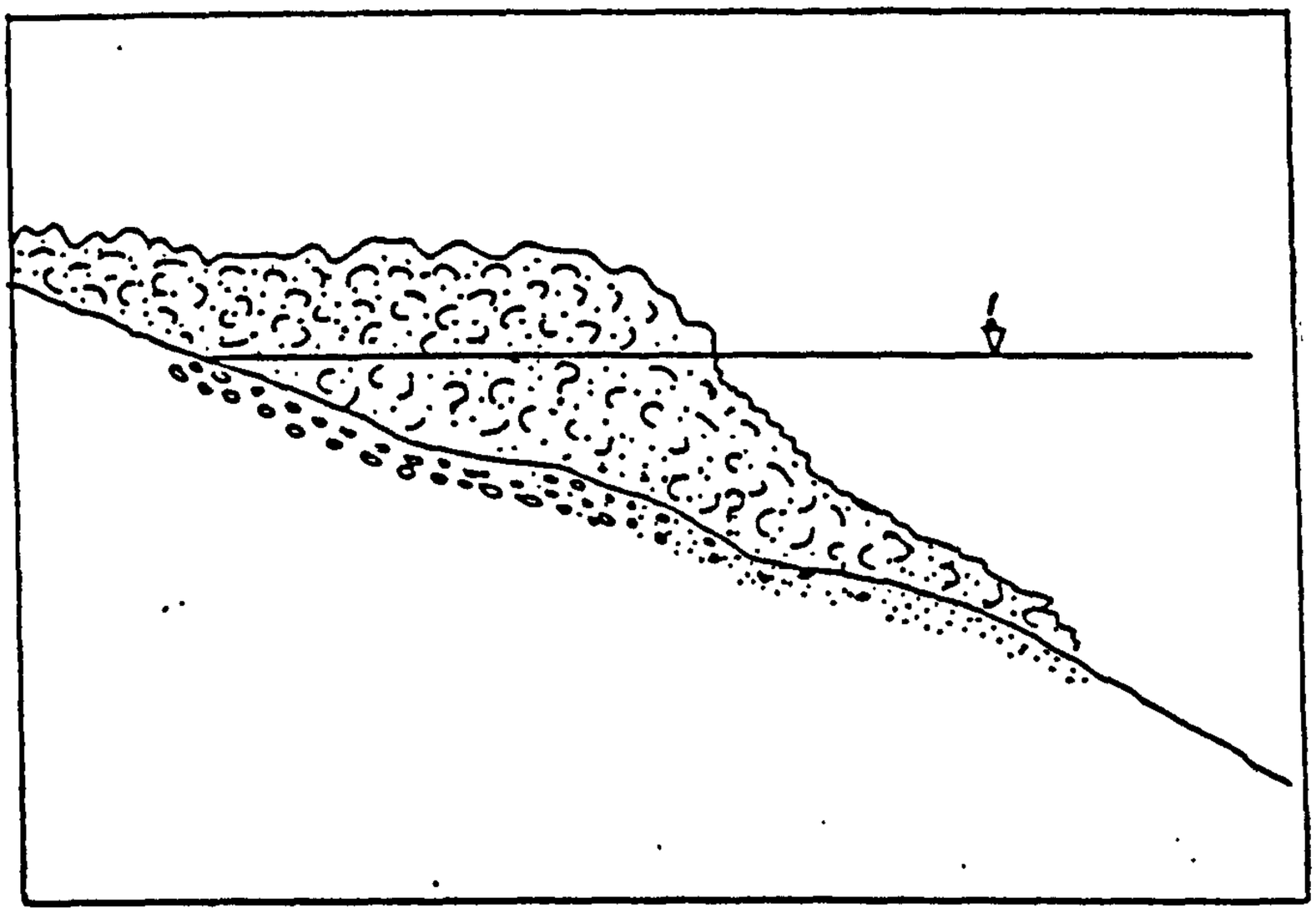

FIGURE 3.11a. Proposed mode of emplacement of the parent rocks in the deposit of Fanara (Kimolos).

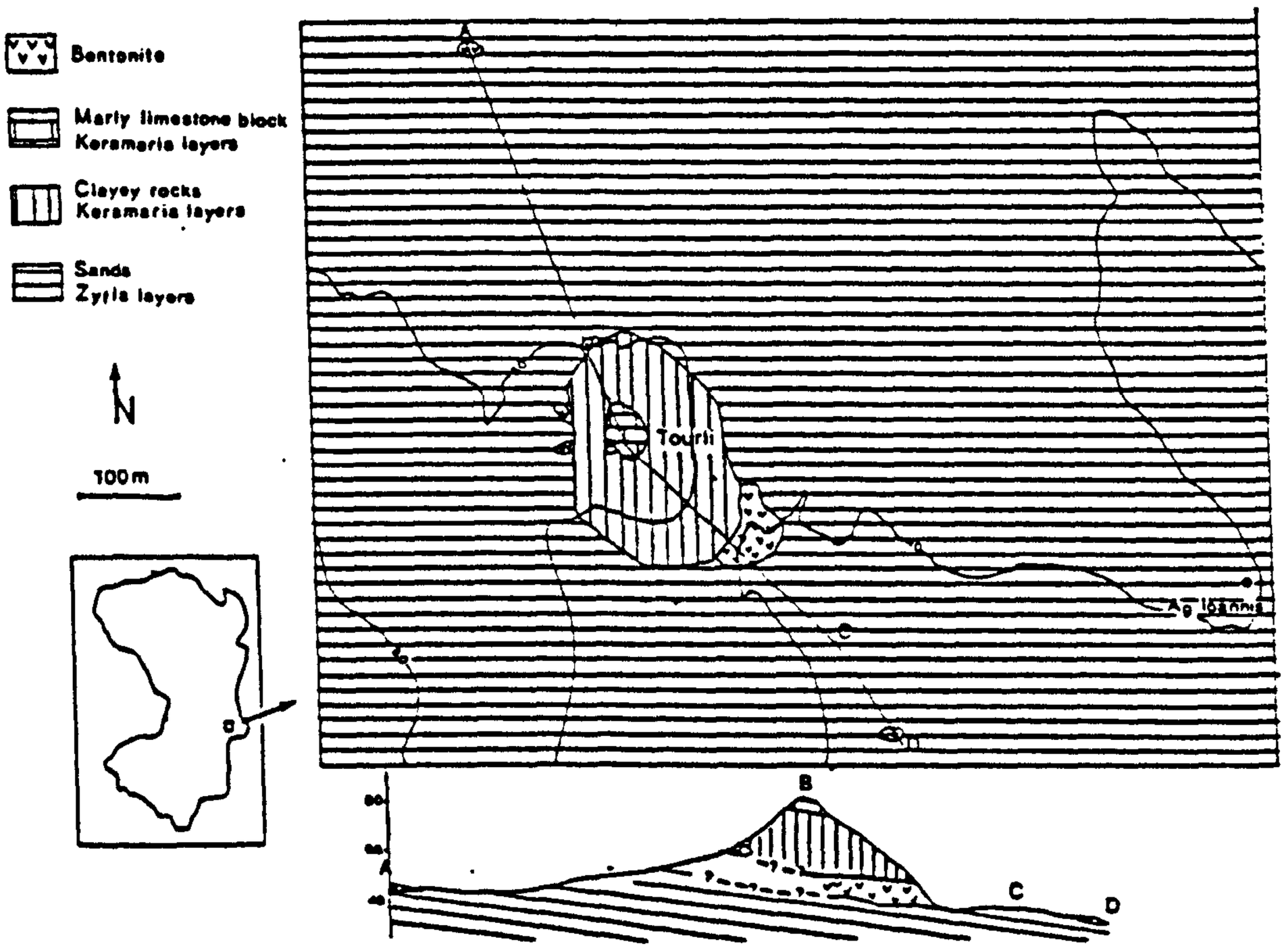

FIGURE 3.11b. Geological map of the bentonite deposit located south of the Thymiana village, Chios Island.

gypsum and kaolinite. In the Loutra deposit the influence of hydrothermal activity is visible in faults cutting the bentonite. It this case the fault planes have been fillled with Fe-rich materials. Tsoli-Katagas & Mavronichi (1989) suggested that the smectite- and kaolinite-type alterations observed in the area of Agios Tryfon constitute distinct zones which are products of the same alteration event. However, the geological evidence contradicts this suggestion since the bentonite deposits are stratiform, have widespread distribution and are usually not associated with kaolinite, while kaolin occurrences are restricted to a small number of areas and are always associated with structural lineations. The development of kaolinite over smectites will be shown in detail in the following chapters.

3.3.3. Chios Island.

The bentonite deposits of Chios island are associated with the Neogene rocks which crop out in the SE part of the island south of the village of Thymiana. Essentially, it is a single tuffaceous horizon of Lower-Middle Miocene age which has been altered to bentonite. The depositional environment of the parent tuff was fluviolacustrine (Besenecker *et al.* 1968, Besenecker 1973). The thickness of the deposit varies substantially from site to site and the maximum outcrop observed is 8m thick. It overlies the sands of the highest horizons of the Zyfia layers and is overlain by the red clays and the intercalated greenish sand beds of the Keramaria layers (see Section 3.1.3). It is a predominately grey (in places green), hard (probably due to the presence of opal) bentonite with abundant grit content (Plate 8). The material does not show any evidence of hydrothermal alteration; it is therefore believed that it was formed from subaqueous devitrification of volcanic ash which had been deposited in a fluviolacustrine environment The geological map of the area in which the bentonite occurrences crop out is given in Figure 3.11b.

Plate 1

1. Southern face of the Tsantili bentonite deposit, Area 1, Milos. The influence of hydrothermal alteration is obvious. The original bentonite has been converted to K-bentonite. The white horizon in the centre of the photograph has been produced from silicification, the silica been released during the smectite-to-illite conversion. The avarage height of the benches is 3m.

2. Aspro Horio deposit, Area 1, Milos. Note the fine bedded bentonite horizons close to the boundary between the yellow and the dark green-blue bentonite. Deposition of silica has taken place in various sites of the yellow horizon.

Plate 1

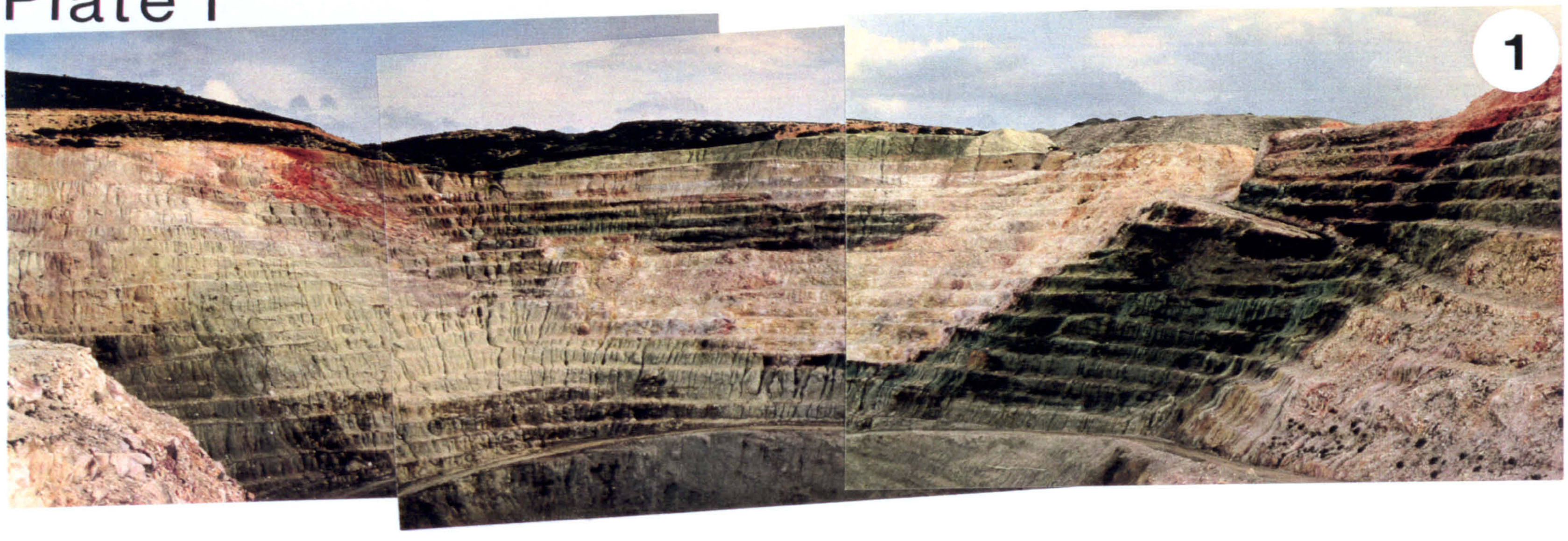

Plate 2

1. Zoulias deposit, Area 1 Milos. Note the composite character of the deposit. The lower blue-dark green bentonite horizon has been derived from an andesitic lava. The influence of hydrothermal alteration is obvious in the lower stratigraphic levels of the deposit (yellow and red colourations). The two grey horizons at the top of the sequence (described as horizons 9 and 10 in the text).

2. Lower bentonite horizon in the Ano Komia deposit, Area 3, Milos. The grey bentonite has been affected by S-bearing hydrothermal solutions which formed stockwerk-like structures. The well bedded lappilli-tuff at the top of the photograph is the parent material of the grey bentonite.

Plate 2

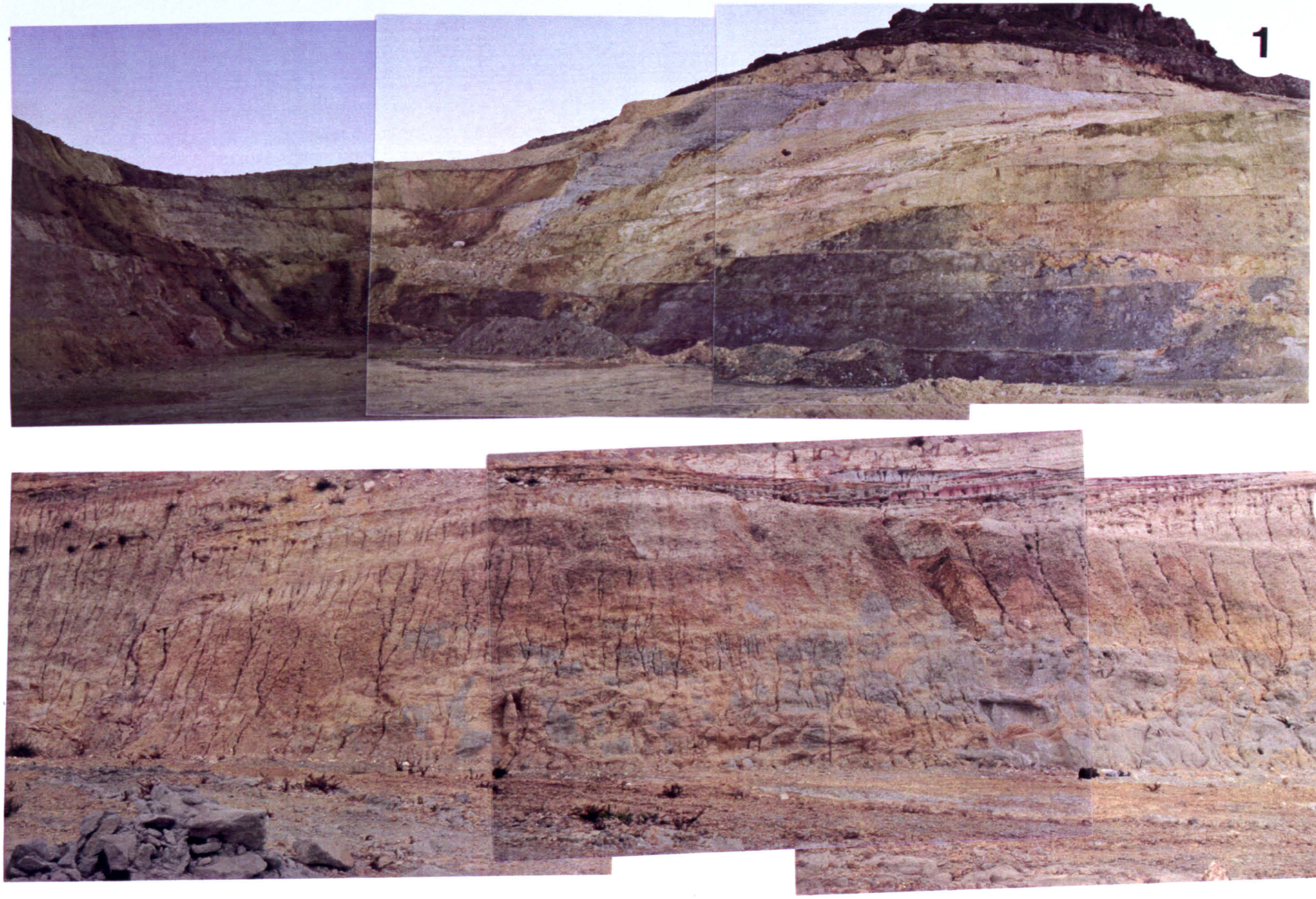

Plate 3

1. Ankeria deposit, Area 2 Milos. Composite deposit consisting of 4 stratiform bentonite horizons. The deposit is currently affected by hydrothermal activity in the form of a solfatara spring (centre of the photograph). The red overburden is fossil-bearing (bivalves) indicating deposition under marine conditions.

2. Koufi deposit, Area 2 Milos. The massive green bentonite is divided into two separate horizons in its lowermost sections. Th uppermost yellow horizon is silicified in several sites.

Plate 3

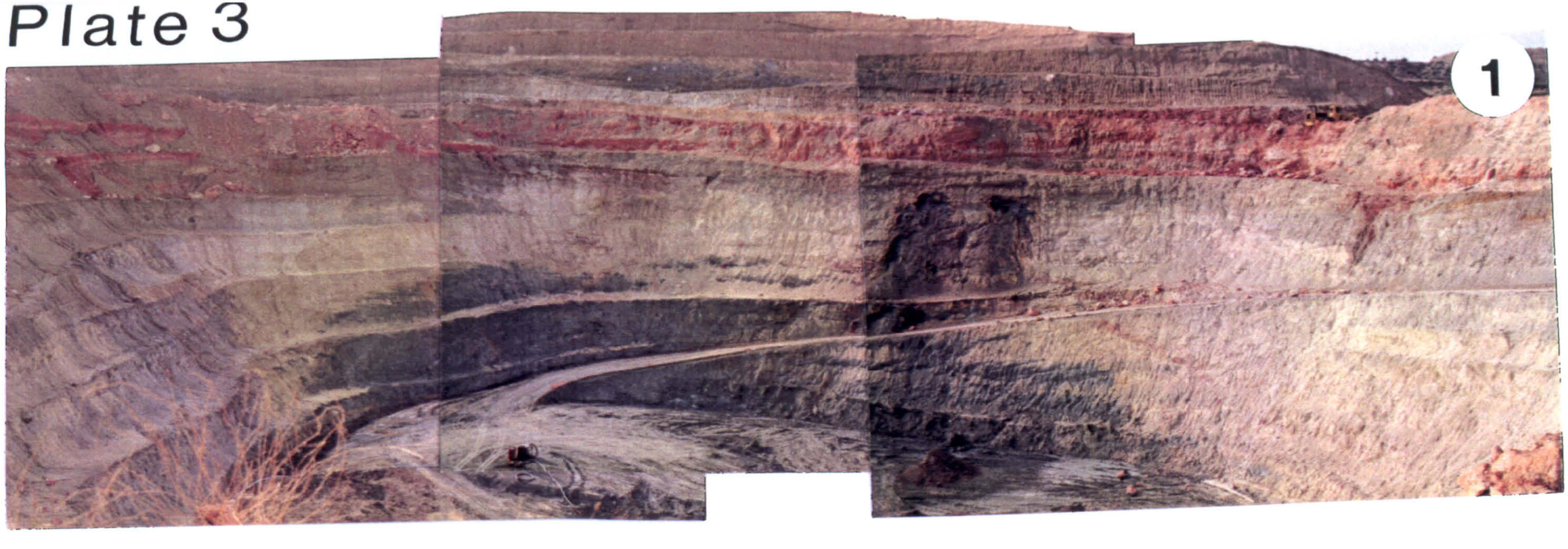

Plate 4

1. Higher bentonite horizon of the Ano Komia deposit, Area 3 Milos. It is white bentonite with red colourations in places due to the presence of iron oxides. The underlying bedded rock belongs to the lower bentonite horizon showed in plate 2. Note the different macroscopic characterics of the two materials.

2. Garyfalakena deposit, Area 3 Milos. The grey bentonite present in the base of the deposit has turned to yellow due to the influence of hydrothermal solutions rich in S. The higher horizons of this deposit display intense silicification.

3. Kato Komia deposit, Area 3, Milos. Grey bentonite which has been subsequently affected by hydrothermal alteration (yellowish-white areas). The alteration is more intense in the right side of the photograph.

Plate 4

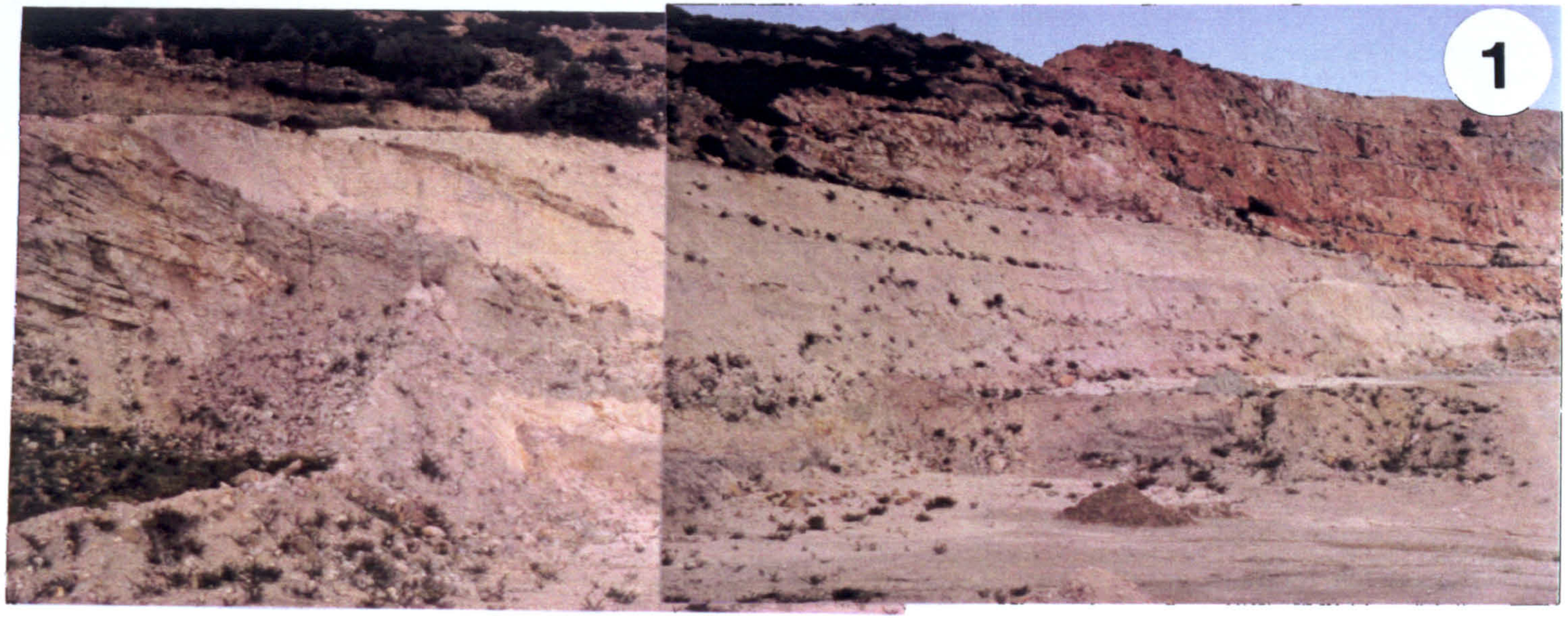

Plate 5

1. Mavrogiannis deposit, Area 3, Milos. The originally grey bentonite (the grey colout is still visible in the lowermost part of the quarry face) has been subsequently affected by hydrothermal alteration. The yellow colourations are due to the inffluence of S-bearing solutions.

2. Rema deposit, Area 3 Milos. Grey bentonite which has been affected by hydrothermal alteration, present in the form of yellow colourations in the grey body.

Plate 5

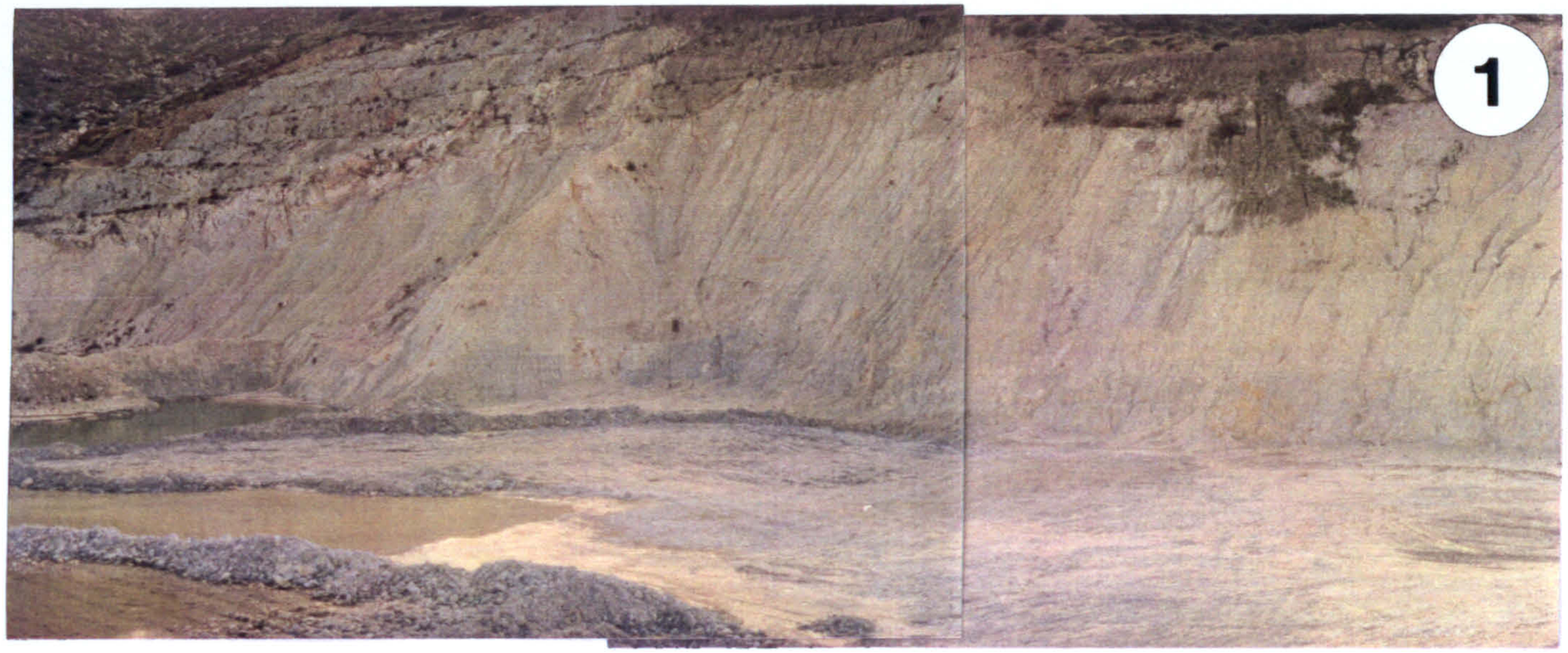

Plate 6

1. Kastriani deposit (poor quality kaolin), Area 3, Milos. The deposit has been formed at the expense of lapilli-tuffs and probably of the "green lahar" (term introduced by Fyticas, 1977) which has very recent age. Similar alteration of the "green lahar" has been observed in the Agia Kyriaki area close to this deposit. The "Green Lahar" overlies the bentonite deposits.

2. The bentonite deposit of Agrilies. The deposit is located next to the barytes deposit of Pikridou and displays ample evidence of influence of hydrothermal alteration. Note the sharp contact between the light coloured bentonite and the dark "Green Lahar".

Plate 6

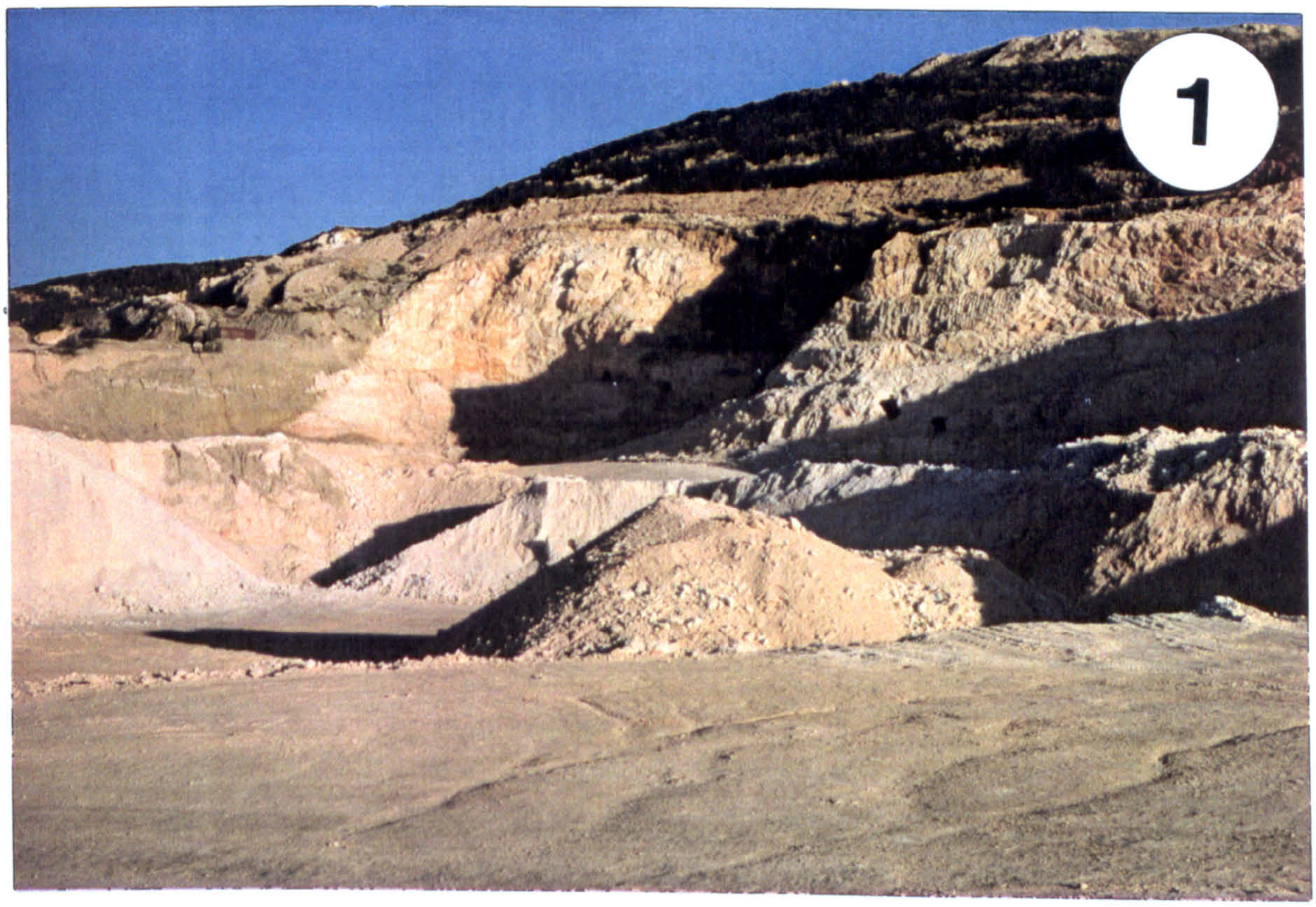

Plate 7

1. Prassa deposit, Kimolos. The deposit has been formed at the expense of an ignimbrite ("Prassa ignimbrite" according to Fyticas & Vougioukalakis, 1992). The grey rock in the centre of the deposit corresponds to the smectite zone, while the white material next to it (left side of the photograph shown by the arrow) to the smectite + mordenite zone. In the far end at the centre of the photograph note the faulted area. Around this area, a minor bentonite body has been formed.

2. Loutra deposit, Kimolos. Well bedded lappilli-tuff altered to bentonite. The deposit is cut by faults (indicated with the arrow), along which the mineral phases carried by hydrothermal solutions have been precipitated.

Plate 7

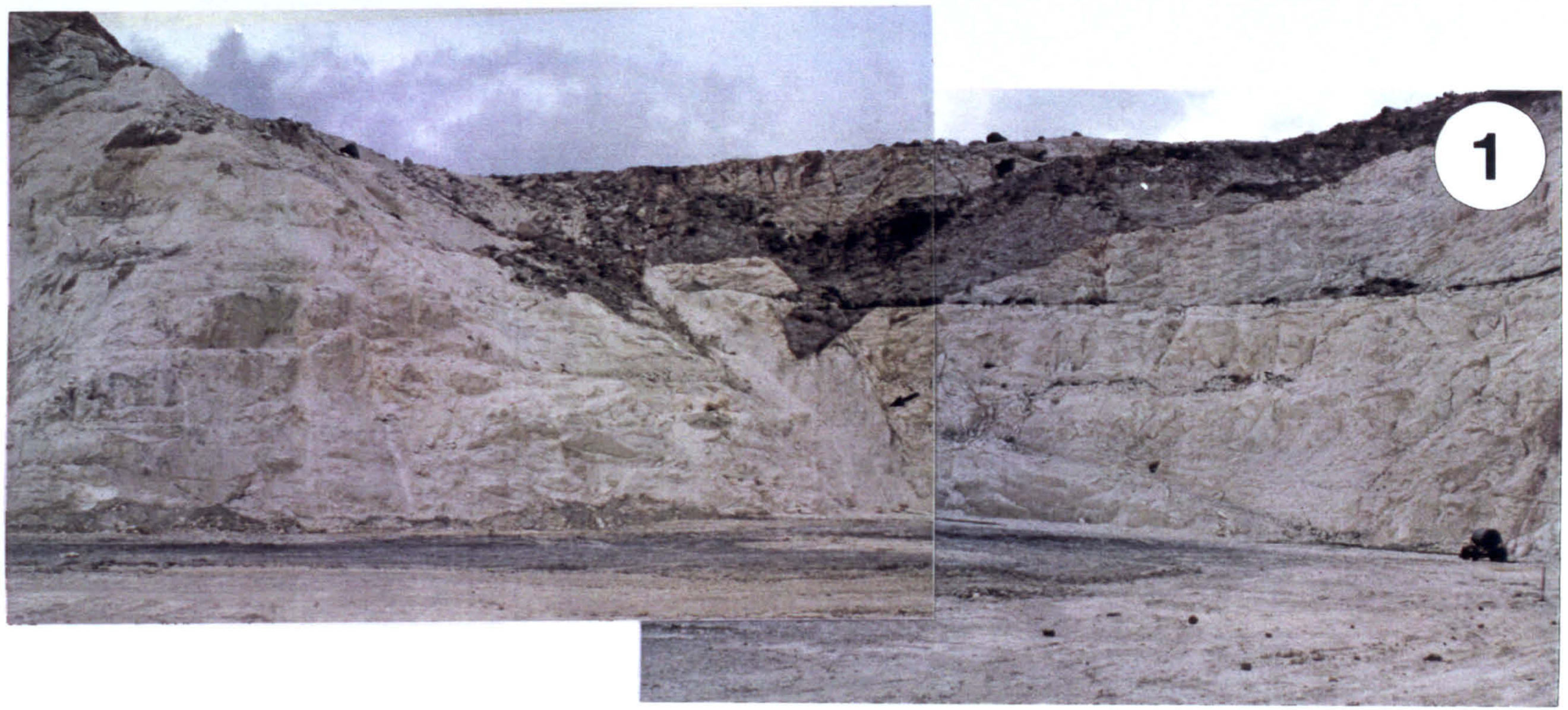

Plate 8

1. Bentonite at the Fanara deposit, Kimolos. The higher horizons of the bentonite have been silicified.

2. Bonatsa deposit, Kimolos. Alteration of a perlitic lava to bentonite. It is obvious that alteration is more pronounced along cracks and faulted zones.

3. Agios Tryfon deposit, Kimolos. It is a poor kaolin deposit. The red colourations are due to the presence of Fe-oxides. The material has undergone small scale underground extraction in the past. The yellowish material in the lower right corner of the photograph is a bentonite partialy kaolinized.

4. Bentonite outcrop in Chios Island. The material is grey-off white.

Plate 8

Plate 9

1. Stockwork textures formed by hydrothermal alteration in the Zoulias bentonite deposit. The grey material forming the background is the andesitic lava in the lowermost sector of the deposit.

2. Syn-sedimentary fault observed in the Zoulias deposit. The lower horizon contains authigenic K-feldspar and zeolites (clinoptilolite and mordenite).

3. Opal C-T-bearing bed deposited amidst the higher grey bentonite horizon of the Ankeria deposit. Such beds cause difficulties during the extraction of the bentonite.

4. Pillow-lava-like texture observed in the Koufi deposit. It os not certain whetehr this texture is primary or due to alteration to bentonite.

Plate 9

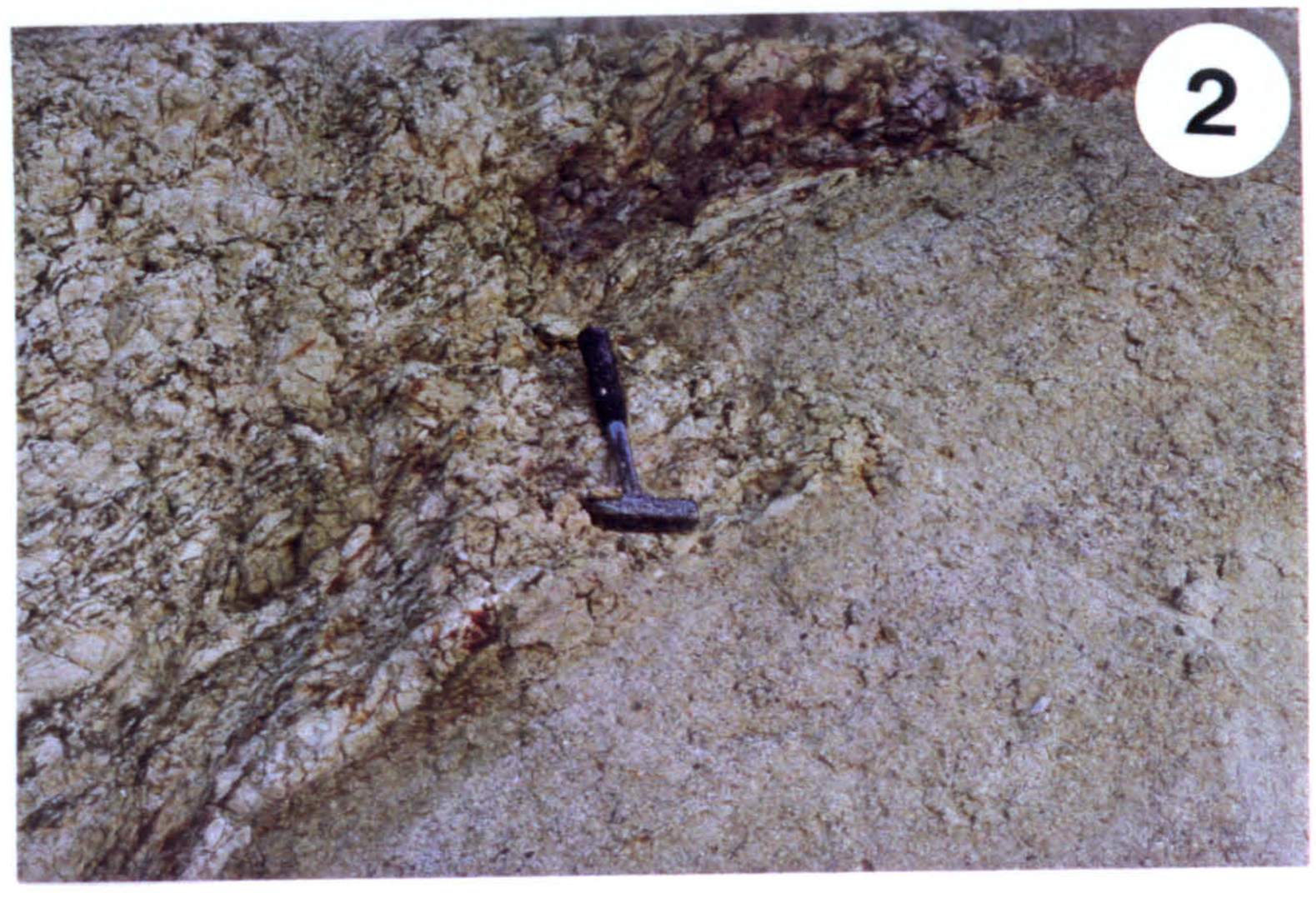

Plate 10

1. Concentric alteration of the original rock to bentonite. The degree of alteration increases from the centre to the rims of the block (Koufi deposit, area 2 Milos).

2. Sedimentary structures (dewatering structures) which have been formed from deformation of the soft volcaniclastic rock. The "pop corn"-like textures in the right hand side of the photograph are due to the presence of smectite (lower bentonite horizon, Ano Komia deposit).

3. Sharp contact between the bentonite and the "Green Lahar" in the Rema deposit, area 3 Milos.

4. Herring bone textures in the volcanic sand overlying the Prassa ignimbrite at the Prassa deposit. This ignimbrite is the parent rock for the bentonite of the Prassa deposit. Note the rounded pebbles above the volcanic sand. The above sedimentary textures support the existence of a marine environment.

Plate 10

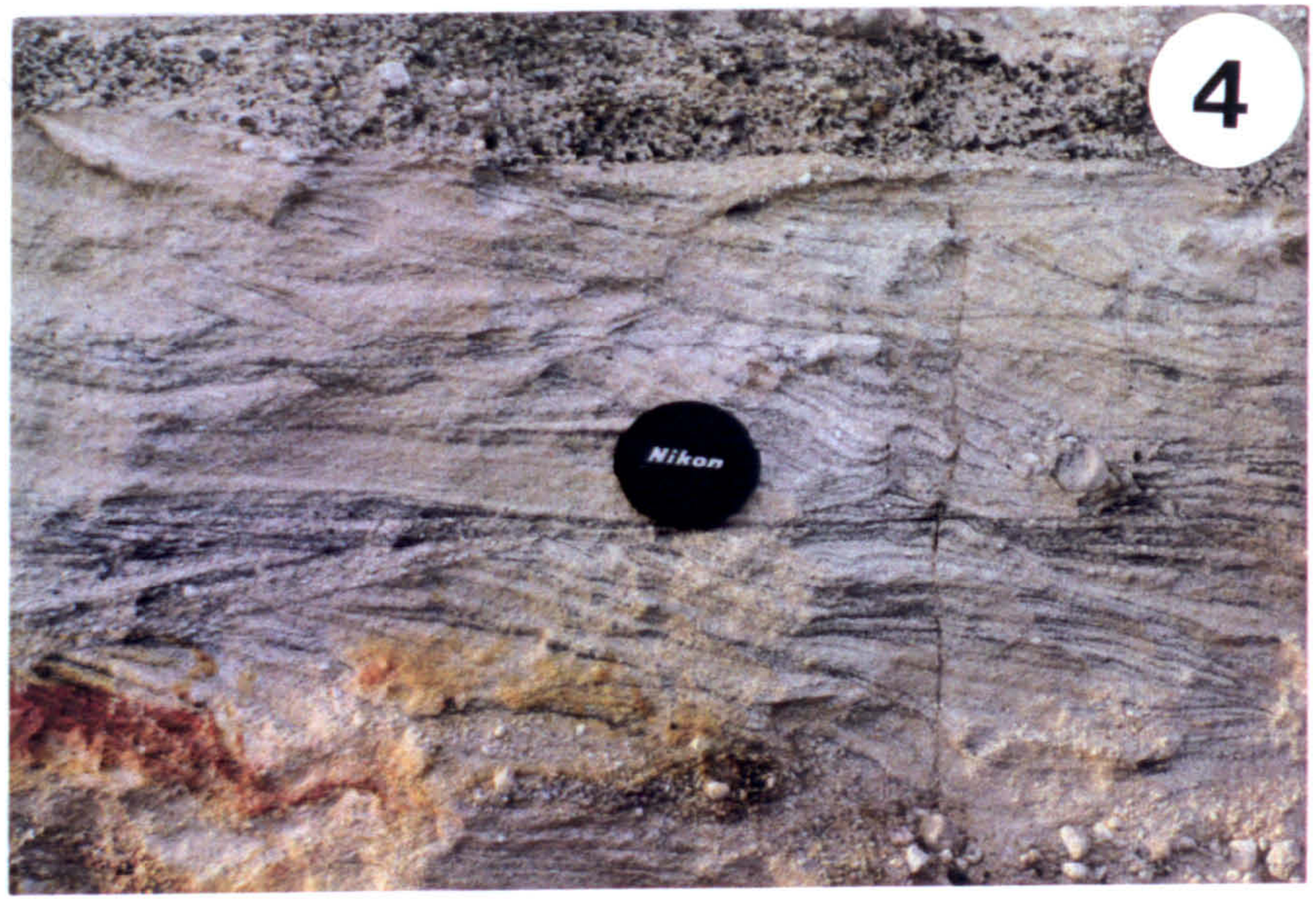

Plate 11

1. Bivalve fossil (shown by the arrow) possibly CARDIUM Sp. in the Loutra bentonite (Kimolos), suggesting that the alteration took place under a marine environment.

2. Typical "pop corn" texture, characteristic of the bentonite outcrops, formed from dehydration of the smectite flakes (Bonatsa deposit, Kimolos).

Plate 11

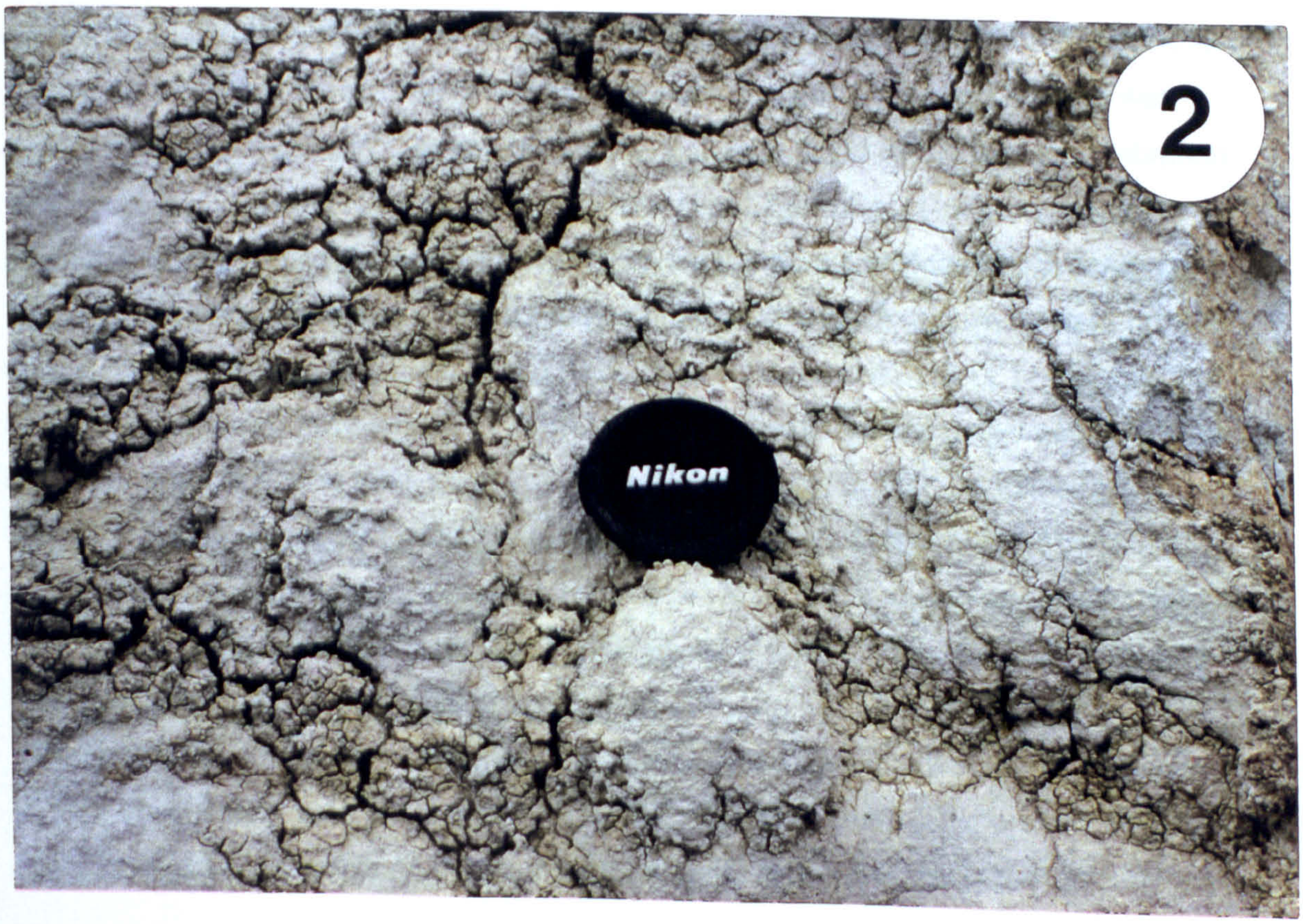

CHAPTER FOUR

MINERALOGY AND MINERAL CHEMISTRY

4.1 Experimental techniques.

The techniques used for the determination of the mineralogy and mineral chemistry of the Greek bentonites are optical microscopy, X-Ray Diffraction (XRD), Scanning and Transmission Electron Microscopy (SEM and TEM respectively), Electron Probe Microanalysis, Differential Thermal Analysis and Thermogravimetric Analysis (DTA and TG respectively), and Infra Red Spectrometry. All analyses unless stated were carried out in the department of Geology, University of Leicester.

X-Ray Diffraction was used for qualitative determination of the bulk mineralogy as well as the mineralogy of the clay fraction. The diffractometer used was a Philips PW 1729 operating at 40kV and 30mA equipped with an automatic sample loading system, controlled by a PW1710 computer control unit. The recording unit was a PM8203A one line recorder. CuKa radiation and Ni-filter was used. A number of samples was examined using a Siemens D500 automatic X-Ray diffractometer operating at similar conditions in the Technical University of Crete, Greece. Bulk mineralogy was examined by means of random orientated powders mounted in Al-holders following the method described by Brown & Brindley (1984, p. 310). The samples were examined in the scanning range 4-65^{o} 2θ. Clay mineralogy was examined using the -2μm fraction of orientated samples prepared by the glass-slide method (see Moore & Reynolds, 1989). In those samples from the Tsantili and Agrilies deposits where mixed layer illite/smectite was present, the -0.5μm fraction was separated as well. The samples were dispersed in distilled water, using ultrasonic vibration for 2 minutes and adding Na-polymetaphosphate as a deflocculant. The separated clay fraction was treated with ethylene-glycol at 70^{o}C for 16 hours and X-rayed immediately. The samples which contained a mineral species with a peak at 7Å and which were not unambiguously identified from the peak in the 3.5-3.6Å and/or the peak at 14Å because of smectite interference were heated at 550^{o}C to clarify whether this mineral was kaolinite or chlorite. Semiquantitative analysis of the clay fraction was carried out using the methods of Reynolds (1989). Finally, the percentage of expandable layers in the mixed-layer illite/smectites was determined using the methods of Srodon (1980, see Appendix 4.1a). For terms of comparison the same determinations were carried out by the peak migration methods of Reynolds (1984, see Appendix 4.1b).

Broken surfaces of selected samples were examined with a Hitachi S520 SEM operating at 20kV accelerating voltage equipped with a Link AN10000 Energy Dispersive Spectrometer for qualitative analyses. The less than 1μm clay fraction of selected samples

was examined by TEM. The samples were mounted on copper grids which had previously been covered with a plastic film and coated with carbon. Selected clay fractions which contained mixed-layer clay minerals were additionaly subjected to Pt-coating (Beutelspacher & van der Marel 1968, Comer 1971 and Nadeau & Tait 1987) for particle thickness measurements. The accuracy of the method is ± 4-5Å (Guven & Pease, 1975, Nadeau *et al.* 1984c) . Finally a small number of selected clay fractions was prepared with the methods described by Lee *et al.* (1975) and examined with High Resolution TEM, to determine details of the smectite structure. The methods used for the preparation of the samples for TEM and HRTEM observation are described in the Appendices 4.2, 4.3 and 4.4. The microscopes used for low resolution TEM observations were a KORINTH 274 TEM operating at 60kV and a JEOL 100CX TEM operating at 80kV at the department of Biology, University of Leicester. HRTEM images were obtained with the JEOL 100CX operating at 100kV.

Microanalyses of smectites and other authigenic minerals were carried out on polished blocks with a JEOL JXA-8600 Superprobe. This was equipped with three wavelength spectrometers (WDS) and one Link series 1 energy dispersive spectrometer (EDS), with a Link 860 series 1 detector having 158eV resolution at 5.8KeV. Analyses were carried out with the EDS at 100 seconds live time for smectites, carbonates and feldspars and 20 seconds for zeolites, using a 15kV acceleration current potential and a 3nA specimen current. Both a focused and an unfocused beam with a 5 or 15µm spot size were applied. The 15µm spot size was used for mordenite. The accuracy, precision and detection limits of the method used have been described by Dunham & Wilkinson (1978). The following standards were used: wollastonite for Si and Ca, jadeite (intensity standard) and NaCl (profile standard) for Na, synthetic MgO for Mg, microcline for K, synthetic Fe_2O_3 for Fe, rutile for Ti and rhodonite for Mn. Co was used as a secondary standard to monitor the overall count rates.

The thermal stability of heulandite/clinoptilolite-type zeolites was determined using the method of Boles (1972), which examines the changes of the 020 peak after heating. The temperature used was 450^{o}C and the duration 16h. The samples were cooled to room temperature in a dessicator and X-rayed. Characterization of the various polymorphs was made using the following assumptions (Boles & Surdam, 1979): If the intensity of the peak was reduced by less than 50% compared to the original one after heating the mineral was characterized as clinoptilolite. If the original peak disappeared completely after heating the mineral was characterized as heulandite. Finally if after heating the intensity of the 020 peak was less than 50% of the original one the mineral was characterized as "intermediate". In this work no heulandite was detected.

Differential Thermal and Thermogravimetric Analyses were carried out on -2µm fractions separated by sedimentation methods, using a Standon Redcroft TG-DTA STA 1000/1500

Thermal Analyser. The atmosphere used was air. The samples were heated from 20 to 1000^{o}C with a heating rate of 10^{o}C/min. The sensitivity for DTA was 20 mV. Finally, Infrared Absorption Spectroscopic Analysis was carried out on -2μm clay fractions mounted on KBr pellets according to the method described by Russel (1987), with a computer controlled BIORAD FTS40 Fourier Transform Infra-red spectrometer in the Department of Chemistry, University of Leicester, in the frequency range between 400 and 4000cm^{-1}. The method used for the preparation of the samples is described in Appendix 4.5.

4.2 Mineralogical characteristics of the bentonite deposits.

The mineralogical assemblages present in the bentonite deposits examined were determined by X-Ray diffraction methods and Scanning Electron Microscopy.. Representative traces of both the bulk samples and the clay fractions are depicted in Figures 4.1 and 4.2 respectively. Mineralogical profiles of the deposits are shown in Figure 4.3, while the complete mineralogical composition is given in Table 4.9 (end of Chapter 4).

4.2.1 Milos Island

4.2.1.1. Ankeria deposit.

The major, and in some sites only, mineral present is dioctahedral smectite as it can be seen from the location of the 060 peak in the XRD traces (Fig. 4.1). Calcite is abundant while quartz, plagioclase, and opal-CT are minor phases. Potassium feldspar, pyrite, marcasite and hematite are accesory minerals. At least some of the K-feldspar present is authigenic (Plate 14). Finally, in the Area affected by the solfatara activity (Plate 3) jarosite, gypsum and native sulphur are also present.

Plagioclase occurs only in the stratigraphicaly higher grey horizon, becoming more abundant away from the contact with the underlying yellow horizon (see Plate 3). K-feldspar is present in the stratigraficaly lowest blue horizon as well as in the lower sectors of the bright yellow horizon. It is more abundant in the SE sector of the deposit. Opal-CT is abundant in the higher and quartz mainly in the western part of the light yellow horizon of the quarry, while calcite is present throughout the entire Area of the deposit. Mordenite aggregates occur in trace amounts in the bright yellow horizon filling pore spaces among the altered shards.

4.2.1.2. Koufi deposit.

In the main horizon of the deposit (higher horizon) dioctahedral smectite and plagioclase

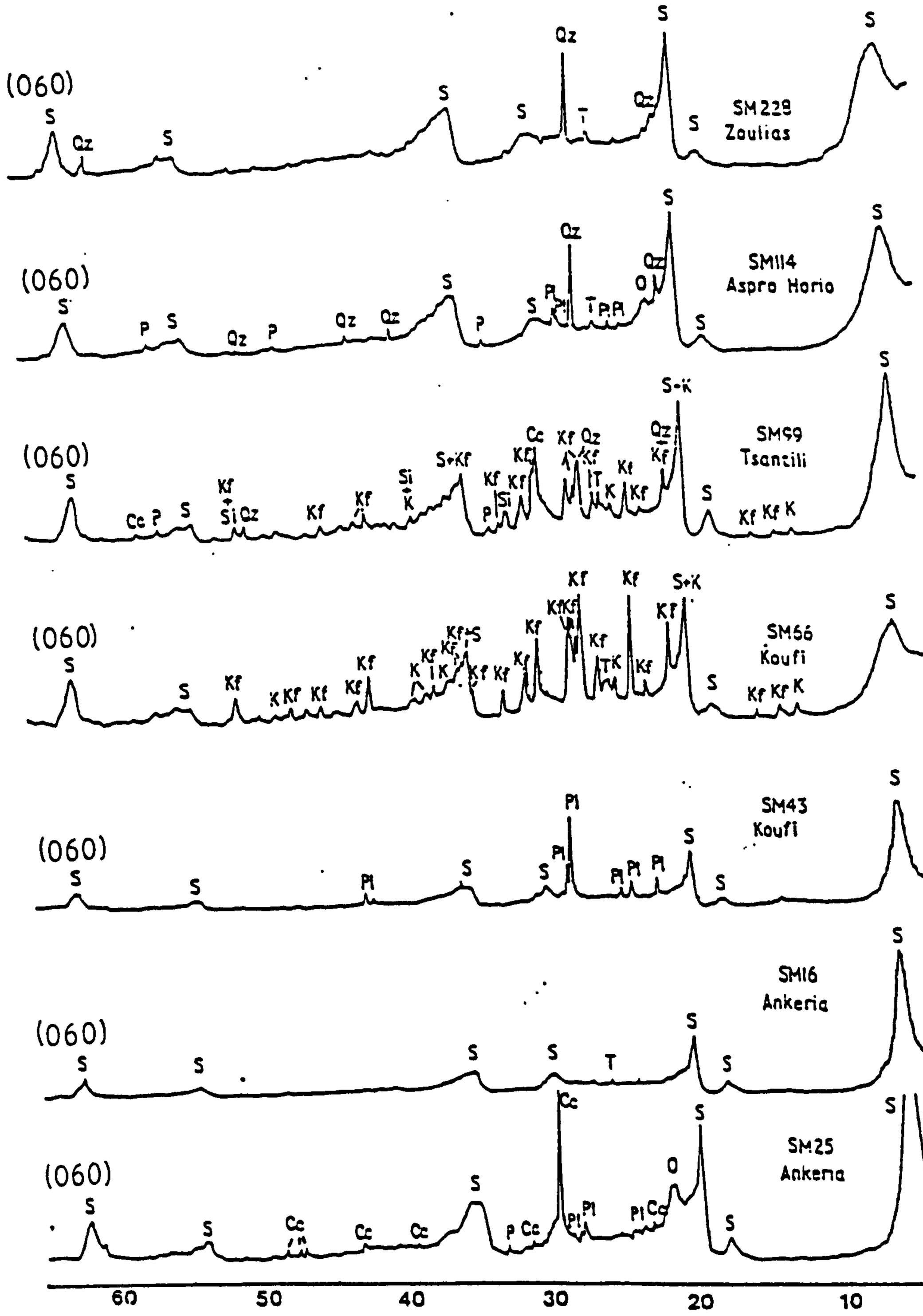

FIGURE 4.1. Representative XRD traces of the Greek bentonites (bulk samples). Key to the symbols: S=smectite, K=kaolinite, M=mica, Chl=chlorite, G=gypsum, Qz=quartz, O=opal C–T, Cr=cristobalite, Kf=K-feldspar, Pl=plagioclase, Cc=calcite, Do=dolomite, Si=siderite, T=Ti-oxides, P=pyrite, J=jarosite, A=apatite.

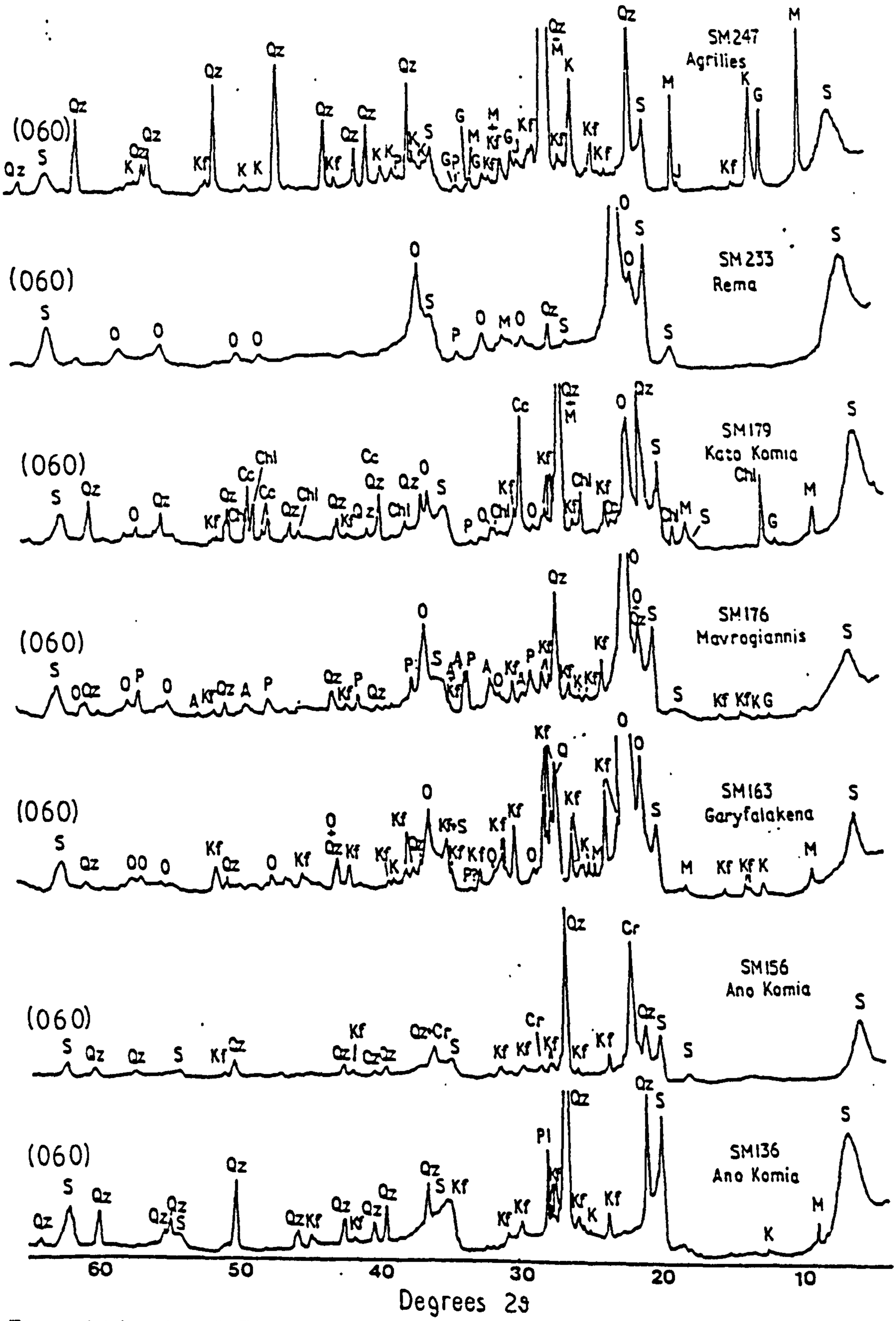

FIGURE 4.1 (continued). Representative XRD-traces from the Greek bentonite deposits (bulk samples).

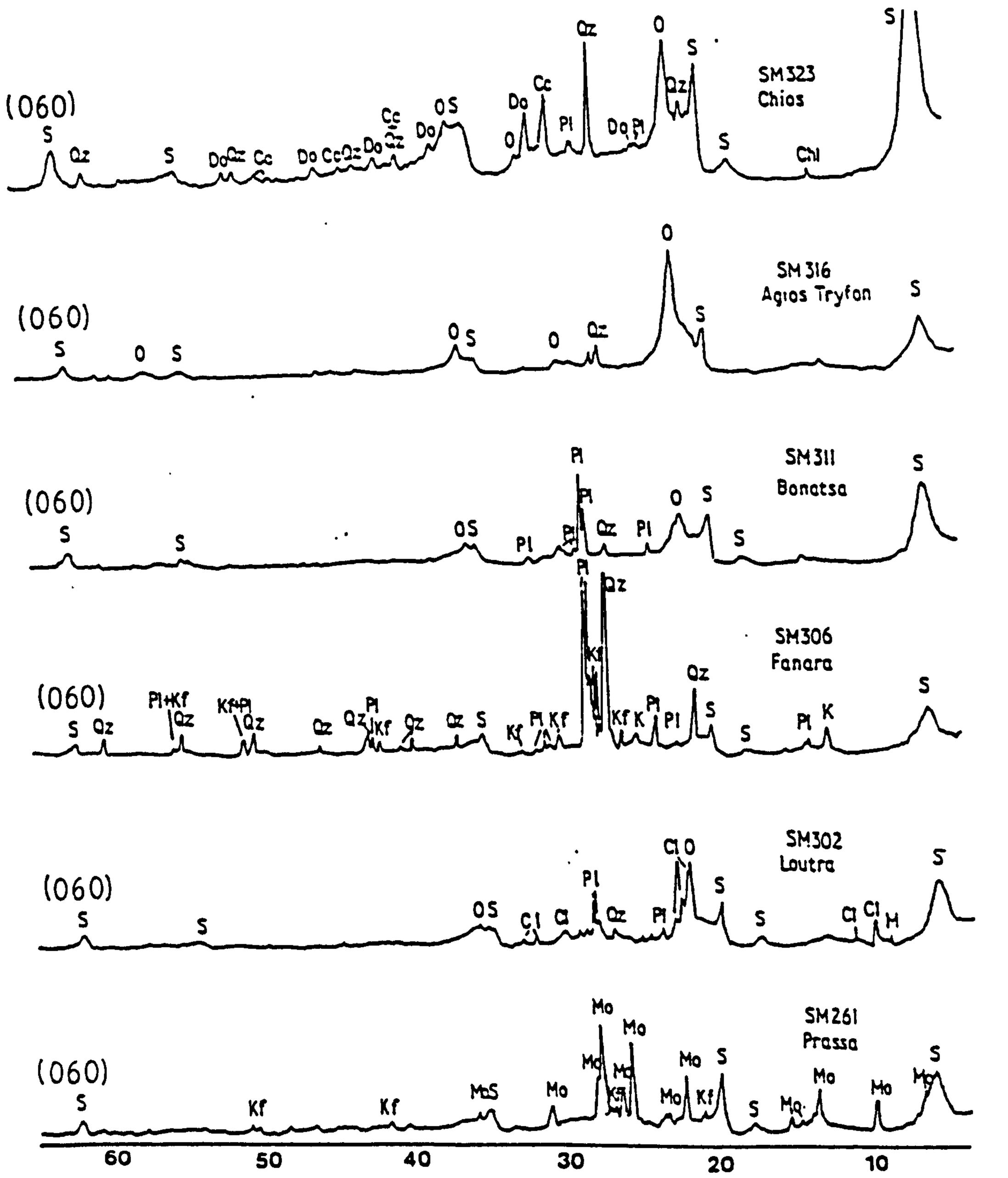

FIGURE 4.1 (continued). Representative XRD-traces from the Greek bentonite deposits (bulk samples).

are the major mineral phases, K-feldspar is a minor phase and sulphides (pyrite and marcasite are trace minerals. Occasionaly, calcite, opal-CT, quartz and gypsum are present. In the lower horizon of the deposit montmorillonite and authigenic K-feldspar (Plate 14) are the major phases, kaolinite is minor and sulphides (pyrite and marcasite) are present as accesory minerals.

Montmorillonite is present throughout the entire Area of the quarry. Plagioclase is abundant in the whole northern face as well as the western sector of the southern part of the deposit (Plate 3). K-feldspar is usually present in the southern face of the quarry while sulphide minerals are dispersed throughout the entire mass of the bentonite. The other mineral phases do not show a distinct distribution pattern. Generally, silica phases (quartz and/or opal-CT) are present only in trace amounts or absent.

4.2.1.3 Tsantili deposit.

Dioctahedral smectite and K-feldspar are the major phases present throughout the entire Area of the deposit. In the southern and SW face of the quarry mixed-layer illite/smectite (I/S) has replaced the smectite minerals (Fig. 4.5). The amount of illite in the mixed-layer mineral increases towards the higher stratigraphic levels of the deposit (Fig 4.4a). In the lower levels the interstratification is of random type (R0, see Appendix 4.1c for explanation) changing to an ordered type (R1, *i.e* I/S) with about 43-45% expandable layers (Fig. 4.5). Random interstratification is present with up to about 51% expandables in good agreement with other workers (Inoue & Utada, 1983, Brusewitz, 1986, Srodon *et al.*,1986, Inoue *et al.*,1987 among others). The presence of both random and ordered interstratification (R0/R1) was also identified in the range 50-45% expandables. Coexistence of both ordered and random interstratification has been reported in natural samples by Brusewitz (1986) and Srodon *et al.* (1986) and in hydrothermal experiments by Whitney & Northrop (1988). In all these cases the existence of both random and ordered intrestratification is present in the range 50-40% expandables, similar to this case. R1 type of ordering is present up to about 24% expandables. The R1 I/S can be classified as fully ordered or partially (1/2 ordered) using the diagrams of Srodon (1980) (Fig. 4.4b). The partially ordered I/S are associated with kaolinite. Finally R3-type ordering (*i.e* ISII) occurs at expandabilities below 18%. The lowest amount of expandable layers found was 13%. The results from the calculation of the illite content in the I/S minerals, using different methods are depicted in Table 4.1. It can be seen that the method of Srodon (1980) gives slightly higher illite contents than that of Reynolds (1984) and that there is a very good agreement between the two methods especially in the ordered I/S. However, there is not good agreement between the two methods in the case of random interstratification. In this case the methods of Srodon are considered more reliable because they take into account the effect of the

Table 4.1.

Expandabilities of the illites/smectites present in the Tsantili deposit, Milos, calculated with the methods of Srodon (1980 and Reynolds (1984).

Sample	Srodon	Reynolds	Ordering
SM75	40	40	R1
SM76	24	27	R1
SM78	16	19	R3
SM79	13	16	R3
SM80	27	28	R1
SM81	16	19	R3
SM82	17	- -	R3
SM83	25	26	R1
SM84	43	44	R1/R0
SM85	81	81	R0
SM86	45	44	R0/R1
SM88	43	43	R1/R0
SM89	47	49	R1
SM90	40	43	R1
SM91	74	76	R0
SM94	35	34	R1
SM95	51	50	R0/R1
SM104	72	83	R0
SM105	65	78	R0
SM107	- -	44	R1
SM108	69	76	R0

ethylene-glycol complex thickness and are less seriously affected by the Lorentz Polarization Factor.

K-feldspar is also a major phase throughout the deposit. There is no indication of an inverse relationship between the amount of K-feldspar present and the expandable layers present in the mixed layer I/S. Minor phases present are kaolinite, carbonates, jarosite and gypsum. Kaolinite is usually absent, or present in small amounts in the western and SW sector of the quarry. The smectite:kaolinite ratio in the samples where kaolinite is present varies between 24:1 and 4.9:1 (from 4% to 17%). Three types of carbonates were identified; calcite, ankerite and siderite. They are present in the lower sections of the deposit, especially in the eastern part, and are usually not associated with the mixed-layered minerals. Gypsum is dispersed in small amounts throughout the entire Area of the deposit, while jarosite occurs in the higher levels of the deposit. It always coexists with gypsum but never with carbonates. Silica phases are observed only in the SE and eastern face of the quarry in the form of quartz. They are abundant in the silicified zone at the higher levels of the deposit (Plate 1). Sulphides are accesory minerals present in small amounts in the lowest levels of the deposit.

4.2.1.4. Aspro Horio deposit.

Dioctahedral smectite and quartz are the major minerals throughout the deposit. Plagioclase is abundant in the lower blue-green horizon and is present in the higher yellowish one, but is absent from the thin reddish horizon which separates the two previous ones (see previous chapter). K-feldspar is present as a minor phase in the red bentonite as well as in the yellowish one. Halloysite is present as an accesory phase (5-7% of the clay fraction, the rest being smectite) in the yellowish bentonite. Pyrite and/or marcasite is disseminated in the mass of blue-green bentonite and in the yellow horizon, but it is absent from the higher yellowish one. Calcite occurs in the blue bentonite while sulphates (gypsum and jarosite) occur in the southern sector of the deposit where the hydrothermal activity is obvious.

4.2.1.5. Zoulias deposit.

The deposit is composed of a large number of horizons some of which have not been converted to bentonite. The mineralogical composition varies from one horizon to another.

The characteristic mineralogical feature of this deposit is the presence of a heulandite/clinoptilolite zeolite in horizon 3. This implies that the presence of this mineral is controlled by stratigraphic criteria. The thermal stability of this mineral indicates

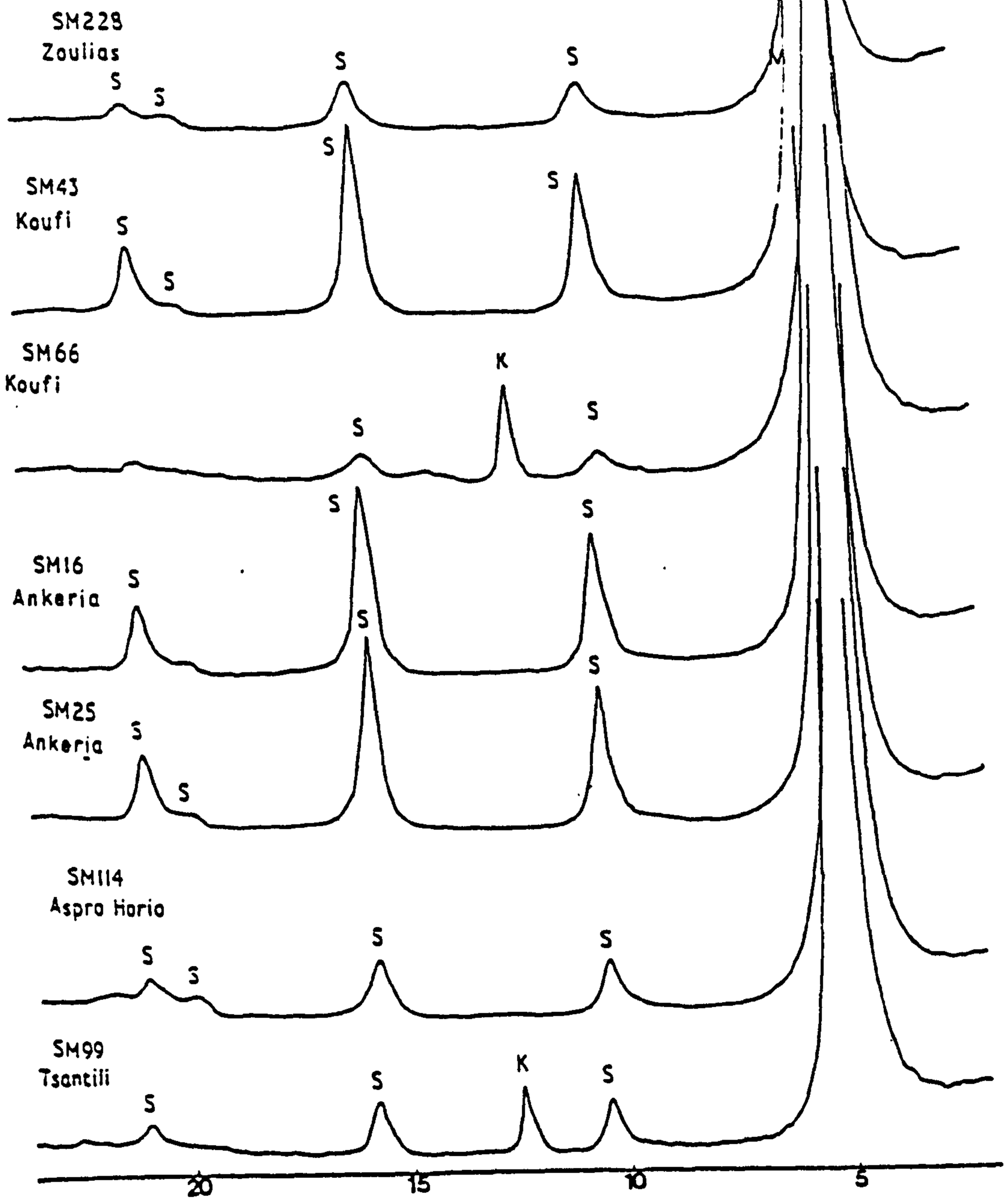

FIGURE 4.2. Representative XRD traces of the less than 2μm fraction of the Greek bentonites. Key to the symbols: S=smectite, K=kaolinite, M=mica, Chl=Chlorite.

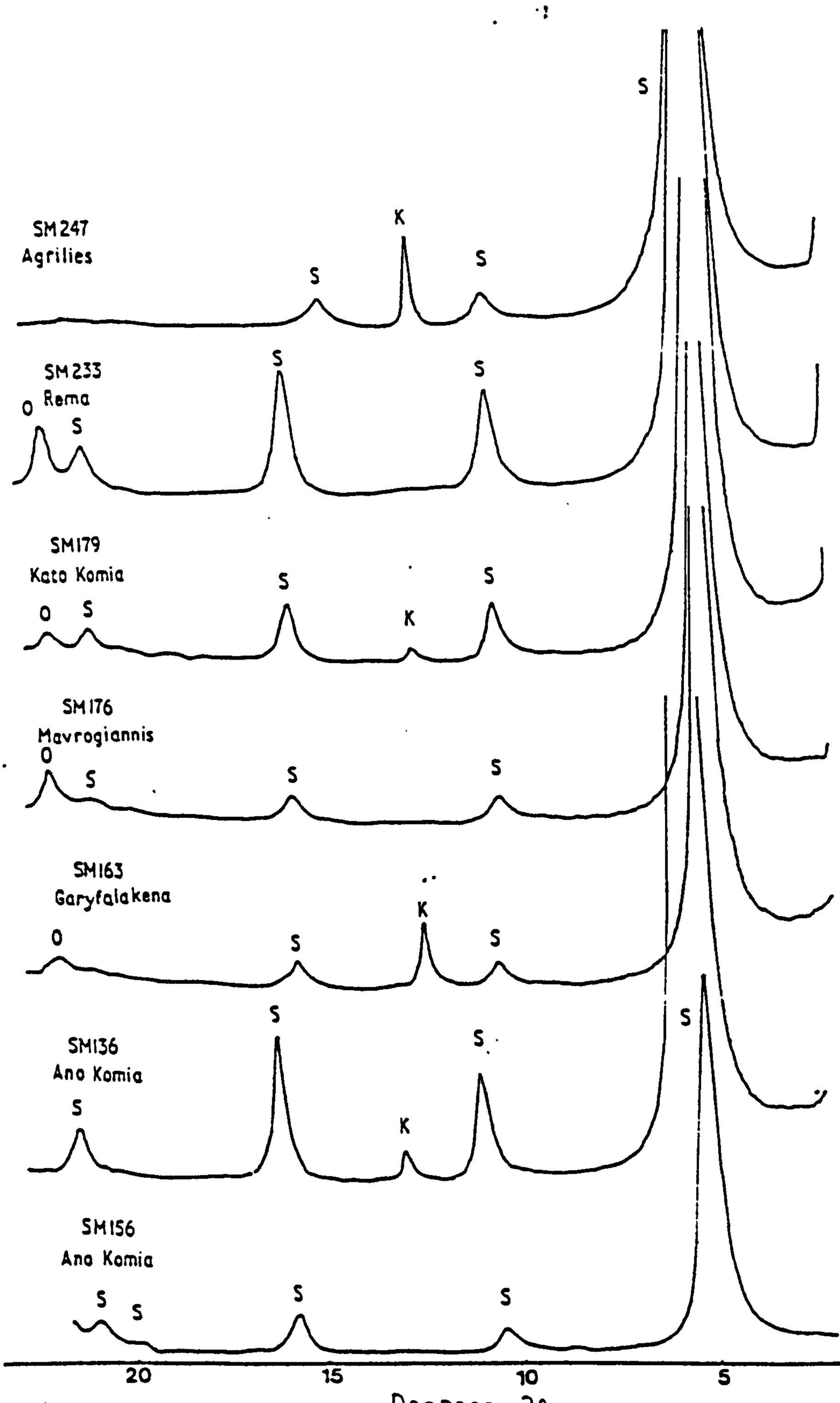

FIGURE 4.2 (continued). Representative XRD-traces of the less than 2μm fraction of the Greek bentonites.

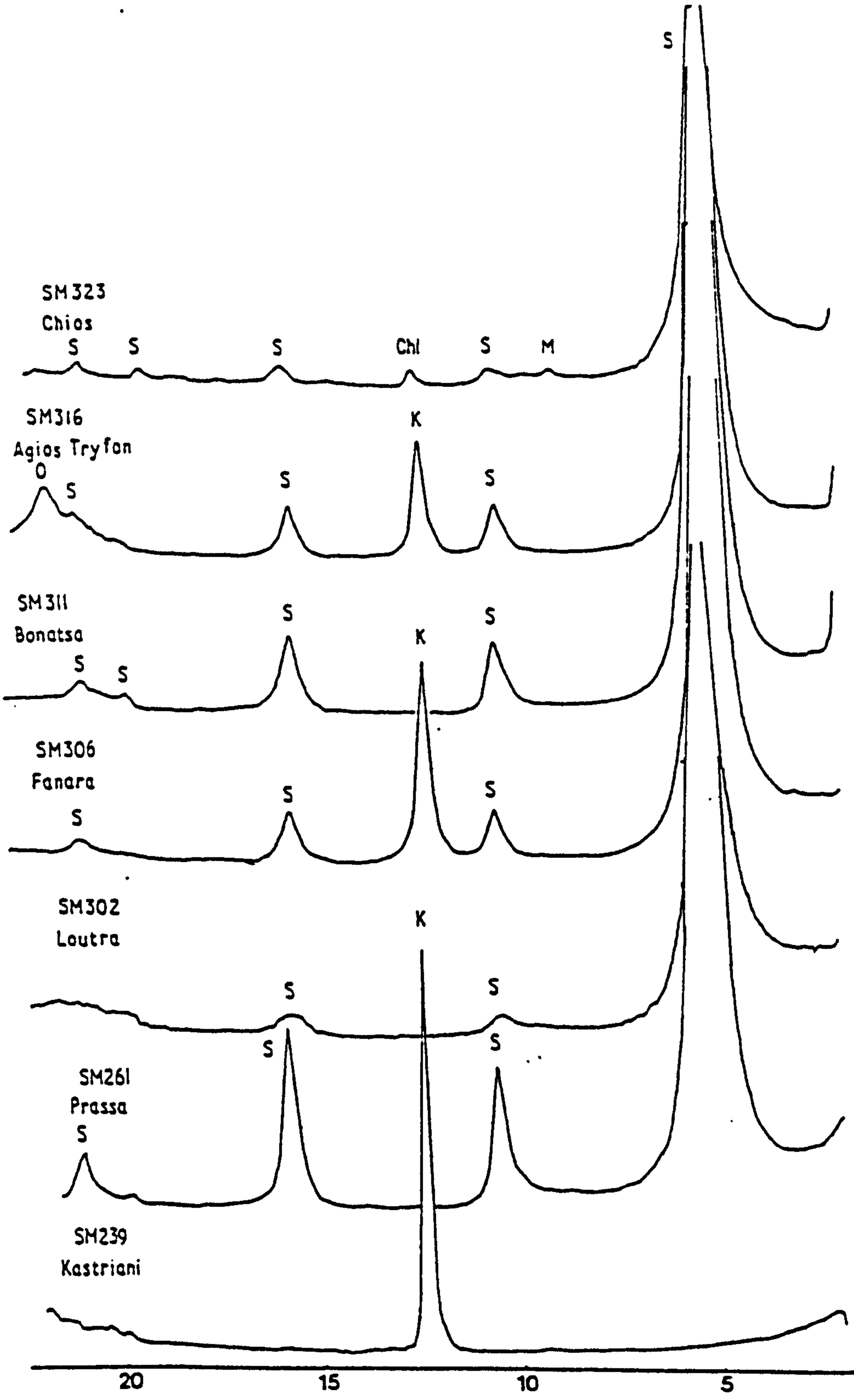

FIGURE 4.2 (continued). Representative XRD-traces of the less than 2μm fraction of the Greek bentonites.

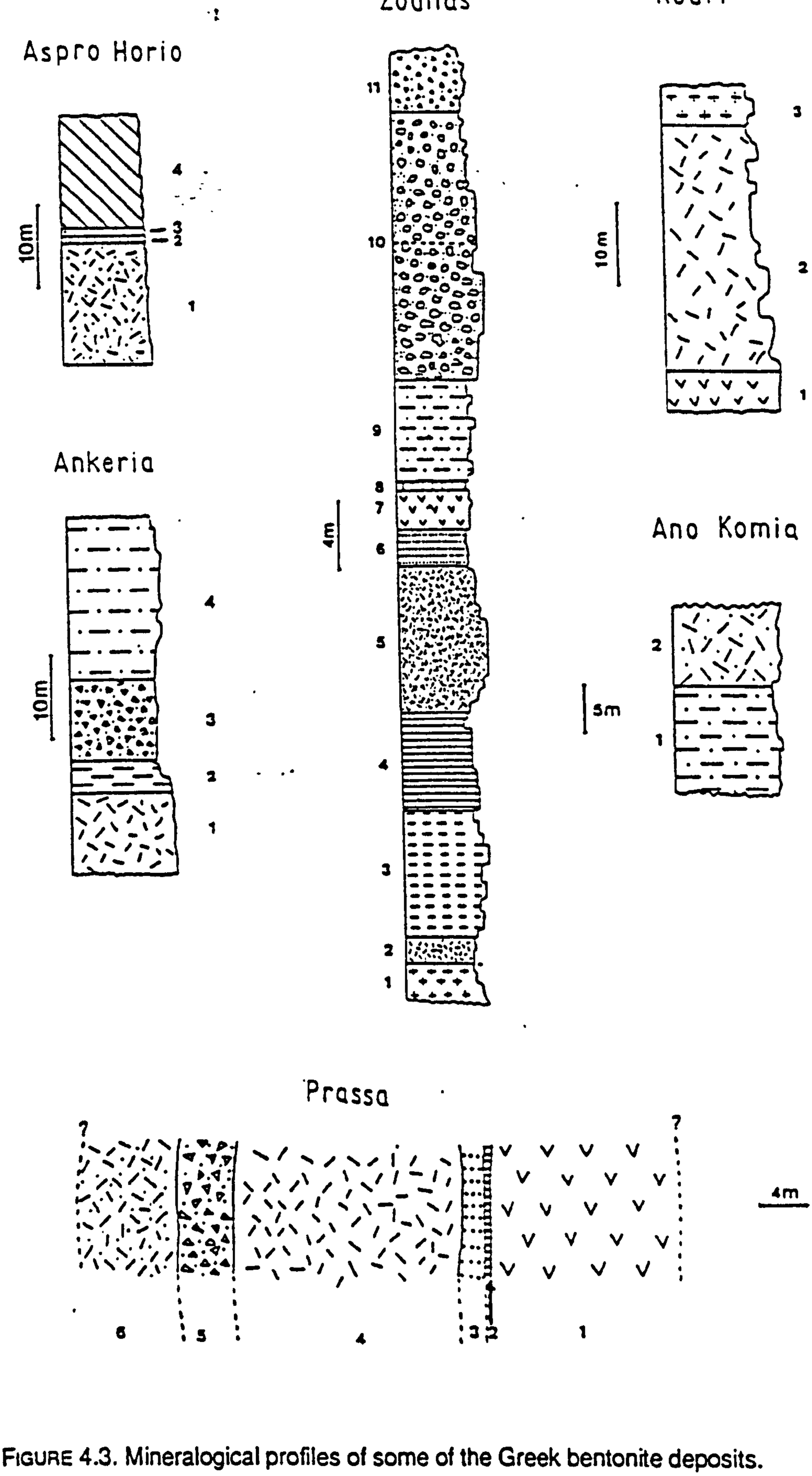

FIGURE 4.3. Mineralogical profiles of some of the Greek bentonite deposits.

Fig. 4.3. Legend

Aspro Horio Deposit.

Horizon 1: Smectite (M) + Quartz (M) + Plagioclase (Min) + Pyrite (T) ± opal C-T ± K-feldspar ± Marcasite ± Calcite.

Horizon 2: Smectite (M) + Quartz (M) + Plagioclase (Min) + K-feldspar (MIn) + Pyrite (T).

Horizon 3: Smectite (M) + Quartz (M) + Plagioclase (Min) + opal C-T (T) + Pyrite (T).

Horizon 4: Smectite (M) + Quartz (M) + Plagioclase (MIn) ± opal C-T ± halloysite ± pyrite.

Zoulias deposit.

Horizon 1: Smectite (M) + Plagioclase (M) + Sanidine (M) + Quartz (Min) + opal C-T (Min) + pyrite (T) ± (marcasite (T) ± gypsum (T)

Horizon 2: Smectite (M) + plagioclase (Min) + Sanidine (Min) + opal C-T (T) + gypsum (T) + pyrite (T) ± marcasite (T).

Horizon 3: Smectite (M) + Plagioclase (M) + Sanidine (M) + Quartz (M) + Clinoptilolite (either M or Min) ± opal C-T (M).

Horizon 4: Smectite (M) + opal C-T (M) ± pyrite (T) ± kaolinite (T) ± quartz (T).

Horizon 5: Smectite (M) + opal C-T (M) ± Plagioclase (Min) ± quartz (T) ± K-feldspar (T) ± Barytes (T).

Horizon 6: It was not sampled.

Horizon 7: Smectite (M) + Plagioclase (M) + Quartz (Min) + opal C-T (T)

Horizon 9: Glass (M) + Smectite (Min) + Plagioclase (Min).

Horizon 10: Smectite (M) + Sanidine (M) + Plagioclase (M) + Quartz (Min) + opal C-T (T) + Pyrite (T).

Horizon 11: Smectite (M) + Plagioclase (M) + Quartz (Min or M) + opal C-T (T) ± Ankerite (M) ± Fe-carbonates (M) ± Pyrite (T) ± K-feldspar (T) ± kaolinite (T).

Ankeria deposit.

Horizon 1: Smectite (M) + Calcite (M or Min) ± Quartz (Min) ± opal C-T (Min) ± K-feldspar (T) ± Pyrite (T).

Horizon 2: Smectite (M) ± Calcite (Min) ± K-feldspar (Min or T) ± Plagioclase (T) ± Pyrite (T).

Horizon 3: Smectite (M) + Calcite (M) ± opal C-T (M) ± Quartz (T) ± K-feldspar (T).

Horizon 4: Smectite (M) + Calcite (M or Min) + Plagioclase (Min) ± opal C-T (Min) ± K-feldspar (T) ± Pyrite or Marcasite (T) ± Hematite.

Koufi deposit.

Horizon 1: Smectite (M) + K-feldspar (M) + Pyrite (T) ± Kaolinite (T) ± Quartz (T)

Horizon 2: Smectite (M) + Plagioclase (Min) + Pyrite or Marcasite (T) ± Calcite (Min) ± Gypsum (Min) ± Quartz (T) ± Barytes (T).

Horizon 3: Smectite (M) + Plagioclase (Min) ± Pyrite (T).

Ano Komia deposit.

Lower Horizon: Smectite (M) + Quartz (M) + Calcite (M) + K-feldspar (Min) + Plagioclase (Min) + Kaolinite (T) + Mica (T) + Chlorite (T) + Pyrite (T) + Gypsum (T).

Higher Horizon: Smectite (M) + Opal C-T + Quartz (M) + K-Feldspar (Min) ± Mica (T).

Prassa deposit, Kimolos.

Zone 1: Glass.

Zone 2: Glass + Smectite.

Zone 3: Smectite + opal C-T.

Zone 4: Smectite + Plagioclase ± Quartz.

Zone 5: Smectite + Mordenite + K-feldspar ± opal C-T.

Zone 6: Smectite + opal C-T ± Mordenite ± K-feldspar.

heulandite/clinoptilolite of intermediate composition (see Section 4.1). The complete mineralogical profile of the deposit is depicted in Figure 4.3.

4.2.1.6. Ano Komia Deposit.

The two horizons observed in the quarry are characterized by different mineralogical assemblages. In the lower horizon the major phases are dioctahedral smectite, quartz and calcite. K-feldspar and plagioclase are minor minerals while kaolinite, gypsum, pyrite, mica and chlorite are present as accessory minerals. Kaolinite is present in variable amounts in the clay fraction ranging from 6 to 38%. There is a tendency for increasing of the kaolinite content from the lower to the higher horizons of the deposits. Since mica and chlorite are absent from the clay fraction i.e they are coarse grained. This implies that their source is the metamorphic basement. The abundance of calcite decreases towards the higher levels and towards the western sector of the deposit i.e towards the Areas where the S-activity is obvious. In the higher stratigraphic levels natroalunite is present while smectite is absent.

The higher white bentonite is dominated by the mineralogical assemblage dioctahedral smectite + opal-CT + quartz (major phases), K-feldspar (minor phase) + mica and kaolinite, which is consistent throughout the entire deposit. In places opal-C is present instead of opal-CT.

4.2.1.7. Kato Komia deposit.

The major mineralogical constituents of the deposit are dioctahedral smectite, opal-CT, quartz and calcite. K-feldspar, chlorite, mica + plagioclase are minor phases while gypsum and pyrite are present as trace minerals. Chlorite and mica are coarse grained and are probably derived from the metamorphic basement. Mica is absent from the clay fraction while chlorite participates with only 1.8%. Kaolinite constitutes 3-5% of the clay fraction, the rest being smectite. In the Area of the deposit which is affected by intense hydrothermal alteration (Plate 4), the mineralogical assemblage is different consisting of alunite + jarosite + opal-CT.

4.2.1.8. Garyfalakaina deposit.

Dioctahedral smectite and opal-CT are the main mineralogical phases. Quartz, K-feldspar and zeolites (clinoptilolite/heulandite and mordenite) are minor phases while plagioclase, kaolinite, gypsum, calcite, and pyrite are accessory phases. Zeolites vary systematically with depth, with clinoptilolite/heulandite predominating over mordenite in the higher stratigraphic levels of the deposit and being less abundant in the lower levels. On

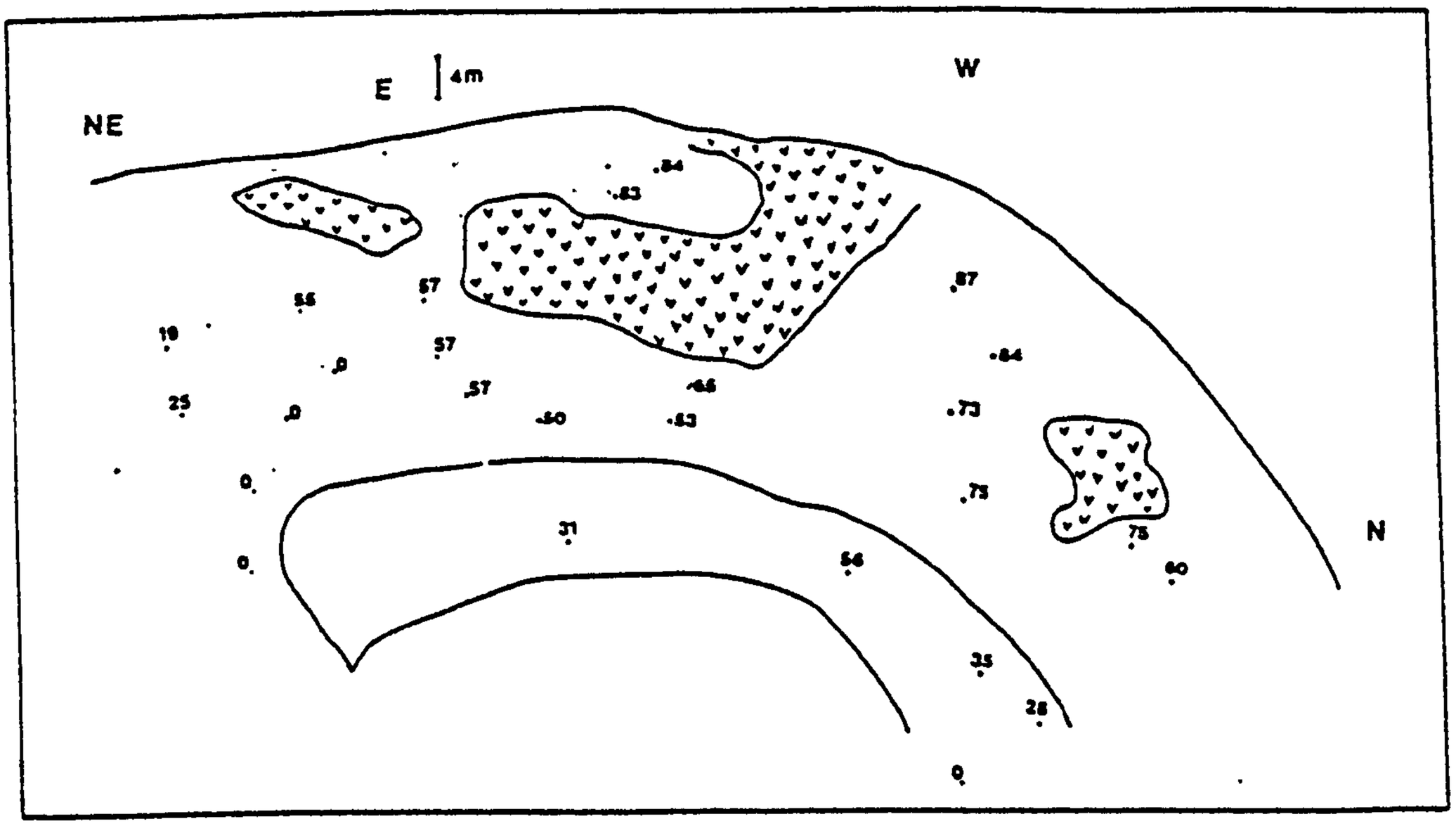

FIGURE 4.4a. Schematic representation of the distribution of illite/smectite in the Tsantili deposit, Milos. The numbers correspond to illite content.

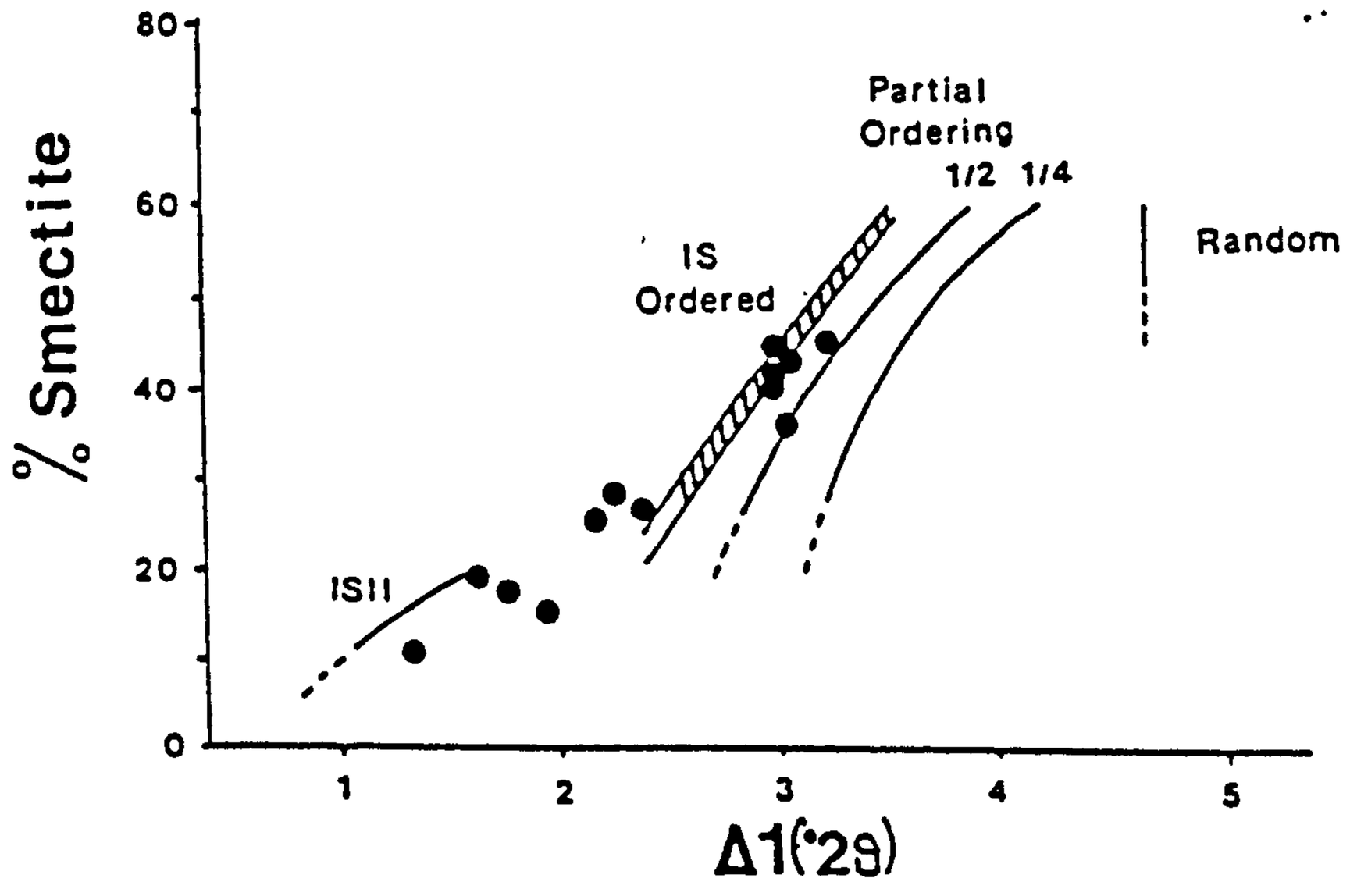

FIGURE 4.4b. Characterization of the ordering of the illite/smectites according to the methods of Srodon (1980).

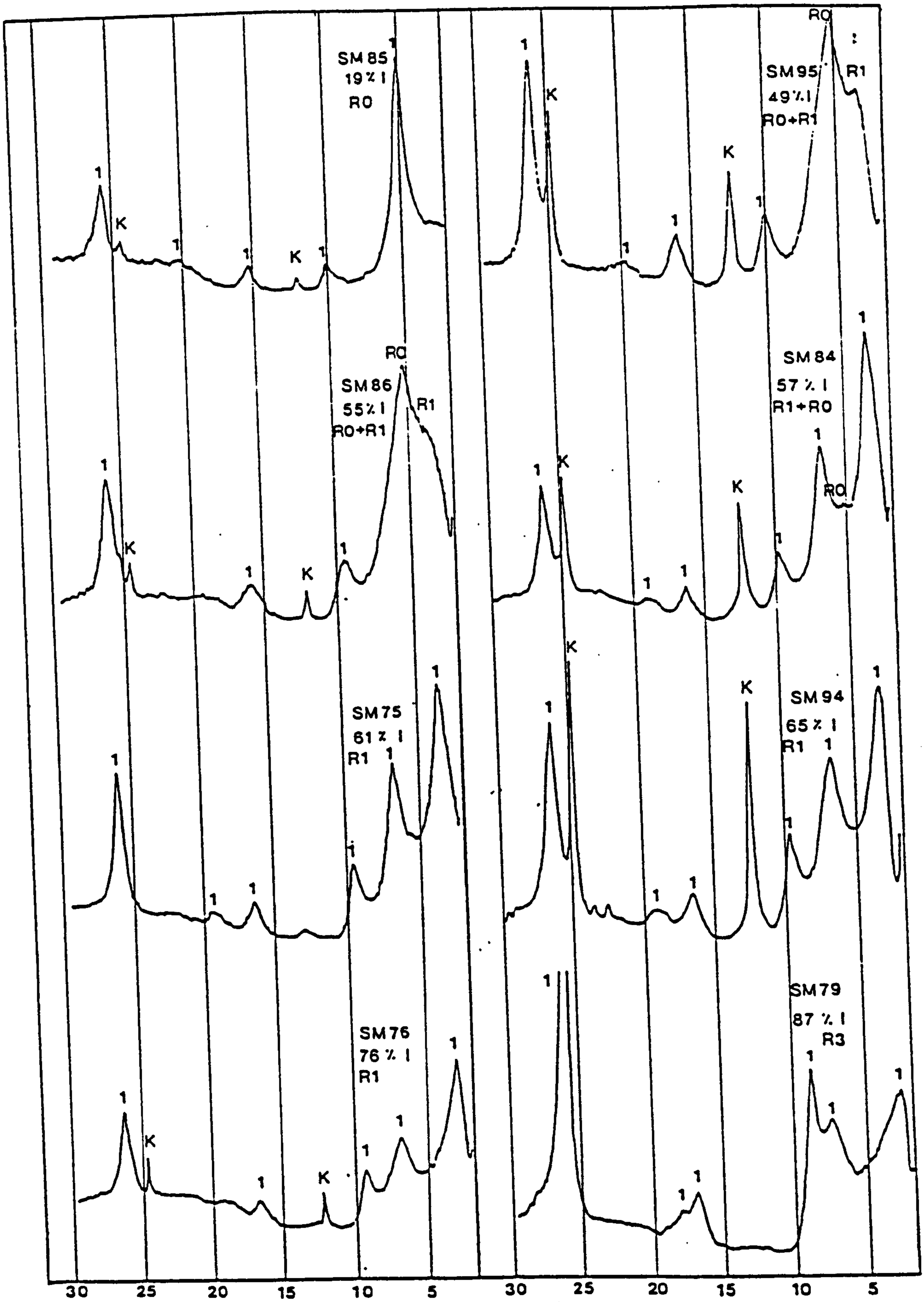

FIGURE 4.5. XRD traces of the less than 0.5μm fraction of the illite/smectites from the Tsantili deposit.

the other hand, mordenite follows the opposite trend being less abundant in the higher stratigraphic levels but predominating over clinoptilolite/heulandite in the lower levels of the deposit. The thermal stability of clinoptilolite/heulandite is indicative of intermediate composition (see Section 4.1). Calcite is abundant only in the higher stratigraphic levels, being absent from the base of the deposit. Gypsum is associated with kaolinite and occur in the lower levels of the southern face of the deposit. Kaolinite constitutes 15-29% of the clay fraction in the southern face of the deposit where it is present.

4.2.1.9. Mavrogiannis deposit.

The mineralogical asseblage is very similar t the Garyfalakaina deposit. Dioctahedral smectite, opal-CT and quartz are the major mineralogical phases present. K-feldspar is a minor phase while plagioclase, gypsum and mica are accessory minerals. Kaolinite occurs in traces (< 2% of the clay fraction). Zeolite minerals are absent. No particular mineralogical trend is displayed in the deposit.

4.2.1.10. Rema deposit.

The mineralogical assemblage is similar to those of the Garyfalakaina and Mavrogiannis deposits. Dioctahedral smectite and opal-CT are the major constituents, quartz and plagioclase are minor phases while K-feldspar, pyrite + marcasite + jarosite are accesory minerals. Fresh glass is also present. The main differences between this deposit and those of Mavrogiannis and Garyfalakaina which have similar characteristics are i) the lower abundance of K-feldspar and ii) the presence of fresh glass.

4.2.1.11 Kastriani deposit.

It is a poor kaolin deposit characterized by the predominance of opal-CT, quartz, alunite and kaolinite. It seems that the spacial relationship between alunite and kaolinite is reverse i.e the abundance of the former is associated with elimination of the latter. Halite is an accessory mineral occuring in places.

4.2.1.12. Agrilies deposit.

The major phases present are dioctahedral smectite and quartz. K-feldspar, kaolinite, gypsum, and white mica are minor constituents while jarosite, pyrite and/or marcasite are accessory phases. Mica is absent from the -2μm fraction. This implies either that it has been derived from the metamorphic basement or that it is the product of alteration

(sericitization) of feldspar. Christidis (1989) has shown that both explanations are possible. The possibility for igneous derivation is rejected because of the incompatibility of muscovite crystallization in volcanic and/or volcaniclastic rocks (Deer *et al.* 1962). In the northern part of the deposit the smectite has been converted to mixed-layer illite/smectite characterized by the coexistence of random and ordered interstratification. The abundance of kaolinite present varies between 3 and 54% of the clay fraction, the higher amounts being associated with the illitization of smectite.

4.2.2 Kimolos island.

4.2.2.1. Prassa deposit.

The deposit is characterized by the existence of 4 bentonite bodies, the larger of which is divided into six distinct zones (Fig. 4.3), each one representing a different mineralogical assemblage. The mineralogical zonation represents a horizontal transition from the fresh glass to a zeolite-rich white tuff. The first zone consists of fresh glass without any authigenic crystalline phase present. Only traces of halite are present in some sites. It is followed by a thin zone (30-50cm thick) characterized by the first appearance of smectite; the paragenesis being glass + smectite. The third zone is dominated by the assemblage smectite + opal-CT, the opal-CT being more abundant towards the previous zone. The thickness of this zone is 1.5-2m. After that the main smectite zone is developed. Smectite comprises 95-98% of the total mass of the rock, the rest being plagioclase and K-feldspar. Tiny monazite crystals are dispersed throughout the entire mass of the rock, while traces of baryte and gypsum were identified by electron microscopy. The smectite zone is followed by the development of the zeolite-bearing one characterized by the domination of the assemblage mordenite + smectite, which comprises 95% of the total mass of the rock. K-feldspar and/or opal-CT are accessory minerals. Baryte, gypsum and monazite are present as trace phases. The zeolite-bearing zone is followed by an opal-CT-rich zone dominated by the assemblage smectite + opal-CT ± mordenite ± K-feldspar.

4.2.2.2. Loutra deposit.

Smectite and plagioclase are the major mineral phases present, while quartz, clinoptilolite (according to thermal stability criteria) and opal-CT are minor phases. Fresh glass is also present. The relative amount of the silica phases varies from site to site with the opal-CT occasionaly becoming a major phase, and in some extreme cases the only phase present.

4.2.2.3. Fanara deposit.

Two different mineral assemblages are present corresponding to the different bentonites horizons observed. The volcanic conglomerate which evolves to volcanic sand (see chapter 3) is dominated by the assemblage smectite + quartz with K-feldspar and plagioclase being minor mineral phases. Kaolinite is present occcasionaly at the higher stratigraphic levels, close to the silicified overlying rocks constituting 18-25% of the clay fraction. In lower levels it is present in amounts less than 3%.

The white bentonite is dominated by the assemblage smectite + opal-CT, with K-feldspar being a minor phase. This assemblage is consistent throughout the entire mass of the rock.

4.2.2.4. Bonatsa deposit.

Smectite + plagioclase + opal-CT are the major minerals present, while quartz and clinoptilolite occur as minor phases. In many Areas volcanic glass is abundant because the original perlitic lava has not been devitrified completely.

4.2.2.5. Agios Tryfon Area.

The characteristic of this deposit is the development of a transition zone from bentonite to kaolin. Two different mineral assemblages can be distinguished in this transition zone; the former having kaolinite + quartz ± gypsum ± opal-CT as major constituents and smectite as a minor one, and the latter having kaolinite + alunite + quartz major mineral phases and opal-CT a minor one. The first assemblage is representative of smectite rich part of the transition zone while the second corresponds to the kaolinite-rich part. Kaolinite varies from 13% of the clay fraction in the smectite-rich Area to 76% in sites in proximity of the kaolinite zone, becoming the only phase of the clay fraction in this zone.

4.2.3. Chios Island.

The bentonite deposit close to the Thymiana Village is dominated by two mineralogical assemblages: the first having smectite, dolomite and opal-CT as minor phases and quartz, plagioclase ± calcite as minor ones and the second with smectite, quartz and plagioclase as major components, chlorite, mica and serpentine as minor components and talc ± dolomite as trace minerals. Aragonite and amphibole are occasionally present. The first assemblage occurs in the lower parts of the deposit while the second is characteristic of the higher parts. It is also observed in the overlying red clay bed. Chlorite and mica are detrital minerals because although they are abundant in the bulk sample they are present

in very small amounts in the clay fraction, the former ranging between 1-5.5% and the latter between 0 and 1.5% of this fraction.

4.2.4. Characteristics of the K-feldspars present.

The XRD-traces of the K-feldspars present in the deposits of Tsantili, Koufi, Ano Komia, Garyfalakaina, Mavrogiannis and Rema (Milos) fit well with those of high-sanidine (JCPDS Card 25-618). They plot in the high-sanidine-orthoclase area (Fig 4.6) in the diagram of Wright (1968). They all are monoclinic and using the criteria of Wright (1968) in most cases they are classified as anomalous K-feldspars (*i.e* the 2θ value of the 201 peak obtained from the diagram in Figure 4.6, agrees within 0.1° 2θ with the 2θ value directly measured on the XRD trace). Examination under the optical microscope revealed that their size is very small, while SEM observation revealed that they are euhedral-subhedral (see next sections). Similar observations were made by Sheppard & Gude (1973) for authigenic K-feldspars. It seems that the feldspars from each individual deposit tend to plot in a particular area in the diagram. It can be seen that the K-feldspars from the Areas 1 and 2 (Tsantili, Koufi and Agrilies deposits) plot in the field between orthoclase and high sanidine, while those of Area 3 close to the high-sanidine corner. However the K-feldspars from Ano Komia deposit plot close to those from the deposits of Areas 1 and 2.

On the other hand, the K-feldspars occuring in the andesitic lava of Zoulias deposit (horizon 1 in Fig 4.3) as well as the Prassa quarry (Kimolos) show different X-Ray patterns being identical to those of sanidine (JCPDS card 19-1227).

4.2.5. Investigation with I.R Specroscopy.

4.2.5.1. Theoretical concepts.

Infrared Radiation is electromagnetic radiation the region of which extends from about 1μm to about 100μm. In infrared spectroscopy the number of waves per cm (wavenumber (cm^{-1})) or Kyser unit is used: $v(cm^{-1})=10000/l(\mu m)$. Hence, 1μm=10000 cm^{-1} and 100μm= 100 cm^{-1} (van der Marel & Bautelspacher 1976). The infrared region is divided into three sectors, the near-infrared, the middle-infrared and the far-infrared.

Since the magnetic conponent of the electromagnetic radiation has very low energy, it is the electric component which is used in I.R. Spectroscopy. The applications of this technique take into account the fact that the atom-members of chemical bonds in the various molecules undergo vibrational and/or rotational transitions. Rotational vibrations have very low energy and occur only in gases. Therefore in the case of clay minerals and other silicates the vibrational transitions are of prime importance. However, from the total

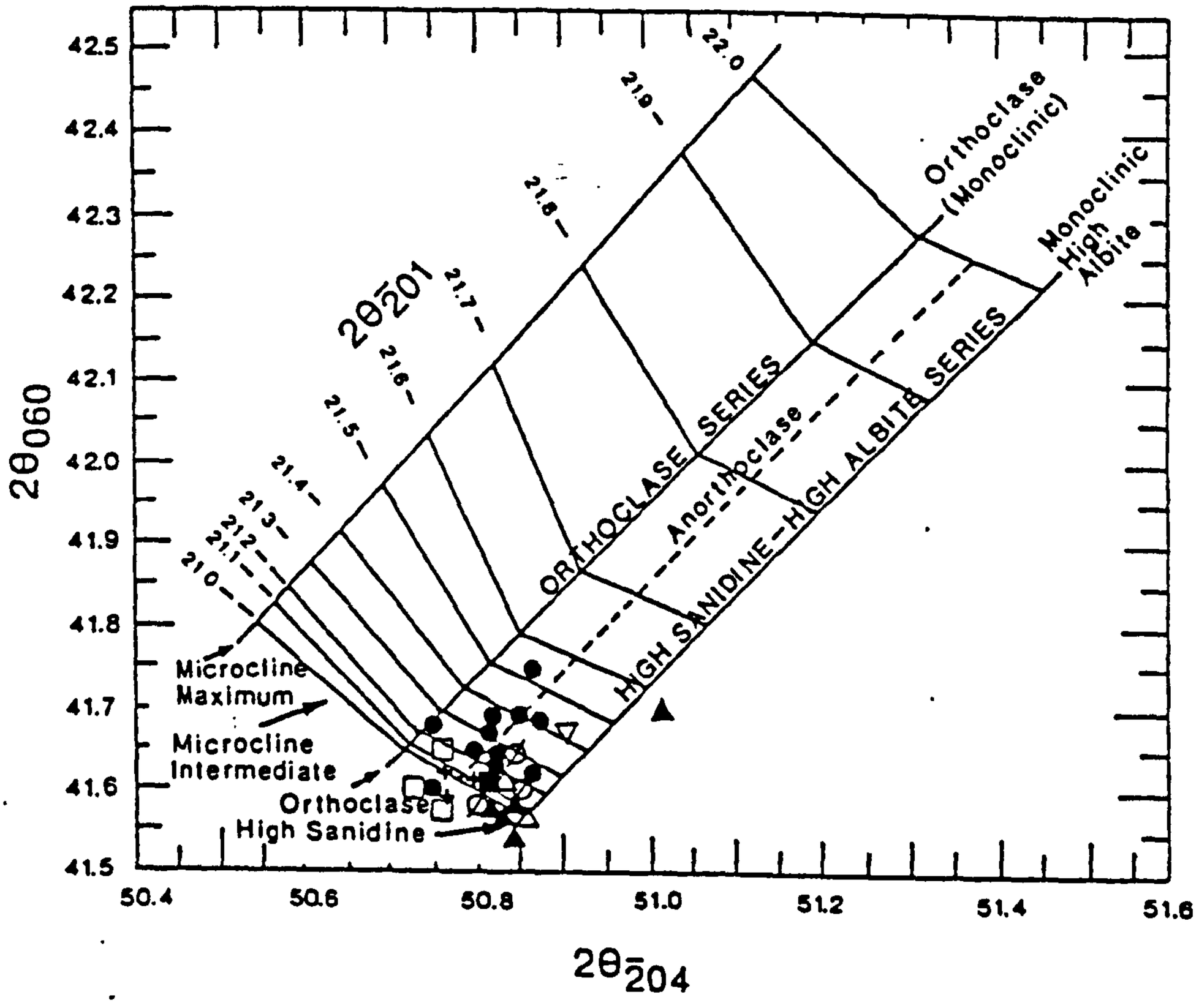

● Tsantili Deposit
+ Kouji -//-
□ Agrilles -//-
▲ Garyfalakena -//-
■ Kato Komia -//-
ø Ano Komia -//-
△ Mavrogiannis -//-
▽ Rema -//-

FIGURE 4.6. Projection of the K-feldspars from the Greek bentonite deposits on the diagram of Wright (1968).

number of vibrations only those that undergo change in dipole moment during the absorption process are active in the infrared.

The absorption of infrared radiation by clay minerals depends on atomic masses, and the lengths, strengths and force constants of interatomic bonds, and is controlled by the overall symmetry of the unit cell as well as the local site symetry of each atom in the unit cell (Russell 1987). The total number of potentially active vibrations is $3n$-6 where n is the number of atoms in the unit cell. When a molecule characterised by active vibrations is irradiated with I.R. radiation it absorbs radiation. Absorption will be maximum when the axis of the bond is parallel to the electric vector of the beam and minimum when the two axes are perpendicular. There are two types of infrared active vibrations, the stretching and the deformation vibrations. The former are of higher energy due to existence of large stretching forces. Therefore they are observed at higher wavenumbers than the corresponding deformation vibrations. There are several types of deformation vibrations namely bending or scissoring, wagging, rocking and twisting (van der Marel & Beutelspacher 1976).

4.2.5.2. I.R. Investigation of the Greek smectites.

The infrared spectra of the -2μm fractions of the samples examined are depicted in Figure 4.7. The allocation of the absorption bands to certain type of bonds was carried out based on information from the work of Farmer & Russel (1964, 1967), Farmer (1968, 1974, 1979), van der Marel & Beutelspacher (1976) and Russel (1987).

i) **Smectites from Area 1, Milos.** The samples examined come from the deposits of Tsantili (SM100), Aspro Horio (SM114 and SM117) and Zoulias (SM228). The spectra of all the smectites have very similar characteristics. The band at 3630 cm^{-1} corresponds to AlAlOH and AlMgOH stretching. The two bands are not resolved in accordance with the data of Farmer (1968, 1974, 1979) and Russel (1987), although Russel & Fraser (1971) and van der Marel & Beutelspacher (1976) assign an absorption band at 3687 cm^{-1} to AlMgOH stretching. The bands at about 3420 cm^{-1} and 3240 cm^{-1} correspond to absorption from the interlayer water (Farmer & Russel, 1967, Farmer, 1979, van der Marel & Beutelspacher, 1976). The former band has been assigned to hydrogen bonding between H_2O molecules in the interlayer region, while the latter is not certain whether it corresponds to a still stronger hydrogen bond or it is simply an overtone of the HOH angle deformation band occuring between 1630 and 1635 cm^{-1} (Farmer & Russel 1967). The band at 1430 cm^{-1} which is present in the samples SM100 amd SM114 belongs to calcite.

The broad absorption area present between 750 and 1200 cm^{-1} provides information about lattice stretching vibrations as well as OH-bending vibrations. The band at about 1110 cm is assigned to Si-O (out of plane) vibration, while the broad band at about 1040 cm^{-1} to Si-O-Si (in plane) vibrations. According to Farmer & Russel (1964, 1967), Farmer

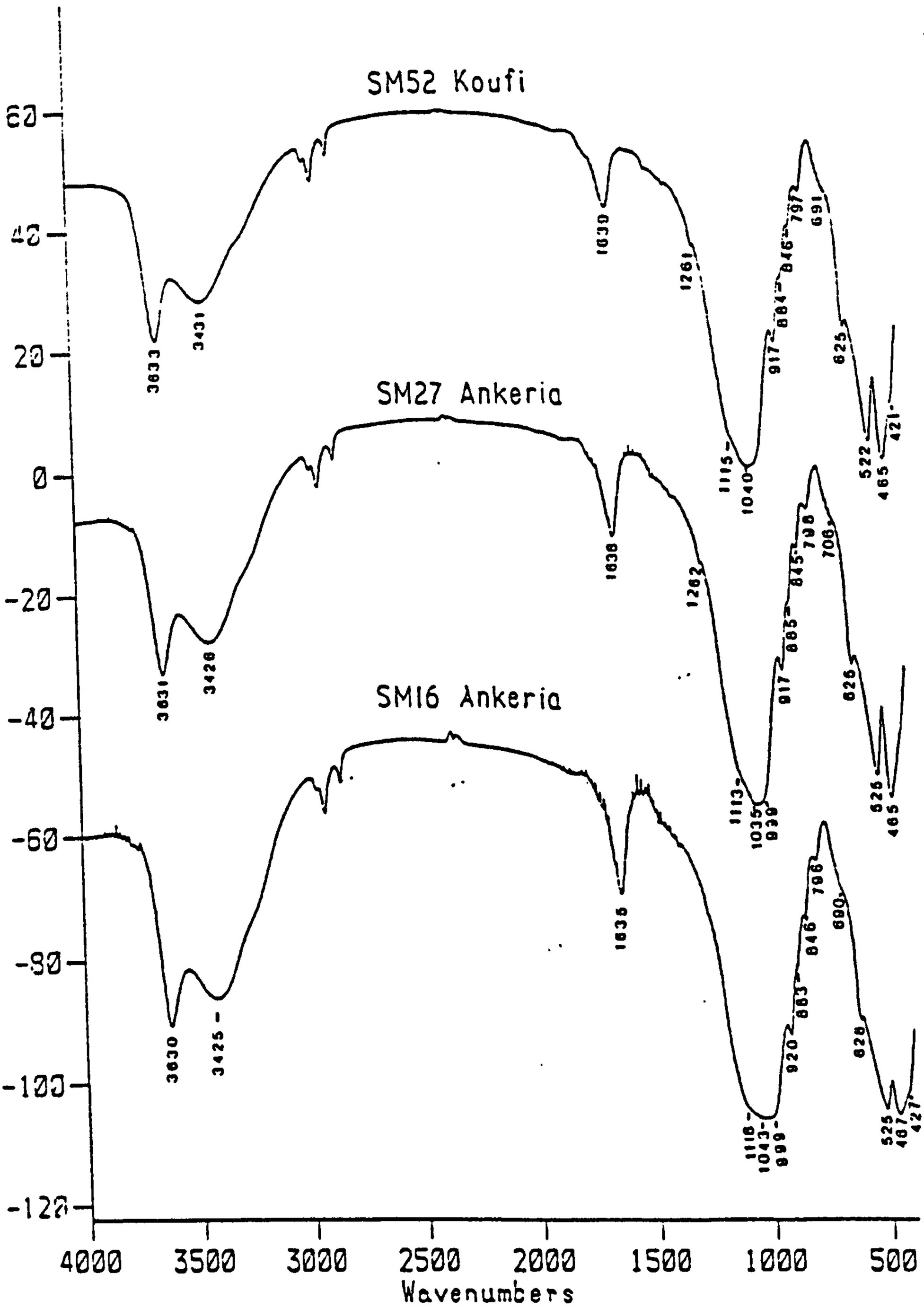

FIGURE 4.7. Representative Infra Red Spectra of the less than 2μm fraction of the Greek bentonites

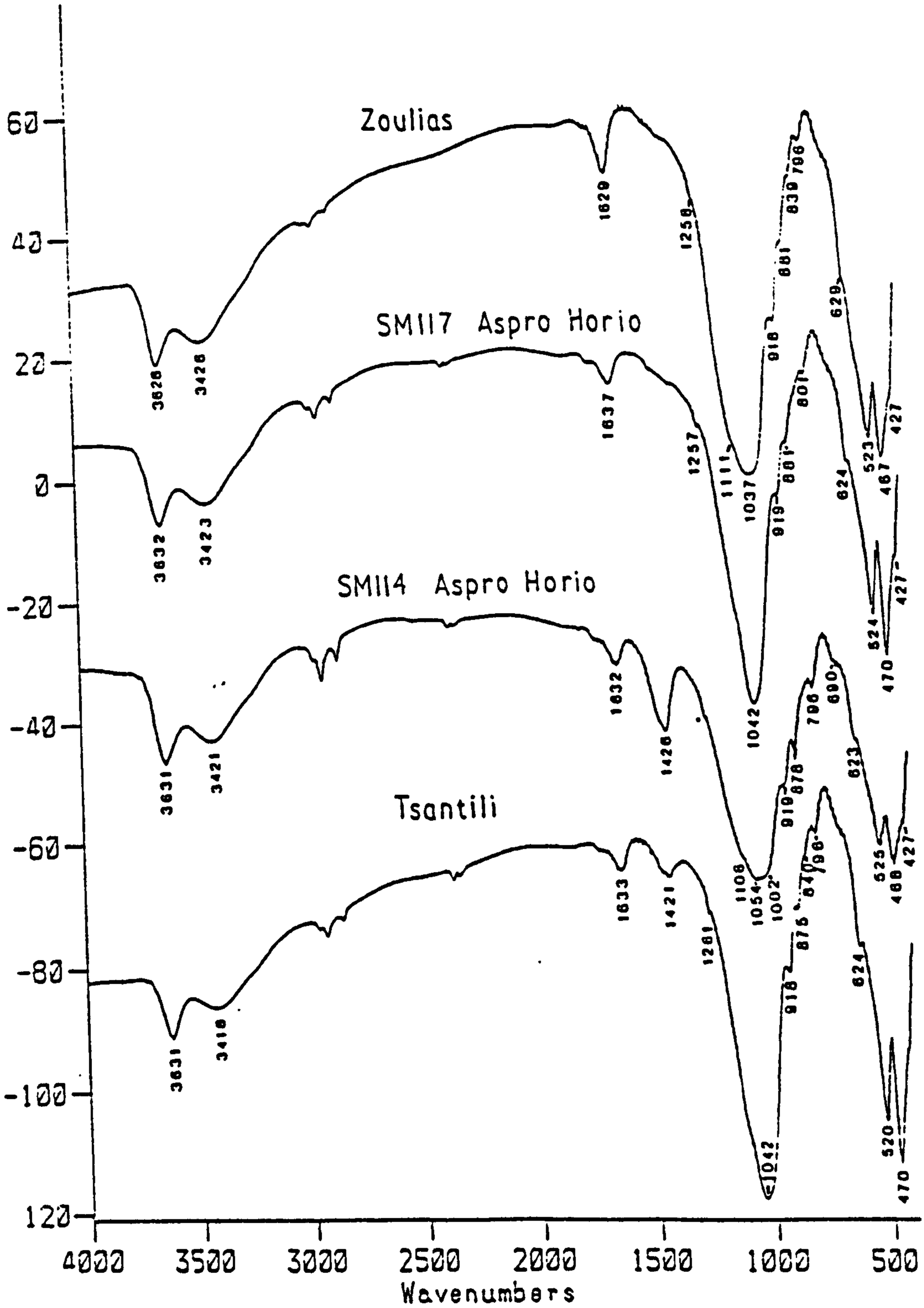

FIGURE 4.7 (continued). Representative Infra Red Spectra of the less than 2μm fraction of the Greek bentonites

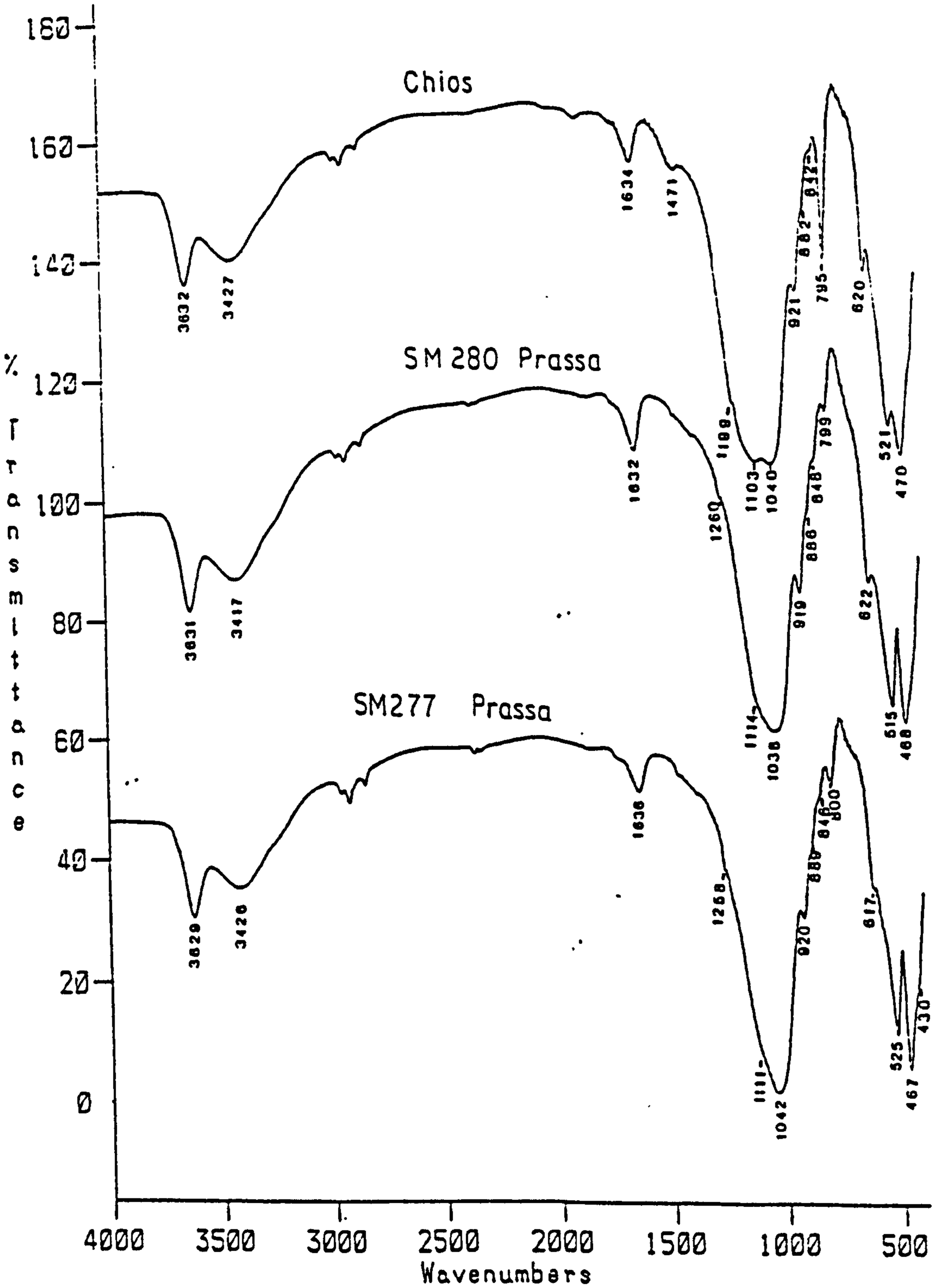

FIGURE 4.7 (continued). Representative Infra Red Spectra of the less than 2μm fraction of the Greek bentonites.

(1968, 1974, 1979), and van der Marel & Beutelspacher, (1976), there are two Si-O-Si stretching vibrations, which however were not resolved. The distinct bands at 918, 875-880 and 840 cm^{-1} correspond to AlAlOH, $AlFe^{3+}OH$ and AlMgOH bending vibrations respectively. In the samples SM100 and SM114 it is highly possible that there is also interfence from calcite in the region of 870-880 cm^{-1}. However, this interference must not be very significant especially in SM114 because the intense $AlFe^{3+}OH$ deformation band is escorted by a decrease of the intensity of the AlAlOH band implying an increased Fe^{3+} for Al^{3+} substitution. The band at about 800 cm^{-1} should be assigned to a silica form, either tridymite or cristobalite present in the clay fraction, or to an AlMgOH deformation vibration (van der Marel & Beutelspacher, 1976).

The bands below 700 cm^{-1} have been assigned to lattice vibrations involving both tetrahedral and octahedral cations coupled by OH vibrations. Hence, the shoulder at 695 cm^{-1} might correspond to Al-O-Si (in plane) vibrations (van der Marel & Beudelspacher, 1976), or to the silica phase (Farmer, 1979). The band at 620-625 cm^{-1} might belong to Al-OH (perpenticular) vibration (Farmer & Russel, 1964, van der Marel & Beutelspacher, 1976). Another possibility is that it belongs to Al-O stretching and Si-O deformation (Farmer, 1979). The bands at 525 and 468 cm^{-1} are assigned to Si-O-Al and Si-O-Mg coupled by OH vibrations (Farmer & Russel, 1964, Farmer 1974, 1979, van der Marel & Beutelspacher, 1976). Finally, the band at 427 cm^{-1} has been assigned to Si-O bending vibrations.

ii) **Smectites from the Area 2, Milos.** The infrared spectra come from the samples SM16 and SM27 from Ankeria deposit and SM52 from Koufi deposit. As it can be seen in Fig 4.7 there are two major differences between the smectites from the two areas:

1) Increased intensity of the AlAlOH band and the subsequent decrease of the AlFeOH band at 920 and 875 cm^{-1} respectively in the smectites of the Area 2. This implies a decreasing substitution of Fe^{3+} for Al^{3+} in the smectites of the Area 2.

2) Increased intensity of the AlMgOH band in the smectites of Area 2 compared to those of Area 1. This in turn implies increasing Mg for Al^{3+} substitution in the smectites from Area 2.

3) Increased intensity of the band at 625 cm^{-1} (possibly Al-OH perpenticular vibration) in the smectites of Area 2.

The aforementioned information imply that the smectites from Area 1 possess characteristics which are typical of Wyoming montmorillonites, while those of Area 2 of Cheto montmorillonites.

iii) **Smectites from Area 3 and the deposit of Agrilies.** The infrared spectra of these smectites are similar to those of smectites from the previous Areas (Fig. 4.7). The important features of these smectites which are distinct from those from the previous Areas are the following:

1) Abundance of a silica phase in the clay fraction which might be either disordered tridymite or disordered cristobalite (intense band at 795-800 cm^{-1}).

2) Almost complete (entirely complete in SM246) elimination of the band at 875-880 cm^{-1}, which implies small scale Fe^{3+} for Al^{3+} substitution. This is coupled with the very small band at 845 cm^{-1} (MgAlOH bending) implying a smectite which is very rich in Al. From the spectra obtained the beidellitic character of the material is not obvious because of lack of the band at about 830 cm^{-1} due to Al-O out of plane vibrations. An exception to that is the sample SM246 with a small band at 825 cm^{-1}. However the existence of a distinct peak at 740-750 cm^{-1} (Al-O-Si in plane vibration characteristic of beidellite) in SM246 and SM235 implies that small amounts of beidellite might coexist with an Al-rich montmorillonite. Taking into account the small substitution of both Fe^{3+} amd Mg for Al^{3+} it follows that the montmorillonite might be a Tatatilla-type one.

3) The bands ay 3693 and 3647 cm^{-1} present in the sample SM246 (Agrilies deposit) belong to kaolinite (Farmer & Russell, 1964, 1967, Farmer, 1968, 1974, 1979, van der Marel & Beutelspacher, 1976, Russell, 1987) which is abundant in this deposit (see Section 4.2.1.12).

iv) **Smectites from Prassa deposit (Kimolos) and Chios.** The infrared characteristics from Prassa deposit (Kimolos) and Chios have similar characteristics to those of the other smectites examined (Fig. 4.7). The absorption bands are assigned in a similar way to that in the previous samples. In SM325 the weak band at 880 cm^{-1} might be due to the presence of dolomite (band at 1442 cm^{-1}) because the Fe^{3+} for Al^{3+} substitution is very limited as this will be shown in the following sections.

The low abundance of Fe^{3+}, the abundance of Mg (MgAlOH vibrations at about 845 cm^{-1}) and the lack of the characteristic bands for beidellite at 830 and 750 cm^{-1} imply that the smectites present might be Cheto-type montmorillonites.

4.2.6. Investigation using thermal techniques (DTA and TG).

Thermal techniques have been used successfully in the past to acquire qualitative as well as quantitative (especially when different methods are combined together) information about clay materials. The thermoanalytical techniques used for mineralogical investigations are: Differential Thermal Analysis (DTA), Differential Thermal Calorimetry (DSC), Thermogravimetry (TG), Evolved Gas Detection/Analysis (EGD/EGA) and Thermodilatometry, Electrical Conductivity, Thermoluminescence, and decripitation. In the present study a combination of DTA and TG was used to obtain information about the changes occuring during the heating of smectite rich material. This will provide an indication about the durability of the various bentonites, which is very important for applications in the foundry industry (Alther 1991). The combined DTA/TG/ curves of the -

2μm fractions of the samples examined are presented in Figure 4.8. The clay fractions used belong to the same samples analysed by Infra-Red Spectrometry. The main characteristics of the thermodiagrams obtained can be summarized in the following points:

1) The removal of the interlayer water takes place in two steps, the first at 115-130^{o}C and the second at 200-215^{o}C. In the samples SM277 and SM280 there is an intermediate step at about 150^{o}C. These temperature ranges are well within the known limits of interlayer water loss i.e 100-250^{o}C (Paterson & Swaffield, 1987).

2) After the complete loss of interlayer water, the gradual increase of temperature up to the dehydroxylation point is coupled by a gradual water loss recorded in the TG curves (Fig. 4.8). This event has been attributed to the fact that not all adsorbed or interlayer water is lost before the dehydroxylation reaction begins (Schultz, 1969). This is observed only when interlayer cations with high hydration energy are present (MacKenzie, 1970). The point where the dehydroxylation reaction begins is considered to be at the midpoint of the inclined plateau (Schultz, 1969). This point is different for the various smectites examied in this study. The smectites from Area 1 exhibit the lowest temperature for the midpoint, which varies between 335 and 350^{o}C. In Area 2 this temperature varies between 360 and 405^{o}C, while in Area 3 between 360 and 425^{o}C. In Agrilies deposit (SM246) the midpoint of the plateau was recorded in the lowest temperature (320^{o}C) due to either kaolinite or beidellite. Finally, smectites from Kimolos and Chios gave plateau-midpoint temperatures similar to those of the Areas 2 and 3. The fact that the smectites from Area 1 have plateau-midpoint temperatures up to 90^{o}C lower than that of the smectites from Areas 2,3 in Milos and those of Kimolos and Chios, means that in the **raw** state they begin to loose their structural water faster. This might affect their durability adversely.

3) The dehydroxylation temperatures of the smectites examined are within the reported values for "ideal" or "normal" montmorillonite (Greene-Kelly, 1957, Schultz, 1969, MacKenzie, 1970). It is known that beidellite (non ideal beidellite of Schultz) gives its main dehydroxylation reaction at about 550-600^{o}C (Greene-Kelly, 1957, Schultz, 1969, MacKenzie, 1970) although Paterson & Swaffield (1987) reported a dehydroxylation temperature close to 700^{o}C. In the sample SM246 a small curvature at 548^{o}C might indicate the presence of beidellite (non ideal beidellite after Schultz, 1969) or/and kaolinite as this has already be shown by infrared methods in the previous section. The temperatures of the major dehydroxylation process were found to be between 715 and 730^{o}C, except for the samples SM114 and SM228 (Aspro Horio and Zoulias deposit respectively) at which the loss of hydroxyls took place between 685 and 690^{o}C. At the same samples the rapid water loss corresponding to the major dehydroxylation reaction was initiated at considerably lower temperatures compared to the other smectites. In other words the inclined plataeu is smaller in these smectites. It is interesting that although smectites from the SM117 and the SM100 (Aspro Horio and Tsantili deposit respectively)

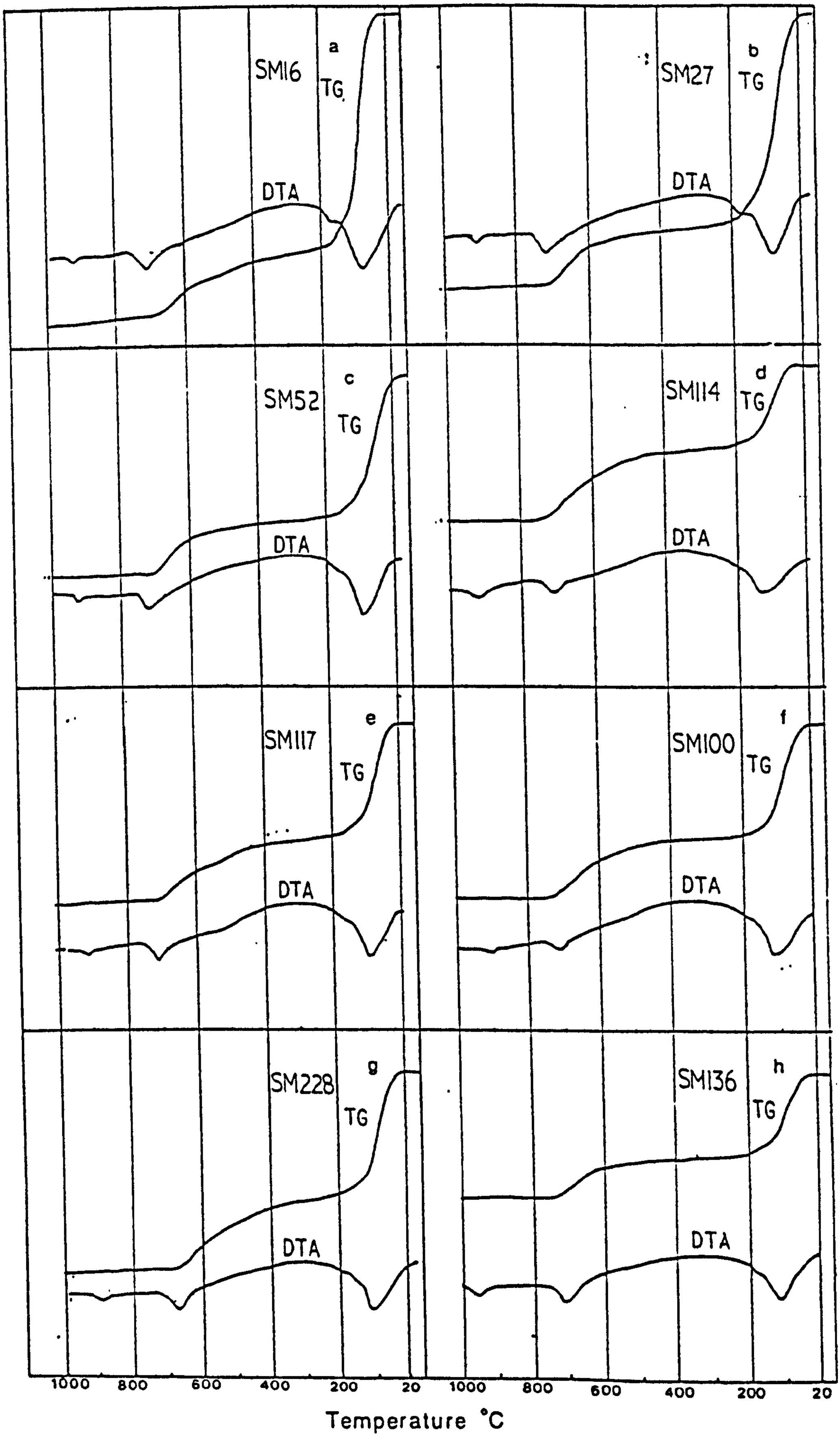

FIGURE 4.8. Representative thermograms of the less than 2μm fraction of the Greek bentonites.

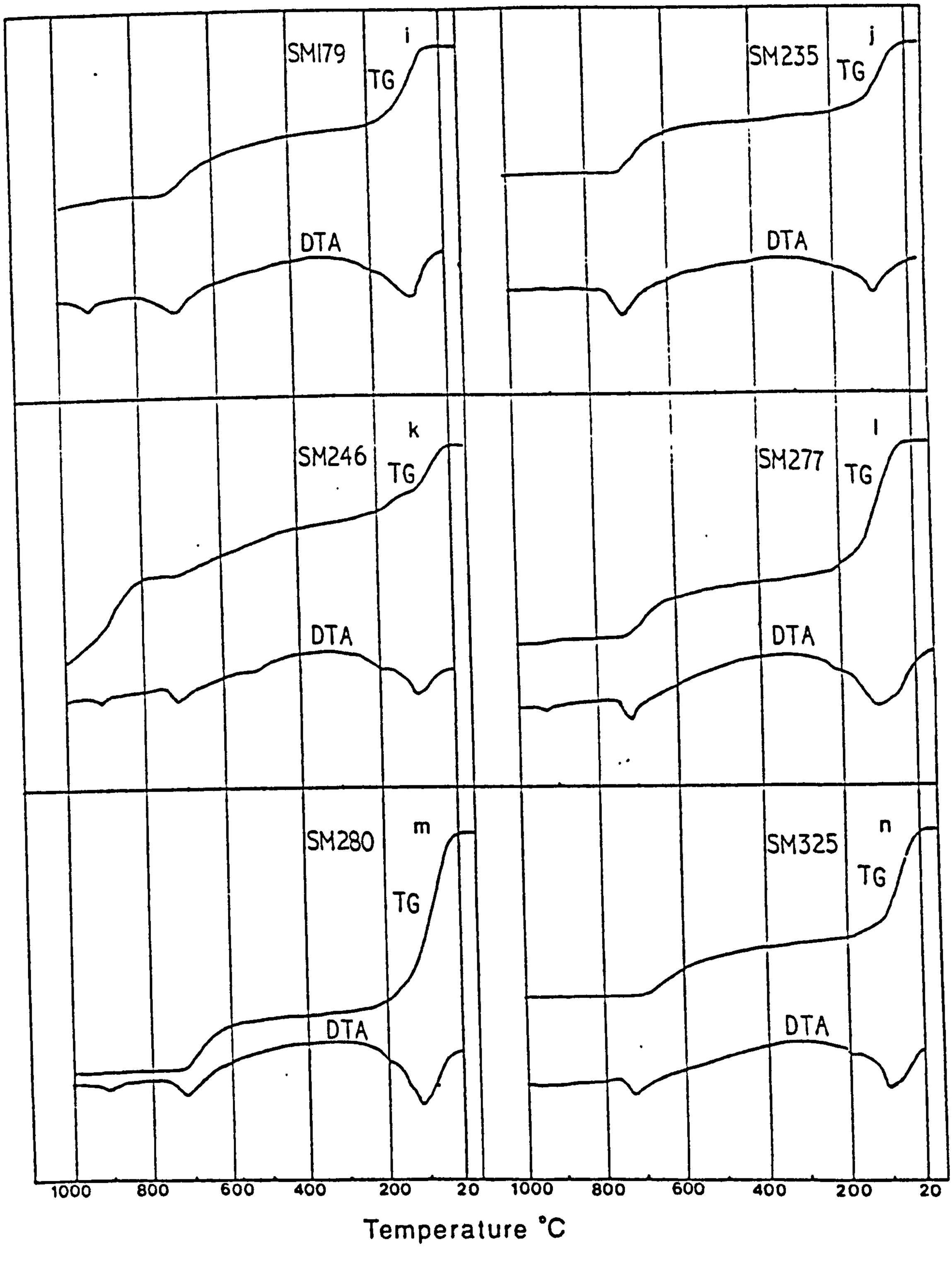

FIGURE 4.8. (continued). Representative thermodiagrams of the less than 2μm fraction of the Greek bentonites. Key to the symbols: Milos bentonites: a,b=Ankeria deposit, c=Koufi deposit, d,e=Aspro Horio deposit, f=Tsantili deposit, g=Zoulias deposit, h=Ano Komia deposit, i=Kato Komia deposit, j=Rema deposit, k=Agrilies deposit. Kimolos bentonites: l,m=Prassa deposit, n=Chios bentonite.

have a similar inclined plateau as the smectites in the samples SM114 and SM228, their major dehydroxylation reaction takes place at a higher temperature (Fig. 4.8).

4) The third endothermic peak at about 900°C has been attributed to the complete destruction of the smectite structure (Greene-Kelly, 1957, MacKenzie, 1970). According to Earley *et al.*, (1953) it represents the absoption of heat during the conversion from a relatively ordered anhydrous state to a disordered amorphous material. This amorphous material constitutes the substrate for the formation of other crystalline phases at higher temperatures (Greene-Kelly 1957, Grim & Kulbicki, 1961). In the samples studied this endothermic peak is weak and occured between 900 and 940°C, while in SM136, SM235 and SM325 the peak did not appear at all. Also the exothermic peak which follows the third endothermic one was not observed. These temperatures are relatively higher than those reported in the literature (see Greene-Kelly, 1957, Schultz, 1969, MacKenzie, 1970, Paterson & Swaffield, 1987). However, there are some smectites which gave their third exothermic peak well above 900°C, like the Texas smectite (MacKenzie & Gaillere, 1979). Moreover, in the detailed work of Schultz (1969) only Wyoming-type montmorillonites gave a weak third endothemic peak at 900 ± 10°C. However, he used considerably lower heating rates (5°C/min instead of 10°C used in this study). It is well known that a decrease in heating rates causes a decrease in the temperature a particular peak is recorded (Holdridge & Vaughan, 1957). Also, Paterson & Swaffield (1987) published DTA thermodiagrams of montmorillonites lacking both the third endothermic peak and the subsequent exothermic peak. It seems therefore that the thermal characteristics of the Greek smectites are not uncommon.

4.2.7. Morphological characteristics of the major authigenic phases present in the Greek bentonites.

The investigation of the morphological and textural characteristics of the authigenic phases occuring in the Greek bentonites was based on observations with SEM and TEM techniques.

4.2.7.1. SEM observations.

a) **Smectite.** Smectite crystals are present in the form of wavy flakes, forming characteristic honeycomb textures very often (Plate 12). No systematic relationship between the smectite morphology and the location of the flakes (*i.e* in the edges or the interior of the glass shards) was found although Konta (1985) has suggested the existence of better developed flakes in the margins of the altered shards. In the deposit of Bonatsa (Kimolos) an iron-rich smectite (possibly nontronite) was determined, having different

morphological characteristics than the other smectites. The flakes are elongated and their length is greater compared to that of the common smectites found (Plate 12). The smectite crystals have been formed mainly at the expense of volcanic glass through the formation of a poorly crystaline phase (Plate 12). The alteration of the glass to smectite has led to characteristic pseudomorphic textures over the parent glass (Plate 12). Similar textures have been reported by Khoury & Eberl (1979) and can be explained by the model of Dibble & Tiller (1981) (see Section 6.1). The formation of smectite through a protocrystalline phase has been reported by Banfield & Eggleton (1990) during the weathering of feldspars. On the contrary, Banfield *et al.*, (1991a) did not observe any intermediate phase during the formation of smectite from weathering of plagioclase. Smectite was also found to form at the expense of pyrogenetic feldspars, both plagioclase and K-feldspar (Plates 13, 17) in agreement with Banfield & Eggleton (1990) and Banfield *et. al.*, (1991a).

The most common authigenic phases associated with smectite are K-feldspar and opal-CT. Alteration of smectite has given rise to kaolinite, halloysite and mixed-layer illite/smectite (Plates 13, 15). Formation of kaolinite at the expense of smectites has been reported by Morgan *et. al.*; (1979) in some English bentonites.

b) **Opal-CT.** Opal-CT occurs in two different types of crystals (Plate 14). One is characterized by spherulitic crystals considered to be a diagenetic by-product formed by co-precipitation during the formation of smectites. The second forms axiolitic crystals and is considered a direct product of the devitrification of the vocanic glass. Coexistence of two types of opal-CT have been reported by Moncure *et. al.*, (1981). In the Area 3 of Milos opal-CT has been transformed to other silica phases like cristobalite or more commonly quartz.

c) **Illite/smectite.** Observations were made in the deposit of Tsantili where a transition from smectite to illite smectite takes place. The mixed-layer phase occurs in the form of both flakes and laths (Plate 15). The illitization process causes two main texture modifications on the original smectite flakes:

i) Flattening of the original curly smectite flakes and

ii) Formation of illite/smectite laths from expandabilities as high as 75%.

Keller *et. al.*, (1986) reported the existence of illite/smectite ribbons only at very low expandabilities close to the pure illite member (12% smectite). This work showed that lath-like illite/smectites are formed at lower expandabilities in good agreement with the TEM observations (Inoue *et. al*, 1988, also see following Sections in this work). They also found that illitization proceeds causing flattening of the smectite flakes and subsequent formation of scallops at the edges of the flakes. These observations are in close agreement with the findings of this work. It is also interesting that the formation of the lath-like illite/smectites seems to take place through an "amorphous-like" phase (Plate 15), thus implying a neoformation process. This will be discussed thoroughly in Chapter 6. Although, in several

examples K-feldspar has been replaced by I/S (Plate 15) it seems that it was not the main provider of K during illitization confirming the observations made from XRD investigation. Illite/smectite is often associated with kaolinite.

d) **Kaolinite/halloysite.** They both form at the expense of smectite or illite/smectite in most cases. An exception to this tendency is the kaolin deposit of Kastriani where there is no obvious precursor for the kaolinite present. Kaolinite is present in the form of well crystallized flakes often with pseudohexagonal habit, forming "books" in places (Plate 13). Halloysite is present in Aspro Horio deposit in the form of small, well- formed, needle-like crystals derived from alteration of smectite (Plate 13). On the contrary, the kaolinite occuring in Kastriani deposit is present in the form of tiny, subhedral crystals which do not form "book"-like aggregates (Plate 13).

e) **K-feldspar.** Two types of K-feldspars were distinguished during the electron microscopy work. One is anhedral-subhedral occuring in relatively large (greater than 30μm in size), corroded crystals embedded in a smectite groundmass (Plate 17) while the second is characterized by small (< 15μm), fresh, euhedral, monoclinic crystals occuring in pore spaces (Plate 14) or/and lining dissolution cavities formed by the dissolution of volcanic glass (Plate 17). The first type has a pyrogenetic origin, while the second is authigenic.

f) **Mordenite.** It was found in the islands of both Milos and Kimolos. It is easily recognized by its fibrous habit although it resembles erionite (Mumpton & Ormsby, 1976). However the latter was not identified by XRD investigation. The fibres have a length/width ratio greater than 50. Three types of mordenite have been recognized in Prassa deposit (Kimolos):

-One characterized by relatively short fibres not more than 10μm long which originate from an amorphous material, possibly an aluminosilicate gel (Plate 16). This confirms the findings of Mariner & Surdam (1970) but not those of Noh & Boles (1989), who suggested that the Al-Si-gel which formed after the dissolution of the original glass gave rise to authigenic K-feldspar.

-A second type characterized by well formed long fibres which in many occassions have been deposited over the smectite substrate (Plate 16). This mode of occurence is also present in Milos island (Garyfalakaina and Ankeria deposits).

-The third morphologic type develops vertical to pore spaces and cavities linking the two parts of the dissolved cavity.

In the deposit of Garyfalakaina (Milos) some mordenite might have been formed at the expense of clinoptilolite in places (Plate 16).

g) **Clinoptilolite/heulandite.** It occurs in the form of small "coffin-type" crystals which are always found in cavities among the altered shards, obviously formed from dissolution of those shards (Plate 16). Occasionally, they are present as pore linings. In the deposit of Garyfalakaina (Milos) it might have been replaced by mordenite.

4.2.7.2. TEM observations.

a) **Smectite.** Smectites are present mainly in the form of subhedral particles (S-type smectites after Güven & Pease, 1975), especially in Milos island. However, lath-shaped (L-type particles) or even euhedral particles (E-type crystals) with polygonal outlines (Güven & Pease, 1975, Grim & Güven, 1978) are present in both Milos and Kimolos islands (Plate 18). In Kimolos the euhedral crystals form foliated and compact-lamellar aggregates (Grim & Güven, 1978) which exhibit face-to-face association (Plate 18). The lath-shaped smectites have been formed mainly by gentle folding of the edges of thin lamellae, although crystals with long unfolded edges are not uncommon. The thickness of the smectite crystals in Kimolos Island was not determined. In Milos the L-shaped smectites have thicknesses ranging from 30 to 50Å. Güven & Pease (1975) found that similar lath-shaped particles were 20Å thick. The subhedral smectites have thicknesses which range between 30 and 90Å. The distribution of the thickness of smectite particles is depicted in Figure 4.10. It can be seen that 30Å was the minimum thickness found for the population examined. The average thickness was 44.5Å ± 11.7Å (Table 4.2). It seems therefore that single smectite particles 10Å thick, were not separated in **pure smectitic** materials. This is in accordance with the findings of Güven (1974), and Güven & Pease (1975), but not with Mering & Oberlin (1971) and Nadeau *et al.*, (1984a,b) who presented 10Å thick particles. The reason for this difference might be attributed to different sample prepararion methods, since in this work the samples were not saturated with sodium. The influence of sample preparation was clearly demonstrated by Güven & Pease (1975). It is interesting that 10Å particles were isolated in random interstratified illite/smectites from the same deposit, using similar separation techniques. This fact is further discussed in Chapter 7.

The other dimensions of smectite particles range between 0.1 and 1.2μm (length) and 0.05 and 0.55μm (width), where length is the maximum and width the minimum dimension of each particle measured (Table 4.2). These values are well within the limits reported by other workers (Mering & Oberlin, 1967, 1971, Güven, 1974, Güven & Pease, 1975, Grim & Güven, 1978).

b) **Illite/smectite.** They occur in the form of both laths and flakes (Plate 19). The abundance of laths increases towards lower expandabilities. An exception to this trend is the sample SM84 which I/S displays ordered R1-type interstratification with 43% expandables but is dominated by flaky particles. Such an existence of flaky I/S crystals has been mentioned recently by Rosenberg *et al.* (1990), and it seems to contradict the suggestion of Inoue *et al.* (1987, 1988) about the relationship between lath-shaped and flaky I/S particles. This sample differs from the others in that it contains abundant kaolinite. The role of kaolinite in the transformation of illite to smectite will be examined in Chapter six.

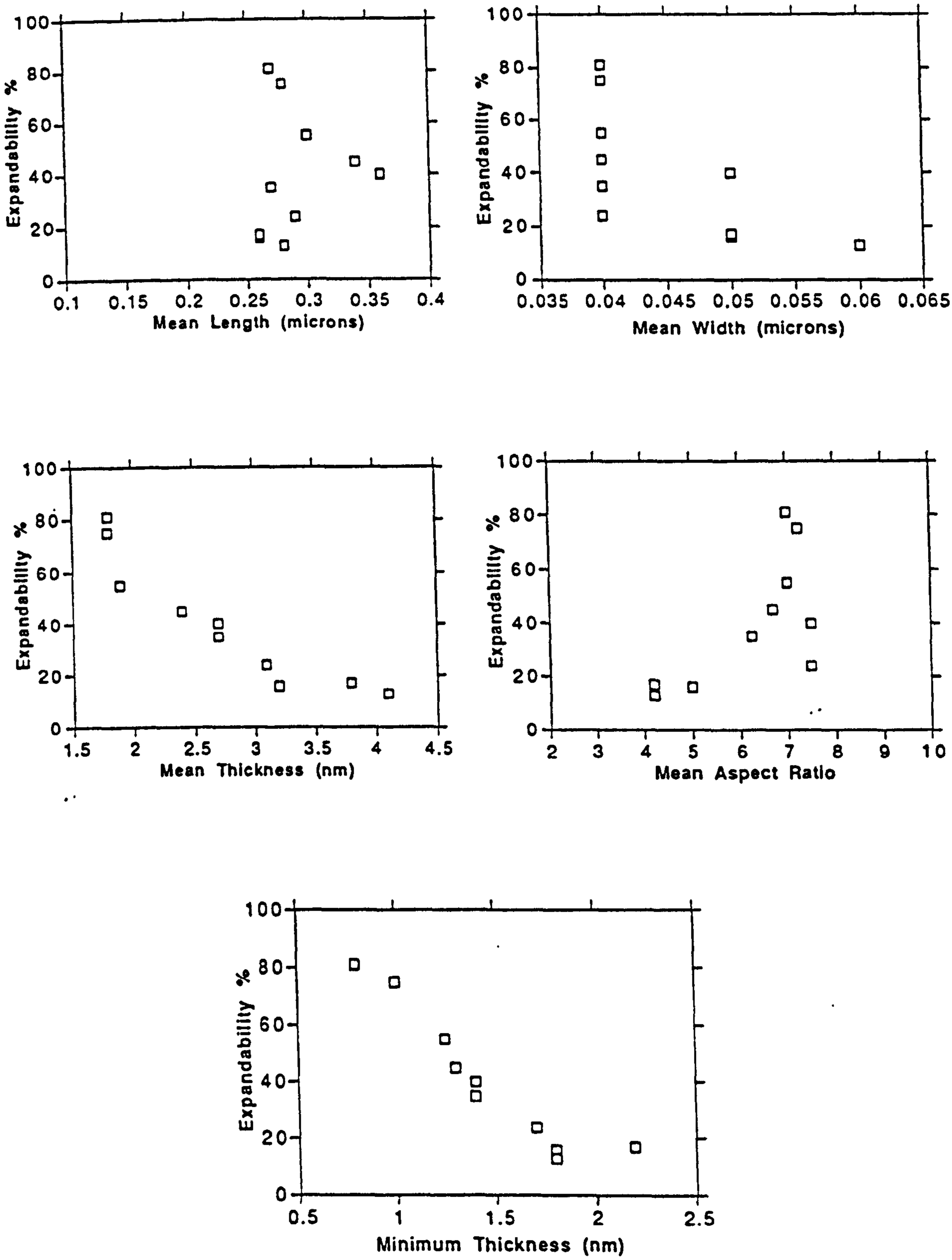

FIGURE 4.9. Evolution of the dimensions of the illite/smectite particles with decreasing expandability. Note the continuous increase of the minimum thickness with increasing illite content.

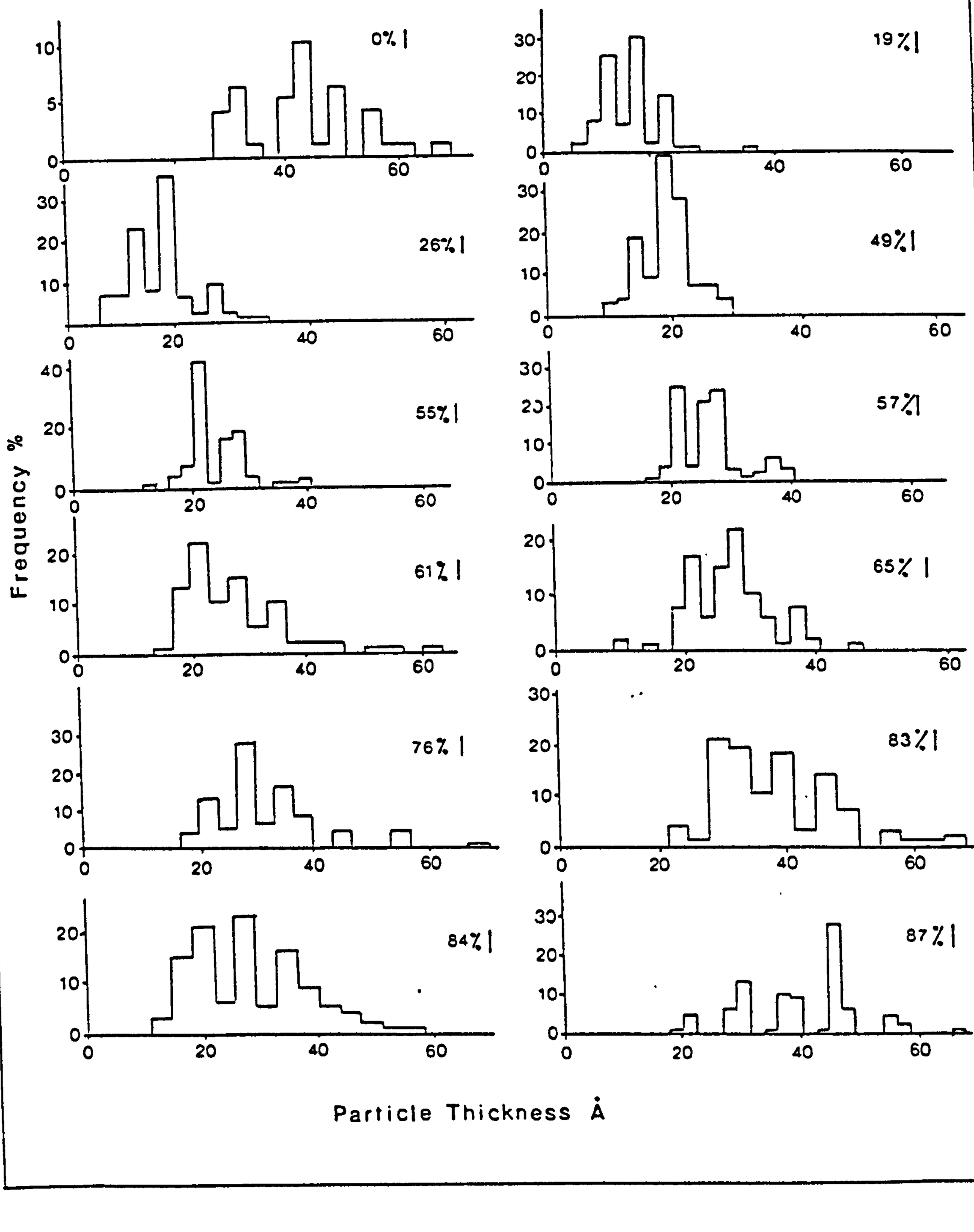

FIGURE 4.10. Histograms showing the distribution of thickness of the illite/smectites and smectites from the Tsantili deposit. Note the maxima at multiples of 10Å. The minimum thickness of the smectite particles is 30Å.

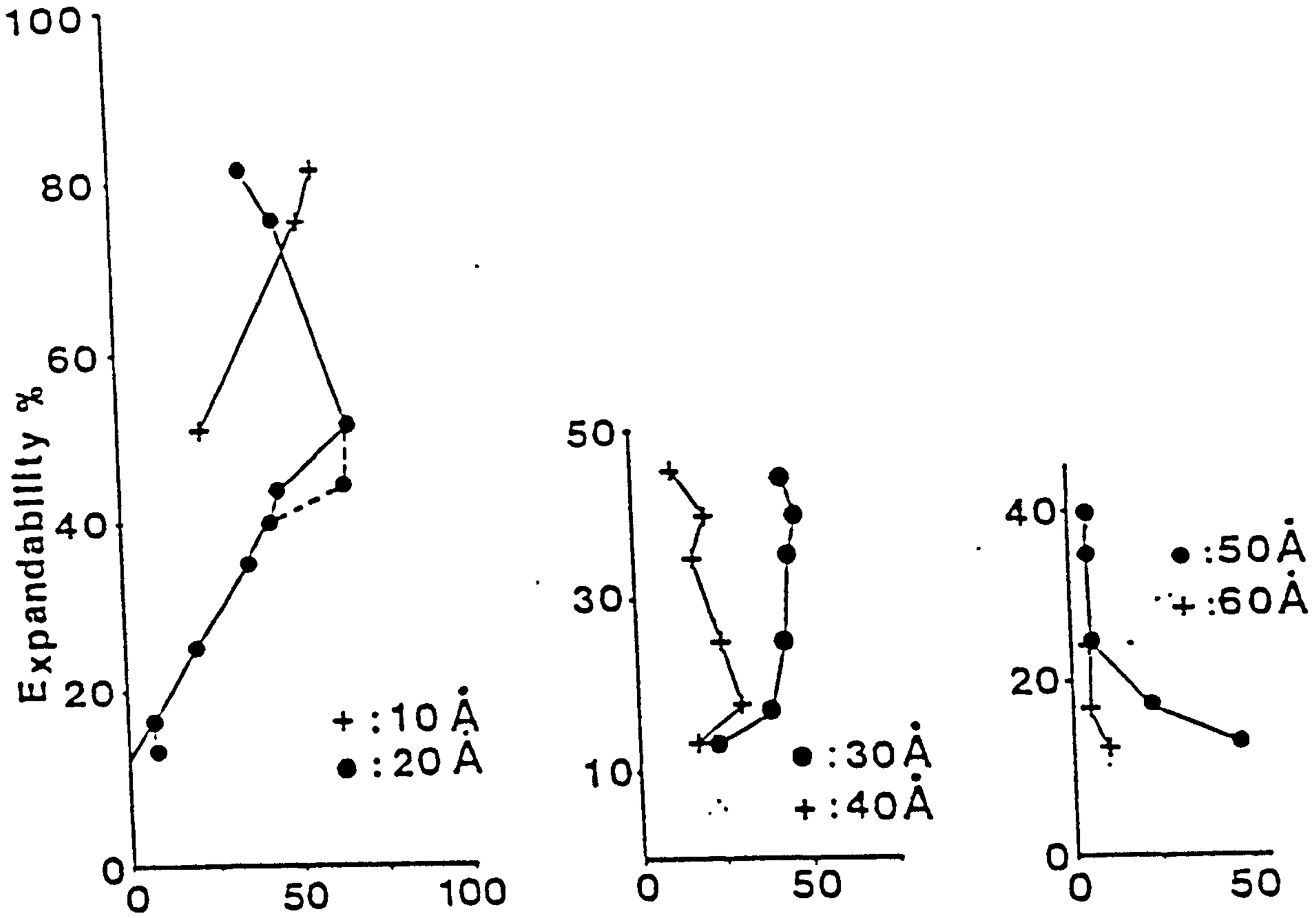

FIGURE 4.11. Evolution of the abundance of the illite/smectite particles having various thicknesses with decreasing expandability. Note that only the population of the 50Å and 60Å thick particles increases continuously.

Table 4.2

Size measurements for smectite particles. Length and width measurements are from smectites from the Prassa deposit, Kimolos and thickness from smectites from the Tsantili deposit Milos. SM259 and SM277 are from the smectite + mordenite zone, while SM278 from the smectite zone. Length and width are in microns while thickness in nanometres.

Dimension	SM93	SM259	SM277	SM278
Average Length	- -	0.44	0.31	0.31
Std. Deviation	- -	0.17	0.13	0.16
Minimum Length	- -	0.12	0.13	0.11
Maximum Length	- -	1.04	0.85	0.94
Average Width	- -	0.27	0.16	0.18
Std. Deviation	- -	0.12	0.06	0.08
Minimum Width	- -	0.08	0.06	0.08
Maximum Width	- -	0.98	0.48	0.56
Average thickness	4.45	- -	- -	- -
Std Deviation	1.17	- -	- -	- -
Minimum thickness	2.76	- -	- -	- -
Maxim Thickness	8.92	- -	- -	- -
No. of particles	42	222	208	233

Table 4.3.

Size (length, width and thickness) measurements of the illite/smectite particles present in the Tsantili deposit, Milos. Length and width are in microns and thickness in nanometers. Expandability refers to the percentage of smectite present in the I/S according to the methods of Srodon (1980).

Dimension	SM75	SM76	SM78	SM79	SM82	SM85	SM86	SM91	SM94	SM95
Expandability	40	24	16	13	17	81	45	74	35	51
Mean Length	0.36	0.29	0.26	0.28	0.26	0.27	0.34	0.28	0.27	0.30
Std Deviation	0.15	0.15	0.13	0.13	0.11	0.11	0.14	0.12	0.12	0.16
Min. Length	0.09	0.07	0.07	0.07	0.09	0.09	0.12	0.07	0.03	0.08
Max Length	0.88	1.04	0.82	0.81	0.87	0.65	0.90	0.77	0.70	1.41
Mean Width	0.05	0.04	0.05	0.06	0.05	0.04	0.04	0.04	0.04	0.04
Std Deviation	0.02	0.02	0.01	0.02	0.02	0.01	0.01	0.01	0.01	0.02
Min Width	0.02	0.01	0.01	0.02	0.02	0.02	0.03	0.01	0.01	0.02
Max Width	0.12	0.19	0.08	0.20	0.13	0.09	0.09	0.10	0.07	0.10
Mean Aspect Ratio	7.20	7.25	5.20	4.70	5.20	6.75	7.60	7.00	6.75	7.50
Mean Thickn	2.70	3.10	3.20	4.10	3.80	1.80	2.40	1.80	2.70	1.90
Std Deviation	0.89	0.93	0.83	1.20	0.99	1.70	0.44	0.46	0.61	0.40
Min Thicknes	1.40	1.70	1.80	1.20	2.20	0.80	1.30	1.0	1.40	1.20
Max Thickn	6.20	6.70	5.80	8.50	7.80	3.50	3.90	3.20	4.70	2.90
Particle No	142	228	157	208	214	159	183	158	170	126

The results from statistical analyses of length, width, thickness and aspect ratio (length : width ratio) of I/S particles of different expandabilities are listed on Table 4.3, while the change of each dimension with increasing expandability is depicted in Figure 4.9. The histograms of thicknesses are shown in Figure 4.10. It is obvious that the total number of thickness measurements can be subdivided into distinct populations with mean thickness multiples of 10Å. This is especially true when the precision of the method applied is taken into account. The mean and mode thickness of the particles increase with increasing expandability. In Figures 4.11and 4.9 it can be observed that with decreasing expandability:

a) The abundance of 10Å thick particles decreases steadily. They disappear completely when the character of interstratification becomes ordered.

b) The abundance of 20Å thick particles increases steadily up to the point where the character of interstatification changes from random to ordered and then decreases almost linearly. Extrapolation of the straight line to 0% 20Å particles gives 12% expandability. It is clear that the I/S with random interstratification are composed of 10Å and 20Å thick particles the relative proportion of which changes reversibly with increasing expandability, in full accordance with Nadaeu *et al.* (1985a).

c) The 30Å thick I/S particles appear at 45% expandables. Their existence in SM86 which is characterized by both random and ordered interstratification must be connected with the ordered I/S layers. Their abundance is nearly constant down to 25% expandables and then decreases suddenly.

d) The population of 40Å particles increases steadily up to about 25% expandables and then suddenly decreases.

e) The population of the 50Å particles is constant up to 25% expandables and then increases suddenly. The 60Å particles are absent at expandabilities higher than 25% increasing steadily. It follows that only particles thicker than 50Å are stable and do not dissolve.

f) The minimum thickness of the illite/smectite particles increases with decreasing expandability (Fig. 4.9).

The mean length of the particles increase steadily up to 50% expandability and then decrease steadily. The maximum mean length coincides with the appearance of ordering in the interstratification. The mean width remain virtually constant until about 20% expandability and then increase rapidly, in accordance with the results of Inoue *et al.*, (1988). It follows that as illitization proceeds the illite/smectite particles become more equant. The hexagonal illite crystals observed by Inoue *et al.* (1988) and Lanson & Champion (1991) close to the illite end were observed at lower expandabilities in this study (Plate 19).

4.2.7.3. HRTEM observations.

The smectite used for HRTEM observation comes from the deposit of Aspro Horio, Area 1, Milos. It is a Wyoming-type montmorillonite (see following section). The lattice fringe images obtained clearly show parallel smectite layers, compact, without disruptions (Plate 20). Similar images for Wyoming montmorillonites from Upton, USA were obtained by Vali & Köster (1986). The thickness of the individual smectite layers varies. In photo 1 (Plate 20) expanded layers about 17Å thick (dark fringes) and about 13Å thick (bright fringes) are present. The thickness of the dark fringes is unreasonably high for untreated smectites. However, it is well known (Guthrie & Veblen, 1989) that the image obtained from HRTEM is highly dependable on the experimental conditions and the type of the electron microscope used; therefore the dark fringes are not the 2:1 layers and should be viewed as "lattice fringes" (Guthrie & Veblen, 1989).

In photo 2 (Plate 20) spacings ca. 11Å (dark fringes) and 10Å (bright fringes) were obtained. These values could be regarded as values corresponding to a collapsed smectite structure. However, the black or white fringes cannot be assigned to the 2:1 layers as mentioned before.

4.3. Mineral chemistry.

4.3.1. Cation assignments in the structural formulas of the authigenic phases.

a) **Smectite** The structural formula of smectites was calculated on an 11 oxygens basis (half unit cell) corresponding to an $O_{10}(OH)_2$ unit cell. The tetrahedral sites were assumed to have 4 cations. All Si cations were assigned to tetrahedral sites, the remaining filled with Al (Al^{IV}). The remaining Al cations were assigned to octahedral sites (Al^{VI}). Iron was assumed to be ferric and was entirely assigned to octahedral positions. Octahedral assignment was assumed also for Mg, although it is known (Foster, 1951, Weaver & Pollard, 1973, Christidis, 1989) that Mg may also be present in interlayer sites. Ca, Na and K were assigned to interlayer sites.

b) **Zeolites.** The structural formula of clinoptilolite/heulandite was calculated on a 72 oxygen basis, while that of mordenite on a 48 oxygens basis. In zeolites, Si and Al are the framework elements, while alkalies and alkaline earth elements occupy the exchangeable sites in open channels and cavities, balancing the charge deficiency generated from the substitution of Al for Si (Mumpton, 1977, Gottardi & Galli, 1985). The structural formulas were controlled with the Error Factor (Gottardi & Galli, 1985), defined as follows:

$$E\% = [(Al+Fe)-Na-K-2(Ca+Mg+Ba+Sr)]/[Na+K+2(Ca+Mg+Ba+Sr)] \times 100.$$

Analyses with E >10% were discarded as imbalanced following the instructions of Gottardi & Galli (1985).

4.3.2. Mineral Chemistry of smectites.

4.3.2.1. Milos island

The bentonites of Areas 1 and 2 (deposits of Aspro Horio, Tsantili, and Zoulias and Ankeria and Koufi respectively) have been formed at the expense of intermediate rocks while those of Ano Komia, Kato Komia Garyfalakaina, Mavrogiannis, and Rema from acidic rocks (see chapter five). Representative microanalyses and structural formulas of smectites from Milos deposits are presented in Table 4.4, while the full set of microanalyses is given in Appendix 4.5. It is obvious that the Greek smectites show large chemical and subsequently structural variation even within the same sample.

4.3.2.1.1. Smectites derived from intermediate glassy rocks (Areas 1 and 2).

They are characterized by a well determined negative relationship between Al and the other octahedral cations (Fig 4.12), which is well shown in the relationship between Fe^{3+} amd Al^{VI}. Such a relationship although expected has not been reported so far. Grim & Güven (1978) and Güven (1988) reported the lack of relationship between Fe^{3+} and Al^{VI}, while Weaver and Pollard (1973) reported a weak negative relationship. The negative relationship observed between Mg and Al^{VI} is in accordance with the data provided by Grim & Güven (1978), Güven (1988) and Weaver & Pollard (1973). Smectites from Zoulias deposit do not follow that trend but display a rather constant Mg content over a range of Al^{VI} values. It seems also that the slope of the line which describes the negative relationship between Al^{VI} and the other octahedral cations is different in the various deposits.

The relationship between Mg and Si does not show a constant pattern (Fig 4.13). These elements display a clear, although relatively weak, positive relationship in Area 2 except for the sample SM16 where no particular relationship is observed, and a lack of any relationship in Area 1. Smectites from the sample SM228 (Area 1) show a different behaviour having a good negative relationship between Mg and Si. It seems therefore that in Area 2 decrease of the tetrahedral charge is accompanied by an increase of the octahedral charge confirming the assumption of Weaver and Pollard (1973). However, this is not the case in Area 1, especially in the Zoulias deposit (SM228) where the opposite trend is implied. A similar lack of a particular trend is is observed between Fe^{3+} and Si (Fig 4.13). Although a positive trend is is observed in Area 2 no particular trend is present in Area 1. An exception to these trends is displayed by sample SM228 (Area 1) in which a weak positive trend is visible and by sample SM16 where Fe^{3+} varies considerably over a long range, with Si remaining essentially constant.

Table 4.4

A selection of microprobe analyses and structural formulae of smectites

Key to the codes:

BMA1=Horizon 2 in the Ankeria deposit (see Fig. 3.8) (Milos).

BMAN=Horizon 4 in the Ankeria deposit (Milos).

BMKF=Main bentonite horizon in the Koufi deposit (Milos).

BMK1=Lower bentonite horizon in the Koufi deposit (Milos).

BMTS=Tsantili deposit (Milos).

BMAH=Aspro Horio deposit (Milos).

BMZL=11th horizon of the Zoulias deposit (see Fig. 3.8) (Milos).

BMRM=Rema deposit (Milos).

BMRS=Mavrogiannis deposit (Milos).

BMAK=Lower bentonite horizon in theAno Komia deposit (Milos).

BMA2=Higher bentonite horizon (white bentonite) in the Ano Komia deposit (Milos)

BMGF=Garyfalakena deposit (Milos).

BKPR=Prassa deposit (Kimolos)

BKLT=Loutra deposit (Kimolos).

BCHT=Chios bentonite.

Table 4.4

A selection of microprobe analyses and structural formulae of smectites

Sample	SM16	SM16	SM16	SM16	SM25	SM25	SM25	SM25	SM43	SM43	SM43	SM43
Quarry	BMA1	BMA1	BMA1	BMA1	BMAN	BMAN	BMAN	BMAN	BMKF	BMKF	BMKF	BMKF
SiO_2	57.01	53.52	55.03	56.05	57.24	55.66	59.27	59.23	58.78	55.76	55.89	56.47
Al_2O_3	21.51	18.19	19.11	22.61	25.14	18.93	22.28	20.89	20.72	23.91	27.17	25.33
Fe_2O_3	1.63	5.08	4.59	0.76	0.88	5.81	2.90	5.17	6.12	2.28	2.33	1.58
MgO	4.47	3.90	4.21	3.65	3.48	4.42	4.72	4.88	3.54	2.93	2.67	2.46
CaO	1.65	1.52	1.78	1.26	1.54	1.88	1.79	2.41	1.20	1.39	1.30	1.33
Na_2O	0.45	0.54	- -	0.41	0.49	0.56	0.51	0.81	0.49	0.46	0.42	0.43
K_2O	0.24	0.51	- -	- -	0.26	0.31	- -	0.28	- -	0.24	- -	- -
Total	86.96	83.26	84.72	84.74	89.03	87.57	91.47	93.67	90.85	86.97	89.78	87.60
Structural formulae based on 11 oxygens												
Si	3.85	3.84	3.85	3.85	3.76	3.81	3.82	3.79	3.85	3.77	3.65	3.76
Al^{IV}	0.15	0.16	0.15	0.15	0.24	0.19	0.18	0.21	0.15	0.23	0.35	0.24
Octahedral cations												
Al^{VI}	1.56	1.38	1.43	1.68	1.71	1.34	1.51	1.36	1.44	1.67	1.75	1.75
$Fe3^{+}$	0.08	0.27	0.24	0.04	0.04	0.30	0.14	0.25	0.30	0.12	0.11	0.08
Mg	0.45	0.42	0.44	0.37	0.34	0.45	0.45	0.47	0.35	0.30	0.26	0.24
VI Cations	2.09	2.07	2.11	2.09	2.09	2.09	2.11	2.07	2.09	2.08	2.12	2.08
Interlayer cations												
Ca	0.12	0.12	0.13	0.09	0.11	0.14	0.12	0.17	0.08	0.10	0.09	0.09
Na	0.06	0.08	0.00	0.05	0.06	0.07	0.06	0.10	0.06	0.06	0.05	0.06
K	0.02	0.05	0.00	0.00	0.02	0.03	0.00	0.02	0.00	0.02	0.00	0.00
Layer Charge	0.32	0.36	0.27	0.24	0.30	0.38	0.31	0.45	0.23	0.28	0.24	0.25
Interl.Charge	0.32	0.36	0.27	0.24	0.30	0.38	0.31	0.45	0.23	0.28	0.24	0.25

Sample	SM66	SM66	SM66	SM66	SM99	SM99	SM99	SM99	SM114	SM114	SM114	SM114
Quarry	BMK1	BMK1	BMK1	BMK1	BMTS	BMTS	BMTS	BMTS	BMAH	BMAH	BMAH	BMAH
SiO_2	50.73	52.09	56.30	54.24	53.02	52.97	56.39	53.76	46.87	46.84	44.35	46.64
Al_2O_3	25.77	27.14	18.29	19.03	16.85	20.99	18.49	20.90	13.41	15.93	13.75	14.68
Fe_2O_3	0.87	1.07	3.95	4.06	3.95	1.76	4.45	1.81	5.19	3.73	5.87	4.15
MgO	1.93	1.53	2.97	4.10	3.25	3.56	3.56	2.71	2.88	3.16	3.86	2.99
CaO	1.00	0.70	0.91	0.69	1.75	1.52	1.58	1.69	1.44	1.25	0.94	1.25
Na_2O	- -	- -	- -	0.98	0.00	0.61	0.54	0.44	0.46	0.63	0.00	0.52
K_2O	- -	0.28	0.84	1.06	0.00	0.46	0.25	0.00	0.25	0.40	2.24	0.32
Total	80.30	82.81	83.26	84.16	78.82	81.87	85.26	81.31	70.50	71.94	71.01	70.55
Structural formulae based on 11 oxygens												
Si	3.67	3.66	3.99	3.84	3.97	3.81	3.92	3.87	3.97	3.87	3.82	3.93
Al^{IV}	0.33	0.34	0.01	0.16	0.03	0.19	0.08	0.13	0.03	0.13	0.18	0.07
Octahedral cations												
Al^{VI}	1.87	1.91	1.51	1.43	1.45	1.59	1.44	1.64	1.31	1.43	1.21	1.39
Fe^{3+}	0.05	0.06	0.21	0.22	0.22	0.10	0.23	0.10	0.33	0.23	0.38	0.26
Mg	0.21	0.16	0.31	0.43	0.36	0.38	0.37	0.29	0.36	0.39	0.50	0.38
VI Cations	2.13	2.12	2.04	2.08	2.04	2.07	2.04	2.03	2.01	2.05	2.09	2.03
Interlayer cations												
Ca	0.08	0.05	0.07	0.05	0.14	0.12	0.12	0.13	0.13	0.11	0.09	0.11
Na	0.00	0.00	0.00	0.13	0.00	0.09	0.07	0.06	0.08	0.10	0.00	0.09
K	0.00	0.03	0.08	0.10	0.00	0.04	0.02	0.00	0.03	0.04	0.25	0.03
Layer Charge	0.16	0.13	0.21	0.34	0.28	0.36	0.33	0.32	0.36	0.36	0.42	0.35
Interl.Charge	0.16	0.13	0.21	0.34	0.28	0.36	0.33	0.32	0.36	0.36	0.42	0.35

Table 4.4 (continued)

Sample	SM119	SM119	SM119	SM119	SM228	SM228	SM228	SM228	SM235	SM235	SM235	SM235
Quarry	BMAH	BMAH	BMAH	BMAH	BMZL	BMZL	BMZL	BMZL	BMRM	BMRM	BMRM	BMRM
SiO_2	52.81	59.93	53.81	52.50	56.21	52.58	56.91	58.31	48.82	47.82	51.94	51.44
Al2O3	19.44	18.43	18.92	17.02	18.91	20.26	23.04	18.94	22.15	20.71	21.65	20.24
Fe_2O_3	1.81	5.95	5.59	4.96	4.02	1.61	2.28	5.03	1.11	1.01	1.08	0.83
MgO	3.62	3.66	3.29	3.04	4.68	3.86	4.84	3.99	2.30	2.38	2.14	2.55
CaO	1.09	1.01	1.06	1.28	1.03	1.13	1.34	1.06	0.96	0.79	0.26	0.98
Na_2O	0.75	0.66	0.70	1.39	0.55	0.00	0.63	0.47	0.41	0.69	0.94	- -
K_2O	0.00	0.74	1.55	1.69	0.00	0.43	0.00	0.00	1.39	0.44	1.21	0.59
Total	79.52	90.38	84.92	81.88	85.40	79.87	89.04	87.80	77.14	73.84	79.22	76.63
Structural formulae based on 11 oxygens												
Si	3.89	3.95	3.82	3.88	3.89	3.85	3.76	3.93	3.73	3.79	3.85	3.91
Al^{IV}	0.11	0.05	0.18	0.12	0.11	0.15	0.24	0.07	0.27	0.21	0.15	0.09
Octahedral cations												
Al^{VI}	1.58	1.38	1.40	1.36	1.43	1.61	1.56	1.43	1.73	1.73	1.74	1.72
Fe^{3+}	0.10	0.30	0.30	0.28	0.21	0.09	0.11	0.26	0.06	0.06	0.06	0.05
Mg	0.40	0.36	0.35	0.33	0.48	0.42	0.48	0.40	0.26	0.28	0.24	0.29
VI Cations	2.08	2.04	2.04	1.97	2.12	2.12	2.15	2.09	2.06	2.07	2.03	2.06
Interlayer cations												
Ca	0.09	0.07	0.08	0.10	0.08	0.09	0.09	0.08	0.08	0.07	0.02	0.08
Na	0.11	0.08	0.10	0.20	0.07	0.00	0.08	0.06	0.06	0.11	0.13	0.00
K	0.00	0.06	0.14	0.16	0.00	0.04	0.00	0.00	0.14	0.04	0.11	0.06
Layer Charge	0.28	0.29	0.40	0.56	0.23	0.22	0.27	0.21	0.35	0.28	0.29	0.22
Interl.Charge	0.28	0.29	0.40	0.56	0.23	0.22	0.27	0.21	0.35	0.28	0.29	0.22

Sample	SM176	SM176	SM176	SM176	SM135	SM135	SM155	SM155	SM155	SM155	SM135	SM135
Quarry	BMRS	BMRS	BMRS	BMRS	BMAK	BMAK	BMA2	BMA2	BMA2	BMA2	BMAK	BMAK
SiO_2	55.34	52.61	53.88	52.55	53.27	51.07	50.59	48.53	54.67	44.80	50.94	49.39
Al_2O_3	20.81	23.11	25.08	24.75	20.23	22.31	21.54	23.51	22.49	21.96	28.04	30.19
Fe_2O_3	1.86	1.19	0.64	0.68	2.46	0.94	2.07	1.56	1.94	1.47	0.86	0.49
MgO	2.24	2.49	2.85	3.06	1.98	1.45	1.27	1.28	1.19	1.57	1.04	0.55
CaO	0.30	0.36	0.34	0.26	0.58	0.34	0.41	1.04	0.56	0.95	- -	0.26
Na_2O	0.92	0.60	0.55	1.18	- -	0.94	0.57	- -	- -	0.62	0.40	- -
K_2O	1.28	0.38	0.36	0.40	0.26	0.48	0.96	1.53	0.56	0.89	0.44	0.35
Total	82.75	80.74	83.70	82.88	78.78	77.53	77.41	77.45	81.41	72.26	81.72	81.23
Structural formulae based on 11 oxygens												
Si	3.93	3.80	3.75	3.71	3.94	3.84	3.84	3.70	3.90	3.66	3.62	3.53
Al^{IV}	0.07	0.20	0.25	0.29	0.06	0.16	0.16	0.30	0.10	0.34	0.38	0.47
Octahedral cations												
Al^{VI}	1.67	1.77	1.80	1.77	1.70	1.81	1.76	1.81	1.80	1.78	1.97	2.07
Fe^{3+}	0.10	0.06	0.03	0.04	0.14	0.05	0.12	0.09	0.10	0.09	0.05	0.03
Mg	0.24	0.27	0.30	0.32	0.22	0.16	0.14	0.15	0.13	0.19	0.11	0.06
VI Cations	2.01	2.10	2.13	2.13	2.05	2.03	2.02	2.04	2.03	2.06	2.13	2.15
Interlayer cations												
Ca	0.02	0.03	0.03	0.02	0.05	0.03	0.03	0.08	0.04	0.08	0.00	0.02
Na	0.13	0.08	0.07	0.16	0.00	0.14	0.08	0.00	0.00	0.10	0.06	0.00
K	0.12	0.04	0.03	0.04	0.02	0.05	0.09	0.15	0.05	0.09	0.04	0.03
Layer Charge	0.29	0.17	0.16	0.24	0.12	0.24	0.24	0.32	0.14	0.36	0.10	0.07
Interl.Charge	0.29	0.17	0.16	0.24	0.12	0.24	0.24	0.32	0.14	0.36	0.10	0.07

Table 4.4 (continued)

Sample	SM158	SM158	SM158	SM158	SM277	SM277	SM302	SM302	SM325	SM325	SM281	SM277
Quarry	BMGF	BMGF	BMGF	BMGF	BKPR	BKPR	BKLT	BKLT	BCHT	BCHT	BKPR	BKPR
SiO_2	51.97	50.86	49.66	51.77	49.14	52.85	60.12	56.75	51.22	61.28	57.53	54.93
Al_2O_3	19.18	20.60	22.98	22.60	17.64	18.12	21.36	18.17	15.71	19.05	20.98	19.13
Fe_2O_3	0.61	- -	- -	- -	1.70	1.56	1.70	3.03	0.41	0.54	1.74	1.58
MgO	1.65	0.99	1.39	1.05	3.67	3.67	4.74	4.37	6.48	7.06	5.23	4.12
CaO	1.18	1.17	1.36	1.45	0.61	0.60	1.14	0.80	0.84	1.03	0.98	0.68
Na_2O	- -	- -	0.48	- -	0.42	0.64	0.00	0.38	0.83	0.39	0.48	0.82
K_2O	1.73	0.97	0.77	0.46	0.87	0.60	0.00	0.55	0.00	0.00	0.00	0.67
Total	76.32	74.59	76.64	77.33	74.05	78.04	89.06	84.05	75.49	89.35	86.94	81.93
Structural formulae based on 11 oxygens												
Si	3.99	3.95	3.78	3.88	3.90	3.97	3.93	3.97	3.97	3.99	3.87	3.93
Al^{IV}	0.01	0.05	0.22	0.12	0.10	0.03	0.07	0.03	0.03	0.01	0.13	0.07
Octahedral cations												
Al^{VI}	1.72	1.84	1.84	1.87	1.56	1.57	1.58	1.47	1.40	1.45	1.54	1.55
Fe^{3+}	0.04	0.00	0.00	0.00	0.10	0.09	0.08	0.16	0.02	0.03	0.09	0.09
Mg	0.19	0.11	0.16	0.12	0.43	0.41	0.46	0.46	0.75	0.69	0.52	0.44
VI Cations	1.95	1.96	2.00	1.99	2.09	2.07	2.12	2.09	2.17	2.17	2.15	2.08
Interlayer cations												
Ca	0.10	0.10	0.11	0.12	0.05	0.05	0.08	0.06	0.07	0.07	0.07	0.05
Na	0.00	0.00	0.07	0.00	0.06	0.09	0.00	0.05	0.12	0.05	0.06	0.11
K	0.17	0.10	0.07	0.04	0.09	0.06	0.00	0.05	0.00	0.00	0.00	0.06
Layer Charge	0.36	0.29	0.37	0.28	0.26	0.25	0.16	0.22	0.26	0.19	0.20	0.28
Interl.Charge	0.36	0.29	0.37	0.28	0.26	0.25	0.16	0.22	0.26	0.19	0.20	0.28

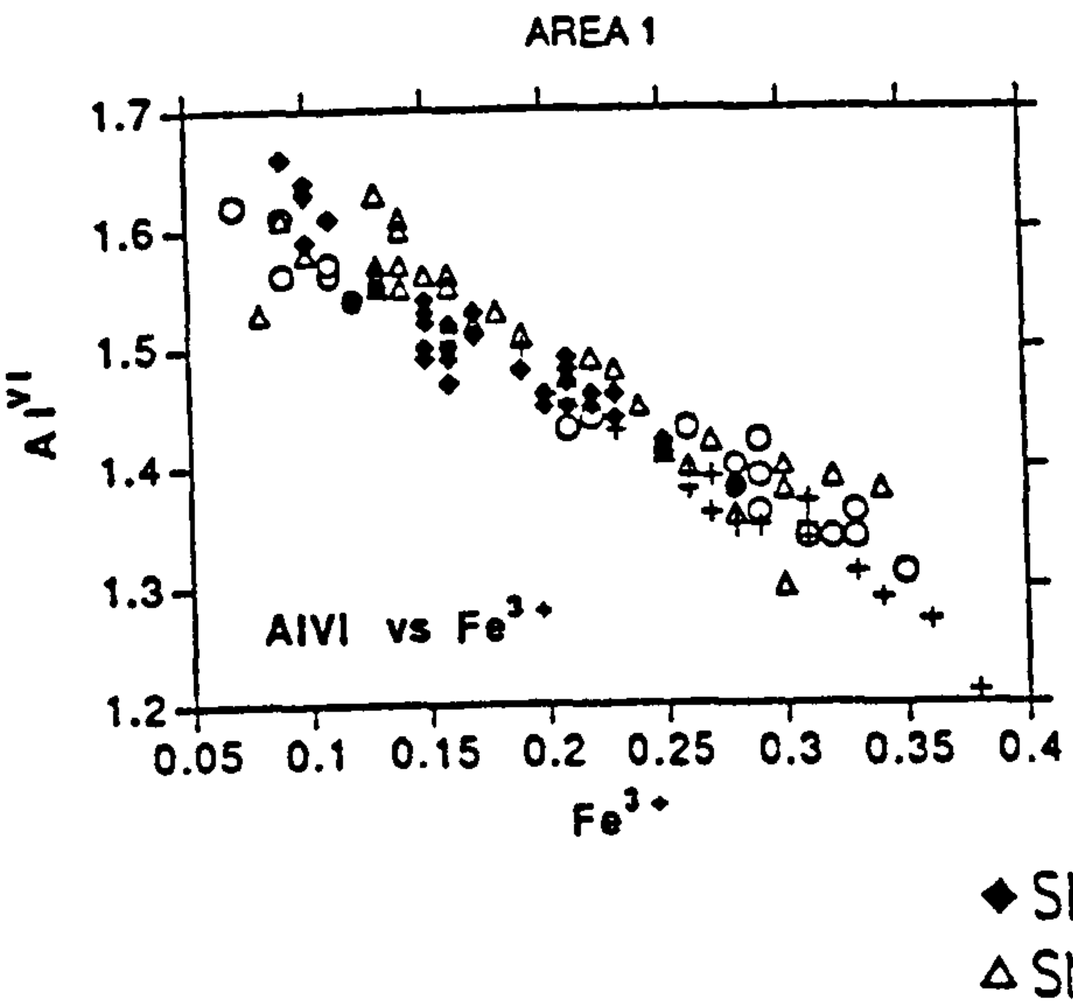

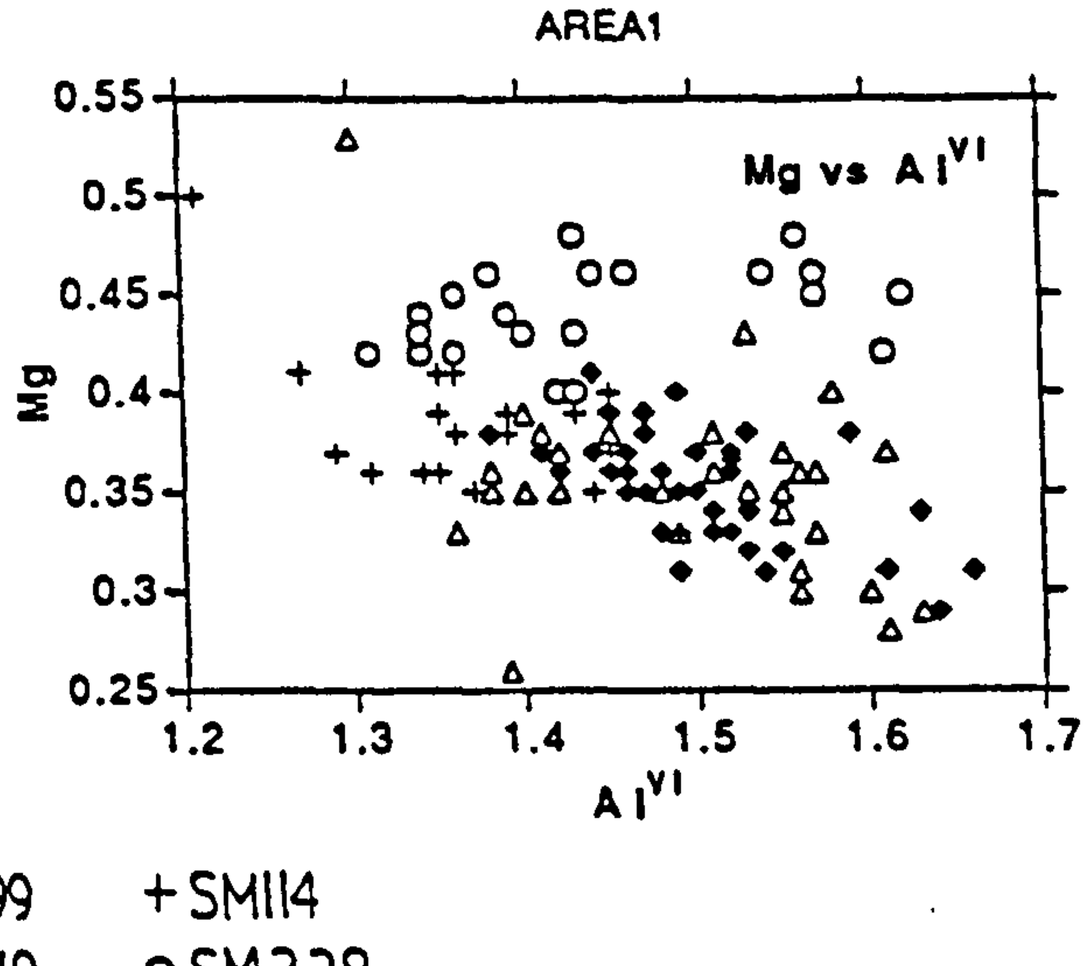

◆ SM99 + SM114
△ SM119 ○ SM228

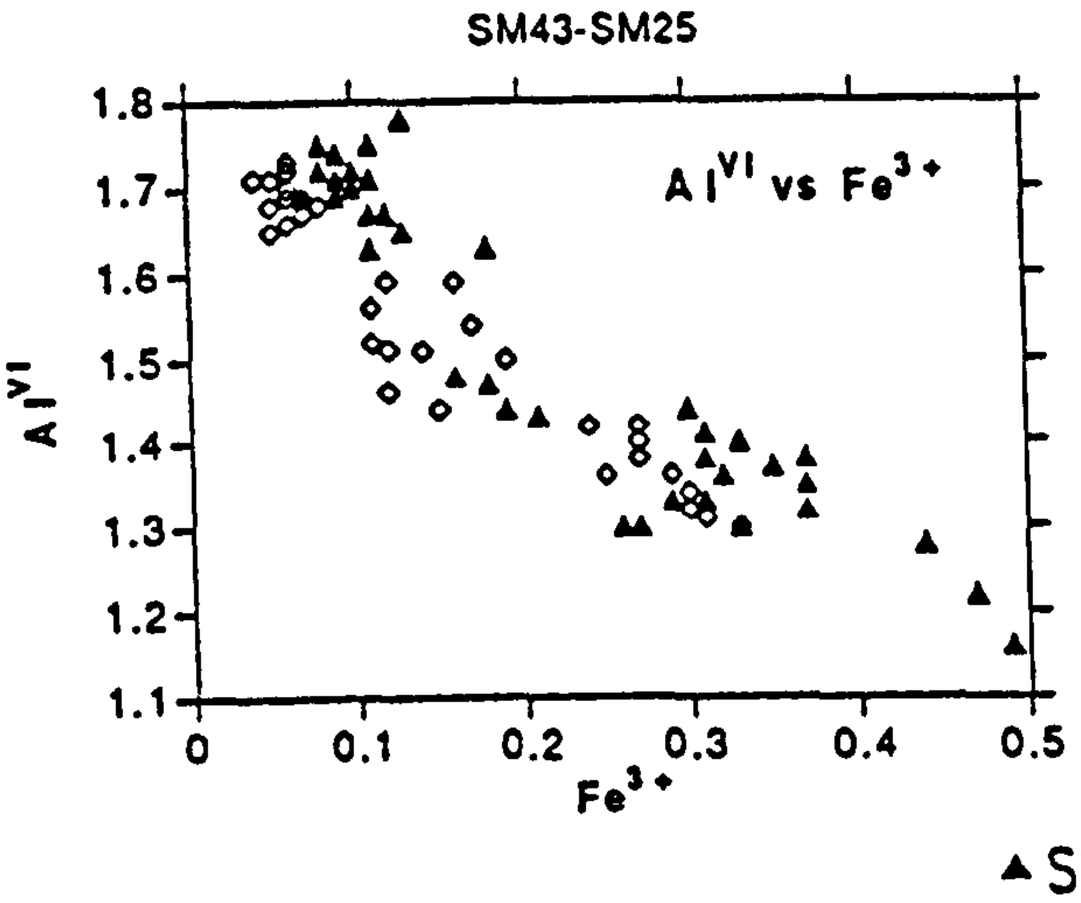

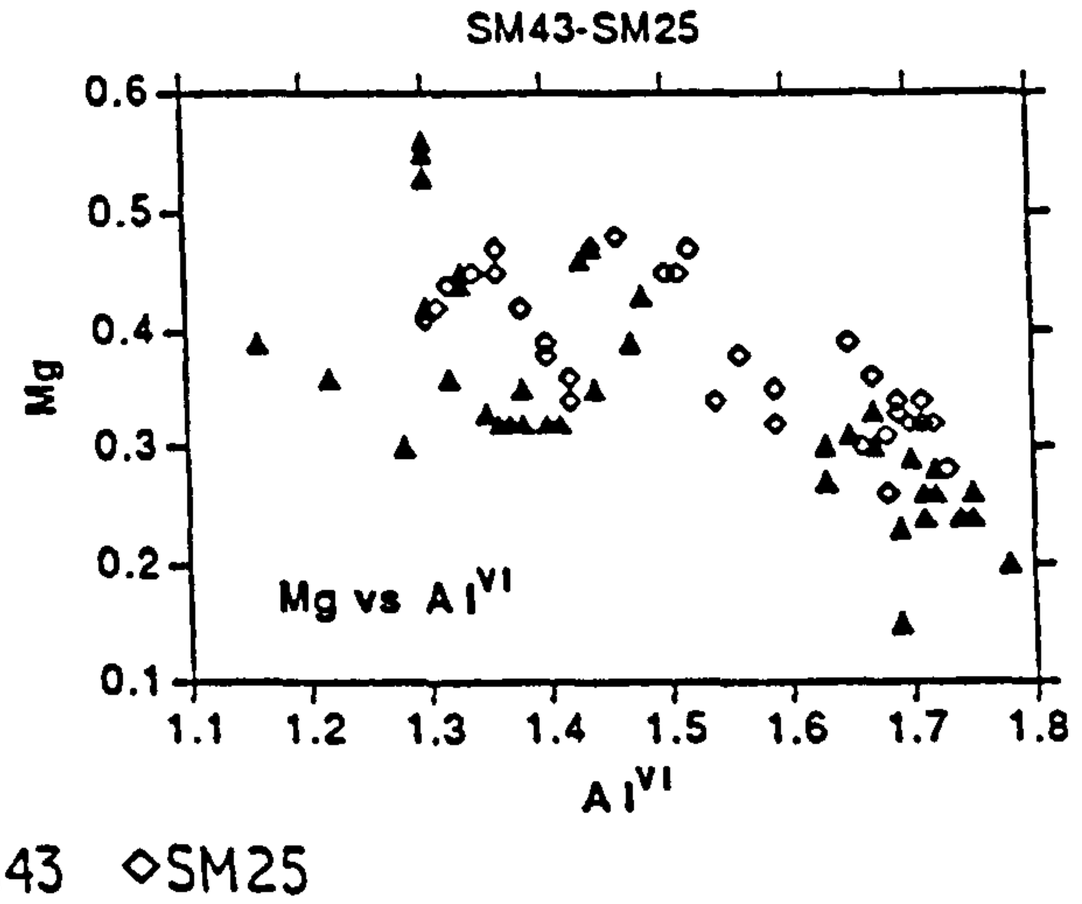

▲ SM43 ◇ SM25

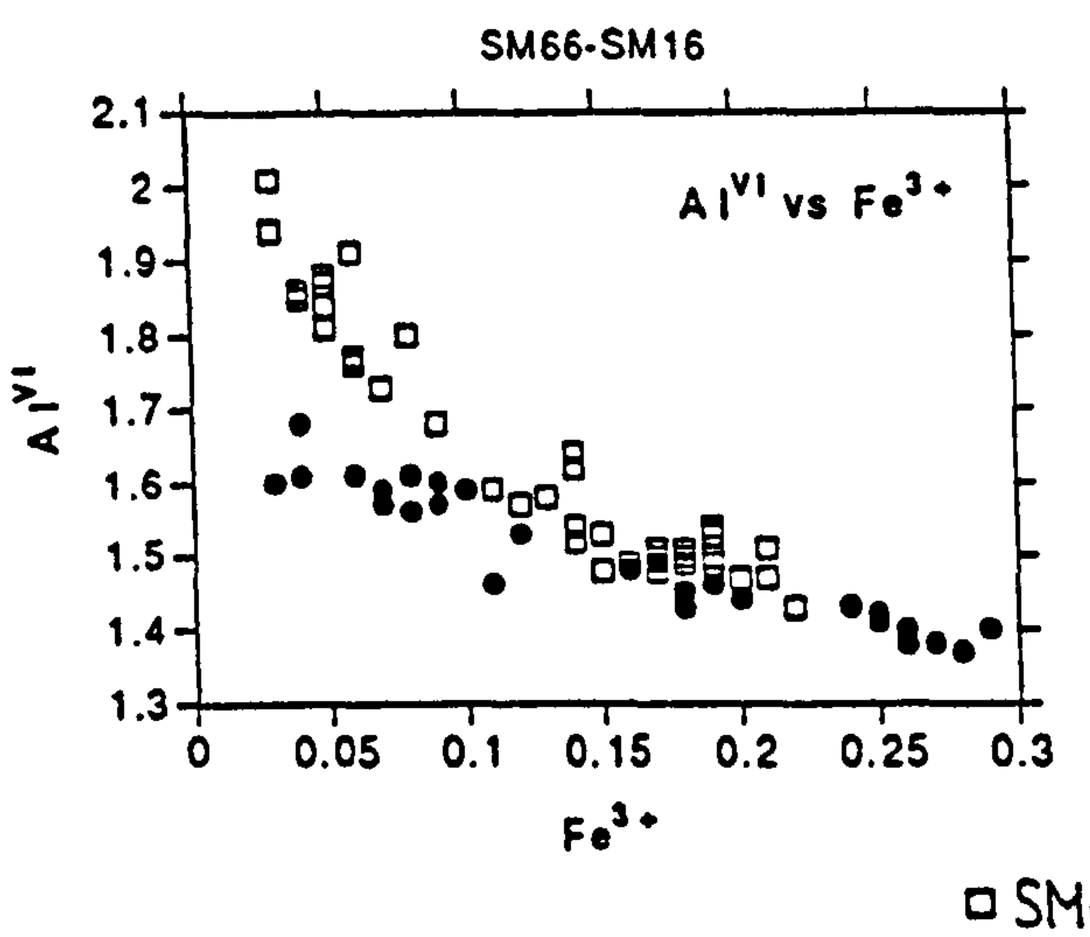

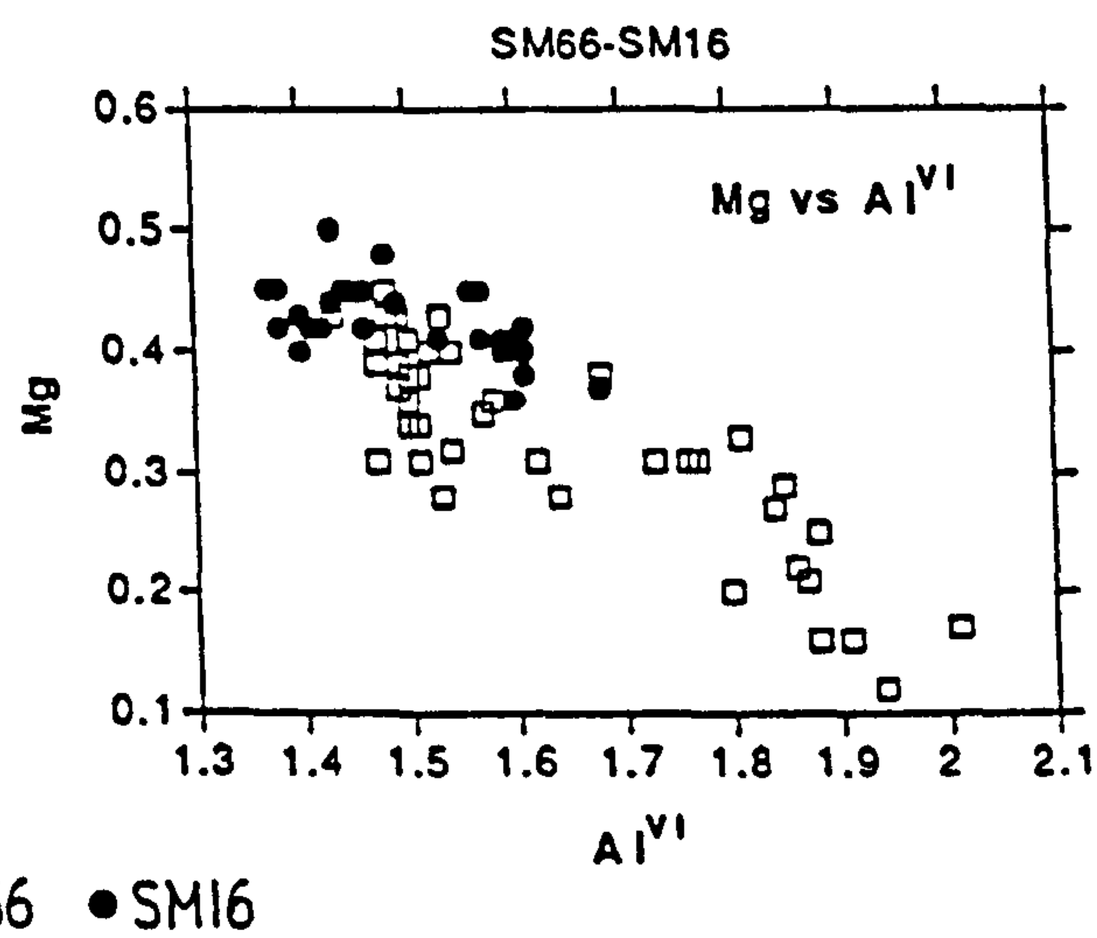

□ SM66 ● SM16

FIGURE 4.12. Diagrams showing the relationship between the octahedral cations of the smectites present in the bentonites from the Areas 1 and 2 of Milos. SM16 and SM26 come from the Ankeria deposit and SM43 and SM66 from the Koufi deposit (Area 2).

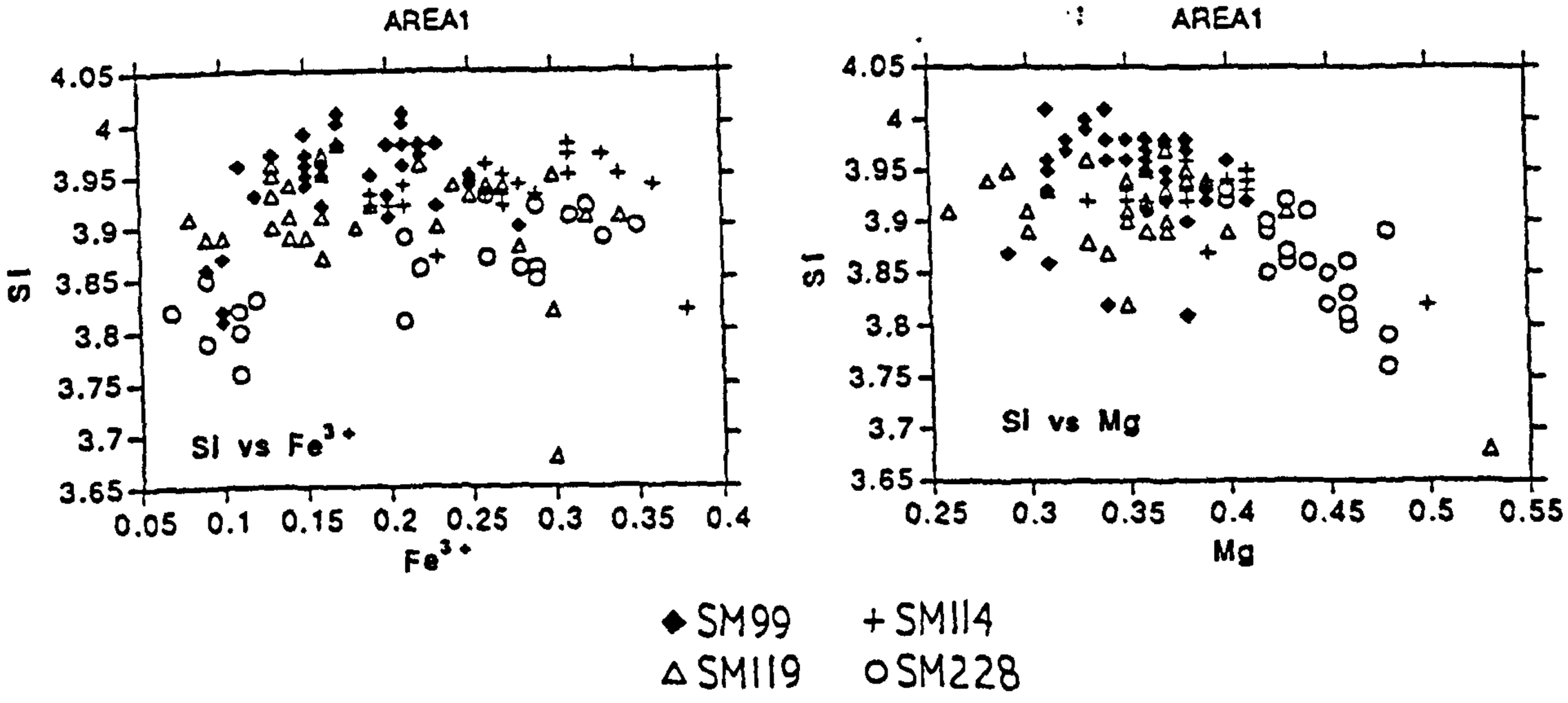

FIGURE 4.13. Diagrams showing the relationship between Si and Fe^{3+} and between Mg and Si in smectites present in the bentonites from the Areas 1 and 2, Milos.

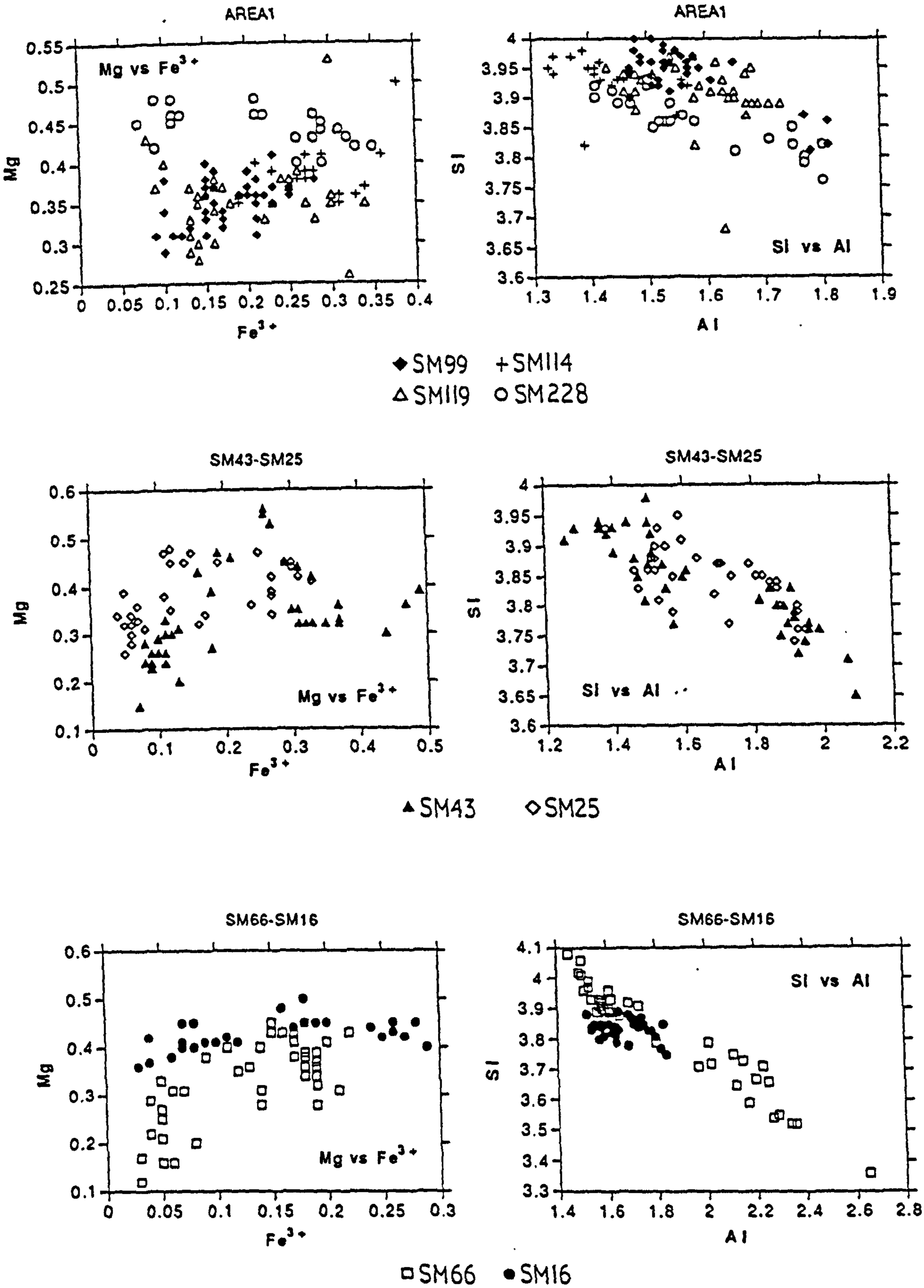

FIGURE 4.14. Diagrams showing the relationship between Fe^{3+} and Mg and betwen Si and total Al in smectites present in the bentonites from the Areas 1 and 2, Milos.

Fe^{3+} and Mg display an interesting positive trend for the smectites in the samples of Area 1 (Fig. 4.14) although Weaver & Pollard (1973) determined a weak negative relationship for these elements. Smectites from SM228 follow a different trend characterized by a negative relationship. This implies that an increase in the substitution of Fe for Al is associated with an increase in octahedral charge. On the other hand, in SM228 substitution of Fe for Al seems to favour a decrease of octahedral charge. No particular trend is observed in smectites from Area 2, except those from sample SM66 which exhibit a good positive relationship complying with the overall trend displayed by smectites in Area 1.

Total Al and Si have an expected negative relationship which is very well displayed in Area 2 (Fig 4.14). In Area 1 the greater scatter is mainly due to smectites from sample SM99 which have higher Si contents. This is considered to be the result of a secondary extensive illization process due to hydrothermal alteration in this deposit, which led to a release of Si from the illitized smectites (see chapter 6 and section 4.2.1.3.).

The effect of different octahedral cation occupancy in the structural formulae of smectites is depicted in the "smectite triangle" (Fig. 4.15), the three angles of which are occupied by the octahedral cations (Güven 1988). It is obvious that the smectite population in each sample: a) does not fall in a single "field" assigned for a particular type, implying coexistence of different smectite types, and b) shows clear compositional trends which are more or less representative for the whole area it comes from. For instance, smectites from Area 1 plot in the field of the Wyoming-type montmorillonite and in an area between the fields of Wyoming and Fe-rich montmorillonite, while those of Area 2 in the field occupied by beidellite and Cheto-type (Grim and Kulbicki's definition). An exception to the trend of the Area 1 is the sample SM228 which does not display the continuous variation observed, but seems to be composed of two distinct populations; one which follows the overall trend of this horizon, and a second which plots in the field of Cheto-type montmorillonites. In addition, in Area 2 it is observed that the smectites from sample SM43 always have higher Fe^{3+} content than their counterparts from sample SM25. In both areas a continuous variation is observed and it seems that both series converge in an area close to the Fe-montmorillonite "field". Although there seems to be a continuous compositional transition from beidellite to Fe-montmorillonite through Cheto-type montmorillonite, such a trend is not observed when Wyoming montmorillonites are present. The coexistence of beidellite and montmorillonite has been reported by Lim & Jackson (1986) and Yamada *et al.* (1991). Also, it seems that although smectites from Tsantili deposit exhibit low tetrahedral charge, they do not plot in the Area of Otay montmorillonite. This might be due to the high Fe^{3+} content and relatively low Mg content i.e low octahedral charge as well.

Similar compositional transitions, although not so clear, are also observed when smectites are plotted in the triangular diagram having MR^3-$2R^3$-$3R^2$ coordinates (Fig.

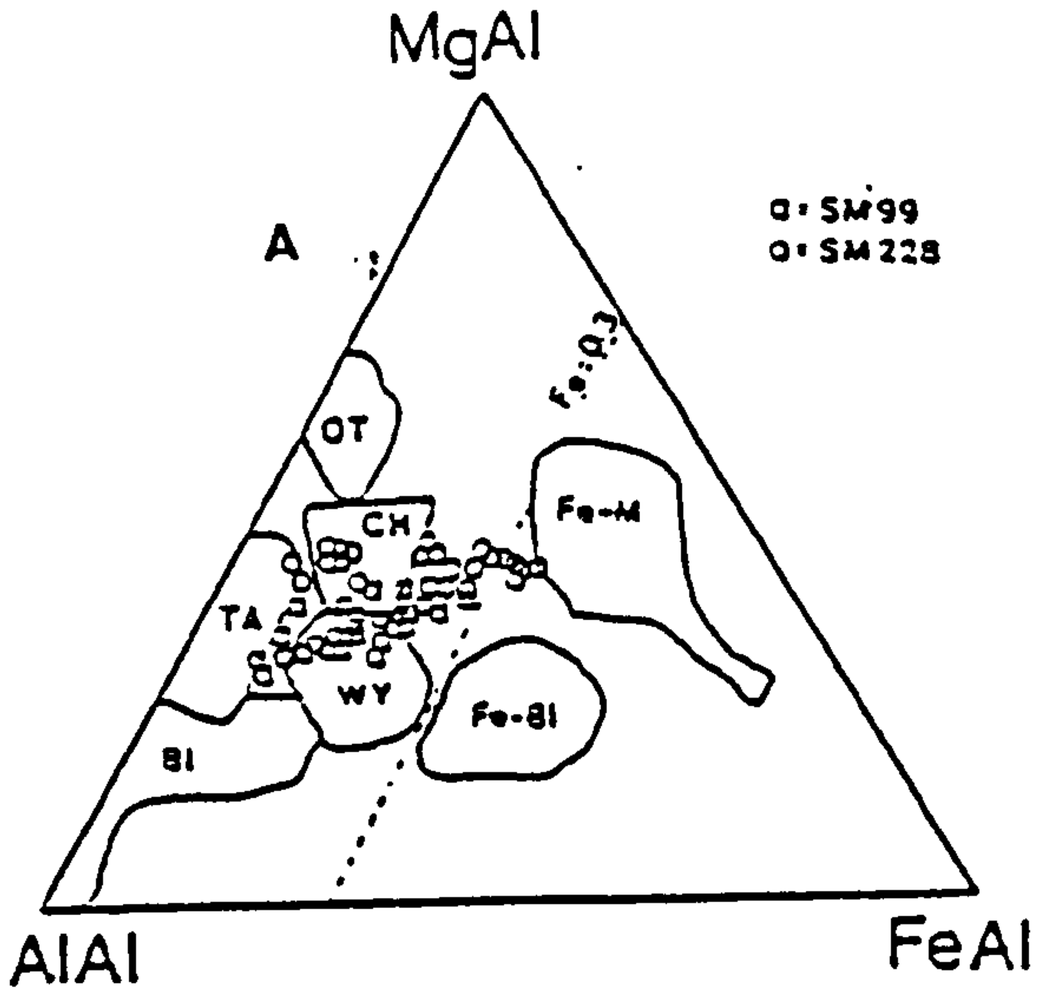

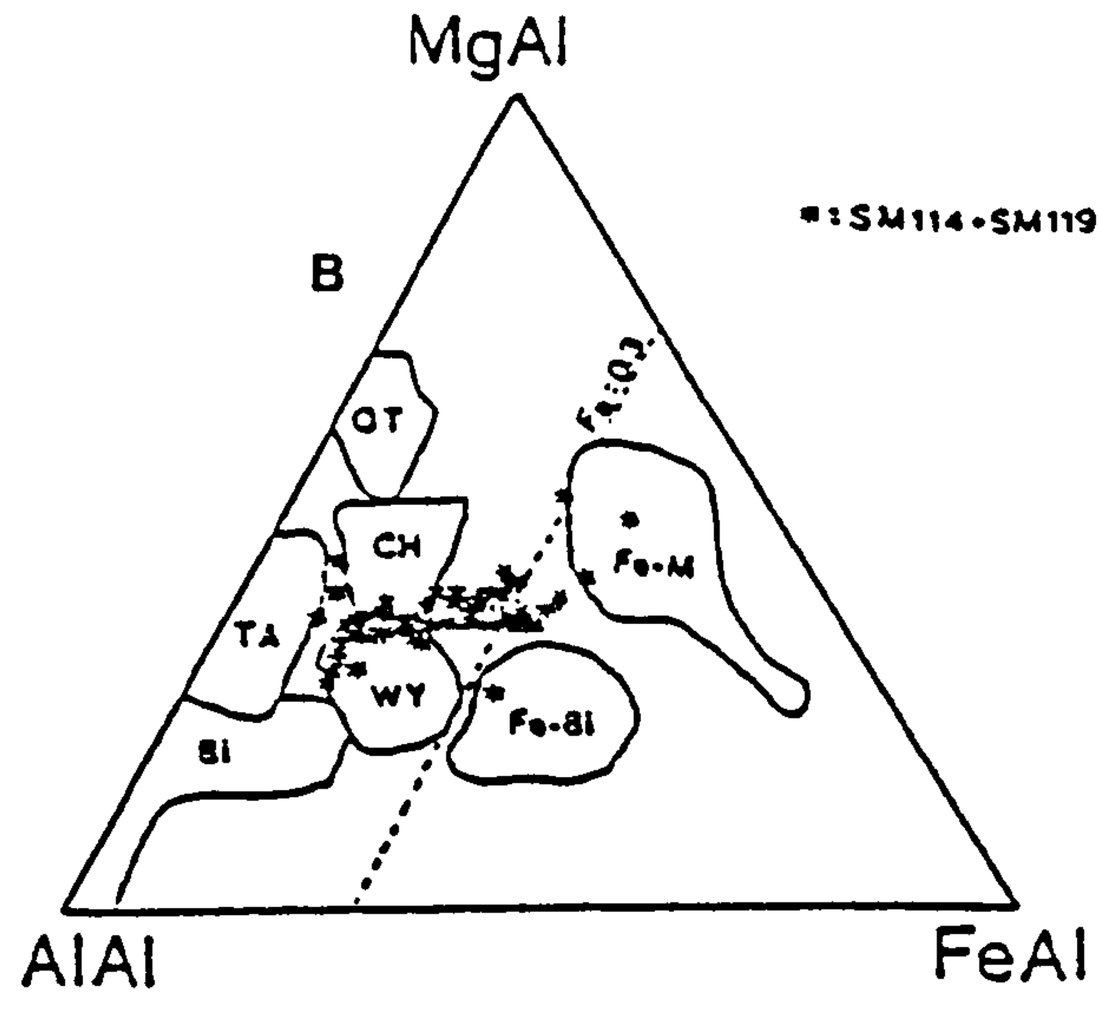

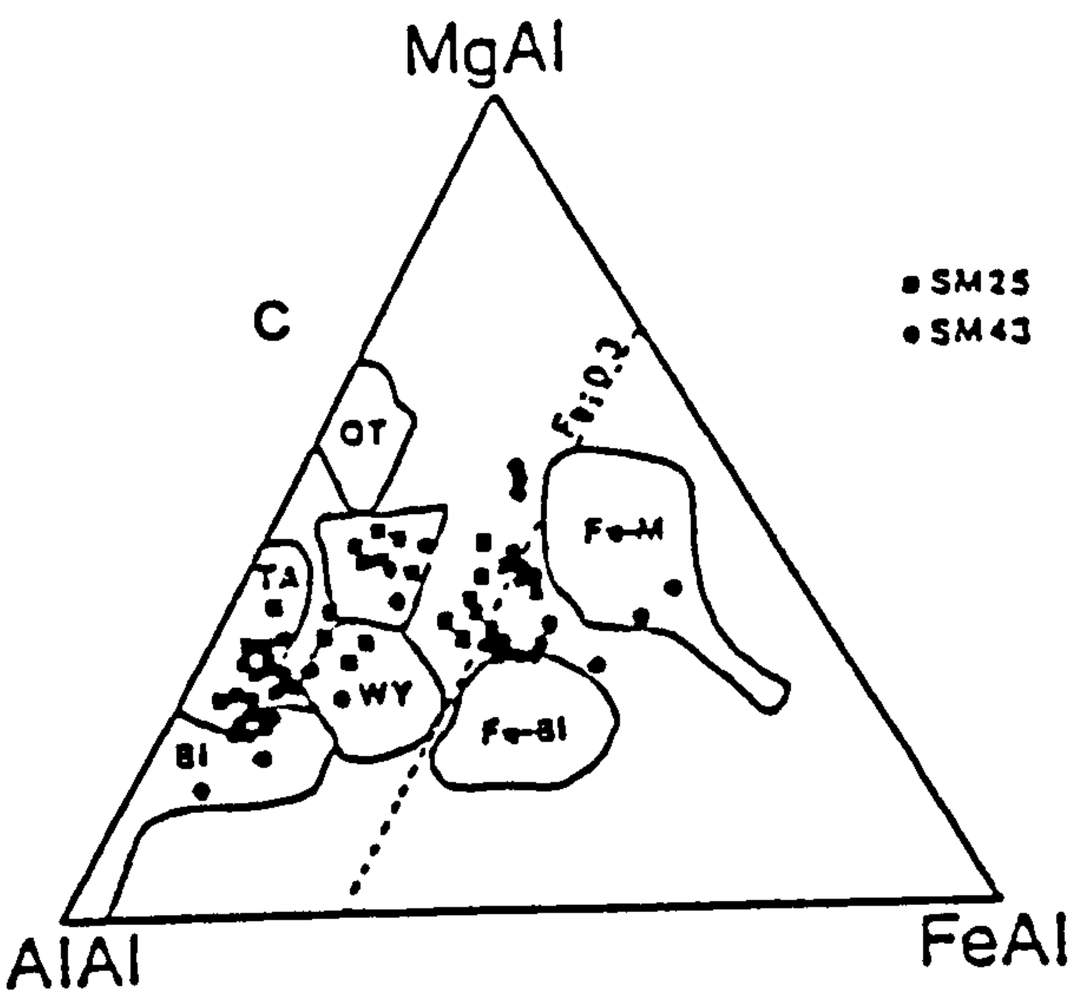

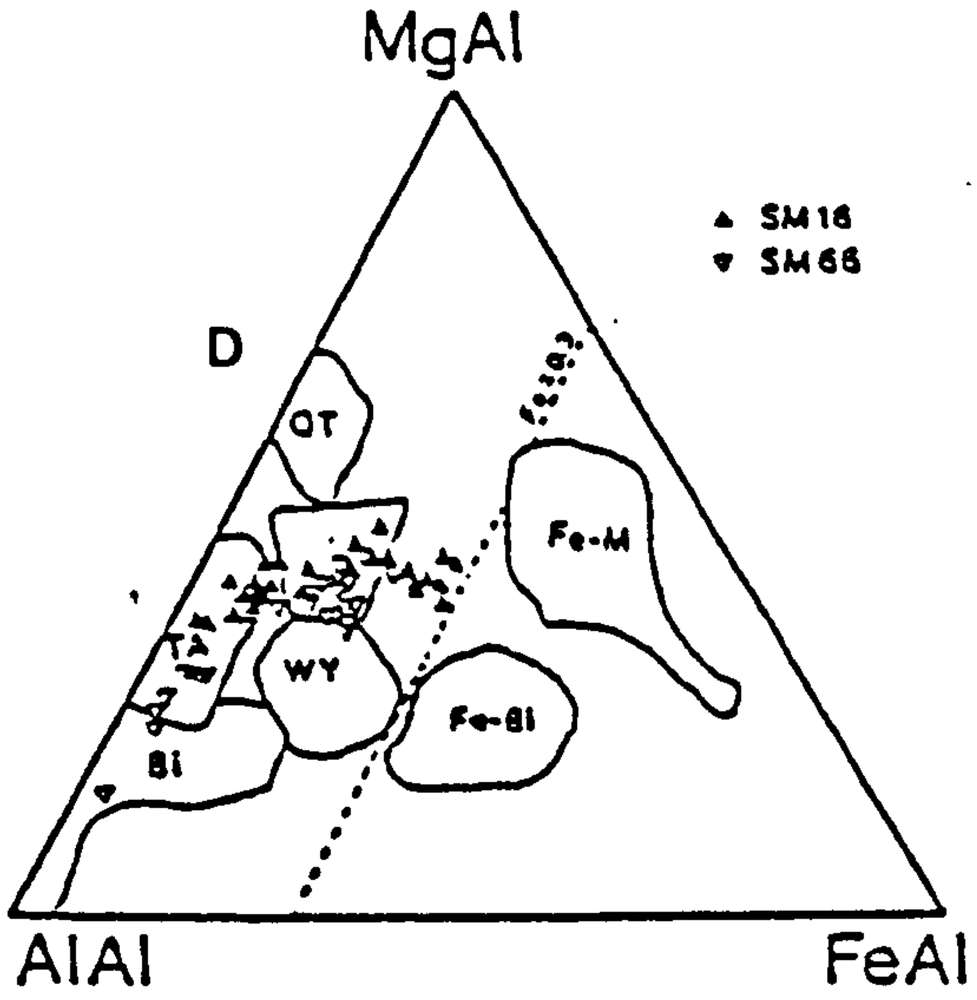

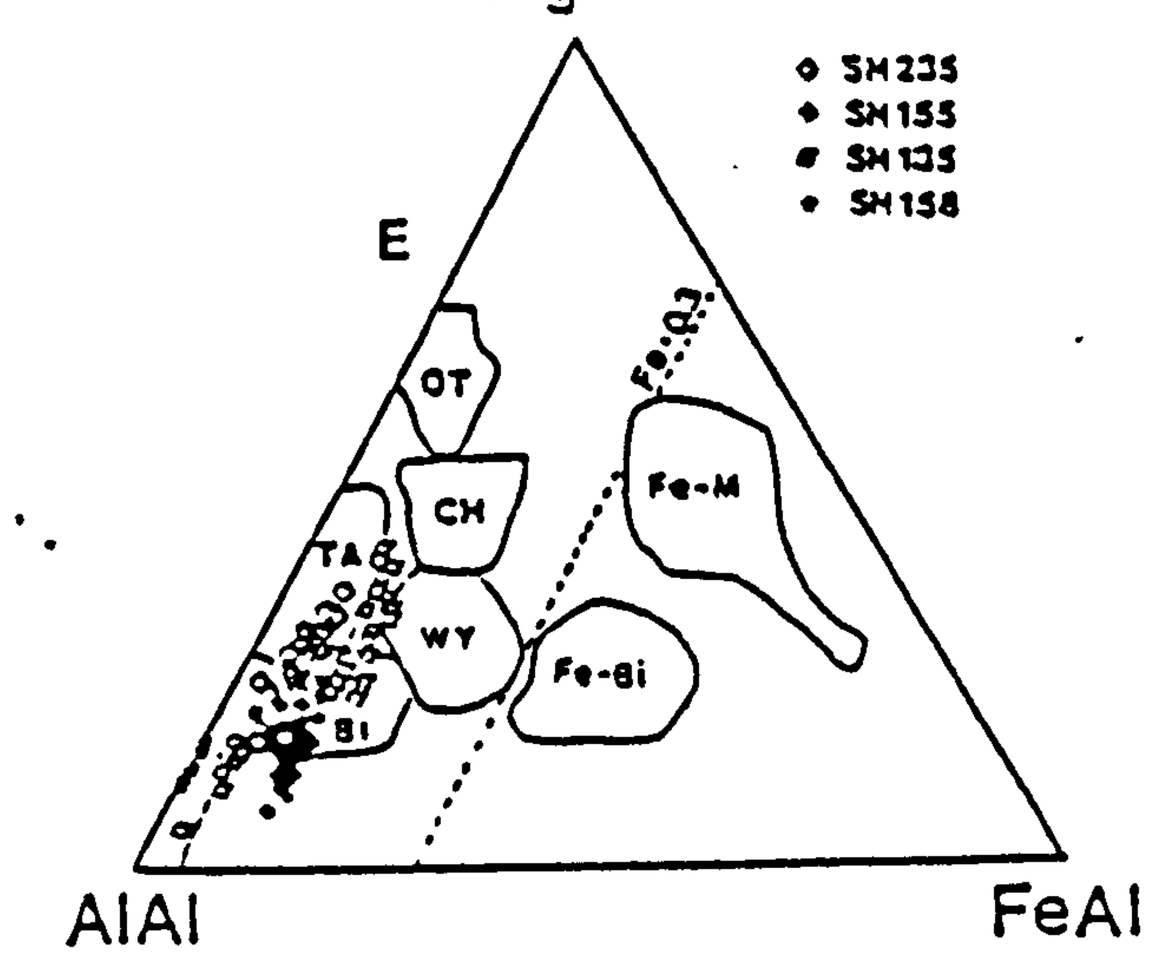

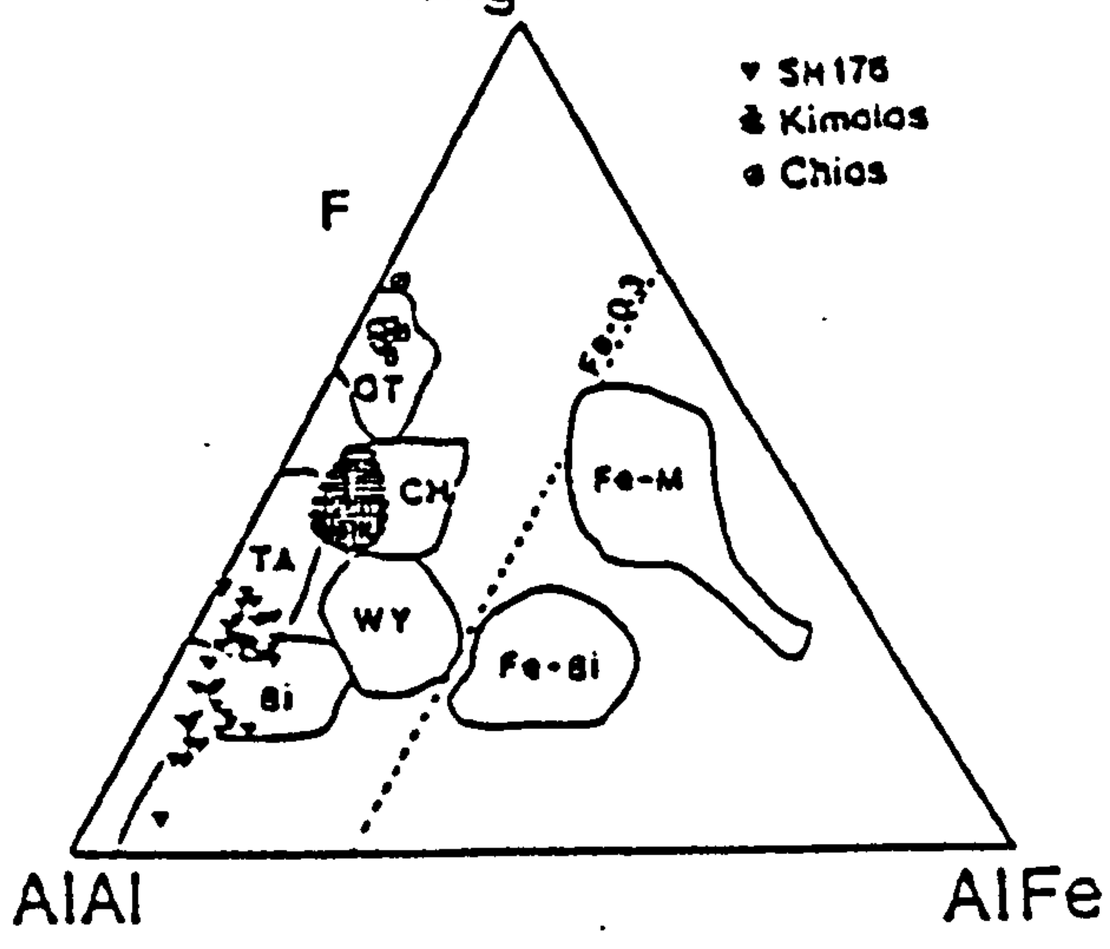

FIGURE 4.15. Projection of the smectites present in the Greek bentonites in the smectite triangle proposed by Güven (1988). a,b= Area 1, Milos, c,d= Area 2, Mllos, e,f= Area 3, Milos, Kimolos and Chios. SM114 and SM119 come from the Aspro Horio deposit, SM99 from the Tsantili deposit, SM228 from the Zoulias deposit, SM16 and SM25 from the Ankeria deposit, SM43 and SM66 from the Koufi deposit, SM135 and SM155 from the Ano Komia deposit, SM158 from the Garyfalakena deposit, SM235 from the Rema deposit and SM176 from the Mavrogiannis deposit. Key to the fields: Bi=beidellite, Ta=Tatatilla montmorillonite, OT=Otay montmorillonite, CH=Chambers montmorilonite, WY=Wyoming montmorillonite, Fe-Bi=Fe-Beidellite and Fe-M=Fe-montmorillonite.

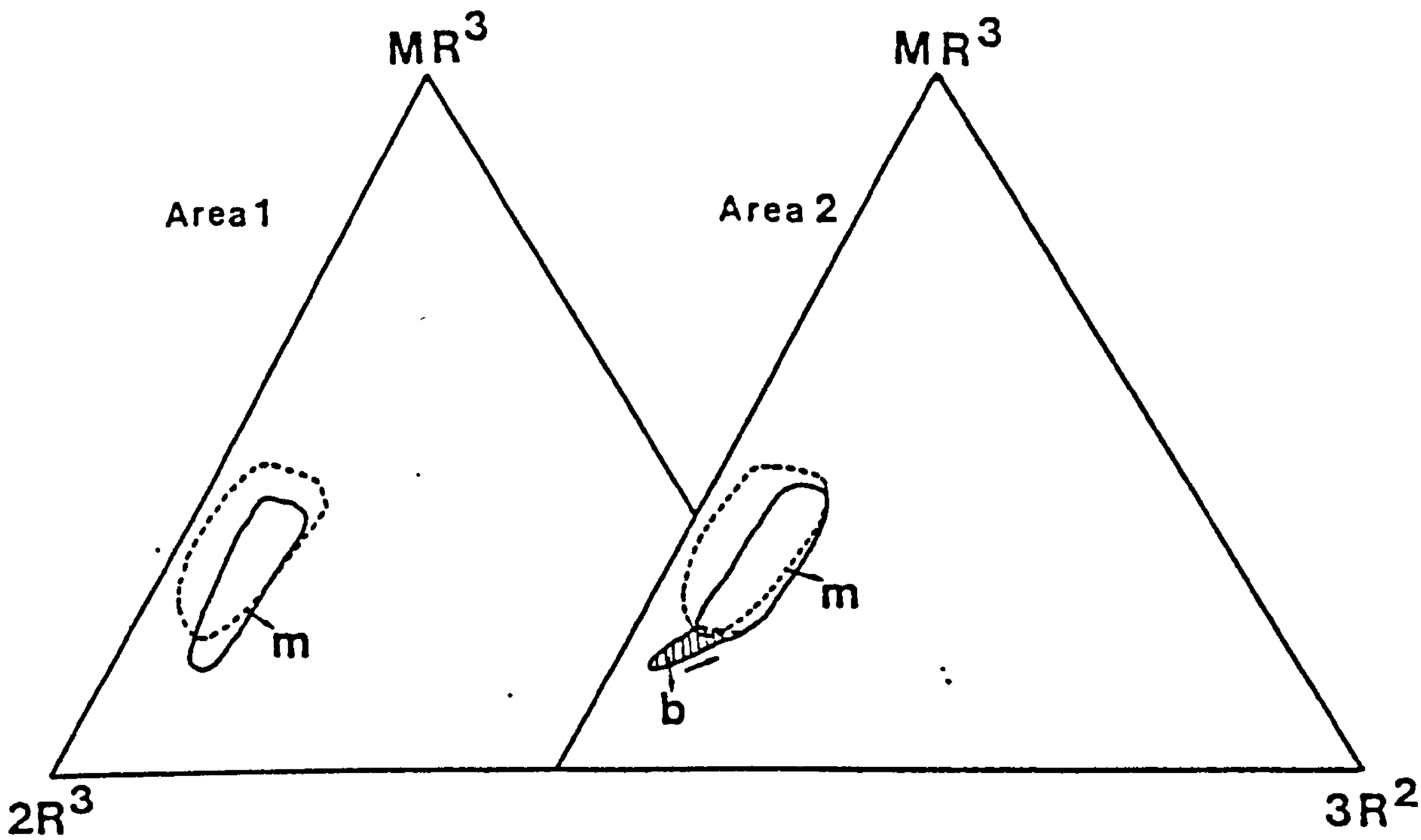

FIGURE 4.16. Projection of the smectites from the areas 1 and 2 of Milos in the M^+R^3-$2R^3$-$3R^2$ triangle proposed by Velde (1985). M^+R^3=Na+K+2Ca, $2R^3$=Al+Fe^3-M^+R^3, $3R^2$=(Mg+Fe^{2+})/3. Key to the symbols: m=montmorillonite, b =beidellite (hatched area). The dashed line indicates the montmorillonite field proposed by Velde (1985), while the thick line shows the range of montorillonite compositions observed in this study.

4.16), using the cation assignments proposed by Velde (1985). Smectites from Area 1 display the same trends in their compositional variation and are plotted within the "field" of fully expandable smectites. They develop variation mainly along the $2R^3$-MR^3 direction having a more or less stable $3R^2$ component. No transition from beidellite to montmorillonite has been observed. Smectites from Area 2 also plot in the "field" of fully expandable smectites but display a somewhat different trend. This trend is dominated by an increase in the $3R^2$ component as the composition moves from beidellitic to montmorillonitic up to a point, beyond which the contribution of the $3R^2$ component remains constant. Consequently, it seems that the transition from beidellite to montmorillonite exists only when Cheto-type montmorillonites are present.

4.3.2.1.2. Smectites derived from acidic glassy rocks (Area 3).

In accordance with their counterparts derived from intermediate rocks, these smectites display a large crystal-chemical variation. However, this variation is not controlled by the same parameters. The major differences observed (Fig. 4.17) can be summarized in the following points:

a) Unlike smectites from Areas 1 and 2 the relationship between Al^{VI} and Fe^{3+} is not well defined although it seems that it is a weak negative one (Fig. 4.17a). There is not a particular tendency within the individual deposits. Fe^{3+} abundance varies between narrow limits.

b) Total Al and Si exhibit a well determined negative relationship, like the smectites derived from intermediate rocks. The slope of the line is constant throughout the deposits, with an exception in the lower horizon of Ano Komia deposit. It seems that the relative proportion of these two elements is the main factor which determines the chemical variations of these smectites. A similar well defined negative relationship exists between Al^{VI} and Mg. The slope of the linear trend is similar for the various deposits except for Mavrogiannis deposit. The well exhibited negative relationship between these two cations indicates that the variations in octahedral occupancy are controlled mainly by the systematic variation between Mg and Al^{VI}, whereas the role of Fe is restricted.

c) The relationship between Si and either Fe^{3+} or Mg is random. An exception to this pattern is shown in the lower horizon of Ano Komia deposit. In this deposit a well defined positive relationship can be observed, until the point where Si has its maximum value. After that Fe^{3+} and Mg increase while Si remains constant. It seems therefore that in this horizon, decrease of the tetrahedral charge is escorted by an increase of Al^{VI} substitution and a concequent increase of the octahedral charge. Finally, no definite relationship exists between Fe^{3+} and Mg in smectites from the various deposits. Again, an exception is displayed by the lower horizon of Ano Komia deposit, in which the two cations display a

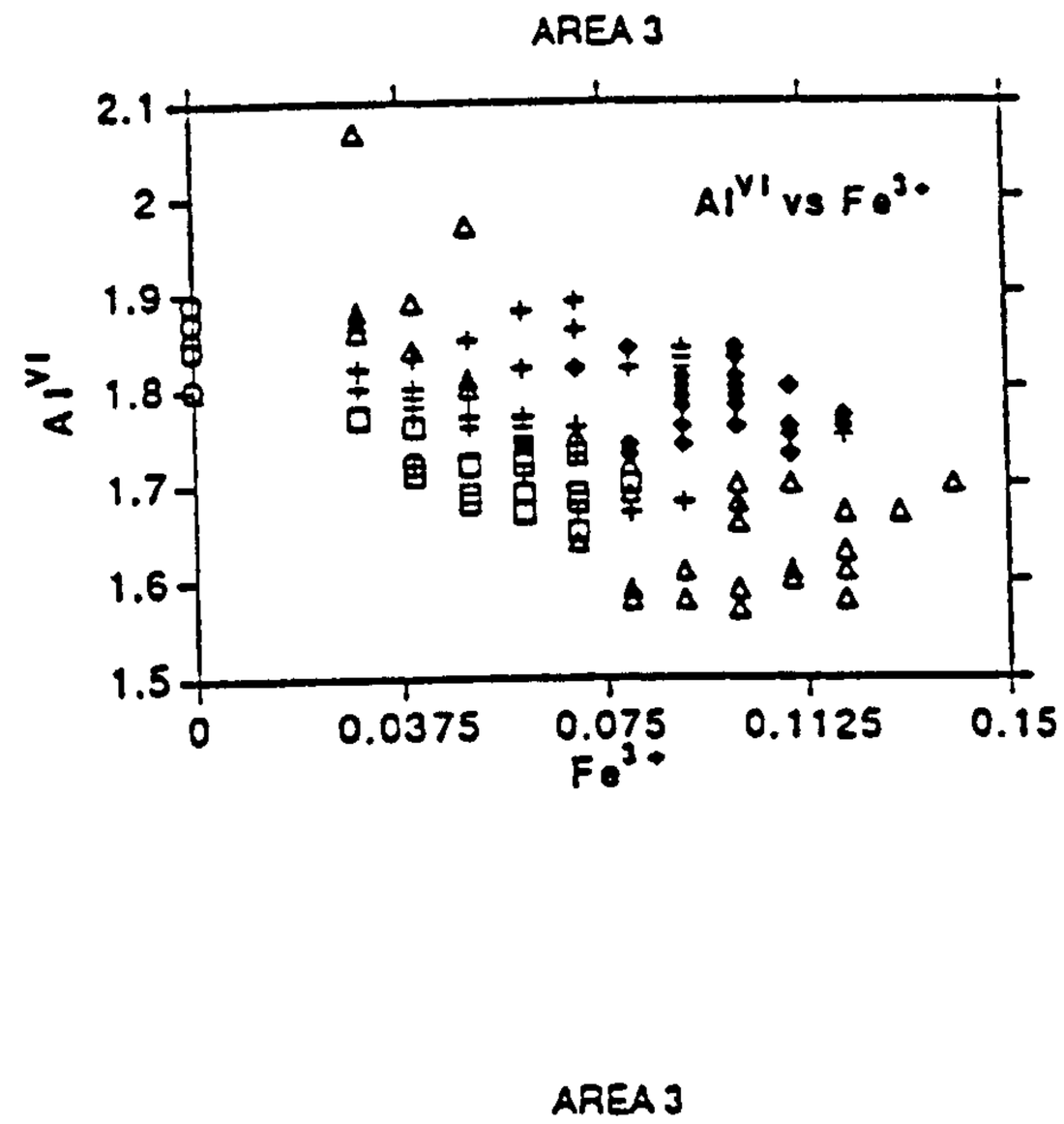

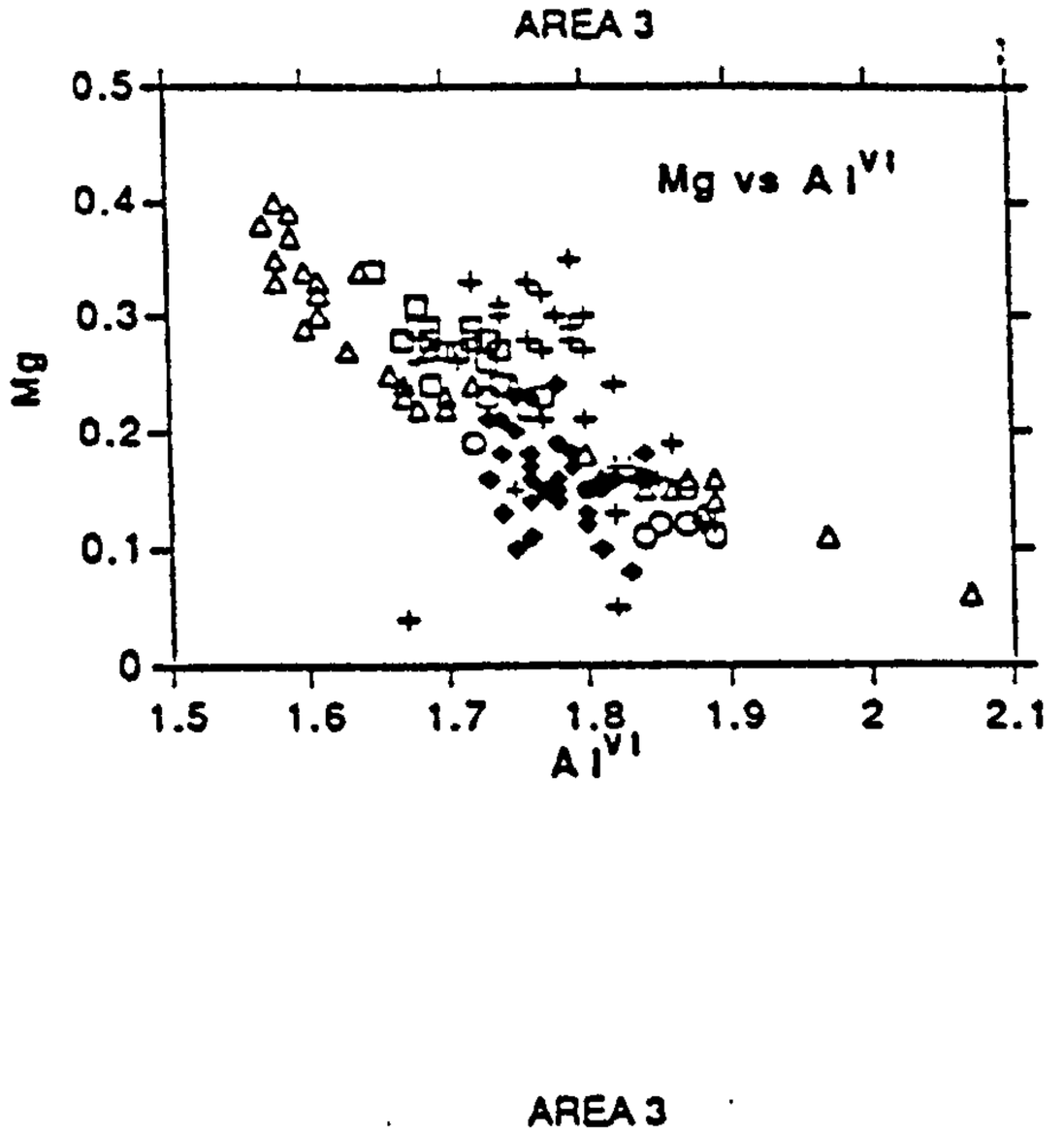

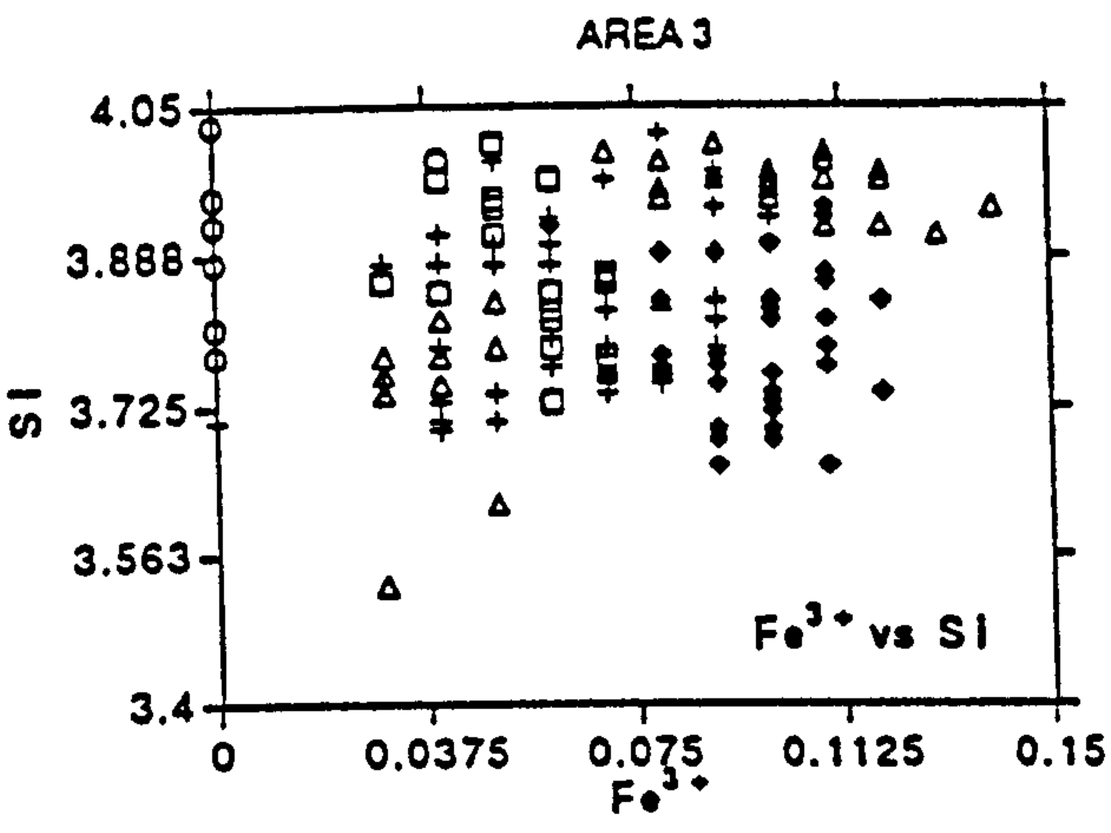

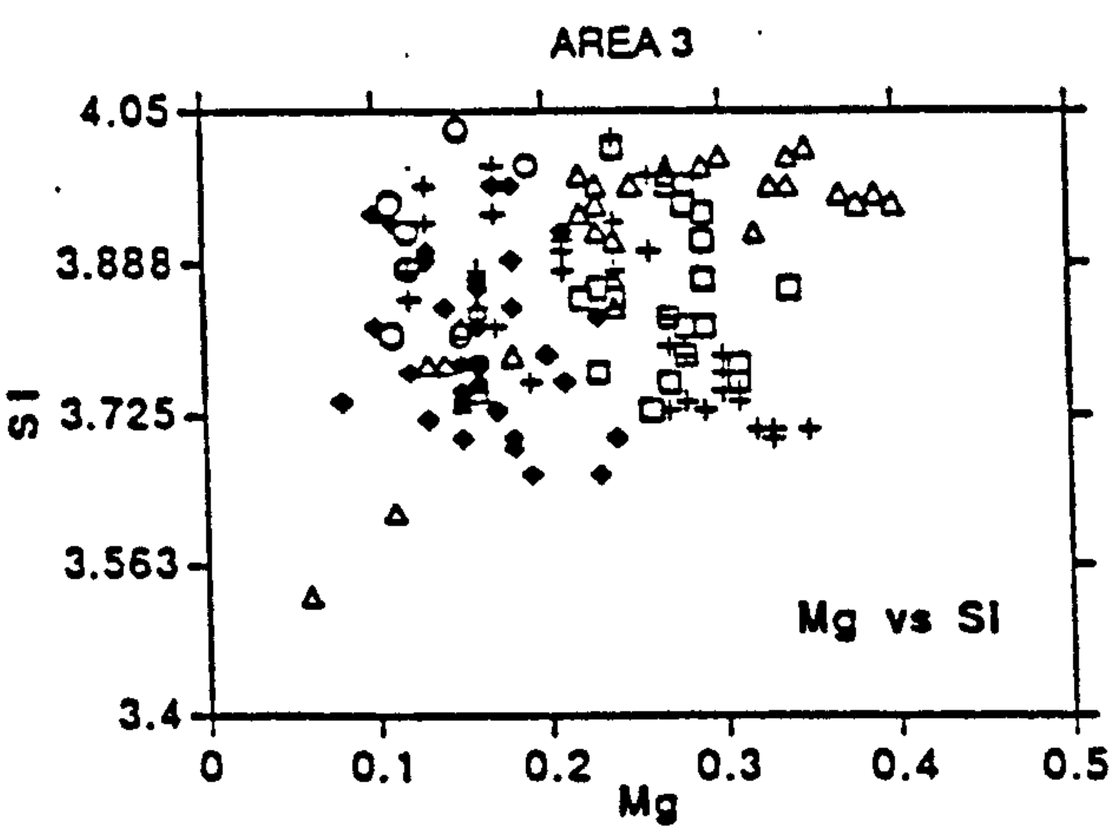

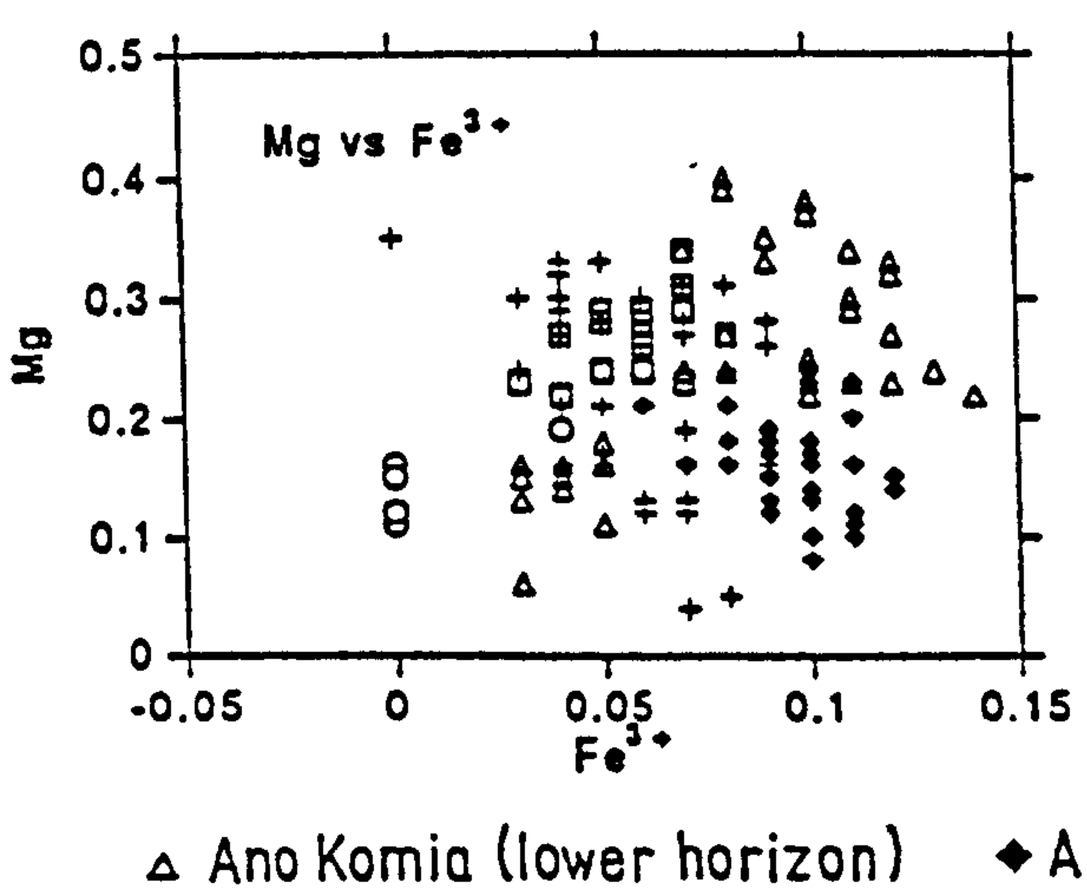

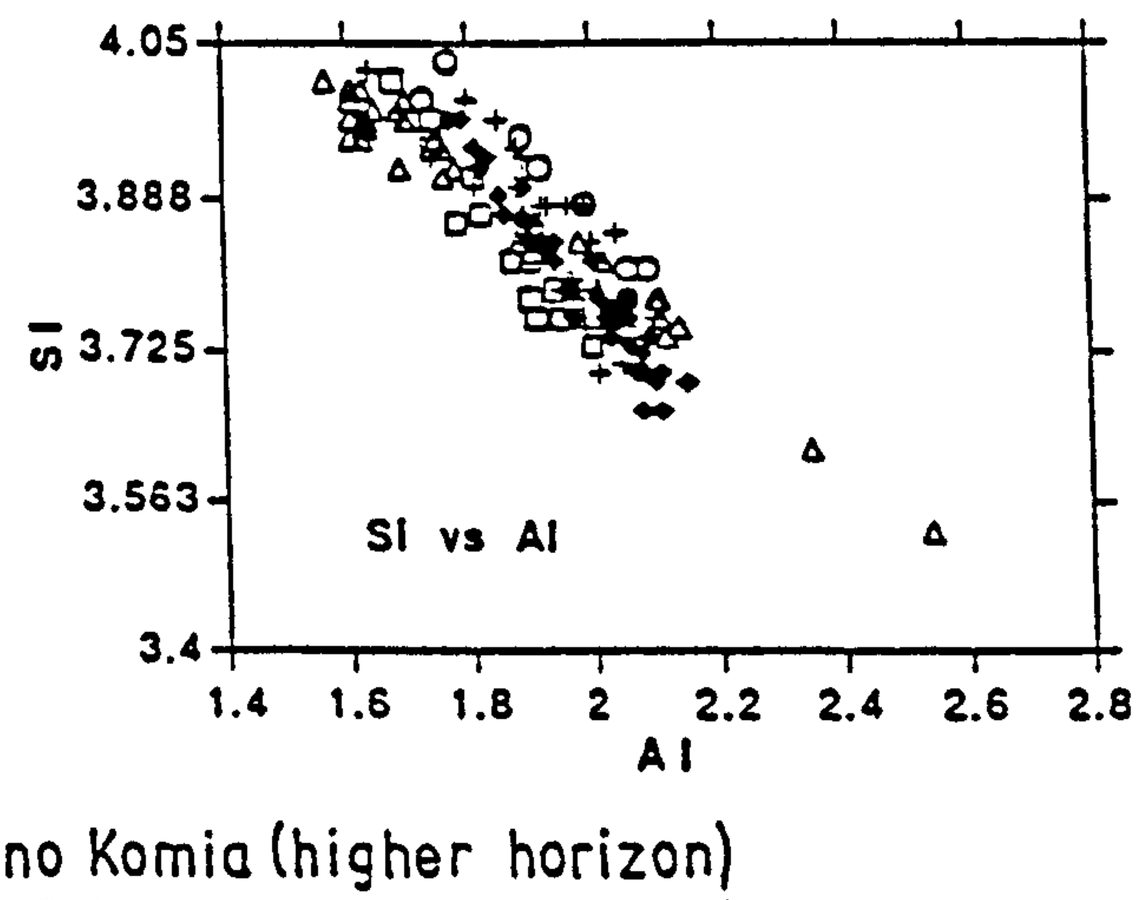

△ Ano Komia (lower horizon) ◆ Ano Komia (higher horizon)

\+ Mavrogiannis □ Rema ○ Garyfalakena

FIGURE 4.17. Orthogonal plots between the octahedral and the tetrahedral cations of the smectites present in the bentonites of the area 3 of Milos

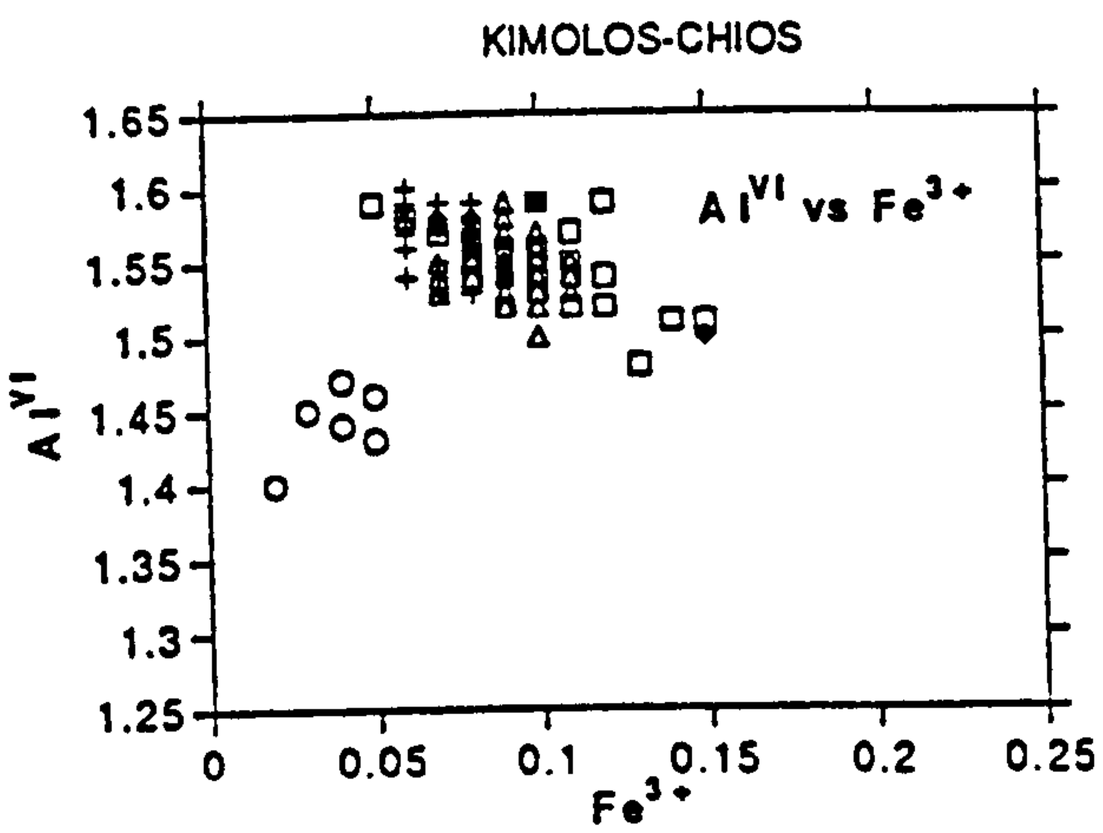

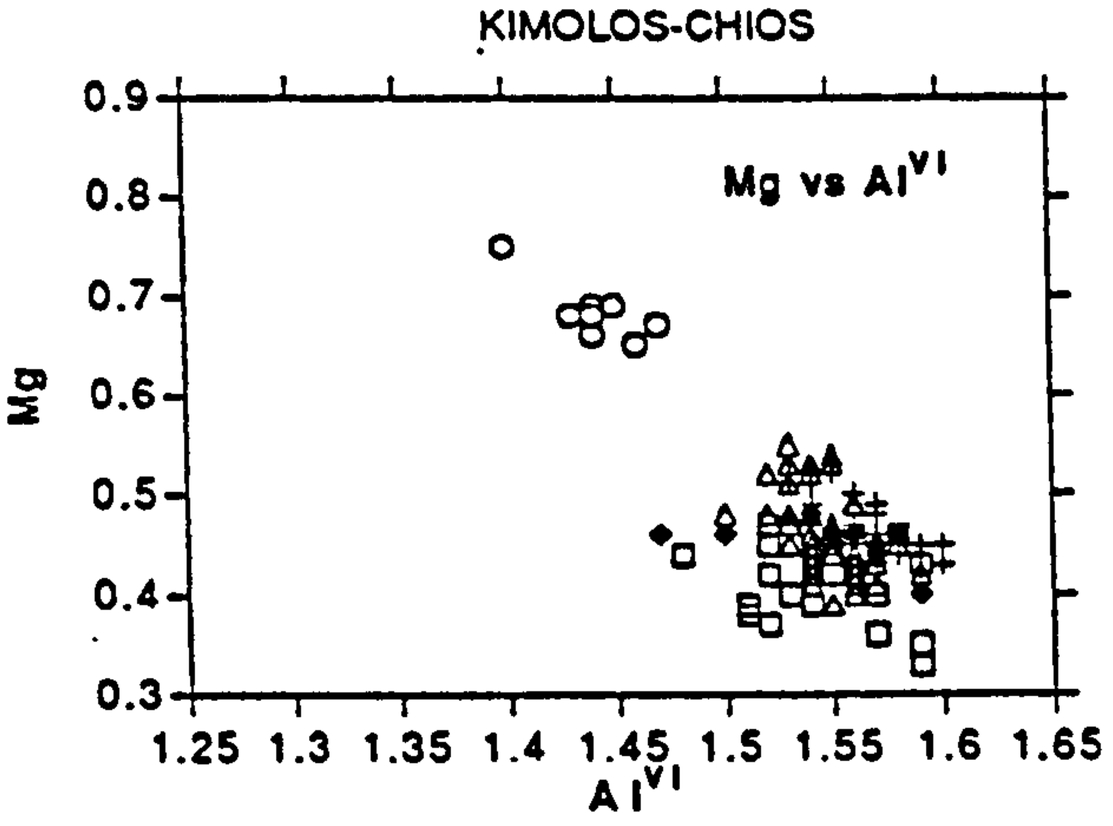

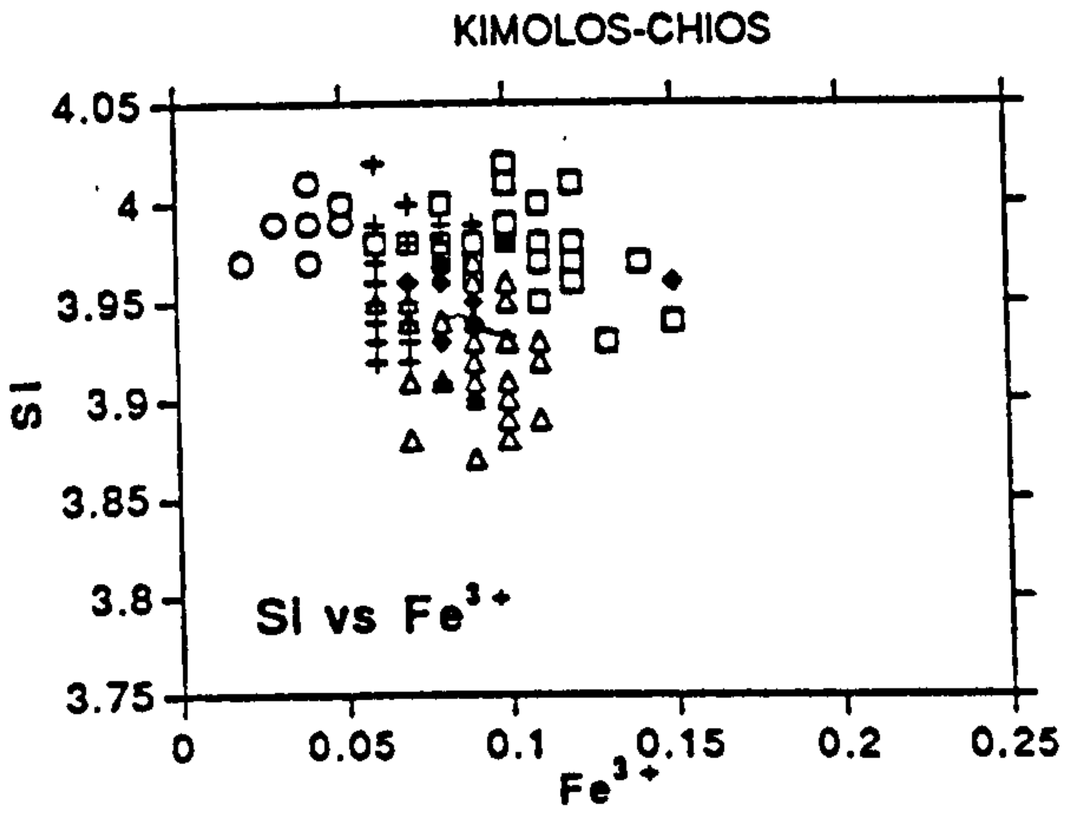

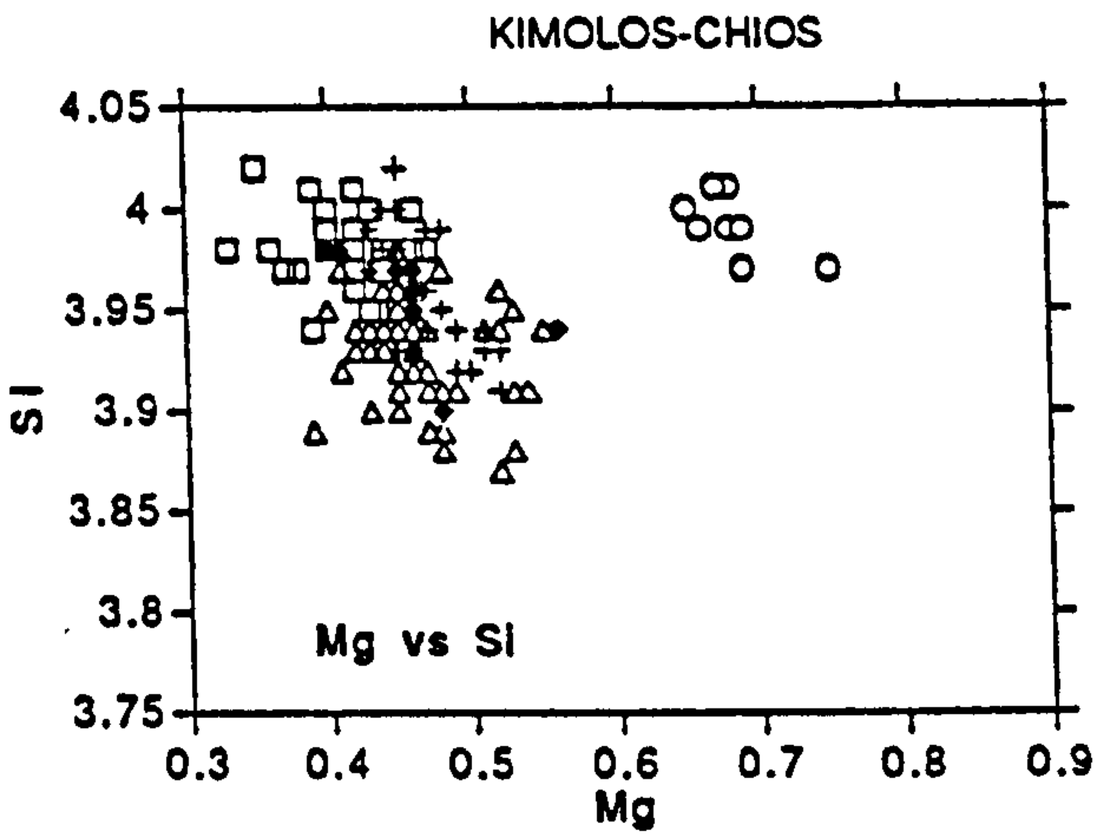

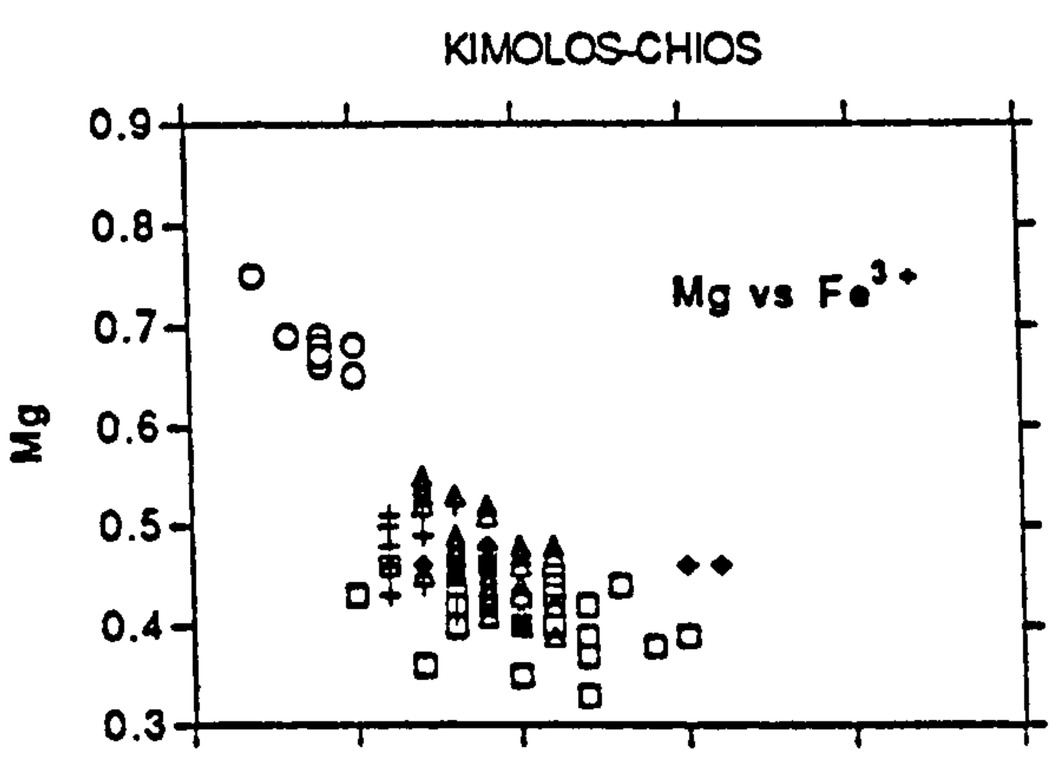

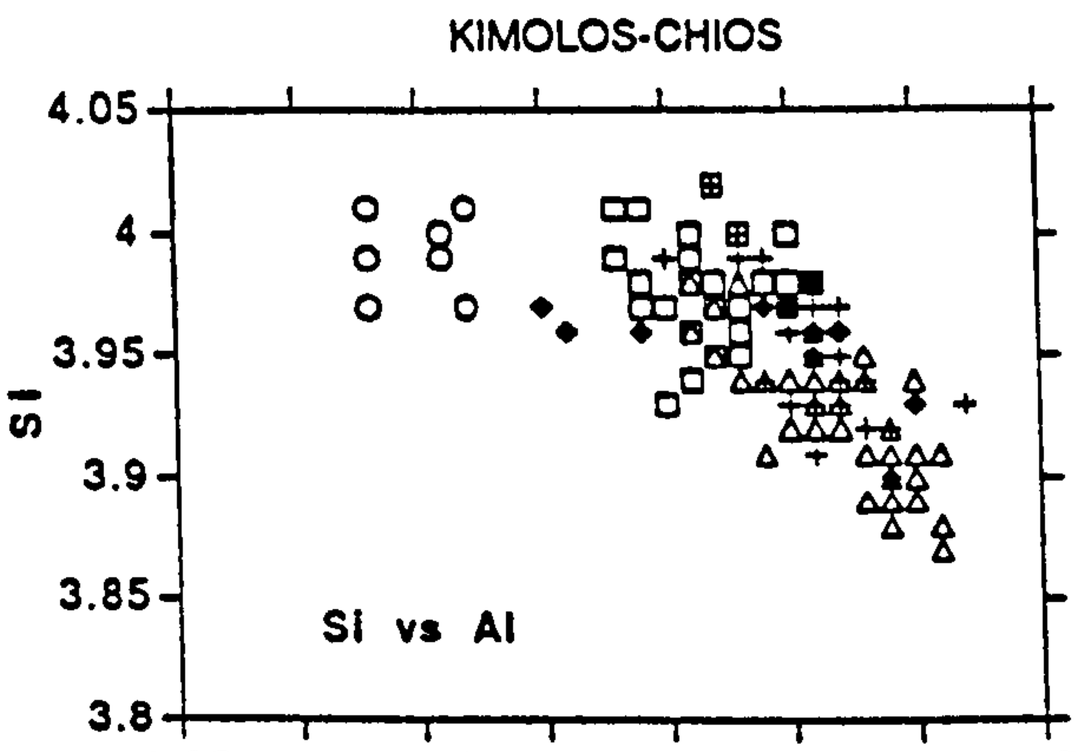

Prassa: □ Smectite+mordenite zone, + Smectite zone, Δ Smectite + opal CT zone
Loutra ◆ Chios ○

FIGURE 4.18. Orthogonal plots between the octahedral and the tetrahedral cations of the smectites present in the bentonites of Kimolos and Chios.

positive relationship until Mg acquires its maximum value, followed by a well defined negative one.

Similar to smectites from Areas 1 and 2 the variation in crystal chemistry of these smectites can be observed when they are projected on the "smectite triangle" of Güven (1988). They do not plot in a single "field" but scatter along a well defined direction parallel to the Al^{VI}-Mg line (Fig. 4.15e). Their composition varies continuously between beidellite and Tatatilla-type montmorillonite. No other Cheto-type smectites are present unlike the deposits of Area 1 (Ankeria and Koufi) confirming the assumption that the compositional signature of smectites from the three different Areas is different.

4.3.2.2. Kimolos Island.

The smectites which were analysed come from the deposits of Prassa and Loutra. In the deposit of Loutra the samples examined come from the main bentonite body, from the zones dominated from the following parageneses: a) smectite + opal-CT b) smectite and c) smectite + mordenite ± opal-CT (see section 4.2.2.1), as well as from one of the small bodies with the following paragenesis smectite + mordenite + K-feldspar. They exhibit characteristics which are between those of the different Areas of Milos, in the sense that although they have been derived from acidic rocks, their iron content is significantly higher than smectites from Area 3 of Milos. Their crystal chemistry is dominated by the following features (Fig. 4.18).

a) Unlike smectites from Area 3 of Milos the negative relationship between Al^{VI} and Fe^{3+} observed for smectites from Areas 1 and 2 of Milos is present here also. However, due to the small variation in Fe^{3+} content, it is not very well expressed. It seems that smectites associated with mordenite have higher Fe^{3+} and lower Al^{VI} content, keeping a more or less constant Al^{VI}:Fe^{3+} ratio. Also, smectites from the smectite + opal-CT zone are more abundant in Fe^{3+} than their counterparts from the pure smectite zone. In the Loutra deposit two different smectite populations can be distinguished on the basis of their Fe^{3+} content; an iron-rich one with Fe^{3+} >0.15 cations per half formula unit and an iron-poor population with less than 0.1 Fe^{3+} cations per half formula unit. A negative relationship is also observed between Al^{VI} and Mg. Smectites from the mordenite-bearing zone are relatively poorer in Al^{VI} compared to those of the mordenite-free zone. Smectites from the small bentonite body follow a different trend which is also characterized by a negative relationship. The slope of this trend is different from that of the main bentonite body. It is obvious that for a constant Al^{VI} content, smectites from the small bentonite deposit are less rich in Mg than those of the main bentonite body.

b) The relationship between Si and Al is a well determined negative one, as was expected. The variation observed for one zone is indicative of the total chemical variation

observed in the deposit. A negative relationship is also present between Mg and Si. It seems, therefore, that decrease of the tetrahedral charge is associated with a concomitant decrease of the octahedral charge. It can also be seen that smectites from the mordenite-bearing zone are relatively poorer in Mg than smectites from the opal-bearing zone. It is interesting that smectites from the small bentonite body which are associated with mordenite are richer in Si than smectites from the mordenite-bearing zone of the nain bentonite body.

c) No significant relationship has been observed between Si and Fe^{3+}. However, an overall negative relationship is observed between Fe^{3+} and Mg. Smectites from the small bentonite body do not follow the overall trend but display a rather constant Mg content over a variable Fe^{3+} content.

d) Smectites coming from different alteration zones plot in different parts of the various diagrams. The relationships between different structural cations describe the overall trend of the total population. In other words, the variation in each alteration zone is not indicative of the total variation of the bentonite deposits unlike Areas 1 and 2 of Milos Island. An exception to this observation is displayed between total Al and Si. The chemical variation of smectites in the Prassa deposit as far as Si and Al are concerned can be described by their variation in one of the different alteration zones. This indicates that in the case of Kimolos Island Si and Al are the main elements controlling the chemical characteristics of smectites, like the case of smectites from Area 3 of Milos.

e) When plotted in the diagram of Güven (1988), smectites from Kimolos fall in the Area between Tatatilla and Chambers montmorillonites (Cheto-type montmorillonites) (Fig 4.15). Alietti & Brigatti (1982) showed with statistical methods that the Kimolian smectites they examined were mainly Otay-montmorillonites. In this study it was observed that the smectites do not possess a high enough octahedral Mg content to be considered as Otay type montmorillonites. Although their tetrahedral charge is small it is impossible to tell whether it is smaller than 15% of the total layer charge, a condition set by Schultz (1969) for the Otay-type montmorillonites, or not, because of the uncertainty in the assignment of the octahedral Mg (see Chapter 6). It seems also that, unlike the smectites of Milos, there is no great compositional variation in these montmorillonites and that beidellite is not present.

4.3.2.3. Chios Island.

Only a small number of reliable analyses were selected (8 out of 53) because the smectites in Thymiana Area are intimately associated with opal-CT and contamination by Si is unavoidable. There is neither any systematic variation in the crystal-chemistry of these smectites nor any systematic relationship between cations which participate in the

crystal structure (Fig. 4.18). The well defined negative relationship between Al and Si has not been observed. The implied positive relationship between Si and Fe^{3+}, negative relationship between Si and Mg and between Fe^{3+} and Mg although expected, are not considered statistically important due to the lack of a significant number of analyses. When projected on the smectite triangle proposed by Güven (1988), the smectites from Chios island plot in the field of Otay-type montmorillonite (Fig. 4.15). This is expected because of their high Mg content and their limited tetrahedral charge.

4.3.3. Mineral Chemistry of Zeolites.

The zeolites analysed come from the island of Kimolos. Two zeolite species were examined: mordenite from Prassa deposit and clinoptilolite from Loutra deposit. Representative analyses of mordenite and clinoptilolite from Kimolos are presented on Table 4.5.

a) **Mordenite from the Prassa deposit.** Two types of mordenite were recognized on the basis of their exchangeable cations: a Na-Ca rich characterized as "normal" mordenite and a K-bearing mordenite. K-bearing mordenites have been described resently by Pe-Piper & Tsolis-Katagas (1991) in the Greek island of Samos. A well determined negative relationship between K and the other exchangeable cations can be observed in Figure 4.19, indicating that K is competing with the other exchangeable cations. It is interesting that the same relationship was observed in the montmorillonites present in the mordenite zone (Fig. 4.19c). The relationship of Ca with the total alkali content clearly shows that there are two distinct populations of mordenites, separated by their total alkali content (Fig 4.19b) while Ca content does not vary substantially. This is probably due to their different K-content. Plotting of mordenites in triangular diagrams describing the composition of the exchangeable sites (Fig 4.20a) confirms that the role of Ca in the variation observed is limited and that the chemical variation of these structural sites is mainly determined by the variation between Na and K (Mg is present in very small amounts).

The Si/Al ratio of mordenites varies between 4.86 and 5.8. No systematic variation between this ratio and the distribution of the exchangeable cations was found. This implies that the relative abundance of these elements in either the gel and/or the fluid phase which they precipitated from (see Section 4.2.7.1) was constant.

b) **Clinoptilolite from the Loutra deposit.** It is dominated by a systematic variation of the exchangeable cations, characterized by a negative relationship between Ca and Ca+Mg and the total alkalis (Fig. 4.19d,e). It has a Si/Al ratio varying between 4.2 and 4.8. It is well known that the higher Si content with respect to Al stabilizes the structure (Alietti, 1972, Boles, 1972) rendering it more thermally stable. Thus, the slight decrease of the

Table 4.5

A selection of microprobe analyses and structural formulae of the mordenites (Mord) and clinoptilolites (Clin).

Sample	SM277	SM277	SM277	SM277	SM277	SM277	SM277	SM277	SM277	SM277	SM277	SM277
Zeolite	Mord	Mord	Mord	Mord	Mord	Mord	Mord	Mord	Mord	Mord	Mord	Mord
SiO_2	65.49	64.76	67.73	71.14	66.09	72.53	71.87	68.06	72.63	73.02	72.89	70.23
TiO_2	- -	- -	- -	- -	- -	- -	- -	- -	- -	- -	- -	- -
Al_2O_3	10.88	10.39	11.13	10.27	10.20	11.11	11.91	10.56	11.78	11.97	11.74	11.98
Fe_2O_3	- -	- -	- -	- -	- -	- -	- -	- -	- -	- -	- -	- -
MgO	0.53	- -	0.47	- -	0.46	- -	- -	- -	- -	- -	- -	0.59
CaO	2.54	2.50	2.43	1.90	2.54	2.59	2.47	2.74	2.82	2.71	2.63	2.71
Na_2O	2.69	3.17	2.99	2.93	1.25	4.02	4.13	2.99	3.79	3.36	1.54	1.69
K_2O	- -	- -	- -	1.62	2.12	- -	- -	0.21	- -	0.91	3.48	2.38
Total	82.12	80.82	84.75	87.86	82.66	90.25	90.38	84.56	91.02	91.97	92.28	89.66
	Structural formulae on the basis of 48 oxygens											
Si	20.11	20.23	20.15	20.53	20.31	20.31	20.12	20.32	20.18	20.15	20.22	20.00
Ti	0.00	0.00	0.00	0.00	0.00	0.00	0.00	0.00	0.00	0.00	0.00	0.00
Al	3.94	3.83	3.90	3.49	3.69	3.67	3.93	3.72	3.86	3.89	3.84	4.02
Fe^{3+}	0.00	0.00	0.00	0.00	0.00	0.00	0.00	0.00	0.00	0.00	0.00	0.00
	Exchangeable cations											
Mg	0.24	0.00	0.21	0.00	0.21	0.00	0.00	0.00	0.00	0.00	0.00	0.25
Ca	0.84	0.84	0.77	0.59	0.84	0.78	0.74	0.88	0.84	0.80	0.78	0.83
Na	1.60	1.92	1.72	1.64	0.74	2.18	2.24	1.73	2.04	1.80	0.83	0.93
K	0.00	0.00	0.00	0.60	0.83	0.00	0.00	0.08	0.00	0.32	1.23	0.86
Si/Al	5.11	5.29	5.16	5.88	5.50	5.54	5.12	5.47	5.23	5.18	5.27	4.97
E%	4.78	6.45	5.74	2.41	0.67	-1.88	5.54	4.27	3.68	4.64	5.94	1.73

Sample	SM302	SM302	SM302	SM302	SM302	SM302	SM302	SM302	SM302	SM302	SM302	SM302
Zeolite	Clin	Clin	Clin	Clin	Clin	Clin	Clin	Clin	Clin	Clin	Clin	Clin
SiO_2	69.45	71.23	69.76	66.84	70.03	69.72	68.21	67.25	70.21	70.02	71.03	68.36
TiO_2	- -	- -	- -	- -	- -	- -	- -	- -	- -	- -	- -	- -
Al_2O_3	13.11	13.87	14.08	12.90	12.55	13.18	12.88	12.43	13.49	13.55	13.62	13.52
Fe_2O_3	- -	- -	- -	- -	- -	- -	- -	- -	- -	- -	- -	- -
MgO	1.34	1.45	1.64	1.12	0.74	0.82	1.16	1.01	0.84	0.83	1.03	1.30
CaO	2.71	2.47	2.38	2.61	2.38	1.80	2.29	2.02	2.09	1.54	1.69	2.61
Na_2O	2.22	2.76	2.50	2.06	2.13	2.95	2.17	2.09	3.68	2.75	3.02	2.52
K_2O	0.35	0.34	1.01	1.10	1.92	2.16	1.76	2.13	0.61	2.88	2.11	0.60
Total	89.18	92.12	91.37	86.63	89.74	90.63	88.47	86.93	90.92	91.57	92.50	88.91
	Structural formulae on the basis of 72 oxygens											
Si	29.53	29.36	29.12	29.41	29.80	29.51	29.48	29.61	29.44	29.42	29.43	29.27
Ti	0.00	0.00	0.00	0.00	0.00	0.00	0.00	0.00	0.00	0.00	0.00	0.00
Al	6.57	6.74	6.93	6.69	6.29	6.57	6.56	6.45	6.67	6.71	6.65	6.82
Fe^{3+}	0.00	0.00	0.00	0.00	0.00	0.00	0.00	0.00	0.00	0.00	0.00	0.00
	Exchangeable cations											
Mg	0.85	0.89	1.02	0.73	0.47	0.52	0.75	0.66	0.52	0.52	0.64	0.83
Ca	1.23	1.09	1.06	1.23	1.09	0.82	1.06	0.95	0.94	0.69	0.75	1.20
Na	1.83	2.21	2.02	1.76	1.76	2.42	1.82	1.78	2.99	2.24	2.43	2.09
K	0.19	0.18	0.54	0.62	1.04	1.17	0.97	1.20	0.33	1.54	1.12	0.33
Si/Al	4.49	4.36	4.20	4.40	4.73	4.49	4.49	4.59	4.42	4.38	4.42	4.29
E%	6.18	6.15	2.91	6.10	6.53	5.12	2.45	3.83	6.73	8.05	5.34	5.39

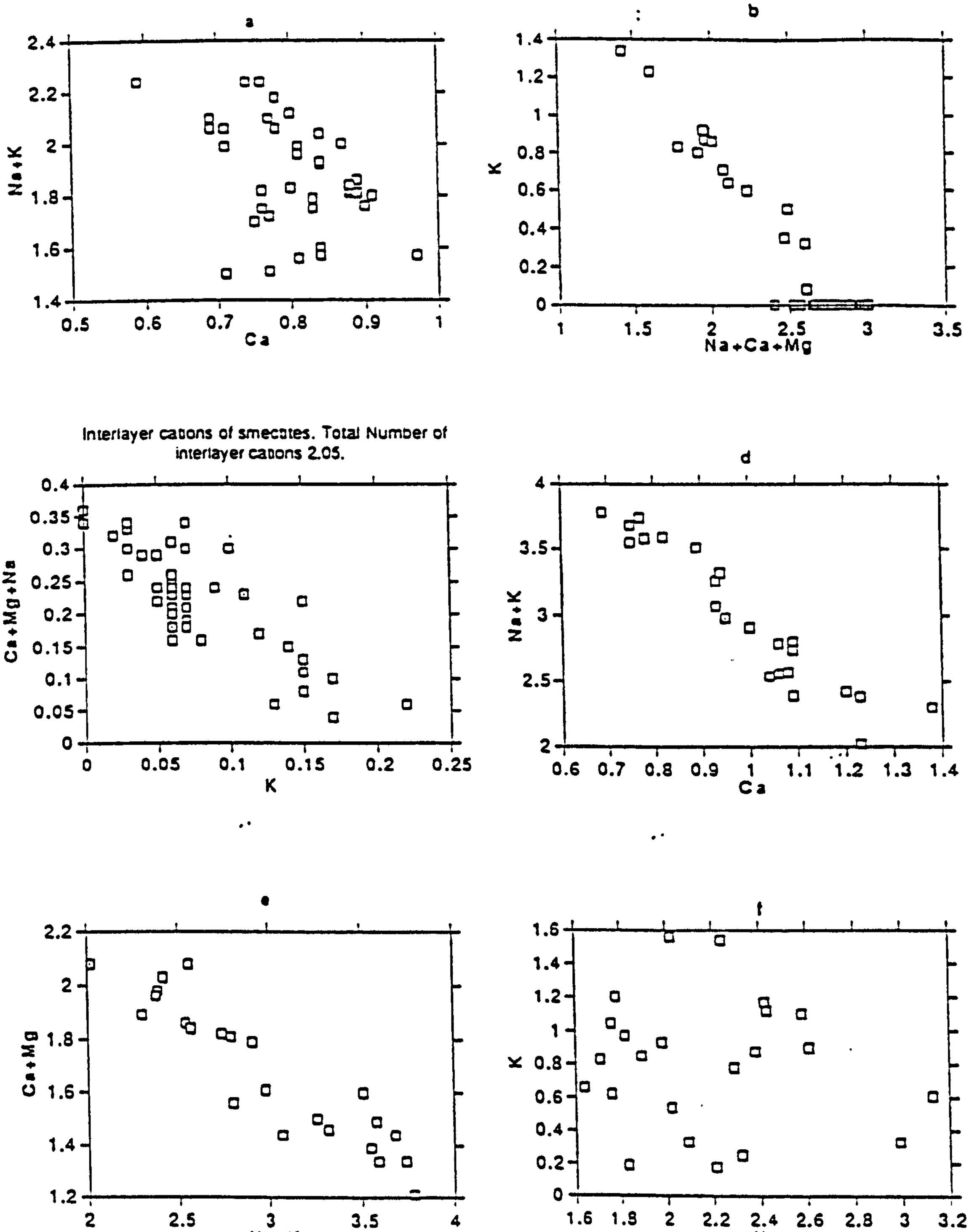

FIGURE 4.19. Diagrams showing the relationships between the exchangeable cations of the zeolites present in the bentonites of Kimolos Island (mordenite from the Prassa deposit 4.19a,b, clinoptilolite from the Loutra deposit 4.19d,e,f), as well as of smectites from the smectite + mordenite zone, Prassa deposit (4.19c).

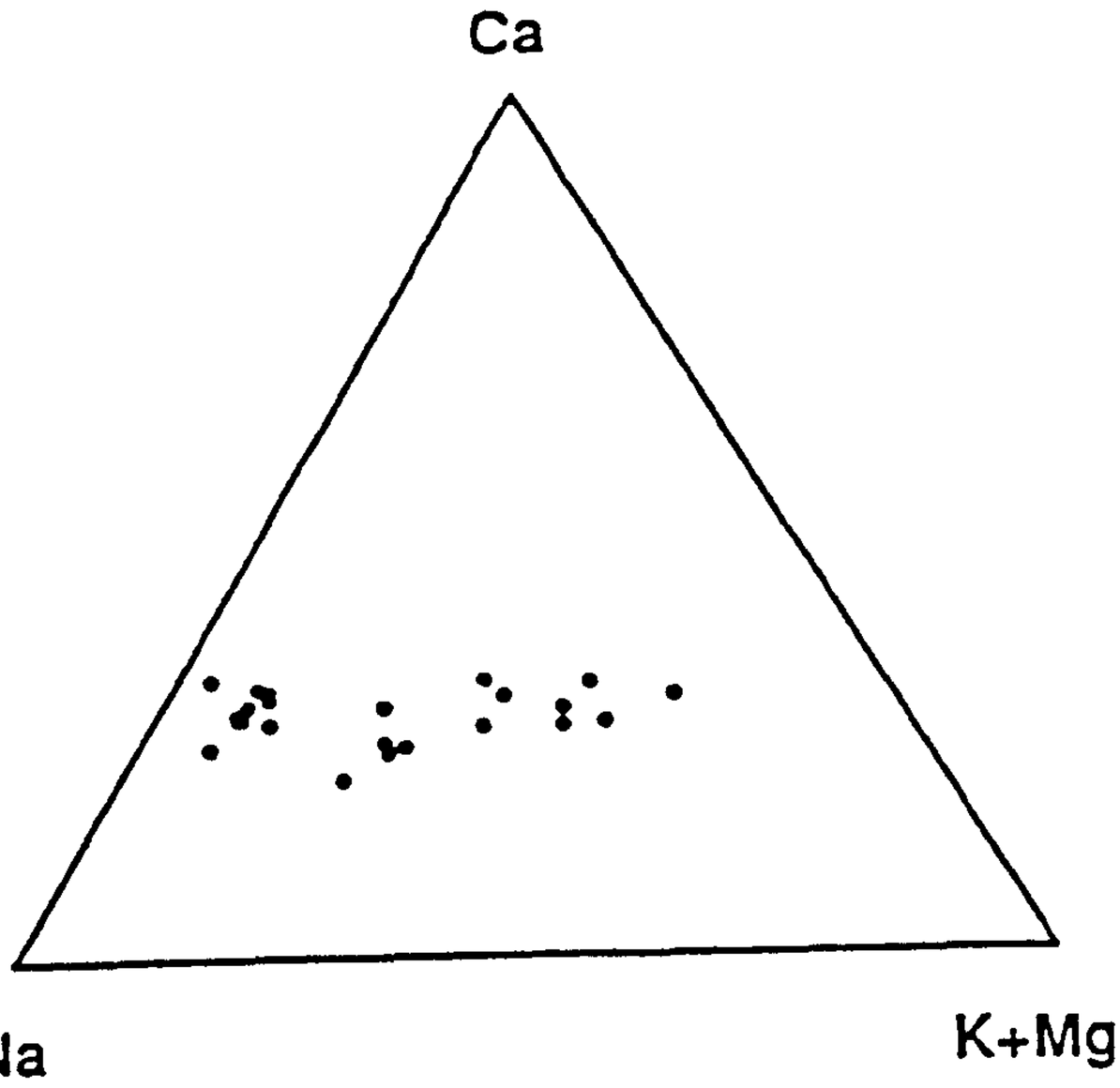

a

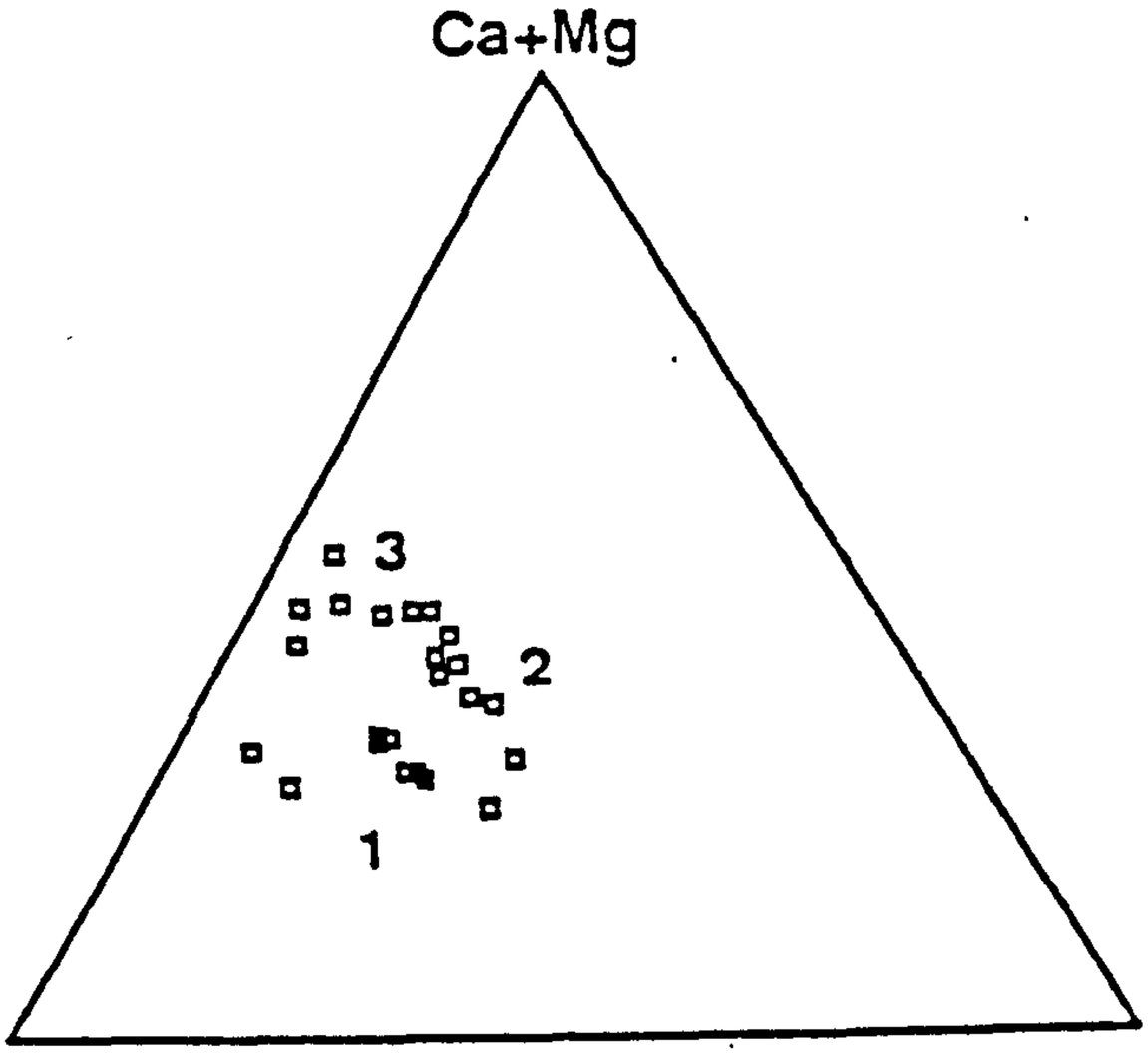

b

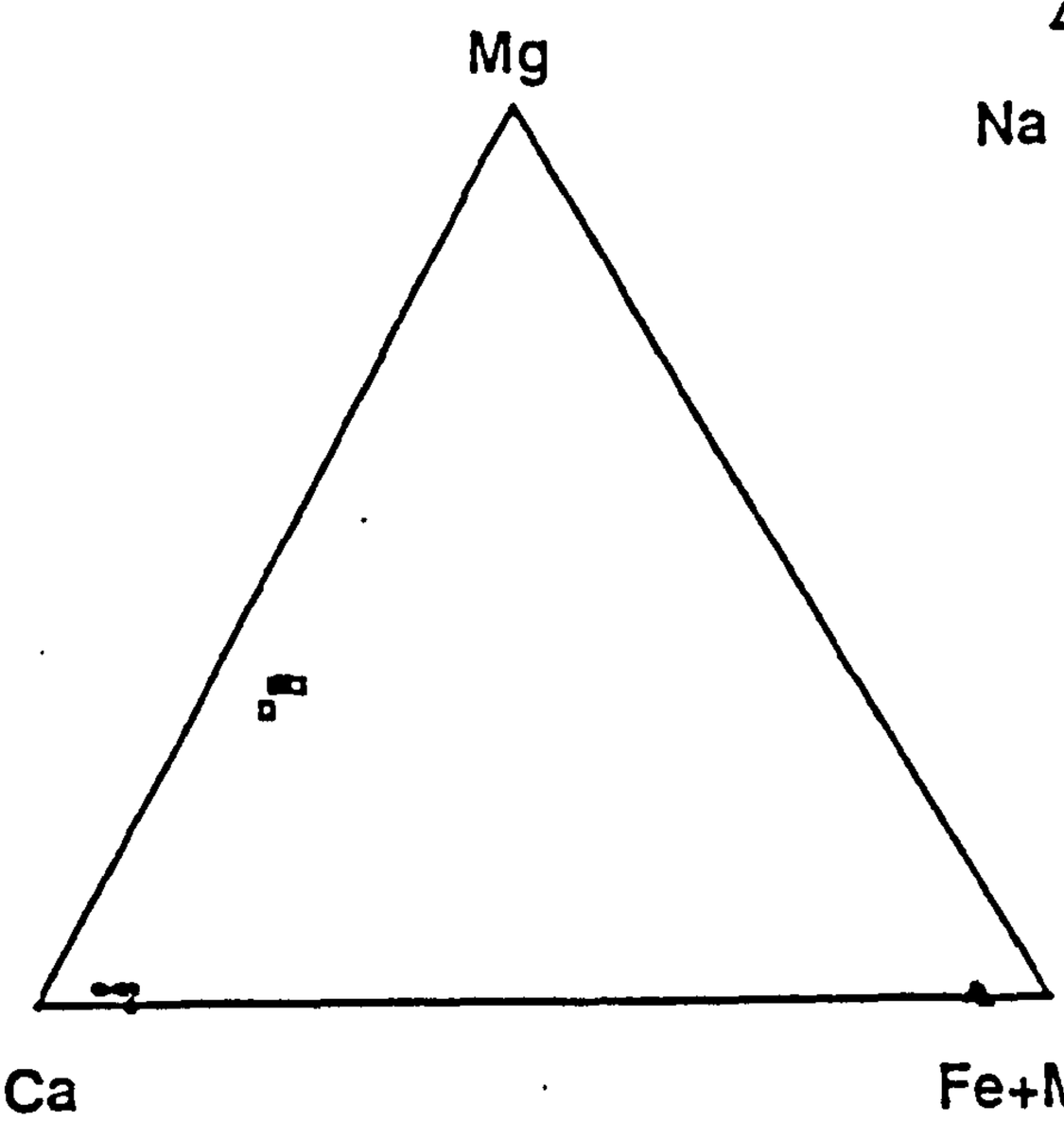

c

FIGURE 4.20. Triangular diagrams showing the relationships between the exchangeable cations of mordenite (a) and clinoptilolite (b) and the main structural cations of the carbonates from the Tsantili deposit (c)

(020) peak intensity after heating might reflect the presence of clinoptilolites with relatively low Si:Al ratios (see Boles, 1972).

In Figures 4.19e,f it is clear that there are two distinct populations, an alkali-rich, Ca+Mg-poor one and a Ca+Mg-rich, alkali-poor one. On the other hand the Si/Al ratio varies within the same limits for both groups (Table 4.5). The variation in bivalent exchangeable cations can also be observed in Figure 4.20b. The two populations (Ca+Mg-rich and Ca+Mg-poor) are separated. It is also obvious that there is a transition betwen the two populations (group 2 on the diagram). It seems therefore, that the chemistry of the clinoptilolites is dominated by two types of exchange:

-1) Ca+Mg for Na+K and

-2) Na for K exchange.

The second type of exchange gradually decreases as the first type becomes increasingly important (group 2) and is limited in the Ca+Mg-poor population (group 3). These variations express the composition of the pore fluids at the time of formation of the different clinoptilolites and are discussed in Chapter 6.

4.3.4. Mineral Chemistry of the feldspars.

Representative microanalyses of pyrogenetic feldspars are given on Table 4.6, while the full set of microanalyses of feldspars is given in the Appendices 4.8 and 4.9. In Milos island the distribution of feldspars exhibits a rather systematic pattern, characterized by the predominance of plagioclase in the deposits of Areas 1 and 2 and K-feldspars in the Area 3. The plagioclases present in the deposits of the Areas 1 and 2 of Milos are andesines (Table 4.6), *i.e* rather on the acid side, if one considers the andesitic-dacitic composition of the parent rocks (see following Chapter).

Abundant K-feldspars have been identified in the lower bentonite horizon of the Koufi deposit (Area 2 Milos) in the Tsantili deposit (Area 1 Milos), in the higher stratigraphic horizon of the Ano Komia deposit, in the Garyfalakena, Rema and Kato Komia deposits (Area 3 Milos) and to a lesser degree in the Ankeria deposit, Milos, and the smectite + mordenite zone in the Prassa deposit, Kimolos. However these K-feldspars have a rather unusual crystal chemistry characterized by the presence of the pure potassium end member, without any Na and/or Ca (see Table 4.7). Chemical purity is a very reliable criterion for the characterization of a K-feldspar as authigenic (Kastner & Siever, 1979). These K-feldspars have substantially different chemistry from their pyrogenetic counterparts which contain significant amounts of Ca and Na in their structure (compare the mineral chemistry of the K-feldspars present in Table 4.6 from those in Table 4.7). Their authigenic origin can be substantiated further, if one takes into account the habit of these feldspars as well as their very small size (see Section 4.2.7.1). According to Kastner

Table 4.6

A selection of microprobe analyses and structural formulae of pyrogenetic plagioclases (Plag) and K-feldspars (KFld). Albite (Albt) comes from the metamorphic basement.

Sample	SM25	SM25	SM25	SM43	SM43	SM43	SM43	SM114	SM144	SM114	SM228	SM228
Quarry	Plag	Plag	Plag	Plag	Plag	KFld	KFld	Plag	Plag	Plag	Plag	Plag
SiO_2	56.86	55.78	58.52	60.06	56.41	65.69	65.39	61.96	59.80	67.84	55.02	58.96
Al_2O_3	27.67	27.66	26.27	24.81	28.02	20.53	20.01	24.02	25.32	19.83	28.98	26.01
Fe_2O_3	- -	0.50	- -	- -	0.56	- -	- -	- -	- -	- -	- -	- -
MgO	0.71	0.88	1.01	0.66	0.79	0.80	0.98	- -	0.85	0.74	- -	0.81
CaO	8.34	8.72	6.82	5.44	8.14	0.83	0.94	4.71	5.81	- -	9.69	5.82
Na_2O	5.93	5.53	6.57	6.99	5.71	4.53	3.57	8.18	7.12	11.17	5.43	6.91
K_2O	0.29	0.30	0.34	0.94	0.51	8.94	9.80	0.67	0.59	- -	- -	0.87
BaO	- -	- -	- -	- -	- -	- -	- -	- -	- -	- -	- -	- -
Total	99.80	99.37	99.53	98.90	100.14	101.39	100.69	99.54	99.59	99.58	99.12	99.38
Structural formulae on the basis of 32 oxygens												
Si	10.19	10.07	10.47	10.79	10.10	11.69	11.73	11.03	10.68	11.88	9.95	10.56
Al	5.84	5.89	5.54	5.25	5.91	4.31	4.23	5.04	5.33	4.09	6.18	5.49
Fe^{3+}	0.00	0.07	0.00	0.00	0.08	0.00	0.00	0.00	0.00	0.00	0.00	0.00
Mg	0.19	0.24	0.27	0.18	0.21	0.21	0.26	0.00	0.23	0.19	0.00	0.22
Ca	1.60	1.69	1.31	1.05	1.56	0.16	0.18	0.90	1.11	0.00	1.88	1.12
Na	2.06	1.94	2.28	2.43	1.98	1.56	1.24	2.82	2.47	3.79	1.90	2.40
K	0.07	0.07	0.08	0.22	0.12	2.03	2.24	0.15	0.13	0.00	0.00	0.20
Ba	- -	- -	- -	- -	- -	- -	- -	- -	- -	- -	- -	- -
Ab	52.59	49.28	57.94	62.85	51.21	39.44	31.62	72.88	62.61	95.15	50.35	61.04
An	45.72	48.97	40.09	31.59	45.79	9.35	11.27	23.19	33.98	4.85	49.65	33.91
Or	1.69	1.76	1.97	5.56	3.01	51.21	57.11	3.93	3.41	0.00	0.00	5.06

Sample	SM228	SM277	SM277	SM277	SM277	SM277	SM277	SM277	SM277	SM281	SM281	SM302
Feldspar	KFld	KFld	KFeld	Plag	Plag	Plag	Plag	KFld	KFld	Albt	Albt	Plag
SiO_2	64.96	65.44	65.78	64.95	66.04	65.13	64.55	63.45	63.04	67.82	68.49	61.87
Al_2O_3	19.07	20.77	20.10	22.54	21.86	22.00	22.94	19.67	18.86	19.90	19.89	24.77
Fe_2O_3	0.44	- -	- -	- -	- -	- -	- -	- -	- -	- -	- -	- -
MgO	1.41	1.57	1.78	0.52	- -	- -	- -	- -	- -	- -	- -	- -
CaO	0.52	0.62	0.98	2.96	2.59	2.84	3.88	0.93	1.98	- -	- -	5.24
Na_2O	1.28	1.47	1.37	5.08	5.61	6.50	7.35	3.96	0.71	11.47	11.38	7.88
K_2O	12.49	10.97	9.74	3.03	4.35	3.90	0.95	9.53	13.71	- -	- -	0.90
BaO	- -	- -	- -	- -	- -	- -	- -	1.28	- -	- -	- -	- -
Total	100.17	100.74	99.75	99.08	100.45	100.41	99.67	98.82	98.30	99.19	99.76	101.12
Structural formulae on the basis of 32 oxygens												
Si	11.81	11.70	11.80	11.51	11.63	11.52	11.38	11.73	11.80	11.93	11.96	10.92
Al	4.09	4.38	4.25	4.71	4.54	4.58	4.77	4.29	4.16	4.13	4.10	5.15
Fe^{3+}	0.06	0.00	0.00	0.00	0.00	0.00	0.00	0.00	0.00	0.00	0.00	0.00
Mg	0.38	0.42	0.48	0.14	0.00	0.00	0.00	0.00	0.00	0.00	0.00	0.00
Ca	0.10	0.12	0.19	0.56	0.49	0.54	0.73	0.18	0.40	0.00	0.00	0.99
Na	0.45	0.51	0.48	1.75	1.92	2.23	2.51	1.42	0.26	3.91	3.85	2.70
K	2.90	2.50	2.23	0.69	0.98	0.88	0.21	2.25	3.27	0.00	0.00	0.20
Ba	- -	- -	- -	- -	- -	- -	- -	0.09	- -	- -	- -	- -
Ab	11.78	14.36	14.14	55.77	56.65	61.12	72.63	36.86	6.56	100.00	100.00	69.32
An	12.62	15.14	19.71	22.35	14.45	14.76	21.19	4.78	10.11	0.00	0.00	25.47
Or	75.61	70.50	66.14	21.89	28.90	24.13	6.18	58.36	83.33	0.00	0.00	5.21

Table 4.6 (continued)

Location of the samples: SM25 Ankeria deposit, Milos, SM43=Koufi deposit, Milos, SM114=Aspro Horio deposit, Milos, SM228=Zoulias deposit, Milos, SM277, SM281=Prassa deposit, Kimolos, SM302=Prassa deposit, Kimolos.

Table 4.7

Microprobe analyses and structural formulae of the authigenic K-feldspars present in the Greek bentonites. Key to the codes: BMKF=Koufi deposit, Milos, BMA1=Higher benotite horizon, Ano Komia deposit, Milos, BMTS=Tsantili deposit, Milos, BKPR=Prassa deposit, Kimolos. Note the purity and the stoichiometry of the K-feldspars.

Sample	SM66	SM66	SM66	SM155	SM155	SM155	SM99	SM99	SM99	SM277	SM277	SM277
Quarry	BMKF	BMKF	BMKF	BMA1	BMA1	BMA1	BMTS	BMTS	BMTS	BKPR	BKPR	BKPR
SiO_2	66.34	65.38	65.87	66.26	65.15	65.51	64.71	65.79	64.30	65.92	66.70	65.15
Al_2O_3	16.78	17.38	18.45	16.86	18.04	17.48	17.71	17.01	18.47	17.33	17.29	17.81
Fe_2O_3	- -	- -	- -	- -	- -	- -	- -	- -	- -	- -	- -	- -
MgO	- -	- -	- -	- -	- -	- -	- -	- -	- -	- -	- -	- -
CaO	- -	- -	- -	- -	- -	- -	- -	- -	- -	- -	- -	- -
Na_2O	- -	- -	- -	- -	- -	- -	- -	- -	- -	- -	- -	- -
K_2O	16.59	16.66	16.11	16.09	16.15	15.97	16.36	16.31	17.03	16.33	15.85	16.31
Total	99.71	99.42	100.43	99.21	99.34	98.76	98.78	99.11	99.80	99.58	99.84	99.27
Structural formulae based on 32 oxygens												
Si	12.28	12.16	12.07	12.29	12.09	12.18	12.10	12.24	11.95	12.20	12.26	12.11
Al	3.66	3.81	3.98	3.68	3.94	3.83	3.90	3.73	4.05	3.78	3.75	3.90
Fe^{3+}	0.00	0.00	0.00	0.00	0.00	0.00	0.00	0.00	0.00	0.00	0.00	0.00
Mg	0.00	0.00	0.00	0.00	0.00	0.00	0.00	0.00	0.00	0.00	0.00	0.00
Ca	0.00	0.00	0.00	0.00	0.00	0.00	0.00	0.00	0.00	0.00	0.00	0.00
Na	0.00	0.00	0.00	0.00	0.00	0.00	0.00	0.00	0.00	0.00	0.00	0.00
K	3.92	3.95	3.77	3.81	3.82	3.79	3.90	3.87	4.04	3.86	3.72	3.87

Table 4.8

Microprobe analyses and structural formulae of the carbonates present in the Tsantili deposit, Milos. Key to the mineral codes: Calc= Mn-calcite, Anke=Ankerite, Side= Mn-siderite.

Sample	SM99	SM99	SM99	SM99	SM99	SM99	SM99	SM99	SM99	SM99	SM99	SM99
Mineral	Calc	Calc	Calc	Calc	Anke	Anke	Anke	Anke	Side	Side	Side	Side
FeO	- -	1.19	- -	0.61	1.54	1.69	1.21	1.18	29.27	28.58	30.98	29.42
MnO	2.61	3.84	5.19	5.00	3.85	3.86	3.83	4.16	22.29	22.65	13.38	18.11
MgO	- -	- -	- -	- -	15.15	15.62	15.08	14.01	2.84	2.94	9.47	6.36
CaO	52.21	51.11	49.84	50.02	32.93	33.06	33.50	34.20	2.69	2.70	2.40	2.96
Total	54.82	56.14	55.03	55.63	53.47	54.23	53.62	53.55	57.09	56.87	56.23	56.85
Structural formulae on the basis of 6 oxygens												
Fe^{2+}	0.00	0.09	0.00	0.04	0.12	0.13	0.09	0.09	2.91	2.87	2.88	2.82
Mn	0.24	0.33	0.45	0.45	0.31	0.33	0.30	0.33	2.25	2.29	1.26	1.74
Mg	0.00	0.00	0.00	0.00	2.17	2.19	2.16	2.01	0.51	0.51	1.56	1.08
Ca	5.76	5.58	5.55	5.52	3.39	3.36	3.45	3.56	0.33	0.33	0.30	0.36

& Siever (1979) pure K-feldspars are indicative of very low temperatures and pressures *i.e* of diagenetic conditions. Pure end members of feldspars have been found also in some pegmatite veins and in low metamorphic conditions (Kastner & Siever, 1979). However, such conditions certainly did not prevail during the formation of the bentonite deposits.

Authigenic K-feldspars might coexist with pyrogenetic and/or metamorphic feldspars. An example is in the Prassa deposit, Kimolos, in which 4 different types of feldspars have been identified: Two of them are pyrogenetic (anorthoclase and intermediate/basic plagioclase; see Table 4.6), one is metamorphic albite derived from the metamorphic basement, and the fourth type is authigenic K-feldspar (Table 4.7).

Both pyrogenetic K-feldspars and plagioclases contain Mg which in many occasions is well in excess of 1%. According to Deer *et al.* (1965) the Mg-content of feldspars is very small, and in their published feldspar analyses the Mg-content does not exceed 0.5% with one exception (0.76%). It is believed that Mg has been introduced during the alteration of the parent volcaniclastic rocks to bentonite, while Ca has been removed. This might explain the relatively low Ca content of the plagioclases present in the bentonites. In Plates 13 and 17 the pseudomorphic replacement of plagioclase by montmorillonite is obvious. Replacement of feldspars by smectite had been assumed by Wetzenstein (1969) and was shown by Christidis (1989) in the bentonites of Milos. Such a replacement has been determined in weathering environments (Banfield & Eggleton, 1990, Banfield *et al.*, 1991a).

4.3.5. Mineral chemistry of the carbonates from the Tsantili deposit.

The X-Ray Diffraction investigation showed that in the Tsantili deposit there are 3 types of carbonates present (Section 4.2.1.3). In agreement with the XRD analyses microprobe analyses (Appendix 4.9) revealed that the three carbonates are:

-a Mn-bearing calcite phase

-an ankerite phase and

-a Mn-siderite phase.

The compositional characteristics of these phases can be observed in the Figure 4.20c., while their textural relationship is depicted in Plate 17. The Mn-siderite phase is always closely associated with the ankerite phase and it may have been derived through exsolution (Plate 17). On the other hand the Mn-calcite does not seem to be texturaly related with the other carbonates. The formation of these carbonates might be closely associated with the illitization of smectite (see Chapter 6).

TABLE 4.9

Mineralogical composition of the Greek bentonite deposits of the Islands of Milos, Kimolos and Chios.

Key to the symbols used

M =Major mineral phase

Min=Minor mineral phase

T =Trace mineral phase

- - = Not detected

(±) =Present is some sectors or horizons of the deposit.

? =Not unambiguous identification of the mineral phase.

Mont/nite=montmorillonite

CH =Chambers (Cheto) montmorillonite

TA =Tatatilla (Cheto) montmorillonite

OT =Otay (Cheto) montmorillonite

I/S =Illite/smectite

R0/R1/R3=ordering type of the illite/smectite interstratification (see Appendix 4.1)

K-feldspar^1= authigenic K-feldspar

K-feldspar^2= pyrogenetic K-feldspar

	AREA 1			AREA 2		AREA 3						
Mineral	Tsantili	Asp. Horio	Zoulias	Ankeria	Kouti	An. Komia	Garyfalakena	Mavrogiannis	K. Komia	Rema	Agrilies	Kastriani
Smectite	M (±)	M	M	M	M	M	M	M	M	M	M (±)	- -
Type	Mont/nite (Wyoming)	Mont/nite (Wyoming)	Mont/nite (Cheto/CH))	Mont/nite (Cheto/TA-CH))	Mont/nite (TA) /beidellite	Mont/nite (TA) /beidellite	Mont/nite (TA) /beidellite	Mont/nite (TA) /beidellite	Mont/nite	Mont/nite Cheto (TA)	Mont/nte (TA) /beidellite	- -
I/S	M (±)	- -	- -	- -	- -	- -	- -	- -	- -	- -	M (±)	- -
Ordering	R0, R1, R3	- -	- -	- -	- -	- -	- -	- -	- -	- -	R0/R1	- -
Kaolinite	T/Min (±)	- -	T (±)	- -	Min (±)	Min/T (±)	T (±)	T	T	- -	Min	M
halloysite	- -	T (±)	- -	- -	- -	- -	- -	- -	- -	- -	- -	- -
Mica	- -	- -	- -	- -	- -	Min (±)	- -	- -	Min	- -	Min	- -
Chlorite	- -	- -	- -	- -	- -	Min (±)	T (±)	- -	Min	- -	- -	- -
Opal-CT	- -	Min/T	Min/M (±)	Min/M (±)	T/Min (±)	M (±)	M	M	M	M	- -	M
Opal-C	- -	- -	- -	- -	- -	M (±)	--	- -	- -	- -	- -	- -
Quartz	Min (±)	M	M/Min (±)	M	T/Min (±)	M	Min	M	M	Min	M	M
Clinoptilolite	- -	- -	Min (±)	- -	- -	- -	Min (±)	- -	- -	- -	- -	- -
Mordenite	- -	- -	- -	T (±)	- -	- -	Min (±)	- -	- -	- -	- -	- -
K-feldspar[1]	M	- -	Min (±)	T (±)	Min (±)	Min (±)	Min (±)	T/Min (±)	Min/T	T/Min	?	- -
Plagioclase	- -	Min	M/Min (±)	Min (±)	Min/M (±)	- -	Min (±)	Min	Min	Min	- -	- -
K-feldspar[2]	- -	Min (±)	M/Min (±)	Min/T (±)	Min/T (±)	Min (±)	T (±)	?	?	?	- -	- -
Calcite	Min (±)	Min/T (±)	- -	M/Min (±)	T (±)	M (±)	T/Min (±)	- -	M	- -	- -	- -
Siderite	Mn (±)	- -	Min (±)	- -	- -	- -	- -	- -	- -	- -	- -	- -
Ankerite	Min/M (±)	- -	Min (±)	- -	- -	- -	- -	- -	- -	- -	- -	- -
Alunite	Min/T (±)	- -	- -	- -	- -	- -	- -	- -	M/Min (±)	- -	- -	M
Jarosite	Min/T (±)	T/Min (±)	- -	Min/T (±)	- -	- -	- -	T (±)	M/Min (±)	T (±)	T (±)	- -
Gypsum	T (±)	T/Min (±)	Min/T (±)	Min/T (±)	T (±)	Min/T (±)	T (±)	- -	T	- -	Min	- -
Baryte	- -	- -	T (±)	- -	T (±)	- -	- -	- -	- -	- -	T (±)	- -
Pyrite/	T (±)	T (±)	T (±)	T (±)	T (±)	T (±)	T(±)	T	T	T	T (±)	- -
Marcasite	T (±)	T (±)	- -	T (±)	T (±)	- -	- -	- -	- -	- -	T (±)	- -
Hematite	T (±)	- -	- -	T (±)	- -	- -	- -	- -	- -	- -	- -	- -
Halite	T (±)	- -	- -	- -	- -	- -	- -	- -	- -	- -	- -	T/Min (±)

	KIMOLOS					CHIOS
Mineral	Presa	Loutra	Fanara	Bonatsa	Agios Tryfon	Thymiana area
Smectite	M	M/Min	M	M	Min/T(±)	M
Type	Mont/nite	Mont/nite	Mont/nite	Mont/nite-Nontronite	Mont/nite	Mont/nite
	Cheto (TA/CH)	Cheto (TA/CH)				Cheto(OT)
Kaolinite	- -	- -	Min/T(±)	- -	M/Min	- -
Halloysite	- -	- -	- -	- -	M/Min(±)	- -
Mica	T(±)	T(±)	- -	- -	- -	Min(±)
Chlorite	- -	- -	- -	- -	- -	Min(±)
Talc	- -	- -	- -	- -	- -	T(±)
Serpentine	- -	- -	- -	- -	- -	T/Min(±)
Opal CT	M/Min	M/Min	M/Min(±)	T(±)	M/Min	M
Quartz	- -	Min	M/Min(±)	Min(±)	M	M/Min
Mordenite	M/Min (±)	- -	- -	- -	- -	- -
Clinoptilolite	- -	Min(±)	- -	T(±)	- -	- -
K-feldspar[1]	T(±)	- -	?	- -	- -	- -
Plagioclase	T/Min	M/Min)	Min	M	Min/T(±)	M/Min
K-feldspar[2]	T	T(±)	M/Min(±)	Min(±)	Min/T(±)	- -
Calcite	- -	- -	- -	- -	- -	Min(±)
Dolomite	- -	- -	- -	- -	- -	M/T
Aragonite	- -	- -	- -	- -	- -	T(±)
Alunite	- -	- -	- -	- -	M/Min(±)	- -
Gypsum	T(±)	- -	- -	- -	Min/M(±)	- -
Halite	T(±)	- -	- -	- -	- -	- -

Plate 12

Microtextures of the smectites present in the Greek bentonites

1. Progressive alteration of volcanic glass (a) to smectite (c) through an intermediate poorly crystalline phase (b). This phase might be a precursor of smectite. The small spherules present belong to opal-CT. Prassa deposit, Kimolos. Scale bar 6μm.

2. Formation of smectite at the expense of volcanic glass shard. The smectite flakes apparently grow at the expense of the volcanic glass. The rhombohedral crystal on the right hand side of the large shard belongs to dolomite. Chios bentonite. Scale bar 20μm.

3. Pseudomorhic replacement of the volcanic glass from smectite (montmorillonite). The oginal texture has been preserved although the volcanic glass has been completely replaced by montmorillonite. The small spherical crystallites present on the top of the smectite flakes belong to opal-CT. Note the small size of the opal-CT crystals. Prassa deposit, Kimolos. Scale bar 20μm.

4. Typical honeycomb texture characteristic of the smectite flakes. Aspro Horio deposit, Milos. Scale bar 4.3μm.

5. Smectite crystals with characteristic honeycomb texture. The small white crystallites in the right hand side of the photo is opal-CT. Ankeria deposit, Milos. Scale bar 6μm.

6. Smectite flakes with a "closed" texture. Although they occupy open space they do not form "open" honeycomb structures as Konta (1985) suggested. The white phase in the centre of the micrograph belongs probably to an Si-Al-gel. Ankeria deposit, Milos. Scale bar 10μm.

7. Nontronite flakes observed in the Bonatsa deposit, Kimolos. The sample was taken next to a faulted zone. Note the elongated shape of these flakes compared to the Al-rich smectites (montmorillonite and beidellite) present in the Greek bentonite deposits. Scale bar 9.3 μm

8. Sphepulitic montmorillonite aggregates present in the Ankeria deposit, Milos. The veilets cutting the smectite mass also consist of montmorillonite. They have probably formed during the reworking of the deposits by hydrothermal alteration. Scale bar 100μm.

Plate 12

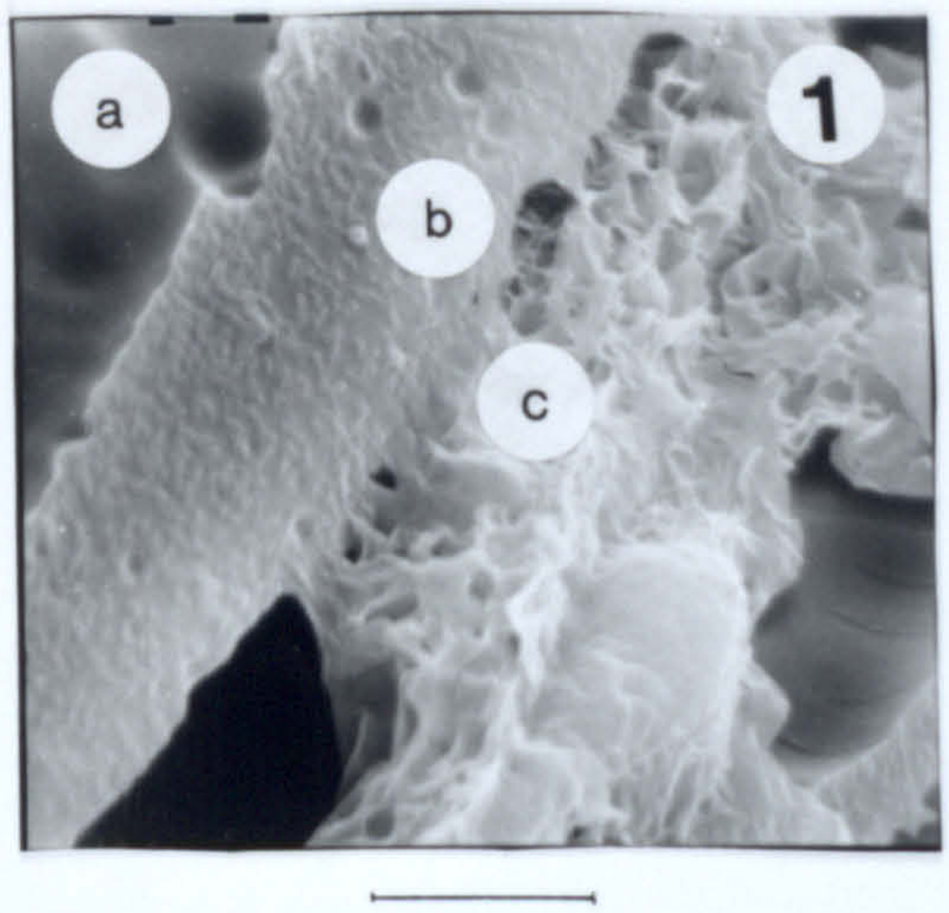

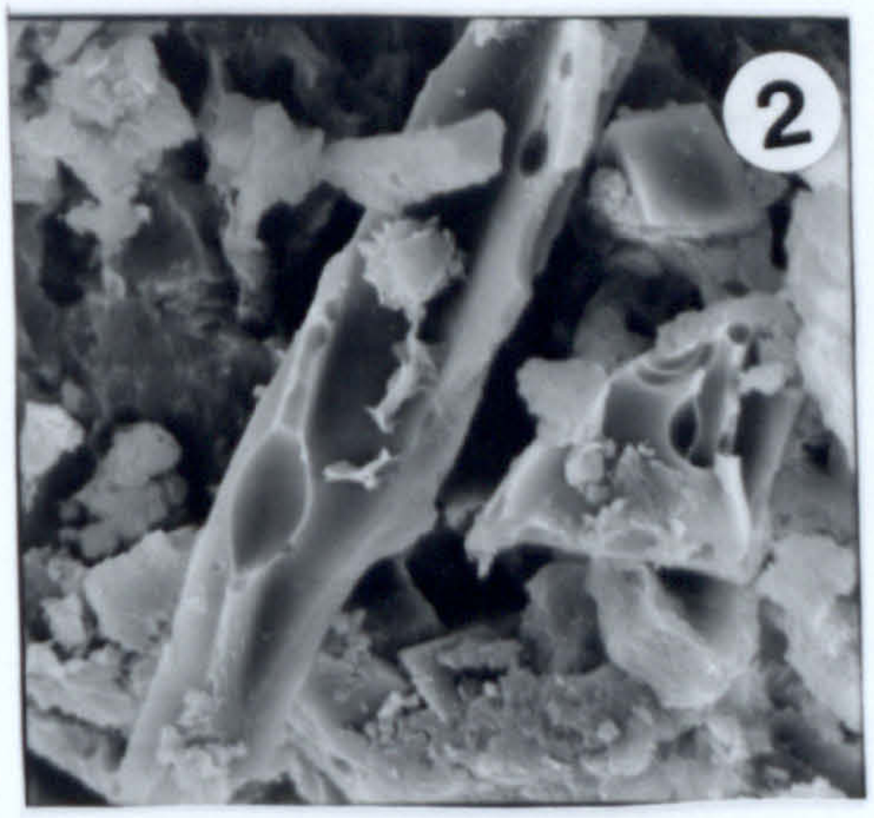

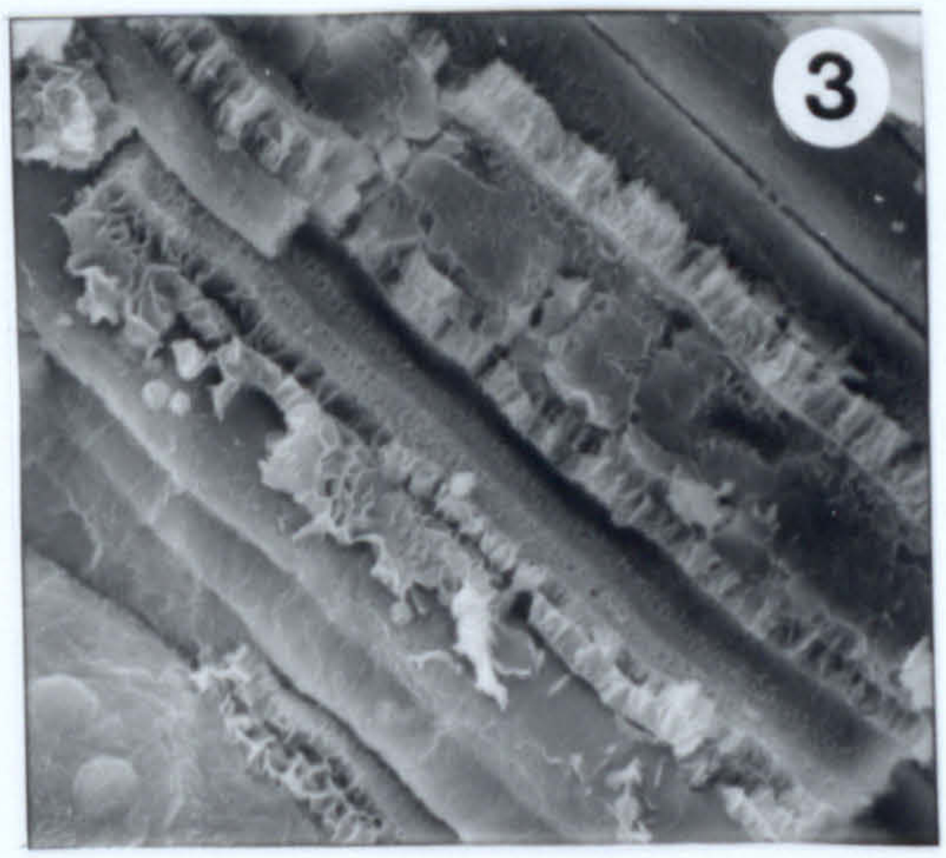

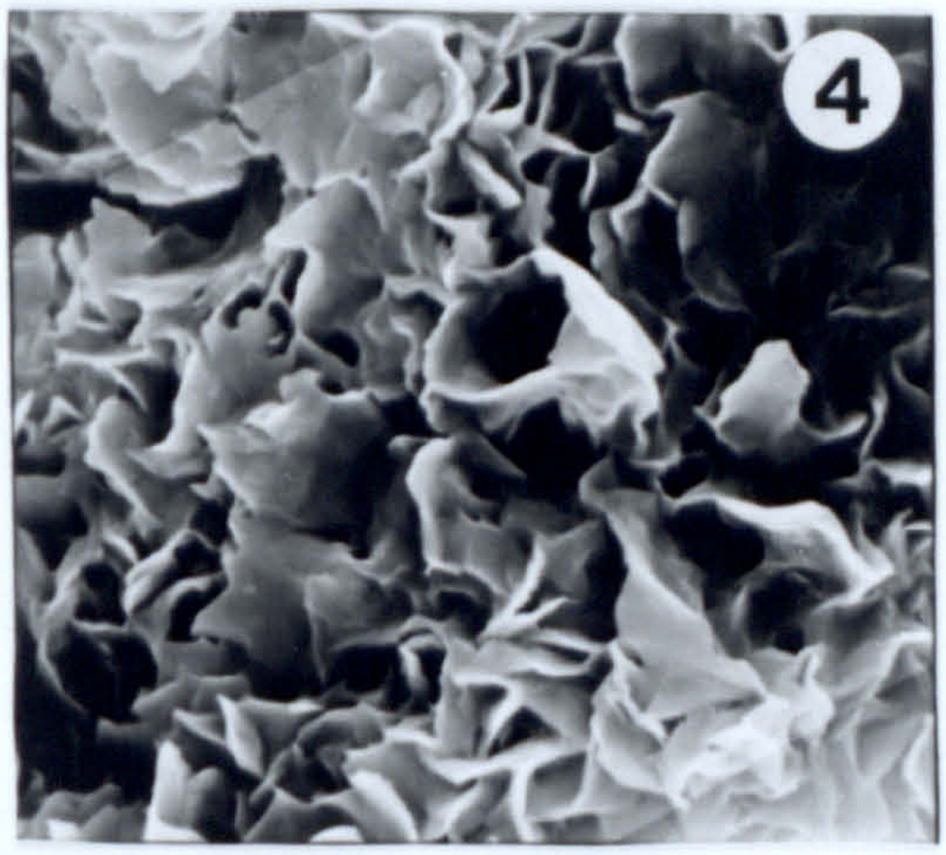

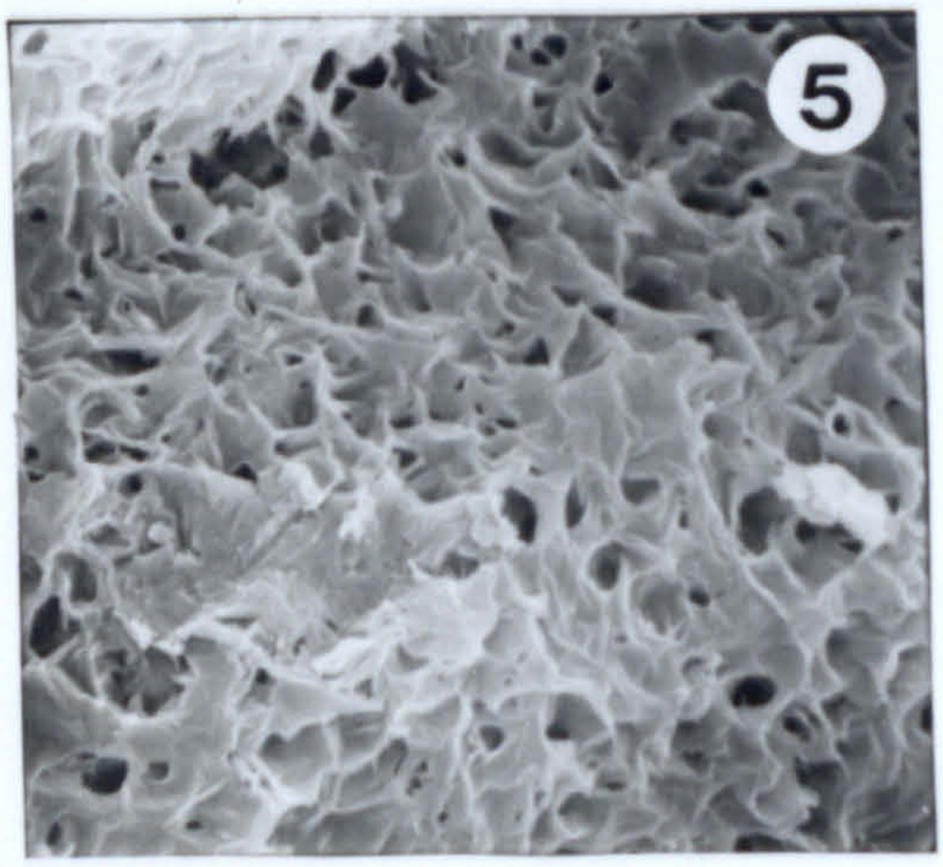

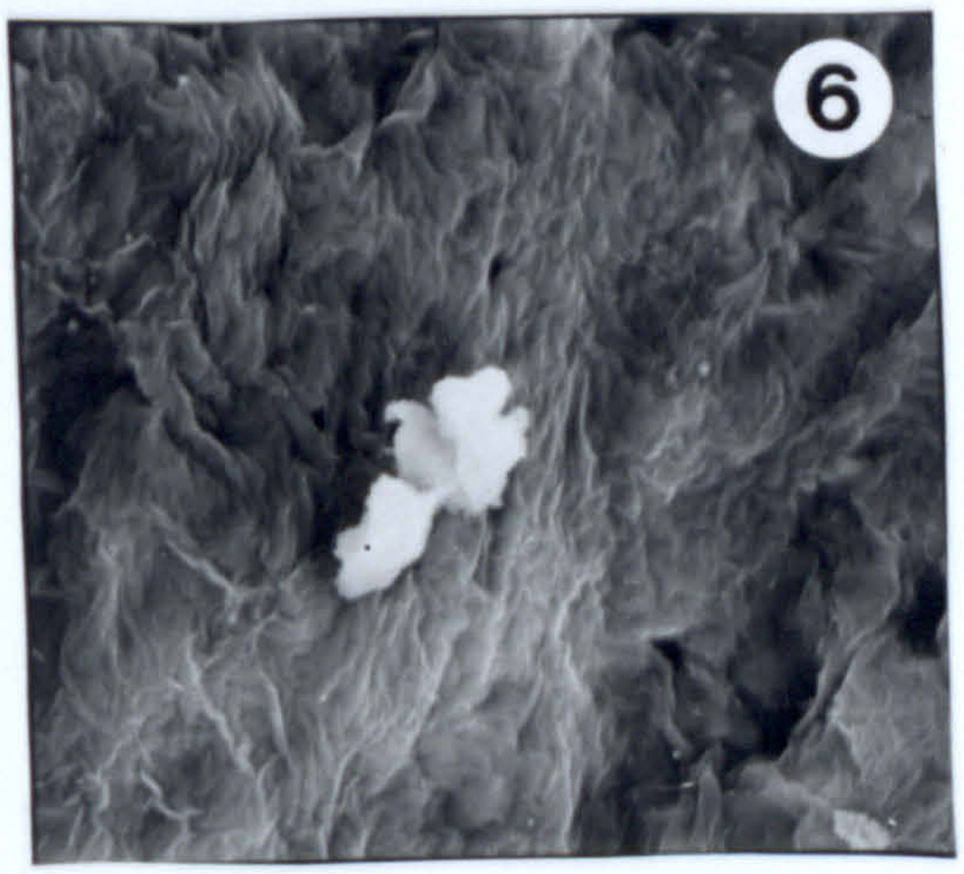

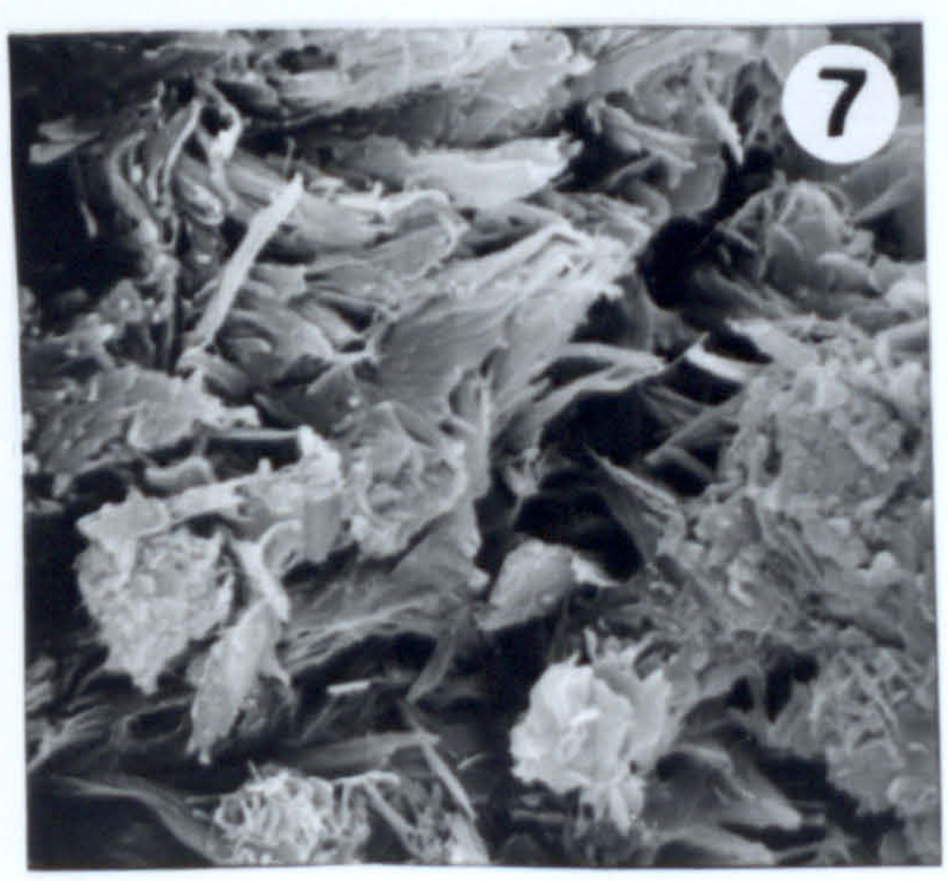

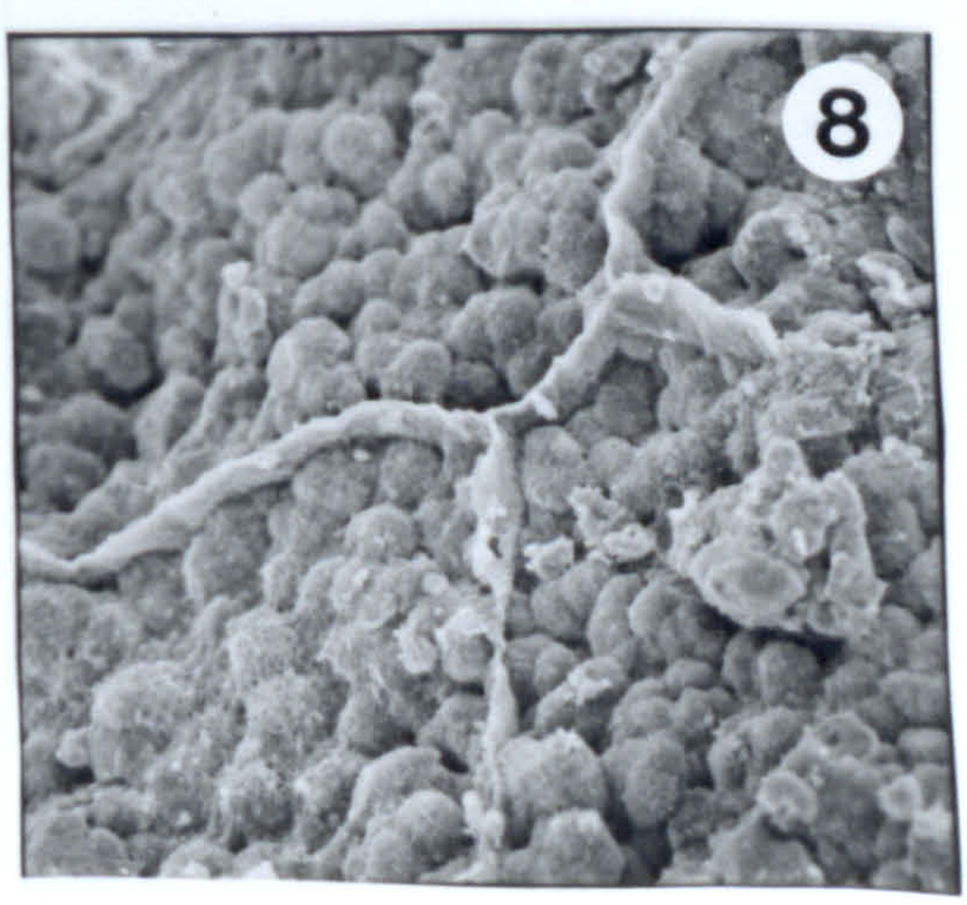

Plate 13

Replacement textures observed in the Greek bentonites.

1. Smectite (shown with the arrow) formed at the expense of pyrogenetic plagioglase. The smectite forms a thin alteration crust on the surface of the plagioclase, but with progressive alteration well developed flakes are formed. The small euhedral crystals drapped over the altered plagioclase belong to apatite. Zoulias deposit, Milos. Scale bar 7.5μm.

2. Smectite formed at the expense of pyrogenetic K-feldspar. Note the different characteristics of this K-fdeldspar compared to the authigenic K-feldspars shown in Plate 14. Ano Komia deposit, Milos. Scale bar 4.3μm.

3. Kaolinite formed at the expense of smectite. It is well crystallized and forms characteristic "books". Agios Tryfon deposit, Kimolos. Scale bar 15μm.

4,5. Kaolinite replacing smectite. Again, kaolinite is well crystallized and forms characteristic books. It is not clear whether kaolinite forms through a mixed layer kaolinite/smectite phase Lower horizon, Ano Komia deposit, Milos. Scale bars: 4= 7.5μm, 5= 15μm.

6. Kaolinite replacing smectite flakes. Tsantili deposit, Milos. Scale bar 7.5μm.

7. Acicular halloysite forming at the expence of smectite (shown by the arrow). The white crystallites present belong to a Si-rich phase (probably opal-CT) have been formed as a by product during the alteration reaction, because the Si:Al ratio of halloysite is considerably lower than this of smectite. Aspro Horio deposit, Milos. Scale bar 3μm.

8. Kaolinite crystals present in the Kastriani kaolin deposit. They have probably precipitated directly from hydrothermal solutions. Note the different size and morphology of these kaolinite flakes compared to the kaolinite formed from a smectite precursor. Scale bar 5μm.

Plate 13

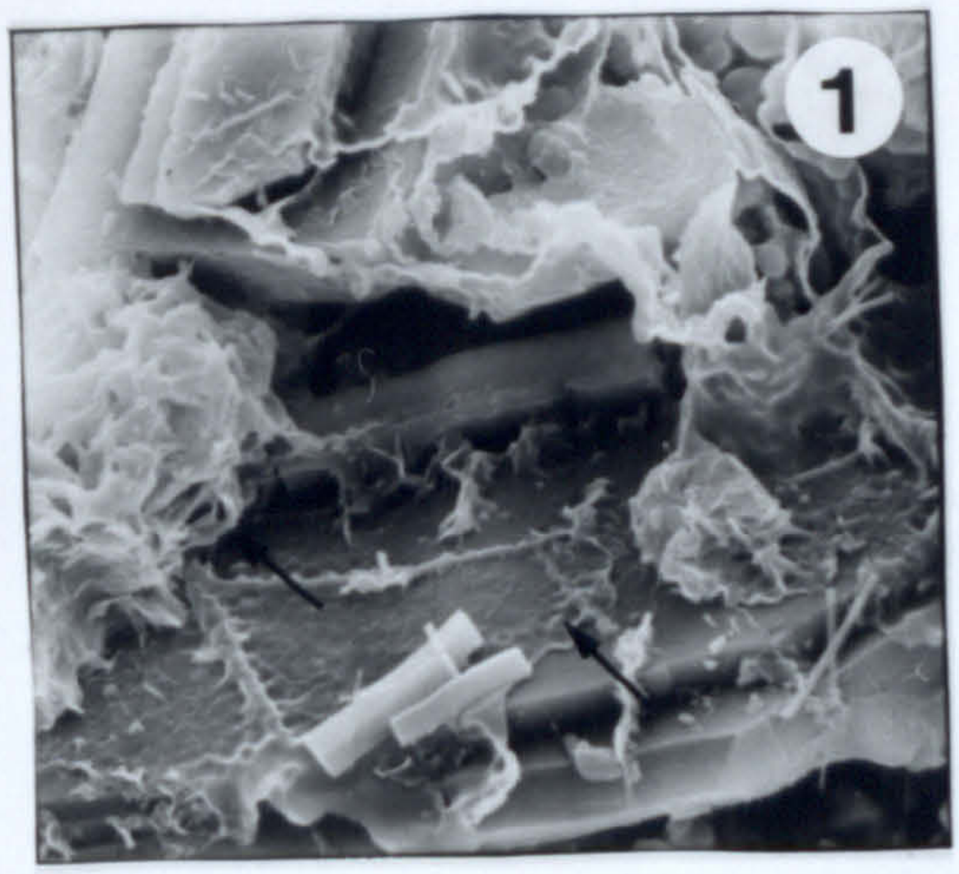

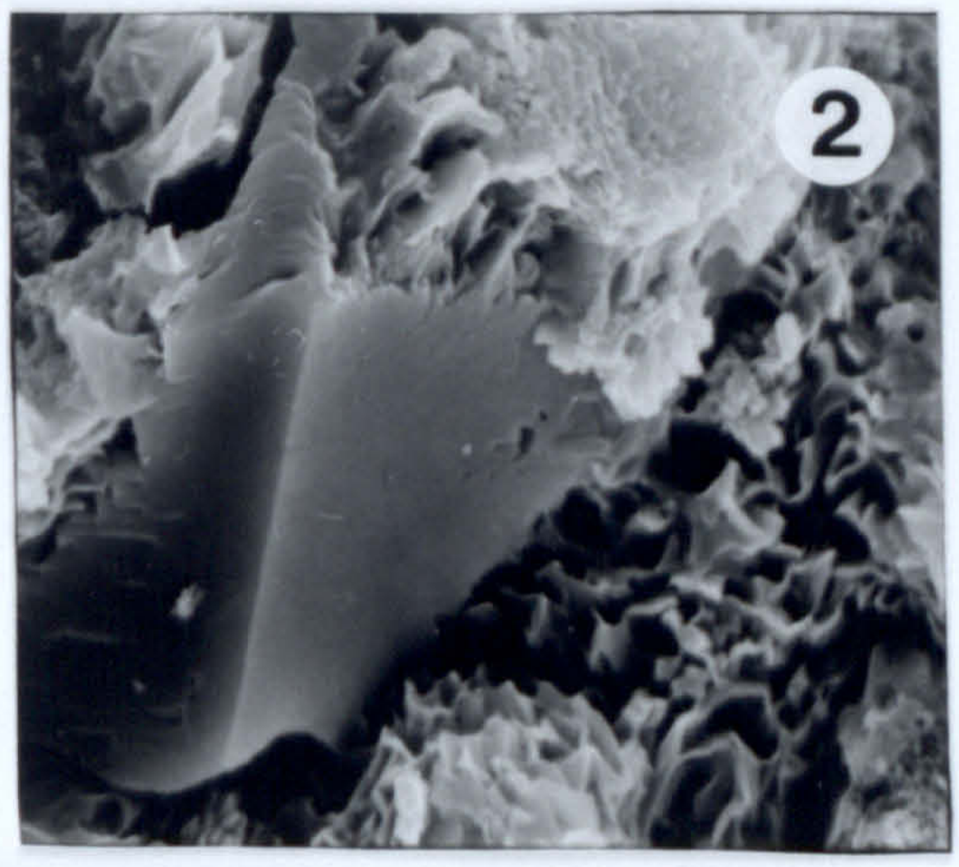

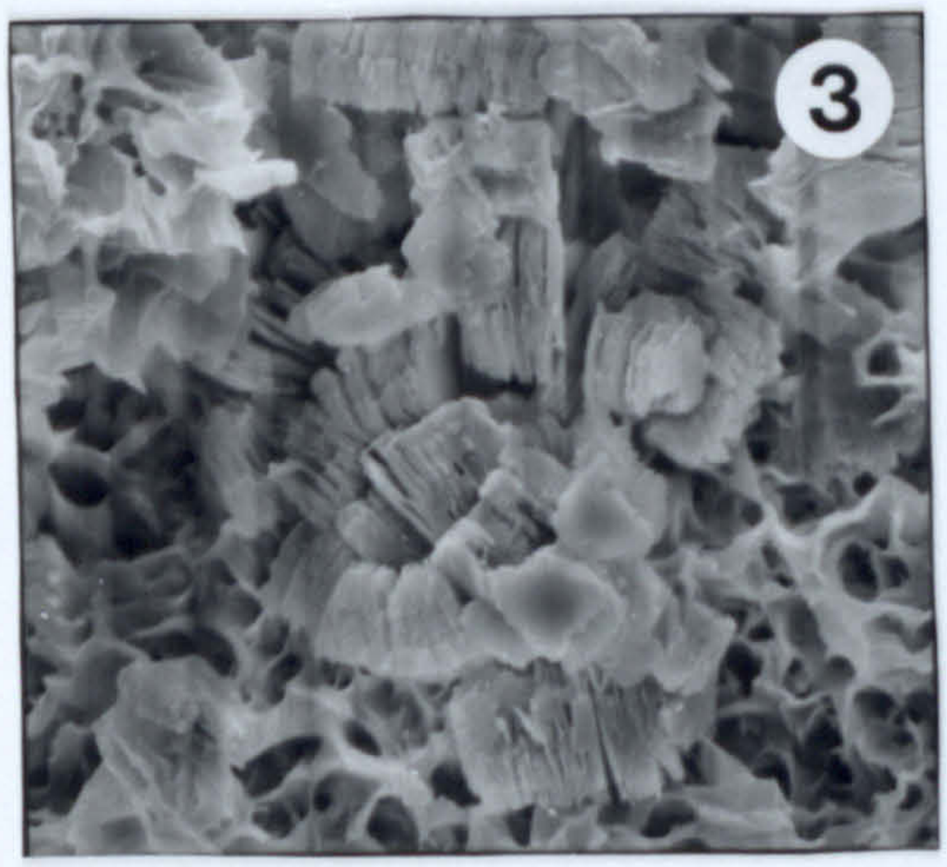

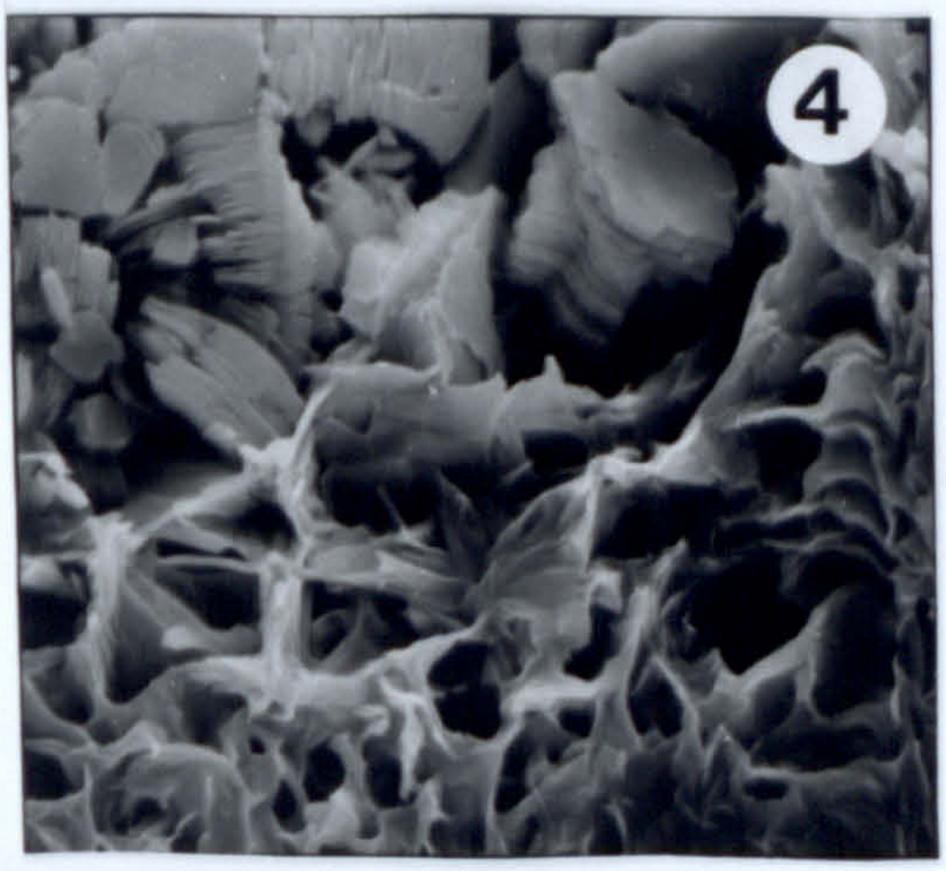

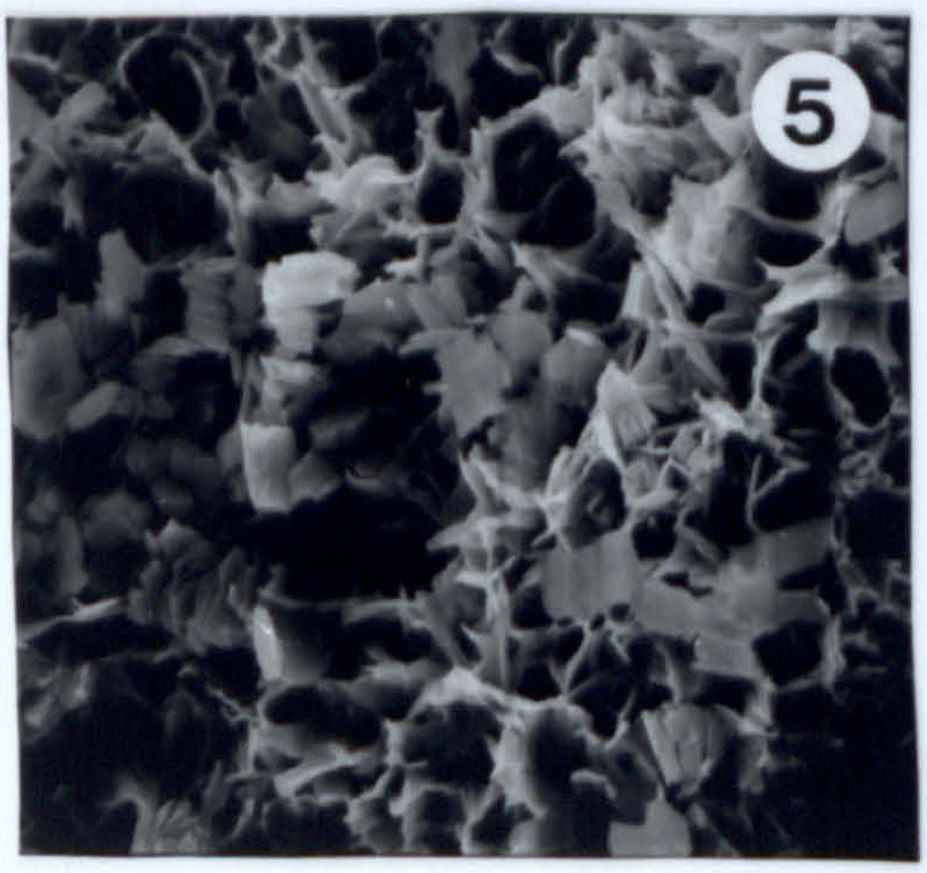

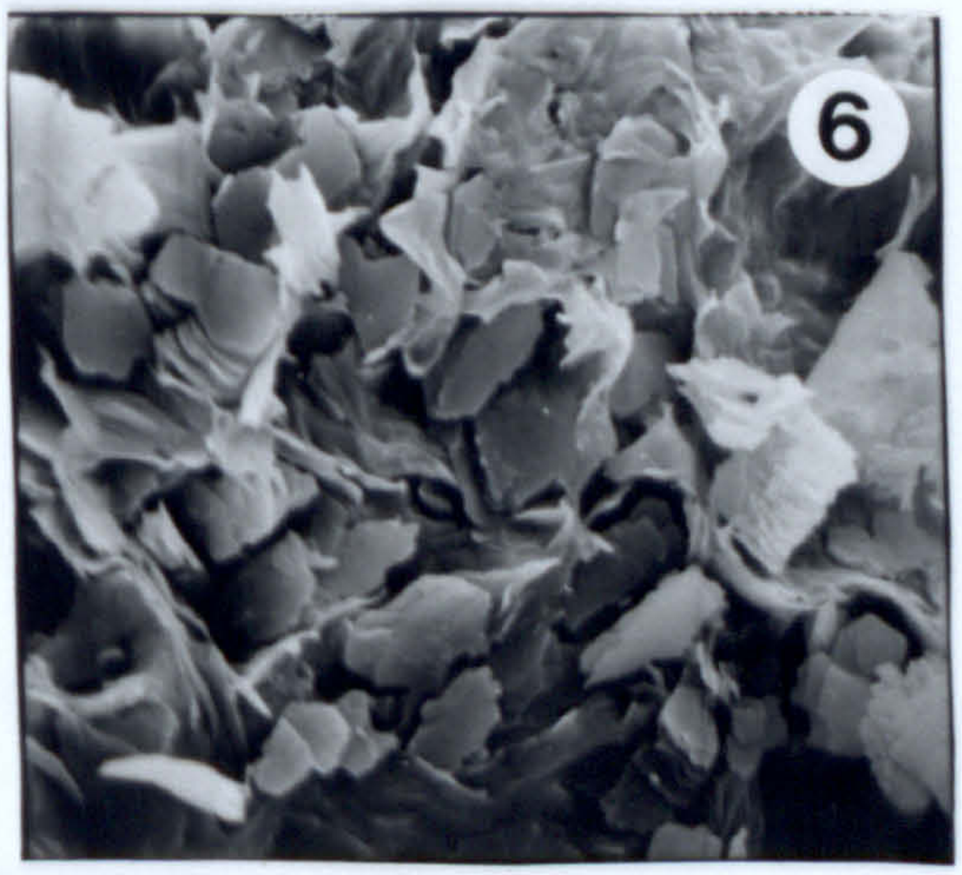

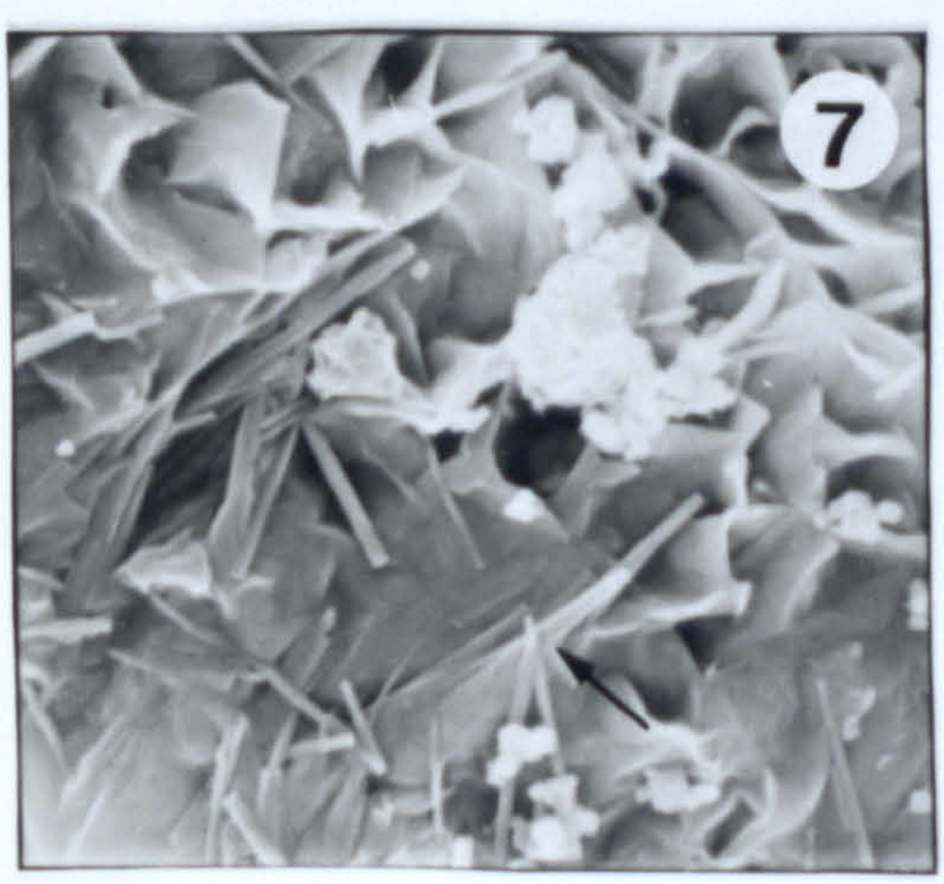

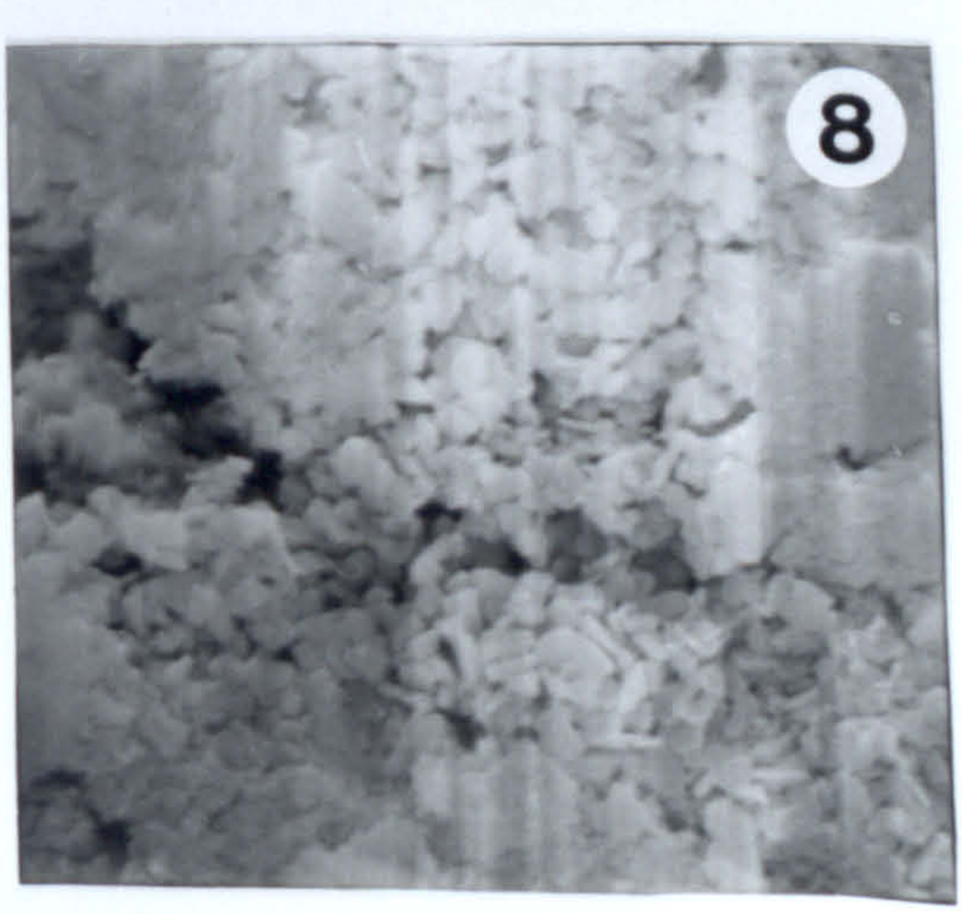

Plate 14

Morphlogical characteristics of the authigenic K-felspars and opal C-T present in the Greek bentonites

1. Euhedral K-feldspar crystals (kf) filling a dissolution cavity, associated with smectite. Lower horizon of the Koufi deposit, Milos. Scale bar 5μm

2. Euhedral K-feldspar crystals lying on a smectite matrix. Tsantili deposit, Milos. Scale bar 8.6μm.

3. Euhedral K-feldspar (kf) present in a cavity formed from dissolution of volcanic glass, among montmorillonite (m) crystals. Ankeria deposit, Milos. Scale bar 2.5μm.

4. Euhedral K-feldspar crystals in a cavity formed from dissolution of the volcanic glass. Higher horizon of Ano Komia deposit, Milos. Scale bar 7.5μm.

5. Euhedral K-feldspar crystals present in a cavity, in close association with opal C-T and smectite. Garyfalakena deposit, Milos. Scale bar 10μm.

6. Euhedral K-feldspar crystals associated with smectite. Rema deposit, Milos.

7. Sherulitic crystal of opal C-T (shown with the arrow) over smectite flakes. Ankeria deposit, Milos. Scale bar 3μm.

8. Opal C-T crystals displaying axiolitic texture. According to Moncure et al. (1981) this texture might be the product of direct devitrification of the volcanic glass. Garyfalakena deposit, Milos. Scale bar 4.5μm.

Plate 14

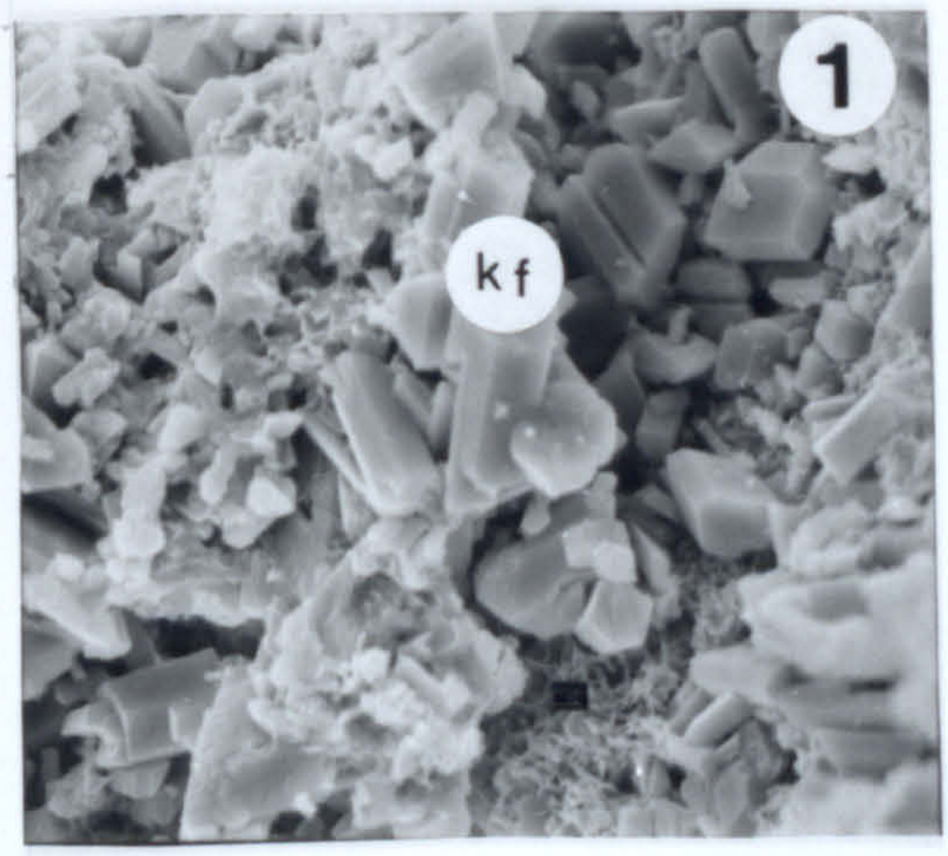

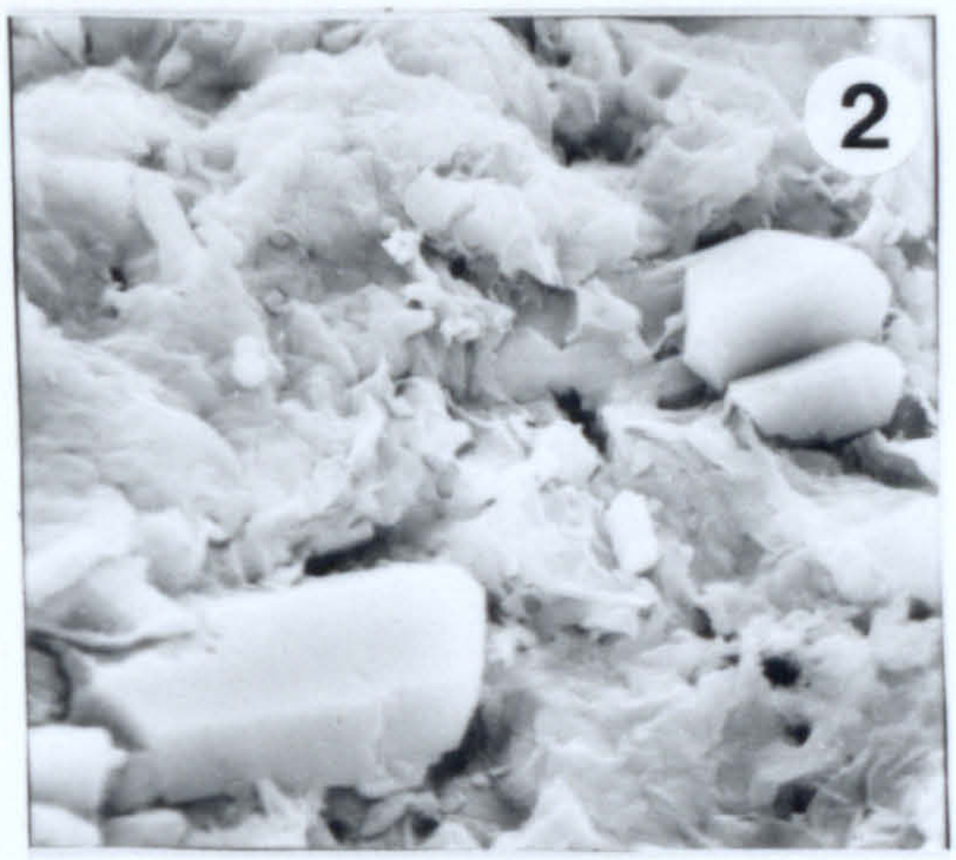

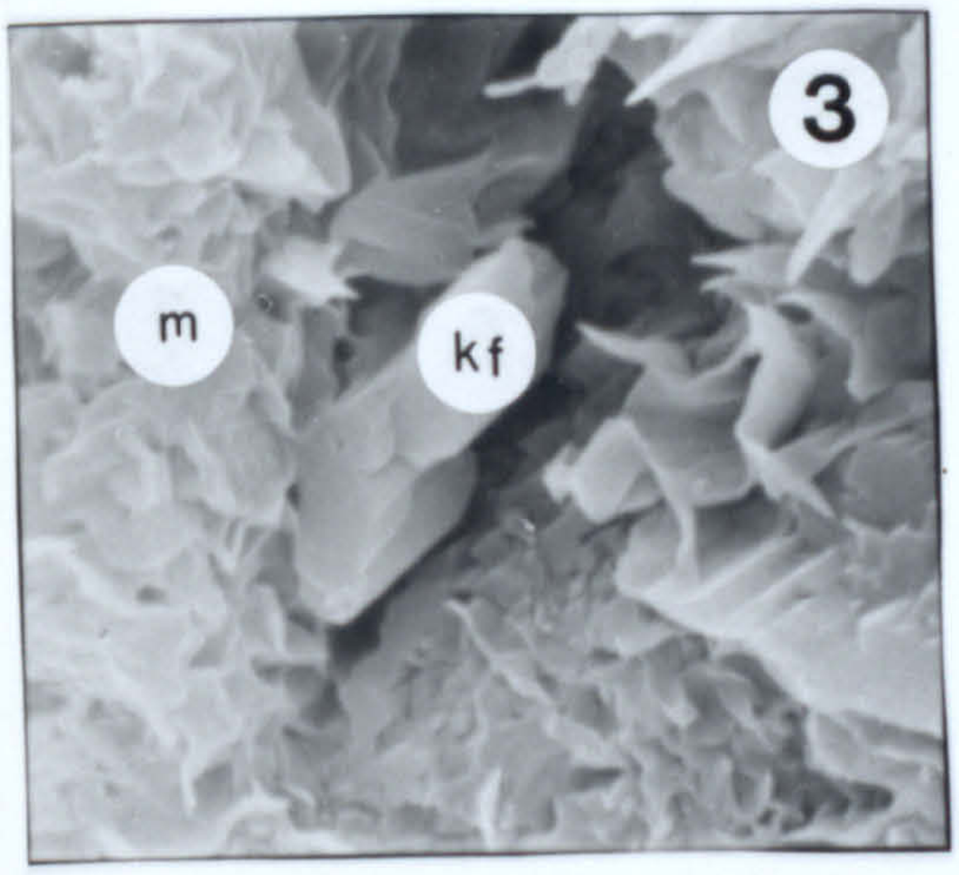

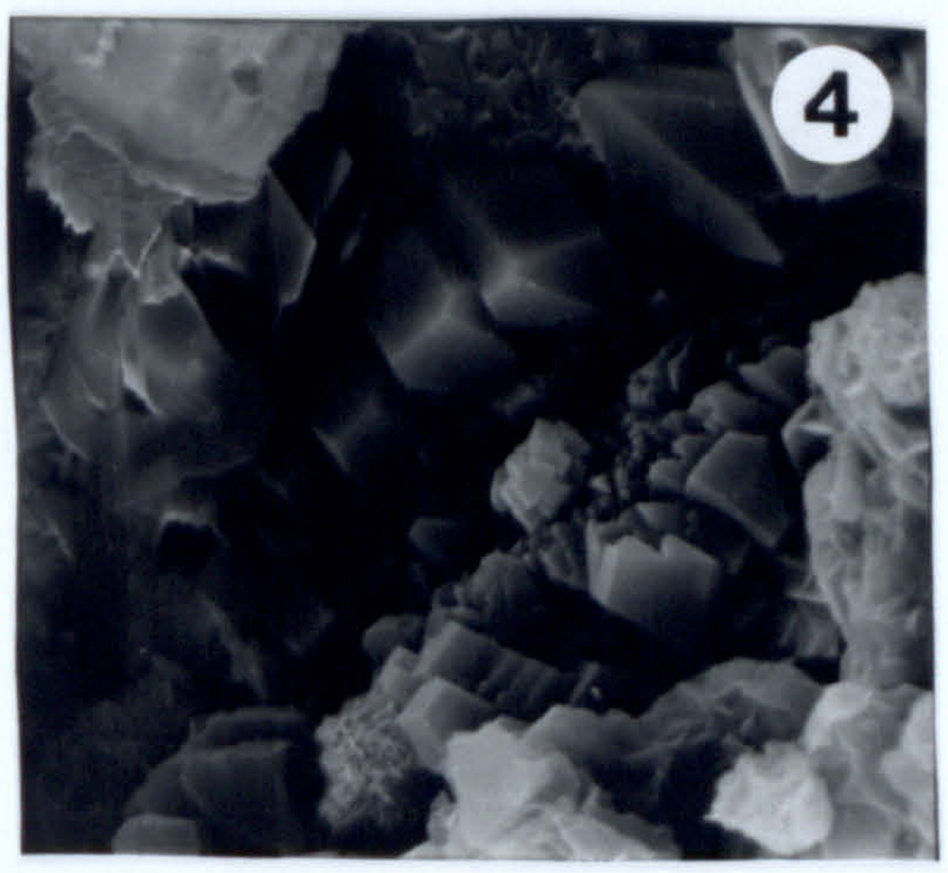

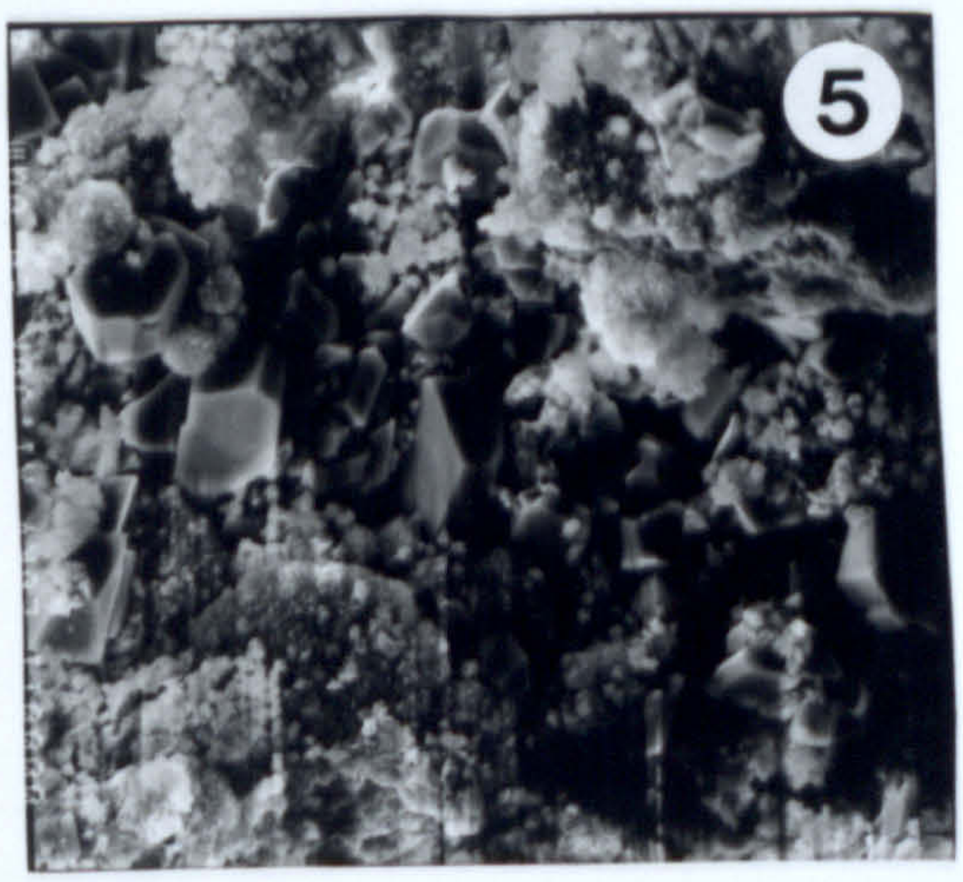

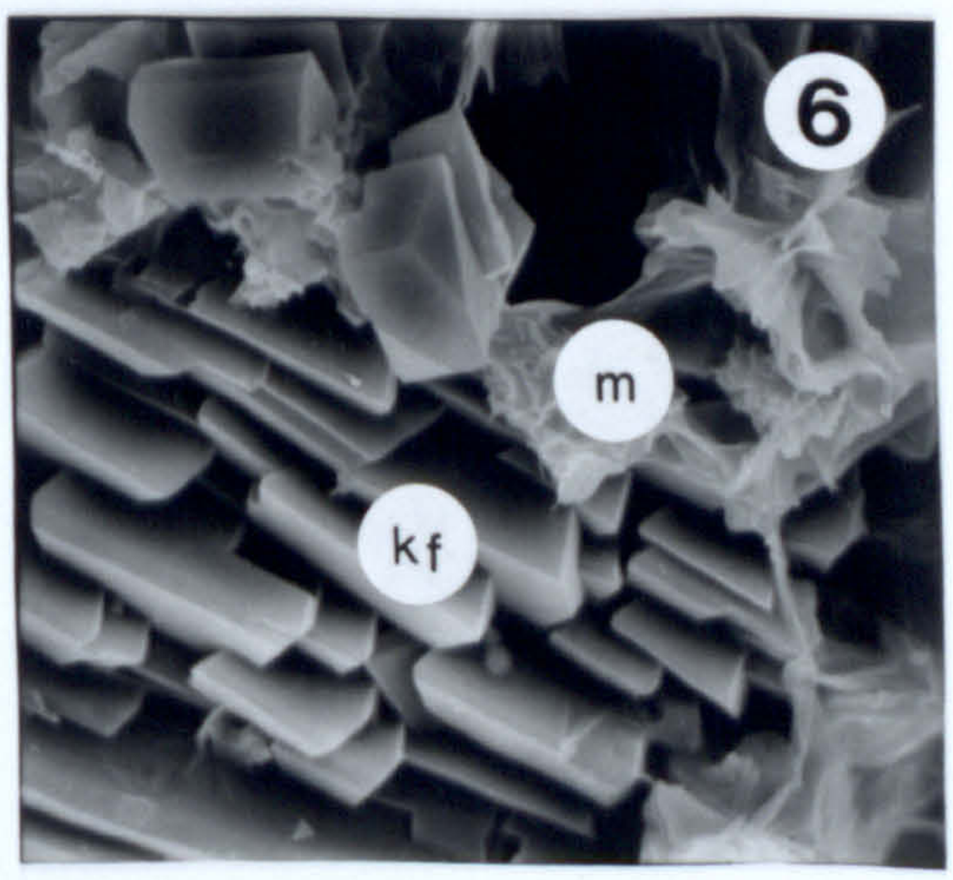

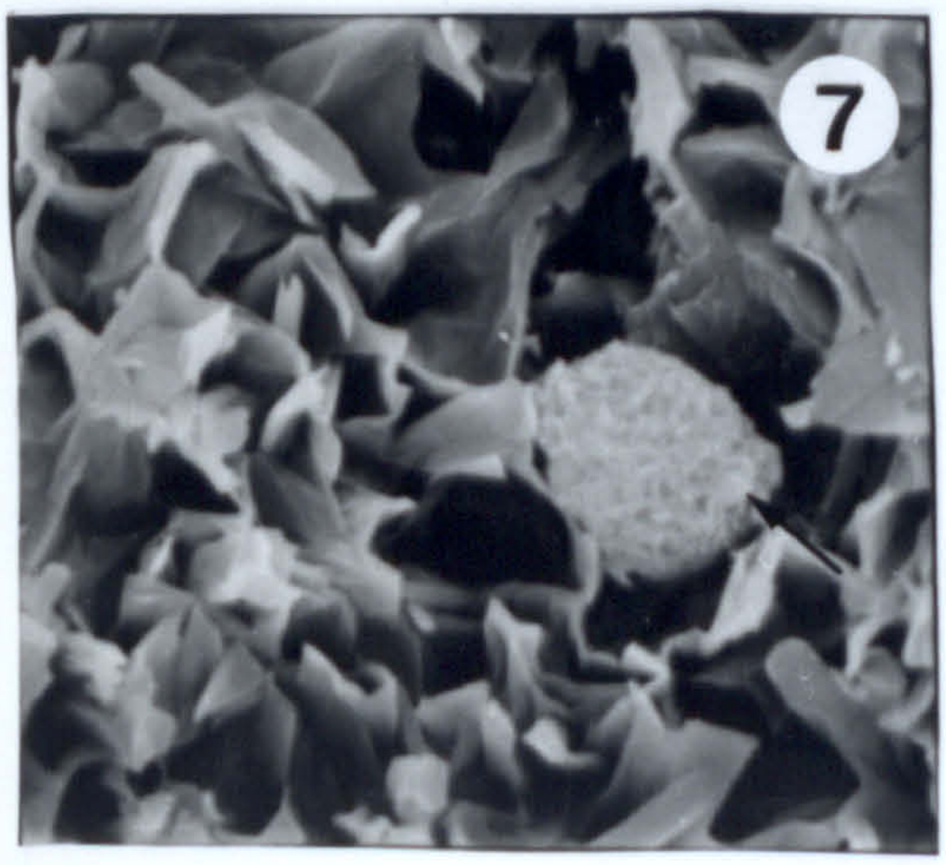

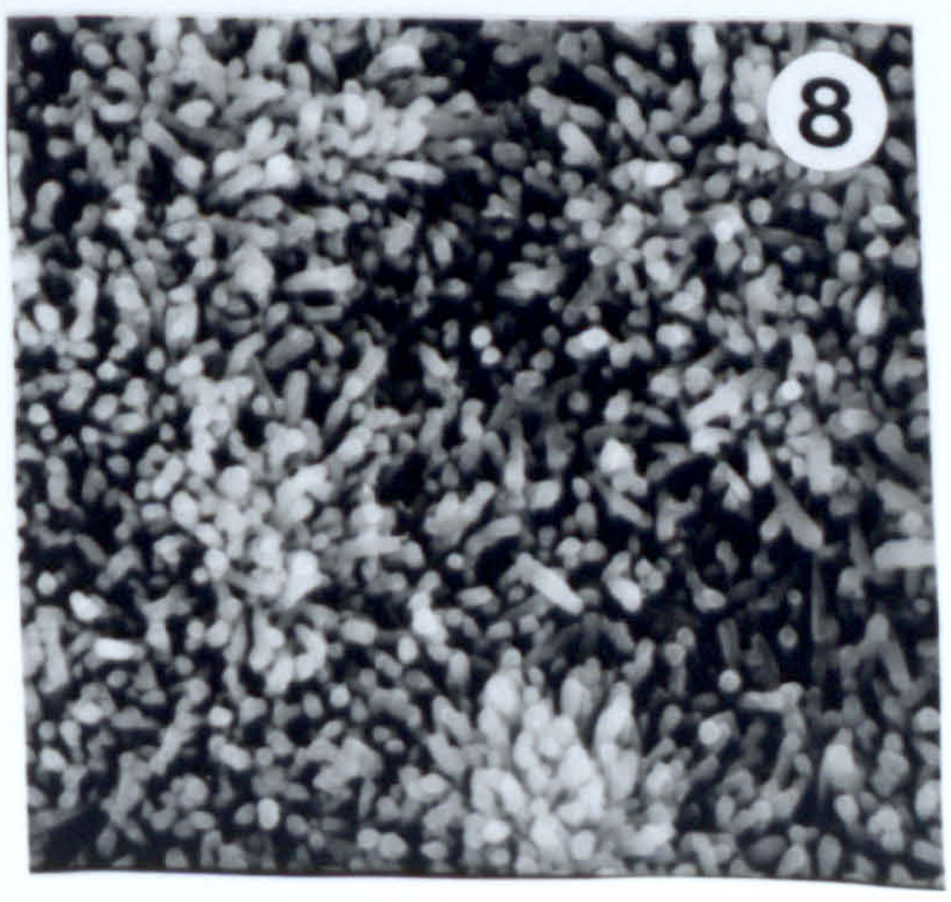

Plate 15

Illite/smectites from the Tsantili deposit, Milos.

1,2. Kaolinite (shown by the arrow) associated with illite/smectite. Kaolinite has probably been formed as a by-product from the illitization of smectite. Scale bar 1= 4.3μm, 2= 2.5μm.

3. Illite/smectite forming at the expense of euhedral K-feldspar crystals. K-feldspar is considered a rather limited source of potassium during to smectite-to-illite formation. Scale bar 4.3μm.

4. Small illite/smectite laths (showed with the arrow) coexisting with flat flakes, which also belong to illite/ smectite. The I/S is characterized by random interstratification (R0). The expandability of the illite/smectite crystallites is 75%. Scale bar 4.3μm.

5. Coexistence of illite/smectite laths and flakes at 26% expandability. Ordered intrestratification (R1 type of ordering). Scale bar 3μm.

6,7. Transition through an intermediate type of crystallites with undetermined morphology (B). 6= 17% expandability, R3 type of ordering, 7= 13% expandability R3-type of ordering. Scale bars: 6= 4.3μm, 7= 6μm.

8. Coexistence of flaky (A and B) and lath-shaped (C) illite/smectite crystallites. There are two types of I/S flakes: well formed wavy flakes (A) and small flakes (B). Both types seem to evolve to the lath-shape crystallites (C). Expandability 13%, R3 type of ordering. Scale bar 7.5μm.

Plate 15

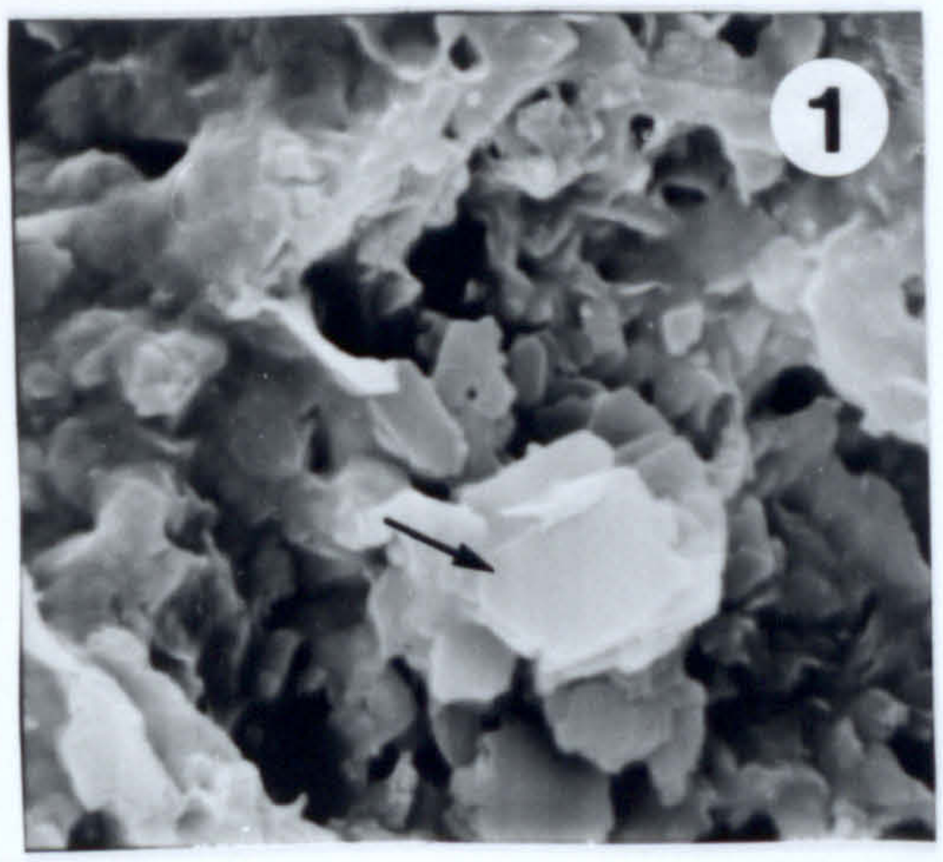

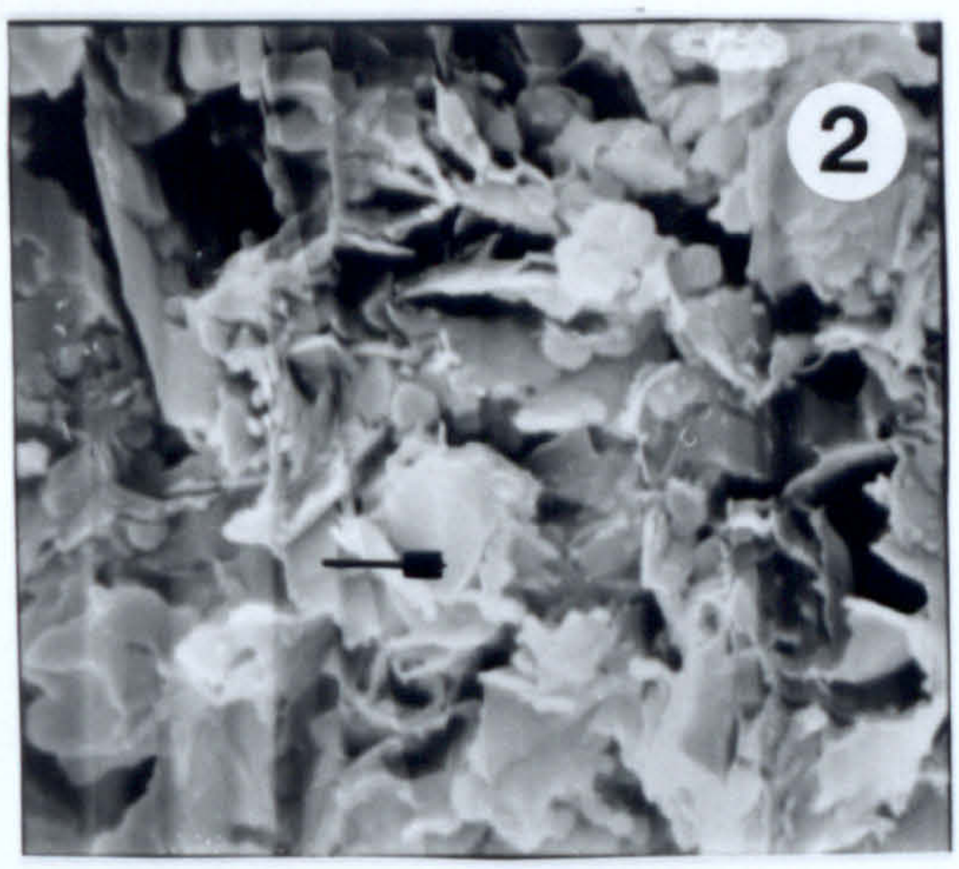

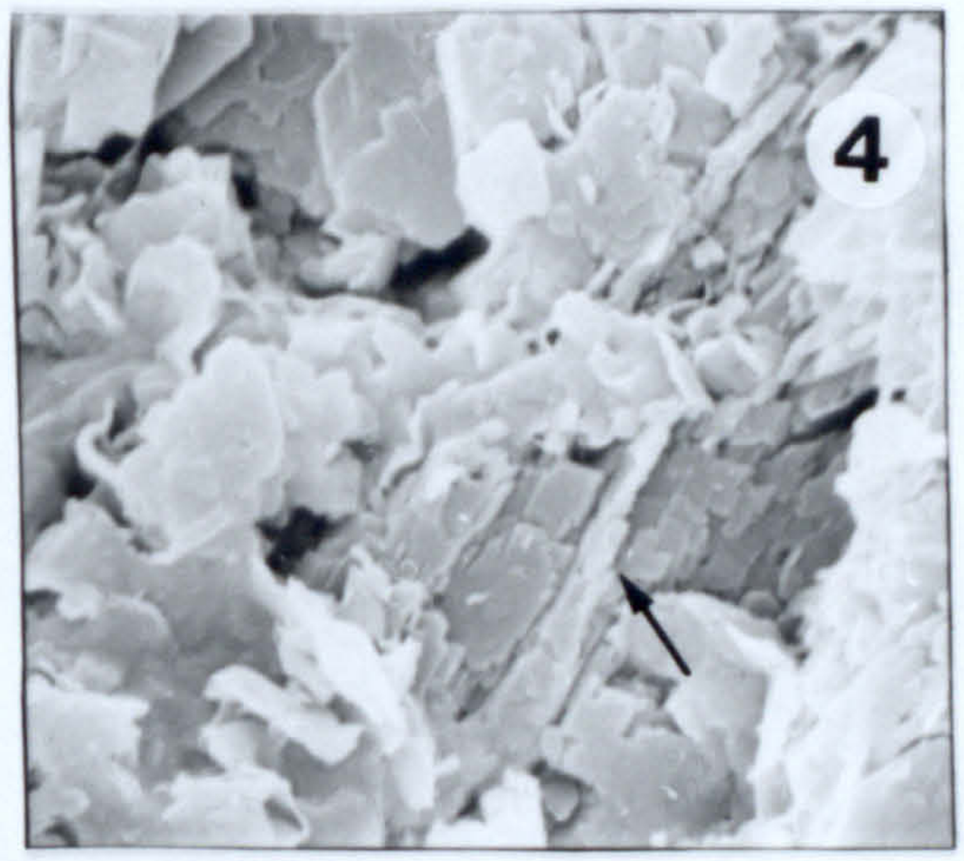

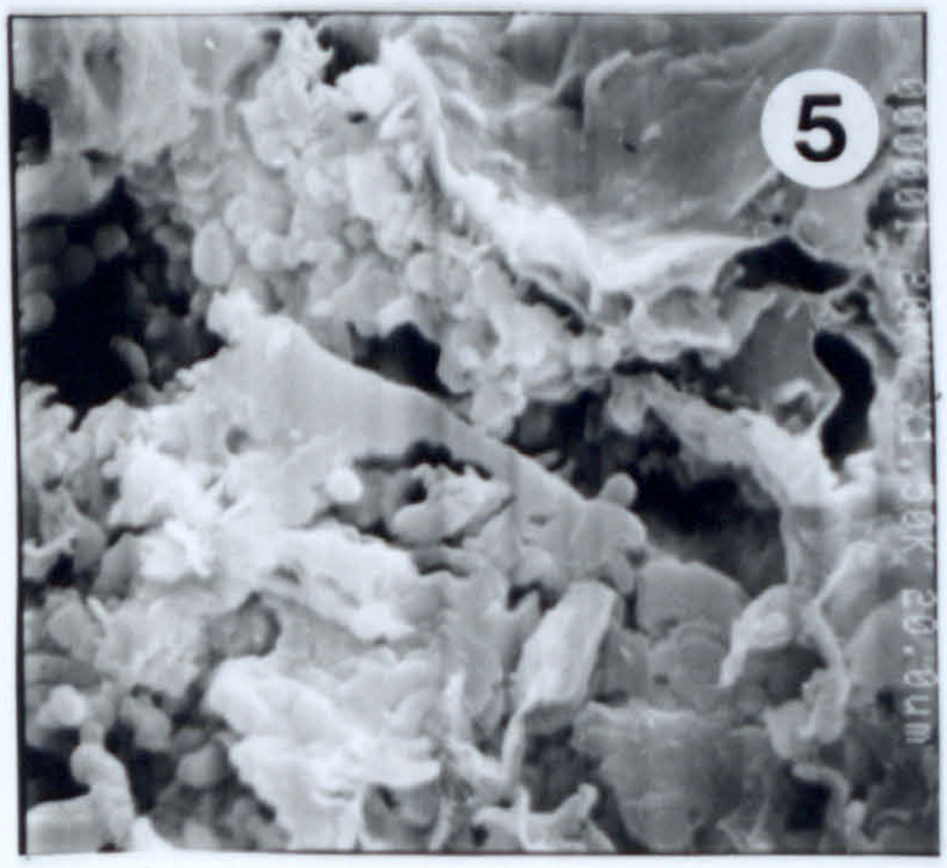

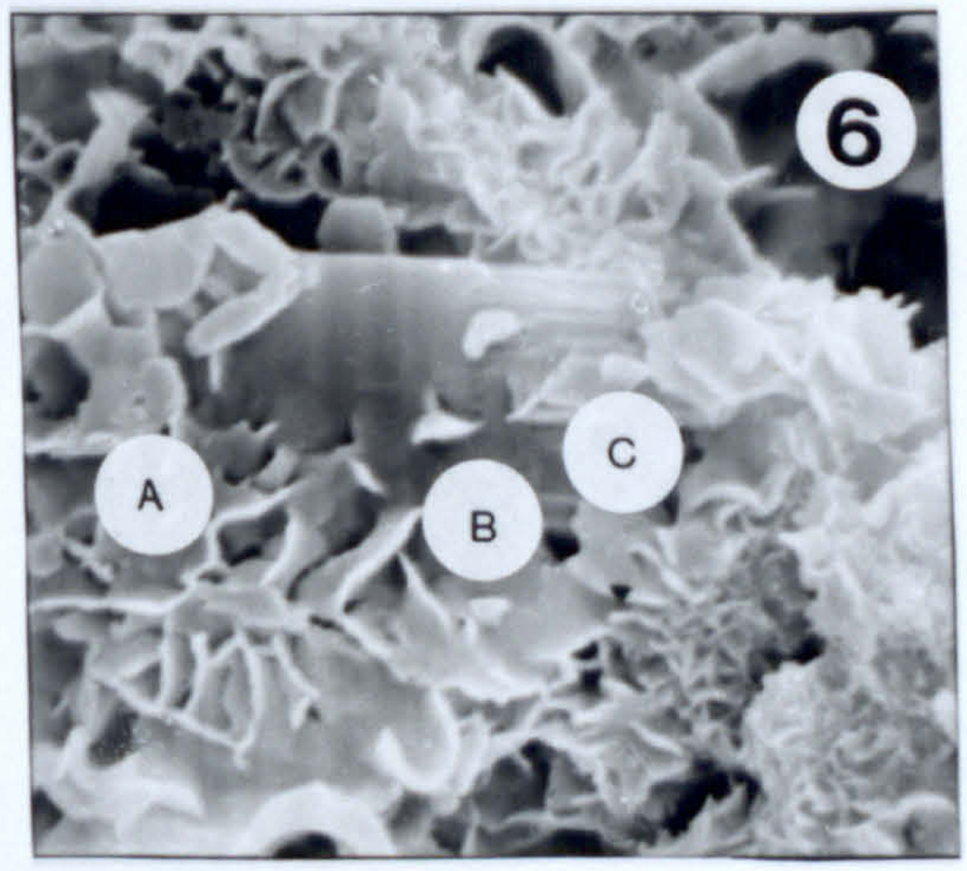

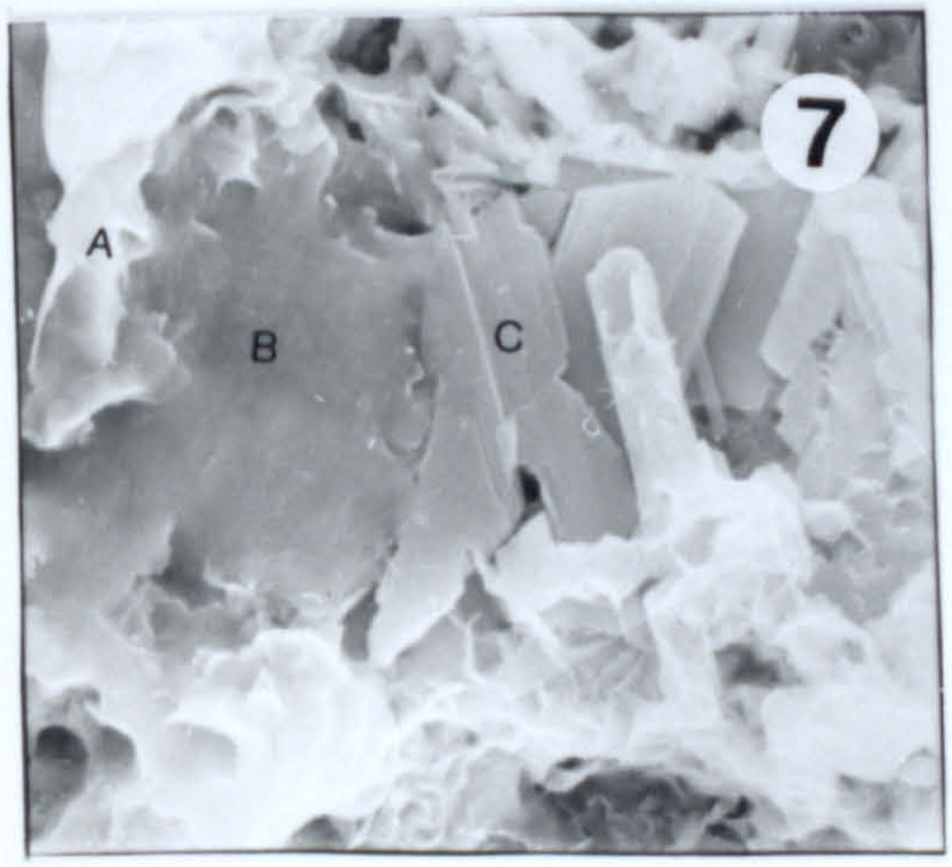

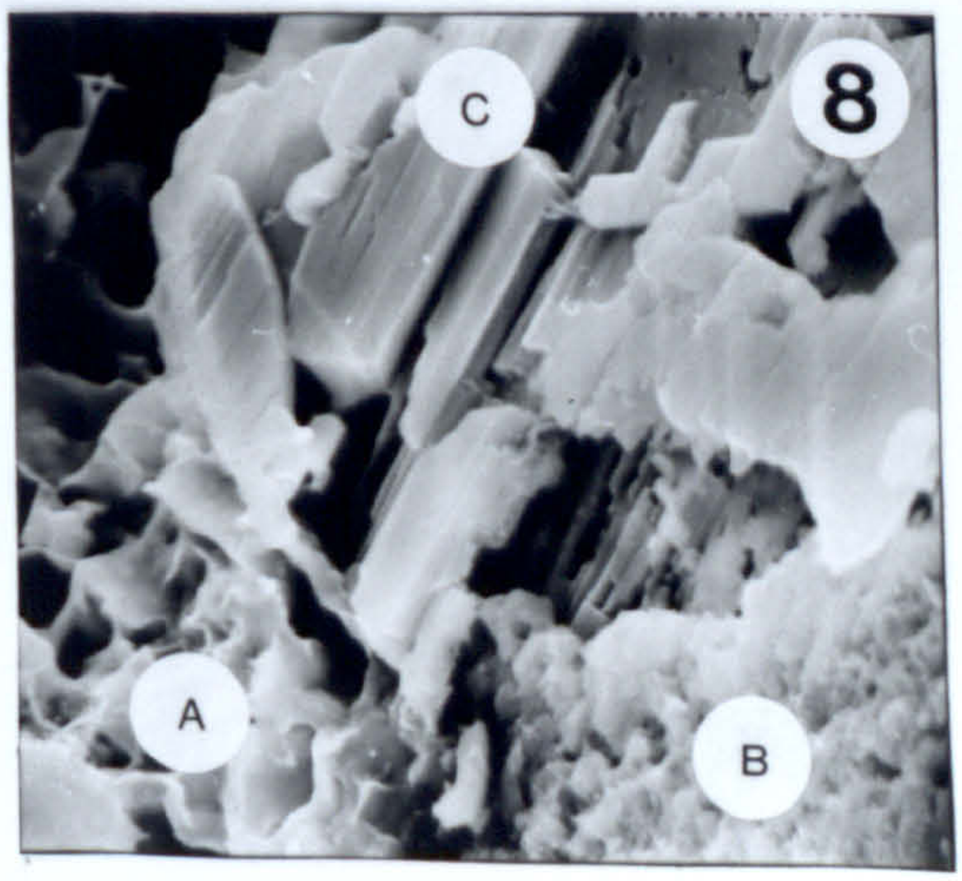

Plate 16

Zeolites in the Greek bentonite deposits

1. Mordenite fibres (a) forming from an amorphous, gel-like precursor (b), associated with montmorillonite flakes (c). No direct association between mordenite and montmorillonite is visible. Smectite + mordenite zone, Prassa deposit, Kimolos. Scale bar 10μm.

2. Mordenite derived from an amorphous precursor (gel). Well developed mordenite flakes are also drapped over smectite flakes. Smectite + mordenite zone, Prassa deposit, Kimolos. Scale bar 20μm.

3. Partly dissolved crystal which probably belongs to clinoptilolite, shown with the arrow, drapped over mordenite fibres. Garyfalakena deposit, Milos. Scale bar 2.5μm.

4. Mordenite fibres drapped over smectite flakes, indicating that its formation postdates at least partly, smectite. The big crystal in the centre of the upper part of the photograph belongs to K-feldspar. Garyfalakena deposit, Milos. Scale bar 7.5μm.

5. Mordenite fibres associated with a poorly crystallised or amorphous phase. The euhedral crystals in the lower part of the photograph belong probably to K-feldspar. Garyfalakena deposit. Scale bar 4.3μm.

6. Well developed mordenite fibres associated with montmorillonite, joining cavity walls formed from the dissolution of the volcanic glass. In several occasions the mordenite fibres are drapped over the montmorillonite flakes. Mordenite + smectite zone, Prassa deposit, Kimolos. Scale bar 10μm.

7. Small cliniptilolite crystals (cl) precipitated in cavities formed by the dissolution of the volcanic glass. There are three types of smectite flakes; one with aggregated flakes (A) one characterized by typical honeycomb texture (C) and one characterized by morphology intermediate between the two previous extreems (B).. Although the type A morphology has been developed in open space, the flakes are aggregated. The spherulitic crystals (O) belong to opal C-T. Note the amorphous material (AP) over the smectite with honeycomb texture. This might be the precursor of clinoptilolite. Loutra deposit, Kimolos. Scale bar 20μm.

8. Clinoptilolite crystals (b) precipitated in a cavity formed by dissolution of the volcanic glass. The principal alteration product is smectite (a). Note the different morphology of the smectite flakes although they have all been formed in open space. Loutra deposit, Kimolos. Scale bar 20μm.

Plate 16

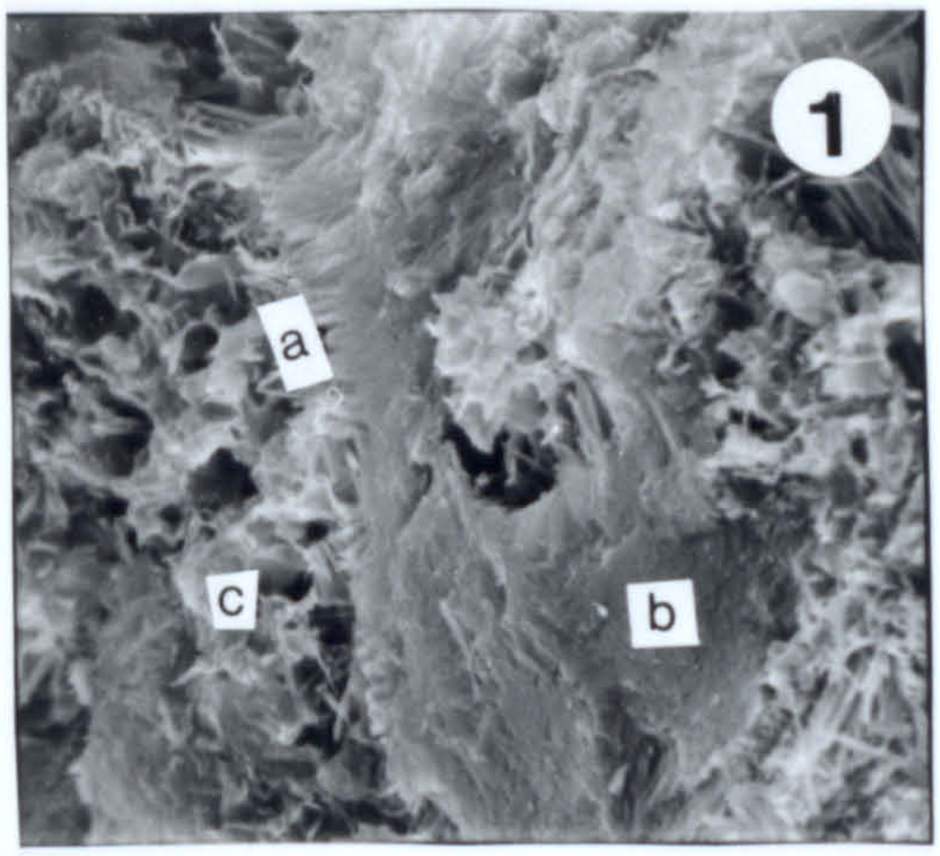

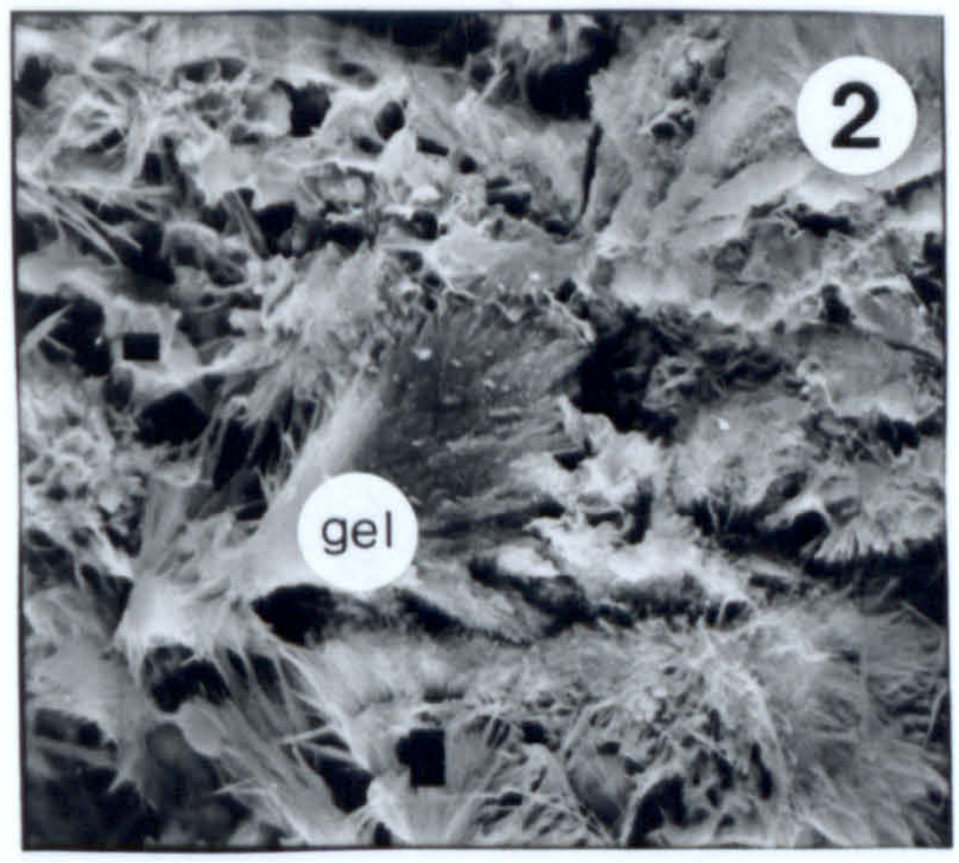

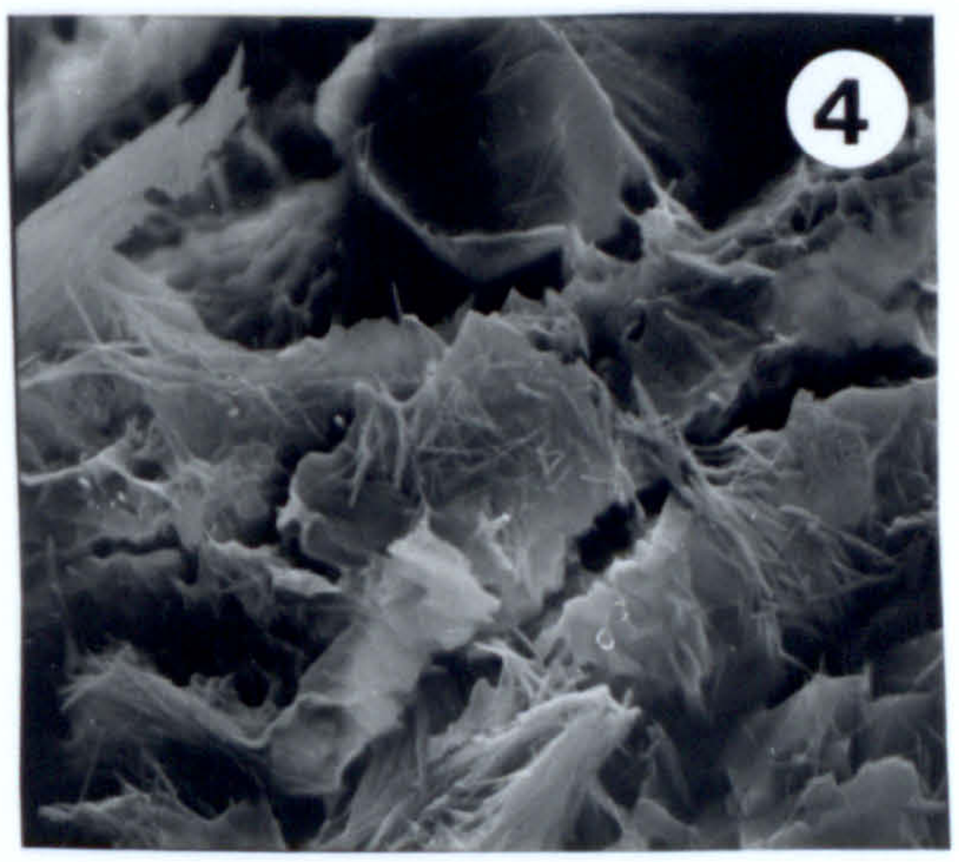

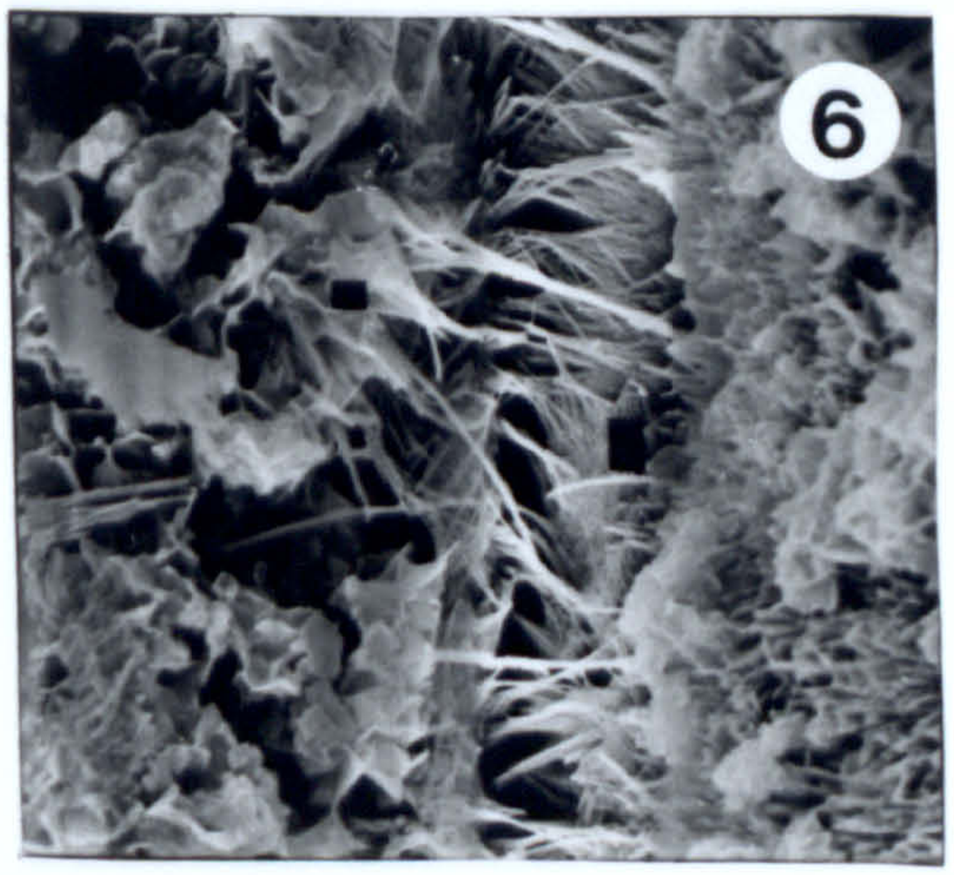

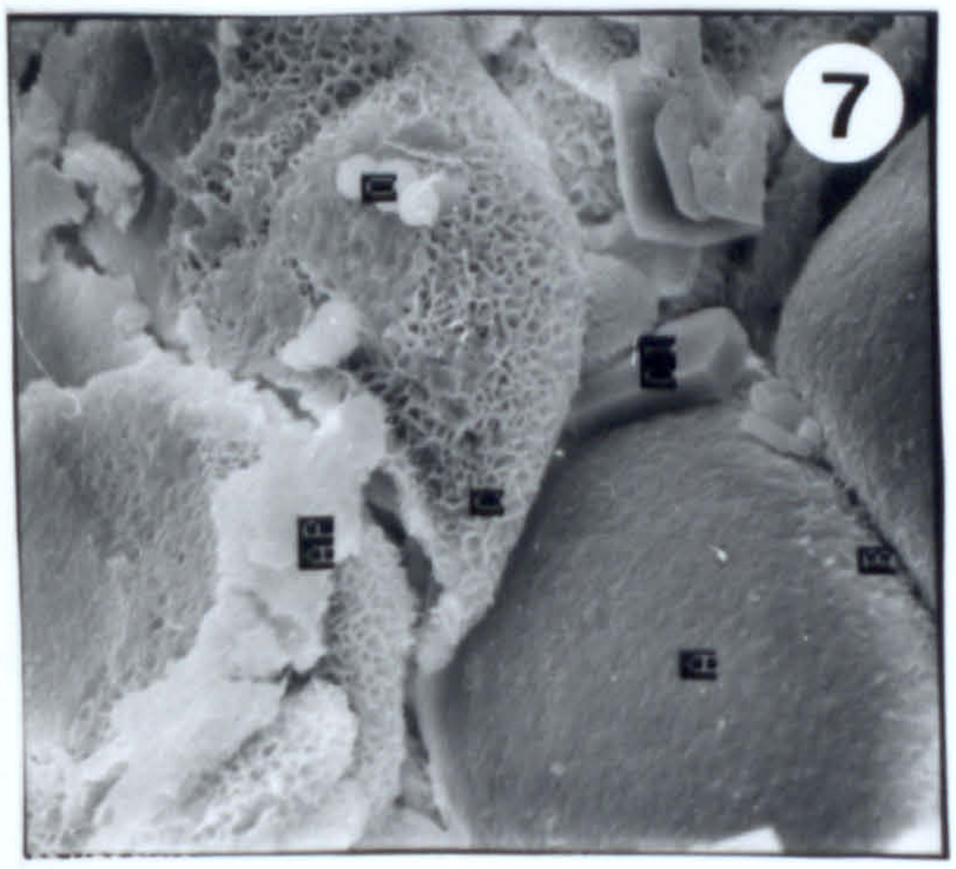

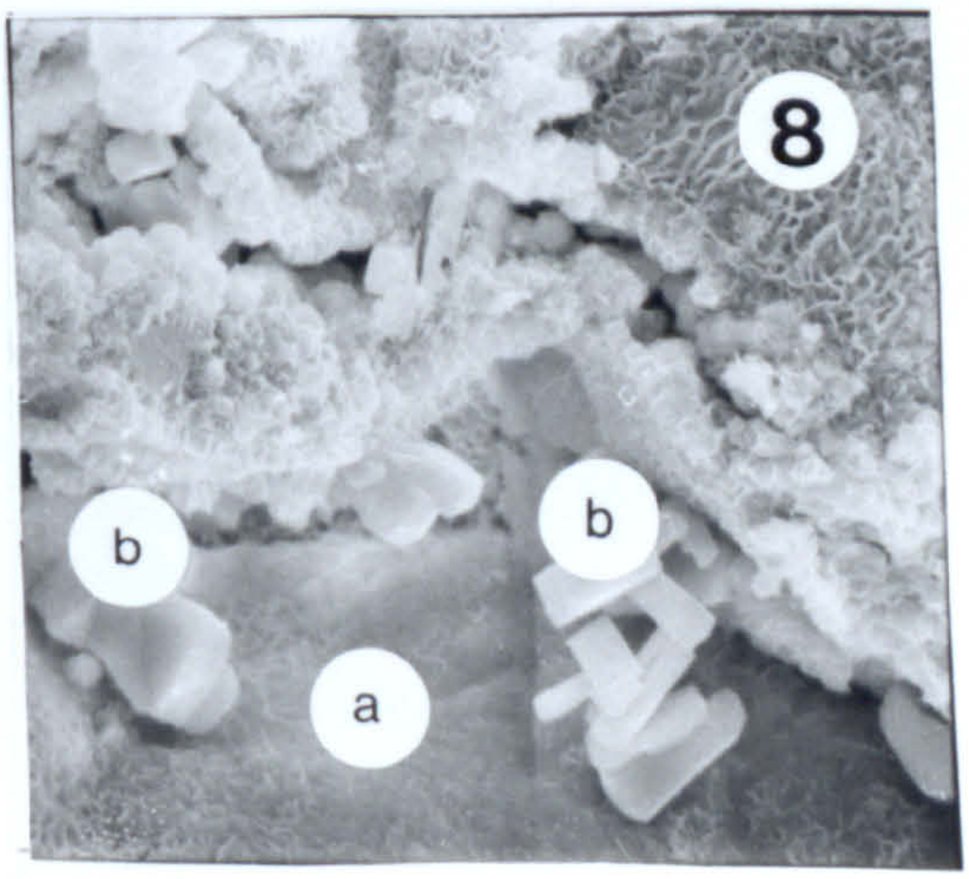

Plate 17

Back scattered electron images from the bentonite deposits.

1. Plagioclase microphenocryst embedded in a montmorillonite groundmess. Montmorillonite is the alteration product of the original volcanic glass. Prassa deposit, Kimolos. Scale bar 10μm.

2. Cryptic zonation in the chemistry of smectites derived from alteration of an acidic rock. In zone (a) beidelite containing 0.8-0.6 AlIV atoms per formula unit is present. Zone (b) contains Tatatilla montmorillonite with 0.20-0.14 AlIV atoms per formula unit, while in zone (c) precipitation of free silica in the form of opal C-T has taken place (more than 8.1 Si atoms per formula unit). Ano Komia deposit, Milos. Scale bar 10μm.

3,4,5. Progressive replacement of plagioclase by smectite. In photo 3 the replacement is not complete and remnants of plagioclase (a) are present, although smectite (b) dominates. In photo 4 plagioclase is present only in some rims of the pseudomorphosed crystal, while in 5 the replacement is almost complete. The black dashed line in photos 4 and 5 displays the probable rims of the original plagioclase crystal. Koufi deposit, Milos. Scale bar 10μm.

6. Carbonates in the Tsantili deposit, Milos. (a) corresponds to oligonite (Mn-siderite) and (b) to ankerite. Oligonite is probably an exsolution product. The grey matrix corresponds to smectite while the small bright crystals occurring in cavities or as pore linings belong to authigenic K-feldspar. Scale bar 10μm.

7. Lapilli-tuff partly altered to bentonite. The centre of the photograph is occupied by a fresh glass shard. The big bright crystals correspond to plagioclase. Loutra deposit, Kimolos. Scale bar 100μm.

8. Corroded plagioclase crystal, partially altered to smectite. The fine groundmass belongs also to smectite. Aspro Horio deposit, Milos. Scale bar 10μm.

Plate 17

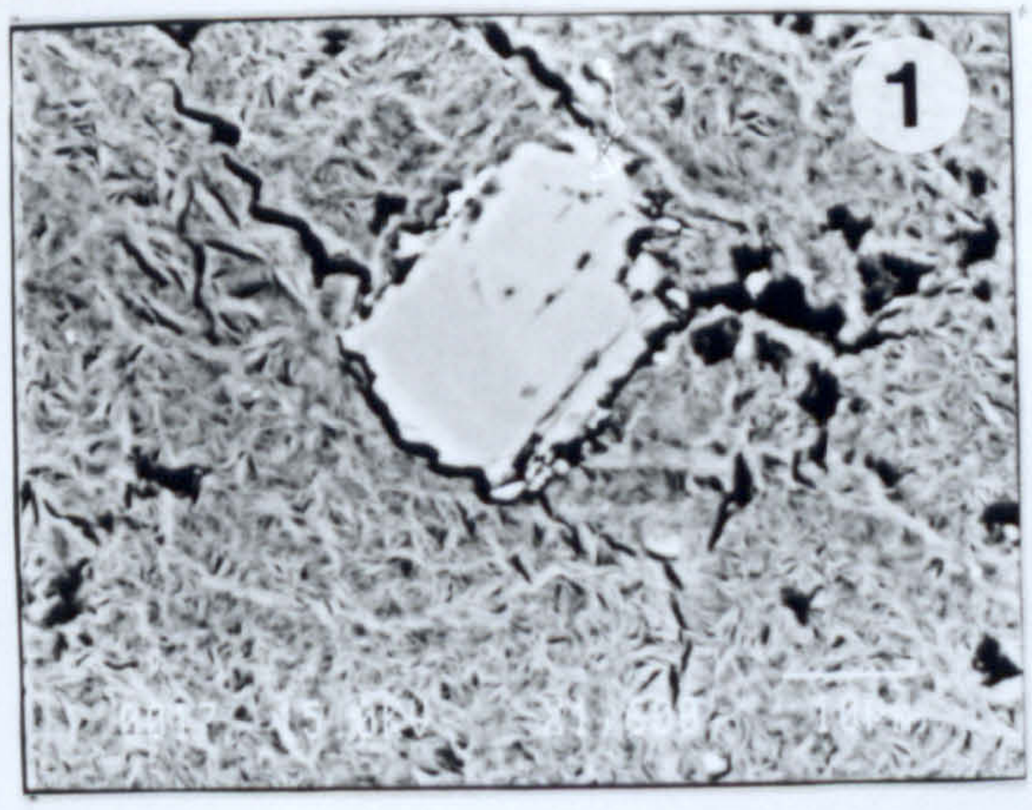
1

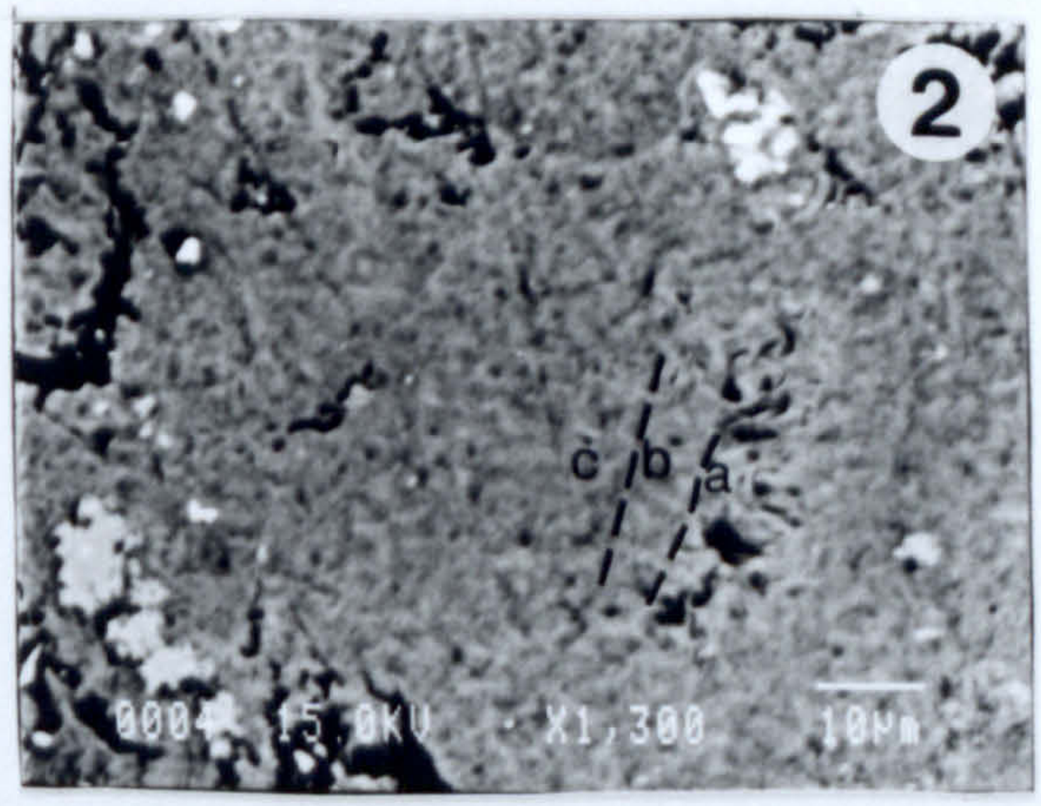
2
c
b
a
0004 15.0KV X1,300 10μm


3
a
b
0025 15.0KV X1,100 10μm

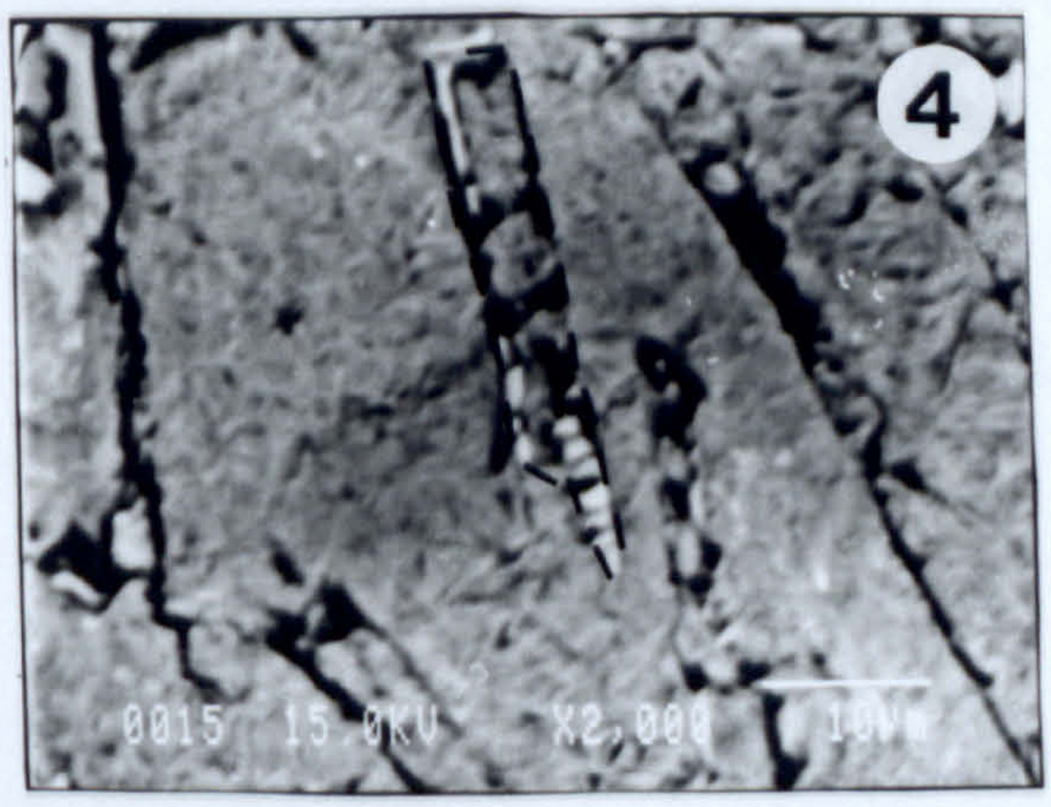
4
0015 15.0KV X2,000 10μm

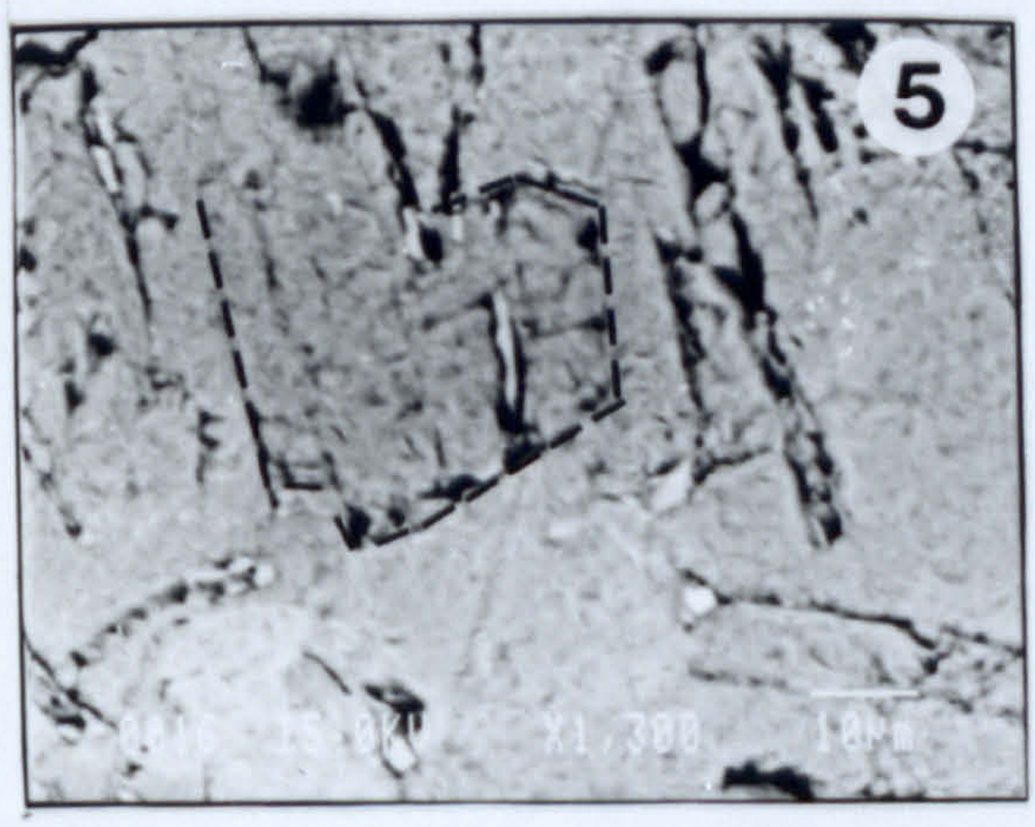
5

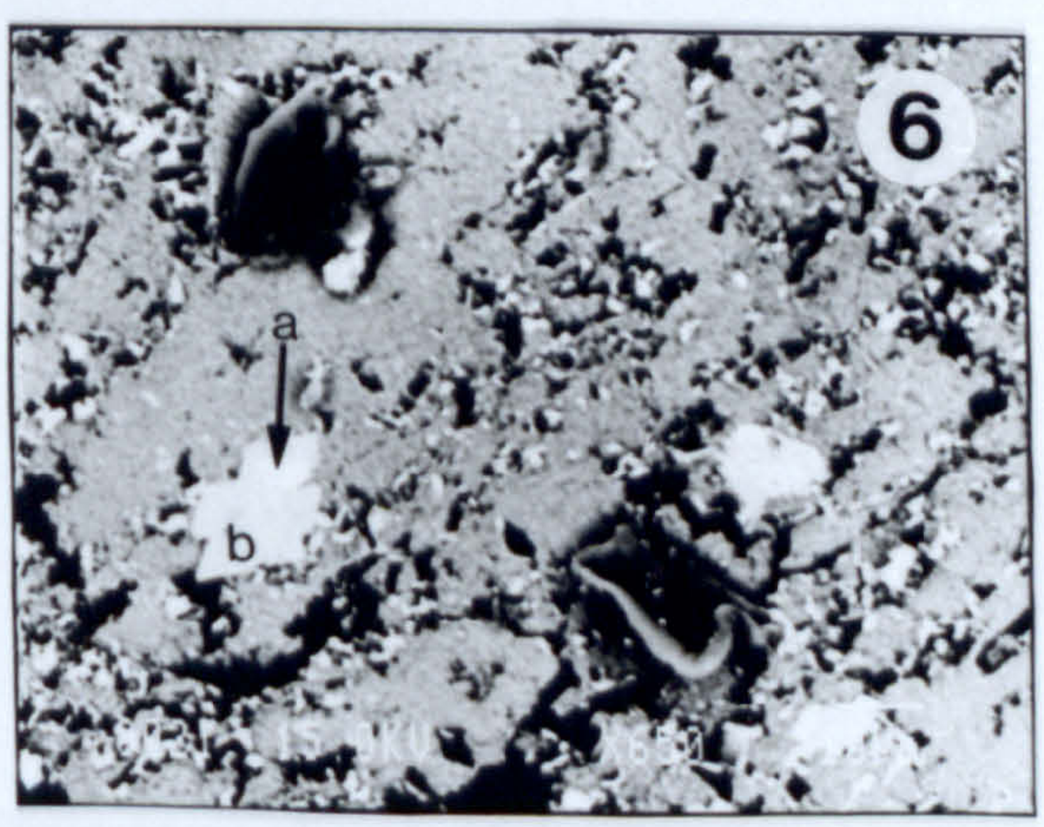
6
a
b

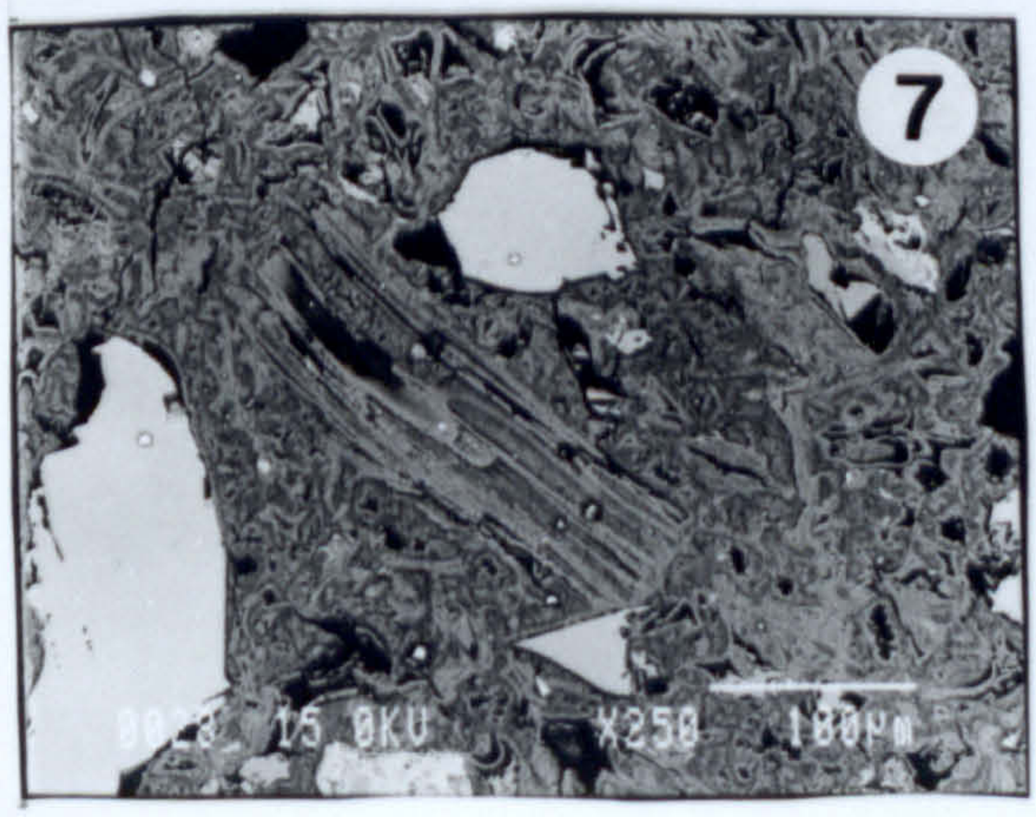
7
15.0KV X250 100μm

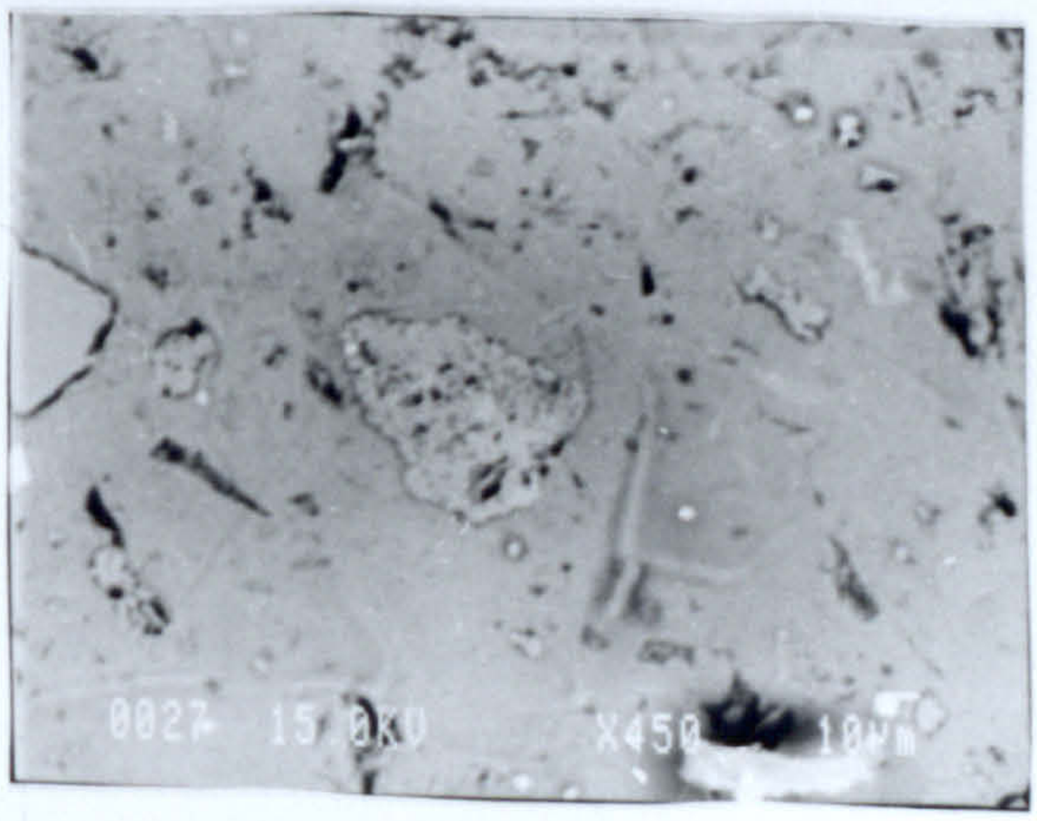
0027 15.0KV X450 10μm

Plate 18

TEM micrographs of the smectites

1,2. Pt-shadowed smectite crystals from the Tsantili deposit, Milos. The average thickness of the smectite crystals is 44.5 ± 11.7 Å. Two types of crystals are present: flakes and laths, the former being predominant. Scale bars 1= 0.5μm, 2= 0.25μm.

3,4. Smectite flakes with different degree of dissagregation. In both photographs the material is unsuitable for particle size measurements. The smectite aggregates can be characterized as compact-lamellar and lamellar aggregates (Grim & Güven, 1978, Güven, 1988). Prassa deposit, Kimolos. Scale bars 3= 0.8μm, 4= 2μm.

5,6,7,8. Disaggregated smectite particles. Both E-type and L-type particles are present. Note the great variety of crystallite sizes. The material is suitable for particle size measurements. Prassa deposit, Kimolos. Scale bars 1μm.

Plate 18

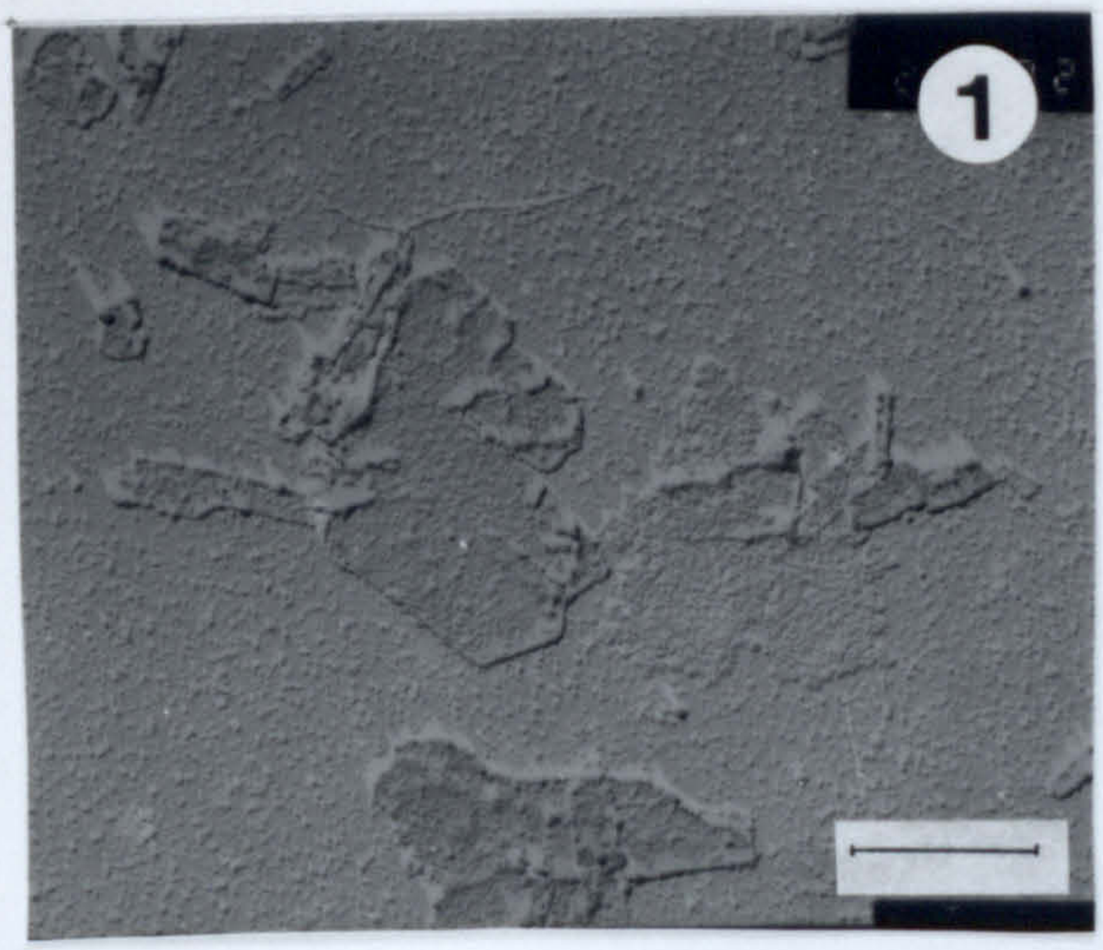

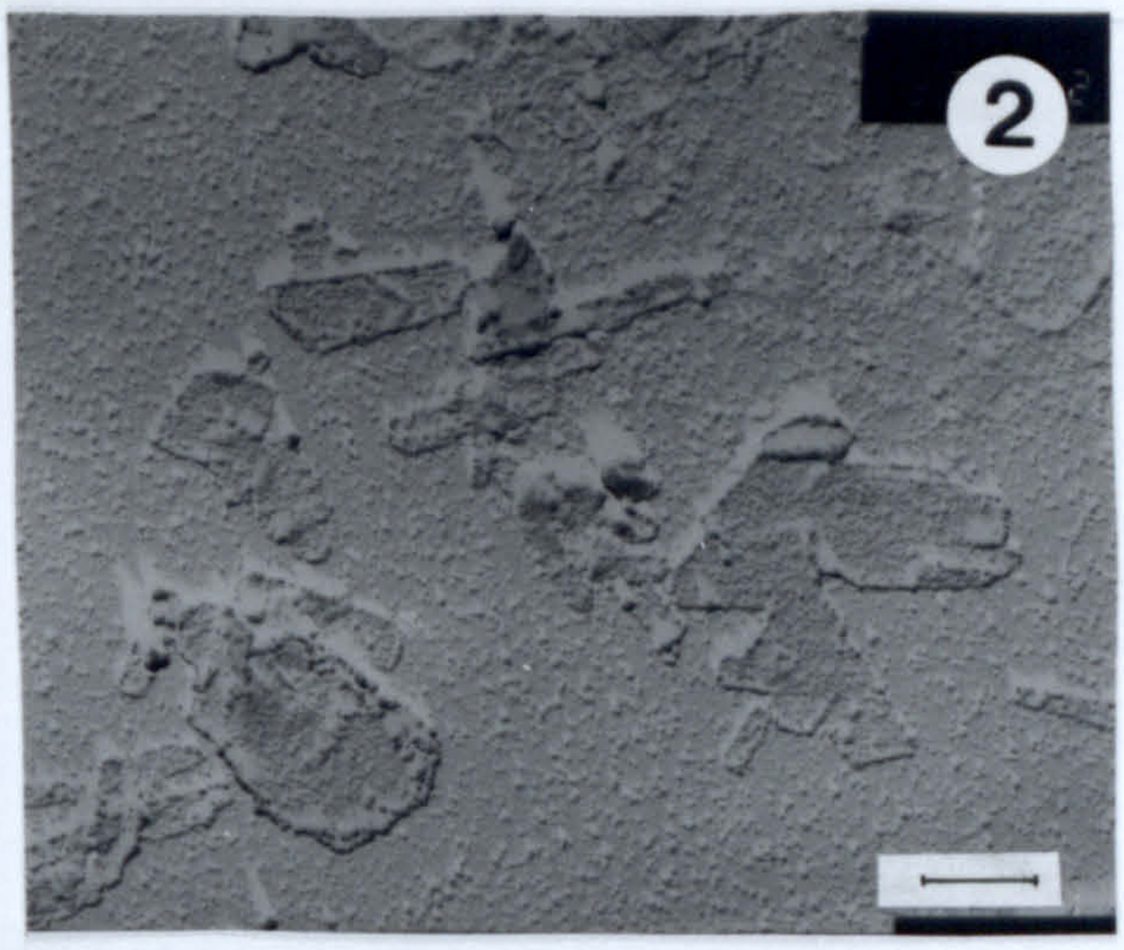

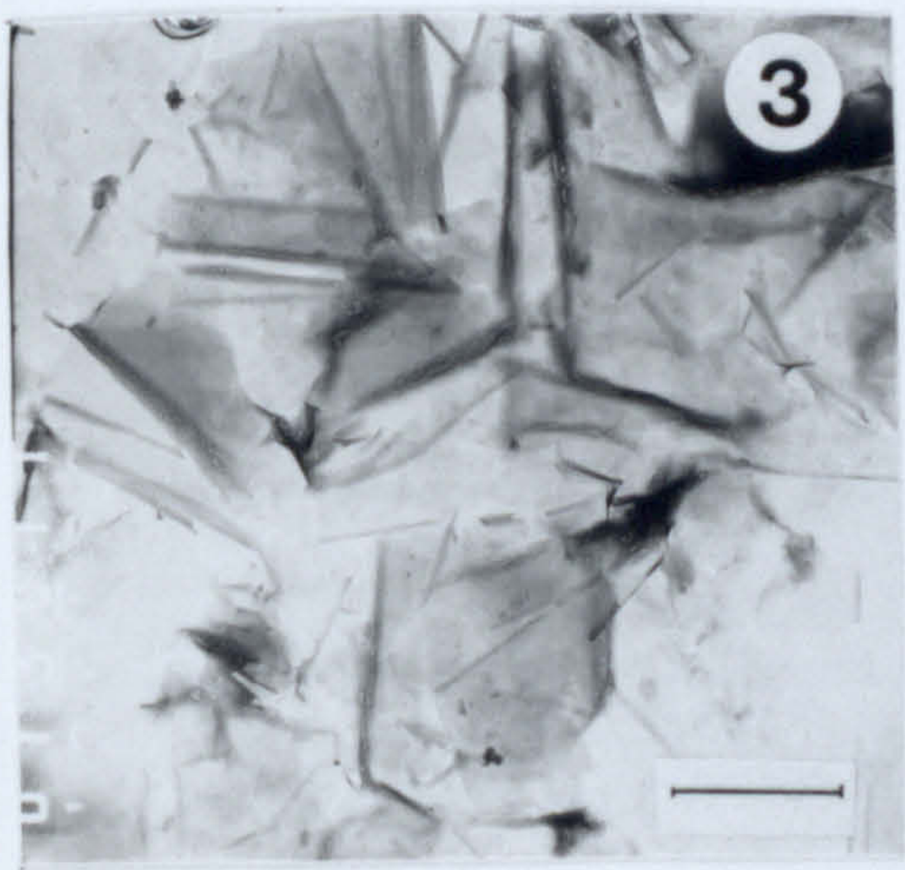

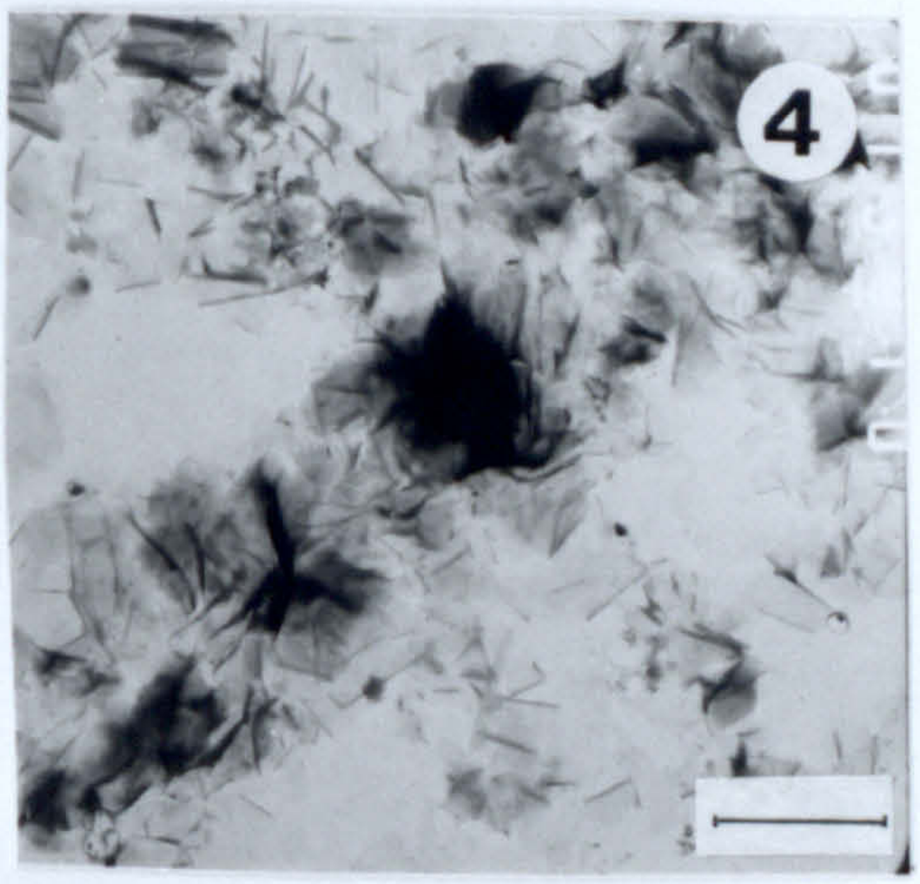

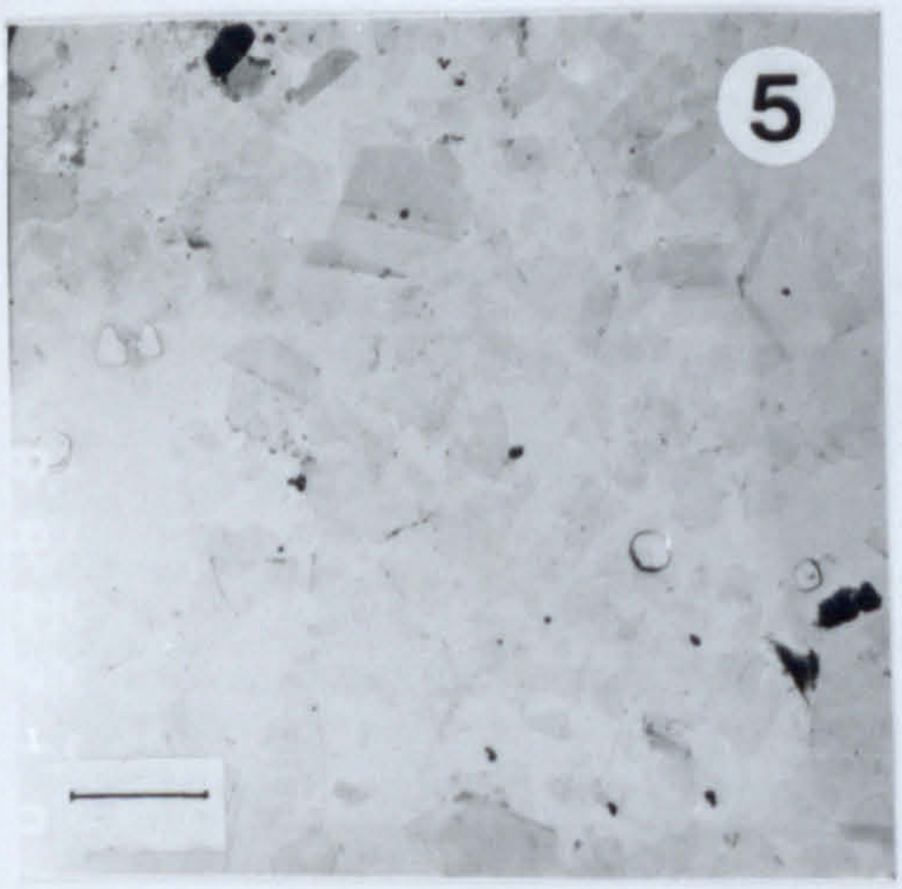

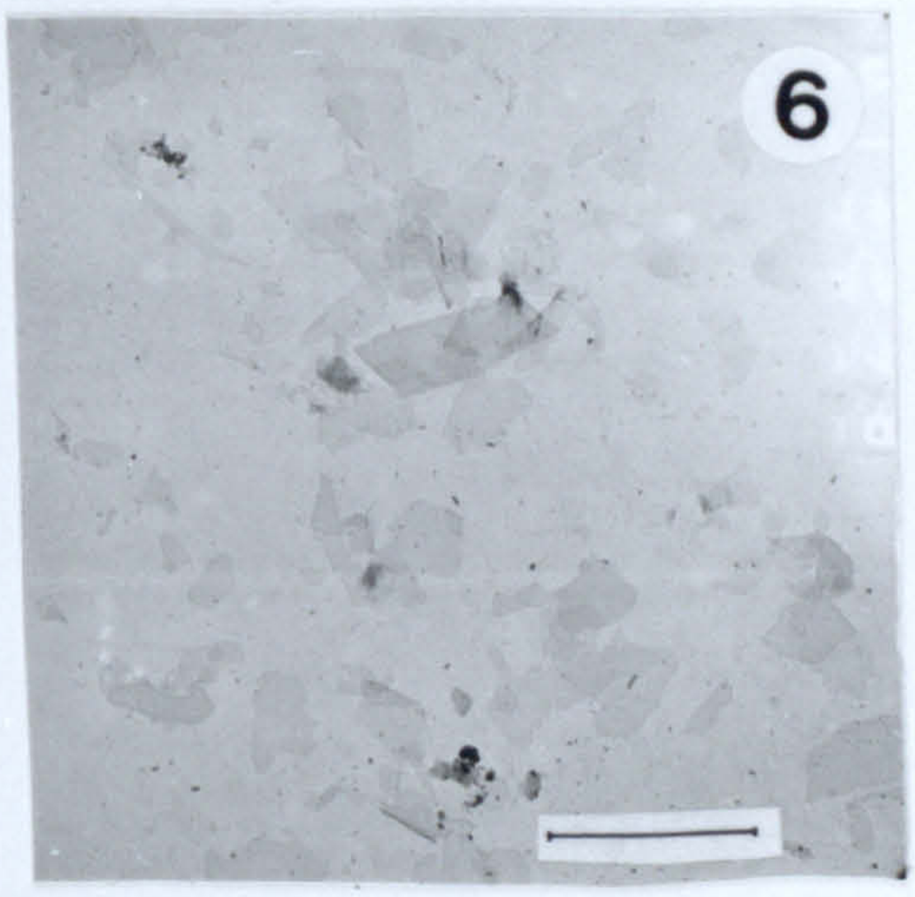

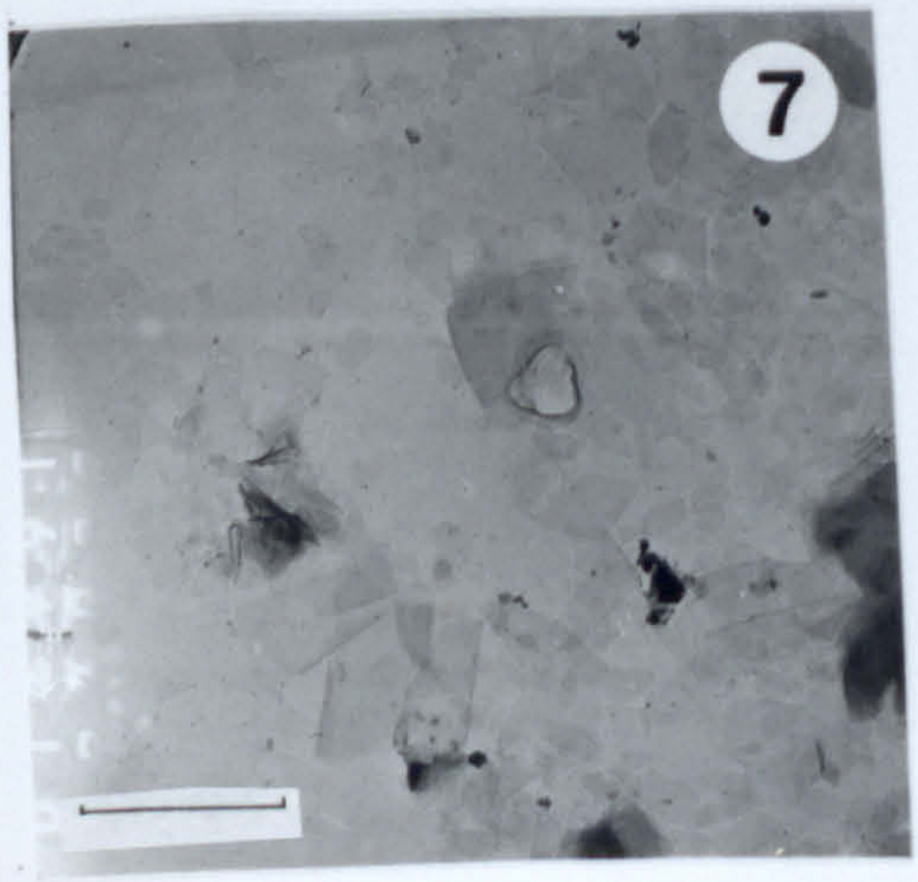

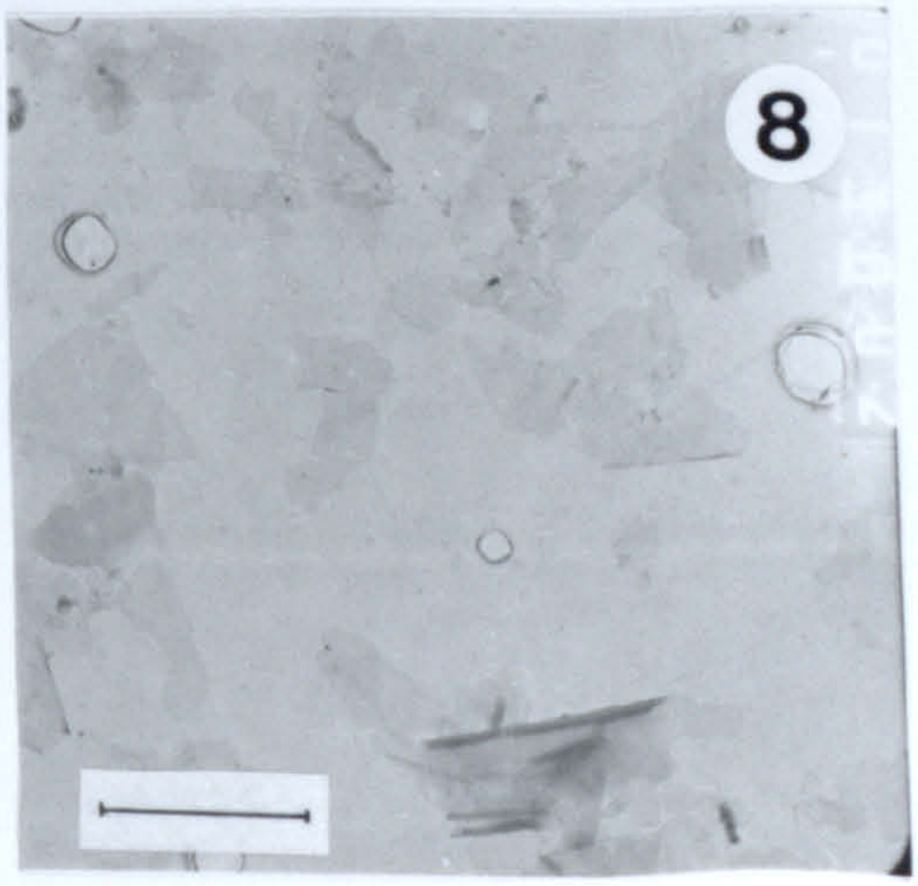

Plate 19

Pt-shadowed smectite and illite/smectite particles from the Tsantili deposit, Milos.

1. S-type (subhedral) smectite flakes (100% expandability). Scale bar 0.25μm.

2. Lath-like particles coexisting with flakes. 70% expandability, R0 type of ordering. Scale bar 0.15μm.

3. Step-like growth (shown by the arrow) of illite/smectite particles with hexagonal shape. It might correspond to spiral growth via screw disslocations. 51% expandability, RO/R1 type of ordering. Scale bar 0.15μm.

4. Predominance of flaky-crystals at 44% expandables. The thickness of the flakes is 20 and 30Å. R1/R0 type of ordering. Scale bar 0.15μm.

5. Predominance of illite/smectite lath-like particles at 40% expandability. R1 type of ordering. Scale bar 0.25μm.

6. Possible step-like growth (see arrow) at 35% expandables. The particles show both face-to-face and edge-to-edge association. Note that the large "flake" in the centre consists of several lath-like particles. R1 type of ordering. Scale bar 0.15μm.

7. Illite/smectite laths at 25% expandables. Flakes are completely missing. R1 type of ordering. Scale bar 0.15μm.

8. Illite/smectite laths at 13% expandables. R3 type of ordering. The particles show face-to-face association. Scale bar 0.25μm.

Plate 19

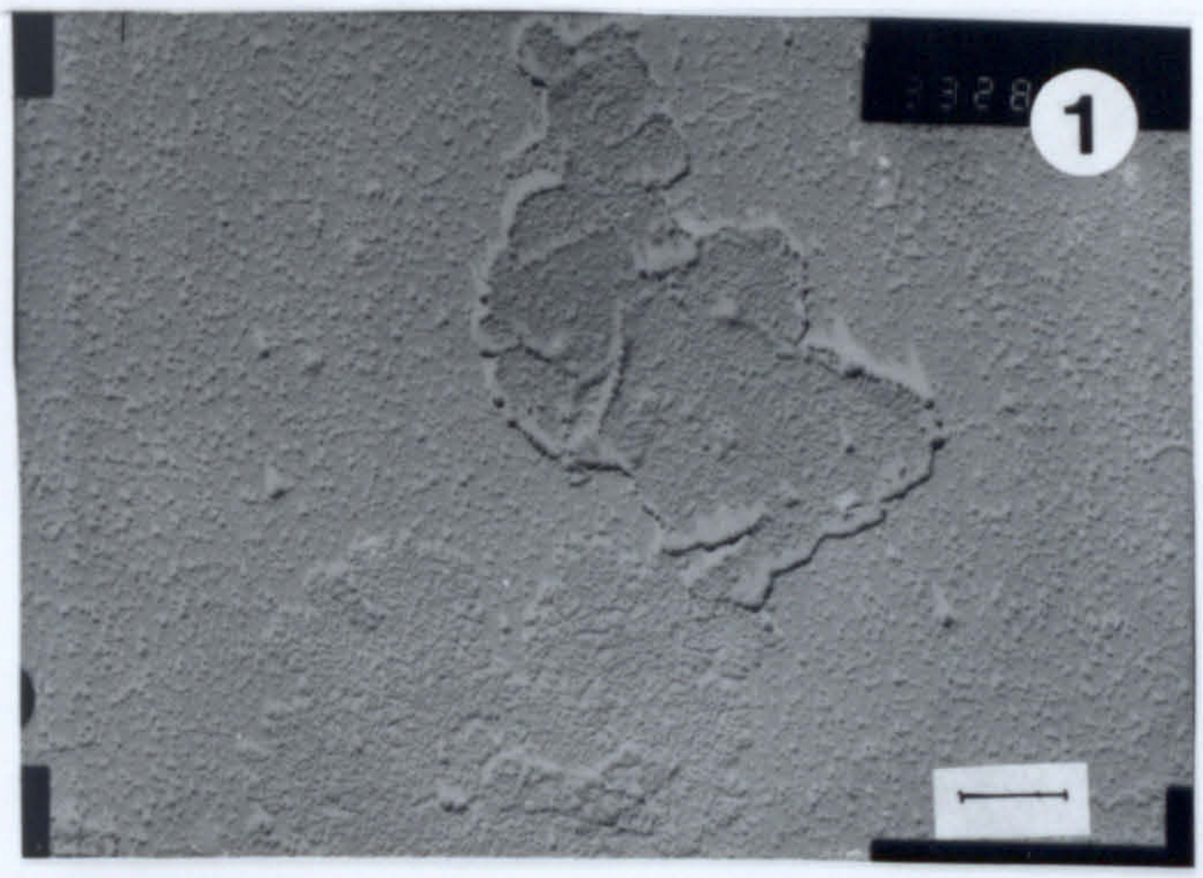

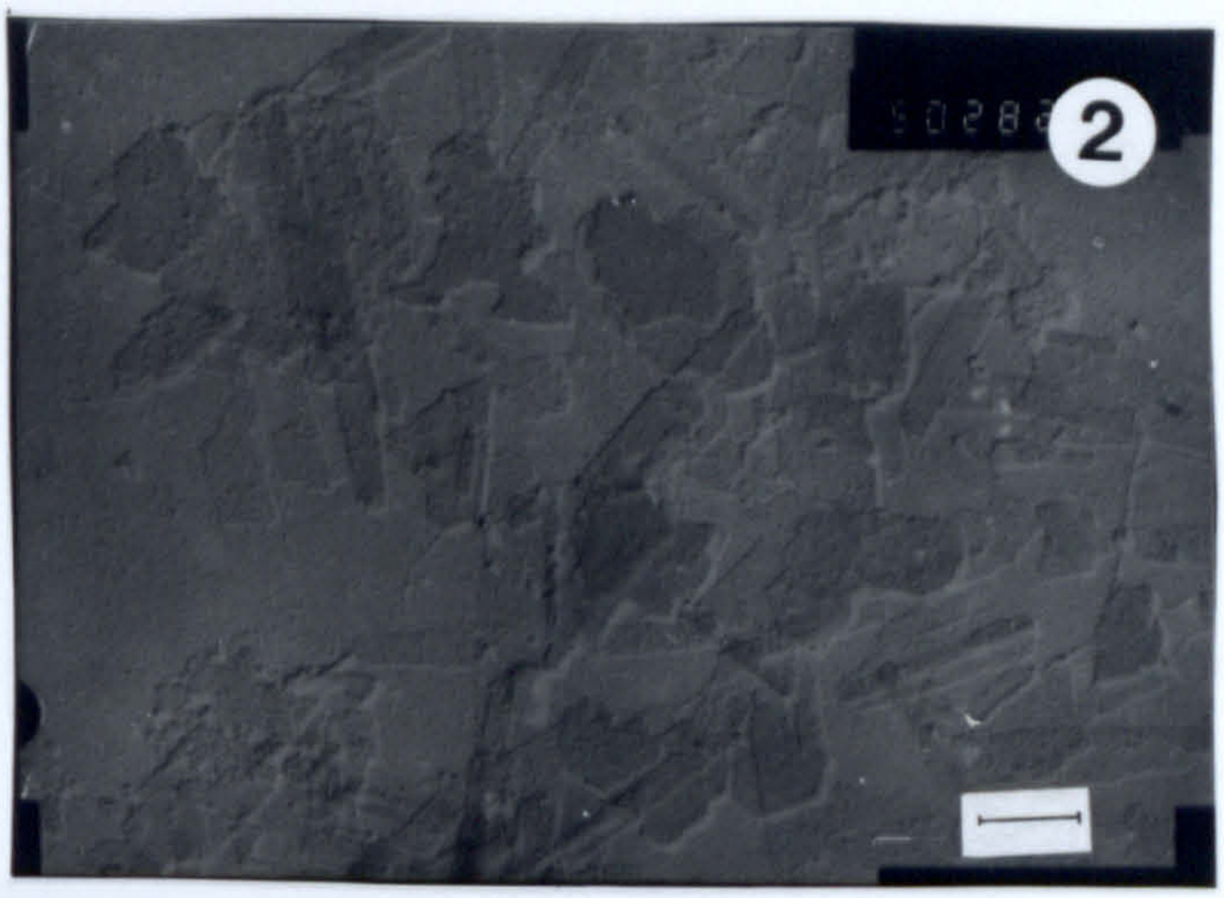

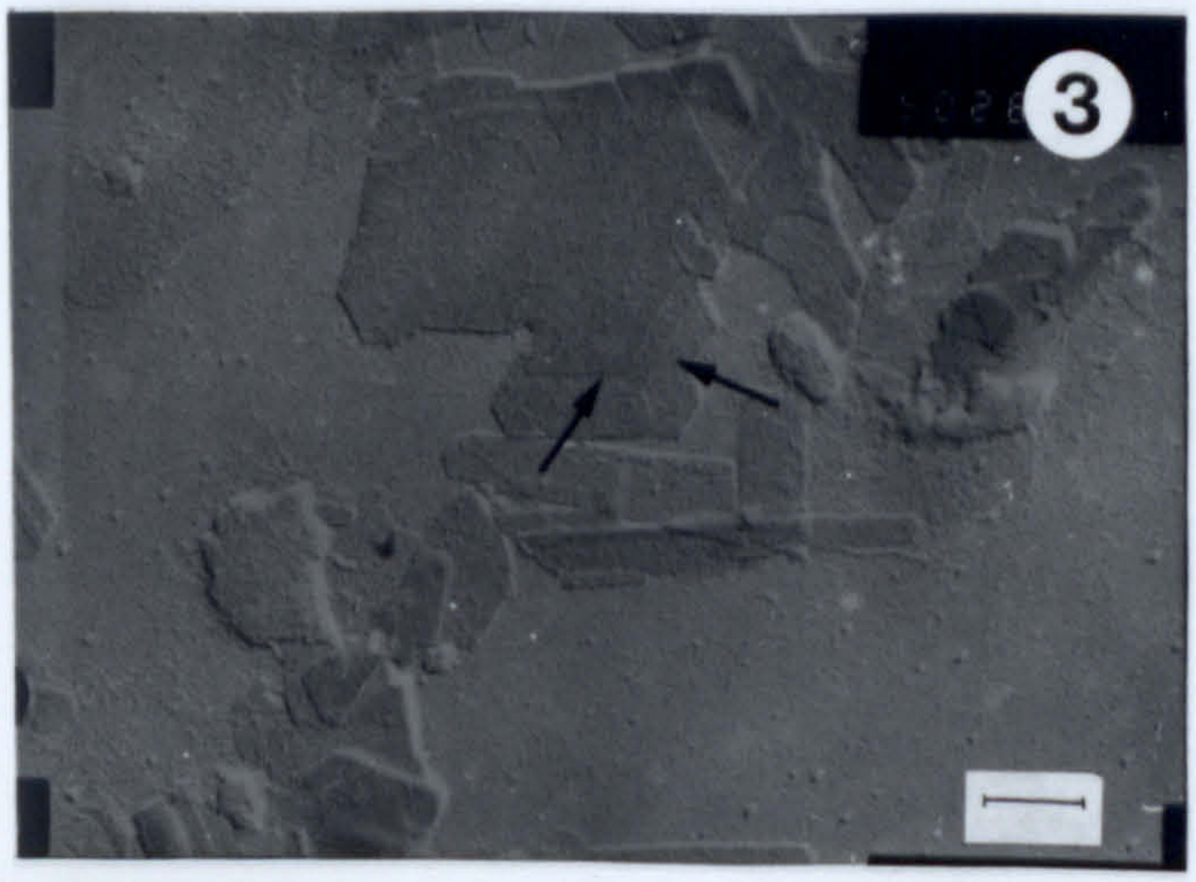

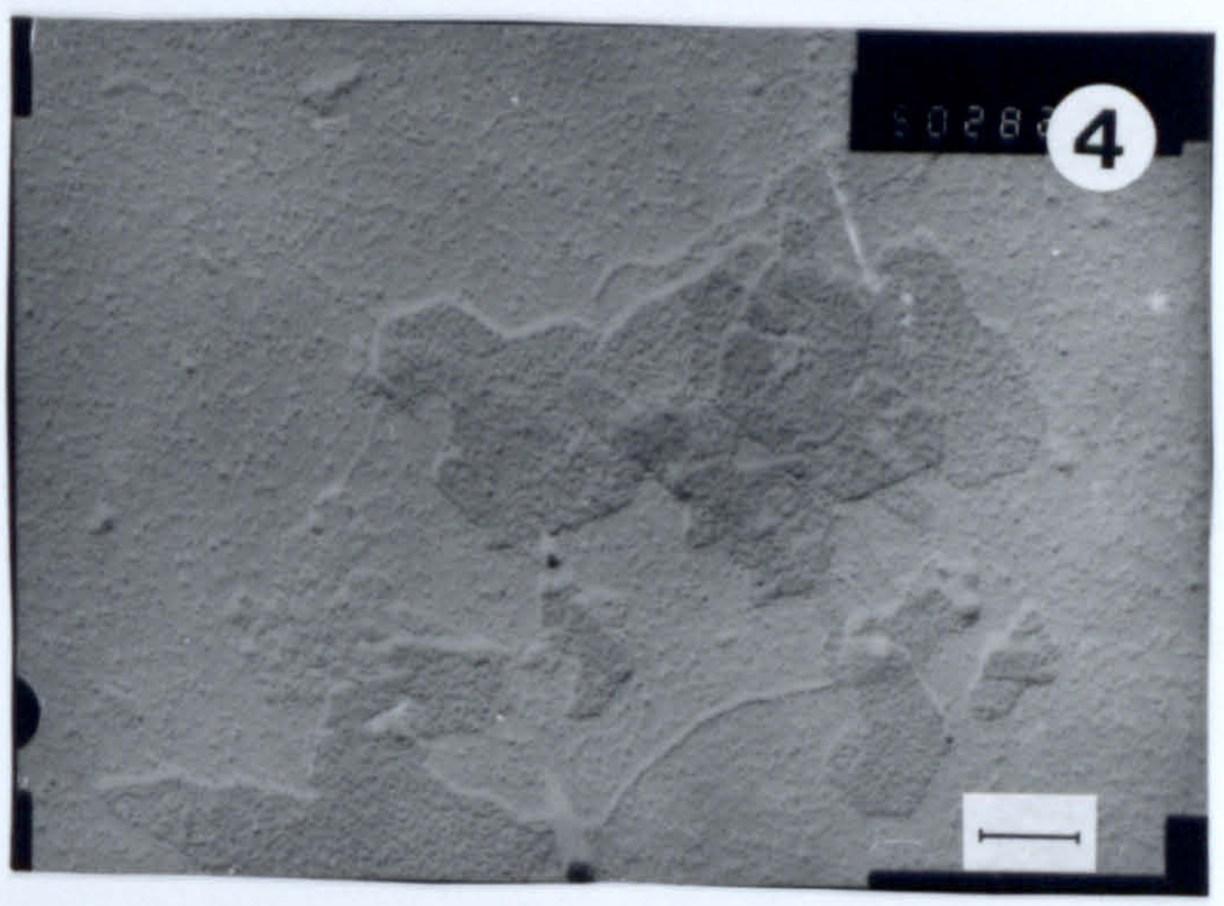

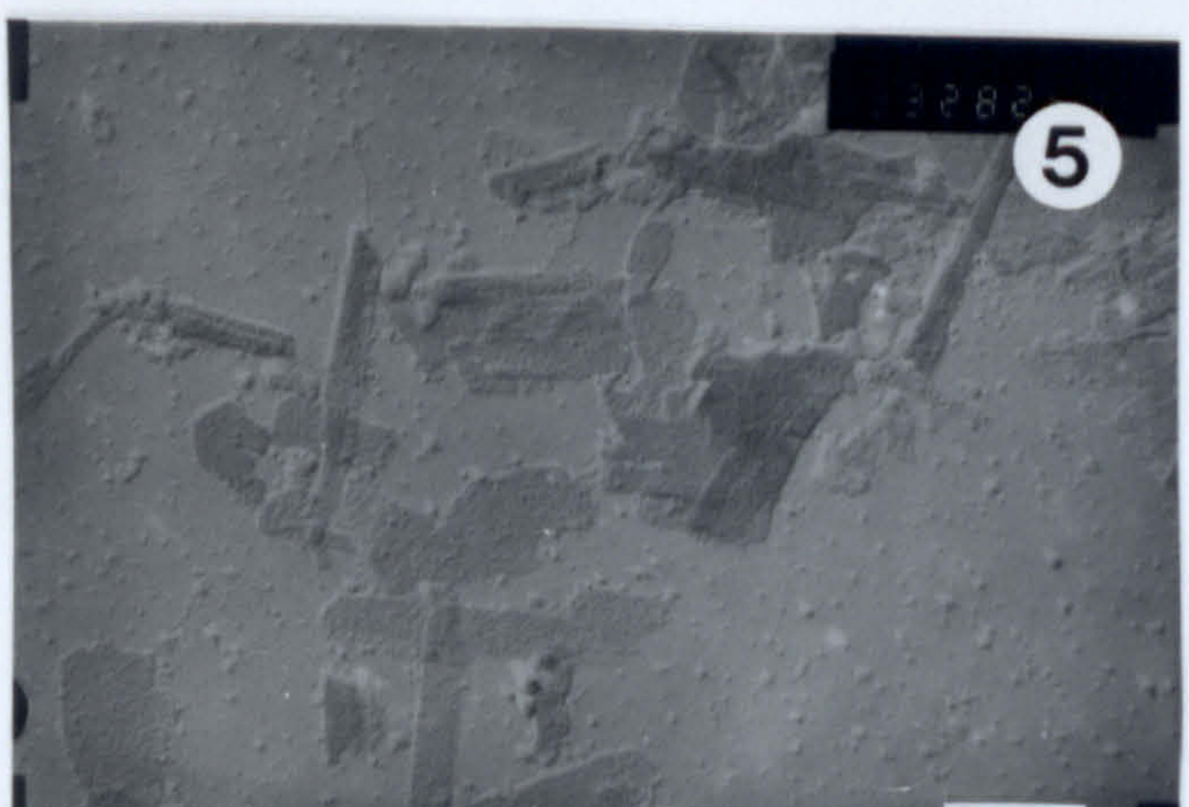

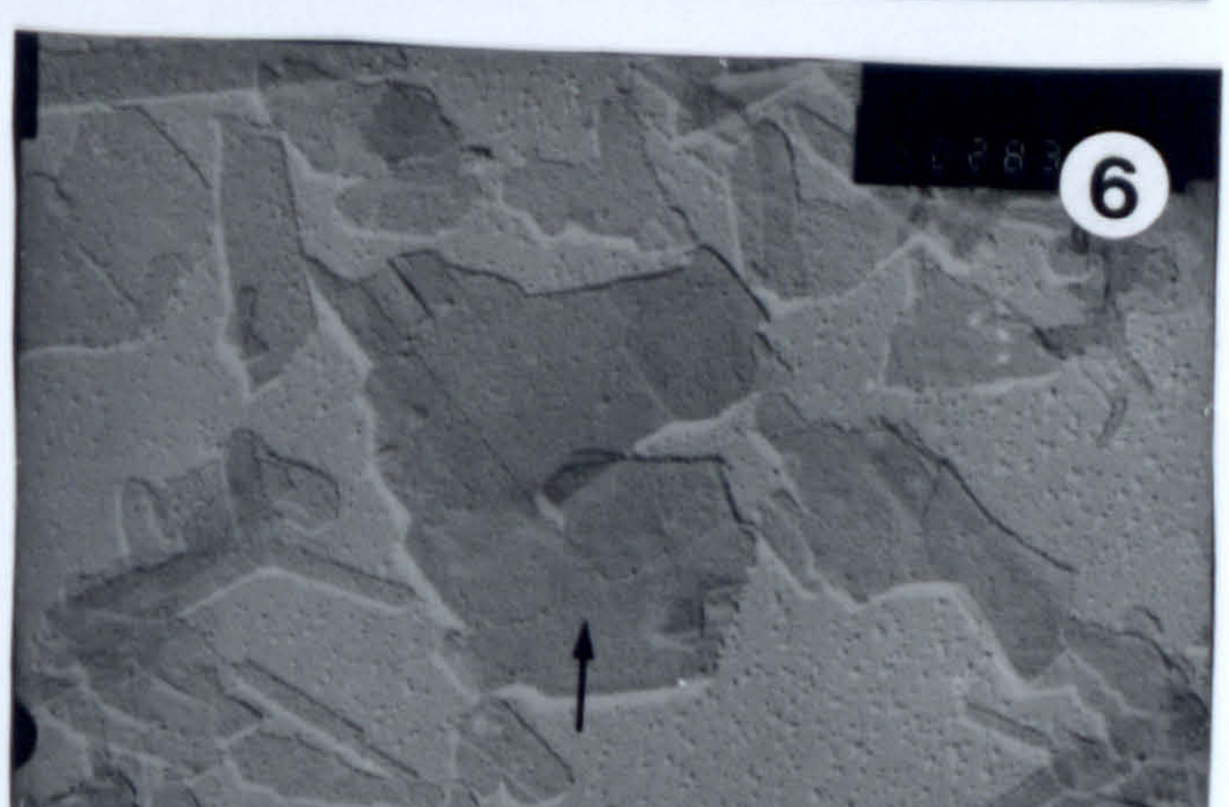

Plate 20

HRTEM images of smectites

1. Partially expanded smectite layers. The dark fringes have an average thickness of 17Å while the bright ones are about 13Å thick. The upper parts of the micrograph show evidence of beam damage. Scale bar 110 Å.

2. Collapsed smectite layers of Wyoming montmorillonite. The thickness of the bright fringes is 10 Å while that of the dark fringes 11 Å. Scale bar 190 Å.

Plate **20**

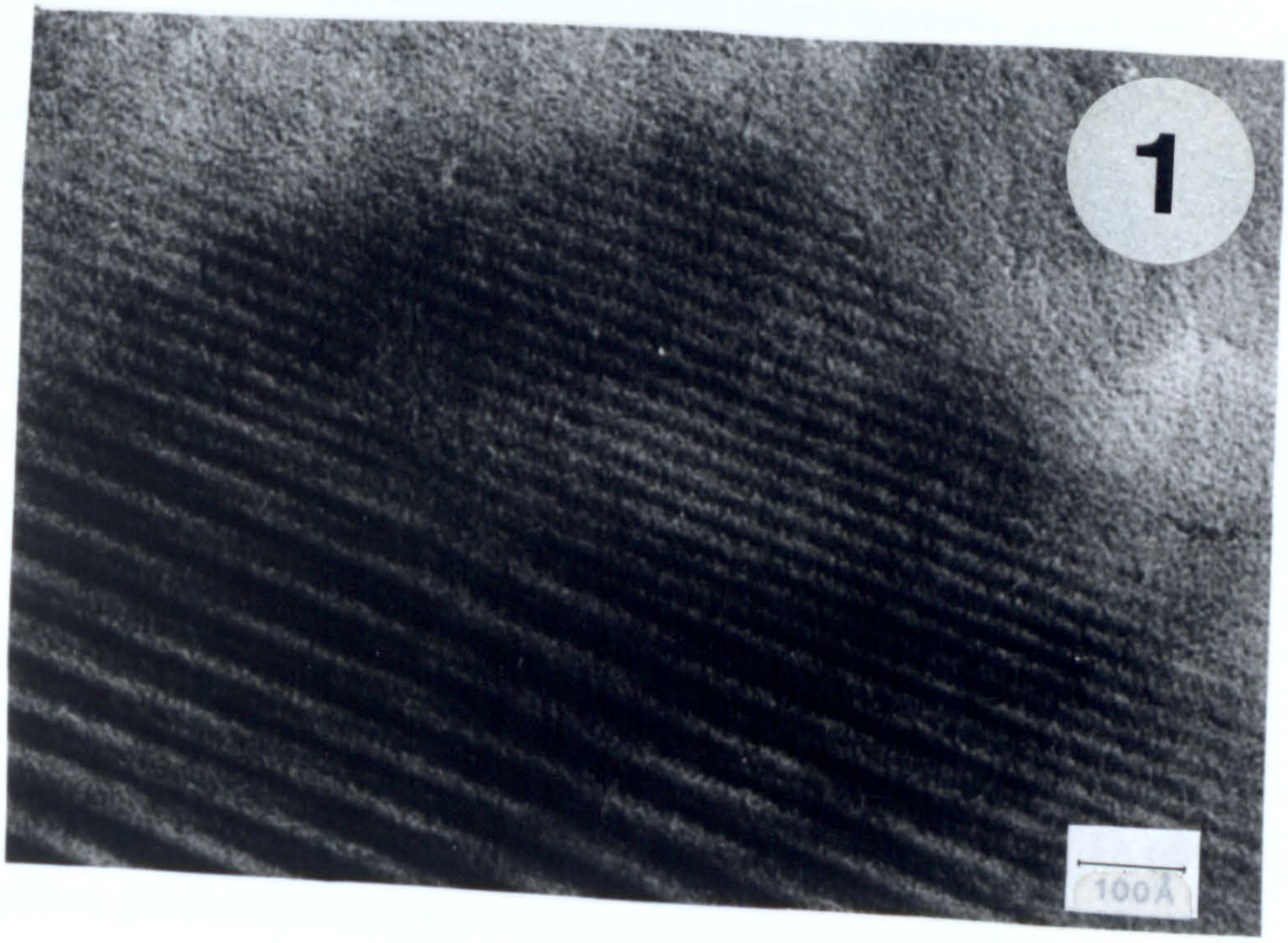

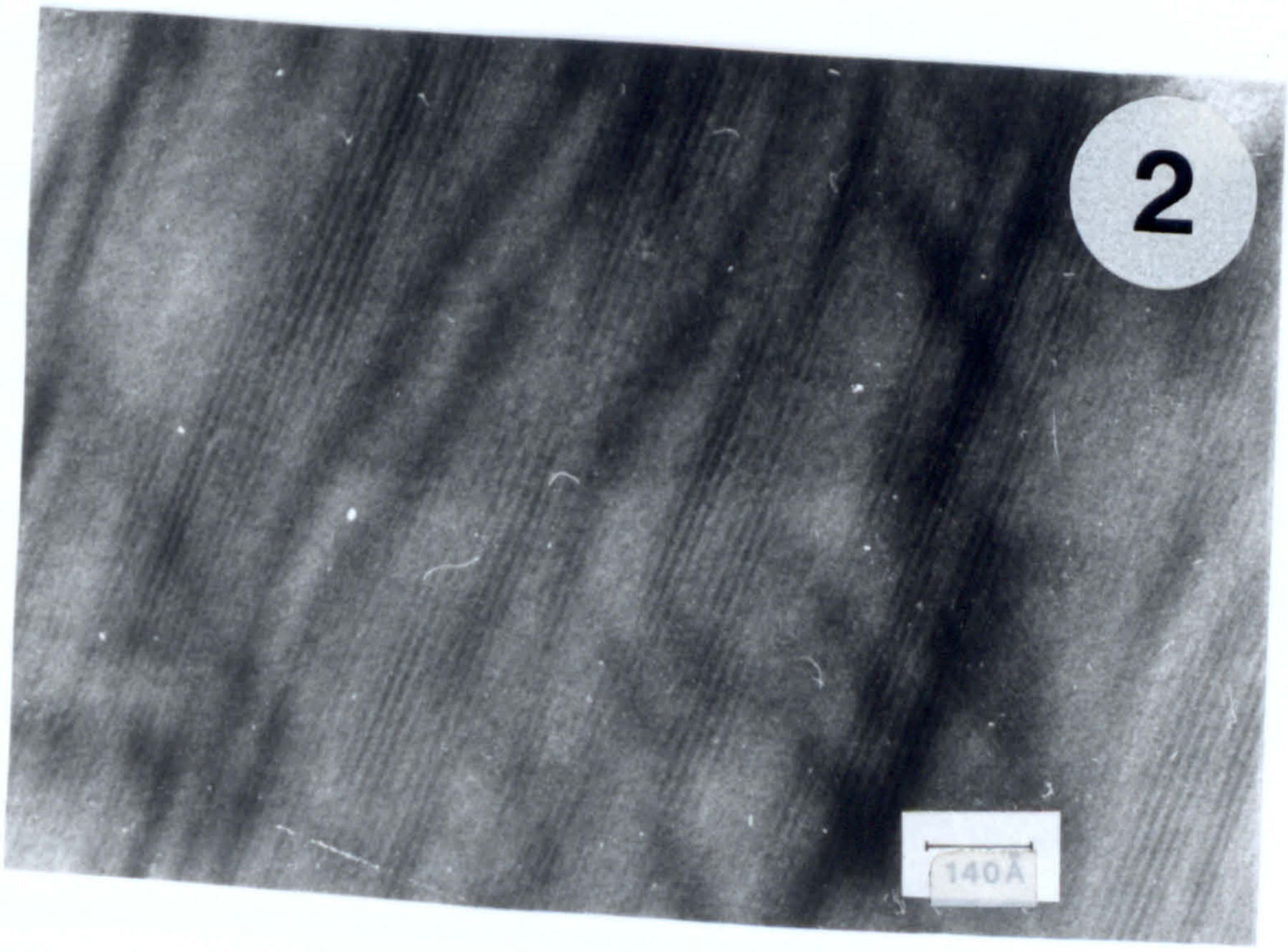

CHAPTER FIVE

GEOCHEMISTRY.

This chapter examines the geochemical characteristics of the Greek bentonites based on major and trace element data. It is organized in five sections. The first section describes briefly the experimental methods used to obtain the geochemical data. The second section examines the correlation between mineralogy and geochemistry. An attempt is made to establish the nature of the parent rocks based on trace element data and to examine the influence of the parent rock geochemistry on the major element geochemistry of bentonites. The third section deals with the mobility of major and trace elements during the process of alteration of a volcanic rock to bentonite. The mobility of chemical elements is examined in three different cases:

-alteration of an acidic rock

-alteration of an intermediate rock

-hydrothermal activity superimposed on an already formed bentonite

The fourth section compares the alteration patterns observed in the three different cases examined and determines the elements which can be considered as relatively immobile. Finally in the fifth section a geochemical correlation between the different bentonite deposits of Milos, based on the relatively immobile elements establised in the previous section, is attempted. The purpose of this correlation is to establish a model, which could be used for exploration of new deposits based on "geochemical-stratigraphic" criteria.

5.1. Experimental methods.

Representative samples of Greek bentonites from Milos, Kimolos and Chios were analysed for both major and trace chemical elements, including rare earth elements. The analysed samples can be subdivided into three groups according to the chemical elements analysed from each of them. The first group includes representative bentonite samples from all the deposits studied. They were analysed for both major and trace elements. The purpose was to determine the overall chemical variation of the Greek bentonites. The second group includes bentonites which were analysed only for trace elements which were used for geochemical correlation purposes, with both conventional triangular plots and multivariate statistics (discriminant function). Finally, the third group consists of samples which were taken from transition zones and represent alteration profiles from fresh glass to bentonite. Those samples were analysed for major and trace elements including the entire range of rare earth elements, in order to determine the relative mobility of the various elements during the alteration of fresh glass to bentonite. In Ankeria deposit which is

currently affected by hydrothermal activity (see Plate 3 and section 3.3.1.2.1 of Chapter 3) a profile from the "fresh" bentonite to the centre of the thermal spring was analysed. The relatively immobile elements from these profiles were used for geochemical correlation, because they represent safe indicators for the signature of the different deposits.

The major elements (Si, Ti, Al, Fe, Mn, Mg, Ca, Na, K, and P) were analysed with X-Ray fluorescence with the method described by Bennett & Oliver (1976) modified by N.Marsh, University of Leicester. The samples were fused using a mixture of 80% Li-tetraborate and 20% Li-metaborate as flux and were casted in Al-dies forming circular glass beads. The flux:sample powder ratio was 1:5. The instrumental conditions used for the determination of major elements are given in Appendix 5.1. Because of the nature of the samples the loss of ignition was calculated during fusion. The method used for the determination of the loss of ignition is described in Appendix 5.2. Chemical analyses of the Greek bentonites are given in Tables 5.1 and 5.2.

Selected samples containing sulphate minerals (baryte, gypsum, alunite, and/or jarosite) and which gave low totals were analysed for SO_3. A series of four standards was prepared by addition of 1, 5, 10 and 20% $BaSO_4$ in the form of barytes, corresponding to 0.34, 1.72, 3.43 and 6.86% SO_3 respectively, to the sample SM336 from Chios island which was SO_3-free. The original Ba-content of this sample was 153.5 ppm (Table 5.1). The calibration curve for SO_3 is given in Appendix 5.3.

Trace element determination was carried out on pressed powder pellets by X-Ray fluorescence. The elements analysed were Nb, Zr, Y, Sr, Rb, Th, Zn, Ni, V, Cr, Ba, La, Ce, and Nd. The results are given in Tables 5.1, 5.2 and 5.3, while the instrumental conditions used are shown in Appendix 5.1. The precision and accuracy of the instruments used for the determinations of the major and trace elements is given in Appendices 5.4.2 and 5.4.3.

Rare earth element determination was carried out by Inductively Coupled Plasma (ICP) analysis. The elements determined were La, Ce, Nd, Sm, Eu, Dy, Er, Yb and Lu. The method used is based on that proposed by Walsh *et al.* (1981) modified at the University of Leicester. The accuracy and precision of the analyses were checked by analysing the Jb-1a international standard (basalt, Geological Survey of Japan) with the samples (Appendix 5.4.4). The sample preparation method is given in Appendix 5.4.1.

5.2. Major and trace element geochemical characteristics of the Greek bentonites.

5.2.1. Milos island.

Milos bentonites can be separated in two different groups according to their major element geochemistry (Fig. 5.1). These diagrams provide an indication about the smectite chemistry and the smectite:Si-phases ratio. This is because Al, Fe and Mg are incorporated mainly in smectites; the feldspar content which includes some Al is small

Legend to Tables 5.1, 5.2 and 5.3

Codes for the bentonite deposits.

BMAN=Ankeria deposit, Milos.

BMKF=Koufi deposit, Milos.

BMTS=Tsantili deposit, Milos.

BMAH=Aspro Horio deposit, Milos.

BMAK=Ano Komia deposit Milos.

BMGF=Garyfalakena, deposit, Milos.

BMRS=Mavrogiannis deposit, Milos.

BMKK=Kato Komia deposit, Milos.

BMZL=Zoulias deposit, Milos.

BMRM=Rema deposit, Milos.

KMKS=Kastriani deposit, Milos (kaolin)

BMAG=Agrilies deposit, Milos.

BKPR=Prassa deposit, Kimolos

BKP1=Main bentonite body, Prassa deposit, Kimolos.

BKP2=Small bentonite body, Prassa depoist, Kimolos

F1,F2=Faulted zone, Prassa depoist, Kimolos

BKLT=Loutra deposit, Kimolos.

BKBO=Bonatsa deposit, Kimolos

BKAT=Agios Tryfon deposit, Kimolos.

BCHT=Chios bentonite

Table 5.1

Major and trace element XRF analyses of the Greek bentonites from the islands of Milos, Kimolos and Chios

Sample	SM8	SM17	SM25	SM35	SM45	SM51	SM64	SM66	SM75	SM78	SM82
Deposit	BMAN	BMAN	BMAN	BMAN	BMKF	BMKF	BMKF	BMKF	BMTS	BMTS	BMTS
Major elements (%)											
SiO_2	55.36	57.11	53.13	66.32	59.41	58.65	58.71	60.37	56.77	53.79	51.49
TiO_2	0.92	0.86	0.77	0.80	0.80	0.69	0.82	0.97	0.88	0.83	1.09
Al_2O_3	18.92	18.07	19.16	15.52	20.87	18.95	22.41	21.42	19.94	19.64	21.58
Fe_2O_3	5.42	2.99	5.02	3.26	5.66	3.92	4.28	2.90	1.91	5.89	2.36
MnO	0.06	0.09	0.03	0.05	0.01	0.01	0.02	0.01	0.01	0.10	0.01
MgO	4.14	3.45	3.37	3.81	2.71	3.59	3.38	2.72	0.79	1.45	1.06
CaO	3.92	6.13	6.42	2.28	2.36	1.45	1.55	1.18	0.34	0.25	0.14
Na_2O	0.51	0.53	0.90	0.54	1.53	0.65	0.53	0.56	0.37	0.20	0.26
K_2O	0.85	0.20	0.32	0.32	0.54	1.37	0.95	4.47	10.10	9.90	8.35
P_2O_5	0.11	0.12	0.17	0.04	0.19	0.20	0.21	0.01	0.09	0.06	0.04
SO_3	- -	- -	- -	- -	- -	1.47	- -	- -	- -	0.50	0.24
LOI	9.32	9.71	10.18	7.64	6.31	6.51	7.13	5.51	8.67	6.50	12.57
Total	99.51	99.26	99.47	100.58	100.39	97.45	99.99	100.12	99.87	99.11	99.19
Trace elements in p.p.m.											
V	132.30	224.00	224.90	149.20	161.80	163.70	182.10	74.10	217.30	211.00	199.30
Cr	17.60	22.90	8.50	23.50	1.30	2.80	5.10	84.10	41.00	44.20	57.20
Ni	15.00	47.00	9.10	10.50	7.50	7.00	12.10	73.90	17.00	14.20	39.30
Zn	58.20	179.30	104.10	31.80	68.90	184.10	32.60	97.90	132.80	115.30	106.00
Rb	50.60	24.10	23.90	22.50	54.40	88.60	62.90	68.00	427.80	538.60	459.70
Sr	89.10	95.50	151.90	77.30	216.40	217.20	58.20	47.30	22.90	18.20	66.80
Y	13.00	17.30	23.60	10.20	19.20	16.40	18.20	14.60	31.60	17.30	27.50
Zr	229.70	214.50	217.90	176.70	281.70	227.80	228.30	159.70	202.10	195.00	170.80
Nb	8.90	8.60	9.00	6.50	12.20	10.00	11.10	6.30	8.10	9.60	8.30
Ba	215.50	929.60	1165.20	66.00	1069.11	0013.70	278.50	1376.10	665.70	308.00	689.80
La	22.01	33.80	35.60	19.80	34.70	40.00	39.70	29.80	42.40	23.20	31.10
Ce	45.84	60.80	69.50	61.20	69.40	51.00	72.10	50.00	80.00	55.70	54.30
Nd	18.66	25.60	29.20	21.00	29.60	17.00	30.50	18.20	46.70	23.10	19.00
Th	10.30	12.90	17.20	7.00	16.80	11.90	18.30	10.80	7.20	10.20	8.40

Table 5.1 (continued)

Sample	SM98	SM100	SM117	SM119	SM127	SM135	SM144	SM148	SM157	SM164	SM168
Deposit	BMTS	BMTS	BMAH	BMAH	BMAH	BMAK	BMAK	BMAK	BMGF	BMGF	BMGF
Major elements (%)											
SiO_2	59.21	58.52	59.02	60.15	59.08	65.42	77.04	75.03	75.71	77.16	70.97
TiO_2	1.06	0.90	0.95	0.79	0.76	0.35	0.66	0.17	0.21	0.28	0.19
Al_2O_3	19.57	19.91	19.13	18.40	18.72	13.63	11.12	13.80	13.72	12.69	12.34
Fe_2O_3	4.14	4.05	6.35	7.26	7.72	2.25	1.22	1.43	1.98	1.60	1.58
MnO	1.08	0.11	0.01	0.02	0.02	0.04	0.01	0.03	0.01	0.01	0.16
MgO	2.52	3.34	3.56	2.79	2.98	1.83	0.78	1.82	1.46	1.44	1.05
CaO	1.09	2.21	1.36	0.84	0.79	4.87	0.39	0.56	0.79	0.46	3.53
Na_2O	0.41	0.48	1.06	1.04	0.36	0.68	1.44	0.29	0.26	0.14	0.47
K_2O	3.23	1.72	0.73	1.28	0.36	0.87	2.99	2.33	1.23	0.32	2.91
P_2O_5	0.16	0.13	0.01	0.09	0.08	0.07	0.20	0.01	0.03	0.03	0.04
SO_3	- -	1.69	0.56	- -	- -	2.69	0.98	- -	- -	- -	- -
LOI	6.92	6.69	6.49	7.32	8.60	6.55	2.76	4.98	4.76	5.14	6.23
Total	99.39	99.75	99.23	99.98	99.47	99.25	99.59	100.45	100.16	99.27	99.47
Trace elements in p.p.m.											
V	280.80	264.20	162.20	136.70	188.80	87.30	87.60	10.00	21.20	19.40	21.40
Cr	52.80	57.50	70.80	78.00	58.60	38.50	174.40	16.30	31.60	39.00	32.90
Ni	24.20	20.60	28.40	40.20	26.40	27.90	12.90	10.70	23.40	30.10	30.80
Zn	199.80	12.50	71.40	92.10	73.30	18.90	149.80	30.60	73.20	94.70	28.30
Rb	171.70	273.10	53.20	94.10	50.40	99.80	113.30	231.50	71.60	23.40	114.10
Sr	13.10	324.10	66.60	97.30	40.80	47.00	22.20	39.80	64.00	31.00	141.70
Y	22.40	30.20	18.60	55.40	22.40	18.00	27.50	18.20	15.30	23.10	15.90
Zr	194.70	138.60	193.50	205.20	186.40	116.90	190.10	136.30	134.90	148.00	121.10
Nb	7.90	10.90	9.10	13.20	7.90	5.10	5.80	7.60	8.10	9.00	6.30
Ba	613.70	413.10	105.10	159.30	376.40	122.90	210.30	94.50	48.00	27.90	883.60
La	34.60	40.90	29.40	49.90	28.40	20.60	33.40	29.60	28.70	37.50	26.60
Ce	55.00	74.10	49.30	131.10	62.70	34.80	71.60	45.10	54.60	73.80	46.30
Nd	30.80	36.90	27.60	57.70	30.80	14.60	33.90	16.60	21.40	32.50	13.50
Th	9.10	9.40	10.20	12.20	10.20	8.10	9.50	14.20	13.90	12.30	12.20

Table 5.1 (continued)

Sample	SM174	SM176	SM179	SM181	SM184	SM205	SM208	SM216	SM228	SM232	SM237
Deposit	BMRS	BMRS	BMKK	BMKK	BMKK	BMZL	BMZL	BMZL	BMZL	BMRM	BMRM
Major elements (%)											
SiO_2	77.27	72.99	65.64	76.93	61.27	61.01	65.61	73.04	60.38	73.62	75.10
TiO_2	0.20	0.21	0.28	0.15	0.34	1.33	0.60	0.18	1.01	0.24	0.25
Al_2O_3	13.13	13.45	12.70	13.49	11.42	17.42	18.08	12.20	18.05	12.33	11.75
Fe_2O_3	1.89	3.30	2.98	1.42	3.13	6.19	3.03	2.73	5.66	1.44	1.53
MnO	0.01	0.02	0.12	0.02	0.12	0.01	0.01	0.01	0.01	0.03	0.04
MgO	1.25	1.18	2.80	1.55	3.12	3.37	2.15	2.28	4.04	1.08	1.23
CaO	0.51	0.45	4.93	0.67	7.14	1.27	1.74	0.70	1.13	1.27	1.59
Na_2O	0.39	0.27	0.62	0.36	0.63	0.95	2.36	0.40	1.00	2.06	0.31
K_2O	1.63	1.68	1.80	1.05	3.47	0.64	1.60	0.19	0.68	2.62	4.36
P_2O_5	0.02	0.03	0.06	0.02	0.06	0.19	0.09	0.01	0.05	0.03	0.04
SO_3	- -	- -	1.02	- -	- -	- -	- -	- -	- -	- -	- -
LOI	4.05	6.41	7.01	4.25	8.91	6.76	5.02	7.37	7.41	5.90	4.09
Total	100.35	99.99	99.96	99.91	99.61	99.14	100.29	99.11	99.42	100.63	100.29
Trace elements in p.p.m.											
V	57.50	18.20	15.60	12.50	74.30	147.60	94.00	85.40	231.70	19.50	26.30
Cr	183.30	24.90	21.90	8.50	249.80	7.70	27.60	3.60	46.70	34.50	50.20
Ni	126.70	47.10	5.70	4.00	130.60	24.40	11.10	5.40	16.70	22.70	24.20
Zn	41.80	53.90	24.10	37.60	42.40	134.20	40.10	31.56	56.80	35.00	26.90
Rb	102.90	82.10	72.20	66.70	144.30	27.90	53.30	14.40	24.80	481.20	176.80
Sr	44.30	75.40	61.90	51.80	109.90	285.30	455.90	56.80	81.60	221.10	42.20
Y	18.60	36.00	10.40	10.10	16.80	65.80	11.80	10.30	75.00	17.70	16.00
Zr	126.50	134.50	135.10	131.00	125.80	382.40	200.00	130.60	184.00	127.90	134.00
Nb	8.40	7.00	6.90	12.50	8.00	20.10	11.10	6.10	7.40	6.80	7.60
Ba	768.00	338.60	153.00	43.80	166.10	554.20	364.40	34.40	123.101	122.40	203.80
La	21.60	28.00	27.70	38.00	29.40	53.30	47.30	9.80	52.40	27.70	23.00
Ce	40.70	50.80	43.70	50.10	46.00	97.60	77.10	33.10	89.20	41.40	43.50
Nd	13.30	19.00	12.20	19.70	17.70	55.30	34.60	11.60	52.10	15.90	14.80
Th	15.30	14.00	14.10	22.00	11.40	23.10	17.40	12.00	8.40	12.70	11.10

Table 5.1 (continued)

Sample	SM238	SM242	SM243	SM247	SM264	SM280	SM281	SM283	BM294	SM299	SM302
Deposit	KMKS	KMKS	BMAG	BMAG	BKPR	BKPR	BKPR	BKPR	BKLT	BKLT	BKLT
Major elements (%)											
SiO_2	75.53	75.02	69.40	66.09	65.68	61.39	63.61	71.78	69.84	76.68	70.78
TiO_2	0.25	0.21	0.45	0.54	0.13	0.16	0.18	0.10	0.28	0.09	0.36
Al_2O_3	14.13	17.94	17.29	16.98	18.18	20.47	19.60	13.21	13.86	12.73	14.08
Fe_2O_3	0.14	- -	2.10	3.16	1.33	1.91	1.85	0.72	2.99	0.74	2.44
MnO	- -	0.01	0.01	0.01	0.03	- -	- -	0.02	0.02	0.03	0.01
MgO	0.07	0.05	1.42	1.53	2.23	5.09	4.53	1.33	2.43	0.40	3.29
CaO	- -	- -	0.76	0.59	1.20	1.10	1.07	0.61	1.81	- -	1.38
Na_2O	0.12	0.07	0.26	0.12	1.49	0.75	0.49	3.00	1.69	0.29	1.33
K_2O	0.17	0.03	1.40	1.92	2.33	0.21	0.12	2.82	1.66	8.21	0.96
P_2O5	0.03	0.04	0.05	0.02	0.02	0.02	0.03	0.02	0.07	0.02	0.08
SO_3	1.43	- -	- -	- -	- -	0.32	0.13	- -	- -	- -	- -
LOI	7.10	6.79	6.39	8.71	7.29	7.85	8.34	4.46	5.39	1.55	5.61
Total	99.27	100.16	99.53	99.65	99.91	99.27	99.95	100.34	100.04	100.74	100.25
Trace elements in p.p.m.											
V	22.00	24.10	80.10	101.10	4.60	0.00	4.70	5.90	33.50	0.00	25.60
Cr	22.00	29.90	84.80	126.20	4.70	6.20	4.80	4.00	6.90	1.40	3.10
Ni	3.00	3.60	9.50	82.10	5.60	6.70	5.30	5.70	7.00	4.90	6.60
Zn	3.00	2.70	19.90	230.80	253.80	257.30	217.40	106.50	78.70	36.30	50.00
Rb	3.90	3.20	67.10	117.30	101.60	12.90	9.80	297.70	190.20	227.50	41.90
Sr	237.60	286.10	103.10	19.00	100.70	113.00	105.60	163.90	152.70	31.40	167.10
Y	3.30	5.90	19.00	18.20	19.30	11.20	18.00	22.60	19.90	19.30	24.40
Zr	133.40	136.00	161.10	164.70	120.50	131.70	136.60	86.90	228.20	84.00	271.10
Nb	7.10	8.20	8.10	7.10	19.10	19.70	22.60	15.00	11.60	12.40	11.30
Ba	139.30	75.20	171.70	432.50	639.30	1246.00	1422.60	255.00	502.10	2259.80	177.40
La	14.80	22.90	48.80	31.20	47.70	36.75	41.48	34.67	34.50	37.00	35.90
Ce	18.20	37.70	86.70	52.40	77.10	61.14	67.25	57.18	54.40	48.70	60.80
Nd	6.60	14.20	35.30	24.80	25.60	19.84	23.95	18.21	19.80	11.90	22.70
Th	7.00	7.70	10.70	9.20	34.70	41.00	38.30	23.50	23.50	23.00	22.50

Table 5.1 (continued)

Sample	SM311	SM314	SM315	SM317	SM324	SM328	SM336	SM338	SM89	BM94
Deposit	BKBO	BKBO	BKAT	BKAT	BCHT	BCHT	BCHT	BCHT	BMTS	BMTS
Major elements (%)										
SiO_2	70.21	70.32	67.49	63.18	56.81	58.63	56.33	65.10	54.43	53.78
TiO_2	0.36	0.21	0.26	0.23	0.09	0.69	0.13	0.18	1.12	1.13
Al_2O_3	14.28	14.65	17.25	16.70	10.84	13.27	11.15	13.51	23.12	22.54
Fe_2O_3	2.89	1.78	1.97	1.35	1.24	7.82	1.37	1.68	1.76	2.47
MnO	0.03	0.04	0.01	0.01	0.05	0.08	0.04	0.04	- -	0.01
MgO	3.12	1.78	1.57	0.13	7.33	6.55	7.63	5.79	1.02	1.10
CaO	1.76	1.47	0.48	0.11	7.83	2.23	7.52	4.01	0.16	0.14
Na_2O	1.36	2.22	1.38	0.23	0.40	1.33	0.43	0.53	0.35	0.28
K_2O	0.78	2.53	0.33	1.54	0.27	1.68	0.26	0.47	8.38	8.71
P_2O_5	0.04	0.02	0.02	0.04	0.03	0.10	0.04	0.05	0.05	0.05
SO_3	- -	- -	0.36	3.04	- -	- -	- -	- -	0.52	0.45
LOI	5.90	5.19	8.12	12.88	14.61	7.36	15.00	9.32	8.82	8.85
Total	100.73	100.21	99.24	99.44	99.50	99.74	99.90	100.68	99.72	99.50
Trace elements p.p.m.										
V	25.30	3.40	11.80	17.30	16.80	139.80	10.60	49.20	- -	- -
Cr	3.20	2.20	14.20	10.80	23.00	534.20	23.80	66.20	- -	- -
Ni	6.30	6.00	15.30	5.30	35.00	519.00	28.20	54.10	- -	- -
Zn	617.90	44.10	318.10	12.00	34.40	90.40	33.90	37.20	- -	- -
Rb	25.70	110.80	22.40	20.30	18.60	105.40	17.60	27.20	- -	- -
Sr	150.50	93.80	51.50	482.40	272.80	111.70	183.40	242.40	- -	- -
Y	15.50	25.70	11.60	0.00	16.00	16.40	28.70	37.80	- -	- -
Zr	257.70	180.80	104.00	160.50	53.50	128.20	66.90	81.10	- -	- -
Nb	8.60	7.80	10.30	15.20	32.10	10.10	32.00	33.60	- -	- -
Ba	691.80	433.00	43.70	375.00	118.30	204.90	153.50	192.60	- -	- -
La	25.50	32.10	42.10	24.50	7.00	14.10	10.70	8.70	- -	- -
Ce	48.20	55.10	73.70	49.00	14.40	26.90	20.60	20.70	- -	- -
Nd	17.30	20.80	33.10	10.40	8.40	12.50	12.70	15.20	- -	- -
Th	19.60	16.90	22.80	30.00	12.50	5.90	14.20	14.30	- -	- -

Table 5.2

Major and trace element analyses, including rare earths, obtained from alteration profiles from the Prassa deposit.

Sample	SM8	SM9	SM10	SM11	SM188	SM193	SM201	SM202	SM203	SM204
Deposit	BMAN	BMAN	BMAN	BMAN	BMZL	BMZL	BMZL	BMZL	BMZL	BMZL
Major elements (%)										
SiO_2	55.36	49.26	57.67	35.89	56.41	60.60	59.20	58.90	59.85	59.99
TiO_2	0.92	0.78	0.90	0.56	1.05	1.12	1.18	1.15	1.17	1.21
Al_2O_3	18.92	16.68	19.56	9.64	20.00	19.68	20.26	20.71	21.15	21.53
Fe_2O_3	5.42	13.28	7.70	24.33	4.30	4.07	4.88	4.79	3.13	3.10
MnO	0.06	0.02	0.01	0.02	0.01	0.02	0.02	0.01	0.01	0.01
MgO	4.14	2.97	3.50	1.62	2.89	1.03	1.05	0.71	0.40	1.28
CaO	3.92	1.78	1.54	2.06	1.69	4.46	3.39	5.24	5.31	4.08
Na_2O	0.51	0.41	0.56	0.40	1.50	3.23	2.46	3.55	3.73	3.15
K_2O	0.85	0.30	0.36	0.18	1.52	2.54	2.23	2.07	2.36	2.23
P_2O_5	0.11	0.10	0.05	0.04	0.17	0.15	0.31	0.24	0.25	0.25
SO_3	- -	4.49	- -	3.09	3.17	- -	- -	- -	- -	- -
LOI	9.32	10.49	8.06	22.60	5.80	3.46	4.12	3.05	2.60	3.62
Total	99.51	100.56	99.91	100.43	98.51	100.37	99.10	100.42	99.96	100.45
Trace elements in p.p.m.										
V	132.30	161.10	154.40	105.00	244.80	305.80	301.70	280.30	334.50	302.20
Cr	17.60	71.10	26.30	13.70	48.60	67.30	67.50	66.40	70.80	72.40
Ni	15.00	47.80	64.80	63.10	30.10	20.60	26.40	13.80	19.50	15.50
Zn	58.20	64.10	298.30	68.00	81.30	20.70	66.20	119.80	187.90	125.90
Rb	50.60	16.80	26.80	8.50	34.80	99.70	63.40	41.90	67.30	52.90
Sr	89.10	448.00	91.20	158.50	174.60	291.40	195.10	295.30	326.70	230.60
Y	13.00	10.60	36.80	21.50	62.70	43.60	51.40	28.80	50.20	27.30
Zr	229.70	169.30	222.60	122.70	211.10	234.20	244.80	219.80	247.70	236.70
Nb	8.90	8.10	8.00	5.10	11.30	9.70	10.70	11.70	12.30	11.30
Ba	215.50	667.30	30.00	353.60	6859.30	664.20	550.60	554.60	651.30	507.30
La	22.01	23.95	34.75	17.31	27.12	22.13	20.17	23.81	21.98	24.09
Ce	45.84	45.52	81.74	37.55	38.90	46.18	46.62	49.11	45.63	50.20
Nd	18.66	22.73	48.51	20.70	19.60	28.65	26.77	25.94	24.20	27.17
Sm	3.01	3.43	9.54	4.08	- -	6.44	5.94	5.20	5.75	5.09
Eu	1.10	1.22	3.21	1.46	1.42	2.57	1.84	1.62	1.87	1.64
Dy	2.69	2.90	4.96	4.55	11.17	7.64	8.00	5.59	8.15	5.69
Er	2.20	1.93	4.95	2.75	4.98	6.23	4.82	3.23	4.95	3.81
Yb	1.38	1.39	3.91	2.50	6.05	4.22	4.02	2.88	4.91	2.75
Lu	0.21	0.19	0.53	0.34	0.91	0.61	0.55	0.40	0.69	0.38
Th	10.30	4.60	9.00	0.60	6.20	10.90	11.10	13.50	13.40	10.00

Table 5.2 (continued)

Sample	SM261	SM277	SM278	SM280	SM279	SM281	SM282	SM283	SM284	SM285
Deposit	BKP1	BKP1	BKP1	BKP1	BKP1	BKP1	BKP1	BKP1	BKP1	BKP1
					Major elements (%)					
SiO_2	67.74	64.47	60.82	61.39	61.67	63.61	76.23	71.78	73.08	72.51
TiO_2	0.13	0.15	0.17	0.16	0.18	0.18	0.11	0.10	0.10	0.09
Al_2O_3	16.79	19.06	20.67	20.47	21.96	19.60	11.66	13.21	12.19	12.06
Fe_2O_3	1.19	1.63	2.18	1.91	1.71	1.85	1.17	0.72	0.58	0.56
MnO	0.02	- -	0.01	- -	- -	- -	- -	0.02	0.01	0.01
MgO	1.99	3.41	5.28	5.09	4.90	4.53	2.79	1.33	0.35	0.27
CaO	1.43	1.08	1.06	1.10	1.11	1.07	0.70	0.61	0.53	0.51
Na_2O	1.94	1.17	0.88	0.75	0.70	0.49	0.39	3.00	3.69	3.51
K_2O	2.30	1.69	0.33	0.21	0.13	0.12	0.12	2.82	4.09	4.19
P_2O_5	- -	- -	- -	0.02	- -	0.03	0.02	0.02	- -	- -
SO_3	- -	- -	0.81	- -	- -	0.13	0.06	- -	- -	- -
LOI	7.29	7.43	6.91	7.85	8.40	8.34	6.10	5.86	5.84	6.48
Total	100.82	100.10	99.12	98.95	100.76	99.95	99.35	99.47	100.46	100.18
					Trace elements in p.p.m.					
V	2.80	4.60	6.70	0.00	6.10	4.70	0.00	5.90	6.50	4.20
Cr	6.30	2.50	5.10	6.20	5.90	4.80	22.40	4.00	1.90	20.80
Ni	4.90	4.50	6.10	6.70	4.90	5.30	3.20	5.70	3.70	4.40
Zn	343.20	363.40	647.80	257.30	283.80	217.40	203.30	106.50	28.60	70.20
Rb	116.50	59.00	20.00	12.90	4.80	9.80	5.90	297.00	320.90	259.30
Sr	97.20	130.70	179.50	113.00	104.90	105.60	56.10	163.00	190.10	172.60
Y	16.50	18.50	31.20	11.20	18.20	18.00	15.20	22.60	22.00	19.80
Zr	94.60	123.40	139.70	131.70	148.20	136.60	88.10	86.90	84.90	78.30
Nb	14.80	17.50	26.70	19.70	24.00	22.60	12.90	15.00	15.40	12.90
Ba	79.70	1830.20	2994.50	1246.00	918.90	1422.60	23.50	255.00	948.70	981.70
La	37.90	41.83	43.80	36.75	35.95	41.48	36.54	34.67	29.51	29.41
Ce	61.26	68.93	69.46	61.14	61.22	67.25	54.80	57.18	48.42	47.47
Nd	18.60	20.48	25.50	19.84	22.93	23.95	18.05	18.21	5.11	15.39
Sm	3.21	2.83	- -	2.29	2.74	3.11	3.02	2.93	2.21	2.18
Eu	0.39	0.42	- -	0.31	0.47	0.49	0.42	0.48	0.34	0.10
Dy	2.90	3.63	- -	2.63	3.41	3.84	3.01	3.41	2.90	2.76
Er	1.84	1.92	- -	1.02	2.16	2.32	1.96	2.80	2.13	2.05
Yb	1.75	1.87	- -	1.26	2.05	1.99	1.74	2.81	2.49	2.30
Lu	0.25	0.28	- -	0.18	0.33	0.29	0.25	0.43	0.38	0.35
Th	33.30	35.70	41.60	41.00	42.90	38.30	25.70	23.50	26.60	21.20

Table 5.2 (continued)

Major element analyses of a small bentonite body and a faulted zone in the Prasa deposit, Kimolos

Sample	SM270	SM273	SM271	SM266	SM268	SM272	SM274	F1	F2
Deposit	BKP2	BKP2	BKP2	BKP2	BKP2	BKP2	BKP2		
SiO2	69.30	76.10	75.30	80.05	74.32	72.75	68.76	68.63	69.32
TiO2	0.12	0.12	0.10	0.08	0.10	0.11	0.12	0.12	0.12
Al2O3	15.43	11.33	12.37	10.31	13.03	13.58	14.95	15.11	14.62
Fe2O3	0.91	1.09	0.98	0.76	1.05	1.21	0.97	1.87	0.94
MnO	0.02	0.01	0.01	0.01	0.01	0.01	0.02	0.02	0.01
MgO	1.70	3.23	2.62	2.57	3.06	3.48	4.33	4.60	2.24
CaO	1.65	0.87	0.94	0.74	0.85	0.93	1.24	1.30	0.98
Na2O	1.90	0.83	0.83	0.50	0.70	0.87	1.85	0.97	2.77
K2O	2.23	0.13	0.77	0.16	0.32	0.10	0.41	0.21	2.46
P2O5	- -	0.02	- -	- -	- -	- -	- -	- -	- -
LOI	7.15	6.29	6.24	5.35	7.30	7.32	7.29	7.50	7.06
Total	100.41	100.02	100.16	100.53	100.75	100.38	99.94	100.33	100.53

Table 5.3

XRF trace element analyses of bentonites from Milos. The values are in p.p.m.

Sample	SM1	SM6	SM16	SM22	SM27	SM36	SM42	SM53	SM54	SM59	SM72	SM103
Deposit	BMAN	BMAN	BMAN	BMAN	BMAN	BMAN	BMKF	BMKF	BMKF	BMKF	BMKF	BMTS
V	152.60	186.60	159.80	290.10	180.20	162.90	178.00	133.50	158.80	142.00	169.00	197.70
Cr	12.70	18.30	27.70	7.50	4.70	21.60	4.60	4.30	3.30	1.80	3.30	37.50
Ni	9.00	11.20	12.30	8.80	8.10	9.80	7.60	7.80	5.70	7.30	6.80	11.30
Zn	74.90	39.00	46.70	60.50	61.70	40.30	78.40	105.10	77.80	54.90	80.70	137.70
Rb	20.90	29.30	42.70	24.20	16.60	27.00	34.00	61.20	48.90	47.80	31.40	286.40
Sr	80.70	83.10	101.70	118.50	132.00	77.80	155.00	58.10	79.10	108.00	136.50	28.20
Y	20.90	32.40	15.90	20.90	22.30	21.00	20.20	20.70	19.10	24.10	19.80	18.20
Zr	232.00	215.10	211.80	252.30	250.00	214.00	262.00	284.70	277.30	270.00	273.20	167.90
Nb	11.20	8.40	6.70	11.00	12.70	7.80	10.10	11.60	12.40	12.00	10.60	6.70
Ba	224.00	152.20	545.20	131.30	712.10	47.50	249.10	27.20	644.70	38.20	146.80	63.20
La	43.10	8.70	22.80	45.80	43.60	25.30	35.80	43.30	37.30	44.00	33.30	21.90
Ce	74.70	65.50	61.40	79.90	76.60	64.40	68.90	88.30	78.70	70.90	66.00	54.90
Nd	33.90	37.50	22.00	35.10	32.20	29.70	29.40	33.10	32.70	31.20	28.00	25.70
Th	15.90	11.20	12.90	17.10	15.30	11.30	16.70	19.80	14.90	16.00	15.10	10.30

Sample	SM107	SM113	SM125	SM125	SM126	SM131	SM132	SM134	SM142	SM143	SM147	SM152
Deposit	BMTS	BMAH	BMAH	BMAH	BMAH	BMAH	BMAH	BMAK	BMAK	BMAK	BMAK	BMAK
V	255.30	168.10	151.30	190.60	195.30	229.70	208.00	80.80	86.50	68.20	8.80	105.40
Cr	40.70	88.80	26.00	60.80	52.80	52.60	50.80	48.60	186.80	124.20	11.90	41.20
Ni	11.00	33.40	37.50	13.70	20.30	73.80	16.20	17.40	24.70	4.90	8.40	6.50
Zn	92.60	64.50	92.30	71.00	73.90	330.60	314.10	16.10	19.20	3.90	29.30	14.90
Rb	401.80	94.50	38.50	24.50	64.50	68.00	59.10	82.60	191.10	53.00	314.80	84.00
Sr	32.10	72.20	165.60	81.40	56.90	163.70	399.60	54.80	25.50	287.60	33.00	96.30
Y	25.50	34.90	28.40	27.00	25.30	269.30	36.90	14.90	18.60	85.50	20.30	6.50
Zr	209.80	184.80	264.00	235.00	184.90	193.80	209.50	106.80	131.40	138.40	131.70	120.00
Nb	9.20	7.50	15.30	11.00	7.30	8.50	8.70	4.00	8.80	7.90	9.20	6.20
Ba	604.60	370.90	317.40	104.40	173.30	204.10	518.10	173.10	183.50	162.40	81.60	148.60
La	28.60	33.10	32.00	42.00	30.50	16.90	43.60	14.80	28.30	33.10	31.00	20.50
Ce	52.50	65.40	51.20	103.80	58.40	26.50	91.80	37.30	49.30	52.00	44.30	37.40
Nd	25.50	31.10	26.30	62.80	30.80	27.70	54.70	15.30	22.70	6.70	17.60	16.00
Th	10.70	9.90	12.30	12.20	12.20	16.60	10.00	8.40	7.20	6.40	14.40	9.30

Sample	SM158	SM159	SM166	SM162	SM171	SM175	SM178	SM180	SM182	SM194	SM197	SM222
Deposit	BMGF	BMGF	BMGF	BMGF	BMGF	BMRS	BMRS	BMKK	BMKK	BMZL	BMZL	BMZL
V	21.30	27.20	22.20	22.60	30.30	16.10	23.90	50.60	9.40	238.40	289.20	69.80
Cr	24.00	44.40	44.90	45.00	41.20	32.50	35.20	180.30	20.10	55.60	55.00	21.50
Ni	26.70	29.60	51.10	14.40	33.00	45.70	25.30	110.40	18.60	20.90	40.40	6.70
Zn	45.10	67.50	95.00	29.40	68.40	71.70	115.60	53.60	249.30	25.80	61.70	23.30
Rb	149.90	36.00	81.60	149.70	172.40	107.50	31.80	108.80	37.90	46.50	31.60	36.20
Sr	53.30	26.10	41.70	78.30	35.80	35.90	132.50	57.101	040.50	256.90	117.50	197.70
Y	18.90	15.70	16.40	27.00	22.60	16.30	9.50	16.90	1.60	58.70	22.80	10.10
Zr	135.00	136.90	133.90	134.10	138.50	136.50	131.20	125.90	0.00	230.60	172.10	214.20
Nb	8.00	7.60	7.40	7.90	6.90	7.00	6.80	8.20	1.90	11.60	6.00	11.50
Ba	39.80	28.50	104.70	83.00	537.60	593.60	403.60	722.001	492.902	286.50	69.40	391.00
La	29.00	24.80	25.40	39.90	26.60	27.00	26.00	24.10	34.70	32.70	22.10	17.60
Ce	51.10	45.40	42.50	60.40	46.30	45.80	48.90	43.80	35.10	67.30	57.40	36.20
Nd	20.60	18.00	14.90	25.80	17.10	16.60	15.80	16.30	3.50	44.20	29.80	15.70
Th	11.10	14.10	12.70	10.50	11.50	13.90	12.70	12.70	4.40	11.60	10.30	10.10

Table 5.3. (continued)

Sample	SM224	SM227	SM230	SM234	SM235	SM236	SM239	SM240	SM244	SM250	SM249	SM287
Deposit	BMZL	BMZL	BMZL	BMRM	BMRM	BMRM	KMKS	KMKS	BMAG	BMAG	BMAG	BKPR
V	46.30	29.60	6.20	27.40	25.20	60.30	31.80	35.60	204.30	88.50	107.30	4.50
Cr	40.50	4.80	0.00	45.50	48.60	82.10	46.50	63.20	29.30	80.20	118.50	7.60
Ni	9.40	12.60	5.80	8.30	8.20	31.70	3.50	3.90	6.60	59.40	26.20	5.30
Zn	49.20	44.50	38.40	28.20	24.60	33.60	2.90	0.70	60.00	91.40	35.70	61.50
Rb	31.40	140.70	164.80	18.20	112.10	45.00	5.40	10.50	158.10	55.40	198.20	140.50
Sr	69.30	250.50	94.50	208.20	84.90	79.40	373.00	826.60	43.20	42.40	37.60	119.00
Y	20.80	54.80	21.60	7.50	15.20	16.90	4.90	18.70	18.80	14.80	15.70	20.00
Zr	168.20	195.90	155.70	131.50	136.20	144.50	125.40	137.10	287.80	159.40	140.20	87.30
Nb	8.50	8.50	8.30	8.00	8.80	8.50	7.80	6.90	8.30	7.20	6.50	16.10
Ba	149.80	722.40	562.80	883.90	58.40	239.20	325.60	814.40	793.80	216.10	417.30	434.00
La	23.00	31.40	28.30	16.80	27.80	25.90	15.30	33.00	26.80	26.00	24.00	38.40
Ce	39.30	46.70	49.80	24.30	51.20	46.10	30.20	56.10	52.50	53.10	40.60	60.10
Nd	19.50	24.10	18.50	4.00	16.70	17.40	12.50	29.20	23.70	22.70	14.40	20.20
Th	16.90	14.10	17.50	9.60	11.90	10.00	13.80	18.10	11.20	11.60	9.40	24.90

Sample	SM69	SM83	SM87	SM90	SM108	SM109	SM217	SM218	SM220	SM221
Deposit	BMKF	BMTS	BMTS	BMTS	BMTS	BMTS	BMZL	BMZL	BMZL	BMZL
V	104.10	197.60	271.10	276.50	257.00	247.30	212.70	208.60	265.90	226.80
Cr	19.80	57.20	75.30	52.30	57.10	45.30	47.20	44.80	63.10	54.70
Ni	5.40	16.80	22.80	29.00	13.50	32.00	16.90	14.50	16.80	34.50
Zn	72.60	149.00	120.90	148.80	88.00	191.40	45.40	39.40	43.60	91.10
Rb	108.20	535.70	157.70	436.50	226.60	152.50	17.70	12.00	17.90	19.30
Sr	51.80	18.20	29.60	29.30	29.40	10.40	531.30	194.40	392.50	354.20
Y	17.00	21.30	19.10	34.00	27.00	20.10	19.80	30.50	17.80	23.50
Zr	277.40	172.80	194.90	212.20	195.10	186.10	169.60	184.90	169.50	183.50
Nb	8.40	9.50	8.40	9.00	8.20	7.00	7.90	8.30	7.40	7.50
Ba	367.40	200.90	606.30	884.80	483.80	487.40	169.80	48.60	102.20	188.30
La	45.00	23.10	27.90	46.50	34.10	30.70	24.80	33.50	31.70	26.40
Ce	79.40	56.50	70.70	78.50	52.80	59.50	56.00	56.10	58.70	51.60
Nd	30.90	28.50	33.60	34.00	31.40	25.50	25.70	25.70	25.10	23.50
Th	10.10	10.30	11.50	10.60	9.50	12.00	10.80	7.70	6.80	8.60

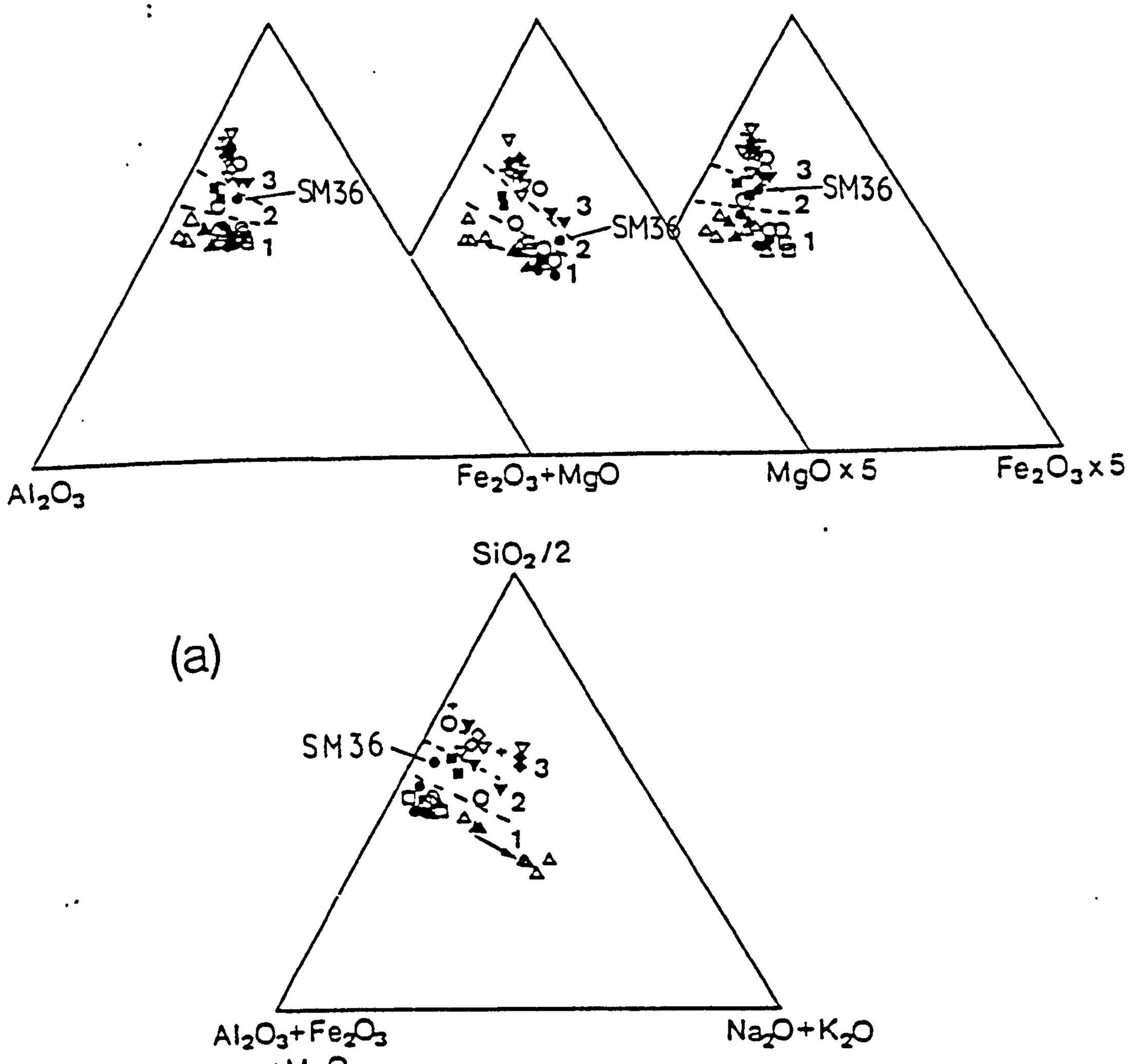

FIGURE 5.1. Projection of the Greek bentonites on triangular geochemical plots involving major chemical elements, (a)=Milos, (b)=Kimolos, Chios. The dashed lines drawn in set (a) separate bentonites from the different areas. 1=Areas 1 and 2, 3=Area 3, 2= other deposits

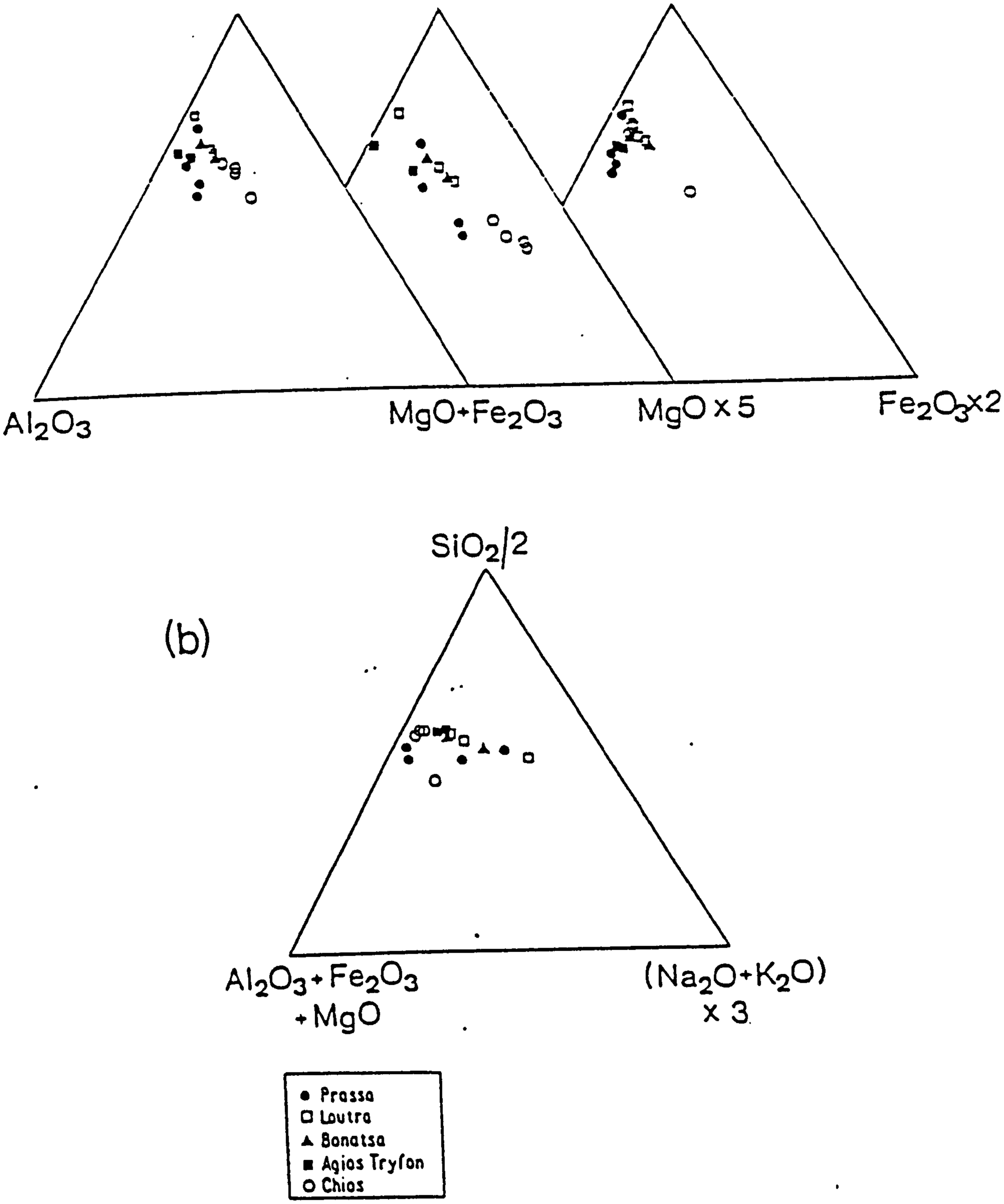

FIGURE 5.1 (continued).

compared to smectites, some Fe-oxides are present, and Si enters both smectite and Si-phases. Inasmuch as calcite and other carbonates, which might not be related to the bentonite formation, are abundant in most deposits, CaO was not included in any of the diagrams.

The first group, which includes the deposits from Areas 1 and 2, is characterized by a higher Al:Si ratio compared to the bentonites from Area 3, which plot separately and are clearly characterized by a lower Al:Si ratio. This is in accordance with the mineralogical investigation which showed that the deposits of group three are abundant in Si-phases (opal-CT, cristobalite, and/or quartz). The deposits from Areas 1 and 2 are generally quartz and/or opal-CT-free.

Exceptions from this trend are shown in the Ankeria deposit (Area 2), in which opal-CT is abundant in the higher horizons of the deposit and in the Zoulias deposit (Area 1) in which some of the bentonite horizons have abundant opal-CT. These exceptions can be observed in Figure 5.1a in which the abundant in opal-CT sample SM36 (Ankeria deposit) plots between the two groups, close to the samples from Agrilies deposit. Similarly, samples from Zoulias deposit which are derived from the lower straticraphic bentonite horizons and are richer in Si compared with those from the "brocken tuff" (highest horizon, see Chapter 3, section 3.3.1.1.3) plot either with samples from Area 3 or between the two groups. Also, the samples from the Tsantili deposit which plot in a different area from the rest of the samples of the same group (pointed by the arrow in Fig. 5.1a), are abundant in mixed layer I/S minerals instead of smectites (see Chapter 4).

The aforementioned observations clearly show that the bentonites of Milos are not parts of a single horizon which extends over a wide area but belong to at least two different ones with distinct Si contents and relatively constant Si:Al ratio in each of them. The latter can be seen in Figure 5.1 in which alkalies are plotted against Si on the one hand and Al_2O_3+MgO+Fe_2O_3 on the other. This is examined in detail in Section 5.4 in which geochemical correlation of the different deposits is attempted.

Projection of the bentonites of Milos in the diagram proposed by Winchester & Floyd (1977), which plots Nb/Y vs Zr/TiO_2,confirms that they are not members of a single horizon but alteration products derived from different precursors (Fig 5.2a). Also, there is a clear distinction between bentonites from Areas 1 and 2. The former seem to have been derived from a more basic precursor (possibly andesite or dacitic-andesite) while the latter from a more acidic rock which was probably of dacitic composition. In the Zoulias deposit (Area 1) it is obvious that the samples from the higher stratigraphic horizon ("brocken-tuff") plot together with samples from the Tsantili and the Aspro Horio deposits, while samples from the lower horizons plot together with those of Area 2 or 3. This indicates that the volcanic activity in the area has changed character as far as the Si-content of the volcanic products

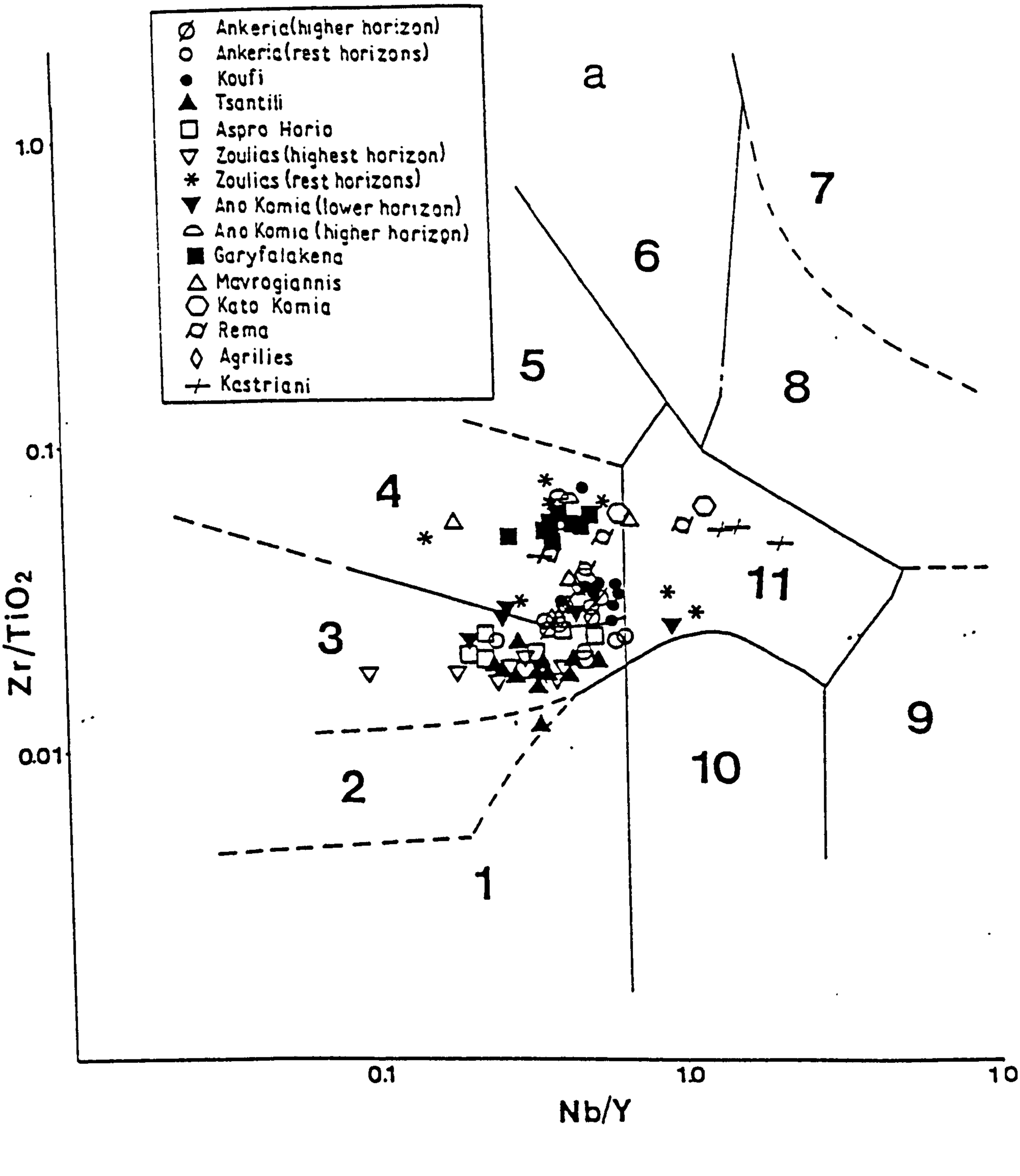

FIGURE 5.2. Projection of the Greek bentonites on the diagrams proposed by Winchester & Floyd (1977). (a) Milos bentonites, (b) Kimolos, Chios bentonites, (c) influence of of the degree of alteration on the proection of the samples. Key to the fields: 1=sub-alkaline basalt, 2=basalt/ andesite, 3=andesite, 4=dacite, rhyodacite, 5=rhyolite, 6=comendite, pantellerite, 7=phonolite, 8=trachyte, 9=basanite, nephelinite, 10=alkal-basalt, 11=trachyandesite.

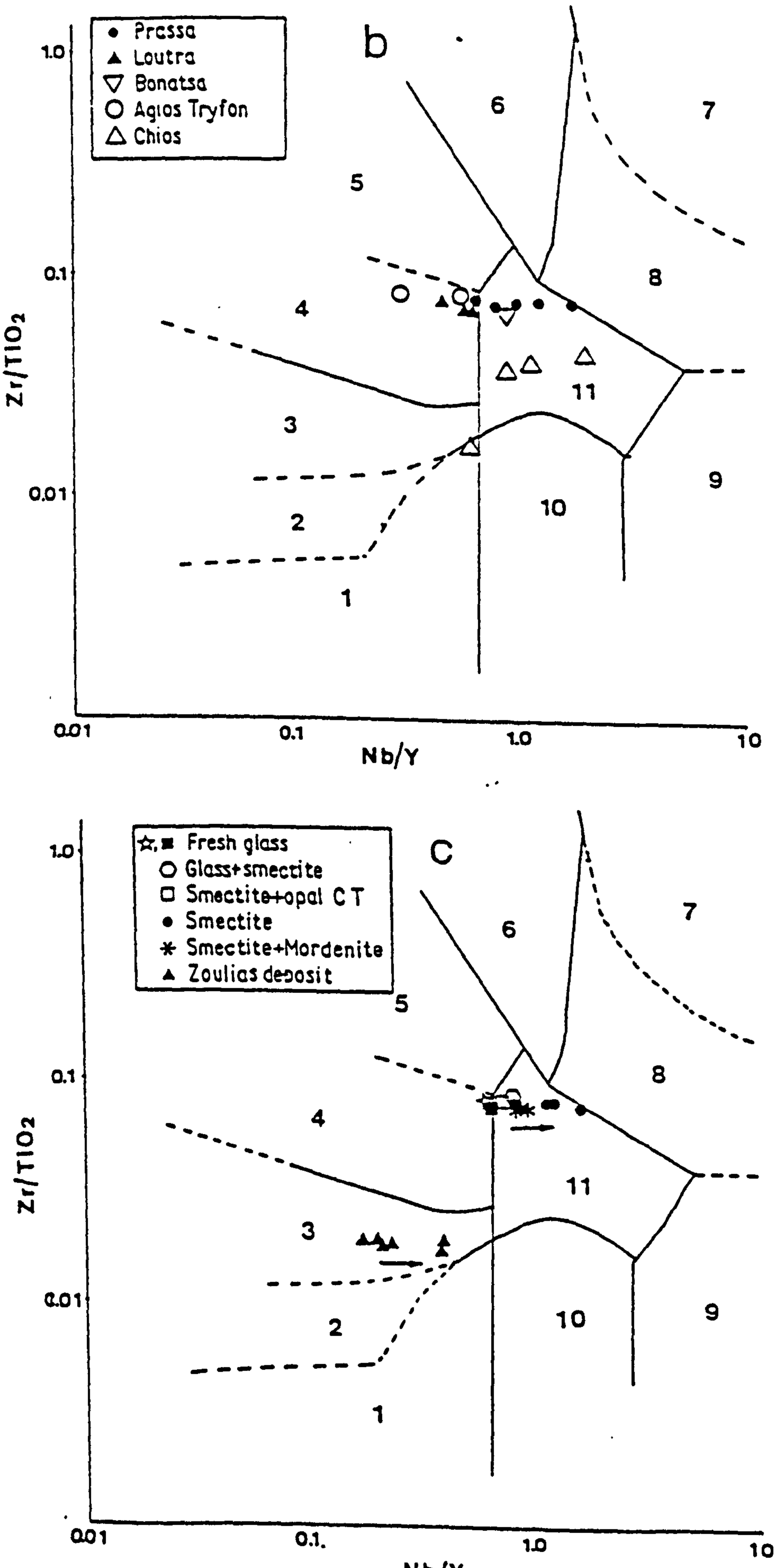

FIGURE 5.2 (continued).

is concerned. On the other hand, the alkaline affinities of the volcanic activity has not changed significantly.

In Figure 5.2a the different character of the bentonites from Area 3 is clearly demonstrated. The parent material was more acidic compared to that of the previous areas and might have been of rhyodacitic-rhyolitic character. This fact supports the idea of a possible derivation of the parent rocks from the acid centre of Demenegaki, as this has already been stated in Chapter 3. However, this does not preclude the possibility for derivation from a different vent (for more discussion see Chapter 3). Four other significant observations can be made on the same diagram concerning the parent rocks of the different deposits:

i) The parent rock of the lower horizon of Koufi deposit was more acidic compared to the overlying horizons.

ii) The two horizons which compose the deposit of Ano Komia have been derived from different precursors. The higher stratigraphic horizon has possibly been derived from a rock very similar to that from which the other deposits of this area have, while the lower has been formed at the expense of a less acidic rock.

iii) The Agrilies deposits might have been derived from a dacitic rock *I.e* similar to the bentonites of Area 2.

iv) Samples coming from the higher stratigraphic horizon of Ankeria deposit seem to have been derived from a more acidic precursor compared to those coming from the underlying horizons. Moreover they plot in the same area as the samples from the Koufi deposit.

The validity of the diagram proposed by Winchester & Floyd (1977) has been discussed by Finlow-Bates & Stumpfl (1981) who concluded that although Zr and Ti are essentially immobile even under conditions of intense hydrothermal alteration, Y and Nb can be removed from the altered zones. Concequently they cannot be considered as very reliable indicators of the parent rocks. However, Huff & Türkmenoglu (1981) and Huff & Morgan (1989) applied the diagram successfully. In the present case it is obvious that the at least in Area 3 the SiO_2-content of the rocks indicates a more acidic rock. It also seems that some rocks from the Zoulias deposit are relatively more alkaline than the others (the Nb/Y ratio provides a good indication for the alkaline character of the rocks).

5.2.2. Kimolos and Chios Islands.

Like the bentonites of Milos, their counterparts on Kimolos and Chios do not seem to follow a single geochemical trend. The bentonites of Chios island are Mg-rich (Fig. 5.1b) confirming the mineralogical and mineral chemistry data which showed the presence of talc, chlorite, serpentine, dolomite and Otay-type montmorillonite in these deposits. The different character shown by sample SM328 (lower Si-content, high Fe-content) is due to

its different mineralogy. It comes from the red-green clayey rock which overlies the bentonite horizon and contains only a moderate amount of smectite, consisting mainly of mica, chlorite, serpentine, talc, plagioclase and quartz, all of which are detrital.

The bentonites from Kimolos, especially those from the Prassa deposit display an interesting trend characterized by the existence of two fields; a Si-rich and a Si-poorer one. Inasmuch all samples come from the same parent rock the existence of the two different poles is considered to be a result of Si-removal from the parent rock during the alteration to bentonite. This indicates that the variation observed is not inherited *i.e* it is not due to the different chemistry of the parent rocks.

In contrast to their counterparts from Milos in the three different areas, the bentonites from Kimolos do not seem to be dominated by a constant Al:Si ratio (Fig 5.1b). This is especially true for the rocks derived from the Prassa deposit which represent different stages of alteration. This might be due to the different behaviour displayed by these elements during the alteration of the parent rock to bentonite.

When plotted in the diagram of Winchester & Floyd (1977) the bentonites from Kimolos clearly show that the different Si-content in the samples from Prassa deposit is not inherited but is due to secondary enrichment of Al accompanied by removal of Si (Fig. 5.2b) This can be proved from the fact that the Zr/Ti ratio which is a good indicator for the acidic/basic character of an igneous rock is constant and close to the boundary between rhyodacite and rhyolite. On the other hand, the highly variable Nb/Y content in those rocks indicates that some Y might have been removed. This can be seen in Figure 5.2c for the whole alteration profile. The Nb/Y ratio varies to such a degree that the samples from the smectite zone reach the trachyandesite-trachyte boundary; the fresh rock is a rhyolite/rhyodacite. Thus, the removal of Y shifted the composition to a more alkaline character. Hence the diagram of Winchester & Floyd (1977) should be used with care in the case of bentonites, as far as the alkalinity factor is concerned.

The bentonites of Chios seem to have been derived from precursors of trachyandesitic character. The different (more basic character of the sample SM328 is attributed to the different mineralogy of this sample. The relatively low Zr and TiO_2 content for parent rocks of such composition might be due to admixture of the volcanic material with sediments. This means that the criteria proposed by Spears & Kanaris-Sotiriou (1979) for the distinction of the parent rocks in similar environments are inapplicable. The scattering of the samples along the alkaline-character axis (*i.e* Nb/Y ratio) might be due either to inhomogeneity of the parent material (inherited or caused by mixture with sediments) or to the mobilization of Y during the alteration process or both. The more alkaline features of these rocks compared to their counterparts from Milos and Kimolos is in accordance with the character of the Neogene volcanism in the area of Central-Eastern Aegean and Western Anatolia, which is associated with crustal extension (see Chapters 2 and 3)

5.3 Mobility of the chemical elements during bentonitization.

5.3.1. Alteration of acidic rocks.

The case-study examined comes from the island of Kimolos in Prassa deposit. This deposit contains several bentonite bodies the location of which is controlled by structural criteria. In the main body the parent rock (ignimbrite) has been altered forming an alteration pattern consisting of six zones (see Chapters 3 and 4).

5.3.1.1. Major elements.

The behaviour of the major elements in this alteration profile is summarized in Figure 5.3a. The conversion of the acidic rock to bentonite is characterized by depletion of alkalies which is almost complete in the smectite zone and enrichment in Mg, Al, Ti, Fe, and Ca. The behaviour of alkalis is the major difference between the smectite and the zeolite-bearing zone. Si is intensively depleted from the smectite zone and is concentrated in the smectite + opal-CT zone. The behaviour of Mn is not well displayed because it is present in amounts close to the detection limits of the analytical method. The depletion of Si is less intense in the zeolite zone because it is accumulated in the siliceous mordenite which has Si:Al ratio between 4.8 and 5.8, *i.e* close to that of the original ignimbrite. Similar trends have been reported by Zielinski (1982). Finally the relatively high LOI of the fresh glass (samples SM285 and SM284) indicates that the rock has undergone some degree of hydration which might be considered as the first indication for alteration. Hydration of a volcanic or artificial glass might involve cation exchange with water which might not lead to devitrification and formation of hydrated minerals (Shiraki & Iiyama, 1990). If this is the case then some alkalies might have been transported to the fluid phase during the Na and/or K for H^+ exchange. However, the alkali-content of what is considered as "fresh glass" does not imply removal of these elements (see Table 5.2)

The enrichment of certain elements might have taken place in situ if they have behaved "residually" *i.e* if they are essentially immobile, or by transportation. If the former has happened, then they should display an almost perfect linear relatioship, with the straight line passing from the origin of the axes. Furthermore, the composition of the fresh rock should plot on the line (MacLean, 1988), because the ratio of the elements remains constant. This is the case for Al_2O_3 and TiO_2 (Fig 5.4a). Ca seems to be enriched in situ although the scattering observed (Fig 5.4b) might indicate some degree of redistribution. On the other hand for both Fe and Mg, although they display a well expressed linear relationship with Al_2O_3, the straight line does not pass from the origin (Fig 5.4c,d). This implies that both Mg and Fe must have undergone enrichment through transportation from an external source or from redistribution during alteration. Zielinski (1982) observed a 13-

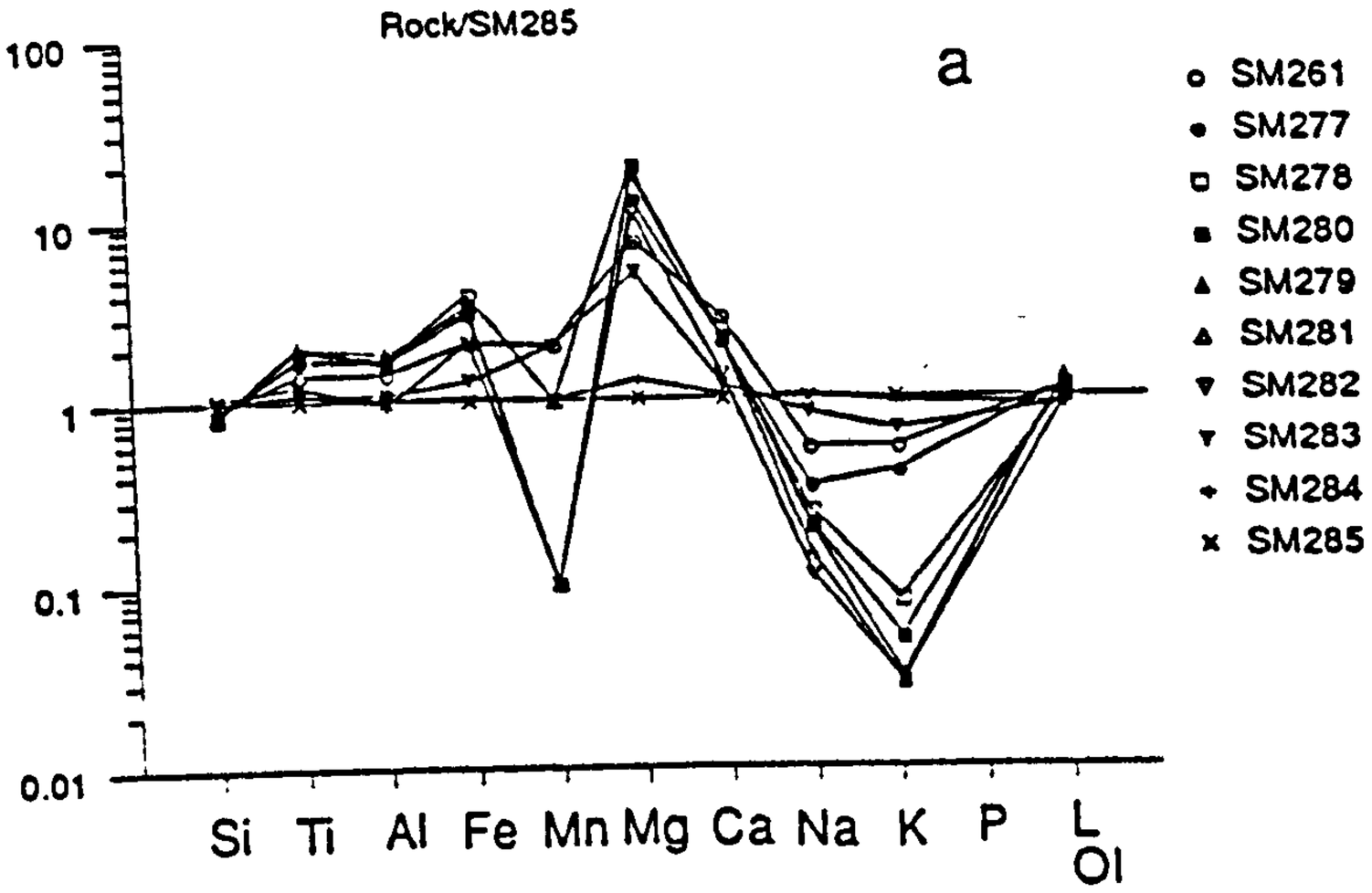

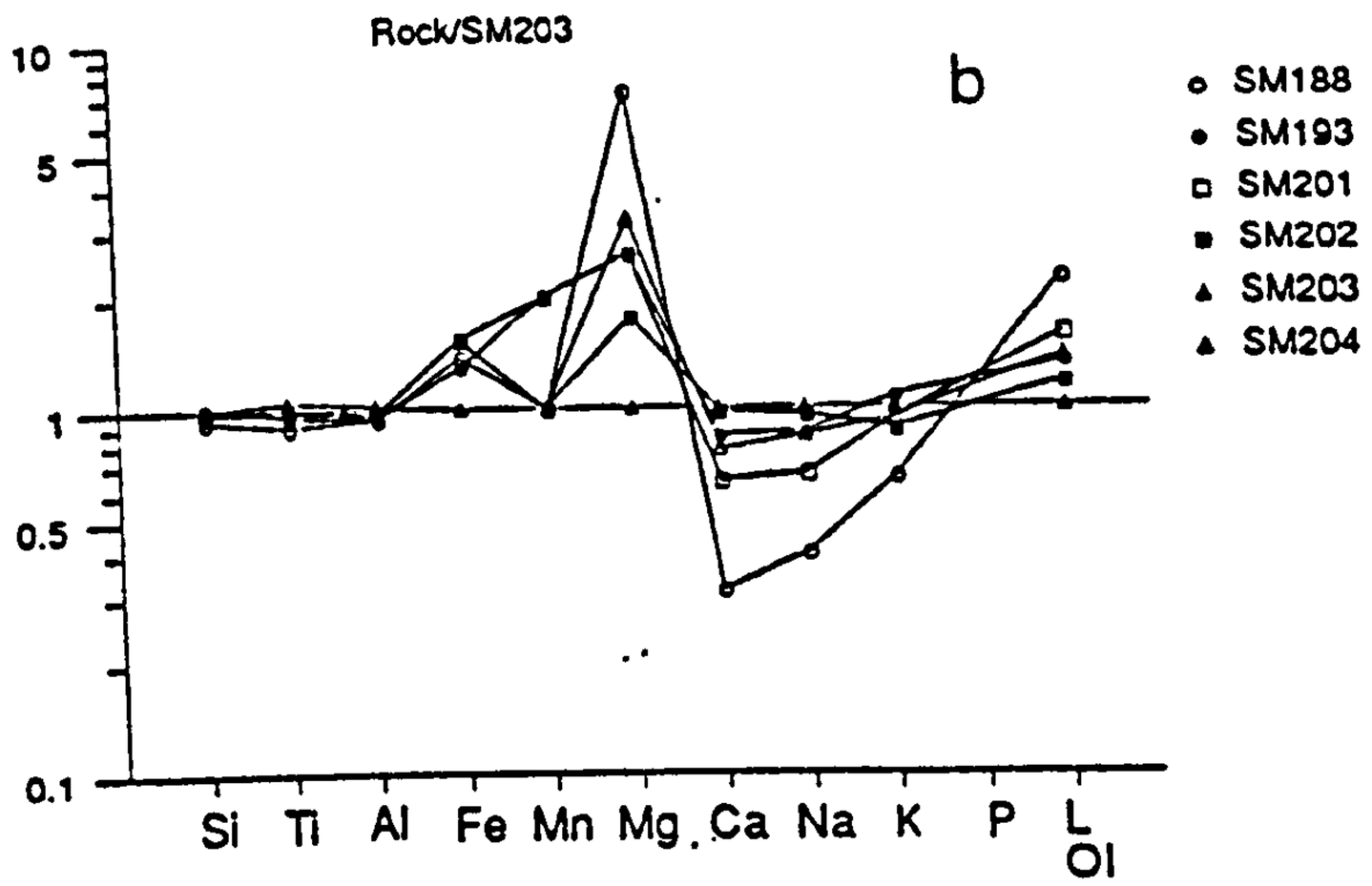

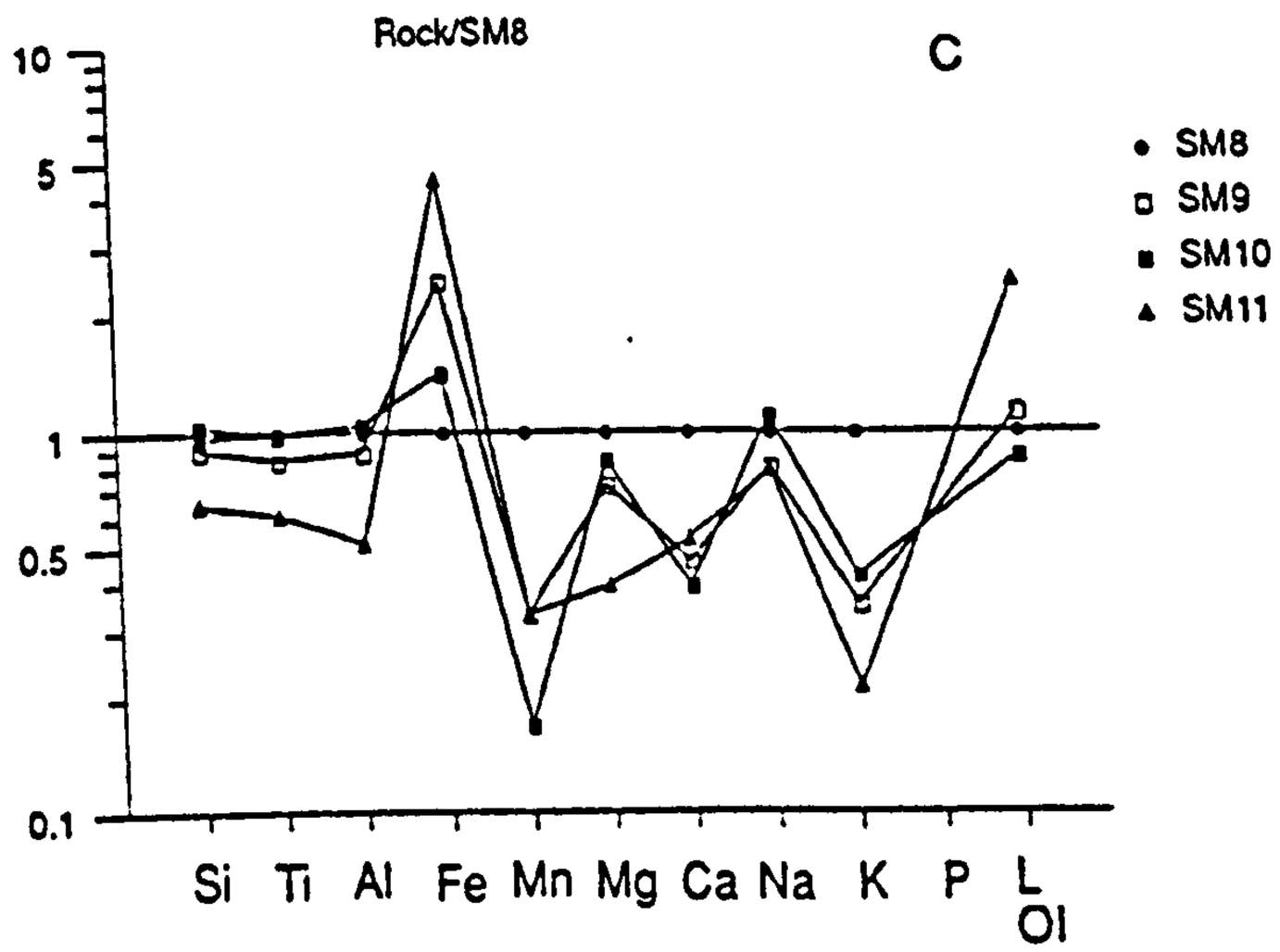

FIGURE 5.3. Multielement diagrams showing the mobility of the major chemical elements during the conversion of (a) an acidic rock (Prassa deposit, Kimolos), (b) an intermediate rock (Zoulias deposit, Milos), and (c) during further alteration of a bentonite through a hydrothermal process (Ankeria deposit, Milos). (a) Normalization over the fresh glass (sample SM285 in the Prassa deposit), (b) over the least altered (almost fresh) glass (sample SM203 in the Zoulias deposit) and (c) over the "fresh" bentonite. In (a): SM285, SM284=fresh glass, SM283=glass+smectite, SM282=smectite+opal C-T, SM281, SM280, SM279, SM278=smectite zone and SM277, SM264 and SM261=smectite+mordenite zone.

15 fold increase in the Mg-content of the parent rocks during conversion to bentonite. Si displays a very well expressed negative relationship when plotted against Al confirming the observation made before about its migration (Fig. 5.4e).

The behaviour of Mg and Fe displays a very interesting two-trend pattern when these elements are plotted versus Al and Si (Fig. 5.4c,d,f,g). The samples which display the first trend are characterized by a significantly lower degree of both Fe and Mg enrichment relative to both Si and Al; those which display the second trend are characterized by a high degree of Mg and Fe enrichment. The two-trend pattern is also visible when Mg is ploted versus Fe. In those diagrams samples from 3 different bentonite bodies are included, one of which corresponds to the main bentonite deposit. In every case the fresh glass plots at the point representing the least mobilization in one of the two trends. It can be seen that every trend includes samples from all three alteration profiles. In the two small bodies the maximum enrichment in both Mg and Fe occurs within the fault zone which is more permeable and thus permits higher water:rock ratios. This implies that in the main horizon also the maximum enrichment in both Mg and Fe must occur within the permeable zone. Inasmuch as the samples of the main horizon which follow that trend come from the smectite zone, it follows that the smectite zone must be in or very close to the centre of the permeable zone. This is also confirmed from the fact that the maximum Si-removal takes place from that zone.

5.3.1.2. Trace elements.

The behaviour of trace elements (Fig. 5.5) displays some interesting trends which are not in accordance with the findings of Zielinski (1982). For instance Cr seems to be mobile, although this might be due to its very low abundance in the parent rock. Sr, with an exception in the very first stages of alteration is mobile and does not follow Ca which presumably participates in the interlayer sites of smectite. A similar trend is displayed by Rb which seems to be a highly mobile element and follows K. Zr, Nb and Th are enriched in situ because they display a well expressed positive linear relationship with Al_2O_3 (Fig. 5.6). Therefore they can be considered as immobile. V and Ni are also enriched but their content is very low. Zn is enriched in every zone especially in the smectite zone. However it appears to have been depleted during the incipient stages of alteration (sample SM284). Also its enrichment does not seem to have taken place in situ (the 5-fold increase of Zn in the smectite zone cannot be explained by residual behaviour because the concentration of Al which displays such a behaviour has increased only twice).

The behaviour of Ba is interesting since it has been removed from the zones of incipient alteration (samples SM283 and SM282, in Fig. 5.5a) and it seems that it has been

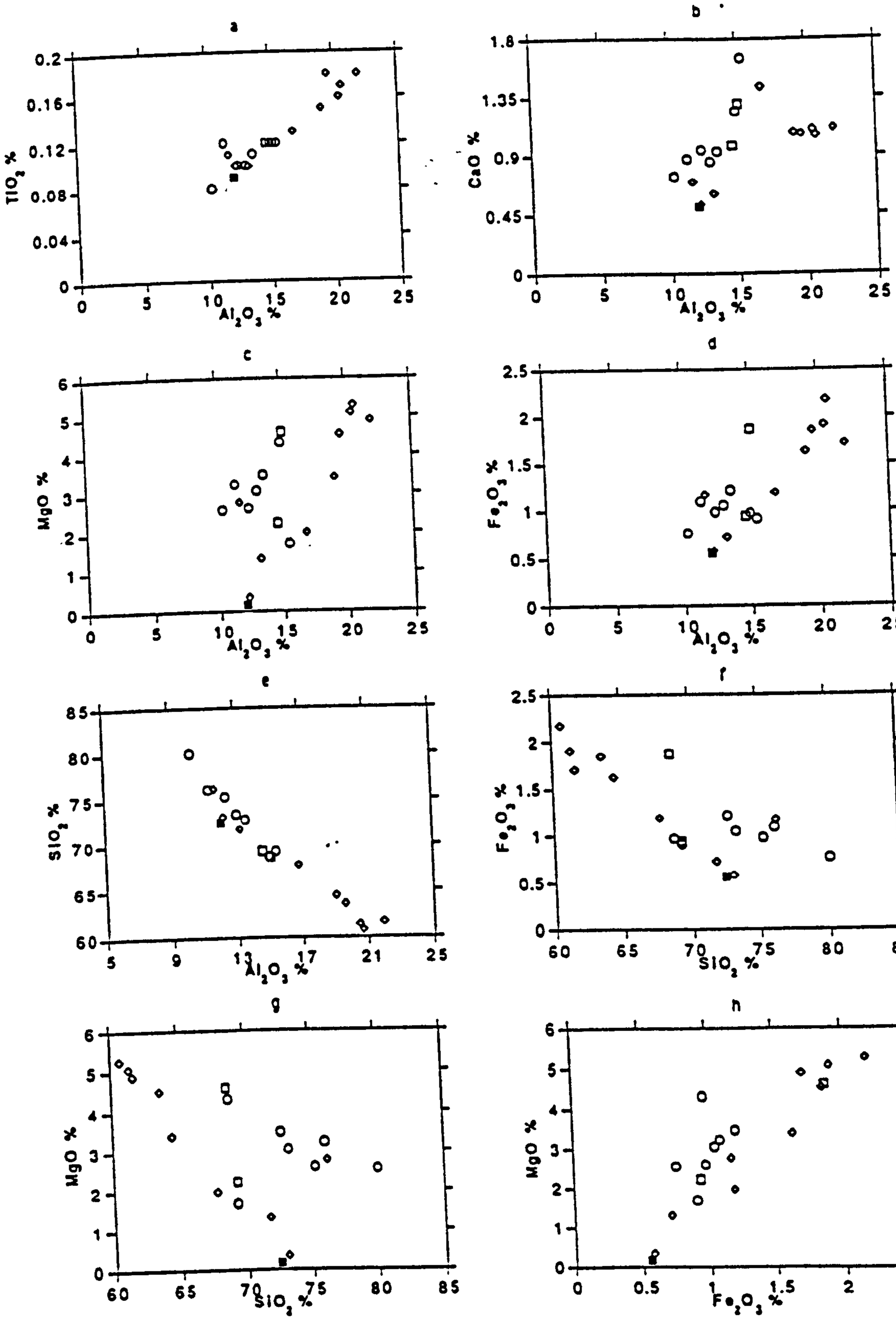

FIGURE 5.4. Mobility of the major hemical elements during the alteration of an acidic rock (ignimbrite) to bentonite as seen whn plotted versus the immobile Al (Prassa deposit, Kimolos). Key to the symbols: Solid square=fresh glass, diamond=main bentonite body, circle=small bentonite body in the same deposit, empty square=faulted zone within the fresh glass.

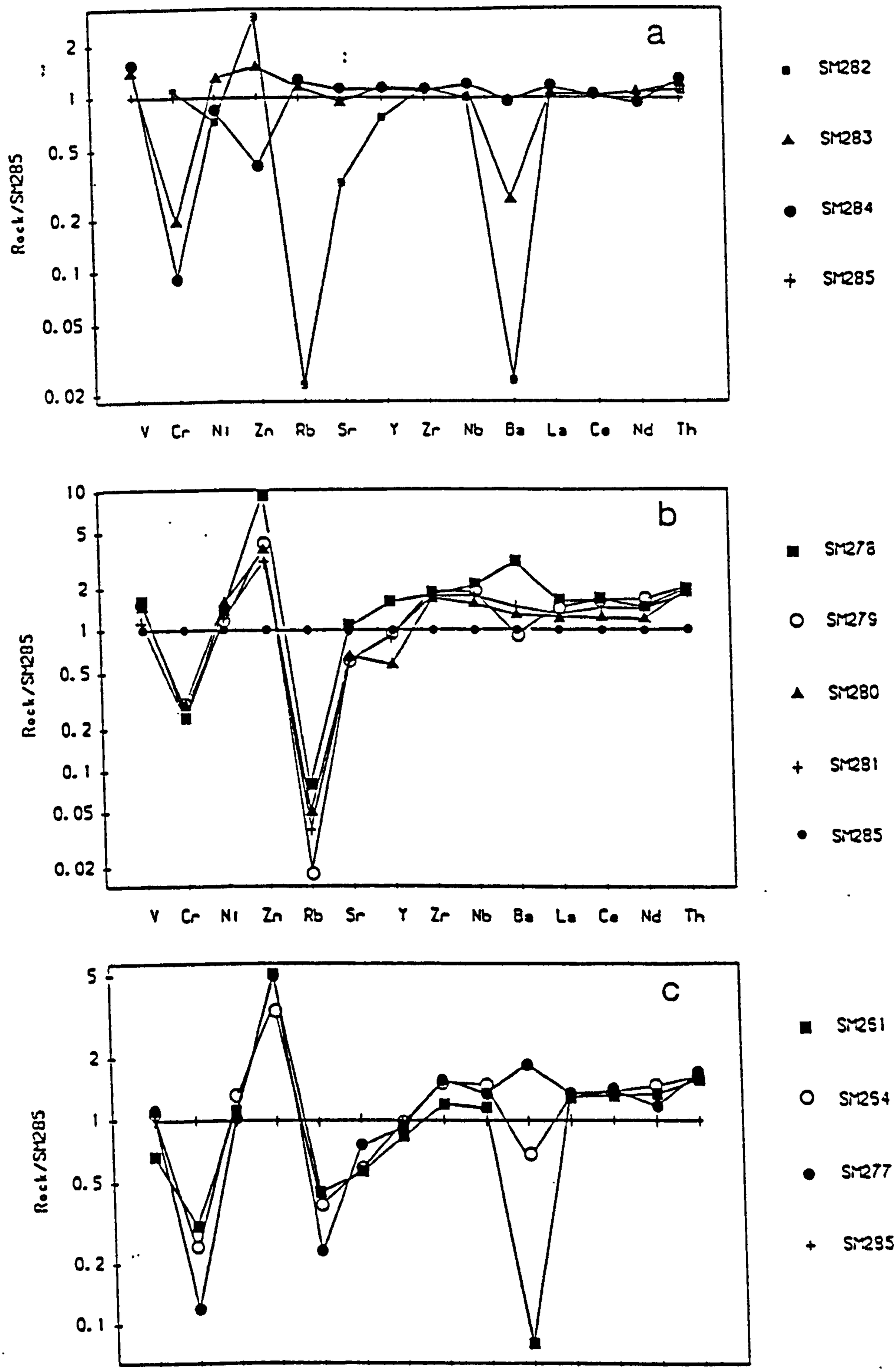

FIGURE 5.5. Multielement diagrams showing the relative moility/immobility of trace elements (the REEs excluded), during the alteration of the ignimbrite in the Prassa deposit, Kimolos. In (a): SM285, SM284 fresh glass, SM283 glass+smectite, SM282 smectite+opal C–T zone, (b): smectite zone and (c): smectite+mordenite zone.

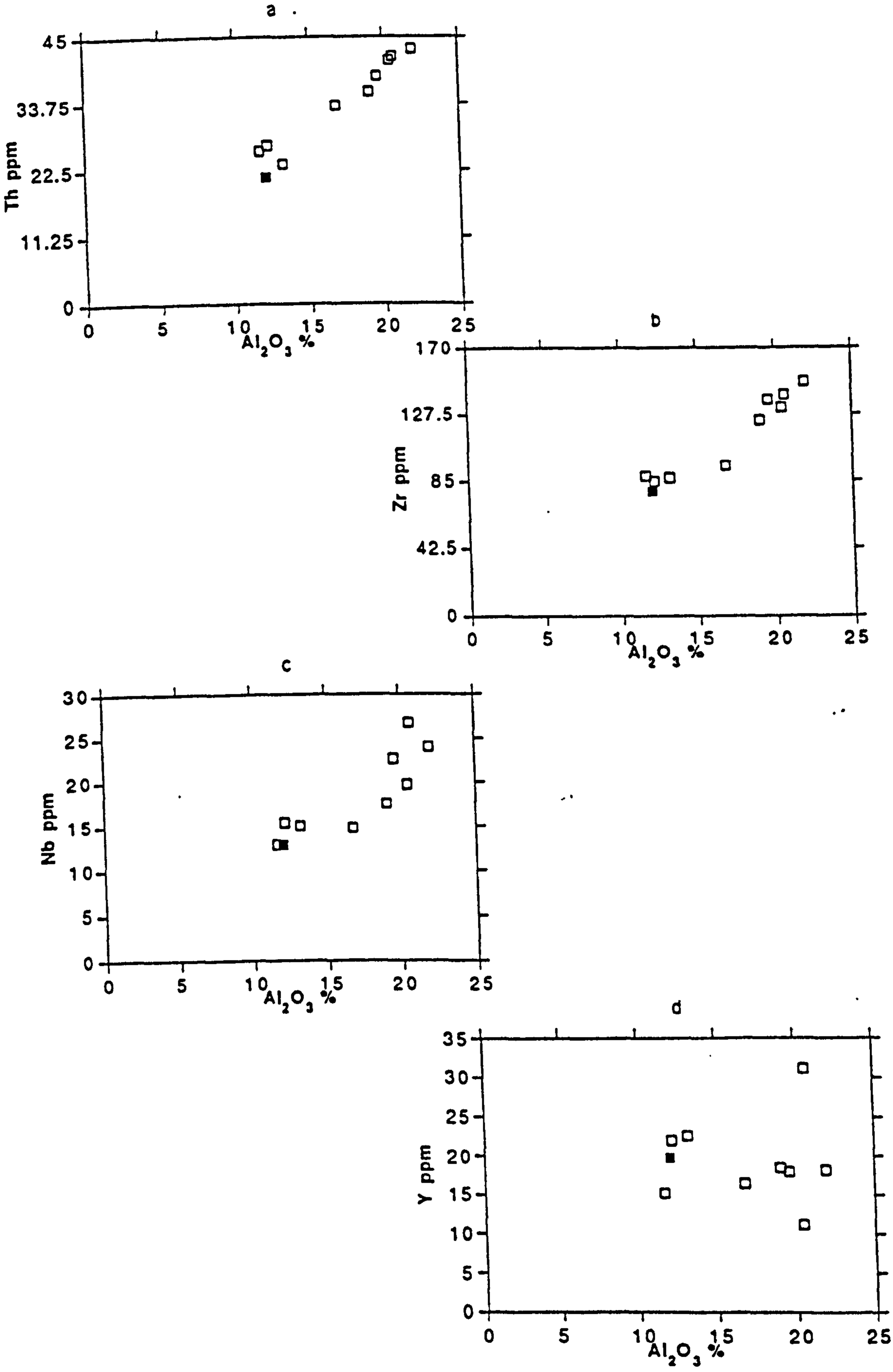

FIGURE 5.6. Relative mobility of Th, Zr, Nb and Y during the alteration of an acidic rock to bentonite, observed when these elements are plotted versus the immobile Al. The solid square correspond to the fresh glass. Prassa deposit, Kimolos.

redistributed in the smectite zone in the main bentonite body. Removal of Ba has also taken place from the zeolite zone (Fig. 5.5c).

The rare earth elements display a trend characterized by an enrichment of the light and depletion of the heavy members of the series (Fig 5.7). When normalized over chondrite the same pattern is visible. The observed trend is characterized by an overall enrichment of the REE in the first stages of alteration (fresh glass and glass + smectite zones) followed by depletion of the HREE and enrichment of the LREE in more advanced stages of alteration (smectite and zeolite zones). The enrichment of the LREE is residual as can be seen when they are plotted vs Al_2O_3 (Fig 5.8). However an amount of the LREE has been removed because the ratio of the individual LREE elements vs Al_2O_3 decreases in the zones of advanced alteration (in order to assume immobility of La in Figure 5.8a, its concentration should be greater than 50ppm at 20% Al_2O_3; hence about 20-25% of La has been removed). The maximum enrichment observed (in absolute terms) has taken place in the smectite zone. Y has ionic radius very similar to Ho (Brookins 1989); therefore it displays behaviour similar to that of the HREE (Fig 5.8) and is removed or redistributed in the system (for example see samples from the smectite zone, Fig 5.5). The removal of the HREE can also be seen in Figure 5.8 from the negative relationship between Lu and both Al_2O_3 and La or Ce.

The different behaviour of the various REE indicates that there must be a "sink" which holds the LREE in the system, but not the HREE. This sinking agent is monazite which must be at least partly secondary (authigenic). If the LREE and Th-content of the parent rock were sufficiently high to support the formation of igneous (pyrogenetic) monazite then this might have been served as the nucleus for monazite overgrowths. If the amounts of Th and LREE were not sufficient then the formation of monazite is entirely auhtigenic. The removal of an amount of the LREE suggests that part of these elements was initially in the glass. In any case, the removal of small amounts of LREE from the system indicates that the growth rate of authigenic monazite might have been low compared to the rate of leaching of the glass so that the part of the LREE was removed.

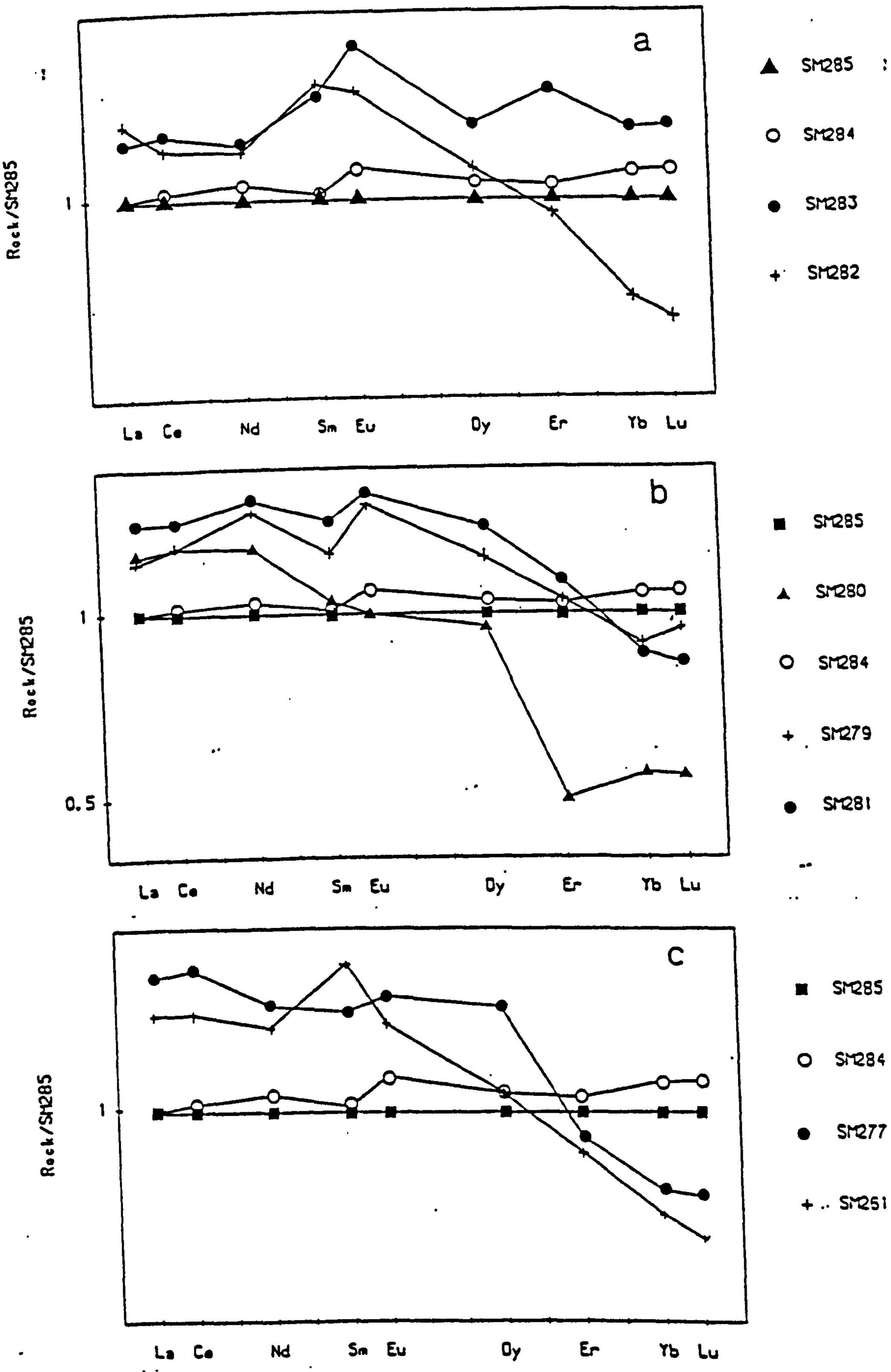

FIGURE 5.7. Multielement diagrams showing the behaviour of the REE at the various stages of alteration of an acidic rock to bentonite (Prassa deposit, Kimolos). In (a): SM285, SM284=fresh glass, SM283=glass+smectite zone, SM282=smectite+opal C–T zone, (b)=smectite zone and (c)=smectite+mordenite zone.

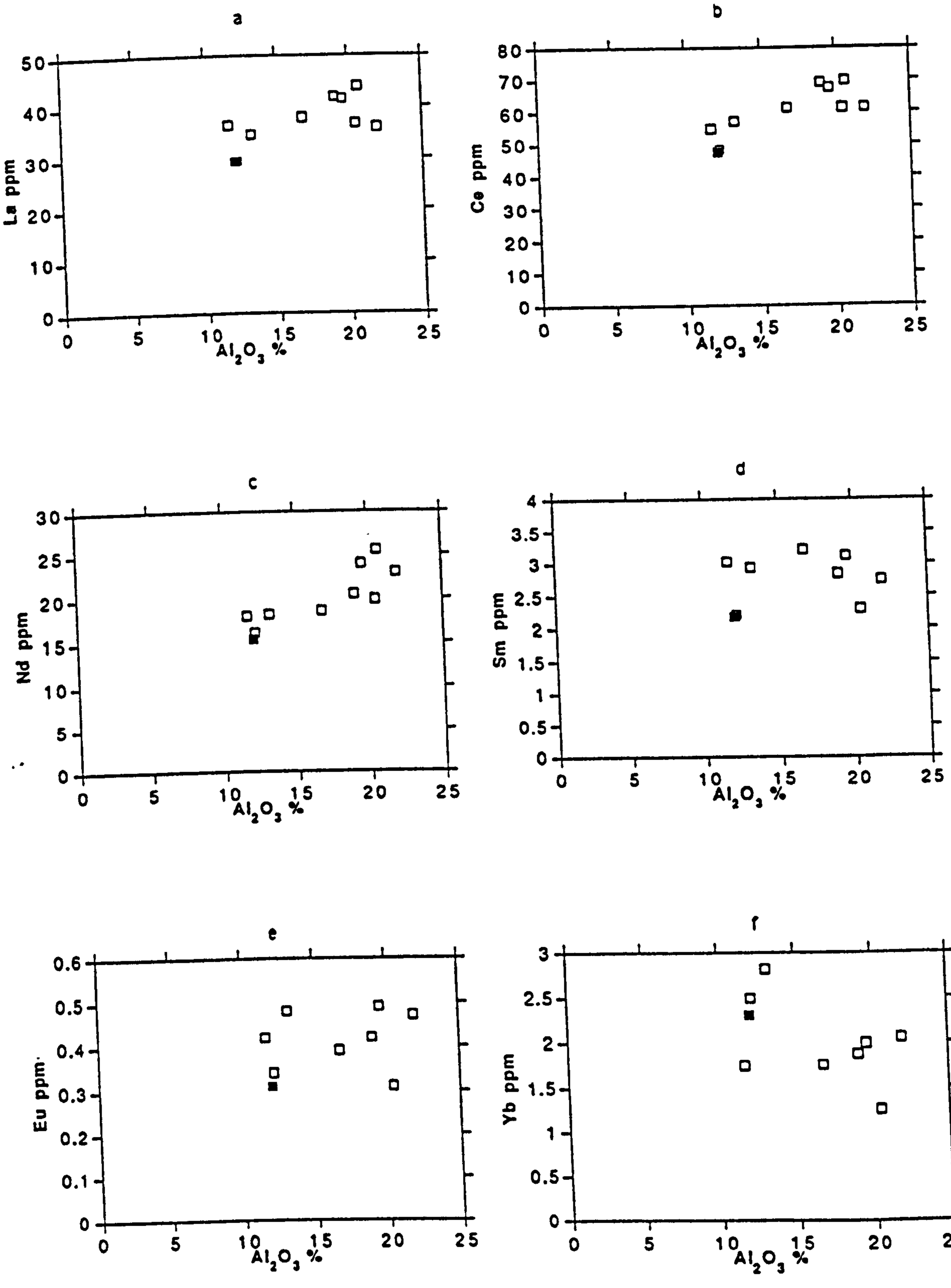

FIGURE 5.8. Relative mobility–immobility of the rare earth elements during the alteration of an acidic rock to bentonite. The solid square corresponds to the fresh glass. Prassa deposit, Kimolos.

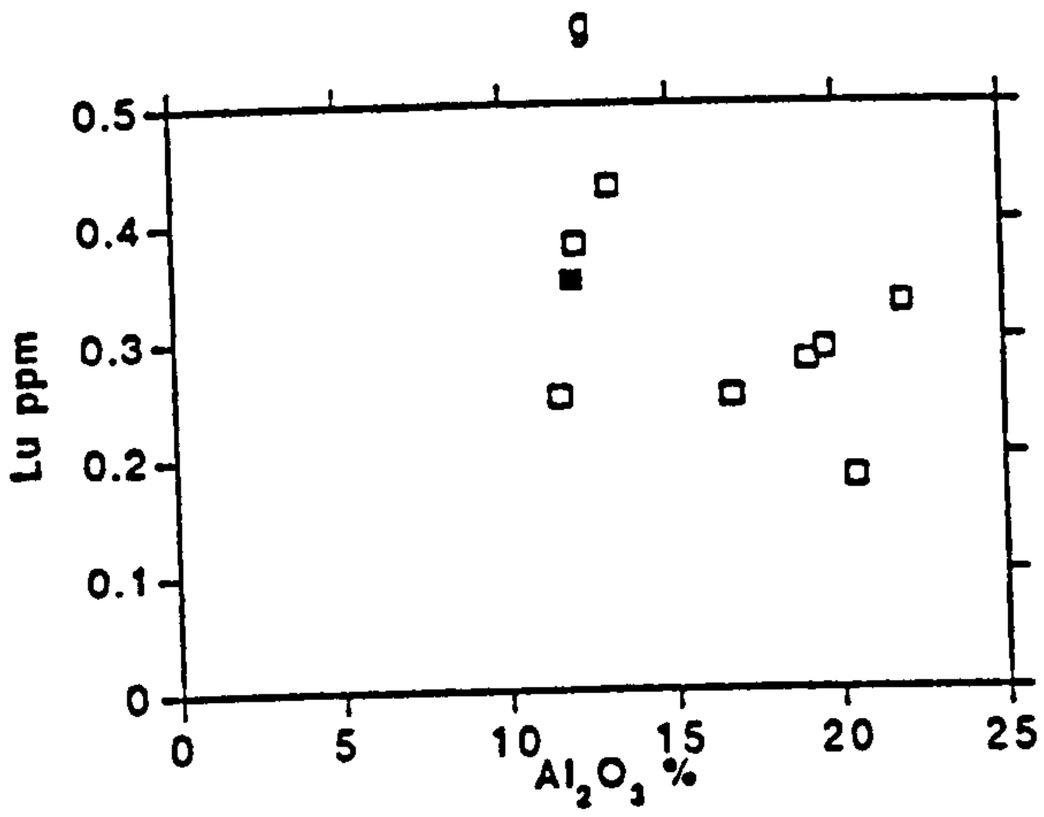

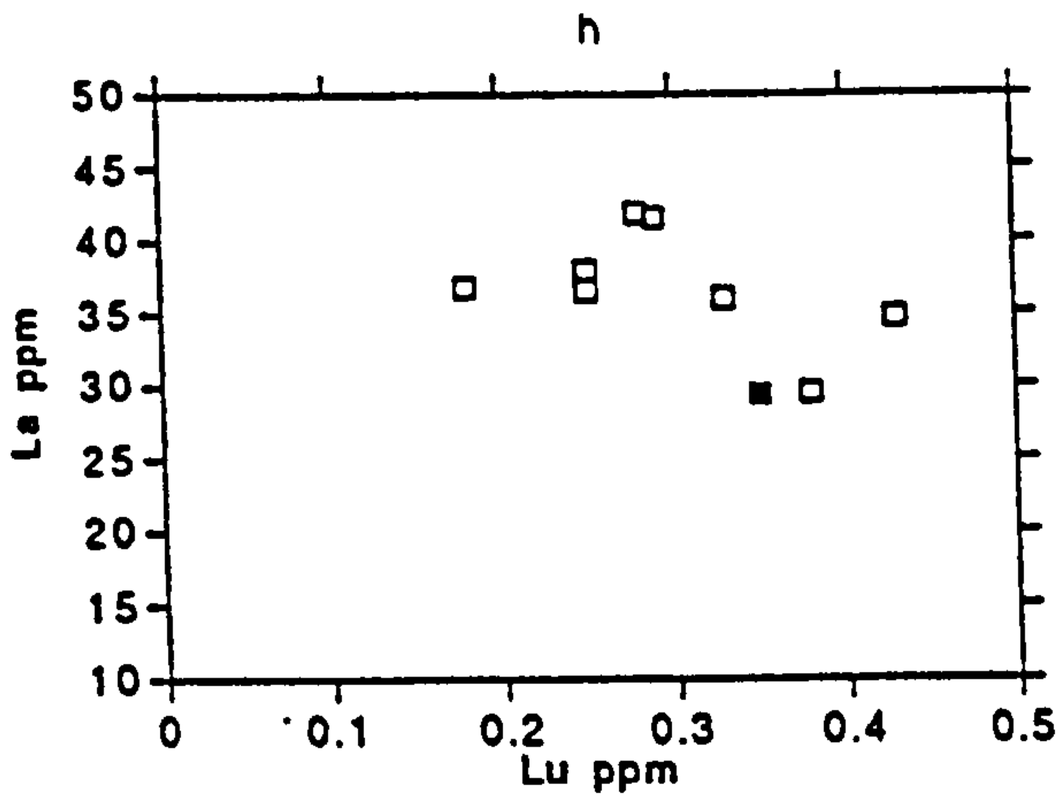

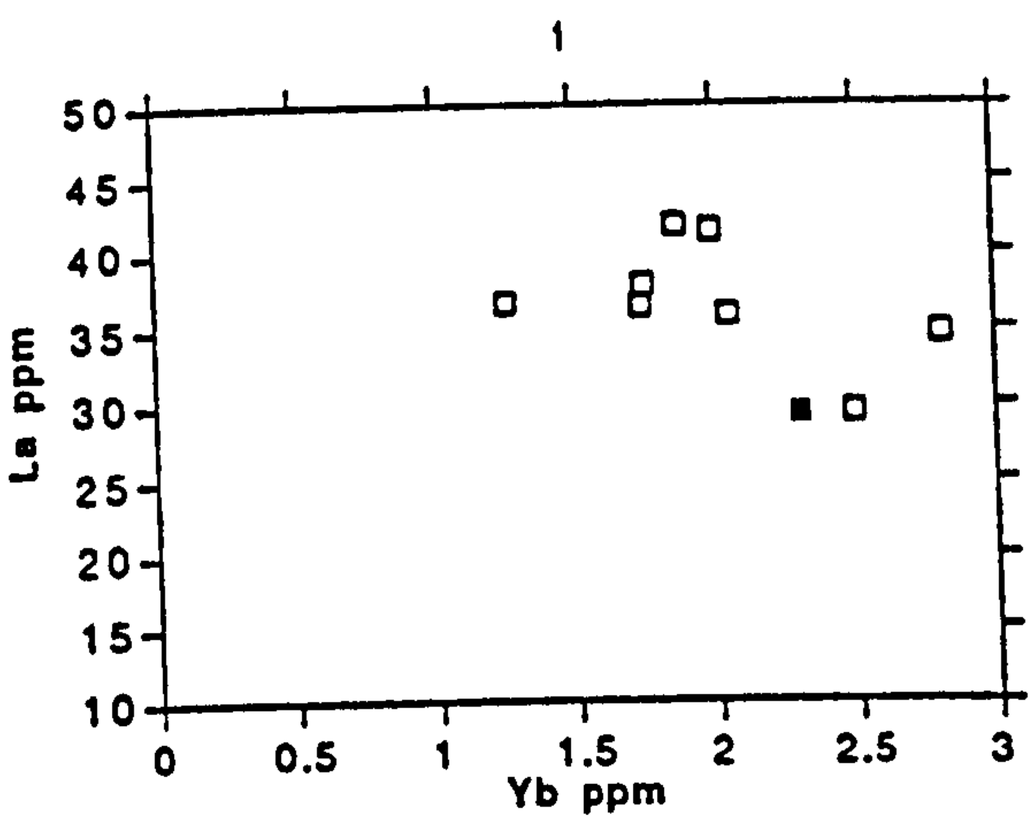

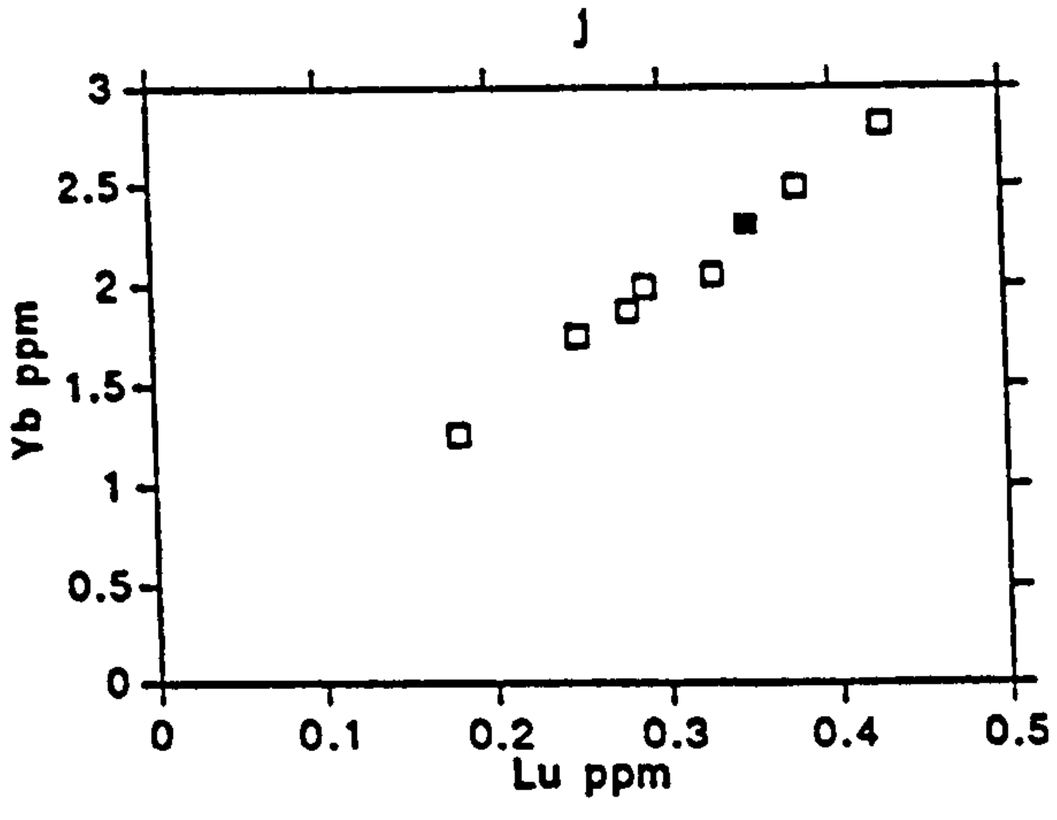

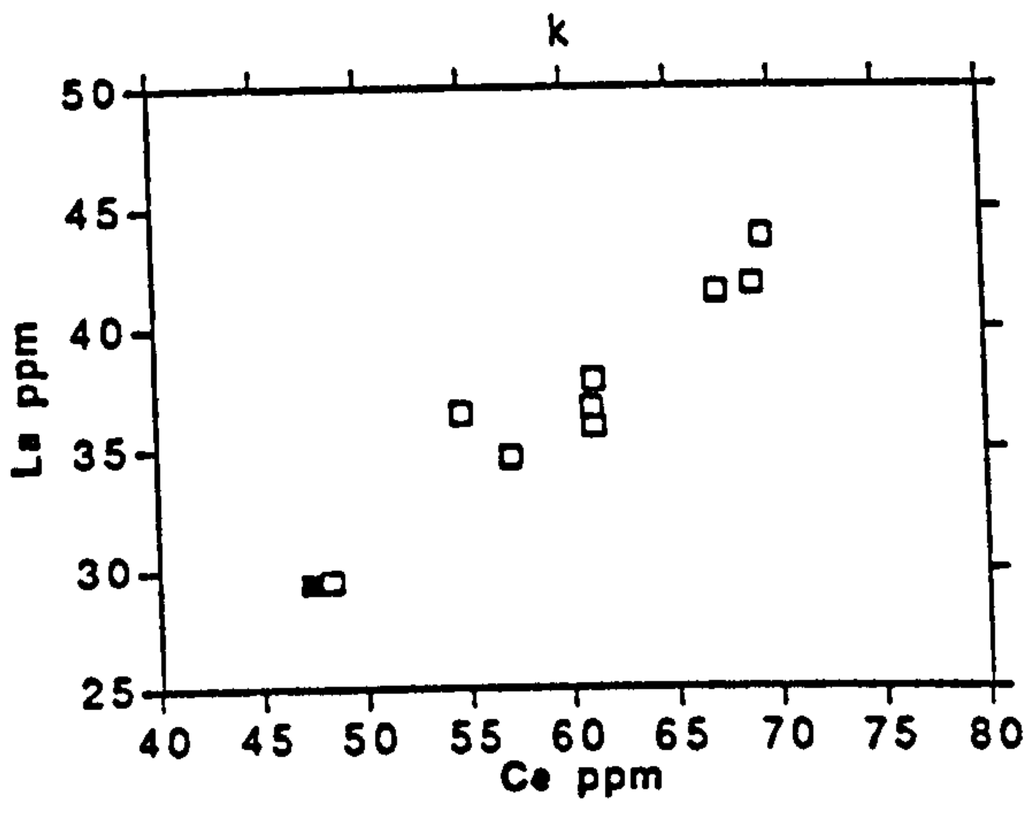

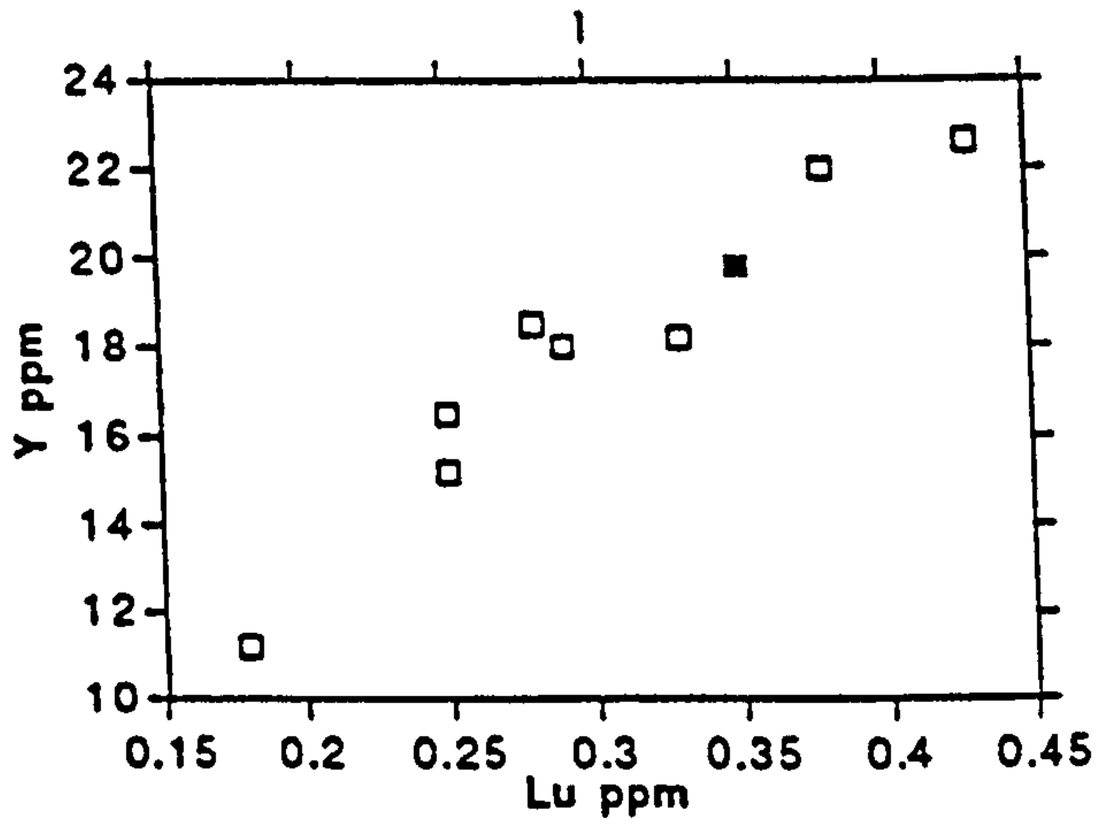

Figure 5.8 (continued).

Secondary minerals like the present monazite may change REE patterns because they are characterized by high mineral/fluid partition coefficients and can accumulate REE (Bau, 1991). Formation of such a phase might be favoured under conditions of infiltration metasomatism characterized by high water/rock ratios (Bau, 1991) like those that might have occured in the Prassa deposit. The almost identical behaviour of the light REE indicates that they were transported in constant proportions in the enriched zones. Similar observations were made by MacLean (1988) but not by Finlow-Bates & Stumpfl (1981) who found that La did not follow Ce in some of the very altered zones they examined.

The geochemical characteristics of this alteration might provide information about the Eh-pH conditions which controlled the mobility of the various elements. The significant increase of the Fe-content, especially in the smectite zone, due to a Fe-supply indicates that iron was transported in its ferrous state either in the form of Fe^{2+} or in that of $Fe(OH)^{-}$ at slightly reducing conditions close to the hematite/magnetite field boundary. This is because, at the neutral to slightly alkaline pH in which the bentonite rocks (see Chapter 8) were formed, ferric iron is not soluble (see Garrels & Christ, 1965, p. 190-191). Also S is present as $SO_4^{=}$. These facts impose some constraints on the valence that the REE (especially Ce and Eu) were transported by the solution. The Eh/pH conditions and the low temperature of alteration (presence of authigenic K-feldspar), suggest that Ce and Eu should be present in their trivalent state (Brookins, 1989, p. 212, 214, Sverjensky, 1984), although the significance of Eu^{2+} in higher temperatures is increased (Wood, 1990b). The presence of Eu^{3+} even at slightly reducing conditions at low temperatures is due to complexation (Wood, 1990b, Bau, 1991).

The behaviour of Eu is similar to that of the LREE in all samples except for the SM280 in which it has been depleted, following the HREE. It is not certain what caused this change in its mobility. Had Eu been present as Eu^{2+} (ionic radius 1.25Å and coordination number 8) in this sample then it would have behaved similar to Sr (ionic radius 1.25Å and coordination number 8) which has also migrated. However, the occurrence of $SO_4^{=}$ in the form of sulphates opposes the existence of Eu^{2+}. In the sample SM280 the HREE underwent maximum depletion, indicating that this might have affected the behaviour of Eu.

It seems therefore that the REE which were initially present in the volcanic glass, were leached and transported in the form of complexes. The mobility of the LREE was restricted because they were bound by the growing monazite. The complexes which might be present at the existing Eh/pH conditions should be carbonates (Cantrell & Byrne, 1987, Wood, 1990a,b). Chloride (Brookins, 1989, Wood, 1990b) sulphate (Brookins, 1989, Wood, 1990a) and especially fluoride (Wood, 1990b) complexes might become important at low pH in some hydrothermal systems (Brookins, 1989, Wood, 1990b), but are not considered

to be important in the physicochemical conditions under which the present alteration took place (Brookins, 1989, Wood, 1990a,b).

The fluid flow observed in the present case raises the question for hydrothermal genesis of this bentonite deposit. Such an argument can be based on the fact that extensive mass transportation and exchange has taken place between the altered rock and the fluid phase. The existence of a zonal pattern in the observed alteration also implies possibility for circulation of a hydrothermal fluid. Hydrothermal alteration involves a hot fluid. However, the presence of pure end member K-feldspar indicates a low temperature of alteration. Furthermore, the increasing content of some elements characteristic of hydrothermal environments (*e.g* Ba or Zn) might be explained by element redistribution, because the fresh rock contains 1000ppm Ba (Ba-bearing K-feldspar is present) and there are zones from which they have both been depleted. The same is expected for iron and the REE. It is believed therefore, that the fluid phase might have been sea water with modified composition after interaction with the volcanic rocks *i.e* evolved sea water. The alteration is more intense within faulted zones because such areas provide better access to the fluid phase.

5.3.2. Alteration of intermediate rocks.

The rocks examined come from the lowest lava horizon in the deposit of Zoulias. The transition represents the first stages of alteration of an andesitic glassy lava to bentonite. The rock has been affected by hydrothermal alteration. It is possible that the conversion to bentonite is at least partially affected by this type of alteration (see Chapters 3 and 4).

5.3.2.1. Major elements.

The mobility pattern of the major elements is depicted in the Figure 5.3b. There are many common features between this alteration and the case in Kimolos Island. Again, the geochemical pattern is characterized by a removal of alkalies and addition of Mg and Fe in the altered rock. However there are some characteristics which were not observed in Kimolos:

i) Ca is removed from the system; the degree of its release increases with the degree of alteration (*i.e* from SM203 to SM188).

ii) Si does not seem to migrate from the system; its content remains constant and only in the more advanced alteration stages its abundance decreases. However its release is relatively insignificant compared to the acid ignimbrite from Kimolos.

iii) The Al and Ti-content does not seem to increase with increasing degree of alteration. On the contrary the Ti-content seems to decrease compared to that of the parent rock in

the most advanced stages of alteration. However this might be due (at least partly) to variations in the Ti-content of the parent rock, since the decrease observed does not exceed 10-15% of the original Ti-content.

iv) P probably migrates from the system in the more advanced stages of alteration. LOI increases systematically as expected with increasing degree of alteration.

The limited changes observed in both Al and Ti which are considered to be stable elements, indicate that the mass transfer during the alteration of this rock was not very significant, and that the loss of alkalies and Ca was counterbalanced entirely by the increase in the Mg, Fe and LOI content of the rock. Also, the two-order increase of the Mn-content of the rock seen in the samples SM193 and SM201 is attributed to the very small abundance of this element (see Table 5.2).

Both Al and Ti can be considered immobile in the Figure 5.3b. The same is true for Si (Fig. 5.9a,b). Whwn Si is plotted vs Al or Ti although the number of plotting points is limited, it can be seen that all of them plot in the same line line which pases from the origin of the axes. On the other hand when Al is plotted against Mg or Fe (Fig 5.9c,d) the plotting points are projected on a line normal to the Al axis indicating that both elements vary over an almost constant Al content. A similar trend is shown when Ca (Fig 5.9e) is plotted versus Al. If the scattering of the points from the line which connects the fresh rock with the origin can be considered a measure of the degree of mobilization of any element present, then in the case of Fe and Mg, an increase of alteration is associated with an increase in the abundances of these elements, while in Ca with a decrease. In any case it is certain that both Mg and Fe have been introduced in the system and at least in the case of Mg this introduction took place in large amounts.

5.3.2.2. Trace elements.

The relative enrichment or depletion of the trace elements is studied with multi-element diagrams (spiderdiagrams). In the Figure 5.10a it can be seen that with increasing degree of alteration V, Cr, Zr Nb and the LREE behave as relatively stable elements in the initial stages of alteration, but V and Cr seem to decrease in more advenced stages. On the other hand it seems that Zn, Rb, Sr, Y and Th are released. The behaviour of Ni is dubious since it does not display a constant pattern but varies unsystematically in the different stages of alteration compared. This might be due to analytical factors or to variations in the original rock. Ba is relatively stable in the first stages of alteration but it displays a sudden increase in concentration in the more advanced ones. Th displays the opposite trend; it is relatively stable in the initial stages of alteration, but it is certainly removed in more advanced stages (sample SM188). This behaviour is opposite to that observed in the alteration in Kimolos.

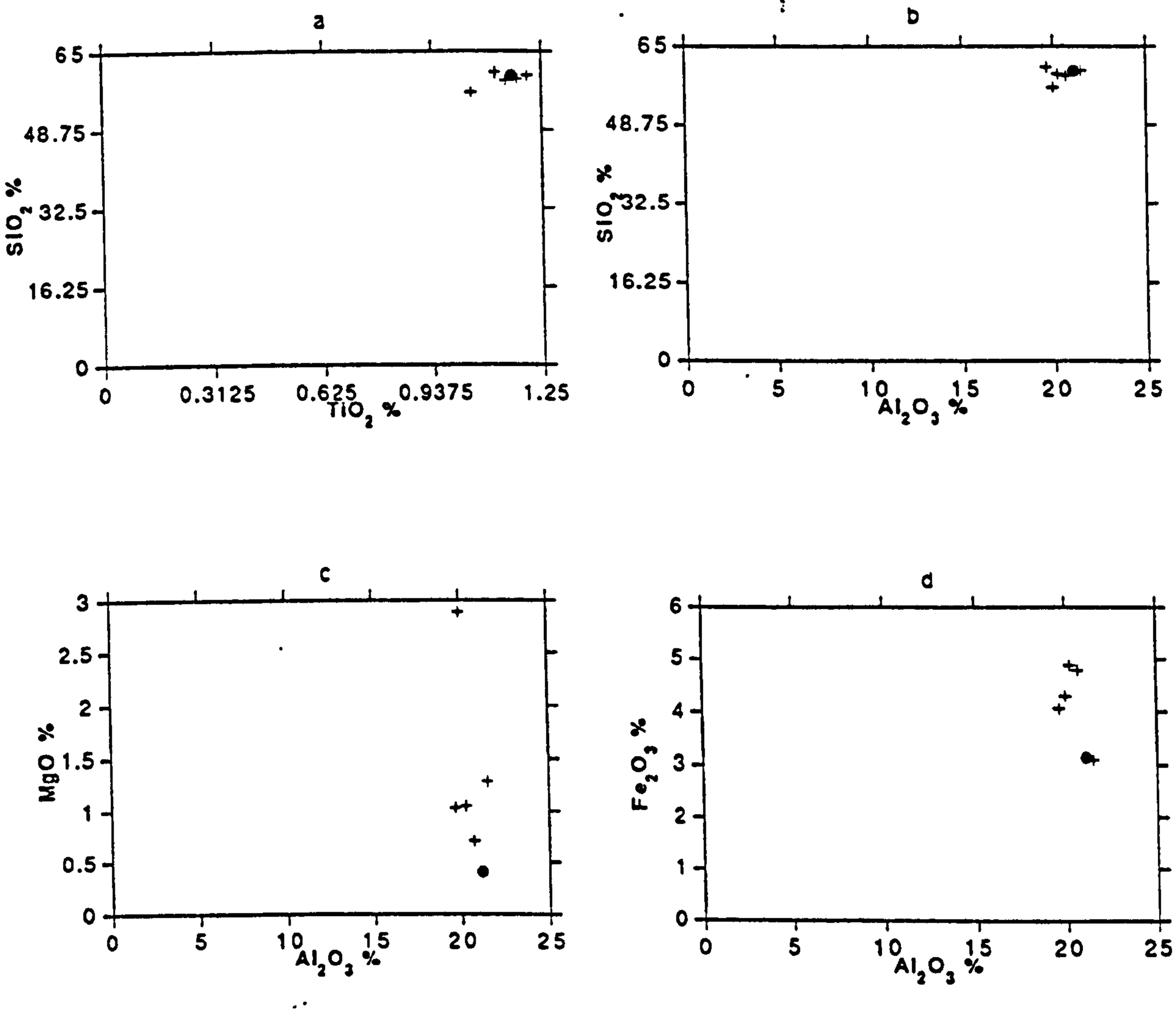

FIGURE 5.9. Relative mobility of the major elements during the alteration of an intermediate rock to bentonite. The solid circle corresponds to the least altered rock. Zoulias deposit, Milos.

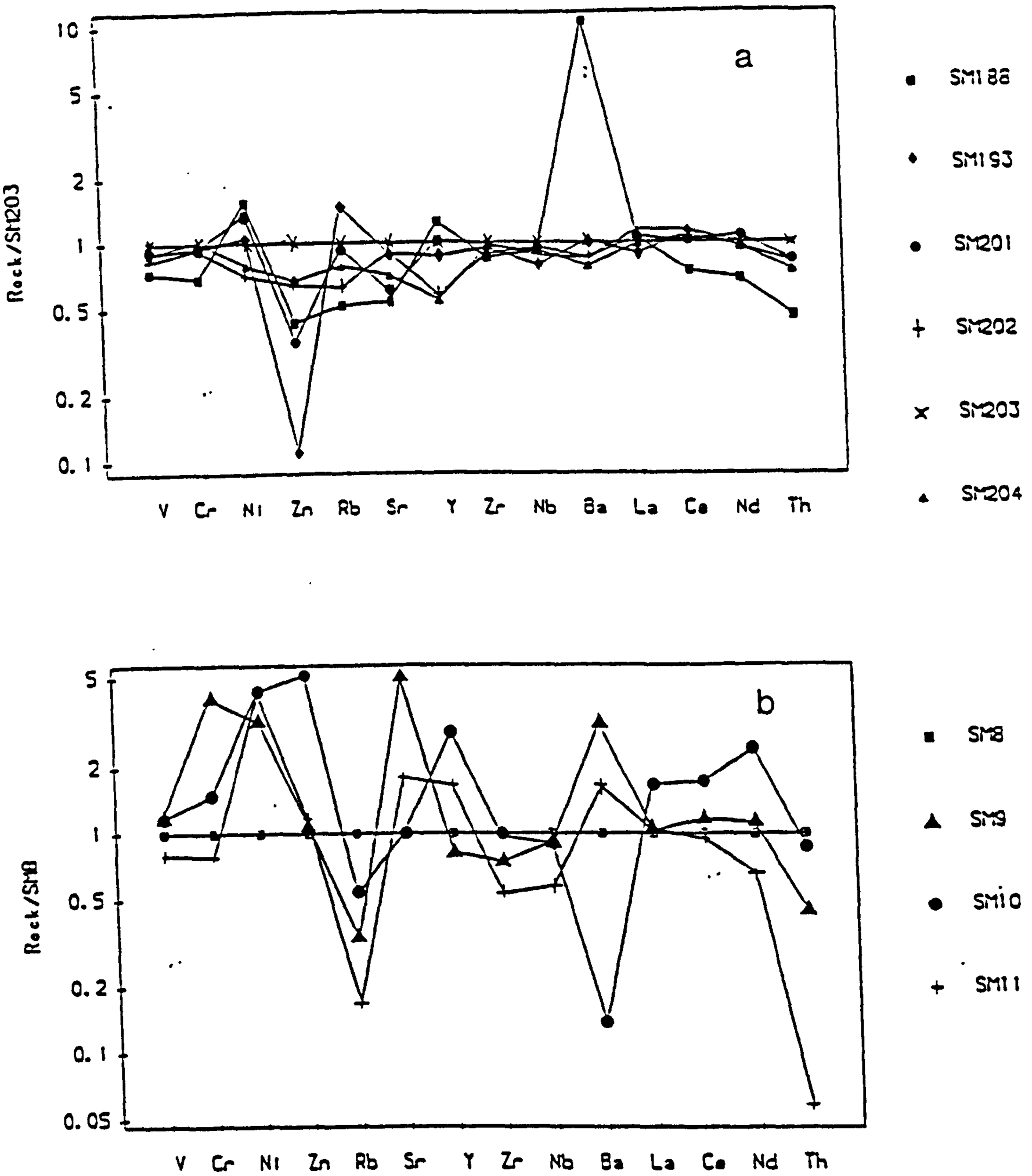

FIGURE 5.10. Multielement diagrams showing the mobility of trace elements (the REEs excluded) during (a) the alteration of an intermediate rock to bentonite (Zoulias deposit, Milos) and (b) during further alteration of a bentonite by hydrothermal processes (Ankeria deposit, Milos).

On the other hand, Y has been removed from the system as in the case of Kimolos and so have Rb and Sr. It can be said therefore, that during the alteration of both acid and intermediate rocks the aforementioned elements are released. In this type of alteration it seems that Sr follows Ca and Rb follows K. This is expected since these elements have very similar chemical characteristics. As can be seen in Figure 5.10a no trace element can be considered as being enriched by transportation in the rock. These results indicate that the alteration of the fresh rock has been affected, at least partially, by fluids which carried certain elements in the system, while simultaneously other elements where removed from the system.

The relative mobility of the trace elements is depicted in the Figure 5.11 where the different elements are plotted versus Al. It can be seen that Nb, Zr and V to some extent plot as a cluster of points in the same Area and can be considered as parts of the line passing from the origin of the axes. On the other hand in the case of both Th and Zn the points are scattered away from the line connecting the fresh rock with the origin of the axes and form a line nearly normal to the Al_2O_3 axis.

The REE elements display an interesting trend characterised by relative immobility of the LREE (Fig. 5.12a) and removal of the HREE. The LREE do not seem to have been enriched by transportation (Fig. 13a,b). The release of the HREE has taken place gradually (Fig 5.12a) and in constant proportions (Fig. 5.13c). Y has followed the HREE out of the system like in the Prassa deposit (Fig. 5.13d). It is interesting that the MREE like Sm, Eu and Dy are stable in the initial stages of alteration but are released in the more advanced ones (Fig. 5.12a). The degree of release of the REE seems to be a function of their atomic number, *i.e* the higher the atomic number the greater the mobility of the elements. The mobility of the HREE relative to Ti which is immobile and the LREE is seen in Figures 5.13e,f. Similar to the Prassa deposit, complexation with carbonate complexes might be reason for the removal of the HREE. The stability displayed by the LREE is probably due to the presence of apatite (Plate 13). In contrast the HREE were either in the glass or in mafic minerals like hornblende and were subsequently leached during the alteration of these phases. It seems therefore, that in both the acidic and the intermediate rock the HREE are mobile during the formation of bentonite.

5.3.3. Influence of the hydrothermal activity on the chemistry of bentonites.

The case studied comes from the deposit of Ankeria, Milos in which the already formed bentonite has been affected by the activity of a hot spring of solfatara type. The alteration is characterized by the deposition of sulphur and various sulphates (see Chapters 3 and 4), while the addition of Fe in the system is obvious (Plate 3).

5.3.3.1. Major elements.

The intensively leaching conditions around the hot spring have caused mobilization of almost every major component, except for iron which has been carried into the system as a result of the hydrothermal activity (Fig. 5.3c). The only element which seems to have been relatively immobile is sodium. This is because the sodium content of the "fresh" bentonite is very low as a result of the conversion of the original parent rock to bentonite (see Table 5.1). Al and Ti seem to be stable even at relatively intense alteration but they are both leached eventually in areas close to the vent where the solutions came from (sample SM11). Similar behaviour is displayed by Mg which is incorporated almost entirely into the smectite, in the octahedral and possibly the interlayer sites. At very advanced stages of alteration smectite is not stable. This is because the conditions are exremely acidic with pH values very close to unity. Instead, minerals like alunite characteristic of such environments, characterized by low pH and high a_{SO4} tend to form (Knight, 1977).

Ca displays a somewhat different trend characterized by a sudden initial drop (sample SM10) recovering later at more acidic conditions. Since Ca is present mainly in smectite which dissolves in such acidic conditions it follows that it must be accommodated in another phase. This phase is gypsum. Phosphorous follows the behaviour of alkalies and Mg and is removed almost completely from the system.

The observed sudden increase in the loss of ignition is due to the presence of native sulphur in the vicinity of the circulation vent. The existence of native sulphur might be attributed to the oxidation of the ascending H_2S gases close to the surface. This oxidation process might also provide the sulphate necessary for the formation of gypsum and alunite which are present close to the vent (Marcopoulos & Katerinopoulos, 1986). The alternative possibility is to assume that Fe is transported in the ferric state in the ascending hydrothermal solutions. This might be feasible at conditions of very low pH where both $Fe(OH)^{++}$ and $Fe(OH)_2^{+}$ in solution are in equilibrium even with magnetite at 25^{o}C and 1 atmosphere (see Garrels & Christ, 1965 p. 190-191). In such a case sulphur might be transported either in the form of dissolved H_2S (magnetite stability field) or in that of HSO_4^{-} (hematite stability field) in slightly oxidizing conditions within the stability field of crystalline sulphur. Consequently precipitation of native sulphur might have taken place without any significant change in Eh or pH conditions.

However, there are some constraints imposed by the transportation and precipitation of vast amounts of iron in the system. More specifically, if iron is present in the hydrothermal solutions then it should be in the $Fe(OH)^{++}$ form, because the amount of iron which can be transported in the $Fe(OH)_2^{+}$ form is too low to account for the enrichment observed (see Garrels & Christ 1965 p. 191). The activity of $Fe(OH)^{++}$ which can be transported at pH 1 (very low for natural systems) is only about 10^{-6} to 10^{-5} *i.e* considerably low; in the case of

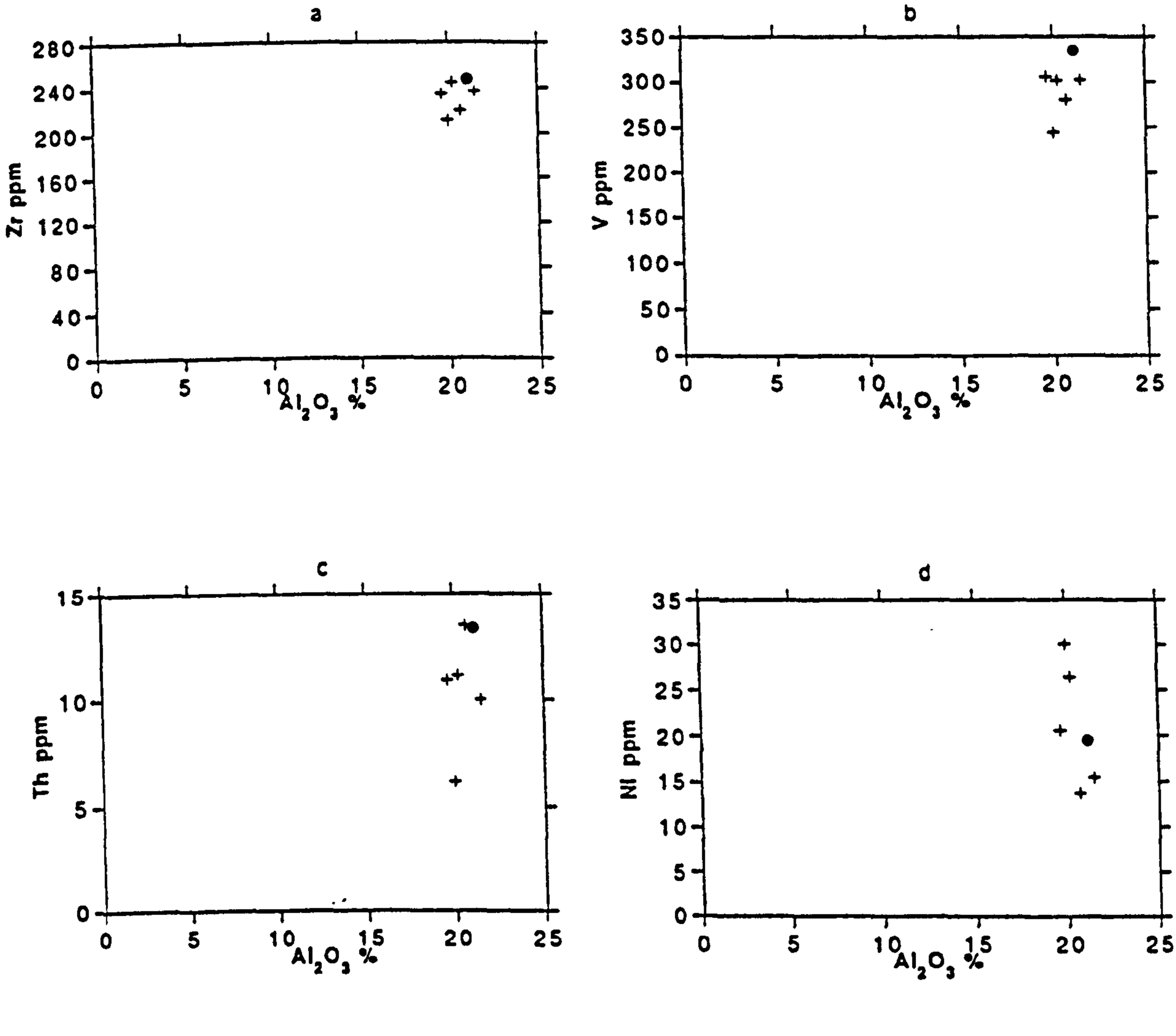

FIGURE 5.11. Relative mobility of the trace elements observed during the alteration of an intermediate rock to bentonite. The solid circle corresponds to the least altered rock. Zoulias deposit, Milos.

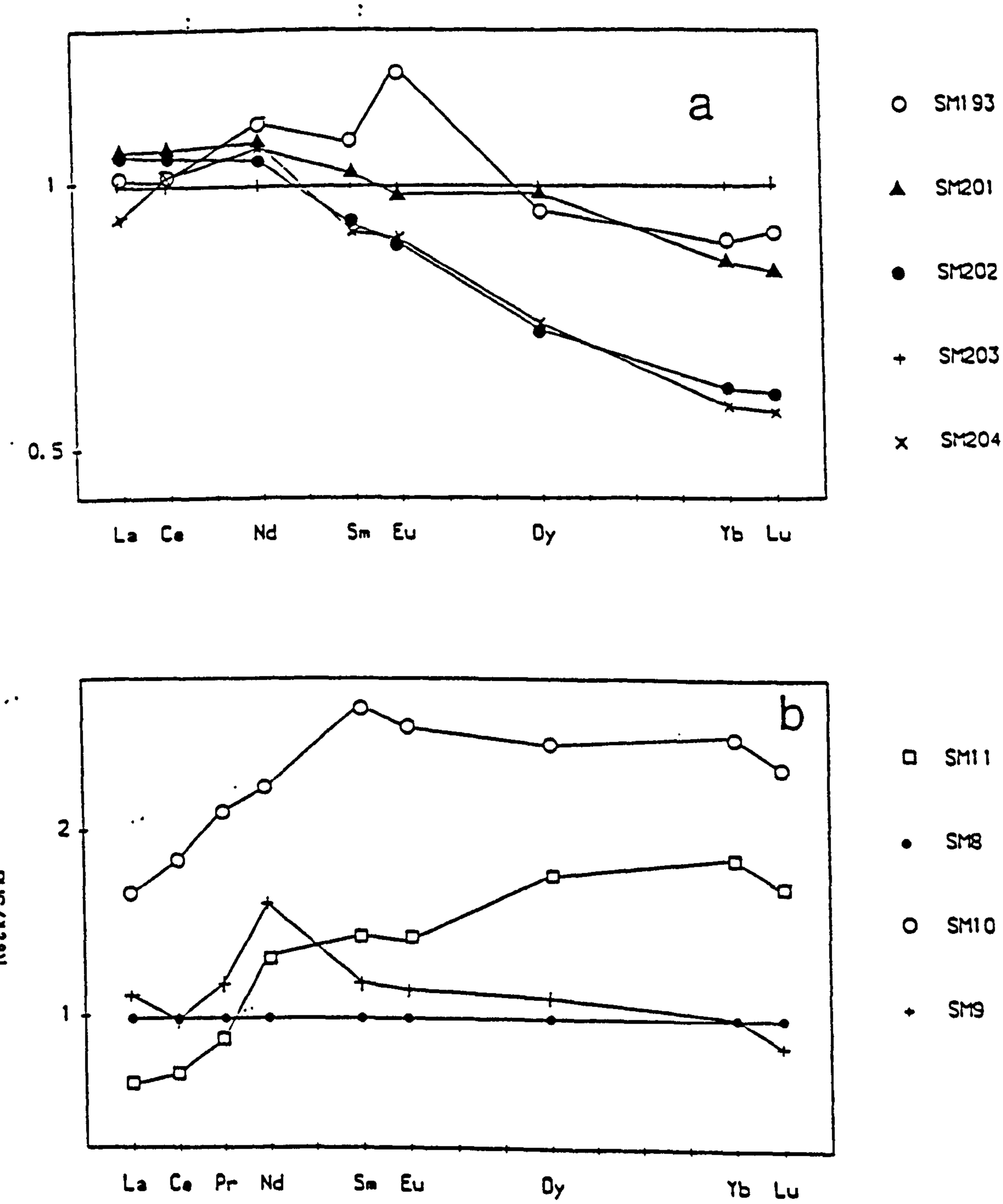

FIGURE 5.12. REE diagrams from the alteration of an intermediate rock ,Zoulias deposit,(a) and the hydrothermally altered bentonite of the Ankeria deposit (b).

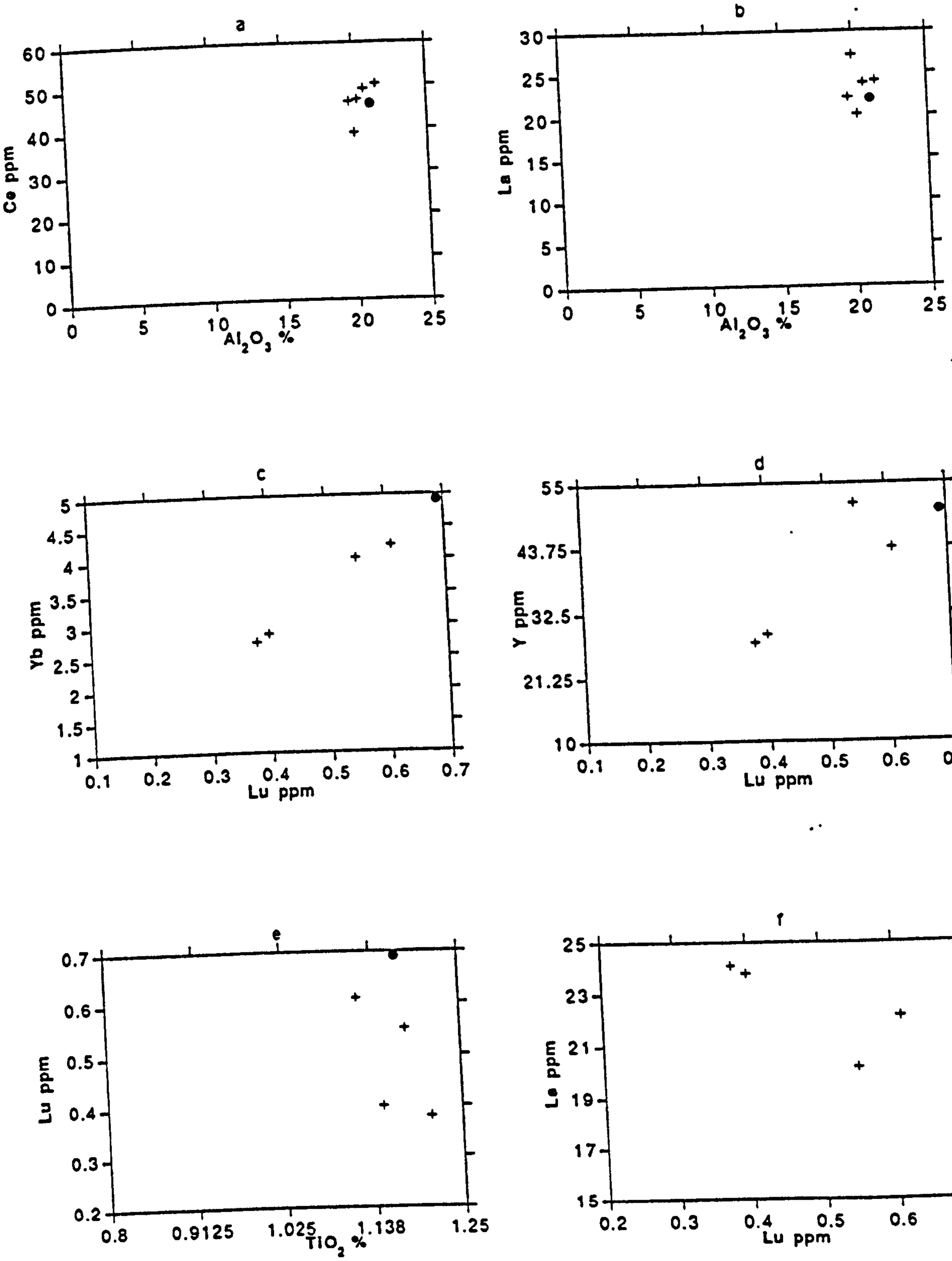

FIGURE 5.13. Relative mobility of the REE elements during the alterarion of an intermediate rock to bentonite. The solid circle corresponds to the least altered rock. Zoulias deposit, Milos.

pH 2 it is even lower (about 10^{-8}). On the other hand if it is assumed that Fe is transported in the ferrous state in the form of $Fe(OH)^+$, then it can be present at activities as high as 10^{-2} at a pH 3-4 and slightly reducing conditions. Such conditions are more likely to occur. This means that the sulphur might be transported in the form of H_2S. As the solution approaches the surface and mixes with more oxidizing fluids the Eh rises and is carried into the field of crystalline sulphur. Native S precipitates according to the reaction (Garrels and Christ, 1965 p.216):

$$H_2S_{aq} = S_c + 2H^+_{aq} + 2e^-$$

The result of this reaction is a drop in the pH of the solution. This event makes the solution more corrosive and accelerates the dissolution of smectite.

5.3.3.2. Trace elements.

All REE seem to increase their absolute concentrations in the first stages of alteration (sample SM10) and to decrease in the more advanced stages of alteration. However it seems that the LREE follow a different pattern characterized by a continuous decrease towards the more advanced stages of alteration while the MREE and the HREE seem to be less affected by the more intense stages of alteration. This can be observed by comparison of the patterns of the samples SM11 which was taken from the hydrothermal vent and SM9 taken 1m away from the vent in Figure 5.12b.

If the different members of the series had been affected in a similar manner by the alteration then the normalized patterns over the original bentonite should be flat. Instead the abundance of the LREE increases with increasing atomic number compared to the original bentonite (Fig.5.12b), while the pattern of both the MREE and HREE is more or less flat in the different degrees of alteration. This indicates that the medium and heavy members of the series behaved in a different way compared to the LREE and that their behaviour was almost identical. If it is assumed that in the sample SM10 (the least altered sample) the enrichment of the HREE and the MREE was due to the residual behaviour of those elements then it follows that the LREE have been mobilized. The inclined normalized pattern of the LREE implies that the observed mobility is controlled by the atomic number of the elements and increases with decreasing atomic number. The HREE have also been mobilized in the more advanced stages, but their removal has taken place in the same degree (Fig. 5.12b).

Alternatively, it might be assumed that the HREE-enrichment in the sample SM10 (the least altered zone) and the SM11 (within the hydrothermal vent) is due to a redistribution of the HREE which were released from the zone around the hydrothermal vent (sample SM9). In any case the HREE cannot be considered as immobile elements in this type of alteration.

As expected, the HREE display a well expressed positive relationship (Fig 5.14a) which is also characteristic for Y (Fig. 5.14b). The same is true for the LREE (Fig 5.14c). On the other hand, no definite relationship is observed between the LREE and the HREE; instead the significant scattering of the plotted points confirms the observation that the behaviour of the LREE during this type of alteration is different from their heavy counterparts (Fig. 5.14d,e). The MREE follow the heavy members of the series (Fig 5.14f) as stated before. This can be seen very clearly in the sample SM9 in which the abrupt decrease in the abundance of the REE with atomic number greater than Nd is obvious (Fig 5.12b).

The behaviour of the remaining trace elements is characterised by mobilization of every element with the exception of V which is relatively stable (Fig 5.10b). Rb, Zr, Nb and Th migrate gradually from the system, while Y follows the rest HREE. The different behaviour of Th compared to the LREE indicates two possible explanations about the source of these elements: i) Th and the LREE were present initially in different phases having different dissolution rates under the conditions the hydrothermal alteration of the Ankeria bentonite took place (Th probably in smectite which was subsequently dissolved while the LREE in apatite, which was more stable) and ii) they were originally present in the same phase (monazite ?) or in different phases having similar dissolution rates. The extremely acidic leaching conditions caused dissolution of these phases; Th was subsequently removed while the LREE were bound in a neoformed phase. This phase might be gypsum, because the ionic radii of the REE in eight-fold coordination are very similar to that of Ca (La^{3+}=1.16Å, Ce^{3+}=1.14Å, Nd^{3+}=1.11Å, Ca^{2+}=1.12Å, Brookins, 1989). If this is indeed the case then the increasing immobility of the LREE with increasing atomic number might be due to the increasing similarity of the ionic radii of the LREE with the ionic radius of Ca (*i.e* the misfit in the structure of gypsum due to the presence of the LREE decreases from La to Nd).

Ba seems to be enriched within the area of maximum alteration but is almost depleted away from it. Elements like Cr, Ni Zn, and Sr seem to have been enriched. However it is not certain whether the observed increase of concentration is a result of residual behaviour or if transportation because there are not any "reliable" elements in this system for comparison. Nevertheless, there are two reasons to suggest that the observed enrichment does not reflect the effect of residual behaviour:

-a) The 5-fold increase observed for Ni Zn and Sr is too large to be explained by residual enrichment without mass transfer. Even in the case of the Prassa deposit in Kimolos, where the conditions were characterized by a removal of large amounts of SiO_2 and alkalies, the elements which exhibited residual behaviour did not increase their concentration by more than twice that of the parent rock.

-b) The enrichment pattern observed, with the exception of Ni, is not characterized by a continuous increase of the elemental abundances with increase of the degree of

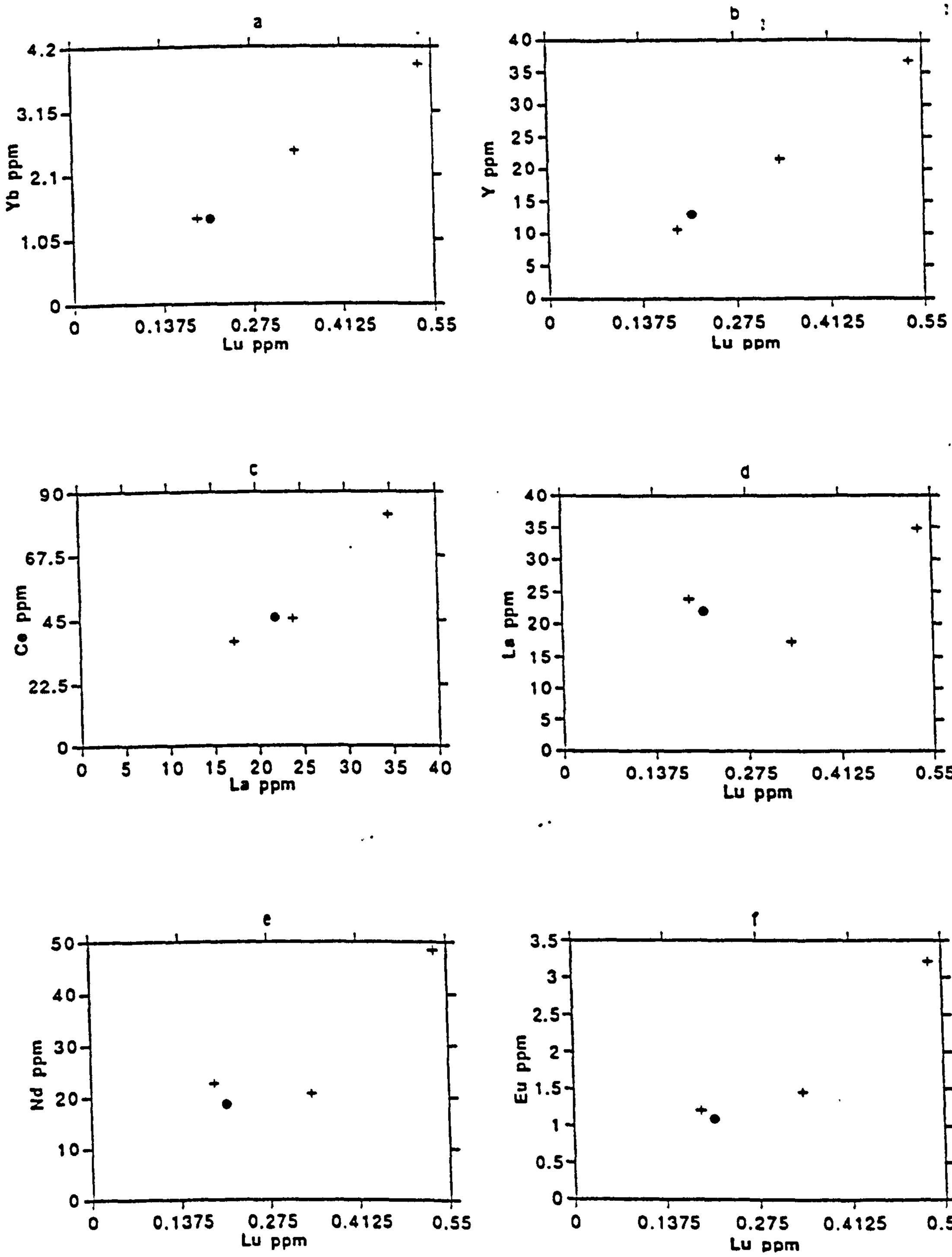

FIGURE 5.14. Diagrams showing the relationships between the REE in a bentonite which has been affected further by hydrothermal alteration. The solid circle belongs to the "fresh" bentonite. Ankeria deposit, Milos.

alteration. The maximum increase of Zn occurs in the least altered zone but its abundance decreases in and close to the hydrothermal vent (Fig 5.10b). Similarly, the maximum increase of the Cr, Sr and Ba content occurs close to but not in the zone of maximum alteration. It is possible that the above elements are released from the more leached Areas and redistributed away from this site. The presence of abundant Sr in the samples SM9 and SM11 is probably associated with the presence of gypsum. Finally, the behaviour of the LREE and Th reflects the effect of the increasing degree of alteration on the materials (Fig. 5.10b).

5.4. Comparison of the alteration patterns of the acidic and intermediate rocks.

5.4.1 Major elements.

The alkalis and the alkaline earth metals are exremely mobile during the alteration. The alkalies are readily released in good agreement with the existing experimental work involving rhyolitic rocks (White & Claasen, 1980, White, 1983, Shiraki *et al.*, 1987, Shiraki & Iiyama, 1990) and basaltic rocks (Seyfried & Mottl, 1982), as well as in natural rocks (Zielinski, 1982). Mg is readily transfered to the solid altered rock, in good agreement with the previous observations. The Mg-increase is greater in the the rhyolite than the andesite.

On the other hand, Ca seems to exhibit a different trend in the different rock-types; its abundance increases in the acidic rock but decreases in the intermediate rock. This behaviour is believed to be closely associated with the mineral phases formed during the alteration (*I.e* smectite) in relation to the original major element geochemistry. Since smectite is the major, and in many cases the only, alteration product and Ca is present only in the interlayer sites of smectite, it should be expected that in a glassy parent rock with an initial 5% Ca content most Ca should migrate from the system. This is because smectites rarely contain more than 1.5% CaO. On the other hand in a rhyolitic rock Ca may behave residually because its abundance in the parent rock rarely exceeds that of smectite.

Al and Ti behave residually in both types of rocks and can be used as guides providing information about the mobility of other elements. In contrast, Si behaves in a different way in the two types of rocks. In the acidic rock the Si:Al ratio is greater than 5:1 (see average rhyolite analyses in Fisher & Schmincke, 1984, and sample SM285 in Table 5.2), while in the smectites studied it varies from about 1.7:1 for beidellites to 3:1 for montmorillonites. This means that during the alteration of an acidic rock Si must be released from its original site in order for smectite to form. It can either migrate from the system under suitable conditions, as in the Prassa deposit of Kimolos, or precipitate as a silica phase, usually opal-CT, as in the deposits of Area 3 of Milos. On the other hand, an andesitic rock has Si:Al ratio much closer to that of smectite. Therefore extensive Si migration is not expected

and Si-phases are not very common, at least in the deposits studied. This explains the immobility of Si in the case of alteration of the Zoulias deposit.

The rest of the major elements are present in small amounts; often below the detection limit of the analytical methods used. Therefore no systematic variation has been observed.

5.4.2. Trace elements.

The trace elements display a very diversified behaviour in the various types of alteration studied. There are certain elements which can be considered immobile and which behaved more or less residually in all cases. These elements are Zr and Nb which even under the extremely acid conditions of the Ankeria deposit retained about 50-60% of their original concentration. Some other elements can be considered fairly immobile although their abundance slightly decreased during the alteration process. These include Th, V, Cr, Ni and possibly the LREE. Th was very stable in the vigorous alteration in Prassa deposit while it lost about 50% of its original content in the case of the Zoulias deposit probably because it was not bound in monazite.

V, Cr and Ni are not as reliable as Zr and Nb but seem to remain in the system. The observed decrease in the Cr content in the Prassa deposit is believed to be mainly due to the low abundance of this element. Ni is stable in the Prassa deposit but varies considerably in the case of the Zoulias deposit. However as stated before, this fluctuation is attributable rather to variations of the parent rock or to limitations of the analytical method than to actual migration of the element. Finally the LREE are immobile in the case of the Zoulias deposit and have slightly been mobilized in the Prassa deposit and under severely leaching conditions in the Ankeria deposit. Therefore they are considered as relatively immobile elements.The nature of the phase which binds these elements also seems to control the behaviour of Th. The latter is not taken by smectite contrary to the proposal of Spears & Kanaris-Sotiriou (1979), but either participates in phosphates (monazite) or migrates from the system.

There are certain elements which are certainly mobile in every case studied. These include Rb, Sr, Zn, Ba and Y. Y follows the HREE which are mobile in all cases studied except perhaps the least altered areas around the thermal spring in the Ankeria deposit. Therefore, these elements cannot be used for geochemical correlation, because it is not certain if the process which led to the formation of bentonites under question was uniform throughout the entire area of Eastern Milos. Moreover, hydrothermal alteration has complicated the alteration pattern of these elements especially in the case of Ba and Rb (see Tables 5.1 and 5.3).

5.5. Geochemical correlation of the bentonite deposits of Eastern Milos.

The geochemical correlation of the bentonite deposits of Eastern Milos was carried out using i) various combinations of elements in the form of triangular diagrams and ii) multivariate statistics and more specifically discriminant functions. The purpose of this correlation is:

-a) To confirm the observations presented in the figures 5.1 and 5.2 about the existence of more than one bentonite horizon.

-b) To establish, if possible, a stratigraphic order and subsequently a chronological order of the bentonite deposits.

-c) To use the stratigraphic data obtained for exploration of possible new deposits.

5.5.1. Correlation using triangular diagrams.

The triangular diagrams used in this study for geochemical correlation always have V and Cr in two apices and a Large Ion Lithophile (LIL) element (one of Th, La, Ce and Nd) or Zr or Nb in the third (Fig 5.15). All the above elements have been characterized as immobile or least mobile in the various types of alteration (see previous sections). Consequently they might provide relatively reliable information about variations between the different deposits if they existed.

The distribution of the points in the V-Cr-Zr diagram (Fig. 5.15a) confirms the assumption made about the existence of more than one bentonite horizon. Furthermore the clear distinction of the two provinces (acidic and basic parent materials), already seen in the Figures 5.1 and 5.2, is obvious. There are several interesting observations as far as the separation of the different deposits in the different Areas is concerned.

-a) The deposit of Ankeria (Area 2) consists of two geochemically distinct horizons. The lower one (encircled points) which is more basic and includes the three lower bentonite horizons (see section 3.3.2.1), while the higher, which corresponds to the higher stratigraphic horizon, is more acidic and plots with the samples from the Koufi deposit.

-b) The lowest horizon of Koufi deposit is significantly different from the other horizons of this deposit and plots with the materials from Agrilies deposit (point showed with arrow).

-c) The samples from the deposits of Tsantili, the lower horizon of Aspro Horio and the highest horizon of Zoulias plot in the same area. In contrast, samples coming from lower horizons of the Zoulias deposit are scattered towards the area occupied by more acidic materials.

-d) The bentonites from the Ano Komia deposit plot in three well distinguished groups. One group, which corresponds to the lower bentonite horizon is associated with the higher horizon of the Aspro Horio deposit. The second, corresponding to the higher stratigraphic

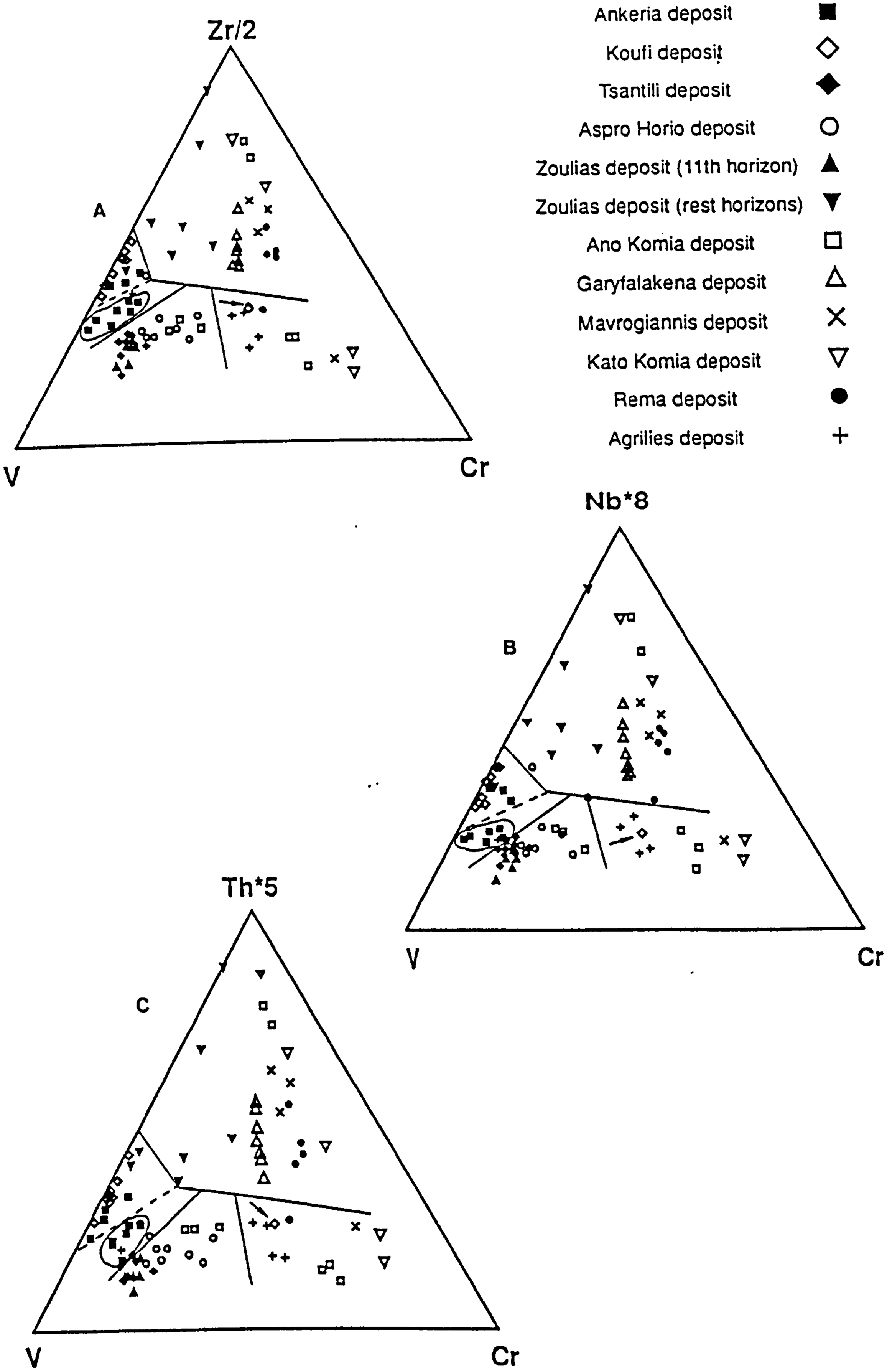

FIGURE 5.15. Triangular diagrams showing the geochemical correlation holding between the bentonite deposits of Milos Island. The lines separate bentonites from diffrent areas. The encircled points correspond to the three lower horizons of the Ankeria deposit, while the arrow points to the lower horizon of the Koufi deposit. The dashed line separates the geochemically different bentonites in the Ankeria deposit.

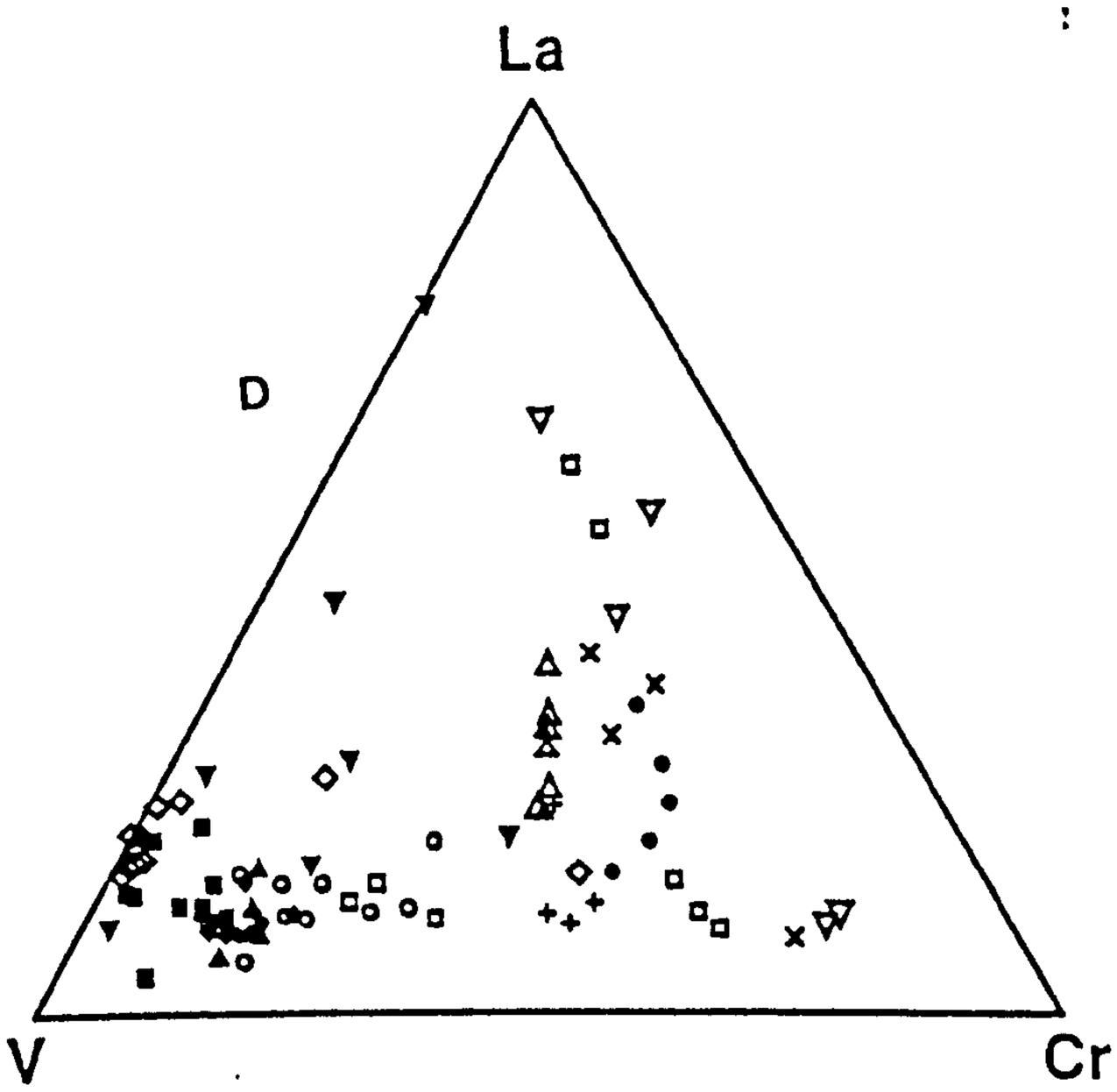

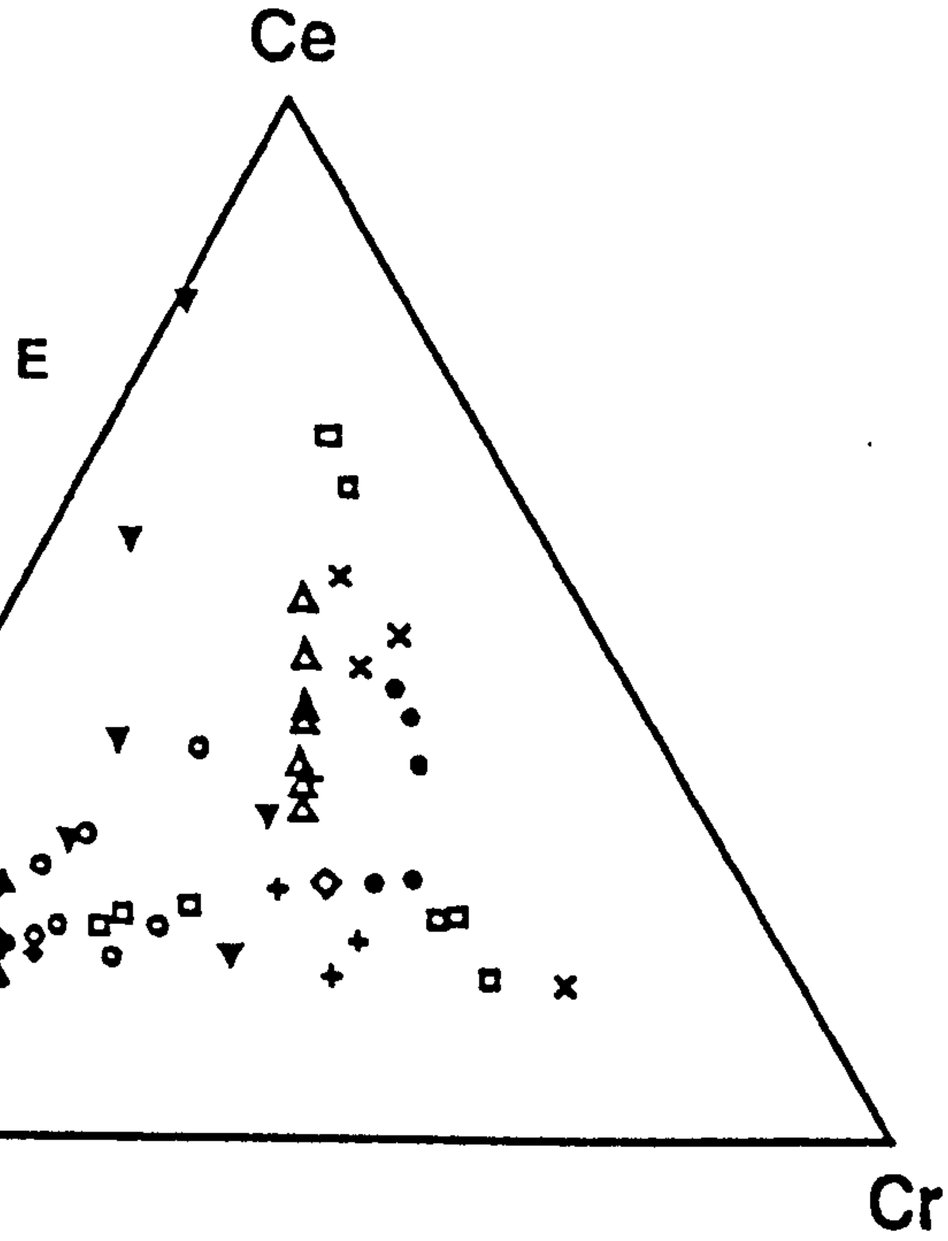

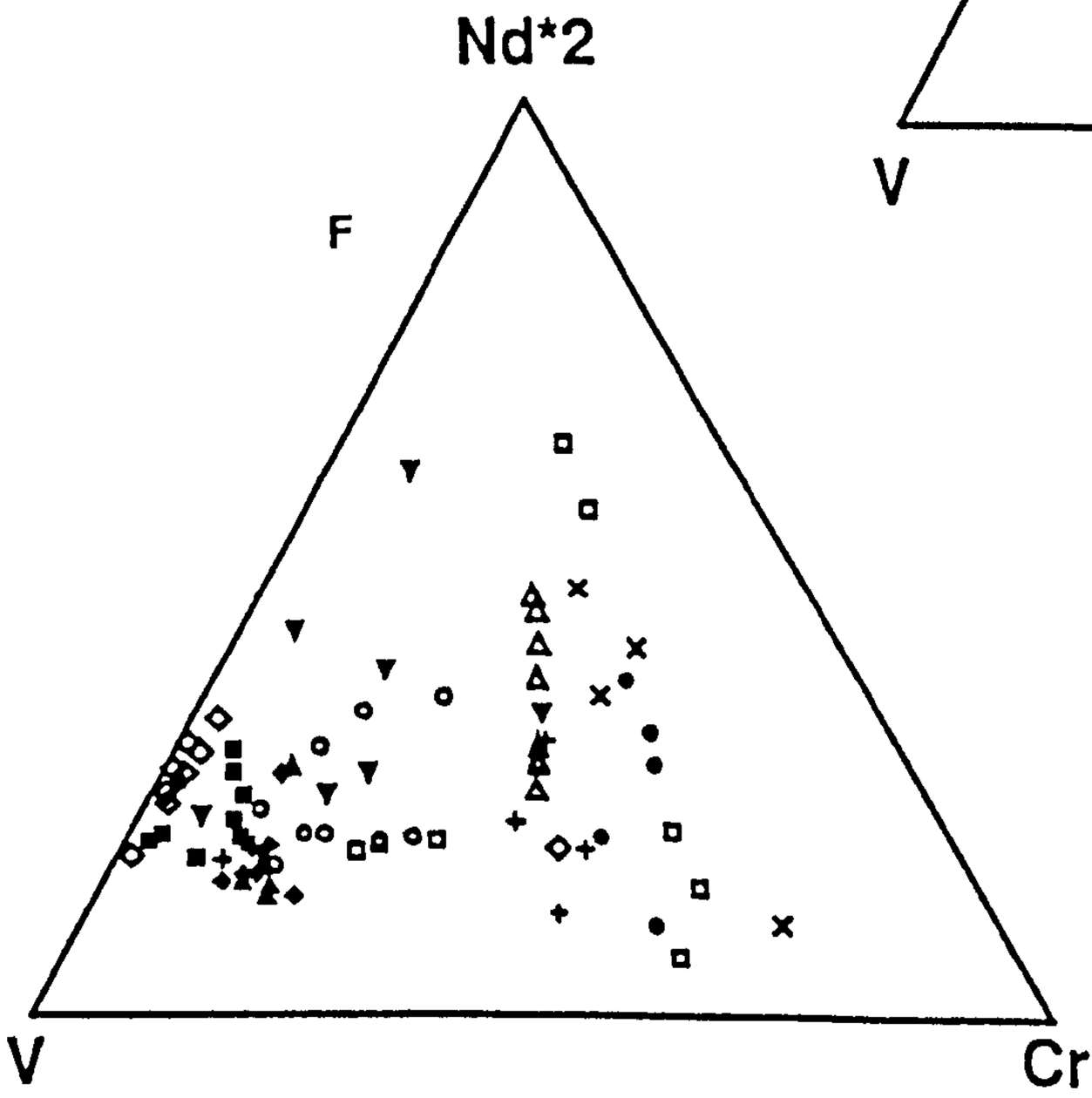

FIGURE 5.15. (continued)

horizon, plots close to the area occupied by the deposits of the Area 3. Finally the third group includes samples which have been affected by hydrothermal alteration. These altered samples come from the parent material of the lower stratigraphic horizon. It seems therefore that the alteration adversely affected the discriminant power of the triangular diagrams.

-e) The deposits from the Area 3 plot in the same field of the diagram. An exception to this trend is exhibited by two samples from the deposit of Kato Komia which plot close to the Cr corner. This is probably due to the presence of metaophiolitic material derived from the metamorphic basement. The intense hydrothermal alteration might also be a further factor affecting the observed scattering

-f) The bentonites from the lower horizons of the Zoulias deposit (inverted solid triangles) are scattered indicating that the characteristics of volcanism in this volcanic centre changed with time.

Similar information is obtained from other diagrams as well. When Zr is replaced by Nb the separation of the bentonites into certain horizons is more obvious. Also, the separation of the bentonites from the Ankeria deposit into two different groups is clear. However, the higher bentonite horizon of this deposit plots close to the the bentonites of the Area 1. Similar information is provided also when Th is used instead of Nb. When the LREE are used the degree of scattering increases and the information obtained is not unambiguous (Fig. 5.15d-f). Nevertheless, the bentonites from the different volcanic centres are separated. The similarity in the distribution of points corresponding to the different deposits in the various diagrams, implies that the separation of the different horizons is not an artifact, but is a result of the different geochemical fingerprinting of these horizons.

5.5.2 Geochemical correlation using discriminant functions.

Discriminant Analysis have been used in the past in several occasions to shed light in geological problems which concern mainly correlation (see Rock, 1988). As far as bentonites are concerned, the method has been used successfully in the past by Huff (1983), Kolata *et al.* (1987), Huff & Morgan (1989) and Huff *et al.*, (1991) for correlation of K-bentonites. The results were used for stratigraphic correlation purposes.

5.5.2.1. Theoretical considerations.

Discriminant analysis is a multivariate statistical technique used for classification purposes. It has the characteristic that it maximizes the separation (*i.e* it discriminates) between two or more groups of data using a set of variables, so called discriminating variables, that measure features in which the groups differ (Klecka, 1975, Rock, 1988).

Discriminant analysis is carried out using the *discriminant functions*. These are linear combinations of the *discriminating variables* and have the following form (Klecka, 1975, Rock, 1988):

$f = a_1x_1 + a_2x_2 + a_3x_3 + ... + a_nx_n$

where, f is the *score* on the discriminant function, $a_1,a_2...a_n$ are weighting coefficients and $x_1,x_2...x_n$ are the discriminant variables. The maximum number of discriminant functions is limited either by the number of groups or variables. It is one less than the number of groups or equal to the number of discriminant variables, whichever is the smaller. The importance of the method is based on the fact that the discriminant functions can be considered as the axes of the geometric space; therefore they can be used for the study of the spatial relationship of the various groups (Klecka, 1975).

The discriminant scores are computed by multiplying each discriminating variable by each corresponding coefficient and adding together all these products. The coefficients may be standardized or unstandardized ("raw coefficients").In the former case the discriminant scores produced are also in standard form. This means that, over all the cases in the analysis, the score from one function will have a mean of zero and a standard deviation of one. Each single score represents the number of standard deviations that case is away from the mean of mean for all cases. The algebric sign of each coefficient shows whether the variable makes a positive or a negative contribution. When the sign is ignored then each coeffient represents the relative contribution of its associated variable to the discriminant function.

The importance of the various discriminant functions for separation is determined by the *eigenvalues*, which are a measure of the relative importance of these functions. In other words, the relative percentage of the eigenvalues is an expression of the discriminant power of the functions. The sum of the eigenvalues is a measure of the variance in the discriminant variables. Usually, a small number of the discriminant functions suffices to provide information about the characteristics of a population. Therefore, using the relative percentage of the eigenvalues we can limit the number of functions to a degree which is sufficient for discriminant puproses.

An additional method to eliminate discriminant functions is the *Wilks' lambda* method. Wilks' lambda is an inverse measure of the discriminating power in the original variables which has not been removed yet; the larger the lambda is, the less information has not been used in the discriminant analysis. Finally an additional way to judge the importance of a discriminant function is its associated *cannonical correlation*. The cannonical correlation is a measure of the association between the single discriminant function and the set of dummy variables which define the group membership, and provide information about how closely the function and the group variable are related. The squared cannonical correlation

may be considered as the proportion of variance in the discriminant function explained by the groups.

5.5.2.2. Geological terms used to replace the corresponding mathematical terms in the use of discriminant analysis. Reasons for choosing the elements used.

The equivalent geological term corresponding to the mathematical term "group" or "class" is bentonite deposit, while the variables are trace elements. Therefore, the discriminant analysis was used to separate 81 samples from 11 deposits with the aid of 9 trace elements. The samples from Zoulias deposit come only from the uppermost bentonite horizon. The elements used were La, Ce, Nd, Th, Zr, Nb, V, Cr, and Ni. The effect of Y, which was found relatively mobile, on the discriminant analysis was tested with the use of a second set of 10 variables (the previous 9 plus Y). The statistical program used is the CANDISC procedure from SAS, provided on the main computer of the University of Leicester. The computer program used to run the CANDISC procedure is given in Appendix 5.5.

The number of elements used is smaller thanthat used by Huff (1983), Kolata *et al.*, (1987), Huff & Morgan (1989) and Huff *et al.*, (1991). Huff (1983) stressed the importance of the number of elements used in the statistical significance of the results obtained, in the sense that the greater the number used the greater the possibility for discrimination. However, since the geological history of the bentonites of eastern Milos is complex and the deposits have been affected to variable extend by more than one alteration events, it was necessary to use only elements which were reliable.

It is believed that some of the elements used by Huff (1983), Kolata *et al.*, (1987), Huff & Morgan (1989) and Huff *et al.*, (1991) (K, Zn, the HREE and especially Rb) must be examined carefully. This is especially true in the case of bentonites which are developed horizontally over large distances. Elements like K can easily be bound in zeolites which act as a sink in some areas, while in others they might migrate from or to the system as in the case of Miloan bentonites. Since Zn, Rb and the HREE seem to migrate even from the very initial stages of alteration of the glass, there is no reason to believe that the degree of their release will be uniform. Consequently, their possible different concentrations might not represent different horizons. Moreover, addition of elements like Zn Ba and/or Rb in some areas through hydrothermal alteration may cause further difficulties. Therefore, it seems imperative to use relatively immobile elements in this type of analysis in deposits with complex history, like those of Milos, and to cross-examine the results obtained with conventional geochemical plots.

The reason for which discriminant analysis was used in this project, was to provide additional information, when used in conjunction with conventional methods, about the

extent of the bentonite deposits. There is no reason to reject the assumption that when the same horizon is detected in two deposits which are located at some distance from one another, then the same horizon might be present in the Area between them. This might be be very helpful in areas like the eastern Milos, which has been intensively affected by tectonism and therefore it is possible to have vertical movements of the various horizons.

5.5.2.3. Use of the discriminant analysis in bentonite deposits of Eastern Milos.

The statistical significance of the between groups differences can be seen in the Table 5.4 from the F ratio and the F probability. The F ratio (between-group mean square / within-group mean square) expresses the extent to which between group variations are due to non- random variation. It can be seen that the probabilty that the between-group differences of Zr, V, Nd, Th, Nb and Cr are not real, but accidental or due to random variations, is almost zero. In the case of Ce and Ni it is slightly higher and only for La and especially for Y the possibility is significant. Thus, the original hypothesis that Y is not a very reliable element at least in the case of Milos bentonites is confirmed again.

Elements like Zr and Nb are probably accommodated in zircon which is not affected by the alteration. Therefore they behave as immobile elements. The same is true for V which is probably present in titanomagnetite. in the original glass. The presence of Ti-oxides (probably anatase or brookite) in the bentonites indicates that the titanomagnetite has partly been altered. In that case it seems possible that V has been incorporated in the Ti-oxides. The LREE have been accomodated in phosphates either igneous (apatite) or authigenic (monazite), while the behaviour of Th has been controlled by the behaviour of the LREE, as stated before. Finally, Ni and Cr which are present in small amounts, are probably accomodated in smectite, because the pyrogenetic phases which originally hosted them (olivine, clinopyroxene) have been altered. The high Ni and Cr contents observed in the Kato Komia deposit (Area 3) are probably due to the presense of ultramafic xenoliths from the basement, as this is indicated by the presence of characteristic minerals in this bentonite (serpentine, talc, chlorite).

The F ratio can be used to determine the relative contribution of each of the elements used to the discrimination (Rock, 1988). The higher the F (and the lower the F probability), the greater the contribution of the element to the discrimination. Under this context, V contributes most followed by Zr, Nd, Th, Nb, Cr, Ce, Ni, La and finally Y (Table 5.4).

In Table 5.5 the eigenvalues, their associated canonical correlations, the squared canonical correlations and the cummulative percent of the discrimination due to each successive function calculation are listed. It can be seen that first function accounts for 66.4% of the discriminating power of the variables used and that the first two account for 86.39% of that power. The third function adds less than 5% being much weaker. Also

Table 5.4

F-statistics for the variables (trace elements) used for discrimination of the Miloan bentonites. See text for discussion of the results.

Element	F-ratios	F-probability
V	45.7454	0.0001
Zr	20.5912	0.0001
Nd	6.2517	0.0001
Th	5.5796	0.0001
Nb	3.7229	0.0005
Cr	3.6965	0.0005
Ce	3.3634	0.0013
Ni	3.1853	0.0020
La	1.7017	0.0975
NY	1.4348	0.1834

Table 5.5.

Results from canonical discriminant analysis of the bentonites from Milos. 10 elements and 82 samples from 11 bentonite deposits were used.

Canonical Function	Eigenvalue	Proportion	Cumulative % of variance	Canonical Correlation	Wilk's Lambda	Approxim F	F-proba-bility
1	9.3833	0.6640	0.6640	0.950627	0.00519479	4.8665	0.0001
2	2.8250	0.1999	0.8639	0.859398	0.05393925	2.8886	0.0001
3	0.6578	0.0465	0.9104	0.629901	0.20632026	1.8190	0.0004
4	0.5484	0.0388	0.9492	0.595115	0.34202900	1.5816	0.0111
5	0.3999	0.0283	0.9775	0.534464	0.52958912	1.2469	0.1658
6	0.1687	0.0119	0.9895	0.379957	0.74136030	0.8278	0.7045
7	0.1035	0.0073	0.9968	0.306208	0.86644683	0.6165	0.8687
8	0.0336	0.0024	0.9992	0.180379	0.95609308	0.3427	0.9593
9	0.0118	0.0008	1.0000	0.108111	0.98824715	0.2045	0.9355
10	0.0001	0.0000	1.0000	0.008107	0.99993427	0.0046	0.9461

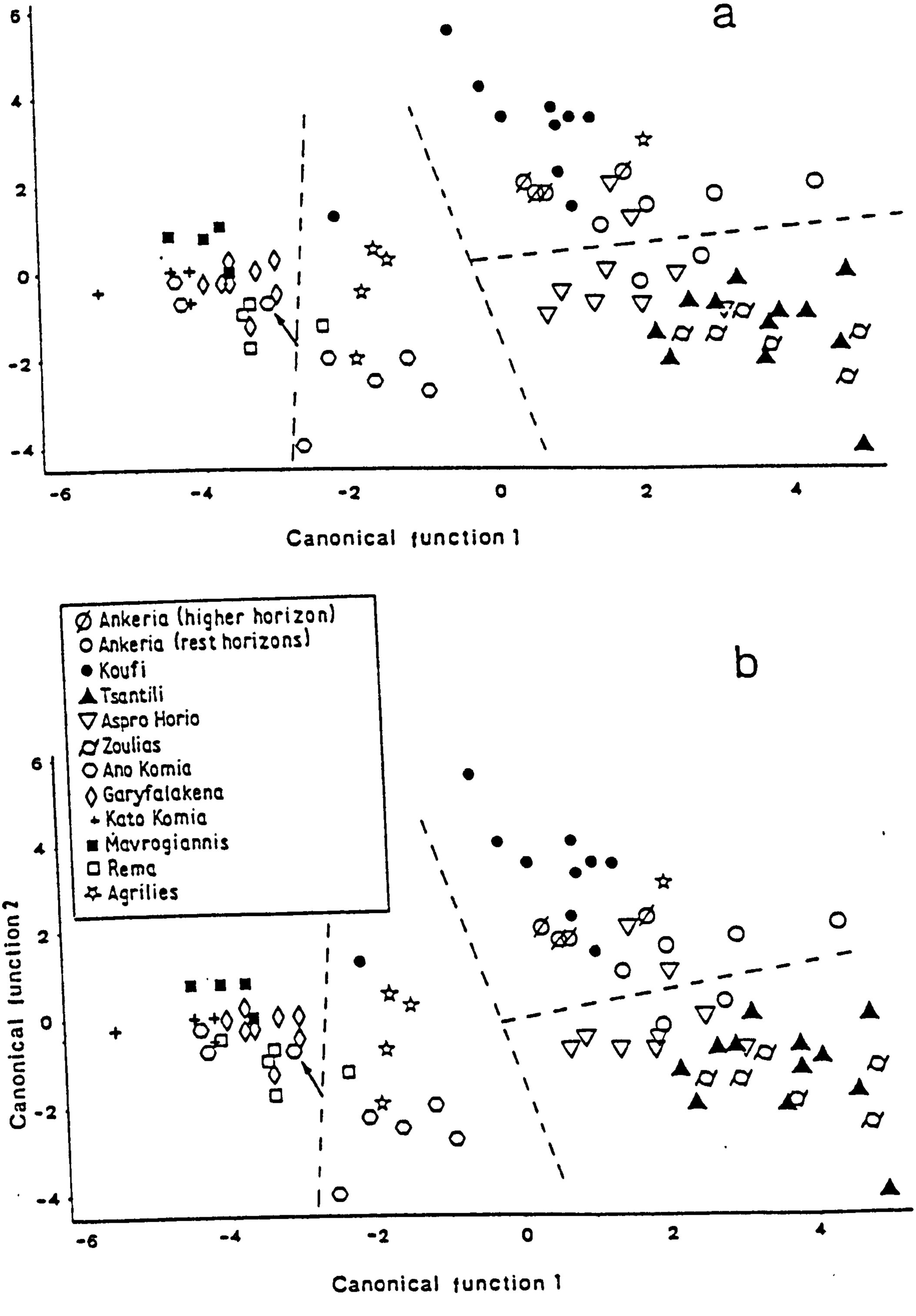

FIGURE 5.16. Territorial plots derived from application of multivariate statistics (discriminant analysis) in the bentonites of Milos. (a) Y is included, (b) is not included. The plots were obtained using the first two discriminant functions. Note the clear separation between the areas 1, 2 and 3. The dashed lines underine the separation of the different groups.

almost 99% of the information can be obtained by using 5 out of nine functions. The canonical correlation results also show that the first two discriminant functions are well correlated with the groups (r=0.95 and 0.86 respectively), while the remaining functions are less correlated.

The results for Wilks' lambda are also presented in Table 5.5. It can be seen that after the introduction of the first discriminant function there is significant discriminating information still existing. With the introduction of the second function much of this information is removed. The multivariate F ratio (Table 5.5) also denotes the importance of the first two discriminant functions. Finally, the F probability (Table 5.5) indicates that the probability that the discrimination of the bentonites into separate groups using the first three functions is accidental, or due to random variations, is virtually zero. Therefore the results obtained are meaningful. The aforementioned observations indicate that the first two functions might be very effective for the separation of the bentonite deposits into different groups, if such discrimination exists. Therefore they were used in the construction of a "territorial map".

In the Figures 5.16a,b the results from the plotting of the discriminant scores in the territorial map are given. Although the variation in the Y content might be accidental (see Table 5.4) its influence in the discriminating power of the total number of elements used does not seem to be significant and is restricted to the greated scattering of the points belonging to a particular group. It can be seen that there is a clear separation between the acidic and the indermediate provinces of the Eastern Milos. This separation takes place along the function 1. Moreover, there are distinct subgroups within the two major provinces which cannot be considered as being parts of the same horizon.

There are many similarities between the results from the use of conventional triangular diagrams and that of discriminant analysis. The deposits from Area 1 plot in the same area and are clearly separated from those of the other areas. An exception to this trend is shown by two samples belonging to the higher horizon of the Aspro Horio deposit which plot in the space occupied by the Ankeria deposit. However, it is obvious that the Aspro Horio deposit is associated much closer with the Tsantili and the Zoulias deposits than with the deposits of Area 2.

The samples from the higher stratigraphic horizon of the Ankeria deposit do not seem to be separated unambiguously from their counterparts of the lower horizons. Similarly, there is not any particular relatinship between the samples from the Koufi deposit and the Ankeria deposit.

In a similar way, the samples from the deposits from Area 3 plot in the same area as in the triangular diagrams. The samples from the higher horizon of the Ano Komia deposit plot in the same area of the territorial map in full accordance with the results shown in the triangular diagrams. Moreover, in the same deposit, the samples from the lower horizon

and those which have undergone hydrothermal alteration and come from the parent rock of this bentonite plot in the same area. This, although expected, is opposite to the results found from the use of the triangular diagrams (see Fig. 5.15). The only exception from this trend is exhibited by the sample SM144 (shown with the arrow in the Fig. 5.16).

The bentonites from the deposit of Agrilies plot in the space among the bentonites from the three other areas except for SM250 which plots in the space occupied by the higher horizon of the Koufi deposit. This trend is in full accordance with that observed in the triangular diagrams. Moveover, the sample from the lower bentonite horizon of the Koufi deposit plots in the same area, in full accordance to observations from the triangular diagrams.

The rejection of a number of elements like Rb or Ba from the discriminamt analysis seems to be justified, if the bentonites from the Tsantili, Aspro Horio and Zoulias deposits are considered. Although these bentonites have very similar geochemical characteristics (practically they cannot be separated) the Rb content of the Tsantili bentonites is at least 20 times higher than that of the rest two deposits. This is probably due to the fact that Rb might have been transported by hydrothermal solutions along with K causing illitization of the bentonite. Some Rb might have been present in the authigenic K-feldspar, which is abundant in this deposit. Also the distribution of Ba is very abnormal within individual deposits, probably due to the different influence of the hydrothermal alteration in the different sectors of the deposits. This is expected because the hydrothermal fluids follow certain paths; therefore their distribution patterns are affected by these paths.

The possible role of other authigenic phases present on the information obtained from the discriminant analysis can be observed in the bentonites of the Tsantili deposit (in the northern phase of the deposit, which has not been affected by hydrothermal alteration) which contain abundant authigenic K-feldspar. These benronites have higher K-contents than their counterparts from the Aspro Horio and the 11th horizon of the Zoulias deposit although they seem to have been derived from the same parent rock (compare the K-content of the samples SM100, Tsantili, with that of SM228, Zoulias). Therefore the use of K in the discriminant analysis (see Huff, 1983) might give misleading results in the case of the Miloan bentonites.

The results obtained might shed some light on the chronological order of the deposition of the parent materials of the various bentonite horizons in Eastern Milos. Thus, in Area 3, the deposition of the parent rock of the Rema, Mavrogiannis, Garyfalakena, Kato Komia and the higher horizon of the Ano Komia deposits, postdated the deposition of the parent rock of the lower horizon of the bentonite of Ano Komia. In Area 1 the volcanic activity which produced the 10 lower horizons of the Zoulias deposits took place before the eruption which produced the parent materials in the 11th horizon of the Zoulias deposit, the Tsantili deposit and the Aspro Horio deposit. Finally, if the higher horizon of the Ankeria

deposit (Area 2), which might be defferent from the three lower horizons of this deposit, is indeed related to the volcanic activity which produced the bentonite in the Koufi deposit, then this activity postdates the eruptions which produced the 3 lower horizons of the Ankeria deposit.

The results from the various methods of geochemical fingerprinting, indicate that, notwithstanding the multiple stages of alteration, the bentonites of Eastern Milos can safely be separated into at least 4 different groups which are not related genetically. Each of these groups consists of deposits which have similar geochemical characteristics which might be used for correlation purposes. This possibility is addressed in the following chapter.

CHAPTER SIX

SYNTHESIS

In this chapter an interpretation of the mineralogical and geochemical characteristics of the Greek bentonite deposits is attempted. The topics which are discussed include:

-a) The phase transformations, the geochemical characteristics of formation of the deposits and the possible relationship between the smectites and zeolites present in the deposits.

-b) The compositional variations of the smectite minerals present, the sources of this variation, the differences in the mineral chemistry of smectites derived from different types of parent rocks and the reasons for the variations observed.

-c) The cause and the influence of the hydrothermal activity on smectites, especially in the Tsantili deposit in which mixed layer illite/smectites were formed. Also, the way that the alteration proceeds and the possibility for Ostwald ripening in the growing illite/smectite crystallites.

-d) The mode of crystal growth of smectites and the influence of zeolites in their growth, followed by an examination of the possibility that a process like Ostwald ripening takes place during the formation of smectites.

-e) The possibility for reliable correlation between the various bentonite deposits of Eastern Milos based on geological, geographical and geochemical criteria. Also the effectiveness of the various methods used for the discrimination of the various bentonite horizons of Eastern Milos and the possible use of these methods for exploration of new deposits.

6.1 Formation of the Greek bentonites. Mineralogical and geochemical control.

In the previous chapters it was shown that the Greek bentonites have been formed at the expense of volcanic glass of acidic-intermediate composition. This range of chemical compositions of the parent rocks is commonly observed in areas where alteration to bentonite is observed (c.f Grim & Güven, 1978).

The alteration of a rhyolitic glass begins with an initial hydration process, which involves a cation exchange between the fluid phase and the rock (White & Claasen, 1980, White, 1983, Shiraki & Iiyama, 1990), and might not necessarily lead to dissolution of the glass (Shiraki & Iiyama, 1990). The elements involved in this exchange are mainly alkalies. The exchange properties of the volcanic glass depend on its thermal history, on the Fe_2O_3 content (network former according to the model of Zachariasen, 1932) and on the H_2O content of the glass (Shiraki & Iiyama, 1990). This initial step is followed by solid state diffusion through the leached layer controlled by parabolic kinetics (White & Claasen, 1980, White, 1983, Hodder *et al.*, 1990). On the other hand Si and Al are removed following first

order kinetics from surface dissociation associated with surface retreat (White, 1983). During the alteration Ca also migrates in the solution (Shiraki *et al.*, 1987). Intermediate rocks display similar alteration patterns (Shiraki *et al.*, 1987).

The release of alkalis is balanced by uptake of Mg and $SO_4^=$ by the altered rock (Mottl & Holland, 1978, Shiraki *et al.*, 1987). This feature has been described in many occasions, both experimental and natural, in acidic rocks (Zielinski, 1982, Shiraki *et al.*, 1987), in intermediate rocks (Shiraki *et al.*, 1987) and in basaltic rocks (Mottl & Holland, 1978, Seyfried & Mottl, 1982). In the rocks studied the Mg-uptake is more intense during the alteration of the acidic rock (see Chapter 5).

These exchange patterns were observed in both the alteration profiles examined in Chapter 5. In the Prassa deposit, Kimolos, the alteration seems to be controlled by a $Mg+Fe+SO_4^=$ for Na+K+Si exchange between the parent rock and the fluid phase, which might be evolved sea water. Al and perhaps Ca behave residually. The uptake of $SO_4^=$ is confirmed by the precipitation of phases like barytes and gypsum. In the Zoulias deposit, Milos, the trends observed are similar as far as the alkalies, Fe and Mg are concerned, but it seems that Si remains in the parent rock and Ca is removed during the alteration process.

In the Prassa deposit, Kimolos, the massive removal of Si and the alkali cations from the parent rock and the uptake of Mg must have taken place through a vigorous reaction, because the exchange between the rock and the fluid phase involved a large mass transfer. This indicates that the water:rock ratio might be high. In this text the term water:rock ratio follows the definition of Mottl & Holland (1978), *i.e* the total amount of water passing through the altered rock divided by the mass of the altered rock. A high fluid:rock ratio indicates permeable zones. This is in accordance with the observation that the altered zones are determined by faulted zones which are compatible with high water:rock ratios and a fully open system.

The ion exchange results in an increase of the alkalinity and the Na, K and Si content of the fluid phase in contact with the glass (*i.e* increase in the $(Na^+ + K^+)/H^+$ activity ratio; that is an increase of salinity and pH), if the system is sufficiently closed (Hay & Sheppard, 1977). Smectite is generally formed in the initial stages of the alteration (c.f Sheppard & Gude, 1968, 1973, Dibble & Tiller, 1981, Hay & Guldman, 1987) in which the $(Na^+ + K^+)/H^+$, *i.e* its salinity and alkalinity, is probably low (Sheppard & Gude, 1968, 1973). This is because the formation of zeolites instead of smectite is favoured by high $(Na^+ + K^+)/H^+$ activity ratios (Hess, 1966). The initial removal of Si and alkalies might provide the favourable physical and chemical conditions to form smectite probably following first order kinetics (Hodder *et al.*, 1990). The formation of smectite took place probably from a poorly-crystalline phase (Plate 9). However, in a siliceous rock the original Si:Al ratio is much higher than that of smectites and much closer to that of zeolites. In an

intermediate rock the ratio is lower, but still higher compared to smectites. The pH of the Greek bentonites (see chapter 8) is neutral to slightly alkaline implying pore waters of similar acidity. Since at such pH conditions Al is not readily released from the glass (Mariner & Surdam, 1970, White, 1983) it follows that:

-a) Si must be removed from the glass in order to keep the optimum Si:Al ratio for the formation of smectite.

-b) The smectites probably did not precipitate from the fluid phase but by reaction between the leached glass and the pore fluid which is rich in Mg.

In the deposits studied smectite is the predominant phase formed during the alteration despite the adversity for their formation in a closed system. On the other hand, zeolites (clinoptilolite/heulandite and mordenite) are present only in a small number of deposits. The pH of the fluids in contact with the parent rock does not seem to be the reason for the predominance of smectite instead of zeolites. This can be seen in the Prassa deposit, Kimolos, where the mordenite rich zone is characterized by pH values very similar to the adjacent mordenite-free zone (see chapter 8).

The non-equilibrium kinetic model proposed by Dibble & Tiller (1981) might explain the formation of smectite instead of zeolites. According to this model the formation of the various authigenic phases is controlled by the Ostwald step rule which states that the most likely phase to form is not nessecarily the most stable thermodynamically, and that equilibrium is gradually approached through a sequence of irreversible steps. If the dissolution rate of the volcanic glass is high relative to the growth rate of the authigenic silicates, then the bulk solution might be supersaturated with respect to many phases, the fastest growing phase being the dominant forming one. Under such conditions the nucleation of a more soluble phase (thus metastable) is favoured over a less soluble one (*I.e* more stable) because it has lower mineral-solution interfacial energy (Steefel & Van Cappellen, 1990).

Whether or not a phase will precipitate depends on the supersaturation of the bulk solution. Under conditions of high supersaturation phases like smectites and Al-silicate gels are favoured over alkali-zeolites or analcime and/or K-feldspars. Alkali-zeolites like mordenite and clinoptilolite/heulandite are favoured by conditions of intermediate to high supersaturation, whereas analcime and K-feldspars, which are the most stable phases are probably formed under low superaturation conditions (Dibble & Tiller, 1981). However, the nature of the parent glass significantly affects the reaction process (Iijima, 1980), because the volcanic glasses of intermediate composition are significantly richer in Ca, Mg and Fe compared to their acidic counterparts (see Fisher & Schmincke, 1984 p. 17).

The system dissolving glass-intermediate pore fluid or *local fluid*-authigenic phase is closed, if the "sink" of the chemical elements released from the alteration of the glass is the authigenic phase. The pore fluid outside the microsystem need not affect the reaction. The

mineralogical assemblage will be affected only if the outside pore fluid act as a sink (*i.e* removes the released components) or is a supplier of chemical components. Under these conditions, smectite formation is favoured only in the primary stages of alteration not only because of the highest supersaturation at that stage (Dibble Tiller, 1981) but also due to the fact that the $(Na^+ + K^+)/H^+$ ratio might be lowest at the incipient stages of alteration of the volcanic glass as stated before.

If the released alkalies are removed (*i.e* the system is fully open and the outside pore water acts as a sink), the formation of smectites instead of zeolites is favoured. In such a case the alteration phases do not form away from the dissolved surfaces (c.f Dibble & Tiller, 1981), leading to the pseudomorphic textures observed in Plate 12. Geochemical evidence (Chapter 5) has shown that the system in which the Greek bentonites were formed was fully open, *I.e* the fluid phase acted as a sink.

The Si released from an acidic rock precipitates as a free silica phase or migrates out of the system. Large scale release of Si has been observed in experiments with acidic rocks at low temperatures (White & Claasen, 1980, White, 1983) and at high temperatures (Shiraki, *et al.*, 1987). However, bentonites derived from intermediate rocks are less rich in free silica. This is expected because the smectite which is the main alteration phase has an Si:Al ratio closer to that of the parent rock. In other words the Si-content which has to be removed from the system and/or to precipitate in the form of a silica phase, in order to keep the proper Si:Al ratio, is smaller. An intermediate rock also has a greater Mg content which is a major constituent of the smectites. This means that the Mg-content which has to be added to the system is significantly less than to an acidic rock.

The above discussion suggests that the predominant alteration products of an acidic rock at low temperatures should be zeolites with minor smectite if the system is closed, and smectite + a silica phase (usually opal-CT) if it is fully open. In the former case smectites are formed only in the incipient stages of alteration. If the system is semi-open zeolites are expected to coexist with smectites and a silica phase is abundant suggesting that alkali-migration has occured to some degree. This situation is believed to have taken place in the deposits of Garyfalakaina and Zoulias (Milos), Loutra (Kimolos) and the minor bentonite bodies in the Prassa deposit (Kimolos). If the excess Si is removed from the system, smectite ± alkali-zeolites are expected to be the alteration products, the presence of zeolites being controlled by the removal of alkalies i.e the $(Na^+ + K^+)/H^+$ activity ratio. Opal might be present in trace amounts. This situation has been observed in the Prassa deposit of Kimolos in the smectite and the mordenite zone. Indeed in Figure 5.3 it can be seen that the smectite zone is chemically distinct from the zeolite zone in that it has been leached of alkalies and Si and is more enriched in Mg. Restricted Si-removal has taken place in the zeolite zone also.

It is expected that bentonites derived from acidic rocks have inferior physical properties due to the presence of abundant opal-CT unless the excess silica is removed (e.g compare the physical properties of the bentonites from the Area 3 of Milos with those of the smectite zone in the Prassa deposit, Kimolos, which are presented in the following chapters). On the other hand, intermediate rocks are expected to be more suitable bentonite precursors in a fully opened system, because their composition is closer to that of smectite after the removal of alkalies. This assumption might explain the fact that most bentonite deposits have been derived from dacitic precursors (c.f Grim & Güven, 1978).

Smectites have also been formed from precursors other than volcanic glass. This study showed that both plagioclase and, less often, K-feldspar have been replaced to various degrees, confirming the findings of Christidis (1989). Similar alteration was reported by Banfield & Eggleton (1990). The alteration might proceed through a Mg for Ca (in plagioclase) or K (in K-feldspar) exchange (see chapter 4). The released Ca might provide the source for a range of Ca-bearing minerals like calcite or gypsum which are abundant in several deposits. This process occurs more often in the deposits of the Areas 1 and 2 of Milos which are intermediate and therefore more abundant in Ca-rich plagioclase. These deposits contain varying contents of calcite.

One of the most interesting features of several bentonite deposits from Milos island is the existence of abundant authigenic K-feldspar, which indicates that the alteration of the parent glass was a low temperature process (Kastner & Siever, 1979). Authigenic K-feldspar is present in all three areas of Milos island regardless the composition of the parent rock and confirms the geological observations about the formation of the Miloan bentonites by devitrification of volcanic glass rather than by hydrothermal activity. The existence of authigenic K-feldspar in bentonites has been reported by Jeans *et al.* (1977), Pablo-Galan (1990) and Altaner & Grim (1990). The occurence of K-feldspar indicates that after the formation of smectite the K/H^+ activity ratio and the Si activity of the pore waters was high (Kastner & Siever 1979). The K-feldspars might have been formed either through the transformation of a zeolite precursor or from a gel precursor, because epitaxial development over a detrital precursor was not found.

The formation of K-feldspar from zeolite precursors has been reported in alkaline environments (Sheppard & Gude, 1968, 1973, Surdam, 1977, Surdam & Sheppard, 1978, Hay & Guldman, 1987), in saline environments (Boles & Surdam, 1979), and in diagenetically altered tuffaceous rocks in open hydrological systems at deep burial depth (Hay & Sheppard, 1977). The formation of K-feldspar from a gel precursor and not from a zeolite has been reported by Noh & Boles (1989). In the Greek bentonite deposits the pH of the pore waters did not reach the high values observed in an alkaline lake. This can be seen from the pH measurements (see Chapter 8), and from the lack of indicative minerals like searlesite, trona and/or gaylussite (c.f Sheppard & Gude, 1968, 1973). This is

expected, because the occurrence of smectite as the predominant phase indicates a fully open system. Also, it is certain that the deposits were never deeply buried. It is thus believed that the formation of K-feldspar took place in a saline and probably slightly alkaline environment similar to that described by Altaner & Grim (1990). Such an environment seems to be similar to that described by Noh & Boles (1989). The difference with the latter case is that in Milos the environment was marine and the alteration extensive. As far as the K-feldspar precursor is concerned, although the conversion of zeolites cannot be rejected, the formation from a gel-like material seems more plausible at least in the case of the Koufi, Tsantili and Ano Komia deposits. This is because in these deposits zeolites were not found. On the other hand, in the deposits of Garyphalakaina and Zoulias formation of the K-feldspar from a zeolite precursor should not be excluded, since in both deposits clinoptilolite and mordenite are present. In any case the formation of K-feldspar is favoured by high K^+/H^+ activity ratio and high Si activity (Sheppard & Gude, 1968, 1973, Boles & Surdam 1979, Kastner & Siever, 1979) as well as increased salinity (Boles & Surdam, 1979).

A high K^+/H^+ activity ratio and a low Na^+ activity might have been favoured by the pH of the solution and/or by the cooling history of the glass. Alteration of glass at neutral-slightly alkaline conditions leads to pore solution composition with high Na^+/K^+ activity ratios compared to the parent rock because Na is preferentially leached (White & Claasen, 1980). This leads to high K^+/Na^+ activity ratios in the altered area of the glass. Since the system was fully open, the leached Na^+ was removed through fluid flow. The leached glass might provide the parent material for the formation of a gel having the high K^+/Na^+ activity ratios necessary for the formation of K-feldspar. Alternatively, if the cooling rates of the glass precursor are high, then the water/rock interaction will lead to high $K^+/(K^+ + Na^+)$ activity ratios in the altered rock and high $Na^+/(Na^+ + K^+)$ ratios in the fluid phase (Shiraki & Iijama, 1990). Such conditions favour K-feldspar especially because the Na-rich fluid phase is removed (the system is fully open). Of course both alternatives might occur simultaneously.

Although there is little doubt that the formation of smectite instead of zeolites took place because of the removal of the alkalies released from the dissolution of the volcanic glass through fluid flow (*i.e* the pore fluid acted as a sink), it is not clear <u>why</u> this fluid flow occured. Since the bentonites were formed under marine conditions gravity-driven flow does not exist because the sea-level is the base level for sediments (c.f Hay & Guldman, 1987). Similarly, compaction is not a plausible reason because the parent rocks were never burried under a large overburden. Pressure-driven flow derived from influx due to compaction of surrounding rocks is also rejected because these rocks are also volcanics which have been burried in similar depths. Furthermore, the basement where it is exposed consists of metamorphic rocks (Wetzenstein, 1969), which were metamorphosed long

before the volcanic eruptions which produced the parent rocks of the bentonites (Altherr *et al.* 1979). The remaining possibility is to assume that the flow is heat-driven. Since the hydrothermal genesis (and thus the possibility for localized heat sources) has been rejected, the reason should be sought elsewhere. Again the possibility for influence of the geothermal gradient is rather small because the thickness of the deposits does not exceed 50-60m.

In most cases the parent rocks of the bentonites are volcaniclastic rocks, probably pyroclastic flows. This has been assumed after examination their geometry, dimensions, and textural features (wherever they have been preserved from the intense alteration). Although it is not certain whether they were erupted under submarine or subaerial conditions and subsequently submerged under the sea level, it is well known that under subaerial conditions the emplacement temperatures may vary between 300 and 850^{o}C (Fisher & Schmincke, 1984, p. 211, Cas & Wright, 1988, p. 97), according to the mechanism of the eruption (Sparks *et al.* 1978). After the eruption little heat exchange takes place, since the pyroclastic flows are good heat-conserving mechanisms (Fisher & Schmincke, 1984).

When a pyroclastic flow enters the sea it reacts with the sea water which is absorbed onto the glass shards (Sparks *et al.* 1980). This reaction causes cooling of the material. Since the temperature of the glass is much higher than that of the sea water a thermal gradient is expected to form. This gradient might be the reason for the existence of the fluid flow during the formation of bentonite. Also a possible temperature variation in the various sectors of the material might cause fluid flow. A possible dissadvantage of this model is that the pyroclastic flow might be coherent and might not allow water to penetrate throughout its entire mass.

If the eruption is subaqueous, then the fragments are expected to react more thoroughly with water. Although temperatures from subaqueous pyroclastic flows have not been reported, a thermal gradient between the colder sea water and the significantly hotter flow might occur. Weaver (1989 p. 378) attributed the lack of alteration in many volcanic glasses present in the oceans to the source of the glass: if the eruption is submarine then alteration takes place easier. This might have happened in the deposits where alteration is complete. In the Prassa deposit, if the ignimbrite was erupted in a subaerial environment and submerged later the sea water might not have found access to the entire rock but only through faulted zones.

In any case, the alteration is believed to be controlled by a vigorous reaction between a relatively warm glassy rock and a cold fluid phase. The water/rock ratio, and the temperature and the composition of the fluid flow during the reaction are believed to be the crucial factors which drove the alteration of a volcanic glass to bentonite and determined

the alteration products in the Greek bentonites. The occurrence of authigenic K-feldspar indicates that the temperature, at least during the precipitation of this phase, was very low.

A rather different situation is believed to have taken place in the case of the bentonites of Chios. Due to the intimate mixing of the volcaniclastic material with the carbonate sediments and the intense alteration which has destroyed any textural evidence, the exact nature of the parent tuffs is not known. The material has been described as "lightweight tuff" (Besenecker *et al.* 1968) and ignimbrite (Besenecker & Pichler, 1974). The composition of the parent material was trachyandesitic-andesitic (see chapter 5). However the Mg content of the rock is much higher than that of the average andesite or trachyandesite (see Fisher & Schmincke, 1984), especially if the contamination with the carbonate sediments is taken into account. Two possibilities for the possible source of Mg can be considered:

a) The parent rock was more basic. In that case the coexistence of aragonite, calcite and dolomite in the bentonite might probably be associated with the formation of the bentonites. The excess Mg which was released from the intermediate-mafic glass shards during the formation of smectite was consumed to convert the Ca-carbonates to dolomite. However, such an assumption is rather unlikely. If it is assumed that the rock was a basalt then it would be richer in Mg. However, its Fe content should also be much higher, and so should the Ti content. Although contamination by sediments has taken place, the ratio of volcanics:sediments should be less than 1:10 to explain the very low Ti-content. However the smectite is a major phase in all samples examined. Since it has been derived from the volcanic glass it follows that the ratio is much higher.

b) The excess Mg has been transported from an external source. Since there is not any evidence for hydrothermal alteration in the area, the origin of the Mg-rich fluids might be looked for in the dissolution of Mg-rich phases like talc, serpentine, Mg-chlorite and/or amphibole which are present in the underlying sands, the overlying red clay beds and/or the bentonite body itself. The presence of such phases suggests that the Neogene basin might have been supplied from an ultrabasic rocks province (probably ophiolites which are very common in both Greece and Turkey). Another possible source is the dolomitic rocks which are abundant in the Alpine basement.

An additional problem is caused by the presence of abundant opal-CT in the bentonite. Such an abundance is not compatible with the composition of the parent rock and it might be explained if it is assumed that the source of the Si was biogenic, *i.e* diatoms. The formation of the opal-CT might have taken place through a transformation of pre-existing opal-A, which had been formed from the dissolution of diatom frustules. If, however, the parent material was a more acidic rock than trachyandesite (i.e rhyolite or rhyodacite), then the source of the silica phase is not nessecarily biogenic. The presence of an acidic rock would explain the low Ti-content and would suggest that the use of the diagram of

Winchester & Floyd (1977) is not reliable for determination of the chemistry of the bentonite precursors. However, as shown in Chapter 5, the intense alteration in Kimolos (Prassa deposit) and Milos (Zoulias deposit) does not seem to affect the ratio Zr/Ti (*i.e* both Zr and Ti were strongly immobile). This suggests that the parent rocks could not be more acidic than a dacite, even in the case that enough Y has been mobilized during the alteration (see figure 5.2). Consequently, at least some of the opal-CT might be biogenic.

6.2. Compositional variations of smectites. Role of the chemistry of the parent material.

6.2.1. Compositional variations of the Greek smectites.

The discovery of a large variation in smectite composition between crystals in the same sample shows that the average structural formulae presented in the literature do not provide sufficient indications about the range of variation of the smectite population in individual samples. Consequently they cannot be considered representative of the total sample in any case and the information they provide must be regarded always with care. It is also evident that the assignment of a particular sample into a certain field in the "smectite triangle" (Güven, 1988) leads to an oversimplification of the smectite compositional variation. Furthermore, a large number of smectites plot outside the proposed "fields". Thus, in the Areas 1 and 2 of Milos a number of points plots between the Wyoming-type and the Fe-rich type montmorillonite "field", while a large number of the montmorillonites from Kimolos plot between the "fields" of Chambers and Tatatilla type. This suggests that it is necessary to obtain a greater number of analyses before the compositional fields of smectites be determined.

The great variation in smectite composition among adjacent crystals, confirms previous reports of heterogeneity of smectites (Byrne, 1954, McAtee, 1958a,b, Grim & Kulbicki, 1961, Tettenhorst & Johns, 1966, Stul & Mortier, 1974, Lagaly & Weiss, 1975, Lagaly *et al.*, 1976, Lagaly, 1981, Goulding & Talibudeen, 1980, Talibudeen & Goulding, 1983, Nadeau *et al.*, 1985, Lim & Jackson, 1986, Goodman *et al.*, 1988). The source for this heterogeneity is located in the following areas:

a) proportion of tetrahedral charge relative to octahedral charge,

b) variable substitutions in octahedral positions

c) relative abundances of the exchangeable cations and

d) variation of the total layer charge.

Although Cheto smectites fullfil the compositional criteria nessecary to be plotted in the appropriate "fields" of Güven's triangle, they do not comply with the layer charge criteria determined by Schultz (1969), but possess a low layer charge. Possible reasons for that may be i) the assignment of the total number of Mg cations to octahedral sites, ii) the

assumption that octahedral Fe is present only in ferric state, and iii) loss of exchangeable Na and/or K cations. Alberti & Brigatti (1985) concluded that there is no reason for Mg cations to be assigned in interlayer positions. However, in many exchangeable cation determination analyses Mg is present in considerable amounts (see Weaver & Pollard 1973). Christidis (1989) found that in montmorillonites from Zoulias quarry, equivalent to SM228, Mg occupies nearly 50% of the exchangeable sites. Although hydrolytic extraction of Mg from octahedral sites is possible (see Alberti & Brigatti 1985), it cannot explain such a large exchangeable Mg content.

The smectites from the Area 3 of Milos, especially the beidellites, are characterized by a high tetrahedral charge and a high occupancy of Al^{VI}. Thus, it is not reasonable to assign all the existing Mg in octahedral sites. Moreover, the assignment of the Mg entirely in octahedral sites gives an unusual low interlayer occupancy which cannot be explained simply by a loss during the microanalysis, unlike the case described by Banfield *et al.* (1991b) who found a high octahedral-Mg occupancy and a high interlayer cation content (K-stevensite). It seems therefore, that a proportion of Mg cations might exist in exchangeable sites, in smectites from Chios, in smectites (particularly in beidellites) from Areas 2 and 3 in Milos and those from Kimolos. However, since the *actual* total number of octahedral cations is not known, it is impossible to determine the exact number of exchangeable Mg.

The oxidation state of iron might also be a possible reason for the low layer charge values. This is certainly the case for the smectites from Area 2 of Milos as well as those from the Prassa deposit of Kimolos. Although it is generally believed that ferrous iron is usually present in small amounts (Weaver & Pollard, 1973, Grim & Güven, 1978, Güven 1988), there are reports (Elzea & Murrey, 1990) of smectites with Fe^{3+}/Fe^{2+} ratios as low as 0.05. It is well known that the oxidation-reduction process is easily triggered, is reversible and is associated with structural changes in smectite (Stucki *et al.* 1984, Lear & Stucki 1985). Since, the bentonites examined were exposed for some time under atmospheric conditions, it is possible that most Fe will be in the ferric state. However, this by no means excludes the possibility that within each sample the degree of oxidation varies, and consequently there might be positions where some Fe is in the ferrous state. This is especially true for the smectites in the Prassa deposit, Kimolos, since it has been shown (see Chapter 5) that the Fe must have been transported in the system in the ferrous state. Unfortunately, it is impossible to determine the exact amount of ferrous iron with microprobe techniques.

The loss of exchangeable alkali-cations, mainly sodium, during microanalyses via volatization and/or evaporation also contributes to a low interlayer charge. The influence of sodium loss to the quality of the microanalyses was determined using the data of one microanalysis from the samples SM16, SM66 SM135 and SM235 and the results are given

in Table 6.1. It is obvious that sodium loss does not affect the relative proportions of the octahedral cations. Therefore the geochemical variations in the smectite triangle (Güven, 1988) are real and are not affected by any loss of sodium. On the other hand, the projections in the diagram of Velde (1985) are affected because alkalies are taken into account. However, for Ca-smectites the loss is not very important; thus the trends obtained for the smectites from the Areas 1 and 2 of Milos are considered to be significant.

6.2.2. Implications for smectite formation

There is a well defined negative relationship between Al^{VI} and the other octahedral cations and between Si and total Al in all smectites analysed from the Areas 1 and 2 of Milos. In the Area 3 of Milos as well as in Kimolos and Chios Al^{VI} is related with Mg but not very well with Fe^{3+}. In these areas it seems that the chemistry of the smectites is controlled by the relative abundance of Si and Al which exhibit a well expressed negative relationship. On the other hand any correlation between other octahedral cations or between octahedral and tetrahedral cations is lacking. Nevertheless, there are some horizons or particular sectors of a horizon (for example SM228 in Area 1 of Milos and the samples from the Prassa deposit, Kimolos) which display definite relationships especially where Mg is involved. This behaviour is believed to be relevant to the conditions which prevail during the formation of bentonites within small domains of the parent rock.

The parent rocks in Area 2 possibly had dacitic-basic dacitic composition, while those in Area 1 were of andesitic composition. On the other hand the bentonites of Area 3, Milos and those of Kimolos were derived from acidic rocks. Interaction of a glassy rock of andesitic or more acidic composition with sea water involves mobilization of alkalies and Ca from the glass, while Mg and $SO_4^{=}$ migrate to the host rock (Shiraki *et al.* 1987). According to Zielinski (1982) the Mg content might increase up to 15 times during conversion of rhyolites to bentonite. In the case of rocks of dacitic-andesitic composition there is considerable Mg present which nevertheless is lower than that present in smectites (see Fyticas, 1977 for representative analyses of andesitic and dacitic rocks from Milos). This means that some Mg must be added from an external source which in this case is sea water. Mg supply is more pronounced in the case of an acidic rock and this is certainly the case in Kimolos.

Interaction of water with a glassy rock involves an ion exchange as described in the previous section. According to the glass model of Zachariasen (1932) alkalies and alkaline earth elements are network modifiers; consequently they might easily be released into the fluid phase. It seems however that although alkalies and Ca readily migrate from the area of dissolution, Mg is essentially immobile. If it is assumed that the Mg-content of sea water reacting with the glass is constant, then the variations in the Mg content of smectites of

Table 6.1

Influence of the loss of sodium on the projection of the smectites on the smectite triangle (Güven, 1988). The first analysis for each sample is the original one. The second represents total loss of Na while the third assumes existence of 1.5% Na in the smectite. The major influence of the Na-loss is in the number of octahedral cations. Note the lack of variation of the octahedral coordinates with variable degrees of Na-loss.

Sample	SM16	SM16	SM16	SM66	SM66	SM66	SM135	SM135	SM135	SM235	SM235	SM235
Deposit	BMAN	BMAN	BMAN	BMK1	BMK1	BMK1	BMAK	BMAK	BMAK	BMRM	BMRM	BMRM
SiO_2	53.52	53.52	53.52	54.24	54.24	54.24	50.94	50.94	50.94	47.82	47.82	47.82
Al_2O_3	18.19	18.19	18.19	19.03	19.03	19.03	28.04	28.04	28.04	20.71	20.71	20.71
Fe_2O_3	5.08	5.08	5.08	4.06	4.06	4.06	0.86	0.86	0.86	1.01	1.01	1.01
MgO	3.90	3.90	3.90	4.10	4.10	4.10	1.04	1.04	1.04	2.38	2.38	2.38
CaO	1.52	1.52	1.52	0.69	0.69	0.69	- -	- -	- -	0.79	0.79	0.79
Na_2O	0.54	- -	1.50	0.98	- -	1.50	0.40	- -	1.50	0.69	- -	1.50
K_2O	0.51	0.51	0.51	1.06	1.06	1.06	0.44	0.44	0.44	0.44	0.44	0.44
Structural formulae based on 11 oxygens												
Tetrahedral cations												
Si	3.84	3.86	3.82	3.84	3.87	3.83	3.62	3.63	3.60	3.79	3.81	3.77
Al^{IV}	0.16	0.14	0.18	0.16	0.13	0.17	0.38	0.37	0.40	0.21	0.19	0.23
Octahedral cations												
Al^{VI}	1.38	1.40	1.35	1.43	1.47	1.42	1.97	1.99	1.93	1.73	1.75	1.69
Fe^{3+}	0.27	0.28	0.27	0.22	0.22	0.22	0.05	0.05	0.05	0.06	0.06	0.06
Mg	0.42	0.42	0.41	0.43	0.44	0.43	0.11	0.11	0.11	0.28	0.28	0.28
VICations	2.07	2.09	2.04	2.08	2.12	2.06	2.13	2.15	2.09	2.07	2.10	2.03
Interlayer cations												
Ca	0.12	0.12	0.12	0.05	0.05	0.05	0.00	0.00	0.00	0.07	0.07	0.07
Na	0.08	0.00	0.21	0.13	0.00	0.21	0.06	0.00	0.21	0.11	0.00	0.23
K	0.05	0.05	0.05	0.10	0.10	0.10	0.04	0.04	0.04	0.04	0.04	0.04
Coordinates for the smectite triangle (Güven, 1988)												
AlAl	1.33	1.34	1.32	1.38	1.38	1.37	1.85	1.85	1.85	1.67	1.67	1.67
$Fe^{3+}Al$	0.26	0.26	0.27	0.21	0.21	0.21	0.04	0.04	0.04	0.06	0.06	0.06
MgAl	0.40	0.40	0.41	0.42	0.41	0.42	0.10	0.10	0.10	0.27	0.27	0.27

adjacent small domains might be due either to small scale migration of the released Mg in the microenvironment or to different degrees of Mg-uptake from the fluid phase in the different domains of the altered glass, or both. In other words, the fluid phase contributes to the variations in the Mg-content.

In the case of the smectites from Areas 1 and 2 of Milos small scale migration is expected also for Fe, which might be either a network former (ferric state) or a network modifier (ferrous state). Since Fe^{2+} is mobile it might be released into solution (Shiraki *et al.* 1987) and migrate for larger distances if the oxygen fugacity is low, or it might be bound in a mineral phase like smectite and/or iron oxides. Since Fe displays a near perfect negative relationship with Al and Al is immobile under the conditions of bentonite formation (Zielinski 1982, White 1983) it follows that some Fe must be released from the original site, and that this release is accompanied by a concomitant migration of other elements like Mg and/or Si (and/or differential selectivity of Mg from the fluid phase in the different domains) keeping the the appropriate cation ratios. To check this possibility Fe^{3+} and Al^{VI} were plotted with Si and Mg in triangular diagrams (Fig. 6.1a,b). It is obvious that the negative relationship displayed by Al^{VI} and Fe^{3+} is controlled by variations of both Si and Mg. Also, the role of Mg is less well defined. In both areas two trends can be observed when Mg is involved. In the sample SM228 (Area 1) it seems that the control of Mg in Fe for Al substitution is of major importance, while in the other samples from this horizon the substitution is mainly controled by the tetrahedral charge since the Mg content is essentially constant over the total range of Al^{VI}/Fe^{3+} ratios.

In Area 2, beidellites display the opposite trend compared to the montmorillonites, since in the former increase in the Mg-content is associated with an increase in the Fe-content while in the latter by a decrease. The above trends indicate that different chemical elements control the formation of different types of smectites. Furthermore, the fact that almost the same extent of chemical variation observed in individual samples characterizes the whole bentonite horizon from which the samples come indicates that the microenvironmental chemistry is very significant for the formation of smectite. It is also interesting that the compositional trend of SM228 follows the path of the smectites from Area 2 and not that of the smectites from Area 1 although it belongs to the same horizon. This indicates that the compositional signature of montmorillonites belonging to a particular type is not affected only by the chemistry of the parent rock.

In the smectites derived from acidic rocks the trends observed using the same diagrams are not well expressed. This might be due to the small amount of Fe present in these smectites (reflecting the small Fe-content of the parent rock), since the role of one of the major factors affecting the chemical variation is removed. When Si is plotted vs Al^{VI} and Fe^{3+} the negative relationship between Al and Fe is associated by a concomitant variation of Si (Fig 6.1d). When Mg is plotted against Al^{VI} and Fe^{3+} no specific trend is observed

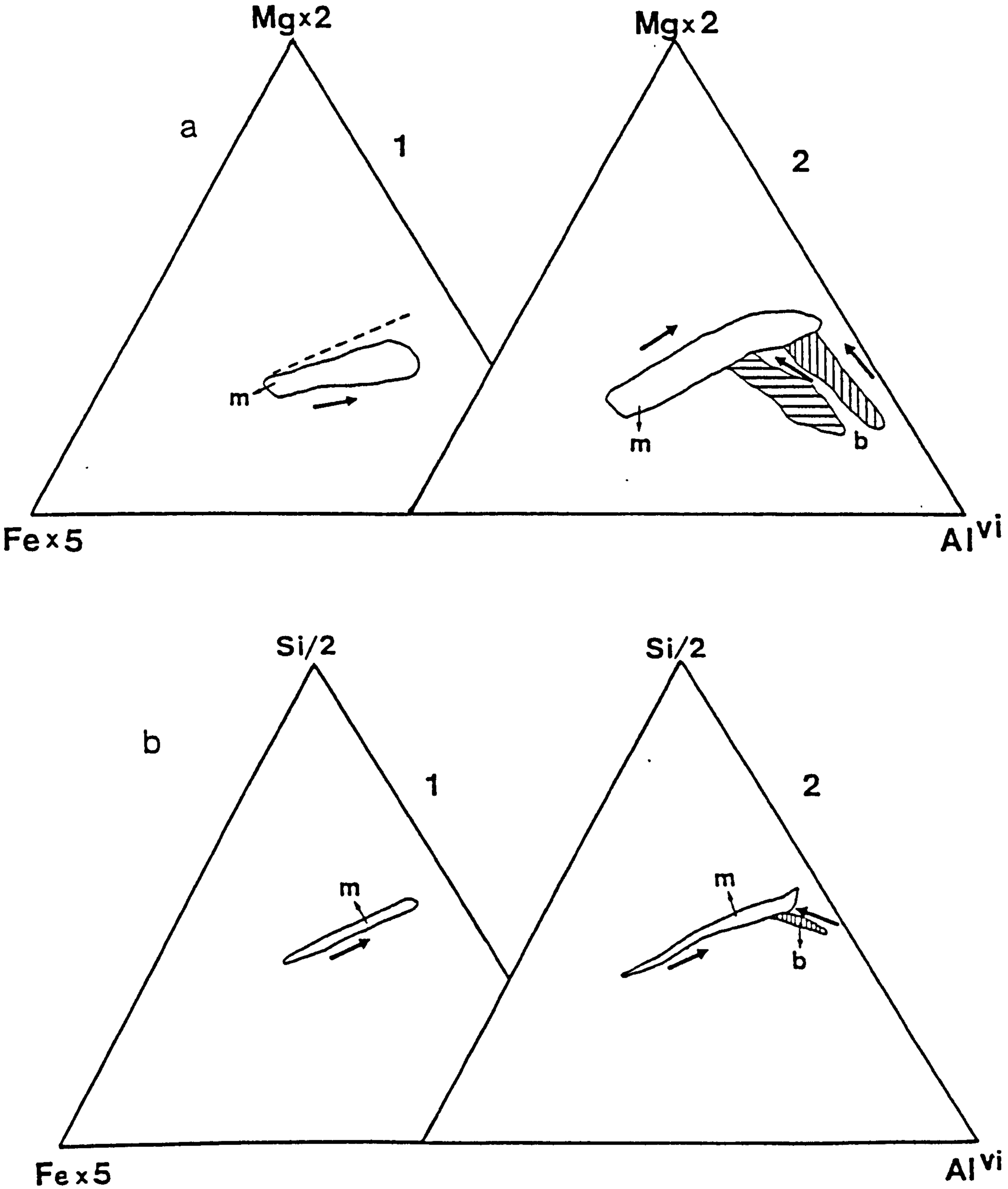

FIGURE 6.1. Triangular diagrams showing the compositional trends of the smectites in Milos (a),(b) and Kimolos and Chios ((c), (d). 1,2,3=Areas 1,2,3 of Milos respectively, 4=Kimolos, Chios. The thick arrows indicate the compositional variations. The empty fields correspond to montmorillonite (m), while the hatched fields to beidelite (b). The vertical and horizontal hatching in (a) (b) correspond to the beidellites from the lower and the main horizon of the Koufi deposit respectively. In (c) vertical and oblique hatching corresponds to beidellites from the lower and higher horizons of the Ano Komia deposit respectively, and horizontal hatching to beidellites from the Mavrigiannis deposit. The dashed line in (a) indicates the trend of the smectites in SM228 (Zoulias deposit).

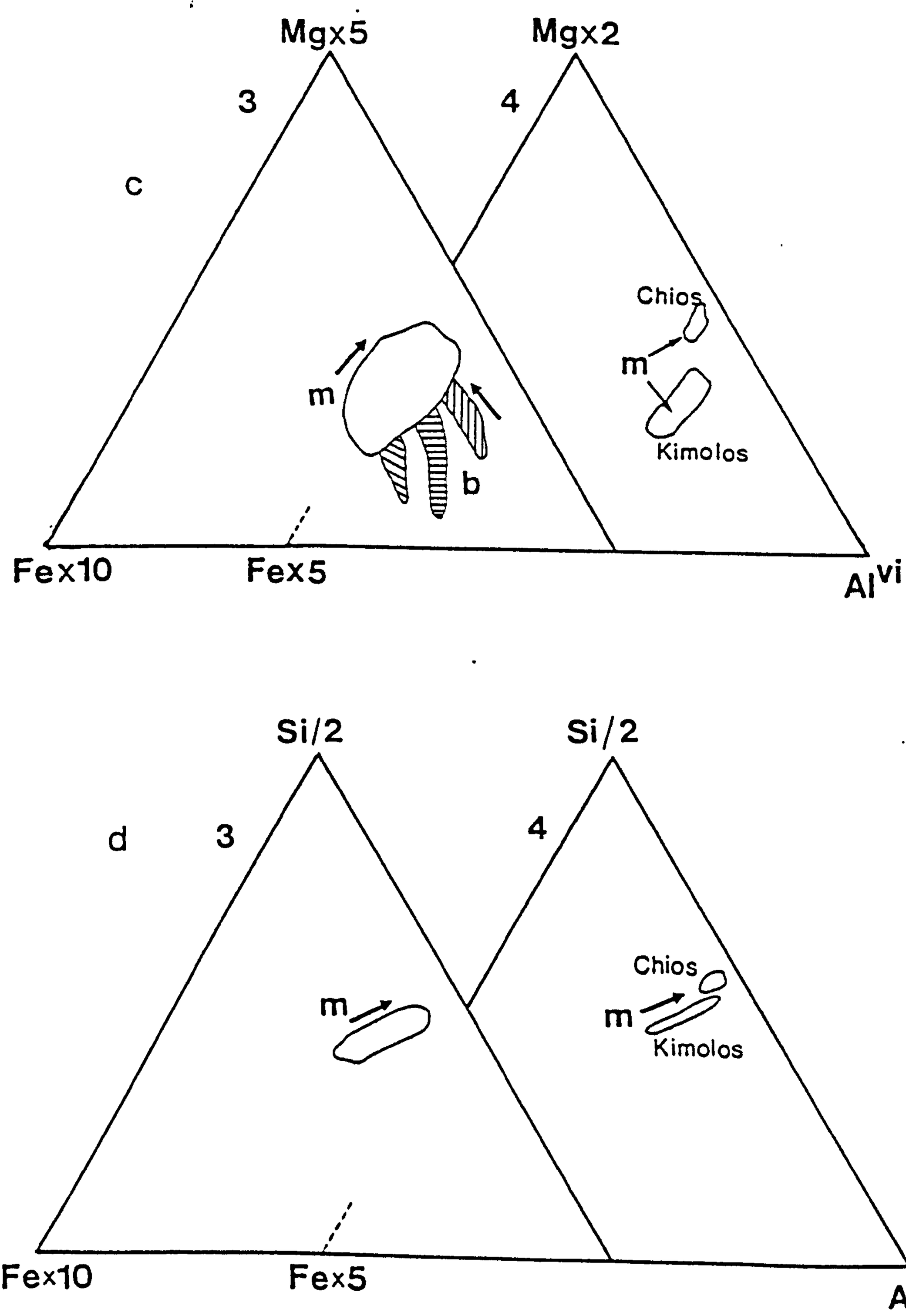

FIGURE 6.1 (continued).

in the samples from Kimolos and Chios (Fig 6.1c), whereas large scattering is observed in Area 3 of Milos (Fig. 6.1c). This scattering is believed to be due to the assignment of the total Mg in octahedral sites. Nevertheless certain trends can be observed, which in general are fairly similar to those from Areas 1 and 2 of Milos. Thus in the beidellites an increase in their Mg content is escorted by an increase in the Fe content, opposite to the trend displayed by the montmorillonites present in the area.

Although the smectites from the Prassa deposit, Kimolos contain about 0.15-0.20 atoms of Fe^{3+} per half unit their Fe content does not vary. The same is also true for Mg. This lack of chemical variation is a significant difference compared with the smectites of Areas 1 and 2 from Milos. A possible reason for this difference is that in Milos the source of Fe and Mg was principally the parent rock (especially for Fe), while in Kimolos both elements were transported into the system in large amounts through fluid flow. It is believed that the ample supply of these elements in the permeable zone due to the high water:rock ratio might have led to a more uniform distribution in the system. On the other hand in Milos small scale migration and/or different degree of uptake from the pore fluid might cause the chemical variations observed. In Area 3 of Milos in which the Fe content of smectites is small, the main source of variation is the distribution between Al and Mg. It is obvious that the variation is much more significant than this of the Prassa deposit. This is related to the fact that in this area the degree of mass flow to the system is small and is associated with a relative small supply of Mg from the fluid as in Areas 1 and 2.

The fluid phase adjacent to the dissolved glass is supersaturated in Mg and perhaps alkalies with respect to smectite. In the case of an intermediate rock with about 60% SiO_2 the amount of silica which must be removed to create the Si/Al ratio nessecary for the formation of smectites observed is relatively low. On the other hand large quantities of Si must be released from an acidic rock to make the optimum Si/Al ratio. The supersaturated fluid might react with the depleted Si-Al network which has lost its initial structure partially or totally providing Mg, and smectites precipitate. Alternatively, after the initial release of cations and diffusion through the leached layer, the Si-Al network is destroyed, Al and Si are released into the solution and smectite precipitates. However, it is known that at neutral pH Al hardly migrates into the solution while Si is released more readily with a linear release rate (White 1983). Consequently the latter is less probable. Since the whole process is fast and is accompanied by a retreat of the dissolved surface of the glass (White 1983), the smectite formation must be controlled by fast growth rates to keep the mass balance (Dibble & Tiller, 1981).

The coexistence of beidellite with montmorillonite and/or montmorillonites with considerable variation in their tetrahedral charge, having Si/Al ratios smaller than that of the parent glass, especially in the case of acidic rocks, within distances not greater than 200-300μm indicates that the reaction rate controlling the release of Si is not of the same

order in the various small domains of the parent rock. This might be due to microscale variations of the factors affecting the rate constant of the glass dissolution reaction i.e pH of the solution (White 1983), and/or fluid/rock ratio (White & Claasen 1980). In Plate 17 (Photo 2) the margin of the glass shard (zone a) has been altered to beidellite (Si:Al ratio = 1.5-1.8:1), and towards the interiors of the shard the Si:Al ratio increases (zone b). Finally in zone c free silica, (probably opal-CT), precipitates. Thus, the variability in the physicochemical parameters of the microenvironment at the time of formation of smectites seems to be very important for their compositional variations.

The compositional variation observed might be attributed to two further alternatives: a) inhomogeous parent glass and b) the results obtained are due to mechanical mixtures of two end members having specific compositions. It is difficult to assess the former possibility because little is known about micro-scale inhomogeneity of the volcanic glasses. The second alternative is based on the fact that since each spot analysed corresponds to a population of several smectite crystals the exact number of which is not known, the chemical data obtained represent average chemical formulas. This means that if only two distinct types of smectites are present *each time i.e* beidellite and montmorillonite, having specific chemistry, then different proportions of them in the area analysed each time, will produce different average compositions. Had this been the case, the compositional trends in the smectite triangle should have been linear. Instead, the trends obtained are curvilinear. This indicates that if mechanical mixtures are the reason for the trends observed then at least 4 end members should be present, which should combine in special ways with each other. It is believed that this possibility is rather small. Recent AEM work by Banfield *et al.*, (1991a,b) confirmed the existence of large compositional variation in smectites. Mechanical mixtures might account for compositional variations only in cases in which the end-members have relatively similar composition.

6.2.3 Solid solution series in smectites

The coexistence of Cheto-type smectites and beidellite with a range of compositions between them also indicates the possibility of a solid solution series between the two species. Weaver & Pollard (1973) assumed a complete solid solution between the two species. On the other hand, Köster (1981) considered that it is not possible for such a solid solution to exist. Brigatti & Poppi (1981) found a miscibility gap between beidellite and montmorillonite using statistical methods, but considered the possibility of solid solutions between the montmorillonite species. There is no particular reason to exclude the possibility of solid solution at least between beidellite and Tatatilla-type montmorillonite, which differ mainly in the distribution of the layer charge. The data in Figure 4.15 display a clear range from a beidellitic to a montmorillonitic component through intermediate

compositions, supporting the idea of a solid solution. However, since the chemical characteristics of beidellite and Tatatilla-montmorillonite are similar the existence of mechanical mixtures might also explain the observed trend. Detailed AEM work is needed to clarify this point.

Nadaeu *et al.* (1985) reported the coexistence of three different beidellite fractions one of which had a more montmorillonitic character. It is possible that this fraction contained a mixed population of montmorillonite and beidellite. It is believed that the coexistence of beidellite and montmorillonite is a rather common event. There is no reason to accept that the physicochemical conditions of the microenvironment where smectites form do not vary so as to favour the formation of one or other mineral. This is especially true for smectites derived from intermediate rocks which have Si/Al ratios closer to beidellite. It is expected that in the future the more extensive use of microprobe will reveal more cases of coexistence between beidellite and montmorillonite.

The fact that different types of montmorillonites having highly variable chemistry coexist within very small distances raises the question of solid solution series among the montmorillonite species. The two series of smectites from the Areas 1 and 2 of Milos seem to converge chemically to a pole close to the iron montmorillonite field. However, there does not seem to be any transition between montmorillonites plotted in the" fields" assigned to Chambers or Tatatilla and Wyoming types. This indicates a possible lack of solid solution between Cheto and Wyoming montmorillonites in accordance with the assumption of Grim & Kulbicki (1961). Nevertheless, the fact that a great number of points from both series plot in an area not assigned to any particular field means that the field boundaries need reconstruction. With the existing data the "common field" cannot be resolved with certainty. Consequently the possibility of a solid solution between Cheto montmorillonites and Fe-rich Wyoming montmorillonites cannot be rejected.

It is not clear why the transition from beidellite to montmorillonite is not observed in the case of Wyoming montmorillonites. A possible explanation is that the higher amount of Fe and the lower layer charge present in Wyoming type montmorillonites, requires more complicated structural rearrangements to obtain a solid solution series. This is indicated from the different substitution pattern Al^{VI}-Fe^{3+}-Mg between Wyoming and Cheto montmorillonites. Also, it seems that in the samples where both smectites coexist (especially in SM66) the transition between beidellite-Tatatilla montmorillonite and Tatatilla-Chambers montmorillonite is questionable. Although this might be due to the relatively small number of microanalyses, the incompatibility of the existence of Mg and Fe in the structure of both beidellite and Tatatilla montmorillonite should not be excluded.

6.3. Influence of the hydrothermal activity on the Greek bentonites. Illitization of smectite.

6.3.1. Hydrothermal activity and its effect on the bentonite deposits.

The influence of the hydrothermal activity in Eastern Milos and Kimolos can be observed in both the macroscopic and and microscopic scale (see Chapters 3 and 4). The macroscopic features include the formation of solfatara springs (c.f Ankeria deposit, Milos), gypsum veins (Tsantili deposit, Milos), barytes veins (Kavos, Pikridou, Tria Pigadia, Pilonisi, Milos) "stockwork" textures characterized by S-metasomatism (Zoulias and Ano Komia deposits, Milos), kaolinite-alunite deposits (*i.e* the Kastriani deposit, Milos, and Agios Tryfon deposit, Kimolos) manganese occurences (Kimolos) and native sulphur deposits (Paleorevma and Thiorychia, Milos). The existence of extensive silica-rich zones is not necessarily associated with the hydrothermal alteration (see previous sections for discussion). As stated in the previous chapters, the spatial relationship between these features and the bentonite deposits suggests that hydrothermal activity is not the reason for the formation of the bentonites.

The study with electron beam devices revealed details of the influence of the hydrothermal activity on the Al-smectites. Alteration products from the reaction between the Al-rich smectites and the hydrothermal fluids produced kaolinite and/or halloysite, mixed layer illite smectite (I/S) and subsequent silicified zones, nontronite (Kimolos) and possibly alunite. The existence of smectite veinlets cutting the bentonite body (Plate 12) might also be a product of the reworking of the deposits during hydrothermal alteration.

Wetzenstein (1969, 1972) proposed a paragenetic model for the deposits of Eastern Milos showing a kaolinite zone overlying a smectite zone. Based on this model, Fyticas (1977) suggested that the smectites were formed through the same hydrothermal event as kaolinites, at higher pH. However, the current research showed that this is not the case. In some deposits (Koufi and Ano Komia deposit, Milos), kaolinite is present only in the lower bentonite horizons. Furthermore, in many deposits kaolinite is absent, although the hydrothermal influence is obvious (Ankeria and Zoulias deposits, Milos). Also in the Kastriani deposit smectites are absent. In general, kaolinite and/or halloysite is dispersed in the bentonites and its distribution does not follow a definite pattern.

The alteration of smectite to kaolinite has been reported in the past by several workers. Altschuler *et al.* (1963), Wilson & Cradwick (1972), Herbillon *et al.* (1981), and Bühmann & Grubb (1991) among others reported that the conversion is a transformation process which proceeds through an interstratified kaolinite-smectite phase. On the other hand Morgan *et al.* (1979) did not report such an intermediate phase. In the present case transition was not observed. Therefore, it is suggested that the conversion to kaolinite and/or halloysite took place under leaching conditions dictated probably by hydrothermal solutions characterized

by low pH. These solutions caused dissolution of the precursor smectite, removal of Si and precipitation of kaolinite. The Si removed might migrate from the system or precipitate in the form of opaline silica (Plate 1). In the case of the Koufi deposit, Milos kaolinite might have been formed by the following reaction:

$$Ca_{0.05}Na_{0.11}K_{0.14}(Al^{VI}_{1.49}Mg^{+2}_{0.37}Fe^{3+}_{0.19})(Si_{3.87}Al^{IV}_{0.13})O_{10}(OH)_2 + 4.29H_2O + 1.66H^+ =$$
$$0.81Al_2SiO_5(OH)_4 + 0.05Ca^{+2} + 0.11Na^+ + 0.14K^+ + 0.37Mg^{+2} + 0.19Fe^{3+} + 2.25H_4SiO_4 \qquad 6.1$$

Under more acidic conditions, combined with $SO_4^=$ supply, alunite instead of kaolinite might be formed. The acidic leaching conditions needed to drive this reaction have been underlined by the presence of hydrogen cations. Fe might migrate or precipitate as ferric oxide according to the redox conditions (reducing or oxidizing respectively), while the released cations pass into the fluid phase. Finally, Si might either precipitate or migrate from the system as stated before.

However, kaolinite might also be formed by another process which is closely associated with the illitization of smectite observed in the Tsantili and Agrilies deposits, Milos. The illitization in the Tsantili deposit is characterized by a continuous transition from smectite to R3-type mixed layer I/S with 13% smectite layers, through R0 (random) and R1-types I/S. The most interesting characteristic of this alteration is that the illite content increases towards lower depths, and the maximum illite content (87%) is observed close to the surface. Also, at lower depths intense silicification is observed (see Plate 1).

The factors affecting the illitization process have been studied extensively over the last twenty years. It is well known temperature, K-availability, pore solution chemistry, smectite composition, permeability and pore water abundance all affect illitization.

a) **K-availability.** It is a very important factor. If the conditions favour the conversion of smectite to illite but the environment is characterized by low K-content, then an increasing layer charge starts to build up, but collapse of smectite layers occurs only if the materials are saturated with K (Howard & Roy, 1985). The relative availability of K might also determine the existence or lack of by-products from the reaction (Whitney & Northrop, 1988). The effect of K-availability in this illitization process can be assessed if the samples SM94 with 35% expandables and abundant kaolinite and SM75 with 40% expandables and without kaolinite are compared. The K-content of the former is 1.5% lower than that of the latter although the I/S present has lower expandability. This suggests that although the temperature was sufficiently high to convert smectite into I/S with 35% expandables (rather higher than for SM75), K^+-supply was not sufficently high to produce only I/S. This was coupled with a greater degree of Si-release (probably due to higher temperature), which led to a higher Al:Si ratio in the residue, thus favouring kaolinite instead of I/S.

The I/S-bearing samples are enriched up to 6 times in K compared to their smectite-bearing counterparts (in Table 5.1 compare the K content of the samples SM75, SM78, SM82, SM89 and SM94 with that of SM100). This implies that an influx of K (K-

metasomatism) might be responsible for the conversion of smectite. K-metasomatism has been postulated in many cases of illitization of bentonites (Huff & Turkmenoglü, 1981, Inoue & Utada, 1983, Altaner *et al.*, 1984, Brusewitz, 1986, Huff *et al.*, 1991). Had the reaction proceeded *mainly* with K from the dissolution of the authigenic K-feldspar, no substantial increase in the K-content of the parent rock would have occured. Nevertheless, it is expected that the K-feldspar might be a limited source of K (see Plate 15).

b) **Temperature.** It is well known that temperature is one of the most important driving forces of the reaction and that there is a strong correlation between the extent of illitization and temperature (Perry & Hower, 1972, Foscolos & Kodama, 1974, Hower *et al.*, 1976, Boles & Franks 1979). The obvious indications for the influence of hydrothermal alteration (see Plate 3) suggest that temperature has played a major role. The conversion of the fully expandable phase to a mixed layer one with only 13% expandables has taken place within less than 40m. This means that the temperature profile must have changed dramatically within a small distance.

The existing data about the temperature of the reaction might provide indications about the temperature variations in the present case. In sedimentary sequences the minimum temperature required to obtain an I/S with 13% expandables is 100^{o}C (see Srodon & Eberl, 1984 Fig. 21). Boles & Franks (1979) reported minimum temperatures of 120^{o}C for 15% expandables in shales. In hydrothermal alteration the appearance of ordering has been reported at 98-135^{o}C in the Salton Sea hydrothermal system (Muffler & White, 1968) and at 85-110^{o}C in the Wairakei hydrothermal system (Srodon & Eberl, 1984). The appearance of illite with less than 5% expandables has been reported at 200^{o}C in the Shinzan area (Inoue & Utada, 1983), at 203-217^{o}C in the Salton Sea system and at 230-240^{o}C in Wairakei. Recently, Harvey & Brown (1991) reported illite formation at 200^{o}C in the Wairakei geothermal field. Since in Milos the illitization did not proceed to more than 13% expandables it follows that the temperature should have been lower than 200^{o}C. Also, the appearance of ordering might have taken place at temperatures around 100-110^{o}C (Hower *et al.*, 1976, Harvey & Browne, 1991).

The thermal source was localized because the alteration is restricted to the southern face of the quarry. Also the fact that the intensity of the alteration decreases towards the surface suggests that the heating source is moving **away** from the deposit. The only geological formation which can supply heat and can have such geometric characteristics is a mineralized vein (Fig. 6.2). Based on the geological characteristics of Milos it is concluded that the vein might contain ore minerals, barytes or might be part of a "barren" thermal conduit which is controlled by tectonics. An indication for the possible nature of the vein is provided from the Agrilies deposit (the only other deposit of Eastern Milos in which mixed layered I/S are present) which is located next to the Pikridou barytes deposit. Kalogeropoulos & Mitropoulos (1983) suggested that the temperature of the baryte vein

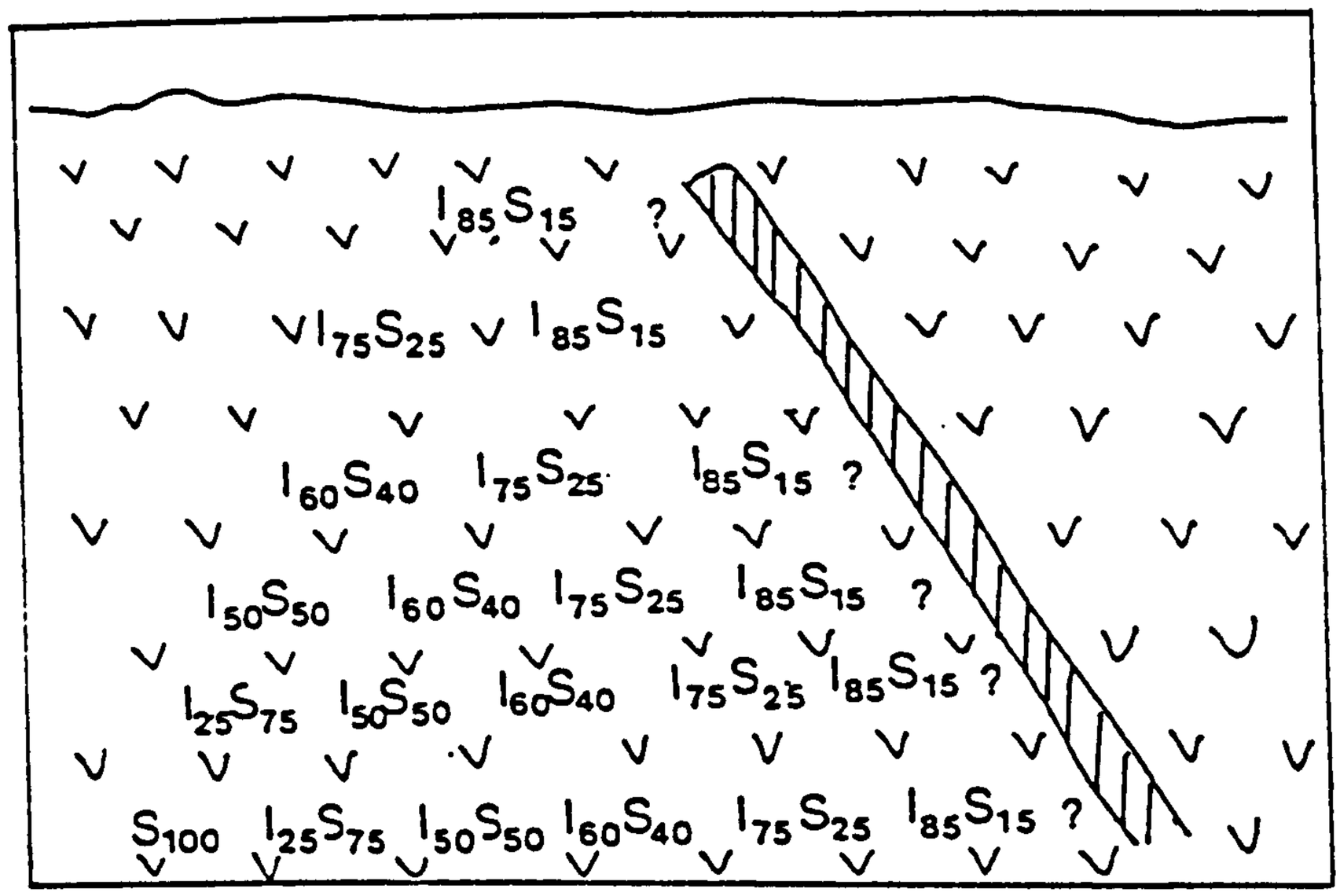

FIGURE 6.2. Model proposed for the cause of illitization and the distribution of the illite content in the Tsantili deposit, Milos.

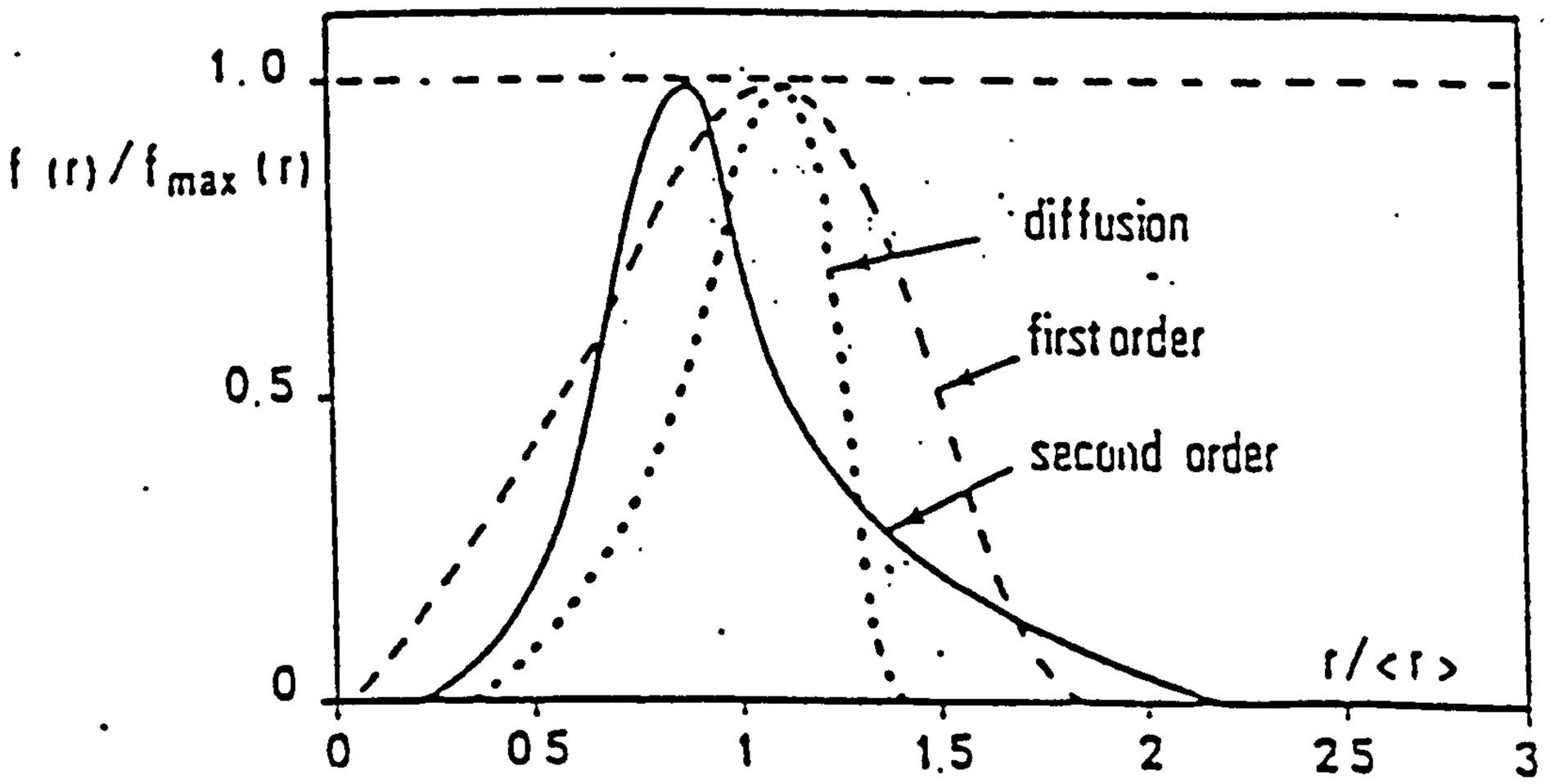

FIGURE 6.3. Theoretical steady state profiles describing the different possible mechanisms of Ostwald Ripening (after Baronnet, 1984).

was between 140 and 170^{o}C. Since the I/S exhibits both random and ordered interstratification it follows that the emplacement of the baryte veins provides a plausible explanation for the heat source which drove the reaction. This might be the case also for the Tsantili deposit, indicating that the emplacement of baryte might be associated with K-metasomatism. Liakopoulos (1987) reported the existence of intense K-metasomatism associated with the Ba-Mn mineralization at cape Vani (NW Milos). If the temperature inferred by Kalogeropoulos & Mitropoulos (1983) is valid, then the baryte-vein should be very close to the most altered bentonites because such low expandabilities are expected at temperatures between 150-180^{o}C. Such a temperature-range is in full accordance with the results of Harvey & Browne (1991) who reported temperatures 155-190^{o}C for I/S with 80-90% illite in the Wairakei hydrothermal field. If this is the case, then the illitization of the bentonite deposits of the Eastern Milos might be used for exploration of other mineral deposits, especially barytes.

c) **Pore chemistry.** The effect of other cations present in the pore fluid has been shown experimentally by Robertson & Lahann (1981). More specifically Ca^{+2} and Mg^{+2} inhibit the reaction rate by an order of magnitude compared with Na^{+} at a fixed K^{+} content. If it is assumed that the pore chemistry played a major role in the reaction then a very intense geochemical gradient should be expected. This gradient should be dominated by an excess of Mg and Ca ion in the pore fluids in the lower sectors of the deposit and a deficiency of these cations in the higher sectors. However, there is no evidence that such a gradient was present in the deposit.

d) **Smectite composition.** It is known that the smectite chemistry affects the reaction substantially. Hydrothermal experiments showed that trioctahedral smectites are more stable than their dioctahedral counterparts (Eberl *et al.*, 1978) and that K-montmorillonites are converted more readily to illite than their Ca or Na-rich counterparts (Eberl, 1978). Also Boles & Franks (1979) showed that smectites with high ratios of octahedral (Fe+Mg)/Al are more stable than Al-rich ones. This assumption was used by Ramseyer & Boles (1986) as one of the possible reasons for differences in the illitization process they studied. In the Tsantili deposit the smectites are dioctahedral. It has been shown that the smectites of Milos are characterized by a remarkable compositional variation. If chemical composition had played a major role then a zonal distribution of smectites having different compositions should be expected. Thus, for constant temperature of alteration, in the lower sectors Fe-Mg smectites (possibly Chambers and Wyoming types) should predominate, while in the upper ones Al-smectites (possibly Tatatilla montmorillonites and/or beidellites) should be present. Alternatively, the smectites in the higher sectors should be K-rich while those in the lower sectors Na and/or Ca rich. Such zonations have not been observed. Instead it has been shown (see chapter 4) that the smectites present in this deposit are Wyoming

montmorillonites and their chemical variation does not exhibit zonation. Consequently it is suggested that the role of variation of the smectite chemistry is rather limited.

e) **Permeability and residence time.** Increased permeability affects the illitization process because it provides access for the pore fluids. In the present case there is no reason to assume that the higher sectors of the deposit were more accessible to the pore fluids than the lower ones. Similarly there is no reason to suggest that the residence time was not different for the materials in the various sectors of the deposit. Therefore both these factors does not seem to have played important role in the illitization process.

f) **Pore water abundance.** Whitney (1990) showed experimentally that the water:rock ratio not only affects the progress of the reaction but it determines the nature of the products as well. Thus illitization was retarded at low water:rock ratios and the inhibition decreased at higher temperatures. Furthermore at low water:rock ratios the only by-product was opal-CT, while at high ratios chlorite, cristobalite and/or quartz were detected. In the present case the by-products observed were either quartz or kaolinite + quartz. Quartz is not present in the samples but has been concentrated in the silicified zone visible in Plate 1. In this case high fluid:rock ratios are expected because a) the initial alteration of the volcanic glass took place in a marine environment and little or no compaction has taken place and b) large amounts of K have been transported in the system through fluid flow. The presence of similar K content in samples with significantly different expandabilities (e.g samples SM75 and SM82 in Table 5.1) suggests that although these samples experienced similar water:rock ratios, temperature played the most important role in the reaction.

It is concluded that in the Easterm Milos illitization of the bentonite deposits is associated with hydrothermal activity. The major controlling factors were temperature, and K-availability which is closely associated with the water:rock ratio because the K-source was the hydrothermal fluid (K-metasomatism). Some of the K consumed in the reaction might have been supplied by the dissolution of K-feldspar. The Al nessecary for the reaction might have been supplied mainly by the dissolution of smectite ("cannibalization" of smectite after Boles & Franks, 1979) and to a much lesser degree by the dissolution of K-feldspar. Therefore the following dual reaction mechanism is proposed:

smectite + K^+ --> I/S + quartz ± kaolinite + Ca^{+2}, Mg^{+2}, Na^+, Fe 6.2

smectite + K^+ + Al^{3+} --> I/S + quartz ± kaolinite + Ca^{+2}, Mg^{+2}, Na^+, Fe 6.3

In the reaction (6.3) K and Al are provided from the dissolution of K-feldspar. Both reactions might proceed simultaneously, although the first is considered to be of primary importance. Also in both rections alunite instead of kaolinite might be formed if the pH is very low and abundant $SO_4^=$ is present. The coexistence of alunite with I/S has been observed in many samples.

The Ca, Na, Mg and Fe elements released from the reactions 6.2 and 6.3 might be diffused in the system and provide the "nutrients" for the precipitation of other phases. It

has been seen (see Chapter 4) that minerals like gypsum and carbonates occur in variable amounts in several sites. It is believed that the formation of these minerals is closely related with the illitization reaction. Boles & Franks (1979) have shown that in sedimentary sequences release of Ca, Mg and Fe through the reaction provides the elements necessary for the precipitation of carbonates which act like cements in sandstones.

The previous discussion showed that illitization proceeded in a way similar to that described by Inoue & Utada (1983) and Inoue *et al.* (1987) *i.e* from a precursor smectite and not like the case studied by Eberl *et al.* (1987) in which sericite was deposited from the hydrothermal solutions. What remains to be answered is whether the reaction involved a solid state transformation in which the smectite layers were transformed layer by layer (c.f Bethke & Altaner, 1986) or is a neoformation process (Nadaeu & Bain, 1986) or both (Inoue *et al.*, 1987).

The morphology of the precursor smectite is dominated by flakes having a minimum thickness of 30μm. The number of the smectite flakes decreases with decreasing expandability, with some exceptions (see Chapter 4). The existence of abundant laths with high expandabilities (random ordering) indicates that dissolution of the smectite laths has started at expandabilities as high as 80%. These lath-shaped crystallites can be considered the product of dissolution of unstable smectite which had fixed potassium (Inoue *et al.* 1987). The presence of I/S laths at high expandabilities has been assumed by Inoue *et al.* (1988) but has not been verified so far. These remarks suggest that illitization proceeded through a dual mechanism similar to that proposed by Inoue *et al.* (1987). In the incipient stages (random ordering), the changes were not significant and were dominated rather by potassium fixation and development of higher layer charge. Since the particle-morphology is dominated by flaky crystals similar to the smectite ones, the reaction might have involved limited dissolution of the original flakes. Solid state transformation is believed to be the dominating mechanism although the most unstable flakes dissolved and laths 20Å thick were formed (neoformation). In the more advanced stages (>50% expandables) the unstable flakes dissolved and I/S laths formed by a neoformation process. The first particles to form were 20Å thick and with advanced illitization the thickness increased. The newly formed particles were increasingly becoming more isometric in shape. Dissolution of the unstable flaky particles was retarded by the formation of kaolinite (sample SM84). In this case it seems that the formation of I/S proceeded through transformation. This might be due to the formation of kaolinite instead of I/S from the dissolution of the unstable I/S flakes. It is interesting that in this sample the transformation led to formation of flaky I/S particles 20 and 30Å thick.

It is not known why hexagonal I/S flakes are abundant at expandabilities as low as 50% in some samples. Also it is not certain if any **pure** illite particles were formed during this alteration process. Nadaeu *et al.* (1984c) considered that the true illite particles are 50μm

thick. If the pure illite particles are the thermodynamically stable products of the illitization reaction, then their thickness should be >50Å because only these particles do not dissolve during neoformation (see Chapter 4). Therefore pure illite began to form at 40% expandables and became abundant at expandabilities lower than 25%.

The Si released from the illitization is present mainly in the form of quartz. However, this by no means excludes the possibility that Si diffuses in the system, is taken up by smectite and facilitates its alteration to kaolinite. In the Tsantili deposit, two main types of montmorillonites have been identified: one with 3.95-4 Si atoms per half structural unit and one with 3.8 atoms per half structural unit. Although the difference observed might be due to "inherited" compositional variation of these smectites, the possibility for secondary uptake of Si should not be ignored. In this case the formation of a Si-rich montmorillonite might have taken place through the following reaction:

$$Ca_{0.10}Na_{0.05}K_{0.05}(Al^{VI}_{1.62}Fe^{3+}_{0.10}Mg_{0.36})(Si_{3.82}Al^{IV}_{0.18})O_{10}(OH)_2 + 0.14Fe^{3+} + 0.02Na^{+} + 0.01Ca^{2+} + 0.39H_4SiO_4 =$$

$$Ca_{0.11}Na_{0.07}K_{0.01}(Al^{VI}_{1.45}Fe^{3+}_{0.24}Mg_{0.36})(Si_{3.93}Al^{IV}_{0.07})\,O_{10}(OH)_2 + 0.14Al_2SiO_5(OH)_4 + 0.04K^{+} + 0.3H_2O + 0.4H^{+} \quad 6.4$$

In this reaction the higher Fe content of the low Al^{IV}- montmorillonite has been attributed to transport probably from the illitized zones (compare the Fe contents of the "fresh" bentonite and that of the K-bentonite). If the higher Fe content of the product smectite is "inherited", the effect of the reaction is restricted to the release of Al from the tetrahedral sites of the smectite. The "product" smectite contains lower number of octahedral cations than the reacting smectite. If the total number of octahedral cations is fixed to a total of 2.05 per half unit (average number given by Grim & Güven, 1978), then the layer charge of the product smectite is lower than that of the parent smectite (0.28 and 0.36 respectively). If reaction 6.4 is valid then it might have taken place at the higher horizons of the deposit where the accesibility of the Si is greater due to the greater degree of illitization.

Meunier *et al.*, (1992) proposed a different mechanism for the replacement of smectite by kaolinite, characterized by consumption of the smectite with lower layer charge and formation of kaolinite, quartz and smectite with higher layer charge. As stated in the previous paragraph, the smectite with higher tetrahedral charge has also higher layer charge, if the total number of the octahedral cations is assumed 2.05 (Grim & Güven, 1978). If the mechanism proposed by Meunier *et al.*, (1992) is valid then the following alternative reaction mechanism might have taken place:

$$2Ca_{0.11}Na_{0.07}K_{0.01}(Al^{VI}_{1.45}Fe^{3+}_{0.24}Mg_{0.36})(Si_{3.93}Al^{IV}_{0.07})\,O_{10}(OH)_2 + 0.03K^{+} + 2.12\,H^{+} =$$

$$Ca_{0.10}Na_{0.05}K_{0.05}(Al^{VI}_{1.62}Fe^{3+}_{0.10}Mg_{0.36})(Si_{3.82}Al^{IV}_{0.18})O_{10}(OH)_2 + 0.62Al_2SiO_5(OH)_4 + 2.8SiO_2 + 0.12Ca^{2+} + 0.09Na^{+} + 0.36Mg^{2+} + 0.38Fe^{3+} + 0.82H_2O \quad 6.5.$$

It is not certain which of the two reaction mechanisms (6.4 or 6.5) might have taken place. The latter is favoured from the fact that the predicted by-product quartz is present in

this sample (see Fig. 4.1, sample SM99). However, this by no means exclude the possibility for precipitation of quartz through a mechanism similar to that of reaction 6.4 from excess H_4SiO_4. The mechanism described in reaction 6.5 also predicts the introduction of K in the system, in accordance with the discussion made in the previous paragraphs. Finally, it assumes substantial release of various cations (Ca, Na, Mg, Fe) which might participate in the formation of carbonates and sulphates present in the Tsantili deposit.

6.3.2 Possible mechanism of the illitization. Ostwald ripening.

6.3.2.1. Theoretical considerations.

The neoformation process in the illitization reaction studied can be separated into three stages: dissolution of the unstable smectite flakes, solute mass transfer, and crystallization which may involve nucleation, crystal growth, Ostwald ripening and/or coalescence of the particles (Whitney, 1990, Baronnet, 1982).

Ostwald ripening is a recrystallization process characterized by simultaneous dissolution and growth of particles in the same medium (Baronnet, 1982). In a closed system after a non-explosive crystallization (nucleation has taken place for a long time, c.f Eberl & Srodon, 1988), the crystallized phase includes particles of different sizes. Although it might be stable in terms of the factors which determine its stability field (e.g temperature, pressure, pore chemistry) it might not be in thermodynamic equilibrium. This is because the surface free energy of the system includes a surface area factor which has not been minimized (Baronnet, 1982). In order to achieve thermodynamic equilibrium, the system must minimize its surface free energy. This is done through dissolution of the smallest particles, mass transfer through the solution and growth of the largest particles (Baronnet, 1982). The process is described by the following equation (Baronnet, 1982, 1984):

$$S_r - S_{r^*} = 2M\gamma S_i (RT\rho)^{-1}(r^{-1} - r^{*-1}) \qquad 6.6$$

where:

S_r = solute concentration close to an equivalent spherical crystal of radius r.

S_{r^*} = solute concentration close to an equivalent spherical crystal of *critical radius* r^*.

M = Molecular weight of the solute.

γ= interfacial tension solid-liquid.

ρ= crystal density.

S_i = standard solubility of a crystal of infinite size (equilibrium concentration around a crystal of infinite size)

R=gas constant

T=temperature

Particles with size equal to the *critical radius* are in unstable size equilibrium with the solution. This means that those particles greater than the critical radius will grow at the expense of particles smaller than the critical radius which will dissolve (Lifshitz & Slyozov, 1961). However, in a closed system the disappearance of the small particles will cause an increase of the critical radius. Therefore, the early supercritical particles will soon become subcritical and dissolve. The end of the reaction will be determined by the survival of the largest initial crystal which will be zoned from an oldest core to a youngest margin (Baronnet, 1982, 1984). However, in real geological systems the end of the reaction is marked by a number of crystals of nearly equal size (Baronnet, 1982). Also, since the relative size relation between particles formed in the original step is maintained during ripening, the recrystallization process will be preserved in the various particle sizes (Eberl *et al.* 1990).

The overall rate law is given from the equation (Baronnet, 1982, 1984):

$$r^n - r_0^n = K_n(t-t_0) \qquad 6.7$$

where r is the mean particle radius for the particle size distribution at time t, r_0 and t_0 are the mean initial particle size and initial time respectively and K is the constant which characterizes the growth rate of the mean radius. n=2 when recrystallization follows first order kinetics (high levels of supersaturation) and n=3 when it follows second order kinetics (low levels of supersaturation) or volume diffusion.

Ostwald ripening can be identified by means of the grain size distribution histogram f(r) as a function of r. The histogram broadens, flattens and shifts toward greater r with time. If this histogram is plotted in reduced coordinates $f(r)/f(r)_{max}$ and r/r_{av} (where f(r) is the frequency of a particle radius, $f(r)_{max}$ is the maximum frequency found, r is the particle radius and r_{av} is the mean particle radius then a normalized grain size distribution is obtained, which is steady in shape. It does not depend on ripening time and on the initial grain-size distribution (Lifshitz & Slyozov, 1961, Baronnet, 1982, 1984) and is indicative of the growth contolling mechanism (Baronnet, 1982,1984). According to Baronnet (1982), the establishment of steady-state profiles may be considered as a criterion to characterize Ostwald ripening in any system.

In Figure 6.3 experimentally derived steady state profiles for bulk diffusion, first order and second order kinetics are given (Baronnet, 1982, 1984).

6.3.2.2. Is illitization in the Tsantili deposit controlled by Ostwald ripening ?

The results obtained from measurement of the length, width and thickness of the I/S particles of different expandabilities were plotted in histograms with reduced coordinates. The steady state profiles obtained (Fig. 6.4) have maxima in the same area (r/r_{av} is 0.9-1) and are comparable to those presented by other workers (Inoue *et al.*, 1988, Eberl &

Srodon, 1988, Eberl *et al.* 1990, Jahren, 1991). Since each profile obtained is composed of particles formed at different temperatures, it follows that the original relative order of particle sizes did not change, even though both the absolute and the relative sizes of the particles changed (Chai, 1974). Although they resemble the profiles of second order kinetics for closed hydrothermal systems (Baronnet 1982, 1984) they do not seem to fit *exactly* with any of the theoretical profiles for first order kinetics, bulk diffusion or second order kinetics. The steady state profile obtained from length measurements fits better with the second order kinetics when compared with the theoretical profiles of Baronnet (1982, 1984). However, the profile from thickness measurements fit better with the second order profiles shown in Eberl & Srodon (1988) and Eberl *et al.* (1990). In any case it seems that the distributions fit between the ideal distribution calculated for second order kinetics and a log-normal distribution (Eberl *et al.*, 1990). Similar profiles were obtained by Jahren (1991) for recrystallized chlorites.

Second order kinetics imply low supersaturation conditions and growth by a screw dislocation mechanism (Baronet, 1982, 1984). On the other hand the growth mechanism which caused the log-normal disrtibution has not been understood so far (Eberl *et al.*, 1990). In plate 19 evidence for spiral growth controlled by screw disslocation is presented. Each step is about 10Å thick. This indicates that second order kinetics might explain to some degree the illitization process in the Tsantili deposit. This implies that the dissolution rate of the subcritical particles was lower than the growth rate of the supercritical particles so as to keep low levels of supersaturation. It seems that growth proceeded initially by a surface nucleation mechanism followed by spiral growth (Baronnet, 1984). However spiral growth was not observed in all the samples examined.

However, is the illitization studied controlled by Ostwald ripening? The factors controlling Ostwald ripening have been determined from hydrothermal laboratory experiments, under conditions which are different from those observed in nature. In the present case the discrepances from the experimental conditions are the following:

a) The system is fully open thermodynamically. Abundant K has been transported into the system through hydrothermal solutions. The sense of alteration through fluid flow itself dictates an open system, because the flow path changes continuously with time (Steefel & Van Capellen, 1990). The chemical components derived from the dissolution of smectite might be transported, affecting the supersaturation in both the area of dissolution and the area of deposition.

b) Potassium might not have been supplied to the same degree in the different sectors of the rock. This suggests that the degree of smectite dissolution will not necessarily be the same in all the sectors of the deposit, under constant temperature.

c) The system is not monominerallic. Except for the dissolving smectite, existing phases like K-feldspar might affect controlling factors of illitization like K-availability. The formation

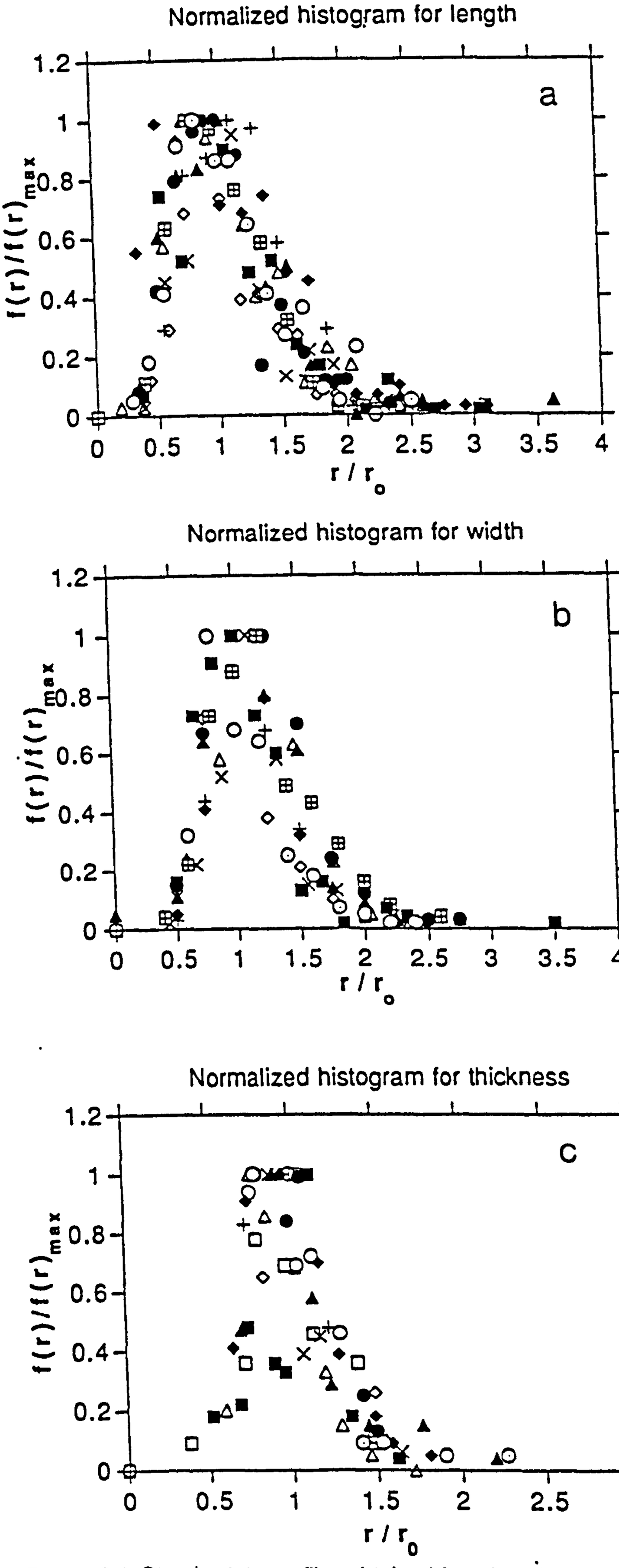

FIGURE 6.4. Steady state profiles obtained from length (a), width (b) and thickness (c) measurements for the illite/smectite particles in the Tsantili deposit. Note that the profiles resemble but do not fit exactly to any of the theoretical profiles shown in Fig. 6.3.

of kaolinite affects smectite dissolution (*e.g* sample SM84), and possibly the crystal growth and recrystallization of the neoformed illite particles. It also indicates that the mass transfer does not take place only fo the neoformed particles but to a second phase as well.

d) A number of other chemical elements like S have been introduced in the system. Their presence might affect the crystallization rate of the I/S (Baronnet, 1984). They might also compete with other chemical components derived from the dissolution of smectite, affecting the reaction rate.

e) The reaction has been triggered by hydrothermal activity. The influence of time on Ostwald ripening although important in geological processes like diagenesis and metamorphism (Eberl *et al.* 1990) and other hydrothermal systems (Eberl & Srodon, 1988) or in experimental conditions (Chai, 1974, Baronnet, 1982, 1984) cannot be estimated in this particular alteration.

f) It is not known whether there was a constant K-supply in the system or K was introduced as pulses. Since the K-transport is associated with hydrothermal activity, thus with temperature, the latter might have been constant or might have been varied. Fluctuations in temperature might affect Ostwald ripening (Baronnet, 1982)

Notwithstanding the above descrepancies from the ideal Ostwald ripening mechanism the illitization reaction is characterized by a disssolution of the smaller (subcritical ?) particles and growth of the larger ones (supercritical ?). The particles evolve towards a larger more isometric shape. Their thickness increases with decreasing expandability (see Chapter 4). Thus, as in the study of Lanson & Champion (1991), even if Ostwald ripening cannot be applied directly, the reaction is directed towards minimization of the surface free energy.

6.4. Growth of smectite crystals from the volcanic glass.

6.4.1 Possible mechanism for crystal growth of the smectite.

Smectite crystals have been formed from volcanic glass and in some deposits are associated with other diagenetic phases like zeolites. In the Prassa deposit the coexistence of the smectite zone close to the mordenite zone offers the chance to study the possible influence of zeolites on smectite growth.

In Figure 6.5 steady state profiles obtained from length measurements of the smectite particles from the smectite and the mordenite zones are presented. It is obvious that the size distribution profiles are different in the different zones. In the smectite zone the profiles obtained are comparable to those from the illitization reaction in the Tsantili. Therefore the distributions fit between the theoretical steady state profile calculated for a second order growth (spiral growth at low supersaturation), and the log-normal profile suggested by Eberl *et al.* (1990). On the other hand the distributions from the mordenite zone fit between the

profile calculated for the first order kinetics (high supersaturation) and that of the second order kinetics.

Apparently, the different steady state profiles obtained are associated with different supersaturation conditions which prevailed at the interface dissolved glass-pore water in the different alteration zones. Again the existence of a well flushed system (especially in the smectite zone), the introduction of chemical elements like Mg, and Fe, and the non-monomineralic character of the system (smectite coexists with zeolites in the zeolite zone) are significant deviations from the ideal Ostwald ripening process. Like the illitization process studied, it can be considered that crystallization of smectite proceeds towards a decrease of the surface free energy of the system.

Smectite is the first phase to form from dissolution of the volcanic glass. Its formation proceeds through nucleation followed by crystal growth and recrystallization. For nucleation to occur a free energy barrier has to be overcome (Steefel & Van Cappellen, 1990):

$$\Delta G^{*} = (16\pi\sigma^{3}v^{2})/3(kT\ln\Omega)^{2} \qquad 6.8$$

where: σ= solid-solution interfacial energy

v= volume of a formula unit of the mineral

Ω= saturation state of the solution

k= reaction constant

T = temperature

The activation energy of the nucleation decreases with increasing solution saturation (increase of the Ω factor) and temperature. In natural systems characterized by reactions in the mineral-water interface, there is a critical value for supersaturation, above which new surface area is created mainly by nucleation of new crystallites (nucleation controlled surface area generation), and below which it is generated by crystal growth (crystal growth controlled surface area generation) (Steefel & Van Cappellen, 1990). However since the nucleation of crystallites is fast, the supersaturation level drops below the critical value and crystal growth begins. A similar process is believed to have taken place in the Prassa deposit.

Stable mineral phases are difficult to nucleate at low temperatures due to their high critical supersaturation values. Their nucleation may take place indirectly through an amorphous precursor with a lower interfacial energy (Berner, 1984, Steefel & Van Cappellen, 1990). For zeolites it has been suggested (Mariner & Surdam, 1970, Surdam, 1977, Taylor & Surdam, 1981) that they probably form from precursor Al-Si gels. Such gels were recognized in the Prassa deposit as precursors of mordenite (Plate 16). Also smectite has probably been formed from a poorly crystalline precursor. These examples of precursor use are known as *cannibalistic* (Steefel & Van Cappellen, 1990).

Since high alkali/H^{+} activity ratios favour the formation of zeolites instead of smectites (Hess, 1966), the precursor of smectites and the first smectite crystals (unstable smectites)

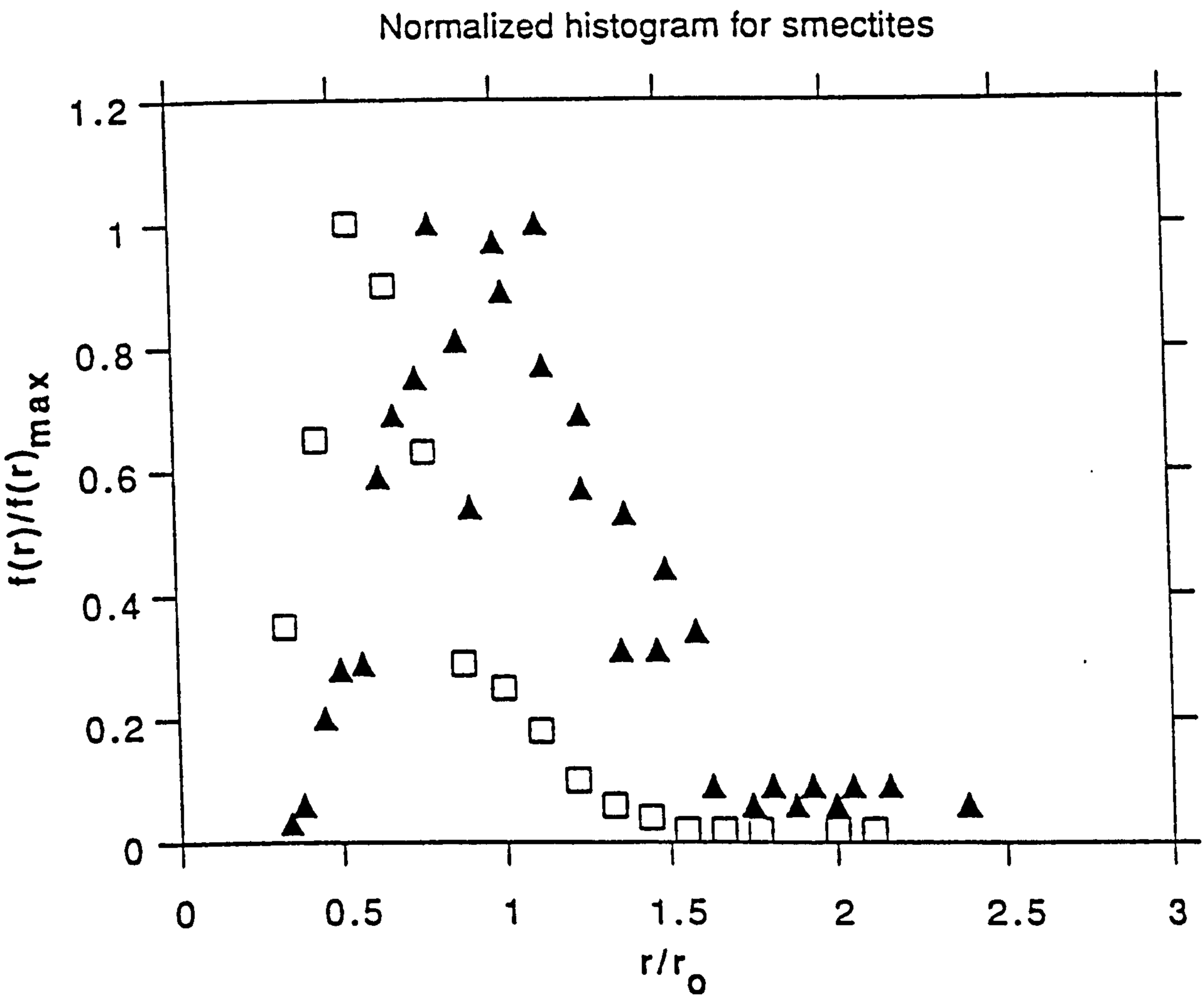

FIGURE 6.5. Steady state profiles obtained from diameter measurements of the smectite particles present in the Prassa deposit, Kimolos. The solid triangles belong to smectites from the smectite+mordenite zone, while the empty squares to smectites from the smectite zone. For discussion of the shpe of the profiles see text.

in the zeolite zone was formed in the initial stages of alteration, under conditions of high supersaturation (see the model of Dibble & Tiller in Section 6.1). Recrystallization through an Ostwald ripening-like process might have taken place at supersaturation higher than the smectite zone if the stable particles were forming at a lower rate than the unstable ones were dissolving. This is expected because smectite growth was probably retarded by the pore fluid chemistry and mordenite was favoured instead. The shape of the steady state profile might be explained in this way.

In the smectite zone, after the growth of the poorly crystallized phase, the first (unstable) smectite crystals probably crystallized through a similar process. However, during recrystallization, the level of supersaturation might have been lower if the unstable smectite particles were dissolving at a lower rate than the more stable ones were forming (Eberl *et al.*, 1990) or if part of the chemical components released from the dissolution of the unstable particles were removed. The fact that the system was well-flushed might have played an important role in the second alterative. Therefore, the steady state profiles from the smectite zone are believed to represent lower supersaturation conditions. Recrystallization of smectite proceeded further because the alkalies were removed from the system.

6.4.2 Possible influence of the smectites on the pore fluid and the chemistry of mordenite. Evidence from the Prassa deposit, Kimolos.

The existence of K-rich mordenite in the Prassa deposit is a rather unusual phenomenon because the dominant exchangeable cations of the mineral are Na and Ca (Gottardi & Galli, 1985). Experimental work (Wirsching, 1976, Hawkins *et al.*, 1978, Hawkins, 1981) has shown that clinoptilolite is favoured over mordenite at lower temperatures and high K:Na ratios. Recently, Pe-Piper & Tsolis-Katagas (1991) described a K-rich mordenite in Samos island, Greece, the formation of which was attributed in the hydrothermal circulation of alkaline waters.

In the Prassa deposit excessive mass transfer has taken place between the altered rock and the fluid phase. However, in Chapter 5 it has been shown that K has not been transported in the system, but released in different degrees from the different alteration zones. This fact rejects the possibility for a K-mordenite genesis through K-influx from a hydrothermal source. The possibility for intense hydrothermal activity has already be questioned because of the presence of pure end member K-feldspar.

The exchangeable cation chemistry of the smectite which coexists with the K-mordenite exhibits variations which are comparable to those of the mordenite (see Chapter 4). Because smectite began to form prior to mordenite, its formation might have influenced the chemistry of the pore solution. If the smectite which crystallized first was K-rich then the

$K^+/(Na^+ + Ca^{2+})$ content of the pore fluid might have been relatively low. The relatively high $Na^+ + Ca^{2+}/H^+$ activity of the pore fluid probably favoured the formation of the Na-Ca-mordenite.

But, how possible is it for the first smectite to be K-rich? It has been shown that smectite probably did not precipitate from the pore solution but was formed rather from a poorly crystalline phase. The chemistry of this phase was probably controlled by the dissolved precursor. Formation of a K-rich smectite might have been influenced either by the pH of the fluid phase or by the cooling history of the parent rock or both (see section 6.1 for details). It is possible that both the previous factors affected the relatively high K-availability in the primary smectites.

After the formation of the first smectite crystallites from the poorly crystallized phase, the free energy of the system was probably high. Consequently dissolution of the subcritical K-rich particles and growth of supercritical smectite, started. This process might have released K to the pore fluid, and removed Ca and Na from it, raising the $K^+/(Na^+ + Ca^{2+})$ activity ratio of the pore fluid. Thus, K-rich mordenite began to form. The Ostwald ripening-like recrystallization process is believed to have played a "purging" role in the smectite chemistry. The smectites produced from this process are characterized by small variation in their interlayer cation population. Such a model does not require nucleation and crystallization of smectite during the formation of mordenite, which would be unlikely due to the unfavourable pore fluid chemistry. Similar assumption for Sr-release during illitization was made by Eberl *et al.*, (1990). Moreover, it is possible that the small amounts of authigenic K-feldspar were formed during this process in areas where the K^+ activity was high.

It is not still clear why K-mordenite instead of clinoptilolite was formed. Three possibilities are addressed here:

a) K-mordenite was favoured by epitaxial growth over a Na-Ca precursor. Although such a "zonal" relationship was not observed it should not be excluded because of the analytical technique applied (a 15μm defocused beam implies the X-ray signal is coming from a large area which might include both types).

b) The Al activity of the pore solution was either high or low. At 25^oC clinoptilolite has a maximum stability field at an intermediate Al-activity which decreases with either increasing or decreasing activities of Al (Bowers & Burns, 1990). Indeed, the Si:Al ratio of mordenites is high (up to 5.8:1) suggesting low Al activity.

c) The composition of the Si-species which were dissolved might have favoured the formation of mordenite. According to Hawkins (1981), if the ratio of Si-monomers ($Si(OH)_4$, $SiO(OH)^-$ or $SiO_2(OH)_2^{2-}$, see Mariner & Surdam, 1970 and Hawkins, 1981) to Si-tetramers ($Si_4O_8(OH)_4^{4-}$) increases, then the formation of Si-pentamers (which are close to the 5-membered ring structure of mordenite) might be formed (tetramer + monomer). In

pH lower than 8.5 alteration of rhyolitic glass yields predominantly $Si(OH)_4$ as Si-monomer, and a very high $Si(OH)_4$:$Al(OH)_4^-$ ratio (Mariner & Surdam, 1970). This confirms the suggestion that the Al-activity was probably low *i.e* not suitable for the formation of clinoptilolite.

In the Loutra deposit the systematic negative relationships of the exchangeable cations found in the clinoptilolite were not observed in smectite. Nevertheless, the possibility that a similar control of the smectite on the chemistry of clinoptilolite to some extent should not be rejected because of the small number of microanalyses (because of the intimate intergrowths between opal-CT and smectite only a small number of smectite microanalyses was considered reliable). However, the existence of two distinct groups of clinoptilolites, suggests a different mode of origin.

The deposit has been affected by hydrothermal activity superimposed on the bentonites, to a certain extent. This is supported from the existence of Fe-oxides- rich zones following fault-planes which "cut" the bentonite body (see Plate 7). It is possible that the formation of one of the two groups of the clinoptilolites took place during this hydrothermal event. Because Ca-clinoptilolites are uncommon diagenetic products in open hydrological systems like that in the Loutra deposit (Altaner & Grim, 1990), a hydrothermal origin is more plausible for them. Since the Si/Al ratios of the total population vary within the same limits, it follows that the hydrothermal alteration has affected only the exchangeable cations of the clinoptilolite.

The previous remarks suggest that after the formation of smectite (Chambers-type montmorillonite) in a hydrologically open system, the $(Na^+ + K^+)/H^+$ activity ratio of the fluid phase was raised and entered the stability field of alkali-rich clinoptilolite. Therefore, Na-K clinoptilolite began to form probably from the dissolution of a gel precursor (Mariner & Surdam, 1970). This clinoptilolite underwent further hydrothermal alteration probably from Ca±Mg-rich fluids (Ca±Mg for Na+K exchange). Similar observations were made by Altaner & Grim (1990) in the clinoptilolite-bearing bentonites they examined.

6.5. Correlation of the bentonite deposits of Eastern Milos. Effectiveness of the various geochemical methods used for discrimination purposes.

All the geochemical methods applied in chapter 5 led to the same conclusion: <u>The bentonite deposits of the eastern Milos are not parts of the same horizon.</u> Therefore any attempt to asign them to a single volcanic event will lead in misleading interpretations. Moreover, several deposits have a composit character and consist of more than one bentonite horizon.

Examination of the diagrams obtained from the bentonite of Milos leads to the following remarks:

a) The deposits of Area 3 (except for the lower horizon of the Ano Komia deposit) have very similar geochemical characteristics. This fact, coupled with the similar geological features of the deposits, indicates that they might have been derived from a similar parent material which was acidic in character. Since they are located in the same area it follows that they might have been derived from the same parent rock. This view is supported from the fact that the composition of the smectites in these deposits varies between the same limits and is controlled by similar parameters. If this is the case then it is very possible that bentonite deposits exist also in the area between the deposits of Ano Komia and Mavrogiannis. Since the potential area of these deposits is within a faulted zone, they might be located at a greater depth.

b) In the same area, the lower horizon of the Ano Komia deposit might continue in the same faulted zone under the previous horizon. The parent material of this bentonite was formed by a volcanic episode clearly distinct from the episode which formed the parent rock of the overlying bentonite.

c) The bentonite deposits of Tsantili, Aspro Horio and the higher horizon of the Zoulias deposit have very similar geochemical and macroscopic characteristics. They might be parts of the same horizon and therefore have possibly been derived from the same parent rock (andesite probably). The very similar crystal chemistry of smectites from these deposits supports this idea. The different behaviour of the smectites from the corresponding horizon in the Zoulias deposit can be explained by assuming different degrees of Mg-uptake. On the contrary, the rest horizons in the Zoulias deposit are distinct and have been derived from different precursors with different chemistry. The presence of rocks with variable Si-content in the Zoulias deposit suggests that the character of volcanism changed with time.

d) The possibility for a common precursor in Area 1 suggests that other bentonite deposits might exist between the existing deposits. This assumption has recently been confirmed from the discovery of a "new" bentonite deposit between the Tsantili and the Aspro Horio deposits at greater depth (Silver & Baryte Ore Mining Co. oral communication, 1990). Since the area between the Tsantili and the Aspro Horio deposits has been influenced by fault tectonism such fluctuations in the location of the bentonite horizon are expected.

e) Although the Ankeria deposit (Area 2) clearly consists of 4 distinct horizons (see plate 1) only two distinct horizons can be separated geochemically by triangular diagrams; the three lower horizons plot separately from the higher one. However, this separation is not obvious when multivariate statistics are used. In any case, it seems that either the different colourations of the 3 lower horizons are due to the different degree of oxidation of Fe (Bates, 1969) or that the 3 parent rocks had very similar characteristics. The similarity in the macroscopic characteristics of the bentonites indicates that the first hypothesis is not impossible.

f) The higher horizon in the Ankeria deposit plots with the samples from the Koufi deposit in the triangular diagrams. In the diagrams of Winchester & Floyd (1977) they also plot in the same area and seem to be more acidic than the 3 lower horizons of the Ankeria deposit. This suggests that they might have been derived from the same precursor. Again, if this is the case, then more bentonite deposits are expected to be found between the two deposits. It is characteristic that smectites from those horizons of the two deposits which might have been derived from the same precursor follow the same compositional trend. However, it seems that the smectites from the Koufi deposit are richer in Fe. This might be explained if it is assumed that the Mg-uptake from the pore fluid was greater for the smectites from the Ankeria deposit.

g) The lower horizon of the Koufi deposit has clearly different geochemical characteristics (it is more acidic) and plots with the bentonites from the Agrilies deposit. Although the possibility exists that these bentonites might be parts of a single horizon, the lack of a large number of representative samples from the lower horizon of the Koufi deposit does not allow a certain determination. However, the smectites from these deposits show different chemical trends. Although this might be due to the different conditions during alteration (see Section 6.2), there are geographical constraints which contradict assignment in the same horizon. This remarks suggest that similar geochemical trends do not necessarily mean a common origin. More parameters must be taken into account before two geochemically similar samples are assigned in the same horizon. In the case of Milos these parameters include:

1) Geological criteria. Similar macroscopic characteristics support a common origin, but should always be examined causiously, because even different colours might be due to different physicochemical conditions (*e.g* Eh in the case of Fe). Moreover, similar macroscopic characteristics might have resulted from similar geological processes which however involved different parent rocks. Thus, the macroscopic characteristics of the bentonites from the Areas 1 and 3 are very similar ("brocken tuff"-type) although the parent rocks are clearly different.

2) Geographical criteria. Geochemical similarity between two different deposits which are located closely in space increases the possibility for an origin from a common precursor.

3) Crystal chemistry of smectites. Most of the chemical components present in smectites, with the partial exception of Mg, are derived from the parent rocks. Therefore it is believed that the chemistry of the parent rock affects the crystal chemistry of smectites in a particular way. Thus, the different compositional trends observed in smectites derived from different precursors are due to the different parent-rock characteristics. However, there are exceptions to this rule in cases where vast mass transfer in the system has taken place. This is certainly the case in the Prassa deposit, Kimolos.

h) Both the triangular diagrams and the discriminant function analysis diagrams used provided similar information about the geochemical characteristics of the deposits. However, there were differences in the information they provided, which should be examined cautiously. For instance in the territorial map the correlation between the higher horizon of the Ankeria deposit with that of the Koufi deposit is not clear. Also some of the samples from the Aspro Horio deposit plot with the samples of Area 2. This might be due to the effect of subsequent hydrothermal alteration on the relative mobility of the elements used, or to the use of a relatively small number of elements (Huff, 1983). Furthermore the hydrothermal alteration might have affected the pattern of the elemental distribution in the various deposits.

On the other hand the territorial map provided more information about the nature of the bentonites in the Ano Komia deposit. Also, the spread of the samples from Area 3 was smaller compared with that observed in the triangular diagrams. It is believed that if both types of diagrams are used together and combined with the existing geological information, they might provide valuable information about the different characteristics of the bentonite deposits and might be used for correlation and exploration purposes.

CHAPTER SEVEN

QUALITY AND GRADE OF THE BENTONITE DEPOSITS

7.1. Introduction-Definitions.

In economic geology in the evaluation of ore deposits the terms grade and quality are used as synonyms and express the concentration of the useful element in the raw material. In these deposits the concentration of the useful element is given in terms of percentage or in absolute quantities, *i.e* gr/metric ton, ounces/long ton, ppm, $/ton, or gr/$m^3$ according to the type of the deposit (Wellmer, 1989). This terminology cannot be applied to bentonite deposits, because their performance in the various industrial applications does not depend only on the absolute amount of the smectite present. Although a smectite-rich bentonite is usually a good bentonite, other inferior materials, in terms of smectite content, can perform equally well. Therefore, the terms grade and quality are used in a different sense. In this context the term grade will refer to the smectite content of the bentonite and quality to the performance of the material in the various applications (Morgan, 1990a). Quality is related to the inherent physico-chemical properties of the material either in its natural or in its modified form (Highley, 1990).

7.2 Quality of the bentonite deposits.

The quality of a bentonite deposit can be assessed in a laboratory by the following methods (Morgan, 1990a):

-Sodium carbonate exchange. It refers to the amount of sodium carbonate required to obtain the optimum property required. This method is applied in the case of the Ca-Mg bentonites because the properties without exchange are inferior. The sodium exchanged bentonites also usually have inferior properties compared to the naturally occuring Na-bentonites (Patterson & Murray, 1983).

-Swelling test. It measures the swelling efficiency of the raw material in distilled water in terms of gel volume of a known amount of clay added into distilled water, or in terms of the mass of absorbed water relative to the clay mass used in the experiment (Davidtz & Low, 1970, Ravina & Low, 1972, Odom & Low, 1978).

-Liquid limit. It refers to the minimum moisture content required for liquid flow in the Casagrande apparatus (Bain & Highley, 1979, Morgan, 1990a). It is a measure of the bonding efficiency of the bentonite (Grimshaw, 1971 p. 514, Morgan, 1990a). The Ca-Mg montmorillonites have liquid limit values between 100 and 200 and their Na-counterparts have liquid limits between 550-700 (Bain, 1971, Morgan, 1990a). Sodium-exchanged

bentonites can develop equally high liquid limit values if they have been disaggregated (Morgan, 1990a).

Usually the assessment of sodium carbonate exchange of bentonites is made using either the swelling test or liquid limit, if the raw material is a Ca-Mg bentonite. In the present project it was combined with the swelling index test. The amount of sodium carbonate which caused maximum swelling of the clay is referred to as the optimum Na-carbonate content.

7.2.1 Swelling of the smectites. Theoretical concepts.

The swelling of the smectites is a result of their structure, *I.e* they are 2:1 layer phyllosilicates characterized by a series of ionic substitutions in both the tetrahedral and octahedral sheet. These substitutions usually create a charge deficiency which is balanced by interlayer, exchangeable cations. The latter readily hydrate in steps and according to the relative humidity up to 2 layer hydrates can be taken up resulting to a basal spacing at about 15Å (Suquet et al., 1975, see also MacEwan & Wilson, 1984, pp. 205-206). Up to 5 steps have been identified in the Li-saponite (Suquet *et al.*, 1975). Immersion in water leads to the formation of a third hydrate or unlimited swelling under certain circumstances (see below). Therefore, two stages of swelling can be distinguished, the crystalline swelling resulting in an increase of the basal spacing up to 19Å and the so-called osmotic swelling resulting in complete separation of the smectite crystallites (Norrish, 1954, Van Olphen, 1977, MacEwan & Wilson, 1984, Madsen & Müller-Vonmoos, 1989).

Swelling varies as a function of the nature of the interlayer cations, the surface charge density, the charge localization, the availability of water (relative humidity) (Suquet *et al.*, 1975, MacEwan & Wilson, 1984) as well as a series of factors associated with the crystal structure (b-dimension, ferrous iron content, specific surface area) discussed below (see the swelling model of Ravina & Low, 1972). Hence, when exposed to the atmosphere up to 60% humidity, univalent cations form one layer hydrates while bivalent cations form mainly two layer hydrates even at humidities as low as 20% (Suquet *et al.*, 1975, MacEwan & Wilson, 1984). When immersed in water Li-smectites, Na-montmorillonites and some Na-beidellites tend to swell indefinitely (osmotic swelling). Other Na-beidellites as well as saponites give a two layer hydrate (Suquet *et al.*, 1975). When immersed in water Ca, Mg and Ba saturated smectites usualy provide a three layer hydrate. Saponites deviate from this trend. Thus Ca-saponite gives usually a two-layer hydrate and more seldom a three-layer hydrate while some Mg and Ba-saponites show the opposite trend. Also, some Ca-beidellites give a monohydrate (Suquet *et al.*, 1975). Furthermore, there are variations among the different types of montmorillonites. Thus Cheto-type montmorillonites give a three layer hydrate even when they are Li- or Na-saturated (MacEwan & Wilson, 1984).

Osmotic swelling is characterized by the development of big basal spacings between the smectite layers which may reach up to complete dissociation (Norrish, 1954) of the smectite layers. Odom & Low (1978) calculated that fully expanded smectites might be separated by a water film about 295Å thick. The transition from the crystalline to the osmotic swelling is abrupt (from 19 to 40Å) and after this transition there is a statistical distribution of the interplanar spacings depended on the electrolyte concentration of the solution (Norrish, 1954). The same worker using Fourier transform analysis found probability maxima for existence of the next smectite layer at λ 50Å, 110Å and 170Å. This means that in a clay/water system there are smectite layers non-expanded, partially expanded and fully expanded. The latter assumption has been addressed by Odom & Low (1978) and Talibudeen & Goulding (1983). The latter authors attributed the different swelling of the smectite layers to the existence of thermodynamically different exchangeable cation sites. This model proposes 6 thermodynamically different sites which vary from "true mica layers" (non expanding) to "true smectite" layers (fully expanding) through a series of intermediate "hydrous mica" layers (partially expanding).

The interlayer water does not behave as a liquid phase and the system smectite-interlayer water has the characteristics of a quasi-crystalline material (Ravina & Low, 1972, Mulla & Low, 1983) . It is associated through hydrogen bonds with the silicate layers and interacts with the interlayer cations (Farmer & Russell, 1971, Prost, 1975, Suquet *et al.*, 1975). The localization of the charge defficiency in the smectite structure is important for the distribution of the interlayer cations (MacEwan & Wilson, 1984). In saponite the distribution of the interlayer cations is controlled by the location of the charge deficiency (tetrahedral charge deficiency). Therefore they form weak chains acting as bridges between the adjacent silicate sheets (Suquet *et al.*, 1975). A similar condition might occur in beidellite, while in montmorillonite in which the layer charge is located mainly in the octahedral sheet the layer charge is distributed in a diffuse manner (MacEwan & Wilson, 1984). Finally, the type of the interlayer cations affects the three-dimensional structural order of the smectites as this is determined by the number of the stacking faults and the multiple b/3 translations (Suquet *et al.*, 1975).

Although the swelling of smectites has been studied extensively, there is not a generally accepted opinion about the mechanisms which drive this property. So far, three different models have been proposed. The first model uses the concept of the *diffuse double layer* (Norrish, 1954, Van Olphen, 1963, 1977, Madsen & Müller Vomoos 1989), the concepts of which have been described in detail by Van Olphen (1963, 1977). According to this model, in a fully dispersed clay suspension each of the negatively charged clay particles is surrounded by an "atmosphere" of positively charged cations, the so called "counter ions" or "gegen ions" which constitute the diffuse or Gouy layer. The concentration of these cations is high close to the clay surface and decreases away from it. Simultaneously, there

is a deficiency of negatively charged ions, the "co-ions", the concentration of which increases away from the clay surface. Thus, there is an adsorption of the counter ions and a negative adsorption of the co-ions from the clay surface.

When two diffuse layers approach each other their interaction outcome is the result of two main types of forces: electrostatic repulsion from the interaction of the two positive diffuse layers and Van der Waals attraction. In the case that the two particles approach each other in an edge-to-face direction then attractive instead of repulsive electrostatic forces may result. Addition of electrolytes like NaCl supresses the diffuse double layers. Two further repulsion forces are efficient only at very short ranges: the Bohr repulsion which resists interpenetration of the crystal lattices and the specific adsorption forces which resists approach closer than that of the inner water shell, to the surface of the particle.

In this model osmotic swelling is related to the formation of the double layer atmosphere when the clay particle enters the water. Due to the difference in the counter ion concentration between the bulk solution and the interlayer space water penetrates that space and the clay swells. The swelling pressure is equal to the osmotic pressure if the double layer repulsion is the only operating force in the system. The most significant attraction force which counteracts and confines the double layer repulsion is a cross linking force due to a negative face-positive edge association of the clay particles.

An important drawback of this model is the admittance of positively charged clay edges when it is known that the point of zero charge of montmorillonite is at much lower pH values than those at which the experiments take place (Rand *et al.*, 1980, Lagaly 1981, Eslinger & Pevear, 1988 table 3-2). Therefore all the clay surface is negatively charged at pH 7. Furthermore it cannot explain why highly charged clay minerals vermiculite or mica do not swell (the former osmotically) (Kleijn & Oster, 1982).

The second model proposes epitaxial (pseudomorphic) development of the water film on the smectite (montmorillonite) surface (Ravina & Low, 1982). Both lattices undergo adjustments with each increment of the water. In the first stages the water lattice is modified in order to conform with that of montmorillonite. As the interlayer water increases in thickness the opposite occurs and the montmorillonite adjusts accordingly. As a result of these adjustments the b-dimension increases (Davidtz & Low, 1970, Ravina & Low, 1972, Odom & Low, 1978) and its final value which is the same for all montmorillonites (about 9.00Å), is governed by the preferred configuration of the water. When the b-dimension reaches the value of 9.00Å swelling ceases (Ravina & Low, 1972). The separation of the clay particles is a function of the swelling pressure (Viani *et al.*, 1983). The latter decreases with an increase in the octahedral ferrous iron content (Stucki *et al.*, 1984). The specific surface areas available to water is a function of both the partially expanded and the fully expanded layers and is a linear function of the b-dimension if only fully expanded particles

are present (Odom & Low, 1978). In an extension of this model it was found that the montmorillonite/water properties obey the following empirical equation (Mulla & Low, 1983):

$$J_i = J_i^0 \exp(\beta_i m_c/m_w) \qquad 7.1$$

where, J_i is the magnitude of any property i of the montmorillonite/water system, J_i^0 is the magnitude of the same property for the pure bulk water, β_i is a constant characteristic of that property and m_c/m_w is the mass ratio of the montmorillonite to water.

The third model proposes an electrostatic source of swelling which is related to the formation of *tactoids i.e* stacks of parallel, equally spaced clay platelets (Kleijn & Oster, 1982). According to this model the average Gibbs free energy of electrostatic interaction, G_e, is a function of the cationic substitution charge σ and the electric potential at the location of the electric substitution charge, in the actual and the reference (single platelets) state. For bivalent counter ions G_e is repulsive at low σ values except for very high electrolyte concentrations. For high σ values G_e is always attractive. For univalent counter ions the trends are similar, but the range of cationic substitution where repulsion occurs is much larger and the repulsion is stronger. A Na-montmorillonite with σ=0.23 will lead to a formation of tactoids only at high electrolyte concentrations, while a Ca-montmorillonite with the same charge will form tactoids at all electrolyte concentrations. This model also explains why minerals with high layer charge like vermiculites do not expand.

The model predicts also the possibility for formation of tactoids, the size of which is determined by G the sum of G_e and G_w (free energy of van del Waals interaction). The tactoid size for which G is minimum will be preferred. The value of G does not depend strongly on the number of platelets for tactoids with more than 4 platelets but is controlled by temperature, because when the decrease of G for an extra platelet approaches kT (k is the Boltzmann constant), the tactoid has reached its maximum size. Therefore, the size of the tactoid is limited by thermal movement unless mechanical forces, like shear forces, break it up. This can explain observations made by Morgan (1990a) about the role of disaggregation, forced by high shear rates, on the liquid limit of some Na-exchanged bentonites.

An alternative electrostatic model for swelling was presented by Farmer & Russell (1971). They attributed the hydration and swelling properties on the type of coordination and the number of the low energy links of the interlayer cation with the surface oxygens. The observed lack of swelling of micas is attributed to the fact that K is coordinated with the maximum number of surface oxygens (12) and that each oxygen is coordinated to two K atoms. Therefore hydration cannot establish new links and water does not penetrate the interlayer space. On the other hand in K-smectites with less than half K-content most oxygens are coordinated to one K atom and some to none. Therefore they hydrate. However, due to the localization of the layer charge, K-saponite and K-beidellite do not hydrate to more than one layer hydrate. For the Na-vermiculite to expand a maximum of

three single water links of Na with surface oxygens must occur. Na-vermiculite does not expand to more than a two layer hydrate due to a larger number of links (4 or 5). For similar reasons K-montmorillonite exhibits osmotic swelling. Similar explanation is given for the behaviour of clays saturated with bivalent interlayer cations.

7.2.2. Swelling properties of the Greek bentonites.

7.2.2.1. Experimental methods.

The swelling properties of the Greek bentonites were assessed by the use of the swelling volume, expressed in ml of gel per 10gr of clay (Morgan, 1990a). A total of 91 samples corresponding to characteristic vertical or horizontal (in the case of the Prassa deposit, Kimolos) profiles of the bentonite deposits were examined. The raw materials were dried at 60^{o}C overnight, reduced in size with a fly press and crushed with pestle and mortar so as they could pass through a 125μm sieve (BS 410). Activation was performed with analytical grade anhydrous sodium carbonate (FISONS) with carbonate content ranging between 1 and 5%. For those samples which did not develop a definite maximum swelling volume, a further treatment with 6% carbonate addition was performed. The method used for the soda activation has been described by Morgan (1990a) and is given in Appendix 7.1.

The swelling volume was determined using a modified version of the method described by Morgan (1990a). The modifications applied include:

-i) Use of 25ml test tubes instead of 10ml measuring cylinders. The larger diameter of the tube compared to that the 10ml measuring cylinders ensures that a smaller contact between the clay and the tube walls occur. These conditions are closer to the free swelling conditions.

-ii) Use of larger volume of distilled water (20ml), in order to avoid calculations of the swelling volume using the residual mass of the material as much as possible. This was necessary since it was found that the bentonites develop very large swelling volumes.

-iii) Addition of the bentonite over a larger time span and in more doses so as to allow the development of the maximum possible swelling.

-iv) Measurement of the swelling volume using a calibration curve in which the column height of the gel was converted to actual volume (Appendix 7.3). This was necessary because of the curvature of the bottom of the test tubes. The relationship between volume and column height is linear for gel volumes greater than 2.8ml (or 28ml/10gr of clay), becoming curvelinear for smaller ones.

The description of the method is given in Appendix 7.2, while the results are presened in Table 7.1.

7.2.2.2. Results.

The swelling volume varies with in the various deposits, but the mode of variation is not the same in the different deposits (Fig. 7.1, 7.2). In the Ankeria deposit (Fig. 7.1a) the swelling properties vary in a rather unsystemetic manner. However, it seems that although no overall trend is observed, swelling decreases from the lower to the higher part of <u>each</u> horizon, for all the bentonite horizons. This profile is observed in the eastern part of the deposit. The swelling volume does not seem to vary substantially within the same horizon (*e.g* compare the swelling volumes of the samples SM1, SM22, SM26 and SM27 in Table 7.1) On the contrary in the Koufi deposit (Fig. 7.1b) there is a well determined overall increase of the swelling properties with decreasing depth. Only in the highest horizon there does the swelling volume decrease. In the same stratigraphic level swelling varies more compared to the Ankeria deposit (*e.g* compare the samples SM54 and SM64 in the Table 7.1). The poor swelling properties (Table 7.1) of the samples SM8 (Ankeria deposit) and SM47 (Koufi deposit) are due to alteration (the SM8 has been affected by the hot spring activity present in Ankeria while the SM47 was taken close to a hydrothermal vein).

In the Tsantili deposit a well determined decrease of the swelling volume with depth is present (Fig. 7.1c). In all three samples smectite is fully expandable. This vertical profile represents the variation at the eastern face of the deposit. Also the effect of the illitization of smectite is visible in Figure 7.1i . As it was expected, the swelling volume decreases with decreasing expandability and becomes essentialy negligible at very low expandabilities. By comparing the Figures 7.1c and 7.1i it is obvious that samples containing mixed layer I/S up to at least 40% expandables (random and/or ordered) have better swelling properties than samples from the upper sector of the deposit containing pure smectite. This event probably represents defferent alteration conditions and will be discussed further in the following section.

In the Aspro Horio deposit the swelling volume increases towards the centre of the lower horizon and then decreases to a minimum value in the thin overlying red horizon. After that it increases to a maximum value in the higher yellowish horizon. Therefore the trends observed in the two main horizons of of this deposit are opposite probably reflecting their different nature.

A very characteristic distribution pattern of the swelling properties is observed in the Zoulias deposit (Fig. 7.1f). A sector characterized by low swelling volumes is "sandwiched" between two sectors of high swelling properties, namely, the lower and the higher stratigraphic levels of the deposit. The low swelling volume of the lowermost horizon (andesitic lava) is probably due to the influence of the hydrothermal alteration (see discussion below).

Table 7.1

Swelling volumes of the Greek bentonites.

Sample	Untreated	Na_2CO_3 1%	Na2CO3 2%	Na2CO3 3%	Na2CO3 4%	Na2CO3 5%	Na2CO3 6%
Ankeria							
SM1	29	52	77	107	151	170	142
SM8	24	39	63	92	113	118	98
SM13	31	51	82	127	162	170	121
SM16	30	43	78	105	165	185	155
SM17	30	67	124	169	183	176	136
SM19	25	42	62	89	127	158	130
SM22	28	51	93	120	158	180	161
SM26	19	44	86	124	169	169	115
SM27	29	57	102	135	165	176	153
SM36	30	67	88	114	193	199	174
Koufl							
SM47	28	65	81	106	101	97	- -
SM51	33	97	125	176	186	170	- -
SM52	32	77	115	163	164	157	- -
SM54	28	65	120	155	161	169	118
SM60	25	76	117	137	169	146	- -
SM64	31	68	121	138	151	132	- -
SM66	22	47	132	149	140	120	- -
SM69	24	71	93	160	155	149	- -
Tsantili							
SM82	10	10	10	10	11	10	- -
SM88	26	28	55	56	49	49	- -
SM93	13	14	14	18	22	25	23
SM95	38	80	82	83	71	60	- -
SM98	24	60	129	154	160	144	- -
SM100	28	51	115	163	186	166	- -
SM108	25	120	102	93	82	71	- -
A. Horio							
SM114	25	69	127	149	168	135	- -
SM115	38	72	145	171	176	138	- -
SM117	35	137	133	173	173	172	128
AM118	30	75	112	138	159	128	- -
SM119	33	77	105	116	121	92	- -
SM120	28	54	73	111	127	121	- -
SM122	10	16	20	22	20	20	- -
SM125	33	65	103	145	204	184	- -

Table 7.1 (continued)

Sample	Untreated	Na2CO3 1%	Na2CO3 2%	Na2CO3 3%	Na2CO3 4%	Na2CO3 5%	Na2CO3 6%
A.Komia							
SM134	16	48	73	72	69	58	- -
SM135	25	51	82	101	88	80	- -
SM136	25	76	122	198	175	131	- -
SM142	16	46	45	39	42	40	- -
SM147	18	81	123	123	112	96	- -
SM148	20	58	110	156	139	121	- -
SM152	29	77	150	142	126	111	- -
SM153	22	47	113	128	98	99	- -
SM156	22	84	151	162	184	115	- -
Garyfala-kena							
SM158	15	35	48	50	51	44	- -
SM159	18	27	50	57	60	43	- -
SM161	18	18	38	54	45	37	- -
SM162	22	36	64	51	46	42	- -
SM163	16	22	44	42	37	36	- -
SM164	20	33	48	59	47	43	- -
SM165	22	52	91	122	104	99	- -
SM167	19	47	80	93	99	80	- -
SM168	15	41	57	48	34	38	- -
Mavrogia-nnis							
SM175	22	40	106	129	122	105	- -
SM176	18	20	24	29	41	61	75
SM178	25	98	125	131	130	123	- -
K.Komia							
SM179	29	68	107	109	84	77	- -
SM180	16	49	66	71	64	63	- -
Zoulias							
SM185	22	25	33	43	44	69	88
SM205	31	105	141	161	187	176	- -
SM207	18	36	120	153	135	110	- -
SM209	30	47	107	152	198	167	- -
SM211	29	57	102	135	165	176	153
SM226	15	32	50	77	68	80	72
SM227	14	27	36	36	24	30	- -
SM228	22	50	81	129	172	143	- -
SM230	13	35	30	29	19	18	- -

Table 7.1 (continued)

Sample	Untreated	Na_2CO_3 1%	Na_2CO_3 2%	Na_2CO_3 3%	Na_2CO_3 4%	Na_2CO_3 5%	Na_2CO_3 6%
Rema							
SM235	32	93	142	145	144	118	- -
SM236	29	54	119	131	140	132	109
SM237	22	68	106	104	89	84	- -
Agrilies							
SM246	18	18	18	18	17	17	- -
SM247	16	16	16	17	27	27	- -
SM248	20	61	121	168	175	127	- -
Prassa							
SM261	42	72	92	110	131	118	- -
SM262	28	62	105	136	136	133	- -
SM264	40	65	110	152	134	154	115
SM265	25	45	90	105	121	99	- -
SM269	37	80	90	108	104	109	107
SM277	39	65	87	101	98	107	94
SM278	41	96	162	189	187	180	- -
SM279	34	71	106	220	250	235	222
SM280	36	74	127	189	206	177	- -
SM281	40	74	123	198	199	205	225
Loutra							
SM295	16	24	33	33	30	30	- -
SM296	10	12	16	16	16	16	- -
SM297	15	38	50	56	59	52	- -
SM298	16	35	54	80	47	56	- -
Fanara							
SM306	15	47	70	58	52	43	- -
SM307	43	112	184	199	215	236	193
Chios							
SM321	18	40	68	75	76	68	
SM324	22	40	62	90	96	97	70
SM336	15	33	60	73	75	68	- -
SM338	25	35	67	94	129	125	99

	7% Na_2CO_3	8% Na_2CO_3
SM185	90	86
SM176	69	70

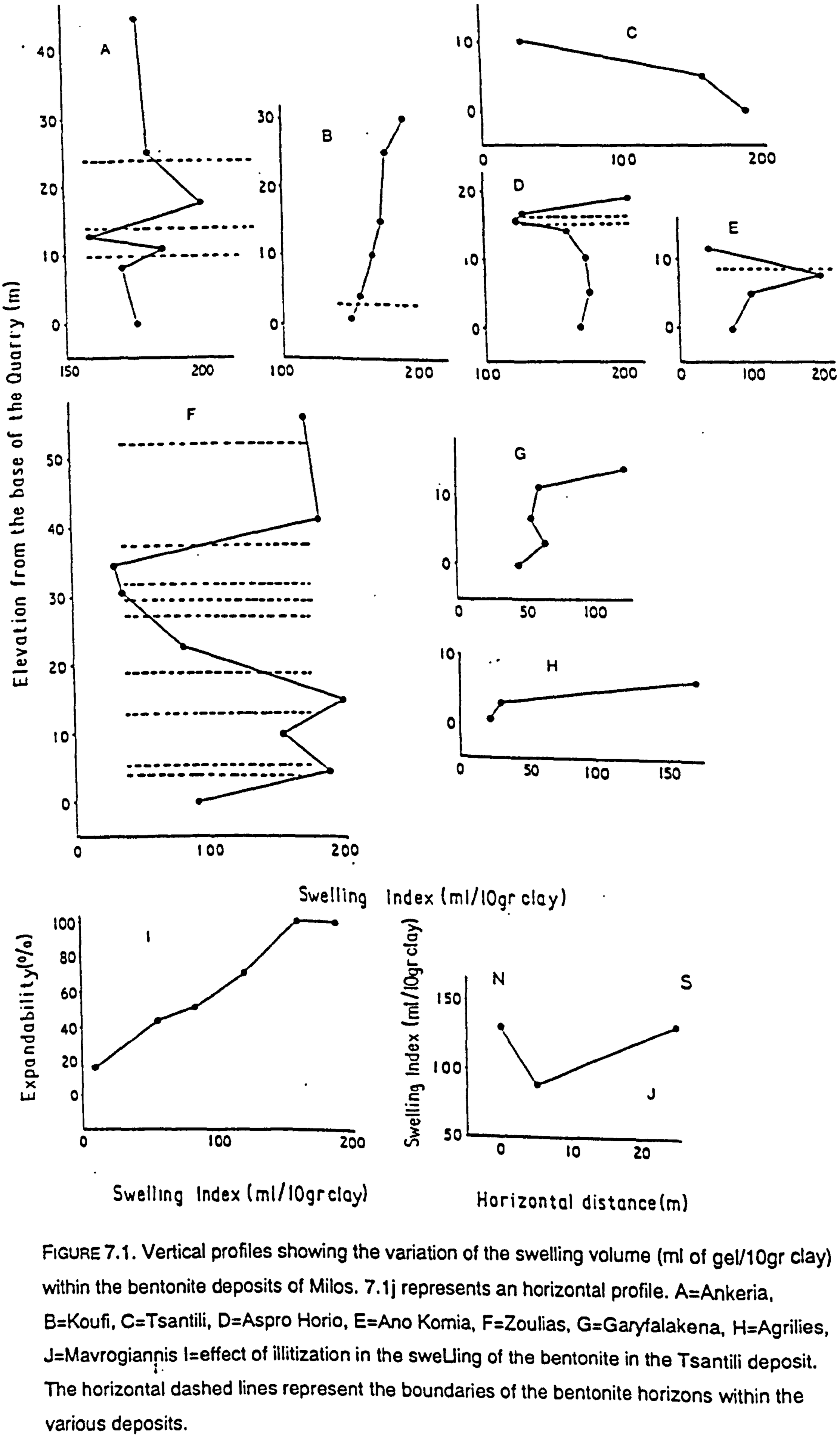

FIGURE 7.1. Vertical profiles showing the variation of the swelling volume (ml of gel/10gr clay) within the bentonite deposits of Milos. 7.1j represents an horizontal profile. A=Ankeria, B=Koufi, C=Tsantili, D=Aspro Horio, E=Ano Komia, F=Zoulias, G=Garyfalakena, H=Agrilies, J=Mavrogiannis I=effect of illitization in the swelling of the bentonite in the Tsantili deposit. The horizontal dashed lines represent the boundaries of the bentonite horizons within the various deposits.

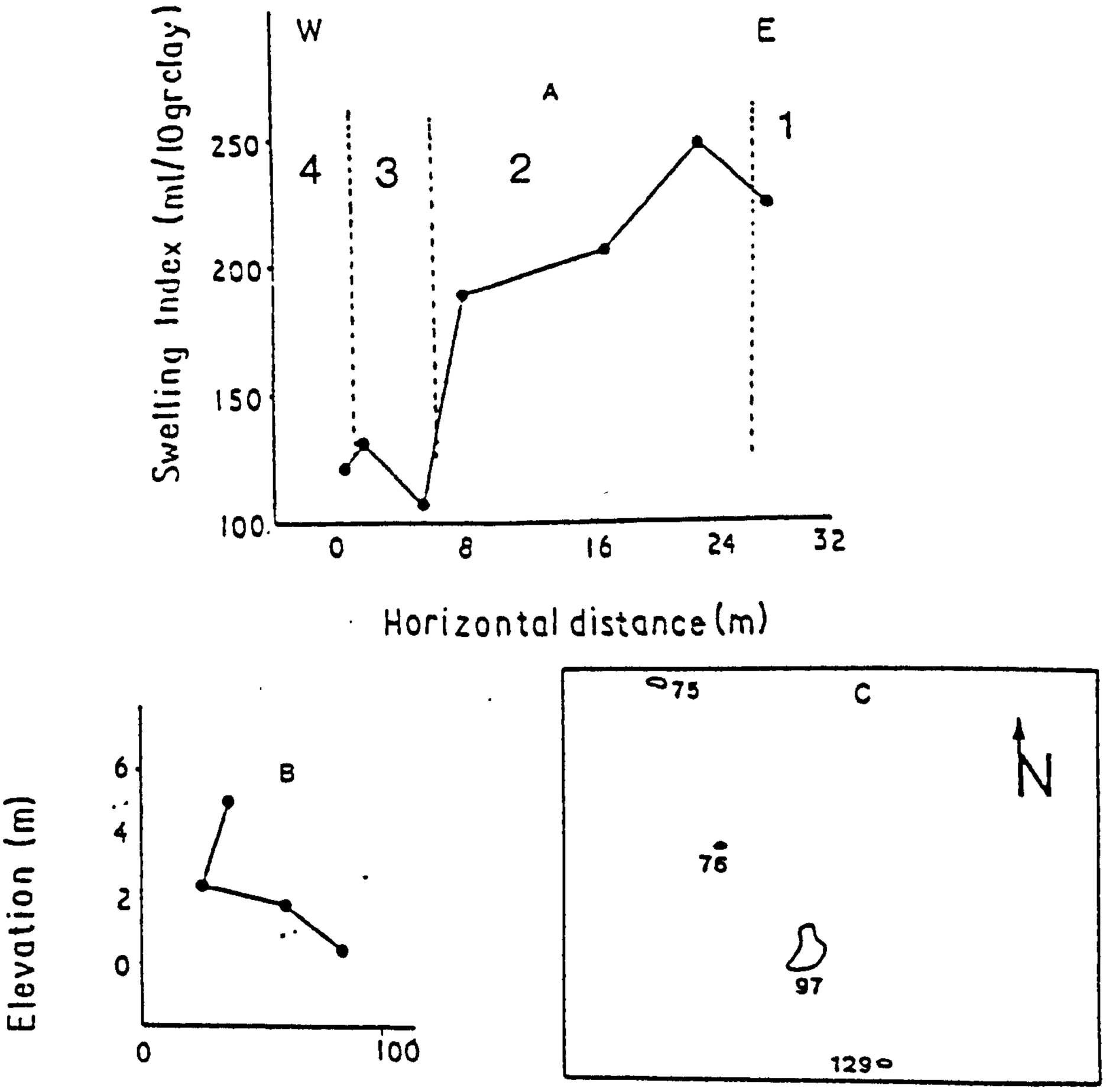

FIGURE 7.2. Profiles showing the variation of the swelling volume (ml of gel/10 gr clay) within the bentonite deposits of Kimolos and the bentonite outcrops of Chios. A=Prassa deposit, Kimolos, B=Loutra deposit, Kimolos, C=Chios. In A: 1= smectite + opal C–T zone, 2= smectite zone, 3= smectite + mordenite zone, 4= smectite + opal C–T ± mordenite zone.

The swelling volumes of the bentonites from the Area 3 of Milos are lower than those from the Areas 1 and 2. In the deposit of Ano Komia the lower horizon is characterized by a continuous increase of the swelling index with decreasing depth (Fig 7.1e). The swelling volume of the overlying horizon which corresponds to the parent material is low due to the small degree of alteration. A rather similar trend is present in the Garyfalakaina deposit (Fig. 7.1g), and in the Kato Komia deposit (in Table 7.1 the sample SM180 overlies SM179). On the other hand in the Mavrogiannis deposit (Fig. 7.1j) and in the Rema deposit (Table 7.1) the swelling volume dues not vary substantially, except for areas affected by hydrothermal alteration. Finally in the deposit of Agrilies (between the Areas 1 and 2) the swelling properties are similar in the lower levels of the deposit increasing suddenly in the higher ones (Fig. 7.1h).

In the Prassa deposit, Kimolos the swelling properties vary substantially in the different alteration zones (Fig. 7.2a). The swelling volumes of the samples from the smectite + mordenite zone and the smectite + opal-CT ± mordenite zone are low while those from the smectite zone are high. The transition between the zeolite-bearing zone and the smectite is abrupt. It also seems that the swelling properties in the smectite zone increase towards the smectite + opal-CT zone.

In the Loutra deposit, Kimolos, the swelling volumes increase with depth but they never reach high values (fig 7.2b). In the Fanara deposit the white bentonite (SM307 in Table 7.1) develops very high swelling volumes while the bentonite in the higher levels of the deposit (see Chapter 3 for the geological description of this deposit) has low quality (SM306 in Table 7.1).

Finally, the bentonites from Chios show an interesting tendency characterized by a steady increase of the swelling volume towards the SE (Fig. 7.2c). Although the swelling properties of these bentonites are not as good as those of many of their Miloan or Kimolian counterparts, they are better than many of the bentonites from the Areas 3 of Milos which have been exploited extensively in the past.

The amount of the sodium carbonate which caused maximum swelling of the bentonites provides an estimation about the nature of the exchangeable cations in the raw material (Morgan, 1990a). Thus in the Areas , Milos, maximum swelling was obtained after addition of 4% Na_2CO_3 in most cases. Some horizons from the Zoulias deposit were activated with 5% carbonate while the lowermost horizon in the same deposit required 7%. It is remarkable that the K-bentonites from the Tsantili deposit required much less carbonate (2-3%) than their unaltered counterparts, indicating that the dominant exchangeable (*i.e* unfixed) cation in the mixed layer I/S is Na. Two possible explanations are proposed:

-a) The K-fixation during the conversion of smectite to illite proceeded through layers containing mainly Ca and/or Mg.

-b) The K-fixation in some layers was coupled by a Na for Ca and/or Mg exchange in others. The Na might have been derived from the replacement of this element by K in those layers where K-fixation occured according to the following reactions (see also Section 6.3):

Smectite + K^+ ± Al^{3+} --> I/S + quartz ± kaolinite + Ca^{2+} + Na^+ + Mg^{2+} 7.2a

(illitization of some of the smectite layers)

$2Na^+$ + (Ca,Mg,Na?)-smectite --> [Na,(Ca?,Mg?)]-smectite + Ca^{2+} + Mg^{2+} 7.2b

(Na for Ca and Mg exchange for the remaining smectite layers)

The latter mechanism is supported from the TEM results (see Chapter 4) in which it was shown that the "smectite" particles in samples containing I/S were 10Å thick. Since complete dissociation of the smectite flakes has been reported only for homoionic Na-smectites (see Mering & Oberlin, 1971, for a discussion) it is believed that the illitization of some of the smectite flakes caused a "natural Na-activation" of the remaining flakes. Nevertheless, the fact that illites/smectites require less Na-carbonate than smectites, should also play an important role on the limited amount of the carbonate used.

The bentonites from the Area 2 in Milos develop their maximum swelling volumes at 4% Na_2CO_3 (Koufi deposit) and 5% Na_2CO_3 (Ankeria deposit). Only the lower horizon of the Koufi deposit was activated with 3% Na_2CO_3. The deposits from the Area 3 of Milos were activated with 3% sodium carbonate. In some samples of the Garyfalakena deposit as low as 2% carbonate was used. In the deposits of Kimolos an average of 4% carbonate was used, with some samples from the Loutra deposit requiring 3% and the poor bentonite of the Fanara deposit only 2%. On the other hand in the latter deposit the white bentonite required 5% carbonate. Finally, the deposits from Chios Island required 4% Na_2CO_3 to develop their maximum swelling volumes.

These results are in accordance with the electron probe microanalytical data for smectites (Appendix 4.3), suggesting that microbeam techniques can provide reliable chemical analyses of clay minerals, even for very sensitive elements, like Na. Indeed in the Areas 1 and 2 the main exchangeable cation of the smectites is Ca. In the lower horizon of the Koufi deposit, the major cation in both the beidellites and the montmorillonites is Na followed by K, while there is little Ca. In the Area 3 of Milos the major exchangeable cation is Na followed by K, while Ca is of minor importance. In the Agrilies deposit almost all the exchangeable cations have been displaced probably by H^+, leading to low pH values in those bentonites (see Chapter 8). In Kimolos the smectites are Ca-rich Cheto montmorillonites with minor Na content. Only in some smectites from the mordenite-bearing zone K is the major exchangeable cation (see chapters 4 and 6). Finally, in the bentonites from Chios sodium is hardly present in the exchangeable sites of the Otay montmorillonites present.

7.2.2.3. Discussion.

Swelling may be considered to consist of two components: a) the "grade component" which reflects the amount of the non-swelling minerals and b) the "pure swelling" component which is the actual result of the swelling capacity of the clay. The latter can be estimated by comparison of the swelling volumes of two bentonites containing similar grit content. Both components can be affected by secondary processes like hydrothermal alteration. The grade component may be affected by the conversion of smectite to other phases like kaolinite, alunite, mixed layer I/S or/and to smectite with lower layer charge, or the precipitation of other phases like carbonates or sulphates by hydrothermal solutions. Both, virtually "dilute" or eliminate the smectite content originally present in the bentonite.

The quality component might be affected by hydrothermal alteration by several mechanisms which are important for all the theories about the cause of swelling. These mechanisms which do not affect the grade component might include:

- Drop of the pH of the gel (influences the formation of positive edges promoting edge-to-face flocculation according to the diffuse double layer theory).
- Formation of smectite with lower layer charge like in the reaction (6.4) (Section 6.3) suggested for the Tsantili deposit (influences the electrostatic models).
- Formation of smectite with different lattice dimensions, caused either by different octahedral occupancy or/and to Fe-oxidation/reduction (influences the epitaxial model).

The influence of the hydrothermal alteration is significant in almost every deposit of Milos island, with most characteristic examples the deposits of Tsantili (Fig. 7.1c,i.), Mavrogiannis (Fig 7.1j), Agrilies (Fig. 7.1h) and Rema (sample SM237 in Table 7.1). In every case it is associated with a substantial decrease of the swelling index. In the Mavrogiannis deposit the material with the low swelling index was taken from a hydrothermal vein rich in sulphates. Also in the Agrilies deposit the lower horizons are influenced by hydrothermal activity associated with S-metasomatism and very acidic conditions.

In the Tsantili deposit the fact that K-bentonites swell more than "normal" ones which are rich in sulphates chacteristic of acidic environments (alunite, jarosite), suggests that pH affects the swelling properties to a certain degree. In this case, the poor swelling properties might be explained by the development of strong edge-to-face links leading to flocculation (Van Olphen, 1963, 1977) at the low pH. Edge-to-face flocculation cannot be rejected because the pH is below that of the point of zero charge.

The effect of pH on the alkali-activation has been examined further in the sample SM185 (2.5 pH in distilled water, see Chapter 8). This sample gave the highest swelling volume only when it was treated with 7% Na_2CO_3, *i.e* only when the pH probably increased from the addition of the carbonate. It is possible that alkali-activation does not improve the

swelling properties of bentonites in acidic conditions because the sodium carbonate is probably consumed in a neutralization reaction:

$$Na_2CO_3 + 2[H_3O]^+ + SO_4^= \text{--> } Na_2SO_4 + 3H_2O + CO_2 \qquad 7.3$$

After neutralization the activation reaction proceeds. This might be a possible reason for the use of large amounts of carbonate in the activation of acidic samples. Only if the pH of the bentonite-water system raises above the point of zero charge, the edge-to-face flocculation is eliminated and the swelling properties improve.

The effect of the grade component can be evaluated in the deposits of the Area 3 in which the bentonite deposits are rich in silica phases like opal-CT or quartz. These bentonites are relatively poorer in smectite compared with their counterparts from the Areas 1 and 2, and develop low swelling index. The presence of the fine grained silica phase (the opal-CT present is usually less than 1μm in size) can also affect the pure swelling component forming fine intergrowths with the smectite crystallites, retarding the separation of the smectite flakes and thus swelling. A similar situation has been observed in the Prassa deposit, Kimolos, in which the mordenite-bearing zone and the smectite + opal-CT ± mordenite zone exhibit significantly lower swelling volumes than the smectite zone.

In several of the Miloan deposits the swelling properties increase with decreasing depth of burial (*i.e* Koufi, Garyfalakaina, Ano Komia). Therefore it seems that compaction influences the swelling properties (Morgan, 1990a). However, this trend is rather exceptional. There are other deposits in which the opposite trend is observed (Aspro Horio deposit, Milos, Loutra deposit, Kimolos) while in other deposits (Ankeria and Zoulias in Milos), no particular trend has been observed. Furthermore, even in the Ano Komia deposit the decrease of the swelling with depth might be due to hydrothermal alteration (see Plate 2). Only in the Koufi deposit compaction might be regarded as the possible reason for the trend observed, because of the thickness of the deposit and the uniform nature of the bentonite.

The nature of the exchangeable cations has been associated with the nature of the parent rock as well as with the concentration of the pore solutions in environments like this in which the Greek bentonites were formed (Odom, 1984). Thus, in the bentonites from the Areas 1 and 2 the existence of Ca as a major interlayer cation is in accordance with the andesitic-dacitic character of the parent rocks. Similarly in the bentonites from the Area 3 the presence of Na as the major interlayer cation is in accordance with the acidic character of the precursors. However, in the case of the Prassa deposit in Kimolos, although the parent rock was acidic, the major interlayer cation is Ca. The same might be true in the white bentonite of the Fanara deposit, which required 5% sodium carbonate to display maximum swelling.

In section 6.2 it was clearly shown that the nature of the parent rock plays an important role in the compositional signature of the smectites present in the Greek bentonites. Since the formation of the bentonites requires removal of the alkali-cations, it follows that in rocks with initially higher Na and K content the possibility for Na-rich smectites is higher. It is also characteristic that in all the deposits the existence of alkali-rich-smectites is associated with another alkali-rich authigenic phase, either K-feldspar, or/and a zeolite (clinoptilolite/heulandite or mordenite). This indicates that although the system was open, fluid flow was not intense enough to prevent the formation of these phases. In the smectite zone in the Prassa deposit although there was an inherited high Na and K concentration, the intensive leaching conditions led to the formation of Ca-smectites and/or Mg-smectites (see following Section and Chapter 10). On the contrary, in the mordenite-bearing zone characterized by less severe fluid flow, Na-K-smectites along with Ca-smectites are present. Therefore, it is believed that the chemical composition of the parent rock, the cooling rate of the glass, the pH of the solution (see Section 6.4), and the conditions of fluid flow prevailing during the formation of the bentonites, might determine the original interlayer cation chemistry of the smectites. The original pattern might be modified later by other events, like recrystallization and crystal growth (Ostwald ripening-like process) and hydrothermal alteration. The latter seems to be the case in several deposits (Agrilies, Tsantili etc.)

7.3. Grade of the bentonite deposits.

Morgan (1990a) suggested that the grade of a bentonite deposit might be evaluated either by measurement of the cation exchange capacity (CEC) or by the surface areas measured by ethylene glycol monoethyl ether (Carter *et al.*, 1965). In the present work the former method was used. The cation exchange capacity of a clayey material can be measured by a variety of methods:

a) Methylene blue absorption (Nevins & Weintritt, 1967) which gives only an estimation of the real CEC because the obtained value corresponds to about 80% of the real CEC (Morgan, 1990a).

b) Saturation of the clay with an index cation and determination of the displaced cations usually with atomic absorption spectrophotometry or flame photometry. The sum of the displaced cations (Na+Ca+Mg+K+exchangeable acidity *i.e* H^+) is the cation exchange capacity (Bain & Smith, 1987).

c) Saturation of the clay with an index cation and subsequent displacement of this cation usually by means of distillation. The cation is collected in a solution containg a combination of indicators, which is subsequently titrated with a weak acid of known strength. The value obtained corresponds to the total CEC.

d) Saturation with an index cation and subsequent radioactivity measurement (c.f Deist & Talibudeen, 1967)

e) CEC determination using exchange resins. The material is allowed to pass through exchange columns where it is saturated with an index cation. The latter is displaced and its concentration is measured by flame photometry (c.f Sansom *et al.*, 1968a,b).

f) Calculation of the CEC from the structural formula, obtained from chemical analysis of the clay fraction. This method is feasible if the clay fraction is monomineralic. It is assumed that the exchangeable cations are Ca, Na and K and that Mg is entirely assigned in the octahedral sites. An extension of this method might include the calculation of the CEC of several smectite crystals the structural formula of which can be obtained by electron-beam techniques. In this case, the average CEC calculated from the microanalyses will be the CEC of the sample. Obviously, the larger the number of the analysed points, the more reliable the CEC determination.

7.3.1. Theoretical concepts.

The cation exchange capacity is the excess of cations over anions present on the surface of a solid (Yariv & Cross, 1979). In similar definition Bain & Smith (1987) considered CEC as the sum of the exchangeable cations a mineral can absorb at a specific pH. It is usually measured in meq/100gr clay. In clay minerals it results from a number of factors associated with their structure. Grim (1962, 1968) considered that CEC is the result of a number of factors:

i) Isomorphous substitutions either in the octahedral (montmorillonite, hectorite) or the tetrahedral (beidellite, saponite) sheet which lead to a charge deficit. This deficit is balanced by the interlayer cations which are readily exchangeable. In the octahedral sheet, the most important substitutions which may lead to cation exchange capacity are Mg^{2+} for Al^{3+} and Fe^{2+} for Al^{3+} in the montmorillonite and to a much lesser degree in beidellite, and Li^{+} for Mg^{2+} in hectorite. In the tetrahedral sheet the most important substitution is that of Al^{3+} for Si^{4+} and sometimes, although seldom, of Fe^{3+} for Si^{4+}. According to Grim (1962, 1968) this type of charge deficit accounts for 80% of the observed CEC in smectites. Sometimes such substitutions may be partially balanced by other lattice changes like OH^{-} for $O^{=}$ exchange.

ii) Broken bonds around the edges of the silica- alumina units may produce charges which are balanced by adsorbed cations. Such bonds usually occur in uncleaved surfaces *i.e* parallel to the *c* axis. The number of the brocken bonds increases with decreasing particle size. It is believed (Grim, 1962, 1968) that they account for about 20% of the total CEC of the smectites.

iii) The hydrogen of the exposed hydroxyls may be displaced by a cation which is replaceable. According to Grim (1968) this type of charge deficiency would be important in kaolinite and halloysite.

Oxidation of the ferrous iron does not decrease the CEC as it might perhaps be expected, because it is accompanied by assimilation of H_2O followed by elimination of a structural H^+ *i.e* a net uptake of an OH^- (Lear & Stucki, 1985).

When the interlayer cations are not replaceable then they are called *fixed*. Such cations have low hydration energy like, K^+, NH_4^+, Rb^+ and Cs^+ (Yariv & Cross, 1979). Fixation is affected by the thermal history of the smectites (Inoue & Minato, 1979) which is closely associated with alternate wetting/drying cycles (Srodon *et al.*, 1986). In a comprehensive review Yariv & Cross (1979) suggested that fixation might occur by sorption onto frayed crystal edges (usual in weathering conditions), by thermal sinking into crystal framework vacancies, by hydrogen bonding between hydrated cations and the oxygen plane, and by polymerization of multivalent cations.

The reaction which describes the mechanism of cation exchange has the following form (Laudelout, 1987):

$$nMZ_m + mN^{n+} = nM^{m+} + mNZn \qquad 7.4$$

where m^+ and n^+ are the charges of the exchangeable cations M and N respectively, and Z is the clay mineral surface *i.e* the exchanger. The reaction rate cannot be described thermodynamically by conventional methods using the activities of the components involved, because in the colloid systems the large colloid particles accumulate larger amounts of smaller ions in their suroundings creating inhomogeneity (Yariv & Cross, 1979). The rate of the exchange reaction is given by the following equation:

$$K = \ln K_N + n\ln f_m - m\ln f_n \qquad 7.5$$

where K is the rate of the reaction, K_N is the selective coefficient of the exchange reaction and f_m and f_n are activity coefficients applying to the exchanger, corresponding to the activity of the exchanger saturated with the different cations (see reaction 7.4). The equation 7.5 can be transformed to the following form (Yariv & Cross, 1979, Laudelout, 1987):

$$\ln K = (m\text{-}n) + \int_L (\ln K_N \, dN_m + n_w \, d\ln a_w) \qquad 7.6$$

where, N_m is the equivalent fraction of the m-valent component defined as: $N_m = I^{(m+)}/\Gamma$ (I is the amount of the cation m^+ *i.e* sorbed in the clay mineral surface and Γ is the *surface excess* of the cation in the clay surface relative to the solvent), a_w is the water activity, n_w is the number of the moles of the water found in the clay surface and L is the reaction path. When ion exchange takes place between cations of the same valency the term out of the integral is 0. If a univalent cation is replaced by a bivalent it is 1 while if the opposite takes

place (like in the case of Na for Ca exchange in the alkali-activation) it becomes -1. The second term in the integral is negligible compared to the other terms and has therefore been omitted in many occasions (c.f Deist & Talibudeen, 1967, Inoue & Minato, 1979). Equation 7.5 is used in the construction of exchange isotherms which depict the selectivity of smectite for different cations (c.f. Deist & Talibudeen, 1967, Inoue & Minato, 1979).

The cation exchange reaction determines the degree of Na-exchange during the alkali-activation of the non-swelling bentonites. This exchange depends on the extent of the charge heterogeneity (Lagaly & Weiss, 1975). Bentonites containing smectites with large charge heterogeneity are more easily activated compared to those with more uniform charge density distribution. During the activation process part of the released Ca ions precipitate as $CaCO_3$ while others are enriched in the contact regions between the particles stabilizing the contacts (Lagaly, 1989).

The preference of montmorillonite is not the same for the different cations. Thus it is known that there is greater selectivity for Ca and Rb (the latter slightly) compared to K (Deist & Talibudeen, 1967, Inoue & Minato, 1979) but not for Na (Deist & Talibudeen, 1967) in the K-Ca, K-Rb or K-Na systems respectively. Also, the layer charge affects the exchange reaction (Maes & Cremers, 1977,1978, Eberl, 1980, Shainberg *et al.*, 1987). Thus, the selectivity of both Ca and Cs over Na (Maes & Cremers, 1977, 1978), and that of K over both Na and Ca (Shainberg *et al.*, 1987) increases with increasing layer charge. On the contrary Shainberg *et al.*, (1987) found that the Ca for Na exchange is not affected by the layer charge. For homovalent cations the cation with the lower hydration energy is preferred (Maes & Cremers, 1978, Eberl, 1980), *i.e* the selectivity sequence for the monovalent cations is $Cs^+ > Rb^+ > K^+ > Na^+ > Li^+ > H^+$ for the same levels of hydration (Eberl, 1980). These observations suggest that the cation excange reaction is very important in sectors like soil science or environmental science, especially in areas like nuclear or urban waste disposal.

Cation exchange capacity measurements depend on a number of factors which include pH, particle size, temperature, grinding and the nature of the cation (Deist & Talibudeen, 1967, Grim, 1968). Therefore, each time, the method used for the determination of the CEC should be mentioned (Bain & Smith, 1987). In the methods involving saturation with an index cation CEC is measured at pH 7.

7.3.2. Experimental methods.

The bentonites were crushed with pestle and mortal, and passed through an 125µm sieve (BS 410). Saturation was obtained with ammonium acetate at pH 7 and the CEC was determined directly by distillation in a Kjeldahl microsteam apparatus. CEC was determined in duplicates. The method of saturation with the index cation and determination of the CEC

has been described in detail by Christidis (1989). The results are given in Table 7.2. Determination of the excangeable cations was made from the microprobe analyses. It was assumed that the exchangeable cations are Ca, Na, and K while all Mg was assigned to the octahedral sites. The problems of the microanalyses have been discussed in Section 6.2. The results are given in table 7.3.

7.3.3. Results.

The precision of the CEC measurements (δCEC) varies between 0 and 0.95 meq/100gr with a mean value of 0.40 meq/100gr and a standard deviation of 0.27 meq/100gr. This deviation might be due to sample dispersion and loss during centrifugation, index-cation hydrolysis and salt retention (Smith *et al.*, 1966), as well as flocculation phenomena (Sansom *et al.*, 1968, Sansom & White, 1970).

The CEC profiles from the various deposits are given in Figures 7.3 and 7.4. In the Ankeria deposit (Fig 7.3a) the CEC in the lower bentonite horizon increases from the bottom to the top and reaches a maximum value in the overlying horizon. Then it drops to a constant value in the two overlying horizons, before it decreases further in the higher levels of the highest horizon. The CEC varies also within the same horizon (*i.e* compare the samples SM1 and SM22 of the highest horizon). In the Koufi deposit (Fig. 7.3b) the variation of the CEC follows a less complicated pattern characterized by a continuous increase from the bottom towards the top of the deposit up to the middle of the thick green horizon (see Chapter 3) and then it decreases slightly in smaller depth. Horizontal variations in the CEC are not observed (*e.g* compare the CEC of the samples SM64 and SM54)

In the Area 1 of Milos in the Zoulias deposit the CEC has great values in the lower and higher stratigraphic horizons decreasing in the intermediate ones (Fig. 7.3d). Similar trend was also observed in the swelling volumes of the bentonites of this deposit. In the Tsantili deposit (Fig. 7.3c) the CEC decreases towards shallower depths following the tendency displayed by the swelling volumes. In the same deposit the influence of the illitization of smectite on the CEC can be observed (Fig. 7.3i). It is obvious that progressive illitization leads to an continuous decrease of the CEC, which dropped to a value about 12% of the initial one. The CEC is not influenced by the transition from random to ordered interstratification as this can be seen from the samples SM95 (51% expandables, R0) and SM88 (43% expandables R1). Finally in the Aspro Horio deposit the variation in the CEC follows the same direction as the swelling index, *i.e* in the lower horizon it increases up to a maximum value, after which it decreases reaching a minimum in the thin red horizon. After that it increases continuously in the overlying yellow horizon.

Table 7.2.

Cation echange capacity of the Greek bentonites.

Sample	CEC (meq/100gr)	1st measurement (meq/100gr)	2nd measurement (meq/100gr)	δC.E.C (meq/100gr)
Ankeria				
SM1	**104.65**	104.00	105.30	0.65
SM8	**86.75**	86.70	86.80	0.05
SM13	**96.8**	97.60	96.10	0.75
SM16	**104.4**	104.90	103.90	0.50
SM17	**82.30**	82.70	81.90	0.40
SM19	**106.2**	105.30	107.10	0.90
SM22	**97.5**	98.10	96.90	0.60
SM26	**71.75**	72.40	71.10	0.65
SM27	**90.75**	91.00	90.50	0.25
SM36	**97.27**	97.00	97.50	0.25
Koufi				
SM47	**82.35**	82.00	82.70	0.35
SM51	**80.35**	81.20	79.50	0.85
SM52	**80.30**	79.60	81.00	0.70
SM54	**84.05**	84.50	83.60	0.45
SM60	**75.45**	74.80	76.10	0.65
SM64	**82.40**	82.80	82.00	0.40
SM66	**59.20**	59.00	59.40	0.20
SM69	**70.10**	69.50	70.70	0.60
Tsantili				
SM82	**10.25**	10.00	10.50	0.25
SM88	**22.00**	21.50	22.50	0.50
SM93	**22.75**	22.50	23.00	0.25
SM95	**22.25**	22.00	22.50	0.25
SM98	**56.90**	56.90	56.90	0.00
SM100	**79.80**	79.50	80.10	0.30
SM108	**38.30**	38.60	38.00	0.30
A. Horio				
SM114	**74.90**	75.00	74.80	0.10
SM115	**80.50**	80.00	81.00	0.50
SM117	**88.25**	88.20	88.30	0.05
AM118	**79.40**	79.60	79.20	0.20
SM119	**67.90**	67.80	68.00	0.10
SM120	**76.80**	77.00	76.60	0.20
SM122	**37.25**	37.50	37.00	0.25
SM125	**92.70**	92.50	92.90	0.20

Table 7.2 (continued)

Sample	CEC (meq/100gr)	1st measurement (meq/100gr)	2nd measurement (meq/100gr)	δC.E.C (meq/100gr)
A.Komia				
SM134	**40.50**	40.00	41.00	0.50
SM135	**43.85**	44.00	43.70	0.15
SM136	**64.05**	63.60	64.50	0.45
SM142	**17.75**	17.50	18.00	0.25
SM147	**41.25**	41.50	41.00	0.25
SM148	**51.80**	52.00	51.60	0.20
SM152	**35.20**	35.00	35.40	0.20
SM153	**47.75**	46.90	48.60	0.85
SM156	**43.45**	43.40	43.50	0.05
Garyfala-kena				
SM158	**33.50**	32.60	34.40	0.90
SM159	**37.25**	37.00	37.50	0.25
SM161	**40.95**	41.00	40.90	0.05
SM162	**36.85**	37.10	36.60	0.25
SM163	**30.70**	31.00	30.40	0.30
SM164	**50.60**	51.20	50.00	0.60
SM165	**52.30**	51.40	53.20	0.90
SM167	**42.45**	42.50	42.40	0.05
SM168	**50.55**	51.00	50.10	0.45
Mavrogia-nnis				
SM175	**40.45**	40.50	40.40	0.05
SM176	**38.05**	38.40	37.70	0.35
SM178	**56.45**	46.40	46.50	0.05
K.Komia				
SM179	**37.50**	37.00	38.00	0.50
SM180	**32.55**	33.00	32.10	0.45
Zoulias				
SM185	**68.45**	68.40	68.50	0.05
SM205	**75.30**	76.00	74.60	0.70
SM207	**51.50**	51.50	51.50	0.00
SM209	**76.50**	76.00	77.00	0.50
SM211	**76.70**	77.30	76.10	0.60
SM226	**54.75**	55.00	54.50	0.25
SM227	**34.25**	34.50	34.00	0.25
SM228	**86.80**	87.10	86.50	0.30
SM230	**23.00**	23.00	23.00	0.00

Table 7.2 (continued)

Sample	CEC (meq/100gr)	1st measurement (meq/100gr)	2nd measurement (meq/100gr)	δC.E.C (meq/100gr)
Rema				
SM235	**48.65**	48.70	48.60	0.05
SM236	**53.50**	52.10	53.50	0.70
SM237	**29.50**	29.90	29.10	0.40
Agrilies				
SM246	**52.65**	53.30	52.00	0.65
SM247	**42.25**	42.50	42.00	0.25
SM248	**51.15**	50.20	52.10	0.95
Prassa				
SM261	**124.80**	125.80	125.80	0.80
SM262	**61.75**	62.00	62.00	0.25
SM264	**112.65**	112.80	112.80	0.15
SM265	**63.95**	94.90	64.90	0.95
SM269	**123.25**	122.70	122.70	0.55
SM277	**126.35**	126.80	126.80	0.45
SM278	**94.90**	94.90	94.90	0.00
SM279	**99.80**	100.30	100.30	0.50
SM280	**99.55**	100.40	100.40	0.85
SM281	**94.30**	94.10	94.10	0.20
Loutra				
SM295	**40.75**	40.50	40.50	0.25
SM296	**46.00**	46.50	46.50	0.50
SM297	**56.55**	56.00	56.00	0.55
SM298	**59.25**	60.00	58.50	0.75
Fanara				
SM306	**35.25**	35.50	35.00	0.25
SM307	**90.25**	91.10	89.40	0.85
Chios				
SM321	**63.55**	64.00	63.10	0.45
SM324	**60.25**	60.60	59.90	0.35
SM336	**53.20**	54.50	52.60	0.95
SM338	**69.50**	69.50	69.50	0.00

In Area 3 of Milos the variation pattern of the CEC follows that of the swelling volume in all the deposits examined. Thus in the Ano Komia deposit (Fig. 7.3f) in the lower bentonite horizon CEC increases steadily towards the top and drops suddenly in the overlying partially altered tuff. In the Garyfalakaina deposit it increases steadily towards the higher horizons (Fig. 7.3g), while in the Mavrogiannis deposit it remains constant throughout the deposit except for areas which are affected by hydrothermal alteration (Fig. 7.3h). However, the decrease in CEC in the altered zone is not so remarkable as in the case of the swelling volume. Similar trends are present in the Rema deposit (compare the Tables 7.1 and 7.2). A different trend is exhibited in the Agrilies deposit in which the CEC remains rather constant (Fig. 7.3i), while the swelling volume is least in the lower horizons.

In the Prassa deposit, Kimolos, the CEC variation pattern exhibits a different character (Fig. 7.4a) dominated by an abrupt increase in the mordenite-bearing zone. This is due to the presence of the zeolite phase itself which has higher CEC than smectite. Also, the CEC in the smectite zone remains constant and does not increase towards the the smectite + opal-CT zone like the swelling properties. In the latter zone the CEC decreases probably due to the presence of small amounts of opal-CT. In the Loutra deposit (Fig. 7.4b) the CEC trend follows that of the swelling volume, increasing with depth. In the Fanara deposit the white bentonite which develops high swelling volumes has also high CEC while the low swelling bentonite is also a low grade bentonite (compare the Tables 7.1 and 7.2). Finally in the Chios Island the grade of the bentonite increases towards a SE direction coupling the swelling volume.

The CEC values of smectites obtained from the microprobe analysis (Table 3) are lower compared with the values reported in the literature (*i.e* 80-150 meq/100gr, according to Grim, 1962,1968), with a few exceptions (Ankeria, Koufi and Garyfalakaina deposits). The descrepancy is smaller for the deposits in which Ca is the major interlayer cation (Table 3). On the other hand, low CEC values were obtained for smectites in which Ca was not the major interlayer cation. This indicates that the low CEC values might be due to the loss of alkalies, especially Na during microprobe analysis. Nevertheless, in the Zoulias deposit (Milos), Prassa deposit (Kimolos) and the Chios bentonites the low CEC values might be due, at least partially, to the presence of interlayer Mg. This is believed to be the case especially in Chios where the smectites are Mg-rich (Otay-type montmorillonites). Furthermore, in the Agrilies deposit, the low CEC value is probably due to the presence of H^+ in the interlayer sites. This view is supported from pH measurements in these deposit (see Chapter 8). The deposit has been affected by intense hydrothermal alteration as this is indicated by the presence of characteristic minerals like alunite, jarosite, gypsum and kaolinite (see Chapter 4).

Notwithstanding the probable loss of alkalis, the results obtained are in full accordance with the swelling tests. Since Ca is not easily lost during the analysis, its abundance

Table 7.3

Exchangeable cations and cation exchange capacity of the smectites present in the Greek bentonites determined by microprobe analysis[1].

Bentonite deposit	Ca (meq/100gr)	Na (meq/100gr)	K (meq/100gr)	Cation excange capacity (meq/100gr)
Milos Island				
Ankeria	64.3	17.4	13.1	**94.8**
Koufi	53.2	21.3	11.9	**86.4**
Koufi[2]	26.8	19.4	16.2	**62.4**
Tsantili	55.0	9.4	8.5	**72.9**
Aspro Horio	42.2	19.0	9.8	**71.0**
Zoulias[3]	38.9	17.7	1.7	**62.6**
Zoulias[4]	31.8	19.0	4.7	**55.5**
Ano Komia	20.7	22.3	9.8	**52.8**
Ano Komia[5]	27.9	17.1	21.3	**66.3**
Garyfalakena	47.9	15.5	18.3	**81.7**
Mavrogiannis	16.1	23.2	12.3	**51.6**
Rema	30.7	26.0	19.2	**75.9**
Agrilies	3.6	16.5	10.0	**30.1**
Kimolos Island				
Prassa	34.3	11.0	8.9	**54.2**
Loutra	34.3	9.4	7.0	**50.7**
Chios Island				
Thymiana area	30.7	13.2	2.6	**46.5**

1: All Mg has been assigned to octahedral sites.

2: Lower bentonie horizon of the Koufi deposit.

3: 4th horizon of the Zoulias deposit.

4: 11th horizon of the Zoulias deposit (i.e same horizon as in the Tsantili and the Aspro Horio deposits.

5: Higher bentonite horizon of the Ano Komia deposit

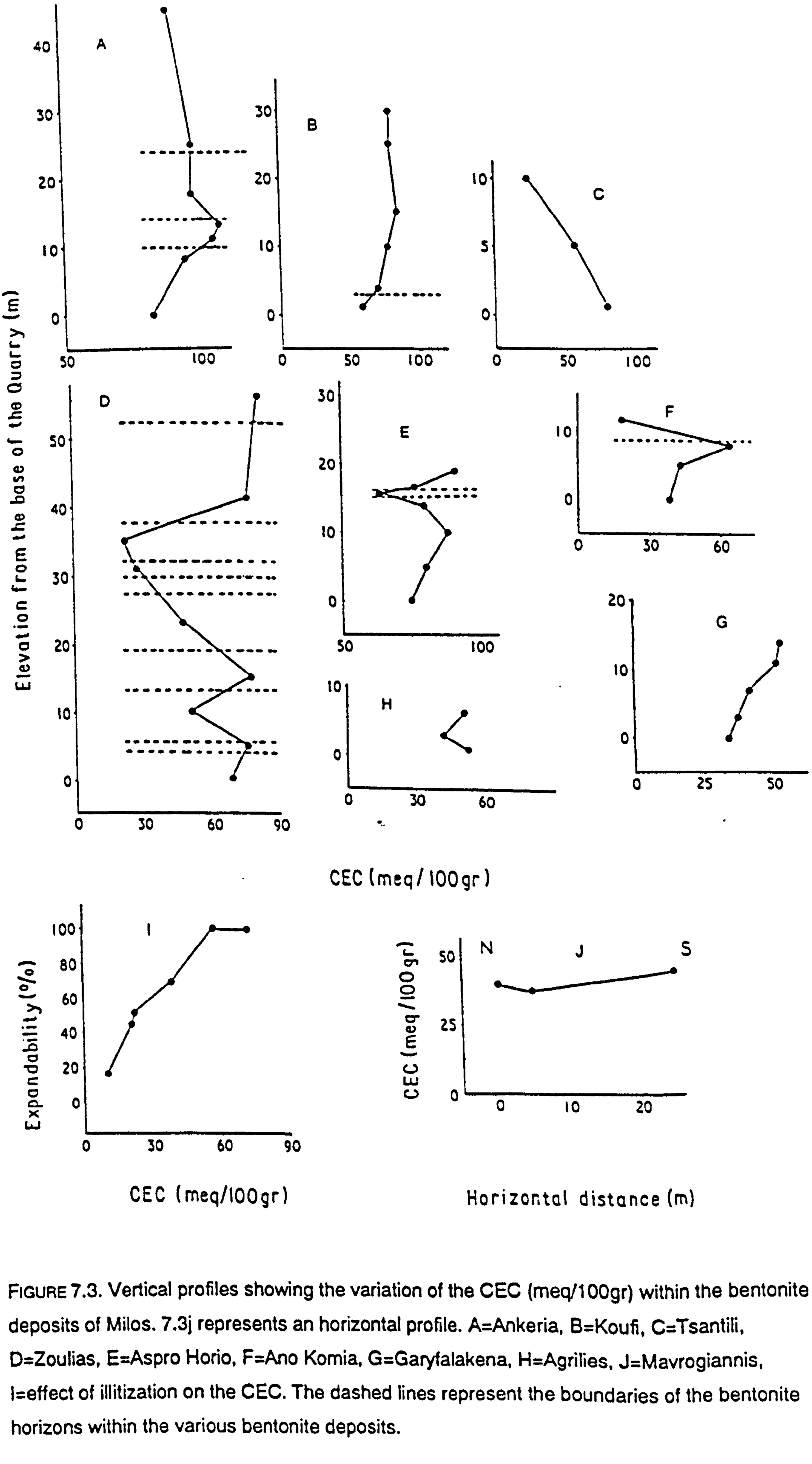

FIGURE 7.3. Vertical profiles showing the variation of the CEC (meq/100gr) within the bentonite deposits of Milos. 7.3j represents an horizontal profile. A=Ankeria, B=Koufi, C=Tsantili, D=Zoulias, E=Aspro Horio, F=Ano Komia, G=Garyfalakena, H=Agrilies, J=Mavrogiannis, I=effect of illitization on the CEC. The dashed lines represent the boundaries of the bentonite horizons within the various bentonite deposits.

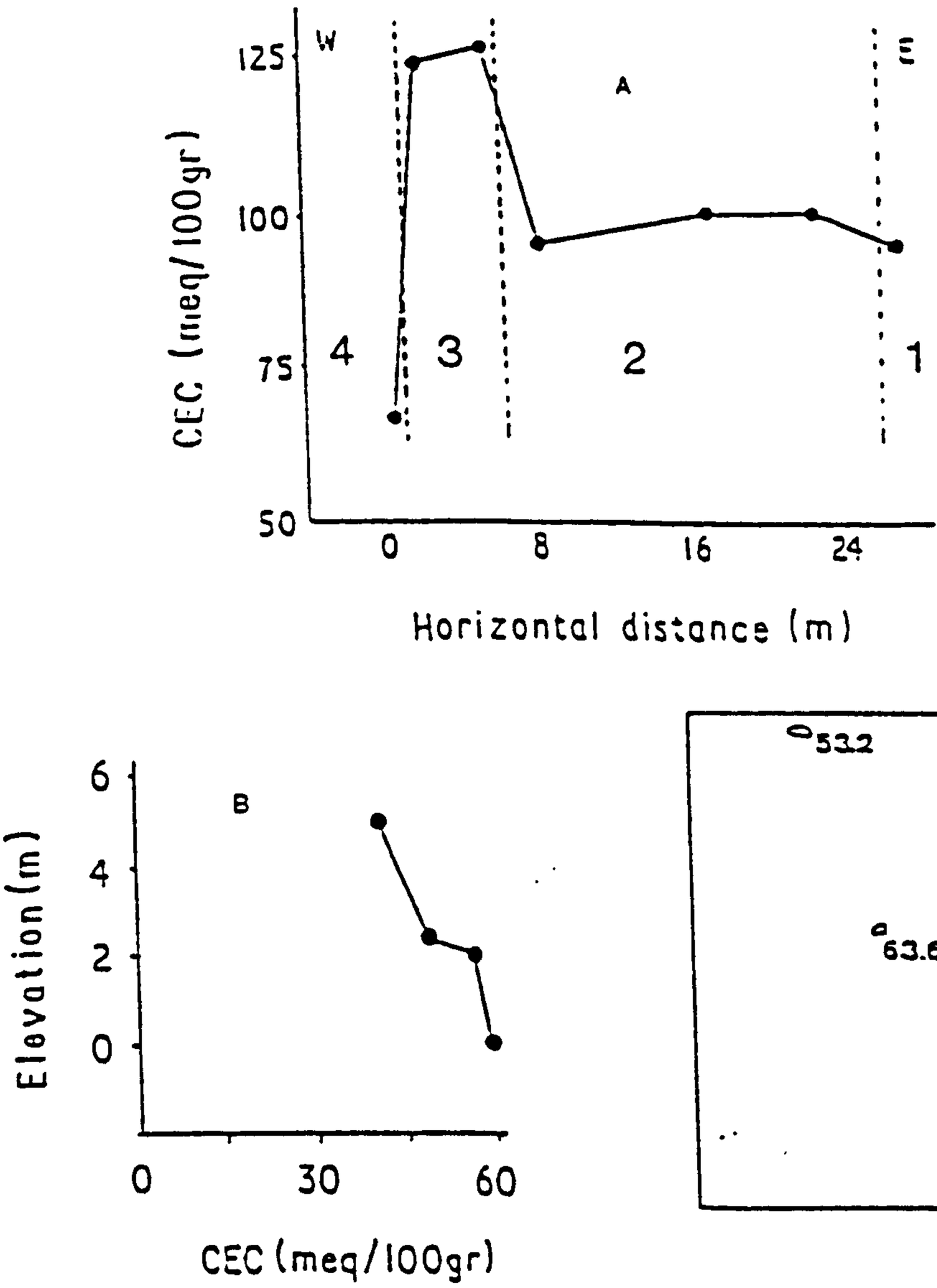

FIGURE 7.4. Profiles showing the variation of the CEC (meq/100gr) within the bentonite deposits of Kimolos and the bentonite outcrops of Chios. A=Prassa deposit, Kimolos, B=Loutra deposit, Kimolos, C=Chios. In A: smectite + opal C-T zone, 2= smectite zone, 3= smectite + mordenite zone, 4= smectite + opal C-T ± mordenite.

provides an estimation of the alkali-content in the interlayer sites. Thus in the deposits of the Areas 1 and 2 in Milos Ca seems to be the major interlayer cation. These bentonites were activated with 4 and 5% Na_2CO_3 indicating that the presence of Na was limited indeed. An exception to this tendency was displayed by the bentonites from the lower horizon of the Koufi deposit which contained limited Ca. This bentonite was activated with 3% Na_2CO_3. Similarly, the Ca-poor bentonites of the Area 3 of Milos were activated with 3% Na_2CO_3, except for the bentonites from the deposit of Garyfalakaina which was activated with 3-4% Na_2CO_3. This bentonite contains smectites with abundant Ca in the interlayer sites.

The bentonites of Kimolos do not contain abundant Ca (only 35% of the CEC estimated for the bulk sample). Nevertheless they were activated with 3-4% Na_2CO_3, indicating that Mg might possibly be present in the interlayer sites. The Mg-content of this sample (>4% MgO) supports this idea. The same may be true for the bentonites of Chios island which contain more than 6% MgO and were activated with 4% Na_2CO_3.

7.3.4. Discussion.

With the exception of zeolites, smectite is the only mineral which displays significant cation exchange properties in the bentonite deposits examined (kaolinite which is the most significant clay mineral coexisting with smectite has very low CEC). Therefore, the CEC gives a good estimation about the presence of grit content. In the deposits containing zeolites (like the mordenite-bearing zone in the Prassa deposit) the high CEC values do not reflect a high smectite content. The effect of the presence of zeolites can be also be observed in the higher horizons of the Garyfalakaina deposit (Fig. 7.3g) which have significantly higher CEC compared to their counterparts from the lower horizons. The higher CEC values are attributed to the presence of heulandite/clinoptilolite and mordenite (see chapter 4). In this deposit the variation of the CEC revealed a cryptic mineralogical variation in this which is not obvious macroscopically.

In addition to the different smectite content CEC may also vary due to the different layer charge of the smectites. Thus, bentonites containing Cheto type montmorillonite (Tatatilla, Chambers or Otay) are expected to show higher CEC compared to a Wyoming bentonite if the non-smectite content is the same, because the layer charge of the smectite of the former is higher (Schultz, 1969). In the Miloan bentonites, the smectites from the Area 1 plot in the field of the Wyoming smectites in the diagram of Güven (1988), while those from the Areas 2 and 3 in the areas of beidellite and the Cheto montmorillonites. However no direct estimation of the "layer charge factor" can be made because of the presence of other mineral phases. Thus, in the Area 3 the low bulk CEC values are due to the abundant opal-CT present in the samples. Also, the bentonites from the Area 1 have on average lower

CEC values compared to their counterparts from the Ankeria deposit but have higher grit content as well. The same is valid for the bentonites from the Koufi deposit. The high CEC values of the bentonites from the Ankeria deposit and those from the smectite zone in the Prassa deposit, Kimolos are in agreement with their the crystal chemistry (Cheto montmorillonite).

Alteration has also affected the CEC of the bentonites. Illitization causes a significant decrease to the CEC due to the collapse of the smectite layers. However, when the alteration is associated with S-metasomatism, unlike the swelling properties, the CEC does not deteriorate substantially (*e.g* the Agrilies and the Mavrogiannis deposits). It seems therefore that in Milos the low pH hydrothermal alteration has affected the swelling of the clay more than the CEC.

7.4. Correlation between quality and grade.

It has been stated (Section 7.1) that in bentonites the terms quality and grade are not used as synonyms because in many occasions low grade bentonites swell equally with others of higher grade. This can be observed in the Figure 7.5a in which the overall relationship between the swelling volume and the CEC is depicted. Notwithstanding the large degree of scattering there is a rather weak positive relationship (r=0.68) between the swelling volume and the CEC. The correlation coefficient increases to 0.75 if the samples from the mordenite bearing zone in the Prassa deposit, Kimolos are not plotted (Fig. 7.5b).

A significantly better correlation is obtained when the CEC and the swelling volume are plotted for bentonites from the same area. In the Area 1 in Milos, the correlation coefficient increases to 0.88 suggesting a closer association between the two properties (Fig. 7.6a). The scattering observed is due to the illitization observed in the Tsantili deposit. Thus, the K-bentonites present, swell more than it is anticipated from their CEC values. This might be explained if it is considered that the illitization proceeded preferentially over the smectites with higher layer charge leaving smectite layers with relative lower layer charge. These layers might have been physically activated through a process described by the reaction 7.1b because low charged smectites display higher selectivity for Na than high-charged ones in a Na-Ca exchange reaction (Deist & Talibudeen, 1967). Also, low charge Na-smectites are expected to swell easier than their Ca-counterparts (Kleijn & Oster, 1982).

In the Area 3 of Milos after the removal of the zeolite-bearing samples from the Garyfalakaina deposit the correlation coefficient increases slightly to 0.78 (Fig. 7.6b). This is due to the high swelling volumes showed by the bentonites from the higher horizon of the Ano Komia deposit. If these samples (SM152 and SM156) are excluded the correlation coefficient increases to 0.83. In the Area 2 of Milos (Fig 7.6c) although a slight positive trend is observed the correlation coefficient is very low (0.3). When only the samples from

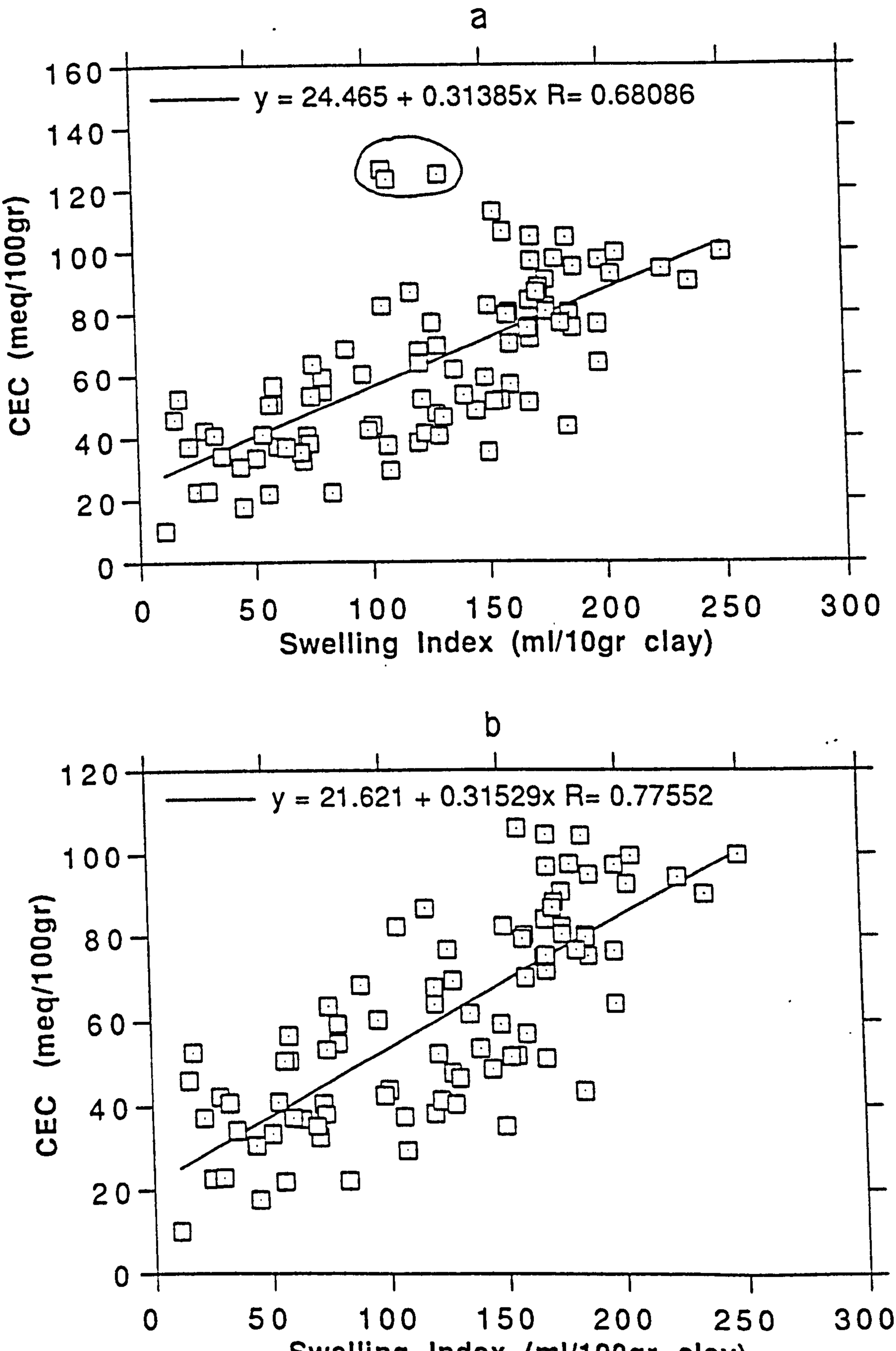

FIGURE 7.5. Correlation between CEC and swelling volume (a) for the total number of samples and (b) the bentonite from the smectite+mordenite zone (Prassa deposit, Kimolos) excluded. The encircled points in (a) correspond to the samples from the smectite+mordenite zone, Prassa deposit, Kimolos.

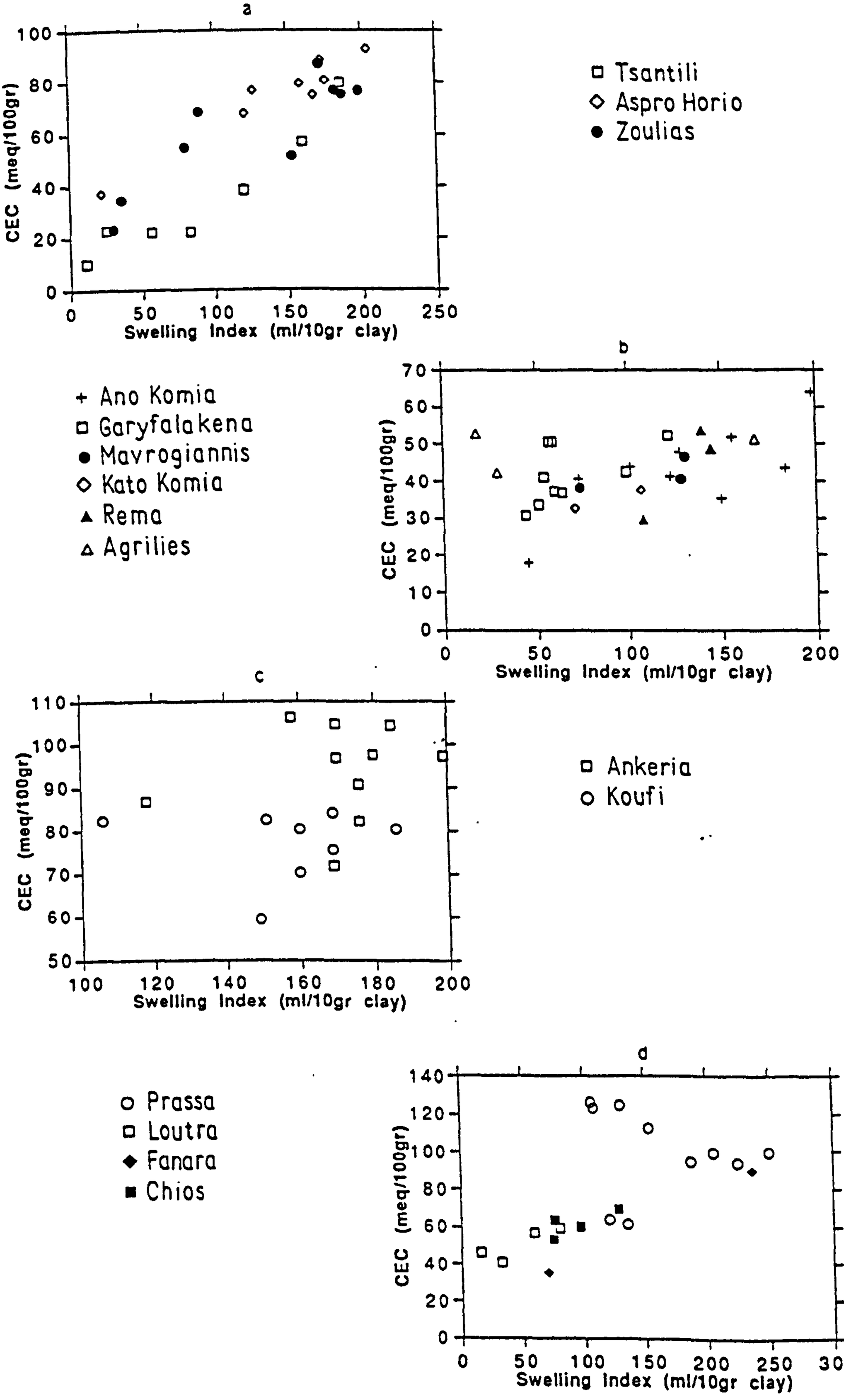

FIGURE 7.6. Correlation between the CEC and the swelling volume in the bentonites from the various areas (a) Area 1 Milos, (b) Area 3, Milos, (c) Area 2, Milos, (d) Kimolos, Chios.

the higher horizon of the Ankeria deposit are ploted the correlation coefficient increases to 0.52 (the hydrothermally affected sample SM47 is excluded). The low correlation coefficient results from the large degree of variation along the swelling axis over constant CEC. It is not certain why this variation of the swelling properties has taken place. A possible contribution from compaction in the Koufi deposit and from the high layer charge in the Ankeria deposit (samples SM16 and SM19) should not be ignored.

In the deposits of Kimolos a high correlation coefficient is obtained (0.94) when the samples from the mordenite-bearing zone in the Prassa deposit are excluded (Fig. 7.6d). The same trend is followed by the bentonites of Chios although the have been derived from different precursors (see Chapter 5). These bentonites unlike their Miloan counterparts have not been affected by any alteration event after their formation. It is therefore believed that the good correlation between these two properties results from the original alteration of the volcanic glass.

Although the bentonites from Kimolos and Chios have been derived from different precursors they have some common characteristics as far as the smectite crystal chemistry is concerned. The smectites present have low tetrahedral charge (less than 15% of the total layer charge in Chios and 15-20% in Kimolos). Also in both areas the compositional variation of smectites is limited. Similarly, in Area 3 of Milos the bentonites of the lower horizon of the Ano Komia deposit have been formed from a different precursor compared with this of the other deposits in this area. Nevertheless, they fit in the same line. Again, the smectites present in this horizon have very similar characteristics to those of the other deposits of the same area, varying in their chemistry between beidellite and Tatatilla montmorillonite with very low iron content. Similar observations can be made for the deposits from Area 1 in Milos (see Section 6.3). On the contrary, in Area 2 of Milos the crystal chemistry of the smectites does not follow the same trend. Thus the smectites from the Koufi deposit are more iron-rich compared to their counterparts from the Ankeria deposit. Moreover, beidellite is present in the former whereas it is absent in the latter.

The above remarks suggest that bentonite deposits in which the smectites present have similar crystal chemical characteristics exhibit a good correlation between CEC and swelling. The parent rock factor is important since it determines the possible chemical variations of the smectites up to a degree (*e.g* Wyoming-type montmorillonites are unlikely to form from a rhyolite), but it does not seem to affect the aforementioned properties *if* the smectites present show similar compositional trends (*i.e* Chios and Kimolos bentonites). Under conditions of similar compositional variations of smectites a bentonite with a higher CEC is expected to swell more than one with a lower CEC. This pattern might be modified by a subsequent hydrothermal alteration event (Ankeria, Koufi, Tsantili, Agrilies, Mavrogiannis, and Ano Komia deposit) or by compaction (Koufi deposit).

These assumptions are not incompatible with any of the models proposed for swelling and the selectivity for Na in the Na-activation. Indeed, a similar compositional variation of smectites suggests a higher possibility for a similar degree of Na-selectivity during the Na-activation because of the higher possibility for a similar distribution in the magnitude of the layer charge (Deist & Talibudeen, 1967), and hence a more uniform swelling according to the model of Kleijn & Oster, (1982). Similar compositional variations in the octahedral sheet might increase the possibility for a more uniform distribution of the b-dimension of the smectites (c.f Radoslovich, 1962). This raises the possibility for uniform swelling according to the epitaxial model (Davidtz & Low, 1970, Ravina & Low, 1972, Odom & Low, 1978). Factors like iron oxidation might affect swelling (Stucki *et al.*, 1984), but if this process affects the whole smectite population to the same degree (*i.e* oxidation is complete), then it is believed that the original tendency will not be affected.

7.5. Conclusions.

The conclusions drawn after examination of the swelling and CEC properties of the Greek bentonites are summarized below:

1) The crystal chemical characteristics (type of smectite, compositional variation, layer charge) of the smectites present in the bentonites are the most important factors controlling both the swelling and the CEC properties. Under similar crystal chemical characteristics a high grade bentonite is expected to swell more than a low grade one.

2) The chemistry of the parent rock is important in the sense that it induces an "inherited" factor in the smectite-type. However, bentonites from different precursors might exhibit similar properties if they possess similar crystal chemical characteristics.

3) Non-smectitic fine grained mineral phases present in the clay fraction, especially opal-CT, affect the quality of the deposits probably because they impede swelling. Also zeolites induce high ion exchange properties on the bentonites due to their high CEC.

4) The original swelling and CEC characteristics of the deposits might be modified by secondary alteration precesses either by "dilution" of the smectite content (formation of minerals phases at the expense of smectite) or by creation of unfavourable physicochemical conditions.

5) The illitization of smectite might cause a by-product "natural Na-activation" of the remaining smectite flakes through a migration of Na-ions released from the altered smectite flakes.

CHAPTER EIGHT

RHEOLOGICAL PROPERTIES

8.1. Introduction.

Rheology examines the flow and deformation behaviour of matter (Shaw, 1980) and has received attention because of its importance in industry and nature (van Olphen, 1977, Shaw, 1980). In clay technology it is important in areas like ceramics (e.g in slip casting) and drilling fluids. The latter is one of the most important applications of bentonites, and in the USA (the largest world producer of bentonite), more than 40% of the 1986 production was consumed in the drilling industry (O'Driscoll, 1988). The role of bentonite in drilling mud has been discussed in Chapter 1.

This chapter deals with the rheological properties of the Greek bentonites. The parameters determined are apparent viscosity, plastic viscosity, yield and filtrate loss. Determination of the pH of the raw materials was also carried out because it affects the rheological properties (Rand *et al.*, 1980, Brandenburg & Lagaly, 1988). For selected samples rheograms and thixotropic loops (see following section for definition of these terms) were also obtained.

8.2. Theoretical considerations-definitions.

The theoretical aspects of rheology in colloidal systems, including clays, have been discussed among others by Goodeve (1939), Gillespie (1960), van Olphen (1963, 1977), Mewis (1979) and Shaw (1980). The rheological behaviour of colloidal suspensions depends on the following factors (Grimshaw, 1971, van Olphen, 1977, Frey & Lagaly, 1979, Rand *et al.*, 1980, Shaw, 1980, Brandenburg & Lagaly, 1988 and Lagaly, 1989 among others): the viscosity of the dispersion medium, the concentration of the suspended material, the size and shape of the particles as well as their distribution and degree of dispersion, the electrolyte type and concentration (*i.e* the zeta potential), the flexibility of the particles in the suspension medium, the existence of particle-particle and particle-dispersion medium interactions, the temperature and the pH of the suspension and in the case of smectites the layer charge and the type of the interlayer cations.

If the flow of a clay suspension, kept between two parallel plates, is laminar[1] (*i.e* the

[1]There are 3 types of flow: the laminar flow described above, *the turbulent flow* due to the inertia of the suspension, which makes it proceed in the changed direction if the frictional forces are small compared to the inertia forces, and *the plug flow* in which the velocity of the various laminar sectors of the suspension is constant.

suspension can be separated into laminar layers parallel to the direction of the flow, each having different speed), then if one plate is kept fixed and a tangential force is applied to the other, a *shear stress* is imparted to the clay suspension. This stress is induced to the rest units of the laminar flow, which, due to friction, move parallel to the direction of the applied stress. When a steady state is reached a *rate of shear* is established in the suspension. In the case that the rate of shear is directly proportional to the shear stress then the flow is *Newtonian* characterized by the following relationship

$$\sigma = n\gamma \qquad 8.1$$

where σ is the shear stress, γ is the shear rate and n is a proportionality factor called *viscosity*. The dimension of viscosity is (mass) (length)$^{-1}$ (time)$^{-1}$ and it is usually measured in Poise. The viscosity of a liquid or a suspension is a measure of its ease to flow. The linear relationship between the shear stress and the rate of shear in the Newtonian flow is depicted in Figure 8.1. Since the clay particles are charged, part of the viscosity is related to their charge, because extra energy is required to overcome the interaction between them. This is known as *electroviscous effect*.

In many occasions, especially in concentrated clay suspensions or in suspensions in which the particles are asymmetric, deviations from the Newtonian flow are observed, and the flow is *non-Newtonian*. If flow occurs only above a finite shear stress it is called *plastic flow* (Fig. 8.1). The value of shear stress that the system begins to yield to the stress is called the *yield stress* (σ_0). In Figure 8.1 three types of plastic flow are depicted (curves 4,5 and 6). In the curve 4 the flow is characterized as *ideal plastic* and obeys the following equation:

$$\sigma - \sigma_0 = n\gamma \qquad 8.2$$

This type of flow is only approximated in real systems. A more common type of flow, called *Bingham flow*, is described by the curve 5, and the linear part of the curve obeys the following equation:

$$\sigma = n\gamma + \sigma_\beta \qquad 8.3$$

where σ_β is the *Bingham yield stress* (see Figure 8.1). In the linear part of the curve the shear stress is proportional to the shear rate. Finally in a third type of plastic flow there is no proportionality between the shear stress and the shear rate (curve 6 in Fig.8.1). Substances that exhibit this behaviour are called Casson bodies and their flow can be described by the following equation:

$$n\gamma = (\sigma - \sigma_0)^{1/2} \qquad 8.4$$

Two more flow curves describing non-Newtonian flow are depicted in figure 8.1. In curve 2 the flow is *pseudoplastic* characterized by *shear thinning i.e* the viscosity decreases with increasing rate of shear. Shear thinning is common in systems containing asymmetric particles, which disturb the flow lines to a greater extenT at low rates of shear (*i.e* when they are randomly orientated), than in higher when they are aligned. *Shear thickening* or

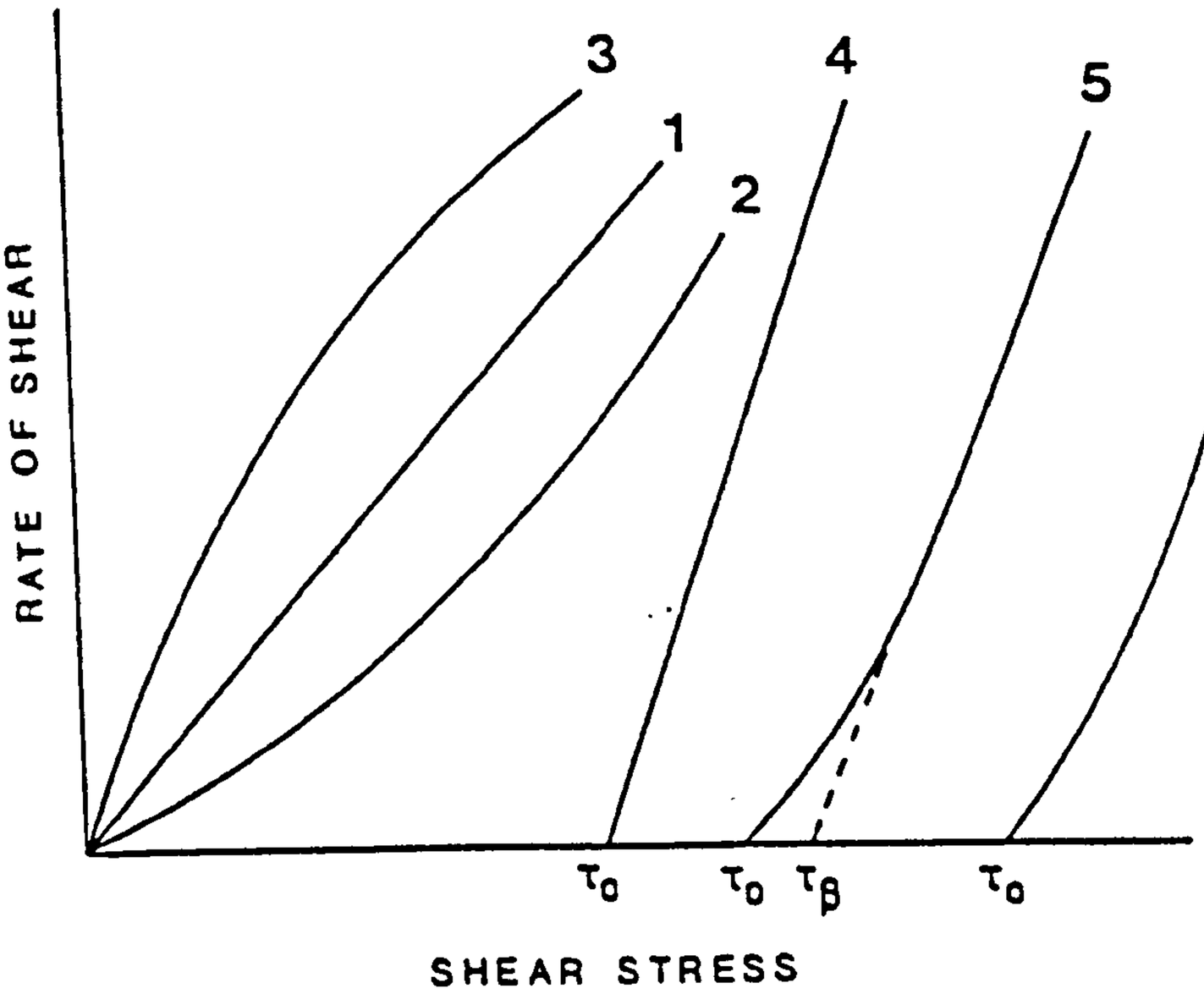

FIGURE 8.1. Rheograms describing the various types of laminar flow (see text for explanation).

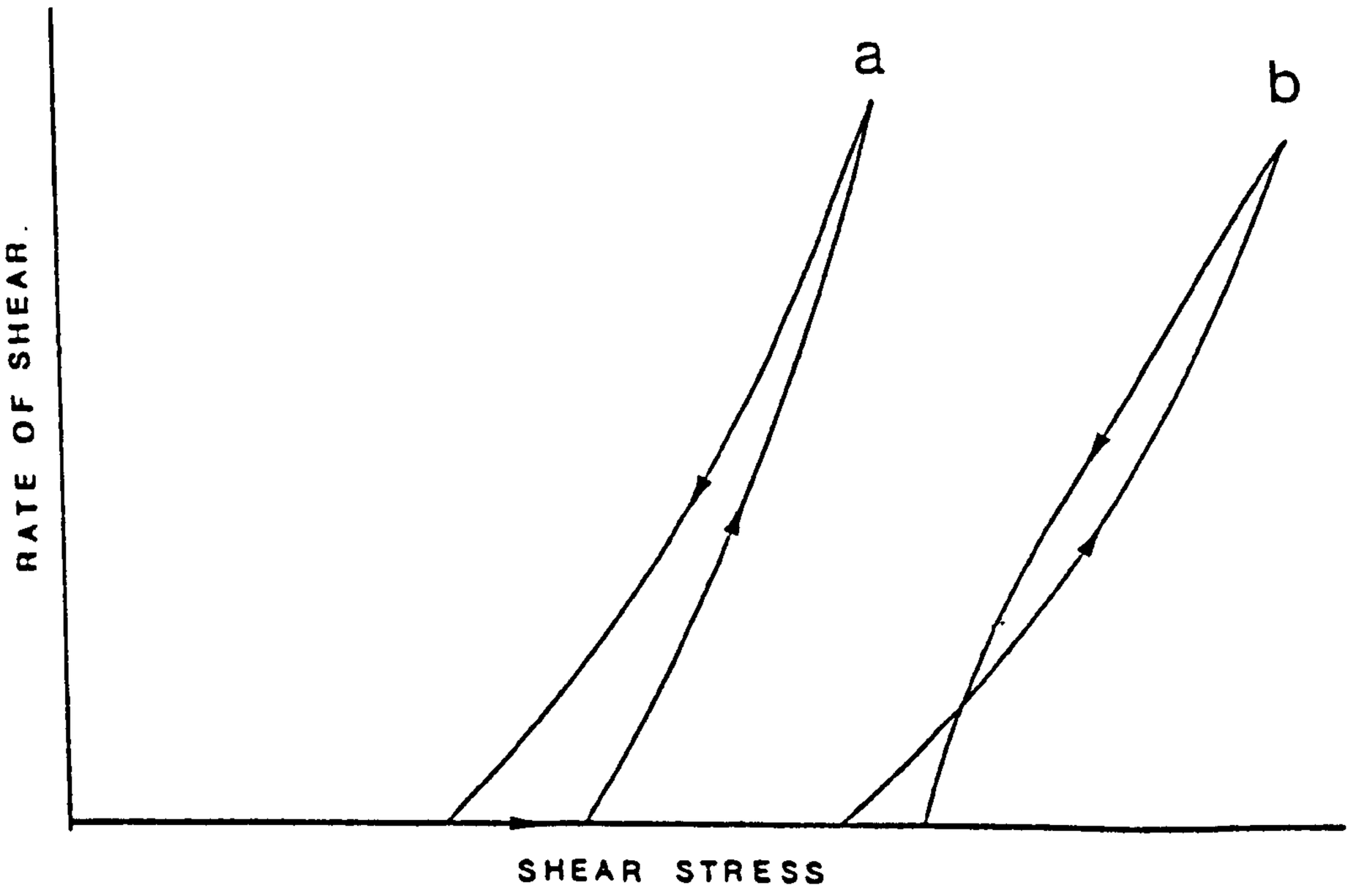

FIGURE 8.2. Rheograms describing (a) thixotropic and (b) antithixotropic rheological properties..

dilatancy (curve 3) is characterized by an increase of viscosity with increasing shear rate. The curves shown in Figure 8.1 are called *rheograms*.

The *differential viscosity* or *plastic viscosity* n_{PL} is the derivative of stress with respect to the rate of shear at a given shear rate (van Olphen, 1977). It is defined as the amount of shear stress greater than the yield stress required to induce unit rate of shear (Elzea & Murray, 1990). The *apparent viscosity* n_{ap} is ratio of shear stress over the rate of shear calculated in experiments, assuming that the flow is Newtonian.

The most important rheological phenomena, from the technological point of view, in clay suspensions are time dependent and depend on the shear history of the system. If the viscosity of a suspension decreases when a finite stress is applied but is recovered at an observable rate when the stress is removed, the suspension is called *thixotropic* and the phenomenon *thixotropy*. Clay suspensions exhibit thixotropy when are more or less flocculated. The thixotropic character of a material can be visualized from the *thixotropic loops* (Fig. 8.2a) which are hysteresis curves obtained by increasing and decreasing rates of shear. Hysteresis loops depend on the previous shear history of both the rate of change and the maximum value of the shear rate (Mewis, 1979). If after removing the stress the decrease of viscosity is permanent, the behaviour is called *work softening*. The permanent increase of viscosity with time induced by shear is called *work hardening*.

Antithixotropy (contrary to thixotropy) is caused by aggregation of the particles in the suspension induced by the shear (Mewis, 1979). It is concluded to exist from an inverse hysteresis loop (Fig. 8.2b). A system might be both thixotropic and antithixotropic under different shear stresses. *Rheopexy* is an increase of the rate of stiffening of a suspension under low shear stress and is sometimes observed as an acceleration of thixotropic recovery. It can be considered as a time dependent shear thickening (Shaw, 1980).

In the Figure 8.1 it is obvious that the Bingham flow consists of two parts; a Newtonian part in which the shear stress is proportional and a non-Newtonian part in which the shear stress is not proportional to the shear rate. The Newtonian part has been ascribed to hydrodynamic effects (Goodeve, 1939) although according to Chen *et al.*, (1990) it is partly due to the strength of the bonds between the particles. The non-Newtonian part has been ascribed to interaction between the particles (shear breaking and making and thermal making and breaking of the links, see impulse theory of Goodeve, 1939, also Gillespie, 1960).

The thixotropic behaviour of clays has been attributed to the linking of the clay particles which form rigid gels. However, there is dispute among the various workers about the nature of that linking, especially in the case of smectites. Van Olphen (1959, 1963, 1977), Brandenburg & Lagaly (1988) and Lagaly (1989) considered that the existence of positive edge-negative face attractive forces could be the reason for the rheological properties of the smectite suspensions. However it has repeatedly been shown that the smectite edges

are not positively charged at any pH (McEwen & Mould, 1957, Rand *et al.*, (1980), Tessier & Pedro (1982). Therefore, a number of alternative models have been postulated for the structure of the smectite gels. Norrish (1954) proposed that the gel structure results from repulsive forces operating among the diffuse double layers of the particles or alternatively by an edge-to-edge contact between the particles. The latter was also proposed by McEwen & Pratt (1957) and has been obserevd in TEM studies (e.g Mering & Oberlin, 1967). Particles in contact (scaffolding structure) have also been postulated by Goodeve (1939).

Callaghan & Ottewill (1974) and Rand *et al.*, (1980) proposed a model similar to the double layer repulsion model of Norrish, in which the clay particles and their electrical double layers fill the available space and mutual repulsive forces are exerted between the negative charged particles. Finally, Chen *et al.*, (1990) stressed the role of the release of Mg on the rheological properties of smectites and supported that it increases the tendency for flocculation because it replaces Na from the interlayer sites (see Kleijn & Oster, 1982 about the role of bivalent cations on the formation of tactoids). Clearly, more work is needed before the smectite-water systems are fully understood.

Most of the above models consider smectites occurring more or less in the form of isolated flakes. However, it has been shown (Güven & Pease, 1975, and also Chapter 4 in this study) that even in very dilute suspensions, smectites form stacks of several layers the thickness of which is not uniform. Only after removing amorphous material and using deflocculants single flakes might be separated (Güven & Pease, 1975). However, such a pretreatment is unlikely to be applied in industrial applications. Therefore it is believed that the interaction between these quasi-crystalline particles must be more complicated than has been proposed in the models presented above.

8.2.1. Measurement of viscosity.

The viscosity of a liquid or a suspension is measured with various types of *viscometers*. In the clay and ceramic industry three types of viscometers are commonly used (Scott, 1990): the Fann viscometer, the Brookfield viscometer and the the simple torsion viscometer. In the drilling industry evaluation of the rheological properties of bentonites is carried out with the Fann viscometer. It is a Couette-type viscometer (rotating cylinder viscometer) consisting of two co-axial cylinders, one of which (the outer) rotates imposing a shear stress on the suspension between the two cylinders. The shear is transported through friction to the various layers of the suspension and eventually to the inner cylinder which is connected to a torsion spring. The resistance to flow displayed by the suspension rotates the inner cylinder. The torsion is transferred to the torsion spring and appears as a

dial deflection of a neddle connected to the spring. The magnitude of the torsion, and thus the deflection of the needle, is indicative of the viscosity of the suspension.

8.3. Experimental methods.

41 bentonite samples were chosen for determination of their rheological properties. The materials were dried overnight at 60^{o}C ground in a Tema mill for 45 seconds and passed through a 250μm sieve (BS410). The rheological properties were determined with a 35S Fann V-G viscometer at the laboratories of the British Geological Survey. The viscometer has been described by Savins & Roper (1954). The experiments were carried out according to the OCMA specifications (OCMA, 1973). Both the OCMA and the American Petroleum Institution (API, 1969) specifications are given in the Table 8.1. The Na_2CO_3 added to the materials was of analytical grade (FISONS) and the amount used corresponds to the optimum amount, *i.e* at which caused maximum swelling (see Chapter 7). The parameters measured for the total number of samples are apparent viscosity, plastic viscosity and yield. The method used for preparation of the materials and the calculations made in order to obtain the various rheological parameters are given in the Appendix 8.1. The results obtained are given in Table 8.2.

The samples were left *to age* overnight before measurement of the rheological properties was carried out. This is important because the viscosity of a bentonite suspension does not develop fully without a sufficient ageing period (Morgan, 1990b). Ageing is also required according to the OCMA specifications. Lebedenko & Plee (1988), on the other hand, using a different activation method, showed that the rheological properties improved with short time of activation but deteriorated later, while in some runs these properties deteriorated immediately.

25 samples were also tested for filtrate loss using a Baroid 1/2-area cell which filters over a $2^{1}/_{2}$" diameter area at a pressure 100lb/in^{2}. The test was performed in order to determine the ability of the bentonites to form impermeable filter cake. The method used is described in the Appendix 8.2 while the results are given in Table 8.2.

Complete rheograms, thixotropic loops and gel strength measurements were obtained for 5 bentonites (samples SM17, SM100, SM235, SM278 and SM280). The first four were chosen because of their high apparent viscosity values. SM280 was chosen because although its mineralogical, chemical, quality and grade characteristics are very similar to those of SM278 its apparent viscosity was substantially lower. The results are given in Tables 8.3 and 8.4. The rheograms obtained are given in Figure 8.3 and the thixotropic loops in Figure 8.4.

Table 8.1.

Specifications of bentonite for drilling mud.

Property	API specifications		OCMA specifications	
	min	max	min	max
Apparent viscosity for 6.42% clay suspension at 600rpm (cp).	15	- -	15	- -
Yield[1]	6 times the plastic viscosity (maximum)		16	- -
Filtrate loss (ml) at 6.42% clay suspension	- -	13.5	- -	15
Moisture content (%)	- -	10	- -	15
Wet sieving (% of material less than 75µm)	- -	2.5	- -	2.5
Dry sieving (% material less than 150µm)	- -	- -	- -	2

[1] = lb/100ft^2 in API specifications, m^3/tonne in OCMA specifications

pH measurements were performed to all 41 samples with a WPA CD30 digital pH-meter equipped with a Russell pH-electrode. The instrument was calibrated with pH-buffers (FISONS) at pH values of 4, 7 and 9. The results are given in Table 8.2.

8.3 Results.

The results obtained show that the rheological properties of the Greek bentonites vary between broad limits even in the same deposit. There are materials which meet the OCMA specifications and others which have very poor rheological properties and cannot be used in the drilling industry.

In Area 1 of Milos the materials have generally poor rheological properties and do not develop high apparent viscosity (Table 8.2). Exception to this trend is exhibited by the bentonites of the Tsantili deposit. Thus SM100 meets the specifications of OCMA while SM98 which has been affected by hydrothermal alteration develops apparent viscosity slightly lower than the limits defined by both the OCMA and the API specifications. However if the two bentonites are blended then the product meets the specifications. On the contrary, the bentonites from the Aspro Horio and the Zoulias deposits have poor rheological properties, although they exhibited high grade and high quality (see Chapter 7). In the Aspro Horio deposit both the apparent and the plastic viscosity increase from the lower to the higher levels of the basal green horizon up to a limit and decrease thereafter (Fig. 8.5b), *i.e* in a way similar to the swelling volume and the CEC. Nevertheless they never meet the specifications required for use in the drilling industry. The highest value of apperent viscosity was 13.8 cpoise (Table 8.2).

The bentonites from the Zoulias deposit developed even more inferior apparent and plastic viscosity (Table 8.2). The sample SM185 has been affected by hydrothermal alteration and its pH is very low.

The pH of the samples vary from acidic for samples affected by hydrothermal alteration, to alkaline for the samples of the Aspro Horio deposit. The pH of the samples SM100 (Tsantill deposit) and SM228 (Zoulias deposit) is neutral. Since the deposits from the Area 1 have probably originated from the same precursor it is very possible that the pH values of the bentonites from the Aspro Horio deposit (*i.e* the least affected by the hydrothermal alteration) are closer to the original ones. Finally all bentonites from this area exhibit low filtrate loss values (Table 8.2) indicating that they develop good filter cakes.

Table 8.2

Rheological properties of the Greek bentonites

Sample	Apparent viscosity (cp)	Plastic viscosity (cp)	Yield ($lbs/100ft^2$)	Filtrate loss (cm^3)	pH
Ankeria					
SM17	19.8	8.0	23.5	7.8	7.5
SM 27	14.5	8.5	12.0	- -	8.5
SM36	17.0	7.5	19.0	8.2	8.6
Koufi					
SM47	6.0	3.0	6.0	- -	8.6
SM52	12.5	7.0	11.0	6.8	8.4
SM60	11.8	5.0	13.5	10.2	8.4
Tsantili					
SM98	13.8	6.0	15.5	7.8	5.9
SM100	17.0	7.5	19.0	8.0	6.7
Aspro Horio					
SM114	7.8	4.0	7.5	- -	8.9
SM115	13.8	7.5	12.5	11.8	8.7
SM117	13.8	6.0	15.5	9.6	8.5
SM118	6.5	3.0	7.0	7.8	8.5
Ano Komia					
SM136	12.5	6.5	12.0	8.0	7.3
SM156	10.3	5.0	10.5	8.2	7.5
Garyfalakena					
SM158	2.3	2.0	0.5	- -	7.2
SM168	3.3	3.0	0.5	- -	8.2
Mavrogiannis					
SM177	5.8	3.5	4.5	13.0	6.2
Kato Komia					
SM 179	5.3	3.0	4.5	11.6	7.8
Zoulias					
SM185	4.0	2.5	3.0	- -	2.5
SM228	6.0	4.0	4.0	- -	6.8

Table 8.2 (continued)

Sample	Apparent viscosity (cp)	Plastic viscosity (cp)	Yield ($lbs/100ft^2$)	Filtrate loss (cm^3)	pH
Rema					
SM235	21.5	3.5	36.0	15.0	6.8
Agrilies					
SM246	1.8	2.0	0.0	- -	2.3
Prassa					
SM260[3]	20.5	6.5	28.0	6.2	7.8
SM264[2]	15.5	7.0	17.0	- -	7.7
SM268[1]	6.3	4.0	4.5	7.6	6.9
SM277[3]	36.0	14.5	21.5	7.2	7.5
SM278[3]	25.0	7.5	35.0	7.6	8.3
SM279[3]	9.8	7.0	5.5	7.0	7.6
SM280[3]	11.3	6.5	9.5	6.8	8.5
SM281[4]	25.0	11.0	27.0	- -	7.7
Loutra					
SM295	1.5	1.5	0.0	- -	8.2
SM296	1.3	1.5	0.0	55.0	8.3
SM297	3.5	2.5	2.0	- -	7.6
SM298	3.7	2.5	2.5	8.2	7.4
Fanara					
SM306	2.5	2.0	1.0	18.0	6.8
SM307	114	68.0	92.0	- -	7.2
Chlos					
SM321	4.3	3.0	2.5	- -	7.6
SM325	3.3	3.0	0.5	- -	8.3
SM332	3.8	3.0	1.5	18.2	8.3
SM336	3.3	3.0	0.5	21.2	7.9
SM337	3.0	3.0	0.5	20.6	8.0

1: Smectite + opal-C-T ± mordenite zone, 2: Smectite + mordenite zone, 3: Smectite zone

4: Smectite + opal-C-T zone (close to the boundary with the smectite zone)

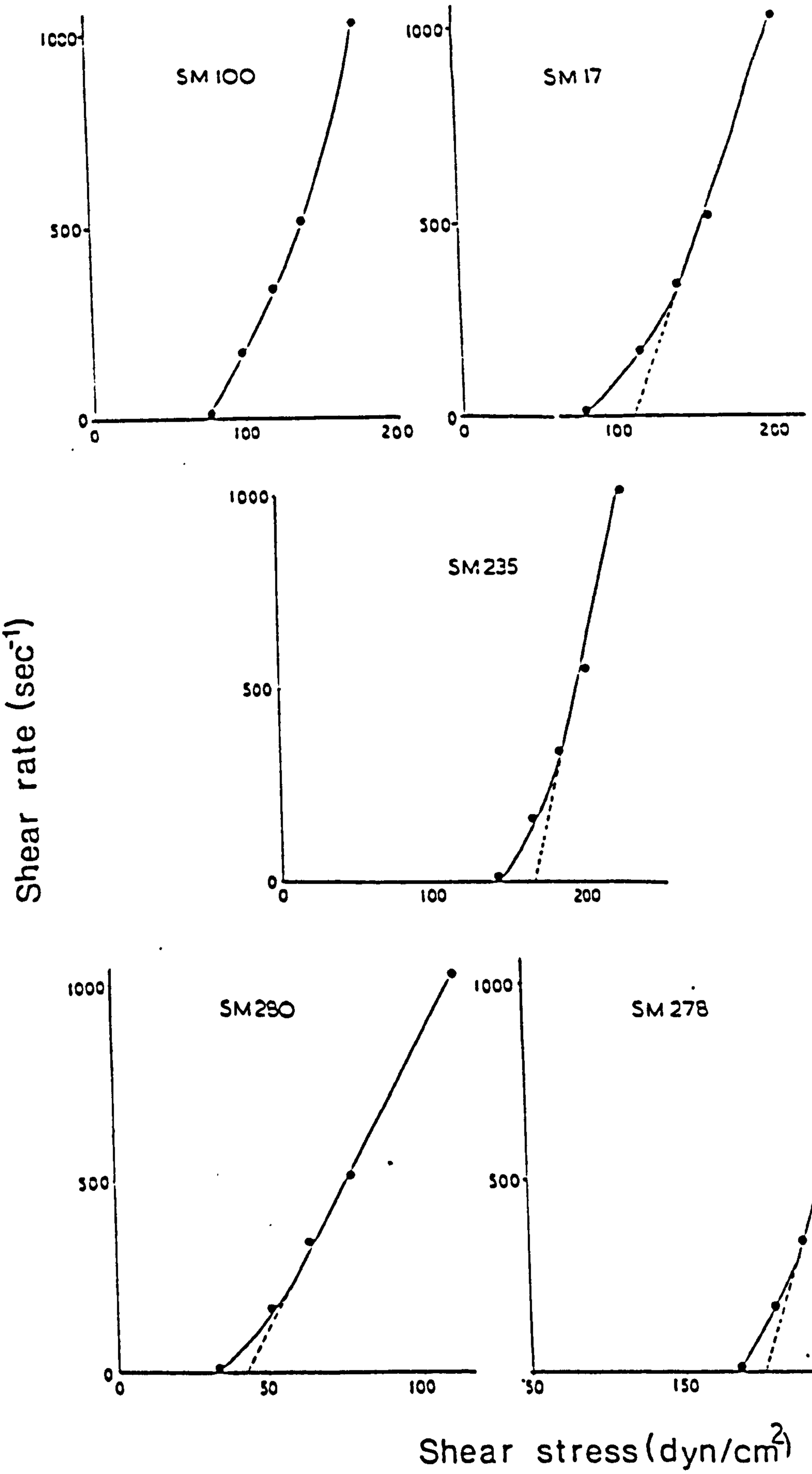

FIGURE 8.3. Rheograms obtained from the bentonites of Milos (Ankeria (SM17), Tsantili (SM100) and Rema (SM235) deposits) and Kimolos (SM278 and SM280 smectite zone from the Prassa deposit)

Table 8.3.

Shear stress values (dynes/cm^2) obtained from the construction of the rheograms of selected bentonite samples .

Shear rate sec^{-1}	SM17	SM100	SM235	SM278	SM280
1022	206	178	223	279	112
511	163	140	203	239	81
340.8	140	119	183	226	64
170.4	114	99	162	208	51
10.2	79	71	143	185	33

Table 8.4.

Shear stress values (dynes/cm^2) obtained during the construction of thixotropic loops of selected bentonite samples.

Shear rate sec^{-1}	SM17	SM100	SM235	SM278	SM280
Increasing shear rate					
10.2	99	80	150	130	43
170.4	114	89	163	178	53
340.8	135	104	170	198	69
511	145	140	196	221	76
1022	185	160	213	169	114
Decreasing shear rate					
511	124	132	188	196	84
340.8	109	109	168	175	71
170.4	84	94	153	168	51
10.2	64	64	124	152	33
Gel strength (lbs/100ft^2)					
10 seconds	26	22	16	45	14
10 minutes	42	35	22	58	26

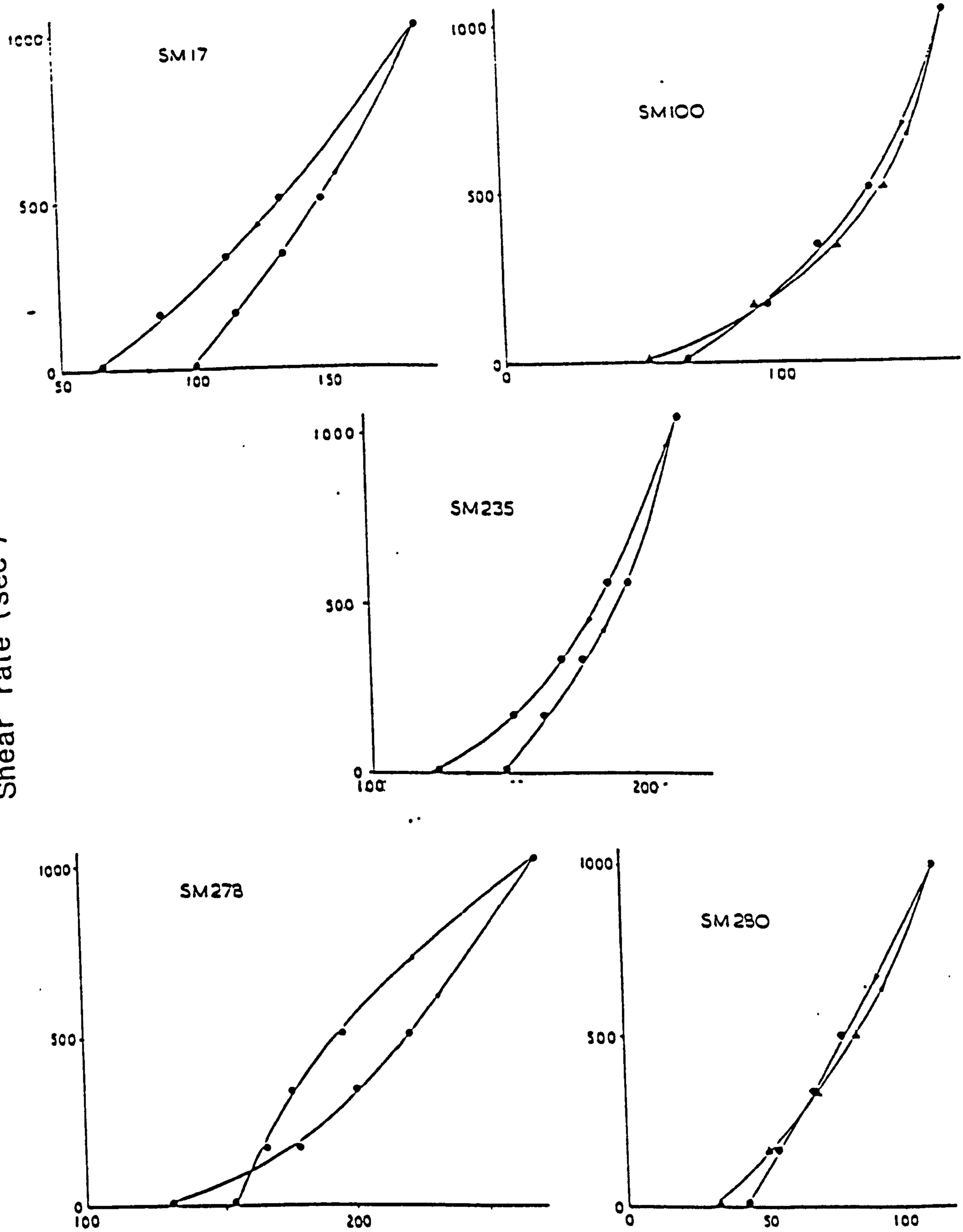

FIGURE 8.4. Thixotropic loops for some of the bentonites of Milos (Ankeria deposit, SM17, Tsantili deposit, SM100, and Rema deposit, SM235) and Kimolos (SM278 and SM280, smectite zone, Prassa deposit)

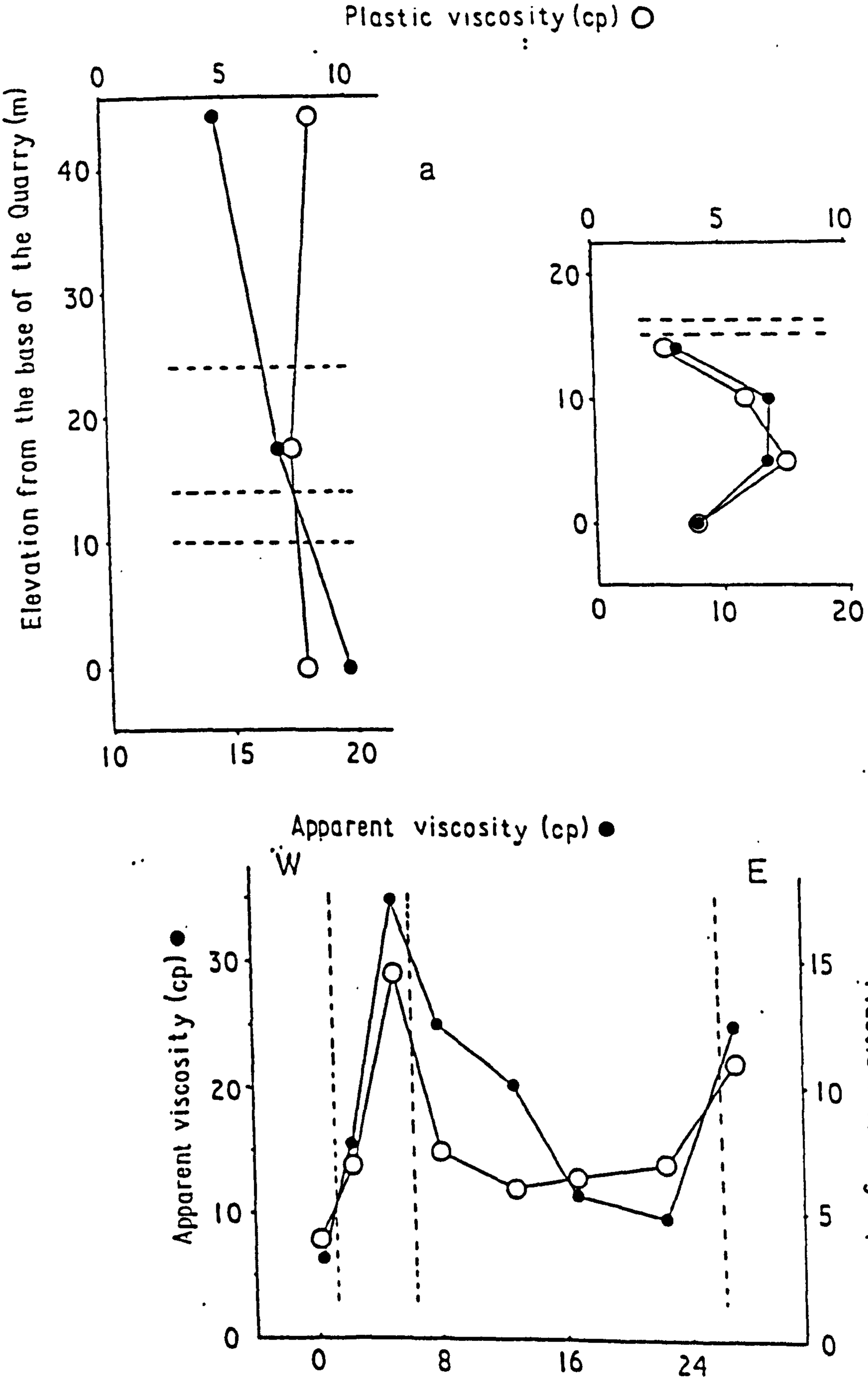

FIGURE 8.5. Variation of the apparent and the plastic viscosity in the deposits of Ankeria (a), Aspro Horio (b), both in Milos and Prassa (Kimolos).

The bentonites from the Ankeria deposit (Area 2) meet the OCMA specifications. The viscosity of the sample SM27 is slightly lower than the minimum value the standards require (see Table 8.2) but when mixed with other bentonites from this deposit it certainly meets the specifications. The apparent viscosity increases towards the bottom of the deposit (Fig. 8.5a), while the plastic viscosity remains constant throughout the vertical profile of the deposit (Fig 8.5a). The bentonites from the Koufi deposit exhibit poor rheological properties and only the sample SM52 develops viscosity close to the lower limit accepted both by the OCMA and the API specifications. The pH of all bentonites from this area is alkaline while the filtrate loss is low indicating good filter cake characteristics (Table 8.2).

The bentonites from Area 3 of Milos have inferior rheological properties compared to their counterparts from Areas 1 and 2. An exception to this tendency is displayed by the bentonites of the Rema deposit (Table 8.2), which however develops very low plastic viscosity. The pH values of these bentonites vary from neutral to alkaline, with the bentonite of the Mavrogiannis deposit being slightly acid (Table 8.2) due to the influence of hydrothermal alteration. The filtrate loss of these bentonites is higher than their counterparts from Areas 1 and 2. An exception to that trend is exhibited by the bentonites of the Ano Komia deposit. The latter develop better rheological properties as well.

The bentonites from the Prassa deposit Kimolos, show a variation in the apparent viscosity characterized by an increase from E to W in the smectite zone, becoming maximum close to the boundary with the mordenite-bearing zone and then decreasing to a minimum value in the smectite + opal-CT ± mordenite zone (Fig. 8.5c). High apparent viscosity values were obtained from the sample SM281 in the smectite + opal-C-T zone (Fig. 8.5c). On the other hand the plastic viscosity does not follow the variations of the apparent viscosity in the smectite zone. Only the samples SM277 (close to the boundary between the smectite and the mordenite-bearing zone) and SM281 (smectite + opal-C-T zone) develop higher plastic viscosity values (Fig. 8.5c).

The pH values range in the neutral-alkaline side, while the filtrate loss is low. The above results indicate that with appropriate blending the bentonites from the smectite zone can be used in the drilling industry. Apparently, the materials from the mordenite-bearing zone can also be used as drilling fluids because they meet both the OCMA and the API specifications.

The bentonites from the Loutra deposit have very poor rheological properties while their filtrate loss values vary from low to very high. Their pH values are in the alkaline side. Obviously these materials cannot be used in the drilling industry.

The white bentonite from the Fanara deposit desplayed the highest viscosity values of all the materials studied (Table 8.2). On the contrary, the other bentonite from this deposit (sample SM306) has poor rheological properties. Both materials are characterized by

neutral pH values. Finally, the bentonites from Chios have poor rheological properties characterized by low appArent and plastic viscosity. Their filtrate loss values are high, above the minimum acceptable values in both the OCMA and the API specifications. Their pH values are on the alkaline side.

The complete rheograms of the samples examined show that they behave like Bingham bodies, except for the sample SM100 which behaves like a Casson body (Fig. 8.3). From the slope of the linear part of the rheograms (the rheogram of the SM100 is excluded) the plastic viscosity increases in the following order SM235<SM278<SM17<SM280. With the exception of SM280 this is the order expected from the plastic viscosity measurements according to the OCMA specifications.

The thixotropic loops obtained (Fig 8.4) indicate that the sample SM17 is more thixotropic than SM235 (the loop is wider). Since both materials were treated in the same way, the "shear history factor" (Mewis, 1979) probably has not affected the loops. The rest materials are thixotropic under high and antithixotropic under low rates of shear. Similar observations were made by Brandenburg & Lagaly (1988) for pH values in the same range as this of the materials examined.

Compared to Wyoming bentonites (e.g see Elzea & Murray, 1990) the plastic viscosity of the Greek bentonite is low. This means that the Na-activation increased only the apparent viscosity. The rheograms of the activated samples have been shifted to higher shear strengths but the linear part must be parallel to that of the raw materials (Morgan 1990b).

8.4. Discussion.

The results obtained revealed large variation in the rheological properties, even among samples belonging to the same bentonite horizon (c.f Aspro Horio and Koufi deposits, Milos, Prassa deposit, Kimolos). In the case of the Prassa deposit the grade of the bentonite is constant throughout the entire horizon. Therefore the abundance of smectite is of secondary importance at least in this case. This is supported from the fact that in this deposit samples from the smectite + mordenite zone, which contain abundant mordenite and have relatively low smectite content, meet the OCMA specifications while samples from the smectite zone very rich in smectites do not.

The role of the pH on the rheological properties of smectites is well known (Rand *et al.*, 1980, Brandenburg & Lagaly, 1988). The pH of the Greek bentonites ranges between values at which poor rheological properties are expected according to both Brandenburg & Lagaly (1988) and Rand *et al.*, (1980). At these pH values Brandenburg and Lagaly consider the "Bandenstruktur" responsible for the rheological properties. It is believed that this theory cannot explain the observed rigidity of the smectite gels. Elzea & Murray (1990) reported high viscosity values at even more alkaline conditions.

In the previous sections it has repeatedly been stated that the house of cards model might not be valid because at this range of pH values the edges of the smectite crystallites must be negatively charged. Also it cannot explain other important features observed in the Greek bentonites. For example although the samples SM278 and SM280 have very similar pH values and similar CEC values their rheological properties are substantially different. pH is probably important in extreme cases like in the samples SM246 and SM185 in which neutralization of the acidic environment probably retarded activation (see Chapter 7). It is believed that the model proposed by Norrish (1954), Callaghan & Ottewill (1974) and Rand *et al.*, (1980) is more plausible (see Section 8.2).

Because the materials were activated with Na_2CO_3, the influence of nature of the interlayer cations (*i.e* the Na/Ca ratio and/or the presence of Mg) should not be important, unless activation was not complete and/or the grade of the deposits is low. In the former case disaggregation of the smectite tactoids should be considered. The problem of disaggregation has been underlined by Lagaly (1989) and Morgan (1990a) and the controlling factors are discussed in the following paragraphs. The rest factors affecting rheological properties, like the shape and size of the smectite particles should also be regarded in association with the degree of disaggregation since the original Ca-rich particles are expected to form long stacks consisting of several layers (Brandenburg & Lagaly, 1989, Lagaly, 1989). Organic matter might affect the rheological properties of the clay suspension by adsorption on the clay surface (van Olphen, 1977); however there is no evidence that organic matter is present in the deposits.

The influence of abundant fine-grained impurities on viscosity is obvious in the Area 3 of Milos, in which, with the exception of the sample SM235, the apparent viscosity of the bentonites is low. These deposits are rich in various polymorphs of silica, especially opal-CT, the size of which is less than 1μm. If opal-CT is intimately associated with smectite then the formation of a rigid gel-structure might be retarded (see also Chapter 7). Furthermore, the close association of the two phases might prevent disaggregation of the smectite tactoids retarding Na-activation.

However, it seems that in the Rema deposit although the bentonite contains abundant opal-CT it develops high apparent viscosity. Also, it seems that in deposits with rather similar Si-phase content the rheological properties vary between broad limits. Thus, the bentonites from the Ano Komia deposit develop significantly better rheological properties than their counterparts from the Mavrogiannis Garyfalakaina and Kato Komia deposits, although they all are abundant in opal-CT. Since the smectite chemistry in these deposits varies between the same limits, the compositional variation of smectite cannot be invoked as a possible reason for the different rheological properties.

The mircoprobe analysis revealed that the Si/Al ratio of these smectites varies between very broad limits (see Chapter 4), indicating that different amounts of Si have been

released from the parent glass. Usually, the rims of the glass shards are more depleted, while their interior is more abundant in Si (Plate 17). As a result, a free Si-phase co-precipitates with smectite in the latter sites, while the Si released from the former sites might precipitate in voids created from the dissolution of the glass, *not* intimately associated with smectite (Plate 17). If the system is characterized by high fluid flow and high water/rock ratios then complete leaching of Si is expected (c.f Prassa deposit, Kimolos). Under such conditions, deposition of a Si-phase not intimately associated with smectite is favoured. If the close association between opal-C-T and smectite imparts a low gel strength, then high fluid flow prevailing during the bentonite formation might lead to materials with better rheological properties.

There is limited evidence that the fluid flow conditions during the formation of these bentonites, which were probably derived from the same precursor (see Chapters 5 and 6), were different. In the Rema deposit and less often in the Ano Komia deposit, the opal-CT usually forms aggregates separated from smectite, while in the rest deposits of this area fine grained intergrowths with smectite are very common. Similar intimate association between opal-C-T and smectite was found in the bentonites of Chios and those of the Loutra deposit, Kimolos, which exhibit very poor rheological properties. These observations support the idea of an existing relationship between rheological properties and smectite-opal-CT association.

However, there is a further factor which should be taken into account. Since all the deposits have been affected by hydrothermal alteration, thermal transformation of opal-CT to quartz or/and opal-C is common (see Chapter 4). This transformation probably involves crystal growth and thus the association of the Si-phase with the fine grained smectite is expected to be less intimate. A combination of these two factors might affect the rheological properties. The fact that both horizons of the Ano Komia deposit and the Rema deposit, which have better rheological properties than the other deposits of this area, contain abundant quartz and/or cristobalite coexisting with opal-C-T might support this view.

In the case of the bentonites from the Area 1 of Milos, although the grade and the quality are high, their rheological properties are poor. Exception to this trend is shown in the Tsantili deposit. This behaviour cannot be explained by the existence of opal -CT because the latter is absent or exists in very small amounts. The smectites in the Tsantili and the Aspro Horio deposits are pobably Wyoming-type montmorillonites, while those of the Zoulias deposit probably Cheto-type montmorillonites and beidellites. Both types of smectites contain abundant iron. Alther (1986) mentioned the influence of the oxidation state of iron in the rheological properties of the bentonites. Thus, if iron is present in the ferrous state then the bentonites develop low viscosity. Recently, Stucki & Tessier (1991) showed that nontronite containing ferrous iron consists of thick stacks of 10Å thick

particles, and has a more ordered structure compared to nontronite containing ferric iron. The latter consists of thin units 1-6 particles thick.

The influence of the oxidation of Fe in terms of the particle thickness might be crucial during the alkali-activation of the bentonites. It is well known that the Na-bentonites have good rheological properties while their Ca-counterparts poor rheological properties (van Olphen, 1959, Patterson & Murrey, 1983, Odom, 1984, Brandenburg & Lagaly, 1988, Lagaly, 1989). This is because the Ca-smectites form thick crystallites several layers thick (van Olphen, 1956, Brandenburg & Lagaly, 1988, Lagaly, 1989). Nevertheless, the optimum rheological properties are exhibited when part of the exchangeable cations is Ca or/and Mg (Grim, 1962, Odom, 1984, Alther, 1986). In any case the presence of ferrous iron is unfavourable because it produces thick tactoids, especially in the presence of Ca ions, retarding disaggregation and thus Na-activation.

In the Area 1 of Milos the original materials are Ca-bentonites (see the swelling tests in Chapter 7). In the evaluation of the rheological properties Na_2CO_3 was added in the high speed stirrer according to the OCMA specifications. If the iron in the particles is present in the ferrous state, activation might not be successful. Morgan (1990a) has shown that prolonged stirring promoted the activation of bentonites. This is probably because the tactolds formed by the original Ca-bentonites are broken by the intensive mechanical action (Kleijn & Oster, 1982). The colour of the bentonites indicate that at least in the Aspro Horio deposit substantial amount of Fe should be in ferrous state. Indeed the HRTEM study (Plate 20) showed that the smectites in this deposit form coherent stacks, several layers thick (Plate 20). In the Zoulias deposit, in as much as the subsequent hydrothermal alteration is characterized by deposition of sulphur-rich compounds, the yellow colour of the highest horizon does not necessarily mean that the iron is present in the ferric state and the poor rheological properties can be explained in a similar way. In the Tsantili deposit the high apparent viscosity values obtained, indicate that if the above speculation is correct then Fe is present mainly in the ferric state. This is expected because the deposit has been affected by hydrothemal alteration and several phases indicative of oxidating environments are present (see Chapter 4).

In the Area 2 of Milos the poor rheological properties of the green bentonites of the Koufi deposit might be explained in a similar way. In the Ankeria deposit however, the lower dark green horizon has the best rheological properties. Since the colour of the bentonite is indicative of the oxidation state of iron (Bates, 1969, Alther, 1986, among others), it follows that the presence of ferrous iron enchanced the rheological properties of this particular material. This however is unlikely. Furthermore, the sharp contact between the bright yellow and the basal green/blue horizon (Plate 3) cannot be explained by the degree of oxidation of Fe.

The alternative explanation is to attribute the green colour to chemical factors other than the presence of ferrous iron. Linares *et al.* (1972) found that the coloured bentonites they studied were more abundant in transition elements, (Cr, Ni and Co) compared to their light coloured counterparts. Therefore they attributed the colour to the presence of these elements. In the present case although the Cr content of the yellow and the green bentonites was the same, the Ni content of the green bentonite was 4 times higher than that of the yellow bentonites (compare the Ni-content of the sample SM17 with that of SM8, SM16 and SM36). However, the Ni-content is relatively low (about 50ppm) to explain such a difference in colour, although it might contribute to some extent. With the existing data this phenomenon cannot be explained.

In the Prassa deposit, Kimolos, the decrease of viscosity towards the smectite + opal-CT zone might be due to a variation in the oxidation state of Fe, because the bentonite is free of opal-CT and the Cr, and Ni content of the rock are minimal. If it is considered that the zone of the more vigorous reaction between the pore fluid and the parent rock is close to the sample SM280, then this zone is more likely to be characterized by more reducing conditions. This is because Fe was transported mainly through this zone in the ferrous state and the fluid/rock ratio was high (see Chapter 5). Indication for a more vigorous reaction in this zone is provided from the fact that the HREE have been leached almost completely from the sample SM280. It is possible that the increase in viscosity towards the mordenite-bearing zone might be due to the gradual increase of the Fe^{3+}/Fe^{2+} ratio in smectite, away from the zone of the highest water/rock ratio.

An alternative explanation for the rheological properties of the bentonites in the Prassa deposit might be provided by the suggestion of Chen *et al.*, (1990), because the smectites present are Mg-rich (see Chapter 4). Had the smectites of the sample SM279 been richer in Mg, then the different degree of Mg release from the octahedral layer during viscosity measurements would have explained the variation observed. However, it is clear that the crystal chemistry of the smectites in the various zones of the deposit is identical (Fig. 4.17). Hence, there is no particular reason to expect a gradual increase in the Mg-release during the viscosity measurements towards the mordenite-bearing zone.

The distribution of the layer charge (charge localization) affects swelling (Suquet *et al.*, 1975); therefore it might affect the rheological properties (Callaghan & Ottewill, 1974, Rand *et al.*, 1980). Thus bentonites which contain beidellite characterized by predominance of tetrahedral layer charge might swell to a lesser degree (charge localization factor). It is interesting that in all bentonites which develop good rheological properties, beidellites are not present. Also, the Rema bentonite which develops good rheological properties is the only bentonite in the Area 3, Milos in which beidellite is not present. It is possible that charge localization might affect the rheological properties to a certain degree. However, in many cases (*i.e* Aspro Horio deposit, Chios bentonite, Zoulias bentonite) where the layer

charge of the smectites is predominately octahedral the materials develop poor rheological properties.

The layer charge density of the smectites might also play some role in the variation of the rheological properties. Lagaly & Weiss (1975) suggested that the charge density between 0.28-0.33 c.u. per half formula and broad heterogeneity favour Na-activation. On the contrary bentonites with smectites having high and low charged smectites and/or smectites with narrow intracrystalline charge distribution are not easily activated. In the present study the smectites in the Rema and the Tsantili deposits which display good rheological properties seem to have the right (according to Lagaly & Weiss, 1975) layer charge density see Table 4.4). However, this is not the case in the bentonite from the Ankeria deposit which develops good rheological properties and in which the layer charge of the smectites varies from very low to high values (see Table 4.4).

An increase of the layer charge results in an increasing tendency for tactoid formation, especially in the case of Ca-smectites (Kleijn & Oster, 1982) affecting disaggregation. Since Wyoming-montmorillonites have lower layer charge than their Cheto counterparts, the smectites from the area 1 in Milos are expected to have better rheological properties than those from the area 2. This might be the case in the Tsantili deposit but not in the Aspro Horio deposit, indicating that the layer charge is either of secondary importance or it acts together with other factors which affect disaggregation.

The second explanation seems more plausible and the layer charge should be considered in conjunction with the oxidation state of Fe, the presence of impurities and the nature of the interlayer cations. Thus, abundance of ferric iron increases the possibility for better disaggregation of the smectite stacks (Stucki & Tessier, 1991). Disaggregation is more efficient if opal-CT is absent or present in small amounts and if the layer charge is lower because the maximum number of layers per tactoid decreases (Kleijn & Oster, 1982). Also, the lower the Ca/Na ratio of the original bentonites the greater the possibility for formation of thinner tactoids. The latter is more important in the case of Ca-bentonites which are activated. The distribution of the layer charge might also be important, with beidellite-rich materials activated less easily. Beidellites contain very little iron, and have large layer charge. This decreases the possibility for formation of thinner tactoids, even after oxidation of the octahedral iron.

All the previous factors affect the accesibility for the Na ions during Na-activation. In other words, Na-activation is successful and the rheological properties good if the smectite stacks are "penetrated" by Na, *i.e* if the disaggregation of the smectite stacks is sufficient. The fact that the Mining Companies in Milos expose the bentonites in flat areas and turn them up and down to facilitate drying and decrease the cost of moisture reduction, probably increases the Fe^{3+}/Fe^{2+} ratio. It is therefore believed that most of the high grade bentonites develop good rheological properties during mineral processing.

The possible role of the smectite mineral chemistry is usually ignored when bentonites are compared with respect to their properties. The materials tested are usually referred to as Na- or Ca-bentonites (e.g see the work of Odom, 1984, Alther, 1986, 1991, Brandenburg & Lagaly, 1989, and Lagaly, 1989 among others). However, it should be taken into account that the Wyoming bentonites which are used as reference materials consist mainly of Na-rich Wyoming-montmorillonite. There is no reason to believe that the bentonites of the Area 1 of Milos which contain Ca-rich Wyoming montmorillonite will behave in a much different way than their Wyoming counterparts *if they are activated successfully.*

Finally, the hydrothermal alteration observed in Milos has certainly affected the original rheological properties of the bentonites in many ways:

a) It reduced the smectite content either by deposition of other phases like sulphates, carbonates and sulphides (see Chapters 4 and 6) or by dissolution of smectite (formation of kaolinite and/or illite/smectite). The presence of gypsum is detrimental for the rheological properties of bentonites (Alther, 1986). On the other hand kaolinite might increase the viscosity of the bentonite suspension because it forms stronger links with smectite than the smectite crystals themselves (Kasperski *et al.*, 1986). It is not certain what type of linking develops between the two clay minerals although Schofield & Samson (1954) considered a negetive smectite face-positive kaolinite edge association. However, the point of zero charge of kaolinite varies between pH 2.5 and 4.6 (Eslinger & Pevear, 1988, Table 3.2) *i.e* higher than almost all the deposits studied, indicating that the edges of kaolinite are also negative charged.

b) It transformed the opal-CT to more coarse grained phases improving the rheological properties of the bentonites. This is more obvious Area 3 of Milos.

c) It possibly led to the formation of smectite with smaller layer charge (see Chapter 6).

d) It might have affected also the oxidation state of Fe. Since in most deposits it is associated with minerals like alunite or jarosite characteristic of oxidising environments, it is expected that the Fe in the smectites might also be in the ferric state. This might be the case in the Tsantili deposit and possibly in the green horizon of the Ankeria deposit. Indeed the pH of these bentonites is lower than that of their counterparts derived from the same precursors (Table 8.2) indicating influence of hydrothermal alteration.

The above discussion indicates that the major reason for the variability in the rheological properties of the Greek bentonites might the different degree of disaggregation of the materials. This might have been caused by a number of reasons as stated before. The crystal chemistry of the smectites probably plays an important role. Thus Wyoming montmorillonites might respond better to the activation process than their Cheto counterparts because their smaller size, the more random distribution of the exchange sites the lack of regular stacking and bonding of the individual layers (Grim & Kulbicki,

1961), the lower layer charge (Shultz, 1969) and their usually higher iron content (Güven, 1988). The unpredictable results of Na-activation noticed by Odom (1984) might be explained in this way.

8.5. Correlation between swelling and rheological properties.

In the previous section the model proposed by Norrish (1954), Callaghan & Ottewill (1974) and Rand *et al.*, (1980) was accepted as the most suitable for understanding of the gelling properties of bentonites. If, as this model proposes, the gel strength is due to the repulsive forces of the interactive double layers, and the formation of the effective double layers is a result of the swelling, then a relationship is expected to hold between the viscosity (both plastic and apparent) and swelling. In this hypothesis, swelling might be the result of *any* of the models presented in the Chapter 7.

In Figure 8.6 swelling volumes are plotted against the apparent (Fig. 8.6a) and the plastic (Fig. 8.6b) viscosity. Notwithstanding the scattering two types of relationship are observed in both cases: for low swelling volumes both the apparent and the plastic viscosity increase slightly with increasing swelling, while for higher swelling volumes they both display a sharp increase. The breaking point is at swelling volumes close to 160ml/10gr of clay. In the case of the apparent viscosity it is believed that the observed relationship is better described by two straight lines with different slopes. The same relationship, although possible, is not certain for plastic viscosity because of the small variation in the values obtained. Thus a curvilinear relationship between plastic viscosity and swelling volume should not be excluded.

The scattering observed in the second part of each curve is probably associated with the various factors affecting both properties (layer charge, oxidation state of iron, compositional variation of smectites, impurities) and the sample preparation. For example the sample SM279 develops very high swelling volume but poor rheological properties. The swelling volumes were measured on materials which had previously been ground by hand to pass through a 150μm sieve and underwent two drying cycles (one before crushing and one after mixing with Na_2CO_3). The possibility that iron oxidation was more complete is thus higher. Alternatively, the high swelling of the smectite particles might have led to weaker interactions between the double layers because of the low electric potential away from the clay surface.

On the other hand the samples SM235 ans SM277 although exhibited poorer swelling properties they developed very good rheological properties. The former is rich in opal-CT while the latter contains abundant mordenite. It seems that in both samples the presence of another phase did not impede the development of a gel with substantial strength. The behaviour of the SM235 has been explained by the relatively small amount of intergrowths

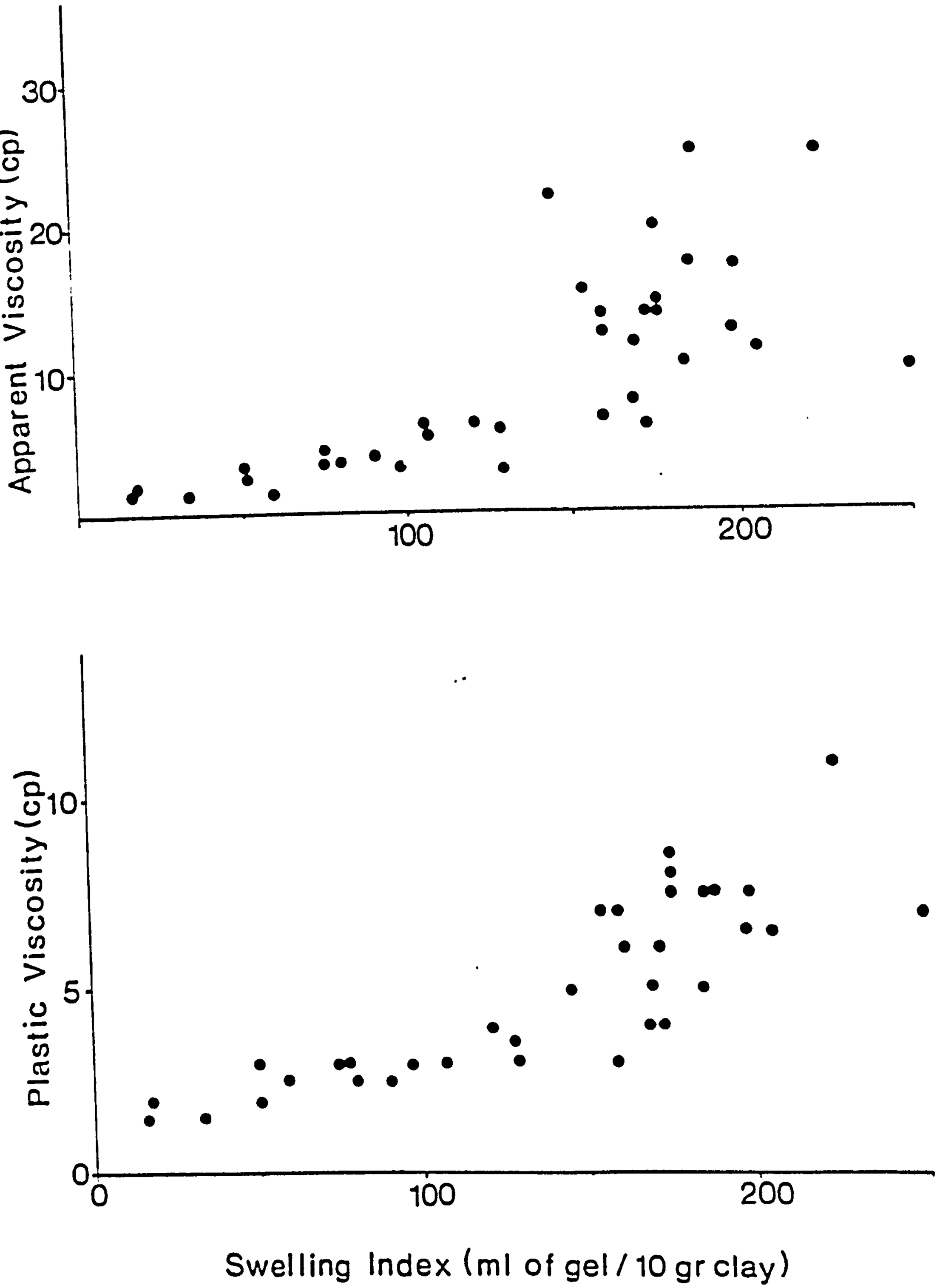

FIGURE 8.6. Correlation between the swelling volume and (a) apparent viscosity and (b) plastic viscosity.

between smectite and opal-CT. On the other hand the properties of the SM277 have not been understood fully so far. Iron oxidation away from the zone of high fluid/rock ratio might explain partly the results obtained.

In any case, for the great majority of the materials examined it is clear that good rheological properties are observed *only* when bentonites develop high swelling volumes. In a smectite-water system most of the water is trapped in the interlayer region (Davidtz & Low, 1970, Low, 1980). Thus the rheological properties are indeed associated with swelling. Whether or not the gel formed will be strong enough to impart high viscosity to the bentonite suspension and render it suitable for use in the drilling industry, depends on the interaction between the double layers of the smectite flocs. If the second explanation for the sample SM279 is valid then it is possible that after a maximum degree of double layer interaction, the repulsive forces are not strong enough to impart a high gel strength. This might occur when the double layers expand beyond a certain limit. If this is the case then the maximum interaction between the smectite particles is not nessecarily associated with maximum swelling. However, the presence of particles with various degrees of swelling makes the interaction more complex. It is believed that the position and the slope of the curve at high sweling/high viscosity values would be different if the disaggregation of the particles was more complete.

8.6 Conclusions.

Examination of the rhological properties of the Greek bentonites has led to the following conclusions:

1) The rheological properties of the bentonites are believed to be a function of the degree of disaggregation of the smectite tactoids.

2) Poor disaggregation leads to insufficient Na-activation imparting poor rheological properties to the clay suspensions, if the parent materials contain Ca-smectites.

3) Disaggregation is influenced by several factors including layer charge density and localization, iron oxidation, presence of clay-size impurities, and probably the original distribution of the interlayer cations.

4) In the case of Wyoming- and Chambers-type montmorillonites iron oxidation is believed to be the most critical factor affecting Na-activation and hence rheological properties. In this sense, it is believed that most of the high grade bentonites of the areas 1 and 2 of Milos might be suitable for the drilling industry after prolonged exposure under oxidizing conditions.

5) Bentonites rich in Ca-Wyoming montmorillonite might develop rheological properties compared to their Wyoming counterparts (*sensu stricto*), if they are activeted successfully.

6) Hydrothermal alteration affects the rheological properties because it modifies the original mineralogical and physicochemical characteristics of the bentonites.

7) Swelling is closely associated with viscosity, and high viscosity values were obtained from highly swollen bentonites.

CHAPTER NINE

ACID ACTIVATION

9.1. Introduction.

In Chapter one it was mentioned that bentonites are highly valued for their absorptive properties, which stem from their high surface area and their tendency to absorb water in the interlayer sites. Their sorptive properties increase when they are treated with various reagents, inorganic and organic (see Odom, 1984). The most important treatment with inorganic reagents is the so- called acid-activation which involves treatment of the raw materials with various acids in order to increase their surface area (Grim, 1962, Rupert *et al*, 1987, Griffiths, 1990, among many authors) and to modify the structure of the smectites present (see following section for details).

Acid activation is a process known since the beginning of the 20th century. According to Robertson (1986) it was applied for the first time in Germany on the 17th November 1909. In the USA bentonites were treated with acids for the first time in 1920. In the U.K bentonites have been activated since the mid 1920's, while in France since 1932 and in Japan since 1937. Finally, in the former Soviet Union the first attempt for acid activation was made in 1928, while acid treated materials were used for the first time in petroleum crackin (1933). According to O'Driscoll (1988) and Griffiths (1990) the current world leader in the production of acid activated bentonites is Germany (165000-180000 tpa) followed by the U.K (130-140000 tpa), Japan (105000) and USA and Canada (102000 tpa). Other European countries which produce acid activated bentonites in small quantities are Italy and Spain. Several third world countries (Mexico, Malaysia, Thailand, Brasil, Peru, India and Pakistan also produce acid activated bentonites, with Malaysia being an ascending power in this market (90000 tpa).

Although Greece is the second bentonite producer in the world after the USA with a production of more than 1.3m.tonnes per annum in 1986 (O'Driscoll, 1988), its needs for acid activated clays are entirely covered by imports. In a first attempt, Christidis (1989) activated bentonites from Milos using sulphuric acid and examined briefly some mineralogical, morphological and physical changes caused by activation on the treated clay. The results were promising since the surface area increased up to about 300 m^2/gr depending on the acid strength and the time of treatment, and the smectite morphology was modified. However, the activated clays were not actually tested for their bleaching properties. Therefore, one of the tasks of this project, examined in this chapter, is the acid activation of some of the bentonites examined, using a large number of combinations of

acid strengths and treating times, and the evaluation of their capacity to decolourize crude edible oil.

9.2. Uses of the acid-activated bentonites.

According to Clarke (1985) and O'Driscoll (1988) the major application areas of the acid activated bentonites are the following:

-a) The foodstuffs industry (refining, decolourizing, purifying and stabilizing of vegetable and animal oils and fats).

-b) Sulphur production (refining, decolourizing, bitumen extraction).

-c) Forest and water conservation (powder fire extinguishing agents and binding agents for oil on water).

-d) The mineral oil industry (refining, decolourizing and purifying mineral oils, fats, waxes, parafin). Also catalysts for oil cracking (limited application).

-e) The beverages and sugar industry (fining of wine must and juices-beer stabilization-purification of saccharine juice and syrup).

-f) The chemical industry (catalyst carriers, insecticides and fungicides, fillers, dehydrating agents, toilet and cosmetic soaps, paints and varnishes)

-g) Environmental protection (water and waste water purification,absorbents for radioactive elements).

-h) The paper industry (pigment and colour developer for carbonless copying paper adsorption of impurities in white water system).

-i) Cleaning and detergents (regeneration of organic fluids for dry cleaning).

In terms of consumption, the most important use of the acid activated bentonites is the purification, decolourization, and stabilization of vegetable oils during refining. They are used to remove impurities (phospholipides, soaps and trace metals), organic compounds and their degradation products which impart undesirable colours to the edible oils (Siddiqui, 1968, Kheok & Lim, 1982, Griffiths, 1990). These compounds are (Siddiqui, 1968): *carotenoids* (especially ß-carotene) and their derivatives, *xanthophylls* which impart the undesirable orange-red colour in most edible oils, *chlorophyll* which imparts the characteristic green colour to olive oil, *pheophytin*, *tocopherols*, and *gossypol*. Other undesirable colouring matters might be the *degradation products* of these compounds. Thus oxidation might convert the unsaturated fatty acids and glycerides to hydroperoxides which are also undesirable and are removed during bleaching.

9.3. Theoretical considerations of activation.

The theoretical aspects of the acid activation reaction have been studied extensively over the last 40 years. The dissolution of smectite is described by pseudo-first order kinetics (Osthaus, 1956, Granquist & Samner, 1959) and is characterized by an initial replacement of the interlayer cations by H^+ (Thomas *et al.*, 1950, Grim, 1962), followed by dissolution of the octahedral sheet and release of the octahedral cations (Thomas *et al.*, 1950, Mills *et al.*, 1950, Brindley & Youell, 1951, Milliken *et al.*, 1955, Osthaus, 1956, Granquist & Samner, 1959, Grim, 1962, Brückman *et al.*, 1976, Novak & Cicel, 1978, Yates, 1986). Tetrahedral aluminium is more resistant and is not removed before substantial octahedral cation removal has taken place (Brindley & Youell, 1951, Osthaus, 1956). Also, several impurities like carbonates or/and sulphates are dissolved, increasing the relative smectite concentration of the bentonite materials (Morgan *et al.*, 1985, Clarke, 1985).

The detailed structural composition of the acid treated smectites has not been published so far (Rupert *et al.*, 1987). Thomas *et al.* (1950) considered the possibility of a change in the coordination of the octahedral aluminium from six-fold to four-fold after the removal of one of a pair of Al^{VI}, and two hydroxyl groups (Fig. 9.1). The new tetrahedron thus formed has extra charge and can serve as proton donor contributing to the acidity of the clay (Brønsted acid centres). If this model is valid then it might be expected that the potential activation of a montmorillonite-rich material depends on its ability to form Al-tetrahedra. However, Rupert *et al.*, (1987) proposed that the newly formed tetrahedra share edges instead of corners, they are uncharged and do not contribute to the acidity of the clay or the CEC.

Osthaus (1956) showed that the rate of release is the same for all octahedral cations, while Stoch *et al.*, (1977) found that the release rate of Mg is greater. The results of Yates (1986) show a faster release of Mg compared to Fe during activation of the Oxfordshire bentonite and slower in the case of the Surrey bentonite. In both bentonites the smectites present are iron rich.

It is well known that not all the bentonites can be activated (Mills *et al.*, 1950, Grim, 1962). According to Grim (1962), bentonites consisting of Cheto montmorillonites seem to be activated successfully; on the contrary, Wyoming bentonites are not activatable by acids. Rupert *et al.*, (1987) proposed that an activatable clay might be characterised by considerable substitution in the tetrahedral layer. On the basis of this proposal Wyoming bentonites should be activatable because their tetrahedral charge ranges between the same limits as those of the Tatatilla and Chambers montmorillonites (see the classification scheme of smectites proposed by Schultz, 1969). In the following sections it will be shown that Otay-motmorillonites which have very low tetrahedral charge were activated very successfully. Therefore it is **imperative** to examine the raw materials *in practice* in order to

characterize them as activatable or not (Morgan 1990c). Also since different oils are bleached by different materials (Stoch *et al.*, 1979a) the fact that an activated clay is effective for one type of oil does not mean that can decolourize other oils.

The most important physical changes in the activated smectites is the increase of their specific surface area and the average pore diameter (Mills *et al.*, 1950, Grim, 1962, Fijal *et al.*, 1975, Morgan *et al.*, 1985, Clarke, 1985, Griffiths, 1990, Srasra *et al.*, 1990 among many others). The increased surface area of the activated smectites and (especially) its acidic properties (*surface acidity* due to the presence of acid centres on the surface of the activated clay) are very important factors controlling the bleaching properties of the clay. Also, the "opening" of the micropores increases the availability of the sites which are active for absorption, thus increasing the bleaching capacity of the clay. The interlayer space of montmorillonite does not contribute to the sorption of colouring matter from crude oils (Stoch *et al.*, 1979b). Interaction with organic compounds (chiefly amines) might also increase the decolourizing efficiency of a smectite clay (Stoch *et al.*, 1979b).

There are two types of acid centres present on the surface of the smectites, namely Brønsted (proton donors) and Lewis (electron pair receivers). Brønsted-type centres are formed due to migration of H^+ resulting from deprotonation of H_3O^+ and NH_4^+ in the interlayer sites at elevated temperatures, as well as from Si-OH and/or Al-OH groups located along crystal edges (Brückman *et al.*, 1976, Stoch *et al.*, 1979a). Migration of H^+ protons to the octahedral sheet might cause disruption of the Si-O-Al bonds, forming new Si-OH or Al-OH bonds (i.e unsaturated Al^{3+} and/or Si^{4+} cations) which serve as Lewis-type acid centres (Brückman *et al.*, 1976, Stoch *et al.*, 1979a). Broken bonds at the edges of crystallites might also give rise to Lewis acid centres.

During activation, the surface area of bentonites increases steadily up to a maximum point beyond which it decreases, due to disruption of the smectite structure (Novak & Gregor, 1969, Kolta *et al.*, 1976, Kheok & Lim, 1982, Morgan *et al.*, 1985, Clarke, 1985, Zaki *et al.*, 1986). Although Novak & Gregor (1969) and Kolta *et al.*, (1976) connected bleaching capacity with the maximum surface area, Morgan *et al.*, (1985) and Zaki *et al.*, (1986) found that this it is not the case. The latter has also been described by Morgan (1990c). This is expected since the bleaching process is not merely a physical adsorption process (Siddiqui, 1968, Khoo *et al.*, 1979, Morgan *et al.*, 1985). The evolution of the surface area as well as that of the bleaching capacity depend in the acid strength and time of treatment (Novak & Gregor, 1969, Kolta *et al.*, 1976, Kheok & Lim (1982), Zaki *et al.*, (1986), Srasra *et al.*, (1990) as well as on temperature (Kolta, *et al.*, 1976).

The mechanism of acid activation is depicted in Figure 9.2. The acid attacks the octahedral layer and removes part of the octahedral cations. This process causes disruption of the smectite stacks and renders some tetrahedral sheets exposed at the edge of the attacked layers, which precipitate in the form of amorphous silica (Fijal *et al.*, 1975,

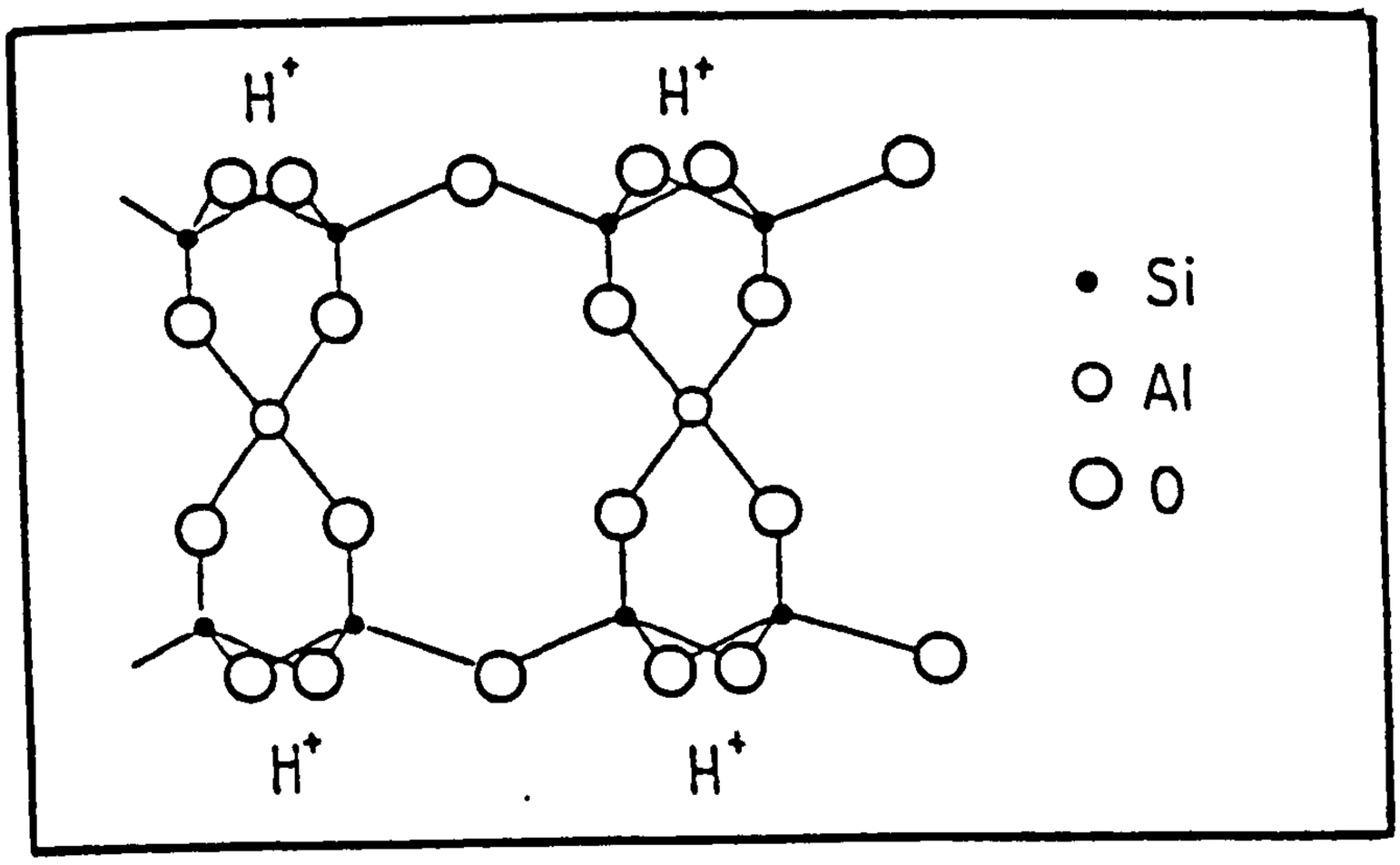

FIGURE 9.1. Theoretical structure of the acid activated smectites (after Thomas *et al.*, 1950).

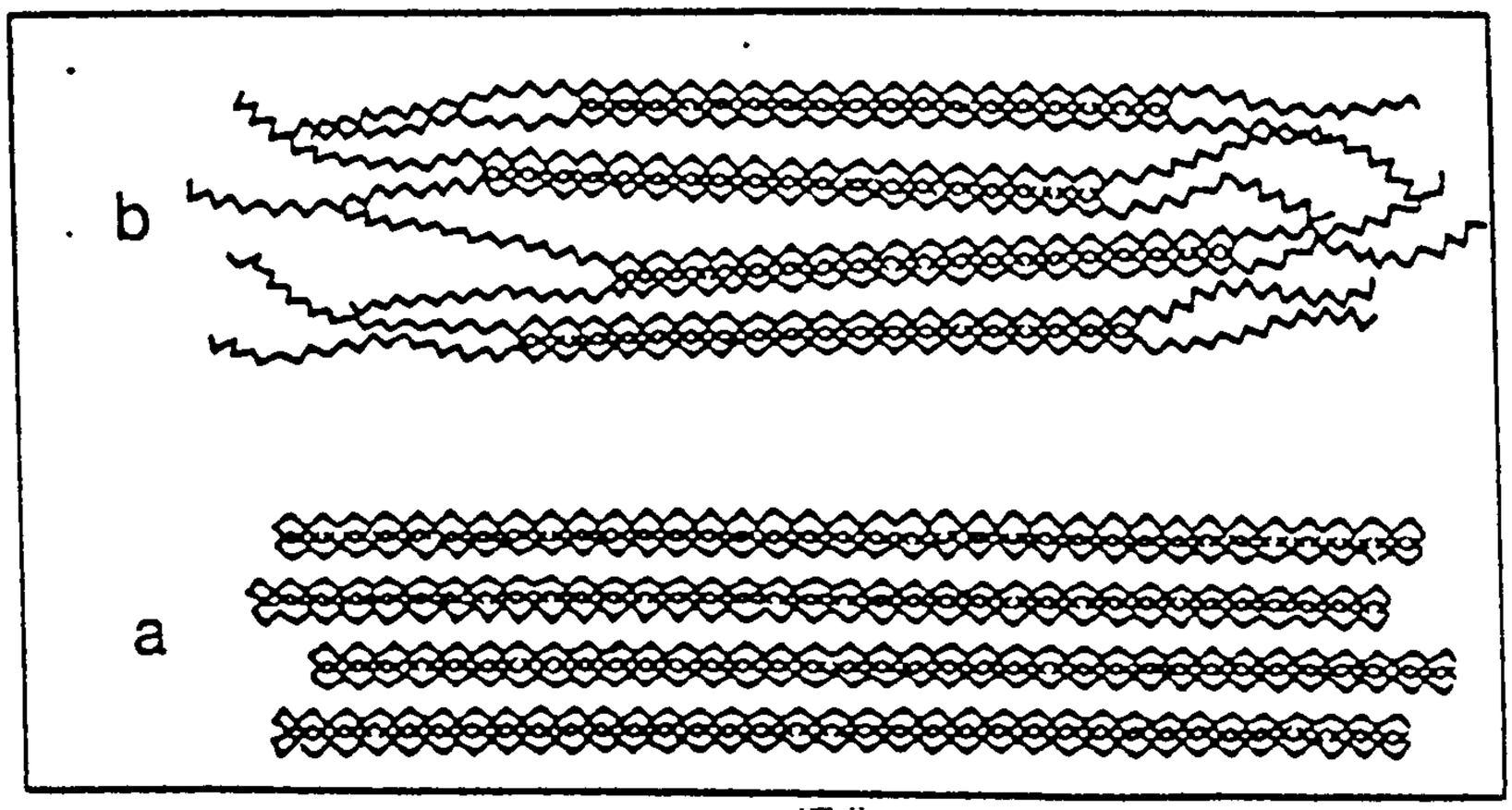

FIGURE 9.2. Effect of the acid activation on the smectite layers. (a)=untreated smectite, (b)=acid activated smectite (after Fahn & Fenderl, 1983).

Brückman *et al.*, 1976, Fahn & Fenderl, 1983, Morgan *et al.*, 1985, Yates, 1986). The acid attacks first in the margins of the smectite flakes leaving the middle of the flakes essentially intact (Fahn & Fenderl 1983, Morgan *et al.*, 1985); progressive treatment affects the interior of the flakes as well. When the octahedral layer has entirely been destroyed the smectite structure collapses (Newman, 1963). The area of the clay surface attacked by acid decreases with time (Rupert *et al.*, 1987). The CEC of the treated smectites *increases* during activation because the original smectite is transformed into a phase which becomes more electrically imbalanced as the reaction proceeds (Granquist & Samner, 1959). The *apparent decrease* of the CEC usually observed for the *total amount of solids* (c.f Yates, 1986, Christidis, 1989) is probably due to the precipitation of amorphous silica *i.e* due to the effective dilution of the smectite present.

9.4. Materials and experimental methods.

9.4.1. Materials

Three bentonites coming from different areas were activated. The materials come from the lower horizon of the deposit of Ankeria (area 2 Milos) designated as SM16, the deposit of Rema (area 3 Milos) designated as SM236 and Chios (SM324). All bentonites contain Cheto-type montmorillonite ± beidellite. More specifically, the bentonite from the Ankeria deposit contains Tatatilla and Chambers type montmorillonites, that from the Rema deposit contains beidellite and Tatatilla-type montmorillonite, while the Chios bentonite consists of Otay-montmorillonite (see Chapter 4).

The bentonite from the Rema deposit and that from Chios contain abundant opal-CT and have similar grade but their quality is significantly different; also, their surface areas are different (Table 9.1). The bentonite from Chios contains abundant dolomite while that from the Rema deposit has small amounts of calcite and traces of pyrite. On the other hand, the bentonite from the Ankeria deposit consists principally of montmorillonite (its grade is much higher) and is free of opal-CT (Table 9.1). All bentonites were dried at 65^{o}C overnight, ground in Tema mill and passed through a 250μm sieve (BS 410).

9.4.2. Experimental methods.

9.4.2.1. Acid activation.

The acid used for activation was HCl of analytical grade (FISONS). The strength varied from 0.5N to 8N (0.5N, 1N, 1.5N, 2N, 3N, 5N and 8N). The strength of the commercially available concentrated (*i.e* 37%) HCl is about 12N. Before preparation of the acids having different normalities (*i.e* strengths) the concentrated HCl acid was titrated with anhydrous

Table 9.1.

Mineralogy, cation exchange capacity and specific surface area of the activated bentonites.

Sample No	Mineralogical composition	Cation exchange capacity meq/100gr	Specific surface area m^2/gr
SM 16	Smectite	104.4	61.76
SM236	Smectite (M), opal-CT (M), calcite (Min), Pyrite and/or marcasite (T)	52.8	24.11
SM324	Smectite (M), opal-CT (M), dolomite (M), quartz (Min), Plagioclase (Min).	60.25	53.47

M = major mineral phase, Min = minor mineral phase, T = trace mineral phase.

Na_2CO_3 of analytical grade (FISONS) using methyl red indicator (FISONS), according to the method described by Vogel (1961).

The time of activation varied between 30 minutes and 6h. For the bentonite from the Rema deposit additional 8h treatments were applied because it was found that the surface area began to increase significantly only after prolonged treatments. For each acid strength each sample was treated for 7 (the Rema bentonite for 8) different time intervals (30 minutes, 1h, 1h30 minutes, 2h, 3h, 4h30 minutes and 6h). Therefore, for the bentonites from Ankeria and Chios 49 and for the Rema bentonite 56 different combinations between acid strength and time of treatment were applied. This was decided for three reasons:

a) To monitor the evolution of the surface area with detail during the different combinations between acid strength and time and to construct three dimensional diagrams (acid strength-time of treatment-surface area diagrams) depicting this evolution. These were named STS diagrams (S stands for acid strength, T for time and S for surface area).

b) It is known that different combinations of acid strength and time of treatment produce bleaching clays having different decolourizing properties (Grim, 1962, Morgan, 1990c, see also the experimental results of Novak & Gregor, 1969, Kolta *et al.*, 1976, Zaki *et al.*, 1986 and Srasra *et al.*, 1990). Therefore it was decided necessary to describe the evolution of the bleaching capacity with detail.

c) To evaluate the relationship between surface area and bleaching capacity with detail. Moreover, to establish the most efficient combination between acid strength and time from both the quality and economic point of view. Apparently, the least time consuming optimum combination will be preferred by the industry.

d) It is believed that in the cases of the Greek bentonites in which the bleaching efficiency has not been evaluated so far a detailed survey is needed.

The clay-acid ratio used was 10gr clay/per 150ml acid. Activation took place at the temperature of $70^{o} \pm 2^{o}C$ in 250ml glass beakers covered with watch-glasses to avoid extensive evaporation which could alter both the acid strength and the clay:acid ratio, especially in the prolonged experiments. After the end of each run the acid was discarded and the clay was washed until the pH of the supernatant liquid was 6. The clay slurry was filtered and the collected material was dried at $100^{o}C$ for 3 hours and subsequently ground gently with pestle and mortar so as to pass through a 125μm sieve (BS410).

9.4.2.2. Surface area measurements.

Single point surface area measurements of the activated materials were obtained with a Strohlein Area Meter II using nitrogen gas. The samples were first degassed overnight at $75^{o}C$, in suitable vessels, at very low pressure, to remove any adsorbed gas. The vessels were immersed in liquid nitrogen and nitrogen gas was allowed in the system. This gas was

adsorbed on the surface of the activated clay. It is assumed that a monolayer of nitrogen was adsorbed.

Since the adsorbed nitrogen does not behave as an ideal gas its pressure is lower than predicted by the gas laws. Therefore a pressure difference between the vessel containing the sample and a blank vessel in which nitrogen gas was also allowed is created; the larger the surface area the greater the amount of the sorbed nitrogen and therefore the greater the pressure difference. The surface area was determined from the following formula:

$$sg=(A * H) / m \qquad 9.1$$

where sg=surface area

A=constant affected by the barometric pressure

H=indication read on the manometer of the instrument and

m=the weight of the sample.

The values of A can be obtained by means of a nomogram (Appendix 9.1). The results obtained are given in Table 9.2, while the three-dimensions STS diagrams are given in Figure 9.6.

9.4.2.3. Investigation of the structural changes of the smectites during acid activation.

The structural changes caused on smectites during acid activation were monitored by means of X-ray Diffraction, Thermal Analysis (DTA and TG) and Infra Red spectrospopy. CEC measurements were also performed in the acid treated samples. Finally SEM was used for observation of the textural changes of the smectite flakes. Both the effect of time of treatment under constant acid strength and that of acid strength over the same time were examined. The CEC measurements were performed on selected experimental runs in all three bentonites, while X-ray Diffraction Thermal Analysis and IR Spectroscopy only on runs of the bentonite from the Ankeria deposit. This was decided since this bentonite consists essentially of Cheto (Tatatilla and Chambers) montmorillonites; therefore the changes observed reflect the structural changes of smectite. In the runs from the Ankeria bentonite the loss of Ignition at 1000^{o}C was also determined.

IR spectroscopy was regarded as a reasonably sensitive and fast technique for the investigation of the removal of the octahedral cations (area between 950 and 820cm^{-1}), and the deposition of the dissolved amorphous Si (800cm^{-1}). The presence of abundant opal-CT in both the Rema and the Chios bentonites would make the observation of the evolution this band, due to deposition of amorphous SiO_2, very difficult in these materials. Other structural changes might also be traced in the area between 1000 and 1200cm^{-1} and between 500 and 600cm^{-1} (Si-O in and out of plane and Si-O-Al vibrations). Also the Thermal Techniques might provide valuable information about the structural changes

Table 9.2 .

Surface area of the acid activated bentonites treated with various combinations of treating time and acid strength (m^2/gr).

Ankeria deposit (SM16)

Acid strength	0.5N	1N	1.5N	2N	3N	5N	8N
Time							
30'	66.7	72.7	77.1	111.3	131.3	156.8	149.8
1h	71.7	78.9	86.7	125.7	145.7	164.0	160.0
1h30'	79.2	88.7	96.7	- -	- -	- -	- -
2h	89.8	102.8	117.0	159.2	168.7	188.3	185.5
3h	98.2	112.1	150.1	186.5	198.4	222.4	186.0
4h30'	114.8	158.4	207.0	214.0	242.3	225.0	196.0
6h	130.1	185.0	227.6	263.4	211.9	201.7	182.0

Chios bentonite (SM324)

Acid strength	0.5N	1N	1.5N	2N	3N	5N	8N
Time							
30'	70.7	78.0	83.0	90.0	92.0	121.0	128.0
1h	86.6	101.0	115.0	129.0	134.0	147.0	137.3
1h30'	- -	106.0	120.0	139.0	145.0	171.0	166.0
2h	- -	115.0	134.0	148.0	164.0	184.0	161.0
3h	- -	126.0	146.0	165.0	178.0	196.0	154.0
4h30'	- -	137.0	161.0	197.0	186.0	180.0	136.0
6h	- -	157.0	194.0	197.0	183.0	145.0	125.0

Table 9.2 (continued)

Rema deposit (SM236)

Acid strength	0.5N	1N	1.5N	2N	3N	5N	8N
Time							
30'	30.4	- -	33.8	37.4	40.5	47.6	53.2
1h	33.1	34.4	39.5	42.3	46.4	55.5	54.2
1h30'	34.1	36.0	41.0	46.0	52.8	59.0	58.0
2h	36.2	39.0	45.0	49.0	56.1	66.0	61.0
3h	37.9	46.3	53.1	57.6	63.5	72.1	67.0
4h30'	40.4	51.9	62.1	69.3	77.0	79.0	74.7
6h	54.2	68.2	89.0	104.0	100.1	100.3	90.0
8h	62.9	84.2	102.4	90.5	88.4	88.8	86.7

during activation through i) the size and shape of the dehydroxylation peak and ii) the rate of the weight loss of the sample, especially close to the dehydroxylation temperature (TG-technique).

The instruments and experimental conditions used for X-ray Diffraction, Thermal Analysis Scanning Electron Microscopy and IR Spectroscopy have been described in Chapter 4 while the method used for determination of the CEC in Chapter 7. The X-ray diagrams are depicted in Figure 9.3. The IR diagrams obtained are given in Figure 9.4 while the thermograms in Figure 9.5. The characteristics of the Thermogiagrams obtained from the treated samples are summarized in Table 9.3, while the results from the CEC measurements are given in Table 9.4. Finally, the results from the loss of ignition are given in Table 9.5.

9.4.2.4. Bleaching experiments.

The crude oil used for determination of the bleaching capacity of the acid activated bentonites was low erucic acid rapeseed oil provided by SEATONS (Hull). 1gr of acid activated clay was added to 20ml of crude oil. The experiments were performed at atmospheric conditions at the constant temperature of $90^{o} \pm 2^{o}C$ under stirring and the time at the top temperature was 20 minutes. These conditions represent atmospheric-type bleaching (Richardson, 1978).

The treated oils were filtered under vacuum and stored in polyethylene bottles. The bleaching capacity of the activated clays was evaluated by means of removal of ß-carotene from the crude oil. For this purpose ß-carotene standards were prepared by dissolving ß-carotene (ALDRICH) in acetone and measuring the absorbance at 450nm using a CECIL CE303 series 2 absorption spectrophotometer, at the Department of Chemistry, University of Leicester. The calibration curve obtained is given in Appendix 9.2.

The colour changes in the treated oils were determined spectrophotometrically at 450nm and 430nm (CECIL CE303 series 2 absorption spectrophotometer) by diluting 5ml of oil in 15ml acetone. For selected runs the full absorption spectrum between 400 and 500nm was obtained. By converting the absorbance units to ß-carotene concentration, the adsorbed amount of the colouring agent was calculated. The bleaching capacity of the activated clays was determined from the following equation:

$$\text{Bleaching capacity} = (C_0 - C / C_0) * 100 \qquad 9.2$$

where C_0=concentration (µg/ml) of ß-carotene in the crude oil and

C=concentration of ß-carotene in the bleached oil.

The concentration of the absorbed ß-carotene was converted to moles per 100gr of clay. For terms of comparison the same bleaching experiment was performed using an industrial

Table 9.3.

Results from the Differential Themal Analysis from some of the runs of the acid activated bentonite from the Ankeria deposit.

Experimental Run	1st endothermic peak (°C)		2nd endothermic peak (°C)	3rd endothermic peak (°C)	exothermic peak (°C)
	1st step	2nd step			
Untreated	120	210	720	910	- -
1N/1h	105	155	680	920	945
2N/1h	105	150	675	930	950
3N/1h	105	150	680	925	940
5N/1h	105	150	675	930	955
2N/3h	105	150	680	930	955
2N/4h30'	105	155	680	930	955
2N/6h	105	155	675	930	- -

Table 9.4.

Cation exchange capacity results from some experimental runs of the acid activated bentonites.

Sample SM16	Cation exchange capacity meq/100gr	Sample SM 236	Cation exchange capacity meq/100gr	Sample SM 324	Cation exchange capacity meq/100gr
Untreated	104.4	Untreated	52.8	Untreated	60.25
1N/1h	88.0	1N/1h	47.0	1N/1h	69.0
2N/1h	87.1	2N/1h	49.0	2N/1h	63.8
3N/1h	79.2	3N/1h	48.0	3N/1h	64.9
5N/1h	73.4	5N/1h	48.0	5N/1h	57.1
2N/3h	79.2	2N/3h	48.2	2N/3h	64.0
2N/4h30'	80.1	2N/4h30'	46.0	2N/4h30'	45.0
2N/6h	72.9	2N/6h	48.0	2N/6h	45.1

Table 9.5

Loss of ignition of the acid activated bentonite (Ankeria deposit)

Experimental run	Loss of ignition %	Midpoint plateau (°C)
Untreated	7.04	360
1N/1h	7.28	390
2N/1h	6.77	370
3N/1h	7.36	360
5N/1h	6.98	370
2N/3h	6.93	370
2N/4h30'	7.31	370
2N/6h	7.16	360

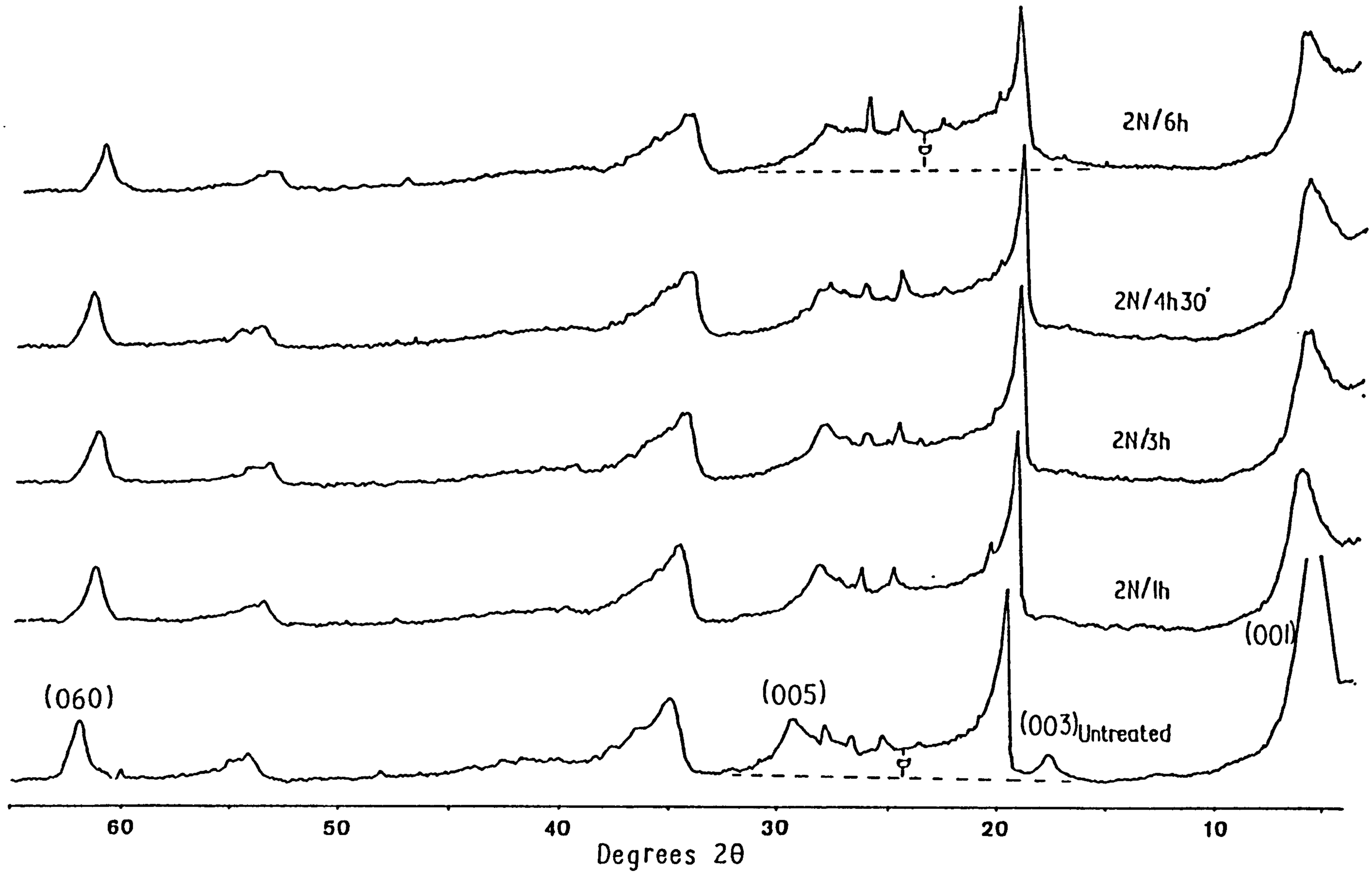

FIGURE 9.3. X-ray traces of the acid activated bentonite from the Ankeria deposit (a) influence of time.

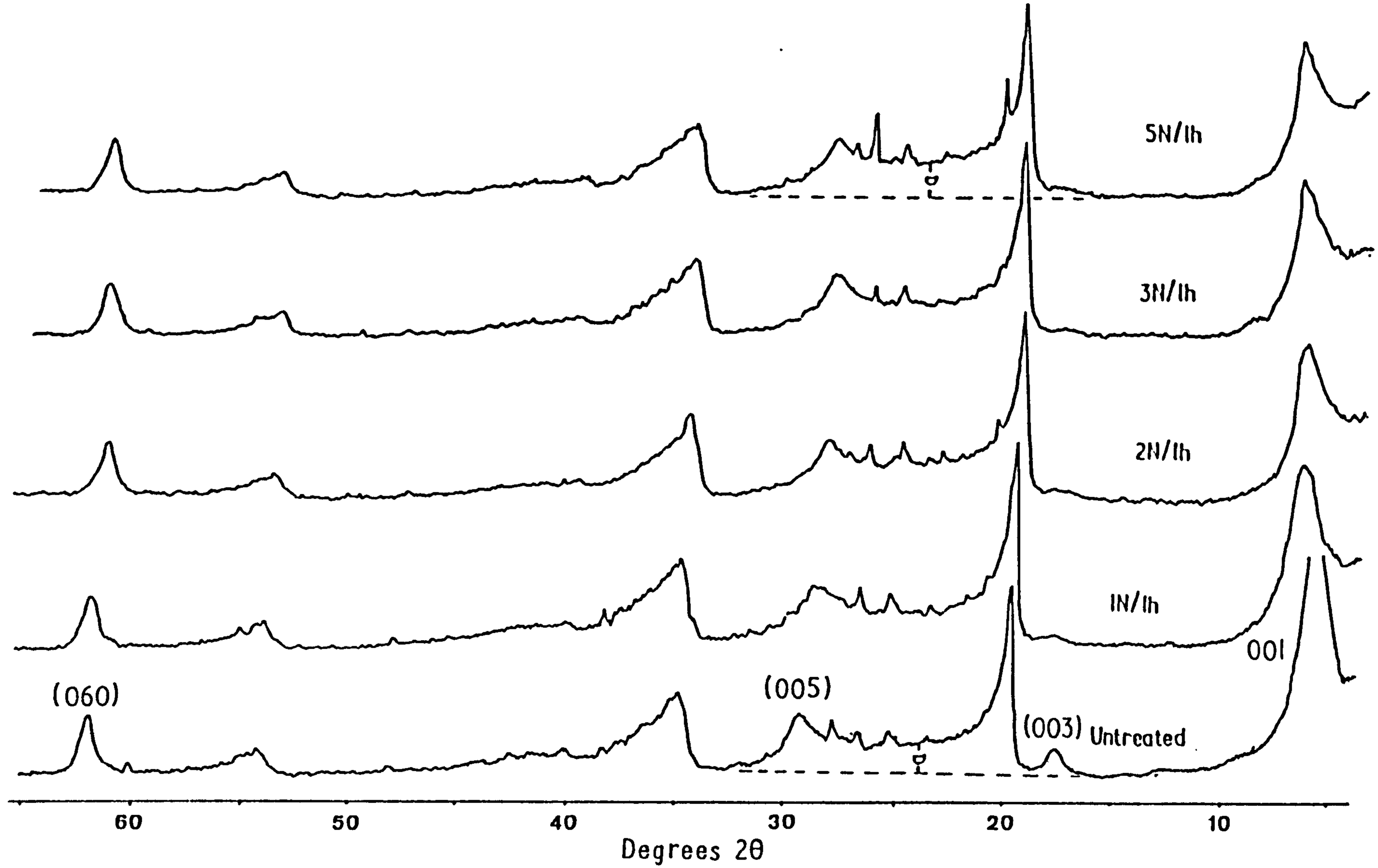

FIGURE 9.3 (continued). X-ray traces of the acid activated bentonite from the Ankeria deposit (b) influence of acid strength.

product available in the market (FULLMONT AA), provided by Laporte Absorbents. The results obtained are given in Table 9.6.

9.5. Results.

9.5.1 Evolution of the surface area during acid treatment.

In all three samples surface area increased with both the time of treatment and acid strength (Fig. 9.6). In the Ankeria and Chios bentonites a four fold increase has been observed, while the surface area of the Rema bentonite increased more than five times. However, in the latter case the maximum value recorded was less than $105m^2/gr$. Also, the maximum surface area of the Chios bentonite is slightly lower than $200m^2/gr$ (see Table 9.2).

The evolution of the surface area follows similar paths in the different bentonites. At first it increases continuously up to a maximum value and then it decreases. This has been observed by several workers (Novak & Gregor, 1969, Kolta *et al.*, 1976, Kheok & Lim, 1982, Zaki *et al.*, 1986), although others have reported either a constant increase with lower increasing rate at more severe treatments (Yates, 1986) or the existence of a plateau after an initial rapid increase (Srasra *et al.*, 1990). In all three cases the surface area evolution paths depend on both the acid strength and time but the dependance is different in the different bentonites. It is obvious (Fig. 9.6) that the maximum surface area values are obtained in more severe treatments in terms of both acid strength and time, in the different materials. The bentonite from Chios develops its maximum surface area faster while the Rema bentonite much latter, at more severe treatments. The Ankeria bentonite behaves in a intermediate way.

The dependance of the surface area on each of the two factors mentioned before is illustrated in Figure 9.7. In the case of the Chios bentonite the surface area increases fast, with the rate of increase decreasing continuously, with both acid strength and time. This has been observed also in the sample SM16 (Ankeria deposit) but is not clear in SM236 (Rema deposit) at least in the case of the acid strength influence. In this sample, the rate of increase up to the maximum surface area value is constant. The observed increase is followed by a decrease at prolonged treatments or treatments with strong acids. In some cases the subsequent decrease is not observed; instead a plateau is present.

Two are the most important features observed in Figure 9.7: a) with increasing acid strength, the time at which the maximum surface area is attained decreases and b) with increasing the time of treatment, the acid strength at which surface area maximum is obtained also decreases. Therefore the maximum values of surface area are attained with treatments characterized by many combinations between acid strength and time, as this is illustrated in the STS diagrams (Fig. 9.6). Also, in all three samples the surface area

TABLE 9.6

Absorption of ß-carotene from the acid activated bentonites during the bleaching process of the crude rape-seed oil.

Sample SM16	Bleaching capacity %	Absorption of ß-carotene at 450nm (Absorbance units)	Absorption of ß-carotene at 430nm (Absorbance units)	Concentration of the absorbed ß-carotene (µg/ml)	Concentration of the absorbed ß-carotene (10^{-4} moles/ 100gr clay)
30'/1N	65.9	1.280	1.160	77.19	7.2
30'/2N	69.1	1.160	1.060	80.95	7.5
30'/3N	89.3	0.400	0.430	104.67	9.7
30'/5N	94.3	0.215	0.270	110.47	10.3
30'/8N	95.3	0.175	0.220	111.71	10.4
1h/1N	86.9	0.490	0.495	101.87	9.5
1h/2N	95.1	0.185	0.230	111.39	10.4
1h/3N	95.6	0.165	0.210	112.03	10.4
1h/5N	96.8	0.120	0.160	113.43	10.6
1h/8N	94.1	0.220	0.270	110.31	10.3
2h/1N	93.9	0.230	0.284	109.99	10.2
2h/2N	90.4	0.360	0.220	105.95	9.9
2h/3N	96.0	0.150	0.200	112.51	10.5
2h/5N	98.4	0.060	0.085	115.31	10.7
2h/8N	98.1	0.070	0.100	114.99	10.7
3h/1N	95.2	0.180	0.220	111.55	10.4
3h/2N	96.3	0.140	0.175	112.83	10.5
3h/3N	96.1	0.145	0.180	112.67	10.5
3h/5N	97.5	0.095	0.125	114.23	10.6
3h/8N	97.1	0.110	0.190	113.75	10.6
4h30'/1N	96.3	0.140	0.175	112.83	10.5
4h30'/2N	98.2	0.067	0.095	115.11	10.7
4h30'/3N	97.3	0.100	0.135	114.07	10.6
4h30'/5N	98.4	0.060	0.087	115.31	10.7
4h30'/8N	98.1	0.070	0.100	114.99	10.7
6h/1N	96.0	0.150	0.195	112.51	10.5
6h/2N	97.6	0.090	0.120	114.39	10.7
6h/3N	96.0	0.150	0.190	112.51	10.5
6h/5N	96.3	0.140	0.175	112.83	10.5
6h/8N	95.9	0.155	0.200	112.35	10.5

TABLE 9.6 (continued)

Sample SM324	Bleaching capacity %	Absorption at 450nm (Absorbance units)	Absorption at 430nm (Absorbance units)	Concentration of ß-carotene (µg/ml)	Concentration of ß-carotene (10^{-4} moles/ 100gr clay)
30'/1N	- -	0.115	0.140	113.59	10.6
30'/2N	- -	0.115	0.105	113.59	10.6
30'/3N	- -	0.135	0.120	112.99	10.5
30'/5N	- -	0.120	0.085	113.43	10.6
30'8N	- -	0.070	0.105	114.99	10.7
1h/1N	94.8	0.195	0.240	111.11	10.3
1h/2N	95.7	0.160	0.230	112.19	10.4
1h/3N	96.5	0.130	0.160	113.11	10.5
1h/5N	97.1	0.110	0.165	113.75	10.6
1h/8N	96.1	0.145	0.180	112.67	10.5
2h/1N	97.2	0.105	0.115	113.91	10.6
2h/2N	98.1	0.070	0.110	114.99	10.7
2h/3N	98.6	0.052	0.085	115.55	10.8
2h/5N	98.7	0.050	0.085	115.63	10.8
2h/8N	97.6	0.090	0.125	114.39	10.7
3h/1N	96.8	0.120	0.185	113.43	10.6
2h/2N	96.9	0.115	0.125	113.59	10.6
3h/3N	98.3	0.065	0.105	115.15	10.7
3h/5N	98.3	0.065	0.095	115.15	10.7
3h/8N	97.2	0.105	0.155	113.91	10.6
4h30'/1N	96.8	0.120	0.290	113.43	10.6
4h30'/2N	96.1	0.145	0.145	112.67	10.5
4h30'/3N	96.1	0.145	0.195	112.67	10.5
4h30'/5N	96.1	0.145	0.195	112.67	10.5
4h30'/8N	95.5	0.170	0.225	111.87	10.4
6h/1N	96.9	0.115	0.155	113.59	10.6
6h/2N	96.4	0.135	0.180	112.99	10.5
6h/3N	96.0	0.150	0.180	112.51	10.5
6h/5N	80.8	0.720	0.685	94.67	8.8
6h/8N	76.0	0.900	0.850	89.07	8.3

TABLE 9.6 (continued)

Sample SM236	Bleaching capacity %	Absorption of ß-carotene at 450nm (Absorbance units)	Absorption of ß-carotene at 430nm (Absorbance units)	Concentration of the absorbed ß-carotene (µg.ml)	Concentration of the absorbed ß-carotene (10^{-4} moles/ 100gr clay)
1h/1N	73.3	1.000	0.900	85.95	8.0
1h/2N	84.9	0.565	0.570	99.55	9.3
1h/3N	85.3	0.550	0.565	99.99	9.3
1h/5N	92.8	0.270	0.310	108.75	10.1
1h/8N	91.5	0.320	0.350	107.19	10.0
2h/1N	72.0	1.050	0.950	84.39	7.9
2h/2N	84.9	0.565	0.570	99.55	9.3
2h/3N	87.5	0.470	0.475	102.51	9.5
2h/5N	93.1	0.260	0.295	109.07	10.2
2h/8N	89.7	0.385	0.345	105.15	9.8
3h/1N	77.3	0.850	0.750	90.63	8.4
3h/2N	87.0	0.490	0.495	101.91	9.5
3h/3N	91.1	0.335	0.380	106.71	9.9
3h/5N	92.7	0.275	0.325	108.59	10.1
3h/8N	92.3	0.290	0.345	108.15	10.1
4h30'/1N	81.9	0.680	0.660	95.95	8.9
4h30'/2N	92.7	0.275	0.310	108.59	10.1
4h30'/3N	93.2	0.255	0.305	109.23	10.2
4h30'/5N	92.3	0.290	0.345	108.11	10.1
4h30'/8N	92.7	0.275	0.325	108.59	10.1
6h/1N	92.8	0.270	0.310	108.75	10.1
6h/2N	95.1	0.185	0.225	111.39	10.4
6h/3N	94.7	0.200	0.245	110.95	10.3
6h/5N	92.3	0.190	0.240	111.27	10.4
6h/8N	96.1	0.145	0.185	112.67	10.5
8h/1N	98.2	- -	- -	- -	- -
8h/2N	97.7	- -	- -	- -	- -
8h/3N	98.0	- -	- -	- -	- -
8h/5N	97.6	- -	- -	- -	- -
8h/8N	95.2	- -	- -	- -	- -
FULLMONT AA	96.8	0.120	0.290	113.43	10.6

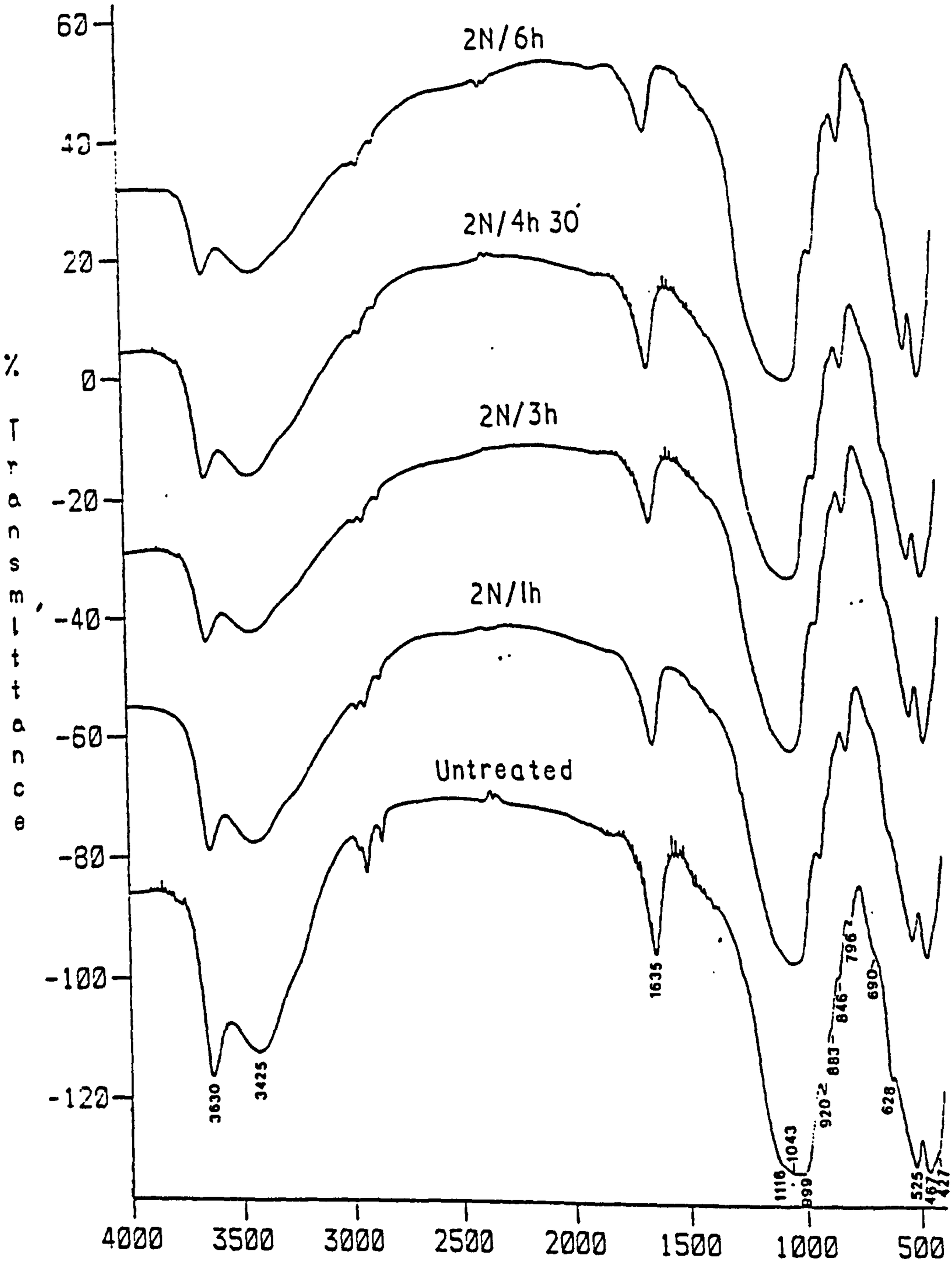

FIGURE 9.4. Infra Red Spectra of the acid activated bentonite from the Ankeria deposit (a) influence of time.

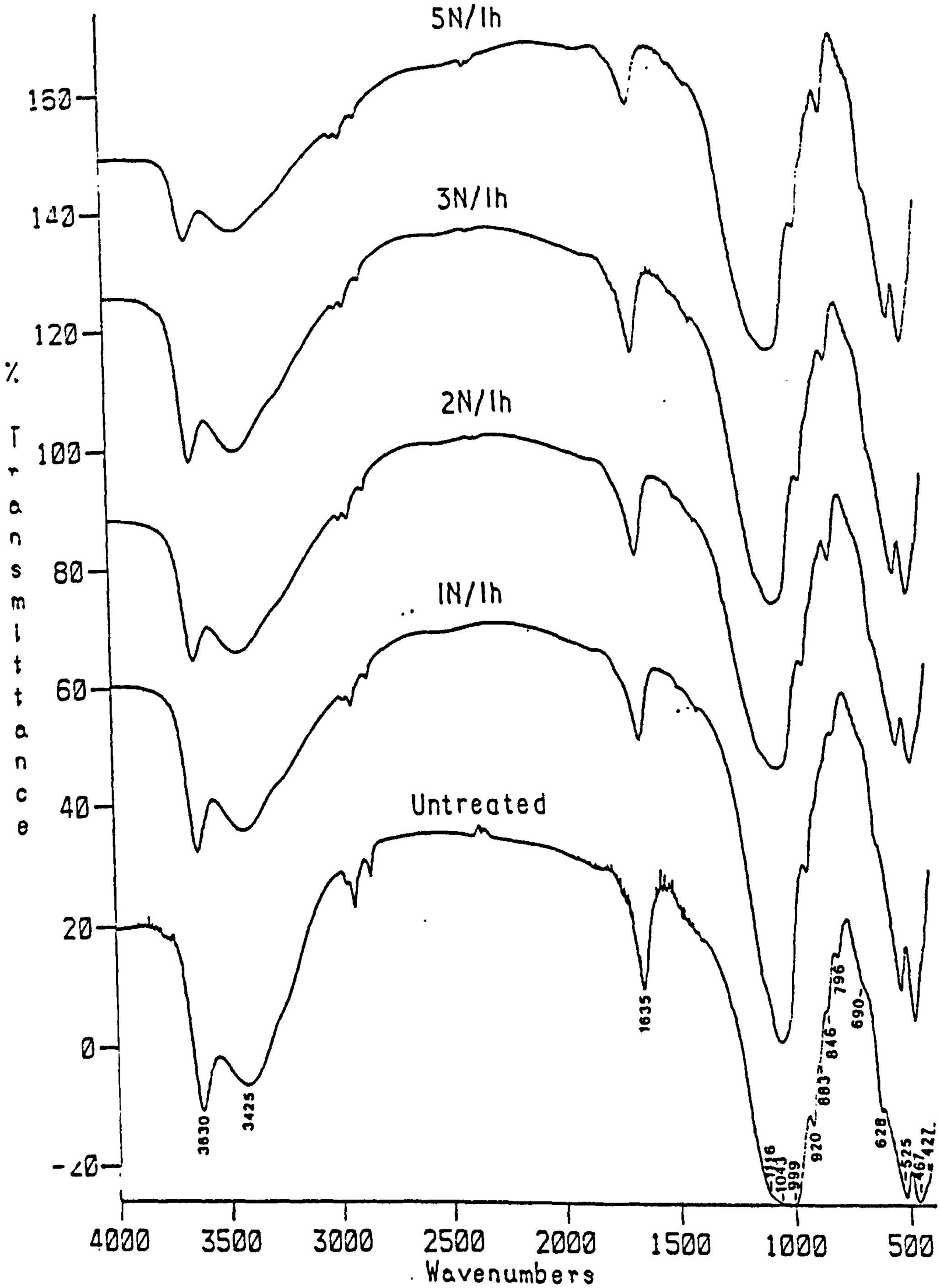

FIGURE 9.4 (continued). Infra Red Spectra of the acid activated bentonite from the Ankeria deposit (b) influence of acid strength.

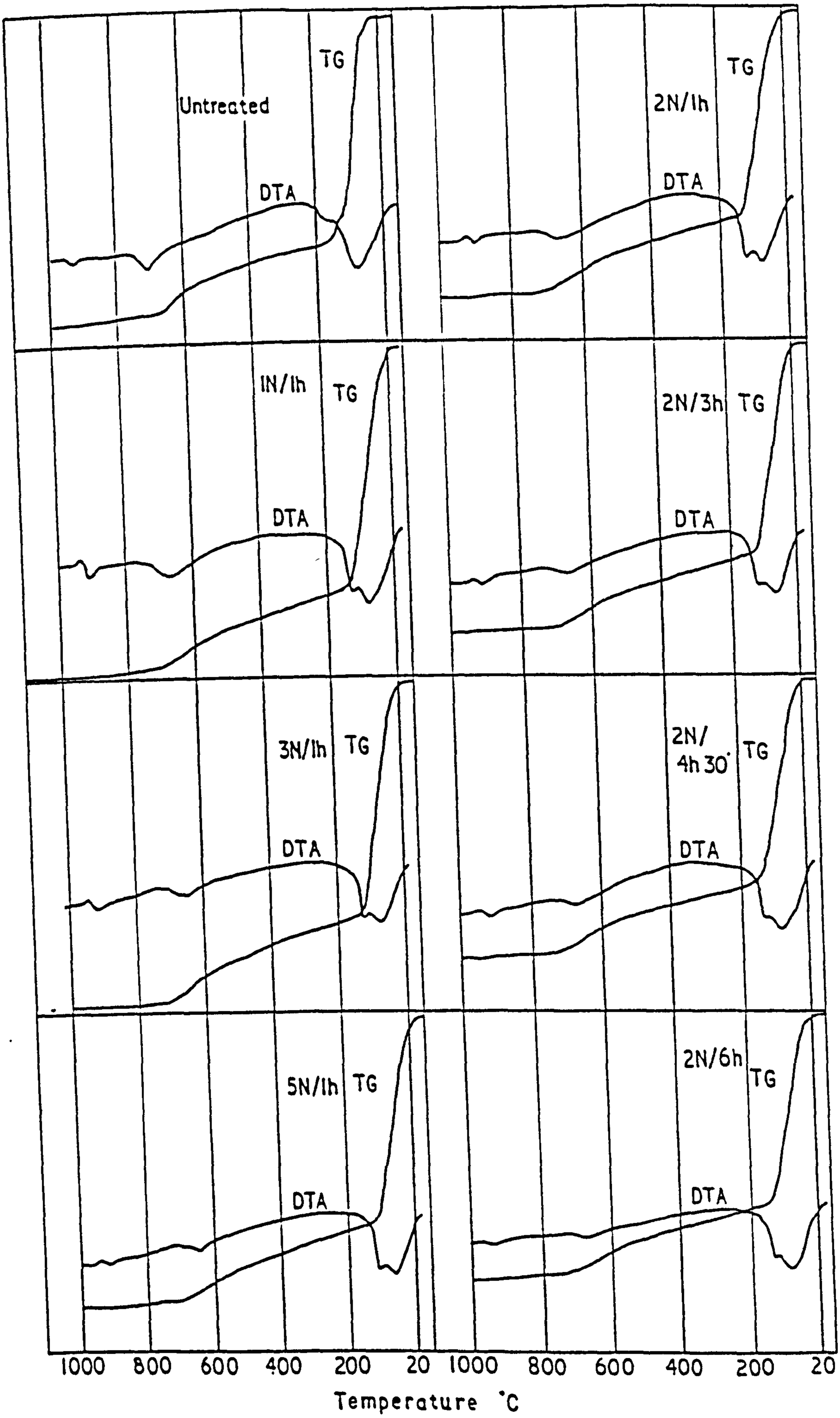

FIGURE 9.5. DTA-TGA thermodiagrams of the acid activated bentonite from the Ankeria deposit. .

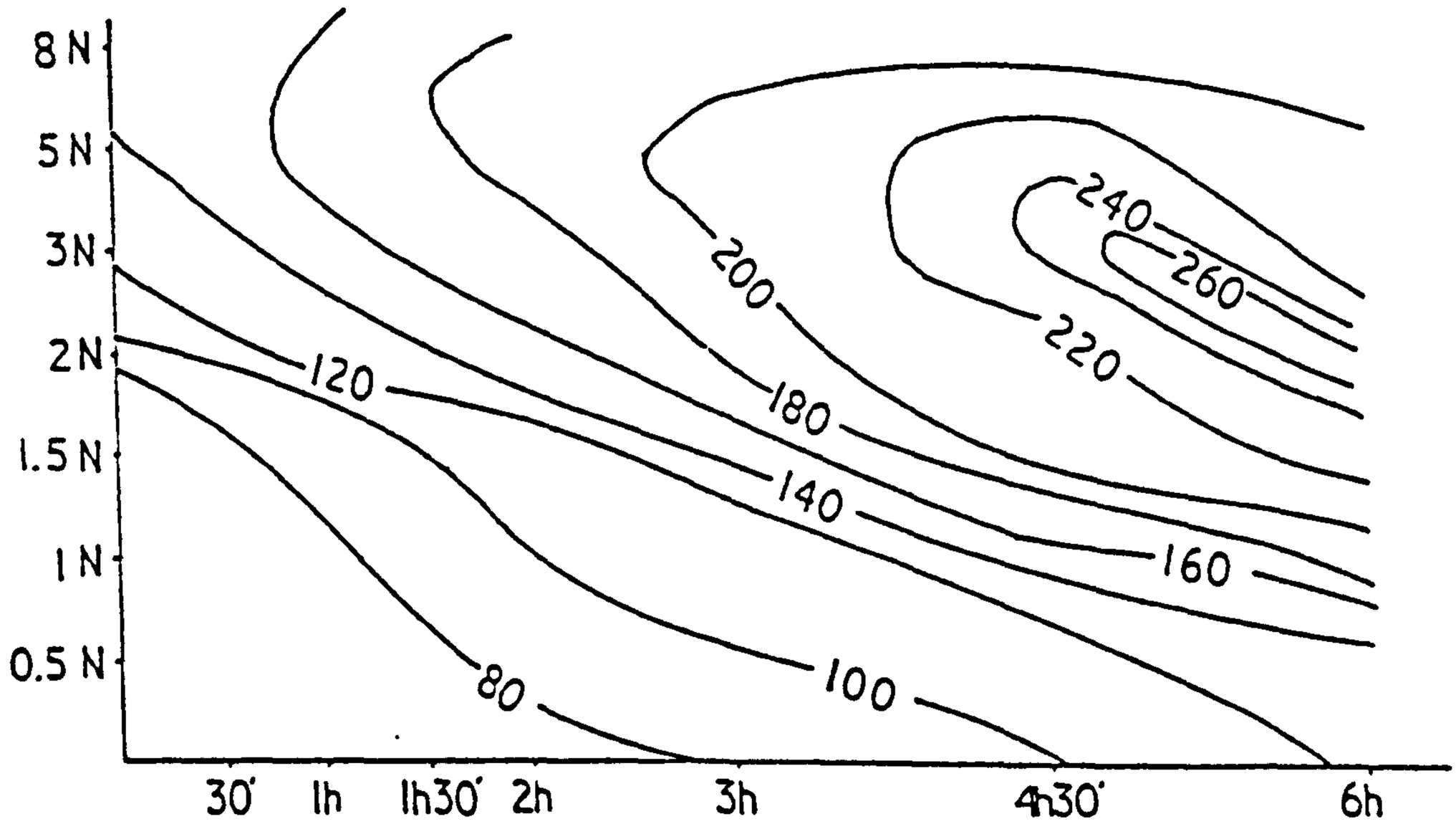

a) SM16

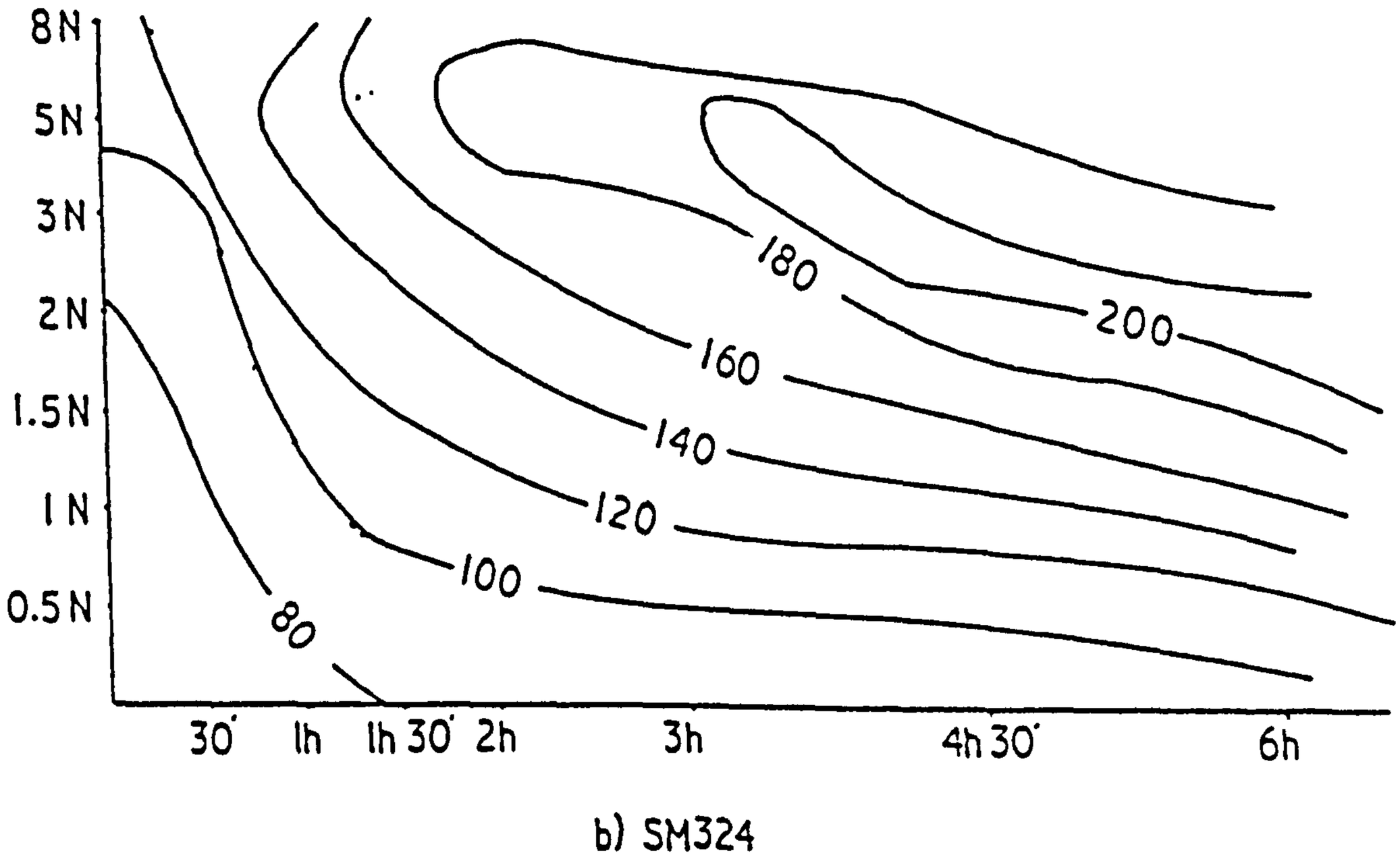

b) SM324

FIGURE 9.6. **STS** (Surface area-Time-Acid Strength) diagrams for the bentonites from (a) Ankeria deposit (Milos), and (b) Chios

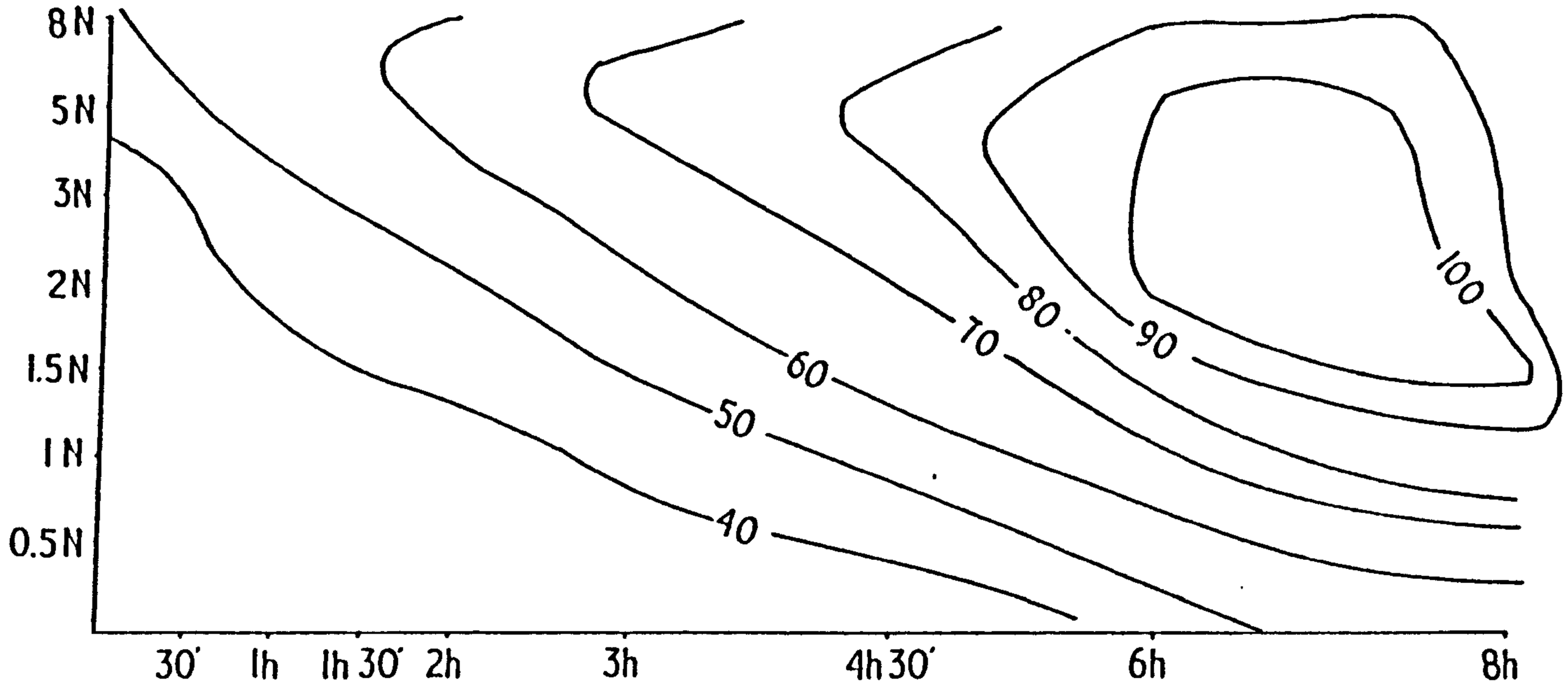

c) SM236

FIGURE 9.6 (continued). **STS** (Surface area-Time-Acid Strength) diagram for the bentonite from the Rema deposit (Milos) (c).

declines if activation has been performed with acid stronger than 5N, unless the treatment is short. For the sample SM324 this is true for even weaker acid. On the other hand, in treatments with dilute (1N) acid the materials do not seem to have developed their maximum surface area, since even after 8h of treatment (SM236) no sign of surface area decrease has been observed.

9.5.2. Bleaching capacity of the activated bentonites.

The evolution of the bleaching capacity of the three bentonites is illustrated in Figure 9.8. Notwithstanding the different smectite content and smectite crystal chemistry as well as the different mineral assemblages present, all three materials display high bleaching capacities (> 95%). Thus, the maximum bleaching capacity of the Ankeria bentonite is very similar to that of the the Rema bentonite, although the grade of the latter is much lower, almost half. However, the maximum bleaching capacities are displayed at different combinations between acid strength and time of treatment for the three materials.

Acid activation seems to have taken place very fast in the bentonite from Chios. For this bentonite the use of a weak acid (1N) for only 1 hour imparts more than 95% of the final bleaching capacity. This is not the case for the other two materials, especially for the Rema bentonite which develops its maximum bleaching properties only at very intense treatment. Acid strengths up to 3N do not seem to develop the adsoptive properties of this material for treating time up to three hours. The bentonite from the Ankeria deposit follows an intermediate path; it is activated faster than the Rema bentonite, but slower than the Chios bentonite after treatment with weaker acid for short times.

The Chios bentonite seems to lose its decolourizing properties after prolonged activation, when treated with acids stronger than 5N. A decrease of a much smaller scale has also been observed in the other two materials. Therefore, two are the most important differences between the three bentonites examined as far as their bleaching capacity is concerned: a) the rate at which they aquire their maximum bleaching capacity b) the ease with which their decolourizing properties deteriorate after prolonged treatment with strong HCl acid.

The bleaching capacity does not follow the variations of the surface area with acid treatment (compare Fig. 9.7 with Fig 9.8). Only in the sample SM324 for prolonged treatments with strong acid (6h/8N) the bleaching properties deteriorate following the decrease of the surface area. Furthermore, in several occasions treatment with weak acid (for instance 1N/3h treatment for SM16 and 1N/1H treatment for SM324) is sufficient for development of most of the bleaching capacity of the clay, although its surface area is less than 50% of the maximum observed at more severe treatments. These results contradict

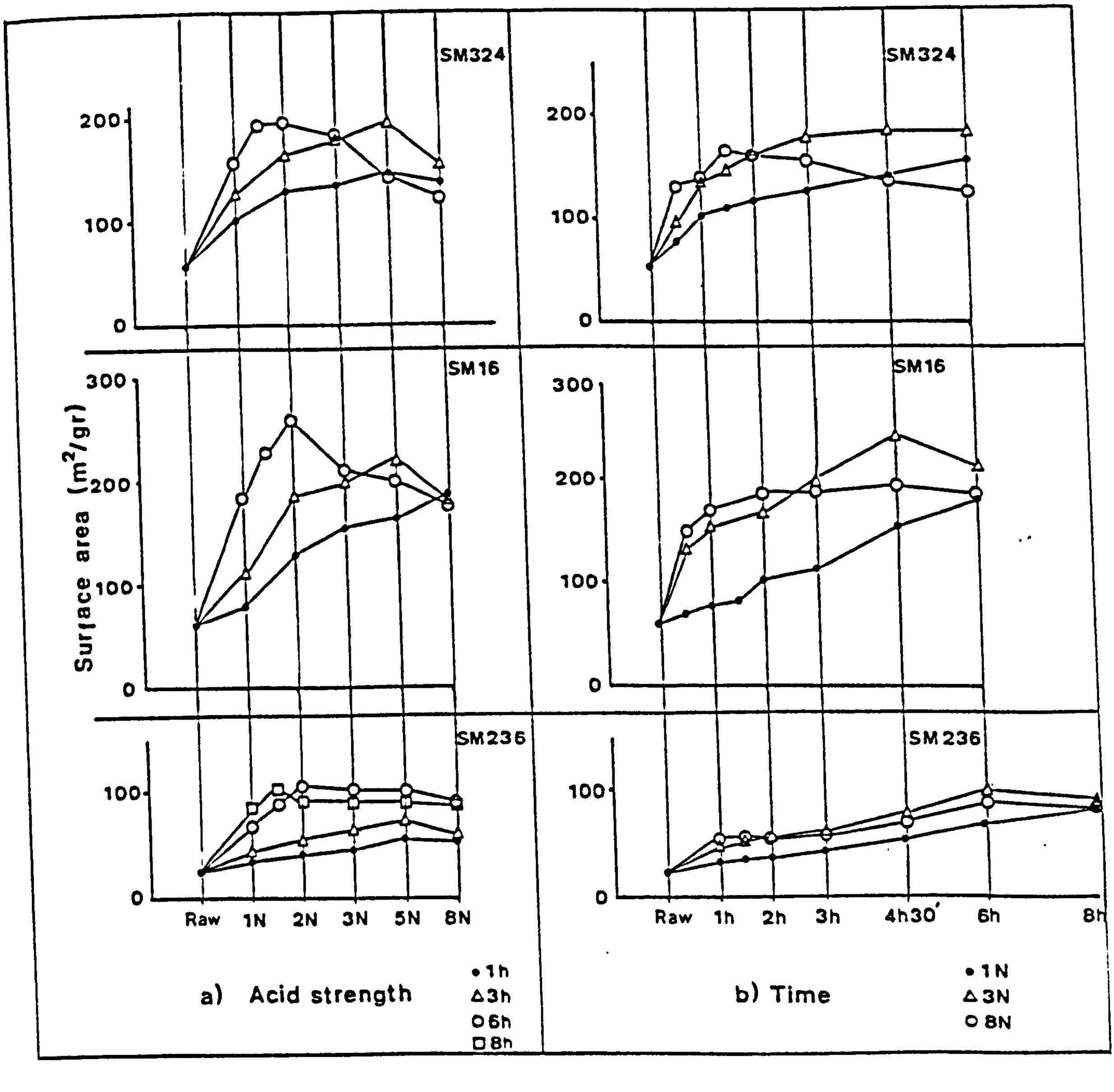

FIGURE 9.7. Influence of the acid strength and the treating time on the evolution of the surface area for the three activated bentonites.

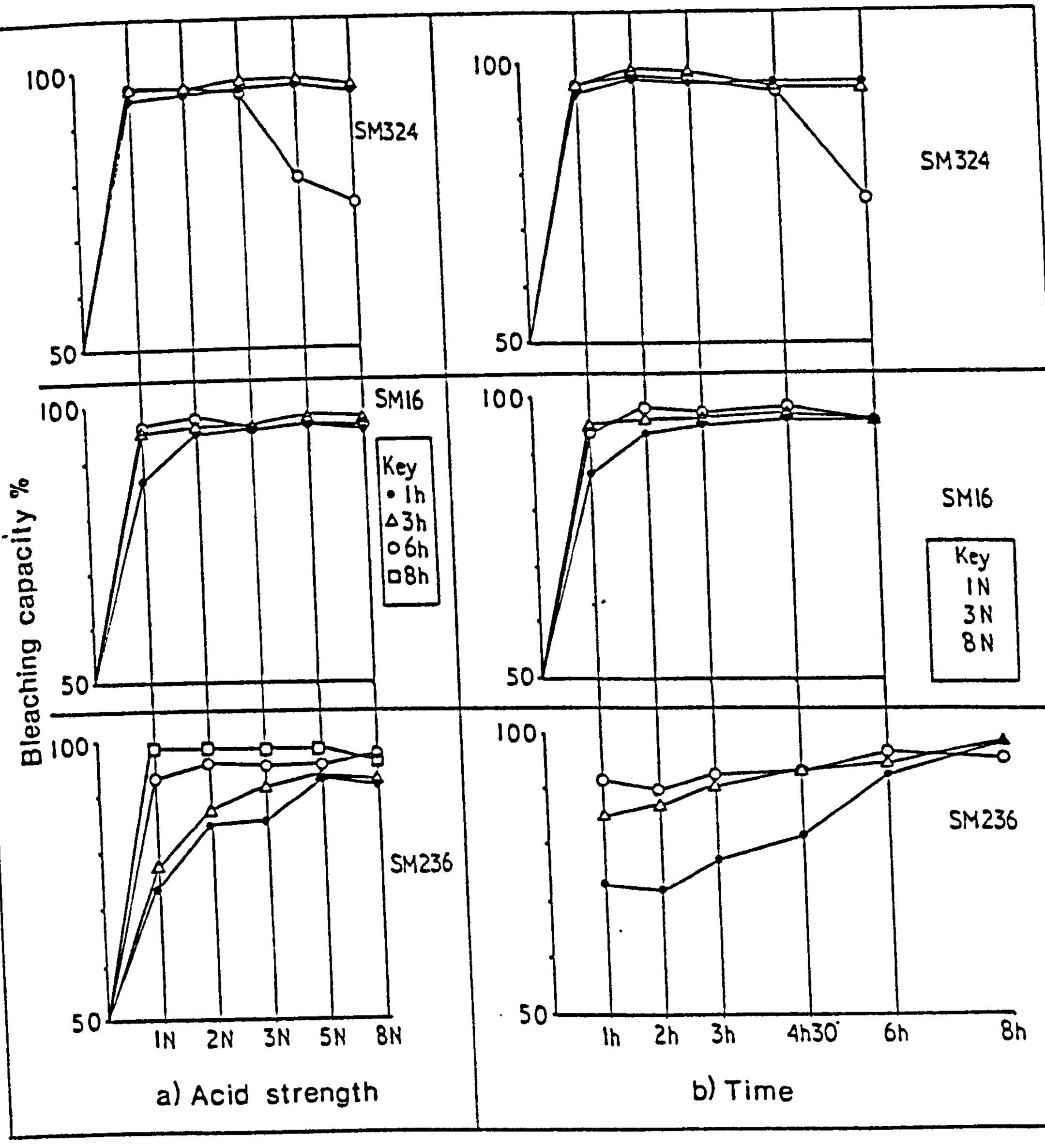

FIGURE 9.8. Evolution of the bleaching capacity of the acid activated bentonites as a function of acid strength and time. See text for definition of the term bleaching capacity.

the findings of Novak & Gregor, (1969) and Kolta *et al.*, (1976), but corroborate the results of Morgan *et al.*, 1985, Zaki *et al.*, (1986) and the report of Morgan (1990c).

The results for absorption of ß-carotene are illustrated in Figure 9.9. The pattern obtained follows that of the bleaching capacity, reflecting this property, as it is expected. It is obvious that the Chios bentonite is rendered suitable to absorb ß-carotene if treated with weak acids for short periods. On the other hand, the other bentonites display a character dominated by a more progressive increase in the absorption of ß-carotene with increasing both time and acid strength. This is more clearly demonstrated by the sample SM236. Also, the amount of ß-carotene adsorbed by Chios bentonite decreases significantly after prolonged treatments (6h) with acids stronger than 5N. The results obtained clearly demonstrate that the absorption of ß-carotene and hence the bleaching capacity as defined in this project, reaches a *plateau* and not a single maximum value. This plateau can be reached by using several combinations of acid strength and time during treatments. Although the same observations were made for the surface area, it has been clearly demonstrated that this property is not associated with the maximum adsorption of ß-carotene.

The degree of adsorption of ß-carotene can also be observed in Figure 9.10 in which the whole absorption spectrum between 400 and 500nm (characteristic for this compound) is illustrated. This spectrum is characterized by the existence of a deflection maximum at about 450nm "sandwiched" between two shoulders. The curve No 1 corresponds to the crude rapeseed oil, while the dashed line to the FULLMONT AA activated clay provided by Laporte Absorbents. The both results for both the Ankeria and the Chios bentonites are better than the commercial product. This is true for a number of products derived from different runs from all three samples as this can be observed in Table 9.2.

The most important characteristic observed in Figure 9.10, except for the decrease in the absorption due to the removal of the ß-carotene, is the elimination of the deflection at 450nm. This deflection appears only in the 4h30 minutes treatment of the sample SM236 (Rema deposit) and the 6h/5N treatment of the SM324 (Chios bentonite). In the former sample the bentonite is *under-activated*, while in the latter it is *over-activated*. This is because in the former more and in the latter less severe treatments cause a decrease in the absorption spectra of ß-carotene and thus produce better products. However, in both cases the spectra obtained from ß-carotene are almost identical.

When the bleaching capacities of the activated bentonites are plotted on the STS diagrams, composite diagrams are produced (Fig 9.11). These composite diagrams have been named STSD diagrams (D stands for decolourization, the other initials have been defined previously). In these diagrams the combination of acid strength and treating time which produce the surface areas necessary for maximum decolourizing properties is depicted. The cut-off limit selected for maximum bleaching capacity is 95% (95% of the ß-

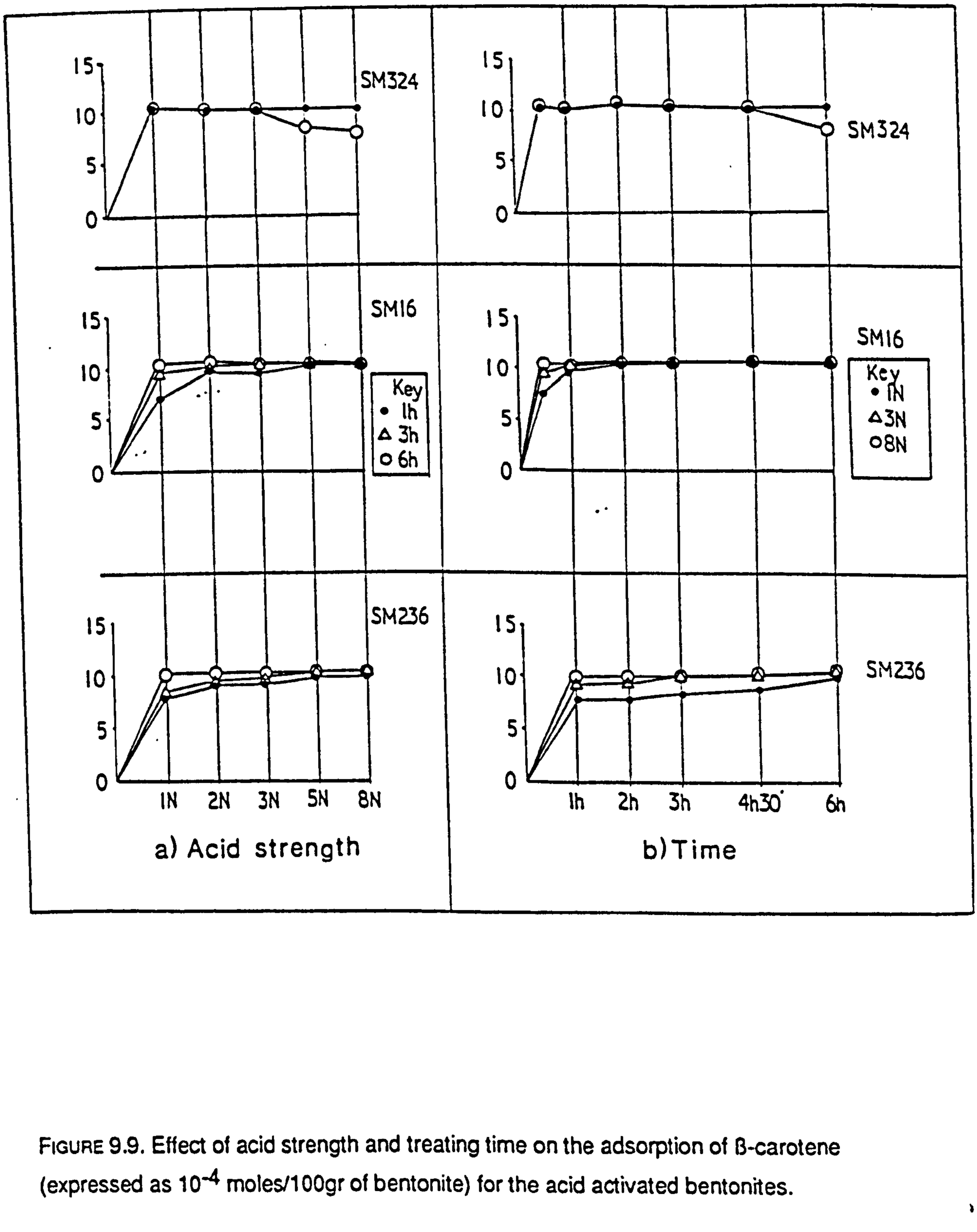

FIGURE 9.9. Effect of acid strength and treating time on the adsorption of ß-carotene (expressed as 10^{-4} moles/100gr of bentonite) for the acid activated bentonites.

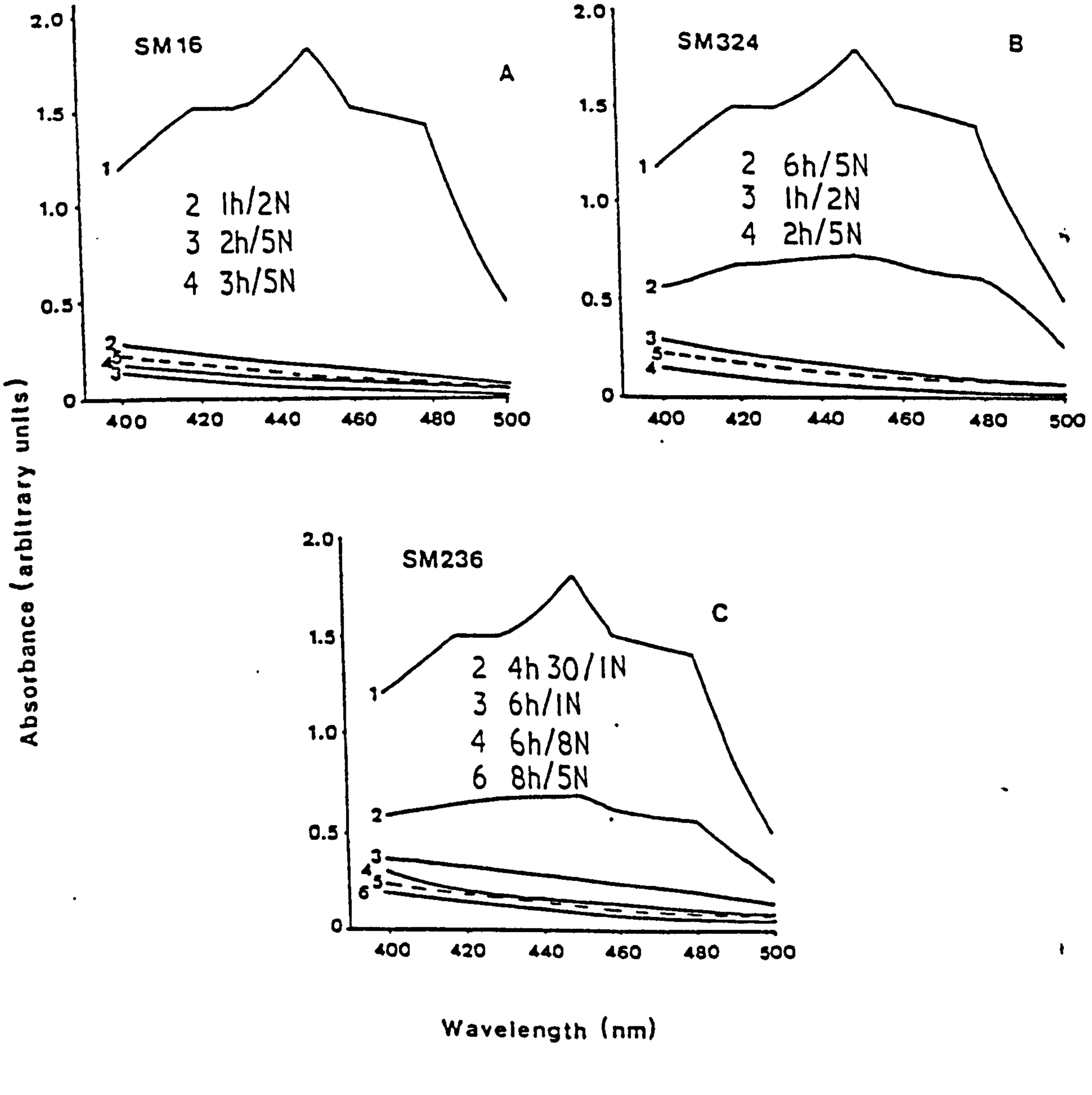

FIGURE 9.10. Absorption spectra obtained from the crude oil and oil treated with acid of different acid strength for variable time. (a) SM16, (b) SM324 (c) SM236. Curve 1 corresponds to the crude oil and curve 5 to the FULLMONT AA in all three diagrams.

carotene present in the crude oil be removed). Two curves have been drawn: one at the cut-off limit and one at the bleaching capacity of the FULLMONT AA (96.8%). Therefore the products encircled by the second curve have higher decolourizing properties than FULLMONT AA. The areas of maximum bleaching properties are shaded.

It is obvious that the same observations made previously can be visualized more completely in these diagrams. In all three samples the maximum decolourizing properties are not observed at maximum surface area. The lack of dependance of the bleaching efficiency on the surface area is obvious since the bleahing contours are not parallel to the surface area ones. However, the important outcome of this detailed diagram is that the combinations of acid strength and treating time which produce the best (in terms of bleaching capacity) products can be easily determined.

In the case of the Chios bentonite treatments longer than 1h with acid stronger than 1.5N produce clays which can remove more than 95% of the ß-carotene present in the crude oil. On the other hand treatments longer than 4h 30' with acids stronger than 5N (and probably even weaker, *i.e* 4N) lead to the deterioration of the decolourizing properties of the clay. In the Ankeria bentonite 1h treatments give the same results provided that the acid is stronger than 3N. For 1N acid a minimum 2h treatment is required to remove 95% of the ß-carotene. Finally, the Rema bentonite is activated only with prolonged treatments.

9.5.3. Structural changes of smectites during activation.

The X-ray Diffraction study (Fig. 9.3) showed that acid activation has caused structural changes in the treated smectite in accordance with other workers (Brückman *et al.*, 1976, Stoch *et al.*, 1979a,b, Yates, 1986, Christidis, 1989, Srasra *et al.*, 1990). The effect of both time under constant acid strength and acid strength under constant time on the smectite structure is similar, although it seems that the variation of time for the acid strength chosen (*i.e* 2N) caused more drastic changes (compare Figures 9.3a and 9.3b). This can also be observed in the Figures 9.6 and 9.11, in which it is obvious that the surface area of the 5N/1h sample is about $100m^2/100gr$ lower than that of the sample 2N/6h.

Activation has affected mainly the *00l*-order (basal) reflections. More specifically, the 003 reflection has completely disappeared, while the intensity of the 001 and 005 reflections has been significantly reduced. On the other hand the "prismatic" reflections (110, 020 band and 060 reflection) do not seem to have been affected by the acid treatment. The 001 reflection has not dissapeared completely as in other reports (e.g Srasra *et al.*, 1990), probably because the acid was not strong enough.

An important feature of the X-ray traces of the acid activated samples is the increase of the background in the interval between 20 and $30^{o}2\theta$ (designated with α in Fig. 9.3). This phenomenon is more pronounced in Figure 9.3b (variation of time at a constant acid

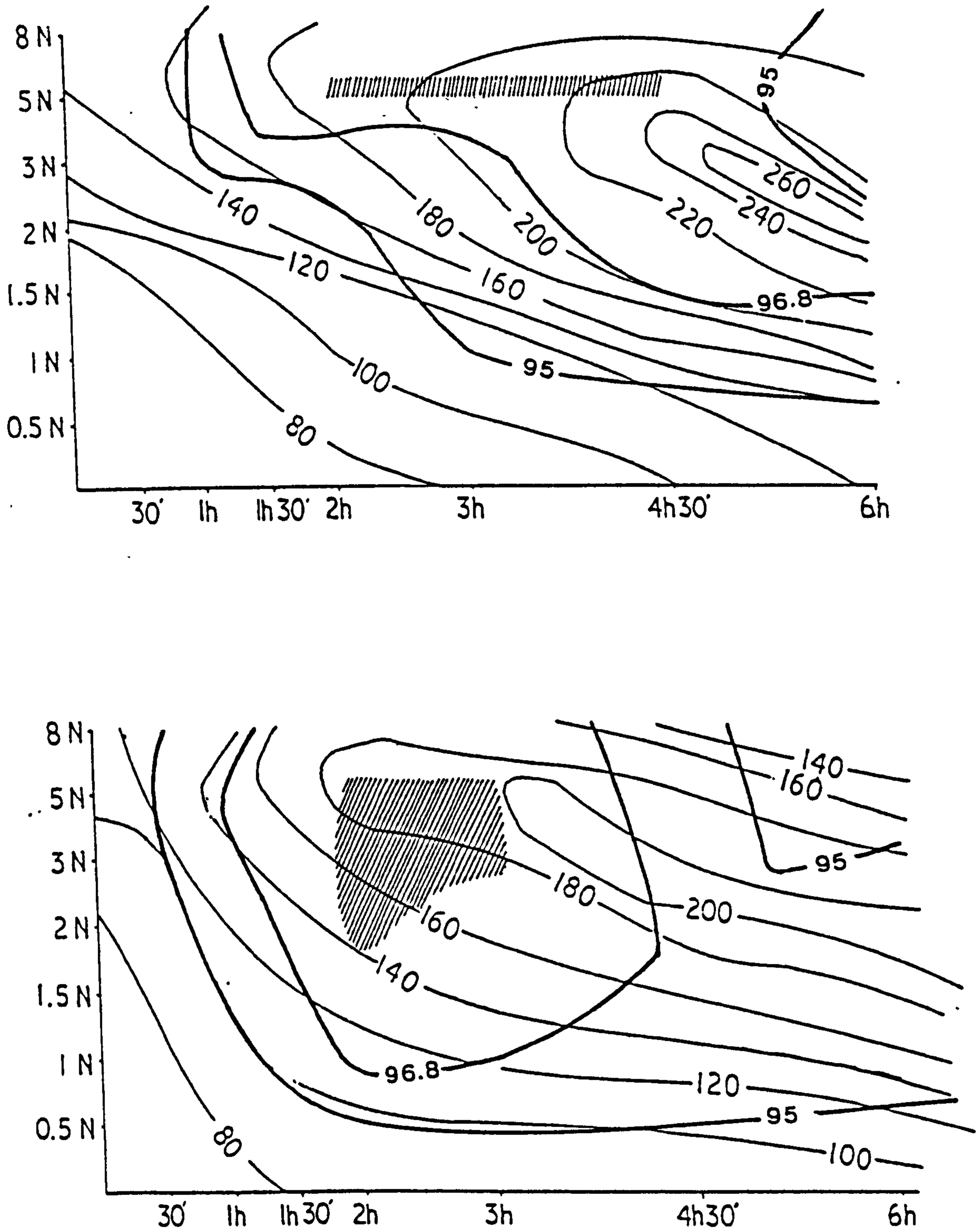

FIGURE 9.11. **STSD** (Surface area–Time–Acid Strength–Dcolourization efficiency *i.e* bleaching capacity) diagrams for the bentonites from (a) Ankeria deposit (Milos), and (b) Chios.

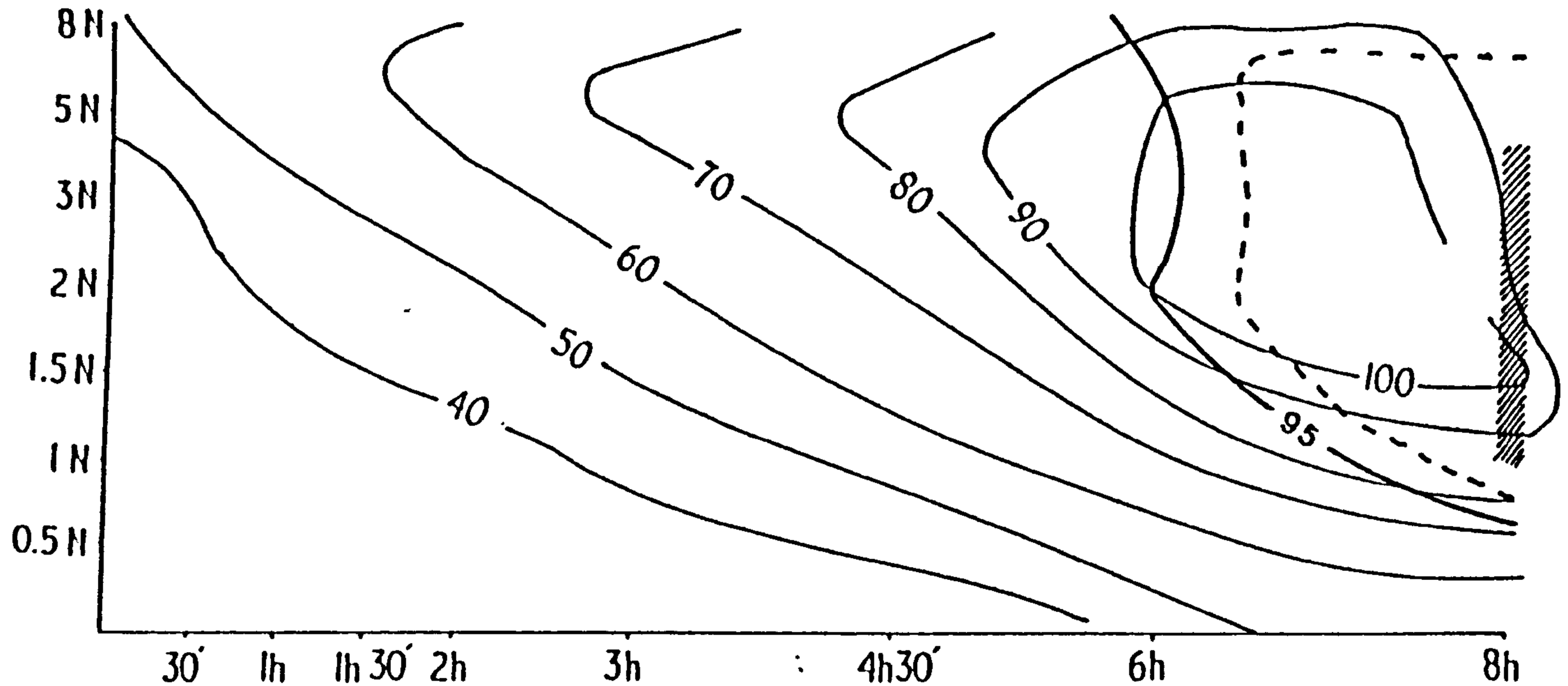

FIGURE 9.11 (continued). STSD (Surface area-Time-Acid Strength-Decolourization efficiency *i.e* bleaching capacity) diagrams for the bentonite from the Rema deposit, Milos (c).

strength, 2N) and has been attributed to the deposition of amorphous silica gel caused after the attack on the octahedral layer and the exposure of the tetrahedral layer (see Section 9.3).

The Infra Red Spectra obtained from the acid activated samples (Fig. 9.4) exhibit significant differences when compared to the untreated sample. The influence of the acid treatment is function of both the acid strength (Fig. 9.4a) and time (Fig. 9.4b). The characteristics of the Infra Red Spectra of the activated samples are summarized in the following points:

-1) The intensity of the absorption band at 3630cm^{-1}, which corresponds to AlAlOH coupled by AlMgOH stretching vibrations (see Section 4.2.5 in Chapter 4) decreases with increasing severity of treatment.

-2) The bands at 3425cm^{-1} and 3200cm^{-1} which correspond to absorption by the interlayer water seems to be more diffuse with increasing severity of treatment.

-3) The intensity of the Si-O out of plane and Si-O-Si (2 bands) in plane stretching bands at 1116, 1043 and 999cm^{-1} do not seem to be affected, although according to Srasra *et al.*, (1990) and Komadel *et al.*, (1990) the intensity of the Si-O (out of plane) band increases.

-4) The AlAlOH (920cm^{-1}), AlFe^{3+}OH (883cm^{-1}) and especially AlMgOH (846cm^{-1}) deformation bands decrease with increasing intensity of treatment. The AlMgOH deformation is almost eliminated in the most severe treatments.

-5) The intensity of the band at 796cm^{-1} which has been attributed to dissordered opal-CT increases significantly with increasing intensity of treatment inn accordance to the findings of other workers (Brũckman *et al.*, 1976, Srasra *et al.*, 1990, Komadel *et al.*, 1990 among many others).

-6) The intensity of the band at 628cm^{-1} which corresponds either to Al-OH vibration or to Si-O bending and/or Al-O stretching gradually decreases with increasing both the time of treatment and acid strength in good aggreement with the findings of Komadel *et al.*, (1990).

-7) The intensity of the band at 467 cm^{-1} (Si-O-Al and Si-O-Mg coupled by OH vibrations or Si-O bending vibrations) is essentially unchanged. On the other hand, the absorption band at 525cm^{-1} which has been assigned to the same kind of vibrations (see Section 4.2.5 in Chapter 4) decreases with increasing severity of treatment.

The effects of the acid activation process on the thermal properties of the treated bentonites (Fig. 9.5) are summarized in the folllowing points:

-1) Both steps of the loss of interlayer water have been preserved in the acid treated samples. However they both occur at lower temperatures compared with the untreated sample. More specifically, the lower temperature step occurs at 105^{o}C (120^{o}C in the untreated sample), while the high temperatutre step occurs at 150-155^{o}C (210^{o}C in the untreated sample). These temperatures remain unchanged throughout the entire range of treatments examined.

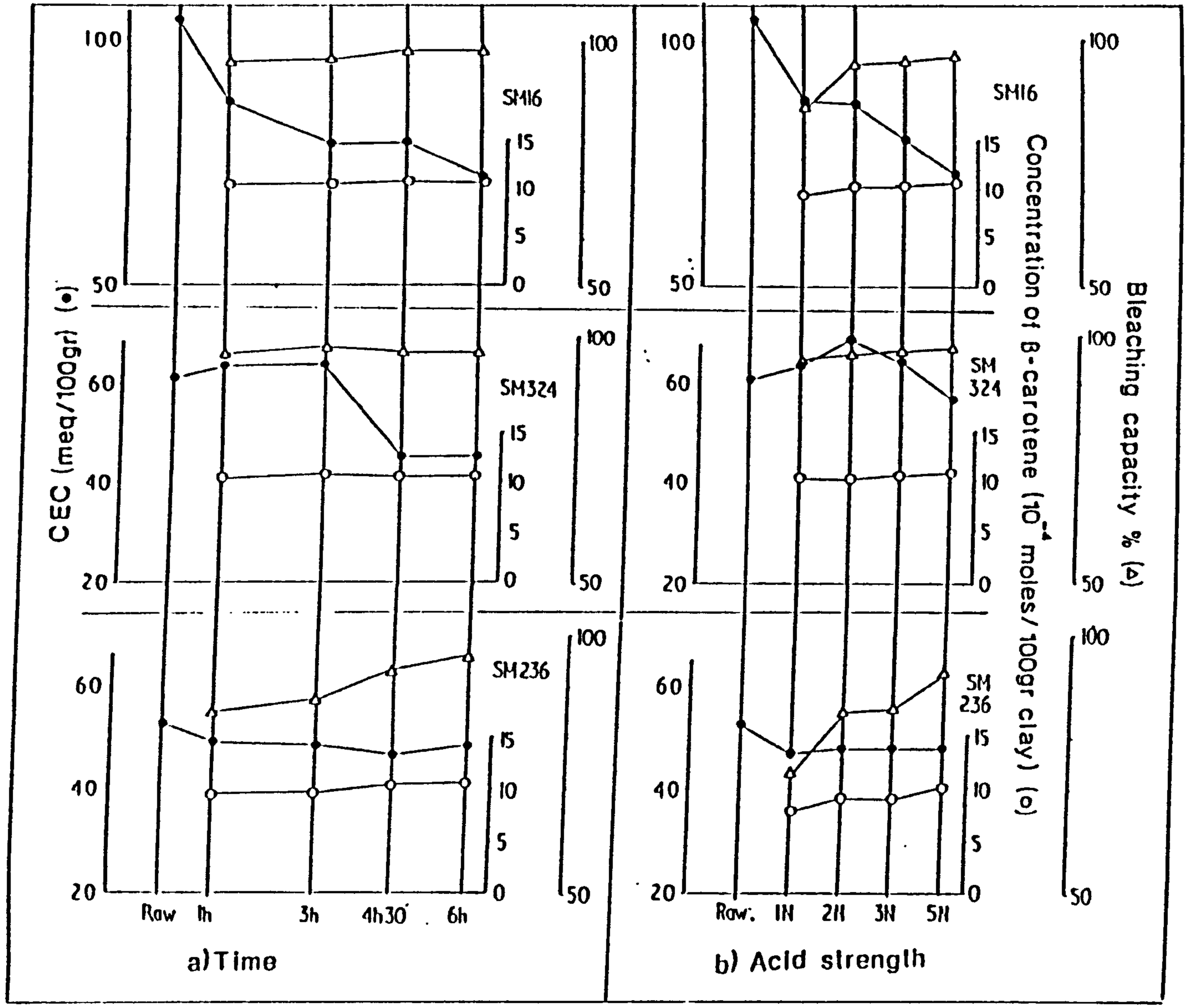

FIGURE 5.12. Evolution of the CEC with treating time and acid strength. In the same diagrams the bleaching capacity and the quantity of adsorbed β-carotene are also plotted. Note the lack of any relationship between the evolution of the CEC and the evolution of the bleaching capacity.

-2) The decrease in the area of the interlayer water peak with increasing severity of treatment reported by Granquist & Samner (1959) was not found in this work.
-3) The main dehydroxylation peak becomes more diffuse with increasing both the acid strength and time of treatment and it shifts to lower temperatures (from 720^{o}C to 675^{o}C). However, there is no systematic variation in the shift of the dehydroxylation peak with increasing treatment like the case reported by Granquist & Samner (1959).
-4) The intensity of the third exothermic peak increases during treatment with weak acids and decreases latter. It also shifts to slightly higher temperatures (925-930^{o}C), with an intermediate step at 920^{o}C (1N/1h run).
-5) The exothermic peak occurring immediately after the third endothermic peak (Greene Kelly, 1957, Grim & Kulbicki 1961 Schultz 1969, MacKenzie, 1970 among many others), which was not observed in the untreated sample is clear and occurs between 950-955^{o}C. Only in the 1N/1h run it occurs at slightly lower temperature (945^{o}C).
-6) The TG curves of the treated materials display an important difference compared to the untreated bentonite as far as the loss of the structural water in the main dehydroxylation reaction is concerned. It is clear (Fig. 9.5) that the rate loss of hydroxyls during the main part of the reaction is much slower in the activated samples compared to the untreated sample.
-7) The slope of the TG curve between the first two endothermic peaks is much greater in the activated samples. This means that the rate of the hydroxyl loss before all the interlayer water has been removed is much greater in the treated samples. The exact mid point cannot be located because of the uncertainty about the initiation of the weight loss due to removal of hydroxyls.

The CEC of the activated materials, determined in the bulk samples, decreases continuously with increasing degree of activation in the Ankeria and Rema bentonites, while increases in the beginning and decreases later in the Chios bentonite (Table 9.4). It seems that the decrease
occurs in steps (Fig. 9.12). This is more apparent in the Ankeria bentonite. Also it is clear that the variations in the CEC are not related either to the bleaching capacity or to the concentration of the adsorbed ß-carotene.

The SEM examination showed that the smectite flakes have undergone significant morphological alteration. The original wavy flakes characterized by honeycomb texture have been replaced by flat flakes (Plate 21). At more advanced stages of alteration vermicular textures also appear (Plate 21). Similar textures were observed by Christidis (1989) for the activated bentonites from the Zoulias deposit.

9.6. Discussion of the results.

The results in Figures 9.6 and 9.11 clearly demonstrate that although the Rema bentonite (Milos) and the Chios bentonite have similar grade the latter is activated very easily while the former only at prolonged treatments with strong acids. Furthermore the evolution of the CEC of the Chios bentonite follows a different path compared to the other materials. Also the performance of the bentonite from Chios deteriorates significantly at prolonged treatments with strong acids. This behaviour is believed to be a function of two factors:

-i) the mineralogical composition of this particular bentonite

-ii) the mineral chemistry of the smectites present in the Chios bentonite.

The Chios bentonite is the only material which contains abundant carbonates, mainly dolomite. In the initial stages of the acid treatment carbonates dissolve during acid activation causing effective enrichment of the smectite content. Simultaneously, the acid attacks the smectite crystallites by releasing octahedral cations in the solution and causing deposition of amorphous silica in the edges of the crystallites. However, because the dissolution of the carbonates by the hot acid is vigorous, it covers the effect of the dissolution of smectite, which probably is a slower process. Hence the faster removal of the carbonates prevails and this subsequently leads to an increase of the cation exchange capacity.

In the more advanced stages of the acid treatment the dissolution of the smectite continues. This leads to a dual result: a) the proportion of the smectite present (*i.e* the grade of the materials) continuously decreases leading to a continuous decrease in the CEC capacity of the activated bentonite (see Table 9.4 and Figure 9.12) and b) with continuous release of the octahedral cations the smectites become increasingly imbalanced in terms of their layer charge, leading to an actual increase of the CEC of the smectite flakes (Granquist & Samner, 1959). In the Ankeria and the Rema bentonites in which carbonates are absent or are present only in places and in subordinate amounts, the CEC of the treated bentonites continuously decreases as a result of the continuous dissolution of the smectite flakes and deposition of amorphous silica (see Infra Red Spectra in Fig. 9.4).

All the three bentonites examined are composed of Cheto smectites. In these smectites the Mg content increases in the following order: Rema smectites (Beidellite, Tatatilla montmorillonite)--> Ankeria bentonite (Tatatilla and Chambers montmorillonite)--> Chios bentonite (Otay montmorillonite). Stoch *et al.*, (1977) found that Mg is released more easily during activation although Osthaus (1956) had proposed that all three octahedral cations are released with the same rate. The Infra Red Absorption spectra of the Ankeria bentonite (Fig. 9.4) showed that the Mg release is more pronounced; the band at 846cm^{-1} OH-

deformation band corresponding to AlMgOH has almost completely disappeared while that at 883cm^{-1} characteristic of AlFe^{3+}OH can be observed even at the most advanced stages of alteration. The smectites present in this bentonite are generally richer in Mg than Fe (see Appendix 4.6). This indicates that Mg might be released at a higher rate than iron.

The faster release of Mg indicates that smectites richer in Mg might undergo structural changes at faster rates compared to more Al-rich ones. Hence the active sites might develop faster and the clay might be activated easier. Novak & Cicel (1978) concluded that it is the substitution of Al by Mg and/or Fe which lowers the stability of the octahedral layer and thus renders the smectite crystals prone to changes imposed by acid attack. Under this context the fact that the Rema bentonite which contains Al-rich smectites is activated only after prolonged treatments with strong acids is not unexpected. Also, the fast activation of the Chios bentonite which is rich in Mg might be understood in this way.

The presence of abundant opal-CT might also play an important role during the acid treatment. If it is intimately associated with the smectite flakes then it might impede the acid attack by blocking part of the exposed octahedral sheet. This might be an additional factor for the inferior performance of the Rema bentonite. This possibility does not seem to be very significant on the basis that the Chios bentonite which was successfully activated contains abundant opal-CT. However, the Chios bentonite is also abundant in carbonates. The vigorous dissolution of the carbonates in the incipient stages of the treatment might have increased the smectite-acid reaction area vastly, thus enhancing activation. Therefore a possible impeding role of the opal-CT might partly account for the slow activation rate of the Rema bentonite.

The stepwise decrease of the cation exchange capacity is another interesting feature of the smectites studied. It indicates that the removal of the octahedral cations and the precipitation of the amorphous silica phase which effectively "dilutes" the smectite present might be a stepwise process. A possible explanation for this feature is that for removal of a certain number of octahedral cations to occur and for the structure to be modified probably through a change in the coordination of the remaining octahedral cations, a free energy level has to be overcome. If the combination acid strength-time of treatment at the given temperature (70 ± 2^{o}C) does not provide the activation energy which is essential for the progress of the reaction, then the removal of the octahedral cations does not proceed. If this is the case, then the treatments 1N/1h and 2N/1h do not cause significantly different imbalance in the structure.

An alternative explanation is to assume that the different treatments cause structural modifications of different degree, increasing the CEC with increasing severity of treatment, but the dissolution of the smectite crystallites and the precipitation of amorphous SiO_2, which dilutes smectite, takes place at a similar rate. This assumption can explain the fact that the bleaching properties caused by the two treatments mentioned before are

significantly different (Fig. 9.12), through the formation of more active absorption sites (Brønsted or Lewis acid centres) during more severe treatments. If this is the case, then the different steps observed in the CEC are due to precipitation of amorphous material at a faster rate than the increase of the imbalance in the smectite structure. This alternative seems more plausible.

In any case, the exact modifications of the structure are not known (Rupert *et al.*, 1987). The possibility that any existing octahedral Fe^{2+} is oxidized during activation without concomitant uptake of OH^- like in the case of oxidation of Fe in the natural state (Lear & Stucki, 1985) is also very possible. In natural samples oxidation of iron is escorted by uptake of OH; therefore the CEC does not decrease (Lear & Stucki, 1985). In the activated samples the situation is more complicated because hydroxyls are probably removed during treatment (Thomas *et al.*, 1950).

Nevertheless, the loss of ignition of the activated bentonites is not lower than that of the untreated sample (Table 9.5), contrary to the results of Granquist and Samner (1959). On the other hand, the TGA curves showed that the weight loss due to the first endothermic reaction is smaller compared to the untreated bentonite. The loss of ignition was determined from samples which has previously been dried at 110^oC for 4 hours, *i.e* at temperature higher than that corresponding to the first step of the removal of the interlayer water. It is possible that due to the prolonged drying time more water than that corresponding to this first step has been removed. In any case in order to display similar or even higher loss of ignition values (Table 9.5), the activated bentonites must have higher hydroxyl-content than the untreated bentonites.

The above discussion suggests that during activation although a number of hydroxyls have probably been removed during the partial dissolution of the octahedral sheet, the migration of H^+ protons from Brønsted acid centres might have caused disruption of Si-O-Si or Si-O-Al or Si-O or Al-O bonds. This might have led to the formation of new Si-OH or Al-OH bonds (Brückman *et al.*, 1976, Stoch *et al.*, 1979a). The structural features of the activated bentonite is unlikely to be similar to those of the untreated material and the new hydroxyls might be bound in a less cohesive manner; therefore they might be removed easier and at a larger temperature range. This might lead to the inclined TG curves and the less well defined second endothermic peak.

Rupert *et al.*, (1987) proposed that the absorptive properties of the bentonite clays are indeed due to the presence of tetrahedrally coordinated Al. However, opposite to the model of Thomas *et al.*, (1950), this Al^{IV} is not formed from conversion of Al^{VI} to Al^{IV} through removal of OH, but from exposure of Al^{IV} which substitutes for Si in the tetrahedral sheet. The results presented in this work clearly demonstrate that the bentonites from Chios, which contain Otay montmorillonite with very low or even without tetrahedral substitution, can be activated very successfully. Hence, at least in this case, the active acid centres do

not exist "waiting to be exposed" as Rupert *et al.*, (1987) proposed, but are formed during activation. Whether these centres will be formed or not might depend on the degree the octahedral cations are removed and thus on the degree of the octahedral substitution (Novak & Cicel 1978).

The observed increase of the intensity of the third endothermic peak at relatively mild treatments and the appearance of the exothermic peak immediately after that has been observed also by Granquist & Samner, (1959). Greene-Kelly (1957) suggested that after the main dehydroxylation peak loss of the structural hydroxyls is not complete. Such a gradual loss might lead to a decrease of the intensity or even complete elimination of the third endothermic peak. In the acid activated samples the partial loss of the hydroxyls during the acid treatment, and the formation of new Si-OH and Al-OH bonds which are probably weak (see the TG curves in Figure 9.5) might cause complete dehydroxylation during the second endothermic peak. This might lead to a more pronounced third endothermic peak which is associated with the total collapse of the smectite structure. In prolonged treatments or treatments with strong acids the structure has already been affected significantly by dissolution. Thus the difference in entropy of the material before and after the reaction (McKenzie, 1970) might not be great; therefore the intensity of the third endothermic peak decreases.

The acid activation tests showed that the bentonites from Chios and from the Ankeria deposit (Milos) can remove ß-carotene successfully from crude rapeseed oil. The Rema bentonite might perfom successfully only at prolonged treatments with strong acid. At these conditions it is possible that other reactions (like oxidation of the carotenoids) might produce undesirable by-products. It is not believed that this bentonite will be an effective bleaching agent at least for crude rapeseed oil, because of the mineral chemistry of the smectites present, its low grade and the abundant opal-CT present.

9.7. Conclusions.

1) Acid activation increased the surface area of the bentonites examined up to a maximum value after which it decreased. The modification of the surface area is associated with changes in the smectite structure which occurred during activation.

2) The acid activated bentonites have been rendered efficient for the decolourization of rape seed oil through removal of colouring agents like ß-carotene. This is possibly due to the formation of active acid centres on the surface of the smectite crystallites due to the structural changes caused during activation.

3) Although increased surface area is an important feature of the acid activated bentonites, the maximum bleaching capacity of all the materials tested is not associated with maximum surface area.

4) The optimum decolourization properties for all three bentonites can be obtained with a variety of combinations between acid strength and treating time. The combination which is likely to be preferred in an industrial scale, is the least energy consuming. Therefore shorter treatments with weaker acid are preferable.

5) The bentonite from Chios was activated faster than the rest materials tested. This is believed to be due to the higher Mg-content of the smectites present (Otay-montmorillonites) as well as to the presence of carbonates which dissolve, thus increasing the effective smectite content. However, the presence of abundant carbonates suggests that some acid will be consumed for the dissolution of the carbonates, thus increasing the cost of the activation.

6) The bentonite from the Rema deposit display good bleaching properties only after prolonged treatment with strong acid. This is believed to be due to the high Al-content of the smectites present and the existence of abundant opal-CT. Under these conditions it is unlikely that it might be used successfuly as a bleaching earth.

7) Both the Chios bentonite and the Ankeria bentonite might be used successfully for decolourization of rape seed oil. However before use, a series of other tests like the determination of the free fatty acid of the bleached oil as well as its acidity might be determined. This is beyond the scope of this project.

Plate 21

SEM micrographs of the acid activated bentonites

1,2. Smectite flakes flattened during activation. Compared to their untreated counterparts the curled flakes showing honeycomb textures have dissapeared. Nevertheless in both micrographs, some of the flakes have slightly curled edges. Sample SM16 (Ankeria deposit). Photo 1= 1N/30' run, photo 2= 1N/2h run. Scale bars 4μm.

3,4. Smectite flakes flattened during acid activation. In micrograph 3 some flakes have slightly curled edges, but their number is smaller than in the previous micrographs. In 4 the flakes with curled edges have disappeared. Instead vermicular and spherical crystallites are present, along with the flat flakes. The spherical crystallites might belong to amorphous Si released during the dissolution of the smectite flakes from acid activation. Sample SM16 (Ankeria deposit). Photo 3= 5N/2h run, photo 4= 8N/6h run. Scale bars: 3 = 4μm, 4 = 3μm.

5,6. Flat smectite flakes products of acid activation of the Chios bentonite. In photo 3 some slightly curled flakes are visible. Note that the carbonates which are abundant in the original rock are absent. Scale bars 4μm.

Plate 21

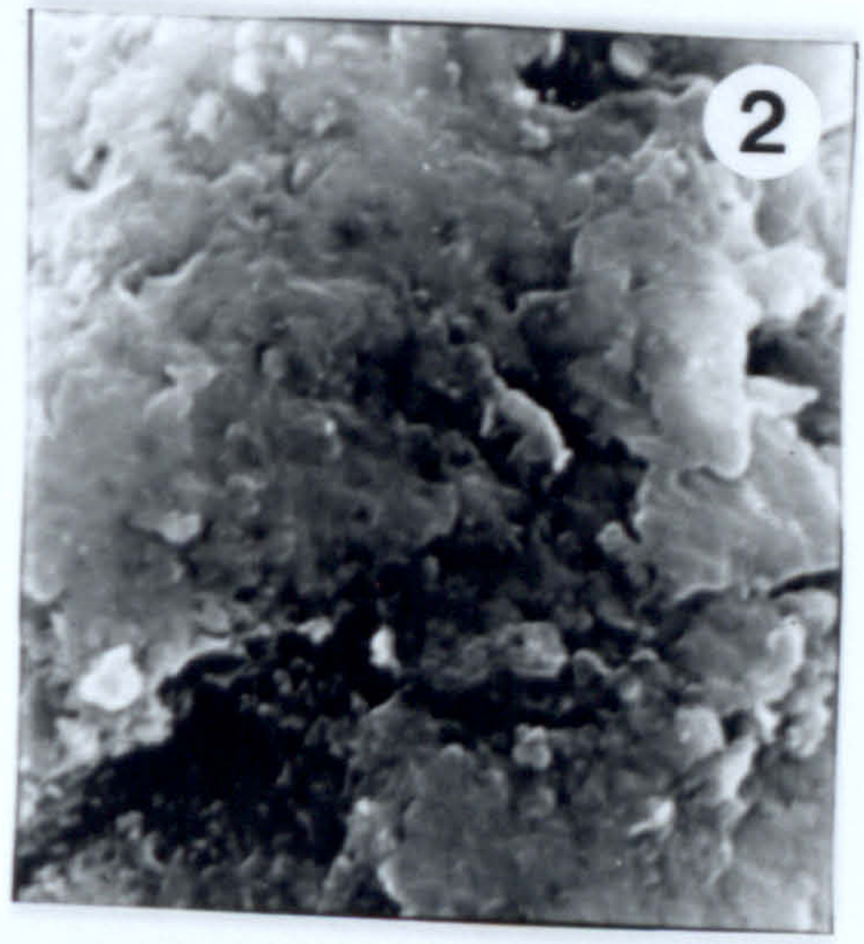

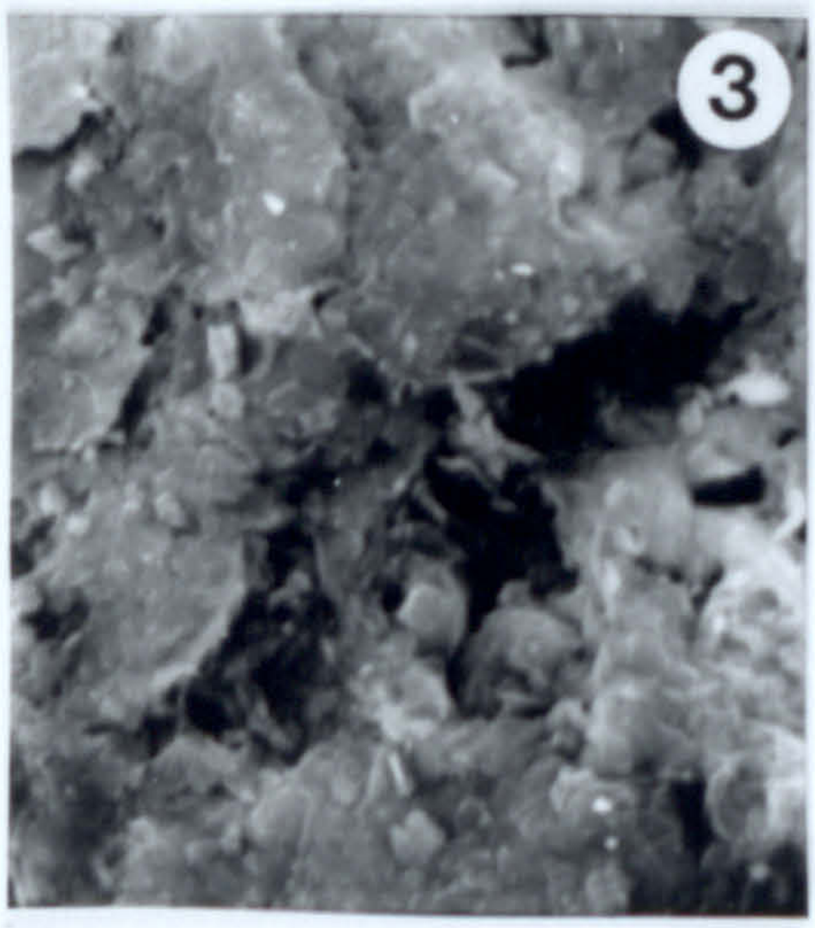

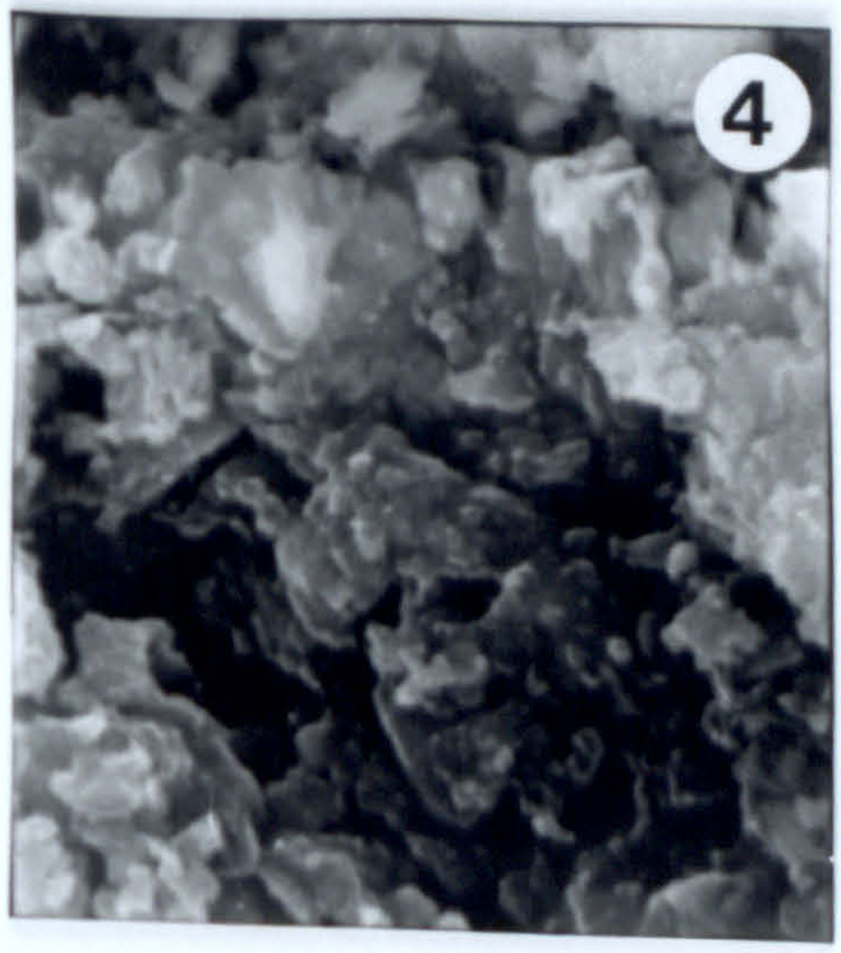

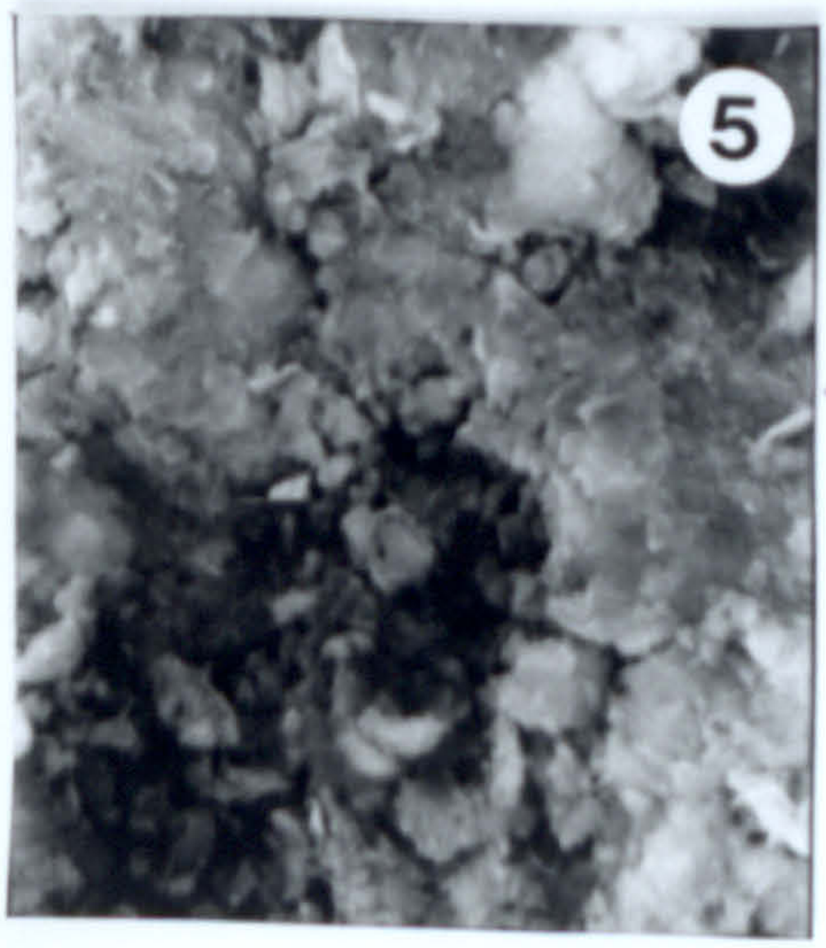

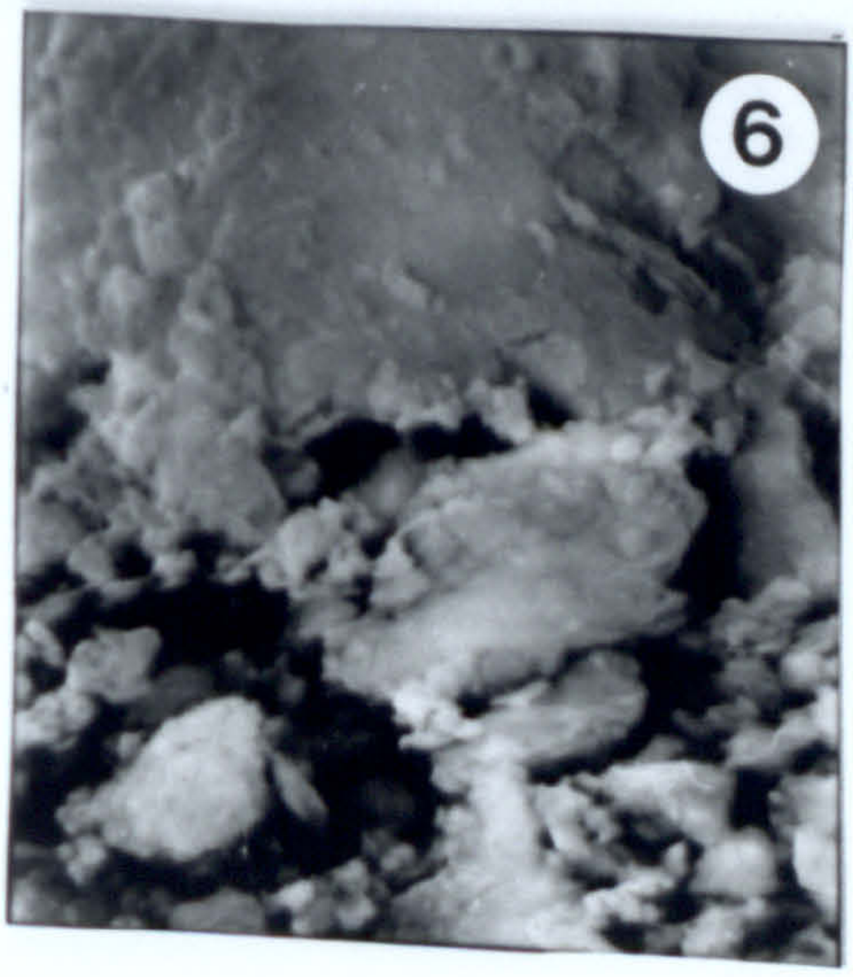

CHAPTER TEN

PROPERTIES OF THE GREEK BENTONITES FOR THE FOUNDRY INDUSTRY

10.1. Introduction.

Bentonites are widely used as binding agents in the construction of moulds used in the shaping of metals by the casting process (Grim, 1962, Highley, 1972, Patterson & Murray, 1983 and Odom, 1984, among others). According to Robertson (1986) Wyoming bentonites were first used as binding agents in foundries in the USA in the 1920's and in the U.K in 1933. Since then their use has expanded and according to Odom (1984) and O'Driscoll (1988), the foundry industry is the first, in terms of tonnage, consumer of bentonites in Europe, and the second in the USA. At present, bentonite bonded sands (synthetic greensands; for a full definition of the terms concerning bentonites in the foundry industry see the following Section 10.2) are broadly used in the iron and steel foundries, although they face competition from chemically bonded sands in areas where high production rates, reduced handling and improved dimensional accuracy are required (BCIRA report, 1985).

The Greek bentonites are sold as binders in the foundry industry all over the world, and the Silver & Barytes Ore Mining Company is the only European firm which exports large amounts of bentonite for this purpose to Canada (Robertson, 1986). However, the data concerning the performance of the raw materials in the various physical tests have not been disclosed by the operating companies. Furhtermore, certain bentonites like those of the Kimolos and of Chios islands have not been tested so far. Therefore the purpose of this chapter is to evaluate the performance of the bentonites with various tests used by the foundry industry and to compare them with commercial products used in this industry.

10.2. Definitions. Theoretical concepts.

Moulding sands used in the foundry industry can be one of the following:

-Natural greensands are silica sands which contain up to 20% clay when quarried (10-24% according to Wilborg & Henderson, 1983), and are used without the addition of other binding agents. They are still used mainly for small castings although they have have progressively been displaced by the synthetic greensands.

-Synthetic greensands are relatively pure silica sands (more than 95% SiO_2), free from clay, which are bound by bentonite with the addition of small amounts of water (tempering water) and organic additives.

-Chemically bonded sands are pure silica sands which are bound by various types of chemical binders (other than bentonite). The methods which have been developed by the foundry industry are (Ashby, 1976): a) The CO_2 process in which sodium silicate is used as binder and the sand is hardened by passing CO_2 through the mould. b) The use of various types of resin binders and their catalyst systems. c) The Na-silicate process in which organic esters are used as hardening agents.

-Olivine and zircon sands are sometimes used because of their refractory properties instead of silica sands.

-Calcined clay sands are refractory sands made of vitrified china clay (molochite), used in the production of investment castings (Ashby, 1976).

The synthetic greensands are preferred from the other types of sands because of their good performance relative to their price. Also, they can be reused with the addition of small amounts of bentonite and sand contributing to a less environmental impact. Lack of recycling is a disadvantage of the olivine and the zircon sands and the naturally bonded sands.

Bentonites are added in amounts ranging between 5 and 10% and are mixed with water and sand (Odom, 1984). The mixture is mulled for sufficient time (according to Sanders & Doelman, 1969, 8 minutes mulling suffices to impart most of the strength in the sand-bentonite-water mixture). Since the physical properties of the moulds (green, dry and hot strength) is affected by the clay and the water content, and the type of exchangeable ions (Grim, 1962, Odom, 1984 Hoffman, 1985, BCIRA report, 1985, Loto & Omotoso, 1990) the tests are performed with a specific sand, at a determined clay and water content. The water used is referred to as *tempering water* and corresponds to the amount of water that must be added to render the sand-clay system somewhat plastic, to develop cohesive strength so that the mixture can be moulded around a pattern, and to maintain the cavity after the pattern is removed and the metal is poured into it (Grim, 1962). The main requirements for bentonites used as binders in the synthetic greensands are:

-Development of strength when mixed with sand.

-High durability.

-High fusion point.

-Good resistance to expansion problems (conversion of α- to β-quartz).

Because natural Na-bentonites or Na-activated bentonites display superior performance compared to their Ca-counterparts (Hoffman, 1958, Grim, 1962, Fahn, 1964, Sanders & Doelman, 1967, 1968, 1969, Highley, 1972, Patterson & Murray, 1983, Odom, 1984, Hoffman, 1985, Alther, 1991), usually Na-bentonites are preferred in the foundry industry.

In practice, the suitability of the bentonites as a binder in the foundry moulding sands is controlled by measurement of the physical properties of specimens which have dimensions determined by the American Foundrymen's Society (AFS, 1978). Since the physical

properties of the moulds (and thus of the specimens) are affected by the clay and the water content, and the type of exchangeable ions of the smectites present in bentonites (Grim, 1962, Sanders & Doelman, 1967, 1968, 1969, Stephens & Waterworth, 1968, Odom, 1984, Hoffman, 1985, BCIRA report, 1985, Loto & Omotoso, 1990) the tests are performed with a specific sand, at a determined clay and water content (Odom, 1984). The physical properties which are routinely determined include the green and dry compression strengths, the shatter index, the compactability, the permeability and the wet tensile strength of the moulding sands (BCIRA report, 1985). Sanders & Doelman, (1967, 1968, 1969) proposed methods to determine the durability of the bentonites which include heating of the clay at different temperatures, measurement of the green, dry and hot compresssion strengths and comparison of the results with those of the raw clays.

The *green compression strength* expresses the strength of a moulded sand-bentonite mixture at a specified tempering water content. It reflects the bonding ability of the clay and is measured by determining the compressive force necessary to cause failure in a specimen of definite size. It depends on the nature of the interlayer cation, the amount of tempering water and the clay content (Fig. 10.1a,b). For a fixed clay content the "working range" of the moulding sands (*i.e* the tempering water range for suitable moulding properties) is always in the wet side of the maximum green strength value. Ca-bentonites develop usually higher green strength than their Na-counterparts (Grim, 1962, Patterson & Murray, 1983, Odom, 1984).

The *dry compression strength* is the compressive force necessary to cause failure to a rammed specimen which has been dried at 110^{o}C in an oven to remove all the tempering water and cooled in a dessicator. It expresses the resistance of the sand-clay mixture to erosion. It is always greater than green strength. The dry compression strength measurements are affected in a great degree by the handling of the specimens; therefore the reproducibility of the results is not always good. Na-bentonites develop much higher dry compession strengths compared to their Ca-counterparts (Fig. 10.1c,d). The former bentonites are very sensitive in the amount of tempering water as far as dry compression strength is concerned. Also, Mg-bentonites tend to develop high dry compression strength (Stephens & Waterworth, 1968).

The *hot compression strength* is the compressive force necessary to cause failure to a rammed specimen heated at elevated temperatures. It varies with the amount of tempering water (Grim, 1962) and it is much higher for Na- than for Ca-bentonites (Fig 10.1e). According to Grim (1962), the compessive strengths of specimens are much higher at high temperatures
than when they are allowed to cool at room temperature, probably due to expansion phenomena.

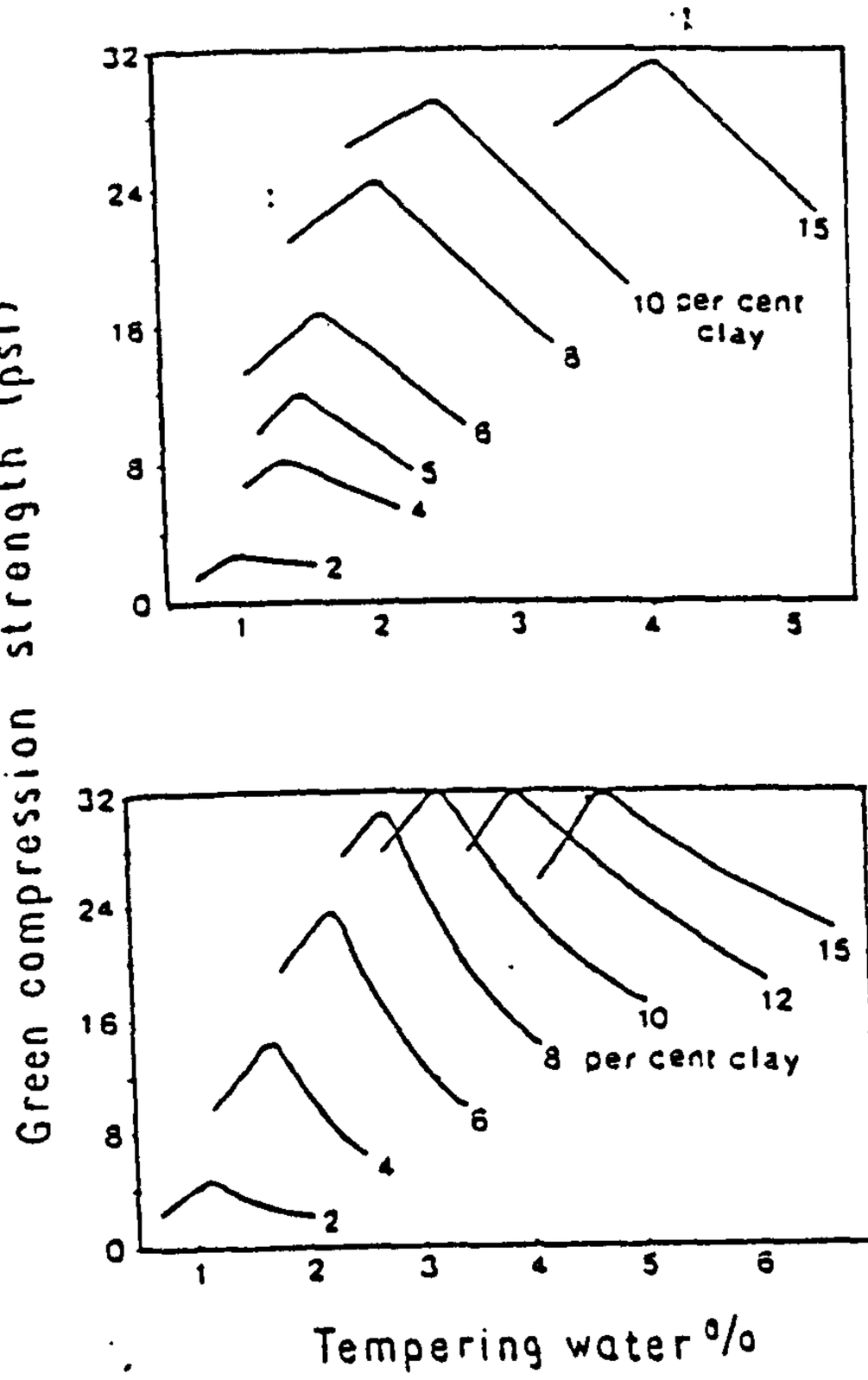

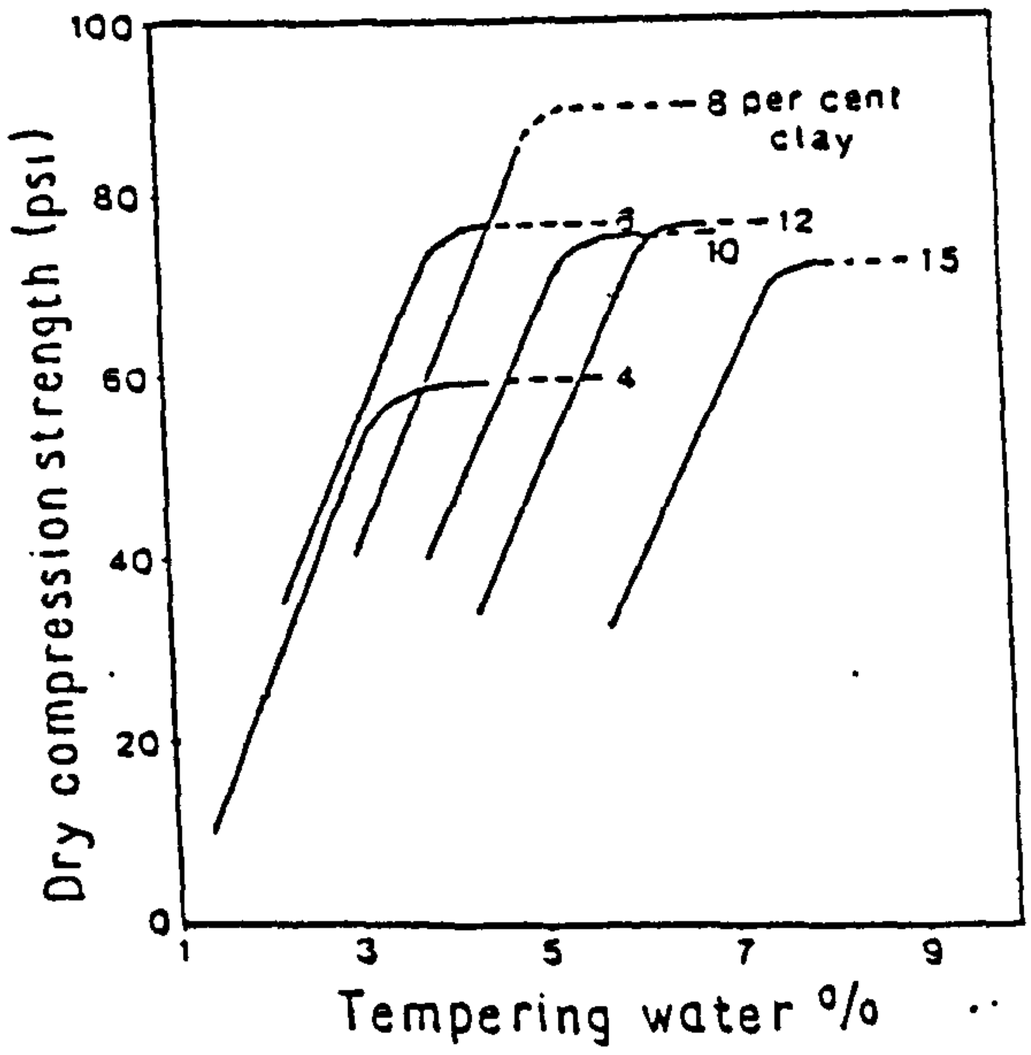

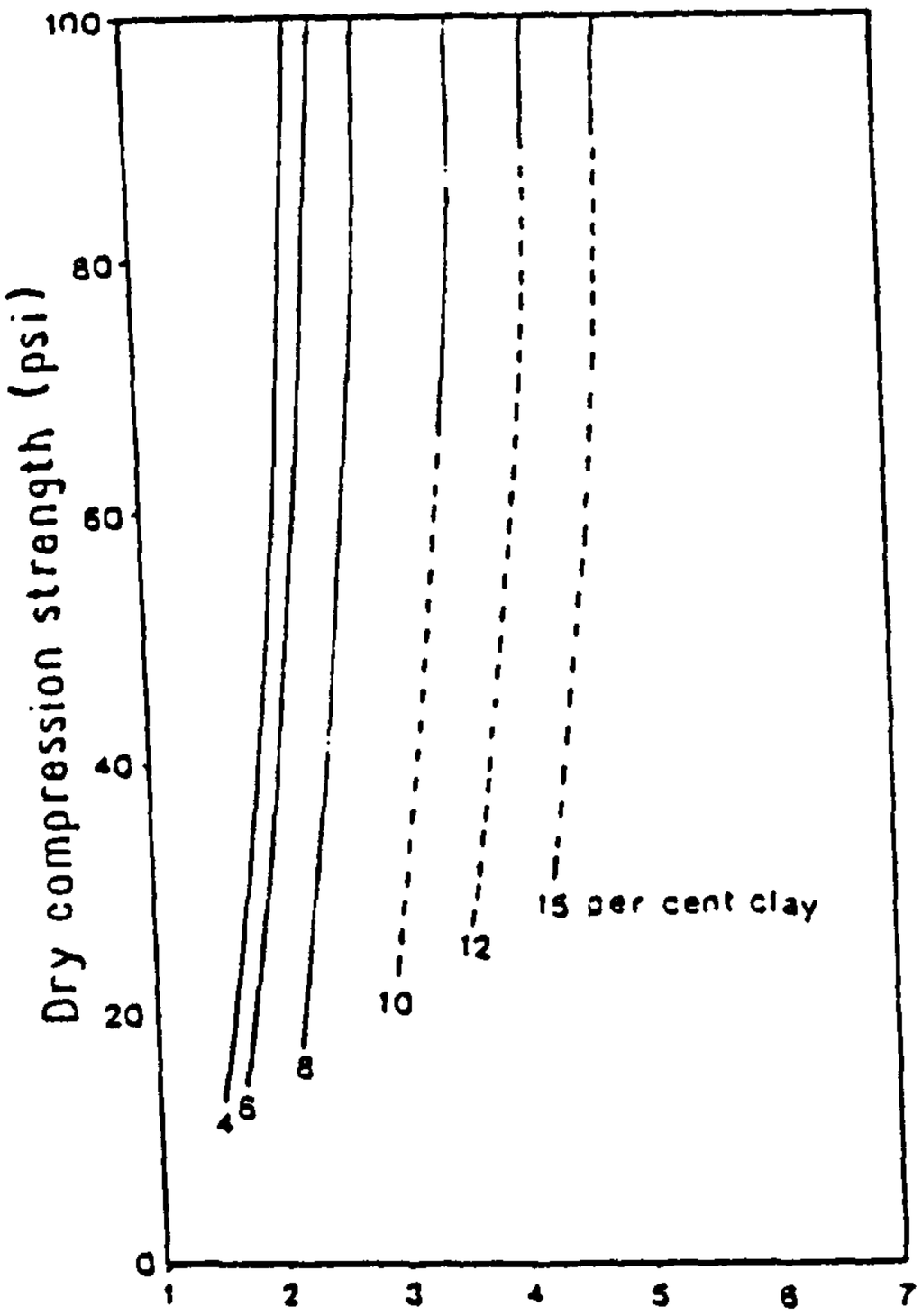

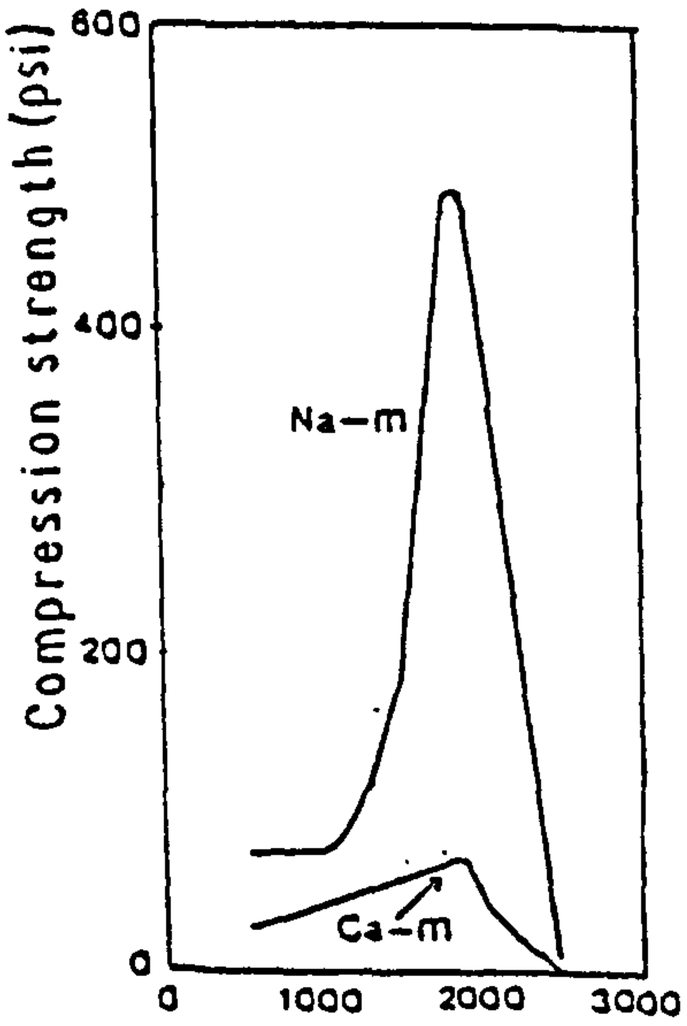

FIGURE 10.1. Green, dry and hot compression strengths for Na- (10.1a,c), and Ca-montmorillonites (10.1b,d), for various clay and tempering water contents.

(modified after Grim, 1962)

Durability is the speed with which bentonites lose their industrial properties due to thermal degradation (Alther, 1991) and should not be confused with thermal stability which reflects the resistance of the mineral phase at the elevated temperature. It is characteristic that most bentonites lose their properties at temperatures much lower than the dehydroxylation temperature of the ideal smectites (see for example, Hoffman, 1958, 1985, Sanders & Doelman, 1967, 1968, 1969, and Alther 1991). The influence of exchangeable cation, in the case of Na and Ca, on the dehydroxylation temperature is minimal (Fahn, 1964, Hoffman, 1958, 1985). This it is expected because the dehydroxylation temperature depends on the ionic radius and not on the valence of the interlayer cations (MacKenzie & Bishui, 1958), and Ca and Na have almost identical ionic radii in both the six- and eightfold coordination (Brownlow, 1979 p. 200).

The durability of a bentonite determines the amount of the clay which has to be added after each casting to replace the "dead burnt" clay so as the sand-clay mixture acquires its original strength (Sanders & Doelman, 1967). According to Hoffman (1985) it depends on the following factors: sand to metal ratio, cooling time of the casting in the mould, pouring temperature, bentonite type, degree and manner of activation (for activated bentonites), the carbonaceous additives, the moisture requirement of the sand, the core binder condensation products and the mould density and heat conductivity of the compacted sand.

Na-bentonites have much greater durability than their Ca-counterparts. Thus the loss of both the green and dry strength with increasing temperature and increasing number of castings is much less for the Na-bentonites than that of the Ca-bentonites (Hoffman, 1958, 1985, Sanders & Doelman, 1967, 1968, Odom, 1984, Alther, 1991). Na-activation of Ca-bentonites does not always improve the durability of the raw materials (Hoffman, 1958, 1985, Sanders & Doelman, 1969, Odom, 1984, Alther, 1991), although usually, the products of Na-activation have intermediate properties (Sanders & Doelman, 1968).

Wet tensile strength is the tensile force which causes failure on a rammed test specimen when it is heated. It is one of the factors affecting the "scabbing" tendency of the greensand (Fig. 10.2a), *i.e* the tendency of creating defects in the cast metal (Boenisch & Paterson, 1967). The heating of the sample creates a weak water condensation zone, due to migration of adsorbed and crystalline water (see Fig. 10.2b). This zone is prone to rupture and causes the failure of the specimen. Natural Na-smectites have high and Ca-Mg smectites very low wet tensile strengths (Stephens & Waterworth, 1968, Odom, 1984).

Flowability is the property of the moulding sand that enables it to flow or conform to the shape of the pattern with a minimum ramming or squeezing (Grim, 1962). It is affected by grain shape, clay and tempering

water content (Grim, 1962, Odom, 1984), and for mixtures with the same amount of clay and tempering water, Ca-bentonites have better flowability than Na-bentonites (Odom,

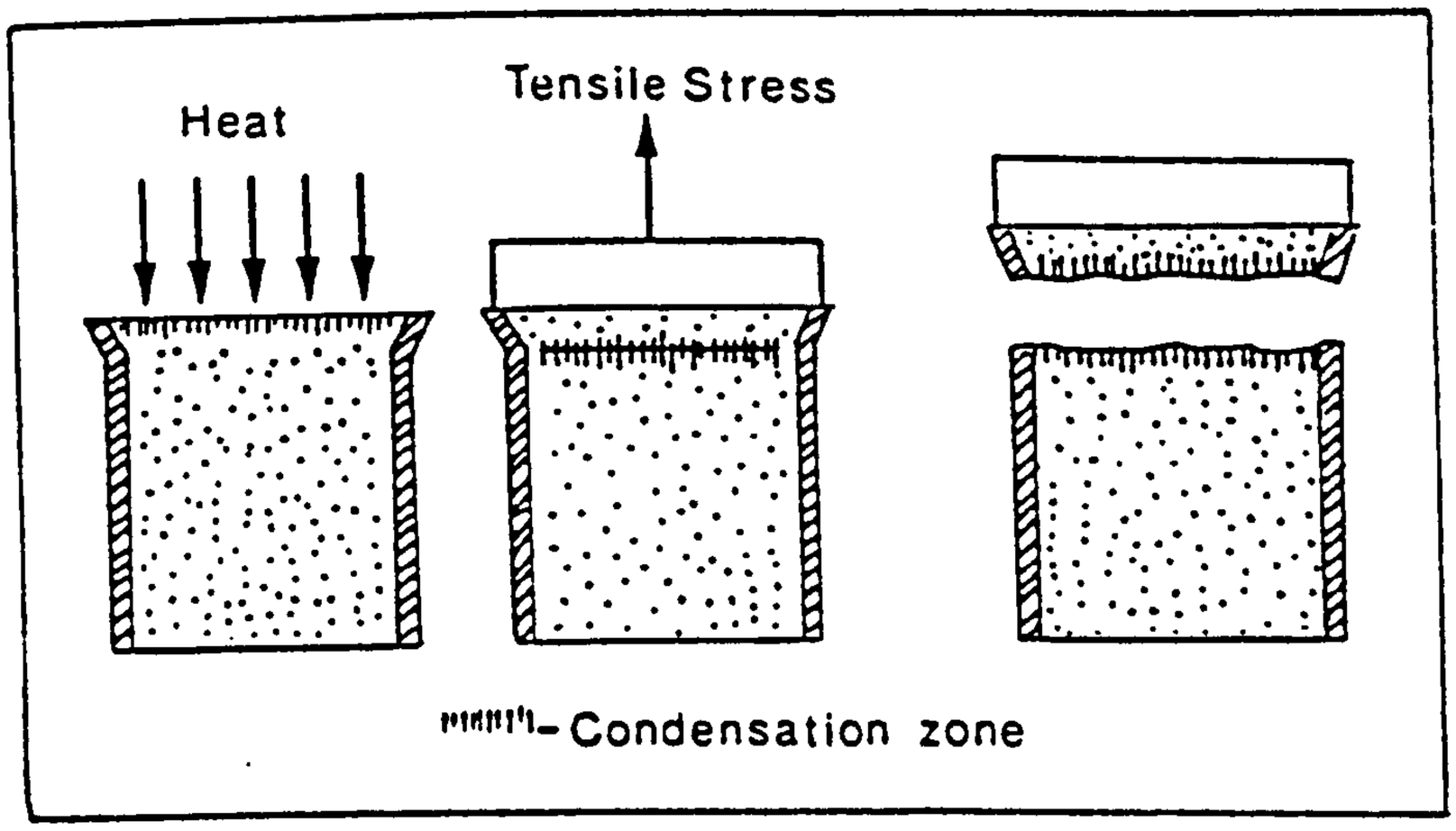

a

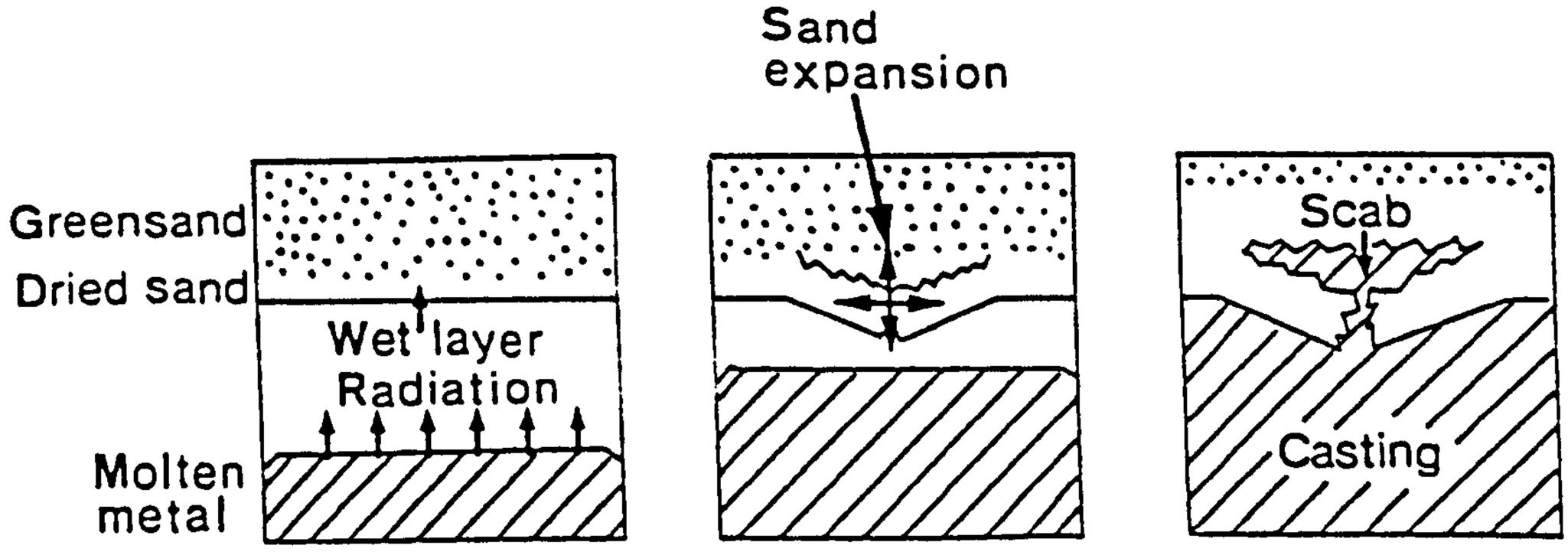

b

FIGURE 10.2. (a) Development of a weak condensation zone from migration of water during the measurement of the wet tensile strength (after Boenisch & Patterson, 1967 and BCIRA, 1985) (b) Possible way of formation of a scab defect during metal casting (BCIRA report, 1985).

1984). In the laboratory, flowability is assessed by measuring the *compactability* of the greensand *i.e* the percentage of the decrease in the height of a riddled volume of sand (BCIRA report, 1985). Normal greensands have 45-50% compactability.

Permeability is the property of the greensand which allows gas to pass through it. Thus it influences the venting properties of the moulds (BCIRA report, 1985). The permeability of the test specimen depends on the size distribution of the sand grains, the tempering water and the bentonite content and the density to which it is rammed. The *density* or *bulk density* according to Grim (1962) is the weight per unit volume of the greensand compacted by ramming. Finally, the *shatter index* is a measure of the toughness of the greensand under impact conditions *i.e* of its ability to be rammed to the required degree of compaction (BCIRA report, 1985). Na-activation does not always improve the performance of the original materials (Sanders & Doelman, 1969).

Na-exchange of the Ca-bentonites usually produces unpredictable results (Stephens & Waterworth, 1968, Sanders & Doelman, 1969, Odom, 1984). It improves the rate of loss of bonding properties, but not the decomposition temperature of the bentonites (Hoffman, 1985). Other factors which might affect the behaviour of the bentonites in the foundry industry are the clay type and the petrological characteristics of the clay (Stephens & Waterworth, 1968, Hoffman, 1985). The process of the Na-activation itself (wet or dry method) is also important (Sanders & Doelman, 1969). According to Parkes (1971) the activation which raises the pH of the clays produces a small change in green strength and shatter index and might or might not affect the dry strength. Like the rheological properties, the degree of disaggregation during the activation process might also be important.

The bonding properties of the bentonite clays have been attributed to the formation of coatings around the sand grains which are connected by clay wedges (Grim, 1962). The maximum green strength is developed when the wedges are rigid and have homogeneous thickness. The bond strength has been attributed to the surface tension of the water surrounding the clay and sand-clay particles and filling the interstices among the clay particles (Loto & Omotoso, 1990). As the water layer becomes thinner by drying the forces holding the particles together increase. This can explain the higher dry strength of the greensands compared to the green strength.

Caine & Toepke (1967, 1968) distinguished two types of bond strength developed between the clay coating and the sand grains namely the *adhesion* strength (ability of the bentonite to adhere to the sand surface) and the *cohesion strength* (strength of the bentonite gel). Both depend on the contact pressure (ramming) and especially the water content because it affects the gel strength of the bentonite. For water contents lower than approximately 25-27% the gel strength is low because bentonite is brittle, the cohesive strength is higher than the adhesive strength and high contact pressures are required for the clay to adhere on the sand grains. For high water contents the gel strength decreases

again due to stiffness (Caine & Toepke, 1967), but the adhesive strength is higher than the cohesive strength (the clay is sticky). At water content of about 35% the clay-sand mixture displays the greater combination of adhesion and cohesion. These systems show *maximum resistance* to compactability.

10.3. Experimental Methods.

The physical properties of 19 representative Greek bentonite samples were measured in the laboratories of the British Cast Iron Research Association (BCIRA). The bentonites tested were prepared after homogenization of the samples belonging in the same horizons, as this was established in Chapter 5. The results are given in Table 10.1. These materials are referred to as untreated bentonites. After the determination of the physical properties of the raw materials, 16 samples were treated with Na_2CO_3 and the same physical properties were measured again. The results are given in Table 10.2. The physical properties which were determined include green and dry compression strength, wet tensile strength, bulk density, shatter index, compactability and permeability. The first three tests are considered as the most important ones for determining the quality of the bonding clay (Stephens & Waterworth, 1968).

The greensands were prepared using 92.5% Chelford 50 silica sand, 5% bentonite and 2.5% tempering water. The bentonites were dried at 65^{o}C, ground in a Tema Mill and passed through a 150μm sieve (BS410) at the University of Leicester. The weight of the bentonite used was corrected for the moisture content with a speedy moisture tester using calcium carbide (see Appendix 10.1). The ingredients of the greensand were mulled for 10 minutes and stored in sealed plastic bags to keep their moisture. Na-activation was performed *in situ* during mulling by adding the optimum percentage of Na_2CO_3, as this was determined by the swelling tests (see Chapter 7). The Na_2CO_3 used was of analytical grade (FISONS). After mulling the activated materials were stored in sealed bags and kept overnight. According to Boenisch & Paterson (1967) *in situ* activation has the same results as far as the wet tensile strength is concerned compared with the conventional method *i.e* activation prior to the evaluation of the foundry properties.

The test specimens for all tests except for the wet tensile strength were prepared using a Ridsdale-Dietert Fischer sand rammer (Appendix 10.2). The same rammer was used for the determination of compactability. The test specimens for determination of the wet tensile strength were prepared with a George Fischer sand rammer Type PRA (Appendix 10.2). Three rammings were applied and the specimen height had always to be within the tolerance allowed. The density of the samples prepared from the Green compression strength was determined using a Ridsdale-Dietert universal pendulum apparatus (Appendix 10.3). The indication obtained from the instrument corresponds to lb/in^2 and can be

converted to KN/m^2 by multiplication with 6.89476. The shatter index was determined with a pneumatically operated shatter-test apparatus (Appendix 10.4). The results are expessed in per cent of weight of the greensand passing through a 12.7mm aperture (BS410). Permeability was measured with a BCIRA direct-reading Permeability Meter using clean and dry compressed air supply. Dry compression strength was measured with a Howden screw driven Universal Strength Tester. The results are expressed in lb/in^2. Wet tensile strength was measured with a George Fischer wet-tensile tester. The surface of the samples was heated at 320^oC for 20 minutes followed by a tensile force applied to the specimen by draw forks. The results are expressed in gr/cm^2.

10.4. Results.

The results obtained for the raw bentonites exhibit clear trends for materials derived from different areas (Table 10.1). Thus, the bentonites from the Areas 1 and 2 of Milos display higher green compression strength (values between 10.2 and 13.0 lb/in^2) compared to the bentonites from the Area 3 (4.8-9.8 lb/in^2) and those form Kimolos (with one exception from the smectite zone in the Prassa deposit, below 10.2 lb/in^2) and Chios (8.9 lb/in^2). The shatter index follows the same trend and indeed in Figure 10.3a, a linear relationship holds between these two properties. On the other hand the density of the materials does not exhibit particular trends in Milos. However the density of the bentonites from Kimolos seems to be higher.

There are certain trends also within the individual deposits. Thus in the Ankeria deposit (Area 1 Milos), the higher horizon exhibits lower green compression strength and shatter index than the lower one. Also in the Prassa deposit (Kimolos), both properties exhibit higher values in the smectite zone (Fig. 10.4a).

The dry compression strength values also vary in a rather systematic way in the various areas. With the exception of the Garyfalakaina deposit, the bentonites from Area 3 of Milos develop higher dry compression strength than those from the Areas 1 and 2. The bentonites of Kimolos, with the exception of the Loutra deposit, develop high dry compression strength values. Finally, the bentonites from Chios display values similar to those of Area 1 of Milos.

The wet tensile strength of the untreated materials, with the exception of the bentonites from the Koufi and the Aspro Horio deposits (Milos) are low. It seems that the bentonites from Areas 1 and 2 of Milos develop higher wet tensile strengths than their counterparts from Area 3. However the deposits of Zoulias (Area 1) and the lower horizon of Ankeria (Area 2) display low values of wet tensile strength. In the Prassa deposit (Kimolos) the smectite zone develops higher wet tensile strength values than the mordenite-bearing and the smectite + opal-CT zone (Fig 10.4b). Weak linear relationships

Table 10.1

Foundry properties of the untreated bentonites.

Quarry	Density	Green compression strength (lb/in^2)	Shatter index (%)	Compact-ability (%)	Permeabi-lity	Wet tensile strength (gr/cm^2)	Dry compression strength (lb/in^2)
Milos							
Ankeria[1]	160	12.5	73	53	110	8.0	55.7
Ankeria[2]	160	10.2	71	59	150	12.0	65.9
Koufi	160	11.0	73	54	140	24.0	62.3
Tsantili	160	10.9	73	55	115	16.0	61.0
A. Horio	160	13.0	73	55	125	23.0	63.3
Zoulias	160	11.9	69	56	150	6.5	43.7
A.Komia[3]	162	4.8	52	53	130	7.0	78.3
A.Komia[4]	160	6.4	48	51	120	7.0	71.3
Garyfala-kena	158	9.8	57	38	140	8.5	35.7
Mavrogia-nnis	160	8.5	63	51	145	6.0	62.7
Rema	160	8.2	61	54	140	9.0	77.3
Agrilies	160	7.8	55	49	150	4.0	48.7
Kimolos							
Prassa i	160	7.6	62	56	135	10.0	100.9
Prassa ii	162	12.7	73	58	120	14.0	86.3
Prassa iii	161	10.2	73	58	135	14.0	86.3
Prassa iv	159	8.1	63	54	140	8.0	68.8
Loutra	160	6.2	43	47	160	3.0	29.0
Fanara	160	8.1	66	57	120	11.0	117.0
Chios							
Thymiana	160	8.9	59	50	160	4.0	55.7

1,2= Lower and higher horizon (respectively) of the Ankeria deposit, 3,4= Lower and higher (respectively) horizon of the Ano Komia deposit. Prassa deposit: i= smectite+ mordenite zone, ii, iii= smectite zone (ii = closer to the smectite + mordenite zone), iv= smectite + opal-CT zone (the sample contains tiny amount of opal-CT).

Table 10.2

Foundry properties of the Na-activated bentonites.

Quarry	Density	Green Compression strength (lb/in^2)	Shatter Index (%)	Compact-ability (%)	Permeabi-lity	Wet tensile strength (gr/cm^2)	Dry compression strength (lb/in^2)
Milos							
Ankeria[1]	160	14.1	73	54	125	28	43.0
Ankeria[2]	160	10.8	68	56	140	31	67.8
Koufi	160	10.2	68	58	130	29	60.5
Tsantili	160	11.4	68	56	155	28	64.0
A. Horio	160	12.6	72	55	135	29	61.1
Agrilies	160	8.9	48	40	120	10	22.6
A.Komia[3]	161	5.5	46	54	105	16	65.3
A.Komia[4]	160	7.7	49	46	120	13	76.7
Garyfala-kena	160	10.1	54	44	140	17	57.6
Mavrogia-nnis	160	10.1	54	44	130	15	62.1
Rema	162	8.7	60	54	135	16	60.2
Kimolos							
Prassa ii	162	14.0	74	57	130	34	55.1
Prassa iii	161	14.0	68	50	110	25	50.0
Prassa iv	160	9.3	66	58	125	30	100.9
Fanara	161	9.4	63	58	120	25	93.4
Chios							
Thymiana	160	8.7	58	54	130	17	58.6

1,2= Lower and higher horizon (respectively) of the Ankeria deposit, 3,4= Lower and higher (respectively) horizon of the Ano Komia deposit. Prassa deposit: ii, iii= smectite zone (ii = closer to the smectite + mordenite zone), iv= smectite + opal-CT zone (the sample contains tiny amount of opal-CT).

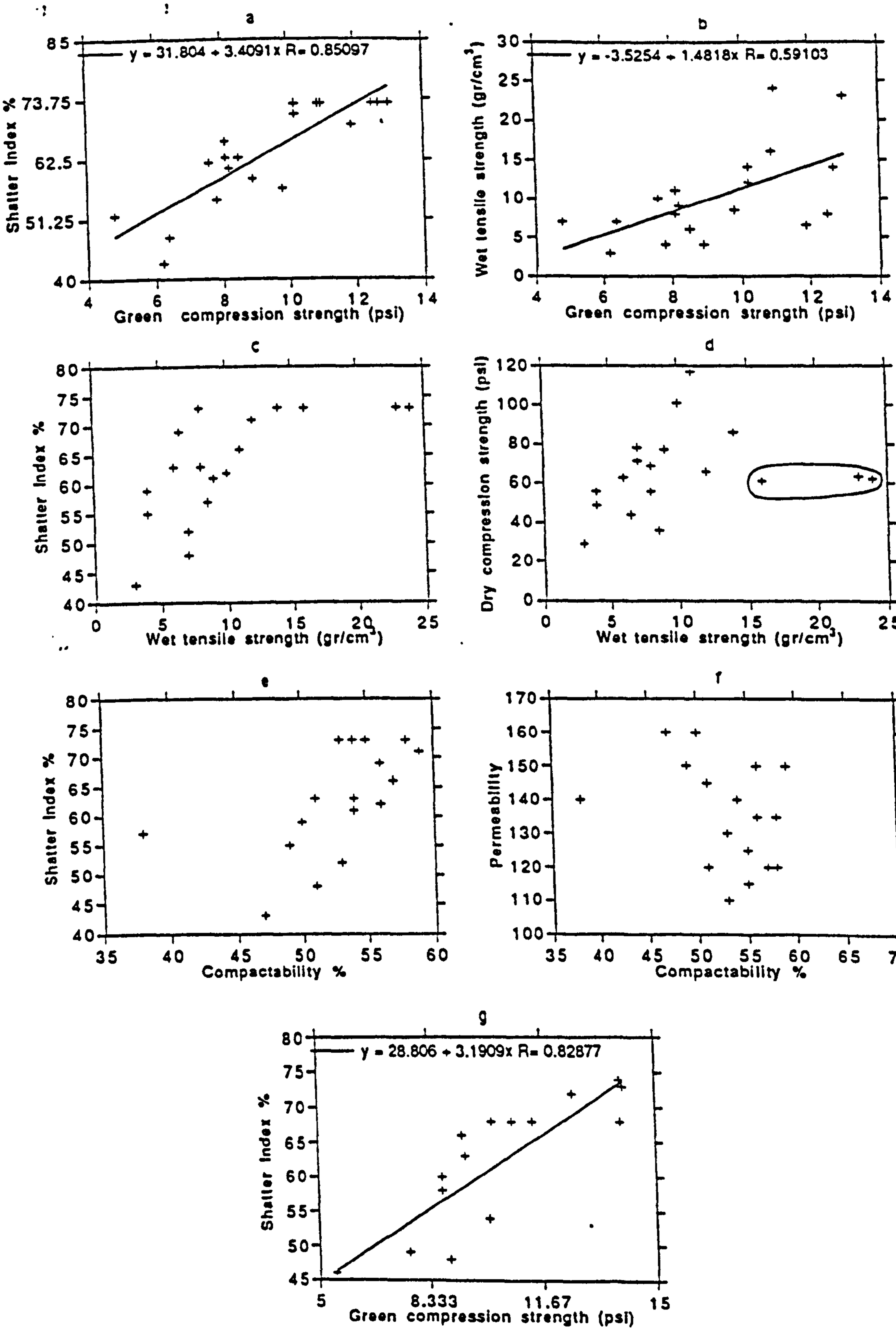

FIGURE 10.3. Orthogonal plots between the various foundry properties of the Greek bentonites. The encircled points in the diagrams 10.3d and 10.3m correspond to materials which do not follow the trends displayed by the other bentonites

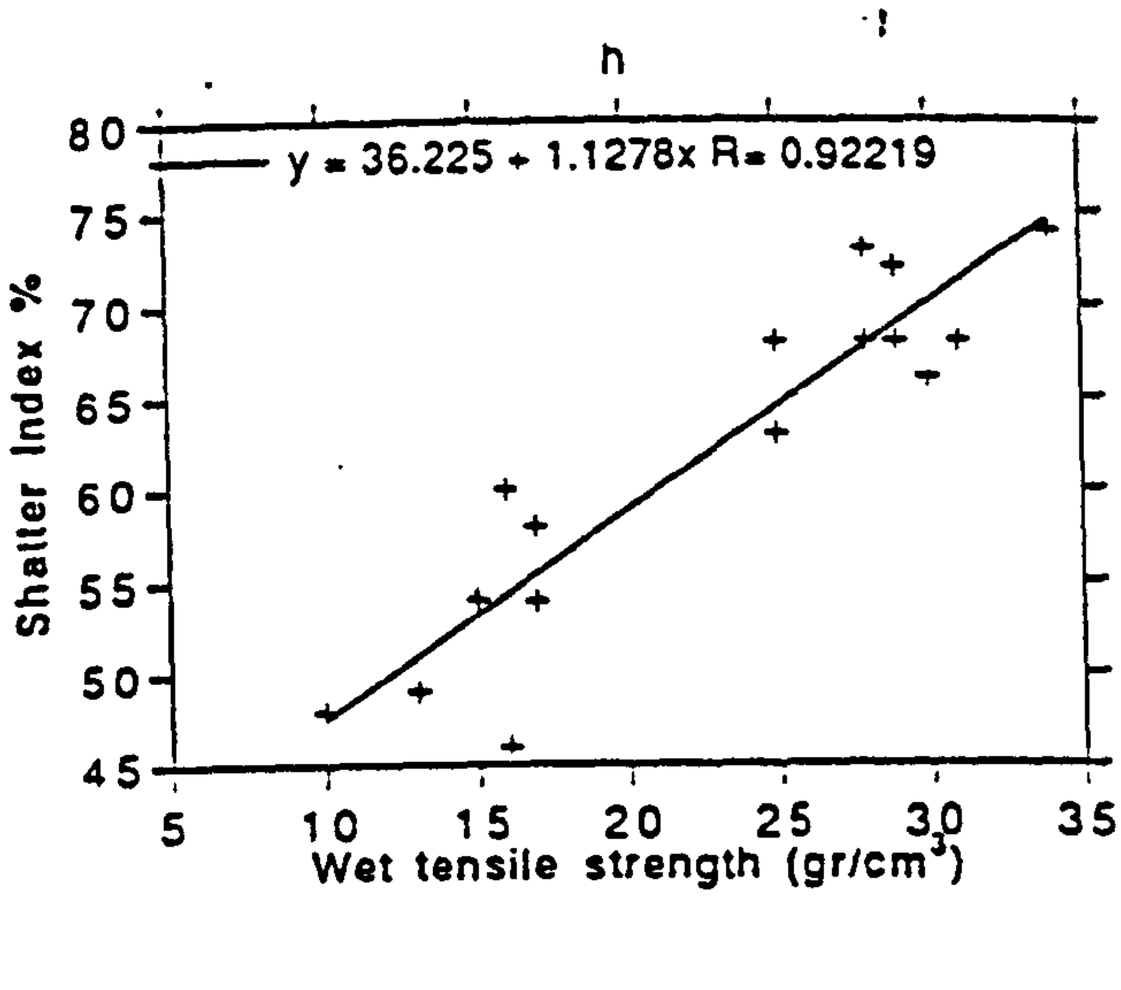

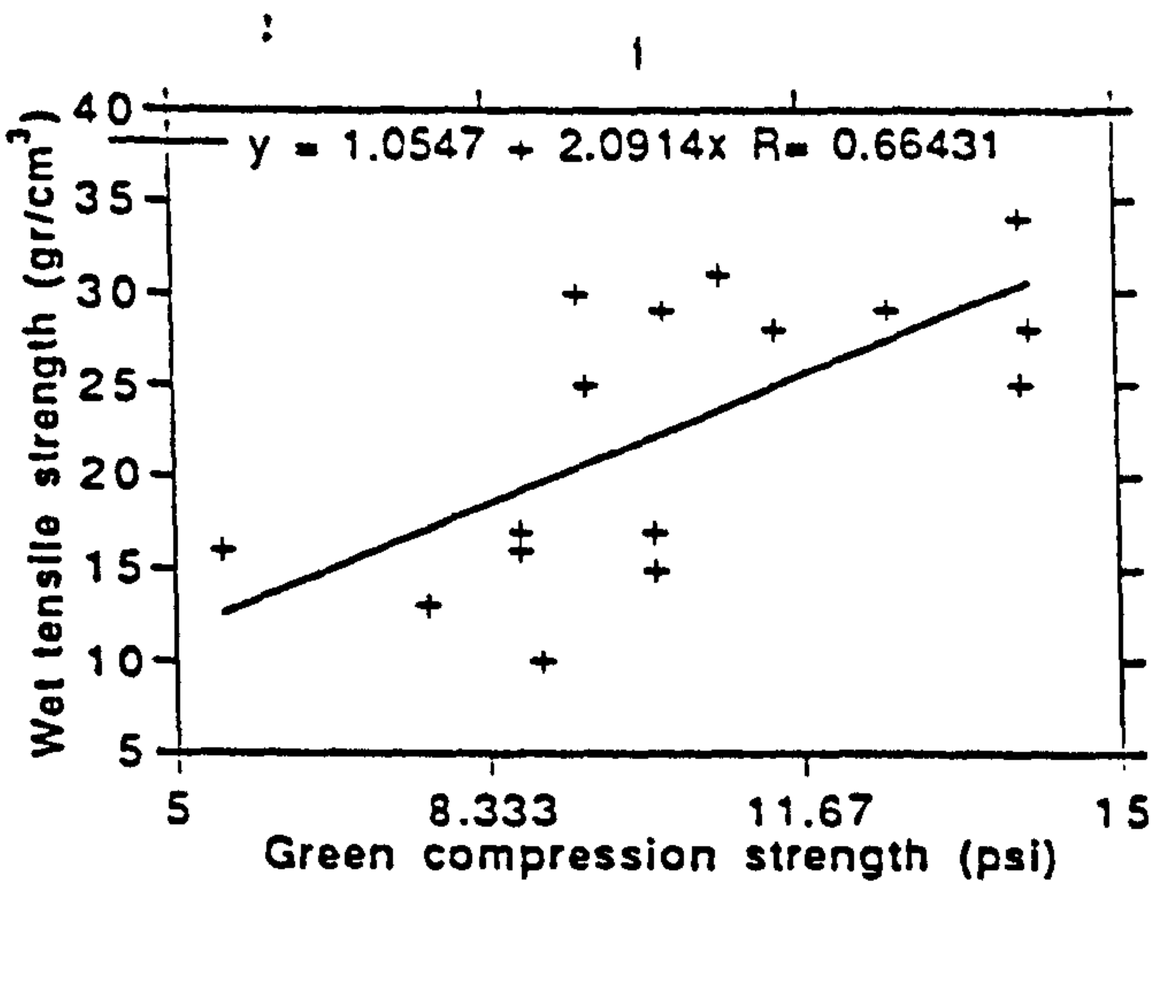

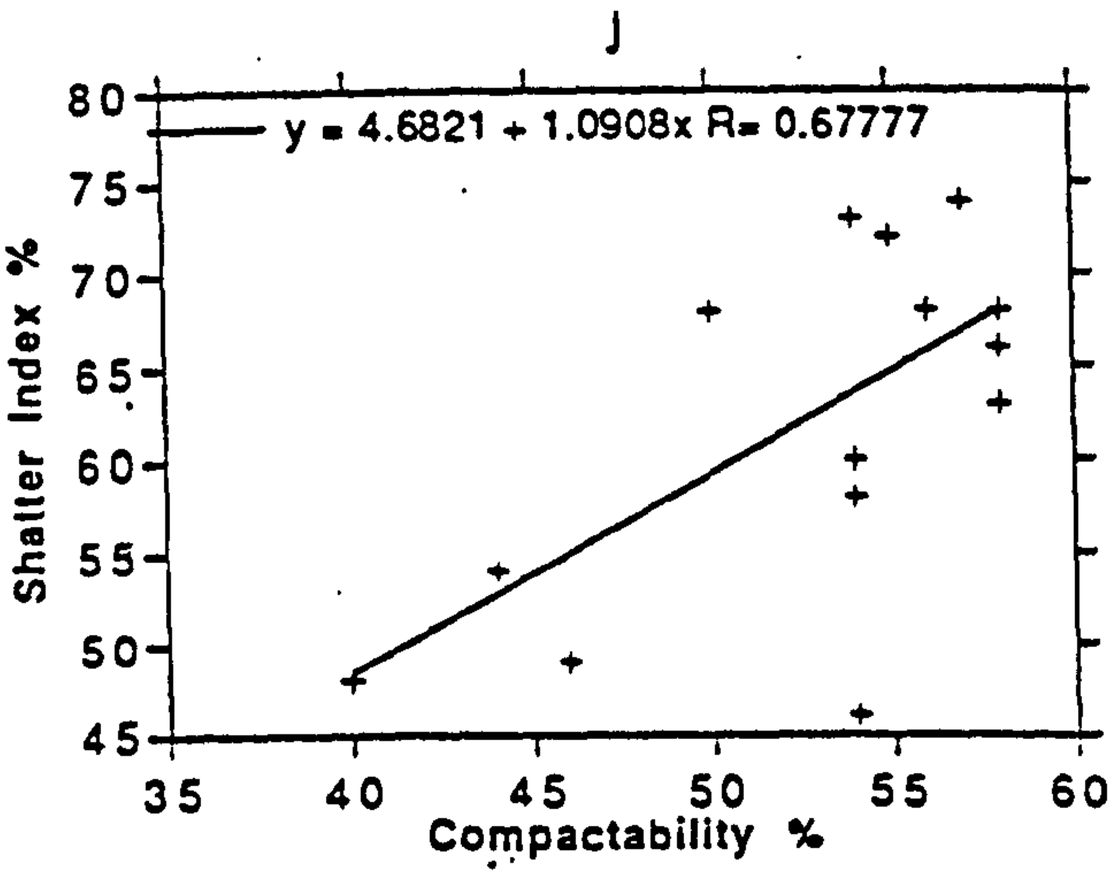

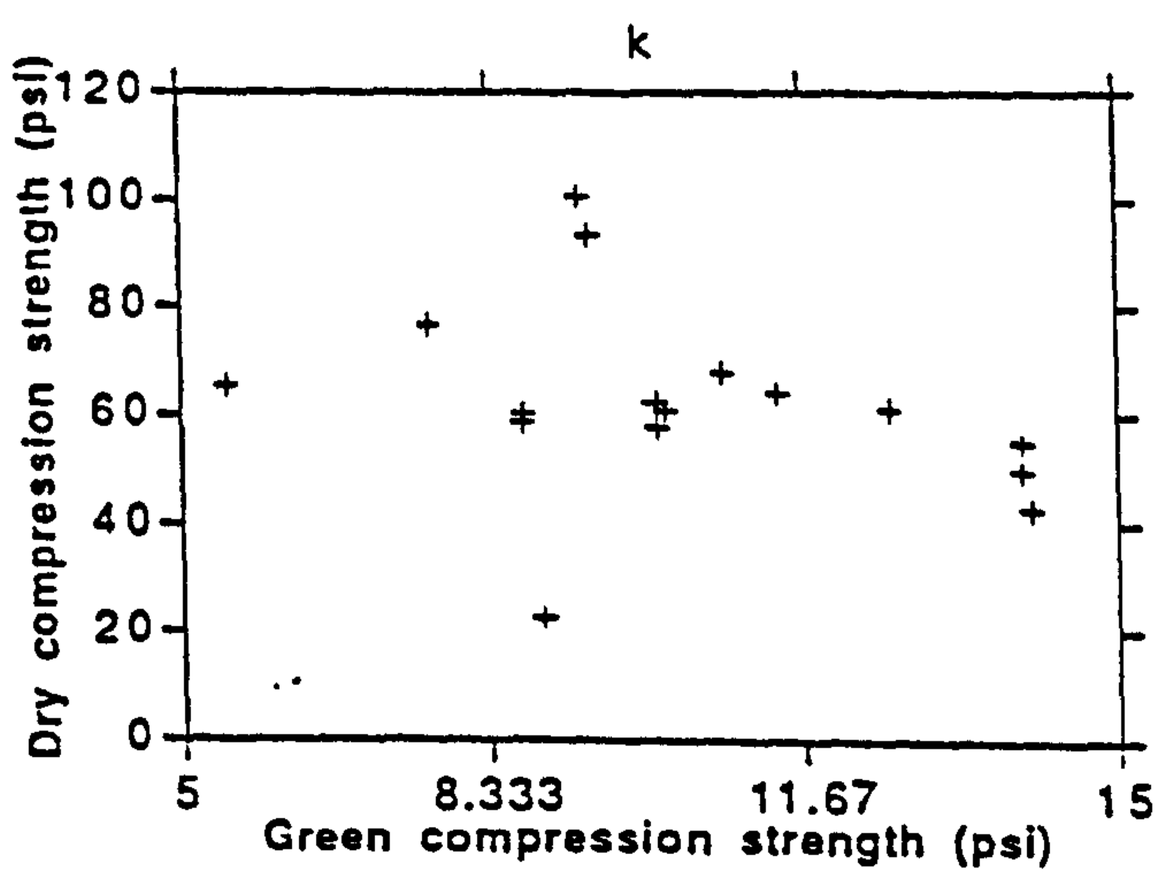

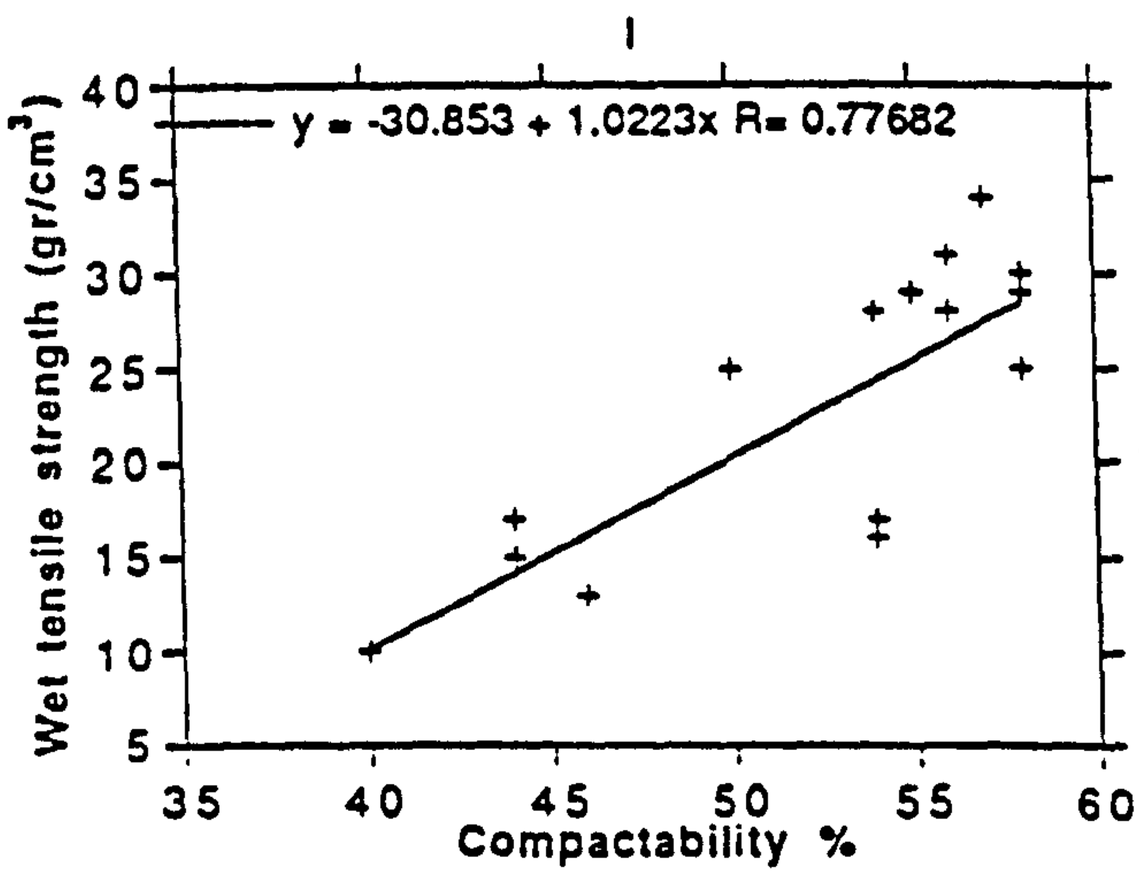

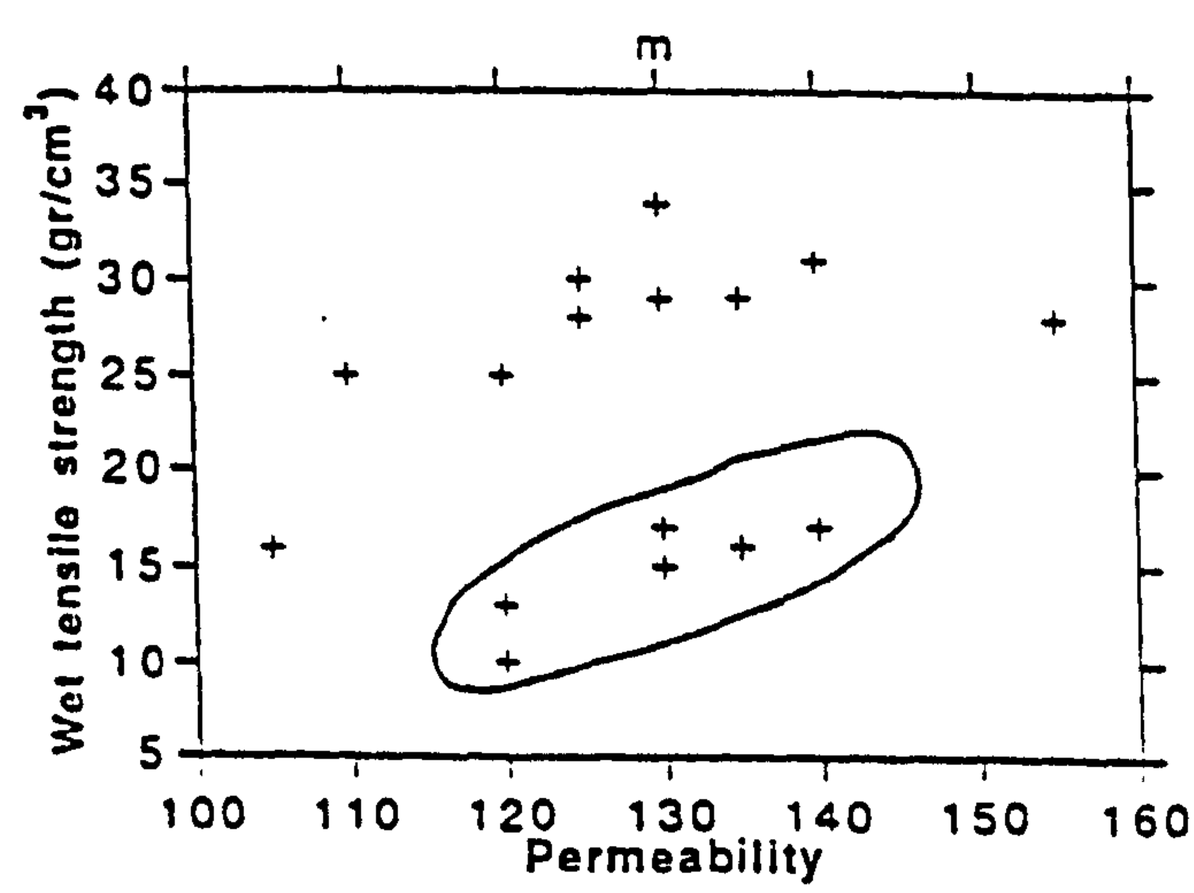

FIGURE 10.3 (continued). Orthogonal plots between the various foundry properties of the Greek bentonites.

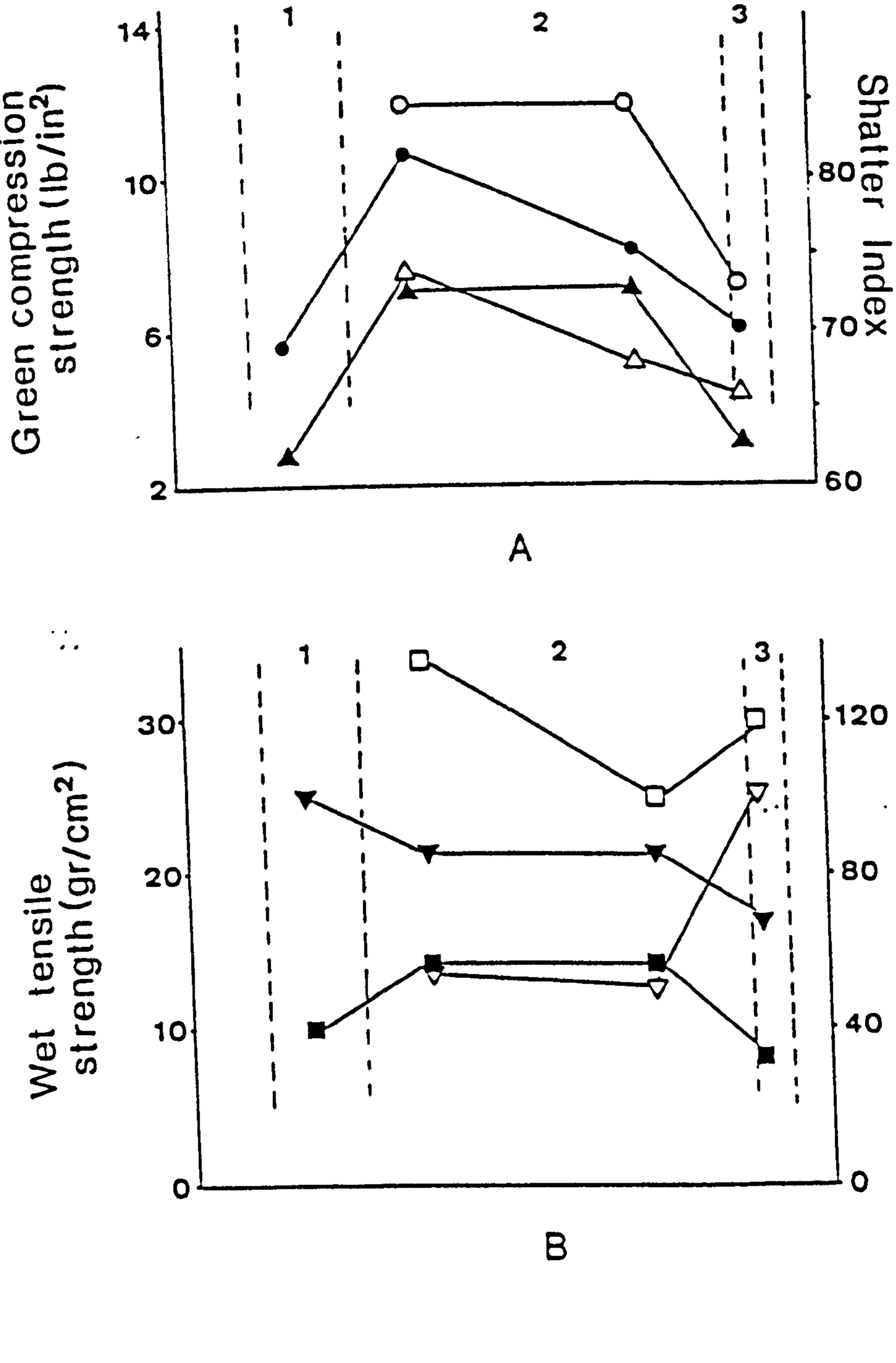

FIGURE 10.4. Variation of the foundry properties in the bentonite in the Prassa deposit Kimolos. 1= smectite + mordenite zone, 2= smectite zone, 3= smectite + opal-CT zone. The solid symbols correspond to the untreated and the empty symbols to the Na-activated bentonites. Key to the symbols: circles = green compression strength, triangles = shatter index, squares = wet tensile strength,inverted trangles = dry compression strength.

hold between the wet tensile strength and the green and dry compression strength (Fig. 10.3 b,d). The wet tensile strength also dislpays a weak linear relationship with shatter index up to the value of 13gr/cm^2. With further increase of the wet tensile strength the shatter index remains constant (Fig. 10.3c). Also in the case of the dry compression strength the samples from the Tsantili, Koufi and Aspro Horio deposits plot separately from the other bentonites (encircled points in Fig. 10.3d).

The compactability of the bentonites is almost always greater than 50% (Table 10.1). Thus, it is higher than the optimum range proposed by the BCIRA (45-50% for the percentage of bentonite and tempering water used in these experiments according to the BCIRA report, 1985). This does not mean that the values obtained are not acceptable for foundry applications, because there are commercial products available in the market like the "BREBOND" with 60% compactability at the same tempering water and bentonite content (Table 10.3). The compactability of the various deposits seems to vary systematically; the bentonites from the Areas 1 and 2 of Milos develop higher compactability than their counterparts from the Area 3 (Table 10.1). Also with the exception of the Loutra deposit, the bentonites of Kimolos have high values of compactability. Finally, the permeability of the Greek bentonites varies between 110 and 160 and does not exhibit systematic trends characteristic of the various areas (Table 10.1)

Compactablity is linearly correlated with shatter index. Thus an increase of compactability is associated by an increase of the shatter index (Fig. 10.3e). The bentonite from the Agrilies deposit which has severely been affected by hydrothermal alteration does not follow the same trend. Compactability is not correlated with permeability. The bentonite from the Agrilies deposit plots away from the other bentonites (Fig. 10.3f). It seems that while permeability varies within broad limits, compactability varies between 45 ans 55%.

Na-exchange modifies the original properties of the bentonites to a certain degree. The most obvious change is the increase of the wet tensile strength up to 350% (Table 10.2). On the other hand permeability systematically decreases in all the bentonites but those from the Tsantili deposit and the lower horizon of the Ankeria deposit. The green compression strength and the shatter index on the other hand do not exhibit a single direction trend. In the areas 1 and 2 of Milos both properties have lower values in the activated samples. Exception to this trend is exhibited by the lower horizon of Ankeria and by the bentonite in the Tsantili deposit, in which the green compression strength is higher in the activated samples. On the other hand, in the Area 3 of Milos the green compression strength increases while the shatter index remains either unchanged or decreases with activation (Table 10.2). In the Kimolos bentonites the green strength increases substantially while the shatter index decreases. Finally in the bentonites from Chios both the shatter index and the green compression strength decrease slightly.

The dry compression strength does not display change in a certain direction. In the Areas 1 and 2 of Milos it increases with the lower horizon of the Ankeria deposit exhibiting the greater increase. The bentonite from the Koufi deposit display a slight decrease which might be explained by the uncertainty introduced by the testing method. In the Area 3 of Milos it decreases in the deposit of Rema and the lower horizon of the Ano Komia deposit and increases in the rest deposits except for that of Mavrogiannis in which it remains unchanged. In the bentonite from Chios it increases slightly while on the contrary in Kimolos it decreases sustantially. An exception to this trend is depicted by the bentonite from the smectite + opal-CT horizon in the Prassa deposit, Kimolos (Fig. 10.4b). Similar to the previous properties change of the compactability after Na-activation does not display a systematic trend (Table 10.2).

The positive linear trend between the shatter index and the green compression strength and between the wet tensile strength and both the shatter index and the green compression strength shown by the untreated bentonites is also observed in their activated counterparts (Fig 10.3g,h,i). Moreover, compactability is correlated with the shatter index (Fig. 10.3j) but not with permeability. Activated bentonites also show a weak negative relationship between the green and the dry compression strength (Fig. 10.3k), Finally a positive linear relationship holds between the wet tensile strength and both the compactability (Fig. 10.3l) and the permeability (Fig. 10.3m). In the latter case the bentonites from the Area 3 of Milos and that of Chios follow a different, although linear trend (encircled points in Fig. 10.3m).

10.5. Discussion.

The results obtained from the Na-exchanged bentonites can be compared with Stephens & Waterworth (1968), Sanders & Doelman (1969) and Hoffman (1985). The process produces materials with unpredictable performance. However it is certain that the wet tensile strength of the activated bentonites is **always** higher compared to that of the raw bentonites which have **different** Ca/Na ratios (see Chapter 7). The same observations were made by Boenisch & Paterson (1967) and Stephens & Waterworth (1968), while Odom (1984) reported that the wet tensile strength of many Ca-bentonites improves with Na-activation.

The significant increase of the wet tensile strength indicates that at least in the case of the Greek bentonites the original Na/Ca ratio does not affect or is not the only factor affecting this property, provided that the activation process is consistent. The same is also true for the untreated bentonites. Thus, the low wet tensile strength developed by the Na-richer bentonites (compared to their countreparts from the other areas) of the Area 3 of Milos might be due to the high opal-CT content in those deposits.

The presence of opal-CT seems to affect the dry compression strength of the untreated bentonites of the Area 3, Milos, in a lesser degree. This might be due to the presence of Mg in the interlayer sites of the smectites present in those deposits (see Chapters 6 and 7). Mg-bentonites are known to develop high dry compression strength but low wet tensile strength (Stephens & Waterworth, 1968). The opal-CT-bearing bentonites behave in exactly the same way, in both the untreated and the activated state, as their counterparts from the Prassa deposit Kimolos which probably contain considerable interlayer Mg, but the values obtained are lower. This is probably due to the absence of opal-CT from the Kimolian bentonites.

Odom (1984) explained the development of higher wet tensile strength by the Na-bentonites assuming that in the Na-smectites the water which migrates from the dehydrated zones forms a rigid structure while in the case of the Ca-Mg smectites it is in a liquid form. Mulla & Low (1983) calculated that the thickness of the water film around Na-smectites which is closely associated with the clay surface, and therefore can be in the Odom's rigid form, is about 40Å. It is also known (see Chapter 7) that smectites saturated with bivalent cations do not swell to more than 19Å in water. Therefore the water film rigidly bound in the Na-smectites is thicker than in the Ca-Mg smectites. It follows that if the water in the condensation zone exceeds the swelling capacity of the Ca-Mg-smectites it probably remains in liquid form leading to a weaker mould as Odom (1984) proposed.

The above discussion indicates that in the Na-activated bentonites the wet tensile strength must be a function of the non-smectite content. Therefore it should be correlated with both the CEC and probably with the swelling index if the smectites have similar crystal chemical characteristics. This will be shown in the following section. Moreover, because the swelling index is affected by the presence of opal-CT the low wet tensile strength of the opal-bearing activated bentonites might be attributed to the presence of this mineral.

The linear relationship between the green compression strength and the shatter index in both the untreated and the activated bentonites is expected because both properties depend on the green bonding properties of the bentonites (BCIRA report, 1985). According to Parkes (1971) an increase of the mould hardness is followed by an increase of the green compression strength, and the shatter index increases first but then it remains constant. This was not observed in this work probably because the limits between which the shatter index varies are rather narrow.

The positive linear relationship between the wet tensile strength and the green compression strength (Fig. 10.3b) has been also reported by Stephens & Waterworth (1968) and implies that the bonding strength of a greensand increases with the ability of the material to withstand collapse in the water condensation zone. Since the green compression strength and the shatter index are linearly correlated, the linear relationship between the wet tensile strength and the shatter index (Fig. 10.3c) is expected. Parkes

(1971) also reported a negative linear relationship between the hardness of the mould and permeability although this was not expected. In this work no definite trend between either the shatter index or the green compression strength and permeability is observed in the untreated bentonites. Finally, the linear positive relationship between shatter index and compactability indicates that the toughness of the mould is related to the flowability of the greensand. This is expected because the bond strength (and therefore the brittleness of the mould) as expressed by both the adhesive and the cohesive strength affects compactability (Caine & Toepke, 1968). Therefore the greensands which provide a denser mould are tougher and can probably withstand handling better than others, which are less compactable. The different behaviour of the bentonite from the Agrilies deposit is probably due to changes caused on the original bentonite by hydrothermal alteration.

The inverse relationship between permeability and compactability at high compactability values observed in the untreated bentonites, might be explained by the assumption that less dense specimens (*i.e*having lower compactability) might have larger pores and thus might be more permeable to gases. Such materials are expected to have lower green compression strength and be less tough.

In the Na-activated bentonites trends between the other properties are also revealed (Fig. 10.3). This possibly indicates that under relatively homogeneous conditions dictated by a more uniform Na/Ca ratio several of the other physical properties measured might be interdependable. Thus the positive linear correlation between the wet tensile strength and both the green compression strength and the shatter index is present also in the activated bentonites, but in the latter case is characterized by higher correlation coefficients.

The negative relationship observed between the dry and the green compression strength in the activated bentonites (Fig 10.3k) has not been explained so far. The scattering of the plotting points observed in this and the other diagrams might be due to the variable degree of Na-activation due to the incomplete disaggregation of the smectite particles. This has been shown in detail in Chapter 8.

In Table 10.3 the physical properties of some industrial products used in the foundry industry at the same bentonite content are presented. Several of the Greek bentonites have properties comparable to those of these products. However, the opal-CT-bearing bentonites (Area 3 of Milos, Chios and Loutra deposit, Kimolos) have inferior properties and it is unlikely to be suitable for use in the foundry industry, in both the raw and the activated state. This is due to the low values of the wet tensile strength the shatter index and to a lesser degree the green compression strength.

On the other hand the Na-activated bentonites from the Areas 1 and 2, Milos, Prassa deposit, Kimolos and Fanara deposit Kimolos can certainly be used in the foundry industry. These bentonites develop lower dry strength than HYBOND (Steetley Minerals Ltd), but higher than both the BREBOND (Brett Bentonite Ltd) and the FULLBOND (Laporte)

Table 10.3.

Foundry properties of some commercial products available in the market

Property	HYBOND 100* (Steetley Minerals Ltd)	FULLBOND STANDARD** (Laporte)	BREBOND*** (Brett bentonite Ltd)
Green compression strength (lb/in^2)	9.8	12	11
Dry compression strength (lb/in^2)	80-100	20 (90)	55
Shatter Index (%)	82	70	80
Wet tensile strength (gr/cm^2)	28	30 (35)	- -
Compactability (%)	- -	40	60

* The values refer to 3% tempering water.

** The values refer to 2.5% temprering water. The values in parentheses refer to 3% tempering water.

*** The values refer to 2.5% tempering water.

industrial products. However the values recorded for the HYBOND correspond to 3.5% tempering water, and it is known that the dry strength (which is lower in the Greek bentonites) increases with increasing tempering water. The shatter index of the Greek bentonites varies between those of FULLBOND and BREBOND while their green compressive strength and the wet tensile strength is of the same order as in these materials.

Some opal-CT bearing bentonites from the Area 3 of Milos (Garyfalakaina and Mavrogiannis deposits) as well as the bentonites from Chios might be usable if mixed with other superior products. Such blending might improve the inferior properties of these materials. It is certain that the companies operating in both Milos and Kimolos produce blended materials which are extracted from different deposits.

Finally, hydrothermal activity has also affected the bonding properties of bentonites. The bentonite from the Agrilies deposit which has been affected by hydrothermal alteration (very low pH, deposition of characteristic sulphates, kaolinization of smectite) develops the worst bonding properties and is not suitable for use in the foundry industry.

10.5 Correlation with the swelling and the cation exchange properties.

In the previous discussion it was proposed that the higher wet tensile strength of the Na-activated bentonites compared to their Ca-Mg-counterparts is probably due to the ability of the former to hold more water layers in a rigid manner. Therefore wet tensile strength might be associated with the higher swelling capacity of the Na-bentonites. If this is the case, then it should be correlated with the swelling index. In Figure 10.5a it is clear that the bentonites with low swelling indices develop also low wet tensile strength. However, it is not certain whether a linear relationship holds among the examined materials or they simply plot to different areas of the diagram. All materials which develop low swelling and low wet tensile strength are abundant in opal-CT.

The swelling volume also seems to be correlated with the dry and the green compression strength and the shatter index of the Na-activated materials (Fig. 10.5b,c,d). The relationship holding between the dry strength and the swelling volume is a weak positive one, with the bentonite from the Agrilies deposit, which has been affected by hydrothermal alteration, characetrized by both low swelling index and dry compression strength. The bentonites from the smectite zone of the Prassa deposit, Kimolos and the lower horizon of the Ankeria deposit do not follow the same trend (encircled points in Fig. 10.5b).

In Figure 10.5c the green compression strength seems to be related with the swelling index. One Kimolian bentonite (smectite zone Prassa deposit) and the bentonites from the deposits of Ano Komia and Rema (Area 3, Milos) do not follow this trend

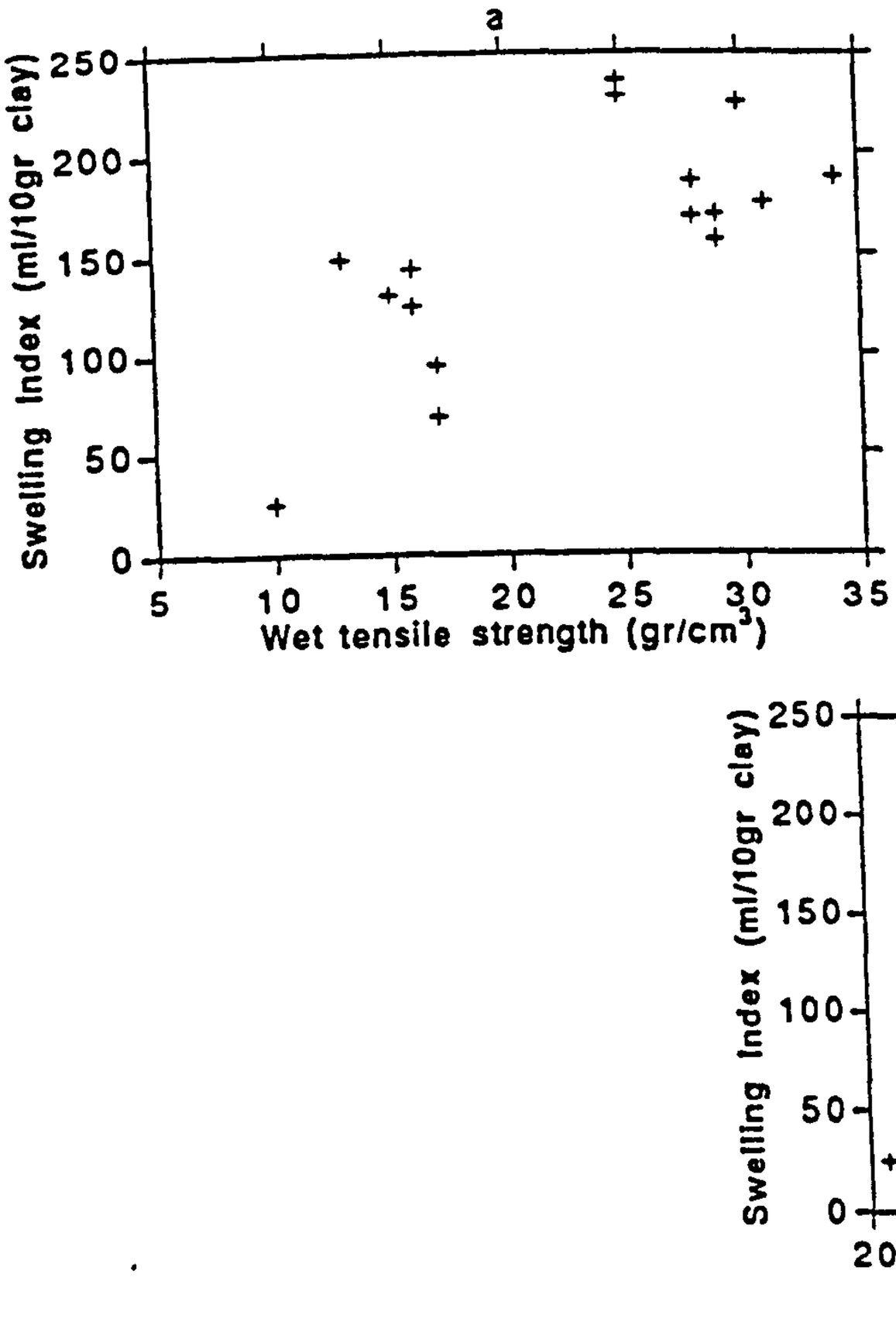

FIGURE 10.5. Correlation between the foundry and the swelling properties of the Greek bentonites. The encircled points in the diagrams 10.5b,c ,d correspond to bentonites which do not follow the trends displayed by the other bentonites.

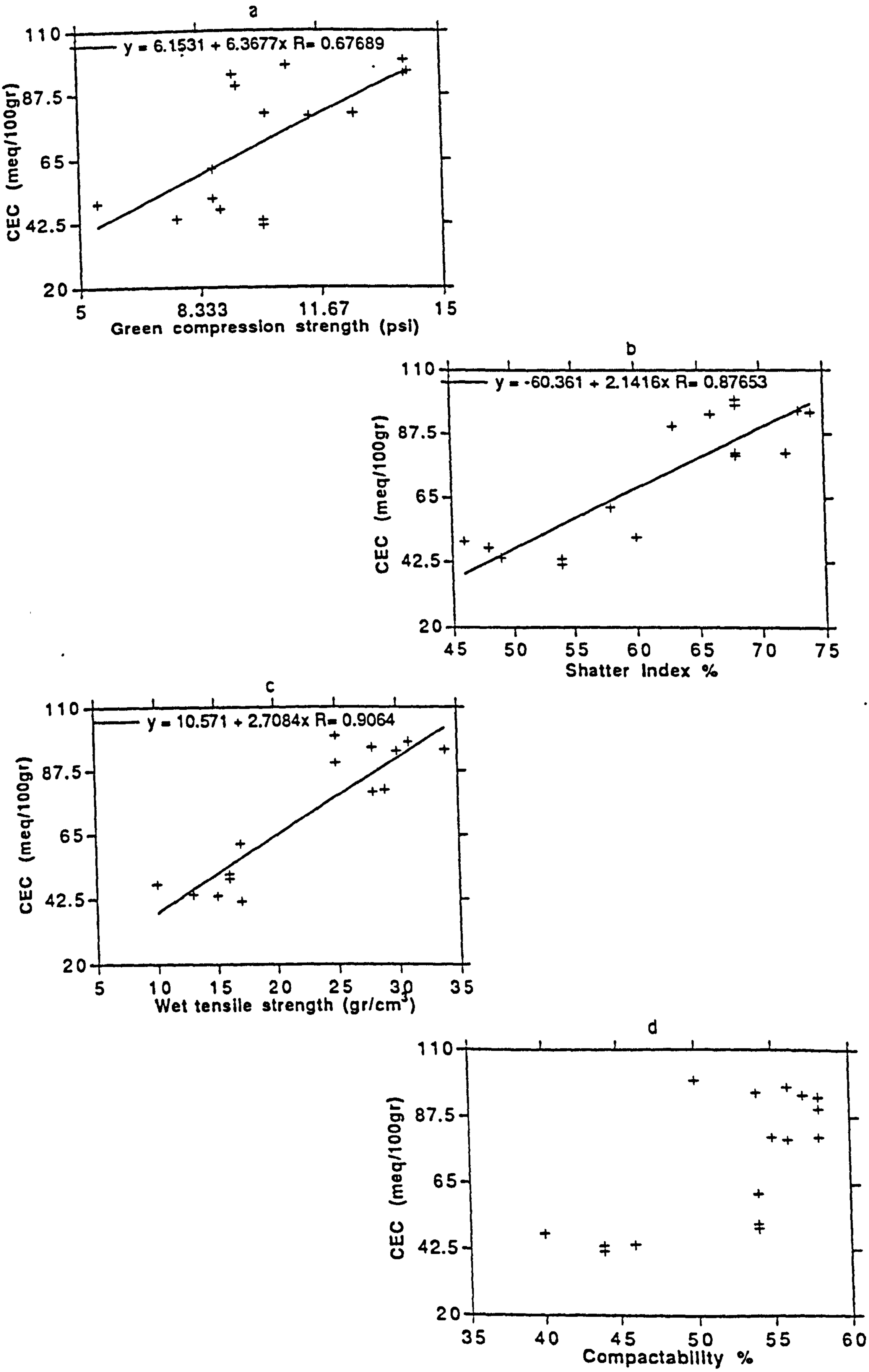

FIGURE 10.6. Correlation between the CEC and the foundry properties of the bentonites.

(encircled points in Fig. 10.3c). A similar weak positive trend seem to hold between shatter index and swelling volume (Fig. 10.5d). Again the bentonites from the Area 3 of Milos (encircled points in Fig 10.5d) do not follow this trend. The same seems to be the case for some Kimolian bentonites characterized by high swelling indices.

The correlation between the swelling volume and the foundry properties of bentonites might be due to the role of swelling on the delamination of the smectite stacks during mulling. For a uniform, even coating of the sand grains to form, the smectite aggregates must be disaggregated (Grim, 1962). Na-smectites swell, promoting disaggregation. Therefore, disaggregation and swelling depend on the success of Na-activation. If activation is successful smectites with better swelling properties might disaggregate easier than others with poorer swelling properties. The bentonites from the Area 3 of Milos which do not follow the linear trends develop swelling volumes higher than expected from their grade. This behaviour has been discussed in detailed in Chapter 8 and is believed to be due to the type of association between the smectite flakes and the opal-CT crystallites which are abundant in these deposits. The behaviour of the Kimolian bentonites has not been explained so far.

The grade of the deposits also affects the properties of bentonites examined in the foundry industry. Positive linear relationships possibly hold between the cation exchange capacity (CEC) and the green compression strength (Fig. 10.6a), the shatter index (Fig. 10.6b) and the wet tensile strength (Fig. 10.6c). No particular relationship holds between the CEC and compactability, although it can be observed that the bentonites which develop low compactability have also low CEC (Fig. 10.6d).

Although due to the small number of samples it is not certain whether the relationships observed in the Figures 10.6a,b,c are indeed linear, it is clear that bentonites with poor grade do not develop good physical properties to be used in foundries. In the present work all the poor grade bentonites are abundant in opal-CT. Therefore it is not known whether the presence of other gangue minerals influence the performance of bentonites in the same manner as opal does. It has been mentioned before that opal crystallites are probably intimately associated with smectite and therefore influence the bonding ability of the clay. It is possible that coarser minerals (feldspars, quartz, zeolites) are not intimately associated with smectite and therefore might not affect the properties of bentonites in the same degree.

10.6. Correlation with the rheological properties.

Fahn (1964), observed a positive relationship between viscosity and durability of a Na-activated bentonite in terms of the green compressive strength. The higher the viscosity of the activated bentonite the higher the thermal resistance of the material. Hoffman (1985)

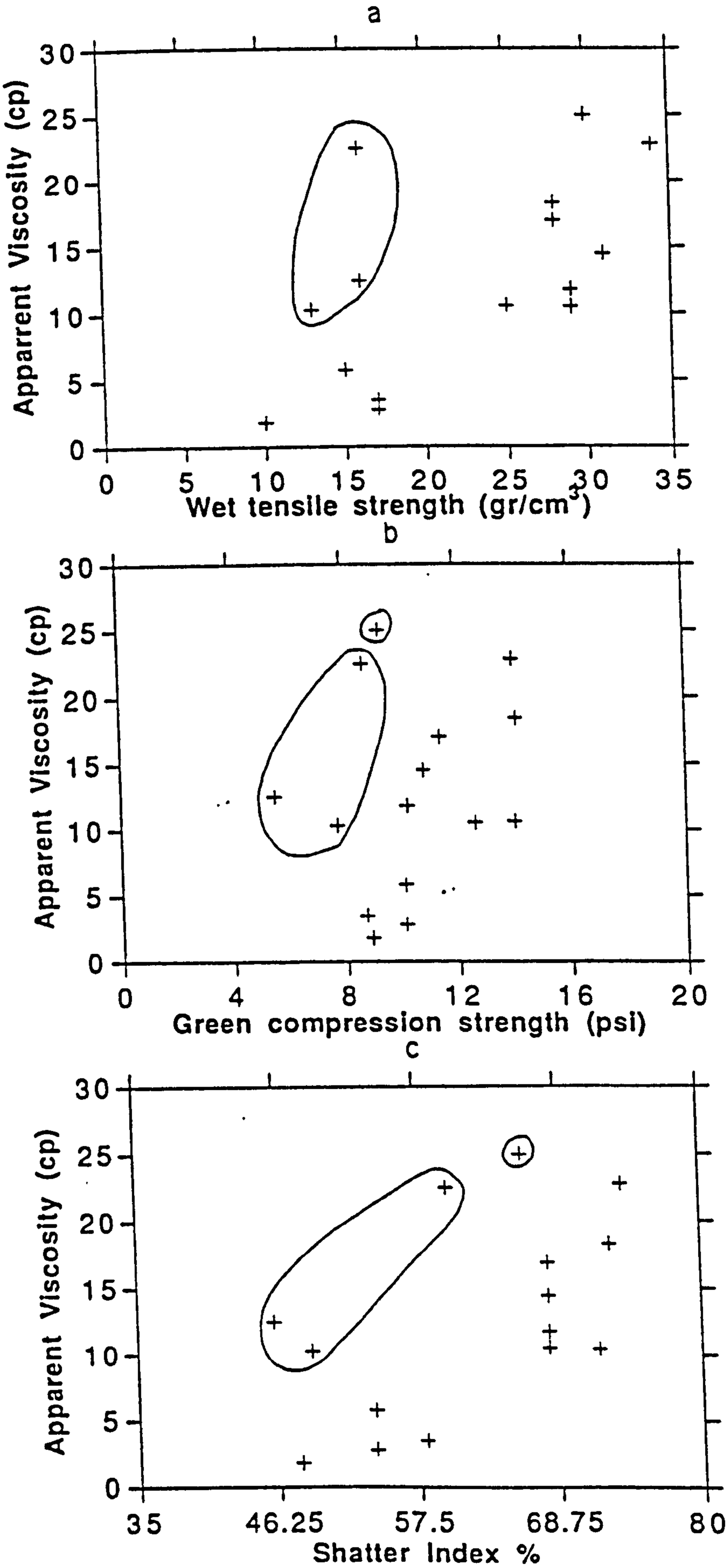

FIGURE 10.7. Correlation between the foundry and the rheological properties of the Greek bentonites. The encircled points correspond to materials which do not follow the trend displayed by the other bentonites.

observed that in the Na-activated state, the high-swelling bentonites are more durable. In this work durability experiments were not performed. However, it has been found that swelling is correlated with various foundry properties (see Section 10.5). Since swelling is also associated with the rheological properties (see Chapter 8), it might be possible that properties like viscosity might be associated with the foundry properties to a certain degree.

In the Figures 10.7a-10.7d apparent viscosity is plotted against the foundry properties of the Na-activated bentonites. Notwithstanding the considerable scattering it seems that an increase of apparent viscosity is associated with increase in the foundry properties of the bentonites. However, the bentonites from both horizons of the Ano Komia deposit and those from the Rema deposit seem to deviate from the overall trend (encircled points). The same is true for one of the Kimolian bentonites. The same samples were found to deviate from the overall trend between the swelling index and the foundry properties, observed for the rest bentonites examined.

The deviation of the Ano Komia and the Rema bentonites from the overall trend might be due to the type of association between the opal-CT crystals and the smectite flakes. In Chapter 8 it was shown that in these bentonites opal-CT forms mainly aggregates isolated from the smectite flakes, while in the rest deposits of the Area 3 of Milos as well as the Chios bentonites it is intimately associated with smectite. However, although they develop relatively high viscosity compared to their grade, their foundry properties are not improved compared to their counterparts from the same area. It is thus inferred that the ability of a bentonite to develop high gel strength does not necessarily affect its bonding properties.

According to the model of Norrish (1954), supported by Callaghan & Ottewill (1974) and Rand *et.al.*, (1980), the development of viscosity depends on the ability of smectite crystallites to swell and form electric double layers repelling each other. On the other hand, the bonding properties probably depend on the ability of the clay to form an even cover around the sand grains and the surface tension between the smectite flakes, as well as the water film surrounding them (Grim, 1962, Caine & Toepke, 1967, 1968, Loto & Omotoso, 1990). If the silica phase is not intimately associated with the smectite flakes then the development of gel strength might not be affected (see Chapter 8). Therefore high viscosity might develop. However in the case of smectite coatings around sand grains, if the silica phase (either in close intimacy with smectite flakes or in the form of aggregates) is intercalated between the clay flakes and the quartz crystals, then the sand-clay bond might not be strong, the linking wedges not rigid, and the clay coating might not be even. It is thus suggested that although the rheological properties might not be affected by the presence of opal-CT (this depending on the type of association between the two phases), the bonding properties always deteriorate. Therefore, although a bentonite of moderate

grade might develop high gel strength, only high grade bentonites might be suitable for the foundry industry.

10.7 Conclusions.

1) The foundry properties of the Greek bentonites vary between broad limits and after Na-activation the performance of most of them is comparable to that of commercial products used in the foundry industry.

2) Na-activation causes rather unpredictable results on the Greek bentonites. From the properties examined only wet tensile strength increases significantly. The other properties do not display a definite increasing or decreasing trend after Na-activation.

3) Green compression strength and shatter index are linearly correlated in both the untreated and the activated bentonites. The same relationship holds between wet tensile strength and both green compression strength and shatter index, and between compactability and shatter index.

4) Bentonites which exhibit high swelling volumes have also good bonding properties. On the contrary, bentonites which do not swell, develop poor bonding properties.

5) The bonding properties of bentonites depend on the grade of the deposits and probably on the type of impurities. The presence of opal-CT is harmful, irrespective of the type of association with the smectite flakes. Only high grade bentonites are suitable for the foundry industry, while bentonites of moderate grade might be suitable in the drilling industry.

CHAPTER 11

SUMMARY-CONCLUSIONS-RECOMMENDATIONS

11.1 Geological characteristics of the Greek bentonite deposits.

The Lower Pleistocene bentonites of Eastern Milos and Kimolos have been formed at the expense of volcaniclastic calk-alkaline rocks, under a submarine environment (presence of bivalve fossils and characteristic sedimentary structures). An exception is the lowermost horizon of the Zoulias deposit and the Bonatsa deposit, Kimolos, in which the parent rock was a lava. The exact nature of the parent rocks is not known with certainty, because the original textural features have been obliterated. However, their geological characteristics indicate that the parent rocks were probably pyroclastic flows. The parent rocks are known with certainty in i) the Prassa deposit, Kimolos (ignimbrite), and ii) the lower horizon of the Loutra deposit, Kimolos (well bedded lapilli-tuff).

Most deposits are composite, consisting of more than one thick bentonite horizons. In all composite deposits the parent rocks were different, indicating that the character of the volcanism changed in geological time. The bentonite horizons are stratiform and several contain pockets of partly devitrified volcanic glass. Opal-rich beds are common and occur at several stratigraphic horizons.

Most the deposits show evidence for the influence of Neogene extensional fault tectonism. Most structural discontinuities postdate the formation of the deposits and many are filled with gypsum and/or Fe-oxides. Syn-sedimentary faults have also been observed in some deposits (*e.g.* Zoulias).

The formation of the bentonite deposits of Milos and Kimolos is probably associated with diagenetic dissolution of the original volcanic glass at low temperature. This is indicated by the existence of abundant authigenic K-feldspar in several deposits. Almost all deposits have been affected by hydrothermal alteration, but this is certainly a later event. Hydrothermal alteration is controlled by structural criteria, mainly faults, and is active still today in the form of solfataras.

The geological characteristics of the bentonite from Chios are significantly different from its counterparts from Milos and Kimolos. The deposit constitutes a particular stratigraphic horizon in the Neogene stratigraphic sequence of the Island. It has a Lower-Middle Miocene age and was formed by subaqueous alteration of volcanic ash deposited in a fluvio-lacustrine environment, at low temperature. The deposit has not been affected by hydrothermal alteration either during or after its formation. The volcanism which produced the parent rocks is associated with the extensional tectonism observed in the Central and Eastern Aegean and Western Anatolia.

11.2. Mineralogical characteristics of the bentonite deposits.

The major mineral phase present in all deposits is dioctahedral smectite, which has been formed both by dissolution of volcanic glass (main source) and by alteration of pyrogenetic phases (Plagioclase and K-feldspar). Except for the Tsantili deposit and the lower horizon of the Koufi deposit, plagioclase is the second most abundant phase in Areas 1 and 2 of Milos. On the other hand opal-CT and/or quartz or cristobalite are abundant in the deposits of Area 3. In the latter deposits K-feldspar is abundant also. In Kimolos the dioctahedral smectite coexists with zeolites, plagioclase and/or K-feldspar. Zeolites have been identified also in Milos in the Garyfalakena deposit, in the Zoulias deposit and in the Ankeria deposit. In the Chios bentonite smectite is associated with carbonates (mainly dolomite) and opal-CT. Carbonates are abundant also in the Tsantili deposit, Area 1, Milos.

Two types of K-feldspar have been recognized in the deposits examined. A pyrogenetic (igneous) one and an authigenic K-feldspar. The former displays variable degrees of replacement by smectite and contains Na and Ca, while the latter occurs in the form of small, euhedral crystals. It contains only K as the main cation balancing the substitution of Si by Al and its XRD pattern has the characteristics of high-sanidine. Its presence indicates that the alteration of the parent material took place at low temperature.

Both plagioclase and pyrogenetic K-feldspar contain abundant Mg in their structure which in several occassions exceeds 1%. This high Mg-content has probably been introduced in the structure of the feldspars during devitrification of the volcanic glass. It probably constitutes the first step of replacement by smectite.

Hydrothermal alteration has contributed to the modification of the original mineralogical assemblages by means of four processes: i) dissolution of the smectite crystals and formation of new phases from the products of the dissolution reaction ii) dissolution of the original smectite and formation of smectite with different layer charge iii) oxidation of the octahedral iron originally present in smectite iv) precipitation of new phases directly from the hydrothermal solutions. The mineral phases which are associated with the hydrothermal alteration are kaolinite, halloysite, illite/smectite, alunite, jarosite, gypsum, barytes and sulphides.

Kaolinite, halloysite, mixed layer illite/smectite and possibly alunite have been formed from dissolution of the smectite. Kaolinite might also been formed as a by-product during the formation of smectite with different layer charge. The product of these dissolution reactions is a) amorphous silica which precipitates in the form of opal-CT or quartz depending on the temperature of the pore solution and b) various cations (alkalis, Ca, Mg, Fe), which form new phases (sulphates, carbonates, sulphides) according to the composition and the Eh/pH conditions of the hydrothermal solution.

Mixed layer illite/smectite has been identified in the Tsantili and the Agrilies deposits in

Milos. Its formation has been triggered by K-metasomatism which is probably associated with the formation of barytes deposits. Temperature and K-availability are believed to be the driving forces for this type of alteration which led to the formation of I/S with R3-type of ordering. The maximum temperature during alteration, estimated from the lowest expandability found, might have been 150-180^{o}C. It is believed that the existence of illite/smectite in a Miloan bentonite might be used for exploration of new barytes deposits.

The zeolites present in the Greek bentonite deposits are mordenite and/or clinoptilolite/heulandite. Mordenite is abundant in the Prassa deposit Kimolos and has variable exchangeable cation chemistry; some mordenites in this deposit are unusually rich in K.

11.3. Crystal chemistry of the smectites.

The crystal-chemistry of the smectites varies between broad limits; therefore, the average structural formulae usually obtained do not provide useful information about the smectites. This compositional variation is believed to be real and not due to mechanical mixture between end-members. This is because the transitions observed are not linear as would be expected had the variation been due to mechanical mixtures, but curvilinear.

In many bentonites transitions between beidellite and Tatatilla montmorillonite and between Tatatilla and Fe-rich montmorillonite through Chambers-montmorillonite has been observed. On the other hand transition between beidellite and Wyoming-montmorillonite and between Wyoming and Cheto montmorillonite have not been found. However, the compositional transition series for both the Wyoming and the Cheto montmorillonite seem to converge close to the Fe-montmorillonite field, indicating the possibility for a common end-member. The compositional trends in beidellites are different than those observed in montmorillonite.

The nature of the parent rocks seems to control the crystal chemistry of the smectites. In the case of intermediate parent rocks Wyoming, Mg-rich Tatatilla, Chambers and Fe-rich montmorillonites are usually formed. Beidellite and Al-rich Tatatilla-montmorillonite are less common. In the case of acidic parent rocks the crystal chemistry usually varies between Tatatilla-montmorillonite and beidellite. Exceptions are the acidic parent rocks in the Prassa and Loutra deposits, Kimolos, in which vigorous water/rock reaction has introduced vast amounts of Mg in the system, thus shifting the composition of smectites to the Tatatilla-Chambers-montmorillonite field boundary. The nature of the parent rock affects mainly the availability of Fe and, to a lesser degree, of Mg.

Smectites derived from intermediate rocks are characterized by almost perfect negative linear relationships between the octahedral cations, especially between Al^{VI} and Fe. A negative relationship has also been observed between Si and Al. On the other hand,

smectites derived from acidic precursors are dominated by an almost perfect negative relationship between Si and Al and to a lesser degree between Al^{VI} and Mg. No systematic relationship has been found between Fe and Al^{VI}.

The compositional variations of smectites observed in the various deposits are believed to represent the significant variations in the pore-water chemistry during the dissolution of the volcanic glass *I.e* the existence of extremely variable microenvironmental conditions. These different conditions might be due to the differential degree of mobility of chemical elements during the smectite formation. This in turn depends on several factors like the f_{O2} (controls the oxidation and thus mobility of iron), pH of the solution, cooling history of the parent rock, permeability of the host rock (especially along fractured zones) and finally composition and temperature of the fluid (sea water, modified sea water, meteoric water, hydrothermal fluid having variable composition).

11.4. Growth mechanisms of smectites and illite- smectites. Possible control of the pore-fluid chemistry by smectite.

Particle size (length, width and thickness) measurements of illite/smectite particles showed that the alteration of smectite to illite begins with dissolution of the smectite flakes and precipitation of lath-like particles 20μm thick. These initially formed particles are unstable and dissolve to more stable ones which are thicker. The smectite-to-illite reaction leads to formation of thicker and wider but shorter particles, characterized by progressively smaller aspect ratios, *I.e* more equant in shape. Lath-like particles having thicknesses smaller than 50Å dissolve progressively probably because they are unstable; the thickness of the unstable particles increases with increasing expandability. Only particles equal to or thicker than 50Å continue to grow. Inasmuch as the illitization reaction proceeds towards the more thermodynamically stable illite, it is believed that the pure illite particles have a minimum 50Å thickness and that they began to form at a maximum expandability of 40% and became abundant at expandabilities lower than 25%.

The use of normalized size histograms with reduced coordinates led to steady state profiles which provide indirect indications about the possibility for an Ostwald-ripening dominating illitization mechanism. The steady state profiles indicate that the precipitation of the illite/smectite laths took place probably under low supersaturation via screw dislocations. TEM evidence indeed showed the existence of growth steps in the illite/smectite crystallites. However, crystal growth proceeding through Ostwald ripening *sensu stricto* is not believed to have taken place because a) the system was fully open, b) K-availability which constitutes one of the major factors for the progress of the reaction is not determined within the system c) existence of other phases except for I/S, like kaolinite, which might be involved in the mass transfer from the dissolving to the grown particles and

d) the introduction of chemical elements other than K might have affected the reaction. Nevertheless, it is believed that the reaction proceeds towards minimization of the surface free energy.

Ostwald ripening-like recrystallization has been observed also in smectites from the various alteration zones of the Prassa deposit, Kimolos, in which smectite was found to have been formed through cannibalistic use of a poorly crystallized precursor. The recrystallization mechanism of smectite has probably been affected by the degree of supersaturation of the pore fluids. This in turn depends on the degree of leaching of the parent glass. In well flushed zones there is a considerable degree of leaching; recrystallization of the smectite crystals takes place at relatively low supersaturation conditions (second order kinetics). On the contrary, in less leached zones indicated by the presence of characteristic phases like zeolites, crystal growth takes place under higher supersaturation conditions, closer to first order kinetics. In the latter case further growth of smectites was retarded by the unfavourable pore fluid chemistry, and mordenite formed instead.

Recrystallization of smectite through an Ostwald ripening-like mechanism might have also affected the pore fluid chemistry and therefore the mineral chemistry of the phases which precipitated out from it. It is possible that the first smectites formed in the Prassa deposit were K-rich and that during recrystallization, they released potassium in the pore fluid. This potassium was consumed during the precipitation of mordenite, which therefore became K-rich. The initially formed mordenite was Na-Ca-rich. It is believed that the control of smectite on the pore fluid chemistry is more important than it is hitherto suggested.

11.5. Chemical changes during the alteration of volcanic glass to bentonite.

The dissolution of volcanic glass by sea water has caused mobilization of several major and trace elements to and from the dissolved glass. On the other hand elements like Al and Ti were found to be essentially immobile. The mobility of all chemical elements is interdependant with the mineral phases which precipitate.

Alkalis are mobile elements and are removed from the dissolved glass during alteration, unless they are bound in zeolites. The relative abundance of alkalies is the main difference between the smectite and the smectite + mordenite zone in the Prassa deposit, Kimolos. In this deposit the almost total depletion of the alkalis from the smectite zone is probably due to the coincidence of this zone with one of the the fractured zones observed in this deposit. The high water/rock ratios prevailing along this zone might have caused mobilization of Na and K. On the other hand, the smectite + mordenite zone is further away from the zone of maximum permeability; therefore water access, and thus alkali-mobilization, has occurred to a lesser degree.

Mg has been introduced in the dissolved area, its source being the sea water. Mg uptake is more pronounced in the case of acidic rocks. However, it is also possible that the degree of Mg-uptake depends on the the water/rock ratio: in the fractured zone of the Prassa deposit the degree of Mg-uptake is very high, while in Area 3 of Milos limited fluid flow led to limited Mg-uptake. The degree of Mg-uptake seems also to control the crystal chemistry of the smectites present and their compositional variation. The behaviour of Ca is different in the different types of rocks: it is depleted from intermediate rocks, but it remains in acidic rocks. Its behaviour is controlled by smectite which does not contain more than 1.5% CaO. Fe was not found to be removed from the system: either it behaves residually or it is redistributed within the system. The product of alteration by sea water is also a gain in $SO_4^=$ and H_2O. The former is bound in sulphates (gypsum, barytes) while the latter contributes to the formation of smectite.

The trace elements, including the rare earths elements, display variable degrees of mobility, controlled by the mineral phases in which they are bound. Zr, Nb, Cr Ni and V are practically immobile, while Zn, Sr, Ba and Rb are very mobile. The behaviour of Th and the LREE is controlled by the presence or/not of characteristic phases (monazite, apatite), while the HREE and Y were found to be mobile.

11.6. Geochemical correlation of the bentonite deposits of Eastern Milos.

The bentonite deposits of the Eastern Milos have been formed from parent rocks which were erupted from different volcanic centres. Therefore they do not constitute parts of a single horizon but of at least five different ones. The bentonites from Tsantili and Aspro Horio deposits, and the higher horizon of the Zoulias deposit have been derived from andesitic precursors, the other horizons from more acidic ones. The bentonites of Ankeria and Koufi deposits, (Area 2), have probably been derived from dacitic precursors. The bentonites from Area 3 of Milos, with the exception of the lower horizon of the Ano Komia deposit have probably been derived from rhyodacitic-rhyolitic precursors. Finally, the lower horizons of the Ano Komia deposit and the Agrilies bentonite have probably been formed at the expense of dacitic rocks.

The deposits of Tsantili, Aspro Horio and the highest (11th) horizon of the Zoulias deposit are probably parts of the same bentonite horizon, and were formed at the expense of the same precursor. The higher horizon of the Ankeria deposit seems to be geochemically different from the 3 lower ones, showing similarities with the massive bentonite horizon of the Koufi deposit, but separation is not unambiguous. The latter bentonite horizon is certainly different from the 3 lower horizons of the Ankeria deposit. The lower horizon of the Koufi deposit is significantly different from the others displaying similarities with the bentonite from the Agrilies deposit. This similarity does not necessarily indicate the

existence of a single horizon because of the existence of constraints like the different character in the smectite compositional variations, unless it is assumed that the microenvironmental conditions causing the differences in the smectite crystal-chemistry were much different in the various part of the horizon during alteration.

The bentonites from Area 3 (the lower horizon of the Ano Komia deposit excluded) have probably been formed at the expense of the same parent material. This assumption is reinforced from the fact that the compositional trends of the smectites present in these deposits are almost identical. This indicates the predominance of almost identical microenvironmental conditions during the alteration of the parent glass.

The previous comments suggest that the areas between the deposits of Aspro Horio, Tsantili and Zoulias (Area 1) possibly contain parts of the same bentonite horizon. It is also possible that bentonite continues under the andesitic dome of Korakia. Similarly, in the Area 3, it is possible that more bentonite deposits exist under the valley between the Garyfalakena and the Ano Komia deposit. It is also very possible that the same bentonite horizon continues under the Demenegaki rhyolitic dome between the deposits of Rema and Garyfalakena, Mavrogiannis and Kato Komia.

11.7. Quality and grade of the bentonite deposits.

The major interlayer cation of the Greek bentonites is calcium. Sodium is abundant in deposits which contain other authigenic alkali-phases, like K-feldspar and/or zeolites. Ca is the main exchangeable cation in the deposits of Ankeria, Tsantili, Aspro Horio, and the main horizon of Koufi, Milos. The lower horizon of Koufi and the deposits from Area 3, Milos contain abundant Na and K. The deposits from Area 3 and the bentonites from Zoulias deposit might also contain Mg. The bentonite in the Agrilies deposit has probably undergone a "natural acid activation" process; the original interlayer cations have been almost completely removed and replaced by H^+. The bentonites of Kimolos contain abundant Mg along with Ca in their interlayer sites, while the role of alkalis is relatively restricted. Finally the bentonite from Chios is a Mg-bentonite.

The crystal chemical characteristics (type of smectite, compositional variation, layer charge) of the smectites present in the bentonites are believed to be very important factors controlling both the swelling and the CEC properties. Under similar crystal chemical characteristics a high grade bentonite is expected to swell more than a low grade one.

The chemistry of the parent rock is important in the sense that it induces an "inherited" factor in the smectite-type. However, bentonites from different precursors might exhibit similar properties if they possess similar crystal chemical characteristics. Since the crystal chemistry of smectites and their compositional variations are probably affected by other factors like the degree of Mg and/or Fe uptake and/or mobilization, the inherited factor

might be obliterated. This is believed to be the reason for the similar behaviour observed between the smectite in the Prassa deposit and the Chios bentonite.

Non-smectitic fine grained mineral phases present in the clay fraction, especially opal-CT, affect the quality of the deposits probably because they impede swelling. Also zeolites induce high ion exchange properties on the bentonites due to their high CEC. Coarse grained authigenic phases like K-feldspars and zeolites do not affect swelling (*e.g.* Tsantili deposit)

The original swelling and CEC characteristics of the deposits might be modified by secondary alteration precesses either by "dilution" of the smectite content (formation of minerals like kaolinite, halloysite, illite/smectite and alunite, at the expense of smectite) or by creation of unfavourable physicochemical conditions (lowering of the pH at very acidic values, thereby increasing edge-to-face flocculation and impeding Na-activation).

The illitization of smectite might cause a by-product "natural Na-activation" of the remaining smectite flakes through a migration of Na-ions released from the altered smectite flakes. This has been assumed because the smectite layers in the illite/smectite phase require considerably less sodium carbonate to obtain their optimum swelling properties than their pure smectite counterparts.

11.8. Rheological properties of the Greek bentonites.

The rheological properties of the bentonites are believed to be a function of the degree of disaggregation of the smectite tactoids. Disaggregation might be influenced by several factors including layer charge, degree of iron oxidation, presence of clay-size impurities, and probably the original distribution of the interlayer cations.

Poor disaggregation leads to insufficient Na-activation imparting poor rheological properties to the clay suspensions, if the parent materials contain Ca-and/or Mg-smectites, like the majority of the Greek bentonites. Under laboratory conditions prolonged high speed stirring might improve disaggregation, but it is unlikely that this technique is applied in practice by the operating companies.

In the case of Wyoming- and Chambers-type montmorillonites iron oxidation is believed to be the most critical factor affecting Na-activation and hence rheological properties. In this sense, it is believed that most of the high grade bentonites of the Areas 1 and 2 of Milos might be suitable for the drilling industry after prolonged exposure under oxidizing conditions. The fact that the operating companies in Greece use the dry climate to reduce the moisture of the original material is believed to lead to a more thorough oxidation of iron. Furthermore, the fact that the viscosity values obtained for several bentonites are close to the lower limits accepted by both the API and the OCMA specifications suggests that with suitable blending, these materials can also be used in the drilling industry.

The bentonites from Area 3 of Milos develop inferior rheological properties, probably due to the presence of opal-CT in close association with smectite, thus impeding the smectite flakes to form a rigid gel. The same is probably the case for the Chios bentonite. The coexistence of abundant beidellite with Tatatilla montmorillonite in most bentonites from Area 3, Milos might also be a reason for the poor rheological properties of these materials (charge localization factor). The significantly improved properties of the Rema bentonite are probably due to the presence of opal-CT aggregates separate from the smectite flakes and to the lack of beidellite. Also, the Kimolian bentonites develop good rheological properties.

Bentonites rich in Ca-Wyoming montmorillonite might develop rheological properties comparable to their Wyoming counterparts (*sensu stricto*), if they are activated successfully. Hence the bentonites from the Aspro Horio deposit, which, notwithstanding their high grade and quality, developed relatively poor rheological properties, might improve their performance.

Hydrothermal alteration affects the rheological properties because it modifies the original mineralogical and physicochemical characteristics of the bentonites. The mineralogical changes include dissolution of smectite and formation of kaolinite, illite/smectite and alunite. Precipitation of phases like baryte and gypsum also takes place. The latter probably deteriorates the rheological properties of the bentonites.

The presence of kaolinite in small amounts does not seem to affect the rheological properties of the bentonites significantly, probably because of the development of strong links between the smectite and the kaolinite flakes. The link between kaolinite and smectite might not be due to a negative face-positive edge attraction, because at the pH ranges that the experiments take place, the clay particles should be entirely negatively charged.

Swelling is closely associated with viscosity, and high viscosity values were obtained from highly swollen bentonites. Such an interdependance between the two properties is expected because the development of gel strength (and thus viscosity) probably depends on the repulsive forces between the expanded smectite particles. However, it is also possible that swelling beyond a certain limit might cause deterioration of the rheological properties.

11.9. Acid activation.

Acid activation increased the surface area of the bentonites examined up to a maximum value after which it decreased. The modification of the surface area is associated with changes in the smectite structure and surface texture and chemistry which occurred during activation. These changes include flattening of the smectite flakes, replacement of the interlayer cations with hydronium (H_3O^+) cations thus increasing the surface acidity,

removal of octahedral cations and dissolution of the exposed silica tetrahedra thus causing precipitation of amorphous silica. The CEC of the bulk sample decreases due to the effective dilution of the smectite content in the sample.

The acid activated bentonites have been rendered efficient for the decolourization of rape seed oil through removal of colouring agents like ß-carotene. This is possibly due to the formation of active acid centres on the surface of the smectite crystallites. These acid centres might be both Brønsted and Lewis; the former formed by deprotonation of hydronium cations present in the interlayer sites, disruption of the Si-O-Al bonds or existence of exposed Al-OH and Si-OH bonds, while the latter from the existence of unsaturated Al^{3+} or Si^{4+} cations.

Although increased surface area is an important feature of the acid activated bentonites, the maximum bleaching capacity of all the materials tested is not associated with maximum surface area. This is probably because dissolution of smectite crystallites beyond a certain point causes collapse of the structure, with subsequent distruction of the active adsorptive sites. The high surface area might partly be due to the amorphous silica, which is by-product of the dissolution reaction.

The optimum decolourization properties for all three bentonites can be obtained with a variety of combinations between acid strength and treating time. The combination which is likely to be preferred in an industrial scale, is the least energy consuming. Therefore shorter treatments with weaker acid are preferable. Under these conditions acid activation of the Chios bentonite might possibly be the easiest and in economic terms the most profitable. It is suggested that the Chios bentonite might provide a well performing bleaching clay. The same is believed to be the case for the bentonite from the Ankeria deposit.

The bentonite from Chios was activated faster than the other materials tested. This might be due to the higher Mg-content of the smectites present (Otay-montmorillonites) as well as to the presence of carbonates which dissolve, thus increasing the effective smectite content and releasing this part of the smectite surface "blocked" along the contact between crystals of these two phases. Mg was found to be the easiest removed element; therefore the active sites for adsorption were created faster. However, the ease with which Mg was removed from the dissolving smectite caused faster collapse of the structure. Hence the optimum combinations of treating time/acid strength are created faster than the rest bentonites tested.

The bentonite from the Rema deposit display good bleaching properties only after prolonged treatment with strong hydrochloric acid. This is believed to be due to the high Al-content of the smectites present (Tatatilla montmorillonites) and the existence of abundant opal-CT. Under these conditions it is unlikely that it might be used successfuly as a bleaching earth, especially when there are materials which can be activated easier.

Both the Chios bentonite and the Ankeria bentonite might be used successfully for decolourization of rape seed oil. However, before use a series of other tests like the determination of the free fatty acid of the bleached oil as well as its acidity might be determined. This is beyond the scope of this project.

11.10. Foundry properties of the Greek bentonites.

The foundry properties of the Greek bentonites vary between broad limits and after Na-activation the performance of most of them is comparable to that of commercial products used in the foundry industry. Hence they can be used successfully as binding agents in the greensands. Also, many of the bentonites which develop relatively poor properties might be blended with superior materials and be used as commercial products. This might be the case for the bentonites from Area 3 of Milos, and the Chios bentonite.

When examined in the raw state, the bentonites from the Prassa deposit, Kimolos, and those from the Ano Komia and the Mavrogiannis deposits, Area 3 Milos, develop high dry compression strength, but low wet tensile strength. This behaviour has been attributed to the presence of abundant exchangeable Mg. With Na-activation it seems to decrease in both Areas with an exception in the Rema deposit (Area 3 Milos).

Na-activation causes rather unpredictable results on the properties Greek bentonites. From the properties examined only wet tensile strength increases significantly. The other properties do not display a definite increasing or decreasing trend after Na-activation.

Green compression strength and shatter index are linearly correlated in both the original and the activated bentonites. This might happen because with increasing bonding capacity of the bentonite the toughness of the mould increases. The same relationship holds between the wet tensile strength and both green compression strength and shatter index, and between compactability and shatter index. The latter indicates that the toughness of the mould is related to the flowability of the greensand, probably because the bond strength affects compactability. Therefore the greensands which provide a denser mould are tougher and can probably withstand handling better than others, less compactable.

Bentonites which exhibit high swelling volumes have also good bonding properties. On the contrary, bentonites which do not swell develop poor bonding properties. Since the swelling properties of the Greek bentonites have been adversely affected by hydrothermal alteration, hydrothermally altered bentonites, like the bentonite of Agrilies, Milos, and the illitized sector of the Tsantili deposit, are not suitable for the foundry industry. The same is the case for bentonites in which devitrification is not complete (Loutra deposit, Kimolos).

The bonding properties of bentonites depend on the grade of the deposits and probably on the type of impurities. The presence of opal-CT is harmful, irrespective of the type of association with the smectite flakes. This might be due to the fact that the presence of

abundant opal-CT either in close association with smectite or present in the form of aggregates affect the development of the bond between adjacent quartz grains. Therefore, only high grade bentonites are suitable in the foundry industry, while bentonites of moderate grade might be suitable in the drilling industry if the development of gel strength is not retarded by the presence of impurities.

11.11. Recommendations for further research.

This research has shed light on several of the characteristics of the Greek bentonite deposits and is believed to have contributed in the understanding of the processes which led to their formation and modified their characteristics thereafter. Moreover, many physical and chemical properties of these deposits have been determined and the acid activation tests showed that the Greek bentonites can be successfully transformed to bleaching earths which can decolourize edible oils. Nevertheless there are certain topics which cannot be exhausted within the limits of the current project. This becomes even more clear if one considers that more than one theoretical models have been proposed in order to explain most of the properties of the bentonites.

The first steps beyond the limits of the current project concern further research on the compositional trends found in the Greek smectites. This can be done by performing a large number of microanalyses on other bentonite materials and compare the results. For example materials like the British smectites (the term bentonite is preferred instead of fuller's earths) might shed light on the obscure relationships observed between the Fe-montmorillonite and the Wyoming and Chambers montmorillonite because they are iron rich. The existence or not of a compositional transition between beidellite and Tatatilla montmorillonite could be established by the use of Analytical Electron Microscopy (AEM). The author's personal opinion is that this transition exists because these two phases are very similar as far as their crystal chemistry is concerned.

The careful preparation of clay samples for TEM examination showed that the illite/smectite particles can be viewed as fundamental particles (Nadeau *et al.*, 1984a,b,c). Since the thickness of the particles is different their composition is expected to be different. Careful EPMA on polished blocks and/or AEM work on specially prepared samples (see Lanson & Champion, 1991, for example) might help to shed light in this field. However the author does not agree with the conclusion of Lanson & Champion (1991) based on AEM techniques about the validity of the fundamental particles' model, merely because even in the AEM techniques the analytical information comes from a depth much greater than the thickness of a fundamental particle.

Pt-carbon coated samples are easily made and with correct interpretation they might provide sufficient information about the nature of the clay materials. On the other hand the

images obtained from HRTEM need to be accompanied by computer simulation images because the lattice fringes obtained depend strongly on the operation conditions. Furthermore the area under observation is restricted and beam damage phenomena are very frequent. However, a combination of the two techniques might assist the solution of the problem concerning the "forced thickness" (during sample preparation) of the fundamental particles. Under this prism, the study of the illitization in the Tsantili deposit will be even more detailed if HRTEM study is performed. This study might be coupled by AEM.

As far as the author can establish the possibility of recrystallization of smectites through an Ostwald ripening-like process has not been reported so far. The same might be said about the influence of this process on the pore chemistry, as was exhibited from the chemistry of the mordenites in the Prassa deposit, Kimolos. Certainly this possibility can be explored further because in the case of the Prassa deposit the mordenite-bearing zone was also abundant in smectite. It is possible that the steady state profiles of smectites from materials richer in zeolites (like the rhyolitic tuffs described by Pe-Piper & Tsolis-Katagas, 1991 in the island of Samos, Greece) are different, matching better the first order profiles because such systems are expected to be relatively closed.

The use of discriminant analysis revealed that the Greek bentonite deposits can be classified into several groups, the members of which cannot be separated. This implies that for several examples a single horizon extends over a large area. The next step is to obtain samples from areas between the deposits to establish the validity of the model proposed. In one case (area between the Tsantili and the Aspro Horio deposits, Milos) a "deposit" has already been developed (see Chapter 6). This is believed to the case in the deposits of Area 3, Milos. Further research is needed to establish the existence of any links between the Agrilies deposit and the lower horizon of the Koufi deposit. It is believed that discriminant analysis might work in the exploration for new bentonite deposits, even in complicated terrains like this of Eastern Milos, provided that the trace elements used are chosen carefully.

The rheological properties of many of the Greek bentonites are poor if their grade and quality are taken into account. For the deposits from the Area 1, and the Koufi deposit, Milos the degree of Fe-oxidation has been invoked as the main factor determining this behaviour. It would be interesting to examine the rheological properties of these materials after various degrees of Fe-oxidation. Further research might also be carried out on the role that the opal-CT with axiolitic texture might exert on the rheological and swelling properties of the bentonites. These textures have been attributed to divitrification of the volcanic glass (Moncure *et al.*, 1981).

The acid activation experiments showed that some Greek bentonites can be used successfully as bleaching earths. It is recommended that the acid treated materials be

treated with acids other than hydrochloric acid. Furthermore they might be tested for their efficiency to decolourize other glyceride oils (*e.g.* soya bean, sunflower, palm, and cotton seed oils). The experiments can be extended to blends of various types of bentonites. For instance it has been found that bentonites containing Al-rich smectites cannot be activated easily. It would be interesting to see the results of acid activation of blends containing bentonites from Chios and bentonites containing Al-rich smectites. Also, an attempt to activate the K-bentonites from the Tsantili deposit would be interesting. At present the materials are not used in any application. Finally, since the structure of the acid activated smectites is not known, techniques like NMR would help to shed light in this obscure field. However care should be taken because the crystal chemistry of the smectites is highly variable.

There is ample field for further research in the foundry properties of the Greek bentonites, especially on their durability. The materials might be heated to high temperatures (500-600^{o}C) and examined for the percentage of loss of their foundry properties. It would be interesting also to try to activate successfully the Wyoming bentonites from Area 1, Milos and compare their durability with the Wyoming bentonites *sensu stricto*. A comparison with the durability of some Na-activated bentonites from Area 2 (contain Cheto montmorillonites and beidellites) should shed light on the role of the crystal chemistry of smectites on the durability of bentonites.

Finally, another area which requires further research is the field of white bentonites. As far as the the author can establish there is little information about the properties of these materials and no information about their mode of origin. There is no published work about the white bentonite deposits of Greece. This research might shed light on the variation of the colour properties of the Greek white bentonites (colour measurement) as well as the reasons for this variation. The latter can be done by examination of the possible factors which might affect colour (particle size and shape, mineralogy, chemistry, organic material). The mode of origin of these materials might be an important factor affecting the quality of these materials. For instance the opal-CT-bearing white bentonite in the Ano Komia deposit, Milos (higher horizon) has certainly been formed through different alteration processes from the opal-CT-free, mordenite-bearing white bentonite in the Prassa deposit, Kimolos (smectite + mordenite zone, in this deposit), although the parent rocks were very similar.

Diagrams used for the determination of the illite content of the illite/smectites present in the Tsantili deposit, Milos (after Srodon, 1980). a, c= random interstratification, b,d= ordered interstratification. The values 16.6, 16.9 and 17.2 correspond to the thickness of the ethylene-glycol complex.

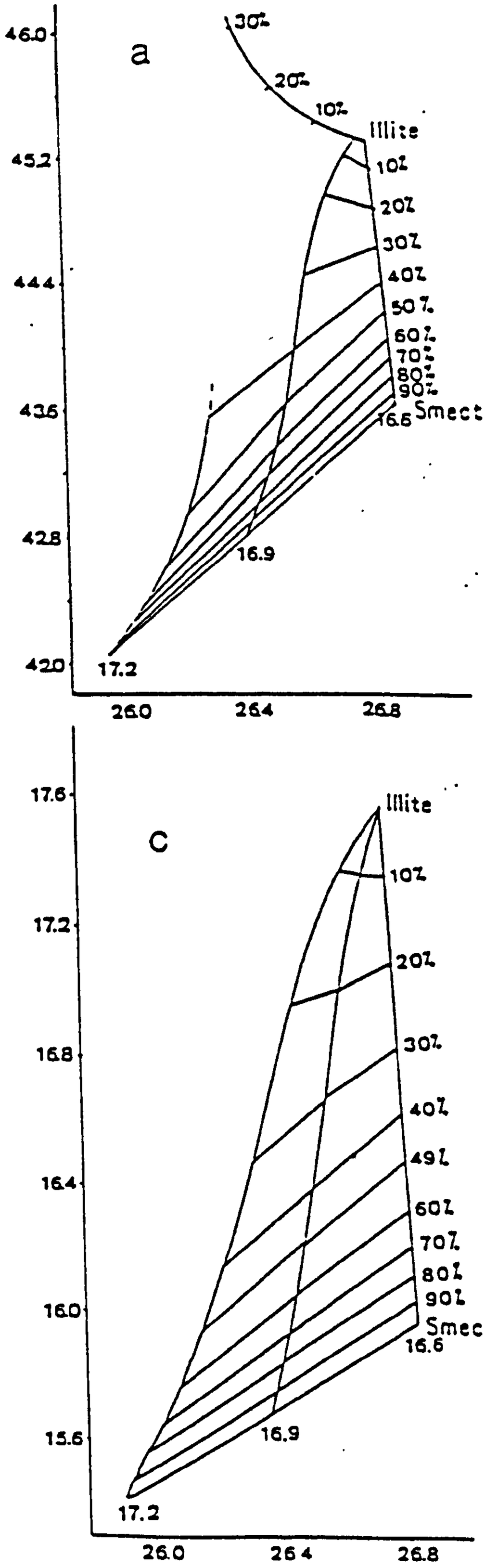

APPENDIX 4.1.1

Relations between compositions and peak positions for illite/montmorillonite interstratification; d spacings in Å (after Reynolds, 1984).

	Random		Ordered	
% Illite	d	d	d	d
0	8.52	5.62	8.52	5.62
10	8.60	5.59	8.60	5.59
20	8.67	5.57	8.71	5.55
30	8.76	5.54	8.82	5.50
40	8.90	5.50	8.93	5.44
50	9.06	5.44	9.03	5.39
60	9.26	5.37	9.21	5.34
70	9.52	5.28	9.40	5.28
80	9.83	5.16	9.66	5.22
90	10.00	5.07	9.99	5.09
100	10.16	5.01	10.16	5.01

APPENDIX 4.1.2

Terminology used to describe the illite-smectite interstratification in orientated, ethylene glycol-treated samples (after Reynolds, 1984, and Moore & Reynolds, 1989).

a) Reichweite (R): Expresses the probability given layer A of finding the next layer B. In the case of a perfectly ordered 50/50 illite/smectite (I/S), given an I (illite) or S (smectite) the other unit should be next in line and the type of ordering is R=1 (designated as R1). The conditions for perfect ordering are also described by the following relationships (Reynolds, 1984):

$P_A + P_B = 1$ (1)

$P_{A.B} = 1$, $P_{A.A} = 0$ and $P_{B.B}=0$ (2)

The relationships in set (2) are called junction probabilities and mean that in the case of perfect ordering the probability of a layer A to be followed by a layer B is 1 **and** the probability of a layer A to be followed by a layer A is 0. If $P_{A.B} = P_{A.A} = P_A$ then the interstratification is random (designated by R0)

In the case that a longer layer sequence is present (*i.e* ISII) then the ordering is R3 meaning that 3 illite layers appear sequentially before the first smectite layer turns up. In other words every smectite layer is surrounded by 3 illite layers. The existence of the intermediate type of ordering (expressed as R2) might not be possible, although (Bethke & Altaner, 1986) there is speculation that it exists. Should this type of ordering exist it would be expressed by the sequence ISI.

b) Recognition of the type of ordering: Random interstratification cannot be identified in terms of migration of the 001 reflection of smectite. Indications for the existence of illite-smectite interstratification are provided from the migration of the 002 and 003 reflections relative to the pure smectite. In other words the reflections are not present in a rational order.

The appearance of a reflection between 6.5 and 8.5^{o} 2θ indicates the existence of ordering. If this reflection occurs at about 6.5^{o} 2θ (*i.e* about 13.3 Å), then the type of ordering is R1. The appearance of this reflection at angles greater than 7^{o} 2θ (especially close to 8^{o} 2θ) indicates the existence of R3 type of ordering. The type and the degree of ordering can also be identified from the digrams of Srodon (1980) (see Fig. 4.4)

APPENDIX 4.2.

Preparation of clay samples for TEM observation.

1. Spread excess liquid celloidin film on one side of a standard microscopic slide. Use 2/3 of the available glass surface and leave the rest 1/3 dry to permit handling. Leave the wet surface for 10 minutes to dry.
2. Use a razor blade to remove the excess celloidin film from the thin sides of the microscopic slide. This is done to enable water penetration between the thin plastic film and the surface of the microscopic slide.
3. **Very carefully,** put the edge of the slide with the film on it into a basin with water. Allow water to penetrate the intersurface slide-film due to surface tension. The film separates from the slide and stays on the water surface.
4. Place the copper grids on the supportive film which stands on the water surface. All grids should be placed with the shiny side in contact with the film. Then using a piece of paper (a piece of newspaper is suitable) cover the grids (the dull side). Water moistens the paper from the edges and advances towards the middle of the paper.
5. When the paper is sufficiently wet the copper grids are visible through its moist surface. Use a pair of twizzers and carefully remove the paper from water. The copper grids are stuck on the surface of the paper having the supportive plastic film on their surface. Allow them to dry. The grids are ready for use.
6. Separate the desired clay fraction with normal sedimentation methods. The suspension should be well dispersed *i.e* stable, to avoid settling of certain particle sizes. In the case of smectites, the use of Na-polymetaphosphate as a deflocculant will help. Dilute the concentrated clay suspension with distilled water. There is not a fixed dilution ratio but it is at least 1:40-1:60,70 according to the concentration of the suspension.
7. With a dropper, remove a small volume of the diluted suspension and put half a drop on an already prepared copper grid. Allow the clay particles to settle for 15 minutes and then use the tip of a sheet of paper to remove the excess water from the grid. Allow the grid to dry, coat it with carbon and examine the grid in the TEM. If the clay particles are not separated, dilute the suspension further and try again. It is a *try and error method.*

APPENDIX 4.3.

Preparation of Pt-shadowed clay samples for TEM observation.

1. The method uses freshly cleaved mica as a supportive substrate for the clay particles on the copper grids, instead of celloidin film.
2. Using two pairs of twizzers, carefully separate a freshly cleaved mica surface. Separation of the mica flakes is facilitated (especially when they are placed into water) if their edges have been previously cut by a pair of scissors to remove any bended areas.
3. Spread the diluted clay suspension on the top of the mica flakes and allow it to dry. Bend a thick tungsten metal wire in "V" shape and wind a small amount of Pt-wire around the tip of the W-wire. Place the W-wire with the Pt-tip in the coating unit and adjust the angle that the Pt-tip faces the mica flakes with a carefully measured angle. Usually 10^{o} is the optimum angle (Nadeau & Tait, 1987). Evaporate the Pt-metal under vacuum to obtain Pt-shadowing.
4. After Pt-shadowing, carbon coating is applied, with the carbon source (graphite) placed perpenticular to the sample-bearing stage. The flakes are ready for separation of their clay-bearing surfaces.
5. The carbon coated an Pt-shadowed cleaved mica faces are placed carefully in a basin with water by means of suitable twizzers. Water penetrates under the mica surface and a thin film floats on the water surface. The rest mica sinks in the water volume.
6. By means of twizzers place one by one the copper grids underneath the floating mica film (in the water volume) and carefully "fish" a part of the film. The delicate film separates easily into segments. Repeat this for the rest of the grids. Allow the grids (with the mica film on their surface) to dry and examine them in the TEM. Pt-shadowing enables the measurement of the clay particle thickness using the shadow of the particle observed under the TEM, by means of the following equation:

$$T=(l \times \tan a)/m$$

where T is the thickness of the particle l is the shadow length a is the shadowind angle and m is the magnification used.

APPENDIX 4.4.

Preparation of clay samples for HRTEM.

1. The sample preparation is based on the method of Lee et al. (1975) and Bell (1986), modified G. Christidis with the help of S. and E. Roberts at the E.M lab of the Biology department, University of Leicester.
2. Precautions: Preparation involves the use of carcinogenic and suspected carcinogenic organic reagents. Attention has to be paid a) as far as the preparation of the embedded resin is concerned and b) about the disposal of the waste, unpolymerized organic liquids.
3. Put Spurr Low-viscosity embedded medium in flat moulds up to the middle of the moulds. Allow the resin to cure at low temperature.
4. Pipette the clay suspensions on the half filled moulds and place them under vacuum for 3 days to remove the excess water by evaporation.
5. Fill the rest of the moulds with Spurr resin up to the top. The clay is now sandwitched between the two layers of resin. The moulds are cured overnight at 60^{o}C under partial vacuum.
6. Remove the embedded clay samples from the moulds and place them in Beem capsules. Fill the capsules with more Spurr resin and cure them for an additional 24-72 hours until the epoxy has the desired hardness. The epoxy embedded clay samples are ready for microtome sectioning.
7. Trim the embedded samples with a razor blade until they aquire the shape of a truncated pyramid. Cut several ultra-thin (500-1000Å) microtome sections using a glass knife. The sections are cut perpenticular to the *00l* planes. Collect the sections on film-coated (see Appendix 4.1.) copper grids and apply a thin carbon coating. The sections are ready for HRTEM observation.

Problems during the preparation of the microtome sections.

Insufficient cure of the resin might impart brittleness on the resin embedded samples, rendering microtome sectioning difficult. Also, insufficient water evaporation from the clay film might cause bubbling which leads to spalling during trimming. It is preferrable to let the resin cure during the various stages, and water to evaporate, for maximum time.

APPENDIX 4.5.

Preparation of clay samples for Infra Red Spectroscopy.

1. Separate the less than 2μm clay fraction using conventional sedimentation techniques. The separated clay powder is dried overnight at 110^{o}C. The clay powder is allowed to cool in a desiccator where it is kept thereafter.
2. Take a fixed amount of the clay fraction (1-3mg is sufficient) and mix it with 150-180mg of an alkali halide (usually KBr is the most appropriate). Thorough mixing is obtained if the clay-halide mix is ground gently with an agate pestle and mortar until a fine powder is obtained. The alkali-halide should be stored in an oven to avoid water adsorption, because it is highly hydroscopic.
3. The clay-halide mix is pressed in an evacuated dye to get a thin 13mm diametr disc. The thin disc is almost transparent.
4. Store the discs in a desiccator to avoid water adsorption. The materials are ready for Infra Red Spectroscopy.
5. It may be necessary to dry the discs in an oven at 150^{o}C overnight to remove absorbed water, the absorption bands of which interfere with some absorption bands important for clay mineral identification. In this case the dried discs are allowed to cool in a desiccator before I.R examination. In the present study this was not necessary.

APPENDIX 4.6

Microprobe analyses of smectites present in the Greek bentonites

Sample	SM16	SM16	SM16	SM16	SM16	SM16	SM16	SM16	SM16	SM16	SM16	SM16
Quarry	BMAN	BMAN	BMAN	BMAN	BMAN	BMAN	BMAN	BMAN	BMAN	BMAN	BMAN	BMAN
SiO2	57.01	52.34	53.52	59.72	58.39	54.91	56.87	50.77	52.19	55.03	57.44	58.72
Al2O3	21.51	18.47	18.19	21.86	21.50	18.70	19.85	18.22	17.82	19.11	20.96	20.85
Fe2O3	1.63	4.75	5.08	3.38	3.61	5.41	4.89	2.13	4.46	4.59	3.97	3.85
MgO	4.47	3.93	3.90	4.98	5.18	4.29	4.21	3.57	3.77	4.21	4.59	4.65
CaO	1.65	1.72	1.52	1.45	1.73	1.62	1.66	1.60	1.80	1.78	1.38	1.57
Na2O	0.45	0.69	0.54	0.64	0.78	0.46	0.59	0.45	0.49	- -	0.90	0.47
K2O	0.24	- -	0.51	0.21	0.41	- -	- -	- -	- -	- -	0.61	- -
Total	86.96	81.90	83.26	92.24	91.60	85.39	88.07	76.74	80.53	84.72	89.85	90.11

Sample	SM16	SM16	SM16	SM16	SM16	SM16	SM16	SM16	SM16	SM16	SM16	SM16
Quarry	BMAN	BMAN	BMAN	BMAN	BMAN	BMAN	BMAN	BMAN	BMAN	BMAN	BMAN	BMAN
SiO2	55.61	56.16	52.34	57.50	49.27	52.32	53.68	53.22	56.05	54.65	54.22	54.95
Al2O3	20.18	19.72	17.41	20.72	18.98	19.55	19.87	20.33	22.61	21.54	20.71	22.88
Fe2O3	3.19	5.18	5.18	3.69	0.52	1.27	1.70	1.47	0.76	0.78	1.32	1.70
MgO	4.30	4.50	3.59	4.54	3.08	4.06	3.81	3.67	3.65	4.04	3.91	3.98
CaO	1.31	1.82	1.43	1.83	1.39	1.45	1.61	1.36	1.26	1.64	1.90	1.88
Na2O	0.60	0.75	0.42	0.87	0.50	0.59	0.46	0.45	0.41	0.55	0.46	0.58
K2O	0.44	- -	- -	0.22	2.47	- -	- -	- -	- -	0.67	0.70	0.36
Total	85.63	88.13	80.37	89.37	76.21	79.24	81.13	80.50	84.74	83.87	83.22	86.33

Sample	SM16	SM16	SM16	SM16	SM25	SM25	SM25	SM25	SM25	SM25	SM25	SM25
Quarry	BMAN	BMAN	BMAN	BMAN	BMAN	BMAN	BMAN	BMAN	BMAN	BMAN	BMAN	BMAN
SiO2	53.31	56.03	53.51	55.03	57.24	56.30	58.64	56.44	55.66	55.85	57.91	59.27
Al2O3	20.20	23.00	21.50	21.55	25.14	24.51	20.32	23.00	18.93	18.46	23.05	22.28
Fe2O3	2.13	1.90	1.18	1.31	0.88	1.12	2.41	1.29	5.81	5.60	0.96	2.90
MgO	4.00	4.07	3.60	3.86	3.48	3.45	4.52	3.26	4.42	4.36	3.98	4.72
CaO	3.49	1.64	1.80	1.44	1.54	1.65	1.76	1.51	1.88	2.08	1.83	1.79
Na2O	0.69	0.71	0.44	0.81	0.49	0.45	0.44	- -	0.56	- -	- -	0.51
K2O	0.29	0.44	0.93	0.68	0.26	- -	- -	- -	0.31	0.22	- -	- -
Total	84.11	87.79	82.96	84.68	89.03	87.48	88.09	85.50	87.57	86.57	87.73	91.47

Sample	SM25	SM25	SM25	SM25	SM25	SM25	SM25	SM25	SM25	SM25	SM25	SM25
Quarry	BMAN	BMAN	BMAN	BMAN	BMAN	BMAN	BMAN	BMAN	BMAN	BMAN	BMAN	BMAN
SiO2	57.10	59.23	53.47	54.68	58.50	54.28	53.90	55.14	57.69	58.41	57.71	54.83
Al2O3	22.31	20.89	22.15	23.52	22.99	17.95	16.93	18.38	21.68	19.33	22.11	17.58
Fe2O3	3.88	5.17	1.00	1.10	1.23	5.08	5.68	5.15	3.18	5.32	2.42	5.60
MgO	4.53	4.88	2.95	2.71	3.08	3.22	3.89	3.64	3.19	3.91	3.51	4.23
CaO	1.83	2.41	1.54	1.81	2.16	2.09	1.92	2.16	1.75	2.19	1.72	1.94
Na2O	- -	0.81	- -	- -	- -	- -	0.44	- -	- -	0.43	0.46	0.50
K2O	0.24	0.28	- -	- -	0.45	- -	- -	- -	- -	- -	- -	0.27
Total	89.89	93.67	81.11	83.82	88.41	82.62	82.76	84.47	87.49	89.59	87.93	84.95

Sample	SM25	SM25	SM25	SM25	SM25	SM25	SM25	SM25	SM25	SM25	SM25	SM25
Quarry	BMAN	BMAN	BMAN	BMAN	BMAN	BMAN	BMAN	BMAN	BMAN	BMAN	BMAN	BMAN
SiO2	54.61	58.68	57.47	56.05	60.66	58.06	57.88	58.48	57.15	57.97	56.57	55.12
Al2O3	20.34	21.01	23.15	24.47	20.40	19.54	19.29	19.99	23.73	25.11	23.72	19.10
Fe2O3	2.01	2.16	0.98	1.49	2.47	2.91	5.30	3.30	1.24	1.14	1.57	4.66
MgO	3.64	4.77	2.64	3.61	4.99	4.71	4.25	3.34	3.21	3.31	3.14	3.48
CaO	1.87	2.05	1.47	1.76	2.31	2.36	1.91	1.69	1.74	1.63	1.55	2.42
Na2O	- -	- -	- -	0.51	0.48	0.46	0.47	- -	- -	- -	0.45	0.49
K2O	0.84	0.23	2.43	- -	- -	- -	0.26	- -	- -	- -	- -	0.26
Total	83.31	88.90	88.14	87.89	91.31	88.04	89.36	86.80	87.07	89.16	87.00	85.53

Sample	SM25	SM43	SM43	SM43	SM43	SM43	SM43	SM43	SM43	SM43	SM43	SM43
Quarry	BMAN	BMKF	BMKF	BMKF	BMKF	BMKF	BMKF	BMKF	BMKF	BMKF	BMKF	BMKF
SiO2	52.69	56.24	59.39	58.78	55.76	56.86	56.81	57.69	52.55	55.89	58.23	56.30
Al2O3	17.20	23.50	19.36	20.72	23.91	17.01	16.64	16.95	18.53	27.17	19.33	24.75
Fe2O3	5.97	2.26	4.19	6.12	2.28	5.06	5.09	4.97	3.33	2.33	6.70	2.69
MgO	3.76	3.26	4.72	3.54	2.93	5.36	5.15	5.47	3.55	2.67	4.27	3.15
CaO	2.58	1.12	1.29	1.20	1.39	1.43	1.49	1.37	1.39	1.30	1.78	1.45
Na2O	0.46	- -	0.46	0.49	0.46	0.48	0.45	0.49	0.98	0.42	1.05	0.71
K2O	0.22	0.32	- -	- -	0.24	- -	0.37	0.42	0.53	- -	0.93	- -
Total	82.88	86.70	89.41	90.85	86.97	86.20	86.00	87.36	80.86	89.78	92.29	89.05

Sample	SM43	SM43	SM43	SM43	SM43	SM43	SM43	SM43	SM43	SM43	SM43	SM43
Quarry	BMKF	BMKF	BMKF	BMKF	BMKF	BMKL	BMKF	BMKF	BMKF	BMKF	BMKF	BMKF
SiO2	57.23	57.18	56.47	55.92	54.80	57.08	55.97	56.06	54.42	54.10	55.98	54.92
Al2O3	17.36	20.16	25.33	17.90	17.98	25.26	24.15	24.78	17.57	25.57	18.40	23.15
Fe2O3	5.65	6.32	1.58	2.98	6.59	1.70	2.20	1.96	3.49	2.44	6.36	1.64
MgO	4.43	4.46	2.46	4.10	2.99	2.84	2.34	2.89	4.33	1.94	3.07	2.19
CaO	1.56	2.01	1.33	1.52	1.54	1.38	1.55	1.48	1.62	1.24	1.19	1.83
Na2O	- -	0.87	0.43	- -	0.52	0.54	0.50	0.68	- -	- -	0.48	0.92
K2O	0.65	0.24	- -	- -	0.25	- -	- -	0.23	- -	- -	0.36	0.26
Total	86.88	91.24	87.60	82.42	84.67	88.80	86.71	88.08	81.43	85.29	85.84	84.91

Sample	SM43	SM43	SM43	SM43	SM43	SM43	SM43	SM43	SM43	SM43	SM43	SM43
Quarry	BMKF	BMKF	BMKF	BMKF	BMKF	BMKF	BMKF	BMKF	BMKF	BMKF	BMKF	BMKF
SiO2	57.48	54.57	59.56	60.50	59.05	60.59	59.35	59.14	56.95	59.61	55.19	52.99
Al2O3	25.36	23.10	24.11	20.83	19.86	16.52	19.47	16.43	18.23	19.30	22.66	22.51
Fe2O3	1.96	1.68	2.21	6.41	6.37	10.07	6.59	9.31	7.21	7.60	1.30	3.37
MgO	2.67	2.28	3.10	3.70	3.30	4.06	3.32	3.68	3.25	3.73	1.44	2.58
CaO	1.42	1.40	1.61	1.42	1.58	1.67	1.97	1.39	1.24	1.51	2.43	1.38
Na2O	0.49	- -	0.93	1.54	0.73	0.46	0.66	- -	0.54	0.78	1.58	0.41
K2O	- -	- -	0.72	0.59	- -	0.86	0.77	0.86	0.60	0.67	0.37	- -
Total	89.38	83.03	92.24	94.99	90.89	94.23	92.13	90.81	88.02	93.20	84.97	83.24

Sample	SM43	SM43	SM43	SM66	SM66	SM66	SM66	SM66	SM66	SM66	SM66	SM66
Quarry	BMKF	BMKF	BMKF	BMK1	BMK1	BMK1	BMK1	BMK1	BMK1	BMK1	BMK1	BMK1
SiO2	59.82	60.85	58.06	54.43	55.56	50.73	57.87	56.64	54.57	52.28	57.74	55.01
Al2O3	25.68	18.55	18.03	18.77	17.61	25.77	19.29	18.58	16.49	24.97	20.18	20.70
Fe2O3	1.82	9.19	7.17	2.37	3.46	0.87	4.00	3.47	3.31	0.71	3.81	2.61
MgO	2.73	3.20	3.16	3.36	3.19	1.93	4.01	3.41	2.48	2.04	3.17	2.64
CaO	1.53	1.21	1.38	0.98	1.03	1.00	0.99	1.17	0.95	0.66	0.89	0.97
Na2O	0.67	0.50	- -	- -	- -	- -	0.51	0.42	- -	- -	- -	- -
K2O	- -	1.14	- -	0.41	0.80	- -	0.39	0.33	0.55	0.30	0.95	0.34
Total	92.25	94.64	87.80	80.32	81.65	80.30	87.06	84.02	78.35	80.96	86.74	82.27

Sample	SM66	SM66	SM66	SM66	SM66	SM66	SM66	SM66	SM66	SM66	SM66	SM66
Quarry	BMK1	BMK1	BMK1	BMK1	BMK1	BMK1	BMK1	BMK1	BMK1	BMK1	BMK1	BMK1
SiO2	52.09	56.44	56.94	53.02	55.36	47.73	47.79	56.30	53.93	54.24	53.64	50.06
Al2O3	27.14	17.77	17.89	25.89	20.25	21.46	24.42	18.29	17.47	19.03	21.65	27.29
Fe2O3	1.07	3.45	3.22	0.99	2.60	1.32	0.57	3.95	3.79	4.06	2.07	0.86
MgO	1.53	3.16	3.25	1.51	2.89	1.71	1.03	2.97	2.81	4.10	3.77	3.12
CaO	0.70	0.69	0.86	0.79	1.07	0.89	0.66	0.91	0.92	0.69	0.71	0.62
Na2O	- -	0.55	- -	- -	- -	- -	- -	- -	0.63	0.98	0.78	0.82
K2O	0.28	0.39	0.50	0.26	0.45	- -	0.30	0.84	1.75	1.06	0.95	0.39
Total	82.81	82.45	82.66	82.46	82.62	73.11	74.77	83.26	81.30	84.16	83.57	83.16

Sample	SM66	SM66	SM66	SM66	SM66	SM66	SM66	SM66	SM66	SM66	SM66	SM66
Quarry	BMK1	BMK1	BMK1	BMK1	BMK1	BMK1	BMK1	BMK1	BMK1	BMK1	BMK1	BMK1
SiO2	51.28	49.08	51.59	50.97	52.03	47.91	41.75	47.55	54.37	54.81	52.18	49.58
Al2O3	25.24	27.86	23.20	26.20	23.94	26.25	27.87	26.82	18.54	19.52	18.30	16.83
Fe2O3	1.13	0.87	1.67	1.21	1.34	0.87	0.50	0.72	3.37	3.65	2.91	3.27
MgO	2.95	2.35	3.57	3.00	2.93	2.42	1.40	2.66	4.21	3.50	3.87	3.06
CaO	0.66	0.54	0.62	0.66	0.79	0.44	0.31	0.58	0.59	0.65	0.60	0.79
Na2O	0.43	0.45	0.43	0.94	- -	0.67	0.50	0.53	0.85	0.83	0.76	0.42
K2O	0.78	0.62	0.78	0.93	0.77	0.82	0.51	0.52	1.11	1.55	0.84	0.63
Total	82.47	81.77	81.86	83.91	81.80	79.38	72.84	79.38	83.04	84.51	79.46	74.58

Sample	SM66	SM66	SM66	SM66	SM66	SM66	SM66	SM66	SM66	SM66	SM244	SM244
Quarry	BMK1	BMK1	BMK1	BMK1	BMK1	BMK1	BMK1	BMK1	BMK1	BMK1	BMAG	BMAG
SiO2	46.10	48.85	53.61	50.92	51.39	53.24	52.43	51.00	49.87	52.31	50.43	51.45
Al2O3	16.66	17.48	18.74	17.64	17.50	18.67	18.01	17.37	17.12	17.81	19.47	19.90
Fe2O3	2.21	2.44	3.55	2.88	3.05	2.52	3.03	2.93	3.10	2.70	1.09	0.94
MgO	3.18	3.60	3.62	3.58	3.35	3.65	3.84	3.27	3.33	4.00	2.61	2.68
CaO	0.95	0.66	0.57	0.82	0.74	0.72	0.58	0.69	0.69	0.66	- -	- -
Na2O	0.42	0.44	0.79	0.55	0.42	0.66	0.63	0.51	0.73	0.69	- -	- -
K2O	0.49	0.52	1.75	0.82	1.16	1.34	1.15	0.84	0.77	1.10	- -	- -
Total	70.01	73.99	82.63	77.21	77.61	80.80	79.67	76.61	75.61	79.27	73.60	74.97

Sample	SM244	SM244	SM244	SM244	SM244	SM244	SM244	SM244	SM244	SM244	SM244	SM244
Quarry	BMAG	BMAG	BMAG	BMAG	BMAG	BMAG	BMAG	BMAG	BMAG	BMAG	BMAG	BMAG
SiO2	49.48	51.22	48.68	47.39	52.71	50.85	52.68	52.26	53.34	52.50	51.02	47.78
Al2O3	20.77	20.05	20.53	20.36	21.29	20.80	21.49	22.22	19.89	20.97	21.02	20.87
Fe2O3	1.20	1.10	1.36	1.01	1.77	1.20	1.66	1.51	1.58	1.32	1.40	0.90
MgO	1.83	2.47	2.42	1.87	2.74	2.76	2.50	2.45	2.46	2.87	2.63	2.98
CaO	- -	- -	- -	0.25	- -	0.24	0.28	- -	- -	- -	- -	0.26
Na2O	- -	- -	- -	- -	- -	- -	- -	- -	- -	- -	- -	- -
K2O	- -	- -	- -	- -	- -	- -	- -	- -	- -	- -	- -	- -
Total	73.28	74.84	72.99	70.88	78.51	75.85	78.61	78.44	77.27	77.66	76.07	72.79

Sample	SM244	SM244	SM244	SM244	SM244	SM244	SM244	SM244	SM244	SM244	SM244	SM244
Quarry	BMAG	BMAG	BMAG	BMAG	BMAG	BMAG	BMAG	BMAG	BMAG	BMAG	BMAG	BMAG
SiO2	48.91	50.85	53.09	50.99	49.20	47.97	48.35	50.22	49.71	49.85	49.79	48.99
Al2O3	21.56	20.63	23.11	18.30	22.22	21.64	20.52	20.97	21.49	20.96	21.80	20.74
Fe2O3	1.18	1.06	1.20	1.43	1.30	1.12	0.88	1.17	1.11	1.58	1.19	1.22
MgO	3.50	2.66	3.23	2.49	3.42	3.06	3.41	3.10	3.08	3.26	3.34	2.83
CaO	0.23	0.23	0.22	- -	- -	- -	0.26	- -	- -	0.23	0.22	- -
Na2O	0.65	0.43	- -	0.46	0.60	0.43	0.50	0.43	- -	0.65	0.42	- -
K2O	- -	- -	- -	- -	- -	0.26	0.22	- -	- -	- -	- -	0.33
Total	76.03	75.86	80.85	73.67	76.74	74.48	74.14	75.89	75.39	76.53	76.76	74.11

Sample	SM244	SM244	SM244	SM244	SM244	SM244	SM244	SM244	SM244	SM244	SM244	SM244
Quarry	BMAG	BMAG	BMAG	BMAG	BMAG	BMAG	BMAG	BMAG	BMAG	BMAG	BMAG	BMAG
SiO2	52.03	48.26	48.97	48.32	49.12	50.90	50.91	52.15	51.74	49.82	51.27	50.38
Al2O3	22.65	20.69	21.07	20.75	21.51	22.37	22.23	21.19	21.79	21.07	21.42	20.70
Fe2O3	1.34	1.21	1.48	1.32	1.27	1.44	1.12	1.49	1.34	1.52	0.82	1.50
MgO	3.51	2.23	2.60	3.62	3.40	3.69	3.26	3.15	3.13	2.95	3.22	2.80
CaO	- -	- -	- -	- -	- -	- -	- -	- -	- -	- -	- -	- -
Na2O	0.45	- -	- -	0.48	0.66	0.61	- -	- -	- -	0.52	0.50	- -
K2O	- -	- -	- -	- -	- -	- -	- -	- -	- -	- -	0.81	- -
Total	79.98	72.39	74.12	74.49	75.96	79.01	77.52	77.98	78.00	75.88	78.04	75.38

Sample	SM99	SM99	SM99	SM99	SM99	SM99	SM99	SM99	SM99	SM99	SM99	SM99
Quarry	BMTS	BMTS	BMTS	BMTS	BMTS	BMTS	BMTS	BMTS	BMTS	BMTS	BMTS	BMTS
SiO2	52.35	53.71	53.02	54.00	56.09	52.41	53.28	54.73	52.85	53.50	52.53	52.97
Al2O3	16.55	17.72	16.85	17.68	18.94	17.51	18.50	18.47	17.81	17.63	17.04	20.99
Fe2O3	3.66	2.92	3.95	2.67	2.91	3.53	2.24	3.06	2.38	2.91	2.64	1.76
MgO	3.31	3.22	3.25	3.69	3.40	3.21	2.82	3.69	2.85	3.15	2.95	3.56
CaO	1.42	1.49	1.75	1.52	1.44	1.73	1.94	1.79	1.67	0.88	1.78	1.52
Na2O	0.00	0.56	0.00	0.39	0.41	0.45	0.42	0.57	0.00	0.67	0.00	0.61
K2O	0.00	0.59	0.00	0.25	0.30	1.09	0.81	0.27	0.60	1.46	0.48	0.46
Total	77.29	80.21	78.82	80.20	83.49	79.93	80.01	82.58	78.16	80.20	77.42	81.87

Sample	SM99	SM99	SM99	SM99	SM99	SM99	SM99	SM99	SM99	SM99	SM99	SM99
Quarry	BMTS	BMTS	BMTS	BMTS	BMTS	BMTS	BMTS	BMTS	BMTS	BMTS	BMTS	BMTS
SiO2	52.97	51.18	56.39	54.28	55.09	54.79	56.02	56.01	53.97	53.07	53.55	54.50
Al2O3	16.92	16.38	18.49	17.09	17.53	18.50	18.45	22.48	17.79	17.63	17.36	17.72
Fe2O3	2.95	4.81	4.45	3.71	3.16	2.75	3.63	1.93	2.98	2.63	3.81	3.11
MgO	2.94	3.31	3.56	2.98	3.12	3.43	3.38	3.38	2.88	3.41	3.14	3.15
CaO	1.34	1.59	1.58	1.76	1.72	1.60	1.72	1.27	1.62	1.23	1.38	1.60
Na2O	0.41	0.60	0.54	0.00	0.00	0.60	0.46	0.41	0.00	0.00	0.43	0.00
K2O	0.28	0.36	0.25	0.00	0.00	0.54	0.00	0.71	0.59	0.39	0.35	0.30
Total	77.81	78.23	85.26	79.82	80.62	82.21	83.66	86.19	79.83	78.36	80.02	80.38

Sample	SM99	SM99	SM99	SM99	SM99	SM99	SM99	SM99	SM99	SM99	SM99	SM99
Quarry	BMTS	BMTS	BMTS	BMTS	BMTS	BMTS	BMTS	BMTS	BMTS	BMTS	BMTS	BMTS
SiO2	56.56	54.35	55.96	55.23	53.57	53.57	53.30	53.76	54.34	54.65	53.97	53.56
Al2O3	18.50	17.32	19.79	17.30	16.96	16.93	16.81	20.90	17.16	18.64	17.07	17.51
Fe2O3	4.46	3.83	2.08	3.78	3.51	4.07	4.56	1.81	3.91	2.78	4.58	3.67
MgO	3.92	3.30	2.91	2.84	3.30	3.15	3.27	2.71	3.27	2.91	3.42	3.60
CaO	1.14	1.52	1.32	1.83	1.72	1.56	1.43	1.69	1.51	1.59	1.59	1.38
Na2O	0.37	0.52	0.00	0.00	0.00	0.00	0.43	0.44	0.36	0.45	0.50	0.52
K2O	0.39	0.31	0.91	0.00	0.50	0.00	0.26	0.00	0.00	0.61	0.23	0.33
Total	85.34	81.15	82.97	80.98	79.56	79.28	80.06	81.31	80.55	81.63	81.36	80.57

Sample	SM99	SM99	SM99	SM114	SM114	SM114	SM114	SM114	SM114	SM114	SM114	SM114
Quarry	BMTS	BMTS	BMTS	BMAH	BMAH	BMAH	BMAH	BMAH	BMAH	BMAH	BMAH	BMAH
SiO2	54.21	54.89	54.56	45.49	46.87	50.17	46.84	46.33	44.67	48.71	45.94	47.18
Al2O3	21.55	18.47	18.39	13.11	13.41	16.49	14.25	13.23	15.05	14.72	15.53	15.36
Fe2O3	1.62	2.81	2.95	5.59	5.19	3.47	4.02	5.22	2.81	4.46	2.99	3.33
MgO	2.89	3.20	3.40	3.17	2.88	3.17	3.01	2.94	2.67	3.40	2.82	3.18
CaO	1.35	1.68	1.29	1.23	1.44	1.50	1.39	1.46	0.86	1.46	1.10	1.29
Na2O	0.00	0.00	0.00	0.48	0.46	0.66	0.64	0.71	0.48	0.40	0.84	0.41
K2O	0.78	0.51	0.75	0.23	0.25	0.36	0.26	0.47	0.67	0.00	0.22	0.00
Total	82.40	81.56	81.34	69.30	70.50	75.82	70.41	70.36	67.21	73.15	69.44	70.75

Sample	SM114	SM114	SM114	SM114	SM114	SM114	SM114	SM114	SM114	SM114	SM114	SM114
Quarry	BMAH	BMAH	BMAH	BMAH	BMAH	BMAH	BMAH	BMAH	BMAH	BMAH	BMAH	BMAH
SiO2	46.84	46.12	47.79	44.35	46.21	49.08	49.48	47.02	47.62	49.28	46.73	46.64
Al2O3	15.93	14.45	14.65	13.75	13.52	16.15	15.05	15.49	14.13	15.30	14.04	14.68
Fe2O3	3.73	4.28	4.70	5.87	4.76	3.22	4.60	3.73	4.90	4.58	4.90	4.15
MgO	3.16	3.03	3.31	3.86	2.80	2.92	3.30	2.82	2.78	3.19	2.84	2.99
CaO	1.25	1.07	1.17	0.94	1.27	1.26	1.29	1.23	1.38	1.58	1.18	1.25
Na2O	0.63	0.48	0.72	0.00	0.57	0.00	0.82	0.60	0.00	0.69	0.55	0.52
K2O	0.40	0.29	0.00	2.24	0.42	0.58	0.68	0.52	0.27	0.41	0.22	0.32
Total	71.94	69.72	72.34	71.01	69.55	73.21	75.22	71.41	71.08	75.03	70.46	70.55

Sample	SM114	SM119	SM119	SM119	SM119	SM119	SM119	SM119	SM119	SM119	SM119	SM119
Quarry	BMAH	BMAH	BMAH	BMAH	BMAH	BMAH	BMAH	BMAH	BMAH	BMAH	BMAH	BMAH
SiO2	45.39	53.84	54.92	54.16	56.69	54.48	54.64	53.44	52.81	53.91	59.93	58.31
Al2O3	15.38	18.65	18.49	20.44	18.69	17.13	18.78	17.63	19.44	17.77	18.43	20.02
Fe2O3	3.21	2.42	2.93	1.68	2.99	4.81	3.52	3.98	1.81	3.09	5.95	4.51
MgO	2.54	3.04	3.43	3.44	3.57	3.65	3.33	2.95	3.62	3.32	3.66	3.53
CaO	1.05	1.03	1.06	1.06	1.22	1.44	1.02	1.21	1.09	1.34	1.01	1.00
Na2O	0.59	0.65	0.00	0.71	0.59	0.49	0.81	0.38	0.75	0.00	0.66	0.50
K2O	0.32	0.00	0.00	0.00	0.00	0.00	0.00	0.00	0.00	0.00	0.74	0.77
Total	68.48	79.63	80.83	81.49	83.75	82.00	82.10	79.59	79.52	79.43	90.38	88.64

Sample	SM119	SM119	SM119	SM119	SM119	SM119	SM119	SM119	SM119	SM119	SM119	SM119
Quarry	BMAH	BMAH	BMAH	BMAH	BMAH	BMAH	BMAH	BMAH	BMAH	BMAH	BMAH	BMAH
SiO2	60.21	61.03	58.14	55.94	59.65	51.41	53.81	50.46	52.33	52.50	54.87	54.15
Al2O3	19.56	19.24	17.88	17.74	19.22	16.49	18.92	18.81	19.19	17.02	19.69	19.10
Fe2O3	4.78	5.19	5.97	6.47	5.12	5.51	5.59	2.49	2.91	4.96	2.56	2.46
MgO	3.94	3.94	3.51	3.36	3.73	2.25	3.29	2.58	3.06	3.04	2.59	2.89
CaO	0.83	0.98	1.08	0.87	1.12	1.15	1.06	1.26	1.20	1.28	1.20	1.34
Na2O	1.03	0.95	0.73	0.47	0.94	0.63	0.70	0.47	0.77	1.39	0.51	0.50
K2O	0.00	0.50	0.50	0.41	0.38	1.67	1.55	0.00	0.26	1.69	0.00	0.77
Total	90.35	91.83	87.81	85.26	90.16	79.11	84.92	76.07	79.72	81.88	81.42	81.21

Sample	SM119	SM119	SM119	SM119	SM119	SM119	SM119	SM119	SM119	SM119	SM119	SM214
Quarry	BMAH	BMAH	BMAH	BMAH	BMAH	BMAH	BMAH	BMAH	BMAS	BMAH	BMAH	BMZL
SiO2	53.49	53.07	56.09	51.18	53.25	60.62	59.75	53.37	58.92	54.62	52.69	52.13
Al2O3	19.19	18.96	20.47	17.91	18.83	19.35	21.31	19.57	21.25	20.52	17.59	18.05
Fe2O3	2.41	2.92	2.82	1.44	2.51	5.46	3.58	2.47	2.52	5.98	2.76	4.18
MgO	3.36	2.70	3.45	3.80	3.20	3.59	3.56	3.28	2.94	5.32	3.42	3.61
CaO	1.35	1.18	1.24	0.45	1.29	1.05	0.96	1.40	0.95	1.13	1.38	0.89
Na2O	0.60	0.45	0.79	0.63	0.75	0.71	0.92	0.51	0.50	0.75	0.53	0.75
K2O	0.33	0.72	0.00	2.27	0.23	0.90	0.36	0.00	0.00	2.04	0.00	0.25
Total	80.73	80.00	84.86	77.68	80.06	91.68	90.44	80.60	87.08	90.36	78.37	79.86

Sample	SM214	SM214	SM214	SM214	SM214	SM214	SM214	SM214	SM214	SM214	SM214	SM214
Quarry	BMZL	BMZL	BMZL	BMZL	BMZL	BMZL	BMZL	BMZL	BMZL	BMZL	BMZL	BMZL
SiO2	54.94	55.35	53.08	53.05	54.90	54.31	53.07	53.49	53.57	51.98	52.64	52.58
Al2O3	17.38	18.62	17.68	16.45	16.54	16.57	16.22	17.85	17.64	16.46	16.83	18.20
Fe2O3	5.59	4.99	4.57	6.11	6.06	4.12	5.85	4.97	4.47	3.80	3.88	3.50
MgO	3.91	3.64	3.83	3.39	3.70	3.55	3.78	3.21	4.02	3.35	4.00	3.77
CaO	0.96	0.86	0.96	0.72	1.07	1.33	0.82	1.07	0.53	0.91	0.89	0.66
Na2O	0.68	0.43	0.00	0.71	0.45	0.72	0.68	0.58	0.67	0.55	0.53	0.71
K2O	0.27	0.41	0.63	0.00	0.25	0.96	0.00	0.24	0.00	0.22	0.00	0.00
Total	83.73	84.30	80.75	80.43	82.97	81.56	80.42	81.41	80.90	77.27	78.77	79.42

Sample Quarry	SM214 BMZL	SM214 BMZL	SM214 BMZL	SM214 BMZL	SM214 BMZL	SM214 BMZL	SM214 BMZL	SM228 BMZL	SM228 BMZL	SM228 BMZL	SM228 BMZL	SM228 BMZL
SiO2	51.36	52.08	54.42	52.98	51.66	53.09	53.09	56.43	56.21	53.28	53.91	52.58
Al2O3	17.19	17.20	17.97	17.12	17.32	17.08	17.08	21.39	18.91	16.81	21.37	20.26
Fe2O3	3.88	3.12	5.58	5.75	3.19	4.10	4.10	2.33	4.02	6.03	1.79	1.61
MgO	3.52	3.46	3.55	3.27	3.75	4.11	4.11	4.58	4.68	3.88	4.59	3.86
CaO	0.87	0.81	0.99	0.81	0.63	0.98	0.98	1.23	1.03	0.91	1.12	1.13
Na2O	0.42	0.51	0.67	0.54	0.78	0.70	0.70	0.69	0.55	0.68	0.80	0.00
K2O	0.00	0.29	0.00	0.71	0.24	0.00	0.00	0.00	0.00	0.00	0.00	0.43
Total	77.24	77.47	83.18	81.18	77.57	80.06	80.06	86.65	85.40	81.59	83.58	79.87

Sample Quarry	SM228 BMZL	SM228 BMZL	SM228 BMZL	SM228 BMZL	SM228 BMZL	SM228 BMZL	SM228 BMZL	SM228 BMZL	SM228 BMZ;	SM228 BMZL	SM228 BMZL	SM228 BMZL
SiO2	57.46	56.91	59.06	55.54	56.57	57.90	58.21	56.49	56.09	56.78	54.20	57.26
Al2O3	22.68	23.04	18.12	18.00	17.63	19.43	19.96	18.77	18.70	22.02	16.58	21.09
Fe2O3	2.27	2.28	7.01	5.37	5.93	5.86	5.13	5.67	5.31	2.08	5.91	4.20
MgO	4.64	4.84	4.30	3.79	4.28	4.39	4.30	4.41	4.51	4.50	3.97	4.64
CaO	1.20	1.34	1.26	0.71	0.99	0.91	0.99	1.24	1.02	1.11	0.98	1.26
Na2O	0.45	0.63	0.86	0.41	0.59	0.67	0.57	0.60	0.78	0.82	0.49	0.58
K2O	0.00	0.00	0.00	0.00	0.32	0.00	0.00	0.28	0.00	0.00	0.31	0.00
Total	88.70	89.04	90.61	83.82	86.31	89.16	89.16	87.46	86.41	87.31	82.44	89.03

Sample Quarry	SM228 BMZL	SM228 BMZL	SM228 BMZL	SM228 BMZL	SM228 BMZL	SM235 BMRM	SM235 BMRM	SM235 BMRM	SM235 BMRM	SM235 BMRM	SM235 BMRM	SM235 BMRM
SiO2	57.71	58.31	55.88	55.55	54.93	52.55	50.79	54.40	52.96	52.21	48.82	53.43
Al2O3	20.12	18.94	18.98	22.13	17.65	18.67	21.59	20.20	22.00	22.97	22.15	22.54
Fe2O3	4.41	5.03	5.40	1.29	6.25	0.89	1.28	0.78	1.14	1.44	1.11	1.20
MgO	4.59	3.99	4.16	4.41	3.96	2.12	2.78	2.48	2.73	2.54	2.30	2.60
CaO	1.05	1.06	1.07	1.07	1.24	0.91	0.90	0.85	0.98	1.00	0.96	0.79
Na2O	0.69	0.47	0.55	0.41	0.00	0.54	0.78	0.42	0.73	0.77	0.41	0.37
K2O	0.00	0.00	0.22	0.00	0.21	0.51	0.94	0.60	0.80	0.98	1.39	1.01
Total	88.57	87.80	86.26	84.86	84.24	76.19	79.06	79.73	81.34	81.91	77.14	81.94

Sample Quarry	SM235 BMRM	SM235 BMRM	SM235 BMRM	SM235 BMRM	SM235 BMRM	SM235 BMRM	SM235 BMRM	SM235 BMRM	SM235 BMRM	SM235 BMRM	SM235 BMRM	SM235 BMRM
SiO2	53.38	51.10	53.91	49.74	47.82	53.39	51.94	51.99	53.02	53.14	52.40	51.44
Al2O3	19.93	22.66	20.26	20.77	20.71	22.63	21.65	20.71	19.37	22.31	20.52	20.24
Fe2O3	0.87	1.27	0.82	0.51	1.01	1.10	1.08	1.23	0.99	0.77	1.23	0.83
MgO	2.50	2.10	2.69	2.01	2.38	2.51	2.14	2.64	2.54	2.06	3.11	2.55
CaO	0.87	- -	- -	- -	0.79	- -	0.26	- -	0.90	0.34	1.08	0.98
Na2O	0.69	1.34	1.34	1.11	0.69	0.88	0.94	1.41	0.45	1.14	0.67	- -
K2O	0.54	1.80	1.14	1.16	0.44	1.13	1.21	0.80	0.69	1.02	0.44	0.59
Total	78.78	80.27	80.16	75.30	73.84	81.64	79.22	78.78	77.96	80.78	79.45	76.63

Sample	SM235	SM176	SM176	SM176	SM176	SM176	SM176	SM176	SM176	SM176	SM176	SM176
Quarry	BMRM	BMRS	BMRS	BMRS	BMRS	BMRS	BMRS	BMRS	BMRS	BMRS	BMRS	BMRS
SiO2	49.82	53.51	55.07	53.43	55.34	51.29	53.07	52.61	49.77	52.12	53.88	52.55
Al2O3	21.46	23.71	19.06	21.94	20.81	20.17	19.14	23.11	22.70	24.41	25.08	24.75
Fe2O3	1.14	1.30	1.49	0.70	1.86	1.11	1.57	1.19	1.29	0.77	0.64	0.68
MgO	2.79	2.61	2.24	1.91	2.24	2.30	2.35	2.49	2.75	2.68	2.85	3.06
CaO	1.30	0.45	0.47	0.63	0.30	0.51	0.50	0.36	0.25	0.45	0.34	0.26
Na2O	0.65	0.42	0.68	- -	0.92	0.71	0.42	0.60	0.89	0.68	0.55	1.18
K2O	0.81	0.38	0.78	0.58	1.28	0.65	0.52	0.38	0.34	0.40	0.36	0.40
Total	77.97	82.38	79.79	79.19	82.75	76.74	77.57	80.74	77.99	81.51	83.70	82.88

Sample	SM176	SM176	SM176	SM176	SM176	SM176	SM176	SM176	SM176	SM176	SM176	SM135
Quarry	BMRS	BMRS	BMRS	BMRS	BMRS	BMRS	BMRS	BMRS	BMRS	BMRS	BMRS	BMAK
SiO2	49.16	50.63	52.15	52.58	49.71	50.19	51.24	49.29	50.05	50.46	48.02	51.37
Al2O3	23.41	23.77	22.08	23.35	22.33	22.30	22.36	22.91	23.62	22.03	22.15	18.04
Fe2O3	0.00	0.88	1.21	0.70	1.37	1.11	1.09	0.90	0.63	1.62	0.63	1.59
MgO	3.12	3.01	2.47	2.78	2.73	2.65	2.50	2.51	2.45	2.49	2.85	2.85
CaO	0.34	0.26	0.32	- -	0.31	0.45	0.29	0.34	0.69	0.55	1.27	0.85
Na2O	0.78	0.81	0.98	0.92	0.65	0.92	0.66	0.55	0.43	0.59	0.92	0.66
K2O	0.34	0.46	0.44	0.41	0.31	0.33	0.51	0.29	0.46	- -	0.36	0.33
Total	77.15	79.82	79.65	80.74	77.41	77.95	78.65	76.79	78.33	77.74	76.20	75.69

Sample	SM135	SM135	SM135	SM135	SM135	SM135	SM135	SM135	SM135	SM155	SM155	SM155
Quarry	BMAK	BMAK	BMAK	BMAK	BMAK	BMAK	BMAK	BMAK	BMAK	BMA1	BMA1	BMA1
SiO2	52.08	48.82	53.27	51.92	53.08	53.99	51.07	49.90	51.01	50.59	51.04	49.22
Al2O3	18.28	23.58	20.23	21.46	19.46	18.86	22.31	17.38	18.47	21.54	22.02	22.91
Fe2O3	2.10	0.68	2.46	1.23	2.24	1.53	0.94	1.91	1.44	2.07	1.98	1.21
MgO	2.37	1.42	1.98	2.16	2.92	3.55	1.45	2.88	2.33	1.27	1.47	1.44
CaO	0.60	0.41	0.58	0.65	0.79	0.61	0.34	0.41	0.32	0.41	0.55	0.89
Na2O	0.79	0.36	- -	0.37	0.53	0.79	0.94	0.70	0.36	0.57	0.41	- -
K2O	- -	0.29	0.26	0.22	0.23	0.43	0.48	0.34	0.40	0.96	0.95	0.95
Total	76.22	75.56	78.78	78.01	79.25	79.76	77.53	73.52	74.33	77.41	78.42	76.62

Sample	SM155	SM155	SM155	SM155	SM155	SM155	SM155	SM155	SM155	SM155	SM155	SM155
Quarry	BMA1	BMA1	BMA1	BMA1	BMA1	BMA1	BMA1	BMA1	BMA1	BMA1	BMA1	BMA1
SiO2	48.53	49.31	52.92	54.67	50.93	51.04	51.98	49.91	52.01	50.77	52.12	48.94
Al2O3	23.51	21.12	20.03	22.49	23.42	23.24	21.19	19.61	20.96	21.32	24.47	23.69
Fe2O3	1.56	1.74	1.58	1.94	2.10	1.83	1.88	0.96	1.36	1.49	1.83	1.59
MgO	1.28	1.17	1.57	1.19	1.34	1.41	1.48	1.76	1.58	1.61	1.56	1.58
CaO	1.04	0.28	0.77	0.56	0.98	1.01	0.64	0.71	0.50	0.85	1.02	1.09
Na2O	- -	0.44	- -	- -	- -	- -	0.42	0.54	0.69	0.52	- -	- -
K2O	1.53	1.32	0.84	0.56	1.52	1.13	1.52	0.68	1.14	1.10	1.10	1.35
Total	77.45	75.38	77.71	81.41	80.29	79.66	79.11	74.17	78.24	77.66	82.10	78.24

Sample	SM155	SM155	SM155	SM155	SM155	SM155	SM155	SM155	SM155	SM155	SM155	SM155
Quarry	BMA1	BMA1	BMA1	BMA1	BMA1	BMA1	BMA1	BMA1	BMA1	BMA1	BMA1	BMA1
SiO2	45.97	44.80	51.10	46.72	47.37	48.07	47.71	46.26	53.18	48.92	48.83	49.27
Al2O3	22.17	21.96	23.09	22.18	21.02	23.74	22.70	20.28	20.35	22.44	20.88	22.61
Fe2O3	1.80	1.47	1.65	1.54	1.38	1.79	1.79	1.73	1.53	1.91	1.72	1.61
MgO	1.91	1.57	1.36	1.49	1.77	1.60	2.08	1.60	1.57	1.05	1.93	1.32
CaO	0.91	0.95	0.93	1.13	0.89	0.39	0.52	0.53	0.52	1.00	0.64	0.82
Na2O	0.56	0.62	- -	0.78	0.71	- -	- -	0.41	- -	- -	- -	0.46
K2O	0.72	0.89	1.11	0.79	1.07	0.39	0.67	0.69	0.43	0.89	0.37	1.45
Total	74.04	72.26	79.24	74.63	74.21	75.98	75.47	71.50	77.58	76.21	74.37	77.54

Sample	SM155	SM155	SM155	SM155	SM155	SM155	SM155	SM155	SM155	SM155	SM135	SM135
Quarry	BMA1	BMA1	BMA1	BMA1	BMA1	BMA1	BMA1	BMA1	BMA1	BMA1	BMAK	BMAK
SiO2	50.06	45.49	49.15	50.37	48.33	48.36	52.26	50.35	48.02	48.41	54.00	50.42
Al2O3	23.16	21.64	21.81	19.64	22.90	22.14	20.70	20.34	22.19	20.16	25.62	17.70
Fe2O3	1.36	1.67	1.77	1.80	1.70	1.53	1.88	1.63	1.64	1.80	0.72	1.62
MgO	1.39	1.06	0.87	0.82	0.66	1.00	0.96	1.11	1.34	1.36	1.31	3.20
CaO	0.71	0.78	0.55	1.17	0.66	1.04	0.76	1.10	0.74	0.80	0.71	0.61
Na2O	- -	- -	- -	- -	0.48	0.42	- -	0.44	- -	- -	- -	0.59
K2O	0.36	1.64	1.53	0.96	1.39	0.90	1.25	1.21	0.94	0.77	0.81	0.32
Total	77.04	72.28	75.68	74.76	76.12	75.39	77.81	76.18	74.87	73.30	83.17	74.46

Sample	SM135	SM135	SM135	SM135	SM135	SM135	SM135	SM135	SM135	SM135	SM135	SM135
Quarry	BMAK	BMAK	BMAK	BMAK	BMAK	BMAK	BMAK	BMAK	BMAK	BMAK	BMAK	BMAK
SiO2	49.82	56.89	50.02	48.85	49.75	49.39	49.22	49.68	50.21	49.59	49.69	53.14
Al2O3	18.09	21.46	17.34	18.68	17.95	16.85	16.95	16.97	22.60	17.42	19.14	18.41
Fe2O3	1.75	2.00	1.66	2.21	1.69	1.84	1.95	1.86	0.90	1.31	1.81	1.23
MgO	2.09	2.20	3.21	1.99	1.84	2.39	2.74	2.48	1.59	3.41	1.99	3.03
CaO	0.66	0.81	0.65	0.62	0.55	0.61	0.46	0.61	0.47	0.72	0.87	0.45
Na2O	0.81	0.44	0.99	0.68	0.96	1.03	1.00	0.69	1.21	0.59	0.38	0.49
K2O	- -	- -	0.38	- -	- -	0.24	0.38	0.36	0.58	0.53	- -	0.53
Total	73.22	83.80	74.25	73.03	72.74	72.35	72.70	72.65	77.56	73.57	73.88	77.28

Sample	SM135	SM135	SM135	SM135	SM135	SM135	SM135	SM135	SM135	SM176	SM176	SM176
Quarry	BMAK	BMAK	BMAK	BMAK	BMAK	BMAK	BMAK	BMAK	BMAK	BMRS	BMRS	BMRS
SiO2	51.48	52.00	53.46	50.80	50.94	55.46	49.39	52.21	52.28	56.79	61.18	49.97
Al2O3	21.32	24.76	24.02	24.48	28.04	26.12	30.19	17.30	18.97	19.85	10.46	21.59
Fe2O3	1.36	0.61	0.74	0.60	0.86	0.68	0.49	1.63	2.09	1.48	1.16	0.89
MgO	2.19	1.52	1.45	1.35	1.04	1.29	0.55	3.03	2.05	0.49	0.34	1.38
CaO	0.67	0.44	0.63	0.63	- -	0.43	0.26	0.55	0.55	- -	- -	- -
Na2O	1.01	0.65	0.43	0.70	0.40	0.63	- -	0.88	0.60	- -	- -	- -
K2O	0.27	0.59	0.70	1.06	0.44	0.81	0.35	0.61	- -	0.68	- -	0.82
Total	78.30	80.57	81.43	79.62	81.72	85.42	81.23	76.21	76.54	79.29	73.14	74.65

Sample	SM176	SM176	SM176	SM176	SM176	SM176	SM176	SM176	SM176	SM176	SM176	SM176
Quarry	BMRS	BMRS	BMRS	BMRS	BMRS	BMRS	BMRS	BMRS	BMRS	BMRS	BMRS	BMRS
SiO2	52.75	53.86	54.86	50.16	49.89	51.00	50.26	54.15	50.19	52.23	53.30	51.89
Al2O3	22.96	19.00	21.73	22.16	23.58	22.80	20.41	22.11	21.21	22.36	20.46	21.20
Fe2O3	1.11	2.04	1.32	1.57	1.22	1.67	1.48	0.99	0.57	0.77	0.91	1.11
MgO	1.10	1.37	1.25	1.37	1.68	1.49	1.48	1.97	2.11	1.49	1.49	1.18
CaO	- -	- -	- -	- -	- -	- -	- -	0.62	0.50	0.40	0.39	0.43
Na2O	- -	- -	- -	- -	- -	- -	- -	0.52	- -	- -	- -	- -
K2O	0.65	0.34	0.83	0.53	0.83	0.74	- -	0.33	- -	1.12	0.95	0.95
Total	78.57	76.61	79.99	75.79	77.20	77.70	73.63	80.70	74.58	78.37	77.50	76.76

Sample	SM176	SM176	SM158	SM158	SM158	SM158	SM158	SM158	SM158	SM158	SM277	SM277
Quarry	BMRS	BMRS	BMGF	BMGF	BMGF	BMGF	BMGF	BMGF	BMGF	BMGF	BKP1	BKP1
SiO2	53.31	50.35	51.97	50.86	55.03	50.87	49.66	51.77	52.26	51.14	49.14	50.98
Al2O3	22.35	22.67	19.18	20.60	20.57	21.14	22.98	22.60	23.95	23.79	17.64	18.02
Fe2O3	0.78	1.19	0.61	- -	- -	0.00	- -	- -	- -	- -	1.70	1.66
MgO	1.93	1.04	1.65	0.99	1.34	1.02	1.39	1.05	1.36	0.96	3.67	4.09
CaO	0.45	- -	1.18	1.17	1.31	1.39	1.36	1.45	1.41	1.43	0.61	0.71
Na2O	- -	- -	- -	- -	- -	- -	0.48	- -	- -	- -	0.42	0.57
K2O	1.14	0.36	1.73	0.97	0.71	0.73	0.77	0.46	0.80	0.71	0.87	0.75
Total	79.96	75.61	76.32	74.59	78.96	75.15	76.64	77.33	79.78	78.03	74.05	76.78

Sample	SM277	SM277	SM277	SM277	SM277	SM277	SM277	SM277	SM277	SM277	SM277	SM277
Quarry	BKP1	BKP1	BKP1	BKP1	BKP1	BKP1	BKP1	BKP1	BKP1	BKP1	BKP1	BKP1
SiO2	48.98	50.86	51.27	51.51	52.66	48.30	49.96	50.64	50.06	52.17	53.79	53.25
Al2O3	17.09	18.31	17.96	18.04	18.13	16.93	17.87	17.66	17.75	18.50	19.20	19.18
Fe2O3	1.64	1.68	1.64	1.61	1.72	1.48	1.85	1.60	1.61	1.59	1.71	2.06
MgO	3.58	4.21	4.02	3.77	4.34	3.43	4.14	3.87	3.52	3.71	4.13	3.62
CaO	0.74	0.85	0.85	0.95	0.96	1.55	0.95	1.47	1.34	0.92	1.43	1.62
Na2O	0.42	0.53	0.49	0.00	0.80	0.51	0.42	0.43	0.38	0.00	0.57	0.38
K2O	1.08	1.03	0.46	0.47	0.79	0.23	0.30	0.00	0.26	0.47	0.00	0.27
Total	73.53	77.47	76.69	76.35	79.40	72.43	75.49	75.67	74.92	77.36	80.83	80.38

Sample	SM277	SM277	SM277	SM277	SM277	SM277	SM277	SM281	SM281	SM281	SM281	SM281
Quarry	BKP1	BKP1	BKP1	BKP1	BKP1	BKP1	BKP1	BKP3	BKP3	BKP3	BKP3	BKP3
SiO2	52.14	52.55	54.58	55.56	52.85	53.65	56.72	60.38	60.28	58.58	60.20	62.16
Al2O3	18.16	18.19	18.92	18.91	18.12	18.71	20.21	21.02	21.16	20.26	20.97	22.42
Fe2O3	1.66	1.76	2.06	1.70	1.56	2.06	1.96	1.66	1.27	1.67	2.01	1.82
MgO	3.76	3.61	4.37	4.41	3.67	3.84	4.64	4.78	4.68	4.45	4.70	4.84
CaO	1.27	1.35	0.56	0.71	0.60	0.75	0.74	1.27	1.01	1.06	0.96	0.85
Na2O	0.00	0.00	0.62	0.76	0.64	0.62	0.80	0.45	0.48	0.00	0.68	0.73
K2O	0.26	0.63	0.59	0.67	0.60	0.69	0.69	0.00	0.00	0.00	0.00	0.00
Total	77.25	78.09	81.70	82.72	78.04	80.32	85.76	89.56	88.88	86.02	89.52	92.82

Sample	SM281	SM281	SM281	SM279	SM279	SM279	SM279	SM279	SM279	SM279	SM279	SM279
Quarry	BKP3	BKP3	BKP3	BKP2	BKP2	BKP2	BKP2	BKP2	BKP2	BKP2	BKP2	BKP2
SiO2	58.80	59.58	61.78	60.59	60.69	64.23	61.83	63.27	60.88	63.42	63.55	61.12
Al2O3	20.27	20.56	21.63	20.43	20.82	21.97	20.51	21.24	21.18	21.77	21.85	21.22
Fe2O3	2.03	1.63	1.42	1.66	1.56	1.52	1.24	1.51	1.46	1.38	1.27	1.27
MgO	4.40	4.80	4.71	4.42	4.21	4.76	4.65	4.73	4.72	5.55	5.07	4.43
CaO	1.06	0.97	1.07	1.23	1.00	1.12	1.02	1.23	1.13	1.28	1.25	1.43
Na2O	0.00	0.64	0.37	0.00	0.41	0.00	0.00	0.00	0.41	0.49	0.47	0.00
K2O	0.00	0.00	0.00	0.00	0.00	0.00	0.00	0.00	0.00	0.00	0.00	0.00
Total	86.56	88.18	90.98	88.33	88.69	93.60	89.25	91.98	89.78	93.88	93.46	89.47

Sample	SM279	SM279	SM279	SM279	SM279	SM269	SM269	SM269	SM269	SM269	SM269	SM269
Quarry	BKP2	BKP2	BKP2	BKP2	BKP2	BKP1	BKP1	BKP1	BKP1	BKP1	BKP1	BKP1
SiO2	60.30	62.16	61.68	61.26	61.89	52.72	53.61	50.02	49.16	53.50	53.46	51.98
Al2O3	20.93	22.39	21.12	20.48	21.37	17.68	18.24	17.06	16.45	17.71	17.58	17.67
Fe2O3	1.22	1.34	1.39	1.40	1.34	1.49	1.36	1.43	1.86	2.15	2.45	1.89
MgO	4.74	4.75	4.65	4.55	4.66	3.73	3.62	3.51	3.61	3.38	3.42	3.78
CaO	1.43	1.22	1.18	1.14	1.13	0.94	0.68	0.69	0.40	0.68	0.68	0.70
Na2O	0.35	0.00	0.00	0.00	0.38	0.62	0.65	0.48	0.00	0.42	0.35	0.48
K2O	0.00	0.00	0.00	0.00	0.00	0.67	0.73	0.64	0.76	1.84	1.62	0.70
Total	88.97	91.86	90.02	88.83	90.77	77.85	78.89	73.83	72.24	79.68	79.56	77.20

Sample	SM269	SM269	SM269	SM269	SM269	SM269	SM269	SM269	SM269	SM269	SM269	SM269
Quarry	BKP1	BKP1	BKP1	BKP1	BKP1	BKP1	BKP1	BKP1	BKP1	BKP1	BKP1	BKP1
SiO2	55.15	52.99	52.12	56.62	51.95	54.88	55.68	53.43	50.55	55.51	54.20	54.62
Al2O3	18.67	17.52	17.60	19.11	17.49	18.42	18.94	17.82	17.35	18.64	17.55	18.07
Fe2O3	2.09	1.41	1.21	1.69	1.83	2.50	1.14	2.17	1.95	2.76	2.10	1.77
MgO	4.19	4.06	3.14	4.42	3.66	4.10	4.35	3.76	2.80	3.65	3.53	3.21
CaO	0.71	0.65	0.63	0.61	0.66	0.77	0.74	0.48	0.39	0.71	0.51	0.49
Na2O	0.63	0.00	0.39	0.59	0.45	0.58	0.00	0.65	0.00	0.54	0.00	0.00
K2O	0.71	0.59	2.26	0.67	0.76	1.59	0.58	1.31	1.68	1.56	1.54	1.38
Total	82.15	77.22	77.35	83.71	76.80	82.84	81.43	79.62	74.72	83.37	79.43	79.54

Sample	SM269	SM269	SM269	SM269	SM269	SM269	SM269	SM269	SM302	SM302	SM302	SM302
Quarry	BKP1	BKP1	BKP1	BKP1	BKP1	BKP1	BKP1	BKP1	BKL1	BKL1	BKL1	BKL1
SiO2	53.65	53.07	51.62	50.71	53.25	53.82	50.56	51.82	59.52	59.16	58.05	59.30
Al2O3	17.50	17.29	17.21	16.96	17.52	18.17	17.11	17.23	20.58	20.52	18.80	19.51
Fe2O3	1.76	1.75	1.70	1.78	1.63	1.52	0.77	1.64	1.81	1.52	3.00	3.05
MgO	3.58	3.69	3.64	3.37	4.20	4.03	3.66	3.67	4.62	4.59	4.50	4.60
CaO	0.84	0.90	0.84	0.64	0.75	0.66	0.84	0.87	1.13	1.15	0.96	0.84
Na2O	0.37	0.00	0.45	0.00	0.41	0.53	0.00	0.00	0.38	0.00	0.60	0.00
K2O	1.58	0.64	0.57	0.59	0.71	0.62	0.72	0.71	0.00	0.00	0.39	0.65
Total	79.28	77.34	76.03	74.05	78.47	79.35	73.66	75.94	88.04	86.94	86.30	87.95

Sample	SM302	SM302	SM302	SM302	SM302	SM302	SM302	SM302	SM302	SM325	SM325	SM325
Quarry	BKL1	BKL1	BKL1	BKL1	BKL1	BKL1	BKL1	BKL1	BKL1	BCH1	BCH1	BCH1
SiO2	57.86	56.23	54.47	60.12	58.00	55.15	62.47	56.75	58.79	53.72	51.22	48.48
Al2O3	20.62	19.17	19.44	21.36	19.87	19.05	21.24	18.17	17.16	16.37	15.71	14.62
Fe2O3	1.68	1.42	3.19	1.70	1.94	1.26	1.63	3.03	3.92	0.88	0.41	0.62
MgO	4.81	4.23	8.03	4.74	3.91	4.31	4.90	4.37	5.60	6.14	6.48	5.48
CaO	0.91	0.88	0.55	1.14	1.05	1.10	0.94	0.80	1.04	0.80	0.84	0.56
Na2O	1.04	0.42	0.00	0.00	0.00	0.00	0.47	0.38	0.48	0.51	0.83	0.50
K2O	0.00	0.00	0.00	0.00	0.00	0.00	0.00	0.55	2.75	0.23	0.00	0.23
Total	86.92	82.35	85.68	89.06	84.77	80.87	91.64	84.05	89.74	78.65	75.49	70.49

Sample	SM325	SM325	SM325	SM325	SM325	SM279	SM279	SM279	SM279	SM279	SM279	SM279
Quarry	BCH1	BCH1	BCH1	BCH1	BCH1	BKP2	BKP2	BKP2	BKP2	BKP2	BKP2	BKP2
SiO2	52.20	61.28	64.16	60.24	61.11	57.38	56.72	56.67	57.19	55.36	56.25	56.70
Al2O3	16.20	19.05	19.92	18.62	19.12	20.21	19.77	19.01	19.84	19.36	19.94	19.81
Fe2O3	0.66	0.54	0.78	1.00	0.83	1.44	1.31	1.11	1.34	1.44	1.08	1.12
MgO	5.76	7.06	7.25	6.61	7.10	4.77	4.99	4.59	4.99	4.90	4.80	4.62
CaO	0.92	1.03	0.91	1.01	0.85	1.05	1.25	1.13	1.17	1.12	1.11	1.39
Na2O	0.54	0.39	0.00	0.00	0.53	0.00	0.00	0.00	0.40	0.55	0.50	0.00
K2O	0.24	0.00	0.00	0.00	0.23	0.00	0.00	0.00	0.00	0.00	0.00	0.00
Total	76.52	89.35	93.02	87.48	89.77	84.85	0.00	82.51	84.93	82.73	83.68	83.64

Sample	SM279	SM279	SM279	SM279	SM281	SM281	SM281	SM281	SM281	SM281	SM281	SM281
Quarry	BKP2	BKP2	BKP2	BKP2	BKP3	BKP3	BKP3	BKP3	BKP3	BKP3	BKP3	BKP3
SiO2	56.70	55.54	55.49	56.87	57.92	58.42	59.56	57.53	59.51	59.46	58.55	60.90
Al2O3	19.81	18.37	19.53	19.63	20.71	21.16	21.17	20.98	21.05	20.56	20.17	20.30
Fe2O3	1.63	1.60	1.34	1.38	1.54	1.41	1.42	1.74	1.53	1.41	1.71	1.90
MgO	4.57	4.36	4.68	4.94	4.91	5.39	5.47	5.23	5.44	5.23	5.08	5.31
CaO	1.28	1.32	1.27	1.26	0.81	0.90	0.85	0.98	0.73	0.90	0.93	1.20
Na2O	0.00	0.00	0.45	0.41	0.58	0.68	0.38	0.48	0.41	0.58	0.39	0.00
K2O	0.00	0.00	0.00	0.00	0.00	0.00	0.00	0.00	0.00	0.00	0.00	0.00
Total	83.99	81.19	82.76	84.49	86.47	87.96	88.85	86.94	88.67	88.14	86.83	89.61

Sample	SM281	SM281	SM281	SM277	SM277	SM277	SM277	SM277	SM277
Quarry	BKP3	BKP3	BKP3	BKP1	BKP1	BKP1	BKP1	BKP1	BKP1
SiO2	61.13	59.16	63.58	53.44	54.05	50.78	54.93	56.18	49.32
Al2O3	20.61	19.80	21.75	18.60	18.01	17.70	19.13	19.44	16.65
Fe2O3	1.38	1.52	1.41	1.89	1.52	1.59	1.58	1.62	1.69
MgO	5.45	4.84	5.93	4.04	4.12	3.80	4.12	4.31	3.41
CaO	1.12	1.05	0.80	1.15	1.28	1.35	0.68	0.59	0.89
Na2O	0.46	0.38	0.68	0.39	0.00	0.00	0.82	0.75	0.00
K2O	0.00	0.00	0.00	0.32	0.31	0.00	0.67	0.52	0.30
Total	90.15	86.75	94.15	79.83	79.29	75.22	81.93	83.41	72.26

APPENDIX 4.7

Microprobe analyses of zeolites.

Sample	SM302	SM302	SM302	SM302	SM302	SM302	SM302	SM302	SM302	SM302	SM302	SM302
Quarry	LTCL	LTCL	LTCL	LTCL	LTCL	LTCL	LTCL	LTCL	LTCL	LTCL	LTCL	LTCL
SiO2	69.45	71.23	69.76	66.84	70.03	70.58	70.58	69.72	68.93	68.21	67.25	70.20
Al2O3	13.11	13.87	14.08	12.90	12.55	12.45	13.64	13.18	12.65	12.88	12.43	12.55
Fe2O3	- -	- -	- -	- -	- -	- -	- -	- -	- -	- -	- -	- -
MgO	1.34	1.45	1.64	1.12	0.74	0.81	1.32	0.82	0.79	1.16	1.01	1.16
CaO	2.71	2.47	2.38	2.61	2.38	2.05	2.32	1.80	3.00	2.29	2.02	2.41
Na2O	2.22	2.76	2.50	2.06	2.13	2.79	2.12	2.95	1.96	2.17	2.09	2.30
K2O	0.35	0.34	1.01	1.10	1.92	1.44	1.56	2.16	1.21	1.76	2.13	1.58
Total	89.18	92.12	91.37	86.63	89.74	90.12	91.54	90.63	88.54	88.47	86.93	90.20

Sample	SM302	SM302	SM302	SM302	SM302	SM032	SM302	SM302	SM302	SM302	SM302	SM277
Quarry	LTCL	LTCL	LTCL	LTCL	LTCL	LTCL	LTCL	LTCL	LTCL	LTCL	LTCL	PRMO
SiO2	71.62	70.21	68.84	70.02	69.80	71.03	68.57	68.36	69.90	68.49	69.58	65.49
Al2O3	13.56	13.49	13.46	13.55	14.03	13.62	13.72	13.52	14.04	13.53	13.58	10.88
Fe2O3	- -	- -	- -	- -	- -	- -	- -	- -	- -	- -	- -	- -
MgO	0.93	0.84	1.20	0.83	1.14	1.03	1.12	1.30	1.27	1.08	0.90	0.53
CaO	2.11	2.09	2.37	1.54	1.98	1.69	1.72	2.61	2.23	1.63	1.71	2.54
Na2O	2.98	3.68	2.81	2.75	3.23	3.02	2.45	2.52	2.44	3.12	3.83	2.69
K2O	1.67	0.61	0.46	2.88	1.69	2.11	2.87	0.60	1.74	2.02	1.13	- -
Total	92.87	90.92	89.14	91.57	91.87	92.50	90.45	88.91	91.62	89.87	90.73	82.12

Sample	SM277	SM277	SM277	SM277	SM277	SM277	SM277	SM277	SM277	SM277	SM277	SM277
Quarry	PRMO	PRMO	PRMO	PRMO	PRMO	PRMO	PRMO	PRMO	PRMO	PRMO	PRMO	PRMO
SiO2	64.76	67.73	71.14	69.03	64.62	66.09	65.83	72.73	72.53	71.87	71.75	73.19
Al2O3	10.39	11.13	10.27	9.41	9.96	10.20	10.09	12.18	11.11	11.91	11.98	12.25
Fe2O3	- -	- -	- -	- -	- -	- -	- -	- -	- -	- -	- -	- -
MgO	- -	0.47	- -	- -	- -	0.46	0.43	0.46	- -	- -	0.55	- -
CaO	2.50	2.43	1.90	2.16	2.86	2.54	2.44	2.39	2.59	2.47	2.68	2.57
Na2O	3.17	2.99	2.93	2.45	2.57	1.25	2.61	3.71	4.02	4.13	3.37	4.21
K2O	- -	0.00	1.62	1.68	- -	2.12	- -	- -	- -	- -	- -	- -
Total	80.82	84.75	87.86	84.73	80.01	82.66	81.40	91.47	90.25	90.38	90.33	92.22

Sample	SM277	SM277	SM277	SM277	SM277	SM277	SM277	SM277	SM277	SM277	SM277	SM277
Quarry	PRMO	PRMO	PRMO	PRMO	PRMO	PRMO	PRMO	PRMO	PRMO	PRMO	PRMO	PRMO
SiO2	73.36	68.68	67.63	68.06	64.89	70.21	68.99	65.67	64.49	64.62	64.43	66.08
Al2O3	12.08	10.87	10.53	10.56	10.06	11.20	10.90	10.03	10.18	10.48	10.25	10.60
Fe2O3	- -	- -	- -	- -	- -	- -	- -	- -	- -	- -	- -	- -
MgO	0.48	0.44	0.46	0.00	- -	- -	- -	- -	- -	- -	- -	- -
CaO	2.54	2.23	2.38	2.74	2.65	2.63	2.57	2.65	2.63	2.69	2.69	2.48
Na2O	3.18	2.62	3.01	2.99	3.07	3.54	3.44	3.02	2.97	2.90	2.96	3.35
K2O	- -	- -	- -	0.21	- -	- -	- -	- -	- -	- -	- -	- -
Total	91.64	84.84	84.01	84.56	80.67	87.58	85.90	81.37	80.27	80.69	80.33	82.51

Sample	SM277	SM277	SM277	SM277	SM277	SM277	SM277	SM277	SM277	SM277	SM277	SM277
Quarry	PRMO	PRMO	PRMO	PRMO	PRMO	PRMO	PRMO	PRMO	PRMO	PRMO	PRMO	PRMO
SiO2	72.63	71.44	71.78	72.35	73.02	72.89	72.63	73.52	70.76	71.05	71.79	70.23
Al2O3	11.78	11.63	11.94	12.63	11.97	11.74	11.80	11.78	11.46	11.74	12.08	11.98
Fe2O3	- -	- -	- -	- -	- -	- -	- -	- -	- -	- -	- -	- -
MgO	- -	0.58	0.57	0.53	- -	- -	- -	- -	- -	- -	0.61	0.59
CaO	2.82	2.53	2.78	2.41	2.71	2.63	2.81	2.60	2.24	2.88	2.54	2.71
Na2O	3.79	2.75	2.59	2.92	3.36	1.54	1.09	2.23	2.51	1.97	1.76	1.69
K2O	- -	- -	0.97	1.43	0.91	3.48	3.78	2.58	1.95	2.55	2.43	2.38
Total	91.02	88.93	90.33	92.27	91.97	92.28	92.11	92.71	88.92	90.19	91.21	89.66

Sample	SM277
Quarry	PRMO
SiO2	73.03
Al2O3	11.97
Fe2O3	- -
MgO	- -
CaO	2.96
Na2O	1.95
K2O	2.27
Total	92.18

Key to the codes: LTCT= Clinoptilolite from the Loutra deposit, kimolos. PRMO= Mordenite from the Prassa deposit, Kimolos.

APPENDIX 4.8.

Microprobe analyses of pyrogenetic feldspars present in the Greek bentonites

Sample	SM25	SM25	SM25	SM25	SM25	SM25	SM25	SM25	SM43	SM43	SM43	SM43
Quarry	ANPL	ANPL	ANPL	ANPL	ANPL	ANPL	ANPL	ANPL	KFPL	KFPL	KFPL	KFPL
SiO2	56.52	56.86	57.99	55.78	57.58	58.52	58.34	58.74	61.02	62.31	60.46	60.01
Al2O3	27.84	27.67	27.69	27.66	26.25	26.27	25.92	26.00	24.22	22.59	24.25	25.69
Fe2O3	- -	- -	- -	0.50	0.53	- -	- -	- -	1.39	0.92	1.09	0.57
MgO	- -	0.71	1.31	0.88	0.79	1.01	0.90	0.90	1.98	1.31	1.24	1.35
CaO	9.10	8.34	7.64	8.72	7.39	6.82	7.15	6.82	4.26	3.56	5.41	5.53
Na2O	6.10	5.93	6.27	5.53	6.19	6.57	6.51	6.17	5.81	5.61	5.53	6.73
K2O	- -	0.29	0.31	0.30	0.30	0.34	0.44	0.32	0.88	3.92	1.06	0.71
Total	99.56	99.80	101.21	99.37	99.03	99.53	99.26	98.95	99.56	100.22	99.04	100.59

Sample	SM43	SM43	SM43	SM43	SM43	SM43	SM43	SM43	SM43	SM43	SM43	SM43
Quarry	KFPL	KFPL	KFPL	KFPL	KFPL	KFPL	KFPL	KFPL	KFPL	KFPL	KFPL	KFPL
SiO2	60.06	56.41	58.53	61.24	61.98	60.49	59.81	60.24	58.96	61.34	65.71	63.82
Al2O3	24.81	28.02	26.05	24.28	24.64	25.37	25.98	25.53	26.21	24.16	21.96	22.17
Fe2O3	- -	0.56	0.88	0.59	1.09	0.69	0.71	- -	0.59	0.66	0.57	- -
MgO	0.66	0.79	1.54	0.83	2.04	1.67	0.91	1.05	- -	1.93	- -	- -
CaO	5.44	8.14	5.57	4.27	3.67	5.20	6.15	5.53	7.08	3.27	3.57	1.68
Na2O	6.99	5.71	6.17	7.00	6.31	6.41	6.70	7.14	7.06	6.77	7.12	5.89
K2O	0.94	0.51	0.46	1.12	1.30	0.58	0.68	0.68	0.48	1.51	2.21	6.36
Total	98.90	100.14	99.20	99.33	101.03	100.41	100.94	100.17	100.38	99.64	101.14	99.92

Sample	SM43	SM43	SM43	SM43	SM43	SM43	SM43	SM43	SM43	SM43	SM43	SM43
Quarry	KFPL	KFPK	KFPR	KFPL	KFKF	KFKF	KFKF	KFKF	KFKF	KFKF	KFKF	KFKF
SiO2	60.20	57.71	58.92	60.69	65.19	65.70	64.89	65.69	64.41	65.55	65.39	65.59
Al2O3	25.57	26.79	25.95	25.07	19.39	19.38	19.32	20.53	19.35	19.78	20.01	18.41
Fe2O3	0.66	0.98	0.65	0.70	0.49	- -	0.49	- -	0.59	- -	- -	0.62
MgO	- -	- -	- -	- -	0.84	1.30	1.03	0.80	1.10	1.05	0.98	0.64
CaO	7.29	8.39	7.11	6.48	0.74	0.87	0.91	0.83	1.01	0.81	0.94	0.60
Na2O	5.98	6.10	6.58	7.06	3.90	3.52	3.21	4.53	3.83	3.79	3.57	3.49
K2O	1.14	0.65	0.89	0.94	9.82	9.82	9.87	8.94	9.08	10.13	9.80	10.50
Total	100.84	100.62	100.10	100.94	100.37	100.59	99.72	101.39	99.37	101.11	100.69	99.85

Sample	SM114	SM114	SM144	SM114	SM114	SM114	SM114	SM228	SM228	SM228	SM228	SM228
Quarry	TSPL	TSPL	TSPL	TSPL	TSPL	TSPL	TSPL	ZLPL	ZLPL	ZLPL	ZLPL	ZLPL
SiO2	59.96	61.96	59.80	59.94	67.84	60.56	61.60	57.56	55.65	55.02	58.96	54.94
Al2O3	25.66	24.02	25.32	25.21	19.83	24.35	24.05	27.91	28.63	28.98	26.01	29.09
Fe2O3	- -	- -	- -	- -	- -	- -	- -	- -	- -	- -	- -	- -
MgO	- -	- -	0.85	- -	0.74	0.73	0.71	1.14	1.26	- -	0.81	- -
CaO	6.52	4.71	5.81	5.77	- -	5.27	4.74	7.93	8.30	9.69	5.82	10.30
Na2O	7.14	8.18	7.12	7.56	11.17	7.68	7.88	6.04	6.01	5.43	6.91	5.07
K2O	0.47	0.67	0.59	0.41	- -	0.52	0.72	- -	- -	- -	0.87	- -
Total	99.75	99.54	99.59	98.89	99.58	99.11	99.70	100.58	99.85	99.12	99.38	99.93

Sample	SM228	SM228	SM228	SM228	SM277	SM277	SM277	SM277	SM277	SM277	SM277	SM277
Quarry	ZLPL	ZLPL	ZLPL	ZLKF	PRKF	PRKF	PRKF	PRKF	PRKF	PLMR	PLCR	PLMR
SiO2	54.21	54.23	55.18	64.96	67.71	65.44	65.64	65.78	67.68	63.96	63.86	63.75
Al2O3	28.78	29.00	28.33	19.07	19.37	20.77	19.54	20.10	18.75	23.58	24.04	23.51
Fe2O3	0.53	0.42	- -	0.44	- -	- -	- -	- -	- -	- -	- -	- -
MgO	0.84	0.66	0.75	1.41	2.09	1.57	1.83	1.78	1.92	1.22	1.04	1.28
CaO	9.78	9.18	8.77	0.52	1.07	0.62	1.03	0.98	0.86	3.02	3.48	2.94
Na2O	5.03	5.37	5.37	1.28	0.77	1.47	1.27	1.37	1.20	6.54	7.05	6.70
K2O	- -	- -	0.95	12.49	9.21	10.97	10.34	9.74	9.03	1.79	1.27	1.94
Total	99.17	98.86	99.35	100.17	100.22	100.74	99.65	99.75	99.44	100.31	100.74	100.12

Sample	SM277	SM277	SM277	SM277	SM277	SM277	SM277	SM277	SM277	SM277	SM277	SM277
Quarry	PLCR	PLCR	PLMR	PLMR	PLCR	PLMR	PLCR	PLMR	PLCR	PLMR	PLCR	PLMR
SiO2	64.08	63.79	64.76	65.08	64.95	66.04	63.99	63.85	64.86	64.01	65.13	64.55
Al2O3	22.90	23.72	23.29	23.06	22.54	21.86	22.34	22.24	21.47	21.86	22.00	22.94
Fe2O3	- -	- -	- -	- -	- -	- -	- -	- -	- -	- -	- -	- -
MgO	1.02	1.14	0.81	0.63	0.52	- -	0.56	- -	- -	- -	- -	- -
CaO	2.55	2.88	3.08	2.98	2.96	2.59	2.98	3.60	2.36	3.47	2.84	3.88
Na2O	6.08	6.78	6.79	7.09	5.08	5.61	6.23	7.17	5.08	8.22	6.50	7.35
K2O	2.64	1.97	1.47	1.48	3.03	4.35	2.65	2.53	4.66	1.59	3.90	0.95
Total	99.27	100.28	100.20	100.32	99.08	100.45	98.75	99.39	98.43	99.15	100.41	99.67

Sample	SM277	SM277	SM277	SM277	SM277	SM277	SM277	SM277	SM277	SM277	SM277	SM277
Quarry	PLMR	PLCR	PLMR	PLCR	PLMR	PLCR	PLMR	PLCR	PLMR	PLCR	PLMR	PLCR
SiO2	64.41	64.28	64.39	64.68	64.53	64.99	64.39	64.12	63.20	63.58	63.53	63.75
Al2O3	21.13	21.72	21.08	21.08	21.43	21.70	21.27	20.28	23.04	22.20	22.92	22.75
Fe2O3	- -	- -	- -	- -	- -	- -	- -	- -	- -	- -	- -	- -
MgO	- -	- -	- -	- -	- -	- -	- -	- -	0.82	- -	- -	- -
CaO	2.89	3.39	3.16	3.05	3.12	3.07	3.12	2.43	3.41	2.62	3.24	3.56
Na2O	7.48	8.06	6.52	6.85	7.25	7.38	6.71	5.46	7.35	7.41	7.95	7.99
K2O	3.13	1.50	4.33	3.57	2.77	2.59	3.84	6.37	2.14	3.11	1.47	1.22
Total	99.04	98.95	99.48	99.23	99.10	99.73	99.33	98.66	99.96	98.92	99.11	99.27

Sample	SM277	SM277	SM277	SM277	SM277	SM277	SM277	SM277	SM277	SM277	SM277	SM277
Quarry	PLMR	PLCR	PLMR	PLCR	KFMR	KFCR	PLMR	PLCR	PRPL	PRPL	PLMR	PLCR
SiO2	63.31	62.89	53.91	54.71	64.34	63.45	63.86	63.97	63.10	64.51	64.15	65.15
Al2O3	23.28	22.53	29.26	28.93	19.49	19.67	22.57	21.77	22.70	21.70	22.65	19.19
Fe2O3	- -	- -	- -	- -	- -	- -	- -	- -	- -	- -	- -	- -
MgO	0.85	- -	- -	- -	- -	- -	- -	- -	- -	- -	- -	- -
CaO	3.54	3.74	11.55	10.79	0.57	0.93	3.20	2.92	4.03	2.99	3.26	1.80
Na2O	7.85	7.95	4.87	5.08	3.39	3.96	7.36	6.93	7.49	8.08	8.38	3.62
K2O	1.23	1.66	- -	- -	10.85	9.53	2.84	3.06	1.86	2.10	1.62	9.60
Total	100.06	98.77	100.26	99.95	99.79	98.82	99.77	98.65	99.18	99.38	100.06	99.36

Sample	SM277	SM281	SM281	SM281	SM281	SM281	SM281	SM281	SM281	SM281	SM281	SM281
Quarry	PRKF	PRMC	PRMC	PRAB	PRAB	PRAB	PRAB	PRAB	PLMR	PLCR	PLMR	PLCR
SiO2	63.04	51.31	51.45	67.82	68.49	68.09	68.47	67.53	59.85	58.93	63.31	62.85
Al2O3	18.86	26.82	25.71	19.90	19.89	19.92	20.42	20.64	25.99	26.37	25.53	23.94
Fe2O3	- -	2.43	2.48	- -	- -	- -	- -	- -	- -	- -	- -	- -
MgO	- -	3.29	3.50	- -	- -	- -	- -	- -	- -	- -	- -	- -
CaO	1.98	0.00	0.33	- -	- -	- -	- -	- -	7.43	7.39	4.44	4.77
Na2O	0.71	- -	- -	11.47	11.38	11.23	11.26	11.04	6.96	6.83	8.41	8.19
K2O	13.71	10.96	11.09	- -	- -	- -	- -	- -	0.48	0.48	0.74	0.89
Total	98.30	94.81	94.56	99.19	99.76	99.24	100.15	99.21	100.71	100.45	101.42	100.64

Sample	SM281	SM281	SM281	SM281	SM281	SM281	SM281	SM281	SM302	SM302	SM302	SM302
Quarry	PLMR	PLCR	PLMR	PLCR	PLMR	PLCR	PLMR	PLCR	LTPL	PLCR	PLMR	LTPL
SiO2	63.45	63.28	63.73	63.64	63.62	62.95	63.83	63.70	60.48	59.44	61.23	59.98
Al2O3	23.50	22.96	23.31	23.16	23.29	23.14	22.91	23.42	25.56	25.14	25.23	26.00
Fe2O3	- -	- -	- -	- -	- -	- -	- -	- -	- -	- -	- -	- -
MgO	- -	- -	- -	- -	- -	- -	- -	- -	- -	- -	- -	- -
CaO	4.55	4.72	5.08	4.89	5.05	4.47	4.86	4.94	7.32	6.77	6.47	7.47
Na2O	8.14	7.71	7.77	7.85	7.69	7.69	7.85	7.81	6.81	6.96	6.86	6.71
K2O	0.97	1.19	0.89	0.88	0.83	1.02	1.13	0.94	0.74	0.66	0.72	0.54
Total	100.61	99.86	100.78	100.42	100.48	99.27	100.58	100.81	100.91	98.97	100.51	100.70

Sample	SM302	SM302	SM302	SM302	SM302	SM302	SM302	SM302	SM302	SM302	SM302	SM302
Quarry	PLMR	PLCR	PLMR	PLCR	PLMR	PLCR	PLMR	PLCR	PLMR	PLCR	PLMR	PLCR
SiO2	60.13	62.68	57.21	57.07	57.77	57.64	61.77	60.40	60.85	61.72	60.21	60.40
Al2O3	25.69	24.01	26.78	27.58	27.78	27.43	24.98	25.17	25.49	24.12	25.24	25.67
Fe2O3	- -	- -	- -	- -	- -	- -	- -	- -	- -	- -	- -	- -
MgO	- -	- -	- -	- -	- -	- -	- -	- -	- -	- -	- -	- -
CaO	7.32	5.63	8.95	9.05	9.34	9.12	5.78	6.68	7.07	6.10	6.44	6.88
Na2O	6.66	7.43	5.94	6.16	6.02	5.85	7.45	7.07	7.18	6.91	6.52	6.66
K2O	0.58	0.83	0.40	0.32	0.25	0.42	0.70	0.70	0.72	1.21	0.85	0.76
Total	100.38	100.58	99.78	100.18	101.16	100.46	100.68	100.54	101.31	100.06	99.26	100.37

Sample	SM302	SM302	SM302	SM302	SM302
Quarry	PLMR	PLCR	LTPL	LTPL	LTPL
SiO2	62.31	60.35	62.00	61.87	61.84
Al2O3	24.43	25.82	24.66	24.77	24.58
Fe2O3	- -	- -	- -	- -	- -
MgO	- -	- -	- -	- -	- -
CaO	5.63	6.93	6.11	5.24	6.08
Na2O	7.61	6.98	7.48	7.88	7.31
K2O	0.91	0.66	0.73	0.90	0.79
Total	100.89	100.74	100.98	101.12	100.60

APPENDIX 4.9.

Microprobe analyses of authigenic K-feldspars present in the Greek bentonites.

Sample	SM66	SM66	SM66	SM66	SM66	SM66	SM66	SM66	SM66	SM66	SM66	SM66
Quarry	BMKF	BMKF	BMKF	BMKF	BMKF	BMKF	BMKF	BMKF	BMKF	BMKF	BMKF	BMKF
SiO2	66.93	65.40	64.58	65.10	65.19	65.23	64.27	65.98	65.73	64.52	65.73	66.06
Al2O3	17.63	17.15	18.80	18.47	18.50	18.61	18.07	18.19	18.68	18.30	18.72	18.22
Fe2O3	- -	- -	- -	- -	- -	- -	- -	- -	- -	- -	- -	- -
MgO	- -	- -	- -	- -	- -	- -	- -	- -	- -	- -	- -	- -
CaO	- -	- -	- -	- -	- -	- -	- -	- -	- -	- -	- -	- -
Na2O	- -	- -	- -	- -	- -	- -	- -	- -	- -	- -	- -	- -
K2O	16.20	16.56	16.81	17.25	16.78	17.09	16.80	16.42	16.75	16.61	16.51	16.66
Total	100.76	99.11	100.19	100.82	100.47	100.93	99.14	100.59	101.15	99.43	100.96	100.94

Sample	SM66	SM66	SM66	SM66	SM66	SM66	SM66	SM66	SM66	SM66	SM66	SM66
Quarry	BMKF	BMKF	BMKF	BMKF	BMKF	BMKF	BMKF	BMKF	BMKF	BMKF	BMKF	BMKF
SiO2	66.26	66.27	66.92	66.16	66.37	66.34	65.08	65.38	65.65	66.22	65.87	66.68
Al2O3	17.33	17.82	17.98	17.61	17.32	16.78	17.75	17.38	18.36	17.24	18.45	17.31
Fe2O3	- -	- -	- -	- -	- -	- -	- -	- -	- -	- -	- -	- -
MgO	- -	- -	- -	- -	- -	- -	- -	- -	- -	- -	- -	- -
CaO	- -	- -	- -	- -	- -	- -	- -	- -	- -	- -	- -	- -
Na2O	- -	- -	- -	- -	- -	- -	- -	- -	- -	- -	- -	- -
K2O	16.77	16.33	15.76	16.44	16.26	16.59	16.38	16.66	16.32	16.41	16.11	16.29
Total	100.36	100.42	100.66	100.21	99.95	99.71	99.21	99.42	100.33	99.87	100.43	100.28

Sample	SM66	SM66	SM66	SM66	SM155	SM155	SM155	SM155	SM155	SM155	SM155	SM155
Quarry	BMKF	BMKF	BMKF	BMKF	BMAK	BMAK	BMAK	BMAK	BMAK	BMAK	BMAK	BMAK
SiO2	65.69	65.35	65.73	65.88	66.26	65.15	66.06	66.60	66.75	65.86	66.87	65.91
Al2O3	17.06	18.31	16.61	17.45	16.86	18.04	17.47	17.62	17.84	17.22	17.09	17.11
Fe2O3	- -	- -	- -	- -	- -	- -	- -	- -	- -	- -	- -	- -
MgO	- -	- -	- -	- -	- -	- -	- -	- -	- -	- -	- -	- -
CaO	- -	- -	- -	- -	- -	- -	- -	- -	- -	- -	- -	- -
Na2O	- -	- -	- -	- -	- -	- -	- -	- -	- -	- -	- -	- -
K2O	15.84	16.02	16.33	16.85	16.09	16.15	16.10	16.03	15.96	16.39	15.91	15.93
Total	98.59	99.68	98.67	100.18	99.21	99.34	99.63	100.25	100.55	99.47	99.87	98.85

Sample	SM155	SM155	SM155	SM99	SM99	SM99	SM99	SM99	SM99	SM99	SM99	SM99
Quarry	BMAK	BMAK	BMAK	BMTS	BMTS	BMTS	BMTS	BMTS	BMTS	BMTS	BMTS	BMTS
SiO2	66.03	65.21	65.51	64.23	64.92	64.97	64.71	64.58	64.38	65.90	65.08	65.79
Al2O3	17.21	17.56	17.48	18.11	17.77	17.91	17.71	18.24	18.48	17.28	17.88	17.01
Fe2O3	- -	- -	- -	- -	- -	- -	- -	- -	- -	- -	- -	- -
MgO	- -	- -	- -	- -	- -	- -	- -	- -	- -	- -	- -	- -
CaO	- -	- -	- -	- -	- -	- -	- -	- -	- -	- -	- -	- -
Na2O	- -	- -	- -	- -	- -	- -	- -	- -	- -	- -	- -	- -
K2O	16.07	16.12	15.97	17.11	16.33	16.66	16.36	16.75	16.78	16.01	16.28	16.31
Total	99.31	98.89	98.76	99.45	99.02	99.54	98.78	99.87	99.64	99.19	99.24	99.11

Sample	SM99	SM99	SM99	SM99	SM277	SM277	SM277	SM277	SM277	SM277
Quarry	BMTS	BMTS	BMTS	BMTS	BKPR	BKPR	BKPR	BKPR	BKPR	BKPR
SiO2	64.53	64.52	64.30	64.40	66.51	65.92	65.24	66.40	66.70	65.15
Al2O3	17.86	18.25	18.47	18.17	17.72	17.33	17.44	17.13	17.29	17.81
Fe2O3	- -	- -	- -	- -	- -	- -	- -	- -	- -	- -
MgO	- -	- -	- -	- -	- -	- -	- -	- -	- -	- -
CaO	- -	0.43	- -	- -	- -	- -	- -	- -	- -	- -
Na2O	- -	- -	- -	- -	- -	- -	- -	- -	- -	- -
K2O	16.31	15.98	17.03	16.90	16.51	16.33	16.29	15.96	15.85	16.31
Total	98.70	99.18	99.80	99.47	100.74	99.58	98.97	99.49	99.84	99.27

APPENDIX 4.10

Microprobe analyses of carbonates present in the Tsantili deposit, Milos

Sample	SM99	SM99	SM99	SM99	SM99	SM99	SM99	SM99	SM99	SM99
Quarry	TSCA	TSCX	TSCA	TSCA	TSCA	TSCA	TSCA	TSCA	TSCA	TSCA
FeO	- -	1.19	- -	0.61	- -	0.56	1.54	1.69	1.21	1.18
MnO	2.61	3.84	5.19	5.00	6.15	2.83	3.85	3.86	3.83	4.16
MgO	- -	- -	- -	- -	0.71	- -	15.15	15.62	15.08	14.01
CaO	52.21	51.11	49.84	50.02	49.22	51.94	32.93	33.06	33.50	34.20
Total	54.82	56.14	55.03	55.63	56.08	55.33	53.47	54.23	53.62	53.55

Sample	SM99	SM99	SM99	SM99	SM99	SM99
Quarry	TSCA	TSCA	TSCA	TSCA	TSCA	TSCA
FeO	2.23	29.27	28.58	30.98	29.42	28.34
MnO	4.17	22.29	22.65	13.38	18.11	21.77
MgO	15.07	2.84	2.94	9.47	6.36	4.43
CaO	32.35	2.69	2.70	2.40	2.96	3.18
Total	53.82	57.09	56.87	56.23	56.85	57.72

APPENDIX 5.1

Instrumental conditions used for determination of the major elements

Element	Radiation	kV	mA	Crystal	Counting time (sec)	Counter	Collimator
Si	Ka_1	50	50	PE	20	FPC	Coarse
Ti	Ka_2	50	50	20	40	FPC	Fine
Al	Ka_1	50	50	PE	30	FPC	Coarse
Fe	Ka_2	50	50	20	25	FPC	Fine
Mn	Ka_2	50	50	22	50	FPC	Fine
Mg	Ka_1	50	50	AX	50	FPC	Coarse
Ca	Ka_2	50	50	20	25	FPC	Fine
Na	Ka_1	50	50	AX	50	FPC	Coarse
K	Ka_2	50	50	20	50	FPC	Fine
P	Ka_1	50	50	PE	50	FPC	Fine

PE= Pentaerythritol

20= LiF_{200}

22= LiF_{220}

AX= AX_{06} (multilayer crystal)

FPC= Flow proportional counter

APPENDIX 5.2

Method used for determination of Loss of Ignition

1. Determination of the loss of ignition takes place during the preparation of the fusion beads. 1gr of air-dried (at 110^{o}C) sample mixed with 5gr of flux (mixture of 80% Li-metaborate with 20% Li-tetraborate) in a 95%Pt/5%Au crucible is placed in a vertical furnace for 10 minutes at the temperature of 1050^{o}C.
2. The crucible is removed from the oven and allowed to cool in a desiccator for 10 minutes. After cooling, the crucible is weighted. The loss of ignition is determined from the following formula:

LOI (%)=((A-C)/(B-C)) X 100

where A=Mass of Pt-crucible+sample before ignition

B=Mass of Pt-crucible+sample after ignition

C=Crucible mass

3. The amount of sample lost during ignition plus the calculated loss of ignition for this addition is added in the crucible, and preparation of the fusion bead proceeds.

APPENDIX 5.3

Calibration curve used for determination of the SO_3.

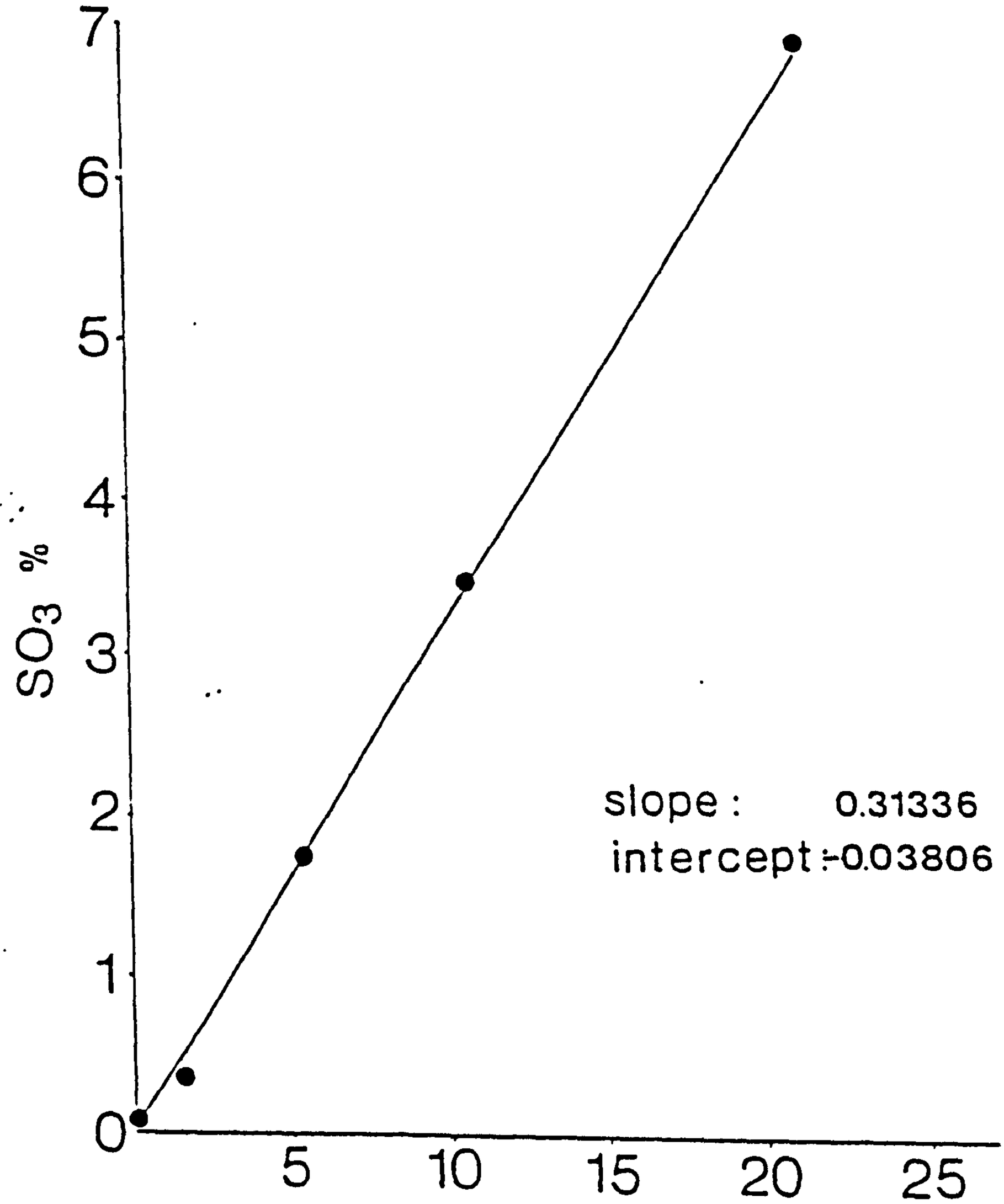

APPENDIX 5.4.

5.4.1. Sample preparation for determination of the REE.

1. Weight out 0.5 gr of finely powdered rock previously ignited for 1.5h at *ca.* 950^{o}C into a 100ml teflon beaker. Use an antistatic gun prior to weighing, to avoid spraying of the sample on the walls of the beaker.
2. Add 15ml 40% HF (hydrofluoric acid) using a polyethylene measuring cylinder, followed by 4ml 67-70% $HClO_4$ (perchloric acid) from a dispenser bottle.
3. Place the teflon beaker on a hot plate at about 180-200^{o}C to digest the sample and evaporate down to incipient dryness. This will take 3-4 hours. Add another 3-4ml $HCLO_4$ and mix by gently swirling the teflon beaker around. Evaporate down to incipient dryness again. The second stage of the digestion is required to ensure that any fluorides produced by the initial digestion are converted to chlorides and perchlorates, by ensuring that all HF has been driven off.
4. The digestion products are re-dissolved in 20ml warmed 25% HCl on the hot plate. The contents of the teflon beaker are then transferred into clean 100ml pyrex beakers, thoroughly rinsing out the teflon beaker with deionized-distilled water. If the solution is free from residues make the volume up to *ca.* 50ml with more HCl. If there appear to be any residues try gently warming the solution again in the pyrex beaker.
5. Before the solution is added on the ion-exchange column the latter should be charged. Charging involves the passage of a series of reagents through the column. These include in turn: a) 250ml of distilled-deionized water b) 250ml of 4N HCl c) 250ml of 1N HCL. The addition of each of the reagents takes place when the level of the previously added reagent is 2-3cm above the column.
6. Immediately after the passage of the 250ml of 1N HCl the sample solution is loaded. When about 2-3cm of sample solution has been left above the resin add 450ml of 1.7N HCl and allow it to pass through the resin. Up to this point all the liquid passing through the resin was collected in a polyethylene bottle and discharged.
7. Replace the polyethylene bottle with a 1l pyrex beaker, cover it with cling film and place it under the column. Now add 600ml 4N HCl and collect the solution passing through the column in the glass beaker. It should contain the REE plus some Sr, Ba and Ca.
8. Remove the cling film an place the beaker on a hot plate (under a fume cupboard) to evaporate the solution down to 50-100ml. Transfer it to a 50ml pyrex beaker which has previously been soaked in 10% HNO_3 and continue to evaporate the solution.
9. When the solution has been evaporated down to 10-15ml add 2ml concentrated HNO_3 and evaporate down to dryness.

5.4.2. Accuracy and precision of the XRF analyses obtained for major elements. Mean values represent average of 5 analyses. The recommended values (R.Value) for the international standards are from Govindaraju (1989).

Standard	Mean BOB1	StDev BOB1	%StDev BOB1	R.Value BOB1	Mean JA1	StDev JA1	%StDev JA1	R.Value JA1	Mean NIMG	StDev NIMG	%StDev NIMG	R.Value NIMG
SiO2	50.59	0.10	0.20	50.57	66.06	0.27	0.41	64.28	77.75	0.49	0.63	76.04
TiO2	1.29	0.05	0.35	1.29	0.88	0.00	0.57	0.87	0.10	0.00	0.20	0.09
Al2O3	16.40	0.04	0.24	16.66	14.35	0.05	0.32	15.03	11.52	0.07	0.63	12.01
Fe2O3	8.55	0.01	0.16	8.67	7.05	0.02	0.23	6.97	2.02	0.02	1.04	2.03
MnO	0.14	0.00	0.96	0.14	0.14	0.00	0.71	0.15	0.01	0.00	15.38	0.02
MgO	7.66	0.03	0.34	7.63	1.61	0.02	0.99	1.62	0.09	0.01	13.33	0.06
CaO	11.13	0.02	0.21	11.29	5.68	0.03	0.48	5.70	0.75	0.00	0.40	0.78
Na2O	3.12	0.01	0.40	3.10	3.30	0.03	0.88	3.87	2.91	0.01	0.34	3.37
K2O	0.37	0.00	0.32	0.36	0.75	0.00	0.40	0.78	4.94	0.01	0.24	5.01
P2O5	0.16	0.00	0.92	0.17	0.17	0.00	1.21	0.16	0.01	0.00	6.00	0.01

Standard	Mean SO1	StDev SO1	%StDev SO1	R.Value SO1	Mean SO2	StDev SO2	%StDev SO2	R.Value SO2
SiO2	59.09	0.53	0.90	58.21	61.47	0.39	0.64	60.19
TiO2	0.91	0.01	0.66	0.92	1.61	0.01	0.37	1.61
Al2O3	18.13	0.10	0.56	18.62	16.15	0.10	0.62	17.01
Fe2O3	9.04	0.01	0.14	9.08	8.96	0.03	0.37	8.89
MnO	0.12	0.00	1.67	0.12	0.01	0.00	10.00	0.10
MgO	4.10	0.03	0.76	4.06	1.05	0.02	1.81	1.00
CaO	2.62	0.01	0.57	2.60	3.10	0.01	0.02	3.12
Na2O	2.34	0.02	0.90	2.86	2.36	0.02	0.97	2.79
K2O	3.28	0.02	0.64	3.37	3.23	0.01	0.28	3.31
P2O5	0.16	0.00	1.25	0.16	0.79	0.01	0.76	0.76

APPENDIX 5.4.3

Precision and accuracy of the XRF measurements for trace elements. The average value quoted is the mean for a total of 5 analyses per standard. The recommended values (R.Value) are from Govindaraju (1989).

Standard	Mean BE-N	StDev BE-N	%StDev BE-N	R.Value BE-N	Mean TYG	StDev TYG	%Stdev TYG	R.Value TYG	Mean GA	StDev GA	%StDev GA	R.Value GA
V	241.90	11.90	4.90	235.00	16.70	1.40	8.40	15.00	38.30	6.90	18.00	38.00
Cr	347.30	15.20	4.40	360.00	4.60	2.40	52.20	8.00	27.20	1.50	5.50	12.00
Ni	274.10	7.10	2.60	267.00	6.30	0.50	7.90	4.00	9.00	2.70	30.00	7.00
Zn	121.40	4.60	3.80	120.00	64.30	4.80	7.50	70.00	71.90	7.10	9.90	80.00
Rb	49.30	2.60	5.30	47.00	63.60	3.70	5.80	67.00	175.30	12.00	6.80	175.00
Sr	1345.00	26.80	2.00	1370.00	63.90	4.00	6.30	65.00	301.00	10.30	3.40	310.00
Y	29.60	1.90	6.40	30.00	47.20	4.20	8.90	46.00	21.00	3.20	15.20	21.00
Zr	266.00	3.40	1.30	265.00	214.10	10.90	5.10	198.00	144.00	4.50	3.10	150.00
Nb	109.30	1.60	1.50	100.00	11.90	1.70	14.30	12.60	11.60	0.60	5.20	12.00
Ba	1095.60	26.00	2.40	1025.00	418.80	11.20	2.70	416.00	847.60	21.40	2.50	840.00
La	79.60	1.80	2.30	82.00	33.40	3.80	11.40	31.00	33.80	2.00	5.90	40.00
Ce	147.10	6.60	4.50	152.00	64.50	4.00	6.20	65.00	61.80	3.70	6.00	76.00
Nd	64.00	4.00	6.30	70.00	29.30	1.40	4.80	28.00	23.10	1.20	5.20	27.00
Th	11.00	1.00	9.10	11.00	14.80	1.20	8.10	16.80	17.60	0.90	5.10	17.00

Sample Deposit	Mean W-2	StDev W-2	%StDev W-2	R.Value W-2	Mean MRG1	StDev MRG1	%StDev MRG1	R.Value MRG1	Mean NIMG	StDev NIMG	%StDev NIMG	R.Value NIMG
V	264.30	3.40	1.30	262.00	536.50	10.70	2.00	526.00	1.00	1.10	110.00	2.00
Cr	92.10	2.90	3.10	93.00	474.50	19.10	4.00	430.00	19.60	1.60	8.20	12.00
Ni	70.30	2.30	3.30	70.00	192.00	9.00	4.70	193.00	10.90	1.25	11.50	8.00
Zn	67.70	2.40	3.50	77.00	204.60	8.00	3.90	191.00	54.70	2.70	4.90	50.00
Rb	24.00	2.20	9.20	20.00	10.70	1.90	17.80	8.50	317.10	7.60	2.40	320.00
Sr	193.40	5.40	2.80	194.00	262.50	4.80	1.80	266.00	118.00	0.60	5.10	10.00
Y	21.40	1.50	7.00	24.00	11.70	1.10	9.40	14.00	145.70	3.90	2.70	143.00
Zr	96.80	3.00	3.10	9.40	107.20	3.10	2.90	108.00	304.70	4.80	1.60	300.00
Nb	7.30	0.80	11.00	7.90	19.30	1.60	8.30	20.00	55.90	3.90	7.00	53.00
Ba	190.20	12.30	6.50	182.00	57.20	3.50	6.10	61.00	120.50	2.50	2.10	120.00
La	10.60	4.60	43.30	11.40	10.00	3.30	33.00	9.80	108.50	5.40	5.00	109.00
Ce	24.10	2.00	8.30	24.00	29.40	4.20	14.30	26.00	198.10	1.30	0.70	195.00
Nd	12.30	1.60	13.00	14.00	18.40	0.80	4.30	19.20	74.60	1.67	2.20	72.00
Th	1.70	0.90	52.90	2.20	2.00	1.70	85.00	0.90	53.00	2.60	4.90	51.00

Sample Deposit	Mean AN-G	StDev AN-G	%StDev AN-G	R.Value AN-G	Mean BOB1	StDev BOB1	%StDev BOB1	R.Value BOB1
V	69.50	4.40	6.30	70.00	225.70	10.10	4.50	234.00
Cr	49.80	2.50	5.00	50.00	276.70	4.50	1.60	304.00
Ni	34.20	5.20	15.20	36.50	112.10	1.80	1.60	115.00
Zn	22.20	4.20	18.90	20.00	86.90	5.60	6.40	63.00
Rb	3.60	1.80	50.00	2.60	8.30	1.60	19.20	6.00
Sr	76.50	3.00	3.90	71.80	195.20	4.60	2.40	190.00
Y	7.20	1.60	22.20	7.70	26.90	1.03	3.80	26.00
Zr	11.10	2.20	20.00	9.60	107.30	3.40	3.20	100.00
Nb	0.50	0.60	120.00	0.60	3.80	1.20	31.60	4.70
Ba	29.80	5.40	18.10	34.00	44.60	2.60	5.80	44.00
La	5.20	2.80	53.80	2.00	7.80	2.40	30.80	5.60
Ce	3.40	1.80	52.90	4.70	15.50	2.40	15.50	14.70
Nd	2.20	3.00	136,00	3.00	11.00	1.24	11.30	10.90
Th	0.70	1.70	243.00	0.00	0.50	0.80	160.00	1.40

5.4.4. Accuracy and precision of the ICP analyses for REE. The mean values represent the average of 5 analyses. The recommended values are from N. Marsh & A. Holmes, University of Leicester (R.Val1) and Ando *et al.*, (1987) (R.Val2).

	Mean	StDev	%StDev	R.Val1	R.Val2
Standard	Jb-1a	Jb-1a	Jb-1a	Jb-1a	Jb-1a
La	34.24	1.07	2.70	37.26	38.00
Ce	66.00	1.36	2.10	63.56	67.00
Nd	29.04	1.09	3.80	26.25	27.00
Sm	4.74	0.35	7.40	5.09	5.00
Eu	1.80	0.11	6.10	1.53	1.52
Dy	4.91	0.30	6.10	4.10	4.20
Er	- -	- -	- -	- -	- -
Yb	2.29	0.06	2.60	2.13	2.10
Lu	0.33	0.01	3.00	0.32	0.31

APPENDIX 5.5.

Computer program used to run the CANDISC procedure in the SAS statistical package.

```
DATA MILOS;
INFILE 'TRCHEM7.DAT';
INPUT Nb Zr Y Th Ni V Cr La Ce Nd Qua_No@@;
If Qua_No=1 THEN Quarry='BMAN';
If Qua_No=2 THEN Quarry='BMKF';
If Qua_No=3 THEN Quarry='BMTS';
If Qua_No=4 THEN Quarry='BMAH';
If Qua_No=5 THEN Quarry='BMAK';
If Qua_No=6 THEN Quarry='BMGF';
If Qua_No=7 THEN Quarry='BMRS';
If Qua_No=8 THEN Quarry='BMKK';
If Qua_No=9 THEN Quarry='BMZL';
If Qua_No=0 THEN Quarry='BMRM';
If Qua_No=11 THEN Quarry='BMAG';
PROC CANDISC ALL OUT=DISC;
CLASSES QUARRY;
VAR Nb Zr Y Th Ni V Cr La Ce Nd;
PROC PLOT;
PLOT CAN2*CAN1=Qua_No;
Title 'Plot of Canonical Discriminant Functions';
RUN;
```

In this program the name of the data file is TRCHEM7.DAT while the initials BMAN, BMKF, BMTS, BMAH, BMAK, BMGF, BMRS, BMKK, BMZL, BMRM and BMAG correspond to the various bentonite deposits of Eastern Milos. The same initials have been used in Chapters 4 and 5.

APPENDIX 7.1

Method used for Na-activation of the Greek bentonites and the determination of the swelling volume (adopted from Morgan 1990a).

1. Weight 5gr of less than 125μm bentonite powder (BS410) which have previously been dried at 60-65^{o}C overnight in a watch glass on a top pan balance.
2. Add 1% anhydrous sodium carbonate on the bentonite powder. Mix them thorougly through grinding in a porcelain pestle and mortar.
3. Add 10ml of distilled of water and using a spatula spread it over the bentonite-Na-carbonate mixture to make a uniform thick paste. Poor quality bentonites, bentonites with high S-content or K-bentonites usually require less than 10ml of water to form the paste. On the contrary, for high swelling bentonites 15ml water might be necessary.
4. Place the watch-glass in a drying oven at 60-65^{o}C overnight. Grind the clay gently with pestle and mortar to pass through a 125μm sieve (BS410). The material is now ready for determination of the swelling volume.
5. Repeat the experiment using 2, 3, 4, 5 and if necessary 6% Na-carbonate.
6. Add 15ml of destiled water in a test tube. Weigh 1 gr of the Na-activated clay, and by means of a funnel, the tip of which is about 1cm above the level of water in the test tube, add the clay in 8-10 small portions over a 2 hours interval. Before the addition of every portion hit gently the bottom of the tube on your palm, to level off the clay sediment at the bottom of the test tube.
7. High quality bentonites develop swelling volumes well in excess of the height of the water column. Therefore the experiment is stopped when the gel volume has risen up to 1cm lower than the water level. The clay left is weighted and the swelling volume is calculated from the amount of clay used to obtain the observed swelling volume.
8. Measure the height of the gel to the nearest millimetre and convert the measured value to volume using the calibration curve shown in Appendix 7.2. The swelling volume per 10gm of clay is found by multiplication of the volume found with the calibration curve by 10.
9. Repeat the experiment using the same bentonite activated with different Na-carbonate contents. The highest value obtained for the clay column corresponds to the maximum swelling volume (or simply swelling volume)

APPENDIX 7.2.

Calibration curve used to convert the volume of the bentonite gel to swelling volume.

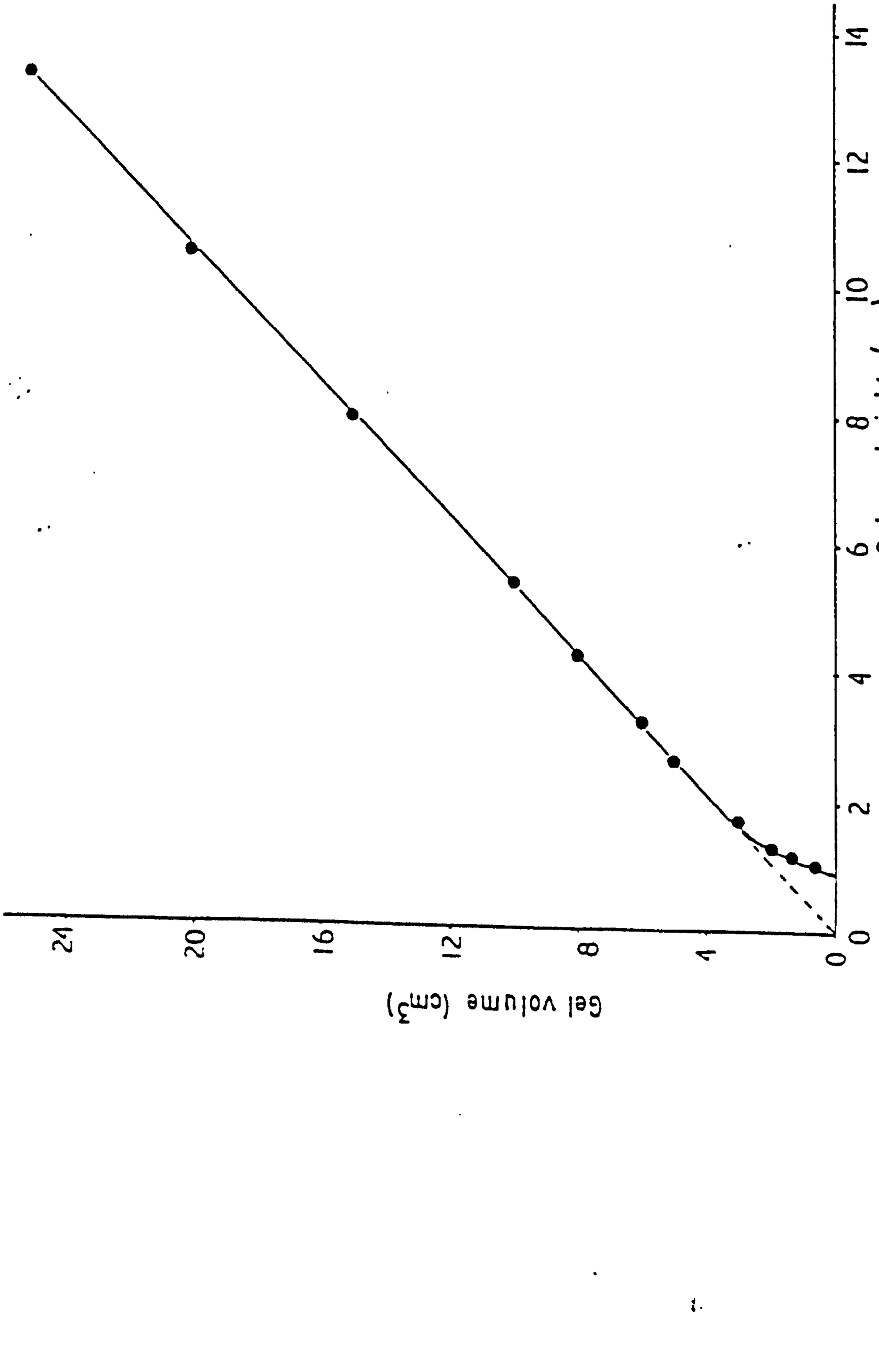

APPENDIX 8.1.

Measurement of the rheological properties using a FANN 35S viscometer.

(Adopted from API specifications, API 1969).

1. Dry the bentonites overnight at 60-65^{o}C, grind them in a TEMA mill for 10-15 seconds to pass through a 250μm sieve (BS410).
2. Weigh out 25.71 gr of the clay on a top pan belance. This amount corresponds to a 6.42% bentonite suspension using 400ml distiled water. However since the method involves the addition of Na-carbonate in amount which corresponds to the maximum swelling (optimum Na-carbonate content), the volume of water used to make the 6.42% bentonite suspension takes into account the carbonate addition too.
3. Switch a high speed mixer on and add the bentonite and the optimum carbonate content, while stirring in the mixer.
4. After 5 minutes remove the container from the mixer scrape sides to dislodge any bentonite adhering to the container by means of a spatula.
5. Replace on mixer and continue stirring for an additional 15 minutes. The total mixing time should be 20 ± 1 minute.
6. Remove the suspension from the container and place it in a 1l beaker. Cover the beaker and let the suspension to age for 16 hours (practically overnight).
7. Remove the aged suspension from the beaker and using a direct-reading FANN viscometer record the dial readings at 600 and 300rpm. The various rheological parameters are calculated as follows:

a) Apparent viscosity (cps): Dial reading at 600rpm :2

b) Plastic viscosity (cps): Dial reading at 600rpm-300rpm.

c) Yield (lbs/100ft^{2}): Dial reading at 300rpm-plastic viscosity.

d) Measurement of yield strength (lbs/100ft^{2}): Stir the sample thoroughly at 600rpm and turn the motor off. Allow desired rest time (in this case 10 seconds and 10 minutes). Using the lowest speed (3rpm) read dial at instant of gel break.

APPENDIX 8.2.

Determination of the filtrate loss of a bentonite suspension using an 1/2 area filter press.

(Adopted from the API specifications for OCMA grade bentonites).

1. Stir the suspension for 1 minute in the high speed mixer after measuring the viscosity.
2. Be sure that each part of the cell, particularly the screen is clean and dry, and that the gaskets are not distorted or worn. Pour the mud sample into the cell to within 13mm of the top and put the filter paper in place.
3. Place a measuring cylinder under the filter press, close the relieve valve and adjust the regulators so that a pressure of 100 ± 5 psi is applied in 30 seconds or less.
4. After 7.5 minutes replace the cylinder with a 10ml dry measuring cylinder and collect the filtrate for another 22.5 minutes (*i.e* the total duration of the test is 30 minutes). It is not necessary to measure the filtrate volume during the first 7.5 minutes of the test.
5. After the end of 30 minutes remove the measuring cylinder and record the volume of the filtrate collected between 7.5 and 30 minutes. The filtrate loss is calculated from the equation:

Filtrate loss in cm^3 = 2 x (volume filtrate cm^3).

APPENDIX 9.1.

Nomogram used for the calculation of the surface area.

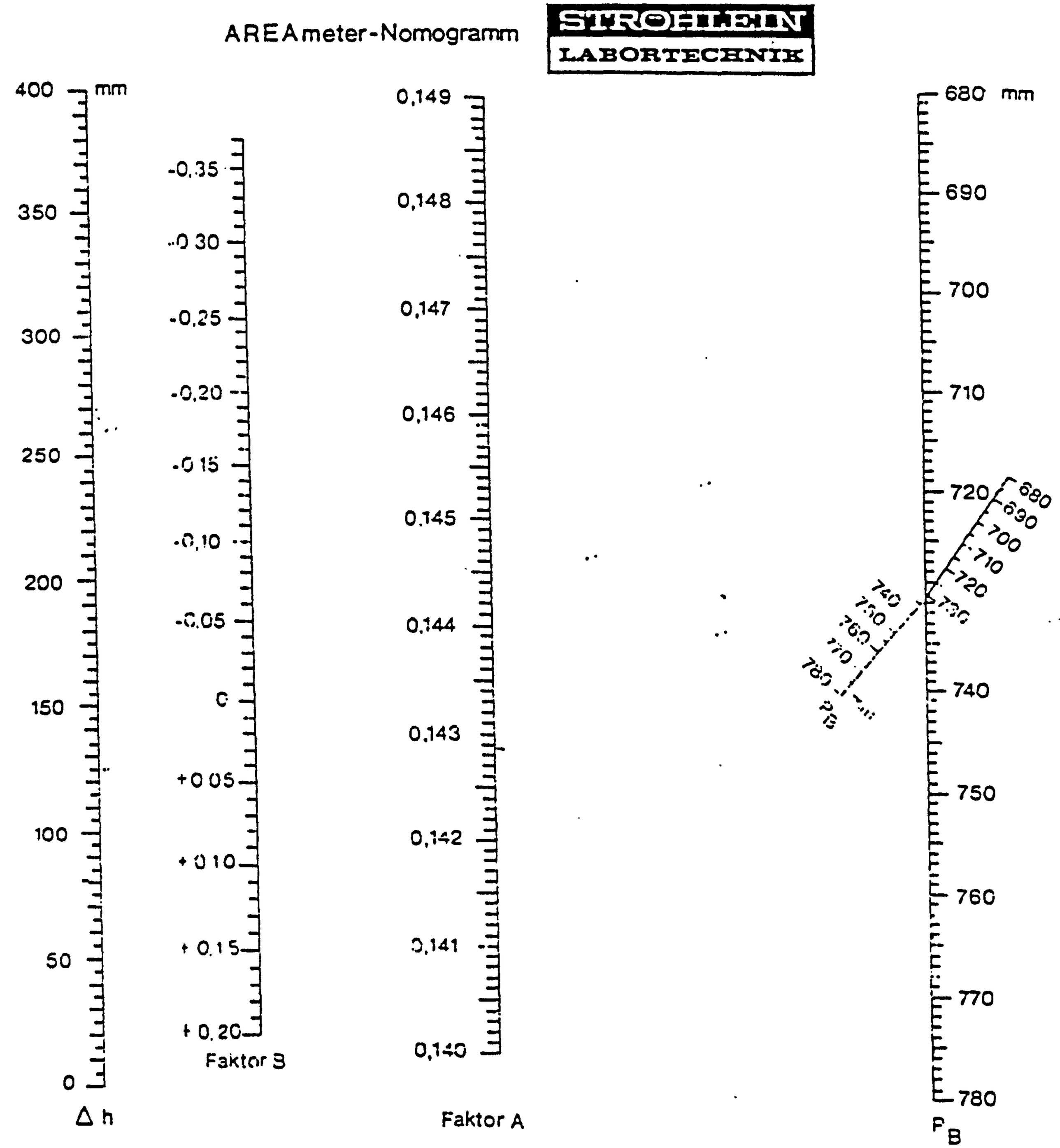

APPENDIX 9.2.

Calibration curve used to calculate the concentration of the a-carotene adsorbed during the decolourization experiments

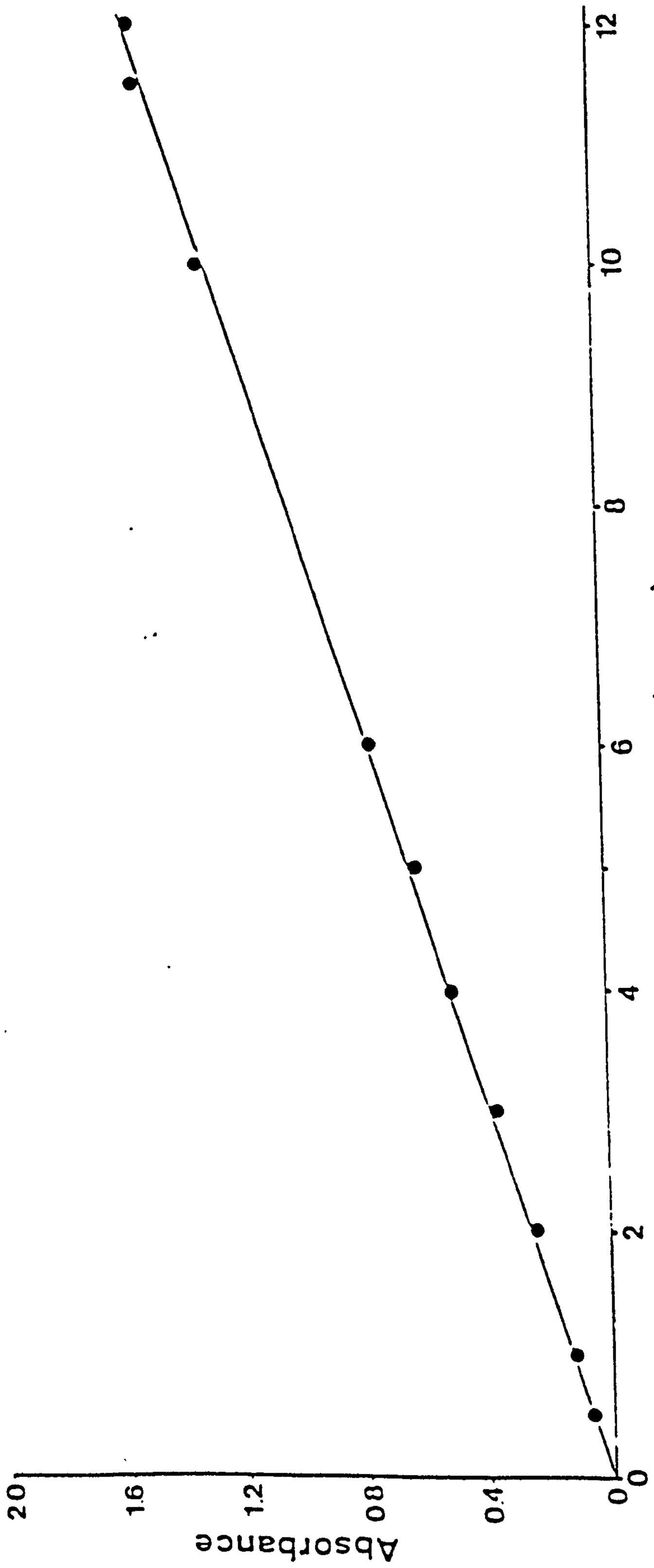

APPENDIX 10.1

Determination of moisture content using a rapid moisture tester.

(Adopted from BCIRA Broadsheet 16-2)

1. Set up the balance provided with the instrument and weigh a sufficient amount of bentonite clay. Place the weighed bentonite in the cap of the metal container of the moisture tester.
2. Using the provided scoop place 1 measure of calcium carbide in the body of the container.
3. Hold the body of the emtal container in a horizontal position and fix the cap tightly in position by means of the stirrup and locking screw. Take care so that the bentonite and the calcium carbide do not mix during this stage.
4. Turn the container into a vertical position with the dial pointing downwards, and mix the carbide and the bentonite thoroughly by shaking the instrument for a few seconds.
5. Invert the container, tap and allow to stand for one minute.
6. Return to the original vertical position and shake for a furher few seconds.
7. Repeat stages 5 and 6 once more.
8. Hold the instrument in a horizontal position and read the moisture content of the sand directly from the pressure-gauge fitted in the base of the instrument.

APPENDIX 10.2.

Preparation of standard test species.

(Methods adopted from BCIRA broadsheet 16-1).

10.2.1. Preparation of 2in diameter x 2in AFS test pieces, using a Ridsdale-Dietert rammer.

1. Weigh out the quantity of greensand (*i.e* mixture of silica sand + 5% bentonite + 2.5% tempering water mulled in a suitable muller) required to form the test piece. 160 gr is a suitable initial trial weight to use.
2. The greensand is placed in a 5 in high spherical tube with an internal diameter of 2 in, the base of which has been sealed by a suitable metal base-plug or metal cup.
3. The weight on the hammer is raised by means of the handle provided on the side of the equipment, and the specimen tube with the base plug or cup are then placed under the ramming head with the centralizing peg on the metal plug located in the hole of the base plate.
4. The rammer head and weight are lowered until they are supported by the sand in the container.
5. The rammer weight is raised and allowed to fall freely through a 2 in height by the cam on the equipment. This is repeated 2 more times (three times in total).
6. After the thitd ramming, the gauge mark on the upper end of the rammer rod should be between the limits set on the tolerance scale, to give a specimen height of 2 ± 1/32 in. If the specimen height is not within the tolerance allowed, the test piece is discarded and another one is prepared using different amount of greensand.
7. The specimen tube is removed from the rammer; the test piece can be removed from the tube by means of a suitable stripping post.

10.2.2. Preparation of 50mm diameter x 50mm DIN test pieces.

1. These test pieces are prepared with a George Fischer sand rammer Type PRA (DIN). They are used only for the determination of the wet tensile strength.
2. The preparation of the test pieces takes place as in the case of AFS test pieces. The difference is in the actual weight of the rammer and the height from which it falls on the sample. The sample weight used is 8 gr less than in the AFS test pieces.

APPENDIX 10.3.

Determination of the green compression strength.

(Adopted from BCIRA broadsheet 16-4)

1. Prepare three AFS test pieces with the method described in Appendix 10.2 using a Ridsdale-Dietert rammer.
2. Place the test speciment between the correct set off compression heads.
3. Place the magnetic rider in position on the scale in front of the pendulum weight. The pendulum weight is raised by switching on the motor of the instrument.
4. At the point the test piece breaks record the value of the green compression strength in lbs/in^2 at the left trailing edge of the magnetic rider on the appropriate scale. This value can be converted to kN/m^2 (SI system) if multiplied by 6.89476.
5. Repeat the test for the rest 2 specimens, record the green compression strength values and take the avarage values. The reproducibility of the test is good.

APPENDIX 10.4

Measurement of the shatter index

(Adopted from BCIRA broadsheet 16-5)

1. Prepare three AFS test-specimens using the Ridsdale-Dietert rammer (see Appendix 10.2).
2. Push the specimen tube upwards onto the stripping post so that the specimen is ejected and falls squarely onto the anvil of the equipment (see Figure below).
3. As test piece shatters on the anvil the fragments fall onto the sieve and the amount of sand passing through the sieve is collected and weighed.
4. The result is expressed as an index, the shatter index, which is the percentage of sand remaining on the sieve calculated from the original weight of the test piece:

Shatter index: (A-B) X 100 / A

where A= specimen weight

B= weight passing the sieve

5. Repeat the test for the rest two test-specimens, record the shatter indices and take the average value. The test is reproducible provided that no impetus is given to the test piece when it is stripped from the specimen tube.

FIGURE 10.4.1. Pneumatic apparatus used for the determination of shatter index

(Modified from BCIRA Report, 1985)

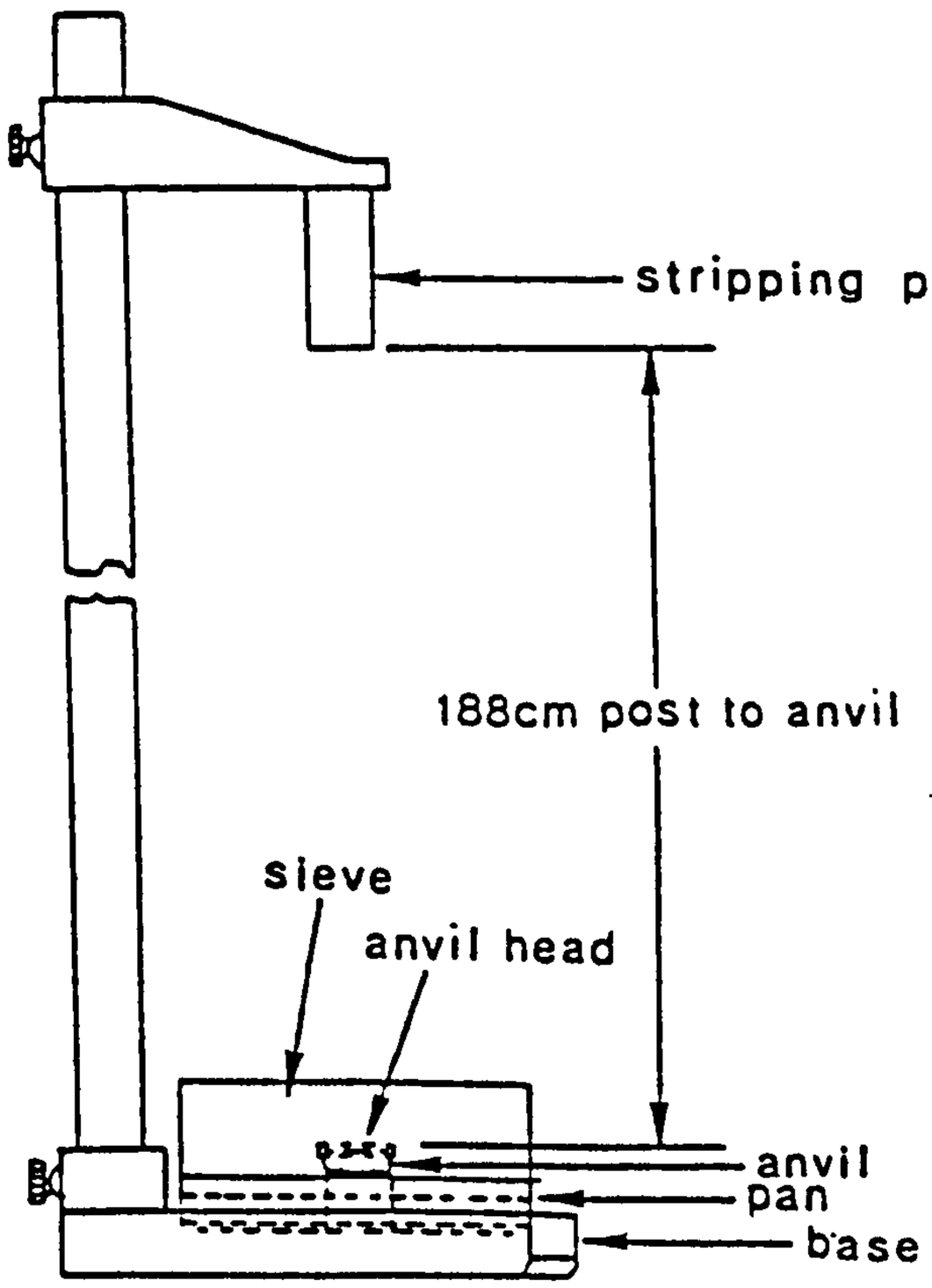

REFERENCES CITED

ALBERTI, A. & BRIGATTI, M.F. (1985). Crystal chemical differences in Al-rich smectites as shown by multivariate analysis of variance and discriminant analysis. *Clays Clay Miner.* **33**, 546-558.

ALLIETI, A. (1972). Polymorphism and crystal-chemistry of heulandites and clinoptilolites. *Am. Miner.* **57**, 1448-1462.

ALLIETI, A. & BRIGATTI, M.F. (1982). Some Grecian montmorillonites and the crystal chemistry of the smectite family. *Miner. Petrogr. Acta* **26**, 39-47.

ALTANER, S.P, HOWER, J., WHITNEY, G. & ARONSON, J.L. (1984). Model for K-bentonite formation: Evidence from zoned K-bentonites in the disturbed belt, Montana. *Geology* **12**, 412-415.

ALTANER, S.P. & GRIM, R.E (1990). Mineralogy, Chemistry and diagenesis of tuffs in the Sucker Creek Formation (Miocene) Eastern Oregon. *Clays Clay Miner.* **38**, 561-572.

ALTHER, G.R. (1986). The effect of the exchangeable cations on the physico-chemical properties of Wyoming bentonites. *Appl. Clay Sci.* **1**, 273-284.

ALTHER, G.R. (1991). Thermal stability of some industrial bentonites. *Appl. Clay Sci.* **5**, 469-488.

ALTHERR, R., SCHLIESTEDT, M., OKRUSCH, M., SEIDEL, E., KREUZER, H., HARRE, W., LENZ, H., WENDT, I. & WAGNER, G.A. (1979). Geochronology of High-Pressure rocks on Sifnos (Cyclades, Greece). *Contrib. Mineral. Petrol.* **70**, 245-255.

ALTHERR, R., KREUZER, H., WENDT, I., LENZ, H., WAGNER, G., KELLER, R., HARRE, W. & HÖHNDORF, A. (1982). A late Oligocene/Early Miocene High Temperature Belt in the Attic-Cycladic Crystalline Complex (SE Pelagonian, Greece). *Geol. Jb.* **E23**, 97-164.

ALTSCHULER, Z.S., DWORNIK, E.J. & KRAMER, J. (1963). Transformation of montmorillonite to kaolinite during weathering. *Science* **141**, 148-152.

AMERICAN FOUNDRYMEN SOCIETY (1978). *Mold and core test handbook.* Des Plaines, Ill., AFS, Sections 3-5 to 3-12.

ANDO, A., NAOKI, M., TERASHIMA, S. (1987). 1986 values for fifteen GSJ rock reference samples "Igneous rock series". *Geostandards Newsletter* **11**, 159-166.

ANDRIESSEN, P., BOELRIJK, N., HEBEBA, E., PRIEM, N., VERDUMEN, E. & VERSHURE, R. (1979). Dating the events of Metamorphism and granitic magmatism in the Alpine orogen of Naxos. *Contrib. Mineral. Petrol.* **69**, 215-225.

ANDRONOPOULOS, B. (1961). Etude d'une argile a montmorillonite de Chios (Grece). *Bull. Soc. franc. Miner. Crist.* **LXXXIV**, 385-387.

ANDSETA, S. (1983). Geomorphological study of Milos, Antimilos, Kimolos, Polyegos

Islands. *Unpub. Report. Electr. Board,* 22p.

ANGELIER, J., CANTAGREL, J-M., & VILMINOT, J-C. (1977). Neotectonique cassante et volcanisme plio-quaternaire dans l'arc egeen interne: l'isle de Milos (Grece). *Bull. Soc. geol. France* (7). t. **XIX**, 1, 119-123.

ANGELIER, J., LYBERIS, N., LEPICHON, X., BARRIER, E. & HUCHON, P. (1982). The tectonic development of the Hellenic Arc and the Sea of Crete: a synthesis. *Tectonophysics* **86**, 159-196.

ANON. (1978). Bentonite, sepiolite, attapulgate, etc.-Swelling markets for active clays. *Ind. Miner.* **126**, 49-91.

A.P.I. (1969). *A.P.I Specification for oil-well drilling-fluid materials.* API std 13A, American Petroleum Institute, Dallas, Texas, 12p.

ASHBY, G. (1976). Minerals in the foundry industry. *2nd Ind. Miner. Int. Congress Munich.* Pp 157-167.

BAILEY, S.W. (1984). Structures of layer silicates. Pp 1-124 in: *Crystal structures of clay minerals and their X-ray identification* (G.W. Brindley & G. Brown editors). Mineralogical Society, London.

BAIN, J.A. (1971). A plasticity chart as an aid to the identification and assessment of industrial clays. *Clay Miner.* **9**, 1-17.

BAIN, J.A & HIGHLEY, D.E. (1978). Regional appraisal of clay resources-challenge to the clay mineralogist. *Proc. Int. Clay Confer. Oxford*, 437-446.

BAIN, D.C. & SMITH, B.L.F. (1987). Chemical Analysis. Pp. 248-274 in: *A handbook of determinative methods in clay mineralogy* (M.J. Wilson, editor). Blackie, Glasgow & London.

BANFIELD, J.F & EGGLETON, R.A. (1990). Analytical transmission electron microscope studies of plagioclase, muscovite, and K-feldspar weathering. *Clays Clay Miner.* **38**, 77-89.

BANFIELD, J.F., JONES, B.R. & VEBLEN, D.R. (1991a). An AEM-TEM study of weathering and diagenesis, Albert Lake, Oregon: I. Weathering reactions in the volcanics. *Geochim. Cosmochim. Acta* **55**,2781-2793.

BANFIELD, J.F., JONES, B.R. & VEBLEN, D.R. (1991b). An AEM-TEM study of weathering and diagenesis, Albert Lake, Oregon: II. Diagenetic modification of the sedimentary assemblage. *Geochim. Cosmochim. Acta* **55**, 2795-2810.

BARONNET, A. (1982). Ostwald ripening in solution. The case of calcite and mica. *Estud. Geol.* **38**, 185-198.

BARONNET, A. (1984). Growth kinetics of the silicates. A review of the basic concepts. *Fortschr. Miner.* **62**, 187-232.

BATES, R.L. (1969). *Geology of the Industrial Rocks and Minerals.* Dover Pub. Inc., New York, pp 117-155

BAU, M. (1991). Rare-earth element mobility during hydrothermal and metamorphic fluid-rock interaction and the significance of the oxidation state of europium. *Chem. Geol.* **93**, 219-230.

B.C.I.R.A. (1985). *Greensand moulding technology*. BCIRA, Alvechurch, Birmingham.

BELLON, H., GRISOLLET, G. & SOREL, D. (1979). Age de l'activite volcanique neogene de l'ile de Chios (Mer Egee, Grece). *C. R. Acad. Sc. Paris* **288**, 1255-1258.

BENNETT, H. & OLIVER, G.J. (1976). Development of fluxes for the analysis of ceramic materials by X-ray Spectrometry. *Analyst* **101**, 803-807.

BERCKHEMER, H. (1978). Some aspects of the evolution of marginal seas deduced from observations in the Aegean Region. Pp. 527-529 in: *Alps, Apennines, Hellenides-Geodynamic Investigations along geotraverses* (H. Closs, D.H. Roedder & K. Schidt editors), Stuttgart.

BERCKHEMER, H. (1980). The geological evolution of the Aegean Region. Pp. 21-32 in: *Thera and the Aegean World, vol.2* (C. Doumas editor).

BERNER, R.A. (1984). Sedimentary pyrite formation: An update. *Geochim. Cosmochim. Acta* **48**, 605-615.

BESENECKER, H. (1973). *Neogen und Quartär der Insel Chios (Ägäis)*. Ph.D Thesis. Univ. Marburg, Germany, 197p.

BESENECKER, H., DÜRR, S., HERGET, G., JACOBSHAGEN, V., KAUFFMANN, G., LÜDKE, G., ROTH, W. & TIETZE, K-W. (1968). Geologie von Chios (Ägäis). Ein Überblick. *Geologica et Paleontologica* **2**, 121-150.

BESENECKER, H. & PICHLER, H. (1974). Die jungen Vulkanite der Insel Chios (östliche Ägäis, Griechenland). *Geol. Jb.* **D9**, 41-65.

BESSON, G., BOOKIN, A.S., DAINYAK, L.G., RAUTUREAU, M., TSIPURSKY, S.I., TCHOUBAR, C. & DRITS, V.A. (1983). Use of diffraction and Mössbauer methods for the structural and crystallochemical characterization of nontronites. *J. Appl. Cryst.* **16**, 374-383.

BETHKE, G.M. & ALTANER, SP. (1986). Layer by layer mechanism of smectite illitization and application to a new rate law. *Clays Clay Miner.* **34**, 136-145.

BEUTELSPACHER, H. & VAN DER MAREL, H.W. (1968). *Atlas of Electron Microscopy of Clay Minerals and their admixtures*. Elsevier, Amsterdam, 333p.

BOCCALETI, M., MANETTI, P. & PECCERILLO, A. (1974). The Balkanids as an Instance of Back-Arc Thrust belt: possible relation with the Hellenids. *Bull. Geol. Soc. Am.* **85**, 1077-1084.

BOENISCH, D. & PATTERSON, W. (1967). Discussion of the scabbing tendencies of green sand. *Brit. Found.* **55**, 438-447.

BOLES, J.R. (1972). Composition, optical properties, cell dimensions and thermal stability of some heulandite group zeolites. *Am. Miner.* **57**, 1463-1493.

BOLES, J.R. & FRANKS, S.G. (1979). Clay diagenesis in Wilcox Sandstones of Southwest

Texas: Implications of smectitediagenesis on sandstone cementation. *J. Sed. Petrol.* **49**, 55-70.

BOLES J.R. & SURDAM, R.C. (1979). Diagenesis of volcanogenic sediments in a Tertiary saline lake, Wagon Red Formation. *Am. J. Sci.* **279**, 832-853.

BOWERS, T.S & BURNS, R.G. (1990). Activity diagrams for cliniptilolite: Susceptibility of this zeolite to further diagenetic reactions. *Am. Miner.* **75**, 601-619.

BRANDENBURG, U. & LAGALY, G. (1988). Rheological properties of sodium montmorillonite dispersions. *Appl. Clay Sci.* **3**, 263-279.

BRIGATTI, M.F. & POPPI, L. (1981). A mathematical model distinguish the members of the dioctahedral smectite series. *Clay Miner.* **16**, 81-89.

BRINDLEY, G. (1984). Order-disorder in Clay Mineral Structures. Pp. 169-180 in: *Crystal structures of clay minerals and their X-ray identification* (G.W. Brindley & G. Brown editors). Mineralogical Society, London.

BRINDLEY, G.W. & YOUELL, R.F. (1951). A chemical determination of "tetrahedral" and "octahedral" aluminium ions in a silicate. *Acta crystallogr.* **4**, 495-496.

BRIQUEU, L., JAVOY, M., LANCELOT, J.R. & TATSUMOTO, M. (1986). Isotope geochemistry of recent magmatism in the Aegean Arc: Sr, Nd, Hf and O isotopic ratios in the lavas of Milos and Santorini-geodynamic implications. *Earth Planet. Sci. Letters* **80**, 41-54.

BRITISH STANDARDS INSTITUTION BS 410 (1976). Specifications for test sieves.

BROOKINS, D.G. (1989). Aqueous geochemistry of rare-earth elements. Pp 201-225 in: *Geochemistry and mineralogy of rare earth elements* (B.R. Lipin & G.A. McKay editors) Reviews in Mineralogy, Vol. 21, Mineralogical Society of America.

BROWN, G. & BRINDLEY, G.W. (1984). X-ray Diffraction procedures for Clay Mineral Identification. Pp 305-360 in : *Crystal structures of clay minerals and their X-ray identification* (G.W. Brindley & G. Brown editors). Mineralogical Society, London.

BROWNLOW, A.H. (1979). *Geochemistry*. Prentice Hall, London. Pp. 191-242.

BRÜCKMAN, K., FIJAL, J., KLAPYTA, Z., WILTOWSKI, T. & ZABINSKI, W. (1976). Infuence of different activation methods on the catalytic properties of montmorillonite. *Mineralogia Polonica*. **7**, 5-14.

BRUSEWITZ, A.M. (1986). Chemical and physical properties of Paleozoic potassium bentonites from Kinnekulle, Sweden. *Clays Clay Miner.* **34**, 442-454.

BÜHMANN, C. & GRUBB, P.L.C. (1991). A kaolin-smectite interstratification sequence from a red and black complex. *Clay Miner.* **26**, 343-358.

BYRNE, P.J.S. (1954). Some observations on montmorillonite-organic complexes. *Clays Clay Miner.* **2**, 241-253.

CAINE, J.B. & TOEPKE, R.E. (1967). An exploratory investigation of some bond-water systems. *Trans. Am. Found. Soc.* **75**, 10-16.

CAINE, J.B. & TOEPKE, R.E. (1968). Water-bond ratios and mouldability of moulding sands. *Trans. Am. Found. Soc.* **76**, 65-69.

CALLAGHAN, I.C. & OTTEWILL, R.H. (1974). Interparticle forces in montmorillonite gels. *Disc. Faraday Chem. Soc.* **57**, 110-118.

CANTRELL, K.J. & BYRNE, R.H. (1987). Rare earth element complexation by carbonate and oxalate ions. *Geochim. Cosmochim. Acta* **51**, 597-606.

CARTER, D.L., HEILMAN, M.D. & GONZALEZ, F.L. (1965). Ethylene glycol monoethyl ether for determining surface area of silicate minerals. *Soil Sci.* **100**, 356-360.

CAS, R.A.F. & WRIGHT, J.V. (1988). *Volcanic successions. Modern and ancient.* Unwin Hyman, London, 528p.

CHAI, B.H.T. (1974). Mass transfer of calcite during hydrothermal recrystallization. Pp 205-218 in: *Geochemical Transport and Kinetics* (A.W. Hoffmann, B.J. Giletti, H.S Yoder Jr & R.A Jund editors), Carnegie Inst. Washington.

CHAMLEY, H. (1989) *Clay Sedimentology.* Springer Verlag, Berlin, pp 411-414.

CHEN, J.S., CUSHMAN, J.H. & LOW, P.F. (1990). Rheological behaviour of Na-montmorillonite suspensions at low electrolyte concentration. *Clays Clay Miner.* **38**, 57-62.

CHRISTIDIS, G. (1989). *Mineralogy, physical and chemical properties of the bentonite deposits of Milos Island, Greece.* M.Sc Thesis. Univ. Hull, UK, 172pp.

CLARKE, G.M. (1985). Special Clays. *Ind. Miner.* **216**, 25-51.

COMER, J.J. (1971). Specimen preparation. Pp 79-108 in: *The Electron Optical Investigation of Clays*, (J.A. Gard editor) Mineralogical Society, London.

DAVIDTZ, J.C & LOW, P.F. (1970). Relationship between crystal-lattice configuration and swelling of montmorillonites. *Clays Clay Miner.* **18**, 325-332.

DEER, W.A., HOWIE, R.A. & ZUSSMAN, G. (1962). *Rock forming Minerals, vol. 3: Sheet silicates.* Longmans, London. Pp 226-245.

DEER, W.A., HOWIE, R.A. & ZUSSMAN, G. (1965). *Rock forming minerals, vol.4: Framework silicates.* Longmans, London. Pp. 6-144

DEIST, J. & TALIBUDEEN, O. (1967). Ion exchange in soils from the ion pairs K-Ca, K-Rb, and K-Na. *J. Soil Sci.* **18**, 125-137.

DEWEY, J.F. & SENGÖR, A.M.C. (1979). Aegean and surrounding regions: Complex multiplate and continuum tectonics in a convergent zone. *Bull. Geol. Soc. Am.* **90**, 84-92.

DIBBLE, W.E.Jr & TILLER, W. (1981). Kinetic model of zeolite paragenesis in tuffaceous sediments. *Clays Clay Miner.* **29**, 323-330.

DUNHAM, A.C. & WILKINSON, F.C.F. (1978). Accuracy, precision and detection limits of Energy Dispersive Electron-microprobe analyses of silicates. *X-Ray Spectometry.***7**, 50-56.

EARLEY, J.W. MILNE, I.H. & MCVEAGH, W.J. (1953). Dehydration of montmorillonite. *Am. Miner.* **38**, 770-783.

EBERL, D.D. (1978). The reaction of montmorillonite to mixed-layer clay: the effect of interlayer alkali and alkaline earth cations. *Geochim. Cosmochim.* Acta **42**, 1-7.

EBERL, D.D. (1980). Alkali-cation selectivity and fixation by clay minerals. *Clays Clay Miner.* **28**, 161-172.

EBERL, D.D., WHITNEY, G. & KHOURY, H. (1978). Hydrothermal reactivity of smectite. *Am. Miner.* **63**, 401-409.

EBERL, D.D., SRODON, J., LEE, M., NADEAU, P.H. & NORTHROP, R. (1987). Sericite from the Silerton Caldera, Colorado: Corelation among structure, origin, and particle thickness. *Am. Miner.* **72**, 914-934.

EBERL, D.D. & SRODON, J. (1988). Ostwald ripening and interparticle-diffraction effects for illite crystals. *Am. Miner.* **73**, 1335-1345.

EBERL, D.D., SRODON, J., KRALIK, M., TAYLOR, B.E. & PETERMAN, Z.E. (1990). Ostwald ripening of clays and metamorphic minerals. *Science* **248**, 474-477.

EDELMAN, C.H., & FAVEJEE, J.C.L. (1940). On the crystal structure of montmorillonite and halloysite. *Z. Krist.* **102**, 417-431.

EHRENBURG, K. (1889). *Die Inselgruppe von Milos.* Unpublished Thesis. Univ. Leipzig, Germany. 121pp.

ESLINGER, E. & PEVEAR, D. (1988). *Clay minerals for petroleum geologists and engineers.* SEPM Shrt course No.22. Pp. 3-1 - 3-24.

ELZEA, J.M. & MURRAY, H.H. (1990). Variation in the mineralogical, chemical and physical properties of the Cretaceous Clay Spur bentonite in Wyoming and Montana (U.S.A). *Appl. Clay Sci.* **5**, 229-248.

FAHN, R. (1964). Zussammenhänge zwischen Viscosität and thermischer Beständigkeit von Aktivbentonit. *Giesserei* **51**, 4-10.

FAHN, R. & FENDERL, K. (1983). Reaction products of organic dye molecules with acid treated montmorillonite. *Clay Miner.* **18**, 447-458.

FARMER, V.C. (1968). Infrared spectroscopy in clay mineral studies. *Clay Miner.* **7**, 373-387.

FARMER, V.C. (1974). The Layer silicates. Pp 331-363 in: *The Infrared Spectra of Minerals* (V.C. Farmer editor). Mineralogical Society, London.

FARMER, V.C. (1979). Infrared spectroscopy. Pp 285-337 in: *Data handbook for clay materials and other non-metallic minerals* (H. van Olphen & J.J. Fripiat editors) Pergamon Press, Oxford.

FARMER, V.C & RUSSELL, J.D. (1964). The infrared spectra of layer silicates. *Spectrochim. Acta* **20**, 1149-1173.

FARMER, V.C. & RUSSELL, J.D. (1967). Infrared absorption spectrometry in clay studies.

Clays Clay Miner. **15**, 121-142.

FARMER, V.C. & RUSSELL, J.D. (1971). Interlayer complexes in layer siliccates, the structure of water in lamellar ionic solutions. *Trans. Faraday Soc.* **67**, 2737-2749.

FERRARA, G., FYTICAS, M., GIULIANI, O. & MARINELLI, G. (1980). Age of the formation of the Aegean active volcanic arc. Pp 37-42 in: *Thera and the Aegean World, vol.2* (C. Doumas editor).

FIJAL, J., KLAPYTA, Z., KWIECINSKA, B., ZIETKIEWITCZ, J. & ZYLA, M. (1975). On the mechanism of acid activation of montmorillonite: II. Changes in the morphology and porosity in the light of electron microscopic and adsorption investigations. *Mineralogia Polonica* **6**, 49-57.

FINLOW-BATES, T. & STUMPFL, E.F. (1981). The behaviour of so-called immobile elements in hydrothermally altered rocks associated with volcanogenic submarine exhalative ore deposits. *Mineral. Deposita*, **16**, 319-328.

FISHER, R.V., & SCHMINCKE, H.U. (1984). *Pyroclastic Rocks*. Springer-Verlag, Berlin, 472pp.

FOSCOLOS, A.E. & KODAMA, H. (1974). Diagenesis of clay minerals from Lower Cretaceous Shales of North Eastern British Columbia. *Clays Clay Miner.* **22**, 319-335.

FOSTER, M.D. (1951). The importance of exchangeable magnesium and cation exchange capacity in the study of montmorillonite clays. *Am. Miner.* **36**, 717-730.

FREY, E. & LAGALY, G. (1979). Selective coagulation in mixed colloidal suspensions. *J. Coll. Interf. Sci.* **70**, 46-55.

FYTICAS, M. (1977). *Geological and geothermal study of Milos Island*. Ph.D Thesis, Univ. Thessaloniki, Greece, 228p (in Greek).

FYTICAS, M., GIULLIANI, O., INNOCENTI, F., MARINELLI, G. & MAZZUOLI, R. (1976). Geochronological data on recent magmatism of the Aegean Sea. *Tectonophysics* **31**, T29-T34.

FYTICAS, M., GIULLIANI, O., INNOCENTI, F., MANETTI, P., MAZZUOLI, R., PECCERILLO, A. & VILLARI, L. (1979). Neogene volcanism of the Northern and Central Aegean Region. *Ann. Geol. des Pays Helleniques* **30**, 106-129.

FYTICAS, M., INNOCENTI, F., MANETTI, P., MAZZUOLI, R., PECCERILLO, A. & VILLARI, L. (1984). Tertiary to Quaternary evolution of volcanism in the Aegean region. Pp. 687-699 in: *The Geological Evolution of the Eastern Mediterranean* (J.E. Dixon & A.H.F. Robertson editors), Geological Society of London, special publication No. 17.

FYTICAS, M., INNOCENTI, F., KOLIOS, N., MANETTI, P., MAZZUOLI, R, POLI, G., RITA, F. & VILLARI, L. (1986). Volcanology and petrology of volcanic products from the island of Milos and neighbouring islets. *J. Volcanol. Geotherm. Res.* **28**, 297-317.

FYTICAS, M. & VOUGIOUKALAKIS, G. (1992). Volcanic structure and evolution of Kimolos and Polyegos (Milos Island group). *6th Congress Geol. Soc. Greece*, Abstracts.

GARRELS, R.M. & CHRIST, C.L. (1965). *Solutions minerals and equilibria*. Freeman Cooper, San Fransisco. Pp 172-267.

GILLESPIE, T. (1960). An extension of Goodeve's impulse theory of viscosity to pseudoplastic systems. *J. Colloid Sci.* **15**, 219-231.

GOODEVE, C.F. (1939). A general theory of thixotropy and viscosity. *Trans. Faraday Soc.* **35**, 342-358.

GOODMAN, B.A., NADEAU, P.H. & CHADWICK, J. (1988). Evidence for the multiphase nature of bentonites from Mössbauer and EPR spectroscopy. *Clay Miner.* **23**, 147-159.

GOTTARDI, G. & GALLI, E. (1985). *Natural zeolites*. Springer-Verlag, Berlin. Pp 1-34, 233-305.

GOULDING, K.T.W. & TALIBUDEEN, O. (1980). Heterogeneity of cation-exchange sites for K-Ca exchange in aluminosilicates. *J. Coll. Inter. Sci.* **78**, 15-24.

GOVINDARAJU, K. (1989). *Geostandards Newsletter* **13**, Special Issue, July 1989.

GRANQUIST, W.T. & SAMNER, G.G. (1959). Acid dissolution of a Texas bentonite. *Clays Clay Miner.* **6**, 292-308.

GREEN-KELLY, R. (1957). The montmorillonite minerals. Pp 140-164 in: *The differential thermal investigation of clays* (R.C. MacKenzie editor). Mineralogical Society, London.

GRIFFITHS, J. (1990). Acid activated bleaching clays. What's cooking in the oil industry? *Ind. Miner.* **276**, 55-67.

GRIM, R.E. (1962). *Applied Clay Mineralogy*. McGraw-Hill, New York, 422p.

GRIM, R.E. (1968). *Clay Mineralogy*. Pp 77-92, 185-233, McGraw-Hill, New York.

GRIM, R.E. & KULBICKI, G. (1961). Montmorillonite: High temperature reactions and classification. *Am. Miner.* **46**, 1329-1369.

GRIM, R.E. & GÜVEN, N. (1978). *Bentonites*. Elsevier, New York, 256pp.

GRIMSHAW, R.W. (1971). *The chemistry and physics of clays and allied ceramic materials*. Ernest Benn Ltd. Pp 140-148, 513-517.

GUTHRIE, G.D. & VEBLEN, D.R. (1989). High resolution transmission electron microscopy of mixed-layer illite/smectite: computer simulations. *Clays Clay Miner.* **37**, 1-11.

GÜVEN, N. (1974). Electron Optical investigations on montmorillonites-I. Cheto, Camp-Bertaux and Wyoming montmorillonites. *Clays Clay Miner.* **22**, 155-165.

GÜVEN, H. (1988). Smectite. Pp 497-559 in: *Hydrous Phyllosilicates*, (S.W. Bailey editor). Reviews in mineralogy, vol. 19. Mineralogical Society of America.

GÜVEN, N. & PEASE, R.W. (1975). Electron Optical investigations on montmorillonites-II: Morphological variations in the intermediate members of the montmorillonite-beidellite series. *Clays Clay Miner.* **23**, 187-191.

HALL, P.L. (1987). Clays: their significance, properties, origins and uses. Pp 1-25 in: *A handbook of determinative methods in clay mineralogy* (M.J. Wilson editor).

Blackie, Glasgow and London.

HARBEN, P.W., & BATES, R.L. (1984). *Geology of the non-metallics*. Metal Bulletin Inc., New York, pp 87-125.

HARBEN, P.W., & BATES, R.L. (1990). *Industrial Minerals Geology and World deposits*. Metal Bulletin Plc, London, 62-89.

HARTWELL, J.M. (1965). The diverse uses of montmorillonite. *Clay Miner.* **6**, 11-118.

HARVEY, C.C. & BROWNE, P.R.L. (1991). Mixed-layer Clay Geothermometry in the Wairakei geothermal Field, New Zealand. *Clays Clay Miner.* **39**, 614-621.

HAWKINS, D.B. (1981). Kinetics of glass dissolution and zeolite formation under hydrothermal conditions. *Clays Clay Miner.* **29**, 331-340.

HAWKINS, D.B., SHEPPARD, R.A. & GUDE, A.J., 3rd (1978). Hydrothermal synthesis of clinoptilolite and comments on the assemblage phillipsite-clinoptilolite-mordenite. Pp 337-343 in: *Natural Zeolites: Occurrence, Properties, Use*. (L.B Sand & F.A. Mumpton editors), Pergamon Press, Elmsford, New York.

HAY, R.L. & SHEPPARD, R.A. (1977). Zeolites in open hydrologic systems. Pp 93-102 in: *Mineralogy and Geology of Natural Zeolites* (F.A Mumpton editor). Reviews in mineralogy vol. 4, Mineralogical Society of America.

HAY, R.L. & GULDMAN, S.G. (1987). Diagenetic alteration of silicic ash in Searles lake, California. *Clays Clay Miner.* **35**, 449-457.

HERBILLON, A.J., FRANKART, R. & VIELVOYE, L. (1981). An occurrence of interstratified kaolinite-smectite minerals in a red-black soil toposequence. *Clay Miner.* **16**, 195-201.

HERGET, G. (1969). *Die Geologie von Nord-Chios (Ägäis)*. Ph.D Thesis, Univ. Marburg, Germany, 206p.

HERGET, G. & ROTH, W. (1968). Stratigraphie des Paläozoikums im Nordwest-Teil der Insel Chios (Ägäis). *N. Jb. Geol. Paläont. Abh.* **131**, 46-71.

HESS, P.C. (1966). Phase equilibria of some minerals in the K2O-Na2O-Al2O3-SiO2-H2O system at 25oC and 1 atmosphere: *Am. J. Sci.* **264**, 289-309.

HIGHLEY, D.E. (1972). *Fuller's Earth*, Mineral Dossier No 3, Mineral Resources Consultative Committee, London, 26pp.

HIGHLEY, D.E. (1990). The occurrence, mining and processing of bentonite. *EC/Asean cource on assessment procedures for clays and ceramic raw materials*. Ipoh, Malaysia, 6p.

HODDER, A.P.W., GREEN, B.E., & LOWE, D.J. (1990). A two-stage model for the formation of clay minerals from tephra-derived volcanic glass. *Clay Miner.* **25**, 313-327.

HOFFMANN, C. & KELLER, J. (1979). Xenoliths of Lawsonite-ferroglaucophane rocks from a Quaternary volcano of Milos (Aegean Sea, Greece). *Lithos* **12**, 209-219.

HOFMANN, F. (1958). Investigations on the effect of heat on the bonding properties of

various bentonites. *Trans. Am. Foundr. Soc.* **66**, 305-311.

HOFMANN, F. (1985). Heat effects on bentonite bonding. *Modern Cast.* June 1985, 53-57.

HOFSTADT, C.E., & FAHN, R. (1976). Bentonite-a valuable and versatile mineral and raw material. *2nd "Industrial Minerals" Int. Congress*, Munich, 95-101.

HOLDRIDGE, D.A. & VAUGHAN, F. (1957). The kaolin minerals (kandites). Pp 98-139 in: *The differential thermal investigation of clays* (R.C. Mackenzie, editor) Mineralogical Society, London.

HOWARD, J.J. & ROY, D.M. (1985). Development of layer charge and kinetics of experimental smectite alteration. *Clays Clay Miner.* **33**, 81-88.

HOWER, J., ESLINGER, E.V., HOWER, M.E. & PERRY, E.A. (1976). Mechanism of burial metamorphism of argillaceous sediment: 1. Mineralogical and chemical evidence. *Bull. Geol. Soc. Am.* **87**, 725-737.

HUCHON, P., LYBERIS, N., ANGELIER, J., LePICHON, X. & RENARD, V. (1982). Tectonics of the Hellenic Trench: A synthesis of sea beam and submersible observations. *Tectonophysics* **86**, 69-112.

HUFF, W.D. (1983). Correlation of Middle Ordovician K-bentonites based on chemical fingerprinting. *J. Geol.* **91**, 657-669.

HUFF, W.D. & TÜRKMENOGLU. A.G. (1981). Chemical characteristics and origin of Ordovician K-bentonites along the Cincinnati Arch. *Clays Clay. Miner.* **29**, 113-123.

HUFF, W.D. & MORGAN, D.J. (1989). Stratigraphy, mineralogy and tectonic setting of Silurian K-bentonites in southern England and Wales. *Proc. 9th Int. Clay Conf. Strasbourg*, 33-42.

HUFF, W.D., ANDERSON, T.B., RUNDLE, C.C. & ODIN, G.S. (1991). Chemostratigraphy, K-Ar ages and illitization of Sillurian K-bentonites from the Central Belt of the Southern Uplands-Down-Longford terrain, British Isles. *J. Geol. Soc. London* **148**, 861-868.

IIJIMA, A. (1980). Geology of natural zeolites and zeolitic rocks. *Proc. 5th Int. Conf. on zeolites.* Pp 103-118.

INNOCENTI, F., MANETTI, P., PECCERILLO, A. & POLI, G. (1979). Inner Arc volcanism in NW Aegean Arc: geochemical and geochronological data. *N. Jb. Miner. Mh.* **4**, 145-158.

INNOCENTI, F. MANETTI, P. PECCERILLO, A. & POLI, G. (1981). South-Aegean Volcanic Arc: Geochemical Variations and Geotectonic implications. *Bull. Volcanol.* **44**, 377-391.

INNOCENTI, F., MANETTI, P., MAZZUOLI, R., PASQUARE, G. & VILLARI, L (1982a): Anatolia and North-Western Iran. Pp. 327-349 in: *Orogenic Andesites and related rocks* (R.S. Thorpe editor) Wiley, New York.

INNOCENTI, F., KOLIOS, N., MANETTI, P., RITA, I. & VILLARI, L. (1982b): Acid and basic Late Neogene volcanism in central Aegean Sea: Its nature and Geotectonic significance. *Bull. Volcanol.* **45**, 87-97.

INOUE, A. & MINATO, H. (1979). Ca-K exchange reaction and interstratification in montmorillonite. *Clays Clay Miner.* **27**, 393-401.

INOUE, A. & UTADA, M (1983). Further investigations of a conversion series of diochahedral mica/smectiites in the Shinzan hydrothermal alteration area, Northeast Japan. *Clays Clay Miner.* **31**, 401-412.

INOUE, A., KOHYAMA, N. KITAGAWA, R & WATANABE, T. (1987). Chemical and morphological evidence for the conversion of smectite to illite. *Clays Clay Miner.* **35**, 111-120.

INOUE, A., VELDE, B., MEUNIER, A. & TOUCHARD, G. (1988). Mechanism of illite formation during smectite-to-illite conversion in a hydrothermal system. *Am. Miner.* **73**, 1305-1334.

JACKSON, J.A., KING, G. & VITA-FINZI, C. (1982). The Neotectonics of the Aegean: an alternative view. *Earth Planet. Sci. Letters* **61**, 303-318.

JACKSON, J.A. & MCKENZIE, D. (1988). The relationship between plate motions and seismic moment tensors and rates of active deformation in the Mediterranean and Middle East. *Geophys. J.* **93**, 45-73.

JAHREN, J.S. (1991). Evidence of Ostwald ripening related recrystallization of diagenetic chlorites from reservoir rocks offshore Norway. *Clay Miner.* **26**, 169-178.

JEANS, C.V. MERRIMAN, R.J. & MITCHELL, J.G. (1977). Origin of Midddle Jurassic and Lower Cretaceous Fuller's earths in England. *Clay Miner.* **12**, 11-44.

JONES, K.G. (1979). Iron ore pelletization. *Ind.Miner.* **138**, 61-73.

JONES, C.E. TARNEY, J. & BAKER, J.H. (1992). Tertiary granitoids of Rhodope, N. Greece: magmatism related to extensional collapse of the Hellenic Orogen? *Tectonophysics*, in press.

JONGSMA, D., WISSMAN, G., HINZ, K. & GARDE, S. (1978). Result of Reflection Seismic surveys in the Southern Aegean Sea. Pp. 532-535 in: *Alps, Apennines, Hellenides-Geodynamic Investigations along Geotraverses* (H. Closs, D.H. Roeder & K. Schidt editors), Stuttgart.

KALOGEROPOULOS, S.I. & MITROPOULOS, P. (1983). Geochemistry of barites from Milos island (Aegean Sea), Greece. *N. Jb. Miner. Mh.* 13-21.

KAUFFMANN, G. (1969). *Die Geologie von Nordost-Chios (Ägäis)*. Ph.D. Thesis, Univ. Marburg, Germany, 213p.

KANARIS, I.T. (1978). Report on the industrial minerals and rocks of the island of Chios. *Unpubl. Report, IGME*, 9p (in Greek).

KANARIS, I.T. & MINOPOULOS, P. (1979). Preliminary report about the reconnaissance for kaolin and bentonite deposits of Milos Island. *Unpub. Report, IGME*, 21p (in Greek).

KASPERSKI, K.L., HEPLER, C.T. & HEPLER, L.G. (1986). Viscosities of dilute aqueous suspensions of montmorillonite and kaolinite clays. *Can. J. Chem.* **64**, 1919-1924.

KASTNER, M. & SIEVER, R. (1979). Low temperature feldspars in sedimentary rocks. *Am. J. Sci.* **279**, 435-479.

KELLER, W.D., REYNOLDS, R.C. & INOUE, A. (1986). Morphology of clay minerals in the smectite-to-illite conversion series by scanning electron microscopy. *Clays Clay Miner.* **34**, 187-197.

KHEOK, S.C. & LIM, E.E. (1982). Mechanism of palm oil bleaching by montmorillonite clay activated at various acid concentrations. *J. Am. Oil Chem. Soc.* **59**, 129-131.

KHOO, L.E., MORSINGH, F. & LIEW, K.Y. (1979). The adsorption of ß-carotene I. by bleaching earths. *J. Am. Oil Chem. Soc.* **56**, 672-675.

KHOURY, H.N. & EBERL, D.D. (1979). Bubble-wall shards altered to montmorillonite: *Clays Clay Miner.* **27**, 291-292.

KISSEL, C., LAJ, C. & MÜLLER, C. (1985). Tertiary geodynamical evolution of northwestern Greece: Paleomagnetic results. *Earth Planet. Sci. Letters* **72**, 190-204.

KISSEL, C., LAJ, C., POISSON, A., SAVASCIN, Y., SIMEAKIS, K. & MERCIER, J.L. (1986a). Paleomagnetic evidence for Neogene rotational deformations in the Aegean domain. *Tectonics* **5**, 783-795.

KISSEL, C., LAJ, C. & MAZAUD, A. (1986b). First paleomagnetic results from Neogene formations in Evia, Skyros and the Volos region and the deformation of central Aegean. *Geophys. Res. Letters* **13**, 1446-1449.

KISSEL, C. & LAJ, C. (1988). The Tertiary geodynamical evolution of the Aegean Arc: a paleomagnetic reconstruction. *Tectonophysics* **146**, 183-201.

KLECKA, W.R. (1975). Discriminant analysis. Pp 434-467 in: *Statistical package for the social sciences* (N.H. Nie, C.H. Hull, J.G. Jenkins, K. Steinbrenner, and D.H. Bent editors) McGraw-Hill, New York.

KLEIJN, W.B. & OSTER, J.D. (1982). A model of clay swelling and tactoid formation. *Clays Clay Miner.* **30**, 383-390.

KNIGHT, J.E. (1977). A thermodynamical study of alunite enargite, luzonite, and tennantite deposits. *Econ. Geol.* **72**, 1321-1336.

KOLATA, D.R., FROST, J.K. & HUFF, W.D. (1987). Chemical correlation of K-bentonite beds in the Middle Ordovician Decorah Subgroup, upper Mississippi Valley. *Geology* **15**, 208-211.

KOLTA, G.A., NOVAK, I., SAMIR, Z. EL-T. & KAMILIA, A. EL-B. (1975). Evaluation of bleaching capacity of acid-leached Egyptian bentonites. *J. Appl. Chem. Biotechnol.* **26**, 355-360.

KOMADEL, P., SCHMIDT, D., MADEJOVA, J. & CICEL, B. (1990). Alteration of smectites by treatments with hydrochloric acid and sodium carbonate solutions. *Appl. Clay Sci.* **5**, 113-122.

KONTA, J. (1985). Textural variation and composition of bentonite derived from basaltic ash.

Clays Clay Miner. **34**, 257-265.

KORNPROBST, J., KIENAST, J. & VILMINOT, J. (1979). The high-Pressure assemblages at Milos, Greece. *Contrib. Mineral. Petrol.* **69**, 49-63.

KÖSTER, H.M. (1981). The crystal structure of 2:1 layer silicates. *Proc. Int. Clay Confer. Pavia Italy*, 41-71.

KREATSAS, K.G. (1964). Contribution to the knowledge of the Neogene of the Island of Chios. *Bull. Geol. Soc. Greece*. **5**, 92-107 (in Greek).

LAGALY, G. (1981). Characterization of clays by organic compounds. *Clay Miner.* **16**, 1-21.

LAGALY, G. (1989). Principles of flow of kaolin and bentonite dispersions. *Appl. Clay Scl.* **4**, 105-123.

LAGALY, G. & WEISS, A. (1975). The layer charge of smectitic layer silicates. *Proc. Int. Clay Conf. Mexico*. 157-172.

LAGALY, G., FERNANDEZ-GONZALEZ, M. & WEISS, A. (1976). Problems in layer-charge determination of montmorillonites. *Clay Miner.* **11**, 173-187.

LAJ, C., JAMET, M., SOREL, D. & VALENTE, J.P.(1982). First Paleomagnetic results from Mio-Pliocene series of the Hellenic sedimentary arc. *Tectonophysics* **86**, 45-67.

LAMBROPOULOS, S. & KAMINARI, M. (1989). Stream sediment geochemical exploration in the Island of Chios. *Unpubl. Report, IGME*, 25p (in Greek).

LANSON, B. & CHAMPION, D. (1991). The I/S to illite reaction in the late stage diagenesis. *Am. J. Sci.* **291**, 473-506.

LAUDELOUT, H. (1987). Cation exchange equilibria in clays. Pp 225-236 in: *Chemistry of clays and clay minerals* (A.C.D. Newman editor), Mineralogical Society, London.

LEAR, P.R. & STUCKI, J.W. (1985). Role of structural hydrogen in the reduction and re-oxidation of iron in nontronite. *Clays Clay Miner.* **34**, 346-352.

LEBEDENKO, F. & PLEE, D. (1988). Some considerations on the ageing of Na2CO3-activated bentonites. *Appl. Clay Sci.* **3**, 1-10.

LEE, S.Y. JACKSON, M.L. & BROWN, J.L. (1975). Micaceous occlusions in kaolinite observed by ultramicrotomy and high resolution electron microscopy. *Clays Clay Miner.* **23**, 125-129.

LePICHON, X. & ANGELIER, J. (1979). The Hellenic Arc and Trench system: a key to the Neotectonic evolution of the Eastern Mediterranean Area. *Tectonophysics* **60** 1-42.

LePICHON, X. & ANGELIER, J. (1981). The Aegean Sea. *Phil. Trans. R. Soc. London A***300** 357-372.

LIAKOPOULOS, A. (1987). *Hydrothermalisme et mineralizations metalliferes de l' ile de Milos* (Cyclades, Grece). Ph.D Thesis, Univ. Pierre & Marie Curie, Paris, 276p.

LIATSIKAS, N. (1955). Geology and mineral deposits of Milos Island. *Geol. Reconnaissance, Rep. No 20, IGSR*, 30p (in Greek).

LIFSHITZ, I.M. & SLYOZOV, V.V. (1961). The kinetics of precipitation from supersaturated

solid solutions. *J. Phys. Chem. Solids.* **19**, 35-50.

LIM, C.H. & JACKSON, M.L. (1986). Expandable phyllosilicate reactions with lithium on heating. *Clays Clay Miner.* **34**, 346-352.

LINARES, J., HUERTAS, F., LACHICA, M., & REYES, E. (1972). Geochemistry of trace elements during the genesis of coloured bentonites. *Proc. Int. Clay Conf. Madrid*, 351-365.

LOTO, C.A & OMOTOSO, E.O. (1990). Analysis and development of Igbokoda Clay as a binder for synthetic Moulding sand. *Appl. Clay Sci.* **5**, 85-97.

LOW, P.F. (1980). The swelling of clay: II. Montmorillonites. *Soil Sci. Soc. Am. J.* **44**, 667-676.

LÜDKE, G. (1969). *Die Geologie von Südwest-Chios (Ägäis).* Ph.D Thesis, Univ. Marburg, Germany, 169p.

LÜTTIG, G. & WIEDENBEIN, F. (1990). Bentonite and related deposits. World economic significance and situation in Greece. *5th Congr. Geol. Soc. Greece.* Thessaloniki, Abstracts.

MACEWAN, D.M.C. & WILSON, M.J. (1984). Interlayer and intercalation complexes of clay minerals. Pp 197-248 in: *Crystal structures of clay minerals and their X-ray identification* (Brindley, G.W. & Brown G. editors). Mineralogical Society, London.

MCEWEN, M.B. & MOULD, D.L. (1957). Gelation of montmorillonite II. The nature of the interparticle forces in soils of Wyoming bentonite. *Trans. Faraday Soc.* **53**, 548-564.

MCEWEN, M.B. & PRATT, M.I. (1957). The gelation of montmorillonite. I. The formation of a structural framework in soils of Wyoming bentonite. *Trans. Faraday Soc.* **53**, 535-547.

MACKENZIE, R.C. (1970). Simple phyllosilicates. Pp 498-537 in: *Differential Thermal Analusis* Vol.1 (R.C. Mackenzie editor) Academic Press, London.

MACKENZIE, R.C., & BISHUI, B.M. (1958). The montmorillonite differential thermal curve. II. Effect of exchangeable cations on the dehydroxylation of normal montmorillonite. *Clay Miner. Bull.* **3**, 276-286.

MACKENZIE, R.C. & CAILLERE, S. (1979). Thermal Analysis, DTA, Tg, DTG. Pp. 243-284 In: *Data handbook for clay materials and other non-metallic minerals* (H. van Olphen & J.J. Fripiat editors) Pergamon Press, Oxford.

MAES, A. & CREMERS, A. (1977). Charge density effects in ion exchange. *Faraday Trans. R. Chem. Soc.* **73**, 1807-1814.

MAES, A. & CREMERS, A. (1978). Charge density effects in ion exchange. *Faraday Trans. R. Chem. Soc.* **74**, 1234-1241.

MCATEE, J.L. (1958a). Heterogeneity in montmorillonite. *Clays Clay Miner.* **5**, 279-288.

MCATEE, J.L. (1958b). Random interstratification in organophilic bentonites. *Clays Clay Miner.* **5**, 308-317.

MACLEAN, W.H. (1988). Rare earth element mobility at constant inter-REE ratios in the alteration zone at the Phelps Dodge massive sulphide deposit, Matagami, Quebec. *Mineral. Deposita* **23**, 231-238.

MADSEN, F.T. & MÜLLER-VONMOOS, M. (1989). The swelling behaviour of clays. *Appl. Clay Sci.* **4**, 143-156.

MAKRIS, J. (1976). A dynamic model of the Hellenic Arc deduced from Geophysical data. *Tectonophysics* **36**, 339-346.

MAKRIS , J. (1978a). A Geophysical study of Greece based on: Deep seismic soundingd, gravity and magnetics. Pp. 392-401 in: *Alps, Apennines, Hellenides-Geodynamic Investigations along Geotraverses* (H. Closs, D.H. Roedder & K. Scmhidt, editors) Stuttgart.

MAKRIS, J. (1978b). The crust and upper mantle of the Aegean region from deep seismic soundings. *Tectonophysics* **46**, 269-284.

MAKRIS, J & VEES, R. (1977). Crustal structure of the central Aegean Sea and the Islands of Evia and Crete, Greece, obtained by refractional seismic experiments. *J. Geophys.* **42**, 329-341.

MAKRIS, J. & STOBBE, C. (1984). Physical properties and state of the crust and upper mantle of the eastern Mediterranean sea deduced from geophysical data. *Marine Geol.* **55**, 347-363.

MARCOPOULOS, T. & KRANIOTIS, A. (1982). Klinoptilolith, Mordenit und Analkim im Bentonit von Milos/Griechenland. *Fortschr. Miner.* **60**, 136-137.

MARCOPOULOS, T & KATERINOPOULOS, T. (1986). Die Alunit-Vorcommen von Milos (Griechenland): Mineralbestand und Genese. *Chem. Erde* **45**, 105-112.

MARCOPOULOS, T. & CHRISTIDIS, G. (1988). Genesis of the industrial rocks and minerals of Kimolos Island. *Bull.Geol. Soc. Greece* **23**, 487-498.

MARINER, R.H & SURDAM, R.A. (1970). Alkalinity and formation of zeolites in saline alkaline lakes. *Science* **170**, 977-980.

MARINOS, G. (1955). *Reconnaissanse survey of the kaolin deposits of NW Milos.* Unpub. Report No 404a, IGME.

MELIDONIS, N. (1980). Geology and metalliferrous outcrops of Tinos Island. *Spec. Studies Geol. Greece*, 13, 1-80 (in Greek).

MERCIER, J.L. (1981). Extensional-cmpressional tectonics associated with the Aegean Arc: comparison with the Andean Cordillera of south Peru-north Bolivia. *Phil. Trans. R. Soc. London A***300**, 337-355.

MERING, J. & OBERLIN, A. (1967). Electron optical study of smectites. *Clays Clay Miner.* **15**, 3-25.

MERING, J. & OBERLIN, A. (1971). The smectites. Pp 193-229 in: *The elctron optical investigation of clays* (J.A. Gard editor) Mineralogical Society, London.

MEUNIER, A., PROUST, D., BEAUFORT, D., LAJUDE, A., & PETIT, J.-C. (1992). Heterogeneous reactions of dioctahedral smectites in illite-smectite and kaolinite-smectite mixed-layers: applications to clay materials for engineered barriers. *Appl. Geochem.* Suppl. Issue No.1, 143-150.

MEWIS, J. (1979). Thixotropy-A general review. *J. Non-Newtonian fluids* **6**, 1-20.

MILLIKEN, T.H., OBLAD, A.G. & MILLS, G.A. (1955). Use of clays as petroleum cracking catalysts. *Clays Clay Miner.* **1**, 314-326.

MILLS, G.A., HOLMES, J. & CORNELIUS, E.B. (1950). Acid activation of some bentonite clays. *J. Phys. Colloid Chem.* **54**, 1170-1185.

MINOPOULOS, P.A. (1980). Bentonitic deposits of Kimolos Island. Discovery of sedimentary zeolite of clinoptilolite-type. *Unpub. Report, IGME*, 15p, (in Greek).

MINOPOULOS. P.A. (1981). Reconnaissance research about the industrial minerals of the Polyegos and Kimolos Islands. *Unpub. report, IGME*, 10p (in Greek).

MITROPOULOS, P., TARNEY, J., SAUNDERS, A.D. & MARSH, N. (1987). Petrogenesis of Cenozoic volcanic rocks from the Aegean Island Arc. *J. Volcanol. Geotherm. Res.* **32**, 177-194.

McKENZIE, D.P (1970). Plate tectonics of the Mediterranean region. *Nature*, **226**, 239-243.

McKENZIE, D.P. (1972). Active tectonics of the Mediterranean region. *Geophys. J. R. Astron. Soc.* **30**, 109-185.

McKENZIE, D.P. (1978). Active tectonics of the Alpine-Himalayan belt: the Aegean Sea and surrunding regions. *Geophys. J. R. Astr. Soc.* **55**, 217-254.

McKENZIE, D.P. & JACKSON, J. (1983). The relationship between strain rates, crustal thickening, paleomagnetism, finite strain and fault movements within a deforming zone. *Earth Planet. Sci. Letters* **65**, 182-202.

McKENZIE, D.P. & JACKSON, J. (1986). A block model of distributed deformation by faulting. *J. Geol. Soc. London* **143**, 349-353.

MONCURE, G.K., SURDAM, R.C. & McKAGUE, H.L. (1981). Zeolite diagenesis below Pahute Mesa, Nevada test site. *Clays Clay Miner.* **29**, 385-396.

MONOD, O. & AKAY, E. (1984). Evidence for a Late Triassic-Early Jurassic orogenic event in the Taurides. Pp 113-122 in: *The Geological Evolution of the Eastern Mediterranean* (Dixon, J.E & robertson, A.H.F. editors). Geol Soc. Spec. Publ. No. 17.

MOORE, D.M., & REYNOLDS Jr. R.C. (1989). *X-Ray Diffraction and the identification and analysis of Clay Minerals.* Oxford University Press, Oxford. Pp 135-138.

MORGAN, D.A., SHAW, D.B., SIDEBOTTOM, T.C., SOON, T.C. & TAYLOR, R.S. (1985). The function of bleaching earths in the processing of palm, palm kernel and coconut oils. *J. Am. Oil Chem. Soc.* **62**, 292-299.

MORGAN, D.J. (1990a). Laboratory assessment of bentonite deposits. *EC/Asean training*

course on assessment procedures for clays and ceramic raw materials. Ipoh, Malaysia, 14p.

MORGAN, D.J. (1990b). Testing bentonite for drilling muds. *EC/Asean training course on assessment procedures for clays and ceramic raw materials, Ipoh, Malaysia*. 7p.

MORGAN, D.J. (1990c). Bentonite for use in edible oil clarification: mechanism of acid activation and assessment of bleaching performance. *EC/Asean training course on assessment procedures for clays and ceramic raw materials, Ipoh, Malaysia*, 7p.

MORGAN, D.J. HIGHLEY, D.E. & BLAND, D.J. (1979). A montmorillonite-kaolinite association in the Lower Cretaceous of South-East England. *Proc. Inter. Clay Conf. Oxford.* 301-310.

MOTTL, M.J. & HOLLAND, H.D. (1978). Chemical exchange during hydrothermal alteration of basalt by seawater.-I. Experimental results for major and minor components of seawater. *Geochim. Cosmochim. Acta* **42**, 1103-1115.

MUFFLER, P.L.J. & WHITE, D.E. (1969). Active metamorphism of Upper Cenozoic sediments in the Salton Sea Geothermal Field and the Salton Trough, southeastern California. *Bull. Geol. Soc. Am.* **80**, 157-182.

MULLA, D.J. & LOW, P.F. (1983). The Molar Absorptivity of Interparticle water in clay-water systems. *J. Coll. Interf. Sci.* **95**, 51-60.

MUMPTON, F.A. (1977). Natural zeolites. Pp 1-17 in: *Mineralogy and geology of natural zeolites* (F.A. Mumpton editor) Reviews in mineralogy vol. 4, Mineralogical Society of America.

MUMPTON, F.A. & ORMSBY, W.C. (1976). Morphology of zeolites in sedimentary rocks by scanning electron microscopy. *Clays Clay Miner.* **24**, 1-23.

NADEAU, P.H., TAIT, J.M., MCHARDY, W.J. & WILSON, M.J. (1984a). Interstratified XRD characteristics of physical mixtures of elementary clay particles. *Clay Miner.* **19**, 67-76.

NADEAU, P.H, WILSON, M.J., MCHARDY, W.J. & TAIT, J.M. (1984b). Interstratified clays as fundamental particles. *Science*. **225**, 923-925.

NADEAU, P.H., WILSON, M.J., MCHARDY, W.J. & TAIT, J.M. (1984c). Interparticle diffraction: a new concept for interstratified clays. *Clay Miner.* **19**, 757-769.

NADEAU, P.H., WILSON, M.J., MCHARDY, W.J. & TAIT, J.M. (1985a). The conversion of smectite to illite during diagenesis: evidence from some illitic clays from bentonites and sandstones. *Miner. Mag.* **49**, 393-400.

NADEAU, P.H., FARMER, V.C, MCHARDY, W.J. & BAIN, D.C. (1985b). Compositional variations of the Unterrupsroth beidellite. *Am. Miner.* **70**, 1004-1010.

NADEAU, P.H., & BAIN, D.C. (1986). Composition of some smectites and diagenetic illitic clays and implications for their origin. *Clays Clay Miner.* **34**, 455-464.

NADEAU, P.H. & TAIT, J.M. (1987). Transmission Electron Microscopy. Pp 209-247 In: *A*

Handbook of determinative methods in clay mineralogy (M.J. Wilson editor) Blackie, Glasgow & London.

NEVINS, M.J. & WEINTRITT, D.J. (1967). Determination of cation exchange capacity by methylene blue adsorption. *Amer. Ceram. Soc. Bull.* **46**, 587-592.

NEWMAN, B.S. (1963). The thermal stability of acid extracted montmorillonites. *Proc. Int. Clay Conf. Stockholm*, Pergamon Press, Oxford.

NEWMAN, A.C.D. & BROWN, G. (1987). The chemical constitution of clays. Pp 1-128 in: *Chemistry of clays and clay minerals* (A.C.D. Newman editor). Mineralogical Society, London.

NICHOLLS, I.A. (1978). Primary Basaltic Magmas for the Pre-caldera volcanic rocks of Santorini. Pp. 109-120 in: *Thera snd the Aegean World vol.2* (C. Doumas editor).

NINKOVICH, D. & HAYS, J.D. (1972). Mediterranean Island Arc and origin of high potash volcanoes. *Earth Planet. sci. Letters* **16**, 331-345.

NOH, H.J & BOLES, J.R. (1989). Diagenetic alteration of perlite in the Guryongpo area, Republic of Korea. *Clays Clay Miner.* **37**, 47-58.

NORRISH, K. (1954). The swelling of montmorillonite. *Disc. Faraday Soc.* **18**, 120-134.

NOVAK, I. & GREGOR, M. (1969). Surface area and decolourizing ability of some acid-treated montmorillonites. *Proc. Int. Clay Conf. Tokyo*, 851-857.

NOVAK, I. & CICEL, B. (1978). Dissolution of smectites in hydrochloric acid: II. Dossolution rate as a function of crystallochemical composition. *Clays Clay Miner.* **26**, 341-344.

O.C.M.A. (1973). *Specification No. DFCP-4, drilling fluid materials (bentonite).* The Institute of Petroleum, London, 5p.

ODOM, I.E. (1984). Smectite clay minerals: properties and uses. *Phil. Trans. R. Soc. Lond. A* **311**, 391-409.

ODOM, J.W. & LOW, P.F. (1978). Relation between swelling, surface area and b-dimension of Na-montmorillonites. *Clays Clay Miner.* **26**, 345-351.

O' DRISCOLL, M. (1988). Bentonite; overcapacity in need of markets. *Ind.Miner.***250**, 43-67.

VAN OLPHEN, H. (1959). Forces between suspended bentonite particles. Part II. Calcium bentonite. *Clays Clay Miner.* **6**, 196-206

VAN OLPHEN, H. (1963). *An introduction to Clay Colloid Chemistry.* Wiley, New York. N.Y., 301p.

VAN OLPHEN, H. (1977). *An introduction to Clay Colloid Chemistry,* 2nd ed. Wiley-Interscience, 318p.

OSTHAUS, B. (1956). Kinetic studies on montmorillonites and nontronite by the acid-dissolution technique. *Clays Clay Miner.* **4**, 301-321.

PABLO-GALAN, L. (1990). Diagenesis of Oligocene-Miocene vitric tuffs to montmorillonite and K-feldspar deposits, Durango, Mexico. *Clays Clay Miner.* **38**, 426-436.

PAPANICOLAOU, D. (1978). Contribution to the Geology of Aegean Sea. The island of

Andros. *Ann. Geol. Pays Hellen.* **29**, 477-553.

PAPANICOLAOU, D. (1986). *Geology of Greece.* Eptalofos, Athens, 240p (in Greek).

PAPANICOLAOU, D. (1988). Structural Analysis of the Milos Geothermal Field. *Unpub. Report, Electr. Board,* 115p.

PAPANICOLAOU, D. & SIDERIS, C. (1983). Le Paleozoique de l'autochthone de Chios: Une formation a blocks de type wildflysch d'age Permien (pro parte). *C. R. Acad. Paris* **297**, 603-606.

PAPAVASILIOU, C.T. & SIDERIS, C. (1982). Geochemistry and Mineralogy of Tertiary lavas of Sappai-Ferrai area (W. Thrace) Greece. Implications on their origin. P. 85 in: *The Geological Evolution of the Eastern Mediterranean* (Dixon, J.E. & Robertson, A.H.F. editors), Edinburgh (1982), Abstracts.

PAPAZACHOS, B.C. (1973). Distribution of seismic foci in the Mediterranean and sourrounding area and its tectonic implication. *Geophys. J. R. Astr. Soc.* **33**, 421-430.

PAPAZACHOS, B.C. (1976). Seismotectonics of the northern Aegean Area. *Tectonophysics* **33**, 199-209.

PARKES, W.B. (1971). *Clay-bonded foundry sand.* Applied Science Publishers, London, 367p.

PATERSON, E. & SWAFFIELD, R. (1987). Thermal analysis. Pp 99-132 in: *A Handbook of determinative methods in clay mineralogy* (M.J. Wilson editor) Blackie, Glasgow & London.

PATTERSON, S.H. & MURRAY, H.H. (1983). Clays. Pp 519-585 in: *Industrial Minerals and Rocks* (S.J Lefond, editor). Am. Inst. Mining Engineers, New York.

PE-PIPER, G & TSOLIS-KATAGAS P. (1991). K-rich mordenite from Late Miocene Rhyolitic Tuffs, Island of Samos, Greece. *Clays Clay Miner.* **39**, 239-247.

PERRY, E. & HOWER, J. (1970). Burial diagenesis in Gulf Coast pelitic sediments. *Clays Clay Miner.* **18**, 165-177.

PORPHYRIS, S. (1955). Untitled, unpublished note to the director of the Greek Geological Survey, 4p (in Greek).

PRICE, S.P. (1989). *Sedimentation and Neotectonics of the Burdur region, Southwest Turkey.* Ph.D Thesis. Univ. Leicester, U.K.

PROST, R. (1975). Interactions between adsorbed water molecules and the structure of clay minerals: Hydration mechanism of smectites. *Proc. Int. Clay Conf. Mexico*, 351-359.

RADOSLOVICH, E.W. (1962). Cell dimensions and symmetry of layer-lattice silicates. *Am. Miner.* **47**, 617-636.

RAMSEYER, K. & BOLES, J.R. (1986). Mixed-layer illite/smectite minerals in tertiary sandstones and shales, San Joaquin Basin, California. *Clays Clay Miner.* **34**. 115-

124.

RAND, B., PEKENC, R., GOODWIN, J.W. & SMITH, R.B. (1980). Investigation into the existence of edge-face coagulated structures in Na-montmorillonite suspensions: *J. Chem. Soc. Faraday. Trans.* **76**, 225-235.

RAVINA, I. & LOW, P.F. (1972). Relation between swelling, water properties and b-dimension in montmorillonite-water systems. *Clays Clay Miner.* **20**, 109-123.

REYNOLDS, R.C. (1984). Interstratified Clay Minerals. Pp. 249-303 in: *Crystal structures of clay minerals and their X-ray identification* (G.W. Brindley & G.Brown editors). Mineralogical Society, London.

REYNOLDS, R.C. (1989). Principles and techniques of quantitative analysis of clay minerals by X-ray powder diffraction. Pp 4-36 in: *Quantitative mineral analysis of clays* (D.R Pevear & F.A Mumpton editors) Clay Minerals Sociery workshop lectures vol. 1.

RICHARDSON, L.L. (1978). Use of bleaching clays in processing edible oils. *J. Am. Oil Chem. Soc.* **55**, 777-780.

RICHTER, I. & STROBACH, K. (1978). Benioff zones of the Aegean Arc. Pp. 410-414 in: *Alps, Appennines, Hellenides-Geodynamic Investigations along Geotraverses* (H. Closs, D.H. Roeder & K.Schidt, editors), Stuttgart.

ROBERTSON, R.H.S. (1986). *Fuller's earth, a history.* Volturna Press, Hythe, Kent, 421p.

ROBERTSON, H.E. & LAHANN, R.W. (1981). Smectite to illite conversion rates: effects of solution chemistry. *Clays Clay Miner.* **29**, 129-135.

ROBERTSON, A.H.F. & DIXON, J.E. (1984). Introduction: aspects of the geological evolution of the Eastern Mediterranean. Pp. 1-74 in: *The Geological Evolution of the Eastern Mediterranean* (J.E. Dixon & A.H.F. Robertson editors) Geological Society of London Special Publication No 17.

ROCK, N.M.S. (1988). *Numerical geology. Lecture notes in Earth Sciences.* Springer Verlag, Berlin, pp 304-311.

ROEN, J.B., & HOSTERMAN, J.W., (1982). Misuse of the term "bentonite" for ash beds of Devonian age in the Appalachian basin. *Geol. Soc. Am. Bull.* **93**, 921-925.

ROSENBERG, P.E., KITTRICK, J.A. & AJA, S.U. (1990). Mixed layer illite/smectite: A multiphase model. *Am. Miner.* **75**, 1182-1185.

ROTH, W. (1968). *Geologie von Nordwest-Chios (Ägäis).* Ph.D Thesis. Univ. Marburg, Germany, 88p.

RUPERT, J.P., GRANQUIST, W.T., & PINNAVAIA, T.J (1987). Catalytic Properties of Clay Minerals. Pp 275-318 in: *Chemistry of Clays and Clay Minerals* (A.C.D. Newman editor). Mineralogical Society, London.

RUSSELL, J.D. (1987). Infrared Methods. Pp 133-173 in: *A handbook of determinative methods in clay mineralogy* (M.J. Wilson editor) Blackie, Glasgow & London.

RUSSELL, J.D. & FRASER, A.R. (1971). IR spectroscopic evidence for interaction between

hydronium ions and lattice OH groups in montmorillonite. *Clays Clay Miner.* **19**, 55-59.

SANDERS, C.A. & DOELMAN, R.L. (1967). Durability of bonding clays. *Trans. Am. Found. Soc.* **75**, 408-427.

SANDERS, C.A. & DOELMAN, R.L. (1968). Durability of bonding clays-Part V. Durability characteristics of twenty nine commercial clays. *Trans. Am. Found. Soc.* **76**, 334-348.

SANDERS, C.A. & DOELMAN, R.L. (1969). Clay technology, durability of bonding clays, Parts VI-X. *Trans. Am. Found. Soc.* **77**, 233-252.

SANSOM, K.G., SMITH, R.G. & WHITE, D. (1968a). The cation-exchange capacity of layer lattice minerals, part I. *Trans. Brit. Ceram. Soc.* **67**, 83-91.

SANSOM, K.G., SMITH, R.G. & WHITE, D. (1968b). The cation exchange capacity of layer-lattice silicate minerals, part II. *Trans. Brit. Ceram. Soc.* **67**, 83-91.

SANSOM, K.G. & WHITE, D. (1970). Aggregation and dispersion in clays with particular reference to the montmorillonites. *Trans. Brit. Ceram. Soc.* **69**, 163-165.

SAUVAGE, M. (1846). Description geologique de l'ile de Milo. *Annales de Mines* **4**, 69-100.

SAVINS, J.G. & ROPER, W.F. (1954). A direct-indicating Viscometer for drilling fluids. *Proc. Amer. Petrol. Inst.* Section IV, 7-22.

SCHOFIELD, R.K. & SAMSON, H.R. (1954). Flocculation of kaolinite due to the attraction of oppositely charged crystal faces. *Disc. Faraday Soc.* **18**, 135-145.

SCHULTZ, L.G. (1969). Lithium and potassium absorption, dehydroxylation temperature and structural water content of aluminus smectites. *Clays Clay Miner.* **19**, 115-149.

SCOTT, P.W. (1990). Brightness and colour measurement. *CEC/Asean training course on assessment procedures for clays and ceramic raw materials, Ipoh Malaysia,* 11p.

SEIDEL, E., KREUZER, H. & HARRE, W. (1982). A late Oligocene/Early Miocene High-Pressure Belt in the external Hellenides. *Geol. Jb.* **E23**, 165-206.

SENGÖR, A.M.C., GÖRÜR, N. & AKKÖK, R. (1985). Strike-slip deformation basin formation and sedimentation: Strike slip faulting and related basin formation in zones of tectonic escape: Turkey as a case study. *Society of Economic Paleontologists and Mineralogists, Special Publication no 37*, 227-264.

SEYFRIED Jr, W.E. & MOTTL, M.J (1982). Hydrothemal alteration of basalt by seawater under seawater-dominated conditions. *Geochim. Cosmochim. Acta* **46**, 985-1002.

SEYITOGLU, G & SCOTT, B. (1991). Late Cenozoic crustal extension and basin formation in west Turkey. *Geol. Mag.* **128**, 155-166.

SHAINBERG, I., ALPEROVITCH, N.I. & KEREN, R. (1987). Charge density and Na-K-Ca exchange on smectites. *Clays Clay Miner.* **35**, 68-73.

SHAW, D.J. (1980). *Introduction to colloid and surface chemistry.* Butterworths, London, 236p.

SHEPPARD, R.A. & GUDE 3rd, A.J. (1968). Distribution and genesis of authigenic silicate minerals in tuffs of Pleistocene lake Tecopa, Inyo County, California. *U.S. Geol Surv. Prof. Paper* No **597**, 38p.

SHEPPARD, R.A. & GUDE 3rd, A.J. (1973). Zeolites and associated authigenic silicate minerals in tuffaceous rocks of the Big Sandy Formation, Mohave County, Arizona. *U.S. Geol. Surv. Prof. Paper*, No **830**, 36p.

SHIRAKI, R., SAKAI, H., ENDOH, M. & KUSHIMA, N. (1987). Experimental studies on rhyolite- and andesite-seawater interactions at 300oC and 1,000 bars. *Geochem. J.* **21**, 139-148.

SHIRAKI, R. & IIYAMA, T. (1990). Na-K ion exchange reaction between rhyolitic glass and (Na,K)Cl aqueous solution under hydrothermal conditions. *Geochim. Cosmochim. Acta* **54**, 2923-2931.

SIDERIS, C. (1986). *Contribution to the knowledge of the geodynamic evolution during the Permo-Triassic in the area of Eastern Greece.* Ph.D Thesis. Univ. Athens, Greece. 212p (in Greek).

SIDDIQUI, M.K.H. (1968). *Bleaching earths.* Pergamon Press, Oxford, Pp 32-55.

SIMEAKIS, K. (1985). Neotectonic evolution of the Island Group of Milos. *Unpub. Report, IGME,* 50p (in Greek).

SKARPELIS, N. (1982). *Genesis of the massive sulphide ore deposits and petrology of the external metamorphic zone of Hellenides (SE Peloponnese).* Ph.D Thesis, Univ. Athens, Greece, 149p (in Greek).

SMITH, H.W., MOODIE, C.D., OKAZAKI, R. & ELLSWORTH, N. (1966). Hydrolysis and salt-retention errors in conventional cation exchange capacity procedures: II. *Soil Sci.* **102**, 94-106.

SONDER, R.A. (1924/25). Zur Geologie und Petrographie der Inselgruppe von Milos. *Z. Volcanologie.* **8**, 181-237.

SPARKS, R.S.J., WILSON, L. & HULME, G. (1978). Theoretical modeling of the generation, movement and emplacement of pyroclastic flows by column collapse. *J. Geophys. Res.* **83**, 1727-1739.

SPARKS, R.S.J., SIGURDSSON, H. & CAREY, S.N. (1980). The entrance of pyroclastic flows into the sea, II. Theoretical considerations on subaqueous emplacement and welding. *J. Volcanol. Geotherm. Res.* **7**, 97-105.

SPEARS, D.A & KANARIS-SOTIRIOU, R. (1979). A geochemical and mineralogical investigation of some British and other European tonsteins: *Sedimentology* **26**, 407-425.

SRASRA, E., BERGAYA, F., VAN DAMME, H. & ARGUIB, N.K. (1989). Surface properties of an activated bentonite-Decolourization of rape-seed oil. *Appl. Clay Sci.* **4**, 411-421.

SRODON, J. (1980). Precise identification of illite/smectite interstratifications by X-ray

diffraction. *Clays Clay Miner.* **28**, 401-411.

SRODON, J. & EBERL, D.D. (1984). Illite. Pp 495-538 in: *Micas* (S.W. Bailey editor). Reviews in Mineralogy, Vol. 13, Mineralogical Society of America.

SRODON, J., MORGAN, D.J., ESLINGER, E.V., EBERL, D.D. & KARLINGER, M.R. (1986). Chemistry of illite/smectite and end-member illite. *Clays Clay Miner.* **34**, 368-378.

STEEFEL, C.I. & VAN CAPPELLEN, P. (1990). A new kinetic approach to modeling water-rock interaction: The role of nucleation, precursors and Ostwald ripening. *Geochim. Cosmochim. Acta* **54**, 2657-2677.

STEPHENS, H.A. & WATERWORTH, A.N. (1968). Significance of the exchangeable cation in foundry bentonite. *Brit. Found.* **61**, 202-219.

STOCH, L., BAHRANOWSKI, K., BUDEK, L. & FIJAL, J. (1977). Bleaching properties of non-bentonitic clay materials and their modification. *Mineralogia Polonica* **8**, 31-49.

STOCH, L., BAHRANOWSKI, K. & GATARZ, Z. (1979a).Bleaching properties of non-bentonitic clay materials and their modification: II. Bleaching ability of natural and activated Krakowiec clays from Machow. *Mineralogia Polonica* **10**, 21-38.

STOCH, L., BAHRANOWSKI, K., EILMES, J. & FIJAL, J. (1979b). Bleaching properties of non-bentonitic clay materials and their modification: III. Modification of bleaching properties of Krakowiec clays from Machow with some organic compounds. *Mineralogia Polonica* **10**, 39-47.

STUCKI, J.W., LOW, P.F., ROTH, C.B. & GOLDEN, D.C. (1984). Effects of oxidation state of octahedral iron on clay swelling. *Clays Clay Miner.* **22**, 391-396.

STUCKI, J.W. & TESSIER, D, (1991). Effects of iron oxidation state on the texture and structural order of Na-nontronite gels. *Clays Clay Miner.* **39**, 137-143.

STUL, M.S., & MORTIER, W.J. (1974). The heterogeneity of the charge density in montmorillonites. *Clays Clay Miner.* **22**, 391-396.

SUQUET H., DE LA CALLE, C & PEZERAT, H. (1975). Swelling and structural organization of saponite. *Clays Clay Miner.* **23**, 1-9.

SURDAM, R.C. (1977). Zeolites in closed hydrological systems. Pp 65-91 in: *Mineralogy and Geology of Natural Zeolites* (F.A. Mumpton editor). Reviews in mineralogy, vol 4, Mineralogical Society of America.

SURDAM, R.C. & SHEPPARD, R.A. (1978). Zeolites in saline, alkaline-lake deposits. Pp 145-174 in: *Natural zeolites* (L.B Sand & F.A. Mumpton, editors).

SVERJENSKY, D.A. (1984). Europium redox equilibria in aqueous solution. *Earth Planet. Sci. Lett.* **67**, 70-78

TALIBUDEEN, O. & GOULDING, K.W.T. (1983). Charge heterogeneity in smectites. *Clays Clay Miner.* **22**, 391-396.

TAYLOR, M.W. & SURDAM, R.C. (1981). Zeolite Reactions in the tuffaceous sediments at Teels Marsh, Nevada. *Clays Clay Miner.* **29**, 341-352.

TESSIER, D. & PEDRO, G. (1982). Electron microscopy study of Na-smectite fabric-Role of layer charge, salt concentration and suction parameters. *Proc. Int. Clay Conf. Pavia*, (van Olphen, H. & Veniale, F. editors) 165-176.

TETTENHORST, R. & JOHNS, W.D. (1966). Interstratification in montmorillonite. *Clays Clay Miner.* **25**, 85-93.

TIETZE, K-W. (1969). *Geologie von Mittel-Chios (Ägäis)*. Ph.D Thesis. Univ. Marburg, Germany, 145p.

THANASOULAS, K. (1983). Reconnaissance geoelectric study in NW Milos. *Unpubl. Report, IGME*, 6p (in Greek).

THANASOULAS, K. & TSOKAS, G. (1985). Geoelectric study of Kimolos Island. *Unpub. Report, IGME*, 8p (in Greek).

THOMAS, C.L., HICKEY, J. & STECKER, G. (1950). Chemistry of clay cracking catalysts. *Ind. Engng. Chem.* **42**, 866-871.

TSIPURSKY, S.I., & DRITS, V.A (1984). The distribution of octahedral cations in the 2:1 layers of dioctahedral smectites studied by oblique-texture electron diffraction. *Clay Miner.* **19**, 177-199.

TSOLIS-KATAGAS, P. & MAVRONICHI, M. (1989). Kaolinization of the Kimolos Island volcanics, Cyclades, Greece. *Clay Miner.* **24**, 75-89.

VALI, H. & KÖSTER, H.M. (1986). Expanding behaviour, structural disorder, regular and random irregular interstratification of 2:1 layer silicates studied by high-resolution images of transmission electron microscopy. *Clay Miner.* **21**, 827-859.

VAN DER MAREL, H.W. & BEUTELSPACHER, H. (1976). *Atlas of Infra Red Spectroscopy of Clay Minerals and their admixtures.* Elsevier, Amsterdam.

VELDE, B. (1985). *Clay Minerals. A physico-chemical explanation of their occurrence.* Pp 38-43. and 104-145. Elsevier, Amsterdam.

VIANI, B.E., LOW, P.F. & ROTH, C.B. (1983). Direct measurement of the relation between interlayer force and interlayer distance in the swelling of montmorillonite. *J. Coll. Inter. Sci.* **96**, 229-244.

VOGEL, A.I. (1961). *A textbook of quantitative inorganic analysis, 3rd edition.* Longmans, London, pp. 235-238.

VOREADIS, G.D., & MOURAMBAS, T.G. (1935). The silver deposits of Milos Island. *Greek Geol Surv.* **22**, 9-54 (in Greek).

VOREADIS G.D. (1958). The kaoline deposits in the area Kontaros-Tria Pigadia, Milos. *Bull. Geol. Soc. Greece* **3**, 157-180.

WALSH, J.N., BUCKLEY, F. & BARKER, J. (1981). The simultaneous determination of the REE's in rocks using ICP source spectrometry. *Chem. Geol.* **33**, 141-153.

WATSON, I. (1982). Minerals in animal feedstuffs-plenty of food for thought. *Ind. Miner.***175**, 71-91.

WEAVER, C.E & POLLARD, L.D. (1973). *The chemisrty of clay minerals.* Pp 55-77. Elsevier, Amsterdam.

WEAVER, C.E. (1989). *Clays, Muds and Shales.* Elsevier, Amsterdam. P 378.

WELLMER, F-W. (1989). *Economic evaluations in exploration.* Springer Verlag, Berlin. Pp. 1-15.

WETZENSTEIN, W. (1969). *Die Bentonitlagerstätten im Ostteil der Insel Milos/Griechenland und ihre mineralogische Zussamensetzung.* Ph.D Thesis, Univ. Stuttgart, Germany, 63pp.

WETZENSTEIN, W. (1972). Die bentonitlagerstätten im Osteil der Insel Milos und ihre mineralogische Zussamensetzung. *Bull. Geol. Soc. Greece* **6**, 144-171.

WETZENSTEIN, W. (1975). Tektonik und Metallogenese der Insel Milos/Kykladen. *Bull. Geol. Soc. Greece* **17**, 31-39.

WHITE, A.F. & CLAASEN, H.C. (1980). Kinetic model for the short-term dissolution of a rhyolitic glass. *Chem. Geol.* **28**, 91-109.

WHITE, A.F. (1983). Surface chemistry and dissolution kinetics of glassy rocks at 25°C. *Geochim. Cosmochim. Acta* **47**, 805-815.

WHITNEY, G. (1990). Role of water in the smectite-to-illite reaction. *Clays Clay Miner.* **38**, 343-350.

WHITNEY, G. & NORTHROP. R (1988). Experimental investigation of the smectite to illite reaction: Dual reaction mechanisms and oxygen-isotope systematics. *Am. Miner.* **73**, 77-90.

WILBORG, H.E. & HENDERSON, G.V. (1983). Foundry sand. Pp 271-278 in: *Industrial minerals and rocks 5th edition* (S.J. Lefond editor) American Institute of Mining Enginners.

WILSON, M.J. & CRADWICK, P.D. (1972). Occurrence of interstratified kaolinite-montmorillonite in some Scottish soils. *Clay Miner.* **9**, 435-437.

WINCHESTER, J.A. & FLOYD, P.A. (1977). Geochemical discrimination of different magma series and their differentiation products using immobile elements. *Chem. Geol.* **20**, 325-343.

WIRSCHING, U. (1976). Experiments on hydrothermal alteration processes of rhyolitic glass in closed and "open" system. *N. Jb. Miner. Mh* **5**, 203-219.

WOOD, S.A. (1990a). The aqueous geochemistry of the rare-earth elements and yttrium. 1. Review of available low-temperature data for inorganic complexes and the inorganic REE speciation of natural waters. Che*m. Geol.* **82**, 159-186.

WOOD, S.A. (1990b). The aqueous geochemistry of the rare-earth elements and yttrium. 2. Theoretical predictions of speciation in hydrithermal solutions at 350°C at saturation water vapour pressure. *Chem. Geol.* **88**, 99-125.

WRIGHT, T.L. (1968). X-ray and optical study of alkali-feldspar: II. An X-ray method for

determining the composition and structural state from measurement of 2_ values for three reflections. *Am. Miner.* **53**, 88-104.

YAMADA, H., NAKAZAWA, H., YOSHIOKA, K., & FUJITA, T. (1991). Smectites in the montmorillonite-beidellite series. *Clay Miner.* **26**, 359-369.

YARIV, S. & CROSS, H. (1979). *Geochemistry of colloid systems.* Springer Verlag, Berlin. Pp 93-155.

YATES, M.H. (1986). Acid treatment of English montmorillonite and its effect on clay structure and properties. *Unpublished paper (Laporte Inorganics, Widnes, UK).*

ZACHARIASEN, W.H. (1932). The atomic arrangement in glass. *J. amer. Chem. Soc.* **54**, 3841-3851.

ZAGALIS, K.P. (1983). *Quantitative analysis of the kaolins and bentonites of Milos Island.* Unpub. Report, IGME, 10p.

ZAKI, I., ABDEL-KHALIK, M. & HABASHI, G.M. (1986). Acid leaching and concequent pore structure and bleaching capacity modifications of Egyptian clays. *Colloids & Surfaces* **17**, 241-249.

ZIELINSKI, R.A. (1982). The mobility of Uranium and other elements during alteration of rhyolite ash to montmorillonite: A case study in the troublesome formation, Colorado, USA. *Chem. Geol.* **35**, 185-204.